Talanta

The International Journal of Pure and Applied Analytical Chemistry

Editors-in-Chief

Professor G.D. Christian, University of Washington, Department of Chemistry, 36 Bagely Hall, P.O. Box 351700, Seattle,WA 98195-1700, U.S.A.

Professor J.-M. Kauffmann, Université Libre de Bruxelles, Institut de Pharmacie, Campus de la Plaine, C.P. 205/6, Boulevard du Triomphe, B-1050 Bruxelles, Belgium

Associate Editors

Professor J.-H. Wang, Research Center for Analytical Sciences, Northeastern University, Box 332, Shenyang 110004, China

Professor J.L. Burguera, Los Andes University, IVAIQUIM, Faculty of Sciences, P.O. Box 542, 5101-A Mérida, Venezuela.

Assistant Editors

Dr R.E. Synovec, Department of Chemistry, University of Washington, Box 351700, Seattle, WA 98195-1700, U.S.A.

Professor J.-C. Vire, Université Libre de Bruxelles, Institut de Pharmacie, Campus de la Plaine, C.P. 205/6, Boulevard du Triomphe, B-1050 Bruxelles, Belgium

Talanta

R. Apak (Istanbul, Turkey)
L.G. Bachas (Lexinton, KY, U.S.A.)
E. Bakker (Auburn, AL, U.S.A.)
D. Barceló (Barcelona, Spain)
K. Booksh (Tempe, AZ, U.S.A.)
C.M.A. Brett (Coimbra, Portugal)
Yi. Chen (Beijing, China)
R. Compton (Oxford, U.K.)
S. Cosnier (Grenoble, France)
P.K. Dasgupta (Lubbock, TX, U.S.A.)
D. Diamond (Dublin, Ireland)
G.A. Eiceman (Las Cruces, NM, U.S.A.)
M.-R. Fuh (Taipei, Taiwan)
K. Grupdan (Chaing Mai, Thailand)
V.K. Gupta (Roorkee, India)
A. Gustavo González (Sevilla, Spain)
I. Gutz (Sao Paulo, Brazil)
E.H. Hansen (Lyngby, Denmark)
P. de B. Harrington (OH, U.S.A.)
W.L. Hinze (Winston-Salem, NC, U.S.A.)
A. Ivaska (Turku, Finland)
B. Karlberg (Stockholm, Sweden)
U. Karst (Enschede, The Netherlands)
R. Lobinski (Pau, France)
C.A. Lucy (Edmonton, AB, Canada)
M.D. Luque de Castro (Cordoba, Spain)
I.D. McKelvie (Victoria, Australia)
E. Morosonova (Moscow, Russia)
J.-M. Pingarron (Madrid, Spain)
E. Pretsch (Zürich, Switzerland)
W. Schuhmann (Bochum, Germany)
M. Shamsipur (Kermanshah, Iran)
K. Suzuki (Yokohama, Japan)
D.L. Tsalev (Sofia, Bulgaria)
Y. Umezawa (Tokyo, Japan)
K. Vytras (Pardubice, Czech Republic)
B. Walzcak (Katowice, Poland)
R. von Wandruszka (Moscow, U.S.A.)
J. Wang (Tempe, AZ, U.S.A.)
J.D. Winefordner (Gainesville, U.S.A)
Xiu-Ping Yan (Tianjin, China)
E.A.G. Zagatto (Piracicaba, SP, Brazil)

Copyright © 2007 Elsevier B.V. All rights reserved

Publication information: *Talanta* (ISSN 0039-9140). For 2007, volumes 71–73 are scheduled for publication. Subscription prices are available upon request from the Publisher or from the Regional Sales Office nearest you or from this journal's website (http://www.elsevier.com/locate/talanta). Further information is available on this journal and other Elsevier products through Elsevier's website: (http://www.elsevier.com). Subscriptions are accepted on a prepaid basis only and are entered on a calendar year basis. Issues are sent by standard mail (surface within Europe, air delivery outside Europe). Priority rates are available upon request. Claims for missing issues should be made within six months of the date of dispatch.

Orders, claims, and journal enquiries: please contact the Customer Service Department at the Regional Sales Office nearest you:
Orlando: Elsevier, Customer Service Department, 6277 Sea Harbor Drive, Orlando, FL 32887-4800, USA; phone: (+1) (877) 8397126 [toll free number for US customers], or (+1) (407) 3454020 [customers outside US]; fax: (+1) (407) 3631354; e-mail: usjcs@elsevier.com
Amsterdam: Elsevier, Customer Service Department, PO Box 211, 1000 AE Amsterdam, The Netherlands; phone: (+31) (20) 4853757; fax: (+31) (20) 4853432; e-mail: nlinfo-f@elsevier.com
Tokyo: Elsevier, Customer Service Department, 4F Higashi-Azabu, 1-Chome Bldg, 1-9-15 Higashi-Azabu, Minato-ku, Tokyo 106-0044, Japan; phone: (+81) (3) 5561 5037; fax: (+81) (3) 5561 5047; e-mail: jp.info@elsevier.com
Singapore: Elsevier, Customer Service Department, 3 Killiney Road, #08-01 Winsland House I, Singapore 239519; phone: (+65) 63490222; fax: (+65) 67331510; e-mail: asiainfo@elsevier.com

USA mailing notice: *Talanta* (ISSN 0039-9140) is published monthly by Elsevier B.V. (P.O. Box 211, 1000 AE Amsterdam, The Netherlands). Annual subscription price in the USA US$ 3,818 (valid in North, Central and South America), including air speed delivery. Application to mail at periodical postage rate is paid at Rathway, NJ and additional mailing offices.
USA POSTMASTER: Send address changes to *Talanta*, Publications Expediting Inc., 200 Meacham Avenue, Elmont, NY 11003.
AIRFREIGHT AND MAILING in the USA by Publications Expediting Inc., 200 Meacham Avenue, Elmont, NY 11003.

Available online at www.sciencedirect.com
ScienceDirect
Talanta 71 (2007) 1103–1109
Talanta
www.elsevier.com/locate/talanta

Spectrophotometric determination of beryllium in water samples after micelle-mediated extraction preconcentration

Abbas Afkhami [a,*], Tayyebeh Madrakian [a], Elaheh Bozorgzadeh [a], Morteza Bahram [b]

[a] Department of Chemistry, Faculty of Science, Bu-Ali Sina University, Hamadan, Iran
[b] Department of Chemistry, Faculty of Science, Urmia University, Urmia, Iran

Received 22 April 2006; received in revised form 1 June 2006; accepted 1 June 2006
Available online 7 July 2006

Abstract

A new micelle-mediated phase preconcentration method for preconcentration of ultra-trace quantities of beryllium as a prior step to its determination by spectrophotometry has been developed. Chrome Azurol S (CAS) and cetyltrimethylammonium bromide (CTAB) were used as chelating agent and cationic surfactant, respectively. The method evaluates and eliminates the blank bias error present in such procedures using mean centering of ratio spectra. This procedure gives more accurate results than the traditional approach using absorbance values against reagent blank. The optimal extraction and reaction conditions were studied and the analytical characteristics of the method (e.g., limit of detection, linear range, preconcentration and improvement factors) were obtained. Linearity was obeyed in the range of 0.9–18.0 ng mL^{-1} (1.00×10^{-7}–2.00×10^{-6} mol L^{-1}) of beryllium. The detection limit of the method is 0.51 ng mL^{-1} (5.66×10^{-8} mol L^{-1}) of beryllium. The interference effect of some anions and cations was also tested. The method was applied to the determination of beryllium in spring water samples.
© 2006 Elsevier B.V. All rights reserved.

Keywords: Beryllium determination; Micelle-mediated extraction; Chrome Azurol S; Spectrophtometry; Mean centering

1. Introduction

Beryllium finds use in alloys, e.g., those of copper, aluminum, magnesium, nickel, zinc and iron, in aircraft materials and as a neutron reflector in nuclear reactors because the oxide shows good thermal conductivity in spite of its high melting point and high electrical insulation. However, beryllium and its compounds are very toxic, especially to the lung, skin and eyes and at high concentration can cause death [1]. For example, the toxic concentration (TC) of beryllium in air for a person is 0.1 mg m^{-3}, the median lethal dose (LDw) of beryllium chloride for a rat, is 86 mg kg^{-1} and the LDw of beryllium sulfate for a mouse is 80 mg kg^{-1}.

The carcinogenic risks to humans of beryllium and beryllium compounds have been considered on a number of occasions by the International Agency for Research on Cancer (IARC) of the World Health Organization (WHO) [2]. Different national guidelines suggested that beryllium concentrations should not exceed a limit of 0.1 μg L^{-1} for tap water and 0.2 μg L^{-1} for surface water [3]. The average beryllium concentration in natural waters is in the ng L^{-1} range [4]. Therefore, sensitive and reliable analytical methods are necessary to determine its concentration.

Different methods including spectrophotometry [5–7], spectrofluorimetry [8], potentiometry [9,10], atomic absorption spectrometry (AAS) [3,11–13], inductively coupled plasma optical emission spectrometry (ICP-OES) [14–17] and inductively coupled plasma mass spectrometry (ICP-MS) [18] have been used for the determination of beryllium.

As the concentration of beryllium in some real samples is very low, suitable enrichment procedures are required for beryllium determination. Several methods have also been reported for the preconcentration of beryllium prior to its determination. Okutani et al. [19] determined beryllium at μg L^{-1} levels in water samples by graphite furnace atomic absorption spectrometry (GF-AAS) after preconcentration and separation as the beryllium acetylacetone complex on activated carbon. Szczepaniak and Szymanski [20] determined trace beryllium by GF-AAS after preconcentration on silica gel with immobilized morin. Beryllium in the range 0.07–0.184 μg L^{-1} could be determined

* Corresponding author. Tel.: +98 811 8272404; fax: +98 811 8272404.
E-mail address: afkhami@basu.ac.ir (A. Afkhami).

0039-9140/$ – see front matter © 2006 Elsevier B.V. All rights reserved.
doi:10.1016/j.talanta.2006.06.004

by this method. Kubova et al. [21] determined trace beryllium in mineral waters by GF-AAS after preconcentration on a salicylate chelating resin. Nasciment and Schwedt [22] used polyethylene powder as an adsorbent for preconcentration of the complex formed between beryllium and Chrome Azurol S prior to the determination by GF-AAS. Yamini et al. [23] preconcentrated beryllium by an octadecyl silica cartridge, modified with quinalizarine as a chelating agent and determined it by atomic absorption spectrometry. Suvardhan et al. [24] used a syringe loaded with sorbent 2-propylpiperidine-1-carbothioate for the separation and enrichment of beryllium, lead, nickel and bismuth prior to their analysis by flame atomic absorption spectrometry. We reported a method for the determination of ultra-trace quantities of beryllium by FAAS after preconcentration of Be^{2+} on an OH-form strong base anion exchange resin [25]. Suvardhan et al. [26] developed a method for the determination of beryllium, lead, nickel and bismuth in various water samples. They loaded a syringe with 2-propylpiperidine-1-carbodithioate as a sorbent for the separation and enrichment of beryllium, lead, nickel and bismuth prior to their analysis by flame atomic absorption spectrometry.

Clouding is a phenomenon familiar in non-ionic surfactants; upon raising the temperature, the system becomes cloudy and phase separate at a well-defined temperature, T_{cp} [27]. For charged micelles, the phenomenon rarely occurs, presumably because electrostatic repulsion prevents phase separation in most cases. In the presence of salt, long-tailed cationic surfactants can self-assemble in aqueous solution into long, flexible worm-like micelles, thus rendering the solution viscoelastic [28,29]. Salts with hydrophobic counterions, such as sodium salicylate (NaSal) and sodium tosylate (NaTos), are particularly effective in inducing micellar growth even at low concentrations. With increasing salt content, complex variations occur in the rheological properties [28–30].

High concentrations of salt also cause cationic surfactant solutions to separate into immiscible surfactant-rich and surfactant-poor phases [31]. This phenomenon, originally termed coacervation, has been investigated since the 1940s and was first observed for mixtures of the cationic surfactant Hyamine 1622 with salts such as potassium thiocyanate (KSCN) and potassium chloride (KCl) [32,33]. The phase separation is typically of the upper consolute type, i.e., it occurs on cooling below a characteristic temperature T_c, which, in turn, increases with salt content [31].

Triphenylmethane dye Chrom Azurol S (3″-Sulfo-2″,6″-dichloro-3,3′-dimethyl-4-hydroxyfuchsone-5,5′-dicarboxylic acid, trisodium salt; CAS) reacts with beryllium to form the anionic complex $Be(CAS)_2$ [34]. Surfactants can interact with the dye and/or the meta–dye complex as an individual molecule or aggregates. For example, cationic surfactants react by ion pair formation with the anionic $Be(CAS)_2$ to form a ternary complex involving surfactant monomers [35].

To the best of our knowledge, there is no report on the cloud point extraction of beryllium. In this paper, a cloud point extraction spectrophotometric method for the determination of ultra-trace beryllium is described. The method is based on the complexation reaction of beryllium with CAS and micelle-mediated extraction of the complex. The cationic surfactant cetyltrimethylammonium bromide (CTAB) was used.

The reagent blank, the response obtained from an analyte-free sample solution, is considered as an integral part of measurement technique and its response usually is subtracted from the standard response. In spectrophotometry, when the product formed and one of the reagents absorb at the same wavelength, the blank absorbance at the end of reaction can be lower than that measured in the beginning, because of the reagent consumption. Therefore, the real absorbance of the formed product will be larger than the measured value. If we consider a calibration line, this difference will increase by increasing the concentration of analyte and therefore affect the accuracy of the analytical response. Furthermore, excess reagents cannot be used in spectrophotometric determination, because if the blank absorbs near the absorbance maximum of product formed, the presence of excess amounts of reagents can affect the molar absorptivities and therefore the calibration line is distorted [36].

Recently Falco et al. [37] have shown that the H-point standard addition method (HPSAM) can be used for the determination of the analyte concentration free from bias error. This method needs to have several standard addition samples. The responses are collected in two selected wavelengths so that blank absorptivity is the same in both wavelengths. The difference of absorbance (absorbance increment) in these wavelengths (ΔA) will cancel the contribution of the reagent blank. The disadvantage of HPSAM is its need for standard addition for every sample. Also when using the absorbance increment instead of one wavelength absorbance we loose some of the method's sensitivity.

Gao [38] has proposed another method for correction of this bias called β-correction absorbance. This method uses some mathematical equations to give correct responses. This method also uses only a couple of wavelengths for calculations.

More recently we have presented some new approaches for simultaneous analysis of binary and ternary mixtures which we called mean centering of ratio spectra [39–42].

In the present work, we used mean centering of ratio spectra for blank bias error elimination. The results related to determination of beryllium after CPE using mean centering of ratio spectra showed that this method can be used where the analyte determination requires the use of an absorbent reagent.

2. Experimental

2.1. Apparatus

A Perkin-Elmer Lambda 45 UV–vis spectrometer was used for recording absorbance spectra. Absorption measurements at λ_{max} wavelength were performed using a Shimadzu UV-mini-1240 V spectrophotometer with 1-cm quartz cells (0.5 mL). A Metrohm pH meter (model 713) with a combined glass electrode was used for pH measurements. A centrifuge with 10-mL calibrated centrifuge tubes (Superior, Germany) was used to accelerate the phase separation process. All calculations in the computing process were done in Matlab6.5 and Microsoft Excel

for windows. A simple program was written for this purpose in Matlab6.5.

2.2. Reagents

All the solutions were prepared using reagent grade substances and triply distilled water. A 1.000 g L^{-1} (1.11×10^{-2} mol L^{-1}) stock solution of Be^{2+} was prepared in 0.10 mol L^{-1} sulfuric acid using $BeSO_4 \cdot 4H_2O$ (Merck). Working solutions were prepared by appropriate dilution of the stock solution every day. A 4.0×10^{-4} mol L^{-1} CAS solution was prepared by dissolving an appropriate amount of CAS (Merck) in water. A 0.1% (w/v) (2.74×10^{-3} mol L^{-1}) CTAB solution in water was prepared. Acetate buffer solution of pH 5 was prepared from 0.5 mol L^{-1} acetic acid and 0.5 mol L^{-1} sodium acetate solutions.

2.3. Procedure

An aliquot of the solution containing 10–250 ng (1.11–27.75 nmol) of beryllium ion, 0.4 mL of 1.0×10^{-4} mol L^{-1} CAS solution, 2 mL of pH 5 acetate buffer solution and 1 mL of 0.1% (w/v) (2.74×10^{-3} mol L^{-1}) CTAB solution were transferred into a 10-mL tube. The solution was diluted to approximately 9 mL with water and allowed to stand for 10 min at room temperature. Then 1 mL of 0.10 mol L^{-1} KI solution was added and made up to the mark with water. Separation of two phases was accelerated by centrifugation for 5 min at 3000 rpm. The aqueous phase was easily decanted by simply inverting the tube. The surfactant rich phase of this procedure was dissolved and diluted to 0.5 mL with ethanol and transferred into a 0.5-mL quartz cell. The absorbance spectrum of the solution was recorded and stored in the range of 350–700 nm. A calibration graph for beryllium was constructed by recording and storing the absorbance spectra for the solutions containing different concentrations of beryllium submitted to the same procedure. The blank solution was submitted to the same procedure and its spectrum was recorded and stored.

The stored sample spectra were divided by the spectrum of the blank solution according to Eq. (2) and mean centering of these vectors with respect to the wavelength was obtained according to Eq. (3). The minimum or maximum of these vectors with respect to wavelength is used for the construction of the calibration graph for beryllium.

3. Results and discussion

The colored complex of beryllium with CAS can be extracted by cloud point extraction method using CTAB as a cationic surfactant. Fig. 1 shows the absorbance spectra for Be–CAS complex and the blank solution in surfactant rich phase. As Fig. 1 shows the absorbance spectra of complex and CAS overlapped. For accurate determination of beryllium by spectrophotometry the accurate absorbance for complex should be determined. Due to the overlapping of the sample and blank spectra the blank signal should subtracted from sample signal. The amount of blank

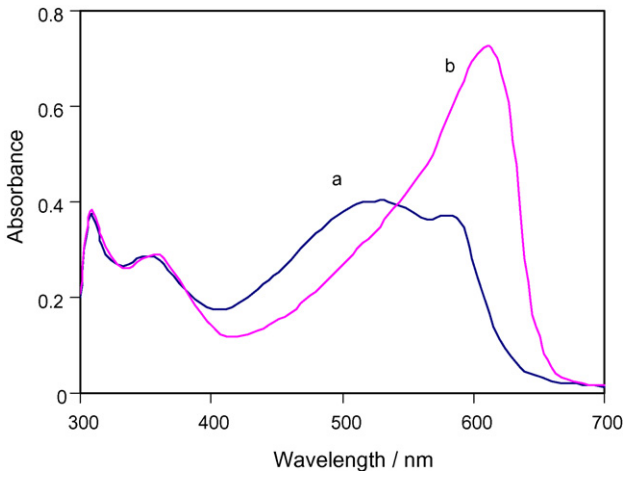


Fig. 1. Absorption spectra for CAS (a) and its complex with beryllium (b) in surfactant-rich phase. Conditions: CAS, 4.0×10^{-6} mol L^{-1}; beryllium, 6.0 ng mL^{-1} (6.66×10^{-7} mol L^{-1}); KI, 0.01 mol L^{-1}; CTAB concentration, 0.01% (w/v) (2.74×10^{-4} mol L^{-1}); pH, 5.

signal at different wavelengths depends on the concentration of beryllium. Therefore, the accurate blank signals for the solutions with different concentrations of beryllium are not the same. For example blank signal decreases by increasing beryllium concentration at 612 nm. By applying mean centering of ratio spectra [39–42] the blank signal can be canceled truly and the accurate sample signal can be obtained.

3.1. Effect of variables

To take full advantage of the procedure, the reagent concentrations and reaction conditions must be optimized. Various experimental parameters were studied in order to obtain optimized system. These parameters were optimized by setting all parameters to be constant and optimizing one each time. This optimization procedure may not lead to the actual optimum, although it certainly leads to an improvement of the analytical method. In the optimization of conditions the absorbance change for the solution (ΔA) at 612 nm was followed.

Effect of CAS concentration on the extraction and determination of beryllium was investigated in the range 1.0×10^{-6} to 1.6×10^{-5} mol L^{-1}(0.9–14.5 molar ratio CAS/Be). As Fig. 2 shows the sensitivity of the method increased by increasing CAS concentration up to 4.0×10^{-6} (3.6 molar ratio CAS/Be) mol L^{-1} and decreased at higher concentrations. It was expected that increasing CAS causes an increase in ΔA because increasing in CAS concentration caused an increase in $Be(CAS)_2$ concentration. At concentrations higher than 4.0×10^{-6} mol L^{-1} (3.6 molar ratio CAS/Be) the concentration of complex did not change significantly but the concentration of uncomplexed CAS increase significantly. Because the blank absorbs near the absorbance maximum of complex, presence of excess amounts of reagents can affect the molar absorptivitiy and therefore much probably, the decrease in ΔA at concentrations higher than 4.0×10^{-6} mol L^{-1} decreases is due to this fact. A concentration of 4.0×10^{-6} mol L^{-1} of CAS was selected as the optimum.

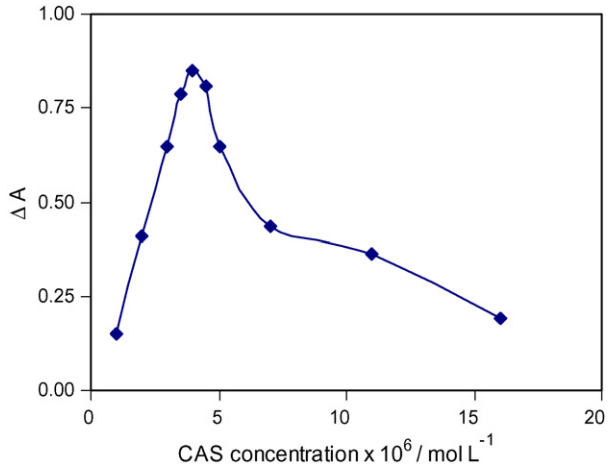


Fig. 2. Effect of CAS concentration on the extraction and determination of beryllium. Conditions: beryllium, 10.0 ng mL^{-1} (1.11×10^{-6} mol L^{-1}); KI, 0.01 mol L^{-1}; CTAB concentration, 0.01% (w/v) (2.74×10^{-4} mol L^{-1}); pH, 5.

Effect of CTAB concentration on the extraction and determination of beryllium was investigated in the range 0.003–0.03% (w/v) (8.23×10^{-5} to 8.23×10^{-4} mol L^{-1}). The results are shown in Fig. 3. The amount of the absorbance for sample increased by increasing in CTAB concentration up to 0.01% (w/v) (2.74×10^{-4} mol L^{-1}) and remained constant at higher concentrations. The blank signal also increased slowly by increasing CTAB concentration. But the difference between the sample and blank signals (ΔA at 612 nm) increased by increasing CTAB concentration up to 0.01% (w/v) and decreased slowly at higher concentrations. Therefore, 0.01% (w/v) CTAB was chosen as the optimum.

As described above, addition of salt can cause cationic surfactant solutions to separate into immiscible surfactant-rich and surfactant-poor phases. Therefore, iodide was added to induce micellar growth and extraction of complex. The effect of iodide concentration was studied in the range 0.002–0.02 mol L^{-1}. The

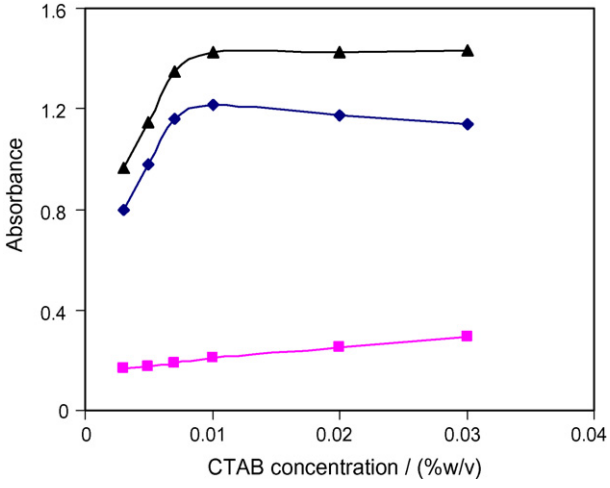


Fig. 3. Effect of CTAB concentration on the extraction and determination of beryllium, sample (▲), blank (■) and their difference (♦). Conditions: beryllium, 15.0 ng mL^{-1} (1.67×10^{-6} mol L^{-1}); KI, 0.01 mol L^{-1}; CAS concentration, 4.0×10^{-6} mol L^{-1}; pH, 5.

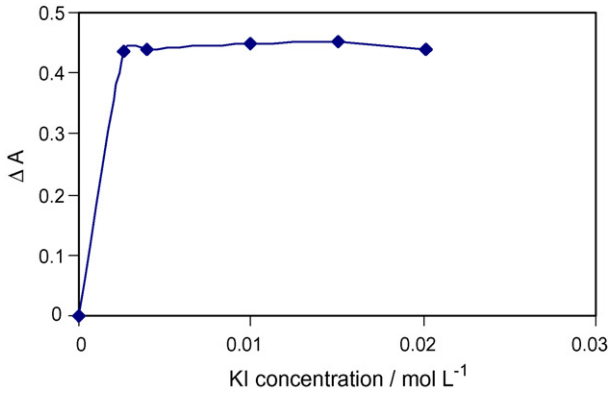


Fig. 4. Effect of iodide concentration on the extraction and determination of beryllium. Conditions: beryllium, 5.0 ng mL^{-1} (5.55×10^{-7} mol L^{-1}); CAS, 4.0×10^{-6} mol L^{-1}; CTAB concentration, 0.01% (w/v) (2.74×10^{-4} mol L^{-1}); pH, 5.

results (Fig. 4) show that at zero point the micellization process does not take place and the amount of ΔA is zero. Addition of 0.002 mol L^{-1} iodide sufficed for maximum extraction of the complex and the signal remained constant at higher concentrations. A concentration of 0.01 mol L^{-1} iodide was selected for further works.

The results of the study of the effect of pH on the complexation and extraction of beryllium show that pH 5 is most suitable [43].

3.2. Mean centering of ratio spectra

Consider a mixture of three compounds X and Y. If there is no interaction among the compounds and Beer's low is obeyed for each compound, it can be written [44]:

$$A_m = \alpha_X C_X + \alpha_Y C_Y \quad (1)$$

where A_m is the vector of the absorbance of the mixture, α_X and α_Y the molar absorptivity vectors of X and Y and C_X and C_Y are the concentrations of X and Y, respectively.

If Eq. (1) is divided by α_Y corresponding to the spectrum of a standard solution of Y in binary mixture, the first ratio spectrum is obtained in the form of Eq. (2) (for possibility of dividing operation, the zero values of α_Y should not be used in the divisor):

$$B = \frac{A_m}{\alpha_Y} = \frac{\alpha_X C_X}{\alpha_Y} + C_Y \quad (2)$$

If the Eq. (2) is mean centered (MC), since the mean centering of a constant (C_Y) is zero, Eq. (3) would be obtained:

$$\mathrm{MC}(B) = \mathrm{MC}\left[\frac{\alpha_X C_X}{\alpha_Y}\right] \quad (3)$$

The absorption spectra for the samples with different concentrations of beryllium were recorded in the wavelength range of 350–700 nm (Fig. 5a) and divided by the normalized spectrum of the CAS and the ratio spectra were obtained. Mean centering of the ratio spectra were obtained in the wavelength range of 480–580 nm (Fig. 5b). The concentration of beryllium was

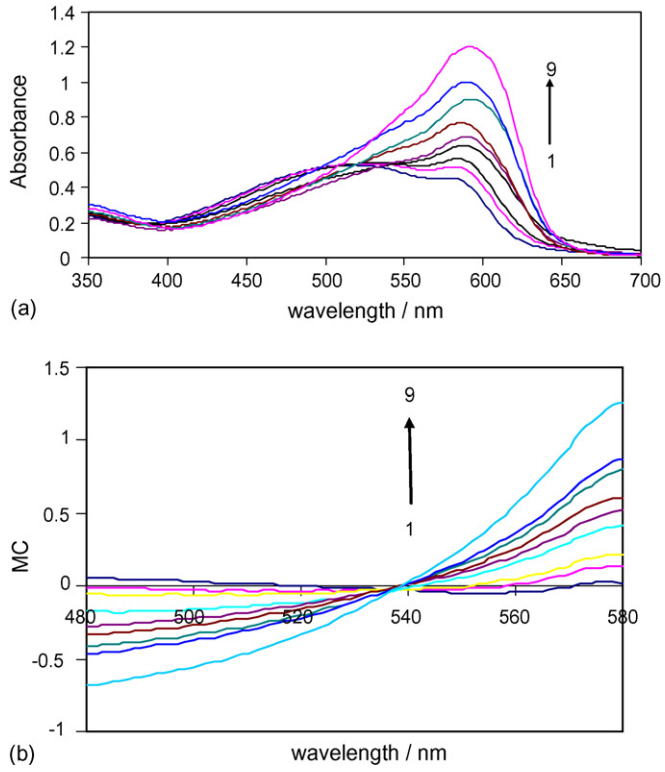


Fig. 5. The zero order spectra for 4.0×10^{-6} mol L^{-1} CAS in the presence of (1) 0.9, (2) 1.8, (3) 3.6, (4) 5.4, (5) 7.4, (6) 9.0, (7) 10.8, (8) 12.6 and (9) 14.4 ng mL^{-1} of beryllium (a) and MC of their ratio spectra (b) as obtained by Eq. (3).

determined by measuring the amplitude at 580 nm corresponding to a maximum wavelength shown in Fig. 5b.

3.3. Analytical characteristics

Table 1 summarizes the analytical characteristics of the optimized method, including regression equation, linear range, limit of detection, reproducibility and preconcentration and improvement factors. The limit of detection, defined as $C_L = 3\ S_B/m$ (where C_L, S_B and m are the limit of detection, standard deviation of the blank and slope of the calibration graph, respectively) [45], was 0.51 ng mL^{-1}. Because the amount of beryllium in 10 mL of sample solution is measured after preconcentration by CPE in a final volume of 0.5 mL, the solution is concentrated by a factor of 20. The relative standard deviation (R.S.D.) for five replicate measurements of 5 ng mL^{-1} beryllium was 1.50%.

A calibration graph was also constructed by measuring the absorbance change for surfactant-rich phase as a function of beryllium concentration at fixed wavelength of 612 nm. The analytical characteristics of the method are summarized in Table 1. The limit of detection was 0.75 ng mL^{-1}. The improvement factor was 36.5 and the relative standard deviation (R.S.D.) for five replicate measurements of 5 ng mL^{-1} beryllium was 2.1%. Table 1 shows the importance of exact removing of reagent response from sample. The ratio of slope/intercept has been increased dramatically when using mean centering of ratio spectra in order to removing the blank absorbance. Comparison of detection limit, regression coefficient, reproducibility (R.S.D.) and linear range of traditionally method with those of mean centering ones slightly improves the figure of merit of the method.

Table 2
Tolerance ratio of diverse ions on the determination of 10 ng mL^{-1} of Be^{2+}

Ion	Tolerance limit (ng mL^{-1})
Na^+, K^+, NH_4^+, Br^-, Cl^-, NO_3^-, SO_4^{2-}, CO_3^{2-}, Mg^{2+}, Ca^{2+} and ClO_3^-	5000
Cd^{2+}, Co^{2+}, Cu^{2+}, Mn^{2+}, Fe^{2+}, Pb^{2+}, Zn^{2+}, V(IV), Zr(IV), Mo(VI), Fe^{3+} and V(V)	5000[a]
PO_4^{3-}, F^- and Citrate	200

[a] After removing as described in text.

3.4. Selectivity

In order to study the selectivity of the proposed method, we tested the effect of various cations and anions on the preconcentration and determination of 10 ng mL^{-1} of Be^{2+} by the proposed method under the optimum conditions. The results are summarized in Table 2. The tolerance limit was defined as the concentration of added ion that caused less than ±3% relative error. The ions Cd^{2+}, Co^{2+}, Cu^{2+}, Mn^{2+}, Fe^{2+}, Pb^{2+}, Zn^{2+}, V(IV), Zr(IV), Mo(VI), Fe^{3+} and V(V) interfered at 50 ng mL^{-1}. The interfering effects of Cd^{2+}, Co^{2+}, Cu^{2+}, Mn^{2+}, Fe^{2+}, Pb^{2+}, Zn^{2+}, V(IV), Zr(IV) and Mo(VI) up to 5000 ng mL^{-1} were completely

Table 1
Analytical characteristics of the method

	MCRAS	Fixed wavelength
Concentration range (ng mL^{-1})	0.9–18	1.8–18
Concentration range (mol L^{-1})	1.00×10^{-7}–2.00×10^{-6}	2.00×10^{-7}–2.00×10^{-6}
Slope (mL ng^{-1})	0.0714	0.0802
Intercept	0.0016	0.0411
Correlation coefficient (r)	0.9995	0.9968
Limit of detection (ng mL^{-1})	0.51 (5.66×10^{-8} mol L^{-1})	0.75 (8.32×10^{-8} mol L^{-1})
Reproducibility ($n = 5$) (for 5.0 ng mL^{-1} beryllium) (%)	1.5	2.1
Preconcentration factor	20	20
Improvement factor	31	36.5

Table 3
Determination of beryllium in water samples by the proposed (MCRS) and standard methods

Sample	Beryllium concentration[a] (ng mL^{-1})			
	Proposed method			Standard method
	Added	Found	Recovery	
Spring water 1	–	4.93	–	5.12
	1.00	5.88	95.0	
	3.00	8.00	102.3	
	5.00	9.85	98.4	
	10.00	15.10	101.7	
Spring water 2	–	5.61	–	5.43
	2.00	7.57	98.0	
	4.00	9.72	102.8	
	6.00	11.91	105.0	
	8.00	13.69	101.0	

[a] Average of three determinations.

removed by the addition of 0.5 mL of 0.1% EDTA solution. The interfering effects of Fe^{3+} and V(V) up to 5000 ng mL^{-1} were completely removed by the addition of ascorbic acid to the solution.

3.5. Application

In order to evaluate the analytical applicability of the proposed method, it was applied to the determination of beryllium in several water samples collected around Hamadan. Water samples were collected and acidified with 0.1 mol L^{-1} sulfuric acid solution and their beryllium concentration were determined by both the proposed method and standard method [46]. The results are given in Table 3. There is good agreement between the results obtained by proposed and standard methods. The recoveries for the addition of different concentrations of beryllium to water samples were in the range 95–105%. The results show that the proposed method is suitable for determination of Be^{2+} in such water samples.

4. Conclusion

The new proposed procedure gives a selective, very sensitive and low-cost spectrophotometric procedure for determination of beryllium that can be applied to real samples. The surfactant has been used for preconcentration of beryllium and thus toxic solvent extraction, has been avoided. Mean centering of ratio spectra has been used to obtain pure analyte response free from absorbent reagent blank. Hence, the calibration lines shows no influence of the free reagent, because at each sample spectra its absorbance is cancelled using mean centering of ratio spectra, even when its contribution to the absorbance value differ from one solution to other. Application of mean centering of ratio spectra provides lower limit of detection, wider linear range and accurate calibration equation. To the best of our knowledge this is the first report on the cloud point extraction of beryllium.

References

[1] L.S. Clesceri, A.E. Greenberg, R.R. Trussell, Standard Methods for the Exarnination of Water and Wastewater, 17th ed., American Public Health Association, Washington, DC, 1989, pp. 3–79.
[2] H.A.M.G. Vaessen, B. Szteke, Food Addit. Contam. 17 (2000) 149.
[3] J.L. Burguera, M. Burguera, C. Rondon, P. Carrero, M.R. Brunetto, Y. Petit de Peña, Talanta 52 (2000) 27.
[4] P. Burba, P.G. Willmer, M. Betz, F. Fuchs, Int. J. Environ. Anal. Chem. 13 (1983) 177.
[5] E.B. Sandell, H. Hnishi, Photometric Determination of Trace Metals, Part 3, Wiley, New York, 1978.
[6] M.Y.Y. Vin, S.M. Khopkar, Analyst 113 (1988) 175.
[7] H.B. Singh, N.K. Agnihotri, K. Singh, Talanta 47 (1998) 1287.
[8] C. Jiang, F. He, Spectrochim. Acta, Part A 59 (2003) 1321.
[9] A. Soleymanpour, N. Ahmadi Rad, K. Niknam, Sens. Actuators, B 114 (2006) 740.
[10] M.R. Ganjali, A. Moghimi, M. Shamsipur, Anal. Chem. 70 (1998) 5259.
[11] C. Moscoso-Perez, J. Moreda-Pineiro, P. Lopez-Mahia, S. Muniategui-Lorenzo, E. Fernandez-Fernandez, D. Prada-Rodriguez, Talanta 61 (2003) 633.
[12] H.-W. Peng, M.-S. Kuo, Anal. Sci. 16 (2000) 157.
[13] S.W. Wu, X.O. Yang, W.W. Chen, M. Yang, Z.Y. Tang, Z.X. Jin, Spectrosc. Spect. Anal. 25 (2005) 785.
[14] S.Q. Tao, Y. Okamoto, T. Kumamaru, Anal. Chim. Acta 309 (1995) 379.
[15] D.S.R. Murty, B. Gomathy, G. Chakrapani, At. Spectrosc. 21 (2000) 123.
[16] A. Profumo, G. Spini, L.M. Cucca, M. Pesavento, Talanta 57 (2002) 929.
[17] D.E. Kimbrough, I.H. Suffet, Analyst 121 (1996) 309.
[18] F. Pilon, S. Lorithioir, J.C. Birolteau, S. Lafontan, J. Anal. At. Spectrom. 11 (1996) 759.
[19] T. Okutani, Y. Tsuruta, A. Sakuragawa, Anal. Chem. 65 (1993) 1273.
[20] W. Szczepaniak, A. Szymanski, Chem. Anal. 41 (1996) 193.
[21] J. Kubova, V. Nevoral, V. Stresko, Z. Fresenius, J. Anal. Chem. 348 (1994) 287.
[22] D.B. Do Nasciment, G. Schwedt, Anal Chim. Acta 283 (1993) 909.
[23] Y. Yamini, J. Hassan, R. Mohandesi, N. Bahramifar, Talanta 56 (2002) 375.
[24] K. Suvardhan, K. Suresh Kumar, D. Rekha, B. Jayaraj, G. Krishnamurthy Naidu, P. Chiranjeevi, Talanta 68 (2006) 735.
[25] A. Afkhami, T. Madrakian, A. Afshar Assl, A. Akbari Sehhat, Anal. Chim. Acta 437 (2001) 17.
[26] K. Suvardhan, K. Suresh Kumar, D. Rekha, B. Jayaraj, G. Krishnamurthy Naidu, P. Chiranjeevi, Talanta 68 (2006) 735.
[27] V. Degiorgio, in: V. Degiorgio, M. Corti (Eds.), Physics of Amphiphiles: Micelles, Vesicles, and Microemulsions, North-Holland Publishers, Amsterdam, 1983, p. 303.
[28] H. Rehage, H. Hoffmann, Mol. Phys. 74 (1991) 933.
[29] H. Hoffmann, Structure, Flow in Surfactant Solutions, in: C.A. Herb, R. Prudhomme (Eds.), ACS Symposium Series 578, American Chemical Society, Washington, DC, 1994, p. 2.
[30] V.K. Aswal, P.S. Goyal, P. Thiyagarajan, J. Phys. Chem. B 102 (1998) 2469.
[31] A.E. Vassiliades, in: E. Jungerman (Ed.), Cationic Surfactants, Marcel Dekker, New York, 1970, p. 387.
[32] H.L. Booij, in: H.R. Kruyt (Ed.), Colloid Science, Elsevier, Amsterdam, 1949, p. 681.
[33] I. Cohen, C.F. Hiskey, G. Oster, J. Colloid Sci. 9 (1954) 243.
[34] K. Hayashi, Y. Sasaki, S. Tagashira, E. Kosaka, Anal. Chem. 58 (1986) 1444.
[35] H. Nishida, Bunseki Kagaku 20 (1971) 1080.
[36] F. Zhou, Fenxi Huaxue 11 (1983) 398.
[37] P.C. Falco, F. Bosch-Reig, J. Verdu-Andres, Anal. Chim. Acta 270 (1992) 253.
[38] H.-W. Gao, Spectrochim. Acta, Part A 51 (1995) 1379.
[39] A. Afkhami, M. Bahram, Talanta 66 (2005) 712.
[40] A. Afkhami, M. Bahram, Anal. Chim. Acta 526 (2004) 211.
[41] A. Afkhami, M. Bahram, Talanta 68 (2006) 1148.

[42] A. Afkhami, T. Madrakian, M. Bahram, J. Hazard. Mater. 123 (2005) 250.
[43] A. Afkhami, A.R. Zarei, Anal. Sci. 20 (2004) 1711.
[44] D.L. Massart, B.G.M. Vandeginste, L.M.C. Buydens, S.D.E. Jong, P.J. Lewi, J. Smeyers-Verbeke, Handbook of Chemometrics and Qualimetrics: Part A, Elsevier Science, 1997.
[45] J.D. Ingle Jr., S.R. Crouch, Spectrochemical Analysis, Prentice-Hall, USA, 1988, p.173.
[46] American Public Health Association, Standard Methods for Examination of Water and Wastewater, 19th ed., Washington, DC, USA, 1995, p. 15.

Available online at www.sciencedirect.com
ScienceDirect
Talanta 71 (2007) 1047–1053
Talanta
www.elsevier.com/locate/talanta

Development of a reversed FIA system for the spectrophotometric determination of Sb(III) and total Sb in antileishmanial drugs

Vanessa G.K. Almeida, Mônica F. Lima, Ricardo J. Cassella *

Departamento de Química Analítica, Universidade Federal Fluminense, Outeiro de São João Batista s/n, Centro, Niterói 24020-150, RJ, Brazil

Received 5 April 2006; received in revised form 29 May 2006; accepted 29 May 2006
Available online 12 July 2006

Abstract

This paper reports the development of a reversed flow injection system for the spectrophotometric determination of Sb(III) and total Sb in antileishmanial drugs. The analytical system is based on the selective reaction between Sb(III) and bromopyrogallol red (BPR) with the decrease of the absorbance at 555 nm. Total Sb concentration was determined after reduction of all Sb(V) to Sb(III) with KI and ascorbic acid. The influence of system variables (chemical and flow type) and the possible interference of high amounts of Sb(V) on Sb(III) was studied as well as the suitable conditions for preparation of samples. It was verified that the use of Triton X-100 enhanced the sensitivity of the methodology and that the previous sonication of the samples was fundamental to achieve accurate results. Under optimized conditions the reversed FIA system was able to process 63 samples per hour with a detection limit of 29 ng ml^{-1} and a R.S.D. of 3.8% (0.25 μg ml^{-1} level). Real samples of commercial antileishmanial drugs were analyzed, being observed no statistical difference between the results obtained by the developed system and FAAS or manual methodology in relation to total Sb concentration.
© 2006 Elsevier B.V. All rights reserved.

Keywords: Antimony; Antileishmanial drugs; Flow injection analysis; Spectrophotometry

1. Introduction

The leishmaniasis is an infectious disease disseminated all over the world with remarkable incidence in developing countries of Asia, Africa and Central/South Americas. It can attack both humans and some animal species, being firstly related by Pedro Pizarro in 1571. In Brazil, the leishmaniasis is found along poorest regions of the country and around 67,000 new cases were diagnosticated in 2003, making leishmaniasis to be classified as an out-of-control disease [1].

Although new drugs are in development [2–5], the treatment of leishmaniasis is usually carried out with antimony-based preparations. Among all antimony-based drugs utilized, maybe the most importants are those prepared with *N*-methylglucamine antimoniate, or simply meglumine antimoniate. In this compound Sb is found in the pentavalent form, which is less toxic when compared with trivalent one, which has great affinity by blood and spleen, being also observed its accumulation in the liver and kidney [6]. This way, the determination of the oxidation state in which Sb is found in the medicine is very important to assess the possible deleterious effect of the drug supplied to leishmaniasis patients.

The determination of Sb in different kinds of samples has been performed by various analytical techniques such as IC-ICP-MS [7], hydride generation-atomic fluorescence [8,9], HG-ICP OES [10–12], spectrophotometry [13–17], HG-AAS [18] and HG-FTIR [19]. Among these works only some of them are applied to the Sb determination in antileishmanial drugs [15–19]. Additionally, very few papers relate the speciation of antimony in such samples [16–18].

Gallignani et al. [19] developed a FIA system for HG-FTIR determination of total antimony in pharmaceuticals. The methodology is based on the on-line treatment of the samples in order to release Sb from organic molecules, and posterior reduction of Sb(V) to Sb(III). From Sb(III), gaseous SbH_3 is formed, which is then transported by a N_2 carrier stream to the flow-cell, after separation from solution in a gas–liquid separator device. The 1893 cm^{-1} band was used for quantification

* Corresponding author. Tel.: +55 21 2629 2222; fax: +55 21 2629 2143.
E-mail address: cassella@vm.uff.br (R.J. Cassella).

0039-9140/$ – see front matter © 2006 Elsevier B.V. All rights reserved.
doi:10.1016/j.talanta.2006.05.093

purposes, providing a detection limit of 0.9 mg l^{-1}, which is adequate for the analysis of total Sb in the samples. It is important to remark that the measurement frequency of such FIA system was 28 h^{-1}.

Flores et al. [18] employed hydride generation-atomic absorption spectrometry for the speciation of Sb in commercial samples of injectable drugs used for leishmaniasis treatment. The procedure is based on the selective hydride generation from Sb(III) in presence of citric acid, used to inhibit the formation of hydride formation from Sb(V). Thus, after addition of a suitable reductant, total Sb is determined and Sb(V) is obtained by difference. Operating at optimum conditions the authors achieved a detection limit of 1.5 ng of Sb, which demanded high dilution factors for analysis since the amount of Sb in the samples varied from 83.5 to 110.3 mg ml^{-1}.

Rath et al. [16] employed the selective reaction between Sb(III) and bromopyrogallol red (BPR) to develop a method for antimony speciation in commercial drugs used in the treatment of leishmaniasis. In a such manual method, Sb(III) reacts with BPR decreasing the absorbance of the solution at 560 nm. At the same conditions, Sb(V) does not react with BPR. In order to determine Sb(V) in the sample, the authors utilized similar approach employed by Flores et al. [18], reducing all Sb(V) to Sb(III) and posterior calculation of Sb(V) by difference. The same research group developed a FIA system for Sb(V) determination with rhodamine B in the same samples. The set-up included a liquid–liquid extraction unit for the measurement of the complex [15].

Recently, a FIA/spectrophotometry system was used for Figueiredo et al. [17] to determine Sb(III) and total Sb in antileishmanial drugs. The method was based on the SbH_3 generation and its posterior reaction with $KMnO_4$ solution which has your color intensity diminished due to reduction by stibine.

In this sense, an interesting paper was published by Petit de Peña et al. [20] regarding to Sb speciation in biological tissues. In this work the authors developed a fully automated procedure for extraction and speciation analysis of Sb by HG AAS. Acetic and sulfuric acids were selected among other acids for extraction of Sb(III) and Sb(V), respectively, and L-cysteine was employed for Sb(V) reduction to Sb(III) in order to make possible stibine generation and Sb detection in the quartz cell. The developed methodology was applied in the Sb speciation in biological tissues like cattle liver and hamster blood and kidney. The detection limits achieved were 1 μg l^{-1} for Sb(III) and 0.5 μg l^{-1} for Sb(V).

The aim of this work was to develop a reversed FIA system for the speciation of Sb in drugs used in the treatment of leishmaniasis also exploring the reaction of the Sb(III) ions with BPR in an organized medium containing Triton X-100. A reversed FIA approach was utilized for reagent saving and due to the high absortivity of BPR solutions. In a normal FIA configuration the high absortivity of BPR would lead to a high blank absorbance, strongly affecting the detector operation and thus increasing the baseline noise. In a reversed FIA mode, such problem is not verified.

2. Experimental

2.1. Apparatus

The set-up consisted of a Femto 700 Plus (São Paulo, Brazil) UV–vis spectrophotometer equipped with a Hellma (Jamaica, NY, USA) standard glass flow-cell of 80-μl internal volume and 10-mm optical path. The instrument was set at 555 nm for all absorbance measurements. A Micronal B-332 (São Paulo, Brazil) peristaltic pump, furnished with flexible PVC tubes (Tygon®), was used to propel all solutions and a Rheodyne 5041 six-port valve was employed to inject the reagents mixture into the system. The manifold was built up with PTFE tubes with 0.8 mm bore and PEEK plastic connections.

All pH measurements were carried out in an Analyzer 300 pHmeter equipped with a combined glass electrode (Ag/AgCl as reference).

Flame atomic absorption measurements were carried out in a Perkin-Elmer (Norwalk, CT, USA). Analyst 100 spectrometer equipped with an antimony hollow cathode lamp. The instrument was operated at optimum conditions suggested by the manufacturer (lean blue air-acetylene flame, wavelength = 217.6 nm and slit width = 0.2 nm).

2.2. Reagents and solutions

All solutions were prepared with analytical grade reagents and high purity deionized water, obtained in a Simplicity Milli-Q (Millipore, Saint Quentin Yvelines, France) water purification system.

Antimony solutions. Antimony(III) solutions were prepared daily by adequate dilution of a 1000 mg l^{-1} Sb(III) stock standard solution that was obtained by dissolution of 2.8082 g of $K(SbO)C_4H_4O_6{\cdot}0.5H_2O$ with 50 ml of a 2 mol l^{-1} HCl solution and posterior dilution to 1000 ml in a volumetric flask. As the same way, Sb(V) standard solutions were prepared by dilution of a 1000 mg l^{-1} stock solution prepared by dissolution of a 2.1592 g of $KSb(OH)_6$ in around 250 ml of purified water under heating of 60 °C. After total dissolution of the solid, the solution was left to achieve ambient temperature and the volume was made up to 1000 ml in a volumetric flask.

BPR reagent solution. A 500 mg l^{-1} stock solution of BPR was prepared by dissolving 50 mg of BPR (Acros, USA) in exactly 100 ml of purified water. The solution was stored in a dark flask and maintained in the dark. Under these conditions the solution remains stable for 2 weeks, at least. All solutions of BPR used throughout the experimental work were obtained by convenient dilution of the stock solution.

Triton X-100 solution. A 5 g l^{-1} Triton X-100 solution was prepared by mixing 0.5 g of Triton X-100 (Vetec, Rio de Janeiro, Brazil) with around 80 ml of purified water. After obtaining a homogeneous solution the volume was filled up to 100 ml in a volumetric flask.

Carrier solution. A concentrated buffer solution of NaH_2PO_4/Na_2HPO_4 with pH 6.8 (total concentration 1 mol^{-1}) was prepared by dissolving 15 g of NaH_2PO_4 (Vetec, Rio de Janeiro, Brazil) and 17.7 g of Na_2HPO_4 (Vetec, Rio de Janeiro,

Brazil) in around 200 ml of purified water. The pH was then adjusted to 6.8 with solid NaOH and the volume was completed to 250 ml. The carrier solution used in the FIA system was prepared by dilution of this concentrated buffer solution, taking 1 ml of it and completing the volume to 100 ml. During this dilution the pH was monitored and re-adjusted to 6.8, when necessary.

KI solution. The 2% (w/v) KI reductant solution was prepared by dissolving 0.5 g of KI (Vetec, Rio de Janeiro, Brazil) in 25 ml of purified water. This solution was daily prepared just before use.

Ascorbic acid solution. The 5% (w/v) ascorbic acid reductant solution was prepared by dissolving 1.25 g of ascorbic acid (Vetec, Rio de Janeiro, Brazil) in 25 ml of purified water. This solution was also daily prepared just before use.

HCl solution. A 4 mol l^{-1} HCl solution was prepared by taking 34 ml of concentrated HCl (Vetec, Rio de Janeiro, Brazil) and diluting this volume to 100 ml with purified water. In order to follow safe conditions, the volume of concentrated HCl was firstly added on 50 ml of water, in a beaker, and then the solution obtained was transferred to the volumetric flask and the volume was completed to 100 ml.

Drug samples. Commercial samples of injectable meglumine antimoniate were analyzed in this work. Such samples were obtained in ampoules of 5 ml containing a declared concentration of 85 mg ml^{-1} of Sb as meglumine antimoniate, in aqueous solution.

2.3. Sample preparation before injection in the FIA system

For the determination of Sb(III) concentration, 100 μl of sample were sonicated for 10 min and diluted to 100 ml with water. After this, 5 ml of the resultant solution was taken, 1 ml of the concentrated buffer solution (1 mol l^{-1} total concentration) was added and the volume was made up to 100 ml. This final solution was injected into the FIA system.

For total antimony (Sb(III) + Sb(V)) determination, 100 μl of sample were sonicated for 10 min. Afterwards, 2 ml of 2% (w/v) KI and 2 ml of 5% (w/v) ascorbic acid solutions were added together with 500 μl of 4 mol l^{-1} HCl solution. After elapsed 15 min, the volume was made up to 100 ml. Five millilitres of this final solution were put into a 100 ml volumetric flask, 1 ml of the concentrated buffer solution was added and the volume was filled up to the mark. This final solution was injected into the FIA system.

2.4. Reversed FIA system operation

A schematic diagram of the reversed FIA system is depicted in Fig. 1. In the set-up, reagent solution of BPR (80 mg l^{-1}, 0.98 ml min^{-1}) merges with the Triton X-100 solution (5 g l^{-1}, 0.98 ml min^{-1}) at the confluence point *x*. After mixing in a coil (500 μl), the mixture obtained is pumped to the injection valve, loading the loop (600 μl). The excess of reagent mixture is discarded, flowing directly to the waste flask. At the same time, the carrier stream (phosphate buffer solution, 0.01 mol l^{-1}, pH 6.8, 2.35 ml min^{-1}) flows through other way in the valve, reaching the confluence point *y*, where it merges with the sample stream (1.48 ml min^{-1}). The mixture obtained is then driven to the reaction coil (125 μl) and, after this, to the flow-cell positioned in the optical path of the spectrophotometer (555 nm). At this time, the baseline is established. Afterwards, the injection valve is switched and the carrier stream drifts the reagent plug to the confluence point *y*, where it merges with the sample stream. The mixture flows to the reaction coil, where reaction between BPR and Sb(III) takes place. Then the analytical zone (sample + reagents) reaches the spectrophotometer, yielding a transient signal of absorbance, which diminishes with the increase of the Sb(III) concentration in the sample. Peak height was always used as quantitative variable.

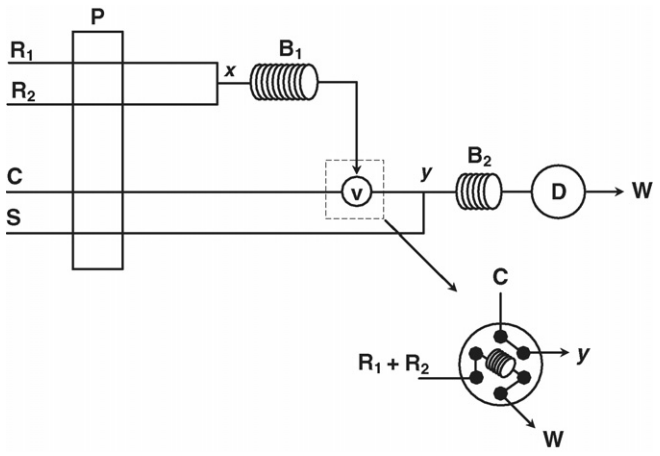


Fig. 1. Reversed FIA manifold for the spectrophotometric speciation of Sb (Sb(III)/Sb(V)) in antileishmanial drugs. S = sample (pH 6.8, 1.48 ml min^{-1}); C = carrier (0.01 mol l^{-1} NaH_2PO_4/Na_2HPO_4 buffer with pH 6.8, 2.35 ml min^{-1}); R_1 = reagent solution (80 mg l^{-1} BPR, pH 6.8, 0.98 ml min^{-1}); R_2 = surfactant solution (5 g l^{-1} Triton X-100, 0.98 ml min^{-1}); B_1 = mixing coil (500 μl); B_2 = reaction coil (125 μl); V = six-port selection valve (loop with 600 μl); *x* and *y* = confluence points; P = peristaltic pump; D = detector (spectrophotometer at 555 nm); W = waste.

3. Results and discussion

In order to attain a best performance for the analytical flow system, the influences of several chemical and flow parameters that could affect it were investigated by univariate method. Also, a study about possible interferents (Sb(V) plus substances present in antileishmanial formulations) and sample pretreatment was performed.

3.1. Investigation of chemical parameters

The first parameter considered as important for the FIA system performance was the reaction pH. According to Rath et al. [16] at neutral range of pH, BPR and Sb(III) react to form a stable complex with 1:1 stoichiometry. On the other hand, Huang et al. [14] performed the reaction of BPR with Sb(III), in a micellar medium, at pH 2.0. At these conditions and maintaining the temperature at 80 °C, the complex Sb(III)–BPR showed maximum absorbance at 538 nm. Taking such informations into account, the reaction between Sb(III) and BPR in micellar medium (Triton X-100 10 g l^{-1}) was tested, in off-line mode, at pH 2.0

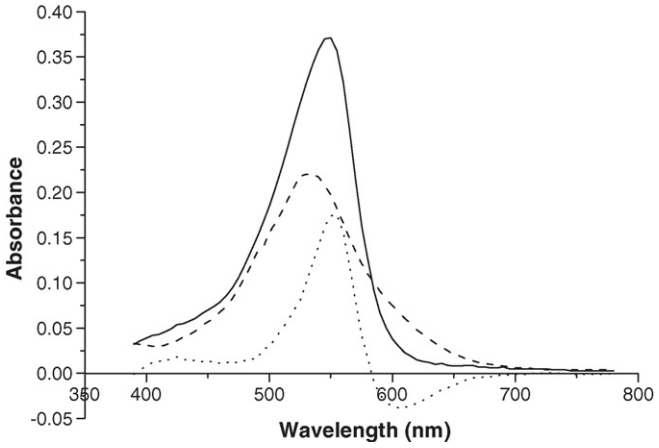


Fig. 2. Spectra of BPR solution (full line), complex BPR–Sb(III) (dashed line) and difference (dotted line). Both solutions were at pH 6.8 and Sb(III) concentration was 1 μg ml^{-1}.

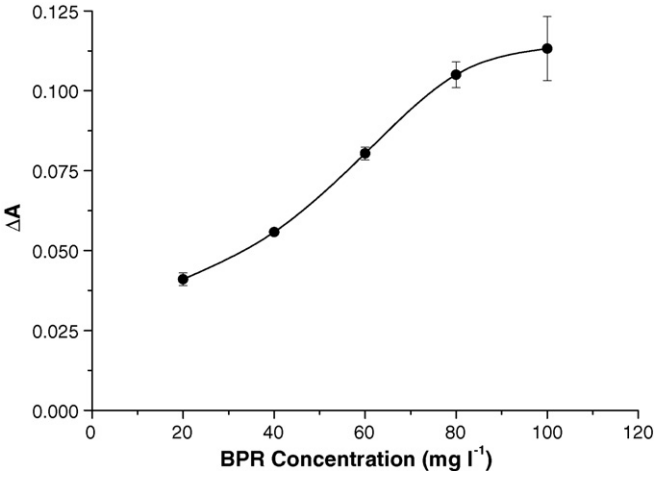


Fig. 3. Effect of BPR concentration on Sb(III) signal. All BPR solutions were prepared at pH 6.8 with 0.01 mol l^{-1} phosphate buffer. Triton X-100 and Sb(III) concentrations were 5 g l^{-1} and 1 μg ml^{-1}, respectively. A loop of 600 μl was employed as well as a sample flow rate of 1.48 ml min^{-1}.

(HCl buffer), 4.5 (acetate buffer) and 6.8 (phosphate buffer). Strong differences between maximum absorbance wavelengths were observed, indicating that different forms of BPR–Sb(III) complex are present in each pH evaluated. Maximum difference between reagent and complex absorbances was verified at pH 6.8. This way, this pH was chosen for the method. Also, analyzing the spectrum of difference at pH 6.8 (Fig. 2), it was possible to realize that maximum difference was obtained at 555 nm, which was elected for all further measurements.

Once established the pH of the reaction, the FIA system was mounted and the influences of other variables were studied. First of all, the effect of BPR concentration was examined. For this purpose, the Triton X-100 concentration was maintained at 2.5 g l^{-1} and the pH of BPR solution was adjusted to 6.8 with phosphate buffer with total concentration of 0.01 mol l^{-1} as well as the carrier solution (0.01 mol l^{-1} phosphate buffer). Solutions with BPR concentration between 20 and 100 mg l^{-1} were tested. Higher analytical signals (difference between absorbances of blank and Sb(III) solutions) were observed with the increase of BPR concentration, as can be seen in Fig. 3. However, although with 100 mg l^{-1} BPR solution the analytical signal was slightly superior to that observed at 80 mg l^{-1}, this BPR concentration was chosen for the method, since the variability of the measurements increased a lot at 100 mg l^{-1}. This high variability resulted from the high blank absorbance verified in the wavelength chosen for the measurements (see Fig. 2), which increased the noise at this condition due to low light power that reaches the detector. Obviously, the poor precision verified for blank measurements affected the analytical signal obtained ($\Delta A = A_{\text{blank}} - A_{\text{Sb(III)}}$).

In order to evaluate the influence of Triton X-100 on analytical signal, its concentration was tested in the range of 0 (pure water)—10 g l^{-1}. As can be seen in Fig. 4, there is a clear influence of the Triton X-100 concentration on analytical signal. It was observed that analytical signals increased up to 5 g l^{-1} and after this value they suffered a soft decrease. So, in order to ensure maximum sensitivity a solution of 5 g l^{-1} Triton X-100 was used in all further experiments. Testing the same reaction at batch mode, a situation where the system reach the equilibrium before absorbance measurement, it was not possible to observe any effect of Triton X-100 on the sensitivity of the Sb(III) measurement with BPR, indicating that the effect of the surfactant could be related to the velocity of the spectrophotometric reaction, which is easily observed in a flow mode. How Triton X-100 accelerates the formation of Sb(III)–BPR complex, higher analytical signals are achieved in presence of the surfactant in the small time between confluence point *y* and the detector.

3.2. Investigation of physical parameters

The first physical parameter investigated was the volume of reagent mixture injected into sample stream. This experiment was carried out varying the loop volume between 250 and 750 μl. Increased analytical signals were verified for volumes up to 750 μl. However, a loop volume of 600 μl was chosen for

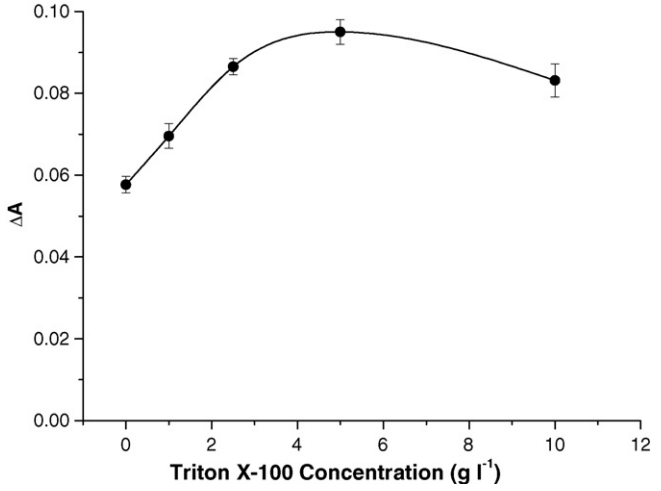


Fig. 4. Effect of Triton X-100 concentration on Sb(III) signal. BPR and Sb(III) concentration were 80 mg l^{-1} and 1 μg ml^{-1}, respectively. A loop of 600 μl was employed as well as a sample flow rate of 1.48 ml min^{-1}.

the system because for volumes higher than this, an undesirable increase of the time elapsed to complete the transient analytical signal occurred, diminishing the measurement frequency of the system with poor gain of sensitivity.

Both flow rates of sample and carrier solution are responsible to control the residence time of analytical zone inside the system, thus controlling the dispersion level of such zone and reaction time between Sb(III) and BPR. So, the influences of both flow rates on system sensitivity were carefully studied since they affect the peak height magnitude.

The carrier flow rate, which was investigated between 0.98 and 4.14 ml min^{-1} (sample flow rate maintained at 2.35 ml min^{-1}), has not presented remarkable influence on the analytical signal, only being observed a slightly decrease when its value was higher than 2.35 ml min^{-1}. This flow rate was then established for the carrier in order to keep the system operating with higher measurement frequency, since at this condition the time required to complete the transient analytical signal was lower without loss of sensitivity.

On the other hand, the sample flow rate, which was also evaluated in the range of 0.98–4.14 ml min^{-1}, showed to have more noticeable effect on analytical signal (Fig. 5). For this variable, a great increase of ΔA was verified from 0.98 to 1.48 ml min^{-1}. After this point, although lower sample dilution, the analytical signal decreased, probably due to the increase of analytical zone dispersion inside the system. How maximum signal was observed for a sample flow rate of 1.48 ml min^{-1}, this value was selected for the method.

As the same way of flow rates, the volume of reaction coil (B_2) influences the residence time of analytical zone inside the system, also controlling the dispersion and reaction time. Reaction coils with volume between 0 μl (no coil) and 500 μl were evaluated. Higher signals were obtained when no coil was connected to the system, indicating that in Triton X-100 medium, the reaction between Sb(III) and BPR is really fast. However, in this situation a soft noise in the baseline was noted because of Schilieren effect. This way, a coil with 125 μl was chosen for the system since with this coil the baseline noise was completely eliminated.

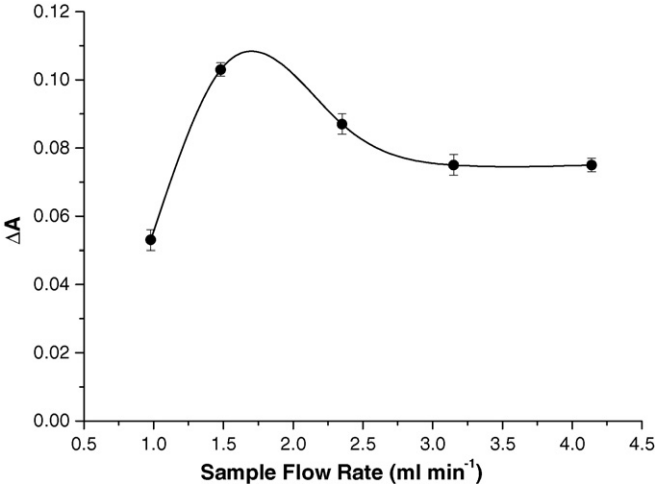


Fig. 5. Effect of sample flow rate on Sb(III) signal. BPR, Triton X-100 and Sb(III) concentrations were 80 mg l^{-1}, 5 g l^{-1} and 1 μg ml^{-1}, respectively. A loop of 600 μl was employed.

3.3. Study of the influence of Sb(V) on Sb(III) signal

All optimization procedure was performed taking into account that BPR only reacts with Sb(III) at pH 6.8, having not any interaction with Sb(V) ion. However, due to the high concentrations of Sb(V) in the real samples – up to 40 times Sb(III) expected concentration – a detailed study was carried out in order to evaluate up to which concentration of Sb(V) the system can support without interference (±5%) on Sb(III) signal. For this purpose two strategies were followed: (i) construction of two analytical curves for Sb(III) (0.25–5 μg ml^{-1}), one without Sb(V) and other with constant 10 μg ml^{-1} concentration of Sb(V); (ii) evaluation of signals for Sb(III) solutions with constant concentrations (0.5 and 2.5 μg ml^{-1}) containing increasing amounts of Sb(V).

In the first study it was possible to realize that the difference between slopes of the curves was not significant, being obtained an equation of $\Delta A = 0.100$ (Sb(III), μg ml^{-1}) + 0.002 ($r = 0.996$) for analytical curve with only Sb(III) and $\Delta A = 0.102$ (Sb(III), μg ml^{-1}) + 0.004 ($r = 0.996$) for the analytical curve with solutions of Sb(III) containing 10 μg ml^{-1} Sb(V). In turn, as can be seen in Table 1, when Sb(III) is measured even in presence of Sb(V) 100 times higher, the analytical signal remains typically the same, indicating, clearly, that is possible to measure Sb(III) in solutions containing high amounts of Sb(V) through reaction with BPR.

Other possible concomitants usually present in the medicine formulations such as EDTA, sodium bissulfite and propylene–glycol were tested as possible interferents but none of them presented any remarkable effect on Sb(III) signal.

3.4. Evaluation of sample preparation conditions

After established all conditions for Sb measurement in the samples, a detailed study about the sample preparation procedure was performed. This study was focused on two points: (i) reduction conditions of Sb(V) to Sb(III) in order to make possible the determination of total Sb in the samples; (ii) effect of the sonication of the sample before analysis in order to release all Sb retained in the meglumine antimoniate structure. In all these

Table 1
Evaluation of Sb(V) influence on Sb(III) signal at different ratios

Solution	Sb(III) (μg ml^{-1})	Sb(V) (μg ml^{-1})	ΔA
1	0.5	0	0.050 ± 0.002
2	0.5	5	0.049 ± 0.002
3	0.5	10	0.051 ± 0.002
4	0.5	25	0.049 ± 0.001
5	0.5	50	0.048 ± 0.002
6	2.5	0	0.248 ± 0.002
7	2.5	5	0.250 ± 0.003
8	2.5	10	0.251 ± 0.002
9	2.5	25	0.247 ± 0.002
10	2.5	50	0.249 ± 0.003

experiments, the tests were performed with a sample containing a known concentration of total Sb (78.5 mg ml^{-1}) previously determined by FAAS.

The reduction process was carried out using a mixture of ascorbic acid (2 ml of a 2% (w/v) solution) and potassium iodide (2 ml of a 5% (w/v) solution) as reducing agents. As well known, these species presents more prominent reducing effect in acidic medium, in contrast with the Sb(III)–BPR reaction that is enhanced around pH 6.8. So, the amount of hydrochloric acid added to the sample for reduction was carefully studied as well as the time required to complete the whole process.

The influence of the volume of 4 mol l^{-1} HCl solution added was studied in the range of 0–1000 μl. For this task, 100 μl of the sample were taken and mixed with 2 ml of a 2% (w/v) ascorbic acid solution and 2 ml of a 5 % (w/v) KI solution. Afterwards, the volume of 4 mol l^{-1} HCl solution was added and the mixture was homogenized and left to react for 30 min before pH adjustment with buffer solution, dilution and injection into the FIA system. Quantitative recovery of Sb was observed for volumes of HCl solution equal or higher than 250 μl. So, in order to ensure that all Sb(V) present would be reduced to Sb(III) even for samples containing high amounts of Sb, a volume of 500 μl of 4 mol l^{-1} HCl was established. It is important to remark that in this test the sample was sonicated for 30 min before addition of ascorbic acid, KI and HCl solutions in order to guarantee that all Sb was released from meglumine antimoniate structure.

The study of the effect of sonication time was important due to be a time-consuming step in the whole process. Therefore, in order to optimize sample preparation the sonication time of sample was examined in the range of 0–30 min. Obtained results (Fig. 6) showed that the sonication of the sample was fundamental to achieve an accurate determination of Sb in the medicines utilized in the treatment of leishmaniosis, since the Sb(V) ions must be released from organic structure of the drug to react with BPR, after reduction. When the sample was not sonicated before addition of reducing substances, the maximum recovery obtained was 88.3%, while after 10 min sonication the recovery was improved to 99.8%.

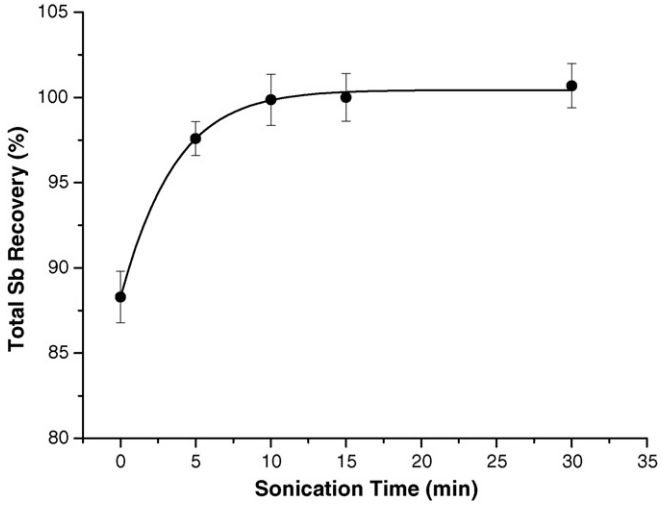


Fig. 6. Effect of sonication time on the determination of total antimony in the samples of antileishmanial drugs. Recovery calculated against the value obtained by FAAS.

4. Method evaluation

4.1. Analytical characteristics

The proposed FIA system was critically evaluated with regard to accuracy, precision, detection limit, quantification limit, linear range and measurement frequency. Operating the system under optimized conditions a linear fit was derived between 0.25 and 5 μg ml^{-1}, with a typical equation $\Delta A = 0.104$ (Sb(III), μg ml^{-1}) + 0.002 with a correlation coefficient of 0.9992, where ΔA is the absorbance signal ($\Delta A = A_{blank} - A_{Sb(III)}$) measured as peak height. The detection limit, estimated as three times the standard deviation of 10 measurements of blank solution [21–23], was 29 ng ml^{-1}. In the same way, the quantification limit, derived from 10 times the standard deviation of the blank [24], was 96 ng ml^{-1}. The R.S.D. observed was 3.8% at the 0.25 μg ml^{-1} level. A measurement of 63 h^{-1} was derived with the FIA system operating at optimum conditions, considering a complete analytical cycle as the time passed between two injections. Another important feature of all methodologies that must be emphasized is the amount of waste generated at the end of their application. In the present case, the system generates around 350 ml of effluent per hour of operation. Table 2 expresses the composition of this effluent in terms of the amount of each substance wasted.

4.2. Application

The applicability of the developed methodology was studied by analyzing three samples of commercial drugs utilized in the treatment of leishmaniasis and comparing the obtained results for total antimony with those determined by flame atomic absorption spectrometry and manual methodology [16]. All results are summarized in Table 3. As can be seen, the results obtained by the reversed FIA method agreed well with those obtained by FAAS employing an external calibration procedure and with those obtained by manual procedure (applying the paired *t*-test with a confidence level of 95%). Taking this fact into account it is possible to affirm that the developed procedure is an excellent alternative to manual procedure, providing a simplest analytical procedure free of matrix interferences and with suitable measurement frequency.

Table 2
Amount of waste generated by reversed FIA system per hour of operation

Reagent	Amount wasted per hour (mg)
BPR	4.7
Triton X-100	294
NaH_2PO_4	138
Na_2HPO_4	163

Table 3
Results obtained for the analysis of commercial samples of antileishmanial drugs

Sample	Sb(III) (mg ml^{-1})	Sb(V) (mg ml^{-1})	Sb total (mg ml^{-1})	Sb total[a] (mg ml^{-1})	Sb total[b] (mg ml^{-1})
I	2.62 ± 0.15	84.0 ± 3.2	86.6	86.3 ± 3.6	85.5 ± 3.5
II	3.01 ± 0.08	75.2 ± 3.5	78.2	81.0 ± 4.6	79.8 ± 2.3
III	2.23 ± 0.05	76.3 ± 1.2	78.5	78.1 ± 2.0	78.5 ± 1.9

Results are expressed as mean ± S.D. ($n = 3$).
[a] Total antimony determined by manual methodology according to Ref. [16].
[b] Total antimony determined by flame atomic absorption spectrometry.

5. Conclusions

The proposed FIA system developed in this work showed good ability, in terms of sensitivity and selectivity, to determine Sb(III) in solution with BPR, being possible apply it in the speciation of Sb in antileishmanial drugs after a suitable treatment of the sample. Such FIA system can be considered an excellent alternative to manual methods like those developed by Huang et al. [14] and Rath et al. [16], since it is able to process a highest number of samples in a shortest period of time with lowest waste generation. Also, the detection limit achieved in this methodology (29 ng ml^{-1}) was better than those reported by Huang et al. [14] and Rath et al. [16] for the same reaction, which were 1.65×10^{-6} mol l^{-1} (0.20 μg ml^{-1}) and 0.04 μg ml^{-1}, respectively.

In the experimental context, the use Triton X-100 in the reaction medium increased the sensitivity of the FIA system, probably due to its catalyst effect on the reaction between Sb(III) and BPR, which was not observed previously by. Also, the 10 min sonication of samples before any other treatment showed to be essential to achieve accurate determination of Sb in the drugs, since this procedure should promote releasing of all Sb bonded to the organic structure of the meglumine antimoniate.

The levels of Sb(III) found in the drugs varied from 2.86 to 3.70% of the total Sb present in the sample. Such results are in agreement with those found in previous works, indicating the developed method is able to perform the quality control of antileishmanial.

Acknowledgements

The authors would like to thank to CNPq (Conselho Nacional de Desenvolvimento Científico e Tecnológico) for the financial support and for the fellowships.

References

[1] L. Goldman, Arch. Dermatol. 119 (1983) 540.
[2] A. Mayence, J.J.V. Eynde, L. LeCour Jr., L.A. Walker, B.L. Tekwani, T.L. Huang, Eur. J. Med. Chem. 39 (2004) 547.
[3] J.C. Macharia, A.J. Bourdichon, M.M. Gicheru, Acta Trop. 92 (2004) 267.
[4] S. Gupta, S. Tiwari, A.P. Bhaduri, G.K. Jain, Acta Trop. 84 (2002) 165.
[5] N.P. Sahu, C. Pal, N.B. Mandal, S. Banerjee, M. Raha, A.P. Kundu, A. Basu, M. Ghosh, K. Roy, S. Bandyopadhyay, Bioorg. Med. Chem. 10 (2002) 1687.
[6] S.A. Felicetti, R.G. Thomas, R.O. McClellan, Am. Ind. Hyg. Assoc. J. 35 (1974) 292.
[7] N. Miekeley, S.R. Mortari, A.O. Schubach, Anal. Bioanal. Chem. 372 (2002) 495.
[8] C. Casiot, M.C.B. Alonso, J. Boisoon, O.F.X. Donard, M. Potin-Gautier, Analyst 123 (1998) 2887.
[9] E. Fuentes, H. Pinochet, I.D. Gregori, M. Potin-Gautier, Spectrochim. Acta B 58 (2003) 1279.
[10] N. Ulrich, Anal. Chim. Acta 417 (2000) 201.
[11] H.B. Hou, H. Narasaki, Anal. Sci. 14 (1998) 1161.
[12] Y.L. Feng, H. Narasaki, H.Y. Chuen, L.C. Tian, Anal. Chim. Acta 386 (1999) 297.
[13] M.S. Bloomfield, A.D. Dow, K.A. Prebble, J. Pharm. Biomed. Anal. 10 (1992) 779.
[14] X. Huang, W. Zhang, S. Han, Y. Yin, G. Xu, X. Wang, Talanta 45 (1997) 127.
[15] L.A. Trivelin, J.J. Rohwedder, S. Rath, Talanta 68 (2006) 1536.
[16] S. Rath, W.F. Jardim, J.G. Dórea, Fresenius J. Anal. Chem. 358 (1997) 548.
[17] E.C. Figueiredo, P.O. Luccas, M.A.Z. Arruda, Anal. Lett. 39 (2006) 543.
[18] E.M.M. Flores, E.P. Santos, J.S. Barin, R. Zanella, V.L. Dressler, C.F. Bittencourt, J. Anal. Atom. Spectrom. 17 (2002) 819.
[19] M. Gallignani, C. Ayala, M.R. Brunetto, M. Burguera, J.L. Burguera, Talanta 59 (2003) 923.
[20] Y. Petit de Peña, O. Vielma, J.L. Burguera, M. Burguera, C. Rondón, P. Carrero, Talanta 55 (2001) 743.
[21] Analytical Chemistry Division, Spectrochim. Acta B 33 (1978) 242.
[22] Analytical Chemistry Division, Pure Appl. Chem. 99 (1976) 99.
[23] Analytical Methods Committee, Analyst 112 (1987) 199.
[24] M. Valcárcel, Princípios de Química Analítica, 1st ed., Springer-Verlag Ibérica, Barcelona, Spain, 1999.

Available online at www.sciencedirect.com
ScienceDirect
Talanta 71 (2007) 1061–1067
Talanta
www.elsevier.com/locate/talanta

Dimerization of thymol blue in solution: Theoretical evidence

Patricia Balderas-Hernández [a,b], Rubicelia Vargas [a], Alberto Rojas-Hernández [a], Ma. Teresa Ramírez-Silva [a], Marcelo Galván [a,*]

[a] *Universidad Autónoma Metropolitana-Iztapalapa, Departamento de Química, Apdo. Postal 55-534, CP 09340, México D.F., México*
[b] *Universidad Autónoma del Estado de México, Facultad de Química, Paseo Colón intersección Paseo Tollocan S/N, CP 50120, Toluca, Estado de México, México*

Received 5 March 2006; received in revised form 30 May 2006; accepted 30 May 2006
Available online 11 July 2006

Abstract

The possibility of dimerization of thymol blue was addressed by ab initio and force field calculations. In agreement with experimental information, a dimer forming symmetrical chemical environments for hydrogen bond formation was determined. This dimer is stable in vacuum and aqueous media and corresponds to the same protonated state proposed by the experiment. A comparison of the CVFF and MM3 force fields and ab initio results shows the suitability of CVFF to qualitatively describe this system.
© 2006 Elsevier B.V. All rights reserved.

Keywords: Thymol blue; Dimerization; Hydrogen bonds; Molecular mechanics calculations; Density functional theory calculations

1. Introduction

Thymol blue is an acid–base indicator from the family of the sulphonephtalein that is used extensively for end-point volumetric determinations. It also has many other field of applications: in the quantitative determination of proteins (γ-globulin, bovine serum albumin) [1], in the study of the effects of the surfactants in proteins [2], in proton exchange in organic reactions [3], in the manufacturing of biosensors used in optic fibers for determining organophosphate pesticides and carbamates [4], in the determination of active substances in pharmaceutical preparations [5], and in the elaboration of culture media for some microorganisms as *Escherichia coli* [6].

Thymol blue (TB) structure, as the indicators of the same family, is formed by three benzene rings bonded to a central carbon, with a sulphonic group bonded to one of the rings, and keto-enol groups bonded to the other rings. The molecule has three sites whose protonation state depends on the pH of the environment. Fig. 1 shows the full protonated structure of TB.

In a previous work [7], we reported some experimental results concerning the determination of the chemical and electrochemical behavior of TB in solution. It was found that a chemical model that describes properly the spectrophotometric, conductimetric, potentiometric and voltammetric information is a model that implicates dimeric structures of the indicator, however, no further details for dimer formation have been provided.

Analysis of the fully protonated TB structure indicates that three usual acidic hydrogen atoms can be recognized; this fact leads to consider that the TB dimer may be stabilized by hydrogen bonds between –OH or $–SO_3H$ groups. Further, it has been proved that theoretical methods are useful to properly describe geometrical parameters and binding energies of hydrogen bond complexes. There are many examples where ab initio methods, such as Moller–Plesset perturbation theory and density functional theory (DFT), are used to describe the electronic structure of hydrogen bond adducts. It is evident from these studies, that high quality basis sets are necessary to study this kind of complexes [8–12]. Then, the size of the systems that could be studied for ab initio methods is limited by the computational cost. Molecular mechanics (MM) methods are a good alternative for large systems, as TB dimer, where applying ab initio methods is not computationally viable.

It is well known that MM methods are successful if the functional form and the parameters used in the force field, describe properly the main interactions in the system under study. In general, protein force field functions (CHARMM, GROMOS, Amber, CVFF) are simpler than more accurate approaches for smaller molecules (MM3), and consequently cheaper. It is not

* Corresponding author. Tel.: +52 55 58046413; fax: +52 55 58046415.
E-mail address: mgalvan@xanum.uam.mx (M. Galván).

0039-9140/$ – see front matter © 2006 Elsevier B.V. All rights reserved.
doi:10.1016/j.talanta.2006.05.084

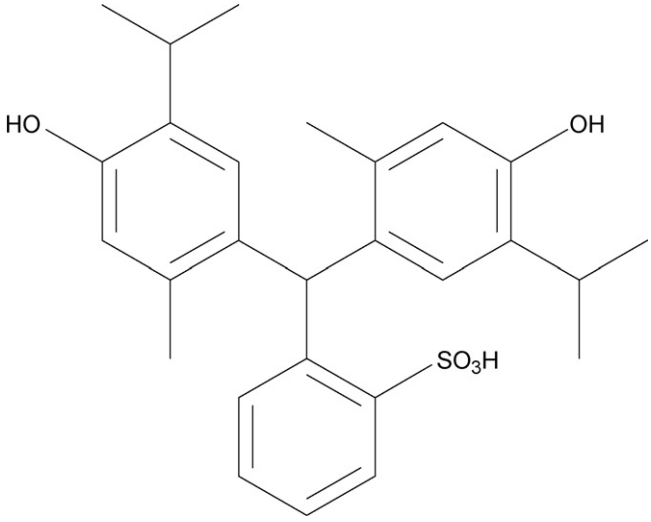


Fig. 1. Schematic representation of the H_3L^+ monomeric structure.

always easy to decide what force field is more suitable for a particular system. In the case we are considering, TB dimerization, we must look for a compromise between accuracy and feasibility.

The main goal of this paper is to use theoretical methods such as MM and ab initio calculations in the study of the thymol blue dimerization, because these methods provide information to support experimental findings in this problem. In the next section, an overview of the experimental facts supporting the dimer formation is presented. Section 3 explains the assortment of techniques used in this work to address the question of dimerization. Section 4 is divided in monomer, dimer and solvent effects on dimer formation. Section 5 gives an overview of the main conclusions obtained.

2. Dimerization of thymol blue, experimental facts

It has been experimentally determined that an acid–base equilibria model involving TB dimers, properly describe spectrophotometric, potentiometric, conductimetric and voltammetric information [7]. The equations that represent the chemical equilibria are

$$H_4L_2 \rightleftarrows H_3L_2^- + H^+; \quad (1)$$

$$H^+ + OH^- \rightleftarrows H_2O; \quad (2)$$

$$H_3L_2^- + OH^- \rightleftarrows 2HL^- + H_2O; \quad (3)$$

$$HL^- + OH^- \rightleftarrows L^{2-} + H_2O; \quad (4)$$

The first titration reaction corresponds to proton neutralization, Eq. (2), because the first dissociation (Eq. (1)) is strong. Eqs. (3) and (4) correspond to the second and third titration reactions. The scope of this paper only deals with the study of the H_4L_2 dimer.

The dimer H_4L_2 could be formed by different combinations between two of the monomeric structures represented in Fig. 2. Due to the fact that the global structure contains four acid protons, the possible combinations are: I–V, I–VI, II–II, I–III, II–IV, III–III, III–IV and IV–IV. The structure IV is discarded, since this molecule is not present in aqueous solution [13].

Previous NMR studies show that it is not possible to distinguish a symmetric dimer from a monomeric species [7]. Therefore, in this work, the possibility of a dimer of the combinations II–II and III–III was assessed because these are good candidates to form symmetric dimers.

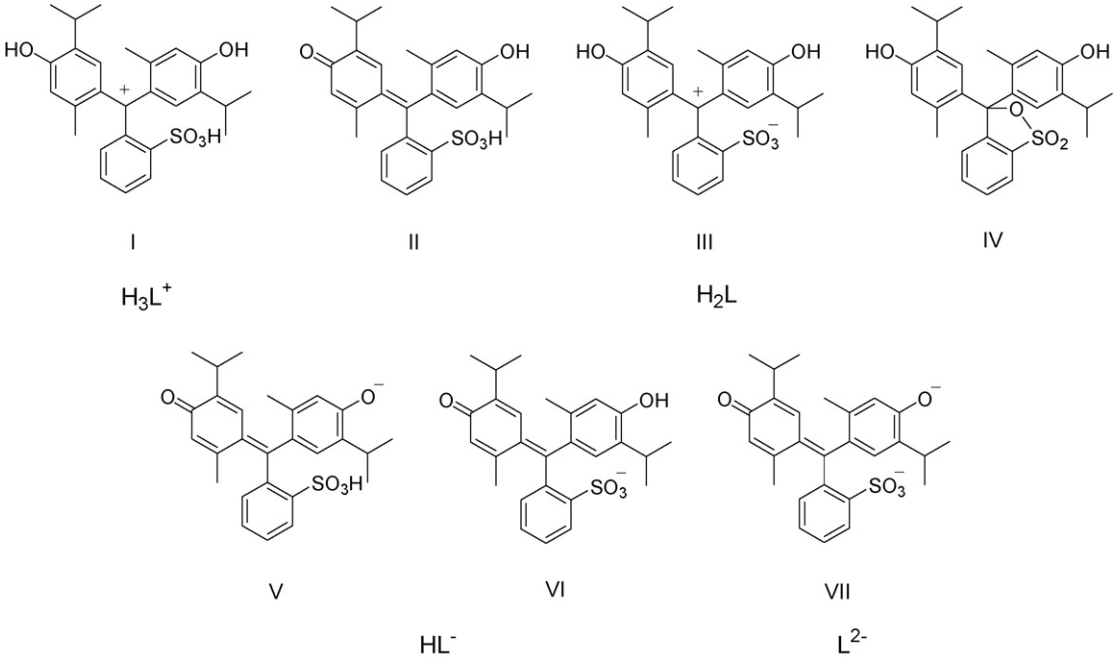


Fig. 2. Representative tautomeric structures for different protonation states of TB. L represents the non-protonated structure.

3. Methodology

To get some insight about the molecular mechanics performance in the geometry description of this kind of systems, two different force fields were tested in the TB monomer: CVFF and MM3. The MM3 calculations were carried out using MM3(96) program with standard atoms [14]. Previous works have shown that C–H···O weak hydrogen bonds can be important in the stabilization of some systems [15–18], the default MM3(96) parameter set was used after the parameters ε^* and r^* were modified for the corresponding atoms in the hydrogen bond to better describe these weak interactions, the values used for the parameters were obtained from prior calculations [19]. The parameters used in the CVFF are the standard ones [20]. Both force field calculations were also compared with the ab initio density functional theory results at the local level [21] and using a polarized double-ξ basis set (LDA/DZVP) as a basis set [22].

For the dimer, the CVFF force field was used to minimize the structures II–IV and also to explore the energy surface for the dimer formation of II–II, III–III and IV–IV structures depicted in Fig. 2. This exploration of the energy surface for the dimer interaction energy includes several simulated annealing steps, starting at 700 K and finishing with a 0 K full geometry optimization. We observed in this procedure that the formation of dimers II–II and IV–IV is possible, but in contrast we did not obtain any III–III stable dimer.

With the same force field, CVFF, a molecular dynamics simulation for the possible II–II dimer was performed for 220 ps at 298 K within the NVT ensemble. To consider solvent effects, our model includes the presence of a surrounding layer of water molecules 20 Å thick, which corresponds to a simulation including 908 water molecules of the first solvation sphere. The first 20 ps were considered as equilibration; therefore the analysis of the molecular dynamics was done on the last 200 ps of the simulation. The time step for integration of the movement equations was 1 fs within a Leapfrog–Verlet scheme.

Ab initio full geometry optimizations were performed on the three molecules corresponding to the structures of the H_2L species in Fig. 2. The level of theory for the optimization was LDA/DZVP. To get a better description of the energy differences between them, single point calculations using a hybrid exchange-correlation functional within DFT (B3LYP) [23–25], were done with the same basis set. All the ab initio calculations were performed with the NWChem program [26].

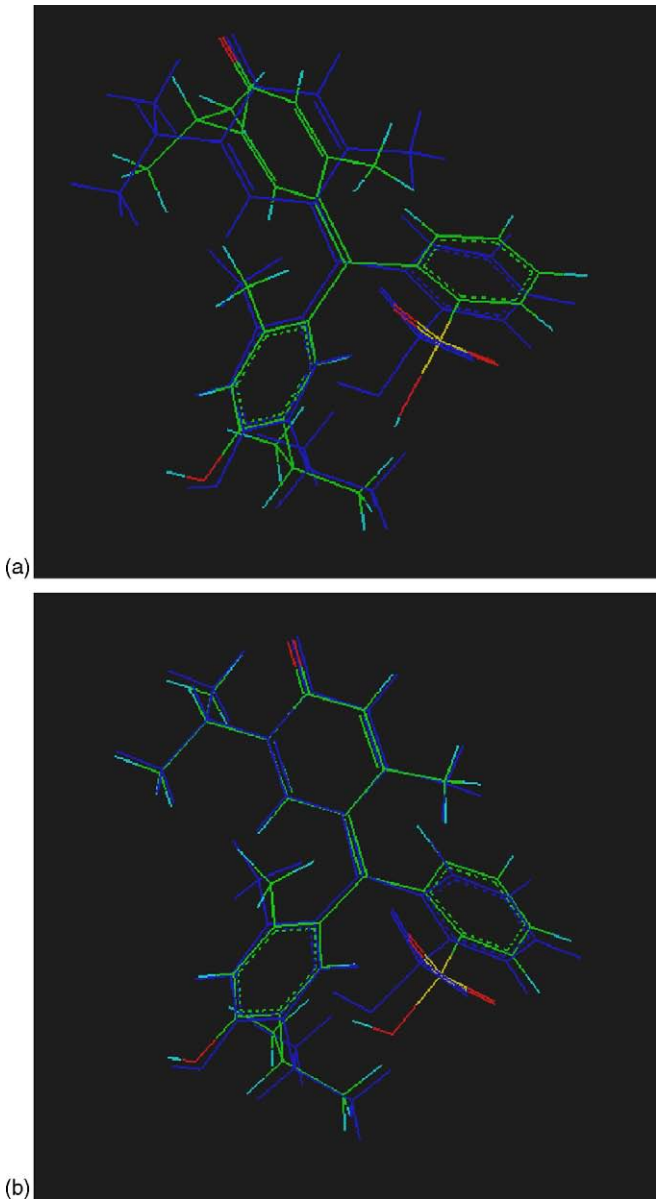


Fig. 3. (a) Comparison of the H_3L^+ monomer structure, obtained by molecular mechanics (CVFF force field) and ab initio calculations (LDA/DZVP). (b) Comparison of the same structure using MM3 force field and ab initio (LDA/DZVP) calculations The molecular mechanics structures are colored by atom: C in green, O in red, S in yellow, H in light blue, and the ab initio structure is colored in blue. (For interpretation of the references to color in this figure legend, the reader is referred to the web version of the article.)

4. Results and discussion

4.1. Monomer

The comparison between the minima obtained with force field and ab initio methods is shown in Fig. 3. In general, one may say that MM3 provides better agreement with respect to LDA calculations. However, CVFF force field maintains the hydrogen bond donors and acceptors in similar positions as MM3 and LDA. This is important because those groups are responsible for the stabilization of the dimer and consequently CVFF is able to describe the dimer formation in our study.

The first two columns in Table 1 display energy differences between the fully protonated species I and structures II and IV, this corresponds to the protonation energies. The energy differences between II and IV tautomers are 11.15 and 14.84 kcal/mol for B3LYP and LDA, respectively, indicating that in vacuum the IV structure is more stable than species II. It is interesting to note that the order of stability is not triggered by the use of LDA approximation and that the protonation energy is in agreement with the order of magnitude for this kind of quantities in vacuum processes.

Table 1
Relative energies in kcal/mol and B3LYP/DZVP HOMO–LUMO gaps in a.u. for three monomer species of TB

Structure	B3LYP/DZVP	LDA/DZVP	HOMO–LUMO gap
IV	232.95	225.53	0.1720
II	244.10	240.37	0.1142
I	0.00	0.00	0.1053

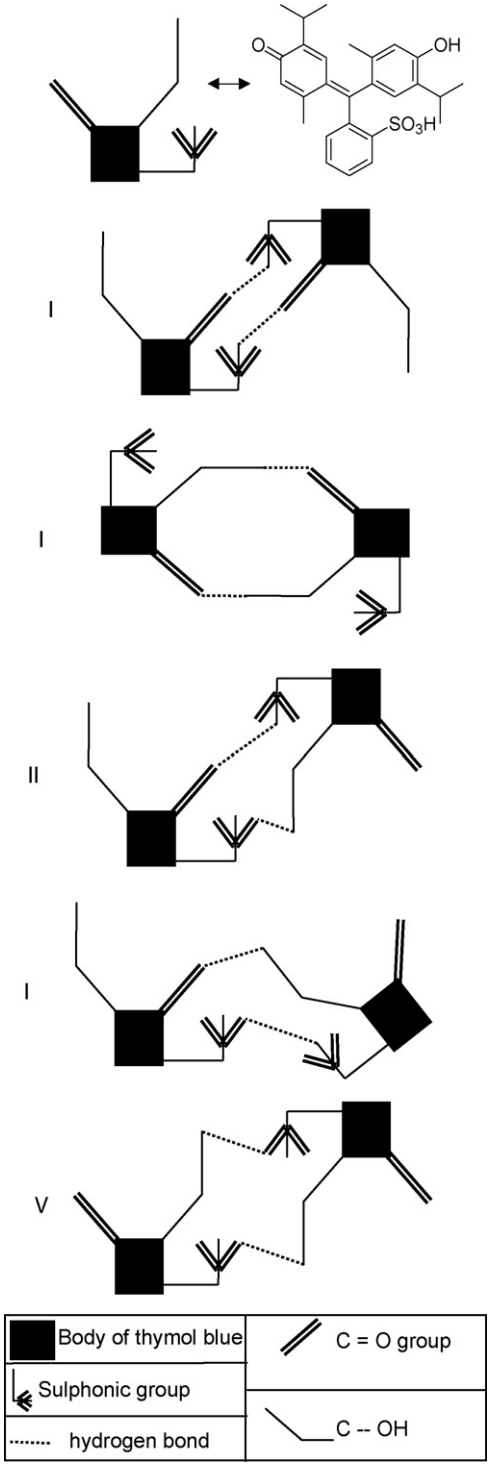


Fig. 4. Representation of possible dimers, linked by hydrogen bonds, formed with H_2L monomers.

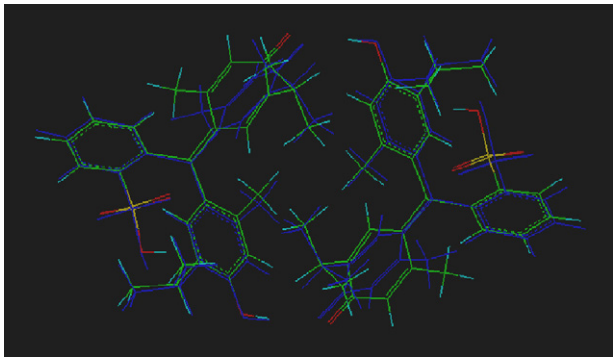


Fig. 5. Comparison of the dimer structure in vacuum optimized using molecular mechanics with MM3 force field and with CVFF force field. The MM3 structure is colored by atom (C in green, O in red, S in yellow, and H in light blue), whereas the CVFF structure is colored in blue. (For interpretation of the references to color in this figure legend, the reader is referred to the web version of the article.)

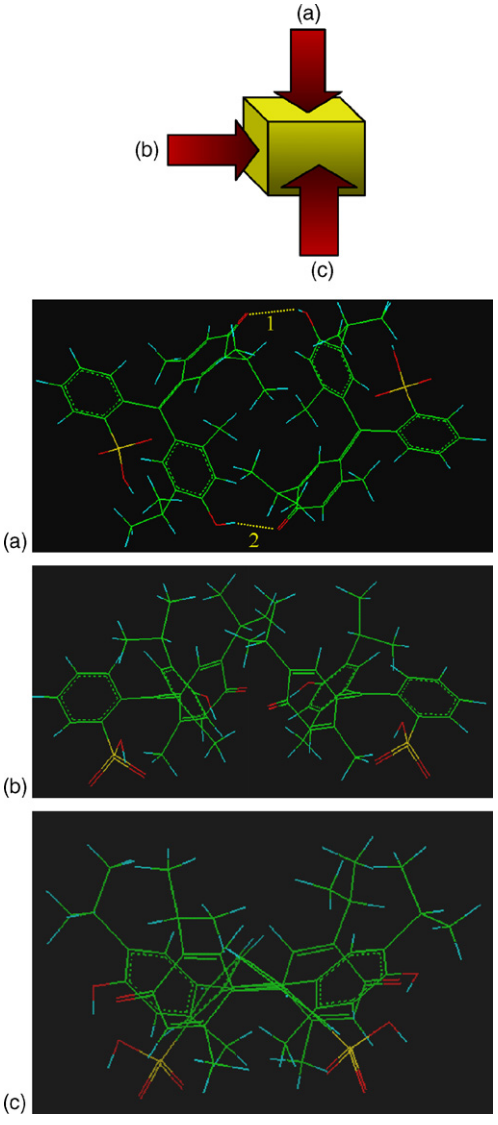


Fig. 6. Three different views of the H_4L_2 dimer configuration in the presence of the solvent (the water molecules are not shown). In the top panel the arrows indicate the three orientations of the views. The dashed yellow lines and numbers indicate the hydrogen bonds formed. (For interpretation of the references to color in this figure legend, the reader is referred to the web version of the article.)

To predict the order of appearance in the UV–vis spectra for species II and IV, the HOMO–LUMO gaps reported in Table 1 are used to estimate the first electronic transitions. Even when this is a crude estimation, it is well known that B3LYP gaps are useful in this context [27] and therefore we only use this level of theory to perform such evaluation. By transforming the gap to wavelength, for structures IV and II, one gets a 265 and 399 nm, respectively. These results indicate that structure IV wavelength corresponds to the UV region and that structure II wavelength is in the visible region. More important for our study is the relative order indicating that structure IV must be colorless.

4.2. Dimer

According to force field simulations, there are two possibilities for dimer formation: II–II and IV–IV. However, it is well known that structure IV is stable in some non-aqueous solutions and that its absorption spectrum does not present any peak in the visible region [13], this is in agreement with the estimated first electronic transition for this species. Also, all the experiments in aqueous media, at the pH in which species II–IV may exist, indicate the presence of a colored solution, consequently, as our work focuses in aqueous media, all dimer simulations were performed on the II–II species. For this dimer, constructed by using H_2L(II) monomers (see Fig. 2), the conformational space was sampled with the CVFF force field, according to the following procedure: (1) the monomer was optimized; (2) several possibilities for the dimer structure were tested according to Fig. 4; (3) for each dimer structure a short molecular dynamics (3 ps) at high temperature (700 K) was run to identify local minima; (4) finally, a full minimization with CVFF force field was done for each minimum. Seven structures were found that correspond to local minima.

The most stable dimer among these minima is shown in Fig. 5, the comparison with the structure obtained using MM3 force field is also displayed. From Fig. 5 one can conclude that the dimer is stabilized by two O–H···O hydrogen bonds formed between by –C=O and –C–OH groups. Also, it is observed that the relative positions of the functional groups implied in the hydrogen bond formation are equivalent for both methods. The interaction energy for this minimum was obtained at the BLYP/DZVP level of theory including the basis set superposition error (BSSE) correction. This calculation was performed using single point calculations in the geometries obtained by the CVFF method for the dimer and monomer. The calculated binding energy of the dimer is −13.5 kcal/mol, which clearly indicates the formation of two O–H···O hydrogen bonds [28].

4.3. The solvent effect on the H_4L_2 dimer formation

The experimental evidence indicates that the dimer is stable in aqueous media. As the molecular mechanics results show, the

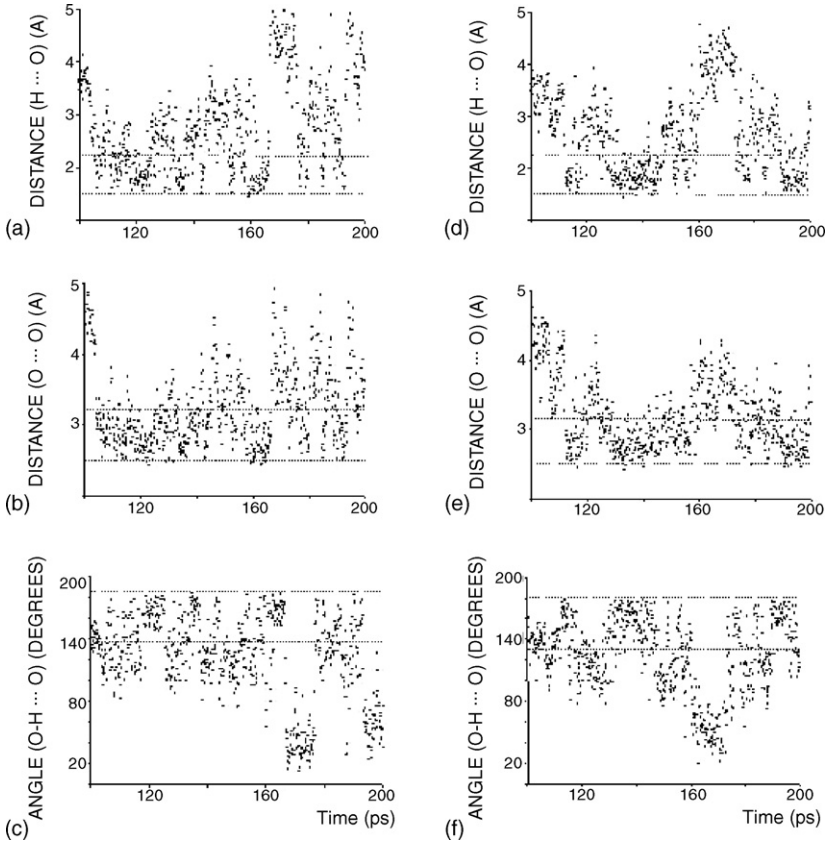


Fig. 7. Fluctuations of the angle O–H···O and distances O···O and H···O, for the stabilizing hydrogen bonds named 1 and 2 in Fig. 6, of the dimer H_4L_2. This figure corresponds to the simulation at 298 K with a layer of solvent built from 908 water molecules. The horizontal dashed lines show the standard limits for hydrogen bond formation for these parameters [28]. Panels (a–c) correspond to hydrogen bond 1 and (d–f) are related to hydrogen bond 2.

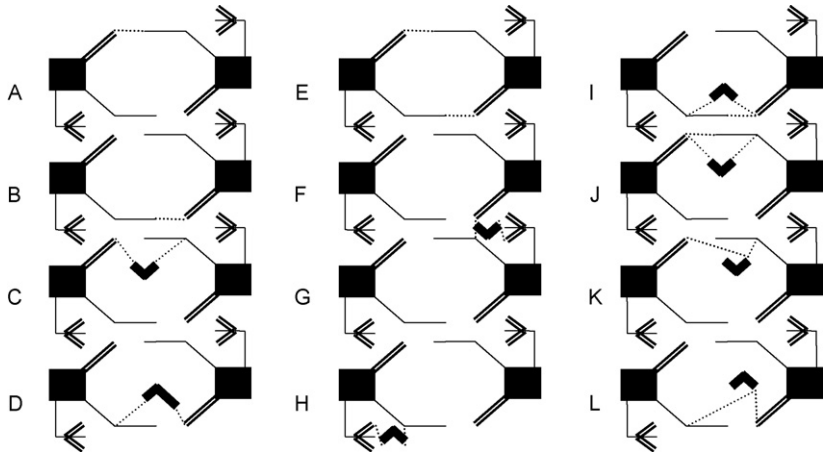


Fig. 8. Schematic representation of typical structures for the H_4L_2 dimer observed during the simulation in the presence of solvent at 298 K. These structures correspond to regions where one or the two hydrogen bonds are broken. In this figure the bold angular solid line indicates the water molecule; see Fig. 5 for other group identification.

dimer is also stable in vacuum. In order to study the dynamical stability of the dimer in aqueous media, a molecular dynamics was performed according to what is described in the methodology section. A typical low energy structure, taken from the molecular dynamics results obtained for the dimer in a layer of water molecules, was fully relaxed to reach a minimum with the CVFF force field. This relaxation includes all the water molecules in the layer; Fig. 6 shows three views of the molecule. It can be seen, by comparing Figs. 5 and 6, that this minimum, which is representative of the structure in the presence of the solvent, is similar to those obtained in vacuum. What is remarkable in Fig. 6 is the "symmetry" of the dimer: the functional groups responsible for the hydrogen bond formation are in equivalent positions in both molecules. Indeed, this "symmetry" implies that equivalent chemical environments surround both hydrogen bonds. This is in agreement with NMR experiments.

A dynamical picture of the hydrogen bonds in the dimer can be extracted from Figs. 7 and 8. These figures show the geometrical fluctuations in the hydrogen bond moiety. From Fig. 7, one is able to see that during the simulation there are periods in which both hydrogen bonds are formed, at approximately 140 ps; during some time only one of the hydrogen bonds is formed, see for example the zone around 160 ps. Also, there is one area, close to 170 ps in which both hydrogen bonds are lost. During the simulation it is seen that some molecules of the solvent form hydrogen bonds with the active groups of the dimer.

The representative structures of these interactions are displayed in Fig. 8; structures A, B, and E represent the situations in which the dimer is stabilized by at least one hydrogen bond without intrusion of water molecules. The structures C, D, I–L correspond to bridge situations where a water molecule form hydrogen bonds with both monomers; sometimes these interactions involve a position of the water molecule in which it is acting as a double donor. Also, some structures show that the presence of water breaks the hydrogen bonds that stabilize the dimer (C, D, K, and L). The water molecules also interact with the sulphonic group as it is indicated in structures G and H. Finally, it is possible to identify the structures such as F, in which both hydrogen bonds are broken. The above discussion shows the variety of hydrogen bonds interactions of the dimer in the solvent and that the dimer is stable for most of the time, which is in agreement with the experimental evidence.

5. Conclusions

The comparison of CVFF with MM3 force field indicates that the former represents appropriately the structure of the relevant hydrogen bond environments for TB molecule and dimer. However, MM3 force field gives a better-detailed description with respect to LDA structure, particularly in the weak hydrogen bonds environments.

In relation to the TB monomers, it can be concluded that, among the species having the possibility of forming dimers, the most stable in vacuum corresponds to structure IV depicted in Fig. 2. Nevertheless this structure is not able to form a dimer in aqueous media. In contrast, the structure II forms a stable dimer in vacuum and aqueous media. The dimer found in our theoretical study generates symmetric hydrogen bond environments, which is in agreement with experimental facts. Therefore, according to our results, the stable dimer proposed by experimental data is of the II–II form. In vacuum, the dimerization energy calculated by ab initio methods corresponds to two O–H···O hydrogen bonds.

Acknowledgments

This research was partially supported by C01-39621 and 36482-E CONACYT projects. PB acknowledges CONACYT for a PhD scholarship.

References

[1] Y. Wei, K. Li, S. Tong, Anal. Chim. Acta 97 (1997) 341.
[2] J. Eley, G. Halbert, A. Florence, J. Pharm. Pharmacol. 41 (1989) 858.
[3] R. Maggini, F. Secco, M. Venturini, J. Phys. Chem. A 101 (1997) 5666.
[4] R. Andres, R. Narayanaswamy, Talanta 44 (1997) 1335.

[5] N. Acar, F. Onur, Anal. Lett. 29 (1996) 763.
[6] K. Chuang, D. Fung, Proceedings of the IFT Annual Meeting E.U., 1995, p. 253.
[7] P. Balderas-Hernández, M.T. Ramírez, A. Rojas-Hernández, A. Gutiérrez, Talanta 46 (1998) 1439;
P. Balderas-Hernández, A. Rojas-Hernández, M. Galván, M.T. Ramírez-Silva, Spectrochim. Acta A 60 (2004) 569.
[8] I.R. Gould, P.A. Kollman, J. Am. Chem. Soc. 116 (1994) 2493.
[9] W. Han, S.J. Suhai, J. Phys. Chem. 100 (1996) 3942.
[10] S.S. Xantheas, J. Chem. Phys. 102 (1995) 4505.
[11] R. Vargas, J. Garza, R.A. Friesner, H. Stern, B.P. Hay, D.A. Dixon, J. Phys. Chem. A 105 (2001) 4963.
[12] J. Sponer, J. Leszczynsky, P. Hobza, J. Phys. Chem. 100 (1996) 1995.
[13] I.M. Kolthoff, M.K. Chantooni, S. Bhowmik, Anal. Chem. 39 (1967) 315.
[14] MM3 (96) may be obtained from Tripos Associates, 1699 S. Hanley Road, St. Louis, MO 63144, for commercial users, and it may be obtained from the Quantum Chemistry Program Exchange, Mr. Richards Counts, QCPE, Indiana University, Bloomington, IN 47405, for noncommercial users.
[15] R. Vargas, J. Garza, D.A. Dixon, B.P. Hay, J. Phys. Chem. A 104 (2000) 5115.
[16] R. Vargas, J. Garza, D.A. Dixon, B.P. Hay, J. Am. Chem. Soc. 122 (2000) 4750.
[17] S. Shceiner, T. Kar, Y.J. Gu, Biol. Chem. 272 (2001) 9832.
[18] W. Bing, J.F. Hinton, P.J. Pulay, J. Phys. Chem. A 107 (2003) 4683.
[19] R. Vargas, J. Garza, D.A. Dixon, B.P. Hay, J. Mol. Struct. (Theochem.) 541 (2001) 243.
[20] Discover version 4.0.0, msi, San Diego, CA, USA.
[21] S.H. Vosko, L. Wilk, M. Nusair, Can. J. Phys. 58 (1980) 1200.
[22] N. Godbout, D.R. Salahub, J. Andzelm, E. Wimmer, Can. J. Chem. 70 (1992) 560.
[23] A.D. Becke, J. Chem. Phys. 98 (1993) 5648.
[24] A.D. Becke, J. Chem. Phys. 98 (1993) 1372.
[25] C. Lee, W. Yang, R.G. Parr, Phys. Rev. B 37 (1988) 78.
[26] D.E. Bernholdt, E. Apra, H.A. Fruchtl, M.F. Guest, R.J. Harrison, R. Kendall, R.A. Dutteh, X. Long, J.B. Nicholas, J.A. Nichols, H.L. Taylor, A.T. Wong, G. Fann, R.J. Littlefield, J. Nieplocha, Int. J. Quantum Chem. Symp. 29 (1995) 475.
[27] U. Salzner, J.B. Lagowski, P.G. Pickup, R.A. Poirier, J. Comp. Chem. 18 (1997) 1943.
[28] G.A. Jeffrey, An Introduction to Hydrogen Bonding, Oxford University Press, New York, 1997, p. 12.

Available online at www.sciencedirect.com
ScienceDirect
Talanta 71 (2007) 1345–1351
Talanta
www.elsevier.com/locate/talanta

Comparison of pressurized liquid extraction and microwave assisted extraction for the determination of organochlorine pesticides in vegetables

M. Barriada-Pereira [a,b], M.J. González-Castro [b], S. Muniategui-Lorenzo [b,*], P. López-Mahía [a,b], D. Prada-Rodríguez [a,b], E. Fernández-Fernández [b]

[a] *University Institute of Environment, Pazo de Lóngora, Liáns, Oleiros, A Coruña, E-15179, Spain*
[b] *Department of Analytical Chemistry, University of A Coruña, Campus da Zapateira, s/n, E-15071, A Coruña, Spain*

Received 10 January 2006; received in revised form 16 June 2006; accepted 6 July 2006
Available online 22 August 2006

Abstract

A method to determine organochlorine pesticides in horticultural samples (lettuce, tomato, spinach, potato, turnip leaf and green bean) using pressurized liquid extraction (PLE) is described and compared with microwave assisted extraction (MAE). Significant parameters affecting PLE procedure such as temperature, static extraction time and extraction solvent were optimised and discussed. Clean-up of extracts was performed by solid phase extraction (SPE) using a carbon cartridge as adsorbent. Pesticides were determined by gas chromatography and electron capture detection (GC–ECD). Analytical recoveries obtained were ca. 100% and the relative standard deviations were lower than 15% for most of the studied pesticides with the proposed methods in each analysed matrix.
© 2006 Elsevier B.V. All rights reserved.

Keywords: Organochlorine pesticides; Vegetable samples; Pressurized liquid extraction; Microwave assisted extraction; Solid-phase extraction

1. Introduction

The preservation of human health from exposure to pesticide residues in foodstuffs, especially in fruits and vegetation, is a problem of increasing public interest [1–3]. The presence of pesticides in the environment has to be controlled due to their high toxicity and their widespread use in agriculture practices [4]. The use of organochlorine pesticides (OCPs) has been banned in more developed countries as they constitute an important group of dangerous organic contaminants due to their low biodegradability and persistence [5]. Besides they are known to induce cancer and have a high endocrine disrupting potential [6–8].

Maximum recommended limits (MRLs) for organochlorine pesticide residues in a variety of agricultural foods were established by the European Union in concentrations which in the most severe cases can be as low as $10\,\mu g\,kg^{-1}$ [1,9]. These concentration values make necessary the development of highly sensitive multiresidue methods to analyze pesticides in different sample matrices.

Although many methods for determining pesticides in fruits, vegetables and other food matrices have been described, the pesticide residues analysis still represents an analytical challenge [10]. Pressurized liquid extraction (PLE) and microwave assisted extraction (MAE) are recent extraction methods that were successfully used during last years in the analysis of a wide range of chemicals from many sample matrices [11–14]. Compared with other traditional extraction techniques they present advantages such as reduction of the volume of extraction solvents and time of analysis, and improvement of the reproducibility of compound recovery [15]. PLE extractions are carried out at temperatures over the boiling point under atmospheric pressure of the solvent extractant, which is possible with the application of high pressures in the extraction cell in order to maintain the solvent in a liquid state [12]. On the other hand commercial microwave equipments with security systems and closed vessels have made MAE an analytical technique of interest since these instruments enable simultaneous extractions of organic pollutants at high pressure and temperature, facilitating rapid and

* Corresponding author. Tel.: +34 981 167 000; fax: +34 981 167 065.
E-mail address: smuniat@udc.es (S. Muniategui-Lorenzo).

0039-9140/$ – see front matter © 2006 Elsevier B.V. All rights reserved.
doi:10.1016/j.talanta.2006.07.012

selective analyte desorption from complexes matrices [16]. The major drawback of PLE and MAE is the high investment cost of the commercialized systems [17].

Although numerous papers have been published on both recent techniques, few of them are related to vegetables. In a previous work we determined OCPs in several vegetables (lettuce, potato, spinach, tomato and pepper) using MAE [18]. In the present study our objective was to develop a method to determine OCPs in horticultural samples using PLE as extraction procedure and compare the obtained results with those obtained with MAE. Furthermore other two matrices (turnip leaf and green bean) are included in this study. In order to minimize the presence of interfering compounds in the GC system, extraction was followed in both cases by a clean-up step with solid phase extraction (SPE) using ENVI^{TM}-Carb as adsorbent. Finally organochlorine pesticides were determined by GC–ECD due its high sensitivity to molecules that contains electronegative atoms [19].

2. Experimental

2.1. Chemicals

2.1.1. Pesticide standards

A mix of organochlorine pesticides named "CLP organochlorine pesticide mix" containing: α-Chlordane; Methoxychlor; γ-Chlordane; Endrin ketone; Aldrin; α-HCH; β-HCH; γ-HCH; δ-HCH; *p*,*p*′-DDD; *p*,*p*′-DDE; *p*,*p*′-DDT; Dieldrin; α-Endosulfan; β-Endosulfan; Endosulfan sulfate; Endrin; Endrin aldehyde; Heptachlor and Heptachlor epoxide (isomer B) and an individual standard of 2,4,5,6-tetrachloro-*m*-xylene (TCMX) were obtained from Supelco (Bellefonte, PA, USA). Isodrin was purchased from ChemService (West Chester, USA).

2.1.2. Solvents

Acetone and *n*-hexane 95% were Super Purity Solvents from Romil (Cambridge, UK). Ethyl acetate (PAR, for analysis of residues) for instrumental analysis was from Panreac (Barcelona, Spain).

2.1.3. Sorbents

ENVI^{TM}-Carb of 100 m^2 g^{-1} Packing 12 ml (1 g) was from Supelco (Bellefonte, PA, USA). Diatomaceous earth, acid-washed, not further calcined, approximately 95% SiO_2 was from Sigma Chemical CO. (St. Louis, MO, USA).

2.1.4. Filters

Cellulose extraction filter of 1.983 cm was from Dionex Corporation (Sunnyvale, CA, USA). Glass fibre filter of 0.6 μm (MN GF-6) was from Macherey Nagel (Düren, Germany). PTFE of 0.45 μm was from Lida, Manufacturing Corp (Kenosha, WI).

2.2. Materials and apparatus

The PLE experiments were performed using an ASE 200 Accelerated Solvent Extractor of Dionex Corporation (Sunnyvale, CA, USA). This instrument features an auto-sampler carousel and a collection tray allowing the unattended extraction of up to 24 samples. Stainless-steel extraction cells and glass collection vials with 11 and 40 ml volumes, respectively, were used. Microwave extraction was carried out using a laboratory microwave oven (Anton Paar Multiwave, Graz, Austria) equipped with a built-in magnetic stirrer, a fiber-optic temperature sensor, a pressure sensor and a basic 6-position extraction rotor.

A rotary evaporator Büchi R-3000 (Büchi Labortechnic AG, Flawil, Switzerland) was used in the evaporation step. A Visiprep® vacuum distribution manifold from Supelco (Bellefonte, PA, USA) was employed in the purification step.

The GC–ECD equipment consisted of a Perkin-Elmer (Norwalk, CT, USA) Autosystem XL chromatograph equipped with a ^{63}Ni electron capture detector (ECD), an auto-sampler, split–splitless injector, programmed pneumatic control and a computer running Turbochrom 4 data processor. For separation a J&W (Folsom, CA, USA) DB-35MS capillary column (length 30 m, i.d. 0.32 mm, film thickness 0.25 μm) was employed.

The GC–MS equipment consisted of a Trace 2000 GC coupled to a Thermo Finnigan (Austin, TX, USA) Polaris-Q ion trap mass spectrometer detector (MS). The gas chromatograph is equipped with a programmed temperature vaporisation (PTV) injector and a J&W DB-XLB (length 60 m, i.d. 0.25 mm, film thickness 0.25 μm) capillary column.

2.3. Sample preparation

Sample preparation is an essential part of a solvent extraction procedure. The ideal sample for extraction is a dry, finely divided solid. For an efficient extraction to occur, solvents must make contact with the target analytes, so high surface areas are recommended.

Fresh vegetables (lettuce, tomato, spinach, potato, turnip leaf and green bean) were purchased at several local markets in A Coruña city, NW Spain. A 1–2 kg sample of each vegetable was chopped and homogenized. An aliquot of about 100 g was weighted on an Erlenmeyer flask and freeze–dried. Then samples were grounded in a mill and stored at room temperature in glass bottles out of light exposure until their analysis.

2.3.1. Pressurized liquid extraction

In the case of PLE the aggregation of sample particles may prevent efficient extraction so samples are dispersed with an inert material such as diatomaceous earth will assist in the extraction process [12]. 0.3 g of each sample were mixed in a mortar with 0.075 g of diatomaceous earth and the mixture was added directly to extraction cells containing cellulose extraction filters to prevent frit blockage of fine powder breakthrough into the collection bottle. With this mixture the extraction chamber is not completely full, there is some free volume for extracting solvents. Afterwards, 50 μl of a standard solution with the studied pesticides in a concentration of 1 μg ml^{-1} were added directly to the sample, sonicated for 5 min and let stay 20 min before extraction procedure.

Samples were extracted under the following conditions—temperature: 110 °C; pressure: 10 MPa (1500 psi); solvent:

approximately 30 ml of hexane:acetone (50:50); heat-up time: 5 min; static time: 5 min; flush volume: 60%; purge: N2, 60 s; number of cycles: 1. Finally the extract was concentrated to ca. 1 ml using a rotary evaporator.

2.3.2. Microwave assisted extraction

In the case of MAE samples were extracted following a procedure previously developed in our laboratory [20]. Briefly, 0.3 g of each sample were weighed into PTFE-TFM extraction vessels and extracted with 15 ml of hexane:acetone (50:50) with stirring using the following microwave program: 1 min ramp from 100 to 800 W, a 4 min hold at 800 W, 0 W for 2 min, 1 min ramp from 100 to 800 W, a 4 min hold at 800 W. After cooling, vessels content was filtered through 0.6 μm glass fibre filter and the filtrate was concentrated to ca. 1 ml using a rotary evaporator.

2.3.3. Clean-up

In both cases the extraction was followed by a clean-up procedure previously optimised which employs SPE ENVI^{TM}-Carb packing cartridges connected to a Visiprep® vacuum distribution manifold [21]. The cartridges were loaded with concentrated extracts and pesticides were eluted with 10 ml of hexane:ethyl acetate (80:20). Finally eluates were evaporated to a drop in rotary-evaporator and got to dryness by a gentle nitrogen stream. Once dissolved in 1 ml hexane, the solution was filtered through a syringe filter PTFE of 0.45 μm and pesticides were determined by gas chromatography and electron capture detection (GC–ECD).

2.4. Chromatographic procedure

2.4.1. GC–ECD conditions

Helium (99.999%) was used as carrier gas. Carrier gas flow: 1 ml min^{-1}. The oven temperature was programmed from 60 °C (1 min) to 220 °C at a rate of 25 °C min^{-1}, 220–300 °C at a rate of 6 °C min^{-1}. The temperature of the injector operating in splitless mode (volume injected 1 μl) was held at 300 °C and electron capture detector temperature was 350 °C. The detector auxiliary gas was nitrogen (99.999%) with a flow of 30 ml min^{-1}. Quantification was performed using TCMX as internal standard. Fig. 1 shows a chromatogram of a standard solution containing of 0.1 mg l^{-1} of each pesticide injected under these chromatographic conditions.

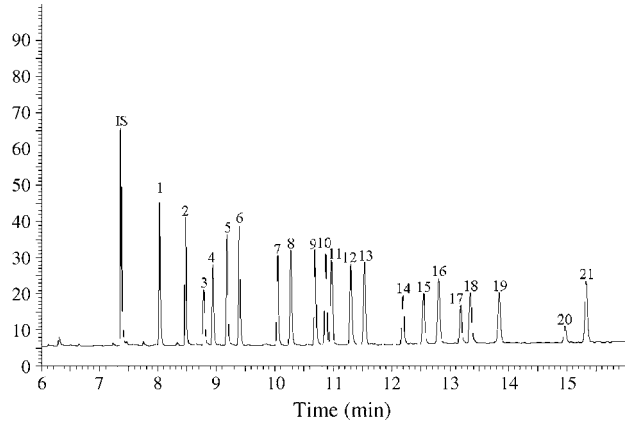


Fig. 1. GC–ECD chromatogram of a standard solution with 0.1 mg l^{-1} of OCPs. Target compounds are numbered as follows: IS TCMX (2,4,5,6-tetrachloro-*m*-xylene); (1) α-HCH; (2) γ-HCH; (3) β-HCH; (4) Heptachlor; (5) δ-HCH; (6) Aldrin; (7) Isodrin; (8) Heptachlor epoxide; (9) γ-Chlordane; (10) α-Chlordane; (11) α-Endosulfan; (12) *p,p′*-DDE; (13) Dieldrin; (14) Endrin; (15) *p,p′*-DDD; (16) β-Endosulfan; (17) *p,p′*-DDT; (18) Endrin aldehyde; (19) Endosulfan sulfate; (20) Methoxychlor; (21) Endrin ketone.

2.4.2. GC–MS conditions

Transfer line temperature 290 °C; ion source temperature 250 °C and multiplier voltage 1450 V. A PTV (programmed temperature vaporisation) injector operating in solvent-split mode was employed. The volume injected was 9 μl, split flow 50 ml min^{-1}, splitless time: 5 min and injection time: 0.50 min, injection flow: 100 ml min^{-1}. Injector temperature programme: 40 °C increased at 4 °C s^{-1} to 290 °C (held for 20 min). The oven temperature program was: 50–150 °C at 10 °C min^{-1}, at 5 °C min^{-1} to 300 °C (5 min). Carrier gas flow: 1 ml min^{-1} constant flow (He). Ion trap mass detection was operated in full scan mode from 50 to 500 amu.

3. Results and discussion

3.1. Optimization of PLE procedure

Extraction temperature, static extraction time, extraction solvent and diatomaceous earth weights were considered to obtain optimised conditions for the pressurized liquid extraction of organochlorine pesticides from vegetables. As pressure is not considered a critical experimental parameter an extraction pressure of 10 MPa was chosen according to literature [22–24]. PLE conditions assayed were selected according with previous studies in our laboratory for the extraction of OCPs in soils [25].

Temperature is the most important parameter used in PLE extraction. The extraction temperature has influence on extraction kinetics and solvents viscosities and therefore also on extraction efficiencies and overall recoveries [23]. The influence of the temperature on the extraction efficiency was investigated by monitoring the range of 80–120 °C. Fig. 2 shows the effect of temperature on the extraction efficiency of PLE for several OCPs extracted from homogenized lettuce samples. Lower recoveries

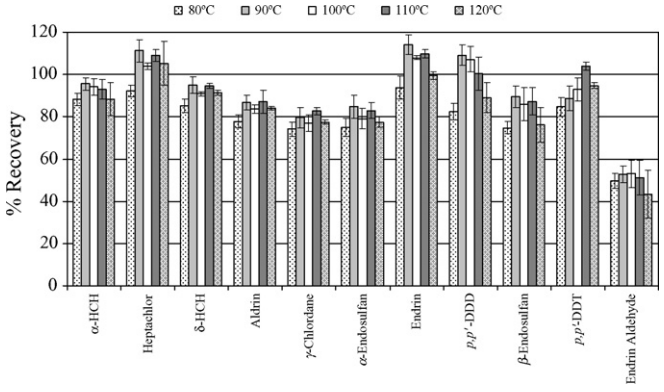


Fig. 2. Effect of extraction temperature on the extraction efficiency of PLE ($n = 3$).

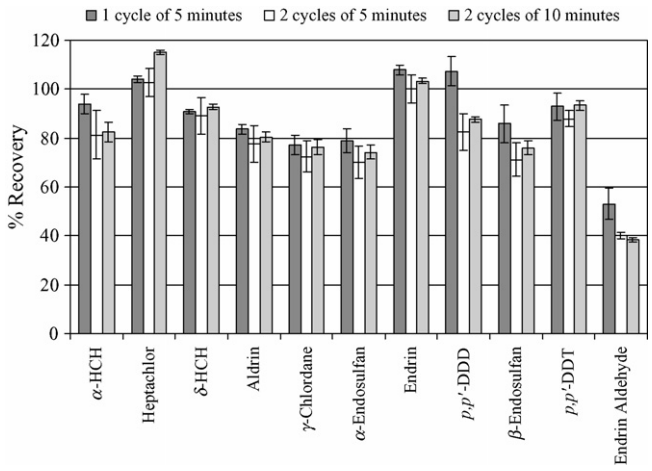


Fig. 3. Influence of number of static cycles and static extraction time on the extraction efficiency of PLE ($n = 3$).

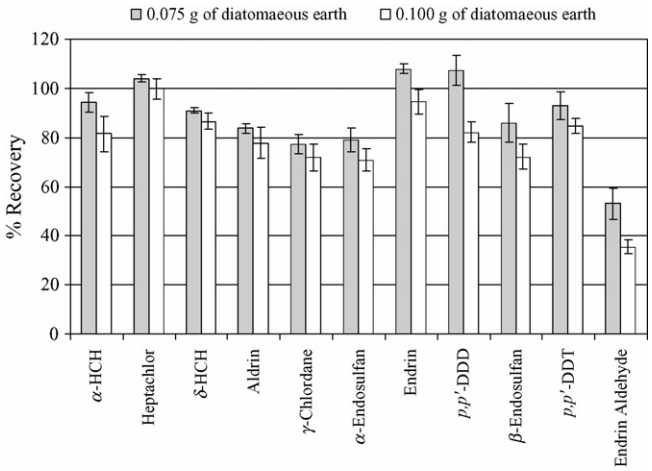


Fig. 5. Effect of percentage of inert material on the extraction efficiency of PLE ($n = 3$).

were achieved with 80 and 120 °C. Although there are no major differences among 90, 100 and 110 °C, a temperature of 110 °C seems to be optimal for the majority of the target compounds.

Certain sample matrices can retain analytes within pores or other structures. These compounds can diffuse into the extraction solvent by increasing the static time at elevated temperatures. The use of static cycles was developed to introduce fresh solvent during the extraction process. The effect of static time should always be explored in conjunction with static cycles, in order to produce a complete extraction in the most efficient way possible. In this work the effect of extraction time was studied between 5 and 20 min, working with one or two cycles of 5 or 10 min. As shown in Fig. 3, the recoveries obtained with these assays were adequate for most of the studied pesticides; thus, a single cycle of 5 min was chosen because it provides a shortened analysis time.

For an efficient extraction, the solvent must be able to solute the target compounds while leaving the sample matrix intact. The polarity of the extraction solvent should closely match that of the target analytes; generally a solvent which provides good results in a conventional procedure works well in PLE. In order to evaluate the extraction solvent efficiency, samples were extracted with hexane and hexane:acetone (50:50). Although similar recovery values were obtained in both cases, the mixture hexane:acetone (50:50) was selected as extraction solvent for the PLE procedure because this is the mixture used in MAE (Fig. 4).

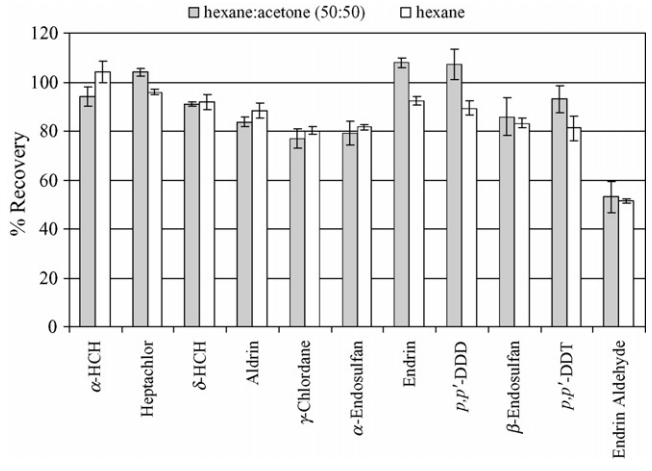


Fig. 4. Effect of solvent composition on the extraction efficiency of PLE ($n = 3$).

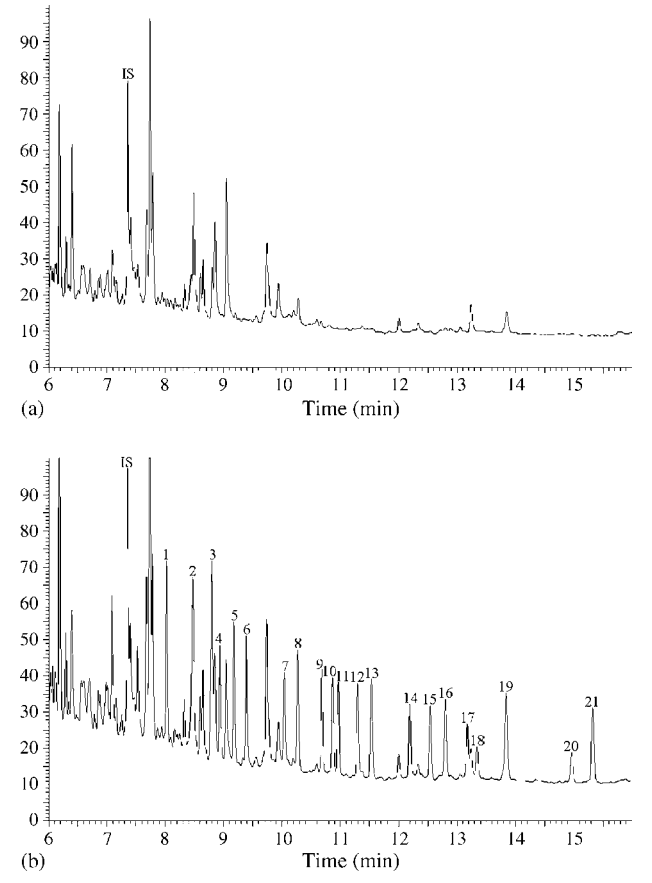


Fig. 6. (a) PLE lettuce extract chromatogram and (b) PLE Spiked lettuce extract chromatogram. Spiked level: 0.17 μg g^{-1}. Target compounds are numbered as follows: IS TCMX (2,4,5,6-tetrachloro-*m*-xylene); (1) α-HCH; (2) γ-HCH; (3) β-HCH; (4) Heptachlor; (5) δ-HCH; (6) Aldrin; (7) Isodrin; (8) Heptachlor epoxide; (9) γ-Chlordane; (10) α-Chlordane; (11) α-Endosulfan; (12) *p,p′*-DDE; (13) Dieldrin; (14) Endrin; (15) *p,p′*-DDD; (16) β-Endosulfan; (17) *p,p′*-DDT; (18) Endrin aldehyde; (19) Endosulfan sulfate; (20) Methoxychlor; (21) Endrin ketone.

The percentage of inert material employed in the matrix dispersion can have influence in the extraction process. Fig. 5 summarize the results obtained with two different weights of diatomaceous earth. It can be seen that the best results were achieved when the 0.3 g of sample were mixed with 0.075 g of diatomeous earth (a 25% of sample weight).

3.2. Comparison of PLE and MAE techniques

As an example GC–ECD chromatograms unspiked and spiked lettuce extracts with the PLE and MAE selected methods are shown in the Figs. 6 and 7. As it can be clearly seen in these figures dirtier chromatograms were obtained in the case of PLE. With PLE more interfering compounds are extracted from the matrix than with those extracted with MAE. In fact, the chromatogram corresponding to PLE extraction (Fig. 6a) shows peaks corresponding to possible traces of pesticides in the non spiked sample.

Confirmation of the results was taken account using GC–MS by its full scan mode and also by selected ion monitoring (SIM). Results obtained by GC–MS showed that these peaks are not pesticides. Cleaner extracts for PLE might be obtained by a larger purification step, but this would make the analysis more expensive and laborious.

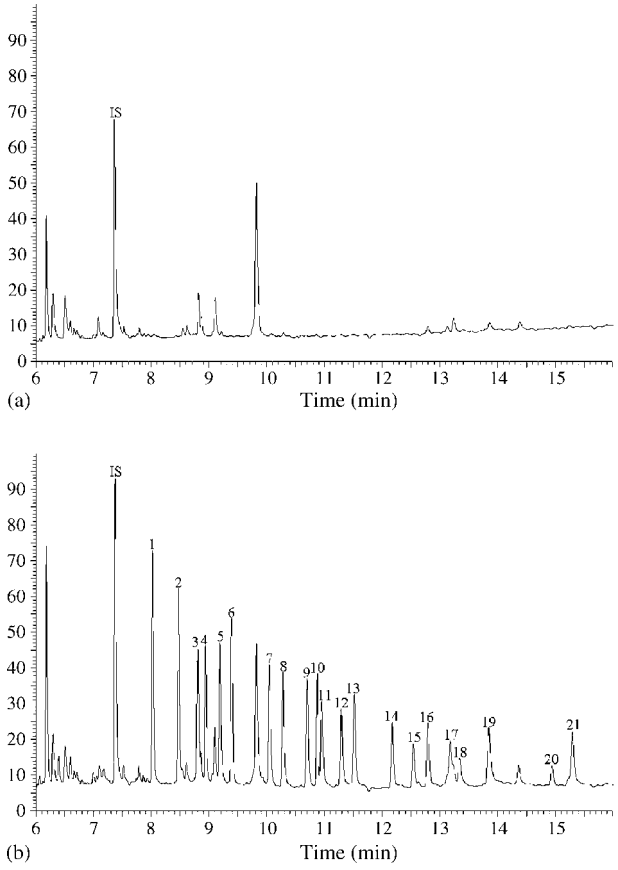


Fig. 7. (a) MAE lettuce extract chromatogram and (b) MAE Spiked lettuce extract chromatogram. Spiked level: 0.17 μg g^{-1}. Target compounds are numbered as follows: IS TCMX (2,4,5,6-tetrachloro-*m*-xylene); (1) α-HCH; (2) γ-HCH; (3) β-HCH; (4) Heptachlor; (5) δ-HCH; (6) Aldrin; (7) Isodrin; (8) Heptachlor epoxide; (9) γ-Chlordane; (10) α-Chlordane; (11) α-Endosulfan; (12) *p,p′*-DDE; (13) Dieldrin; (14) Endrin; (15) *p,p′*-DDD; (16) β-Endosulfan; (17) *p,p′*-DDT; (18) Endrin aldehyde; (19) Endosulfan sulfate; (20) Methoxychlor; (21) Endrin ketone.

Table 1
LOD and LOQ in ng g^{-1} of fresh lettuce extracts (wet percentage 94.6%)

Pesticides	PLE		MAE	
	LOD	LOQ	LOD	LOQ
α-HCH	1.8	4.9	0.7	1.9
γ-HCH	2.1	5.5	0.9	2.2
β-HCH	4.1	10.9	1.8	4.3
Heptachlor	3.5	9.3	1.4	3.6
δ-HCH	2.3	6.0	1.0	2.4
Aldrin	2.0	5.2	0.8	2.0
Isodrin	2.5	6.5	1.1	2.6
Heptachlor epoxide	2.5	6.3	1.1	2.6
γ-Chlordane	2.4	6.2	1.1	2.5
α-Chlordane	2.3	6.5	0.9	2.5
α-Endosulfan	2.5	6.6	1.1	2.6
p,p′-DDE	2.3	6.5	0.8	2.5
Dieldrin	2.4	6.4	1.0	2.5
Endrin	4.2	11.1	1.7	4.4
p,p′-DDD	3.8	10.2	1.5	4.0
β-Endosulfan	1.2	6.6	1.3	3.4
p,p′-DDT	5.5	15.2	2.0	5.8
Endrin aldehyde	3.6	9.8	1.4	3.8
Endosulfan sulfate	2.4	8.4	0.2	2.6
Endrin ketone	2.6	7.3	0.9	2.7

3.2.1. Linearity of the chromatographic method

Linear calibration curves for all pesticides over six calibration levels, from 0.005 to 0.100 mg l^{-1} were constructed using TCMX as internal standard. The calibration curves were linear over the whole concentration tested for all the OCPs with correlation coefficients (R^2) ranging between 0.9955 for β-Endosulfan and 0.9993 for Dieldrin.

3.2.2. Limits of detection and quantification

Limit of detection (LOD) and limit of quantification (LOQ) were calculated at 3 and 10 times the standard deviation above the blank signal in a GC–ECD injection. Table 1 shows these values in ng g^{-1} of fresh samples calculated with PLE and MAE blank lettuce extracts analysed by GC–ECD. As it could be predicted by the aforementioned chromatograms, worse LOD and LOQ were obtained with PLE because matrix interferences were increased with this extraction method. The obtained values show that both methods provide adequate LOQ for the analysis of vegetables with the target analytes at the concentrations established by the EU in the maximum residue levels (MRLs) although LOQ of some pesticides with PLE are close to these MRLs.

3.2.3. Comparison of PLE and MAE recoveries

Recovery efficiency is an important factor when an analytical method is evaluated. The optimisation experiments were performed using spiked lettuce sample (at levels of 0.17 μg g^{-1} of each compound in freeze dried samples). Table 2 shows analytical recoveries (%) and R.S.D. (%) of OCPs extracted from spiked vegetable samples with both techniques. In most cases

Table 2
Analytical recoveries (%*R*) and R.S.D. (%) of OCPs added to vegetable samples[a] ($n = 4$)

Pesticides	Lettuce				Tomato				Spinach				Potato				Turnip leaf				Green bean			
	PLE		MAE		PLE		MAE		PLE		MAE		PLE		MAE		PLE		MAE		PLE		MAE	
	%R	R.S.D. (%)	*%R*	R.S.D. (%)	*%R*	R.S.D. (%)	*%R*	R.S.D. (%)	*%R*	R.S.D. (%)	*%R*	R.S.D. (%)	*%R*	R.S.D. (%)	*%R*	R.S.D. (%)	*%R*	R.S.D. (%)	*%R*	R.S.D. (%)	*%R*	R.S.D. (%)	*%R*	R.S.D. (%)
α-HCH	93	4	89	8	106	3	99	3	97	4	87	3	107	7	92	2	92	4	92	3	83	6	97	4
γ-HCH	114	12	82	9	130	1	92	3	99	12	81	4	95	12	93	5	109	12	87	5	114	14	81	10
β-HCH	144	7	95	12	134	10	104	13	83	2	108	15	116	8	112	9	80	10	145	3	84	11	125	13
Heptachlor	109	4	90	7	128	4	106	4	112	8	109	12	108	5	110	2	116	14	132	2	107	8	106	4
δ-HCH	95	1	88	8	107	4	93	3	97	8	89	2	100	3	86	3	95	8	97	5	89	8	85	5
Aldrin	87	6	85	5	105	1	94	3	92	8	74	8	87	3	91	3	107	3	80	4	94	6	92	2
Isodrin	92	5	92	2	103	4	102	3	111	13	86	3	88	2	94	4	89	3	93	1	89	8	103	4
Heptachlorepoxide	99	2	90	4	107	3	103	4	80	11	86	5	90	2	96	4	79	10	100	15	90	13	92	3
γ-Chlordane	83	2	94	5	102	1	108	5	86	7	91	2	85	2	101	5	86	5	79	4	84	6	85	4
α-Chlordane	82	4	93	5	102	2	106	4	86	8	84	2	87	2	95	5	85	6	81	2	83	6	87	3
α-Endosulfan	83	5	91	5	106	3	108	5	89	7	89	3	86	2	97	4	96	6	90	4	86	6	86	3
p,p′-DDE	86	2	91	10	103	1	110	5	89	9	99	7	86	3	110	3	94	5	87	5	87	10	88	3
Dieldrin	94	3	104	7	114	2	112	6	94	7	101	4	87	2	113	5	88	6	89	4	91	8	92	4
Endrin	110	2	111	4	121	2	115	7	111	8	120	7	116	4	120	4	117	9	120	10	95	12	104	3
p,p′-DDD	100	6	89	10	114	2	99	4	109	7	114	6	105	3	117	3	104	6	108	5	88	9	88	2
β-Endosulfan	87	6	88	6	97	1	104	3	89	9	89	4	80	4	99	4	81	1	85	5	82	1	82	4
p,p′-DDT	104	3	129	7	117	3	132	4	103	12	98	10	133	4	99	6	121	7	126	7	114	13	117	4
Endrin aldehyde	51	14	53	13	80	5	95	5	<LOD	<LOD	12	42	4	25	86	9	15	20	40	10	29	10	66	2
Endosulfan sulfate	97	10	88	5	102	8	104	5	83	4	80	9	103	5	87	8	85	7	88	6	81	4	88	7
Endrin ketone	94	4	116	9	107	2	117	10	98	6	107	8	98	3	114	5	86	6	102	6	84	10	93	3

[a]Spiked level: 0.17 μg g^{-1} in freeze dried samples.

analytical recoveries were between 80 and 120% and R.S.D. lower than 15%.

As it can be seen, in most cases analytical recoveries below 70% were obtained for Endrin aldehyde especially when the extraction is taken account with PLE. Satisfactory recoveries, higher than 80%, were obtained for this compound when tomato and potato were extracted with MAE while lower values were recovered from green vegetables especially from the leafy ones, which are covered by an epicuticular wax that could have influence on the extraction and clean-up process. In the case of PLE extraction, satisfactory recoveries were obtained only for tomato, although it was lower than the MAE value. Recoveries lower than 50% for this analyte were obtained for the other matrices. These results show that the sample matrix strongly affects the behaviour of Endrin aldehyde in the extraction procedure used, as it has been previously reported for some authors, who have observed that differences in the plant material (such as water, fat and pigment contents) and the texture of the samples influence extraction efficiency [26,27].

With PLE extraction β-HCH recovery was over 130% in lettuce and tomato. This fact could be attributed to several causes. The first reason might be the poor separation of β-HCH from interferents which would provide an overestimation of its peak. The second reason could be explained by the matrix effect on the transfer of compounds in the injection port as samples components may compete for the active sites of the liner allowing the transfer of a larger amount of analytes to the chromatographic system [22,28].

3.2.4. Comparison of the analysis process in PLE and MAE

Concerning the volume of organic solvents required both techniques are clearly better than traditional procedures although MAE has a lower solvent consumption than PLE. Regarding the total time of analysis, which nowadays is becoming one of the most important factors, MAE is faster than PLE, because although MAE requires further cooling and filtration to obtain the final extract, simultaneous extractions can be performed in a microwave oven while only sequential extractions can be conducted with the accelerated solvent extractor used in this work. Besides prior to extraction, PLE sample preparation is more tedious and time consuming, since the dispersion of the sample with the diatomaceous earth implies the weight of this material and the homogenisation of the mix with a mortar.

4. Conclusions

Factors influencing the extraction efficiency of PLE were optimised. The best results were obtained with the extraction of 0.3 g of sample homogenised with 0.075 g of diatomaceous earth with hexane:acetone (50:50) in one static extraction cycle of 5 min at a temperature of 110 °C.

PLE and MAE were compared as powerful techniques for the extraction of organochlorine pesticides from vegetables. The proposed methods provide simple and rapid procedures for the determination of pesticides in vegetables with good reproducibility and low detection limits, in the requirements of European Union Legislation. Accuracy and precision obtained by PLE and MAE are similar, but MAE has demonstrated to be more sensitive than PLE. Moreover, compared with PLE, MAE presents another advantages related to cost, analysis time and solvent consumption.

Acknowledgements

The authors wish to thank the University of A Coruña for their financial support. This work was also supported by Xunta de Galicia (PGIDT01PXI10301IF).

References

[1] A. Agüera, M. Contreras, J. Crespo, A.R. Fernández-Alba, Analyst 127 (2002) 347.
[2] P. Manirakiza, A. Covaci, P. Schepens, Chromatographia 52 (2000) 787.
[3] R. Sanghi, V. Tewari, Bull. Environ. Contam. Toxicol. 67 (2001) 587.
[4] D. Ortelli, P. Edder, C. Corvi, Anal. Chim. Acta 520 (2004) 33.
[5] D. Ueno, H. Iwata, S. Tanabe, K. Ikeda, J. Koyama, H. Yamada, Mar. Pollut. Bull. 45 (2002) 254.
[6] C. Basheer, H.K. Lee, J.P. Obbard, J. Chromatogr. A 968 (2002) 191.
[7] N. Furusawa, Anal. Bioanal. Chem. 378 (2004) 2004.
[8] N. Kajiwara, M. Watanabe, S. Tanabe, K. Nakamatsu, M. Amano, N. Miyazaki, Mar. Pollut. Bull. 44 (2002) 1089.
[9] J.L. Martínez-Vidal, M.C. Pablos-Espada, A. Garrido-Frenich, F.J. Arrebola, J. Chromatogr. A 867 (2000) 235.
[10] C. Blasco, G. Font, Y. Picó, J. Chromatogr. A 970 (2002) 201.
[11] V. Camel, Analyst 126 (2001) 1182.
[12] H. Giergielewicz-Mozajska, L. Dabrowski, J. Namiesnik, Crit. Rev. Anal. Chem. 31 (2001) 149.
[13] M. Letellier, H. Budzinski, Analusis 27 (1999) 259.
[14] B.E. Richter, J.L. Ezzell, D. Felix, K.A. Roberts, D.W. Later, Am. Lab. 24 (1995) 26.
[15] A.M. Carro, R.A. Lorenzo, Analyst 126 (2001) 1005.
[16] N. Carro, I. García, M.-C. Ignacio, M. Llompart, M.-C. Yebra, A. Mouteira, Anal. Bioanal. Chem. 374 (2002) 547.
[17] V. Camel, Anal. Bioanal. Chem. 372 (2002) 39.
[18] M. Barriada-Pereira, M.J. Gonzalez-Castro, S. Muniategui-Lorenzo, P. Lopez-Mahia, D. Prada-Rodriguez, E. Fernandez-Fernandez, Int. J. Environ. Anal. Chem. 85 (2005) 325.
[19] C. Blasco, C.M. Lino, Y. Picó, A. Pena, G. Font, M.I.N. Silveira, J. Chromatogr. A 1049 (2004) 155.
[20] M. Barriada-Pereira, E. Concha-Graña, M.J. González-Castro, S. Muniategui-Lorenzo, P. López-Mahía, D. Prada-Rodríguez, E. Fernández-Fernández, J. Chromatogr. A 1008 (2003) 115.
[21] M. Barriada-Pereira, M.J. González-Castro, S. Muniategui-Lorenzo, P. López-Mahía, D. Prada-Rodríguez, E. Fernández-Fernández, J. Chromatogr. A 1061 (2004) 133.
[22] K. Adou, W.R. Bontoyan, P.J. Sweeney, J. Agric. Food. Chem. 49 (2001) 4153.
[23] P. Suchan, J. Pulkrabová, J. Hajslová, V. Kocourek, Anal. Chim. Acta 520 (2004) 193.
[24] L. Wennrich, P. Popp, G. Köller, J. Breuste, J. AOAC Int. 84 (2001) 1194.
[25] E. Concha-Graña, M.I. Turnes-Carou, S. Muniategui-Lorenzo, P. López-Mahía, E. Fernández-Fernández, D. Prada-Rodríguez, J. Chromatogr. A 1047 (2004) 147.
[26] H. Obana, K. Akutso, M. Okihashi, S. Hori, Analyst 126 (2001) 1529.
[27] J. Tekel, S. Hatrík, J. Chromatogr. A 754 (1996) 397.
[28] J.L. Tadeo, C. Sánchez-Brunete, Chromatographia 57 (2003) 793.

Available online at www.sciencedirect.com
ScienceDirect
Talanta 71 (2007) 1022–1030
Talanta
www.elsevier.com/locate/talanta

Voltammetric characterisation of silicon-based microelectrode arrays and their application to mercury-free stripping voltammetry of copper ions

Alfonso Berduque, Yvonne H. Lanyon, Valerio Beni, Grégoire Herzog, Yvonne E. Watson, Kenneth Rodgers, Frank Stam, John Alderman, Damien W.M. Arrigan *

Tyndall National Institute, Lee Maltings, University College, Cork, Ireland

Received 22 February 2006; received in revised form 17 May 2006; accepted 26 May 2006
Available online 18 July 2006

Abstract

This paper describes the electrochemical characterisation of a range of gold and platinum microelectrode arrays (MEAs) fabricated by standard photolithographic methods. The inter-electrode spacing, geometry, numbers and dimensions of the electrodes in the arrays were found to influence the voltammetric behaviours obtained. Excellent correlation was found between experimental data and theoretical predictions employing published models of microelectrode behaviour. Gold MEAs were evaluated for their applicability to copper determination in a soil extract sample, where agreement was found between the standard analytical method and a method based on underpotential deposition—anodic stripping voltammetry (UPD-ASV) at the MEAs, offering a mercury-free alternative for copper sensing.
© 2006 Elsevier B.V. All rights reserved.

Keywords: Microelectrode array; Voltammetry; Micro-square and micro-band electrodes; Stripping voltammetry; Metal ion detection

1. Introduction

Electrochemical sensors are of increasing importance in analytical chemistry due to their sensitivity, selectivity, fast and accurate analyses, portability and inexpensive cost [1]. The applications for such sensors vary widely from environmental and medical diagnostics to biotechnology and food and beverage analysis [2]. Improvements in electrochemical sensors include the development of modified electrodes (using chemical or biological recognition layers to improve the sensitivity and selectivity) and microelectrodes [3–5]. A microelectrode can be defined as an electrode in which at least one of its dimensions is in the μm range [3] or an electrode with at least one dimension smaller than the diffusion length of the analyte [6].

One of the main benefits of using a microelectrode in a sensor application is the greater sensitivity that arises from the enhanced mass-transport at these small electrodes [7,8]. Hemispherical diffusion layers are formed at such electrodes [7,9] and much faster diffusion of electroactive substances occurs due to the multi-dimensional nature of this process, resulting in sigmoidal (or steady-state) cyclic voltammograms (CVs) [3,8,10,11]. The end result for the sensor is improved response time (faster response), a greater sensitivity and increased response per unit electrode surface area (greater current density, increasing the signal to noise ratio). However, the extremely low current values can be problematic [7,12,13]. A solution to this is the use of an array of microelectrodes, yielding a substantial improvement in the signal to noise ratio under steady-state conditions [14–17]. Nevertheless, the spacing between the electrodes in the array then becomes important. As long as the individual electrodes in the MEA are spaced sufficient distances apart so as to experience individual, non-interacting diffusion profiles [8,14,18–22], then steady-state behaviour can be achieved, which is best for sensor applications. The best properties of MEAs can be assumed for (i) smaller microelectrodes, (ii) situations when the number of electrodes in the microelectrode array is increased because the signal to noise (*S*/*N*) ratio increases [19] and (iii) when the distance between electrodes is large.

The improved signal to noise ratio accruing from the enhanced mass transport rate and decreased double layer capacitance at microelectrodes and MEAs enables them to be applied to trace analysis, improving the reliability of the determinations

* Corresponding author. Tel.: +353 21 4904079; fax: +353 21 4270271.
E-mail address: damien.arrigan@tyndall.ie (D.W.M. Arrigan).

0039-9140/$ – see front matter © 2006 Elsevier B.V. All rights reserved.
doi:10.1016/j.talanta.2006.05.090

Table 1
MEA designs, characteristics and voltammetric responses

Chip	Design	l (μm)	w (μm)	d (μm)	x	xA (cm^2)	Voltammetric shape	
							5 mV s^{-1}	50 mV s^{-1}
1	1.1	50	50	500	6	1.5×10^{-4}	*s*	*s*
	1.2	40	40	400	9	1.44×10^{-4}	*s*	*s*
	1.3	30	30	300	15	1.35×10^{-4}	*s*	*s*
	1.4	20	20	200	35	1.4×10^{-4}	*s*	*s*
2	2.1	15	15	150	54	1.215×10^{-4}	*s*	*s*
	2.2	10	10	100	126	1.26×10^{-4}	*s*	*s*
	2.3	5	5	50	486	1.215×10^{-4}	*s*	*s*
	2.4	3[d]	3[d]	30[d]	1426	1.010×10^{-4}	*p*	*p*
3	3.1	500	50	500	4	1×10^{-3}	*s*	*p*
	3.2	500	40	400	5	1×10^{-3}	*p*	*p*
	3.3	500	30	300	6	9×10^{-4}	*p*	*p*
	3.4	500	20	200	9	9×10^{-4}	*p*	*p*
4	4.1	500	15	150	12	9×10^{-4}	*p*	*p*
	4.2	500	10	100	18	9×10^{-4}	*p*	*p*
	4.3	500	5	50	36	9×10^{-4}	*p*	*p*
	4.4	500	3	30	60	9×10^{-4}	*p*	*p*
5	5.1	20	20	100	9	3.6×10^{-5}	*p*	*s*
	5.2	20	20	200	9	3.6×10^{-5}	*s*	*s*
	5.3	20	20	300	9	3.6×10^{-5}	*s*	*s*
	5.4	20	20	400	9	3.6×10^{-5}	*s*	*s*
6	6.1	20[h]	20[h]	100[h]	9	3.6×10^{-5}	*s*	*s*
	6.2	20[h]	20[h]	200[h]	9	3.6×10^{-5}	*s*	*s*
	6.3	20[h]	20[h]	300[h]	9	3.6×10^{-5}	*s*	*s*
	6.4	20[h]	20[h]	400[h]	9	3.6×10^{-5}	*s*	*s*
7	7.1	500	20	100	3	3×10^{-4}	*p*	*p*
	7.2	500	20	200	3	3×10^{-4}	*p*	*p*
	7.3	500	20	400	3	3×10^{-4}	*p*	*p*
	7.4	500	20	600	3	3×10^{-4}	*p*	*p*
8	8.1	500	20	800	3	3×10^{-4}	*s*	*s*
	8.2	500	20	400	7	7×10^{-4}	*s*	*p*
	8.3	500	20	200	9	9×10^{-4}	*p*	*p*
	8.4	500	20	100	17	1.1×10^{-3}	*p*	*p*
9	9.1	20	20	100	117	4.68×10^{-4}	*p*	*s*
	9.2	20	20	200	35	1.4×10^{-4}	*s*	*s*
	9.3	20	20	300	20	8×10^{-5}	*s*	*s*
	9.4	20	20	400	12	4.8×10^{-5}	*s*	*s*
10	10.1	20[h]	20[h]	100[h]	113	4.52×10^{-4}	*p*	*s*
	10.2	20[h]	20[h]	200[h]	35	1.4×10^{-4}	*s*	*s*
	10.3	20[h]	20[h]	300[h]	18	7.2×10^{-5}	*s*	*s*
	10.4	20[h]	20[h]	400[h]	11	4.4×10^{-5}	*s*	*s*
11	11.1	20	20	450	9	3.6×10^{-5}	*s*	*s*
	11.2	20[h]	20[h]	450[h]	9	3.6×10^{-5}	*s*	*s*
	11.3	20	20	450	12	4.8×10^{-5}	*s*	*s*
	11.4	20[h]	20[h]	450[h]	11	4.4×10^{-5}	*s*	*s*
12	12.1	3[dh]	3[dh]	100[dh]	174	1.2×10^{-5}	*s*	*s*
	12.2	3[dh]	3[dh]	200[dh]	53	3.8×10^{-6}	*s*	*s*
	12.3	3[dh]	3[dh]	300[dh]	20	1.4×10^{-6}	*s*	*s*
	12.4	3[dh]	3[dh]	400[dh]	12	8.5×10^{-7}	*s*	*s*

(h) Electrode arrays with hexagonal layout; (d) micro-disc electrode arrays; (l) electrode length; (w) electrode width; (d) inter-electrode distance; (x) number of electrodes in the array; (xA) total electrode area for each array; (*s*) sigmoidal and (*p*) peak-shaped. All unmarked micro-square and disc arrays in square layout.

and facilitating speciation [7]. The determination of trace metals is of concern not only in environmental matrices, but also in biological materials, due to the toxicity of heavy metals. Metals such as copper, lead, cadmium and zinc are important pollutants that can be present in foods, drinking water and other beverages [14,23] as well as in the aquatic environment [1,14,24]. Consequently, their detection and quantification has been an essential target in recent years. Microelectrodes and MEAs have

been used for the detection of metals at parts per billion (ppb, $\mu g\,dm^{-3}$) concentrations by anodic stripping voltammetry (ASV) [8,18,24,25], but always with a mercury film coating, thus harnessing the beneficial electroanalytical performance of mercury as an electrode material. However, the toxicity of mercury has compromised its widespread continued use as an electrode material and worldwide research is directed toward the finding of new electrode materials suitable for trace analytical applications.

In this work, a range of platinum and gold MEAs were fabricated and electrochemically characterised, and their application as sensing devices investigated. The MEAs were fabricated on silicon substrates in square, disc and band geometries using standard photolithographic techniques, and characterised using redox-active probe compound solutions. An application for trace metal analysis was based on the determination of copper in a soil extract solution using under potential deposition-anodic stripping voltammetry (UPD-ASV) [26–29] at gold MEAs, offering a mercury-free alternative for trace metal sensing.

2. Experimental

2.1. Microfabrication

Arrays of platinum and gold squares, discs and bands were fabricated by standard deposition, etching and lithographic techniques used in microfabrication technology. The first step involved growth of a thermal oxide on a silicon wafer. This was followed by plasma enhanced chemical vapour deposition (PECVD) of a silicon dioxide layer. Photoresist was then spun onto the wafer and patterned, and the exposed oxide layer was then wet etched. For the fabrication of the platinum MEAs, platinum was sputtered onto the wafer after an intermediary titanium adhesion layer, and the remaining silicon dioxide was removed by a buffer oxide etch (HF and NH_4F). This was followed by deposition of a Si_3N_4 passivation layer. The recessed microelectrode array (500 nm recess depth) was then obtained using a photolithographic etch process (Pt-EKC solvent). For the fabrication of the gold MEAs, the same procedure was adopted except that the gold was deposited by evaporation of Ti:Pt:Au multilayers in the proportion 30:50:250 nm. Following fabrication, the wafers were diced and the electrodes packaged on printed circuit boards (PCB) by attaching the individual chips to the PCB with silver epoxy die attach (Ablebond 8484, Ablestik), wire bonding the bondpads on the chips to the PCB with 25 μm aluminium wires and finally protecting the wirebonds and chip edges by covering in a polymeric selective encapsulant (Amicon 50300 HT, Emerson and Cuming).

Table 1 presents the silicon-chip electrode designs, including the electrode lengths, widths, inter-electrode distance, number of electrodes in the array and the total electrode surface area of each MEA. The inter-electrode spacing is defined as the edge–edge distance between neighbouring electrodes in the array. Table 1 also describes two different array layouts defined as hexagonal (h) or square (all unmarked micro-square designs, including the micro-discs (d)).

2.2. Electrochemical measurements and reagents

A CHI620A Electrochemical analyser with Picoamp Booster & Faraday Cage (CH Instruments, TX, USA) was used for all of the electrochemical studies. All experiments were performed in a three-electrode cell, where the platinum and gold MEAs were used as working electrodes with a Ag|AgCl reference electrode and platinum wire counter electrode (both from CH instruments). Prior to electrochemical testing, the MEAs were treated with oxygen plasma for 10 min at 100 W to remove any residual organic matter. Cyclic voltammograms (CVs) were recorded at the Au and Pt microelectrode arrays in 0.1 M H_2SO_4 (de-aerated by bubbling with nitrogen for 10 min) and in 1 mM ferrocene monocarboxylic acid (FcCOOH) in phosphate buffered saline (PBS) solution (all purchased from Sigma–Aldrich). For the studies of copper determination by underpotential deposition-anodic stripping voltammetry (UPD-ASV) in linear sweep mode, 1 μM $CuSO_4$ (Fluka) in 0.1 M H_2SO_4 (Sigma–Aldrich) was used. The applicability of the Au MEAs for copper determination in soil extract samples was demonstrated by analysis of copper in an acetic acid soil extract sample (from Prof. M. Valiente, UBA, Barcelona, Spain) with no added electrolyte. Calibration was by standard addition [27–29].

3. Results and discussion

3.1. Electrochemical characterisation in sulphuric acid

Cyclic voltammetry (CV) in sulphuric acid was employed as an initial test to determine if the microelectrode arrays were

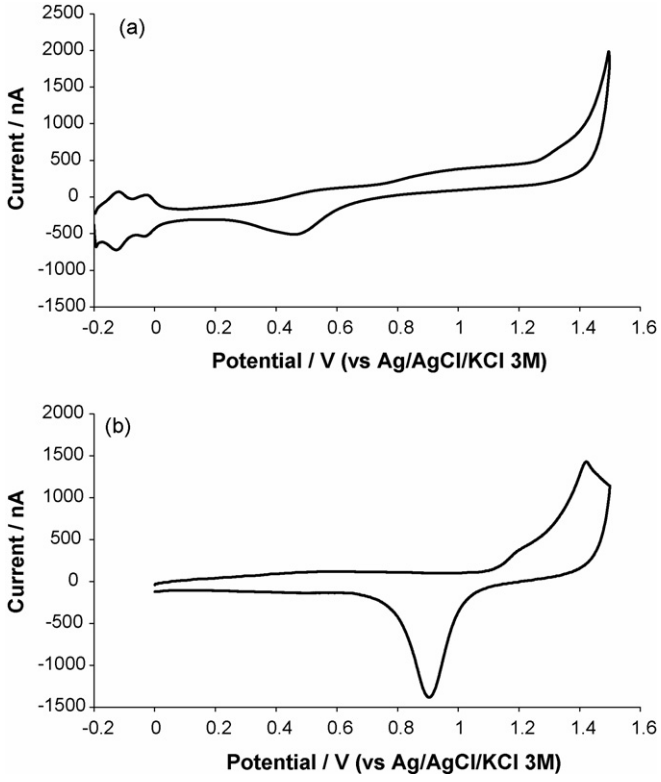


Fig. 1. Cyclic voltammograms recorded using MEAs (design 3.1) in 0.1 M H_2SO_4 from −0.2 to +1.6 V at 200 mV s^{-1} (a) Pt MEAs and (b) Au MEAs.

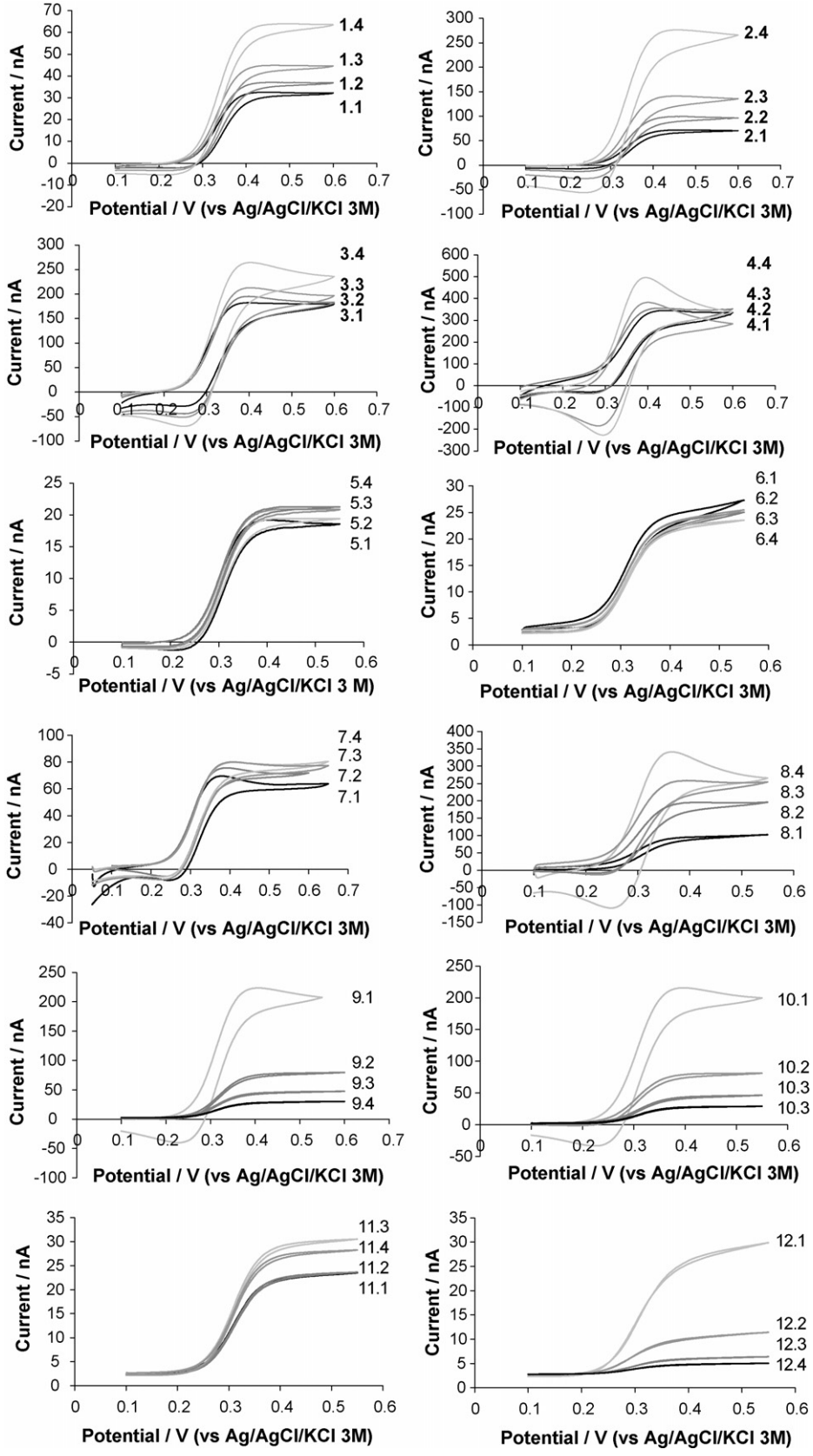


Fig. 2. Cyclic voltammograms using Pt MEAs (see Table 1 for geometrical characteristics) in 1 mM FcCOOH in PBS, from 0.1 to +0.6 V at 5 mV s^{-1}.

operational and as a measure of the cleanliness of the metal surfaces. Both electrode materials used in this development have characteristic CVs in sulphuric acid media that can be used as a simple diagnostic test of quality. The CVs can also be used as a surface activation method or additional cleaning method, since the MEAs cannot be polished as with macro-electrodes or single disc microelectrodes sealed in glass capillaries. Typical CVs recorded in 0.1 M H_2SO_4 for the Pt and Au MEAs are shown in Fig. 1(a and b), respectively. The characteristic Pt oxide formation (ca. 0.9 V) and reduction (ca. 0.5 V) and hydrogen adsorption and desorption peaks [30] are an indication of the cleanliness of Pt electrode surfaces (Fig. 1a). For the Au MEAs, the gold oxide formation and reduction was also clearly visible (Fig. 1b). The characteristic CVs of both electrode materials in sulphuric acid are in agreement with data in literature [30].

3.2. The influence of MEA electrode critical dimension

The electrochemical behaviour of the MEAs was assessed by voltammetry of ferrocenecarboxylic acid (FcCOOH). Experiments showed no significant difference between the electrochemical responses for the Pt and Au MEAs under the same experimental conditions. Hence, for simplicity, only the experimental results obtained from the Pt MEAs are discussed in Sections 3.2–3.5. Fig. 2 presents the CV analyses for the Pt MEAs with varying electrode dimensions (the various designs are summarised in Table 1).

Each of the MEAs differ in their electrode dimensions, but have a constant inter-electrode distance equal to ten times the width in the case of bands or squares (or the diameter in the case of discs). Differences in the electrochemical behaviour were found as a function of the geometrical characteristics of the microelectrode arrays. Micro-square electrode arrays showed steady-state (sigmoidal) voltammograms, which is indicative of hemispherical (3-D) diffusion (Fig. 2, designs 1.1–2.3). An increase in the electrochemical response was observed on going from designs 1.1 to 2.3, due to the decrease in the size of the elements of the arrays while maintaining a constant electrode area, by increasing the number of elements per array (Table 1). This condition was achieved by increasing the elements per array in line with the inverse square of the electrode dimension. Smaller electrode dimensions result in an enhanced mass transport or diffusion rate. The smaller 3-μm disc arrays showed peak-shaped voltammograms (design 2.4, Fig. 2), which is indicative of monodimensional diffusion resulting from insufficient spacing between electrodes in the array (discussed in Section 3.3).

A similar trend was obtained for the micro-band MEAs (designs 3.1–4.4, Fig. 2), but to a different degree as diffusion at micro-band electrodes is a mixture of hemispherical and hemicylindrical diffusion [25]. The occurrence of sigmoidal CVs decreases from the 50 μm × 500 μm bands (design 3.1) to the 3 μm × 500 μm bands (design 4.4). In this case, an inter-electrode spacing ratio of 10 times the width of the micro-band did not yield steady-state voltammograms even at the smallest micro-bands, showing an increase in peak-shaped voltammograms and signifying the importance of one-dimensional diffusion at micro-band arrays.

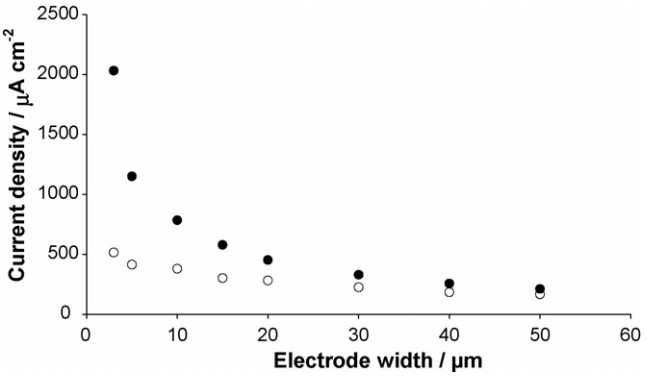


Fig. 3. Current density for the Pt micro-discs (design 2.4), micro-squares (designs 1.1–2.3) (●) and micro-bands (designs 3.1–4.4) (◯) against the electrode width. The current densities were calculated from the current values in Fig. 2.

In order to directly compare all of the above-mentioned electrodes and take into account slight differences in electrode surface area dimensions, the current density was plotted against the electrode width (Fig. 3). This shows that a greater current density is obtained with the micro-square (designs 1.1–2.3) and micro-disc (design 2.4) arrays than with the micro-band arrays (designs 3.1–4.4). Comparisons between micro-squares/discs and micro-bands also revealed a mass transport enhancement as the size of the electrodes in the array decreases (Fig. 3), as expected. The smaller the electrode, the faster the mass transport to that electrode and hence greater current density. Fig. 3 nicely illustrates the benefits of miniaturisation on electrochemical systems.

3.3. The influence of MEA inter-electrode spacing

In this section, the effect of inter-electrode spacing on MEA CV responses is discussed.

Sigmoidal voltammograms were observed for all of the micro-square designs where the ratio of interelectrode spacing to electrode width was ≥10 (designs 5.2–5.4 and 9.2–9.4, Fig. 2). Where the spacing ratio was reduced to 5, peak-shaped voltammograms were observed for design 5.1 and to a greater extent with design 9.1 due to the higher density of (and number of centrally-situated) electrodes in the latter case, causing a greater degree of diffusion-layer overlap. No significant differences were observed between the square and hexagonal micro-square electrode arrangements (designs 9–11, Fig. 2).

The same spatial dimensions were investigated using 3 μm diameter discs, however due to the reduced dimensions of the discs, the interelectrode spacing/electrode width (diameter in this case) ratio was greater, with spacing ratios in the range 33–133 (designs 12.1–12.4). In this case, sigmoidal voltammograms were recorded for all of the arrays due to the reduced electrode dimensions and increased spacing between them, hence no diffusion overlap occurred between neighbouring electrodes in the array.

The micro-band electrodes were affected to the greatest extent by the inter-electrode spacing, due to the prevalence of hemicylindrical diffusion at these electrodes, caused largely by the length of the bands. Peak-shaped voltammograms were

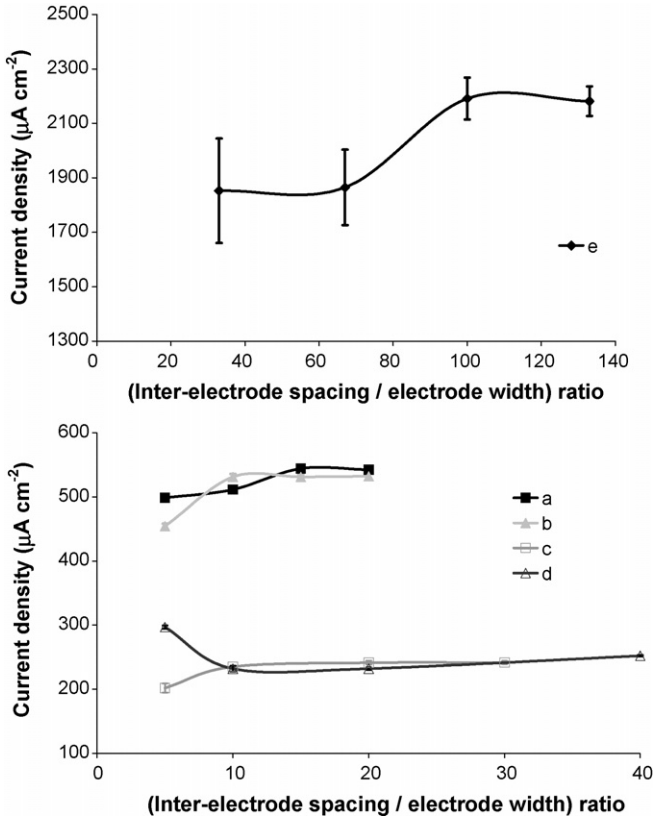


Fig. 4. Current density with increasing ratio of inter-electrode spacing/electrode width. All data based on the CV values from Fig. 2. Series a and b based on micro-square designs 5 and 9, respectively; series c and d based on micro-band designs 7 and 8, respectively; and series e based on micro-disc design 12.

observed for most of the inter-electrode distances investigated where the spacing was 5–30 times the width of the band (designs 7.1–7.4 and 8.3–8.4, respectively, Fig. 2) with the exception of design 8.1, where the spacing ratio was 40 times the band width. Sigmoidal voltammograms were also observed for design 8.2 at a spacing ratio of 20, in contrast to the peak-shaped voltammograms obtained for design 7.3 with the same spacing ratio but fewer bands. This can be attributed to the higher number of band outer edges in design 8.2, causing an increased amount of radial diffusion at those parts of the bands, in accordance with Davies and Compton [21].

Evaluation of the current density enables direct comparison of the MEAs and their inter-electrode spacings. Fig. 4 shows the current density against the spacing/electrode dimension ratio for all of the MEAs. The general trend is that the smallest electrodes, the micro-discs, give the highest current densities, followed by the micro-squares and then the micro-bands. In general, the spacing between electrodes of each MEA, in the range of 5-times the width upwards, had little influence on the current density, indicating that all values of spacings chosen here were sufficient to ensure individual diffusion profiles at each element of the MEA. However, a notable increase in the current density was observed for the smallest dimension (3-μm disc) arrays at a spacing ratio ≥100 times the disc diameter, highlighting a shift in the spatial requirements for optimal performance of micro-disc arrays with reduced critical dimensions (line E, Fig. 4). These results support the theory of Davies and Compton [21] who suggest that as the dimensions of the microelectrodes in an array decrease, their individual diffusion zones will not decrease accordingly, and hence overlap will occur unless there is sufficient spacing between the electrodes. In contrast, the highest current density observed at the closest spacing of the band arrays (line D, Fig. 4) could be attributed to the greater amount of radial diffusion arising from the higher number of band outer-edges in this design, in accordance with Davies and Compton [21].

3.4. The influence of CV potential sweep rates

The influence of the CV sweep rate on the electrochemical response was studied as a function of the geometrical microelectrode array characteristics, summarised in Table 1. Micro-square arrays with larger electrode dimensions were not greatly affected by the scan rate, as expected from MEAs with sufficiently large inter-electrode distances, in accordance with Eq. (1) (Section 3.5). Where the spacing was insufficient (5 times the electrode width, design 9.1), a change from peak-shaped to sigmoidal voltammograms was observed with increasing scan rates (Table 1). These results are consistent with findings by Compton and co-workers [22] who suggested that where the spacing is insufficient, decreasing scan rates cause an increase in the timescale of the measurement, creating larger diffusion zones and a greater extent of diffusion overlap. For the micro-disc arrays with insufficient spacing (10 times the disc diameter), more profound peak-shaped voltammograms with increasing scan rate were observed, which is typical of macro-electrode behaviour (design 2.4, Table 1). Such results suggest that the smaller micro-disc arrays are affected by the inter-electrode spacing to a greater extent. The micro-disc arrays with sufficient spacing (33–133 times the disc diameter) were unaffected by scan rate (designs 12.1–12.4, Table 1, respectively).

Most of the micro-band designs were affected by the scan rate due to the predominance of hemicylindrical diffusion, in accordance with Eq. (2). However, at low scan rates (0.005 V s^{-1}) sigmoidal voltammograms were observed from the largest micro-band arrays with the greatest spacing and fewest number of electrodes in the array (designs 3.1, 8.1 and 8.2, Table 1). Peak-shaped voltammograms became predominant with increasing scan rate, suggesting a greater extent of diffusion overlap at higher scan rates, in contrast to the micro-square geometries.

3.5. Comparison with theory

The results from the above electrochemical characterisation of the MEAs were compared directly with data generated from published models of microelectrode behaviour. Comparisons between theoretical and experimental current were made using the following equations for limiting currents at microelectrodes. Each model takes into account the different geometries of the MEAs investigated and their associated diffusion regimes. For inlaid micro-disc electrodes under steady-state conditions, the limiting current i_L is given by [4,15]:

$$i_L = \left(\frac{4nFACD}{\pi r}\right) x = 4nFDCrx \quad (1)$$

where n is the number of electrons transferred, F the Faraday constant (96485 C mol^{-1}), D the diffusion coefficient of FcCOOH (cm^2 s^{-1}), C the bulk concentration of FcCOOH (mol cm^{-3}), r the radius (cm) and x is the number of electrodes in the array. As an approximation, r can be taken as half the width in the case of micro-square arrays [31].

For inlaid micro-band electrodes under steady-state conditions [3,32] the limiting current is given by:

$$i_L = \left(\frac{2n\pi FCDl}{\ln(64Dt/w^2)}\right)x \quad (2)$$

where l is the micro-band length (cm), w the micro-band width (cm) and t is the time and is equal to RT/Fv, where R is the gas constant (8.314 J mol^{-1} K^{-1}), T the temperature (K) and v is the scan rate (V s^{-1}). The other parameters have their previous definitions.

In contrast to inlaid electrodes, recessed electrodes are located in a recess or well that affects the diffusion of the electro-active species to the electrode surface, depending on their geometrical characteristics. For recessed micro-disc electrodes, the current is defined as [18,33,34]:

$$i_L = \left(\frac{4\pi nFCDr^2}{4L+\pi r}\right)x \quad (3)$$

where, L is the depth of the recess (cm) and the other parameters have their previous definitions.

Fig. 5 shows the variation of the experimentally measured current with the calculated current for the micro-discs, squares and bands of this study. For designs 1–2, the recessed disc model (Eq. (3)), which takes into account the effect of the recess on the current, yielded a better fit to the line of perfect agreement than the inlaid disc model (Eq. (1)) for these MEAs, showing that the smaller electrodes are affected to a greater extent by the depth of the recess. This model was also used for the 3-μm disc arrays (design 12), which gave better agreement with experimental data than use of the inlaid disc model (Eq. (1)). However, the inlaid disc model produced a good correlation for design 9 (20 μm × 20 μm squares), because the recess:electrode width ratio is small. Moreover, no significant differences were found between the inlaid and recessed disc mathematical models for these micro-squares, suggesting a negligible influence from the depth of the recess on the larger microelectrodes.

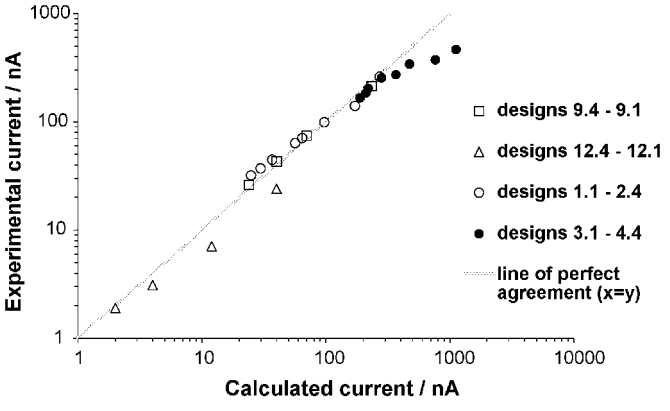


Fig. 5. Comparison of calculated and experimental current for the micro-squares, bands and discs. Theoretical current based on Eqs. (1)–(3) (respectively), and all experimental data based on the CV values from Fig. 2. Data from designs 9 and 12 based on the current obtained from increasing numbers (and spacing) of micro-squares and discs (respectively) in the array. Data from designs 1–4 based on the current obtained from decreasing micro-square and band electrode width, respectively (with increasing numbers of electrodes in the array).

The current values from micro-band designs 3 and 4 were compared to theoretical values based on Eq. (2) (inlaid band electrodes). The theory for inlaid band arrays agrees reasonably well with the experimental data obtained for designs 3 and 4, however, it considerably deviates away from the experimental data as the electrode width decreases (Fig. 5). In this case, the inlaid band model does not take into account the depth of the recess, which will have more of an effect on the bands with smaller widths; i.e., as the ratio L/w increases (where L is the recess depth and w is the band width) with smaller band widths, the depth of the recess approaches the electrodes' critical dimension, thus affecting the electrochemical response to a greater degree. Additionally, the current obtained at the design 7 micro-band arrays was influenced by the scan rate, according to Eq. (2).

Tomes criterion values for the sigmoidal voltammograms obtained from six selected MEA designs compared well with the theoretical values for both gold and platinum, with an average potential separation of 56.4 mV (±2.4 mV) between the quarter and three-quarter sections of the steady-state wave.

The investigations described in Sections 3.2–3.5 show that the smallest electrode dimension (3-μm diameter disc) arrays with sufficient inter-electrode spacing (≥33 times the disc diameter) yielded the highest current densities, and retained the desirable attributes of MEAs arising from the predominance of radial diffusion. The mean coefficient of variation of CV responses for designs 1–11 was 1.1% (±0.7) and the mean for design 12 was 3.7% (±1.8), based on triplicate measurements of each design.

3.6. UPD-SV of copper at gold microelectrode arrays

Microelectrode arrays find large application in environmental analysis such as heavy metal determination [35–40]. The use of a bare noble metal as the material for microelectrode arrays allows the use of under potential deposition-anodic stripping voltammetry (UPD-ASV) [41] as an analytical detection technique [26]. UPD results in deposition of up to a monolayer of metal onto a surface. In order to verify the influence of different microelectrode array designs on the deposition process, a series of UPD-ASV experiments was performed. The electrochemical model adopted was the UPD of Cu^{2+} from aqueous sulphuric acid solution [42]. The electrochemical deposition of the Cu onto the microelectrode arrays was performed by applying 0.0 V (versus Ag/AgCl) for a defined time at the working electrode. Fig. 6a shows the typical response recorded during a series of UPD-ASV experiments. It can be seen that an increase of the deposition time yielded an increase in the electrochemical signal, as expected. An increase of the deposition time should result in an increase of Cu deposited onto the electrode surface. The quantity of Cu deposited onto the electrode can be evaluated from the charge of the stripping voltammetric peaks, which

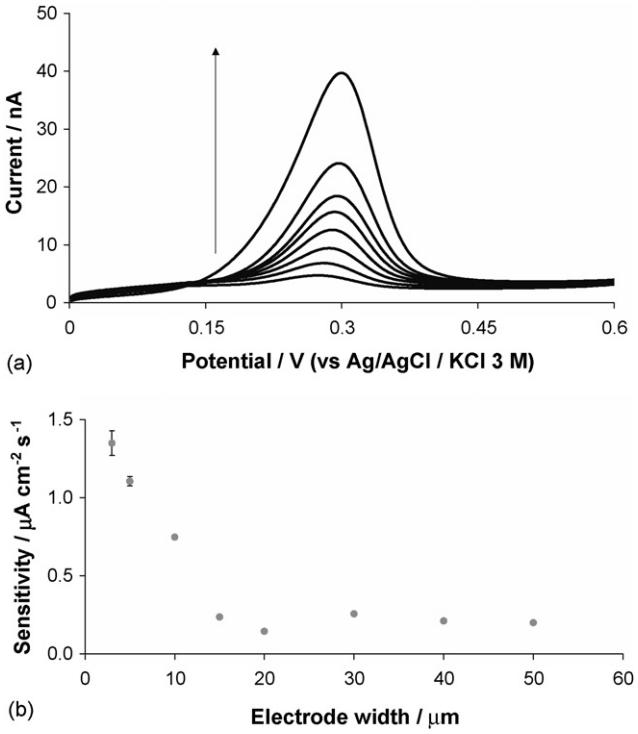


Fig. 6. (a) UPD-SV (scan rate 100 mV s^{-1}) of 1 μM Cu in 0.1 M sulphuric acid using Au micro-band arrays (design 7.2). Deposition times: 0, 5,15, 30, 45, 60, 90 and 180 s. (b) Evaluation of micro-band array sensitivity to deposition time (designs 3 and 4).

yields the surface coverage (Γ) [41]:

$$\Gamma = \frac{Q}{(nFA)} \quad (4)$$

where Q is the charge (C), n the number of electrons exchanged, F the Faraday constant) and A is the surface of the electrode (cm^2).

The surface coverage values recorded for the different microelectrode array designs ranged between 2×10^{-11} mol cm^{-2} and 1×10^{-9} mol cm^{-2}. These values were lower than those reported in literature for the deposition of a complete monolayer of metal onto a metal surface (2×10^{-9} mol cm^{-2}) [41]. All of the surface coverage values generated in the present evaluation were calculated by using the theoretical electrode area. A close analysis of the surface coverage values obtained highlighted that the surface coverage increased with a reduction of the electrode width. Moreover, the surface coverage increased from the band electrode design to the square electrode design (with the same width) and also increased with the increase of the inter-electrode separation. All of these observations are consistent with the enhanced mass transport rate that comes with use of smaller electrodes and use of micro-squares rather than micro-bands.

In order to evaluate and compare the influence of the different microelectrode layouts, the sensitivity of each array design was calculated. Here, the sensitivity is defined as the speed with which the current density increases with deposition time. This sensitivity is given by the slope of stripping current versus

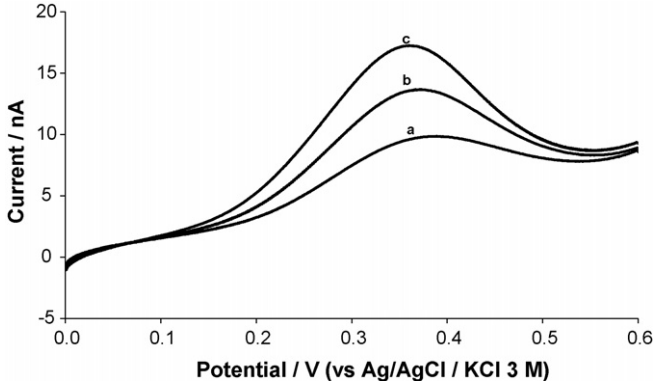


Fig. 7. UPD-SV (scan rate 100 mV s^{-1} deposition time 15 s) of a real sample (0.11 M acetic acid soil extract) using Au micro-band arrays (design 4.1). Curve (a) sample only; curve (b) after addition of 1 μg of Cu; and curve (c) after addition of 2 μg (in total) of Cu.

deposition time plots, and, in this case, for deposition times of between 0 and 60 s (with $n = 6$). This time interval was chosen in order to avoid saturation of the MEA surface that occurs at longer deposition times. Fig. 6b shows the typical sensitivity trends recorded for different micro-band arrays with a constant inter-electrode separation of 10 times the electrode width. A decrease in the critical dimension (electrode width) resulted in an increase of the sensitivity. Moreover, the sensitivity recorded for the micro-square/disc electrode arrays (with the same width) is higher than those recorded for the micro-band arrays (results not shown). These results are in agreement with those obtained from the CV experiments (Fig. 2) and with those presented by others [25]. These results suggest that a different diffusion regime occurred with the different microelectrode array designs. In the case of the micro-band electrodes the diffusion largely follows a mono-dimensional profile (except at the edges where a multi-dimensional diffusion process can occur), while at the micro-square electrodes the diffusion mainly follows a multi-dimensional profile. This multi-dimensional diffusion results in a higher efficiency of the mass transport and, as a consequence, in a better sensitivity of the electroanalytical process.

The use of MEAs for mercury-free analysis was assessed by determining copper concentration in a soil extract sample, which is the first fraction of the BCR (the European Commission's Bureau Communautaire de Reference) extraction sequence [43]. The protocol adopted in this analysis was the same as that previously optimised for the detection of copper using gold macro-electrodes in the same medium [27–29]. Fig. 7 illustrates the results of the standard addition analysis performed on a real soil sample. The concentration of copper in the real sample was determined to be 1.25 ± 0.06 ppm. These results are consistent with those obtained by the reference analytical technique of atomic spectroscopy (1.24 ± 0.04 ppm).

4. Conclusions

A range of gold and platinum microelectrode arrays fabricated by photolithographic techniques were characterised by cyclic voltammetry. The inter-electrode spacing, geome-

try, numbers and dimensions of the electrodes in the array were found to influence the current density and voltammograms obtained, which has allowed the determination of the most suitable configurations for optimal MEA performance. The smallest electrode dimension (3-μm diameter disc) arrays with sufficient inter-electrode spacing (≥33 times the disc diameter) yielded the highest current densities, and retained the desirable attributes of MEAs arising from the predominance of radial diffusion. The electrode responses were reproducible and provided very good agreement with theoretical data calculated from existing microelectrode models. The MEAs were tested for their applicability for copper detection in a real soil extract sample, where agreement was found between the standard analytical method and the UPD-ASV method using MEAs. This technique offers a mercury-free alternative for metal ion sensing in the environment.

Acknowledgements

Aspects of this work were supported in part by Enterprise Ireland (ATRP-336), the European Commission (EVK1-CT-1999-20001) and the Royal Society of Chemistry (Analytical PhDs).

References

[1] J. Wang, Acc. Chem. Res. 35 (2002) 811.
[2] G. Schmitt, J.-W. Schultze, F. Faßbender, G. Buß, H. Lüth, M.J. Schöning, Electrochim. Acta 44 (1999) 3865.
[3] C. Amatore, Electrochemistry at Ultramicroelectrodes, in: I. Rubinstein (Ed.), Physical Electrochemistry: Principles, Methods and Applications, Marcel Dekker, New York, 1995, p. 131.
[4] C.G. Zoski, Electroanalysis 14 (2002) 1041.
[5] M. Koudelka-Hep, P.D. van der Wal, Electrochim. Acta 45 (2000) 2437.
[6] G. Wittstock, Anal. Bioanal. Chem. 372 (2002) 16.
[7] K. Štulík, C. Amatore, K. Holub, V. Mareček, W. Kutner, Pure Appl. Chem. 72 (2000) 1483.
[8] M. Wittkampf, K. Cammann, M. Amrein, R. Reichelt, Sens. Actuators B 40 (1997) 79.
[9] P.M. Kovach, W.L. Caudill, D.G. Peters, R.M. Wightman, J. Electroanal. Chem. 185 (1985) 285.
[10] A.M. Bond, Analyst 119 (1994) 1.
[11] J.A. Alden, J. Booth, R.G. Compton, R.A.W. Dryfe, G.H.W. Sanders, J. Electroanal. Chem. 389 (1995) 45.
[12] P.M.S. Monk, Fundamentals of Electroanalytical Chemistry, Wiley, Chichester, 2001.
[13] S. Fletcher, M.D. Horne, Electrochem. Commun. 1 (1999) 502.
[14] R. Feeney, S.P. Kounaves, Electroanalysis 12 (2000) 677.
[15] A.J. Bard, L.R. Faulkner, Electrochemical Methods: Fundamentals and Applications, second ed., John Wiley & Sons, New York, 2001, p. 168.
[16] K. Aoki, Electroanalysis 5 (1993) 627.
[17] R. Feeney, S.P. Kounaves, Talanta 58 (2002) 23.
[18] C. Belmont, M.-L. Tercier, J. Buffle, G.C. Fiaccabrino, M. Koudelka-Hep, Anal. Chim. Acta 329 (1996) 203.
[19] R.S. Freire, J.J.R. Rohwedder, C. Pasquini, Analyst 124 (1999) 1657.
[20] M. Sandison, N. Anicet, A. Glidle, J.M. Cooper, Anal. Chem. 74 (2002) 5717.
[21] T.J. Davies, R.G. Compton, J. Electroanal. Chem. 585 (2005) 63.
[22] T.J. Davies, S. Ward-Jones, C.E. Banks, J. del Campo, R. Mas, F.X. Muñoz, R.G. Compton, J. Electroanal. Chem. 585 (2005) 51.
[23] A.L. Kukla, N.I. Kanjuk, N.F. Starodub, Yu.M. Shirshov, Sens. Actuators B 57 (1999) 213.
[24] D. Desmond, B. Lane, J. Alderman, M. Hill, D.W.M. Arrigan, J.D. Glennon, Sens. Actuators B 48 (1998) 409.
[25] B. Le Drogoff, M.A. El Khakani, P.R.M. Silva, M. Chaker, A.K. Vijh, Electroanalysis 13 (2001) 1491.
[26] G. Herzog, D.W.M. Arrigan, Trends Anal. Chem. 24 (2005) 208.
[27] V. Beni, H. Newton, D.W.M. Arrigan, M. Hill, W.A. Lane, A. Mathewson, Anal. Chim. Acta 502 (2004) 195.
[28] G. Herzog, V. Beni, P.H. Dillon, T. Barry, D.W.M. Arrigan, Anal. Chim. Acta 511 (2004) 137.
[29] V. Beni, V.I. Ogourtsov, N. Bakunin, D.W.M. Arrigan, M. Hill, Anal. Chim. Acta 552 (2005) 190.
[30] R.T. Kissinger, W.R. Heineman, Laboratory Techniques in Electroanalytical Chemistry, second ed., Marcel Dekker, New York, 1996, p. 353.
[31] S.L. Caston, R. McCarley, J. Electroanal. Chem. 529 (2002) 124.
[32] J. Heinze, Angew. Chem. Int. Ed. Engl. 32 (1993) 1268.
[33] C.S. Henry, I. Fritsch, Anal. Chem. 71 (1999) 550.
[34] A.M. Bond, D. Luscombe, K.B. Oldham, C.G. Zoski, J. Electroanal. Chem. 249 (1988) 1.
[35] R.J. Reay, A.F. Flannery, C.W. Stormen, S.P. Kounaves, G.T.A. Kovacs, Sens. Actuators B 34 (1996) 450.
[36] A. Uhlig, U. Schnakenberg, R. Hitsche, Electroanalysis 9 (1997) 125.
[37] J. Herdan, R. Feeney, S.P. Kounaves, A.F. Flannery, C.W. Storment, G.T.A. Kovacs, R.B. Darling, Environ. Sci. Tech. 32 (1998) 131.
[38] S.B. Saban, R.B. Darling, Sens. Actuators B 61 (1999) 128.
[39] X.D. Xie, D. Stuben, Z. Berner, J. Albers, R. Hitsche, E. Jantzen, Sens. Actuators B 97 (2004) 168.
[40] X.S. Zhu, C. Gao, J.W. Choi, P.L. Bishop, C.H. Ahn, Lab Chip 5 (2005) 212.
[41] D.M. Kolb, in: H. Gerischer, C.W. Thomas (Eds.), Advances in Electrochemistry and Electrochemical Engineering, vol. 11, John Wiley & Sons, New York, 1978, p. 125.
[42] H. Hagenström, M.A. Schneeweiss, D.M. Kolb, Electrochim. Acta 45 (1999) 1141.
[43] Ph. Quevauviller, A. Ure, H. Muntau, B. Gripink, Internat. J. Environ. Anal. Chem. 51 (1993) 129.

Available online at www.sciencedirect.com
ScienceDirect
Talanta 71 (2007) 1226–1232
Talanta
www.elsevier.com/locate/talanta

Selective preconcentration and determination of iodine species in milk samples using polymer inclusion sorbent

P.R. Bhagat [a], A.K. Pandey [b], R. Acharya [b], A.G.C. Nair [b], N.S. Rajurkar [a], A.V.R. Reddy [b,*]

[a] *Department of Chemistry, University of Pune, Pune 411007, India*
[b] *Radiochemistry Division, Bhabha Atomic Research Centre, Trombay, Mumbai 400085, India*

Received 16 May 2006; accepted 12 June 2006
Available online 18 July 2006

Abstract

A method to determine low levels of iodine species namely I^- and IO_3^- in aqueous samples was developed and applied to milk and milk powder samples. It is based on selective preconcentration of I^- in polymer inclusion sorbent (PIS) and neutron activation analysis (NAA) of I^- sorbed in PIS. The PIS was found to be highly selective for I^- in presence of IO_3^- and other anions commonly present in the milk samples. In order to preconcentrate total $I^- + IO_3^-$ content in the PIS, IO_3^- was reduced to I^- using a mixture of acetic acid and ascorbic acid. It was found that total iodine content in milk could be determined with epithermal neutron activation analysis (ENAA). A scheme was developed to determine I^-, IO_3^- and total iodine. The developed method was applied to milk reference materials (NIST SRM-1549 and IAEA-RM-153 milk powder) and a commercially available milk powder. The scheme for estimation of iodine in different forms was validated by using reference material NIST SRM-1549.
© 2006 Elsevier B.V. All rights reserved.

Keywords: Iodine species; Milk; Polymer inclusion sorbent; Selective preconcentration; Neutron activation analysis

1. Introduction

Iodine is an important trace element required for normal thyroid functioning in human beings. Deficiency or excess intake of iodine leads to disorders commonly referred to as iodine disorders. Therefore, accurate data of total iodine concentrations in diet and water are of considerable scientific interest. Iodate, iodide, iodine and organic iodine are the main species of iodine that may be present in the food or water samples. It is important to know the chemical forms of iodine to know its nutritional efficiency and bioavailability.

Determination of specific iodine species as well as total iodine has been carried out using analytical techniques like spectrophotometry [1–6], gas chromatography-mass spectrometry (GCMS) [7], ion chromatography [8,9], high performance liquid chromatography (HPLC) [10], inductively coupled plasma mass spectrometry (ICP-MS) [11] and isotope dilution resonance ionization mass spectrometry [12]. An adsorption chromatography method has been developed [13] based on difference in sorption properties of iodide and iodate species. Neutron activation analysis (NAA) hyphenated with chemical separation methods is also used for iodine determination [14,15]. The membrane-based methods have also been reported for the determination of iodine species. These membranes were converted to chemical sensors by incorporating a suitable response mechanism in the membrane [16–19]. However, this methodology is applicable to a specific iodine species (I^-, I_3^- or IO_3^-) in the sample. In our earlier work, polymer inclusion sorbent (PIS) has been found to be effective for the selective preconcentration of Cr(VI) from aqueous samples [17,18]. One of the important features of this methodology is the possibility of direct quantitative analysis of species preconcentrated in the PIS. Thus, this class of solid sorbents provides a high enrichment factor with minimum sample manipulation. The iodine species selective sorbent is needed not only to provide chemical selectivity to NAA but also reliable one step sample preparation method as target iodine species bound in polymer sorbent can be directly subjected to NAA.

* Corresponding author. Tel.: +91 22 2559 3862; fax: +91 22 2550 5151.
E-mail address: avreddy@barc.gov.in (A.V.R. Reddy).

0039-9140/$ – see front matter © 2006 Elsevier B.V. All rights reserved.
doi:10.1016/j.talanta.2006.06.018

NAA is an isotope specific nuclear analytical technique for simultaneous multielement analysis. NAA is highly sensitive for determination of many elements including iodine. [20,21]. However, NAA using whole reactor neutrons for the determination of low levels of iodine suffers from spectral interferences from the activation products of major elements like Na, Cl, Br, Mn and K, present in the food samples. This problem can be overcome by epithermal neutron activation analysis (ENAA) [22] in reactor neutron flux by means of covering the sample with a filter consisting of cadmium or boron or some other material which has a high thermal neutron absorption cross section allowing selective activation of iodine with epithermal neutrons. This method has been used for non-destructive determination of iodine in food and food products [14,15].

In the present work, the hydrophobic polymer inclusion sorbent (PIS) was prepared by physical immobilization of Aliquat-336 in the cellulose triacetate (CTA) matrix plasticized with dioctyl phthalate (DOP). The uptake of I^- in this PIS was examined in aqueous samples in the presence of IO_3^- and other anions in varying concentrations. In order to provide better discrimination between I^- and IO_3^- anions, the uptake studies were carried out using two different counterions (Cl^- and NO_3^-) in the membrane. Both $I^- + IO_3^-$ in the aqueous sample were preconcentrated in the PIS as I^- after reducing IO_3^- to I^-. A possible scheme for the determination of I^-, IO_3^- and total iodine species in milk and milk powder samples was developed using PIS-NAA methods. A controlled experiment was carried out using ^{131}I marker to estimate possible loss of I^- in manipulations of milk powder samples. Milk and milk powder samples were studied, as they are the major food items for infants and other aged group. Total iodine concentration in the sample, was estimated by instrumental epithermal neutron activation analysis (ENAA). This method was validated using standard reference material (NIST SRM-1549). Finally, this was applied for the determination of I^-, $I^- + IO_3^-$ and total iodine in the reference material (IAEA RM-153, milk powder) and other commercially available milk powder samples. The results of these studies are described in this paper.

2. Experimental

2.1. Reagents and apparatus

Analytical reagent (AR) grade chemicals and ultrapure water (18 MΩ cm^{-1}) were used throughout the present studies. Cellulose triacetate (CTA) (Molecular weight 72000–74000, acetyl value = 43.2%) (Alfa Biochem), dioctyl phthalate (DOP) (BDH), glacial acetic acid (Thomas Baker) and ascorbic acid (Thomas Baker) were used as obtained. Trioctylmethylammonium chloride (Aliquat-336, mixture of C_8–C_{10}; C_8 is dominating) and triisooctylamine (Fluka) were used as obtained. Aliquat-336 was found to contain 85 mol% exchange sites as estimated by chlorine analysis using NAA. Carrier free ^{131}I tracer was obtained from BRIT, India. The aqueous solution of carrier free $^{131}I^-$ ion was purified from I_2 by equilibrating the $^{131}I^-$ aqueous solution with chloroform. The stock solution was prepared by spiking 0.1 M KI solution with $^{131}I^-$. Sample irradiations for neutron activation analysis were carried out at the APSARA reactor in BARC, Mumbai, India that has a neutron flux of 5×10^{11} cm^{-2} s^{-1}. The γ-activity of ^{128}I (443 keV) and ^{131}I (364 keV) were monitored by using HPGe detector connected to a multi-channel analyzer. All the samples and standard containing radioactivity were counted in identical sample to detector geometry. The pH of equilibrating solution was monitored by the pH meter (420 A, Thermo Orion, USA), which was calibrated using pH 4, 7 and 10 standard buffer solutions (Hamilton).

2.2. Preparation of PIS

CTA (0.4 g) was dissolved in 10 ml of dichloromethane. A separate dichloromethane solution containing Aliquat-336 or triisooctylamine (0.1 g) and DOP (0.6 g) was prepared. These solutions were mixed and ultrasonicated for 2 min to form the casting solution. The casting solution was spread on a 9 cm diameter flat bottom petri dish. After evaporation of solvent, (overnight) the transparent PIS was peeled off from the petri dish. The details of PIS preparation are described in ref [17]. The PIS samples were converted to appropriate Cl^- and NO_3^- forms by equilibrating it with 0.25 M potassium salt solutions. The size of PIS samples was kept 1 cm × 2 cm throughout the experiments.

2.3. Characterization of PIS for I^- uptake

The ion-exchange capacity of the PIS was measured by equilibrating membrane sample for 24 h with 0.1 M KI containing known activity of ^{131}I. After equilibration, the membrane samples were thoroughly washed with deionized water to remove equilibrating solution clinging to the surface of the samples. The amount of I^- ion in the PIS sample was obtained by comparing the γ-activity of ^{131}I in the membrane samples with standards prepared on filter paper, having identical shape and size of the membrane samples, from the stock solution containing same active ($^{131}I^-$) to stable iodide ($^{127}I^-$) ratio.

The effect of pH on iodide up-take in PIS was studied by equilibrating PISs with 4 ml aqueous solutions of pH 2–7. The equilibrating aqueous solutions contained a constant amount of iodide ions (5×10^{-3} mM) spiked with ^{131}I radiotracer. The pH adjustments were carried out using HCl. The uptake of I^- ions at different pH was estimated by radioactivity balance.

The uptakes of I^-, IO_3^- and ($I^- + IO_3^-$) in the PIS samples in different ionic forms were studied by equilibrating the samples (1 cm × 2 cm) with 4 ml of aqueous solutions having known amounts of I^- and/or IO_3^- for a period of 24 h. After loading iodine species, the samples were washed with distilled water and sealed in alkathene for neutron irradiation. The standard samples were prepared by drying known volume of standard KI and KIO_3 solutions on filter paper as described above. The PIS and standard samples were irradiated in reactor for 30 min. The concentrations of iodine species in the PIS samples were obtained by counting the γ-activities by HPGe detector for appropriate time and comparing γ-activities with those obtained in the standards.

The interference of anions like Cl^-, CO_3^{2-}, HCO_3^-, CH_3COO^- and SO_4^{2-} on the uptake of I^- in the PIS was studied by equilibrating the membrane samples with solutions having known amounts of anions and I^- spiked with ^{131}I tracer. The uptake of I^- was measured from the difference in radioactivity of ^{131}I before and after the sorption of I^- in PIS samples from the solutions.

2.4. Conversion of iodate to iodide

The conversion of IO_3^- to I^- was carried out by using a mixture of ascorbic acid and acetic acid as described elsewhere [8]. A known volume of IO_3^- solution (238 μg of IO_3^- in 1 ml) was mixed with 1 ml of 3% acetic acid and 1 ml of 0.5 M of ascorbic acid. The resulting solution was stirred for 30 min and then PIS sample was immersed in it for overnight. The uptake of I^- in the PIS was monitored by NAA of equilibrated samples using similar procedure as described above for uptake of I^-.

2.5. Applications to milk samples

In order to apply PIS for preconcentration of I^- from actual samples, a controlled experiment was carried out to monitor the loss of iodine species during different stages of sample manipulations using ^{131}I radiotracer. Accurately weighed amount of a milk powder (0.5 g) was dissolved in 5 ml of water and known radioactivity of ^{131}I radiotracer was added to it. The solution was homogenized by ultrasonicating it for 2 min. The acetic acid (1 ml of 3% solution) was added to separate protein part from milk powder solution and the resulting solution was kept for 15 min for allowing protein to coagulate [23]. This mixture was filtered through a Whatmann 41 filter paper. The solid part obtained was discarded and the aqueous part was used for equilibrating with the PIS sample. The γ-activity of ^{131}I radiotracer in the discarded solid part, remaining aqueous solution before and after equilibration with PIS and PIS sample was measured to monitor the possible loss of iodine species during sample manipulation.

Similar procedure was used for determining the I^- content in the milk (5 ml) and milk powder (0.5 g in 5 ml) samples except that NAA was used instead of ^{131}I radiotracer for measuring I^- in the PIS. The IO_3^- content in food samples was determined by converting IO_3^- to I^- and estimating total I^- by NAA of PIS sample equilibrated with resulting milk powder solution. The procedure used in these studies is shown in Scheme 1. This method was applied for measuring I^- and IO_3^- contents in standard reference material obtained from the National Institute of Standards and Technology (NIST SRM-1549 milk powder), reference material from the International Atomic Energy Agency (IAEA-153 milk powder) and commercially available milk powder samples.

2.6. Total iodine content in milk sample by epithermal neutron activation analysis

The procedure used for epithermal neutron activation analysis (ENAA) was similar to that described above for NAA of PIS samples, except that solid samples were wrapped with a boron carbide (B_4C) sheet having a thickness of 2 mm. About 100 mg milk powder samples and 1 ml of milk sample dried on 1 cm × 2 cm Whatmann-42 filter paper were neutron irradiated in the reactor along with the standards for 1 h. The amounts of iodine in the food samples were obtained from the measured γ-activity in the samples and comparing it with the standards.

3. Results and discussion

The design of PIS was based on the physical inclusion of the hydrophobic liquid anion-exchanger (Aliquat-336 or tri iso octylamine) in DOP plasticized CTA matrix. The triisooctylamine can act as anion-exchanger only in quaternized form which exists in the acidic medium. Therefore, the effect of pH of the solution was studied on the uptake of I^- in the PIS samples containing these two different anion-exchangers and the results are as shown in Fig. 1. As can be seen from this figure, the uptake of I^- in the triisooctylamine based PIS was sensitive to the pH of the equilibrating solution. The uptake of I^- was optimum (90%) from the solutions having pH range of 2–2.5 and gradually starts decreasing above the pH value of 2.5. In the case of Aliquat-336 based PIS, the uptake of I^- increases from pH 2 and reaches a fairly constant value of about 95 ± 2% in the pH range of 4–8. Most of the food samples studied in the present work are expected to have pH in the range of 4–8. Therefore, the PIS based on Aliquat-336 would be more suitable for these samples. Additionally, extraction efficiency for I^- in this pH range is better (95 ± 2%). The ion-exchange capacity in the Aliquat-336 based PIS was found to be $(1.29 \pm 0.06) \times 10^{-4}$ Mol g^{-1}. This indicates that up to 492 μg of I^- can be preconcentrated into the PIS of dimension 1 cm × 2 cm. In order to study the uptake of I^- as a function of its concentration, the PIS samples were equilibrated with aqueous samples having varying amounts of I^-. The neutron activation analysis (NAA) of PIS samples indicated that γ-activity due to neutron activated iodine isotope ^{128}I

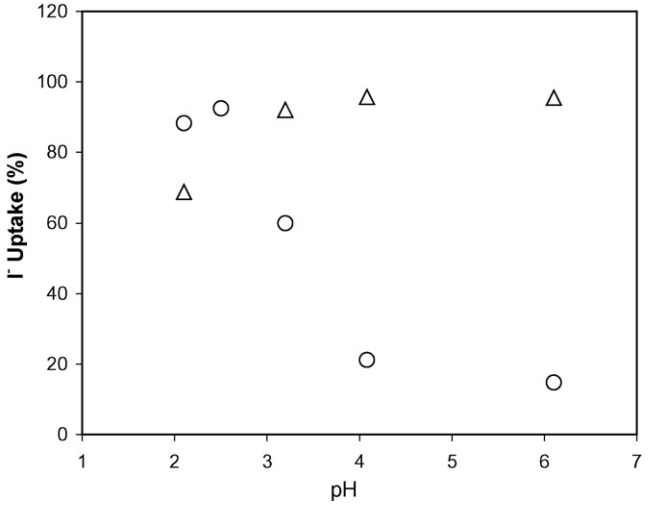
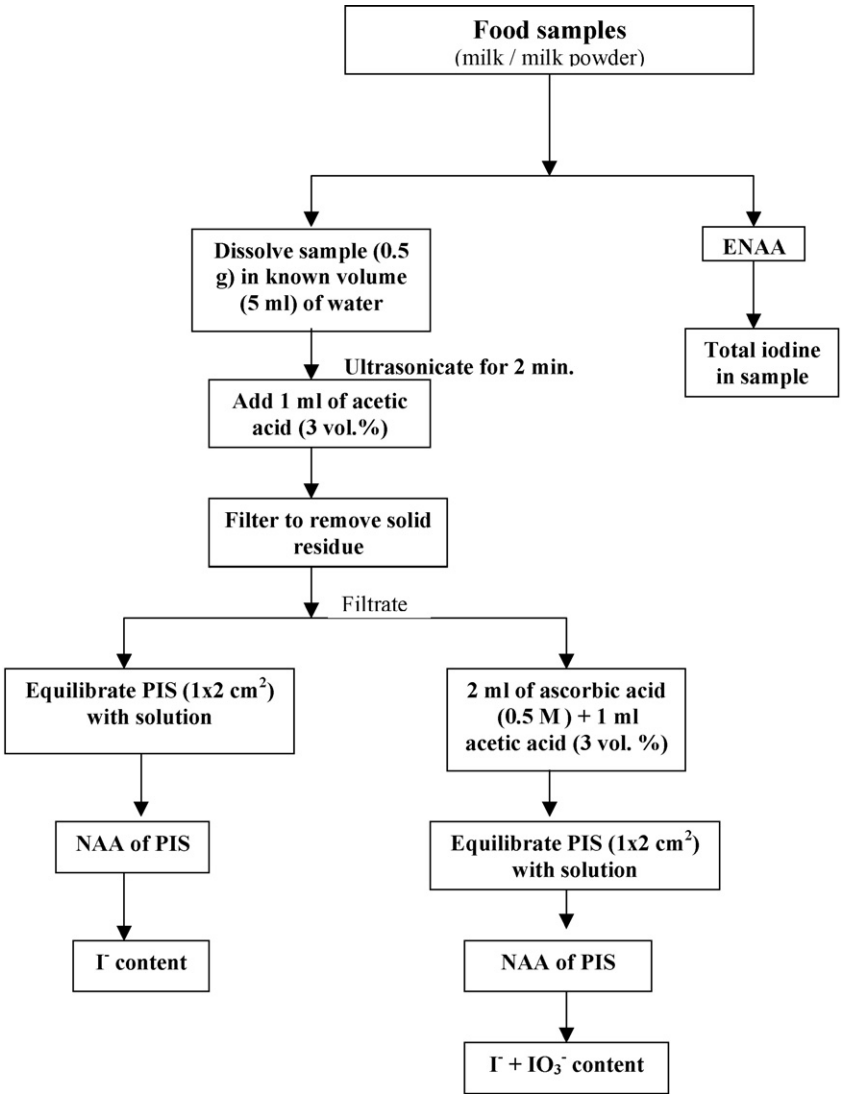


Fig. 1. Variation of uptake of I^- in PIS as a function of pH in equilibrating aqueous sample. Symbols Δ and O represent Aliquat-336 and triisooctylamine based PIS's, respectively.



Scheme 1. PIS-NAA scheme for iodine species.

in PIS samples varies linearly as a function of concentration of I^- in equilibrating solution, as shown in Fig. 2. This indicated that extraction of I^- in PIS samples is linear till all the available ion-exchange sites are used in the PIS sample.

In most of the aqueous samples, the major iodine species are expected to be I^- and IO_3^- and depending on the samples other minor species may be I_2, I_3^- and organic bound iodine [24]. In order to study the selectivity of Aliquat-336 based PIS towards IO_3^-, the PIS samples were equilibrated with aqueous solution containing varying amounts of IO_3^- and the amounts of IO_3^- sorbed in the PIS were measured by NAA. This experiment was carried out by using Aliquat-336 based PIS in two different ionic forms namely Cl^- and NO_3^-. The amount of IO_3^- sorbed in PIS samples as a function of its amount in equilibrating solution is shown in Fig. 3. The uptake of IO_3^- in the PIS samples was found to be of the order of 5.2 and 2.5% in Cl^- and NO_3^- ionic forms of PIS, respectively. The extraction efficiency of IO_3^- did not change on increasing the amount of IO_3^- in the equilibrating aqueous sample. However, the extraction of I^- in both the forms Cl^- and $N0_3^-$ of PIS was $95 \pm 2\%$. In order to study the uptake

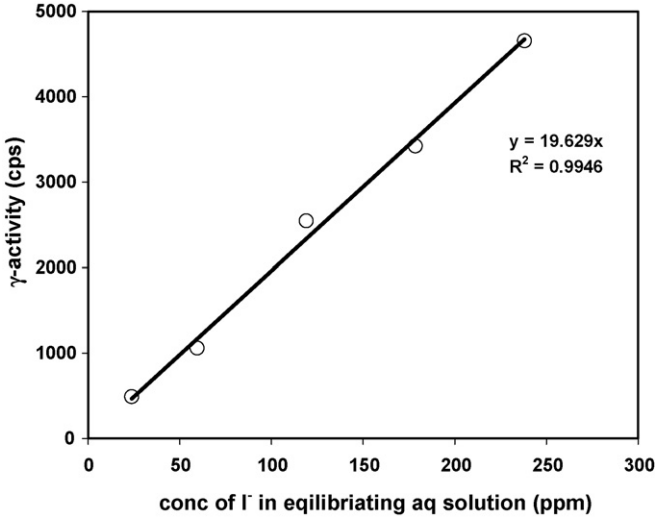


Fig. 2. γ-Activity of $^{128}I^-$ in PIS samples equilibrated with varying amounts of I^- in aqueous samples and neutron activated for 30 min in APSARA reactor.

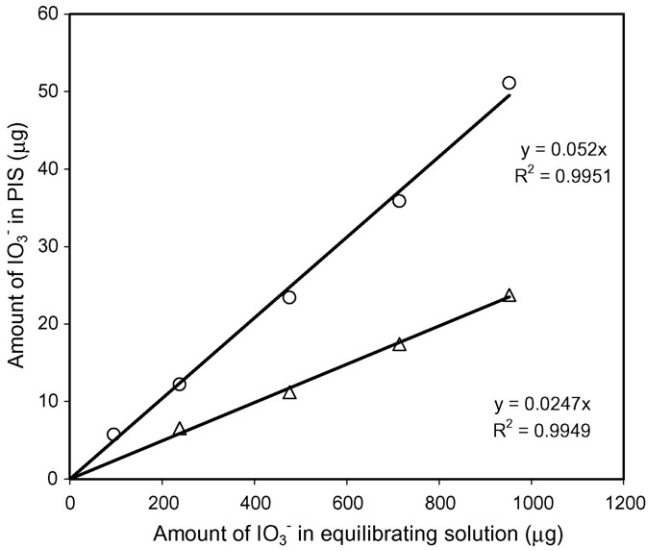


Fig. 3. Variation of uptake of IO_3^- in PIM as a function of IO_3^- in the equilibrating solution. Symbols o and Δ represent chloride and nitrate forms of the PIS, respectively.

of Iodine species in PIS from an aqueous solution of a mixture of I^- and IO_3^-, PIS samples were equilibrated with a solution containing 31.8 µg of I^- and 63.5 µg of IO_3^-. The total iodine content in PIS was found to be 34.9 ± 0.3 µg. This amount was higher than the amount of I^- in the equilibrating solution and approximately corresponds to 5% of IO_3^- in the equilibrating solution. When PIS was equilibrated with a solution having only iodate, the extraction efficiency of iodate was found to be 5%. This suggests that the extraction of the I^- was unaffected by the presence of IO_3^- species.

The lower uptake of IO_3^- in the membrane can be attributed to the fact that its Molar Gibbs free energy of hydration (ΔG_h) is −400 kJ/M while ΔG_h for I^- is −275 kJ/M [25]. Therefore, energetically it is easy for I^- to enter highly hydrophobic matrix as compared to hydrated IO_3^- ions. The order of ΔG_h values for different anions is $I^- < NO_3^- < Cl^- < IO_3^-$ [25]. The lower extraction efficiency of IO_3^- in NO_3^- form of PIS as compared to Cl^- form could be due to its inability to replace more hydrophobic counterions from the PIS. As described in our earlier work, the selectivity of the PIS can be related to the solubility of anions in the hydrophobic organic medium of PIS which is dependent on hydration of anions [17]. The tolerances to anions commonly present in the natural aqueous systems on I^- sorption in the PIS was studied and data are summarized in Table 1. In this experiment, the amount of I^- in aqueous sample was kept as 2×10^{-6} M, which was lower than the available ion-exchange sites (5×10^{-6} M) in the equilibrating PIS sample. It can be seen from the ratio of M of interfering anion [X^-] to M of I^- ([X^-]/[I^-]) that there is no significant interference of anions up to 80–500 times excess of X^- ($X^- = Cl^-$, CH_3COO^-, HCO_3^-, CO_3^{2-} and SO_4^{2-}). This indicates that the selectivity of PIS is based on the hydration characteristics of competing anions. This is related to the fact that I^- is least hydrated among the anions listed in Table 1. In order to study the uptake of I^- in the presence of excess of anions likely to be encountered in the

Table 1
Interference of anions on uptake of I^- in PIS

Interfering ion (X^-)	Ion-exchange sites (µM)	[I^-][a] (µM)	[X^-]/[I^-][b]	Extraction of I^- (%)
None	5.1 ± 5%	2.0	–	97 ± 2
CH_3COO^-	6.0 ± 5%	2.5	160	96 ± 2
HCO_3^-	4.9 ± 5%	2.0	500	92 ± 3
CO_3^{2-}	5.7 ± 5%	2.5	80	93 ± 2
Cl^-	4.5 ± 5%	2.0	200	93 ± 2
SO_4^{2-}	6.6 ± 5%	2.0	200	95 ± 4

[a] I^- concentration.
[b] Mole ratio of interfering anion to iodide concentration.

food samples, the variation of uptake of I^- in the PIS sample as a function of increased ratio of ([X^-]/[I^-]) ($X^- = Cl^-$ and HCO_3^-) was studied and plotted in Fig. 4. It is evident from the figure that even on increasing concentration of Cl^- or HCO_3^- up to 3000 times with respect to I^-, the uptake of I^- is still more than 80%. This seems to suggest that the PIS can be used for I^- preconcentration even in the presence of large excess of Cl^- and HCO_3^-.

In order to study the possibility of estimating IO_3^- in the form of I^- using PIS, the IO_3^- in aqueous sample was reduced to I^- using a mixture of acetic acid and ascorbic acid [8]. The conversion of IO_3^- to I^- in the resulting aqueous solution was estimated by equilibrating it with PIS samples and subsequently subjecting the PIS samples to NAA. It was observed in this experiment that the extraction of IO_3^- after reduction with mixture of 1 ml of 3% acetic acid and 2 ml of 0.5 M ascorbic acid was 97%. This seems to suggest that IO_3^- in the equilibrating solution was fully converted to I^- as the extraction efficiency of iodide in the PIS was expected to be 95 ± 2%.

The total concentration of iodine from milk and milk powder samples was determined by ENAA covering the samples with flex boron carbide having a thickness of about 2 mm and irradiating the samples into reactor neutrons for 1 h. As shown

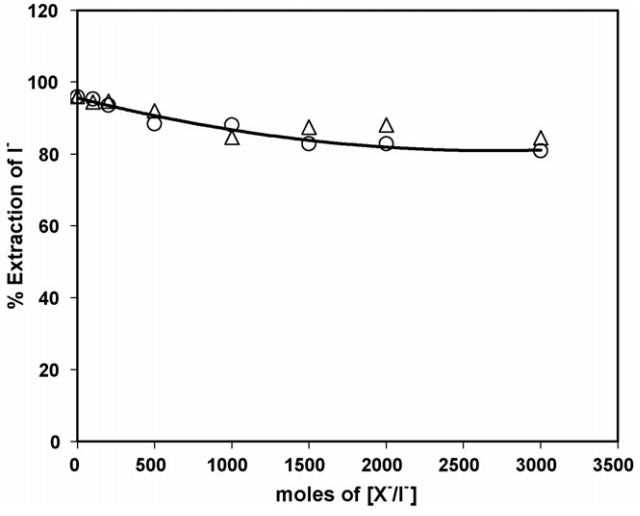


Fig. 4. Variation of percentage extraction of I^- as a function of ratio of concentrations of interfering anion X^- to I^-, where symbols (o and Δ) represent chloride and bicarbonate anion, respectively.

Table 2
Iodine contents in milk samples

Sample	Iodine content by NAA of PIS[a]		Total iodine by ENAA ($\mu g\,g^{-1}$)	Certified value ($\mu g\,g^{-1}$)
	I^- ($\mu g\,g^{-1}$)	Total iodine^{-b} ($\mu g\,g^{-1}$)		
NIST SRM-1549	1.31 ± 0.17	3.54 ± 0.21	3.41 ± 0.03	3.38
IAEA-153	1.15 ± 0.08	1.69 ± 0.19	1.67 ± 0.23	–
Commercial milk powder	1.47 ± 0.06	5.63 ± 0.27	5.55 ± 0.16	–
Low fat milk	0.14 ± 0.03	0.15 ± 0.07	0.17 ± 0.01	–

[a] These values were not corrected for the extraction efficiency and contribution due to IO_3^- in the PIS. The PIS samples were in Cl^- form.
[b] Total iodine($I^- + IO_3^-$) after conversion of IO_3^- to I^-.

in Fig. 5, the γ-spectrum of epithermal neutron activated samples showed ^{128}I peak, which was not distinct in the spectrum of milk powder samples irradiated into reactor without covering with boron carbide. The γ-spectrum of I^- in PIS is also free from spectral interferences as PIS does not contain elements that can be activated by neutrons to a significant extent (Fig. 5).

3.1. Application to milk samples

Based on the studies carried out in the present work, the determination of iodine species was applied to milk powder samples is shown in Scheme 1. In order to estimate possible losses of iodine species at different stages given in Scheme 1, a study was carried out to monitor the uptake of iodide from milk and milk products using ^{131}I marker as described in the experimental section. The uptake of iodide in PIS was found to be quantitative (95 ± 2%). The uptake of I^- in triisooctylamine based PIS was not quantitative from the filtrate obtained after removal of organic part from milk solution.

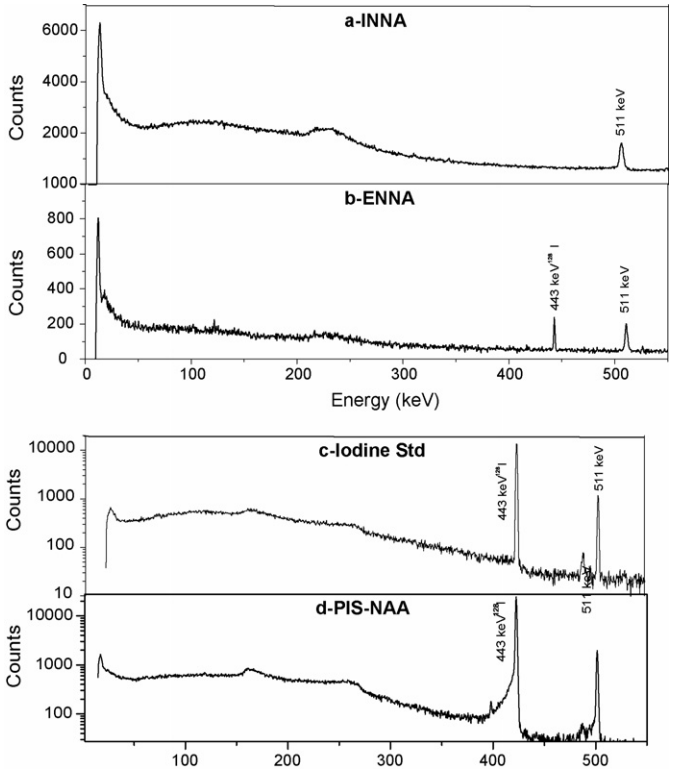


Fig. 5. Gamma ray spectra of (a) INAA of milk powder (b) ENAA of milk powder (c) INAA of iodine standard and (d) PIS-NAA of milk powder.

The iodine contents in different milk powder samples obtained by using Scheme 1 are given in Table 2. As can be seen from this table, the total iodine contents obtained in standard reference material NIST-1549 by ENAA and NAA of PIS (after conversion of IO_3^- to I^-) are in close agreement with the certified value of iodine content. However the uncertainty in the values of iodine contents obtained by NAA of PIS samples was higher than those obtained by ENAA. This can be attributed to the number of steps involved in this method as compared to ENAA. The agreement of value of total iodine content in NIST-1549 obtained by ENAA with NAA of PIS indicates that most of the iodine in this sample is present in I^- and IO_3^- forms. Similar conclusions are drawn from the data given for standard material IAEA-153 milk powder and commercially available milk powder. However, the low fat milk powder seems to contain most of the iodine in the form of I^-. The iodine content obtained from ENAA in this sample is slightly higher than those obtained by PIS-NAA. This may be due to the fact that some of the iodine is organic bound. In order to confirm the absence of organic bound iodine in other sample (commercal milk powder), the organic part separated after coagulation of milk was subjected to ENAA. The iodine peak was not visible in the γ-spectrum of this ENAA activated sample. This indicated that organic bound iodine in this sample might be very low, below sub-microgram detection limit of ENAA method.

4. Conclusions

The PIS was found to be effective in selective preconcentration of I^- from aqueous sample with minimum interference from IO_3^- and other commonly present anions in the milk powder sample. The IO_3^- content in the aqueous sample could also be preconcentrated quantitatively in PIS after converting it to I^- using a mixture of acetic acid and ascorbic acid. A scheme for estimation of different iodine species was developed using PIS. This scheme involves NAA of I^- sorbed in the PIS from aqueous sample and direct ENAA of solid sample without manipulation. The good agreement of the certified value of iodine in NIST SRM-1549 with those obtained in the present work using PIS-NAA and ENAA validated the present approach for the determination of iodine species in the milk samples.

Acknowledgements

Authors thank Dr. V.K. Manchanda, Head, Radiochemistry Division, Bhabha Atomic Research Centre (BARC), Prof. S. B. Padhye, Head, Department of Chemistry, Pune University and Prof. B.S.M. Rao, former Head Department of Chemistry, Pune University for their constant support and encouragement. The authors are thankful to D. Parthasarathi, J.R.F., GITAM for his help during the experiments. Authors are thankful to the personnel of Apsara reactor for their cooperation during irradiation of samples. One of the Authors (P.B.) thanks Board of Research in Nuclear Sciences (BRNS), DAE, India for the financial assistance to the project under BARC-Pune University MoU.

References

[1] G. Lopez-Cueto, J.M. Santiago, N. Grane, Talanta 39 (1992) 349.
[2] T. Tomiyasu, M. Nonaka, M. Uchikadu, K. Anazawa, H. Sakamoto, Anal. Sci. 20 (2004) 391.
[3] S.B. Niazi, M. Mozammil, Anal. Chim. Acta 252 (1991) 115.
[4] A.A. Ensafi, S. Zakeri, Anal Lett. 32 (1999) 1643.
[5] M. Kamburova, Talanta 39 (1992) 997.
[6] Z. Xie, J. Zhao, Talanta 63 (2004) 339.
[7] H.S. Shin, Y. Suk, Y. Oh-Shin, J. Kim, J. Ryu, J. Chromatogr. A 732 (1996) 327.
[8] K. Ito, E. Shoto, H. Sunahara, J. Chromatogr. 549 (1991) 265.
[9] S.D. Kumar, B. Maite, P.K. Mathur, Talanta 53 (2001) 701.
[10] K.A. Schwehr, P.H. Santschi, Anal. Chim. Acta 482 (2003) 59.
[11] E.H. Larsen, M.B. Ludwigsen, J. At. Spectrosc. 12 (1997) 435.
[12] J.D. Fasset, T.J. Murphy, Anal. Chem. 62 (1990) 386.
[13] E.C. Machado, L.F. Bellido, J Radioanal. Nucl. Chem. 249 (2001) 653.
[14] J. Kucera, Z. Randa, L. Soukal, J. Radioanal. Nucl. Chem. 249 (2001) 61.
[15] R. Rao, A. Chatt, Analyst 118 (1993) 1247.
[16] X. Zhao, W. Chan, M. Wong, D. Xiao, Z. Li, Am. Lab. (2003) 13.
[17] Y.M. Scindia, A.K. Pandey, A.V.R. Reddy, S.B. Manohar, Anal. Chem. 74 (2002) 4204.
[18] Y.M. Scindia, A.K. Pandey, A.V.R. Reddy, S.B. Manohar, Anal. Chim. Acta 515 (2004) 311.
[19] A. Rouhollahi, M. Shamsipur, Anal. Chem. 71 (1999) 1350.
[20] Y. Shi, R. Acharya, A. Chatt, J. Radioanal. Nucl. Chem. 262 (2004) 277.
[21] T. Balaji, R.N. Acharya, A.G.C. Nair, A.V.R. Reddy, K.S. Rao, G.R.K. Naidu, Sci. Total Environ. 253 (2000) 75.
[22] R. Rao, J. Holzbecher, A. Chatt, Fresenius J. Anal. Chem. 352 (1995) 53.
[23] Dionex Application Note 37.
[24] J.S. Edmonds, M. Morita, Pure Appl. Chem. 70 (1998) 1567.
[25] Y. Marcus, J. Chem. Soc. Faraday Trans. 87 (1991) 2995.

Available online at www.sciencedirect.com
ScienceDirect
Talanta 71 (2007) 1333–1338
Talanta
www.elsevier.com/locate/talanta

Use of NIR spectroscopy in the production of modified industrial resins

M. Blanco *, V. Villaescusa

Departamento de Química Analítica, Facultad de Ciencias, Universidad Autónoma de Barcelona, 08193 Bellaterra, Barcelona, Spain

Received 5 December 2005; received in revised form 9 June 2006; accepted 6 July 2006
Available online 22 August 2006

Abstract

Natural resins are scarcely used, but after appropriate modification processes they acquire characteristics of viscosity, point of softening, stability, etc. that facilitate their application in fields such as paintings, varnishes, cosmetic, etc. The complexity of resins makes it very difficult to monitor the reactions involved in their modification, the extent of which is usually determined via more experimentally accessible parameters. However, the methods typically used to determine such parameters are slow and produce environmentally unfriendly waste.

In this work, we assessed the potential of NIR spectroscopy, as an alternative to the traditional analytical methods, for monitoring the industrial processes involved in the production of modified resins. To this end, we developed PLS calibration models that were used to quantify physical (viscosity and cloud point) and chemical parameters (acid and hydroxyl numbers), with a view to characterize the evolution of the resins during the reaction that take place throughout the fabrication process.

Samples were withdrawn at different times stages of the process for analysis with the proposed quantitation models; the data thus obtained were compared with those provided by reference methods. Based on the results, NIR spectroscopy is an effective choice for the accurate, expeditious monitoring of industrial resin modification processes.
© 2006 Elsevier B.V. All rights reserved.

Keywords: Near infrared spectroscopy; Natural resins modification; PLS calibration; Physico-chemical properties; Load control

1. Introduction

Natural resins are secretions of mostly vegetable, but also animal, origin that consist of complex mixtures of various types of organic substances. They are solid or semi-fluid amorphous products that are normally insoluble in water and soluble in organic solvents. Colophony, also known as rosin, is a major natural resin obtained from pine resin and commercially available as three different products depending on their origin, namely: gum rosin, which is obtained by processing oleoresin exudates from living trees; wood rosin, which is an organic extract from aged pine logs; and tall oil, which is obtained by purifying the acid byproducts of paper manufacturing. The three types of resin contain a wide variety of compounds (particularly C_{20} monocarboxylic diterpenic resinic acids in addition to some neutral materials, water and other acid substances). The content in neutral compounds, which dictates the way the resin is processed, can range from less than 5% to more than 15%.

Most natural resins cannot be directly used as paints, varnishes, adhesives or cosmetics, for example, even though they are included in many of their formulations [1]. In fact, they usually require a chemical reaction to acquire the required properties (e.g. degree of reticulation, softening point, viscosity, chemical stability) for each specific use. The reactions used for this purpose vary widely in nature.

Industrially, resin modification reactions are monitored via some physical (viscosity, turbidity, refractive index, colour) or chemical parameter (acid number, hydroxyl number, resinic and fatty acids). The analytical methods typically used for this purpose are based on the classical techniques recommended by the American Society for Testing and Materials (ASTM) [2]. Such methods are usually time-consuming, use large amounts of reagents and produce waste. In fact, analysis times can range from a few minutes to several hours; this lengthens production cycles, raises costs and lowers outputs.

Updating production processes entails improving their efficiency and productivity. This can be accomplished by using fast analytical techniques enabling effective, complete analytical control of the processes concerned. The instrumental analytical techniques most frequently used to identify and characterize

* Corresponding author.
E-mail address: marcel.blanco@uab.es (M. Blanco).

0039-9140/$ – see front matter © 2006 Elsevier B.V. All rights reserved.
doi:10.1016/j.talanta.2006.07.028

resins [3–5], which include mass spectrometry (MS), nuclear magnetic resonance (NMR), IR spectroscopy and high performance liquid chromatography (HPLC), are ineffective for monitoring resin modification processes as the need to treat samples for analysis detracts from expeditiousness.

Near infrared spectroscopy (NIRS) is one of the most effective alternatives in this context. In fact, it is fast and non-destructive, requires no sample treatment and affords in situ measurements by use of fiber-optic probes, which makes it especially suitable for controlling industrial processes [6].

However, NIR spectra typically contain unselective, extensively overlapped bands that require the use of multivariate chemometric analytical tools [7] such as partial least squares (PLS), principal component regression (PCR) or multiple linear regression (MLR) for quantitation. A NIR spectrum contains both physical information about the sample and chemical information about its components. The chemical composition of a sample can be modeled by using those wave number ranges where some sample component exhibits high absorption. Determining physical properties, however, requires a different method as such properties usually affect the whole spectrum; one case in point is scattering, which arises from differences in particle size [8].

In this work, we assessed NIR spectroscopy as an alternative to the fast determination of physical and chemical parameters with a view to monitoring the industrial modification of natural resins. To this end, appropriate models for determining both physical (viscosity and cloud point) and chemical parameters (acid and hydroxyl numbers) were developed.

2. Experimental

2.1. Resin modification process

Resinic acids in gum rosin contain two reactive groups, namely: carboxyl groups, which are acidic and conjugated double bonds. These groups must be altered differently depending on the physico-chemical properties the end-product is to possess. The modification process involves several steps. Thus, natural gum rosin is mixed with a phenol and melted in a reactor in order to obtain a homogeneous mass that is then supplied with paraformaldehyde. Below 200 °C, the phenol undergoes the addition of formaldehyde and the subsequent condensation of the conjugated double bonds of resinic acids. The functionality of the resin is increased by adding an unsaturated acid anhydride that also adds to double bonds via a Diels–Alder reaction. Subsequently, a polyol is added to esterify the carboxyl groups above 230 °C and obtain the desired degree of reticulation in the resin. The duration of each step and its validation depend on the variation of the acid and hydroxyl numbers, cloud point and Gardner viscosity—the last is an indirect measure of the mean molecular weight of the resin.

The initial acid and hydroxyl numbers were used to establish the initial reactor load, which was measured when the reactor contents (resin plus phenol) were homogeneous. Subsequent measurements allowed the course of the phenolic condensation reaction to be monitored. Viscosity and cloud point measurements were additionally made at the late stages of the process.

All studied parameters were mutually related and in the final stage tended to decrease the acid number, hydroxyl number and cloud point (facilitated the dissolution of the resin in mineral oils); nevertheless the viscosity tend to increase.

2.2. Samples

A total of 270 samples that were either prepared in the laboratory or obtained from a production plant were studied.

2.2.1. Industrial samples

An overall 179 samples were obtained at different stages of various industrial processes. Thus, 37 samples were used in models for control charge and 142 in models for following the parameters of process. The samples differed in composition depending on the particular stage at which they were withdrawn; sample withdrawal times coincided with those industrially used to monitor the process.

2.2.2. Laboratory samples

An overall 91 samples were prepared by weighing of their components and treated similarly to production samples. Also, their composition was similar to those of the samples withdrawn at each stage during an industrial process. These samples, which were used to expand the concentration ranges of the target components, were of either of two types. Thus, 46 samples were prepared by mixing the resin and phenol in the laboratory in order to mimic the initial reactor load; however, the concentrations of resin and phenol spanned a range of ±25% around the theoretical value. These samples were not reacted; rather, they were melted to obtain a homogeneous mixture and used to develop the load control models.

The resin modification process, which involved the addition of an unsaturated diacid anhydride, was studied by using a laboratory reactor to reproduce three industrial processes; the reactor was loaded with resin concentrations around ±10% the theoretical value and variable concentrations of the anhydride (the dienophile for the Diels–Alder reaction) from 0 to 4%. A total of 45 samples of this type were prepared.

2.3. Reference methods

2.3.1. Acid number

The acid number (AN), which is defined as the number of milligrams of potassium hydroxide required to neutralize 1 g of sample, was determined in accordance with ASTM D-465-01 [9] (*viz.* by titration of the non-volatile acid fraction with an alkaline standard).

2.3.2. Hydroxyl number

The hydroxyl number (OHN), which is defined as the number of milligrams of KOH required to neutralize the acetic acid formed during the acetylation of 1 g of sample, was determined in accordance with ASTM D-1957-86 [9]. This method involves acetylating hydroxyl groups with acetic anhydride in pyridine,

using 4-dimethylaminopyridine (DMAP) as catalyst. After the reaction, excess acetic anhydride is hydrolysed with water and titrated with an alkaline standard.

2.3.3. Gardner viscosity

Gardner viscosity (GV) was determined in accordance with ASTM D-1545-98 [9]. This involved measuring the viscosity of a solution of known concentration in a specific solvent (xylene, toluene) and comparing the time taken by an air bubble to rise in the viscosity tube with reference standards. The reference standards used were a test kit of Gardner-Holdt tubes labeled with the pertinent letters and previously checked using the CA/04 method. The typical standard scale ranges from A to Z10 and spans the viscosity range from 0.5 to 1000 stokes. This method is applicable to transparent liquids containing no crystalline or gel particles.

2.3.4. Cloud point

The cloud point was determined in accordance with ASTM D-6038-05 [9], which involves measuring the ease of dissolution of the resin in aliphatic compounds such as mineral oils (specifically, 69 Af New). This parameter was measured with a Chemotronic Cloud Point Tester from Novocontrol (Hundsangen, Germany), using a solution containing 10% resin in the oil and heating it until a clear solution was obtained. The cloud point was taken to be the temperature at which the solution became turbid during its slow cooling.

2.4. Apparatus and software

NIR spectra were recorded on a Spectrum One NTS instrument from Perkin-Elmer (Norwalk, CT) equipped with a near infrared reflectance accessory (NIRA). Spectra were obtained in the transflectance or reflectance mode depending of the physical properties of the samples. Data were acquired at 2 cm^{-1} interval over the wavenumber range 4000–10,000 cm^{-1}. Each individual spectrum was the average of 30 scans.

The instrument was controlled via its bundled software. Multivariate calibration models were constructed and spectral pretreatments applied using the software Unscrambler V. 9.1 from CAMO (Trondheim, Norway).

2.4.1. Recording of NIR spectra

The samples initially withdrawn from the reactor were highly viscous liquids at ambient temperature, so their spectra were recorded in the transflectance mode. As reticulation increased, viscosity and melting points also increased, and the cooled samples were solid, so their spectra were recorded in the reflectance mode.

Transflectance measurements were made by placing the viscous samples in glass Petri dishes that were heated to clear melt on a hotplate and compressed with an aluminium reflector of 0.5 mm path length, after which they were placed in the capsule of the recording module in order to acquire their spectra before they solidified.

Reflectance measurements of the solid samples were made in the interleaved mode. To this end, they were previously powdered and placed in a capsule that was accommodated over the recording module.

2.5. Data processing

The first- and second-derivative spectral pretreatments were applied by using the Savitzky–Golay algorithm with a second-order polynomial and a 19-point window.

PLS1 calibration models were constructed by cross-validation, using the leave-one-out method; the optimum number of factors was taken to be the minimum in a plot of residual variance *versus* number of factors. The initial model was refined by using the number of factors leading to the lowest R.S.E.P. for the validation model as the optimum value.

The goodness of calibration and prediction was measured in terms of the relative standard error of calibration (R.S.E.C.) and prediction (R.S.E.P.), respectively, defined as:

$$\text{R.S.E.}(\%) = \sqrt{\frac{\sum_{i=1}^{n}(Y_{\text{pred}} - Y_{\text{ref}})^2}{\sum_{i=1}^{n} Y_{\text{ref}}^2}} \times 100$$

where n is the number of samples used, Y_{ref} the parameter value provided by the reference method and Y_{pred} the estimated by the NIR method.

The goodness of each model was assessed from a graph of NIR-predicted *versus* reference values that was used to calculate the confidence intervals for the slope and intercept at a significance level of 95%.

3. Results and discussion

The course of the resin modification process was monitored via the NIR spectra for samples withdrawn at different times. Fig. 1 shows the spectra for various such samples obtained at different stages of the process, namely: initial loading of the reactor, initial esterification-reticulation, formation of the Diels–Alder adduct and formation of the end-product. As can be seen, some bands increased as the reaction developed.

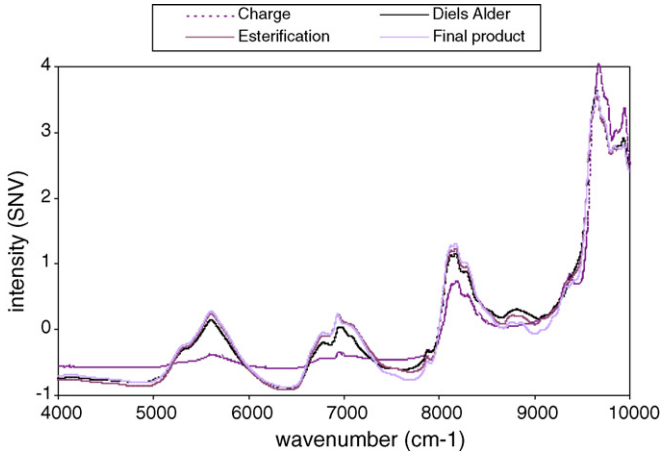


Fig. 1. NIR spectra (SNV) for samples withdrawn at different stages of the production process.

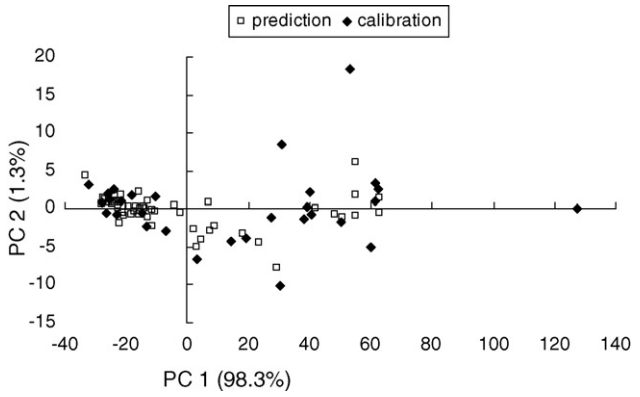


Fig. 2. Scatter plot of PCA from second derivative, 4000–10,000 cm^{-1} spectra for process samples. *Note:* calibration and prediction samples used to develop the AN calibration model are marked.

For construction of different models we use production simples as well laboratory samples. The body of samples was split into a calibration set and a validation set with a view to constructing calibration models for the different target parameters. The samples included in the calibration set should encompass the maximum possible variability and span the whole range of values of the property to be measured. Such samples were selected from a scatter plot of PC1 *versus* PC2 scores that was constructed from the results of a Principal Component Analysis (PCA) of NIR spectra recorded throughout the wavenumber range (4000–10,000 cm^{-1}). The scatter plot is shown in Fig. 2, which first two factors accounted for 99.6% of the total variance and was used in the selection of the samples of process used in the construction of the model for AN (process). Various calibration models based on diverse spectral pretreatments (*viz*. SNV, first and second derivative), spanning variable wavenumber ranges were tested.

In the construction of different models for each parameter, the samples that present high values of the residuals were considered outliers and were suppressed of the model. Models for determining the acid and hydroxyl numbers in samples withdrawn immediately after the reactor load became homogeneous were developed for load control. Table 1 summarizes the characteristics of each model and lists its calibration and prediction errors. Table 2 shows the figures of merit the calibration and prediction curves. As can be seen, the acid number was accurately predicted, but the hydroxyl number was not—which can be ascribed to the lesser accuracy and precision of the reference values for the latter. Also, modeling the hydroxyl number required using more factors.

For a given resin composition, the acid and hydroxyl numbers exhibit virtually identical differences between samples withdrawn at different time stages. The average difference for the reference resin was 33.1 ± 2.4 mg/g. This led us to construct a calibration model allowing the difference between the acid number and hydroxyl number to be determined for load control purposes. Table 2 lists the most salient statistical results regarding the calibration and prediction of the difference between the previous two numbers. With this model, load control can be accomplished by determining a single parameter.

The late stages of the resin modification process were monitored via the acid number, viscosity and cloud point, which govern the properties of the end-product.

At the start of the final stage, the resin had an acid number of 122 ± 2 mg KOH/g; such a number should be reduced to less than 25 mg/g by the end of the process. The model was constructed from production samples alone on account of the broad range of values they spanned. The calibration model for the acid number at this stage of the process was more complicated than that for the previous one by effect of the intrinsic complexity of this stage.

A joint 95% confidence region test for slope and intercept was evaluated and revealing that can accept simultaneously that the slope to be 1 and the intercept to be 0 (for calibration and prediction sets). Also, both curves had a correlation coefficient higher than 0.99, which suggests a highly linear relationship between the target property and the spectral response. Based on the results, the model used to quantify the acid number provided accurate predictions.

The model for the Gardner viscosity was constructed from laboratory samples spanning a viscosity range similar to that for the end-product (3–5.5 stokes); this was accomplished by using samples with viscosity values of 2.9–8.7 stokes in the calibration

Table 1
PLS1 models for the acid number (AN), hydroxyl number (OHN), their difference (AN − OHN), viscosity and cloud point

Parameter	Spectral pretreatment	Calibration			Prediction
		PLS factors	Y-explained variance (%)	R.S.E.C. (%)	R.S.E.P. (%)
Load control					
AN	Second D	1	99.0	0.6	1.6
OHN	First D	4	98.0	1.1	2.5
AN − OHN	Second D	3	98.9	4.3	6.4
Process					
AN	Second D	4	99.6	2.8	5.1
Viscosity	Second D	3	97.2	2.5	5.7
Cloud point	Second D	2	99.5	1.1	3.5

All models were constructed by using the full spectral range (4000–10,000 cm^{-1}).

Table 2
Statistical figures of merit for the regresion line of predicted NIR values *vs.* reference values for each parameter

	Samples	Range	Slope	Intercept	Correlation coefficient
Load control					
AN					
Calibration	22	106.4–138.0 mg/g	0.99 ± 0.05	1.10 ± 5.56	0.995
Prediction	28	106.5–124.2 mg/g	1.10 ± 0.12	−11.30 ± 14.57	0.965
OHN					
Calibration	18	74.7–102.5 mg/g	0.98 ± 0.07	1.81 ± 6.67	0.990
Prediction	18	75.2–101.2 mg/g	0.73 ± 0.18	23.53 ± 16.16	0.910
AN − OHN					
Calibration	19	12.3–75.2 mg/g	0.99 ± 0.05	0.40 ± 2.09	0.994
Prediction	20	21.0–74.9 mg/g	0.97 ± 0.08	2.34 ± 3.23	0.986
Process					
AN					
Calibration	27	17.6–86.2 mg/g	1.00 ± 0.03	0.14 ± 1.03	0.998
Prediction	63	18.4–59.7 mg/g	1.02 ± 0.04	−0.30 ± 1.02	0.991
Viscosity					
Calibration	19	2.95–8.67 stokes	0.97 ± 0.08	0.02 ± 0.06	0.990
Prediction	19	3.68–7.66 stokes	0.90 ± 0.23	0.51 ± 1.22	0.900
Cloud point					
Calibration	29	129.0–207.0 °C	1.00 ± 0.03	0.82 ± 4.47	0.998
Prediction	45	129.0–207.0 °C	0.99 ± 0.07	1.17 ± 11.33	0.972

±Confidence level for means ($p = 0.05$).

set. The model was constructed from decimal logarithms of the viscosity values to avoid non-linearity.

Table 2 shows the statistical figures of merit of the calibration and prediction models for the viscosity. The regression plots of calculated *versus* reference values were obtained by using the antilogarithms of the values calculated by the model. Based on the confidence intervals, the slope and intercept were not significantly different from unity and zero, respectively, for the calibration and prediction curves. The small slope obtained for the predicted values reflects the poor repeatability of the reference values.

The cloud point is typically determined at the last stage of the process in order to confirm that it meets the requirements (125–135 °C). The model for this parameter was constructed from production samples alone as they spanned a wide enough range of values. The model with the highest predictive ability was that obtained by using two PLS factors; as can be seen from Table 2, its predictions were subject to no systematic error.

Table 3
Student's *t*-test on the residuals ($p = 0.05$) of the production samples

	N	Average	S.D.	t_{exp}	t_{crit}
Load control					
AN	24	0.6	1.5	1.9	2.07
OHN	12	−1.0	2.3	1.6	2.20
AN − OHN	11	1.6	2.5	2.1	2.22
Process					
AN	63	0.2	1.5	0.9	2.00
Viscosity	22	0.1	0.6	1.2	2.08
Cloud point	45	−0.5	5.2	0.7	2.02

The previous calibration models were applied to samples obtained from the production process in order to assess their predictive ability. A *t*-test on the body of production samples at the 95% significance level revealed that the residuals for the six PLS models were not significantly different from zero (Table 3). This confirms the accuracy of the models in predicting the target parameters typically used to monitor the production process.

4. Conclusions

Near infrared spectroscopy is an effective alternative to traditional wet analytical methods for controlling industrial resin modification processes as it affords the simultaneous determination of the parameters typically used to assess the status of the evolving system. Also, it substantially reduces analysis times and improves production cycles.

The PLS calibration models developed in this work allow the determination of the physical (viscosity and cloud point) and chemical parameters (acid number and hydroxyl number) used to monitor changes in resins during the reactions involved in their industrial modification.

The relationship between the acid number and hydroxyl number allowed the development of an alternative model based on their difference that reduces load control to the determination of a single parameter. The predictive ability of the PLS models was assessed with production samples not employed in their construction; the predictions exhibited no significant differences from the reference values, which testifies to the accuracy of the proposed models.

In summary, NIR spectrometry is an effective tool for monitoring the industrial modification of natural resins.

Acknowledgements

The authors are grateful to Spain's Ministry of Science and Technology for funding this research within the framework of Project BQU2003-04247. CRAY VALLEY IBÉRICA, S.A. (Sant Celoni, Spain) is also gratefully acknowledged for valuable discussions and kindly supplying the resin samples.

References

[1] P.M. Mandaogade, P.M. Satturwar, S.V. Fulzene, B.B. Gogte, A.K. Dorle, React. Funct. Polym. 50 (3) (2002) 233–242.
[2] D.F. Zinkel, J. Rusell, Naval Stores: Production, Chemistry, Utilization, Pulp Chemicals Asociation, Inc., New York, 1989.
[3] S. Sadhra, C.N. Gray, I.S. Foulds, J. Chromatogr. 700 (1997) 101–110.
[4] Xing Hong Zhang, Hong Mei Wan, Yu Qin Min, Guo Rong Qi, J. Appl. Polym. Sci. 96 (3) (2005) 723–731.
[5] P.A. Smith, P.S. Son, P.M. Callaghan, W.W. Jederberg, K. Kuhlmann, K.R. Still, Toxicology 111 (1996) 225–238.
[6] B.J. Kip, T. Berghmans, P. Palmen, A. Van der Pol, M. Huys, H. Hartwing, M. Sceepers, D. Wienke, Vib. Spectrosc. 24 (2000) 75–92.
[7] D.L. Massart, B.G.M. Vandeginste, L.M.C. Buydens, S. De Jong, P.J. Lewi, S. Smeyers-Verbeke, Handbook of Chemometrics and Qualimetrics: Part B, Elsevier, The Netherlands, 1998, pp. 349–379.
[8] M.C. Pasikatan, J.L. Steele, C.K. Spillman, E. Haque, J. Near Infrared Spectrosc. 9 (2001) 153–164.
[9] Annual Book of ASTM Standards, Section 06.03, American Society for Testing and Materials, Philadelphia, 2005.

Available online at www.sciencedirect.com
ScienceDirect
Talanta 71 (2007) 1276–1281
Talanta
www.elsevier.com/locate/talanta

A temperature-jump stopped-flow system for monitoring chemical kinetics triggered by rapid cooling

Brian L. Boys, Lars Konermann *

Department of Chemistry, The University of Western Ontario, London, Ontario N6A 5B7, Canada

Received 16 June 2006; received in revised form 27 June 2006; accepted 27 June 2006
Available online 25 July 2006

Abstract

This work reports the implementation of a stopped-flow system for studying the kinetics of protein folding triggered by rapid cooling. The transition from denaturing temperatures to ambient conditions is achieved by rapid mixing of pre-heated protein solution with cold refolding buffer. The estimated dead-time of the apparatus is 8 ms. Folding kinetics are monitored by fluorescence spectroscopy. Careful tuning of the solution mixing ratio is required for the elimination of baseline artifacts that could mask fluorescence signals originating from protein conformational changes. The viability of the rapid cooling method is demonstrated by applying it to monitor the refolding of thermally denatured cytochrome *c*. Following a heat exposure time of 3 min, the protein shows multi-exponential folding kinetics, ultimately resulting in a fluorescence level that is virtually indistinguishable from that of the native state. In contrast, incomplete refolding is observed when the heat exposure time is extended to 30 min. This effect may be due to aggregation phenomena affecting the thermally denatured protein. It appears that the rapid cooling approach reported in this work may become a useful tool for temperature-jump studies in various areas of chemistry and biochemistry.
© 2006 Elsevier B.V. All rights reserved.

Keywords: Temperature jump; Rapid cooling; Cytochrome *c*; Thermal denaturation; Protein aggregation

1. Introduction

Proteins have to fold into a highly ordered native conformation in order to be biologically active. Exploring the mechanisms underlying these folding processes continues to be a main focus of research in numerous laboratories [1–4]. In vitro folding experiments normally start with largely disordered polypeptide chains produced by exposing the protein to chemical denaturants such as urea or guanidinium hydrochloride. A disruption of the native structure may also be induced by extremes of temperature or pH. Refolding of these disordered polypeptide chains can be initiated by switching back to physiological solvent conditions, i.e., to low concentrations of chemical denaturants, ambient temperature, and near-neutral pH.

There are two main approaches to protein folding studies [5]. (i) In *equilibrium experiments* the conformation is monitored under stationary conditions, as a function of denaturant concentration. Measurements of protein structural changes are taken only after the protein has adjusted to the solvent environment. (ii) *Kinetic studies* are carried out under non-equilibrium conditions. Structural changes are monitored as a function of time, following a rapid alteration of the protein environment. The latter type of experiment is particularly important for studies on folding mechanisms; it provides information on rate constants, short-lived intermediates, and transition states [6]. Key to the viability of every kinetic experiment is the type of trigger used to initiate refolding, because this will ultimately determine the time resolution of the measurement. Most commonly, refolding is initiated by a concentration jump, i.e., a mixing step that results in a sudden reduction of denaturant concentration by dilution. Manual mixing is suitable for kinetic studies in the range of tens of seconds to hours. However, most proteins fold on much faster time scales, thus necessitating the use of stopped-flow [7,8] or quench-flow [9–11] rapid mixing schemes. Typically, these techniques provide a time resolution on the order of milliseconds. Measurements in the sub-millisecond range have become feasible with the introduction of modern continuous-flow instruments [12–14] and micro-channel mixing devices [15,16]. Time scales down to nanoseconds are accessible in studies employing

* Corresponding author. Tel.: +1 519 661 2111x86313; fax: +1 519 661 3022.
E-mail address: konerman@uwo.ca (L. Konermann).
URL: http://publish.uwo.ca/~konerman/.

0039-9140/$ – see front matter © 2006 Elsevier B.V. All rights reserved.
doi:10.1016/j.talanta.2006.06.032

laser-based photochemical triggers [8,17]. Another interesting possibility is the use of rapid heating methods. The parabolic free energy versus temperature profile of most proteins leads to unfolding at both high and low temperatures. Thus, heating of a cold-unfolded protein by a laser pulse or by an electric discharge can provide a very rapid (nanosecond) refolding trigger [8,17].

A survey of the protein folding literature reveals that, surprisingly, one particular folding trigger that is used only very rarely in kinetic experiments is the cooling of heat-denatured proteins. It is important to point out the conceptual difference of this approach to freeze-quench studies, where a temperature jump to extremely low temperatures (e.g., liquid nitrogen) is used to *stop* the process of interest. In the context of this work, rapid cooling refers to a temperature change from elevated temperature down to ambient conditions that *initiates* a folding reaction. The apparent scarcity of studies using such an approach is in stark contrast to the fact that heating and cooling are commonly used to induce protein conformational changes under equilibrium conditions, e.g., for calorimetric experiments [18]. Theoretical studies have devoted considerable attention to modeling kinetic folding triggered by rapid cooling [19–22]. Yet, the number of reported experiments using a "temperature-jump down" approach is miniscule when compared to the vast number of reports that employed other kinetic triggers. Probably the simplest way to implement a rapid cooling strategy is the manual mixing of heated protein solution with cold refolding buffer, resulting in the desired final temperature [23–27]. As with most manual techniques, the time resolution of these experiments is very limited. One notable exception is the work of Nakatani [28], who developed an apparatus capable of rapid heating and cooling with a dead time of about 60 ms.

Interestingly, the refolding of heat-denatured proteins is often not completely reversible. The reasons for this behavior are poorly understood; possible explanations involve the occurrence of aggregation, disulfide shuffling, or other covalent modifications [22,27,29,30]. In addition, apparent irreversibility can be caused by the accumulation of metastable conformations [18]. It appears that a better understanding of these processes could yield important insights into the general mechanisms of protein folding, in particular for cases involving kinetic folding/aggregation partitioning phenomena [31,32]. A major hurdle for experimental studies on the refolding of heat-denatured proteins is the apparent lack of reliable instrumentation capable of performing rapid cooling experiments. This is in contrast to the situation for concentration-jump measurements, where a large variety of techniques is readily available.

In this work, we describe the modification of a commercial stopped-flow system with fluorescence detection for rapid cooling experiments with a time resolution of a few milliseconds. The functionality of this system is demonstrated by applying it to monitor the refolding of heat-denatured cytochrome *c* (cyt *c*), a protein that has served as model system in numerous folding studies [33–36]. The fluorescence intensity of the single tryptophan (Trp59) in cyt *c* provides a sensitive probe for the overall conformation of the protein. In the native state, Trp59 is in close proximity to the heme group. Quenching by resonance energy transfer causes Trp59 to be virtually non-fluorescent, as long as the protein retains its native structure. Unfolding increases the tryptophan-heme distance, thereby diminishing the quenching efficiency and causing a high fluorescence intensity [37]. It appears that the "temperature-jump down" approach introduced in this work could become a useful tool for millisecond time-resolved studies on protein folding and other (bio)chemical processes.

2. Experimental

2.1. Chemicals

Cytochrome *c*, arginine, and urea were obtained from Sigma (St. Louis, MO) and used without further purification. All solutions used for the experiments in this work contained 40 mM phosphate buffer at pH 7.2.

2.2. Rapid cooling stopped-flow measurements

The temperature-jump system developed for this work is based on a Biologic SFM 4S/Q (Molecular Kinetics, Indianapolis, IN) stopped-flow system. In the commercial version of this instrument, the mixer and optical observation cell are directly coupled to the outlets of stepper motor-driven syringes. For the purpose of this work, this assembly was divided (Fig. 1). The mixer/cell unit was mounted on a separate bracket, and linked to the outlets of the two syringes (termed A and B) via stainless steel tubes (i.d. 1.17 mm, o.d. 1.59 mm). The connections from the lines to the mixer/cell consisted of custom-made PEEK assemblies, designed to result in minimal thermal exchange of the reactant solution during injection. A tubular reservoir was inserted into the tube leading from syringe A to the mixer, resulting in total transfer line volumes of 5 mL and 1.1 mL for syringes A and B, respectively. Each of the two lines were embedded in a poly(vinyl chloride) jacket (i.d. 1.1 cm) through which ice-cold and heated water were circulated as indicated in Fig. 1. The observation cell compartment was thermostated at 26 °C by flushing with dry nitrogen. Syringe A (containing protein solution) and syringe B (containing refolding buffer) were kept at room temperature throughout the entire experiment. Heating of the protein solution, and cooling of the refolding buffer commenced only upon pushing them into the transfer lines. The reservoir connected to syringe A allowed heat exposure of the protein for various amounts of time prior to refolding. Control experiments were carried out to ensure that the contents of the transfer lines were completely temperature equilibrated before injecting them into the mixer/cell assembly. Kinetic measurements were performed in standard stopped-flow mode of operation: liquid was transferred through the transfer lines, through the mixer, and into the observation cell, thereby replacing previously reacted mixture. The total flow rates used were around 3 mL s^{-1} at a pushing pulse duration of 120 ms. Subsequently, the flow was stopped by an electronically controlled hard-stop valve. Reaction kinetics were monitored by fluorescence spectroscopy, using an excitation wavelength of 280 nm. The emission intensity was integrated over the entire wavelength range above 320 nm by mounting a cut-on filter in front of the

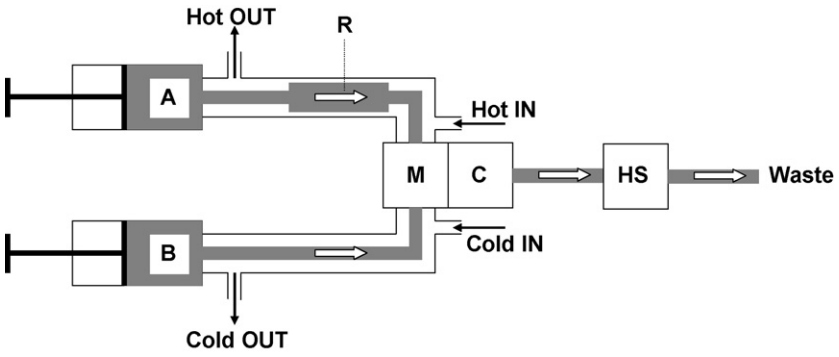


Fig. 1. Schematic representation of the rapid-cooling stopped-flow system used for this work. Syringes A and B are kept at room temperature, they contain protein and refolding buffer, respectively. The contents of the transfer lines connecting the syringes and the mixer (M) are embedded in counter-flow jackets for temperature control. R represents a reservoir that allows the heat exposure of protein solution for various amounts of time. Refolding is initiated by rapid mixing at M, prior to transferring the reaction mixture into the observation cell (C), where the kinetics are monitored optically. The previous contents of C are flushed out to waste. Closing of the hard stop valve (HS) stops the flow of the liquid column after each shot. White block arrows indicate the flow direction from the syringes through the observation cell to waste, thin black arrows represent the flow of the heating fluid and coolant.

PMT detector. Early attempts to obtain reliable kinetics were frustrated by the occurrence of scattering artifacts caused by bubbles in the observation cell. This problem was solved by extensive helium sparging of all reactant solutions [38].

3. Results and discussion

3.1. Optimization of instrument performance for fluorescence detection

Tryptophan fluorescence intensity measurements are a convenient and widely used probe for conformational changes taking place during protein folding [10,39]. The spectral properties of this chromophore are highly dependent on its local environment, access to solvent water, and the proximity of functional groups that can act as quenchers [40]. An aspect that has to be taken into account for the current work is that the fluorescence intensity is strongly influenced by the solution temperature. Free tryptophan in aqueous solution shows a dramatic decline in fluorescence intensity when heated from 20 to 95 °C (Fig. 2) [41]. This effect has important implications for temperature-jump studies, as it can give rise to baseline artifacts, if not properly controlled.

For the experiments described below, the temperatures of hot and cold solutions within the transfer lines were $T_h = 93.5\,^{\circ}C$ and $T_c = 0.5\,^{\circ}C$, respectively, whereas the observation cell was kept at 26 °C. In order to maintain a constant temperature throughout the experimental time window, the freshly injected mixture from the two syringes must match the pre-equilibrated temperature of the cell. Ideally, the final temperature after mixing, T_m, should be given by $T_m = (V_h \times T_h + V_c \times T_c)/(V_h + V_c)$, where V_h and V_c are the volumes of hot and cold solution, respectively. For a final temperature of 26 °C and $V_h = 100\,\mu L$, this relationship predicts a V_c value of 260 μL. To test the validity of this prediction, tryptophan solution was injected into the observation cell using the calculated 260 μL:100 μL ratio. These conditions result in a rapidly dropping fluorescence response that levels off after roughly 3 s (Fig. 3). This observation implies that the actual solution temperature is initially below that of the observation cell, such that thermal equilibration within the cell leads

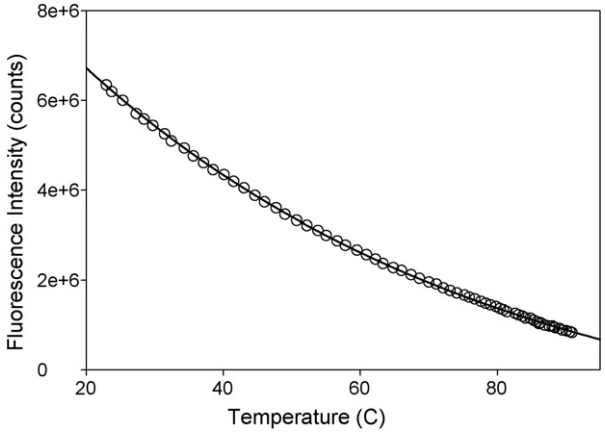


Fig. 2. Fluorescence intensity of 5 μM tryptophan in phosphate buffer as a function of temperature. The solid line represents a regression curve according to $I(T) = I_0 + a \times \exp(-b \times T)$, where $I_0 = -1.8e+6$ counts, $a = 1.2e+7$ counts, $b = 0.016\,^{\circ}C^{-1}$. T is the temperature in degree Celsius.

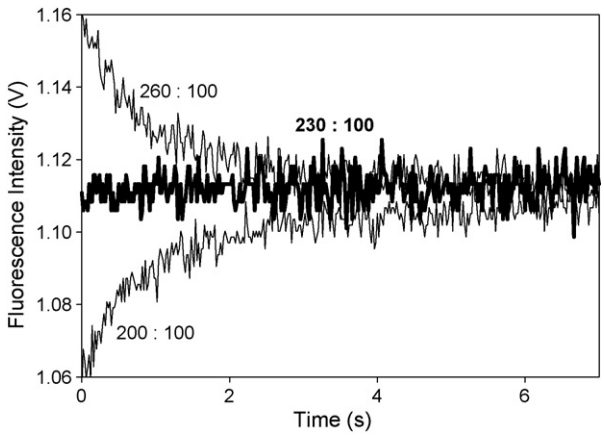


Fig. 3. Fluorescence response observed upon stopped-flow mixing of cold and hot aqueous solutions, each containing 5 μM tryptophan. The V_c:V_h ratios (each number reflects the volume in μL) used for the three data sets are indicated.

to a temperature increase of the solution. According to the data depicted in Fig. 2, such a temperature rise will be accompanied by a fluorescence decrease. Using a cold-to-hot volume ratio of 230 μL:100 μL leads to a flat baseline, which indicates that the temperature of the mixture under these conditions matches that of the cell. The discrepancy in V_c (230 μL versus 260 μL) is attributed to inadvertent cooling of the hot solution upon transfer into the mixer/observation cell assembly. Based on the volume ratio needed for reaching a flat baseline, the actual temperature of the hot solution upon injection into the cell is estimated to be 85 °C. This corresponds to a temperature drop of 8.5 °C, down from the initial value of T_h = 93.5 °C during the ~30 ms needed for the hot solution to reach the mixer. The effects of this slight cooling on the kinetics of folding will be negligible, as long as the reduced temperature of 85 °C is still within the unfolded baseline region. The temperature-jump from 85 down to 26 °C by mixing with the cold solution occurs with a dead-time of approximately 8 ms. The time estimates given here are based on solution flow rates, and on the volumes of transfer lines, mixer, and observation cell. For completeness, Fig. 3 also shows data recorded at an even lower V_c:V_h injection ratio of 200 μL:100 μL which should result in an initial temperature higher than that of the observation cell. As expected, the fluorescence response in this case shows a signal increase, caused by gradual cooling of the mixture. In summary, fluorescence-based temperature-jump experiments require a careful adjustment of the solution mixing ratio. Any temperature mismatch will give rise to baseline artifacts that could mask the occurrence of fluorescence signals arising from conformational changes in protein folding experiments.

3.2. Thermal unfolding of cytochrome c

The midpoint of a heat-induced protein unfolding transition, referred to as melting temperature (T_m), provides a measure for the thermal stability of the native state. Whereas many proteins exhibit melting points around 60–70 °C, others have their T_m values at significantly higher temperatures. The thermal unfolding of these more stable species is commonly studied in solvents containing chemical denaturants, but at concentrations that in themselves are insufficient for inducing unfolding. The presence of these denaturants results in a lowering of T_m, such that unfolding can be induced at temperatures that are more readily accessible [6,18,42]. The melting point of cyt *c* in aqueous solution is around 90 °C [42]. Exposure of the protein to 4 M urea lowers T_m to 67 °C (Fig. 4). The fluorescence versus temperature data in Fig. 4 are the result of two opposing trends, namely the breakdown of Trp59 quenching upon unfolding, and the general tendency of tryptophan to decrease its fluorescence intensity with increasing temperature. To compensate for the latter, the original unfolding curve (solid symbols in Fig. 4) was corrected according to the tryptophan temperature profile depicted in Fig. 2. When applying this correction, the Trp59 unfolding curve (open symbols in Fig. 4) exhibits an end point at 86 °C that coincides with the fluorescence intensity of free tryptophan at 26 °C.

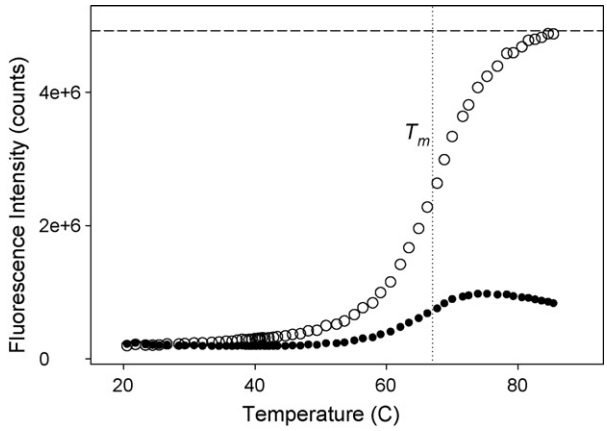


Fig. 4. Temperature-induced unfolding of 5 μM cytochrome *c* measured by monitoring the tryptophan emission of the protein. The original data are indicated by the filled symbols. Open symbols reflect the profile obtained after correcting the profile for the gradual loss of tryptophan intensity with increasing temperature, using the $I(T)$ function determined in Fig. 2. The dashed horizontal line represents the fluorescence intensity of free tryptophan at 26 °C. The midpoint of the corrected unfolding profile is indicated by a dotted vertical line (corresponding to T_m = 67 °C).

3.3. Refolding of cytochrome c triggered by rapid cooling

Although cyt *c* has served as model system for numerous folding studies employing chemical denaturants [33–36], the folding kinetics of the thermally denatured protein have not been investigated yet. For this work the refolding of thermally denatured cyt *c* was initiated by rapid cooling from 93.5 to 26 °C at a constant urea concentration of 4 M. The conformational changes of the protein were followed by monitoring the Trp59 emission intensity as function of time. Initial experiments resulted in kinetic traces that exhibited poor reproducibility (data not shown). This behavior was tentatively attributed to aggregation phenomena. The addition of arginine is known to suppress aggregation to a significant extent, while not affecting protein stability [43–45]. Kinetic data measured in the presence of 1 M arginine were highly reproducible. Refolding of the protein under these conditions results in a kinetic response that exhibits multi-exponential behavior (Fig. 5A). Roughly 60% of the total signal change occurs within the dead time of the stopped-flow experiment, giving rise to a pronounced burst phase. The fluorescence profile within the experimental time window of ~8 s is well described by a bi-exponential fit with relaxation times of 150 ms and 2.1 s that both possess a relative amplitude of 10%. The remaining signal amplitude is recovered with a very slow relaxation time that is beyond the time frame accessible to the rapid mixing experiment. The fluorescence intensity measured 2.5. h after a manually induced temperature jump is virtually zero, and thus indistinguishable from that of the native protein.

As indicated earlier, the instrument used for this study allows refolding kinetics of thermally denatured proteins to be monitored for various heat exposure times. The data depicted in Fig. 5A were collected on cyt *c* that had been in the thermally unfolded state for merely 3 min. An extension of this heating period to 30 min leads to a dramatically different fluorescence response (Fig. 5B). Following a burst phase similar

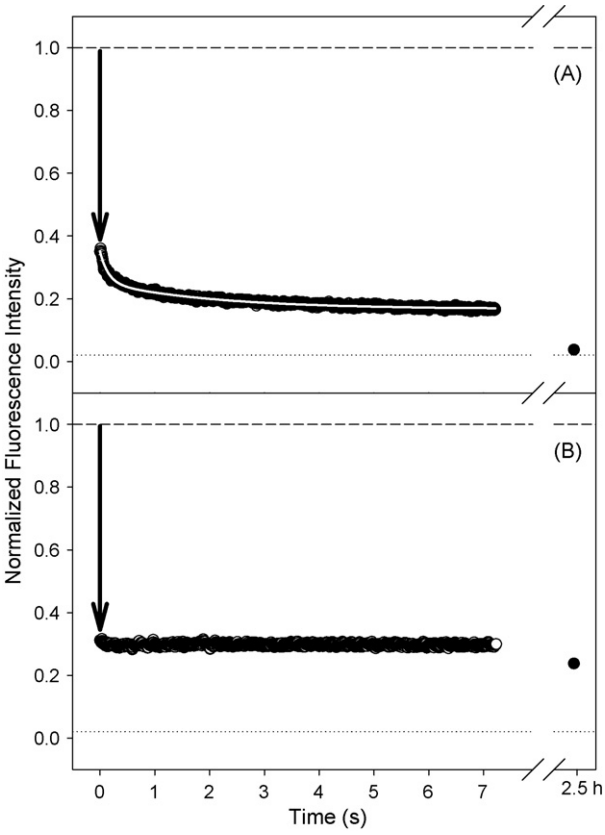


Fig. 5. Refolding of cytochrome *c* triggered by a temperature-jump from 93.5 to 26 °C monitored by measuring the tryptophan emission intensity of the protein as a function of time. The reaction mixture contained 4 M urea and 1 M arginine, the final protein concentration was 1.5 μM. (A) Kinetics obtained after exposing the protein to 93.5 °C for 3 min. The white line represents a bi-exponential fit to the experimental data, fitting parameters are given in the text. (B) Kinetics obtained after exposing the protein to 93.5 °C for 30 min. Horizontal dashed lines indicate the fluorescence intensity of 1.5 μM tryptophan at 26 °C, dotted lines indicate the fluorescence intensity of the native protein. Vertical arrows represent burst phase amplitudes. Also shown in both panels is the fluorescence intensity measured 2.5 h after the temperature jump. The kinetic data shown in each panel are the average of three measurements.

to that observed in the previous experiment, the Trp59 emission intensity remains almost constant at a relative level of 0.3, even for measurements taken 2.5 h after the temperature jump.

The kinetic data depicted in Fig. 5 reveal that the heat exposure duration has a profound effect on the recoverability of the cyt *c* native state conformation after thermal denaturation. An exposure time of 3 min leads to a fluorescence signature that suggests complete refolding on a reasonably fast time scale. In contrast, refolding does not go to completion within several hours when heating the protein for 30 min. This result implies that the thermally unfolded protein at 93.5 °C is subject to a relatively slow process that results in conditions which strongly interfere with refolding. This phenomenon is consistent with earlier studies that have proposed the occurrence of covalent modifications or aggregation upon heat exposure [22,27,29,30]. The formation of non-native disulfide bonds in heat-denatured cyt *c* seems unlikely, as both cysteines present in the protein (at positions 14 and 17) are involved in thioether bridging to the heme. Although aggregation was apparently suppressed by the presence of arginine to the reaction mixture, it cannot be ruled that some aggregation still occurs under the conditions of the current work. As with many other folding processes, it appears that the key to understanding the observed kinetics is a careful characterization of the unfolded state [34,46]. We are currently investigating the effects of various other solvent additives, as well as pH, which controls factors such as the tendency of the heme iron to undergo misligation during folding [47]. The results of these experiments will be reported elsewhere.

4. Conclusions

This work demonstrates how a stopped-flow device can be modified for experiments requiring the rapid cooling of heated solutions down to ambient temperature. Previous kinetic studies on the refolding of thermally denatured proteins were hampered by the fact that "temperature-jump down" methods were not readily accessible, necessitating the use of manual mixing approaches with a very limited time resolution. The approach presented here allows these studies to be carried out with an estimated dead time of about 8 ms. A further improvement of this time resolution would require the use of a more powerful syringe drive system for the injection of the reactant solutions into the observation cell at higher flow rates. The implementation of detection methods other than fluorescence, such as absorbance or circular dichroism spectroscopy, should be straightforward. The cyt *c* folding kinetics reported in this work serve the primary purpose of demonstrating the viability of the experimental approach used. Future studies are required to elucidate the structural changes underlying the heat exposure time dependence of the folding kinetics. In any case, it is clear that the method introduced here represents a kinetic tool that can provide valuable insights into the properties of thermally denatured proteins and their refolding behavior. In addition, it may prove useful for temperature jump studies in many other areas of chemistry and biochemistry. The performance of our setup appears to be comparable to the custom-built device of Nakatani [28]. However, the approach proposed here seems to be more readily accessible for most potential users since it is based on a simple modification of a commercial instrument.

Acknowledgements

We thank Derek J. Wilson for valuable discussions and critical reading of the manuscript. Financial support for this study was provided by the Natural Sciences and Engineering Research Council of Canada (NSERC), the Canada Foundation for Innovation (CFI), the Provincial Government of Ontario, and by the Canada Research Chairs Program.

References

[1] C.B. Anfinsen, Science 181 (1973) 223–230.
[2] C.M. Dobson, Methods 34 (2004) 4–14.
[3] J.N. Onuchic, P.G. Wolynes, Curr. Opin. Struct. Biol. 14 (2004) 70–75.
[4] V. Daggett, A. Fersht, Nat. Rev. Mol. Cell Biol. 4 (2003) 497–502.
[5] T.E. Creighton, Biochem. J. 270 (1990) 1–16.

[6] A.R. Fersht, Structure and Mechanism in Protein Science, W. H. Freeman & Co., New York, 1999.
[7] K.L. Maxwell, D. Wildes, A. Zarrine-Afsar, M.A. De Los Rios, A.G. Brown, C.T. Friel, L. Hedberg, J.-C. Horng, D. Bona, E.J. Miller, A. Vallée-Bélisle, E.R.G. Main, F. Bemporad, L. Qiu, K. Teilum, N.-D. Vu, A.M. Edwards, I. Ruczinski, F.M. Poulsen, B.B. Kragelund, S.W. Michnick, F. Chiti, Y. Bai, S.J. Hagen, L. Serrano, M. Oliveberg, D.P. Raleigh, P. Wittung-Stafshede, S.E. Radford, S.E. Jackson, T.R. Sosnick, S. Marqusee, A.R. Davidson, K.W. Plaxco, Protein Sci. 14 (2005) 602–616.
[8] H. Roder, M.C.R. Shastry, Curr. Opin. Struct. Biol. 9 (1999) 620–626.
[9] J.B. Udgaonkar, R.L. Baldwin, Nature 335 (1988) 694–699.
[10] H. Roder, G.A. Elöve, S.W. Englander, Nature 335 (1988) 700–704.
[11] T.M. Raschke, S. Marqusee, Nat. Struct. Biol. 4 (1997) 298–304.
[12] M.C.R. Shastry, S.D. Luck, H. Roder, Biophys. J. 74 (1998) 2714–2721.
[13] S. Akiyama, S. Takashi, K. Ishimori, I. Morishima, Nat. Struct. Biol. 6 (2000) 514–520.
[14] E. Welker, K. Maki, M.C.R. Shastry, D. Juminaga, R. Bhat, H.A. Scheraga, H. Roder, Proc. Natl. Acad. Sci. U.S.A. 101 (2004) 17681–17686.
[15] J.B. Knight, A. Vishwanath, J.P. Brody, R.H. Austin, Phys. Rev. Lett. 80 (1998) 3863–3866.
[16] O. Bilsel, C. Kayetekin, L.A. Wallace, C.R. Matthews, Rev. Sci. Instrum. 76 (2005) 014302.
[17] M. Gruebele, Annu. Rev. Phys. Chem. 50 (1999) 485–516.
[18] A.L. Privalov, in: T.E. Creighton (Ed.), Protein Folding, W. H. Freeman & Co., New York, 1992, pp. 83–126.
[19] M. Skorobogatiy, H. Guo, M. Zuckermann, J. Chem. Phys. 109 (1998) 2528–2635.
[20] H.D. Nguyen, C.K. Hall, Biotechnol. Bioeng. 80 (2002) 823–834.
[21] A. Hansen, M.H. Jensen, K. Sneppen, G. Zocchi, Physica A 250 (1998) 355–361.
[22] S.A. Potekhin, E.L. Kovrigin, Biophys. Chem. 73 (1998) 241–248.
[23] H. Reiersen, A.R. Clarke, A.R. Rees, J. Mol. Biol. 283 (1998) 255–264.
[24] D. Nohara, T. Yamada, A. Watanabe, T. Sakai, Biotechnol. Bioeng. 44 (1994) 276–282.
[25] J. Backmann, H. Fabian, D. Naumann, FEBS Lett. 364 (1995) 175–178.
[26] D. Reinstädler, H. Fabian, J. Backmann, D. Naumann, Biochemistry 35 (1996) 15822–15830.
[27] F. Tani, N. Shirai, T. Onishi, F. Venelle, Y. Kyoden, E. Doi, Protein Sci. 6 (1997) 1491–1502.
[28] H. Nakatani, Anal. Biochem. 149 (1985) 87–90.
[29] D.I. Kreimer, V.L. Shnyrov, E. Villar, I. Silman, L. Weiner, Protein Sci. 4 (1995) 2349–2357.
[30] S. Miller, B. Schuler, R. Seckler, Protein Sci. 7 (1998) 2223–2232.
[31] F. Chiti, N. Taddei, F. Baroni, C. Capanni, M. Stefani, G. Ramponi, C.M. Dobson, Nat. Struct. Biol. 9 (2002) 137–143.
[32] I.V. Baskakov, G. Legname, S.B. Prusiner, F.E. Cohen, J. Biol. Chem. 276 (2001) 19687–19690.
[33] H. Maity, M. Maity, M.M.G. Krishna, L. Mayne, S.W. Englander, Proc. Natl. Acad. Sci. U.S.A. 102 (2005) 4741–4746.
[34] E.V. Pletneva, H.B. Gray, J.R. Winkler, J. Mol. Biol. 345 (2005) 855–867.
[35] E. Chen, R.A. Goldbeck, D.S. Kliger, J. Am. Chem. Soc. 126 (2004) 11175–11181.
[36] N.P. Prabhu, R. Kumar, A.K. Bhuyan, J. Mol. Biol. 337 (2004) 195–208.
[37] L. Konermann, D.J. Douglas, Biochemistry 36 (1997) 12296–12302.
[38] O.S. Degenhadt, B. Waters, A. Rebelo-Cameirao, A. Meyer, H. Brunner, N.P. Toltl, Dissol. Technol. 11 (2004) 6–11.
[39] P.R. Callis, Methods Enzymol. 278 (1997) 113–150.
[40] Y. Chen, M.D. Barkley, Biochemistry 37 (1998) 9976–9982.
[41] G.G. Guilbault, Practical Fluorescence: General Aspects of Luminescence Spectroscopy, New York, 1990.
[42] T.E. Creighton, Proteins, W. H. Freeman & Co., New York, 1993.
[43] B.M. Baynes, L.T. Bernhardt, Biophys. J. 87 (2004) 1631–1639.
[44] T. Arakawa, K. Tsumoto, Biochem. Biophys. Res. Commun. 304 (2003) 148–152.
[45] M. Ishibashi, K. Tsumoto, T. Arakawa, Protein Expr. Purif. 42 (2005) 1–6.
[46] D. Shortle, FASEB J. 10 (1996) 27–34.
[47] S.W. Englander, T.R. Sosnick, L.C. Mayne, M. Shtilterman, P.X. Qi, Y. Bai, Acc. Chem. Res. 31 (1998) 737–744.

Available online at www.sciencedirect.com
ScienceDirect
Talanta 71 (2007) 1298–1303
Talanta
www.elsevier.com/locate/talanta

Voltammetric analysis of the acaricide amitraz and its degradant, 2,4-dimethylaniline

R. Brimecombe, J. Limson *

Department of Biochemistry, Microbiology and Biotechnology, Rhodes University, P.O. Box 94, Grahamstown 6140, South Africa

Received 4 July 2005; received in revised form 13 May 2006; accepted 29 June 2006
Available online 26 July 2006

Abstract

Amitraz is a formamide acaracide used in the control of ticks and mites in livestock. An electrochemical method for the determination of total amitraz residues and its final breakdown product, 2,4-dimethylaniline, is presented. Cyclic voltammetry at a glassy carbon electrode showed the irreversible oxidation of amitraz and of 2,4-dimethylaniline. A linear current response was obtained with an extrapolated limit of detection of 2×10^{-8} M for amitraz and 1×10^{-8} M for 2,4-dimethylaniline. The biological degradation of amitraz and subsequent formation of 2,4-dimethylaniline was readily monitored in spent cattle dip. Amitraz and 2,4-dimethylaniline was also monitored in milk and honey samples.
© 2006 Elsevier B.V. All rights reserved.

Keywords: Amitraz; 2,4-Dimethylaniline; Pesticide; Degradation; Cyclic voltammetry

1. Introduction

Amitraz (*N*-(2,4-dimethylphenyl)-*N*′-[(2,4-dimethylphenyl)-imino]methyl-*N*-methylinethanimidamide) is a formamide acaricide that is applied as a topical spray or dip on cattle, pigs and sheep to control infections caused by ectoparasites [1,2].

Amitraz (Fig. 1) is readily hydrolysed under the following conditions: exposure to sunlight (UV exposure) [3], low pH [2], and bioaugmentation, through metabolism by bacteria such as *Escherichia coli* and *Pseudomonas* species present in cattle faeces [4]. In addition, solution properties such as ionic strength, temperature and solubility affects the stability of amitraz [5]. Amitraz hydrolyses through a series of intermediate compounds to form the environmentally stable compound 2,4-dimethylaniline (2,4-DMA) (Fig. 1) [2] which is mutagenic, oncogenic and genotoxic [6]. The degradation of amitraz to stable aniline products may contribute significantly to the environmental and health risks of this pesticide's application and use [6].

A common form of amitraz administration is through plunge dipping or spraying of livestock. Both of these techniques are subject to shortcomings in terms of dosing livestock at the correct concentrations. The plunge dipping method in particular is problematic, as dipwater is frequently re-used for further dosing of animals, with users adding additional pesticide to water that may contain unknown residual amounts of pesticide, or potentially harmful degradation products. There is much room for error in maintaining effective dosages if residual concentrations of pesticides are unknown. Researchers have shown that incorrect dosing of amitraz has led to ticks and mites gaining resistance to the pesticide [7].

The potential for pesticide resistance coupled with the toxicity of amitraz and 2,4-DMA to humans, livestock and the environment has lead to a demand for a portable analytical device that can relay information regarding the concentration of active pesticides on-site.

Conventionally, high performance liquid chromatography (HPLC) and gas chromatography (GC) have been employed as the analytical techniques for amitraz and 2,4-DMA analysis [2,3]. These techniques are, however, not readily adapted for on-site use. While water samples from livestock dipping tanks can be sent to laboratories for analysis, this leads to delays in the relay of analytical results and potential inaccuracies as the pesticide composition of the dipping tanks is subject to alteration during long analysis times.

Limited research has been conducted on the utilisation of voltammetry as an analytical tool for the determination of amitraz. Ibrahim et al. [8] obtained sensitivities in the nanomolar

* Corresponding author. Tel.: +27 46 622 5593; fax: +27 46 622 3984.
E-mail address: j.limson@ru.ac.za (J. Limson).

0039-9140/$ – see front matter © 2006 Elsevier B.V. All rights reserved.
doi:10.1016/j.talanta.2006.06.037

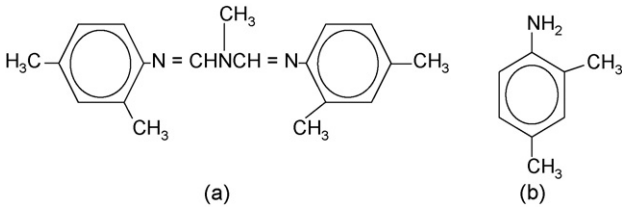


Fig. 1. Structures of (a) amitraz [(*N*-(2,4-dimethylphenyl)-*N*′-[(2,4-dimethylphenyl)-imino]methyl-*N*-methylinethanimidamide)] and (b) 2,4-dimethylaniline.

range for the analysis of amitraz in water and soil using adsorptive stripping voltammetry at a hanging mercury drop electrode (HMDE). No studies have been conducted on the voltammetric analysis of amitraz and 2,4-DMA in the matrix of a livestock dipping tank. Amitraz has been used in beehives to control the mite *Varroa jacobsoni*. Amitraz degradant 2,4-DMA has been found to be present in honey [9]. Amitraz and 2,4-DMA may also be present in animal flesh and milk intended for human consumption [10]. In this study we explore the cyclic voltammetric behaviour of amitraz and 2,4-DMA at a glassy carbon electrode, given the promise shown by these analytical methods towards future development of portable and cost-effective devices for on-site measurement.

2. Experimental

2.1. Reagents

Amitraz and 2,4-dimethylaniline (2,4-DMA) standards were obtained from Sigma–Aldrich. The stability of amitraz in a range of solvents has been examined by several authors [2,3,5,11], with amitraz reportedly most stable in the solvent acetonitrile [2,11]. The ideal solvent for dissolution of amitraz and 2,4-DMA, in terms of sensitivity and reproducibility of the current response, was determined to be acetonitrile in our studies as compared to studies using dimethylsulphoxide, methanol and ethanol. Adequate dissolution of amitraz and 2,4-DMA was shown in 20% acetonitrile. From a selection of buffers, sodium acetate, sodium carbonate, sodium phosphate and Britton–Robinson (BR) buffer, the ideal buffering system for analysis of amitraz and of 2,4-DMA in terms of sensitivity and reproducibility of current response was determined to be BR buffer. BR buffer was also selected for electrochemical studies of amitraz by Ibrahim et al. [8]. BR buffer had been freshly prepared using equimolar amounts of 0.04 M orthophosphoric acid, 0.04 M acetic acid and 0.04 M boric acid. The pH was adjusted accordingly using 0.2 M sodium hydroxide. Amitraz and 2,4-DMA were dissolved in 20% acetonitrile prior to dilution with BR buffer. Triply distilled water was used to prepare all solutions.

For experiments on the effect of pH in which acetonitrile was used, pH values reported were recorded after addition of acetonitrile as apparent pH. All chemicals used were of analytical grade and not further purified. Samples of spent cattle dip from a cattle dipping trough in which solely amitraz was employed as the acaricide (in the form of the commercial preparation of amitraz, Ecotraz^{TM}), were obtained as required, from Cold Springs Farm, Grahamstown, South Africa. The proprietary formulation Ecotraz^{TM} was diluted with water prior to application in the dipping vat. Samples of Ecotraz^{TM} used in these experiments was also obtained from Mr. Chris Brooke, Cold Springs Farm. Milk and honey samples were purchased from commercial outlets.

2.2. Methods

Cyclic voltammograms and differential pulse voltammograms were recorded on the Autolab PGSTAT 30 equipped with a Metrohm VGA stand. All CVs were recorded at a scan rate of 100 mV/s. A 3 mm diameter glassy carbon electrode (GCE) was used as the working electrode, a Ag|AgCl electrode (3 M KCl) was used as the reference electrode and a platinum wire was employed as the auxiliary electrode in all voltammetric analyses. All potential values were referenced against the Ag|AgCl reference electrode. The GCE was thoroughly cleaned before use and between scans by polishing with alumina on a Buehler felt pad, followed by a rinse with water, then dilute acid, ethanol, distilled water, followed by a rinse with the buffer solution. For CV experiments, buffered solutions of amitraz and 2,4-DMA were placed in a glass cell and degassed for 5 min with nitrogen gas prior to scanning a potential window. A gentle flow of nitrogen was maintained over the solution during experimentation. The method was applied for the detection of amitraz and 2,4-DMA in three matrices namely: spent cattle dip, milk and honey.

The limit of detection (LOD) was calculated as the concentration that corresponds to the mean current of the baseline three times the standard deviation of the baseline [12].

2.3. Procedure for the analysis of amitraz and 2,4-dimethylaniline in environmental samples

In order to assess whether amitraz and 2,4-DMA could be detected in spent cattle dip, a sample of the spent dip (pH 3.2) to which amitraz in the form of Ecotraz^{TM} had been applied was obtained from Cold Springs farm after dipping of the livestock. BR buffer of equivalent pH was added to this sample to yield a final ratio of 50:50 (v/v). CV was performed as above. The identity of the resultant oxidation peaks were confirmed by spiking the sample with known concentrations of amitraz and of 2,4-DMA.

CV were also performed on a sample of spent cattle dip to which no Ecotraz^{TM} had been applied in the absence and presence of amitraz and 2,4-DMA. CV of amitraz and 2,4-DMA were performed directly in milk, while the honey sample was diluted with 0.2 M BR buffer of equivalent pH in a 50:50 (v/v) ratio and CV performed in the absence and presence of added amitraz and 2,4-DMA. For these studies in environmental samples, CV were compared with analysis of amitraz and 2,4-DMA in BR buffer of equivalent pH. The linearity of the current response in the environmental samples were determined through standard curves of current versus concentration. For the sake of clarity, return cathodic waves are not presented in certain CV figures.

3. Results and discussion

The CV of 2,4-DMA (Fig. 2) shows two anodic waves at 0.50 V and 0.74 V. The potential and current strength of the anodic peaks depend on the concentration and pH of the medium. On the cathodic scan a broad reduction wave at −0.70 V is observed. A weaker cathodic wave is also observed at −0.50 V depending on the concentration of the solution.

CVs of increasing concentrations of pure 2,4-DMA showed that the anodic peaks (the first, pa_1, at lower potentials, and second, pa_2, at higher potentials), increased with increase in concentration of 2,4-DMA with slight potential shifts towards more positive potentials. A standard curve plot of current versus concentration for the secondary anodic peak showed a linear relation, with $R^2 = 0.9889$. An extrapolated limit of detection of 1×10^{-8} M was determined for CV analysis of 2,4-DMA. By using differential pulse voltammetry, an experimental limit of detection for 2,4-DMA in 0.2 M BR buffer pH 7 was determined as 2.0×10^{-8} M.

Little reference to published information on the voltammetric behaviour of 2,4-DMA was found. CV studies by Marques et al. [13] showed double anodic waves for 2,3-DMA; 2.5-DMA; 2,6-DMA; 3,4-DMA and 3,5-DMA only in anhydrous dimethylformamide solution and without any cathodic waves observed. These authors attribute the first oxidation wave to the formation of a cation radical following oxidation of the arylamine nitrogen and then followed by another one-electron oxidation to form a dication. Studies by Mizoguchi and Adams [14] showed CVs of *N*,*N*-dimethylaniline (pH 2–3) with a reversible couple with $E_{1/2}$ approximately 0.5 V at a platinum electrode. In concurrence with [14,15], these authors report that the oxidation of *N*,*N*-DMA involves the oxidation of the amine to produce a cation intermediate which reacts with unoxidised DMA to form tetramethylbenzidine (TMB). As proposed by these authors, TMB then oxidizes to produce a quinine diimine, TMBox, which may explain the origin of the double anodic waves observed in this study.

The current response and potentials of pa_1 and pa_2 for 2,4-DMA analysis were pH dependent. At pH 2 and 3 pa_1 was dominant while at pH 4 and higher pa_2 for CV of 2,4-DMA was dominant. The second anodic wave pa_2 was masked at pH 2 while pa_1 was absent at pH 8 and higher. Current strength of

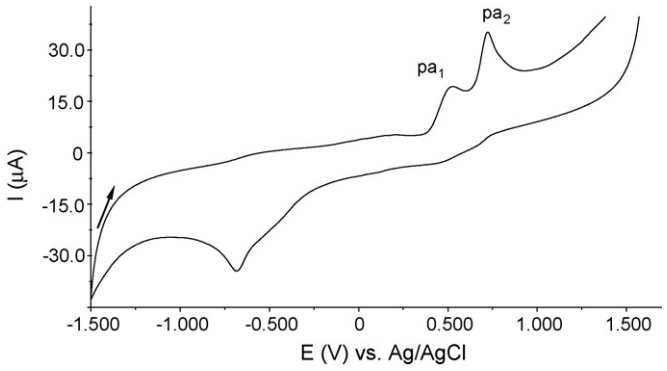


Fig. 2. CV of 2,4-DMA (3.8×10^{-5} M) in 0.2 M BR buffer (pH 7.0). Scan rate: 100 mV/s.

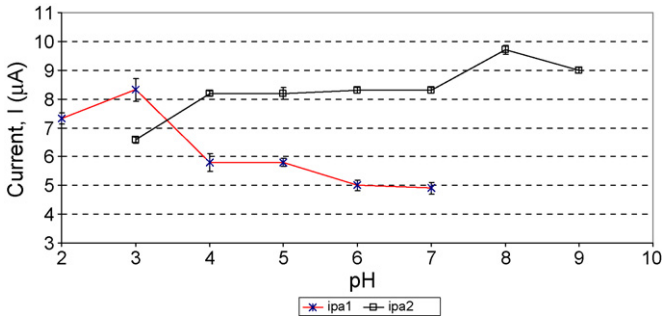


Fig. 3. Effect of pH on current response for the primary (pa_1) and secondary anodic waves (pa_2) for 10 μM 2,4-DMA with pH.

the first anodic wave decreased with increasing alkalinity while the second anodic wave increased with alkalinity (Fig. 3). The potentials of both pa_1 and pa_2 shifted towards more positive values with increase in acidity, from 0.53 V (pH 9) to 0.86 V (pH 3), for pa_2, and 0.48 (pH 7) to 0.77 V (pH 2) for pa_1 (Fig. 4). In [13] their studies on 2,3-DMA; 2,5-DMA; 2,6-DMA; 3,4-DMA and 3,5-DMA also exhibited shifts in anodic waves towards positive potentials with increase in acidity of the electrolyte solution.

Standard curves of current versus concentration for 2,4-DMA in the pH range from 2 to 10 showed that the greatest sensitivity is obtained at more alkaline conditions. Good linearity of current response versus concentration was obtained at all pH values with no particular trend observed. The highest reproducibility of the current response was observed at pH 7.

The electrochemical polymerisation of monomeric and substituted aniline to form a conducting polymer at an electrode has been well studied. Studies of aniline at a glassy carbon electrode [16] show increasing oxidation and reduction waves owing to the electropolymerisation of the polymer at the electrode. In our studies, successive CVs in the potential windows examined showed increases in peak height also suggesting the electropolymerisation of 2,4-DMA at the electrode.

Fig. 5 shows the CV obtained for pure amitraz at a GCE. An anodic peak was observed at +1.13 V and is attributed to the irreversible oxidation of amitraz.

The behaviour of amitraz at a GCE observed in our studies differs from that observed earlier at a hanging mercury drop electrode (HMDE) [8]. In those studies, the authors observed an irreversible cathodic peak at highly negative potentials between approximately −0.9 V and −1.4 V, with the potential being

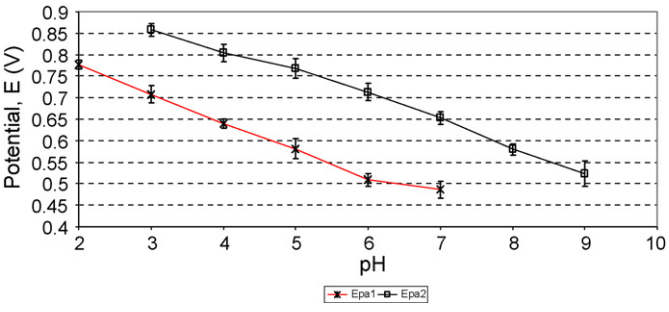


Fig. 4. Effects of pH on potential for the primary (pa_1) and secondary anodic waves (pa_2) for 10 μM 2,4-DMA.

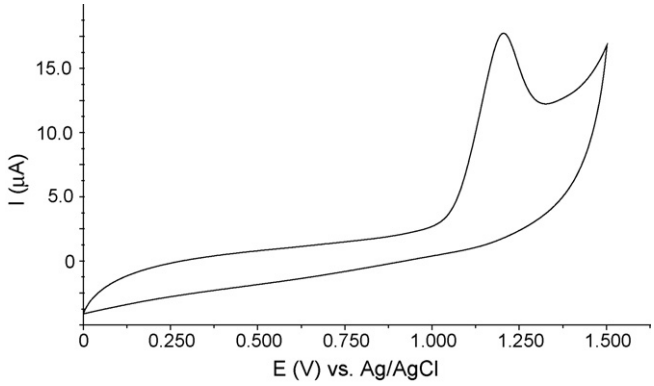


Fig. 5. CV of amitraz (2.0×10^{-5} M). Britton–Robinson buffer (pH 7.0). Scan rate: 100 mV/s.

dependent on the pH of the solution. Our studies of amitraz at a HMDE concurred with this finding.

CVs of increasing concentrations of amitraz showed a linear increase in peak current for the anodic peak observed at 1.13 V. A standard curve plot of current versus concentration showed a linear relation, with $R^2 = 0.9973$. An extrapolated limit of detection of 2×10^{-8} M was determined for CV analysis of amitraz. By using differential pulse voltammetry, an experimental limit of detection for amitraz in 0.2 M BR buffer pH 7, was determined as 8.5×10^{-8} M. This compares favourably with previous studies [3] where the LOD for amitraz by GC–MS was determined as 5.1×10^{-6} M.

The electrode surface was cleaned in between each scan for amitraz owing to the fouling of the electrode surface. The fouling of the electrode is attributed to the irreversible electrochemical oxidation of amitraz and the accumulation of the oxidation products at the GCE surface. The oxidation peaks were, however, reproducible on cleaning of the GCE.

The anodic oxidation of amitraz was observed at all pH's studied between 2 and 10. The current strength of the anodic oxidation wave for amitraz increased with increasing acidity, while potentials shifted to more positive values (Fig. 6).

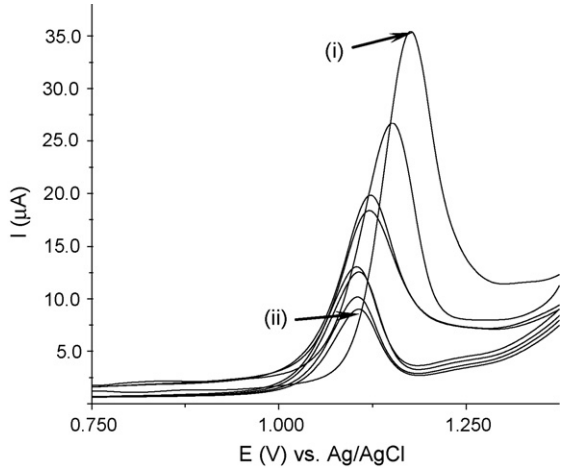


Fig. 6. CVs showing the shift in oxidation potential and change in current response of 15 μM amitraz in 0.2 M BR from (i) pH 2 and (ii) pH 10. Scan rate: 100 mV/s. Peak shown is the primary oxidation peak for amitraz. Cathodic waves not shown.

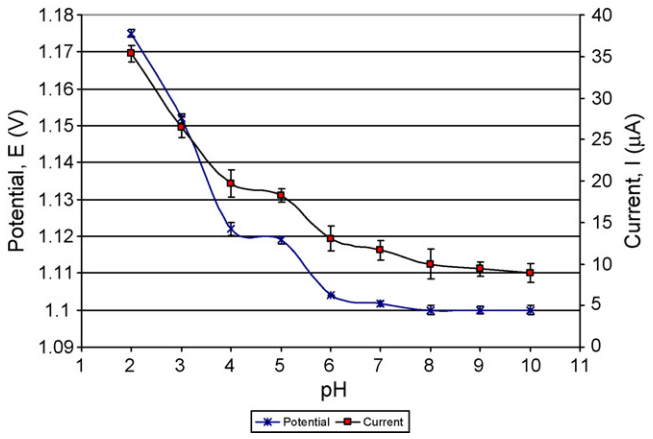


Fig. 7. Current decrease and potential shift with pH for 15 μM amitraz in 0.2 M BR buffer.

Fig. 7 shows the shift in potential to less positive potentials and a decrease in current response with an increase in alkalinity.

Standard curves of amitraz concentration versus current at pH 3 through pH 10 were generated. Amitraz had hydrolysed almost instantaneously at pH 2 and so standard curves at this pH were rendered impractical. The standard curves at more acidic pH conditions yielded a greater current response, with a steeper gradient. The average reproducibility of the current response of the primary oxidation curve is greatest at studies conducted at pH 7.

Amitraz degradation was observed at all pH's studied, with the most rapid degradation observed at pH 2 and the slowest at pH 10. Fig. 8 shows CVs of a solution of pure amitraz at pH 2 taken over a period of 15 min, with CV performed at 5 min intervals. The anodic wave at 1.21 V attributed to amitraz decreased with time until undetectable, while the peaks at 0.73 V and 0.86 V increased with time. The latter peaks are attributed to the formation of 2,4-DMA. The hydrolysis of amitraz to the stable 2,4-DMA concurs with the findings of Corta et al. [2]. These studies then show the ability to monitor the degradation of amitraz and the production of 2,4-DMA simultaneously. A sample at pH 10 was left open to the air and sunlight and it is postulated here that sunlight was the main factor leading to the degradation of amitraz, corresponding with Bernal et al. [3].

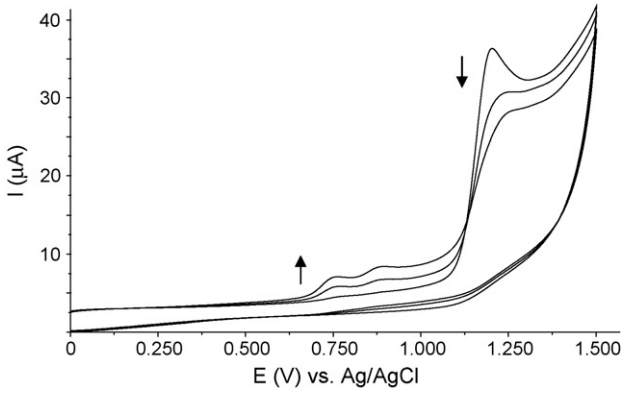


Fig. 8. CVs of amitraz (5.7 μA) taken at 5 min intervals. Britton–Robinson buffer (pH 2.0). Scan rate: 100 mV/s.

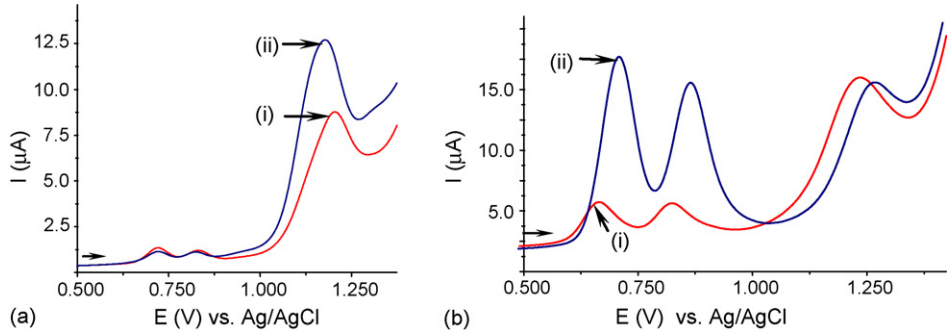


Fig. 9. (a) CV of spent cattle dip (pH 3) (i), spiked with 10 μM amitraz (ii). (b) CV of spent cattle dip (pH 3) (i), spiked with 15 μM 2,4-DMA (ii).

A sample of spent cattle dip was obtained from a dipping tank to which amitraz had been applied. A CV of this sample (Fig. 9a) shows an anodic peak at 1.18 V, which concurs with the anodic wave for amitraz previously described. This was confirmed by spiking the sample with 10 μM amitraz, as is represented by (ii) in Fig. 9a. A slight shift towards less positive potentials was noted for the amitraz peak when the dip was spiked with amitraz.

The anodic couple at 0.66 V and 0.83 V in Fig. 9b concurs with the characterisation of 2,4-DMA, and was confirmed by spiking the spent cattle dip sample with 15 μM 2,4-DMA (ii).

Amitraz and 2,4-DMA were also readily detected in honey and in milk. The current strength for amitraz and 2,4-DMA detection in spent cattle dip, honey and milk were compared with CVs of these compounds performed in BR buffer of equivalent pH.

For analyses in spent cattle dip, minimal current strength decrease and potential shift was observed when compared to that in 0.2 M BR buffer. In the honey:BR buffer (50:50) (v/v) mixture the amitraz peak exhibited a 24.3% decrease in the current strength, as compared to the analysis of amitraz in 0.2 M BR buffer of equivalent pH. Comparison of the current strength of 13 μM amitraz in spent cattle dip, honey and milk, shows that the highest current response obtained was that in spent cattle dip, with the lowest in milk. This is in keeping with expected results as before, where current response for amitraz was shown to be dependent on pH.

However, the relative sensitivity for each compound compared to the equivalent analyses in 0.2 M BR buffer of the same pH, shows that additional factors for the decrease in sensitivity are involved. The decrease in current strength observed for amitraz in milk and honey could be attributed to low ionic strength of these media. Reproducibility of 93.1% for analysis of amitraz in spent cattle dip was favourable, compared to 78.2% in honey and 76.8% in milk. A comparison of the correlation coefficients for standard curves generated showed that the most linear standard curve for amitraz was obtained in spent cattle dip ($R^2 = 0.9972$), with the least linear being that in milk ($R^2 = 0.9841$). For honey the deviation from linearity could be attributed to the viscosity of the solution, while in milk the decrease in linearity could be interference from milk constituents.

Similarly for analysis of 2,4-DMA in spent cattle dip, milk and honey, decreases in anodic strength for all environmental samples compared to analyses in 0.2 M BR buffer were accompanied by slight potential shifts. The relative sensitivity of 2,4-DMA as compared to an equivalent analysis in 0.2 M BR buffer in spent cattle dip was 91.0%, followed by honey, 56.4% and milk, 82.6%. The decrease in current strength can be attributed to lower ionic strength in the milk and honey environmental samples as compared to the spent cattle dip, and 0.2 M BR buffer. Reproducibility of the current response was similar to that for amitraz, 95.6% in spent cattle dip, 75.68% in honey and 71.61% in milk. A comparison of the linearity of the standard curves generated for 2,4-DMA shows that the most linear curve, with $R^2 = 0.9959$, was obtained in spent cattle dip. The standard curve generated in milk (pH 7) yielded a favourable R^2 of 0.9905, whereas the standard curve generated in honey: 0.2 M BR buffer (50:50) (v/v) (pH 4) yielded the lowest R^2 value of 0.9844. In milk, a 37.5% decrease in current strength was observed.

4. Conclusions

This study showed the efficacy of a glassy carbon electrode for direct analysis of amitraz and 2,4-DMA by cyclic voltammetry with sensitivities in the order of 10^{-8} M, respectively. Amitraz and 2,4-DMA could be determined in spent cattle dip with negligible interference from the composition of the sample, requiring little in the way of sample pretreatment. Weaker current and reproducibility observed in milk and honey could be attributed to low ionic strength. The viscosity of honey provides interference in that it hinders the free passage of ions to the electrode surface. This suggests that factors such as ionic strength of the buffer introduced could improve analyses in this medium. In our studies we showed that cyclic voltammetry is capable of providing information on both the concentration of amitraz as well as its final breakdown product. Concurring with the findings of Ibrahim et al. [8], electrochemical methods are well-suited for the analysis of amitraz and, as shown in this research, for the analysis of both amitraz and its degradant, 2,4-DMA in the matrix of spent cattle dip. The ability to monitor the toxic 2,4-DMA is also of environmental and health significance.

Acknowledgements

This material is based on work supported by the National Research Foundation (NRF) of South Africa and Rhodes University.

References

[1] J.J. Jiménez, J.L. Bernal, M.J. del Nozal, C. Alonso, Anal. Chim. Acta 524 (2004) 271.
[2] E. Corta, A. Bakkali, L.A. Berrueta, B. Gallo, F. Vicente, Talanta 48 (1999) 189.
[3] J.L. Bernal, M.J. del Nozal, J.J. Jiménez, J. Chromatogr. A 765 (1997) 109.
[4] P.B. Baker, D.R. Woods, J. Appl. Bacteriol. 42 (1977) 187.
[5] C.M. van Eeden, W. Liebenberg, J.L. du Preez, M.M. de Villiers, J. Environ, Sci. Health Part B 39 (2004) 33.
[6] O. Osano, W. Admiraal, H.J.C. Klamer, D. Pastor, E.A.J. Bleeker, Environ. Pollut. 119 (2002) 195.
[7] N.N. Jonsson, D.G. Mayer, P.E. Green, Vet. Parasitol. 88 (2000) 79.
[8] M.S. Ibrahim, M.S. El-Maazawi, K.M. Al-Magboul, M.M. Kamal, Mikrochim. Acta 137 (2001) 215.
[9] A. Martel, S. Zeggane, J. Chromatogr. A 954 (2002) 173.
[10] C. Bolognesi, Mutat. Res. 543 (2003) 251.
[11] A.C. Pierpoint, C.J. Hapeman, A. Torrents, J. Agric. Chem. 45 (1997) 651.
[12] Analytical Methods Committee, Analyst 112 (1987) 199.
[13] M.M. Marques, L.L.G. Mourato, M.T. Amorim, M.A. Santos, W.B. Melchior Jr., F.A. Beland, Chem. Res. Toxicol. 10 (1997) 1266.
[14] T. Mizoguchi, R.N. Adams, J. Am. Chem. Soc. 84 (1962) 2058.
[15] A.A. Athawale, B.A.D. Milind, V. Kulkarni, Mater. Chem. Phys. 60 (1999) 262.
[16] D. Bejan, A. Duca, Croat. Chem. Acta 71 (1998) 745.

Available online at www.sciencedirect.com
ScienceDirect
Talanta 71 (2007) 1387–1392
Talanta
www.elsevier.com/locate/talanta

Evaluation of the antioxidant power of honey, propolis and royal jelly by amperometric flow injection analysis

S. Buratti *, S. Benedetti, M.S. Cosio

Dipartimento di Scienze e Tecnologie Alimentari e Microbiologiche, Università degli Studi di Milano, Via Celoria 2, 20133 Milano, Italy

Received 31 March 2006; received in revised form 15 May 2006; accepted 6 July 2006
Available online 22 August 2006

Abstract

In this paper is described the applicability of a flow injection system, operating with an amperometric detector, for measurement in rapid and simple way the antioxidant power of honey, propolis and royal jelly. The proposed method evaluates the reducing power of selected antioxidant compounds and does not require the use of free radicals or oxidants. Twelve honey, 12 propolis and 4 royal jelly samples of different botanical and geographical origin were evaluated by the electrochemical method and the data were compared with those obtained by the DPPH assay. Since a good correlation was found ($R^2 = 0.92$) the proposed electrochemical method can be successfully employed for the direct, rapid and simple monitoring of the antioxidant power of honeybee products. Furthermore, the total phenolic content of samples was determined by the Folin–Ciocalteau procedure and the characteristic antioxidant activities showed a good correlation with phenolics ($R^2 = 0.96$ for propolis and 0.90 for honey).
© 2006 Elsevier B.V. All rights reserved.

Keywords: Antioxidant power; Honeybee products; Flavonoids; Amperometric detection; Flow injection system

1. Introduction

In recent years there has been a renewed interest in the study of honey and propolis composition and biological properties. The use of honey and propolis in the treatment and prevention of numerous diseases has been documented [1–3]. This beneficial role is partially attributed to honey and propolis antibacterial activity. However, since some of these diseases are a consequence of oxidative damage, it seems that part of the therapeutical properties of honeybee products is due to their antioxidant capacity. Furthermore, honey, as a source of antioxidants, has been proven to be effective against deteriorative oxidation reaction in food [4,5].

Honey and propolis typically contain more than 150 polyphenolic compounds, including flavonoids and cinnamic acid derivatives. It is well known that the chemical properties of phenolic acids or flavonoids, in terms of the availability of the phenolic hydrogens as hydrogen donating radical scavengers, predict their antioxidant properties. Bors [6], by first, proposed three key determinants in the chemical structure of flavonoids: (1) the 3′,4′-dihydroxy catechol configuration on the B ring; (2) the 2,3-double bond in conjugation with the 4-carbonyl group on the C ring; (3) the 3-hydroxy group in combination with the 2,3-double bond. More recently other studies about structure and antioxidant power relationships of flavonoids and phenolic acids were published. In all these works the rule of 3-OH group attached to the 2,3-double bond and adjacent to the 4-carbonyl in C ring was confirmed, and also the importance of the B ring hydroxylation on the antioxidant activity of flavonoids was demonstrated [7–9].

In literature, several studies for the identification and quantification of antioxidant components of honeybee products are reported [10,11]. The studies for the evaluation of the antioxidant capacity of honey and propolis involved the use of different methods such as the ORAC, FRAP and DPPH assays [12,13]. Little information is available on the antioxidant capacity and chemical composition of royal jelly [14].

The principal aim of our work was to develop a simple and rapid method to examine the total antioxidant power of honeybee products. This method is based on the electrochemical behaviour of flavonoids that depends on their chemical structure. In previous works [15–17] we have demonstrated that the electrochemical behaviour of phenolic acids, carotens and xanthophylls can provide a chemical basis for describing their antioxidant

* Corresponding author. Tel.: +39 02 50316623; fax: +39 02 50316632.
E-mail address: susanna.buratti@unimi.it (S. Buratti).

0039-9140/$ – see front matter © 2006 Elsevier B.V. All rights reserved.
doi:10.1016/j.talanta.2006.07.006

functionality and the results obtained on wine, olive oil and vegetables were perfectly in accordance with those obtained by the application of the ABTS radical cation decoloration assay [18].

The proposed method evaluates the overall reducing power of antioxidant compounds present in samples. In despite of other assays, it does not involve reactive species, and can be considered a direct test of the total antioxidant power since it is based only on the chemico-physical properties of antioxidant compounds. This is important since the dependence on free radical or oxidant is one of the major drawbacks of currently used methods.

The proposed method was applied to honey, propolis and royal jelly samples of different botanical and geographical origins, since these factors greatly influence the chemical composition and consequently the antioxidant power of honeybee products. In particular, unifloral honey samples coming from different Italian regions, propolis and royal jelly samples of different nations of origin were considered.

In addition, we investigated whether the variation in antioxidant content among unifloral honey and propolis samples is correlated significantly with their phenolic contents.

2. Experimental

2.1. Reagents

Caffeic acid, *p*-coumaric acid, ferulic acid and DPPH were purchased from Sigma (St. Louis, MO, USA). Isorhamnetin, kaempferol, quercetin, galangin, hesperitin, naringenin were obtained from Extrasynthese (Genay, France); chrysin and pinocembrin from Funakoshi (Tokyo, Japan). All other chemicals were supplied by Sigma.

2.2. Samples

Twelve different Italian unifloral honey samples, four royal jelly samples and six crude propolis samples of specific geographical origins were analysed. All these samples were produced in the same year and were provided by the Istituto Nazionale di Apicoltura (Bologna, Italy). The honey unifloral authenticity was verified in the accredited laboratory of this institute by pollen, organoleptic and chemical analyses. Data were in accordance with the unifloral honey characterization established by the Italian Minister of Agriculture [19]. Other six commercial hydroalcoholic propolis preparations were obtained from local markets. The year of production and the origin of the commercial propolis samples were not known. Samples, once received, were stored at 4 °C until analysis. In Table 1 the list of samples and their geographical and/or botanical origins is reported.

Table 1
List of samples and their geographical and/or botanical origins

	Geographical origin	Botanical origin
Honey		
H1	Sicilia	*Citrus* spp.
H2	Sicilia	*Citrus* spp.
H3	Campania	*Citrus* spp.
H4	Sardegna	*Citrus* spp.
H5	Lombardia	*Rhododendron* spp.
H6	Trentino	*Rhododendron* spp.
H7	Piemonte	*Rhododendron* spp.
H8	Val d'aosta	*Rhododendron* spp.
H9	Toscana	*Rhododendron* spp.
H10	Lombardia	*Robinia pseudoacacia* L.
H11	Lombardia	*Robinia pseudoacacia* L.
H12	Piemonte	*Robinia pseudoacacia* L.
Propolis		
P1	Italy	–
P2	Germany	–
P3	Italy	–
P4	Hungary	–
P5	China	–
P6	China	–
P7[a]	–	–
P8[a]	–	–
P9[a]	–	–
P10[a]	–	–
P11[a]	–	–
P12[a]	–	–
Royal jelly		
RJ1	China	–
RJ2	China	–
RJ3	Italy	–
RJ4	Italy	–

[a] Commercial hydroalcoholic propolis extracts.

2.3. Sample preparation

Before injection in the Flow Injection (FI) system the honeybee products were diluted with methanol as described below:

- honey samples 1:10 (w/v);
- royal jelly samples 1:20 (w/v);
- commercial propolis samples 1:50 (w/v).

After dilution samples were sonicated and centrifugated at 10,000 × *g* for 10 min. One gram of crude propolis samples was extracted with ethanol at room temperature for 24 h. The ethanol solution was filtered through a 0.45 μm filter (Whatman, Maidstone, England) and diluted 1:50 with methanol before injection.

2.4. Electrochemical method

The flow injection apparatus consisted of a Jasco (Tokyo, Japan) model 880 PU pump an EG&G Princeton Applied Research (Princeton, NJ) model thin-layer electrochemical detector equipped with a single glassy carbon electrode operating at a potential of +0.5 V, a reference electrode (Ag/AgCl saturated), and a platinum counter electrode. The connecting tubes were of PEEK (1.5 mm o.d. × 0.5 mm i.d). Data were recorded using a Philips (Eindhover, Netherlands) PM 8252 recorder. Analyses were performed at room temperature using a carrier solution composed of methanol 700 ml l^{-1}, sodium acetate–acetic acid buffer (0.1 M, pH 4.5) 300 ml l^{-1}, sodium perchlorate monohydrate 20 g l^{-1}. A flow rate of 0.7 ml min^{-1} was employed. The FI experiments were performed operating in amperometric mode and the antioxidant power of honeybee products was evaluated by measuring the current resulted from

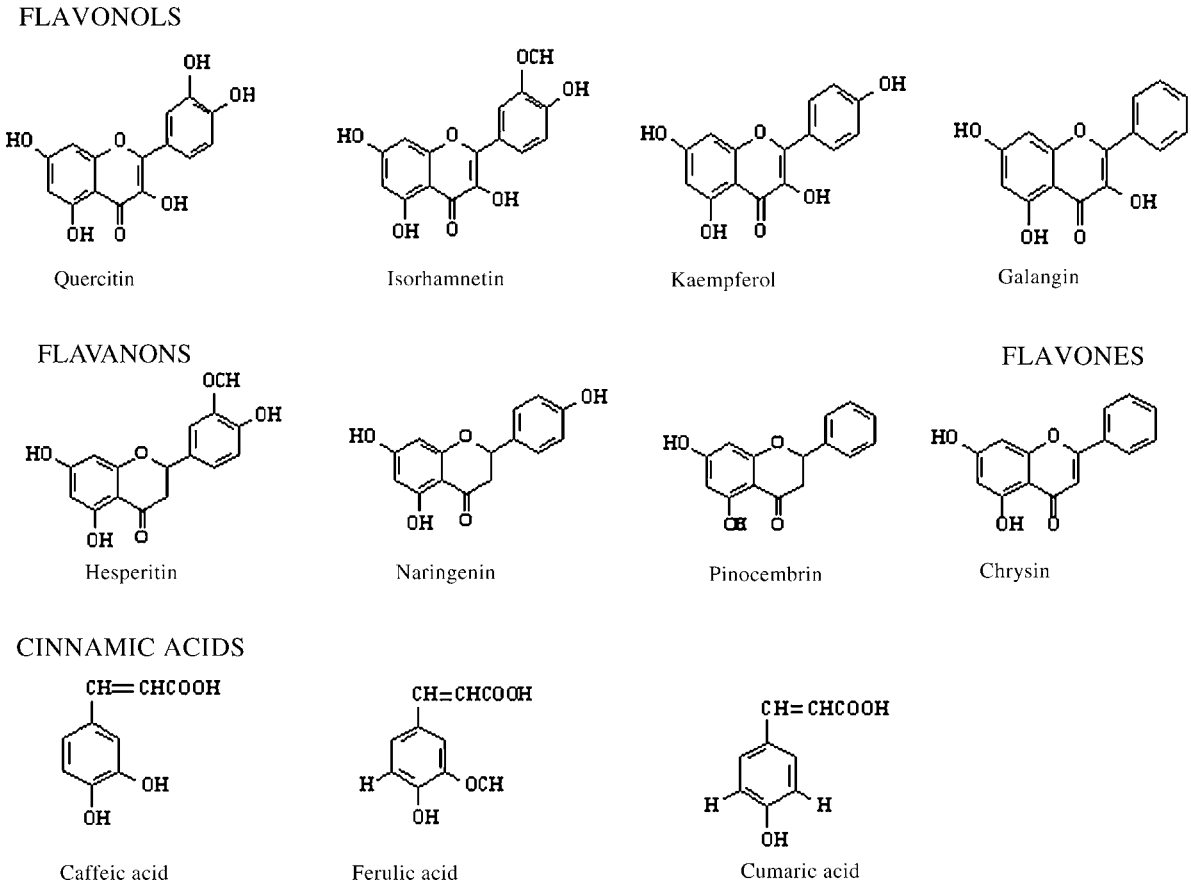


Fig. 1. Chemical structures of flavonoids and cinnamic acids analysed.

the oxidation of electroactive compounds present in the samples, at the established potential of +0.5 V (versus Ag/AgCl). Furthermore, hydrodynamic voltammetric experiments were carried out in order to investigate the electrochemical behaviour of the main phenolic compounds identified in honeybee products. The hydrodynamic voltammograms of these compounds were obtained by running a series of FI experiments in which the potential was increased in the range between +0.2 V and +0.8 V (versus Ag/AgCl) by step of 0.1 V and the current was measured.

2.5. DPPH radical scavenging activity

The antioxidant activity of honey, propolis and royal jelly samples was also evaluated using the DPPH (2,2-diphenyl-1-picrylhydrazyl free radical) assay according to the method of Brand-Williams [20]. Different dilutions of honeybee samples dissolved in methanol were added to 3.9 ml of a 6.1×10^{-5} M DPPH$^{\bullet}$ methanolic solution. The exact initial DPPH$^{\bullet}$ concentration ($C_{DPPH^{\bullet}}$) in the reaction medium was calculated by a calibration curve ($Abs_{515} = 11771 \times (C_{DPPH^{\bullet}}) + 0.01$). The bleaching of DPPH$^{\bullet}$ was monitored at 515 nm (Spectrophotometer Uvidec-610, Jasco, Tokyo, Japan) for 30 min against a blank constituted by the honeybee solution containing all reagents except DPPH$^{\bullet}$. The scavenging activity of the samples on the DPPH$^{\bullet}$ was expressed as IC_{50} (mg ml^{-1}) and was extrapolated from a dose–response curve. All analyses were carried out in triplicate.

2.6. Determination of total phenolics in honey and propolis

Honey and propolis samples were extracted with ethyl acetate, as described by Floris [21]. The total phenolic contents were determined by the Folin–Ciocalteau procedure [22]. Absorbance was read at 760 nm, and phenols were determined using a calibration curve for 0.5 mg kg^{-1}, 1 mg kg^{-1}, 2.5 mg kg^{-1}, 5 mg kg^{-1}, 10 mg kg^{-1} of caffeic acid.

3. Results and discussion

A preliminary study on the electrochemical behaviour of flavonoids and phenolic acids typically present in honeybee products was performed in order to establish the best electrochemical conditions for the evaluation of the total antioxidant power of propolis, honey and royal jelly.

In Fig. 1 the chemical structures of the assayed compounds are reported.

The hydrodynamic voltammetric profile of these compounds (Fig. 2) shows their oxidative behaviour in relation to the established potential. Since the oxidation potential provides an estimate of the energy required to donate an electron, the lowest the oxidation potential the most easily the compound will donate an electron and the highest will be its expected antioxidant power. As it is possible to see at potential lower than +0.5 V (versus Ag/AgCl), only the flavonols and the cin-

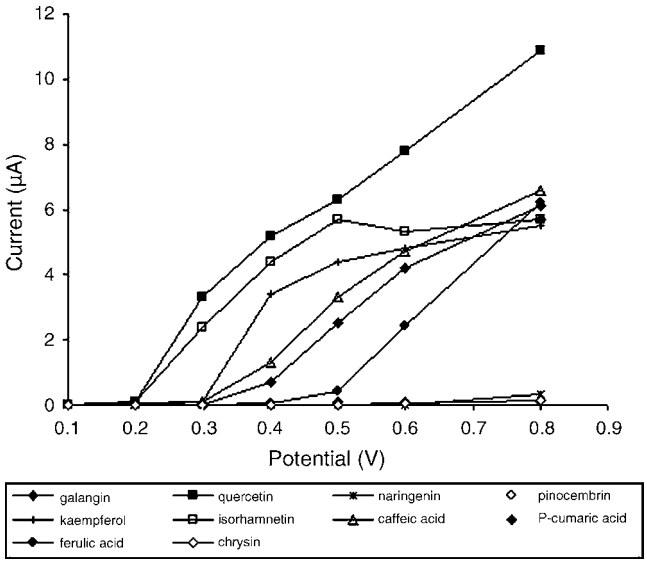


Fig. 2. Hydrodynamic voltammetric profiles of flavonoids and cinnamic acids. *Operative conditions*: standard concentrations, 3.7×10^{-5} mol l^{-1}; flow rate, 0.6 ml min^{-1}; carrier solution—methanol, 700 ml l^{-1}; sodium acetate–acetic acid buffer, 300 ml l^{-1}; sodium perchlorate monohydrate, 20 g l^{-1}; injection volume, 20 μl.

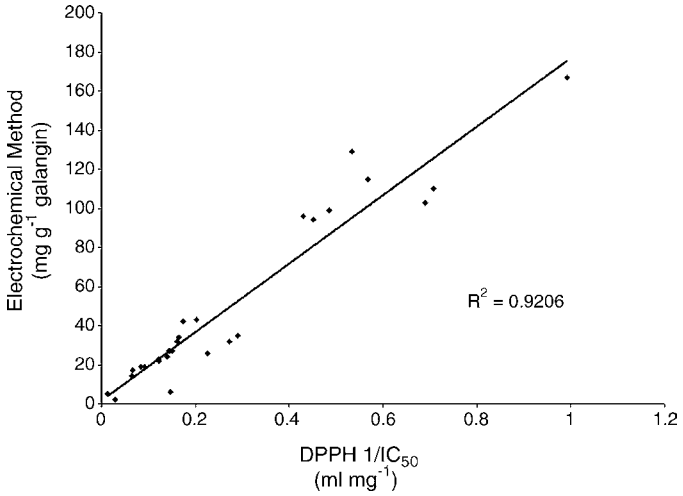


Fig. 3. Linear correlation plot of the DPPH assay ($1/IC_{50}$) and the electrochemical method.

namic acid derivatives can be detected while flavones and flavanons are oxidizable only at potential greater than +0.6 V (versus Ag/AgCl). The potential of +0.5 V appears to be selective to discriminate only the compounds having effective antioxidant power and at this potential the reducing power decreases in order: quercetin > isorhamnetin > kampferol > caffeic acid >

Table 2
Antioxidant power and total phenols content of honeybee samples (average ± *s*) (*n* = 3)

	Electrochemical method (mg g^{-1} galangin)	DPPH method IC_{50} (mg ml^{-1})	Total phenols (mg 100 g^{-1} caffeic acid)
Honey			
H1	17 ± 1	15.1 ± 0.4	20.4 ± 0.5
H2	27 ± 1	6.9 ± 0.4	29.2 ± 0.9
H3	43 ± 3	5.0 ± 0.3	60 ± 1
H4	19 ± 1	11.0 ± 0.4	24.7 ± 0.9
H5	34 ± 2	6.1 ± 0.5	38 ± 2
H6	24 ± 4	7.1 ± 0.5	31.2 ± 0.9
H7	42 ± 3	5.7 ± 0.3	56 ± 1
H8	32 ± 2	6.2 ± 0.3	37 ± 1
H9	14 ± 1	15.5 ± 0.8	17.1 ± 0.7
H10	23 ± 3	8 ± 1	36.8 ± 0.7
H11	19 ± 1	12.0 ± 0.6	20.9 ± 0.4
H12	22 ± 1	8 ± 1	30.8 ± 0.9
Propolis			
P1	167 ± 5	1.0 ± 0.1	181 ± 4
P2	103 ± 3	1.5 ± 0.1	105 ± 3
P3	99 ± 2	2.1 ± 0.2	108 ± 3
P4	115 ± 3	1.8 ± 0.1	114 ± 3
P5	94 ± 2	2.2 ± 0.1	99 ± 3
P6	27 ± 0.3	6.6 ± 0.5	29.0 ± 0.6
P7[a]	129 ± 3	1.9 ± 0.1	170 ± 3
P8[a]	35 ± 1	3.4 ± 0.2	55.0 ± 0.6
P9[a]	2 ± 0.1	36 ± 1	2.0 ± 0.1
P10[a]	26 ± 0.4	4.4 ± 0.4	45 ± 1
P11[a]	6 ± 0.3	6.8 ± 0.1	7.6 ± 0.1
P12[a]	5 ± 0.3	79 ± 2	7.3 ± 0.1
Royal jelly			
RJ1	32 ± 1	3.7 ± 0.2	–
RJ2	27 ± 1	7.0 ± 0.5	–
RJ3	110 ± 3	1.4 ± 0.1	–
RJ4	96 ± 2	2.3 ± 0.2	–

[a] Commercial hydroalcoholic propolis extract.

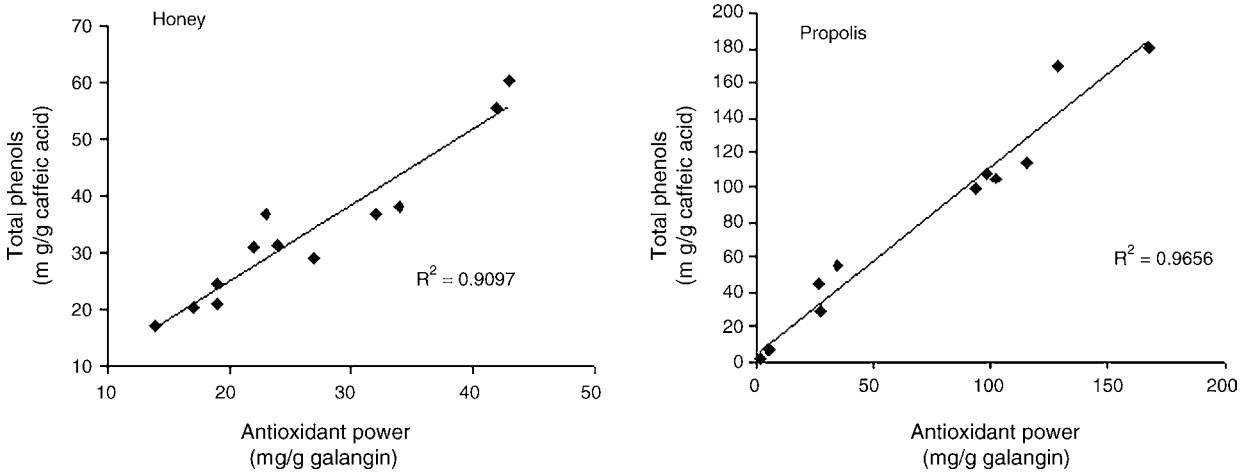


Fig. 4. Linear correlation plots of antioxidant power of propolis and honey vs. total phenols.

galangin > ferulic acid > *p*-cumaric acid. Hesperetin, naringenin, chrysin and pinocembrin are not revealed and presumably they have very little or no antioxidant effect. As it is possible to notice flavonols show a reducing power higher than flavons and flavanons. These results are in accordance with other works [23,24] and are explained by their chemical structures.

Among the cinnamic acid derivatives caffeic acid shows an antioxidant power stronger than ferulic acid and *p*-cumaric acid. The same result has been obtained in other works in which the hydrocinnamates were screened for their radical scavenger activity [25].

On the basis of these preliminary results, a FI system with electrochemical detector operating at a potential of +0.5 V (versus Ag/AgCl) was used for the determination of the antioxidant power of honeybee products.

The antioxidant power was quantified using galangin as reference. Quantification was based on peak height. The amperometric detection resulted in well-defined linear concentration dependence in a range between 1 mg l^{-1} and 10 mg l^{-1} of galangin. The relative standard deviation at the concentration level of 5 mg l^{-1} was 2.5% ($n = 15$) and the estimated detection limit, calculated in accordance to Miller and Miller [26], was 0.15 mg l^{-1}.

Several samples of honey, propolis and royal jelly were analysed by the proposed procedure and the results were expressed as mg g^{-1} galangin equivalent. The same samples were also analysed by the DPPH assay and their total phenolic content was determined by the Folin–Ciocalteau procedure.

In Table 2 the total phenolic content and the antioxidant power of the honeybee products evaluated by the electrochemical method and by the DPPH assay are reported. The data obtained by the proposed method were substantially confirmed by the DPPH assay since a good correlation ($R^2 = 0.92$) was observed between the two methods (Fig. 3).

Considering the data obtained by the electrochemical method it can be notice that there is a great variation in the antioxidant power among the investigated honeybee products. In particular the antioxidant power of propolis samples varies from 2 mg g^{-1} to 169 mg g^{-1} galangin equivalent, crude propolis samples exhibit an antioxidant power higher than commercial hydroalcoholic propolis preparations except for sample P7. The two Chinese propolis have an antioxidant power lower than Italian and German samples.

The antioxidant power of honey samples varies from 14 mg g^{-1} to 43 mg g^{-1}. Except for a *Citrus* sample (H3), *Rhododendron* samples (H5–H8) exhibit the highest antioxidant power while *Robinia* (H9–H12) the lowest. The variation in the antioxidant power among unifloral honeys with different geographical origin can be due to climate and environmental factors such as humidity, temperature and soil composition.

The antioxidant power of the two Italian royal jelly appears to be higher than the two Chinese samples.

Total phenolic content ranges from 2.0 mg g^{-1} to 181.0 mg g^{-1} caffeic acid equivalent for propolis, and from 17.1 mg g^{-1} to 60.3 mg g^{-1} for honey.

Regression analysis between antioxidant power and total phenols content shows a linear correlation (Fig. 4). Coefficients of $R^2 = 0.96$ and 0.90 have been obtained for propolis and honey, respectively. These results suggest that the antioxidant power of propolis and honey samples is especially due to phenolic compounds that are the major constituents having reducing power. The antioxidant power of honey probably can be related also to other reducing agents present at low concentration and not revealed by the Folin–Ciocalteau procedure.

4. Conclusion

The results suggest that the electrochemical method can be successfully used for monitoring the antioxidant power of honeybee products. With respect to the other reported methods, the proposed offers significance improvement since it is rapid (60 determinations h^{-1}), simple and does not require the use of free radicals or oxidants since it evaluates the overall reducing power of antioxidant compounds present in the sample. Furthermore, the data collected demonstrate that within the honeybee products the crude propolis has the highest antioxidant power followed by royal jelly and honey. Among honey samples, *Rhododendron* exhibits the highest antioxidant power; among commercial propolis there is a great variation in the

antioxidant power probably due to conditioning and storage time.

References

[1] M.C. Marcucci, Apidologie 26 (1995) 83.
[2] S. Castaldo, F. Capasso, Fitoterapia 73 (2002) S1.
[3] P.C. Molan, Bee World 80 (1999) 80.
[4] J. McKibben, N.J. Engeseth, J. Agric. Food Chem. 50 (2002) 592.
[5] M.R. McLellan, R.W. Kime, C.Y. Lee, T.M. Long, Food Process. Preserv. 19 (1995) 1.
[6] W. Bors, W. Heller, C. Michel, M. Saran, Methods Enzymol. 186 (1990) 343.
[7] C.A. Rice-Evans, N.J. Miller, G. Paganga, Free Radic. Biol. Med. 20 (1996) 933.
[8] H.L. Madsen, C.M. Andersen, L.V. Jorgensen, L.H. Skibsted, Eur. Food Res. Technol. 211 (2000) 240.
[9] M. Foti, M. Piattelli, M.T. Baratta, G. Ruberto, J. Agric. Food Chem. 44 (1996) 497.
[10] N. Gheldof, X.H. Wang, N.J. Engeseth, J. Agric. Food Chem. 50 (2002) 5870.
[11] J.S. Bonvehí, M.S. Torrentó, E.C. Lorente, J. Agric. Food Chem. 49 (2001) 1848.
[12] A.M. Aljadi, M.Y. Kammaruddin, Food Chem. 85 (2004) 513.
[13] S. Kumazawa, T. Hamasaka, T. Nakayama, Food Chem. 84 (2004) 329.
[14] T. Nagai, M. Sakai, R. Inoue, H. Inoue, N. Suzuki, Food Chem. 75 (2001) 237.
[15] S. Mannino, O. Brenna, S. Buratti, M.S. Cosio, Electroanalysis 10 (1998) 908.
[16] S. Mannino, S. Buratti, M.S. Cosio, N. Pellegrini, Analyst 124 (1999) 1115.
[17] S. Buratti, N. Pellegrini, O. Brenna, S. Mannino, J. Agric. Food Chem. 49 (2001) 5136.
[18] N. Pellegrini, R. Re, M. Yang, C. Rice-Evans, Methods Enzymol. 299 (1999) 379.
[19] L. Persano Oddo, A.G. Sabatini, M. Accorti, R. Colombo, G.L. Marcazzan, M.L. Piana, M.G. Piazza, P. Pulcini, I Mieli Uniflorali Italiani-Nuove Schede di Caratterizzazione, Ministero delle Politiche Agricole e Forestali, Tipografia Benedettucci Carlo, 2000.
[20] W. Brand-William, M.E. Cuvelier, C. Berset, Lebensm. Wiss. U-Technol. 28 (1995) 25.
[21] I. Floris, V. Vacca, M.A. Franco, A. Del Caro, P.M. Marras, F. Reniero, Apicoltura 9 (1994) 119.
[22] K. Slinkard, V.L. Singleton, Am. J. Enol. Vitic. 28 (1977) 49.
[23] S. Burda, W. Oleszek, J. Agric. Food Chem. 49 (2001) 2774.
[24] G. Cao, E. Sofic, R.L. Prior, Free Radic. Biol. Med. 22 (1997) 749.
[25] M.E. Cuvelier, H. Richard, C. Berset, Biosci. Biotechnol. Biochem. 56 (1992) 324.
[26] C. Miller, J.N. Miller, Statistics for Analytical Chemistry, Ellis Horwood Limited, Chichester, UK, 1991.

Available online at www.sciencedirect.com
ScienceDirect
Talanta 71 (2007) 1444–1448
Talanta
www.elsevier.com/locate/talanta

Short communication

A new analytical approach for humin determination in sediments and soils

N. Calace *, B.M. Petronio, S. Persia, M. Pietroletti, D. Pacioni

Department of Chemistry, University "La Sapienza", P.le A. Moro 5, 00185 Rome, Italy

Received 17 March 2006; received in revised form 15 May 2006; accepted 30 June 2006
Available online 14 August 2006

Abstract

In this work a new analytical approach is proposed for the recovery of humin present in soil and sediments. The procedure is based on microwave oven treatment for humin deashing. In this way both the treatment time and the concentration of the HCl/HF mixture are significantly reduced (minutes rather than hours, 10% rather than concentrated). By means of the proposed scheme organic matter present in sediment and soil samples can be subdivided into the different fractions (hydrophobic and hydrophilic compounds, fulvic and humic acids, humin) making up the balance of organic carbon. Results obtained for samples characterised by different organic carbon content showed a loss of carbon ranging between 20% and 30%, consistent with previous reports about humin deashing.
© 2006 Elsevier B.V. All rights reserved.

Keywords: Humin; Separation; Microwave oven

1. Introduction

Natural organic carbon can be divided up into labile forms, subjected to bioassimilation and biotransformation, and non-labile forms. Since labile forms are subject to microbial attack, it is more likely that refractory materials, present in uncharacterised organic matter pool, are buried. The study of factors that control organic matter burial and preservation in sediments and soils has led to the development of several techniques to characterise bulk organic matter [1–3]. Nevertheless knowledge in this field is not exhaustive, and so quantifying and structurally elucidating the uncharacterised organic matter pool remains one of the greatest challenges in marine and terrestrial organic geochemistry today.

Humic substances represent a fraction of this uncharacterised organic matter pool and consist of a complex mixture of molecules whose molecular weight varies from 0.5 to 300 kDa. They can be subdivided into three categories that are operationally defined and based upon their solubility in water: (a) fulvic acids, tend to be smaller in molecular weight, soluble in water at all pHs; (b) humic acids are larger and often colloidal, insoluble at pHs lower than two; (c) humin, the highest in molecular weight and carbon content, is strongly associated with the mineral matrix and insoluble at any pH. Humic and fulvic acids are subjected to chemical transformations whereas humin is highly refractory.

As a consequence of humin insolubility, the physical and chemical nature of humin is the least understood of the three fractions. Moreover, it is known that humin includes unaltered and less-altered biopolymers such as lignin and polysaccharides [4], mineral-bound lipids and humic acid-like materials [5], kerogen and black carbon [6]. It also contains acid-hydrolysable structure segments, carbohydrates, proteins and esters that can be removed by acid treatment [7].

By definition, humin consists of the solid residue that remains after centrifugation of the alkali extract of the sample. To separate humin from the inorganic matrix (mainly clays and oxides) the residue is generally subjected to deashing. The ideal treatment should be capable of dissolving a substantial proportion of the mineral matrix without significantly altering the chemical structure of organic compounds.

Durand and Nicaise [8] carried out the demineralisation process with a concentrated HCl/HF mixture, but in this case a loss of organic matter was observed. Consequently, the HF concentration was reduced (10%), increasing the number of treatments, depending on organic matter concentration [9,10]. Generally six treatments were found to be enough. Using 15% HF the loss of organic matter increased [11]. The number of extractions can be reduced by increasing the extraction time. Two treatments with HF 10% at room temperature for 12 h are

* Corresponding author. Tel.: +39 0649913723; fax: +39 0649913723.
E-mail address: nicoletta.calace@uniroma1.it (N. Calace).

0039-9140/$ – see front matter © 2006 Elsevier B.V. All rights reserved.
doi:10.1016/j.talanta.2006.06.040

generally sufficient, while three extractions are necessary for samples with low organic carbon content and high concentration of hard oxide minerals [11,12]. Silicates were also eliminated by dissolution in hot HCl/HF mixture: at 70 °C for 24 h [13] and at 60 °C for 20 h [6].

For the above treatments the loss of organic matter ranges from 5% to 20.5%. Often subsequent treatment with HCl 6 M is carried out to hydrolyse labile biopolymers not removed by HF/HCl [14] and to remove CaF_2 formed during the demineralisation procedure [6].

Mineral residues are also separated from organic matter by HCl (10%) and HF (70%) mixture shacking, centrifuging, ultrasonic vibration and $ZnBr_2$ floatation [15]. Densimetric separation after exhaustive treatments with concentrated HF/HCl was also employed by Augris et al. [16]. It should be noted that all the above reported procedures are characterised by a significant number of extractions and long extraction times.

In recent years there has been growing interest in the use of microwave heating in analytical chemistry. Microwave-assisted acid solubilisation is a highly suitable method for the digestion of complex matrices such as soil and sediments. Operationally, the procedure allows shorter digestion times and needs smaller quantities of acids, and so a number of potential applications of microwave processing have been investigated. These include microwave-assisted ore grinding, microwave assisted reduction of metal oxides, microwave assisted drying and anhydration; microwave assisted mineral leaching, etc. [17–23].

In this paper we propose a new procedure in which a microwave energy is employed for the digestion of the inorganic fraction present in the matrix alone. In particular the HF/HCl treatment for humin deashing [15] was carried out in a microwave oven. In this way treatment time lasts minutes rather than hours.

Finally, sediment and soil samples were analysed according to the fractionation scheme proposed by us, making up the balance of organic carbon. The scheme allows subdivision into different fractions of organic compounds present both in sediments and in soils. In particular hydrophobic and hydrophilic compounds, fulvic and humic acids, and humin are separated [24–30].

2. Experimental

2.1. Materials

Marine sediments were taken from cores sampled in the Ross Sea (Antarctica). Antarctic sediments are characterised by a high silica content due to the presence of siliceous diatoms and silicoflagellates, and a low organic carbon content, prevalently associated with minerals. In particular, the superficial layer of a core characterised by non-transformed biogenic silica and soluble in basic medium (sediment 1) was used, and two lower layers of other cores in which siliceous minerals prevail (sediments 2 and 3). Sediment 1 (74°00′S, 174°48′E), located in the centre of the northern part of the Joides Basin at a depth of 582 m, represents a setting characterised by high biosiliceous sediment accumulation. Sediment 2 (75°54′S, 177°34′E), was collected at a depth of 628 m in an area near the continental shelf break in a central Ross Sea basin and sediment 3 (75°04′S, 164°138′E), located in the western Ross Sea at a depth of 950 m, was collected in an area representative of an environment with high energy and reworked sediments. A soil sample collected in an agricultural area located near Rome was also analysed.

2.2. Methodology for sediment and soil characterisation

A Labconco 77400 lyophiliser (Labconco, Kansas City, MO) was used for sample lyophilisation.

Grain size composition was obtained using common sieving methods (Table 1). Total organic carbon (TOC) content was determined with a Carlo Erba EA11110 CHNS-O Element Analyser (Carlo Erba, Milan, Italy). A 100 mg aliquot of dried sediment was acidified with 500 μl of concentrated HCl (Merck, Germany) in order to eliminate the carbonate fraction, then freeze-dried and re-weighed. The freeze-dried residue was then analysed for TOC. The measurements were repeated six times and the relative standard deviations were less than 5%. Carbonate content was determined as difference between the total carbon content of sample, determined with elemental analyser, and TOC.

2.3. Methodology for humin deashing

Humin deashing optimisation was carried out using 8.0 g aliquots of lyophilised sediment 3 (Table 1) after extraction of soluble organic fractions (hydrophobic, hydrophilic, humic and fulvic fractions). The total organic carbon remaining in the insoluble residue was 2.0 ± 0.12 mg g^{-1}. The decision to optimise the humin deashing procedure with sediment 3 was due to the low organic carbon and high silicates content.

The insoluble residue was treated with 50 ml of a 1 N HCl and 10% HF (v/v) solution in a microwave oven (10 min at 30 W power, 12 min at 80 W). The maximum temperature reached in the vessels was 70 °C. In order to test this procedure, the humin deashing methodology based on HF/HCl solution maintained at room temperature for 24 h [15], was also performed.

In order to eliminate the minerals associated with the humin fraction as far as possible, a further step based on densimetric separation was performed [31]. The residue was thus treated:

(1) with $ZnCl_2$ solution in order to separate humin (lighter fraction) from residual minerals. The $ZnCl_2$ treatment (10 ml

Table 1
Grain size composition of sediments and soil samples

% of	Sediment 1	Sediment 2	Sediment 3	Soil
Coarse sand	0	3.5	10.1	18.0
Fine sand	32.6	50.5	36.7	34.4
Silt	0	0	0	25.0
Clay	67.4	46.5	52.3	22.6
Carbonate	0	0	0	n.d.
Total organic carbon	0.89	0.54	0.36	4.9
Total nitrogen	0.13	<0.1	<0.1	0.48

solution) was repeated as long as the light fraction was present. The organic fraction was precipitated by diluting the $ZnCl_2$ solution with distilled water;

(2) with $ZnCl_2$ solution. The organic fraction precipitated by diluting the $ZnCl_2$ solution with distilled water was then separated and treated three times with HCl 6 M (each time 10 ml);

(3) three times with HCl 6 M (each time 10 ml), then the residue was treated with $ZnCl_2$ ($d = 2\ g\ cm^{-3}$) solution.

The humin (Hm) obtained as precipitate from (1) to (3) was dried under vacuum at 100 °C and then analysed for organic carbon content.

The water used for rinsing and dilution was organic-free UV-oxidised water dispensed by a Milli-Q Gradient A10 instrument from (Millipore, Bedford, MA). Glassware was cleaned by soaking in a 10% HNO_3 bath for 24 h, rinsing thoroughly with water and muffling at 350 °C for 3 h. All reagents were analytical grade.

2.4. Fractionation of organic carbon

Fractionation of organic carbon was carried out according to the following procedure:

(1) To obtain the hydrophobic (Hb) fraction, lyophilised sediment (ca. 10 g) was extracted for 24 h at room temperature with a CH_2Cl_2/CH_3OH (2:1, v/v) mixture in a 1:5 (w/v) solid/liquid ratio. Two consecutive extractions of 24 h were carried out in a continuous rotating agitator. After centrifugation for 30 min at 4000 rpm, the supernatants were dried at 60 °C in a crucible under vacuum in a desiccator, previously brought to constant weight in a desiccator at 100 °C, and then weighed. The organic carbon content of the Hb fraction was determined by elemental analysis.

(2) To obtain the hydrophilic (Hp) fraction, the residual sediment was treated with 90 ml of a 0.5 N HCl solution for 24 h in a continuous rotating agitator and, after centrifugation for 30 min at 2000 rpm, the acid solution was made up to a volume of 100 ml with distilled water. Aliquots of 20 ml were dried under vacuum in a desiccator at 60 °C in a pre-weighed crucible.

(3) To obtain humic materials the residual sediment was treated with 90 ml of a 0.5 N NaOH solution for 24 h in a continuous rotating agitator. After centrifugation for 30 min at 2000 rpm, the alkaline supernatant, containing humic and fulvic acids, was acidified at pH 1 by dropwise addition of concentrated HCl in order to separate acid-soluble fulvic acids (FA) from precipitating humic acids (HA).

Both acid (step 2) and alkaline extractions (step 3) were alternatively repeated on residual sediment until the alkaline solution was colourless. The organic carbon content of the Hp fraction was determined by elemental analysis and only the first 20 ml aliquot yielded a detectable organic carbon content. In the case of humic substance extraction all the alkaline solutions were mixed. Humic acids, precipitated after acidification to pH 1 of the alkaline solution, were separated, suspended in deionised water and purified by dialysis against deionised water using tubular membranes (Spectra/Por®, Spectrum Laboratories Inc., Rancho Dominguez, CA) with a molecular weight size of 1000 Da. They were then freeze-dried and analysed for organic carbon content by elemental analysis. Fulvic acids remaining in solution after acidification at pH 1 were purified using an Amicon stirred ultrafiltration cell, model 8400 (Millipore, Milan, Italy) fitted at the bottom with a 500 Da membrane disc.

(4) To obtain the humin (Hm) fraction the residual sediment was treated twice with 50 ml of a 1 N HCl and 10% HF (v/v) solution in a microwave oven (10 min at 30 W power, 12 min at 80 W). The residue was then treated with $ZnCl_2$ solution and humin (light fraction $d < 2\ g\ cm^{-3}$) was separated from mineral residue (heavy fraction $d > 2\ g\ cm^{-3}$). The Hm fraction was then treated three times with 6 M HCl (each time 10 ml at room temperature), rinsed with distilled water and dried under vacuum at 100 °C. The organic carbon content of the humin fraction was determined by elemental analysis.

3. Results and discussion

3.1. Humin deashing

The results for the solid/liquid ratio needed for humin deashing are presented in Fig. 1. Results highlighted that the liquid amount used for humin deashing did not influence the yield of the treatment. For this reason we chose to use a solid/liquid ratio of 1:5 (w/v).

The time and power values for microwave oven operation were selected so as to reach the maximum temperature of 70 °C in the vessels. This temperature was chosen to take into account that the addition of the HF/HCl solution to sediment would increase the temperature in the mixture up to 70 °C due to the exothermic reaction of silicate dissolution and so that the temperature value would not exceed 70 °C in order to prevent the possible oxidation of organic compounds [32].

Fig. 2 shows the deashing results obtained from the microwave oven treatment. After two treatments with 50 ml of a 1 N HCl and 10% HF (v/v) solution in a microwave oven,

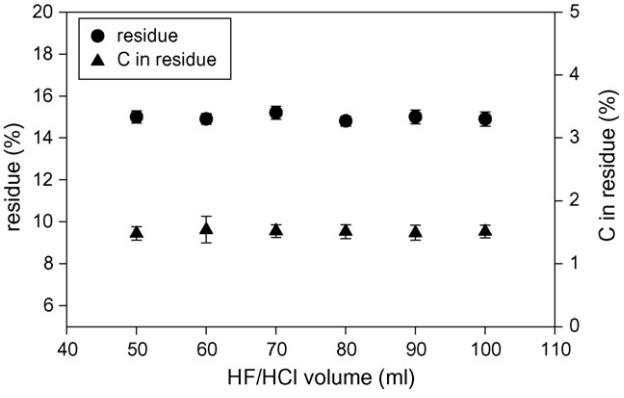


Fig. 1. Residue percentage vs. the liquid amount used for humin deashing.

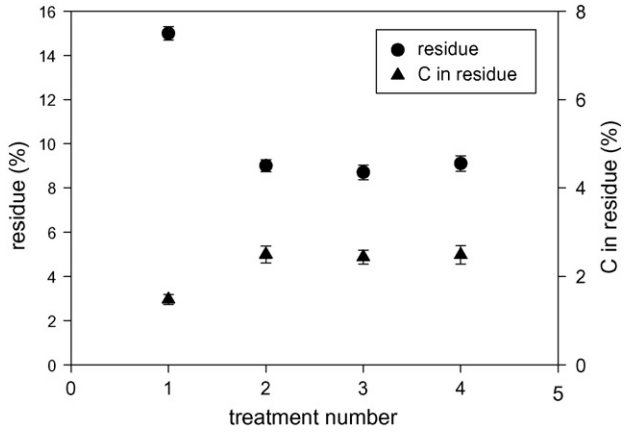


Fig. 2. The residue percentage and the carbon percentage as function of the number of treatments with HF/HCl solution in microwave oven.

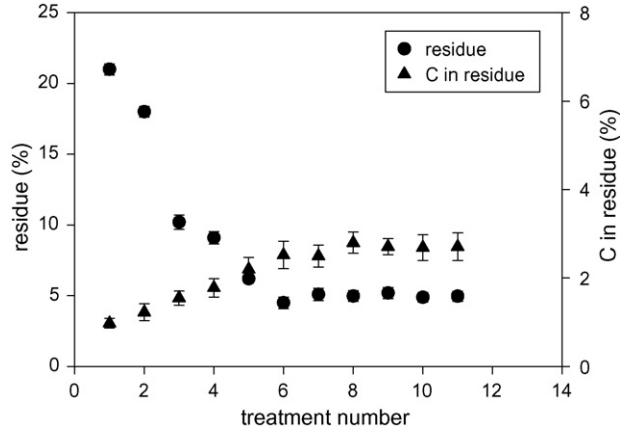


Fig. 3. The residue percentage and the carbon percentage as function of the number of treatments with HF/HCl solution at room temperature.

the residue and the carbon percentage (9% and 2.2%, respectively) of the insoluble residue did not change. The calculated amount of organic carbon of the humin fraction was about $1.5 \pm 0.064\ mg\ g^{-1}$, which accounts for 75% of the total organic carbon content of the sample (2.00 ± 0.12).

On the other hand, the residue and carbon percentage of the residue obtained by treatments with HF/HCl solution at room temperature reached a plateaux after six treatments (Fig. 3). The residue and carbon percentage of the residue were 5% and 2.8%, respectively, which correspond to a humin carbon amount of $1.1 \pm 0.042\ mg\ g^{-1}$. Results obtained from two procedures do not show any significant differences (95% at the confidence level) in humin deashing yield but comparing the results of the two procedures it is evident that the employment

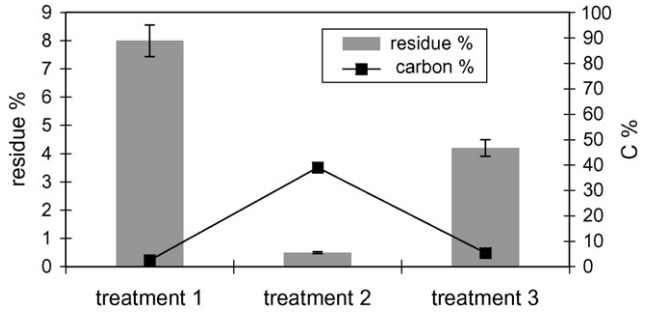


Fig. 4. The residue percentage and the carbon percentage after densimetric separation according to treatment 1 ($ZnCl_2$), treatment 2 (HCl before $ZnCl_2$) and treatment 3 (HCl after $ZnCl_2$).

of the microwave oven merely speeds up the dissolution of the mineral matrix.

However, even if the amount of recovered humin carbon is higher, the carbon percentage of the residue is also low (~2.2%), indicating a strong presence of the mineral fraction. Consequently, to increase the purification level a further step was taken, based on a densimetric separation of organic and inorganic fractions and on treatment with HCl 6 M to remove the CaF_2 formed during the demineralisation process.

With densimetric separation alone no increase in carbon percentage is observed, while carbon percentage significantly increases when HCl is employed (Fig. 4). The best results are obtained with the procedure (2), performing HCl treatment after densimetric separation.

The amount of calculated organic carbon was practically the same ($1.4 \pm 0.18\ mg\ g^{-1}$) for the procedures (1)–(3) and was the same as that calculated after microwave deashing treatments. This finding showed that the different treatments take effect only on the mineral fraction and that the recovery percentage of humin organic carbon depends mainly on microwave assisted acid treatment.

3.2. Organic carbon fractionation procedure

Results obtained by the organic carbon fractionation (Table 2) on matrices characterised by different organic carbon content showed a loss of carbon ranging between 20% and 30%, this is consistent with previous reports by several researchers for humin deashing [6,8,11,13]. A large part of the carbon loss is due to the humin deashing step. As a result, elemental carbon analysis of all the samples studied were carried out soon after the alkaline extraction and before the humin deashing treatment (Table 3) and results show that the loss of carbon after humic substance extraction is negligible.

Table 2
Total organic carbon and carbon amount in the different fractions

	TOC ($mg\ g^{-1}$)	Hb ($mg\ g^{-1}$)	Hp ($mg\ g^{-1}$)	HA ($mg\ g^{-1}$)	FA ($mg\ g^{-1}$)	Hm ($mg\ g^{-1}$)	C loss (%)
Sediment 1	8.9 ± 0.3	0.170 ± 0.008	0.16 ± 0.01	1.5 ± 0.1	4.0 ± 0.4	0.64 ± 0.09	28 ± 10
Sediment 2	5.4 ± 0.4	0.080 ± 0.005	0.11 ± 0.01	0.75 ± 0.06	2.1 ± 0.4	0.71 ± 0.09	31 ± 18
Sediment 3	3.6 ± 0.4	0.070 ± 0.004	0.11 ± 0.01	0.45 ± 0.03	0.9 ± 0.3	1.4 ± 0.2	19 ± 25
Soil	48.9 ± 0.2	0.26 ± 0.01	0.42 ± 0.01	8.6 ± 0.1	16.7 ± 0.5	12.3 ± 0.3	22 ± 2

Table 3
Total organic carbon, organic carbon before humin deashing and after alkaline treatments, and organic carbon as the sum of the fractions before humin deashing

	TOC	OC_{after}	$TOC - OC_{after}$	OC Hb + Hp + FA + HA
Sediment 1	8.9 ± 0.3	2.9 ± 0.1	6.0 ± 0.4	5.8 ± 0.5
Sediment 2	5.4 ± 0.4	2.8 ± 0.2	2.6 ± 0.6	3.0 ± 0.5
Sediment 3	3.6 ± 0.4	2.0 ± 0.1	1.6 ± 0.5	1.5 ± 0.4
Soil	48.9 ± 0.2	26.1 ± 0.5	22.8 ± 0.7	26 ± 1

It should be considered that during the humin deashing procedure, some hydrolysable fragments of organic compounds could be solubilised. Moreover, organic molecules strictly bound to mineral matrix can be solubilised following dissolution of the inorganic matrix, which eliminates their protective support and so may release organic compounds into solution. Some researchers [33,34] have pointed out that the potential for alteration and losses is particularly significant for 'immature' organic matter in aquatic environments such as that found in surface sediments, which are usually younger than deep sediments. Indeed the trend in the organic carbon losses was found to be related to the age of sediments (samples 1 and 2 are much younger than sediment 3) although tests were performed on only a few samples.

4. Conclusion

The results obtained with the approach proposed for the solubilisation of the inorganic matrix of sediments and soils show that microwave-assisted deashing is a viable alternative to traditional systems. The deashing procedure, based on the use of a microwave energy, makes the dissolution process faster and the treatment time is significantly reduced from hours to minutes.

The fractionation scheme proposed could be applied also to samples in which organic carbon content is low. The balance of organic carbon shows that a large part of the carbon loss is due to the humin deashing step. Carbon loss, does not differ from the values reported by certain authors, cannot be ascribed to the use of the microwave oven and can probably be ascribed to hydrolysis processes related to the HF/HCl mixture.

Acknowledgement

This work was funded by the Italian National Research Programme for Antarctica (PNRA), Sector 9: Chimica degli ambienti polari. Research Project 2004/9.1.

References

[1] R.G. Keil, F.S. Hu, E.C. Tsamakis, J.I. Hedges, Nature 369 (1994) 639.
[2] S.G. Wakeham, C. Lee, J.I. Hedges, P.J. Hernes, M.L. Peterson, Geochim. Cosmochim. Acta 61 (1997) 5363.
[3] J.I. Hedges, F.S. Hu, A.H. Devol, H.E. Hartnett, R.G. Keil, Am. J. Sci. 299 (1999) 529.
[4] P.G. Hatcher, I.A. Breger, G.E. Maciel, N.M. Szeverenyi, in: G.R. Aiken, D.M. McKenight, R.L. Wershaw, P. MacCarty (Eds.), Humic Substances in Soil, Sediment and Water. Geochemistry, Isolation and Characterisation, John Wiley & Sons, New York, 1985, pp. 275–302.
[5] J. Rice, P. MacCarthy, Environ. Sci. Technol. 24 (1990) 1875.
[6] J. Song, P. Peng, W. Huang, Environ. Sci. Technol. 36 (2002) 3960.
[7] M.H. Engel, S.A. Macko, Organic Geochemistry: Principles and Applications, Plenum Press, New York, 1993.
[8] B. Durand, G. Nicaise, in: B. Durand (Ed.), Procedures for Kerogen Isolation, Kerogen. Techniq, Paris, 1980, pp. 35–53 (Chapter 2).
[9] C.M. Preston, R.H. Newman, Geoderma 68 (1995) 229.
[10] J.O. Skjemstad, P. Clarke, J.A. Tailor, J.M. Oades, R.H. Newman, Aust. J. Soil Res. 32 (1994) 1215.
[11] Y. Gelinas, J.A. Baldock, J.I. Hedges, Org. Geochem. 32 (2001) 677.
[12] M.W.I. Schmidt, H. Knicker, P.G. Hatcher, I. Kögel-Knabner, Eur. J. Soil Sci. 48 (1997) 319.
[13] M. Khaddor, M. Ziyad, J. Joffre, A. Ambles, Chem. Geol. 186 (2002) 17.
[14] H. Knicker, J.C. del Rio, P.G. Hatcher, R.D. Minard, Org. Geochem. 32 (2001) 397.
[15] H.K. Karapanagioti, J. Childs, D.A. Sabatini, Environ. Sci. Technol. 35 (2001) 4684.
[16] N. Augris, J. Balesdent, A. Mariotti, S. Derenne, C. Largeau, Org. Geochem. 28 (1998) 119.
[17] A. Abu-Sambra, J.S. Morris, S.R. Koirtyohann, Anal. Chem. 47 (1975) 1475.
[18] H.M. Kingston, L.B. Jassei, Introduction to Microwave Sample Preparation: Theory and Practice, 1st ed., American Chemical Society, Washington, DC, 1988.
[19] H. Matusiewicz, R.E. Sturgeon, Prog. Anal. Spectrosc. 12 (1989) 21.
[20] M.H. Feinberg, Analysis 19 (1991) 47.
[21] H.M. Kingston, S.J. Haswell, Microwave-enhanced Chemistry, Fundamentals, Sample Preparation and Applications, American Chemical Society, Washington, DC, 1997.
[22] S.M. Bradshaw, E.J. Vanwyk, J.B. Deswaedt, J. Microw. Power Electromag. Energy 32 (1997) 131.
[23] M.F. Diprose, Plant Soil 229 (2001) 271.
[24] M.Y. Sun, S.G. Wakeham, C. Lee, Geochim. Cosmochim. Acta 61 (1997) 341.
[25] E.M. Thurman, R.L. Malcolm, Environ. Sci. Technol. 15 (1981) 463.
[26] R.V. Tyson, Org. Geochem. 32 (2001) 333–339.
[27] M. Vandenbroucke, R. Pelet, Y. Debyser, in: G.R. Aiken, D.M. McKnight, R.L. Wershaw, P. McCarthy (Eds.), Humic Substances in Soil, Sediment and Water, John Wiley & Sons, New York, 1995, pp. 249–273.
[28] Y. Zegouagh, S. Derenne, C. Largeau, P. Bertrand, M.A. Sicre, A. Saliot, B. Rousseau, Org. Geochem. 30 (1999) 83.
[29] N. Calace, F. De Paolis, F. Minniti, B.M. Petronio, Talanta 47 (1998) 803.
[30] N. Calace, M. Capolei, M. Lucchese, B.M. Petronio, Talanta 49 (1999) 277.
[31] N. Poirier, S. Derenne, J.N. Rouzaud, C. Largeau, A. Mariotti, J. Balesdent, J. Maquet, Org. Geochem. 31 (2000) 813.
[32] A. Ambles, P. Jambu, J.C. Jacquesy, E. Parlanti, B. Secouet, Soil Sci. 156 (1993) 49.
[33] L.M. Mayer, Geochim. Cosmochim. Acta 58 (1994) 1271.
[34] R.G. Keil, E. Tsamakis, C.B. Fuh, J.C. Giddings, J.I. Hedges, Geochim. Cosmochim. Acta 58 (1994) 879.

Available online at www.sciencedirect.com
ScienceDirect
Talanta 71 (2007) 1417–1423
Talanta
www.elsevier.com/locate/talanta

Pesticide analysis in herbal infusions by solid-phase microextraction and gas chromatography with atomic emission detection

Natalia Campillo, Rosa Peñalver, Manuel Hernández-Córdoba *

Department of Analytical Chemistry, Faculty of Chemistry, University of Murcia, E-30071 Murcia, Spain

Received 23 February 2006; received in revised form 21 June 2006; accepted 7 July 2006
Available online 17 August 2006

Abstract

A direct immersion solid-phase microextraction (SPME) procedure was used in combination with capillary gas chromatography with atomic emission detection (GC–AED) for the determination of 10 pesticides (organochlorines, organophosphorus compounds and pyrethrins) in herbal and tea infusions. Ionic strength, sample dilution and time and temperature of the absorption and desorption stages were some of the parameters investigated in order to select the optimum conditions for SPME with a 100 μm PDMS fiber-coating. Element-specific detection and quantification was carried out by monitoring the chlorine (479 nm) and bromine (478 nm) emission lines, which provided nearly specific chromatograms. Calibration was carried out by using a spiked sample infusion. The detection limits varied between 11.9 ng ml^{-1} for deltamethrin and 0.03 ng ml^{-1} for *p,p′*-DDE and *p,p′*-DDD. The recoveries ranged from 73.5% for deltamethrin to 108.3% for *p,p′*-DDT in a spiked white tea infusion. Two of the eight samples analyzed contained low levels of some the pesticides considered.
© 2006 Elsevier B.V. All rights reserved.

Keywords: Pesticides; Herbal infusions; Tea; Solid-phase microextraction (SPME); Gas chromatography–atomic emission detection (GC–AED)

1. Introduction

Many types of plants are consumed throughout the world as infusions for both pleasure and therapeutic purposes. Like other agricultural products, the materials used for infusions must be subject to control because of the pesticides used for their cultivation, in order to minimise possible risks to human health. Tea is one of the most popular drinks in the world, the total daily intake per person in some countries reaching 31 [1], so that such water-based drinks could represent an important share of total human exposure to pesticides. Several countries have set their own maximum residue limits (MRLs) of pesticides for tea and other plants consumed as infusions. Thus, for example, the European Community legislation establish the MRLs for the pesticides considered in the present study at between 0.02 μg g^{-1} for tetradifon and 5 μg g^{-1} for deltamethrin [2] in a wide variety of vegetables, although no MRL is specified in the case of others such as coumaphos.

The literature shows different analytical procedures for the determination of pesticides in medicinal plants and tea [1,3–7]. However, considering that these plants are not consumed as such, and taking into account that the transfer of these compounds from the solid material to the infusion is not total [8], the interest should be focused to the analysis of infusions instead of the plants used for their preparation. Gas chromatography (GC) is a suitable technique for such a purpose [8–12] but, due to the low concentrations to be determined, the compounds of interest have to be separated from the matrix and concentrated to reach the minimum level required for the particular detector used. This separation/concentration stage, which is essential to obtain reliable results, is, at the same time, an important source of errors, and need be carefully optimized. Solid-phase extraction (SPE) [8], liquid–liquid extraction (LLE) [9], stir bar sorptive extraction (SBSE) [10] and solid-phase microextraction (SPME) [11,12] have been used for the separation and preconcentration of pesticides from the infusion matrices. The use of organic solvents and the multiple operational steps involved are important disadvantages of SPE and LLE. However, SPME [13–15] is an interesting, easily available, low-cost alternative to common extraction methods since it integrates sampling, extraction, preconcentration and clean-up into a single step, avoiding the use

* Corresponding author. Tel.: +34 968 367406; fax: +34 968 364148.
E-mail address: hcordoba@um.es (M. Hernández-Córdoba).

0039-9140/$ – see front matter © 2006 Elsevier B.V. All rights reserved.
doi:10.1016/j.talanta.2006.07.014

of organic solvents. As regards the detector to be used, it should be noted that pesticides almost always contain heteroatoms, so that the atomic emission detector (AED) could be advantageous. Since AED is a highly selective detector, it facilitates very simple chromatograms to be obtained, in this way representing an alternative choice to the use of mass spectrometric detectors.

As far as we know, there are no previous references to the use of AED in this type of sample and only one previous paper [12] tackled the determination of pesticides in herbal infusions by SPME using a commercial fiber coating. However the study only applied to organochlorine pesticides, whereas in the present study compounds of three different chemical families (organochlorine and organophosphorus pesticides and pyrethrins) are simultaneously determined.

2. Experimental

2.1. Chemicals

Pesticide standards (aldrin (HHDN), dieldrin, captan, chlorfenvinphos, *p*,*p*′-DDE, *p*,*p*′-DDD, *p*,*p*′-DDT, bromopropylate, tetradifon, coumaphos and deltamethrin) with a purity higher than 96% were provided by Dr Ehrenstorfer (Augsburg, Germany). Standard stock solutions of each pesticide at 1000 mg l^{-1} were prepared in methanol and stored in the dark at 4 °C. Working standard solutions were prepared daily by diluting the stock solutions with Milli-Q water (Millipore, Bedford, USA). Analytical-reagent grade methanol was purchased from Lab-Scan (Dublin, Ireland).

The phosphate buffer solution (1 M) was prepared by dissolving potassium dihydrogen phosphate (Fluka, Buchs, Switzerland) in water and then adjusting the pH to 7 with sodium hydroxide. The buffer solution was stored in the refrigerator at 4 °C.

The plasma gas and carrier gas used for GC was helium. The reagent gas for the AED was oxygen. Nitrogen was used for purging the AED system. All the gases were supplied by Air Liquide (Madrid, Spain).

2.2. Instrumentation

The SPME device for manual sampling was obtained from Supelco (Bellefonte, PA, USA) and consisted of a holder assembly and several replaceable fibers. SPME fibers coated with non-bonded polydimethylsiloxane (PDMS) of 100 μm thickness and partially cross-linked polyacrylate (PA) of 85 μm thickness were obtained from Supelco. The fibers were conditioned prior to their first use as recommended by the manufacturer by heating in the injection port of the chromatographic system for 0.5 h at 250 °C for the PDMS coating and for 2 h at 300 °C for the PA coating. A clean-up step was carried out weekly by heating them in the injection port overnight at 260 °C, with the split vent open. All analyses were performed in 15 ml clear glass vials and the solutions were stirred with a magnetic stirrer (RH KT/C IKA-werke GmbH, Germany) using PTFE-coated magnetic stir bars (10 mm × 6 mm o.d.). To prevent analyte evaporation, vials sealed with hole-caps and PTFE/silicone septa were used. To control vial temperature, a homemade heating system was used.

An Agilent 6890 gas chromatograph was directly coupled by a transfer line to a G2350A microwave-induced plasma atomic emission detector (Agilent). The updated G2070AA ChemStation application with the G2360AA GC–AED software was used to control and automate many features of the GC and AED systems, and for data acquisition and treatment. The chromatograph was fitted with a 30 m × 0.32 mm i.d. HP-5, 5% phenyl 95% dimethyl polysiloxane capillary column from Agilent with a 0.25 μm film thickness. Desorption of the fibers into the injection port was carried out in the splitless mode at 280 °C. The internal volume of the inlet liner was 900 μl. The fiber exposure time was 7 min at the maximum permitted depth. The experimental conditions for the chromatographic separation and the detection system are summarized in Table 1. Helium was used as the carrier gas at 4 ml min^{-1}, in the constant-flow mode. The helium make-up flow-rate was set at 45 ml min^{-1}, being measured with the window purge gas flow on. Solvent venting was switched on immediately after starting the desorption step and switched off 3.5 min later. Filter and backamount adjustment in the AED were set according to Agilent default specifications. The chromatograms for Cl-479 nm and Br-478 nm were obtained simultaneously using oxygen as the only scavenger gas. Table 2 shows the emission lines selected for quantification purposes for each pesticide. The total time for one GC run was 50 min, including the extraction step.

Some GC–MS measurements were carried out for confirmation purposes. A combination of an Agilent 6890N gas chromatograph and an Agilent 5973N mass selective detector equipped with an inert ion source was used. The separation was carried out with a 30 m × 0.25 mm i.d. HP5-MS (Agilent) capillary column (0.25 μm film thickness), and with a helium constant flow-rate of 1 ml min^{-1}. The mass spectrometer was

Table 1
Experimental conditions of the SPME–GC–AED system

SPME conditions	Absorption step	20 min at 90 °C (immersion mode)
	Desorption step	7 min at 280 °C (splitless)
	Fiber material	Polydimethylsiloxane, 100 μm
GC conditions	Capillary column	HP-5 (30 m × 0.32 mm i.d. × 0.25 μm)
	Carrier gas	Helium, 4 ml min^{-1}
	Oven program	40–150 °C at 30 °C min^{-1} (2.5 min), 150–195 °C at 5 °C min^{-1} (5 min), 195–300 °C at 10 °C min^{-1} (0.3 min)
GC–AED interface	Transfer line	HP-5
	Transfer line temperature	325 °C
AED conditions	Reagent gases	O_2 at 15 psi
	Spectrometer purge flow	Nitrogen, 2.5 l min^{-1}
	Helium make-up flow	45 ml min^{-1}
	Cavity temperature	325 °C
	Solvent vent off	0–3.5 min

Table 2
List of pesticides

Pesticide	Molecular formula	Purity (%)	Monitored emission line (nm)	Retention time (min)
Aldrin	$C_{12}H_8Cl_6$	98.0	Cl-479	13.30
Captan	$C_9H_8Cl_3NO_2S$	99.4	Cl-479	15.00
Chlorfenvinphos	$C_{12}H_{14}Cl_3O_4P$	97.0	Cl-479	15.37
Dieldrin	$C_{12}H_8Cl_6O$	99.0	Cl-479	17.12
p,p′-DDE	$C_{14}H_8Cl_4$	98.5	Cl-479	17.40
p,p′-DDD	$C_{14}H_{10}Cl_4$	98.0	Cl-479	19.69
p,p′-DDT	$C_{14}H_9Cl_5$	99.5	Cl-479	21.76
Bromopropylate	$C_{17}H_{16}Br_2O_3$	96.2	Br-478	23.74
Tetradifon	$C_{12}H_6Cl_4O_2S$	98.0	Cl-479	24.46
Coumaphos	$C_{14}H_{16}ClO_5PS$	96.0	Cl-479	26.63
Deltametrin	$C_{22}H_{19}Br_2NO_3$	99.0	Br-478	29.67

operated in the scan mode using electron-impact ionization (electron-accelerating voltage: 306 V). The scan range was from *m/z* 30 to 500 (scan speed: 0.35 s).

2.3. Samples and SPME analysis procedure

Samples of four types of tea (white, oolong, green and the variety of black tea known as Early grey) (*Camellia sinensis*), two samples of camomile (*Matricaria chamomilla*) and two samples of pennyroyal (*Mentha pulegium* L.) were purchased in a supermarket in the bag format. No indication as regards the geographical origin of the plant samples was given in the labels.

Infusions of each different type were prepared on the same day of use by immersing the bag (approximately 1.5 g of plant material) in 100 ml of boiling water for 3 min, reproducing as closely as possible the conditions in which herbal teas are consumed. Infusions were not filtered before being submitted to the SPME procedure. Seven millilitres of the infusion and 3 ml of phosphate buffer solution were placed in 15 ml SPME-vials, which were sealed by the caps after adding the magnetic stir bars. With stirring set at 1400 rpm, the fiber was totally immersed in the sample solution for 20 min at 90 °C. To proceed to the desorption step, the fiber was retracted into the holder needle and transferred without delay to the injection port of the GC in the splitless mode at 280 °C for 7 min. The fiber was then kept in the injector for 10 min after opening the split valve, to ensure total desorption and no memory effects. Each sampling was performed in triplicate.

GC and AED parameters were optimized by using a fortified black tea infusion, ranging between 5 ng ml^{-1} and 2 μg ml^{-1}, depending on the compound, being 10 ml volumes submitted to direct immersion solid phase microextraction with a PDMS fiber.

For recovery studies, 25 ml volume aliquots of recently prepared infusions were spiked with 0.05 ml of a working methanolic solution containing the pesticides at between 100 ng ml^{-1} and 100 μg ml^{-1}, depending on the compound, corresponding to fortification levels of approximately 0.2 and 200 ng ml^{-1}, respectively. The fortification procedure was applied to infusions of four different plant samples at two concentration levels and three replicates were analyzed in each case.

3. Results and discussion

3.1. Chromatographic and AED parameters

The optimized program temperature elutes the eleven pesticides between 13 and 30 min, as shown by their respective retention times (Table 2). Separation was carried out using a constant helium flow-rate of 4 ml min^{-1}. Chlorine and bromine were the two heteroatoms monitored for quantification purposes, and both were detected simultaneously in one GC run because they require oxygen as the only scavenger gas. An oxygen pressure of 15 psi was selected, providing the best sensitivity for all the pesticides in the studied range (15–30 psi). The helium makeup gas flow rate was studied between 35 and 50 ml min^{-1}. When monitoring the chlorine emission line, a reduction in the makeup gas flow increased the peak area, but also the peak width. In the case of the two pesticides monitored in the bromine emission line, a light increase in sensitivity was observed at 40 ml min^{-1}. A compromise value of 45 ml min^{-1} was adopted. The transfer line and the cavity temperatures were optimized in the range 250–350 °C, the best results being obtained at 325 °C.

3.2. Optimization of the SPME conditions

The SPME operational conditions were optimized using fortified black tea infusions. The non-polar poly(dimethylsiloxane) polymeric and the medium-polarity polyacrilate coatings were investigated. It was verified that because of the non-polar character of the studied pesticides, they were partitioned more readily into the PDMS fiber coating. Direct immersion and headspace modes were compared using absorption time and temperature of 20 min and 80 °C and desorption time and temperature of 5 min and 280 °C. When using the headspace mode, sensitivity increased for five pesticides (i.e. aldrin, dieldrin and *p,p′*-DDT and its metabolites). For the rest of the compounds the signals decreased or even were lost (i.e. coumaphos and deltamethrin). Therefore, the immersion mode was adopted.

Other parameters investigated were the ionic strength, the stirring speed, and times and temperatures of both the absorption and desorption stages. Several pH values between 5.5 and 8 were assayed by adding 0.5 ml of 1 M phosphate buffer solutions to 10 ml of the infusion. In all cases maximum sensitivity was attained at pH 7, as can be observed in Fig. 1A, and this value was selected. No salting-out effect was observed when the extraction medium contained sodium chloride concentrations ranging between 5 and 15% (w/v); the signals decreased or were even lost, with the exception of chlorfenvinphos, whose peak area doubled in the presence of the salt at the 15% (w/v) concentration level. Similar results were observed when sodium sulphate was used instead of sodium chloride. Consequently, no salting out agent, other than the buffer solution, was added to the extraction vial.

When the absorption time was varied between 10 and 90 min, maximum signals were reached after 20–75 min for most of

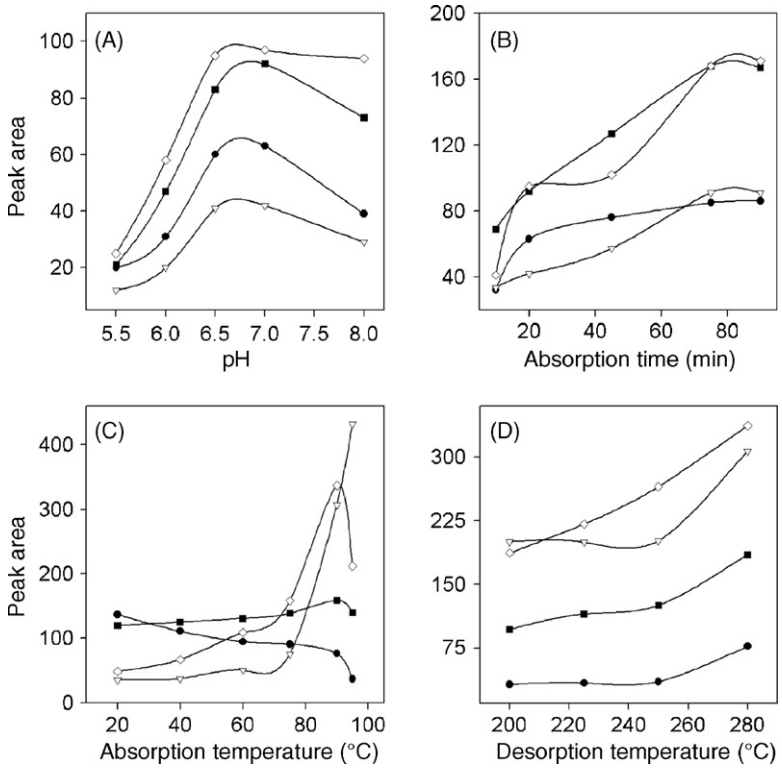


Fig. 1. Effect of (A) pH, (B) absorption time, (C) absorption temperature and (D) desorption temperature on the SPME process of chlorfenvinphos (●), *p*,*p*′-DDT (▽), tetradifon (■) and bromopropylate (◊).

the compounds (Fig. 1B) using 1000 rpm as the stirring speed, these time intervals being reduced when the stirring speed was increased to 1400 rpm. From a practical point of view, an absorption time of 20 min was selected in order to increase the frequency of analysis.

It is known that the addition of hydrophilic solvents can modify the matrix and subsequently the extraction effect. The presence of methanol in the extraction medium was investigated in a low level concentration range (1–5%, v/v), because it is known that high concentrations of organic solvents may decrease the analyte extraction efficiency. Peak area for most of the pesticides hardly varied in the studied range, but it decreased in the case of dieldrin and bromopropylate. Therefore, the addition of methanol was discarded.

The absorption temperature was varied in the range 20–95 °C (Fig. 1C). Whereas aldrin, deltamethrin and *p*,*p*′-DDT and its metabolites were more readily absorbed with increasing temperature, chlorphenvinfos, captan and coumaphos showed the opposite dependency. For the rest of the compounds maximum sensitivity was attained at 90 °C, and this was the temperature adopted as a compromise value.

The desorption temperature was studied between 200 °C and the maximum value recommended by the manufacturer for 100 μm PDMS fiber coatings, i.e. 280 °C (Fig. 1D). As expected, considering the low volatilities of the compounds under study, sensitivity increased with temperature in all cases, and 280 °C was selected. When the desorption time was varied in the range 1–10 min, it was observed that the signals slightly increased with time up to 7 min and then remained constant; therefore, a desorption time of 7 min was selected. The position of the fiber inside the injector is important as the temperature varies along the length of the injector. As expected, considering the high boiling point of the studied compounds, when the fiber was totally exposed at the maximum depth permitted in the injection port, maximum sensitivity was attained for all the compounds.

The influence on sensitivity of diluting the sample dilution with different volumes of buffer solution was also considered since a beneficial effect caused by sample dilution has already been described in the literature for different food matrices [10,16]. To this purpose, an infusion previously checked to be free of any of the studied compounds, was spiked and then mixed in different proportions with the buffer solution. The best results were obtained for all the compounds when the infusions were diluted in the proportion 70:30 (sample:buffer solution), as shown in Fig. 2.

Fig. 3 shows the SPME–GC–AED chromatograms obtained from an unspiked camomile infusion and a spiked black tea infusion under the experimental conditions finally selected.

3.3. Analytical characteristics of the method

The standard additions calibration method was applied to infusions of four different types of plants and the obtained data compared with those provided by the standards in the absence of the sample matrix. In all cases, six spiking levels were analyzed and two replicates for each calibration level were made. The results obtained are summarized in Table 3. Taking into account that the slopes of standard addition calibration graphs were sim-

Table 3
Slopes of the standard addition calibration graphs for four different samples

Pesticide	Slope[a] (ml ng^{-1})				
	Aqueous standard	White tea	Early grey tea	Camomile	Pennyroyal
Aldrin	29 ± 2	28 ± 1	28 ± 1	29 ± 2	29.6 ± 0.5
Captan	0.041 ± 0.004	0.04 ± 0.02	0.047 ± 0.007	0.055 ± 0.003	0.056 ± 0.005
Chlorfenvinphos	0.682 ± 0.007	1.11 ± 0.01	0.99 ± 0.03	0.96 ± 0.02	0.94 ± 0.02
Dieldrin	21.5 ± 0.8	25.9 ± 0.9	24.3 ± 0.3	24.3 ± 0.8	27 ± 2
p,p′-DDE	40 ± 2	32 ± 4	27.0 ± 0.9	28 ± 2	36 ± 3
p,p′-DDD	39 ± 1	37 ± 4	35 ± 2	42 ± 3	44 ± 2
p,p′-DDT	48 ± 1	45 ± 2	39 ± 1	41 ± 2	55 ± 4
Bromopropylate	24 ± 1	19 ± 2	16.3 ± 0.9	18.5 ± 0.5	20.9 ± 0.7
Tetradifon	22.9 ± 0.7	15.2 ± 0.8	19 ± 1	17 ± 1	18.6 ± 0.7
Coumaphos	0.685 ± 0.004	0.467 ± 0.005	0.415 ± 0.004	0.477 ± 0.003	0.497 ± 0.006
Deltametrin	0.080 ± 0.003	0.086 ± 0.002	0.078 ± 0.005	0.060 ± 0.004	0.098 ± 0.009

[a] Mean value ± standard deviation ($n = 2$).

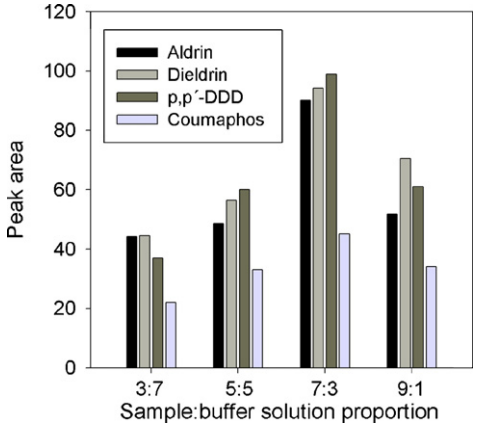


Fig. 2. Influence of the sample dilution of a black tea infusion for some of the pesticides studied under the finally selected conditions.

ilar for the different matrices studied, the convenience of using for calibration purposes an infusion prepared from a tea sample exempt from the analytes was studied. A paired *t*-test was applied between the slopes obtained from this blank infusion and each one of the slopes obtained from the standard addition method to the samples, the "*p*" values obtained being higher than 0.05, thus validating this way of calibration. It should be noted that the sensitivity for each compound depends not only on the number of atoms of the heteroatom contained in the molecular formula, but also (and to a great extent) on the affinity of the compound for the coating of the SPME-fiber. Thus, bromopropylate measurement was more sensitive than that of deltamethrin, even though both compounds contain two bromine atoms in their molecula, and the final results for captan proved the procedure was unsuitable for its determination due to a poor sensitivity. Correlation coefficients higher than 0.995 were obtained in all cases.

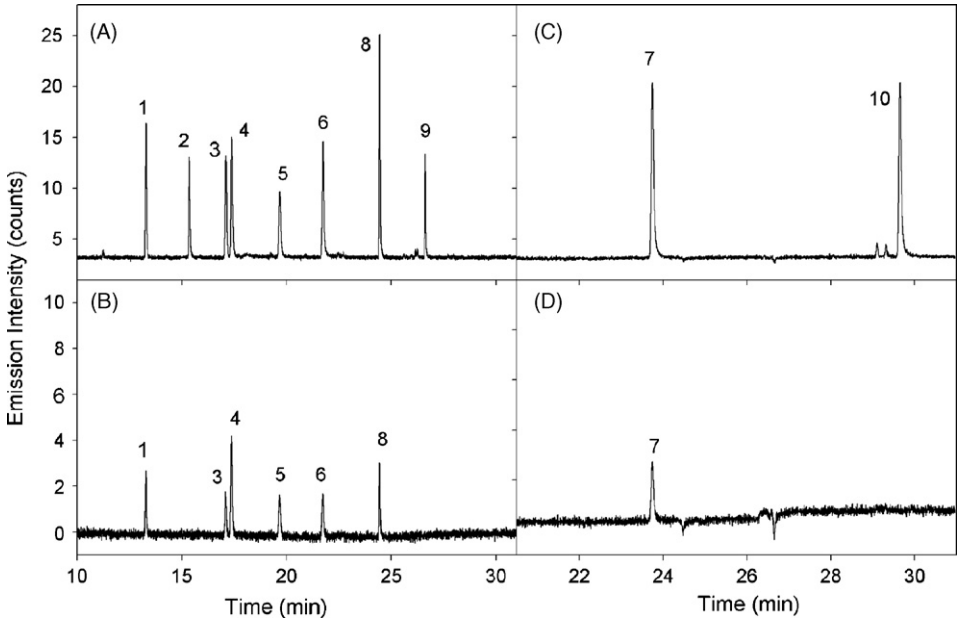


Fig. 3. SPME–GC–AED chromatograms obtained from (A and C) a black tea infusion spiked with the pesticides and (B and D) a non-spiked camomile infusion. (A and B) Cl 479 nm and (C and D) Br 478 nm. (1) Aldrin (2 ng ml^{-1}); (2) chlorfenvinphos (50 ng ml^{-1}); (3) dieldrin (2.7 ng ml^{-1}); (4) *p,p′*-DDE (2.5 ng ml^{-1}); (5) *p,p′*-DDD (1.7 ng ml^{-1}); (6) *p,p′*-DDT (1.9 ng ml^{-1}); (7) bromopropylate (4.5 ng ml^{-1}); (8) tetradifon (5.4 ng ml^{-1}); (9) coumaphos (75 ng ml^{-1}); (10) deltamethrin (800 ng ml^{-1}).

Table 4
Analytical characteristics of the proposed method

Pesticide	Linearity (ng ml^{-1})	Detection limit[a] (ng ml^{-1})	Quantification limit[b] (ng ml^{-1})	R.S.D.[c] (%)	R.S.D.[c] (%)
Aldrin	0.2–10	0.04	0.12	11.5	15.4
Chlorfenvinphos	3–200	1.08	3.81	6.8	7.4
Dieldrin	0.1–10	0.04	0.15	5.4	8.7
p,*p*′-DDE	0.1–10	0.03	0.12	7.2	9.1
p,*p*′-DDD	0.1–10	0.03	0.11	6.4	10.2
p,*p*′-DDT	0.1–10	0.04	0.12	10.0	12.1
Bromopropylate	0.1–10	0.05	0.18	4.3	4.6
Tetradifon	0.1–10	0.06	0.19	5.5	6.8
Coumaphos	5–500	1.95	6.49	7.5	9.5
Deltamethrin	25–2000	11.9	39.6	7.4	10.4

[a] Corresponding to S/N = 3.
[b] Corresponding to S/N = 10.
[c] Calculated for concentrations of 10-fold the corresponding quantification limits.

The detection limits were calculated using a signal-to-noise ratio of three and considering the slopes of the calibration graphs obtained from a blank sample infusion. The quantification limits were calculated using a signal-to-noise ratio of 10 (Table 4). No data for captan have been included due to the mentioned low sensitivity of this compound. The repeatability was calculated using the relative standard deviation of the peak areas found for 10 successive fortifications of a camomile sample infusion at concentration levels of 10 times the corresponding quantification limits (Table 4). Using the same sample infusion, the relative standard deviation for 10 injections carried out on different days was used to estimate the reproducibility of the procedure, obtaining R.S.D. values lower than 15%. The R.S.D.s obtained show good reproducibility for the proposed procedure (Table 4).

3.4. Real samples and recovery studies

Eight different samples of tea and herbal infusions were submitted, in triplicate, to the optimized procedure, and none of the pesticides studied were detected in five of them. However, 0.9 ng ml^{-1} of *p*,*p*′ DDE were found in an infusion prepared from a pennyroyal sample and variable amounts of seven pesticides (aldrin, bromopropylate, tetradifon and *p*,*p*′-DDT and its metabolites) in the 0.2–0.8 ng ml^{-1} range were found both in a white tea and a camomile sample. The identity of these compounds was in addition in this case verified by GC–MS.

The reliability of the optimized procedure was checked by recovery studies for four different sample infusions spiked at two concentration levels, subtracting the analyte content for the white tea sample containing some of the pesticides. The recov-

Table 5
Mean recovery efficiencies and R.S.D. obtained in fortified herbal infusion samples by using the proposed procedure

Pesticide	Recovery[a] (%)				
	Spike level (ng ml^{-1})	White tea	Black tea	Camomile	Pennyroyal
Aldrin	0.5	99.6 (10.1)	85.3 (8.2)	88.1 (5.6)	88.4 (6.9)
	1	99.3 (8.5)	88.9 (7.2)	96.0 (5.4)	91.2 (5.8)
Chlorfenvinphos	5	74.5 (9.9)	75.5 (9.8)	103.1 (10.2)	102.1 (11.4)
	10	98.5 (8.1)	81.4 (8.6)	97.6 (8.9)	95.8 (7.6)
Dieldrin	0.2	83.5 (9.4)	101.3 (7.9)	96.4 (7.8)	100.2 (9.9)
	0.5	92.8 (7.0)	96.2(6.9)	102.7 (7.0)	94.6 (8.7)
p,*p*′-DDE	0.2	81.2 (7.4)	88.4 (6.3)	97.2 (11.1)	105.4 (7.2)
	0.5	95.2 (5.9)	91.3 (6.8)	92.8 (8.7)	99.5 (6.9)
p,*p*′-DDD	0.2	105.4 (7.0)	102.9 (11.1)	93.1 (6.2)	103.6 (11.0)
	0.5	86.3 (6.3)	98.3 (7.3)	89.8 (6.9)	101.2 (9.7)
p,*p*′-DDT	0.2	108.3 (7.8)	90.4 (10.5)	88.4 (8.3)	91.8 (5.9)
	0.5	89.4 (7.1)	96.3 (8.2)	103.5 (6.9)	94.1 (6.7)
Bromopropylate	0.5	73.7 (14.2)	75.8 (10.1)	88.4 (12.3)	92.5 (10.1)
	1.0	103.4 (10.8)	89.4 (9.4)	90.2 (7.9)	103.2 (8.4)
Tetradifon	0.5	74.9 (5.9)	81.6 (9.3)	73.6 (6.3)	74.9 (7.9)
	1.0	86.2 (8.8)	91.5 (6.6)	100.2 (5.4)	88.2 (7.1)
Coumaphos	10	83.3 (9.2)	79.6 (10.8)	99.3 (11.2)	79.8 (13.2)
	20	99.3 (10.4)	77.4 (10.1)	99.9 (7.5)	94.7 (9.7)
Deltamethrin	50	73.5 (9.4)	89.2 (12.1)	82.1 (14.1)	90.2 (14.1)
	100	75.9 (14.3)	91.5 (9.7)	81.3 (8.7)	95.5 (9.1)

[a] Values in brackets are R.S.D. values for $n = 3$.

eries of pesticides from spiked sample infusions varied between 73.5 and 108.3%, with an average recovery ± S.D. ($n = 88$) of 91.4 ± 9.1, as can be seen in Table 5. No significant differences were observed in the R.S.D. values obtained for the recoveries of the different pesticides in each of the herbal infusions analyzed in this study, the values ranging between 8.7 and 12.5% ($n = 22$) for camomile and white tea infusions, respectively.

4. Conclusion

The optimized DI-SPME–GC–AED method permits the rapid and simultaneous determination of 10 pesticides in herbal infusions of different origins. Because no significant differences were found between the slopes of the standard addition calibration graphs for the different types of herbal infusions studied, the tedious standard addition quantification method can be avoided by preparing the standard mixture solution in a pesticide-free sample infusion which is diluted in the proportion 7:3 with a buffer solution. The analytical characteristics and recovery data prove the reliability of the method. Considering the relatively low absorption time required for the preconcentration stage, the procedure represents a valid alternative to other methods based on classical sample treatments, with the possibility of being applied for routine analysis.

Acknowledgements

The authors are grateful to the Spanish Ministerio de Educacion y Ciencia, MEC (Project BQU2003-01731) for financial support. R. Peñalver acknowledges a fellowship from MEC.

References

[1] H. Fiedler, C.K. Cheung, M.H. Wong, Chemosphere 46 (2002) 1429.
[2] http://www.mapya.es, accessed in February 2006.
[3] C. Matos Lino, M.I. Norohna da Silveira, J. Chromatogr. A 769 (1997) 275.
[4] W. Ho, S. Hsieh, Anal. Chim. Acta 428 (2001) 111.
[5] V.G. Zuin, J.H. Yariwake, C. Bicchi, J. Chromatogr. A 985 (2003) 159.
[6] L. Cai, J. Xing, L. Dong, C. Wu, J. Chromatogr. A 1015 (2003) 11.
[7] N. Ochiai, K. Sasamoto, H. Kanda, T. Yamagami, F. David, B. Tiempont, P. Sandra, J. Sep. Sci. 28 (2005) 1083.
[8] J.C. Molto, B. Lejeune, P. Prognon, D. Pradeau, Int. J. Environ. Anal. Chem. 4 (1994) 81.
[9] S. Jaggi, C. Sood, V. Kumar, S.D. Ravindranth, A. Shanker, J. Agric. Food Chem. 49 (2001) 5479.
[10] C. Bicchi, C. Cordero, C. Iori, P. Rubiolo, P. Sandra, J.H. Yariwake, V.G. Zuin, J. Agric. Food Chem. 51 (2003) 27.
[11] V. Gomes Zuin, A. Leite Lopes, J. Harumi Yariwake, F. Augusto, J. Chromatogr. A 1056 (2004) 21.
[12] M.V.N. Rodrigues, F.G.R. Reyes, V.L.G. Rehder, S. Rath, Chromatographia 61 (2005) 291.
[13] H. Lord, J. Pawliszyn, J. Chromatogr. A 885 (2000) 153.
[14] J. Beltran, F.J. López, F. Hernández, J. Chromatogr. A 885 (2000) 389.
[15] H. Kataoka, H.L. Lord, J. Pawliszyn, J. Chromatogr. A 880 (2000) 35.
[16] D.A. Lambropoulou, T.A. Albanis, J. Agric. Food Chem. 50 (2002) 3359.

Available online at www.sciencedirect.com
ScienceDirect
Talanta 71 (2007) 1166–1171
Talanta
www.elsevier.com/locate/talanta

In situ continuous monitoring of chloride, nitrate and ammonium in a temporary stream Comparison with standard methods

S. Capelo *, F. Mira, A.M. de Bettencourt

Grupo de Biogeoquímica-IMAR, Departamento de Ecologia, Universidade de Évora, Rua Romão Ramalho, 59, 7000-671 Évora, Portugal

Received 11 January 2006; received in revised form 24 May 2006; accepted 7 June 2006
Available online 11 July 2006

Abstract

A multi-parameter probe was used for *in situ* chloride, nitrate and ammonium measurements in a temporary stream (Ribeira da Pardiela, in the South of Portugal). Comparison with standard analytical methods was performed for all elements. For chloride, the results of the probe depicted the same behaviour as that obtained with the standard method, although it is clear that the matrix effects were present. For nitrate, the results obtained with the probe were in agreement with the other standard methods used, except for samples collected during drought, when the stream water became brownish and exhaled an offensive smell, due to the decomposition of organic matter. For ammonium, surprisingly the probe show to be the best option, the phenate method being affected by matrix effects. The results still suggest an interference of the bicarbonate ion on nitrate determination, but standard additions approach was shown to minimize most of the matrix effects. Recoveries were reasonable to good for all the three anions under scrutiny.
© 2006 Elsevier B.V. All rights reserved.

Keywords: Ion selective electrodes; Chloride; Nitrate; Ammonium; Temporary stream; Environmental analysis

1. Introduction

Water quality monitoring is usually performed by sampling followed by storage, handling and analysis in the laboratory. This is a cumbersome process and often does not provide the required spatial discrimination and/or the large sets of data necessary to describe the temporal evolution of the parameters of interest. It is also known that during storage the integrity of the sample may not be preserved, due to a number of effects that include biological activity and matrix effects, even when correct sample handling protocols are strictly followed. An alternative approach consists in performing the measurements at the location of interest, i.e., *in situ*. This approach is likely to has a significant impact in the future on (i) our understanding of the ecosystem functioning, and (ii) our ability to monitor, model and therefore to efficiently protect these ecosystems [1]. As a matter of fact *in situ* measurements is probably the best way to overcome a major problem facing aquatic analytical chemists, i.e., how to maintain the sample in its original state during sampling and handling, without stimulating any of the very dynamic chemical, biological and physical processes which may continue after sample collection. Indeed, in their natural environment, aquatic samples are not at thermodynamic equilibrium. In fact, at best, they may be in steady state conditions due to the continuous input (e.g., soil leaching, atmospheric inputs, cell growth) and output (e.g., coagulation/sedimentation, cell death) of colloids and microbes [2,3].

The major advantages of the *in situ* approach compared with laboratory analysis are the following [4]: (1) elimination of contaminants due to sample handling, i.e., no or minimum sample transformation; (2) minimization of the overall cost data collection (in particular, due to a reduction of time for collection, handling and analysis of the sample); (3) possibility of real-time analysis, allowing the rapid detection of pollutant inputs (e.g., monitoring of industrial wastes or water quality in water treatment plants); (4) ability to obtain detailed spatial and temporal

* Corresponding author. Tel.: +351 266 740800; fax: +351 266 745395.
E-mail address: scapelo@uevora.pt (S. Capelo).

0039-9140/$ – see front matter © 2006 Elsevier B.V. All rights reserved.
doi:10.1016/j.talanta.2006.06.013

data banks of complete ecosystems (lakes, aquifers, etc.); (5) possibility of performing measurements in locations which are difficult to access (deep lakes or oceans) and (6) possibility of measuring concentration gradients and fluxes at environmental interfaces (sediment water; air–water), at high (sub-mm) spatial resolution.

There has been an extensive effort to design chemical sensors and analysers that are capable of operating *in situ*. Much of this work has been summarized in a recent volume on chemical sensor systems for aquatic sciences, which describes a variety of continuous flow analysers, electrochemical sensors and optical sensors for *in situ* measurements of dissolved chemical species [1]. All of these systems are affected by interferences due to sample composition, i.e., matrix effects. In fact, even the standard methods when applied to real samples are subject to interferences [5].

Among the *in situ* chemical sensors, the ion selective electrodes (ISE) are able to continuously monitor a system, which is invaluable when it is necessary to use large sets of data to calibrate mathematical models capable to describe the behavior of complex ecosystems and when the sample matrix can be altered by sampling and storage and/or by inflow of nutrients or elements from various sources (as for example, wastewater and agriculture). In this work, we analyse chloride, nitrate and ammonium concentration using the corresponding ion selective electrodes placed *in situ* in a multi-parameter probe [6,7].

Chloride is one of the major inorganic anions in water and wastewater. A higher value of chloride may indicate the inflow of wastewater or industrial effluents into the river. The chloride concentration is higher in wastewater than in raw water because sodium chloride is a common constituent of the diet and passes unchanged through the digestive system [8]. Nitrate and ammonium are important because they are the major forms of nitrogen which are directly assimilated by plants and organisms. Nitrate is one of the most common contaminants of groundwater, originating mainly from agricultural fertilizer application and release of sewage [8]. In fact, nitrogen dynamic plays a key role in determining the ecological status and health of lowland rivers, estuaries and coastal waters as limiting factor of primary production. Eutrophication is, indeed, a major concern in these ecosystems, and is strongly influenced by factors such as agricultural practices and demographic change, and its control requires intensive sampling, with high temporal and spatial collections in catchment areas [9].

In the Mediterranean region, the dominant types of streams are the temporary [8]. The hydrologic and biogeochemical processes that occur during the wetting and drying periods, in this type of stream, are far from being well understood [10–13]. Ribeira da Pardiela is a temporary stream on the right shore of the Degebe river which is one of the main tributaries of the Guadiana river (in the South of Portugal).

The aim of this work was to compare the *in situ* determination of chloride, nitrate and ammonium with well-established laboratory procedures, in a temporary stream (Ribeira da Pardiela).

2. Experimental

2.1. Instrumentation

A multi-parameter probe (Yellow Spring–YSI 6600) was used to *in situ* monitor parameters such as depth, temperature, conductivity, pH, oxidation–reduction potential, dissolved oxygen, chlorophyll, turbidity, chloride, ammonium/ammonia and nitrate. Chloride, ammonium and nitrate were measured using three ion selective electrodes (ISE) incorporated in the probe. The probe chloride ISE employs a solid state membrane attached to a conductive wire. When the probe is immersed in water, a potential is established across the membrane that depends on the relative amounts of chloride in the medium. This potential is read relative to the reference pH electrode of the probe. The probe ammonium ISE employs a silver/silver chloride (Ag/AgCl) wire electrode in a custom filling solution. Nonactin membrane separates the internal solution from the sample medium and this membrane selectively interacts with ammonium ions. When the probe is immersed in water, a potential is established across the membrane that depends on the relative amounts of ammonium in the sample and the internal filling solution. This potential is also read relative to the reference pH electrode of the probe. The probe nitrate ISE consists of a silver/silver chloride wire electrode in a custom filling solution. The internal solution is separated from the sample medium by a polymer membrane, which selectively interacts with nitrate ions. When the probe is immersed in water, a potential is established across the membrane that depends on the relative amounts of nitrate in the sample and the internal filling solution. This potential is read relative to the pH reference electrode of the probe [6].

A Unicam UV/vis spectrophotometer was used for all measurements of nitrate and ammonium with the cadmium reduction method and the phenate method, respectively [5]. An Inolab WTW potentiostat with a nitrate selective electrode (Methrom 6.1241.050) and a reference Ag/AgCl electrode (Methrom 6.0726.100) was used for the nitrate electrode method [5], which was compared with the probe nitrate ISE.

2.2. Reagents and standards solutions

All solutions were prepared from analytical reagent grade chemicals using distilled and deionised water from a Milli-Q water purification system. The deionised water had a specific conductivity less than 0.1 $\mu S\,cm^{-1}$.

Chloride standard solutions (YSI) of 10 and 1000 $mg\,l^{-1}$, nitrate standard solutions (YSI) of 1 and 100 $mg\,l^{-1}$, and ammonium standard solutions (YSI) of 1 and 100 $mg\,l^{-1}$ were used for probe calibration. A two-point calibration was performed for all elements.

3. Analytical procedure

3.1. Sampling and storage

Water samples were regularly collected at the study site between 9 and 10 a.m., maintained at 4 °C during transporta-

tion and filtered through 0.47 μm glass fibre filters (Schleicher & Schuell) immediately at the arrival in the laboratory. Sample conservation was done as specified in [5].

3.2. Probe procedure

The probe was cleaned with distilled water (and soft paper) and calibrated for all parameters before being placed in the field, inside a metal structure for security reasons. This metal structure was partially immersed in Ribeira da Pardiela at the following coordinates: latitude 41°10′45″N, Longitude 8°36′23″W and altitude 178 m.

3.3. Methods

The methods used for comparison, in the laboratory, were the argentometric method for chloride (4500-Cl^- B), the phenate method for ammonium (4500-NH_3 F), and the cadmium reduction (4500-$NO_3{}^-$ E) and the nitrate electrode methods (4500-$NO_3{}^-$ D) for nitrate [5]. The argentometric method is based on the precipitation of the silver chloride, which is indicated by the formation of the red silver chromate. The phenate method consists in the formation of indophenol, an intensely blue compound, that results from the reaction of ammonia, hypochlorite and phenol, which is catalyzed by sodium nitroprusside. For the cadmium reduction method, nitrate is reduced almost quantitatively to nitrite in the presence of cadmium treated with copper sulfate and packed in a glass column. The nitrite thus produced is determined by diazotizing with sulfanilamide and coupling with *N*-(1-naphthyl)-ethylenediamine dihydrochloride to form a highly colored azo dye that is measured colorimetrically. A correction may be made for any nitrite present in the sample by analysing without the reduction step. The nitrate electrode method consists in using an ion selective electrode. This nitrate ion electrode is a selective sensor that develops a potential across a thin, porous and inert membrane. A solution of ammonium sulphate 1 M (1:1) was added to standard solutions and samples in order to keep constant the ionic strength and the pH during measurements. Replicates were done for all the methods.

4. Results and discussion

4.1. Analysis of simple and real samples with the probe and the respective standard methods

To establish the validity of our procedure, before using the multi-parametric probe in real samples we compare the ISE results with the standard methods [5], using standard solutions.

Fig. 1 shows that the values obtained for chloride using a standard solution of 121 mg l^{-1} Cl^-, were the same for the probe ISE and for the argentometric method, within the experimental errors. Nevertheless when the chloride concentration was determined in real samples the probe ISE results were higher than those obtained with the argentometric method, both for filtrated and non-filtrated samples. Filtration does not seem to influence the chloride measurement by the two methods (Fig. 1).

The results obtained with the probe and the phenate method on standard ammonium solutions (0.16, 0.39 and 0.78 mg l^{-1} $NH_4{}^+$-N) agreed, within experimental error (Fig. 2). On the other hand, in real samples, the values obtained with the probe ISE were higher than the values obtained with the phenate method. Moreover the ammonium concentrations determined in non-filtrated samples were higher than in filtrated samples, and these differences are not within the experimental errors. A likely explanation is that ammonium ions adsorb on the suspended particles, and therefore non-filtrated samples present an higher ammonium concentration [8].

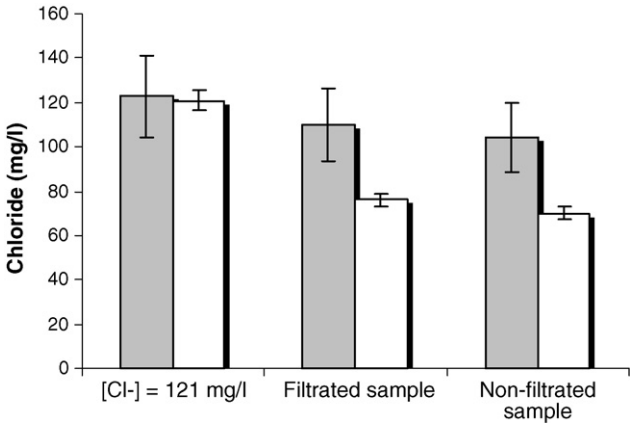


Fig. 1. An example of chloride determinations in standard and field samples, using the probe (▒) and the argentometric method (□). *Note*: The errors presented are not due to replicates but to the uncertainty of the method used.

For nitrate, the probe ISE was compared with two standard laboratory methods, one of them also an ion selective electrode (ISE), the nitrate electrode method, and the other the cadmium reduction method. Fig. 3 depicts the results obtained with these methods in a standard solution and in filtrated and non-filtrated real samples. It can be seen that in a solution with a known concentration of nitrate (1.4 mg l^{-1} $NO_3{}^-$-N) the values obtained are in close agreement for all the three methods, considering the experimental errors associated with each method. For real samples, similar results were obtained with the probe and the nitrate electrode method [5]. However the values obtained with the cadmium reduction method showed to be lower.

For filtrated and non-filtrated real samples the results were again within the experimental errors for each method used. How-

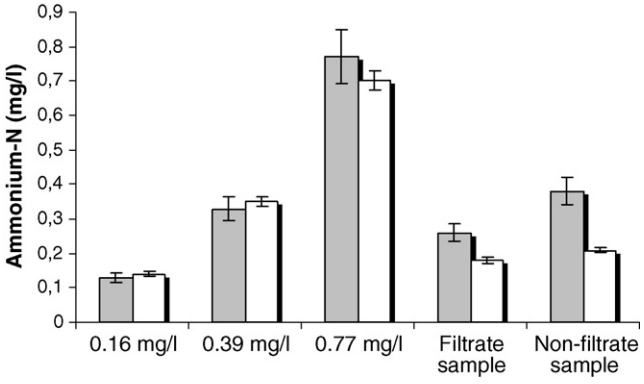


Fig. 2. An example of ammonium determinations in standard and field samples, using the probe (▒) and the phenate method (□). *Note*: The errors presented are not due to replicates but to the uncertainty of the method used.

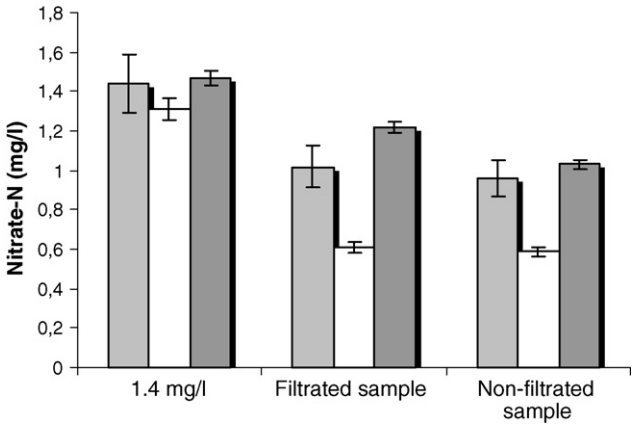


Fig. 3. An example of nitrate (NO_3^--N) determinations in standard and field samples, using the probe ( ), the cadmium reduction method (□) and nitrate electrode method ( ). *Note*: The errors presented are not due to replicates but to the uncertainty of the method used.

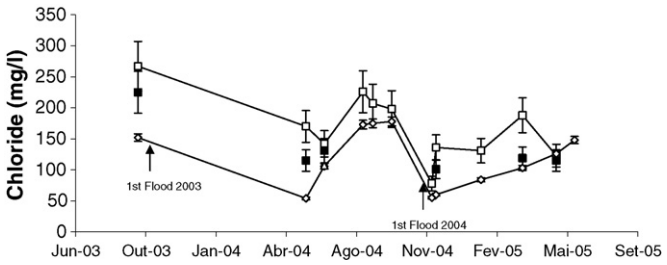


Fig. 4. Chloride determinations vs. time (months) with the probe (□), the probe with standard addition approach (■) and with the argentometric method (◊). *Note*: the values were connected only to demonstrate that the probe behaviour was the same as obtained with the argentometric method. The errors presented are not due to replicates but to the uncertainty of the method used.

ever, the values obtained for nitrate by the three methods with filtered samples appear to be higher than those obtained for non-filtered samples. The filters were therefore tested for nitrate contamination, passing ultra pure Millipore water through them, and analysing the resulting operational blanks, but no contamination could be detected.

4.2. Analysis of real samples with the standard additions method

The standard additions method is known to overcome most of matrix effects, i.e., interferences due to sample composition. It consists in adding known concentrations of the analyte to the sample, and to compute its concentration by extrapolation and interception with the *x*-axis, after a linear correlation. All the readings are taken in the same sample matrix, which avoids or minimizes matrix effects [14].

In order to avoid sample matrix effects, we used the standard additions approach and compared the results obtained with the probe ISEs and the reference methods adopted for comparison for each species (chloride, ammonium and nitrate), using samples collected in the field.

The results obtained for chloride showed that, when the standard additions approach was applied with the argentometric method, no matrix effects could be detected, i.e., the results obtained with standard additions ($107 \pm 4\%$ mg l^{-1} Cl^-) and without standard additions ($106 \pm 4\%$ mg l^{-1} Cl^-) were the same, within the experimental errors. When measuring chloride with the probe ISE, matrix effects were present, as expected, the standard additions approach considerably reducing their interference in most of the samples, though not always.

As can be seen in Fig. 4, the behaviour of chloride concentrations along time, with considerably varying discharge, depicted by the results obtained with the probe ISE is essentially the same as that obtained with the argentometric method determinations, even being affected by sample composition. The initial higher values corresponding to the dry season, decrease abruptly with the onset of the wet season, and rise again with drought until attaining the values of the next dry season. As a matter of fact the first values of Fig. 4, were determined just before the wet season began with the flood of the 30 September 2003. The chloride concentration decreased considerably then and it began to increase in May attaining a maximum value at the end of the summer of 2004 (389 mg l^{-1} Cl^- probe, 27 October 2004; 9–10 a.m.) just before the flood of the 27 October 2004 (1.15–1.30 p.m.). It attained the lowest measured value at the time (28 mg l^{-1} Cl^- probe; 28 October 2004; 9–10 a.m.) and began to rise in November (44 mg l^{-1} Cl^- probe; 06 November 2004; 9–10 a.m.) along the dry season of 2005 until the beginning of the next wet season. The dry season began exceptionally early this year, concentrating chloride earlier. In Fig. 4 the values were connected only to show that the behaviour depicted by the results obtained with probe ISE is essentially the same as the behaviour that follows from the results obtained with the argentometric method.

The results obtained for ammonium showed that the phenate method was affected by sample composition, i.e., the results obtained with standard additions ($0.27 \pm 4\%$ mg l^{-1} NH_4^+-N) and without standard additions ($0.18 \pm 4\%$ mg l^{-1} NH_4^+-N) were significantly different. In this case, the probe ISE seemed to be unaffected by sample composition, i.e., the results obtained with standard additions ($0.26 \pm 10\%$ mg l^{-1} NH_4^+-N) and without standard additions ($0.26 \pm 10\%$ mg l^{-1} NH_4^+-N) converge within experimental error. However, comparing the ammonium values obtained with the standard additions approach when applied to the probe ($0.26 \pm 10\%$ mg l^{-1} NH_4^+-N) and to the phenate method ($0.27 \pm 4\%$ mg l^{-1} NH_4^+-N) there is close agreement, within the experimental errors. In this case, we observed that the standard addition approach is important for the phenate method, since it is affected by matrix effects.

As can be seen in Table 1, the results obtained for nitrate showed that, when the standard additions approach was applied to the cadmium reduction method, no matrix effects could be observed, i.e., the results obtained with standard additions (e.g., $0.48 \pm 4\%$ mg l^{-1} NO_3^--N) and without standard additions (e.g., $0.50 \pm 4\%$ mg l^{-1} NO_3^--N) were the same, within the experimental errors. However, matrix effects could be observed when using the probe ISE and the nitrate electrode method, particularly when dealing with samples colleted during the summer drought. The standard additions approach considerably reduces this effect. For example in the sample collected the 12 May 2005 (Table 1), without standard additions, the values obtained

Table 1
Nitrate (NO_3^--N) determinations in filtrated samples with and without standard additions approach, for all the methods used

Date	Probe NO_3^--N ($mg\,l^{-1}$) (%)	Probe with standard addition NO_3^--N ($mg\,l^{-1}$) (%)	Cadmium reduction method[a] NO_3^--N ($mg\,l^{-1}$) (%)	Cadmium reduction method with standard addition NO_3^--N ($mg\,l^{-1}$) (%)	Nitrate electrode method NO_3^--N ($mg\,l^{-1}$) (%)	Nitrate electrode method with standard addition NO_3^--N ($mg\,l^{-1}$) (%)
25 September 2003	2.21 ± 10	–	0.47 ± 4	–	–	–
16 November 2004	0.61 ± 10	–	0.42 ± 4	–	–	–
24 November 2004	0.51 ± 10	–	0.31 ± 4	–	–	–
25 January 2005	0.45 ± 10	0.42 ± 10	0.30 ± 4	0.48 ± 4	–	–
25 March 2005	0.49 ± 10	0.43 ± 10	0.50 ± 4	0.48 ± 4	–	–
12 May 2005	1.87 ± 10	0.60 ± 10	0.44 ± 4	0.40 ± 4	1.79 ± 2.5	0.83 ± 2.5

Note: The errors presented are not due to replicates but to the uncertainty of the method used.
[a] Nitrite concentration in samples was negligible.

with the probe ISE and the nitrate electrode method were 1.87 and $1.79 \pm 2.5\%\ mg\,l^{-1}$, respectively, whereas with standard additions these results lowered to 0.60 and $0.83 \pm 2.5\%\ mg\,l^{-1}$, respectively.

In fact, the major discrepancies were observed for the dry season samples. This is probably due to the high concentration of decomposing organic matter in the water, that may interfere with the functioning of the nitrate electrode. The water of the drying pools, that were sampled at the time, was deep brown, of oleaginous consistency and exhaled an offensive smell. It seems clear that the conditions were not ideal for accurate chemical determinations and that the chemistry of drying waters poses a considerable analytical challenge. In 2005, as the dry season began exceptionally early, discrepancies were evident in May, which were expected to be observed only in the August and September samples (Table 1).

However some samples collected during the wet season, and therefore less prone to matrix effects, still showed a difference of almost $0.2\ mg\,l^{-1}$ NO_3^--N between the results obtained with the probe and the cadmium reduction methods, when applied without standard additions (e.g., samples of 16 and 24 November 2004). It is also known that if the conductivity in the sample was all due to sodium bicarbonate, the sensor output would indicate $0.2\ mg\,l^{-1}$ of non-existent nitrate due only to the bicarbonate interference [6]. The values obtained in Table 1 suggest that, in these field samples, the predominant anion could be the bicarbonate. In fact, the bicarbonate concentration, in these samples, was about $100\ mg\,l^{-1}$, whereas the chloride concentration is on the range of $50\ mg\,l^{-1}$.

The other results obtained, for samples collected during the wet season, are in good agreement, comparing the probe with the column reduction method, with or without standard additions approach. It should be noticed that at this time of year the water is cleaner, presenting a low solid suspended particle concentration, and posing fewer matrix problems (Table 1).

4.3. The study of interferences

The effect of potential interfering ions normally found in association with chloride and nitrate was studied. A given ion was considered to significantly interfere with the determination when a mean change was observed in the results that reached at least 5%.

4.3.1. Bicarbonate interference

In order to study the possible interference of the bicarbonate ion on the determination of nitrate we measured nitrate, by the three methods under scrutiny, using standard solutions of $1\ mg\,l^{-1}$ (NO_3^--N) in the absence and in the presence of bicarbonate ion, with known concentrations (100 and $200\ mg\,l^{-1}$). These bicarbonate ion concentrations were chosen according to the range found in previous field sample analysis.

For the cadmium reduction method the changes observed were lower than 5%. However, the bicarbonate ion contributed to increase the values given for the concentration of nitrate when using the probe ISE and the nitrate electrode method, by a relative change of 100% and 27%, respectively. Moreover the probe ISE measurements were more affected by the increase in the bicarbonate concentration.

In order to study the influence of bicarbonate ion on the determination of chloride we determined chloride using standard solutions with $70\ mg\,l^{-1}$ (Cl^-) in the absence and presence of bicarbonate ions in two concentrations (100 and $200\ mg\,l^{-1}$). The bicarbonate ion does not interfere with the determination of chloride, the relative error associated being lower than 2%, both for the probe or the argentometric methods.

4.3.2. Chloride interference

To test the influence of chloride in the determination of nitrate we measured nitrate using standard solutions of $1\ mg\,l^{-1}$ (NO_3^--N) in the absence and presence of several chloride concentrations (50, 100, 150, 200, 250 and $300\ mg\,l^{-1}$ Cl^-). These concentrations were chosen according to the range of concentrations likely to be expected from our previous knowledge of chloride measurements in the *Pardiela* samples. It was observed that the presence of chloride in such concentrations enhances the nitrate measured values by about 10%, for all the three methods used. It can be concluded that chloride indeed interferes with the measurement of nitrate by such methods, but because such interference goes in the same sense and is of the same range for all the methods used, it may be not particularly relevant if our goal is the determination of trends or the understanding the gen-

eral biogeochemical behaviour of the river, more than absolute quantitation.

4.4. Recovery analysis with probe and standard methods

We have studied the response of the probe and of the adopted standard methods using field samples. For chloride the recovery obtained in real samples was 100% ($n = 3$; R.S.D. = 4%) using the probe and 97% ($n = 3$; R.S.D. = 0.3%) using the argentometric method. For ammonium the values obtained were 73% ($n = 3$; R.S.D. = 0.4%) with the probe and 98% ($n = 3$; R.S.D. = 2%) with the phenate method. For nitrate the values obtained with the probe were 105% ($n = 3$; R.S.D. = 4%), with the cadmium reduction method they were 97% ($n = 3$; R.S.D. = 3%) and with the nitrate electrode method they were 109% ($n = 3$; R.S.D. = 8%). The recoveries obtained were therefore good, with the exception of the recovery obtained for ammonium determined with the probe, which can only be considered as reasonable.

5. Conclusions

Although great emphasis is given in this work to the study of matrix effects, the results obtained supports the idea that, most of the time, the field monitoring of chloride, nitrate and ammonium, can be performed with ion selective electrodes, with all the advantages of *in situ* determinations. The probe is quite stable and robust, and provides very important information, that would be unavailable otherwise, particularly in what concerns the chemical response of the river to the first flood in the beginning of the wet season. The study of such response with the probe was in fact, the initial goal of this work, and this was accomplished. During dry season the conditions were adverse for all probe ion selective electrodes considered, particularly for the nitrate and the chloride electrodes.

It can also be concluded that a background correction is necessary, especially in the summer due to the complex and largely unknown matrix, if acceptable results are to be obtained. This can be done by regularly comparing the values obtained with the probe and the respective standard methods in the laboratory. Although not being always effective for chloride, the standard additions approach considerably reduces the matrix effects. Particularly when applied to nitrate, the results obtained with the probe and the cadmium reduction method shows a reasonable good agreement.

Acknowledgements

The authors are gratefully to the European Union and to the Fundação da Ciência e Tecnologia (FCT) for financial support under the Projects TempQsim EVK1-CT2002-00112 and ENVI-CHEMICA, respectively, and to the University of Évora for the use of laboratory facilities.

References

[1] J. Buffle, G. Horvai (Eds.), In Situ Monitoring of Aquatic Systems: Chemical Analysis and Speciation, Wiley, New York, 2000.
[2] J. Buffle, G.G. Leppard, Environ. Sci. Technol. 29 (1995) 2169.
[3] Y. Chen, J. Buffle, Water Res. 30 (1996) 2185.
[4] J. Buffle, K.J. Wilkinson, M.-L. Tercier, N. Parthasarathy, Ann. Chim. 87 (1997) 67.
[5] American Public Health Association (APHA), American Water Works Association and Water Environment Federation, Standard Methods for Examination of Water and Wastewater, 20th ed., American Public Health Association, Washington DC, USA, 1998.
[6] YSI Environmental Operations Manual—Environmental Monitoring Systems 6-Series.
[7] EPA/625/R-02/018, Delivering Timely Water Quality Information to Your Community—The Chesapeake Bay and National Aquarium in Baltimore, United States Environmental Protection Agency–EPA, Cincinnati, 2002.
[8] J.B. Jones, P. Mulholland (Eds.), Streams and Groundwaters, Academic Press, 2000.
[9] R. Wetzl, Limnology: Lake and River Ecosystems, 3rd ed., Academic Press, 2001.
[10] C.N. Dahm, M.A. Baker, D.I. Moore, J.R. Thibault, Freshwater Bio. 48 (2003) 1219.
[11] N. Prat, A. Munné, Water Res. 34 (2000) 3876.
[12] J.M. Holloway, R.A. Dahlgren, J. Hydrol. 250 (2001) 106.
[13] A.M.C. Belmonte, F.S. Beltrán, Catena 45 (2001) 229.
[14] R. Reeve, Introduction to Environmental Analysis. Analytical Techniques in the Sciences (Ants), Wiley, New York, 2002, p. 120.

Available online at www.sciencedirect.com
ScienceDirect
Talanta 71 (2007) 1016–1021
Talanta
www.elsevier.com/locate/talanta

Precise and accurate quantitative ^{13}C NMR with reduced experimental time

Elsa Caytan, Gérald S. Remaud *, Eve Tenailleau, Serge Akoka

Nantes University, LAIEM-UMR-CNRS 6006, Faculty of Science and Technology, 2 rue de la Houssinière, BP 92208, F-44322 Nantes Cedex 3, France

Received 9 February 2006; received in revised form 23 May 2006; accepted 26 May 2006
Available online 30 June 2006

Abstract

In order to detect small variations in ^{13}C isotopomers concentrations, high sensitivity, accuracy and precision have to be achieved. To assess such criteria, when using ^{13}C NMR, ^{13}C bi-labelled ethanol has been proposed as a molecular probe. Advantage has been taken of the pre-established structural relationship between the peak areas of the ^{13}C NMR spectrum of this molecule, i.e. the ratio of signal areas is set to a fixed value. It is shown that the quality performance, required by quantitative ^{13}C NMR spectroscopy, is not affected by a large reduction of the repetition delay using relaxation reagents.
© 2006 Elsevier B.V. All rights reserved.

Keywords: Quantitative NMR; SNIF NMR; ^{13}C NMR; Isotopomers; Accuracy; Precision; Relaxation reagents

1. Introduction

Quantitative NMR spectroscopy (qNMR) shows growing interest as illustrated by applications in several areas [1]. One of them has got a particular response in analytical chemistry: the SNIF NMR^{TM} method [2] (Specific Natural Isotope Fractionation by Nuclear Magnetic Resonance, a trade mark of EUROFINS, Nantes, France). This method, which is based on quantitative ^{2}H NMR, was proposed by Martin and Martin [3] in the early 80's as a technique to detect and to quantify the illegal chaptalization of wines. It was then possible to assay the amount of ethanol from the fermentation of sugar beet into ethanol from fermentation of grape sugar (wine) [4]. The use of ^{2}H NMR for quantifying isotopomers was extended to other molecules and other matrices for authenticity [5,6], forensic [7] and metabolic [8,9] studies.

Even though the ^{13}C content is a very valuable information, very few similar approaches for the determination of ^{13}C isotopomer concentrations, at natural abundance level, were published [10–15]. Among these works, kinetic isotopic effects were studied in order to probing mechanisms of organic reactions and/or transition states [13–15]. Unfortunately, only precision was addressed, there was no mention of accuracy and the influence of the stability of the spectrometer on the results. Although, the ^{13}C NMR spectroscopy has the advantage to be much more sensitive than ^{2}H NMR, two main difficulties are encountered in quantitative ^{13}C NMR for isotopic measurement purposes [16]: (i) the nuclear overhauser effect (NOE) should be eliminated by inverse-gated decoupling sequence leading to long experimental time, since the repetition period should be set to at least $7 \times T1$ (longitudinal relaxation time) and (ii) the variation of the ^{13}C content is small in natural products (∼5%) compared to the scale of ^{2}H content (∼50%) [17]. To appreciate such small variations in $^{13}C/^{12}C$ ratios, analytical methods must be very sensitive, accurate and precise. Isotope ratio mass spectrometry (IRMS) matches these requirements [18]: the sensitivity, accuracy and precision of this technique are better than 0.1%. Therefore, IRMS is usually employed to obtain the ^{13}C content of organic material. However, it provides only the global mean value: the carbon atoms of the whole molecule are transformed in CO_2 prior to introduction into the source of the mass spectrometer [19]. Hence the ^{13}C distribution information within the molecule is lost. Site-specific data are obtained only following time-consuming chemical degradations into smaller molecules and the isolation of these fragments [20]. On a routine basis, ^{13}C NMR appears as the only technique, which allows the determination of the $^{13}C/^{12}C$ ratios at each site of a given molecule.

Recently our work has been focussed on the use of quantitative ^{13}C NMR for site-specific ^{13}C distribution (^{13}C SNIF NMR) [21,22]. In order to reach a performance of about 0.1%, several

* Corresponding author. Tel.: +33 2 51 12 57 19; fax: +33 2 51 12 57 12.
E-mail address: Gerald.Remaud@univ-nantes.fr (G.S. Remaud).

0039-9140/$ – see front matter © 2006 Elsevier B.V. All rights reserved.
doi:10.1016/j.talanta.2006.05.075

technical points were tackled, such as decoupling problems. Our goal does not lie in the ability to assay an analyte at a concentration level of 1‰, but rather, it focuses on the possibility to assess, by ^{13}C NMR, variations of the order of 1‰ of the analyte concentrations (i.e. concentration of ^{13}C isotopomers). In a previous work, we proposed a two-carbon bi-labelled molecule for probing the accuracy of ^{13}C SNIF NMR [23]. In such a molecule, the relative signal areas ratio between the resonances is structurally defined. Therefore, it is a very valuable experimental model to explore the quality capabilities of the NMR spectrometer, which could be transposed latter on target molecules at natural abundance. In the present investigation, we aimed to use in more detail this concept to study the reduction of the experimental time, due to long repetition delays encountered in quantitative ^{13}C NMR, by addition of paramagnetic reagents.

2. Experimental

2.1. Material

^{13}C bi-labelled ethanol (99% ^{13}C), aceton-d_6 and $CDCl_3$ were purchased from Eurisotop. Vanillin ex-lignin was purchased from Aldrich. Tris(2,4-pentadionato)chromium (III) (97%), CrAcac was purchased from AcrosOrganics.

2.2. Sample preparation

For ethanol samples: 100 μL of ^{13}C bi-labelled ethanol, 200 or 0 μL of 0.1 M CrAcac solution in $CDCl_3$ and 800 or 1000 μL of $CDCl_3$, respectively. For vanillin samples: 500 mg of solid vanillin, 500 μL of aceton-D_6, 200 or 0 μL of 0.1 M CrAcac solution in aceton and 300 or 500 μL of aceton, respectively.

2.3. NMR experiments

Quantitative ^{13}C NMR spectra were recorded using a Bruker DRX 500 spectrometer fitted with a 5 mm-i.d. dual probe $^{13}C/^{1}H$ carefully tuned at the recording frequency of 125.76 MHz. The temperature of the probe was set at 303 K. The experimental parameters for ^{13}C NMR spectral acquisition were the following: pulse width 4.3 μs (90°), spectral width 10,000 Hz, sampling period 1 s. For ethanol samples, 8 scans were recorded leading to a signal/noise ratio of 5000, and for vanillin samples, 92 scans leading to a signal/noise ratio of 3000. Inverse-gated decoupling techniques were applied in order to avoid NOE. The decoupling sequence employed a cosine adiabatic pulse with appropriate phase cycles, as described in ref [24]. The decoupling power was corresponding to $\gamma B_2/2\pi = 75.16$ kHz. The offset of the decoupler was placed at the middle of the proton frequency range.

For the study of the two-carbon bi-labelled molecule, repetition delay times (RD) were 12, 30 or 100 s for sample with CrAcac, and 150 s for sample without CrAcac. Twelve spectra were recorded for each measurement of sample with relaxation agent (acquisitions distributed over 24 h), and 25 spectra were recorded for each measurement of sample without CrAcac (acquisitions distributed over 6 h). T_1 values were determined by using an inversion recovery sequence, with 14 or 16 inversion-time values of τ ranging from 10 ms to 80 or 180 s (for samples with or without CrAcac, respectively) and by using the T_1 processing software of the spectrometer. NOE values were determined by comparing peak areas from spectra with inverse-gated decoupling and from spectra with high decoupling power during acquisition and low decoupling power during relaxation delay in order to maintain NOE. The normalisation of the signal area was achieved by using the electronic internal reference method ERETIC™ (electronic reference to access in vivo concentrations, a trade mark of BRUKER Biospin, Wissembourg, France) [25,26].

For isotopic measurements of vanillin samples, five spectra were acquired for each sample.

2.4. Data processing

Free induction decay was submitted to an exponential multiplication inducing a line broadening of 2 Hz. The curve fitting was carried out in accordance with a Lorentzian mathematical model using Perch Software (Perch NMR Software, University of Kuopio, Finland).

2.5. Isotopic data

The isotopic distribution into a molecule is characterised by the actual ^{13}C molar fractions f of a specific site i, $f_i = S_i/S_T$ where S_i is the area of the ^{13}C NMR signal of i and S_T is the sum of the areas of all the signals of the molecule. The shift from the random distribution of ^{13}C, which is the main discrimination factor of the origin of the molecule, may be expressed as the f_i/F_i ratio named the reduced molar fraction, where F_i is the statistical molar fraction (for further information on these parameters, see ref. [2]).

3. Results and discussion

3.1. The analytical performance to be reached

The ^{13}C content is usually presented by the isotopic deviation δ ‰ (which should not be confused with the NMR chemical shift), defined as [19]:

$$\delta_i = (R_i/R_{VPDB} - 1) \times 1000 \quad (1)$$

with $R_i = {}^{13}C/{}^{12}C = A_i/(1-A_i)$ (R_i = isotopic ratios, A_i = isotopic abundance of a site i), where the reference product is the V-PDB (Vienna-Pee Dee Belemnite, the international standard, $R_{VPDB} = 0.0112372$) [27]. For natural products, various ^{13}C contents are observed according to the metabolism of the plant and the climatic conditions. As an illustration [28], $\delta^{13}C$ of ethanol samples, fermented from beet sugar, is found around −28‰ ($^{13}C/^{12}C = 0.010923$), while ethanol issued from corn or cane sugar shows $\delta^{13}C$ around −12‰ ($^{13}C/^{12}C = 0.011102$). These values are currently measured by IRMS with a sensitivity and a precision better than 0.1% (1‰ on the $\delta^{13}C$ scale).

Nowadays, in NMR, the quantification limit (described as the lowest concentration of an analyte that can be determined with acceptable precision) can be as low as 0.1%. This represents, in fact, around 1/5 of ^{13}C satellite peak areas, which are detected on both sides of the main resonance in a ^{1}H NMR spectrum [16]. With sufficient signal-to-noise ratio, this limit is technically currently observable [29]. The challenge we address in the present work requires an higher performance. The sensitivity (ability of the instrument to detect small changes of the analyte concentrations) [30] of the NMR spectrometer has to be around 1‰. Ideally, ^{13}C SNIF NMR should distinguish $^{13}C/^{12}C$ ratios of a molecular site which differ by 1‰, e.g. distinction between $^{13}C/^{12}C = 0.01055$ and $^{13}C/^{12}C = 0.01056$, as an example. In practice, the internal distribution of ^{13}C within a molecule is a more powerful phenomenon for discriminating origin than is the global value [21,22,31]. Therefore, a ^{13}C NMR sensitivity of about 2‰ would be, as a start, of a great importance in isotopic analyses.

The NMR precision, in term of repeatability and reproducibility, should be suitable with the above sensitivity, i.e. below 2‰. This can be expressed by the standard deviation calculated from replications of experiments. The remaining quality parameter, the accuracy, should not show a bias larger than 2‰. The ^{13}C SNIF NMR accuracy would not be assessed in the isotopic deviation scale, but rather it will be achieved when the measured internal ^{13}C distribution defined by the reduced molar fraction (see Section 2) will be in agreement with the theoretical one.

3.2. Two-carbon bi-labelled molecular probes

The checking of the above performances is not straightforward. Indeed, it is difficult to define the accuracy of the site-specific isotope ratios, since SNIF NMR is the only method by which they are directly accessible. As mentioned, this information is also achieved by IRMS, but it is too tedious and time-consuming for a general application to multi-site molecules. Nonetheless, it is conceivable to study by ^{13}C NMR a blend of molecules with precise concentrations and for which the ^{13}C content has been measured previously by IRMS. However, the requirements of such a design, i.e. purity of these molecules, uncertainties of weighing, uncertainties of IRMS data, would be a hard task to be achieved.

We have chosen the bi-labelled ^{13}C ethanol molecule as a probe to sensitivity and accuracy for ^{13}C SNIF NMR. Fig. 1 shows the proton decoupled ^{13}C NMR spectrum (NOE suppressed) of bi-labelled ^{13}C ethanol. Four isotopomers constitute the molecule (see Scheme 1). Among these, isotopomer 1 is not visible in NMR since the ^{12}C nucleus has a nuclear spin equal to zero. Isotopomers 2 and 3 appear as a single peak, for which the intensity is dependent on the isotopic abundance of the methylene and methyl sites, respectively. The signal of each ^{13}C in isotopomer 4, is described by a doublet, due to carbon–carbon coupling. Therefore, the area of both doublets should be strictly identical, independently of the real ^{13}C abundance of each site of bi-labelled ethanol. On other words, the ratio of the integral of the "CH_2" doublet over the integral of the "CH_3" doublet should be equal to 1.000. If the phenomenon is described in term of

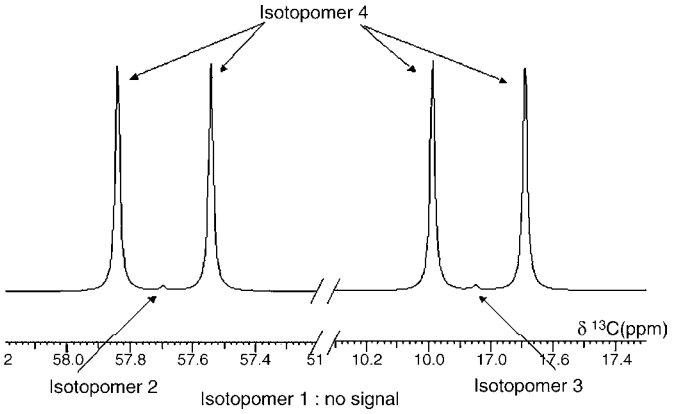


Fig. 1. ^{13}C NMR spectrum of ^{13}C bi-labelled ethanol, recorded with inverse-gated pulses sequence for NOE suppress. The numbering of isotopomers refers to Scheme 1.

experimental molar fractions f and statistical molar fractions F, a new parameter Δ may be set, described by

$$\Delta‰ = (f_{CH2}/F_{CH2} - 1) \times 1000 \quad (2)$$

where f/F are the reduced molar fractions (see experimental). It should be noted that, for this molecule, Δ could also be described using the CH_3 site, as $\Delta‰ = (f_{CH3}/F_{CH3} - 1) \times 1000$. In ^{13}C bi-labelled ethanol (isotopomer 4), Δ should be 0 ‰, since $f_{CH2} = F_{CH2} = f_{CH3} = F_{CH3}$. Thus, Δ is a suitable parameter for gauging the sensitivity and the accuracy of ^{13}C NMR.

3.3. ^{13}C SNIF NMR on bi-labelled ^{13}C ethanol

The measurement conditions are of prime importance for reliable results in ^{13}C SNIF NMR. The classical inverse-gated pulses sequence is designed for the suppression of the nuclear overhauser effect (NOEs), provided that the sampling period (acquisition time) is short enough and the repetition delay (RD) is appropriate [16]. Accordingly, we have chosen an acquisition time of 1 s to limit the heating of the probe and to reduce the size of NOE. Full theoretical descriptions indicate that the RD should allow the recovery of the magnetization to its initial value and should annul the NOEs [16,32,33]. RD is usually set to a value between $7 \times T1_{max}$ and $10 \times T1_{max}$ (the longest longitu-

Isotopomer 1 : $^{12}CH_2OH^{12}CH_3$

Isotopomer 2 : $^{13}CH_2OH^{12}CH_3$

Isotopomer 3 : $^{12}CH_2OH^{13}CH_3$

Isotopomer 4 : $^{13}CH_2OH^{13}CH_3$

Scheme 1. Carbon isotopomers of ^{13}C bi-labelled ethanol.

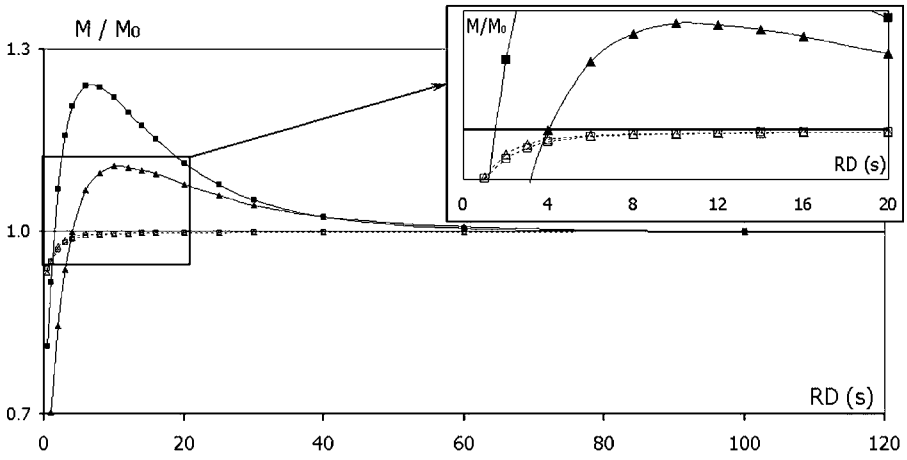


Fig. 2. Normalised M/M_0 (magnetization/thermal equilibrium magnetization) with respect to the repetition delay RD. The normalisation between each experiment is ensured by the ERETIC methodology (see Section 2). The zoom box shows that M/M_0 of CH_3 and CH_2 groups in sample containing CrAcac is reaching an asymptote for RD = 12 s. (▲) M/M_0 of CH_2 group in sample free of CrAcac. (△) M/M_0 of CH_2 group in sample containing CrAcac. (■) M/M_0 of CH_3 group in sample free of CrAcac. (□) M/M_0 of CH_3 group in sample containing CrAcac.

dinal time in the system under investigation), for a pulse angle of 90°. The actual RD value can be further calculated, once the NOE factor and the $T1$ values are measured [32]. Other experimental parameters could influence the performances of the ^{13}C NMR. Among them, we have demonstrated [23] that the ^{1}H decoupling efficiency should be optimised in term of frequency range and of homogeneity over that range.

For the present work, we have used the best conditions so far established [34]. The $T1$ values of the carbon 13 of the bi-labelled ethanol are 16.2 s for CH_2 and 11.9 s for CH_3. Here, the optimum RD cannot be simply calculated from $T1$s and NOEs. The fragment ^{13}C–^{13}C–^{1}H of the molecule introduces additional factors such as the ^{13}C–^{13}C dipole effect and dipolar shift anisotropy [34]. Nevertheless, we have experimentally determined the best RD value for our molecular probe. Fig. 2 shows the evolution of the relative signal intensity of the carbon atoms (after normalisation) with respect to the RD. It is clear that the recovery of the magnetization to its initial value, for both carbons, is reached when the RD value is set to about 120 s (experimentally, we have chosen RD = 150 s, as a safe latitude). The decoupling mode was provided by adiabatic pulses sequences [35,36].

Once these experimental conditions (optimised RD and decoupling scheme) have been selected, Δ values have been calculated on several spectra. As shown in Table 1, the experimental value of Δ is 1‰, which is very close to the target value of 0‰. Other parameters than the decoupling mode and the efficiency of NOE suppress could be at the origin the shifts of the Δ values. The precision is assessed by the standard deviation calculated over 25 replicates. The standard deviation indicates that the variability of the ^{13}C NMR measurements are lower than 2‰ as expected. These results, in terms of accuracy and precision, are in full agreement with the criteria, which should be achieved.

Table 1
Δ values (Eq. (2)) and standard deviations (S.D.) found for ^{13}C bi-labelled ethanol samples, with a repetition delay RD = 150 s without paramagnetic reagent, and RD = 100, 30 or 12 s with the presence of a 20 mM solution of CrAcac as relaxation reagent

Sample	No CrAcac	With CrAcac		
RD (s)	150	100	30	12
Δ (‰)				
Mean	−1.0	−0.8	−0.8	−0.8
S.D.[a]	0.2	0.2	0.2	0.2

[a] Standard deviation over 25 or 12 measurements for sample without or with CrAcac, respectively.

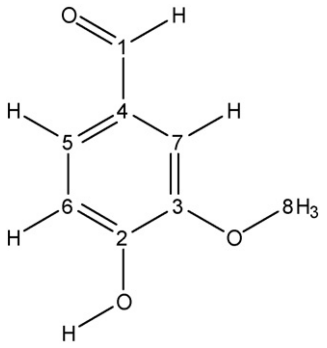
3.4. Applications at natural abundance and paramagnetic reagent effects

A RD value of 150 s would lead to very long experimental times for studies performed at natural abundance. For molecule with quaternary carbons, this delay can even be dramatically longer. This is the main drawback of the methodology for a routine application. A solution consists in shortening of the relaxation times by the addition of a paramagnetic reagent [16,33]. The relaxation is then governed by the efficient electronic dipolar mechanism instead of the much less efficient proton-carbon dipolar one. The questions we have addressed in the present study are the influence of the paramagnetic reagents on the sensitivity, the accuracy and the precision on ^{13}C SNIF NMR. The suitable answer should be brought by the behaviour of the two-carbon bi-labelled model under these new constraints. Upon addition of Tris(2,4-pentanedionato)chromium(III) (CrAcac), the $T1$ values of the bi-labelled ethanol are reduced to 1.3 s for CH_2 and 1.8 s for CH_3. This reducing of the relaxation time is associated to an increase of the line width [16]. Therefore, the amount of added CrAcac is a compromise between the desired shortening of $T1$ and the excessive line broadening counterpart. Subsequently, solutions of bi-labelled ethanol containing 20 mM of CrAcac were used to probe the performance of the ^{13}C NMR experiments. Since the proton-carbon dipolar contribution to $T1$ is not suppressed (it is only overwhelmed by the electronic dipolar contribution) [33], RD is not simply $7 \times T1_{rel}$ to $10 \times T1_{rel}$ (where $T1_{rel}$ is $T1$ after addition of CrAcac). The optimised RD could be retrieved from simulations. Again mathematical calcu-

Table 2
*T*1 values and ^{13}C internal distribution on vanillin, expressed as fi/Fi and as $\delta\,^{13}C$ ‰ (Eq. (1)), for each carbon of the molecule (see Scheme 2), without paramagnetic reagent and with the presence of a 20 mM solution of CrAcac as relaxation reagent

Parameter	Carbon	1	2	3	4	5	6	7	8
*T*1 (s)	No CrAcac	2.8	11.7	18.7	13.4	2.0	2.4	2.4	2.9
	With CrAcac	1.1	1.3	1.5	1.6	0.9	0.9	1.0	0.9
f_i/F_i: Mean	No CrAcac	0.9905 (0.0006)	0.9990 (0.0005)	0.9993 (0.0025)	1.0041 (0.0015)	1.0008 (0.0021)	0.9990 (0.0008)	1.0033 (0.0032)	1.0032 (0.0025)
S.D.[a]	With CrAcac	0.9915 (0.0011)	1.0011 (0.0020)	1.0001 (0.0023)	1.0026 (0.0019)	0.9989 (0.0006)	1.0001 (0.0013)	1.0043 (0.0015)	1.0009 (0.0022)
$\delta\,^{13}C$ (‰)[b]: Mean	No CrAcac	−35.9 (0.6)	−27.5 (0.5)	−27.2 (2.4)	−22.5 (1.4)	−25.7 (2.1)	−27.5 (0.8)	−23.3 (3.2)	−23.3 (2.4)
S.D.[a]	With CrAcac	−34.8 (1.1)	−25.4 (2.0)	−26.4 (2.2)	−23.9 (1.8)	−27.5 (0.6)	−26.4 (1.3)	−22.3 (1.5)	−25.6 (2.1)

[a] Standard deviation over five measurements.
[b] Calculated from the f_i/F_i ratio and the global $\delta\,^{13}C$ of the vanillin sample, see ref. [21].



Scheme 2. Molecular structure of vanillin with numbering of carbons (decreasing ^{13}C chemical shift).

lations are very complicated in our model with the ^{13}C–^{13}C–^{1}H fragment [34]. Therefore, we have preferred to chose the actual RD from experimental data based on the control of the recover of the magnetization to its initial value as shown in Fig. 2. Thus, a RD value of 12 s can be safely used. This is further confirmed by the results of Table 1: the Δ parameter is not affected when RD is set to 12 s or to higher values with respect to the CrAcac free experiment. The data clearly demonstrate that the paramagnetic reagent CrAcac does not influence the accuracy of the quantitative ^{13}C NMR spectroscopy. Similarly, the precision which has been assessed from the standard deviation obtained from 12 replicates is not significantly different with respect to the CrAcac free reference experiment: $\Delta \leq 1.0$‰, with a standard deviation of 0.2‰.

Therefore, a reduction of the experimental time by a large factor (12.5 for bi-labelled ethanol) may be achieved. This is further illustrated by the study of a molecule at natural abundance. We have chosen vanillin (see Scheme 2) as an example, since this product has been intensively investigated by ^{13}C NMR [21]. A large reduction of the *T*1 values for each carbon in vanillin upon addition of CrAcac is found (Table 2). The corresponding RD values are calculated from at least $10 \times T1_{max}$: 20 or 200 s, respectively. The ^{13}C SNIF NMR results obtained either with or without CrAcac are summarised in Table 2. The values obtained in the present work for the relaxation reagent free vanillin sample are in agreement with those previously measured on the same sample [21]. No significant difference is observed when using CrAcac, with a reduction factor of RD of the order of 10.

4. Conclusion

^{13}C SNIF NMR should be a very valuable method for quantifying the $^{13}C/^{12}C$ content of isotopomers. Although, quality performance, such as sensitivity, accuracy and precision of the analytical method are essential for a routine use. The present work has shown that these parameters can be separately studied by using bi-labelled ethanol as a molecular probe. Thus, the best experimental conditions for quantitative ^{13}C NMR may be set: NOE suppress, multi-pulses decoupling scheme. Using this concept, we have shown that the long experimental time, which is associated to long longitudinal relaxation times (*T*1) of ^{13}C signals, could be efficiently reduced by addition of CrAcac.

Thus, it is expected that in routine use, valuable information on the ^{13}C internal distribution can be retrieved in a short time by ^{13}C SNIF NMR. Other instrumental parameters may also be source of uncertainty. Among them, the hardware and the sample temperature variations are known to be potential sources of ^{13}C NMR variability and instability [37]. The two-carbon bi-labelled molecule approach will also be beneficial to assess the effect of these phenomena on the accuracy and precision of NMR experiments.

Acknowledgment

We are grateful to Dr. R. Robins for reviewing the manuscript and for fruitful discussions.

References

[1] See for example: V. Rizzo, V. Pinciroli, J. Pharm. Biomed. Anal. 38 (2005) 851.
[2] G.J. Martin, M.L. Martin, Annu. Rep. NMR Spectrosc. 31 (1995) 81.
[3] G.J. Martin, M.L. Martin, Tetrahedron Lett. 22 (1981) 3525.
[4] Council regulation EEC No. 2676/90, Official Journal of the European Communities L272 (1990) 64.
[5] G.S. Remaud, Y.-L. Martin, G.G. Martin, G.J. Martin, J. Agric. Food Chem. 45 (1997) 859.
[6] G.S. Remaud, A.A. Debon, Y.-L. Martin, G.G. Martin, G.J. Martin, J. Agric. Food Chem. 45 (1997) 4042.
[7] P.A. Hays, G.S. Remaud, E. Jamin, Y.-L. Martin, J. Forensic Sci. 45 (2000) 552.
[8] B.-L. Zhang, I. Billault, X. Li, F. Mabon, G.S. Remaud, M.L. Martin, J. Agric. Food Chem. 50 (2002) 1574.
[9] R.J. Robins, I. Billault, J.-R. Duan, S. Guiet, S. Pionnier, B.-L. Zhang, Phytochem. Rev. 2 (2003) 87.
[10] V. Caer, M. Trierweiler, G.J. Martin, M.L. Martin, Anal. Chem. 63 (1991) 2306.
[11] B.-L. Zhang, S. Buddrus, M. Trierweiler, G.J. Martin, J. Agric. Food Chem. 46 (1998) 1374.
[12] B.-L. Zhang, M. Trierweiler, C. Jouitteau, G.J. Martin, Anal. Chem. 71 (1999) 2301.
[13] D.A. Singleton, A.A. Thomas, J. Am. Chem. Soc. 117 (1995) 9357.
[14] N.J. Saettel, O. Wiest, D.A. Singleton, M.P. Meyer, J. Am. Chem. Soc. 124 (2002) 11552.
[15] J.K. Lee, A.D. Bain, P.J. Berti, J. Am. Chem. Soc. 126 (2004) 3769 (and references therein).
[16] R.R. Ernst, G. Bodenhausen, A. Wokaun, Principles of Nuclear Magnetic Resonance in One and Two Dimensions, Clarendon Press, Oxford, 1987.
[17] G.J. Martin, S. Hanneguelle, G. Remaud, Ital. J. Food Sci. 3 (1993) 191.
[18] J.P. Jasper, Rapid Commun. Mass Spectrom. 15 (2001) 1554.
[19] A. Barrie, S.J. Prosser, Automated analysis of light-element stable isotopes by isotope ratio mass spectrometry, in: T.W. Boutton, S. Yamasaki (Eds.), Mass Spectrometry of Soils, Marcel Dekker Inc., New York, 1996, pp. 1–46.
[20] D. Weber, H. Kexel, H.-L. Schmidt, J. Agric. Food Chem. 45 (1997) 2042.
[21] E.J. Tenailleau, P. Lancelin, R.J. Robins, S. Akoka, J. Agric. Food Chem. 52 (2004) 7782.
[22] E. Caytan, G.S. Remaud, Poster: global methodology for ^{13}C-SNIF-NMR on glycerol, in: 8th International Symposium Authenticity and Safety of Fruit-Based Products and Beverages, Nantes, France, October 19 and 20, 2005.
[23] E.J. Tenailleau, G.S. Remaud, S. Akoka, Instrum. Sci. Technol. 33 (2005) 391.
[24] S. Akoka, E.J. Tenailleau, Poster: precise and accurate quantitative 13C-NMR at natural abundance, in: 46th ENC, Providence, Rhode Island, USA, April 10–15, 2005.
[25] S. Akoka, L. Barantin, M. Trierweiler, Anal. Chem. 71 (1999) 2554.
[26] V. Silvestre, S. Goupry, M. Trierweiler, R. Robins, S. Akoka, Anal. Chem. 73 (2001) 1862.
[27] R. Gonfiantini, W. Stichler, K. Rozanski, IAEA, reference and intercomparison materials for stable isotopes of light elements, in: Proceeding of a consultant meeting held in Vienna, IAEA-Techdoc-825, December 1–3, 1993, pp. 13–29.
[28] M.L. Martin, G.J. Martin, C. Guillou, Mikrochim. Acta (II) (1991) 81–91.
[29] P. Soininen, J. Haarala, J. Vepsäläinen, M. Niemitz, R. Laatikainen, Anal. Chim. Acta 542 (2005) 178.
[30] R. Ekins, P. Edwards, Clin. Chem. 43 (1997) 1824.
[31] A. Rossmann, M. Butzenlechner, H.-L. Schmidt, Plant Physiol. 96 (1991) 609.
[32] D. Canet, J. Magn. Reson. 23 (1976) 361.
[33] D.J. Cookson, B.E. Smith, J. Magn. Reson. 57 (1984) 355.
[34] D. Canet, H. Nery, J. Brondeau, J. Chem. Phys. 70 (1979) 2098.
[35] M. Garwood, L. DelaBarre, J. Magn. Reson. 153 (2001) 155.
[36] Z. Starcuk, K. Bartusek, Z. Starcuk, J. Magn. Reson. A 107 (1994) 24.
[37] P.J. Bowyer, A.G. Swanson, G.A. Morris, J. Magn. Reson. 152 (2001) 234.

Available online at www.sciencedirect.com
ScienceDirect
Talanta 71 (2007) 1246–1251
Talanta
www.elsevier.com/locate/talanta

Rapid and sensitive determination of proteins by enhanced resonance light scattering spectroscopy of sodium lauroyl glutamate

Zhanguang Chen *, Jinbin Liu, Yali Han

Department of Chemistry, Shantou University, Shantou 515063, China

Received 15 April 2006; received in revised form 18 June 2006; accepted 18 June 2006
Available online 27 July 2006

Abstract

A rapid and sensitive method for the determination of proteins is proposed based on the measurements of the enhanced resonance light scattering (RLS) spectroscopy of sodium lauroyl glutamate (SLG). Under the optimum conditions, the interaction between SLG and proteins occurred rapidly, resulting in greatly enhanced RLS intensity with the maximum peak located at 394 nm. It was found that the enhanced RLS intensities were in proportion to the concentrations of proteins in the range of 0.01–3.1 μg ml^{-1} depending on the kind of proteins. The detection limits were below 6 ng ml^{-1}. Compared with some other methods for the determination of proteins, this method shows high sensitivity, low detection limit and simplicity. This is an inexpensive, simple and fast one-step procedure which requires only measuring the RLS intensities. Human serum samples were determined with satisfactory results.
© 2006 Elsevier B.V. All rights reserved.

Keywords: Resonance light scattering (RLS); Sodium lauroyl glutamate (SLG); Acylamino acid-type surfactant; Proteins

1. Introduction

The development of novel methods for the determination of proteins is of great importance in a number of areas, such as chemical and biochemical analysis, clinical diagnosis and biotechnology. Spectrophotometric methods, such as Biuret [1], Lowry [2], and Bradford [3], which are based on the distinct color change of dyes on binding proteins, have been widely used for the determination of proteins. However, these methods have their defects in terms of sensitivity, selectivity and simplicity. In order to solve some of these problems, chemiluminescence [4] and fluorescence [5] methods were developed. At present, resonance light scattering (RLS) technique has become the preferred choice for the study and determination of proteins.

RLS technique as an analytical method has the distinct advantages of speed, convenience and sensitivity. RLS is an elastic scattering occurs when the incident beam is close in energy to an absorption band. RLS is an extremely sensitive and selective technique for monitoring molecular assemblies. Since Pasternack et al. established the RLS technique to study biological macromolecules with a common fluorescence spectrometer [6–8], it has been increasingly applied to the study and determination of nucleic acids [9–13], proteins [14–17], amino acid [18], saccharide [19,20], medicines [21,22] and metal ions [23,24]. In this paper, we have developed a novel method for the direct determination of the trace amount of total protein based on the interaction between sodium lauroyl glutamate (SLG) and proteins by RLS technique.

This assay is based on the observation that the RLS intensity of SLG is strongly enhanced by proteins. SLG is an acylamino acid-type surfactant that can be easily purchased from the market. The acylamino acid-type surfactants display high foam stability and are less irritating to the skin than many other ionic surfactants [25]. Because of these useful characteristics, they are often combined with other surfactants in many consumer products, such as cosmetics, health care products, and pharmaceuticals. Some anion surfactants have been used for the determination of proteins by RLS technique with good sensitivity [26]. But the use of acylamino acid-type surfactant as the probe for the direct determination of proteins has not yet been reported. Its excellent and special properties would prove SLG

* Corresponding author. Tel.: +86 7542903330.
E-mail address: kqlu@stu.edu.cn (Z. Chen).

0039-9140/$ – see front matter © 2006 Elsevier B.V. All rights reserved.
doi:10.1016/j.talanta.2006.06.025

a much better protein probe than some other anion surfactants. Our experiments showed that this method has the merits of simplicity, high sensitivity and relative absence of interferences. The samples of human serum were analyzed with satisfactory results. The mechanism of the reaction between SLG and proteins was also discussed.

2. Experimental

2.1. Apparatus

The RLS spectra and fluorescence spectra were measured with a Perkin-Elmer Model LS-55 spectrofluorometer equipped with a quartz cuvette (1 cm × 1 cm). An SA 720 instrument (Orion Research) was used to measure the pH of the solution.

2.2. Reagents

The stock solutions of proteins were prepared by dissolving commercially purchased proteins in doubly distilled water. The concentration of the working solution was 20.0 μg ml^{-1} by diluting the protein stock solutions. Proteins in this work included bovine serum albumin (BSA), human serum albumin (HSA) (Sino-American Biotechnology Company, China) and γ-globulin (γ-G), lysozyme and hemoglobin (bovine) (Sigma, St. Louis, MO, USA). They were all stored at 0–4 °C.

Sodium lauroyl glutamate (SLG) was obtained from Shanghai Leasun Chemical Co. Ltd. (China). Its stock solution was prepared by dissolving the product in the doubly distilled water and the concentration of its working solution was 1.0×10^{-3} mol l^{-1}.

The Britton-Robinson (BR) buffer solution, being made up of 0.04 mol l^{-1} phosphoric acid, 0.04 mol l^{-1} acetic acid, 0.04 mol l^{-1} boric acid, 0.2 mol l^{-1} sodium hydroxide, was used to control the acidity of the solution. 0.05 mol l^{-1} NaCl solution was used to adjust the ionic strength of the aqueous solution.

Human serum samples were bought from Shantou Central Hospital and diluted with doubly distilled water.

All chemicals used were of analytical grade or the best grade commercially available and doubly distilled water was used throughout.

2.3. General procedures

Into a 10-ml calibrated flask were added 1.0 ml Britton-Robinson buffer, 1.2 ml the working solution of SLG and appropriate proteins (or samples), then diluted to 10.0 ml with doubly distilled water and stirred thoroughly.

All RLS spectra were obtained by scanning simultaneously the excitation and emission monochromators ($\Delta\lambda = 0.0$ nm) from 250.0 to 700.0 nm with the excitation and emission slits 8.0 nm wide. The RLS intensities were measured at 394 nm. The enhanced RLS intensity of the system by proteins was represented as $\Delta I_{RLS} = I_{RLS} - I^0_{RLS}$ (I_{RLS} and I^0_{RLS} were the RLS intensities of the systems with and without proteins).

3. Results and discussion

3.1. Spectral characteristics and reaction

The RLS spectra of the reagent blank and the SLG–BSA system under optimum conditions (1.2×10^{-4} mol l^{-1} SLG; pH 4.0) are shown in Fig. 1. It can be seen that the RLS intensity of the reagent blank is very weak in the wavelength range of 250–700 nm. However, the enhanced RLS intensity can be clearly observed with a maximum peak located at 394 nm when a trace amount of BSA was added. Enhanced RLS shoulder peaks at 454 and 485 nm can also be observed, and moreover, the enhanced RLS intensity increases with the increasing BSA concentration. Therefore, 394 nm was selected as the analytical wavelength. It can be consequently concluded that SLG reacted with BSA and produced a complex of which RLS intensity was much higher than that of BSA or SLG when they existed separately.

The fluorescence excitation (line 1) and emission (line 2) spectra of BSA are shown in Fig. 2. It can be seen only one emission peak located at 344 nm in the emission spectra (b) and two excitation peaks located at 224 and 281 nm. Fig. 3a displays the effects of SLG at variable concentrations on the fluorescence

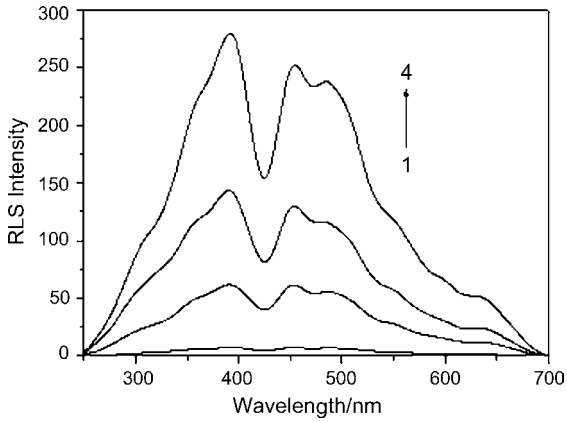


Fig. 1. The RLS spectra of the SLG (line 1) and SLG–BSA system (lines 2–4). Conditions: $C_{SLG} = 1.2 \times 10^{-4}$ mol l^{-1}, C_{BSA} (μg ml^{-1}): (1) 0.0; (2) 0.4; (3) 1.0; (4) 2.0; pH 4.0.

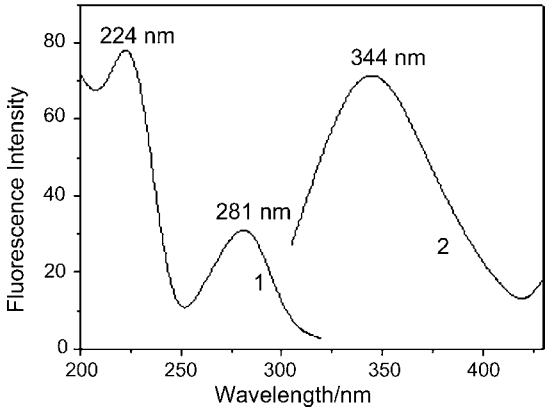


Fig. 2. The fluorescence excitation (line 1) and emission (line 2) spectra of BSA. Conditions: $C_{BSA} = 1.0$ μg ml^{-1}; pH 4.0.

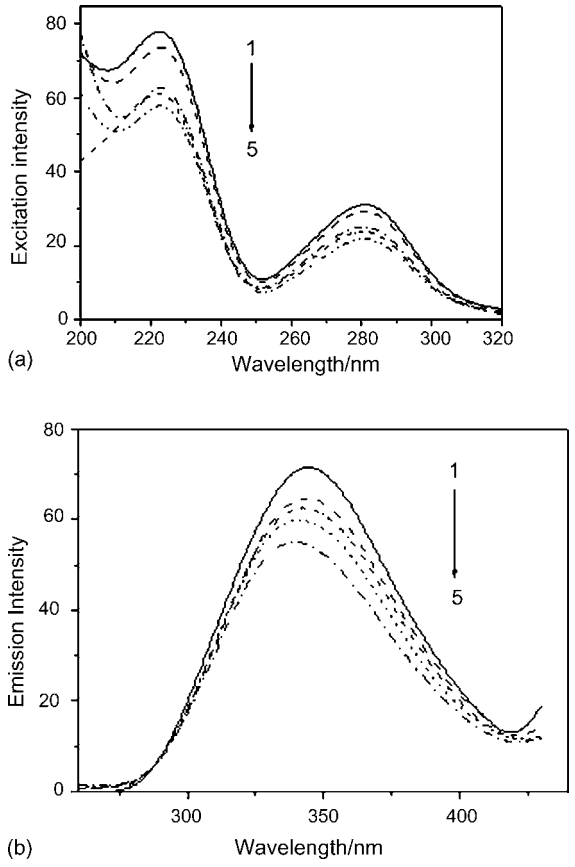


Fig. 3. The effect of SLG at variable concentrations on the fluorescence excitation (a) and emission (b) spectra of BSA. Conditions: $C_{BSA} = 1.0\ \mu g\ ml^{-1}$, C_{SLG} ($mol\ l^{-1}$): (1) 0; (2) 0.4×10^{-4}; (3) 0.8×10^{-4}; (4) 1.2×10^{-4}; (5) 1.6×10^{-4}; pH 4.0.

excitation spectra of the BSA system ($\lambda_{em} = 344$ nm). The results show that the intensity of the excitation spectra was affected by the addition of the SLG, together with a gradual red shift. This phenomenon indicated that the interaction between the SLG and the protein occurred. The presence of SLG also modified the wavelength of maximum emission. In particular, as shown in Fig. 3b, it was observed a decrease in the intensity of the fluorescence emission intensity concomitant with a blue shift of the emission maximum in the presence of SLG. Fluorescence quenching has been a powerful tool to reveal the accessibility of fluorophores in the protein matrix to quenchers. Static quenching refers to formation of a nonfluorescent fluorophore–quencher complex [27]. The changes in the emission spectra suggested for the formation of a SLG–protein complex. The association of SLG to proteins with their hydrophobic groups can produce changes in the position or orientation of the amino acid residues, altering their exposure to the solvent water, leading to alterations on the quantum yield, and thus resulting in a quenching of the fluorescence.

3.2. The effect of pH

As Fig. 4 shows, the RLS intensity of the assay system was affected by pH. Variation of pH from 2.1 to 6.0 at the concentration of 1.0 $\mu g\ ml^{-1}$ of BSA was studied. At pH 4.0, the enhanced

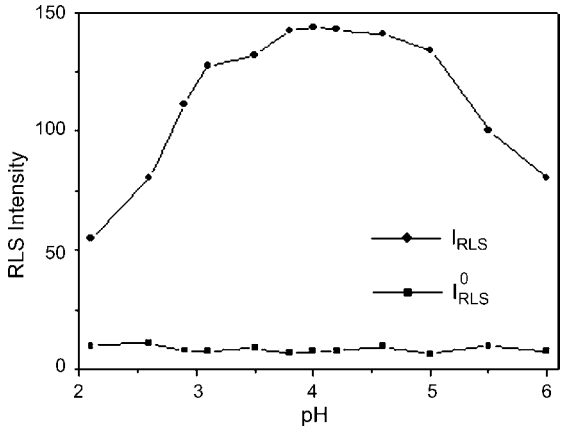


Fig. 4. The effect of pH on the RLS intensity. Conditions: $C_{SLG} = 1.2 \times 10^{-4}\ mol\ l^{-1}$, $C_{BSA} = 1.0\ \mu g\ ml^{-1}$.

RLS intensity reached its maximum. This is possibly related to the isoelectric point of proteins. Proteins are positively charged when the pH is lower than their isoelectric points. SLG contains two carboxylic acid groups, which carries strong negative charges. In acidic medium, the electrostatic interaction between SLG and proteins can be very strong, which is favorable for the RLS intensity enhancement. So pH 4.0 was chosen for the determination.

3.3. The effect of SLG concentration (C_{SLG})

As shown in Fig. 5, the concentration of SLG influenced significantly on the RLS intensity of the system. It can be clearly seen from Fig. 5 that SLG concentration in the range of $2.0 \times 10^{-5}\ mol\ l^{-1}$ to $2.0 \times 10^{-4}\ mol\ l^{-1}$ had a great influence on the RLS intensity. With increasing SLG concentration, the ΔI_{RLS} increased and reached a maximum at $1.2 \times 10^{-4}\ mol\ l^{-1}$. Then an increase of SLG concentration led to a reduction of the RLS intensity. So $1.2 \times 10^{-4}\ mol\ l^{-1}$ SLG was selected in this assay. Because the critical micelle concentration (CMC) of SLG is 9.44×10^{-4} to $1.02 \times 10^{-3}\ mol\ l^{-1}$ [28], the interaction between surfactants and proteins can be interpreted in the framework of molecule-to-molecule interaction.

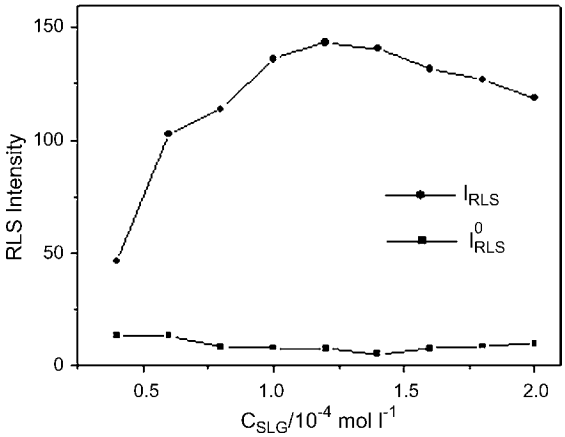


Fig. 5. The effect of SLG concentration on the RLS intensity. Conditions: $C_{BSA} = 1.0\ \mu g\ ml^{-1}$; pH 4.0.

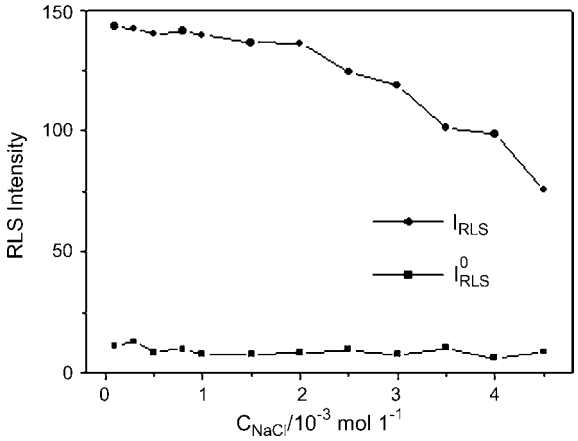


Fig. 6. Effect of ionic strength on the RLS intensity. Conditions: $C_{SLG} = 1.2 \times 10^{-4}$ mol l^{-1}, $C_{BSA} = 1.0$ μg ml^{-1}; pH 4.0.

3.4. The effect of ionic strength

The effect of ionic strength on the RLS intensity of the system is presented clearly in Fig. 6. It can be seen that the RLS intensity of the system SLG–BSA decreased with the increasing of NaCl concentration. The control of ionic strength of the solution is very important, indicating that electrostatic interaction is also one of the main driving forces governing their combination. When the concentration of the NaCl increases, the effects of the electrostatic shielding of charges, including the shielding of protein molecules from SLG or the shielding of SLG from protein molecules, reduce the combination of SLG with protein and result in a decreased RLS signal.

3.5. Incubation time and stability

The stability of the SLG–BSA system was studied by measuring the RLS intensity every 2 min for 2 h immediately after mixing. Our results show that the reaction between SLG and proteins occurred rapidly at room temperature (<4 min) and the RLS intensity of the system reached the maximum. Moreover, the RLS intensity remained stable for at least 90 min. Thus, this assay is rapid and does not require crucial timing.

3.6. Interference of foreign substances

The effect of the foreign substances on the determination of only 1.0 μg ml^{-1} BSA was tested by pre-mixing BSA with compounds such as common ions, sugars and amino acids under the optimum conditions of the general procedure. The criterion for an interference was an I_{RLS} value varying by more than 5% from the expected value for BSA alone. There was no interference from the following ions: 500 μmol l^{-1} of K^+, 100 μmol l^{-1} of Na^+, 50 μmol l^{-1} of Ca^{2+} and Mg^{2+}, 25 μmol l^{-1} of Zn^{2+}, Al^{3+} and Fe^{2+}, 20 μmol l^{-1} of Mn^{2+} and Cu^{2+}, 15 μmol l^{-1} of Cr^{2+} and Co^{2+}, 10 μmol l^{-1} of Cd^{2+}, Hg^{2+} and Pb^{2+}, 25 μmol l^{-1} of $H_2PO_4^-$, 5.0 μmol l^{-1} of PO_4^{3-}. Especially, glucose, ethanol, and urea could be allowed at very high concentration. On the contrary, some other ions such as I^- and Fe^{3+} only can be tolerated at relative low concentration levels (less than 5.0 μmol l^{-1}).

Table 1
Effects of amino acids on the determination of BSA (1.0 μg ml^{-1}) under the optimum conditions

Amino acids (50.0 μg ml^{-1})	Change in I_{RLS} (%)	Amino acids (50.0 μg ml^{-1})	Change in I_{RLS} (%)
L-Proline	+0.5	L-Histidine	+0.9
L-Cysteine	+1.1	L-Lysine	+7.9
L-Asparagine	+0.6	L-Phenylalanine	+2.3
L-Leucine	−1.7	L-Serine	−5.3
L-Arginine	+2.8	L-Tryptophan	+4.8
L-Glutamine	−1.4	L-Tyrosine	−1.2

As shown in Table 1, most of the amino acids also do not interfere with the determination. Dilution with water can minimize all these interferences, which offers this method with the possibility of determination of trace amount of proteins in real samples.

3.7. Calibration curves and sensitivities

According to the above standard procedure, the RLS intensities were obtained under the optimum conditions. The analytical parameters of the determination are listed in Table 2. The limits of detection (LOD) are given by $3S_0/S$, where 3 is the factor at the 99% confidence level, S_0 the standard deviation of the blank measurements ($n = 10$), and S is the slope of the calibration curve. Satisfactory linear relationship with low detection limits (below 6 ng ml^{-1}) and relatively wide linear ranges were obtained. As shown in Table 3, compared with other methods of determination of proteins, this method has the advantages of high sensitivity, low detection limit and fine simplicity.

3.8. Application to sample analysis

Table 4 displays the determination results for human serum samples with HSA as the standard. The samples were diluted 2000-fold with doubly distilled water without further purification. The results displayed in Table 4 are in good agreement with the data provided by the hospital. As shown in Table 2, the protein-to-protein variability cannot be strictly avoided with RLS technique, but the responses for some of the proteins such as BSA, HSA and γ-G, are approximately equal with this method. It is obvious that this method for the determination of the total protein is reliable, sensitive and practical. This measurement system can be encouraged their practical use in chemical and biochemical applications.

Table 2
Analytical parameters of this method under the optimum conditions

Protein	Linear range (μg ml^{-1})	Regression equation	Detection limit (ng ml^{-1})	Correlation coefficient (r)
Lysozyme	0.08–3.1	$\Delta I = 4.3 + 121.1C$	4.6	0.9986
BSA	0.01–2.7	$\Delta I = 2.1 + 134.6C$	1.4	0.9991
HSA	0.04–2.2	$\Delta I = 3.7 + 131.2C$	1.7	0.9997
γ-G	0.08–1.7	$\Delta I = 6.1 + 129.3C$	2.8	0.9989
Hemoglobin	0.01–1.3	$\Delta I = 1.8 + 109.7C$	5.8	0.9981

Table 3
Comparisons with some other assays of proteins

Method	Reagents	Protein	Detection limit (ng ml^{-1})	References
Abs	Lowry		1.0×10^5	[2]
Abs	CBB		5000	[3]
Flu	Chrome azurol S	HAS	100	[29]
Flu	ECR[a]	HAS	500	[30]
RLS	$TPPS_4$[b]	BSA/HSA	18.0/53.5	[14]
RLS	Quercetin	BSA/HSA	59.8/44.4	[31]
RLS	EBBR[c]	BSA/HSA	33.0/25.0	[32]
RLS	Alizarin Red S	BSA/HSA	9.59/9.51	[33]
RLS	Ponceau 4R	BSA/HSA	6.96/5.71	[15]
RLS	SDBS[d]	BSA/HSA	1.8/2.8	[26]
RLS	SLS[e]	BSA/HSA	12.8/21.6	[26]
RLS	SLG	BSA/HSA	1.4/1.7	This work

[a] Eriochrome Cyanine R.
[b] α,β,γ,δ-Tetrakis 4-(sulfophenyl) porphine.
[c] Eriochrome Blue Black R.
[d] Sodium dodecyl benzene sulfonate.
[e] Sodium lauryl sulfate.

3.9. Mechanism of the reaction

Proteins and surfactants share the property of having both charged groups and hydrophobic portions. This implies that the interactions between surfactants and proteins are intrinsically complex processes, involving different types of intermolecular forces. In order to clarify the mechanism of the interaction between them, dependence of the RLS intensity on pH was carefully studied (see Fig. 4). The results show that the RLS intensity was sensitive to the solution pH. It is particularly relevant to the characteristics of both SLG and proteins. In pH < 2.9, both of the two carboxylic acid groups of SLG would be protonated, so the RLS intensity was relatively small. Whereas, in pH > 4.6, proteins were negatively charged. In pH 3.8–4.2, SLG carried strong negative charges, and proteins carried positive charges. So the RLS intensity was strong. The presence of two negative charged hydrophilic groups in the same SLG molecule leads to the better combination with the proteins by their electrostatic interactions. The dependence of the RLS intensity on the pH and the ionic strength is fully compatible with this interpretation. Besides the properties mentioned above, SLG possesses the acylamino group, which can easily form strong hydrogen bonding with proteins [25]. It thus performed better as protein RLS probe than other anion surfactants.

Table 4
Analytical results of human serum samples[a]

Samples (no.)	This method ($n = 6$, mg ml^{-1})	R.S.D. (%)	Clinical data[b] (mg ml^{-1})
Serum 1	69.4 ± 0.76	1.1	71.1 ± 1.4
Serum 2	67.9 ± 0.61	0.9	69.8 ± 0.94
Serum 3	84.1 ± 1.7	2.1	81.3 ± 1.5

[a] Data shown are average ± S.D. from six independent experiments.
[b] Obtained from the Shantou Central Hospital, average from three measurements.

As evidenced from the fluorescence excitation and emission spectra changing with the variable SLG concentrations, it can be concluded that the change of the fluorescence spectra resulted from the changes in the orientation of the protein structures [34]. The change of the protein structures would lead to a better combination with their hydrophobic groups. The data obtained in the present work support a SLG–protein interaction in which hydrophobic forces also play an important role in the RLS intensity enhancement. The surfactant SLG with special characteristics favors better interaction, thus SLG was shown better performance over other surfactants for the determination of proteins.

4. Conclusion

The study of the interaction between surfactants and proteins is of significant scientific and technological importance. The acylamino acid-type surfactants with special properties and advantages are attractive molecules to probe proteins by RLS technique. The results of this study show that SLG played an effective role as a protein probe in the determination of trace amount of proteins using RLS technique. This is an inexpensive, simple and fast one-step procedure which requires only measuring the RLS intensities. It was applied to determine human serum samples satisfactorily. Therefore, it is a useful method to be used in practical applications.

Acknowledgements

All authors express their sincere thanks for the support from the National Natural Science Foundation of China (no. 30271033) and the Municipal Science Foundation of Shantou (no. S02023).

References

[1] L.X. Zhang, G.L. Wu, Advanced Biochemical Experiments, Advanced Education Press, Beijing, 1989, p. 192.
[2] O.H. Lowry, N.J. Rosebrough, A.L. Farr, R.J. Randall, J. Biol. Chem. 193 (1951) 265.
[3] M.M. Bradford, Anal. Biochem. 72 (1976) 248.
[4] T. Hara, M. Toriyama, K. Tsukagoshi, Bull. Chem. Soc. Jpn. 61 (1988) 2779.
[5] N. Li, K.A. Li, S.Y. Tong, Anal. Biochem. 233 (1996) 151.
[6] R.F. Pasternack, C. Bustamante, P.J. Collings, A. Giannetto, E.J. Gibbs, J. Am. Chem. Soc. 115 (1993) 5393.
[7] R.F. Pasternack, P.J. Collings, Science 269 (1993) 935.
[8] R.F. Pasternack, K.F. Schaefer, P. Hambright, Inorg. Chem. 33 (1994) 2062.
[9] C.Z. Huang, K.A. Li, S.Y. Tong, Anal. Chem. 68 (1996) 2259.
[10] Z.P. Li, K.A. Li, S.Y. Tong, Talanta 55 (2001) 669.
[11] Z.G. Chen, W.F. Ding, F.L. Ren, J.B. Liu, Y.Z. Liang, Anal. Chim. Acta 550 (2005) 204.
[12] Z.G. Chen, W.F. Ding, F.L. Ren, Y.Z. Liang, J.B. Liu, Microchim. Acta 150 (2005) 34.
[13] Z.G. Chen, W.F. Ding, F.L. Ren, Y.L. Han, J.B. Liu, Anal. Lett. 38 (2005) 2301.
[14] R.P. Jia, L.J. Dong, Q.F. Li, X.G. Chen, Z.D. Hu, Talanta 57 (2002) 693.
[15] H. Zhong, J.J. Xu, H.Y. Chen, Talanta 67 (2005) 749.
[16] Z.G. Chen, T.Y. Zhang, F.L. Ren, W.F. Ding, Microchim. Acta 153 (2006) 65.

[17] Z.G. Chen, W.F. Ding, F.L. Ren, J.B. Liu, Y.L. Han, Can. J. Anal. Sci. Spect. 50 (2005) 54.
[18] Z.G. Chen, J.B. Liu, Y.L. Han, L. Zhu, Anal. Chim. Acta 570 (2006) 109.
[19] S.Z. Zhang, F.L. Zhao, K.A. Li, S.Y. Tong, Anal. Chim. Acta 431 (2001) 133.
[20] S.Z. Zhang, F.L. Zhao, K.A. Li, S.Y. Tong, Talanta 54 (2001) 333.
[21] C.Z. Huang, X.B. Pang, Y.F. Li, Y.J. Long, Talanta 69 (2006) 180.
[22] P. Feng, W.Q. Shu, C.Z. Huang, Y.F. Li, Anal. Chem. 73 (2001) 4307.
[23] S.P. Liu, Q. Liu, Z.F. Liu, M. Li, C.Z. Huang, Anal. Chim. Acta 379 (1999) 53.
[24] X.F. Long, S.P. Bi, H.Y. Ni, X.C. Tao, N. Gan, Anal. Chim. Acta 501 (2004) 89.
[25] C. Liu, X.M. Jiang, B.Z. Li, W.F. Zhang, Application Encyclopedia of Surfactants, Beijing Industry University Press, Beijing, 1992, p. 43.
[26] R.T. Liu, J.H. Yang, C.X. Sun, X. Wu, L. Li, Z.M. Li, Anal. Bioanal. Chem. 377 (2003) 375.
[27] E.L. Gelamo, M. Tabak, Spectrochim. Acta A 56 (2000) 2255.
[28] X.L. Wei, B.L. Yin, Q. Sang, H.B. Zhang, Liaocheng Shiyuan Xuebao 14 (2001) 66.
[29] Y. Saito, Y. Inden-Okazaki, S. Wada-Yano, A. Kanetsuna, K. Miyazaki, M. Mifune, Y. Tanaka, Anal. Chim. Acta 178 (1985) 337.
[30] Y.X. Ci, L. Chen, Analyst 113 (1988) 679.
[31] P. Feng, X.L. Hu, C.Z. Huang, Anal. Lett. 32 (1999) 1323.
[32] Y.K. Zhao, W.B. Chang, Y.X. Ci, Talanta 59 (2003) 477.
[33] H. Zhong, N. Li, F.L. Zhao, K.A. Li, Talanta 62 (2004) 37.
[34] G.V. Lubarsky, M.M. Browne, S.A. Mitchell, M.R. Davidson, R.H. Bradley, Colloid Surf. B 44 (2005) 56.

Available online at www.sciencedirect.com
ScienceDirect
Talanta 71 (2007) 1083–1087
Talanta
www.elsevier.com/locate/talanta

Determination of four kinds of carbamate pesticides by capillary zone electrophoresis with amperometric detection at a polyamide-modified carbon paste electrode

Xi Cheng, Qingjiang Wang, Shan Zhang, Weidong Zhang, Pingang He, Yuzhi Fang *

Department of Chemistry, East China Normal University, Shanghai 200062, PR China

Received 22 March 2006; received in revised form 31 May 2006; accepted 1 June 2006
Available online 11 July 2006

Abstract

In this paper, a polyamide-modified carbon paste electrode in capillary zone electrophoresis with amperometric detection (CZE–AD) was firstly applied to the determination of four carbamate pesticides: fenobucarb, isoprocarb, metolcarb and carbaryl. The four carbamates were hydrolyzed in alkalescent aqueous solutions, resulting in the formation of 2-sec-butylphenol, 2-isopropylphenol, m-cresol and α-naphthol, which could be determined by amperometry after capillary electrophoretic separation. Under the selected optimum conditions, the four analytes could be perfectly separated within 23 min. The linear ranges of 2-sec-butylphenol, 2-isopropylphenol and m-cresol were from 1.0×10^{-7} to 2.0×10^{-5} mol L^{-1} and that of α-naphthol was from 2.0×10^{-7} to 2.0×10^{-5} mol L^{-1} and their detection limits were 3.0×10^{-8}, 3.0×10^{-8}, 3.0×10^{-8} and 6.0×10^{-8} mol L^{-1}, respectively ($S/N = 3$). Fenobucarb, isoprocarb, metolcarb and carbaryl can be indirectly determined by this CZE–AD method with recovery of 105, 104, 110 and 98% and R.S.D. of 4, 3, 4 and 3%, respectively. Above results demonstrated that this method was of high sensitivity, good repeatability and could be used in the rapid determination of the pesticide residues.
© 2006 Elsevier B.V. All rights reserved.

Keywords: Capillary zone electrophoresis; Amperometric detection; Polyamide-modified carbon paste electrode; Carbamate pesticides

1. Introduction

Carbamate compounds were introduced as pesticides in the early 1950s and are still used extensively in pest control due to their relative short lifetime, effectiveness and broad spectrum of biological activity [1,2]. Their structures (Table 1, Part A) are based on *N*-substituted carbamic acid esters ($R_1OCONHR_2R_3$), in which R_1 is typically a phenyl or a heterocyclic aromatic ring, R_2 is usually a methyl substituent and R_3 is either a hydrogen, methyl, or a more complex group. Fifteen *N*-methylcarbamates form an important family of insecticides [3].

Many carbamates are acutely toxic and can be hazardous to health if care is not taken. Moreover, the determination of pesticide residues is an intricate problem because of the large number of chemicals involved. The methods applied should be able to simultaneously determine multi-component pesticide mixtures with good reproducibility, high recovery and low limit of detection (LOD) [4].

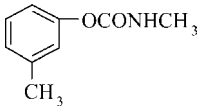
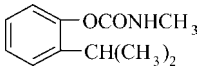
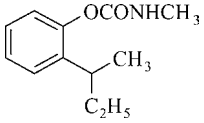
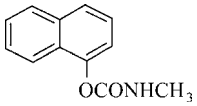
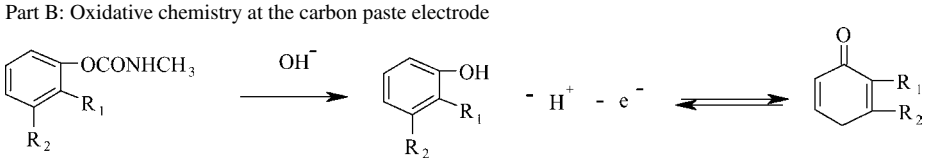
Analysis of pesticides is generally carried out by gas chromatography (GC) [5] or liquid chromatography (LC) coupled to different detectors, especially to mass spectrometer (MS) [6,7]. However, alternative and/or complementary methods, using capillary electrophoresis (CE), have emerged recently [8,9,17]. The prospects for CE in pesticide analysis are very promising because of its advantages, such as higher separation efficiency, shorter analysis times and very small consumption of expensive reagents and toxic solvents. In addition, its capability to conduct analysis in a miniaturized format (microchip technology) is interesting for the routine analysis of samples containing hazardous pesticides [4,10].

Many detection techniques can be coupled with CE, such as UV–vis absorbance spectroscopy [11], fluorescence [12], indirect techniques [13], refractive index detectors [14], mass

* Corresponding author. Tel.: +86 21 62233510; fax: +86 21 62451921.
E-mail address: yuzhi@online.sh.cn (Y. Fang).

0039-9140/$ – see front matter © 2006 Elsevier B.V. All rights reserved.
doi:10.1016/j.talanta.2006.06.001

Table 1
Chemical structures of four carbamates pesticides (Part A) and the oxidation of their hydrolysis products at the carbon paste electrode (Part B)

Pesticides	Molecular formula	Structure
Part A: Chemical structures		
Metolcarb	$C_9H_{11}NO_2$	
Isoprocarb	$C_{11}H_{15}NO_2$	
Fenobucarb	$C_{12}H_{17}NO_2$	
Carbaryl	$C_{12}H_{11}NO_2$	
Part B: Oxidative chemistry at the carbon paste electrode		

spectrometry [15], electrochemical detection (EC) [19] and so on. Although the UV detector is easy to handle, the relatively low sensitivity is an intrinsic drawback. LIF detectors are more sensitive and selective than UV–vis absorption detectors, but only a few different laser sources (488 nm Ar–ion, 442 nm He–Cd and 324 nm He–Ca) are available. Of course, pesticides are not fluorescent and the need for fluorescent labelling prior to analysis is an inherent disadvantage [4]. MS detectors can solve these problems in the majority of applications, but it is more expensive. While electrochemical detection (particularly amperometric) offers many desirable features for CE systems because of high sensitivity, high efficiency, low cost and miniaturized instrumentation. With the development of this method, some other types of electrodes and chemically modified electrodes (CMEs) have been exploited to extend its application area and to improve the detection sensitivity [16].

Fei et al. analyzed metolcarb, carbaryl and other two organophosphate pesticides by capillary zone electrophoresis with amperometric detection (CZE–AD) at a carbon disc working electrode and the detection limit was 0.04 and 0.02 mg L^{-1} [17]. However, the method of determination of carbamates with CZE–AD at a CME, has not been reported.

In this paper, we demonstrated the first application of polyamide-modified carbon paste electrode in CZE–AD to indirectly detect four carbamates: fenobucarb, isoprocarb, metolcarb and carbaryl. The four carbamates can be hydrolyzed in alkalescent aqueous solutions, resulting in the formation of 2-sec-butylphenol, 2-isopropylphenol, m-cresol and α-naphthol, which can be determined amperometrically after capillary electrophoretic separation (Table 1, Part B). It is known that hydroxybenzene has an affinity for carbonyl groups (>C=O) under the formation of hydrogen bonds. Accordingly, hydroxybenzene can be accumulated on the electrode as the hydrogen bond product by the use of an electrode modified with a substance containing the carbonyl group (>C=O) to improve the detection sensitivity. Polyamide was selected because of its >NH and >C=O groups, stability, insolubility in water and the electroinactivity on the organic ligand part [18].

From experimental results, it was found that these four analytes could be perfectly separated within 23 min and the detection limit was as low as 5.0×10^{-8} mol L^{-1}. Moreover, the results also show that simultaneously determining the four analytes by this method is of low-volume sampling, simple instrument and operation and high reproducibility.

2. Experimental

2.1. Apparatus

CZE–AD system was laboratory-built [19,20]. Electrophoresis was driven by a high voltage supplier (±30 kV, Shanghai Institute of Nuclear Research, Shanghai, China). Separations were performed in a fused silica capillary (Hebei Yongnian Laser-fiber factory, China) with 25 μm i.d., 360 μm o.d. and 68 cm long. Potential control and current output were employed by a CH-2 amperometric detector (Jiangsu Electrochemical Analytical Instrumental Factory, China). Electropherograms were recorded by a chart recorder (Shanghai Dahua Instrument Factory, China). Electrochemical experiments were carried out by a CHI 830b electrochemical analyzer (CH Instruments, USA). A three-electrode system, which consisted of a polyamide-modified carbon paste electrode, a saturated calomel reference electrode (SCE) and a platinum wire counter

electrode, was used in both electrochemistry and detection experiments.

2.2. Reagents

The four pesticides: fenobucarb, isoprocarb, metolcarb and carbaryl and their hydrolysis products: 2-sec-butylphenol, 2-isopropylphenol, m-cresol and α-naphthol were obtained from Sigma without further purification. The stock solutions of four hydrolysis products with a concentration of 1.0×10^{-2} mol L^{-1} were prepared by dissolution in 25 mmol L^{-1} sodium hydroxide, stored at 4 °C and diluted with running buffer to the needed concentrations in CZE experiments. All other reagents were of analytical reagent grade. All solutions were prepared with double distilled water. Before CZE experiment, all used solutions were filtered through 0.22 μm polypropylene acrodisc syringe filter and sonicated for 5 min to remove bubbles.

2.3. Procedure

2.3.1. Preparation of polyamide-modified carbon paste electrode

Polyamide-modified carbon paste was prepared by mixing weighed amounts of specpure carbon powder, paraffin oil and polyamide (55:35:10%, w/w) thoroughly in an agate mortar until perfect homogenization was attained. A portion of the ready-prepared paste was then packed firmly into the cavity of a Teflon tube (0.5 mm i.d., 3 mm o.d.). Electrical contact was established via a copper wire, which was threaded into the opposite end of the electrolyte body and embedded into the carbon paste. It is not recommended to employ freshly made CPEs immediately, but they should be left unused for a certain time (12–24 h) to allow their final homogenization to proceed [21].

Prior to use, the surface of the modified carbon paste electrode was smoothed by polishing on weighing paper. After a day's experiment the surface was renewed by removing the top of the used paste. And this type of CPE could be used for 2 months without compromising its analytical performance.

2.3.2. CZE experiments

Before CZE experiments, the three-electrode system was fixed in the corresponding holes of the electrochemical cell and the modified carbon paste electrode was positioned straightly opposite the capillary outlet as close as possible by a three dimension positioner. Before each run in CE experiments, the capillary was sequentially rinsed with 0.1 mol L^{-1} hydrochloric acid, doubly distilled water, 0.1 mol L^{-1} sodium hydroxide, 3 min for each and with running buffer till the inside current of the capillary reached stability. This was important to get a reproducible electroosmotic flow. CZE was performed at the separation voltage of 15 kV with 15 mmol L^{-1} borate solution (pH 11.0) used as running buffer. The potential applied to the working electrode was 1.0 V (versus SCE). Samples were electrokinetically injected at 15 kV for 10 s.

3. Results and discussion

3.1. Optimization of experiment conditions

3.1.1. Conditions of amperometric detection

Since 2-sec-butylphenol, 2-isopropylphenol, m-cresol and α-naphthol can be electrochemically oxidized at a relatively moderate potential, electrochemical detection was used in this work. Fig. 1 shows the hydrodynamic voltammograms (HDVs) of the above analytes, which were obtained by monitoring the current responses after CZE separations within the applied potential range from 0.7 to 1.1 V. It was found that the current responses of these analytes increased with the applied potential increasing. However, the noise was too high when the applied potential was more than 1.1 V. In order to determine above analytes together and obtain the best signal-to-noise ratio, 1.0 V was selected as the most suitable detection potential in this experiment.

3.1.2. Effects of pH and concentration of running buffer

In order to improve the resolution and sensitivity, borate, phosphate, borate–phosphate mixture were employed as running buffer, respectively, in this CZE separation and the best results were got with borate buffer.

The pH effect was investigated within the pH range from 7.0 to 12.0. It was found that when pH value reached 11.0, the baseline separation for the four analytes could be achieved. With the increase of the pH value, the migration time of the four analytes prolonged, the response current reduced and the signal-to-noise ratio decreased. In this experiment, pH 11.0 was selected as the optimum pH.

In addition, the effect of the concentration of borate buffer was investigated. The results show that with the increase of the concentration of borate buffer, the migration time of the four analytes increased obviously. It was because the increase of ionic strength of borate buffer resulted in the decrease of electroosmotic flow in the capillary. While, their current responses decreased but were not effected as much as that of migration

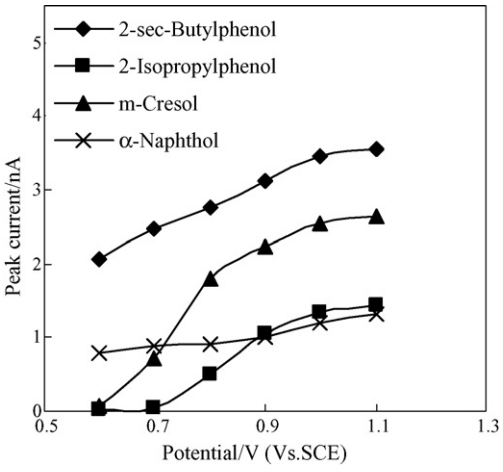


Fig. 1. Hydrodynamic voltammograms for 2-sec-butylphenol, 2-isopropylphenol, m-cresol and α-naphthol with a concentration of 5×10^{-6} mol L^{-1}; the CZE conditions are as the optimal.

time. Hence, 15 mmol L^{-1} borate buffer was chosen as the running buffer in this experiment.

3.1.3. Effect of separation voltage and injection time

The separation efficiency of CZE was investigated within the separation voltage range from 8 to 18 kV. The migration time of the analytes were significantly shortened and their corresponding current peaks were sharpened when the separation voltage was increased. However, if the separation voltage was too high, more Joule heat was produced because of the higher current inside the capillary, which caused peak broadening and reduced separation efficiency. For a comprehensive thought, 15 kV was selected as the optimum separation voltage in this experiment.

Electrokinetic injection was used in the CZE experiment. The effect of injection time was investigated by selecting different injection time (4, 6, 8, 10 and 12 s at a voltage of 15 kV). It was found that when the injection time was prolonged, the peak current increased correspondingly. However, the current response peaks of the analytes were obviously broadened if the injection time was more than 12 s. So, 10 s was selected as the injection time in this experiment and satisfactory results were obtained under this condition.

Through the experiments above, the optimum conditions of CZE–AD for determining the four hydroxybenzenes were detection potential 1.0 V (versus SCE), separation voltage 15 kV, electrokinetic injection time 10 s (15 kV) and 15 mmol L^{-1}borate buffer (pH 11.0). Fig. 2 shows the electropherogram of a standard 2-sec-butylphenol, 2-isopropylphenol, m-cresol and α-naphthol mixture solution with the concentration of 1.0×10^{-6}, 2.5×10^{-6}, 2.5×10^{-6}, 2.5×10^{-6} mol L^{-1} under the optimum conditions. A base-lined separation for the four analytes could be achieved within 23 min.

3.1.4. Reproducibility, linearity and detection limits

A standard mixture solution of 5.0×10^{-6} mol L^{-1} 2-sec-butylphenol, 2-isopropylphenol, m-cresol and α-naphthol was used to determine the reproducibility of the current response and migration time under the optimum conditions in this experiment. The relative standard deviations (R.S.D.) of peak current and migration time were 2 and 1% for 2-sec-butylphenol, 3 and 1% for 2-isopropylphenol, 2 and 1% for m-cresol, 3 and 1% for α-naphthol, respectively, when the analysis was repeated for five times under the same conditions, which demonstrated that this method was of good repeatability.

To determine the linearity for the four hydroxybenzenes by this method, a series of mixed standard solutions with different concentrations were tested. The linear ranges, regression equations, correlation coefficients and detection limits are listed in Table 2. The linear ranges of 2-sec-butylphenol, 2-isopropylphenol and m-cresol were from 1.0×10^{-7} to 2.0×10^{-5} mol l^{-1} and that of α-naphthol was from 2.0×10^{-7} to 2.0×10^{-5} mol L^{-1}. Their detection limits were 3.0×10^{-8}, 3.0×10^{-8}, 3.0×10^{-8} and 6.0×10^{-8} mol L^{-1}, respectively ($S/N = 3$). Above results showed that this method was very sensitive.

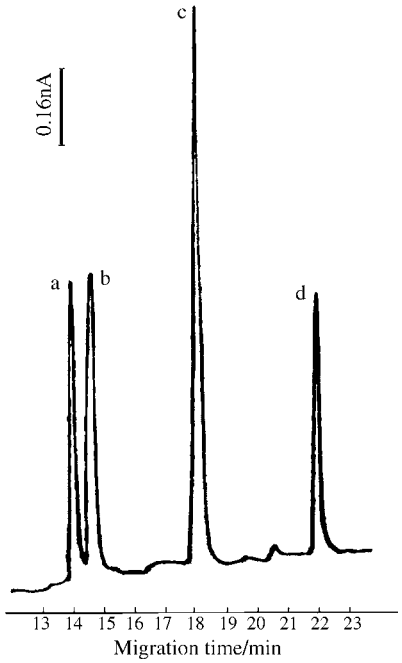


Fig. 2. Electropherogram of a standard solution containing 2-sec-butylphenol (1.0×10^{-6} mol l^{-1}), 2-isopropylphenol (2.5×10^{-6} mol l^{-1}), m-cresol (2.5×10^{-6} mol l^{-1}) and α-naphthol (2.5×10^{-6} mol l^{-1}) under the optimal CZE–AD conditions: (a) 2-sec-butylphenol; (b) 2-isopropylphenol; c, m-cresol; d, α-naphthol.

3.2. Validation of the method

3.2.1. Recovery

The four standard carbamate pesticides, metolcarb, isoprocarb, fenobucarb, carbaryl were hydrolyzed in 1 mol L^{-1} sodium hydroxide, placed in a hot water bath and allowed at least an hour to be hydrolyzed completely. Under the optimum conditions, the determination was carried out according to the procedures described above. Recovery test was performed in this experiment too and the results are listed in Table 3, which indicated that this method was accurate and practical for determining the four carbamate pesticides.

Table 2
The regression equations and the detection limits of m-cresol, 2-isopropylphenol, 2-sec-butylphenol and α-naphthol

Analytes	Regression equation C (M); I (nA)	Correlation coefficient	Linear range (M)	Detection limit[a] (M)
2-sec-Butylphenol	$I = 6.92 \times 10^5$C-0.013	0.9983	1.0×10^{-7}–5.0×10^{-5}	3.0×10^{-8}
2-Isopropylphenol	$I = 2.63 \times 10^5$C + 0.030	0.9987	1.0×10^{-7}–5.0×10^{-5}	3.0×10^{-8}
m-Cresol	$I = 5.12 \times 10^5$C-0.015	0.9979	1.0×10^{-7}–5.0×10^{-5}	3.0×10^{-8}
α-Naphthol	$I = 2.41 \times 10^5$C-0.003	0.9984	2.0×10^{-7}–5.0×10^{-5}	6.0×10^{-8}

[a] Detection limit was estimated according to three times of signal-to-noise.

Table 3
Recoveries of metolcarb , isoprocarb, fenobucarb, carbaryl ($n = 5$)

Analytes	Added amount ($\times 10^{-6}$ M)	Found amount ($\times 10^{-6}$ M)	Recovery (%)	R.S.D. (%)
Fenobucarb	2.0	2.1	105	4
Isoprocarb	5.0	5.2	104	3
Metolcarb	5.0	5.5	110	4
Carbaryl	5.0	4.9	98	3

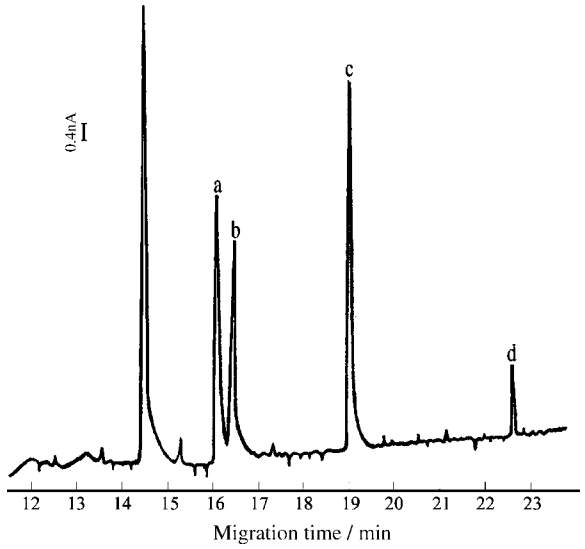


Fig. 3. Electropherogram of lettuce sample solution under the optimal CZE–AD conditions: (a) 2-sec-butylphenol; (b) 2-isopropylphenol; (c) m-cresol; d, α-naphthol.

3.2.2. Sample analysis

The greengrocery purchased from market, was checked for the absence of pesticides using this method. It was cleared and the esculent part was mashed to be analytic sample. The sample was weighed out 5.0 g to a centrifuge tube (50 mL), then double distilled water (1 mL) and acetone (10 mL) were added, sonicated for 10 min and centrifuged at a speed of 5000 r min^{-1} for 5 min. The supernate was filtered through 0.22 μm polypropylene acrodisc syringe filter twice, analyzed according to the procedure in Section 3.2.1 and the content of pesticides were not found.

Lettuce was sprayed with four kinds of pesticides, then detected according to the procedure above 2 hours later. Typical electropherogram of sample is shown in Fig. 3. The contents of fenobucarb, isoprocarb, metolcarb and carbaryl were determined by internal standard method and were calculated as 1.1×10^{-5}, 1.9×10^{-5}, 2.0×10^{-5} and 8.7×10^{-6} mol L^{-1}, respectively.

4. Conclusions

Determination of four carbamate pesticides by CZE–AD at a polyamide-modified carbon paste electrode was performed in this experiment and the results showed that this method was of high separation efficiency, short analysis time, convenience of analysis. Under the optimum conditions, the four hydrolysis products were separated completely within 23 min and good linearity, reproducibility and recovery results were obtained. Their detection limits were 3.0×10^{-8}, 3.0×10^{-8}, 3.0×10^{-8} and 6.0×10^{-8} mol L^{-1}, respectively, which were lower than using a carbon disc working electrode.

Acknowledgment

This work is financially supported by the Natural Science Research Foundation from Shanghai Science and Technology Committee (No. 04ZR14041).

References

[1] Y. Ni, P. Qiu, S. Kokot, Anal. Chim. Acta 537 (2005) 321.
[2] S. Sole, A. Merkoci, S. Alegret, Crit. Rev. Anal. Chem. 33 (2003) 89.
[3] Y. Zhang, Z. Zhang, Pesticides, Chinese Material Press, Beijing, 1997.
[4] Y. Picó, R. Rodríguez, J. Mañes, Trends Anal. Chem. 22 (2003) 133.
[5] K. Maštovská, S.J. Lehotay, J. Hajšlová, J. Chromatogr. A 926 (2001) 291.
[6] H. Li, J. Li, G. Li, J. Jen, Talanta 63 (2004) 547.
[7] L.L.E. Atrache, S. Sabbah, J.P. Morizur, Talanta 65 (2005) 603.
[8] V. Andreu, Y. Picó, Trends Anal. Chem. 23 (2004) 772.
[9] C.L. Silva, E.C. Lima, M.F.M. Tavares, J. Chromatogr. A 1014 (2003) 109.
[10] G. Chen, L. Zhang, J. Wang, Talanta 64 (2004) 1018.
[11] P. Mikuš, I. Valášková, E. Havránek, Talanta 65 (2005) 1031.
[12] J. Zhang, Z. Hu, X. Chen, Talanta 65 (2005) 986.
[13] X. Yang, X. Wang, X. Zhang, J. Sep. Sci. 29 (2006) 677.
[14] K. Swinney, J. Pennington, D.J. Bornhop, Microchem. J. 62 (1999) 154.
[15] H.J. Issaq, G.M. Janini, K.C. Chan, T.D. Veenstra, J. Chromatogr. A 1053 (2004) 37.
[16] S. Hu, M. Zhang, D. Pang, J. Cheng, Anal. Sci. 16 (2000) 807.
[17] X. Fei, L. Wang, S. Zhang, X. Yang, J. Instrumental Anal. 23 (2004) 70.
[18] Y. Zou, J. MO, Anal. Chim. Acta 353 (1997) 71.
[19] Q. Wang, F. Ding, N. Zhu, H. Li, P. He, Y. Fang, J. Chromatogr. A 1016 (2003) 123.
[20] C. Fu, L. Song, Y. Fang, Anal. Chim. Acta 371 (1998) 81.
[21] I. Švancara, K. Schachl, Chem. Listy 93 (1999) 490.

Available online at www.sciencedirect.com
ScienceDirect
Talanta 71 (2007) 987–1000
Talanta
www.elsevier.com/locate/talanta

Review

A review on molybdenum determination in solid geological samples

Arabinda K. Das [1], Ruma Chakraborty, M.Luisa Cervera *, Miguel de la Guardia

Department of Analytical Chemistry, Research Building, University of Valencia, 50 Dr. Moliner St., E-46100 Burjassot, Valencia, Spain

Received 19 December 2005; received in revised form 21 June 2006; accepted 6 July 2006
Available online 22 August 2006

Abstract

This review highlights the necessity for the development of proper sampling and storage, fast pretreatment methodology followed by highly sensitive detection for the determination of molybdenum in geological samples. Distribution of concentration and chemical speciation of molybdenum analysis in solid geological matrices have also been discussed.
© 2006 Elsevier B.V. All rights reserved.

Keywords: Review; Molybdenum; Soil; Sediment; Geological samples

Contents

1. Introduction 987
2. Concentration of molybdenum in solid geological matrices 988
3. Sampling, handling and storage 990
4. Sample preparation 991
   4.1. Digestion of geological samples for Mo determination 991
   4.2. Preconcentration of Mo from geological samples 991
   4.3. Alternative sample preparation method for Mo determination based on slurry 992
5. Molybdenum speciation in solid matrices 992
6. Detection 993
   6.1. UV–vis spectrophotometry 993
   6.2. Atomic absorption spectrometry 995
   6.3. Atomic emission spectrometry 995
   6.4. Mass spectrometry 996
   6.5. Nuclear techniques 997
   6.6. X-ray fluorescence spectrometry 997
   6.7. Electrochemical detectors 998
7. Conclusions 998
   Acknowledgements 998
   References 998

1. Introduction

Molybdenum is a trace element in the earth's crust and the estimated abundance is in the range of 0.05–40 $\mu g\,g^{-1}$ with a mean value of 1.5 $\mu g\,g^{-1}$ [1]. Mo has seven naturally occurring isotopes, e.g. ^{92}Mo, ^{94}Mo, ^{95}Mo, ^{96}Mo, ^{97}Mo, ^{98}Mo and ^{100}Mo with relative abundances ranging from 9.2 to 24.2% [2]. World production of Mo ores is more than 100,000 tonnes per year. Mo is obtained both, as a primary product and as a by product in the production of copper. Eighty-five percent of Mo consumption is in the manufacture of stainless steel and high-speed tools. Pure Mo finds important applications as a catalyst in a variety of petrochemical processes. Besides its widespread

* Corresponding author. Tel.: +34 963 543158; fax: +34 963 544838.
E-mail address: m.luisa.cervera@uv.es (M.Luisa Cervera).
[1] On leave from Department of Chemistry, University of Burdwan, Burdwan 713104, West Bengal, India.

0039-9140/$ – see front matter © 2006 Elsevier B.V. All rights reserved.
doi:10.1016/j.talanta.2006.07.017

industrial importance, Mo is essential to all living organisms, especially plants, animals and microorganisms, because of its important role in enzymatic redox reactions and its specific geochemical behaviour [3]. However, excess concentrations of Mo have adverse effects. Thus either a deficiency or an excess of Mo can cause damage to plants and its routine control is highly important for healthy plant growth [4]. This is why Mo is added in trace amounts to fertilizers to stimulate plant growing. On the other hand, excess exposure causes problems to all organisms. For example, high concentration of Mo in soil causes abnormal growth of some plants. Furthermore, it becomes harmful to rumitants, since adsorption of Cu by the liver is depressed. Mo poisoning results in severe gastrointestinal irritation and death due to cardiac failure [5]. Its excess may also cause bone deformation, teeth vulnerable to caries and disturbances in the metabolism of fats and proteins [6]. Chronic exposure to excess molybdenum in humans is characterized by high uric acid levels in serum and urine, loss of appetite, diarrhea, anaemia and slow growth. A gout-like disease has been observed in inhabitants of a high-molybdenum area in a province of Russia [7].

The behaviour of Mo in the hydrosphere is closely related to various biogeochemical processes. Hence its concentration may change with microbial activity or possibly limit the nitrogen fixation of an ecosystem [8,9]. However the effect of microbial activity is mostly indirect, since the amount of Mo that is directly involved in metabolic process is relatively small. The key parameter that controls Mo concentrations in the various earth reservoirs is oxygen, which itself is controlled by biological activity.

In the context of aqueous geochemistry, a field of rapid development of research on Mo, it has been observed that Mo in marine and fresh water sediments is a powerful paleoproxy for oxygen content and redox state in waters at the time of sediment formation [10,11]. This application makes use of the unusual chemistry of Mo. Although Mo compounds exhibit all oxidation states from −2 to +6, thermodynamic data suggest that Mo should have an oxidation state of Mo(VI) in oxygenated waters. MoO_4^{2-} anion has conservative way of behaviour and interacts weakly with suspended particulate matter. Surprisingly, Mo is the most abundant transition metal in sea water and has an oceanic residence time of about 8×10^5 years much longer than the mixing time of the oceans [12]. The presence of Mo in an anoxic environment is also important. It has been reported that its concentration in water drastically decrease in anoxic conditions, while sediment below the anoxic water is enriched in Mo compared to normal oxic sediments or continental crust [13,14]. Thus Mo enrichment in sediment may be used as an indicator of a reducing depositional condition in the geological past [15,16].

The interest of analysing geological samples for their contents of metals like Mo lies in the fact that they constitute concentrated reservoirs of an analyte, exhibiting higher concentrations as compared to other adjacent samples like water, plants, air and so on [17]. In addition to that it is important to evaluate the metal content in sediments because under certain environmental conditions, sediments can act either as a sink or as a source of it. One reason why the Mo scavenging mechanism remains obscure is that the chemical forms of Mo in sediments have eluded efforts to their characterization [18]. Nevertheless, following legislation governing the use of sewage sludge in agriculture, the determination of Mo in soil and other geological samples has become increasingly important [19].

So far we could know, the only review work that has been presented on the estimation of Mo in a wide variety of samples including soil, sediments and geological matrices is based on thiocyanate methods of molecular absorption spectroscopy. They include conventional thiocyanate methods in which Mo forms an orange red complex with the thiocyanate ions and improved thiocyanate methods where the sensitivity is increased through the formation of ternary ion association complexes [20].

The present review aims to assimilate the extensive literature on the determination of trace molybdenum in geological samples and the source is mainly the Analytical Abstracts database starting from 1990. The present article has been organized in the following manner. It deals with (i) distribution of molybdenum concentration in different geological solid matrices, (ii) methods for sample collection and storage, (iii) sample treatment, (iv) speciation and (v) detection techniques, followed by conclusions.

2. Concentration of molybdenum in solid geological matrices

Mo as a microelement is of great interest. High concentrations of Mo in soils, sediments and sludges, either from natural sources or through pollution, can enter the food chain through plant uptake, direct ingestion of soil by animals or via water supplies, for which reason strict control of Mo concentrations in environmental samples is necessary. Investigation of the sources of molybdenum in the geological matrices indicates an increased awareness of the potential exposure arising from environmental pollution. Concentration of molybdenum in geological samples has been reported by various workers. Typical levels in solid geological matrices are presented in Table 1.

The Mo concentration in sediments and sedimentary rocks formed in anoxic environments provide valuable information about local redox conditions at the time of sediment formation [43,44]. Mo concentrations may also place constraints on the average global redox state of the ocean over geological time [45]. It is well known that sediments deposited from oxygen-deficient marine waters are enriched in Mo as compared to ordinary sediments or to continental crust [46]. On the other had black shales, the geologic descendants of euximic sediments, retain high Mo concentrations [47].

In rocks, the Mo content is in the 1.12–4.8 $\mu g\,g^{-1}$ level with higher values in shale (32–34 $\mu g\,g^{-1}$). The Mo content of soil (0.034–43 $\mu g\,g^{-1}$) usually resembles that of the parent rocks, with the addition of industrial activities and sewage sludge used as fertilizer. In igneous rocks, molybdenum is found mainly as molybdenite while in residual soils it is completely oxidized and present as molybdate, which is largely associated with ferric oxide minerals and also with organic matter [1].

High Mo contents (10–111 $\mu g\,g^{-1}$) have been found in all 43 sediment samples collected as gravity cores in depths from 70

Table 1
Reported molybdenum concentration in geological samples, both, natural and certified materials

Matrix	Concentration ($\mu g\, g^{-1}$)	Reference
Soil		
BCR CRM 142 (Light sandy soil)	0.22 ± 0.0082	[19]
BCR CRM 143 (Over fertilized soil)	6.2 ± 0.1031	
NIST SRM 1832	0.6	[21]
NIST SRM 1833	14	
NIST SRM 613	43	
NIST SRM 2710 (Montana soil)	19 ± 2 (17 ± 3)[a]	[22]
IAEA Soil 7	2.42 ± 0.03 (2.5)[b]	[23]
Soil (5 samples from Murcia, Spain)	1.05 ± 0.10 (1.18 ± 0.08)[a], 0.83 ± 0.08 (0.78 ± 0.05)[a], 1.25 ± 0.10 (1.04 ± 0.10)[a], 0.56 ± 0.05 (0.71 ± 0.11)[a], 0.32 ± 0.06 (0.37 ± 0.02)[a],	[24]
NIST SRM 2711 (Montana soil)	1.4 ± 0.3 (1.6)[c]	
NIST SRM 2709 (San Joaquin soil)	2.0 ± 0.1 (2.0)[c]	
Soil (2 samples from UAS, Dharwad, India)	2.55 ± 0.94 (2.54)[b], 1.90 ± 1.02 (1.91)[b]	[25]
IAEA Soil 7	1.8 ± 0.5 (2.5)[b]	
NIST SRM 2711 (Montana soil)	1.90 ± 0.15 (1.6)[c]	[26]
Soil (Egypt, water soluble part)	0.407	[27]
Soil (Red laterite soil, Raipur, India)	2.9 (3.1)[a]	[28]
Soil (Yellow soil, Raipur, India)	2.4 (2.5)[a]	
Soil (Yellow-gray soil, Raipur, India)	1.3 (1.2)[a]	
Soil (Gray soil, Raipur, India)	0.8 (1.0)[a]	
Soil (Yellow soil, Raipur, India)	1.4 (1.3)[a]	
Soil (Red laterite soil, Raipur, India)	2.1 (2.4)[a]	
Soil (Gray soil, Raipur, India)	0.3 (0.35)[a]	
Soil (Jaen, Spain)	0.235 (0.230)[a]	[29]
Soil (5 Samples from Cordoba, Spain)	0.034, 0.035, 0.031, 0.123, 0.069	[30]
Soil (2 samples from Wuhan, Chaina)	1.92 (1.89)[c], 2.60 (2.62)[c]	[31]
Cultivated soil (Western Macedonia, Greece)	0.81 ± 0.13	[32]
Uncultivated soil: 0–10 cm (Western Macedonia, Greece)	1.25 ± 0.44	
Uncultivated soil: 10–20 cm (Western Macedonia, Greece)	0.90 ± 0.25	
BCR CRM 141R (Calcareous loam soil)	4.2 ± 0.8 (3.7 ± 0.5)[a]	[33]
BCR CRM 142 (Light sandy soil)	0.5 ± 0.1 (0.4 ± 0.14)[a]	
BCR CRM 143 (Sewage sludge amended soil)	8.3 ± 0.2 (8.0 ± 0.4)[a]	
Sediment		
NMIJ CRM 7302a (Marine sediment)	2.3 ± 0.4 (1.98 ± 0.24)[b]	[34]
NMIJ CRM 7303a (Lake sediment)	0.8 ± 0.3 (0.96 ± 0.07)[b]	
IAEA–SLI (Lake sediment)	1.18 ± 0.11 (1.3)[b]	[35]
Oxted sediments (Surrey, UK)	3.9 (Silt trap: front), 4.7 (Silt trap: out flow); 3.3 (out flow interceptor: front); 2.1 (out flow interceptor: back); 0.9 (Deer park)	
JLK-1 (Lake sediment)	2.08 ± 0.22 (2.19)[b]	[36]
Seal beach, California	2.5–10.8	[37]
Tijuana slough, California	<5	
NRCC BCSS-1 (Marine sediment)	1.8 ± 0.1 (1.9)[c]	[24]
NRCC PACS-1 (Marine sediment)	12.7 ± 1.6 (12.9 ± 0.9)[b]	
NIST SRM 2704 (River sediment)	5.00 ± 0.08 (4.94 ± 0.39)[a]	
Antarctic marine sediments (at 21 different locations of coastal area and its surroundings)	1.1, 0.52, 1.02, 0.54, 0.9, 0.84, 1.1, 1.27, 0.45, 0.59, 0.71, 1.6, 0.45, 0.72, 0.89, 0.46, 0.85, 0.56, 0.41, 0.74, 0.88	[38]
Sediment core samples at different depths from 20 locations of southern part of the Black Sea	86 ± 9, 85 ± 8, 64 ± 7, 80 ± 8, 111 ± 12, 68 ± 7, 60 ± 7, 80 ± 9, 55 ± 6, 100 ± 11, 22 ± 3, 34 ± 5, 33 ± 4, 36 ± 4, 37 ± 4, 36 ± 5, 32 ± 4, 20 ± 3, 11 ± 2, 30 ± 3, 12 ± 2, 11 ± 2, 10 ± 2, 40 ± 4, 105 ± 11, 101 ± 12, 103 ± 11, 92 ± 9, 50 ± 6, 55 ± 6, 50 ± 5, 80 ± 8, 85 ± 9, 35 ± 4, 16 ± 3, 16 ± 2, 30 ± 2, 17 ± 2, 40 ± 3, 77 ± 8, 29 ± 4, 24 ± 3, 22 ± 3	[39]
NRCC PACS-1	10.7 ± 1.2, 12.6 ± 0.5 (12.3 ± 0.9)[b]	[40]
NRCC MESS-2	2.89 ± 0.13, 3.04 ± 0.13 (2.85 ± 0.12)[b]	

Table 1 (*Continued*)

Matrix	Concentration ($\mu g\,g^{-1}$)	Reference
NIST SRM 1646a (Estuarine sediment)	2.5 ± 0.3 (1.8)[b]	[41]
Sediments from 5 locations of Spanish Mediterranean Coast	0.15 ± 0.04, 0.78 ± 0.02, 0.41 ± 0.09, 0.83 ± 0.08, 5.9 ± 0.4	
BCR CRM 277 (Estuarine sediment)	4.78 ± 0.61, 3.62 ± 0.33 (1.43–1.47)[c]	[33]
BCR CRM 320 (River sediment)	0.73 ± 0.30, 0.67 ± 0.31 (0.63–0.65)[c]	
USGS MG-1 (Marine sediment)	1.28 ± 0.04	[26]
NIST SRM 1646 (Estuarine sediment)	2.3 ± 1.14 (2.0)[c]	
Rocks and minerals		
GSJ JR-1 (Rhyolite)	3.27 ± 0.04 (3.25)[b]	[36]
JB-2 (Basalt)	1.12 ± 0.41 (1.08)[b]	
USGS SGR-1 (Shale)	32 ± 2, 34 ± 3 (36)[b]	[42]
USGS STM-1 (Syenite)	4.8 ± 0.7 (5.2)[b]	
USGS QLO-1 (Quartz latite)	2.4 ± 0.1 (2.6)[b]	

[a] Other value.
[b] Certified value.
[c] Indicative value.

to 150 cm, from the 20 sampling sites of the continental slope of the southern part of the Black sea [39]. On the other hand, low Mo concentration (0.031–0.235 $\mu g\,g^{-1}$) has been reported in the soils of Spain by different workers [29,30] and thus it seems of interest to establish reference values about the geographical distribution of Mo in soils specially for agriculture.

3. Sampling, handling and storage

As applicable to all trace element determination, sample manipulation prior to Mo determination should be minimized in order to avoid contaminations, losses or other changes. Considering the low concentration levels of molybdenum in geological samples, extreme precaution should be taken during sample collection and storage to avoid cross sample contamination. Location of sampling points, kinds of sample and sampling apparatus for soil and sediment and presence of moisture are also important parameters to be considered.

Reports on the preparation and certification of two types (viz. marine and lake) of sediment reference materials for trace element analysis including Mo have been made by Inagaki et al. [34]. Approximately 300 kg of each surface sediment were sampled and water was removed by filtration, then they were air dried for 2 weeks at room temperature (25–28 °C). After removing visible external materials (e.g. shells), the materials were ground in a high purity alumina ball-mill. Sediment powder that passed through a 104 μm sieve was homogenized using a pan type mixer. The sediment powder was placed in glass bottles (60 g each) and radiation sterilized (^{60}Co, 20 kGy).

Waheed et al. [38] collected Antarctic marine sediments from depths ranging between 100 and 250 m. The samples were stored in precleaned polyethylene containers and later on handled in a laminar flow cupboard to avoid contamination. They were oven dried, homogenized and 100 mg portions were sealed in precleaned polyethylene capsules. The homogeneity of each sample was checked by analysing manganese content.

Oxted sediment (Surrey, UK) samples were homogenised manually by mechanical shaking for a few min and stored at less than 4 °C in a fridge, then they were dried at 105 °C in an oven for 12 h, homogenized in a polypropylene container and sieved (<125 μm). A 10 g sub-sample of dried sediment was weighed in a plastic capped glass bottle [35].

According to Townsend et al. [48], sediment samples from a temperate stratified estuary were collected using a box corer. Cores were sub-sampled, with the top 2.5 cm sections being extruded into acid-washed polyethylene sealed containers. Sediments were stored in the dark in a cool room until digestion.

Portions of dry, homogenized sediment samples collected from Spanish Mediterranean coast [41] were taken in glass vials and placed in a desiccator for 15 days. After that the vials were covered and stored at room temperature.

In order to collect soil samples from agricultural fields in Aomori Prefecture, Japan [49], a plastic core sampler of 15 cm in diameter and 5 cm in depth was used to collect from 8 points in each sampling field. The soil core samples were dried at 60 °C and passed through 2 mm sieve. The sieved soil samples from 8 soil cores in each field were thoroughly mixed and pulverized with an agate ball mill.

By some workers [32] soil samples were collected by using a 10 cm diameter manual corer, in accordance to ASTM C 998-83 standard recommendations [50]. After being collected, all samples were air dried, sieved with a 2 mm mesh and homogenized.

Sampling from two fresh water lakes for sediments was performed in the deepest part of each lake by using a gravity corer that permits collection of a sediment column. Immediately after sampling, the sediment cores were sliced into 1 cm thick layers, which were placed in acid-washed petridishes and kept frozen until analysis [51].

Prior to sampling, litter layers and organic horizons were removed until uppermost mineral horizon was exposed. Soil columns with 66 mm diameter and 50 mm length were collected using home-built sampling device. Five to seven replicates were collected from an area of about 1 m^2. Soil profiles were sampled according to genetic horizons or predefined depths. The samples were packed in airtight bags in order to prevent drying and stored at 4 °C until analysis [52].

4. Sample preparation

Sample preparation is an important step in the analytical determination of geological samples because of the refractory nature of some of these materials (which contain silicate or aluminosilicate structures and the reduced concentration of Mo). This can be accomplished by either of the following ways including digestion and in some cases, preconcentration steps. Additionally it has been considered the use of slurries as an alternative sample preparation strategy.

4.1. Digestion of geological samples for Mo determination

The mineralization of geological samples for the total determination of trace amounts of molybdenum has been performed using wet acid digestion. Now-a-days, the availability of microwave digestion in pressurized sealed containers leads to reduce digestion time and risks of contamination and also to avoid analyte losses.

There are various official methods for the analysis of soils and sediments which use different acid mixtures and microwave heating: ASTM D5258-92 [53], US EPA Method 3050B [54], US EPA Method 3051 [55]. However, the microwave-assisted acid digestion of EPA method 3051 using exclusively concentrated nitric acid does not provides a total digestion of many samples. Because of that, after microwave digestion, not only the vessel content must to be filtered or centrifuged to remove any residual undissolved solid particles, but also some analyte elements attached to silicate structures may not be dissolved.

Acid digestion of soil and sediment samples performed with a Milestone microwave digestion system has been reported by various workers [26,34] under more or less similar conditions. The method of Falciani et al. [26] is as follows: to 0.1 g sample in a PTFE vessel 1 mL H_2O, 5 mL HNO_3 and 3 mL HF were added and the vessel was sealed. The microwave robust digestion program that was developed to give quantitative recoveries was as follows: 250 W for 10 min, 400 W for 10 min, 650 W for 10 min and 250 W for 10 min. An additional care was taken in this sample preparation. When less than 12 samples had to be digested, the remaining vessels were filled with the acid mixture used for the sample digestion in order to provide an appropriated energy balance; since the absorbed microwave power is proportional to the total mass in the cavity. In another microwave acid digestion procedure developed by Inagaki et al. [34] following the time programme of 250 W for 15 min, 400 W for 15 min, 600 W for 5 min and 250 W for 15 min, 3 mL HF and 1 mL $HClO_4$ were added to a PTFE vessel and the microwave irradiation was repeated. The solution in the vessel was evaporated in a PTFE guarded evaporation chamber using an infrared lamp (375 W) and a clean air pump. Finally, the residue was dissolved in 1 mL HNO_3 and diluted with ~30 mL pure water.

Conventional open wet digestion for soils and sediments has been reported by different groups [35,40] using concentrated HNO_3:HF acid mixture. Using a hot plate set at around 70 °C, the whole digestion process normally takes 8 days to be completed, sometimes more if HCl addition was required for samples that retained undissolved residues. However the time may be reduced to about 3 days when high pressure digestion vessels were used [40].

A procedure for the digestion of geological samples using aqua regia by reflux boiling has been described by several research groups [19,56,57] and this method is particularly recommended for samples such as rocks, soils or sediments. For many types of such samples it does not achieve total sample dissolution and aqua regia digestion may, therefore, only be suitable where most of the Mo is present in non-silica phases.

Fusion of the geological samples with lithium metaborate or anhydrous sodium carbonate in a platinum crucible followed by dissolution in HCl has been reported by workers like Melwanki et al. [25], Harita et al. [36], Monte and Curtius [42]. No doubt there is potential for contamination from lithium flux for samples with trace amounts of Mo.

By applying different leaching procedures it is possible to liberate selective fractions of Mo from its total content in a sample. A reductive hydroxylamine hydrochloride leaching was used in order to dissolve Mn and Fe oxide minerals while not attacking the detrital silicate phase [58]. For example, Mn and Fe oxides are important hosting phases for Mo in freshwater sediments. Replicated pseudo-total microwave-assisted digestion of subsamples of these sediments by using a mixture of aqua regia and HF demonstrated that Mo associated with the non-detrital phase (organics and Fe–Mn oxides) constitutes more than 95% of pseudo-total content. Prior to leaching, the sediment samples were washed in order to decompose organic carbon. Organic matter was found to affect negatively the performance of subsequent ion-exchange purification of Mo.

4.2. Preconcentration of Mo from geological samples

This step depends on the detection limit of the method of choice used for Mo determination and the potential for matrix interferences. Preconcentration and separation of the analyte followed by detection is mandatory particularly when the analyte is present at trace and ultra-trace level. Matrix effects and contamination of sample-introduction systems will be minimized after analyte separation. Solvent extraction (SE) and solid phase extraction (SPE) are the two most common methodologies used for the said purpose. SE is inconvenient due to the requirement of large volumes of solvents which may create environmental side problems as well as health hazard problems to the operator. SPE using chelating resins is the method of choice due to its high separation efficiency, good reproducibility of retention parameters and operational simplicity.

Coprecipitation and sorption of Mo have been, together with SE and SPE the most commonly used preconcentration procedures: solvent extraction of Mo is easily do after formation of a thiocyanato complex in acid media in the presence of reducing agents in conventional thiocyanate method or in modified thiocyanate method through the formation of a ternary ion association complex. The solvents used by different workers include butyl acetate, tributyl phosphate in chloroform, 4-methyl pentan-2-ol in benzene, amyl alcohol, isoamyl alcohol + carbon tetrachloride, tribenzylamine in chloroform, tributylphosphate + benzene, acetophenone, isoamyl alcohol,

ethylacetate, ethylmethylketone, butylacetate, isobutyl methyl ketone, chloroform, hexadecyl methyl ammonium bromide in chloroform, toluene + ethanol, dichloroethane, nitrobenzene, isopropylether, chloroform + benzophenone, polyvinyl alcohol and so on. The outlines of such more than 100 solvent extraction procedures, proposed in the literature can be obtained in the review article of Basak et al. [20].

Some variations of the modified thiocyanate methodology for Mo determination in geological samples have been reported by other workers [25,28]. The method of Melwanki et al. [25] is based on the formation of chloroform soluble mixed ligand complexes of Mo(V) with thiocyanate and isothipendyl hydrochloride or pipazethate hydrochloride in hydrochloric acid medium. Again the work of Chikhalikar and Patel [28] involves the extraction of Mo(V)–SCN^- complex with a toluene solution of *N*-octylacetamide and subsequent heating of the extract at 60 °C for about 10 min which eliminates the interference of iron upto 1000 μg mL^{-1} with increased preconcentration.

The use of SPE through ion exchange has been reported for the determination of Mo in soils, sediments, etc. For example, Mo was preconcentrated as its Mo(V)–thiocyanate complex using a column containing Amberlite XAD-7 resin. In this method thiourea was used as the reducing agent [23]. Again in the method of Molina-Diaz et al. [29] the solid phase used was a dextran type anion exchange resin (Sephadex QAE-A-25). An air-segmented continuous flow method has been developed by Harita et al. [36] for the determination of molybdenum at ultra-trace levels using the catalytic effect of molybdate during the oxidation of L-ascorbic acid by H_2O_2. The incorporation of an online ion exchange column (Chelex 100, Na^+ form) improved the tolerence limit for various ions in the determination of Mo.

Although not many references have been cited preconcentration of Mo by coprecipitation reports on that [34] and sorption on activated carbon [42] have been published. For example, to geological sample solutions having a relatively high content of iron(III), 20 mg of ascorbic acid were added, then 1 mL of a 10% (m/v) solution of the ammonium diethyl dithiophosphate was added. After stirring, the solution containing the Mo complex was passed through the filter covered with the activated carbon (0.5%, m/v suspension). After drying at 110 °C for 15 min, the carbon was scraped into a 25 mL beaker, 1 mL concentrated HNO_3 was added and evaporated to dryness. The residue was treated with 1–2 mL 20% HNO_3 at room temperature and centrifuged. Molybdenum was measured in the supernatant [42].

Determination of the isotopic composition of Mo and its isotopic geochemistry have become new and rapidly growing field of Mo research. But prior to Mo isotopic analysis Mo should be separated and purified. Following 2 examples will reveal that it is analytically interesting.

For geological samples with high Fe and low Mo contents, such as fresh water sediments, the separation of Mo from Fe while providing quantitative yield of Mo was made by ion-exchange chromatography using the chelating resin, Chelex 100 after dissolution of the samples in aqua regia [51].

On the other hand, the isotopic composition ($^{95}Mo/^{97}Mo$) in molybdenite (MoS_2), a mineral of Mo in which Fe is present in negligible level can be determined directly without the need for preconcentration or puridication of Mo. To do it molybdenite was dissolved in aqua regia, dried to approximately 20 μL drop and reconstituted in 0.05 M HNO_3 to a molybdenum concentration approximately of 6 μg mL^{-1} [59].

4.3. Alternative sample preparation method for Mo determination based on slurry

The use of suspensions is a well recognized method for introducing solid samples into atomic spectroscopy analysis, thereby avoiding conventional mineralization-based procedures which, in addition to being time consuming, are prone to contamination and analyte losses. The slurry approach is particularly suitable for soil, sediment and sludge samples [60,61] because these materials have fine particle sizes which can be further lowered by simple grinding.

As it has been confirmed by other workers [62,63] making slurry of samples with high silica contents in a HF medium provides additional advantages. For example, the presence of HF not only mobilizes a significant fraction of the analyte towards the liquid phase but also provides the removal of silicon during the heating step. This approach has been used by Campillo et al. [24] where suspensions were prepared by taking 10–25 mg of soil or sediment and adding 25 mL of a solution containing 50% concentrated HF for Mo determination. In order to get reliable results, the sample preparation and ion-exchange separation of Mo was carried out in a clean environment (class 1000) [51].

5. Molybdenum speciation in solid matrices

Modelling of biogeochemical cycles of elements which is important from agrochemical and environmental view points requires the chemical speciation, i.e. the identification and quantification of the Mo compounds in real samples [64].

Molybdenum in sedimentary rocks and sediments has created interest as a paleo-environmental indicator of reducing conditions. This application demands clear knowledge of Mo deposition mechanisms and vice-versa demands better understanding of 'operationally defined' Mo speciation in anaerobic natural waters [65].

Marine plankton bioconcentrate trace MoO_4^{2-}, the dominant Mo species in sea water [46]. Solid surfaces like clay minerals and ferric aluminium oxyhydroxides weakly fix MoO_4^{2-} at slightly alkaline pH [66]. Thus particle-inert MoO_4^{2-} is conservative in the oxic ocean. MoO_4^{2-} can be transformed in sulfidic waters into thiomolybdates, $MoO_xS_{4-x}^{2-}$ [67]. Thiomolybdates are particle-reactive [18] and associated with the chemical pathway leading to stable Mo in anoxic sediments. Thus polysulfide ions facilitate Mo scavenging [68].

A speciation scheme of trace Mo was proposed for river water based on size fractionation by filtration and ultrafiltration [69]. Based on speciation results, most of the Mo was found to be reactive species. About 50% of the Mo was found to be reactive MoO_4^{2-} in the molecular fraction ($MW < 10^3$). The residual part was characterized as reactive Mo adsorbed or complexed on humic iron aggregates in the colloidal fraction and in the presence of a low concentration of humic acid.

Soils, sediments and other geological samples all vary in their moisture content depending on the location and the time of sampling. Provided that the metal species are stable, the matrix should be dried either by freeze-drying or by air drying at 40 °C. Most trace organics associated with them are bound to the organic surfaces of the matrix. Sequential extraction provides valuable information about the speciation of elements in geological samples by adding the chemical reagents that extracts the different compounds selectively from solid matrices. A large number of sequential extraction procedures have been developed in which the element content is partitioned by sequential treatment with a series a reagents [70].

About a decade ago an attempt was made to assimilate various methodologies for sequential extraction procedures among EU member states [71]. The BCR has developed a simple three-stage sequential extraction and prepared a sediment reference material (CRM 601) certified for metals including Mo extractable by the procedure shown in Fig. 1 [72].

In the study of Sanei et al. [73] from the uppermost 50 cm of 5 g sediment from 2 locations of Pigeon Lake, (Alberta, Canada) samples were subjected to a 7-step sequential extraction experiment using the following sequence of chemical treatments: (i) 25 mL of deionized water (for water soluble species); (ii) 50 mL of 1 M $MgCl_2{\cdot}6H_2O$, pH 7 (for exchangeable species); (iii) 50 mL of 1 M NaAc, pH 5, 90 °C (for carbonate species); (iv) 25 mL of 0.1 M $NH_2OH{\cdot}HCl$ at 25% (v/v) CH_3COOH, 90 °C (for reducible species); (v) 25 mL of H_2O_2, pH 2, 100 °C (for oxidizable species); (vi) 20 mL of aqua regia, 120 °C (for sulfide species) and (vii) hot digestion with HF–HCl–HNO_3 to dryness (for residual elemental fractions).

An important speciation technique has been presented for identification and quantification of species with boiling points between −88.5 and 250 °C for various elements including molybdenum in soil samples based on hydride generation low temperature gas chromatography with detection by ICP-MS [74]. A sequential extraction procedure for waste water sediment was developed by Heltai et al. [75] based on CO_2 and water extractants using supercritical fluid extraction and the procedure gives information on water soluble, carbonate bound and

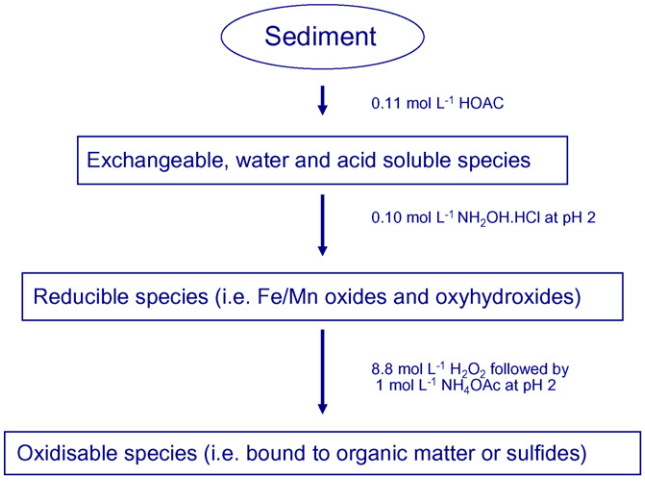


Fig. 1. Scheme for the sequential extraction of Mo in geological samples.

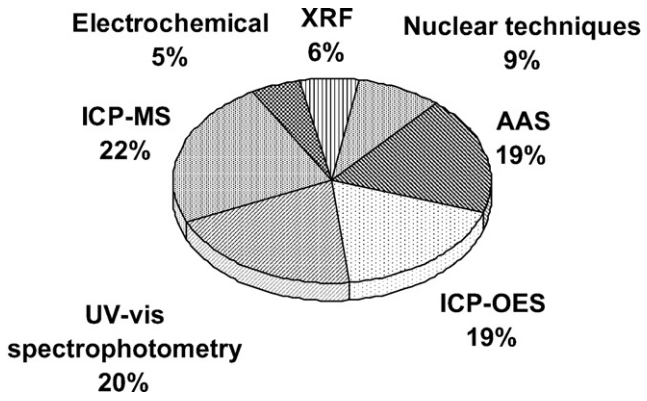


Fig. 2. Distribution of the literature about determination of Mo in geological samples as a function of the techniques employed.

mobile organic bound trace metal fractions including those of molybdenum based on sequential extraction.

Sarkar and O'Connor [76] estimated available Mo in biosolids-amended soil using iron oxide impregnated filter paper. For this study they treated the filter paper by immersion for 1 h in 10% $FeCl_3{\cdot}6H_2O$ solution, air drying and then putting in 2.7 M ammonia. The papers were air dried and cut into strips. Air dried soil was mixed with ground biosolid residues and a portion (1 g) together with a prepared strip, were shaken for 16 h in 1 mM $CaCl_2$. The strip was removed, rinsed and air dried. The retained Mo was extracted with 1 M HCl for 1 h.

6. Detection

Various detection methodologies using UV–vis spectrophotometry, atomic spectrometry, mass spectrometry, X-ray fluorescence (XRF), nuclear and electrochemical techniques have been reported for Mo determination in geological samples. Fig. 2 presents the distribution of such methods.

It is clear that inductively coupled plasma mass spectrometry (ICP-MS) has the highest users for Mo determination in geological samples together with UV–vis spectrophotometry, atomic absorption spectrometry, and atomic emission. The use of nuclear techniques, XRF and electrochemical methods is scarcely.

6.1. UV–vis spectrophotometry

The determination of Mo by its complexation with SCN^- is one of the most commonly used techniques wherein Mo(VI) is reduced to Mo(V) which forms the coloured complex with an absorption maximum in the range of 460–470 nm. Normally the complex is extracted into an appropriate solvent before such measurement. In the modified thiocyanate methods, a third reagent is added which forms a ternary ion association complex followed by the solvent extraction of the complex for absorbance measurement. The thiocyanate methods have been used to determine Mo in rocks, soil, ores, sediment, etc. [20].

Outlines of some of the other spectrophotometric methods are presented here. To the soil solution containing Mo, 2 M thiourea, 3 M KSCN and approximately 0.05 g solid cuprous

chloride were added. Then 2 mL concentrated HCl were added and diluted to 50 mL and left at room temperature for approximately 5 min to allow complete formation of the Mo(V)–SCN complex. The resulting solution was passed through a solid phase extractor containing Amberlite XAD-7 at a flow rate of around 2.5 mL min^{-1}. Then it was eluted with 2.5 mL acetone at a flow rate of 1 mL min^{-1} and Mo directly measured at 461 nm. The calibration graph for Mo was linear up to 5 μg mL^{-1} with a detection limit of 38 μg L^{-1}. The recovery percentage and precision were better than 97% and 4% relative standard deviation (R.S.D.), respectively [23].

The associate formed by triiodide ion (6.6×10^{-2} M) and cetylpyridinium chloride (CPC, 1.4×10^{-3} M) micelles was used to enhance the kinetic spectrophotometric determination of Mo(VI) in soil by its catalytic action on the oxidation of iodide with H_2O_2 in an acid medium. The reaction was monitored at 500 nm which is the λ_{max} of the I_3^-–CPC associate. The micellar medium allowed the determination of Mo(VI) concentrations between 2 and 150 ng mL^{-1} with a detection limit of 1.3 ng mL^{-1} and R.S.D. of 2.6%. The selectivity towards interferents, yielding yellowish solutions was significantly enhanced; although tolerated concentrations of W(VI), Cr(VI) and Ti(IV) were really low [30].

Oxidation of ascorbic acid by H_2O_2 is catalysed by molybdate ion and the reaction product, dihydroascorbic acid is successively condensed with *o*-phenylene diamine to form 3-(1,2-dihydroxy ethyl)-furo [3,4-b] quinoxalin-1-one which is measured spectrophotometrically at 340 nm. An air segmented continuous flow analysis was combined with this reaction to develop high-speed automated system for Mo determination in rock and sediment after alkaline fusion. On-line separation was achieved by using the cation exchange column. The detection limit with the use of the column was 1.6 pg mL^{-1} and the R.S.D. was 0.2% [36].

Other spectrophotometric methods are summarized in Table 2. The literature survey indicates that most of the authors

Table 2
UV–vis spectrophotometric methods for the determination of molybdenum in geological samples

Reagents and conditions	Analytical characteristics	Matrix	Reference
10 M HCl, 20% ammonium thiocyanate, 5% ascorbic acid, 0.5% isothipendyl hydrochloride (IPH) or pipazethate hydrochloride (PPZ), extraction in chloroform, interference due to W(VI) and U(VI), λ_{max} = 461 nm (IPH), 465 nm (PPZ)	Beer's law = 0.5–5.9 μg mL^{-1} (IPH), 0.5–6.9 μg mL^{-1} (PPZ), ε = 32,800 (IPH), 40,000 (PPZ), sensitivity = 9.8 ng mL^{-1} (IPH), 10.9 ng mL^{-1} (PPZ), R.S.D. = 0.88% (IPH), 0.95(PPZ)	Soil	[25]
10 M HCl, 20% ammonium thiocyanate, 10% ascorbic acid, 2% *N*-octylacetamide, extraction in toluene, λ_{max} = 470 nm	Calibration graph = 30–600 ng mL^{-1}, ε = 35,000, detection limit = 4 ng mL^{-1}, R.S.D. = 1%	Soil	[28]
1.29×10^{-4} M pyrocatechol violate, phthalate buffer (pH 2.9), solid phase extraction using Sephadex QAE A25, first derivative spectra with peak at 716 nm, interference due to W(VI)	Linear range = 2–8 ng mL^{-1}, detection limit = 0.024 ng mL^{-1}, R.S.D. = 4.3%	Soil	[29]
Buffer (pH 1.5), 0.01% 3-hydroxy-2-(2-thienyl)-4H-chromen-4-one, 10% Triton X-100, λ_{max} = 410 nm, complex is stable for >2 h	Beer's law = 0.01–0.4 μg mL^{-1}, R.S.D. = 1.3%	Soil	[77]
0.01 M 3,4,5-trihydroxy benzoic acid, 1.2 M HCl, 0.1 mM nitrobluetetrazoliumchloride, saturated ammonium fluoride, extraction in chloroform, λ_{max} = 260 nm	Beer's law = 0.5–5 μg mL^{-1}, ε = 150,000, R.S.D. = 1.4–2.1%	Soil	[78]
10 mM 3,4,5-trihydroxy benzoic acid, 1 mM thiazolyl blue tetrazolium bromide, extraction in 1,2-dichloroethane, λ_{max} = 245 nm	Beer's law = 0.15–3 μg mL^{-1}, ε = 16,700 ± 900	Soil	[79]
6 mM sodium boro hydride, 3–7 M HCl, 28 μM cetylpyridinium chloride + 15 μM Triton X-100, 0.7 M ammonium thiocyanate, extraction in benzene, toluene, chloroform, λ_{max} = 460 nm	Beer's law = up to 2.5 μg mL^{-1}, ε = 23,000, detection limit = 125 ng g^{-1}, R.S.D. = 0.7%	Soil	[80]
Phthalate buffer (pH 3), 1.5% cetylpyridinium chloride, 0.5% 4,5-dibromo-2,3,7-trihydroxy-9-piperonyl-6-fluorone, λ_{max} = 541.5 nm	Beer's law = up to 0.6 μg mL^{-1}, R.S.D. = 0.91–3.17%	Soil	[81]
4 M HCl, 0.2% *N*-*p*-chlorophenyl-alpha-phenylstyryl-acrylohydroxamic acid, extraction with 2% Aliquat-336 in chloroform, λ_{max} = 388 nm	Beer's law = 1–28 μg mL^{-1}, ε = 5000	Soil	[82]
Separation through a column of silica gel pretreated with tributyl phosphate and ethyl ether, eluted with 0.5 M HCl, 0.02% pyrocatechol violet, 0.038% hexadecyltrimethyl ammonium bromide, acetate buffer (pH 3.85), λ_{max} = 6.75 nm	–	Sediments, minerals, rocks, ores	[83]
Quercetin, hexadecyltrimethyl ammonium bromide, KCl–HCl buffer (pH 2.3), λ_{max} = 420 nm	Beer's law = up to 0.3 μg mL^{-1}, ε = 203,000	Silicate rocks	[84]
5 mM Mandelohydroxamic acid, 10 M HCl, 10 mM methyltrioctyl ammonium chloride, extraction in toluene, λ_{max} = 375 nm	Beer's law = up to 4.5 μg mL^{-1}, ε = 16,200, detection limit = 0.05 μg mL^{-1}, R.S.D. = 0.5%	Soil	[85]
40% KSCN, 3% thioacetanilide, extraction in benzene, λ_{max} = 470 nm	ε = 19,000, R.S.D. ≤ 1.5%	Ore	[86]

performed extractive spectrophotometric determination of this element for the analysis of soils.

6.2. Atomic absorption spectrometry

Atomic absorption spectrometry (AAS) is an important sensitive atomic spectrometric method that is suitable for the determination of selected elements at the trace and partly at the ultra-trace level. AAS is perhaps the most commonly used detector for the determination of Mo in geological samples. The techniques employed are essentially two: flame atomic absorption (FAAS), and electrothermal atomization (ETAAS). The FAAS results for Mo show some positive interferences. Mo is a refractory element that requires the use of ion suppressants such as aluminium. Laboratories not using this will have a positive bias in their data [87]. It has been reported that the recovery of Mo is reduced (approximately 60%) using ETAAS as the detection system in comparison to discrete nebulization FAAS. This fact cannot be attributed to the preconcentration procedure, which is the same for both techniques [42]. However, the limit of detection for Mo by both FAAS and ETAAS are, respectively, 30 and 0.005 ng mL^{-1} thus indicating the comparatively high sensitivity of ETAAS.

Analysis using ETAAS, in general requires more care than to do it by FAAS and it is necessary to spend sometime optimizing instrument conditions before analysis in order to avoid various problems. Owing to its refractory nature, high ashing temperature (around 1700 °C) may be used without loss of the element. Several authors reported a plateau in the ashing temperature graph for Mo from 1000 to 1600 °C [19].

Background correction is essential when geological samples are analysed by AAS due to the significant residual background absorbance signal. At the Mo wavelength (313.3 nm) used, the value can be easily corrected by the D_2 arc device [57].

Pyrolytic graphite coated tubes are recommended, because uncoated tubes can easily interact with refractory elements to produce non-volatile carbides, e.g. Mo_2C, MoC (having melting points of 2692, 2687 °C, respectively), a phenomenon which alters the atomization process. Additionally, graphite is porous and the atomizer wall is, therefore, subject to infiltration by the solution and at higher temperatures vapors can diffuse through the atomizer wall. Thus the pyrolytic graphite coating on a tube significantly improves the performance obtained for Mo determination [57].

In the interest of economy, nitrogen may be used as the purge gas during the drying and cooling steps in ETAAS, with argon which provides greater sensitivity replacing nitrogen during ashing and immediately prior to atomization [19].

Table 3 gives the outlines of the methodologies including the AAS operating parameters used for the determination of Mo in geochemical samples. A characteristic mass as low as 9 pg has been reported by such method [24].

6.3. Atomic emission spectrometry

The general trend observed worldwide is that the use of AAS for single-element analysis is being replaced by ICP-OES and ICP-MS in many laboratories for the elemental analysis of samples concerning several elements per sample. Inductively coupled plasma optical emission spectrometry (ICP-OES) is one

Table 3
Atomic absorption spectrometric methods employed for the determination of molybdenum in geological samples

Outline of the method	Analytical characteristics	Reference
Soil extracted with 1 M NH_4Ac for 16 h or digested with aqua regia under reflux for 2 h; GFAAS programme: (step 1) 100 °C for 3 s, (step 2) 200 °C for 30 s, (step 3) 200 °C for 25 s, (step 4) 1000 °C for 10 s, (step 5) 1000 °C for 10 s, (step 6) 1000 °C for 1 s, (step 7) 2900 °C for 1 s, (step 8) 2900 °C for 2 s, (step 9) 2900 °C for 1 s, (step 10) 90 °C for 13 s	Practical range = 0.4–7.0 μg g^{-1}, detection limit = 0.086 μg g^{-1}, R.S.D. = 0.42–7.4%, recovery = 100.5–111%	[19]
Soil or sediment slurry introduced in ETAAS with programme: (drying) 160 °C for 30 s, (atomization) 2650 °C for 5 s, (clean) 2650 °C for 3 s	Calibration = 0–60 ng mL^{-1}, characteristic mass = 9 pg, R.S.D. = 1.9%	[24]
Geological samples dissolved by using lithium metaborate fusion chelated with ammonium diethyl dithiophosphate and sorption on to activated carbon, Mo eluted with HNO_3, analysed by flame and furnace in presence of $Mg(NO_3)_2$ chemical modifier; ETAAS programme: (step 1) 90 °C for 10 s, (step 2) 120 °C for 15 s, (step 3) 1600 °C for 15 s, (step 4) 2650 °C for 5 s, (step 5) 2650 °C for 5 s, (step 6) 20 °C for 10 s	Analytical graphs = up to 69 μg mL^{-1} (flame) and up to 0.18 μg mL^{-1} (furnace)	[42]
Soil digested with aqua regia; ETAAS programme: (drying) 120 °C for 40 s, (ashing) 1700 °C for 20 s, (atomization) 2650 °C for 5 s, (clean) 2650 °C for 3 s	R.S.D. = 2.1–10.5%, recovery = 97.5–108.5%	[57]
Soil digested with aqua regia, HF, $HClO_4$, complexation with thiocyanate, reduced with ascorbic acid, extracted in isobutyl methyl ketone and introduced into GFAAS; temperature programming from 70–2600 °C in five stages	Calibration = linear up to 64 ng mL^{-1}, recovery = 95.5–107.4%	[88]
Sediment treated with HNO_3, $HClO_4$, HCl; solution adjusted with pH 2, mixed with 5 M $NaClO_4$, 0.05 M 5,5′-methylenedisalicylohydroxamic acid; extracted with 1 M tributyl phosphate in isobutyl methyl ketone; extract analysed by N_2O/C_2H_2 FAAS at 313.3 nm with a slit width of 0.7 nm	Calibration curve = 0.1–0.6 μg mL^{-1}	[89]
Soil extracted in hot water; liquid-liquid extraction with ethyl acetate and 8-hydroxyquinoline in chloroform; organic phase analysed by ETAAS	Calibration curve = linear up to 10 ng mL^{-1}, detection limit = 0.5–1.5 ng g^{-1}	[90]
Soil extracted with Tamm's solution (ammonium oxalate + oxalic acid, pH 3.3), analysed by ETAAS	–	[91]
Soil extract treated with HNO_3, introduced into ETAAS with programming: drying at 100 °C for 30 s, ashing at 1900 °C for 10 s, atomization at 2500 °C for 1 s, cleaning at 2500 °C for 4 s	–	[92]

of the most widely used technique for multielement determinations. Its sensitivity for Mo can reach the parts per billion level and the calibration graphs are linear over a range spanning three to five decades of concentration. Adequate preconcentration and separation techniques, however, are necessaries prior to ICP-OES measurements because serious interferences are caused by iron, aluminium and other concomitants of geological samples present at high concentration levels.

Various authors have reported Mo determination in the extracts of geological samples by ICP-OES. Few typical methodologies may be cited below. In the sediment extracts made by supercritical fluid extraction, 15 elements including Mo were determined by ICP-OES using 1.1 kW incident power and the following conditions: a plasma argon gas flow 12 L min^{-1}, a sheath argon gas flow 0.2 L min^{-1}, a nebulization argon gas flow of 0.35 L min^{-1}, nebulizer Babington type and sample uptake rate of 1.5 mL min^{-1} [75].

The Digi PREP digestion system was applied for soil reference material preparation and the temperature probe measures the solution temperature normally at sub-boiling 95 °C. Results are reported for the determination by ICP-OES of μg mL^{-1} levels of 15 elements including Mo with R.S.D. values between 1.6 and 4.7% [93].

An ICP-OES instrument for simultaneous major and minor multielement soil analysis in the wavelength range from 165 to 1050 nm has been described by Marquardt and Wolff [94]. The instrument is controlled by user-friendly TEVA software and the emission beam can be scanned axially and radially for sensitive and less sensitive determinations.

Soil sample was treated with 0.1 M oxalic acid and 0.175 M ammonium oxalate and resulting solution injected at 5.7 mL min^{-1} into a micro ion exchange column packed with Dowex 1 resin for dual-column on-line ion exchange preconcentration in a FIA system with 1.9 M ammonium chloride/0.1 M ammonium citrate as the eluent at 0.5 mL min^{-1} and 60 °C for 5 min. The eluate was raised at 0.5 mL min^{-1} to ICP-OES with argon as carrier gas for Mo measurement at 281.62 nm. The observation height was set at 12 mm and plasma power was fixed at 1.2 kW. Recoveries and R.S.D. were 90–110 and 5.3%, respectively. An enrichment factor of 50 was achieved at a sampling frequency of 12 samples per hour [95].

6.4. Mass spectrometry

The use of inductively coupled plasma mass spectrometry (ICP-MS) has grown in the last 2 decades as a simultaneous multielement specific detection method. This method possesses excellent selectivity and sensitivity and there is the possibility of performing isotopic determinations. Matrix effects and spectral interference cause problems in case of the quadrupole ICP-MS [96] but they can be reduced or even eliminated using sector field ICP-MS (ICP-SFMS) [39]. ICP-MS instruments with multi-collector systems (MC ICP-MS) are advantageous for precise isotope-ratio measurements and the R.S.D. (0.002%) was better in comparison to double-focusing ICP-SFMS with a single ion detector [59]. Outstanding capability of ICP-MS is of interest in trace and ultra-trace analysis for the application of isotope dilution analysis (IDA), providing the possibility of absolute quantification for elements with two or more isotopes in any sample material in order to obtain accurate trace-element concentration [97]. In relation to total molybdenum determination, ICP-MS has been coupled with several pretreatment techniques. Few examples are given below.

Sediment analysis was performed for the determination of ^{98}Mo by ICP-MS. A high solids nebulizer (V-groove) was used for sample nebulization with on-line internal standardisation using ^{115}In. A detection limit of 5 ng g^{-1} was obtained for acid digested sediments [35].

After microwave-assisted digestion of sediment materials for isotope dilution ICP-MS determination of Mo, a coprecipitation-separation technique was developed to remove the matrix concomitants that cause significant spectral interferences with the measured isotope pairs $^{98}Mo/^{96}Mo$ [34].

ICP-MS possesses the unique capability of measuring precise accurate isotope ratios, which is applied in the precise determination of element concentration by the isotope dilution (ID) technique. The Mo concentration in two meteorites (C1 Chondrites) has been measured using the stable IDMS technique incorporating thermal ionization mass spectrometry. The IDMS technique was also used to measure the Mo concentration in the metallic and sulfide phases of the iron meteorite (Mundrabilla). In this present experiment, Mo samples enriched in ^{94}Mo and ^{100}Mo, respectively, were gravimetrically combined to form a double spike with a known $^{94}Mo/^{100}Mo$ isotope abundance ratio. The Mo concentration of the double spike was calibrated by IDMS against an accurate gravimetric laboratory standard [98].

Highly precise and accurate results for traces of Mo were attained using ID ICP-MS, although authors [99] reported the interference from $^{40}Ar^{39}K^{16}O^{+}$ on ^{95}Mo in plant digests due to the high concentration of K. The combination of solvent extraction followed by ion chromatography has been described to remove matrix elements for Mo isotopic analyses by multi-collector ICP-MS [100]. The cloud point extraction (CPE) of trace elements using surfactants like Triton X-114 has been performed as an alternative to solvent extraction [101].

Multielement analysis (including Mo) of soil and sediments by ICP-MS after microwave-assisted digestion has been described by Falciani et al. [26] using ^{103}Rh internal standard. A very low limit of quantification viz. 0.05 μg g^{-1} was obtained. Precision values, as relative standard deviation, in the range 2–14% were obtained (14% at the level of 1.2 μg g^{-1} Mo).

Sector field ICP-MS was used to analyse Mo in HNO_3-leached sediment samples. ^{95}Mo with 300 instrumental resolution was used in such analysis. The measured Mo concentration in the sediment leachates was generally <0.2 ng g^{-1} [48]. The same detection methodology has been applied for quasi-simultaneous multielement analysis of trace elements including Mo after percolation of soil samples using H_2O, 1 M NH_4NO_3 and 0.1 M $NH_4H_2PO_4$. Concentration level of the measured element was in the ng mL^{-1} level [52].

A method using MC ICP-MS for precise measurements of Mo isotopic composition in fresh water sediments and molybdenite samples has been developed by Malinovsky et al. [51]. Purifi-

cation of Mo for isotope ratio measurements was realized by ion exchange chromatography using the chelating resin Chelex-100. This technique allows an efficient separation of Mo from an excess of Fe in samples and, at the same time, provides a quantitative recovery of Mo.

The major potential interferences on Mo isotopes as well as on the normalizing $^{105}Pd/^{104}Pd$ ratio include Zr, Ru, Fe, Mn, Zn, Cu, Ni, Co and Cr. Except for Ru, which has extremely low concentrations in most matrices, these elements are abundant in natural geological samples. According to the authors [51] Mo purification procedure described above is adequate for reducing the aforementioned elements to insignificant concentration levels. The long-term reproducibility has been evaluated as 0.06, 0.04, 0.06, 0.08 and 0.14% for $^{94}Mo/^{95}Mo$, $^{96}Mo/^{95}Mo$, $^{97}Mo/^{95}Mo$, $^{98}Mo/^{95}Mo$ and $^{100}Mo/^{95}Mo$, respectively. The MC ICP-MS sensitivity reported by Dauphas et al. [100] was approximately 7×10^{-5} ions analysed by atom injected.

The technique of diffusive gradients in thin films (DGT) is a truly interesting and useful tool for in situ measurements of 55 elements in water, including Mo, by high resolution ICP MS. LOD value obtained for Mo by this technique was 0.057 ng mL^{-1} [102].

On-line continuous-leaching of soils that produces real-time data takes advantage of the resolution and high sensitivity of high resolution ICP-MS. Elements like Mo present at very low concentrations can be detected and interferences that often occur on using low resolution can be solved. Leaching agents (water, 1% HNO_3, 10% HNO_3 and 30% HNO_3), which are sequentially pumped through a column containing the sample, are scanned continuously at low, medium and high resolution for release of trace and major Mo concentrations [103].

Laser ablation (LA) has become a very fast and popular sample introduction method for ICP based instrumentation. LA ICP-MS has the potential to directly determine the concentrations of around 80 elements in solid soil samples using a laser operating at 266 nm. In the work of Rodushkin et al. [104] limestone and sediment samples were placed in the ablation chamber and analysed for Mo. It has been suggested that the basic requirement for an internal standard in LA ICP-MS is that it exhibits similar ablation characteristics to the analyte (Mo). This behaviour can be established from the shapes of flow rate plots using solid standard materials for calibration.

6.5. Nuclear techniques

Instrumental neutron activation analysis (INAA) allows the simultaneous determination of trace elements giving sensitive and reliable results, in the range of very low concentrations, because it is not much affected by interferences if samples are properly prepared and in some cases permits the determination of elements difficult to be measured by other techniques. Nevertheless, it requires a laboratory with the adequate safety conditions to use a nuclear reactor. This technique has been employed for Mo analysis in geological samples.

INAA was used for the determination of 40 elements including Mo in 21 coastal and marine sediments of Antarctica. For the majority of the radioisotopes of interest, interference free photo peaks were obtained by appropriate selection of irradiation and decay times for the quantitative analyses. Radio-assay schemes for 3 sets of elements after neutron irradiation and cooling were evolved to avoid matrix effects. Data have been compared with those for sediments of various stations at Antarctica and two other regions in different continents. The quality assurance of data was performed using standard reference materials of a similar matrix [38].

Homogenized estuarine sediment samples were dried and approximately 200 mg were sealed in polyethylene capsules irradiated in a 27 kW neutron source reactor with thermal neutron flux of 1.2×10^{12} n cm^{-2} s^{-1} under specified irradiation conditions. Irradiated samples were counted using an HPGe detector and a PC-based multichannel analyser. The resolution was 1.9 keV for the 1332.5 keV peak of ^{60}Co. Trace elements including Mo were detected at the tabulated gamma ray energies [105].

Soils were dry-ashed for 2 h at 500 °C irradiated in polyethylene phials in a thermal neutron flux of 2×10^{13} n cm^{-2} s^{-1} for 20–180 min and allowed to decay for 2–5 days. Each sample was fused with NaOH and the melt extracted with water, then treated with 9 M $HClO_4$. After that Mo(VI) was extracted into 1.7 mM zinc diethyldithiocarbamate in chloroform. The organic phase was washed with 1 M HCl and treated with 12 M HCl and 10 M H_2O_2 for several min. Water was added and Mo back-extracted into the aqueous phase. The extract was evaporated to dryness and the residue dissolved in 13 M ammonia. The sample was allowed to reach secular equilibrium (>2 days) and then counted at the 104 keV gamma-photopeak of ^{99m}Tc with a well-type Ge(Li) detector and multichannel analyser. With irradiation for 3 h the detection limit was approximately 1 ng. The chemical yield was 97–100.5% [106].

Volcanic glass samples were sealed into fused silica ampoules, placed in Al capsules and irradiated in a thermal neutron flux of 3×10^{13} n cm^{-2} s^{-1} for 8 h under cadmium cover, allowed to decay for 9 days, fused with K_2CO_3–Na_2CO_3–$NaNO_3$ and dissolved in HCl. Quantitative coprecipitation of Mo(VI) was carried out with Bi_2S_3 from 1.2 to 2 M HCl. Gamma spectrometric measurements were made with a 70 cm^3 Ge(Li) detector having a resolution of 2.4 keV for the 1332.5 keV peak of ^{60}Co and a multichannel analyser. A computer program was used to calculate peak areas and concentration and values for Mo were corrected for the contribution of uranium. Detection limit for Mo was 1.8 μg g^{-1} volcanic glass [107].

6.6. X-ray fluorescence spectrometry

X-ray fluorescence spectrometry (XRF) offers a fantastic tool for the determination of major and minor components in solid samples. Unfortunately, there is a reduced sensitivity of this procedure. Instrumental methods for improving the detection limits of XRF include the use of total reflectance XRF and polarized radiation based XRF. XRF spectrometry can be performed on powder pellets or fused glass bead and has been routinely applied to the analysis of Mo in geological samples. Only few reports can be found on the analysis of Mo by these methods. The analytical

line used is Mo Kα(0.0709 nm) and the detection limit is about 10 μg g^{-1} [1]. Synchrotron XRF has been described to be the best technique for producing extensive analytical data from the view point of speed, ease of application, cost, non-destructive nature and sensitivity. The technique allowed to obtain data on more than 20 elements (including Mo) of geological interest to be analysed using sample sizes of 10–40 mg [108].

Sediment samples collected as gravity cores in 1978 from the continental slope of the Black Sea were quantitatively analysed by radioisotope excited energy dispersive XRF. Analytical results indicate that samples contain 21 elements including Mo. The data can be used as references for monitoring future metal pollution along Turkish coastline of Black sea [39].

6.7. Electrochemical detectors

These detectors offer good sensitivities for Mo determination with simple and inexpensive instrumentation. Adsorptive cathodic stripping voltammetric determination of Mo in soil has been described by Ali et al. [27]. In this work, the cathodic adsorptive preconcentration at hanging mercury drop electrode in presence of a mixture of 0.01 M ($NaH_2PO_4 + Na_2HPO_4$) and 0.01 M $NaNO_3$ was used for the determination of Mo(VI). The detection limit and R.S.D. were found to be 0.96 ng mL^{-1} and 1.4%, respectively.

A differential pulse stripping voltammetric method for trace determination of Mo(VI) in soil was developed by Zhao et al. [31]. In 0.048 M oxalic acid and 6×10^{-5} M Toluidine Blue (pH 1.8) solution, Mo(V) the reduction product, can form a ternary complex, which can be concentrated by adsorption on a static mercury drop electrode at −0.1 V (versus Ag/AgCl). The adsorbed complex gives a well-defined cathodic stripping current peak at −0.30 V, which can be used for determining Mo(VI) in the range 0.048–0.672 ng mL^{-1}, with a detection limit of 9.59 pg mL^{-1}.

Rocks and soils were treated with anhydrous ethanol before fusing with NaOH at 600 °C for 5 min. The cooled extract was diluted with water, adjusted to neutrality followed by 3 drops H_2SO_4 in excess, treated with supporting electrolyte mixture containing 20% NaCl + 0.05% diphenylglycolic acid (4:1), then added 0.02% 1,3-diphenyl guanidine (1:1). The resulting mixture was set aside for 30 min and analysed by oscillopolarography with wave height at −0.2 V for Mo [109].

Soil samples were boiled with water for 15 min, cooled and treated with 2.5 M $CaCl_2$ solution. A blank polarogram was measured with 0.2 M acetic acid–potassium acetate–0.01 mM cupferron (pH 2.7–3.0), then soil extract was added and the polarogram was recorded. Thereafter, the polarograms were again recorded after adding standard Mo(VI) solution, scanning from 0 to −1.2 V versus SCE by differential pulse polarography [110].

7. Conclusions

In common laboratories, Mo determination in geological samples makes ETAAS the method of choice because of low cost of the instrument and running expenses confined with sufficient sensitivity. Unfortunately, the formation of thermally stable carbides and numerous interference effects influence the analytical results using this technique [57]. ICP-OES has been used by a good number of researchers but has not the necessary sensitivity for trace and ultra-trace analysis and the use of a separation-preconcentration procedure is inevitable [26]. XRF and INAA allow the direct determination of Mo without a previous digestion of samples but require the use of high cost instrumentation. For some reasons electrochemical methods have not been popular for Mo determination but in our opinion offer good alternatives. On the other hand, the very common classical UV–vis absorption method is suitable to be applied in Mo analysis and for example, an air-segmented continuous-flow analysis has been developed for spectrophotometric determination of Mo with an excellent sensitivity [36].

If one is concerned with precise and accurate Mo determination, then modern ICP-MS is the method of choice because this method gives additional advantages such as high sample throughout and multielement determination, and to offer the possibility of isotope discrimination. Microwave digestion in sealed containers followed by ICP-MS is probably one of the most versatile methods for the analysis of Mo in geological samples [26]. The significance of ICP-MS in precise isotope-ratio measurements for the isotope-dilution technique is increasing. Future trends should be devoted to separation and preconcentration techniques, particularly in the light of Mo isotopic analysis and speciation of Mo.

Acknowledgements

Authors acknowledge the financial support of The Ministerio de Ciencia y Tecnología, Project No AGL 2002-00729 and The Generalitat Valenciana Grupos 03/118 and a grant (CTESIN/2005/057) from The Generalitat Valenciana. The authors also thank the reviewers of the paper for critical comments and helpful suggestions which have been to improve the quality of this work.

References

[1] A. Townshend (Ed. in-chief), Encyclopedia of Analytical Sciences, vol. 6, Academic Press, London, 1995.
[2] J.R. De Laeter, J.K. Bohlke, P. De Bievre, H. Hidaka, H.S. Peiser, K.J.R. Rosman, P.D.P. Taylor, Pure Appl. Chem. 75 (2003) 683.
[3] Y.C. Sun, J. Mierzwa, C.R. Lan, Talanta 52 (2000) 417.
[4] L.S. Hurliy, in: P. Bratter, P. Schramel (Eds.), Trace Element Analytical Chemistry in Medicine and Biology, Walter de Gruyter, Berlin, 1984.
[5] S. Langard, T. Norseth, in: L. Friberg, G.F. Nordberg, V.B. Vouk (Eds.), Handbook on the Toxicology of Metals, Elsevier, Amsterdam, 1986.
[6] D. Perez-Bendito, S. Rubio, Environmental Analytical Chemistry (Comprehensive Analytical Chemistry), vol. 32, Elsevier, Amsterdam, 1999.
[7] S. Chan, B. Gerson, S. Subramanian, Clin. Lab. Med. 18 (1998) 673.
[8] B. Magyar, H.C. Moor, L. Sigg, Limnol. Oceanogr. 38 (1993) 521.
[9] J.C. Evans, E.E. Prepas, Limnol. Oceanogr. 42 (1997) 461.
[10] W.E. Dean, J.V. Gardiner, D.Z. Piper, Geochim. Cosmochim. Acta 61 (1997) 4507.
[11] A.D. Anbar, Rev. Miner. Geochem. 55 (2004) 429.
[12] K.W. Bruland, in: J.P. Riley, R. Chester (Eds.), Chemical Oceanography, vol. 8, Academic Press, London, 1983.

[13] H.J. Brumask, J.M. Gieskes, Mar. Chem. 14 (1983) 89.
[14] M. Koide, V.F. Hodge, J.S. Yang, M. Stallard, E.G. Goldberg, Appl. Geochem. 1 (1986) 705.
[15] J. Crusius, S. Calvert, T. Pedersen, D. Sage, Earth Planet Sci. Lett. 14 (1996) 565.
[16] J.L. Morford, S. Emerson, Geochim. Acta 63 (1999) 1735.
[17] A.K. Das, R. Chakraborty, M.L. Cervera, M. de la Guardia, Talanta 42 (1995) 1007.
[18] G.R. Helz, C.V. Miller, J.M. Charnock, J.F.W. Mosselmans, R.A.D. Patrick, C.D. Gardner, D.J. Vaughan, Geochim. Cosmochim. Acta 60 (1996) 3631.
[19] W.H. Rowbottom, J. Anal. At. Spectrom. 6 (1991) 123.
[20] A.C. Basak, K.C. Ghosh, A.R. Paul, S. Bhattacharjee, L.P. Pandey, Talanta 42 (1995) 497.
[21] I. Uzonyi, Gy. Szoor, B. Vekemans, L. Vincze, P. Rózsa, Gy. Szabó, A. Somogyi, F. Adams, A.Z. Kiss, Spectrochim. Acta Part B 59 (2004) 1717.
[22] P. Kump, M. Necemer, J. Drinovec, X-ray Spectrom. 33 (2004) 107.
[23] A. Tunceli, A. Rehber Türker, Microchim. Acta 144 (2004) 69.
[24] N. Campillo, I. Lopez-Garcia, P. Viñas, I. Arnau-Jerez, M. Hernández-Córdoba, J. Anal. At. Spectrom. 17 (2002) 1429.
[25] M.B. Melwanki, J. Seetharamappa, S.P. Masti, Anal. Sci. 17 (2001) 1121.
[26] R. Falciani, E. Novaro, M. Marchesini, M. Gucciardi, J. Anal. At. Spectrom. 15 (2000) 561.
[27] A.M.M. Ali, M.A. Ghandour, S.A. El-Shatoury, S.M. Ahmed, Electroanalysis 12 (2000) 155.
[28] S. Chikhalikar, K.S. Patel, Fresenius' J. Anal. Chem. 357 (1997) 355.
[29] A. Molina-Diaz, M.I. Pascual-Reguera, E. Liñán-Veganzones, M.L. Fernández de Córdova, L.F. Capitán-Vallvey, Talanta 43 (1996) 185.
[30] M.L. Lunar, S. Rubio, D. Pérez-Bendito, Analyst 118 (1993) 715.
[31] Z. Zhao, J. Pei, X. Zhang, X. Zhou, Talanta 37 (1990) 1007.
[32] L.I. Tsikritzis, S.S. Ganatsios, O.G. Duliu, C.V. Kavouridis, T.D. Sawidis, J. Trace Microprobe Tech. 20 (2002) 269.
[33] M. Bettinelli, C. Baffi, G.M. Beone, S. Spezia, At. Spectrosc. 21 (2000) 60.
[34] K. Inagaki, A. Takatsu, T. Kuroiwa, A. Nakama, S. Eyama, K. Chiba, K. Okamoto, Anal. Bioanal. Chem. 378 (2004) 1271.
[35] R. Kamalakkannan, V. Zettel, A. Goubatchev, K. Stead-Dexter, N.I. Ward, J. Environ. Monit. 6 (2004) 175.
[36] Y. Harita, T. Hori, M. Sugiyama, Microchim. Acta 142 (2003) 71.
[37] C.A. Hui, S.L. Goodbred, D.B. Ledig, C.A. Roberts, Bull. Environ. Contam. Toxicol. 68 (2002) 870.
[38] S. Waheed, S. Ahmad, A. Rahman, I.H. Qureshi, J. Radioanal. Nucl. Chem. 250 (2001) 97.
[39] T. Akyüz, S. Akyüz, A. Bassari, J. Radioanal. Nucl. Chem. 250 (2001) 129.
[40] W. Diegor, H. Longerich, T. Abrajano, I. Horn, Anal. Chim. Acta 431 (2001) 195.
[41] M.J. Marqués, A. Salvador, A.E. Morales-Rubio, M. de la Guardia, Microchem. J. 65 (2000) 177.
[42] V.L.A. Monte, A.J. Curtius, J. Anal. At. Spectrom. 5 (1990) 21.
[43] J. Crusius, T.F. Pedersen, S.E. Calvert, G.l. Cowie, T. Oba, Paleoceanography 14 (1999) 248.
[44] Y. Zheng, R.P. Anderson, A. VanGeen, J. Kuwabara, Geochim. Cosmochim. Acta 64 (2000) 4165.
[45] S.R. Emerson, S.S. Huested, Mar. Chem. 34 (1991) 177.
[46] H.J. Brumsack, Geol. Rundschau. 78 (1989) 851.
[47] D.J. Vaughan, M. Sweeney, G. Friedrich, R. Diedel, C. Haranczynk, Inorg. Chem. 24 (1985) 3132.
[48] A.T. Townsend, J. OïSullivan, A.M. Featherstone, E.C.V. Butler, D.J. Mackey, J. Environ. Monit. 3 (2001) 113.
[49] H. Tsukada, H. Hasegawa, J. Radioanal. Nucl. Chem. 252 (2002) 219.
[50] ASTM, Standard Method for Sampling Surface Soil for Radionuclides C998-83. Annual Book of ASTM Standards, West Conshohocken, Pennsylvania, PA, USA, 1983.
[51] D. Malinovsky, I. Rodushkin, D.C. Baxter, J. Ingri, B. Ohlander, Int. J. Mass Spectrom. 245 (2005) 94.
[52] C. Latkoczy, T. Prohaska, G. Stingeder, W.W. Wenzel, Fresenius' J. Anal. Chem. 368 (2000) 256.
[53] ASTM 5258-92: Standard Practice for Acid Extraction of Elements from Sediments Using Closed Vessel Microwave Heating: The American Society for Testing and Materials, Philadelphia, PA, USA, 1992.
[54] SW-846 EPA Method 3050B: Acid Digestion of Sediments, Sludges and Soils, Test Methods for Evaluating Soil Waste, third ed., 3rd update; US Environmental Protection Agency, Washington DC, 1995.
[55] SW-846 EPA Method 3051: Microwave Assisted Acid Digestion of Sediments, Sludges, Soils and Oils, Test Methods for Evaluating Soil Waste, third ed., 3rd update; US Environmental Protection Agency, Washington DC, 1995.
[56] Plan d'Exploration Minerale, Rapport Technique, Methods et Procedes de Laboratoire, DP/UN/COL-72-001/10.
[57] A. Lechotycki, J. Anal. At. Spectrom. 5 (1990) 25.
[58] M. Kersten, U. Forstner, in: G. Batley (Ed.), Trace Element Speciation: Analytical Methods and Problems, CRC Press, 1989.
[59] A.D. Anbar, K.A. Knab, J. Barling, Anal. Chem. 73 (2001) 1425.
[60] N.J. Miller-Ihli, Spectrochim. Acta Part B 50B (1995) 477.
[61] J. Mierzwa, Y.C. Sun, M.H. Yang, Spectrochim. Acta Part B 53B (1998) 63.
[62] C. Bendicho, M.T.C. de Loos-Vollebregt, Spectrochim. Acta Part B 45B (1990) 695.
[63] I. López-Garcia, M. Sánchez-Merlos, M. Hernández-Córdoba, J. Anal. At. Spectrom. 11 (1996) 1003.
[64] S. Caroli, Element Speciation in Bioorganic Chemistry, Wiley, New York, 1996.
[65] B.E. Erickson, G.R. Helz, Geochim. Cosmochim. Acta 64 (2000) 1149.
[66] S. Goldberg, C. Su, H.S. Forster, in: E.A. Jenne (Ed.), Adsorption of Metals by Geomedia, Academic Press, 1998.
[67] T.P. Volicek, G.R. Helz, Geochim. Cosmochim. Acta 66 (2002) 3679.
[68] T.P. Volicek, M.D. Khan, Y. Kasuya, G.R. Helz, Geochim. Cosmochim. Acta 68 (2004) 547.
[69] S. Kawakubo, S. Ichikawa, M. Iwatsuki, Anal. Sci. 18 (2002) 651.
[70] M. Kersten, M. Förstner, in: M.A. Ure, C.M. Davidson (Eds.), Chemical Speciation in the Environment, Blackie Academic and Professional, Glasgow, 1995.
[71] Ph. Quevauviller, H.A. vander Sloot, A.M. Ure, H. Muntau, A. Gomez, G. Rauret, Sci. Total Environ. 178 (1996) 133.
[72] A.M. Ure, Ph. Quevauviller, H. Muntau, B. Griepink, Int. J. Environ. Anal. Chem. 51 (1993) 135.
[73] H. Sanei, F. Goodarzi, E. Vander Flier-Keller, J. Environ. Monit. 3 (2001) 27.
[74] U.M. Gruter, J. Kresimon, A.V. Hirner, Fresenius J. Anal. Chem. 368 (2000) 67.
[75] Gy. Heltai, K. Percsich, I. Fekete, B. Barabaás, T. Józsa, Microchem. J. 67 (2000) 43.
[76] D. Sarkar, G.A. O'Connor, Commun. Soil Sci. Plant Anal. 32 (2001) 2033.
[77] A.K. Malik, V. Sharma, M. Nijhawan, A.L.J. Rao, Ann. Chim. (Rome) 92 (2002) 115.
[78] M. Kamburova, A. Alexandrov, Chem. Anal. (Warsaw) 44 (1999) 745.
[79] M. Kamburova, Anal. Lett. 31 (1998) 2255.
[80] S.G. Aggarwal, K.S. Patel, Mikrochim. Acta 129 (1998) 265.
[81] X.C. Li, B.G. Zhou, D.Q. Wang, Fenxi Kexue Xuebao 14 (1998) 122.
[82] Y.K. Agrawal, S.K. Menon, K.R. Patel, Mikrochim. Acta 122 (1996) 259.
[83] Z.H. Zhou, X.Y. Yue, Fenxi Shiyanshi 11 (1992) 26.
[84] M.T.M. Zaki, A.Ay. El-Sayed, Mikrochim. Acta 106 (1992) 153.
[85] J.L. Martinez-Vidal, A.R. Fernandez-Alba, F. Salinas, Analyst 115 (1990) 329.
[86] N. Mishra, A. Ghosh, R.K. Mishra, K.S. Patel, Anal. Sci. 6 (1990) 407.
[87] D.E. Kimbrough, J. Wakakuwa, Analyst 119 (1994) 383.
[88] M. Zhang, Lihua Jianyan Huaxue Fence 36 (2000) 10.
[89] M. Sanchez-Vinas, G.M. Bagur, D. Gazquez, M. Camino, R. Romero, J. Anal. Toxicol. 23 (1999) 108.
[90] J. Zbiral, Commun. Soil Sci. Plant Anal. 23 (1992) 817.
[91] J. Fazakas, P.V. Botha, A. Harles, R. Lacatusu, Magy Kem Foly 97 (1991) 241.
[92] I.V. Mironov, Pochvovedenie 3 (1990) 156.
[93] A. Ross, P. Kainrath, B. Conrads, Laborpraxis 26 (2002) 48.

[94] D. Marquardt, W. Wolff, LaborPraxis 25 (2001) 38.
[95] L. Guo, G.L. Zhang, Z.L. Fang, Guangpuxue Yu Guangpu Fenxi 13 (1993) 73.
[96] J. Goossens, L. Moens, R. Dams, Anal. Chim. Acta 304 (1995) 307.
[97] J.S. Becker, Tr. Anal. Chem. 24 (2005) 243.
[98] M.E. Wieser, J.R. De Laeter, Fresenius J. Anal. Chem. 368 (2000) 303.
[99] J.I. Garcia Alonso, M. Gutierrez Cambhor, M. Montes Bayon, J.M. Marchante Gayon, A. Sanz Medel, J. Mass Spectrom. 32 (1997) 556.
[100] N. Dauphas, L. Reisberg, B. Marty, Anal. Chem. 73 (2001) 2613.
[101] A. Favre-Regullion, M. Draye, G. Lebuzitt, S. Thomas, J. Foos, G. Cote, A. Guy, Talanta 63 (2004) 803.
[102] O.A. Garmo, O. Royset, E. Steinnes, T.P. Flaten, Anal. Chem. 75 (2003) 3573.
[103] D. Chipley, T.K. Kyser, D. Beauchemin, B. MacFarlane, Can. J. Anal. Sci. Spectrosc. 48 (2003) 269.
[104] I. Rodushkin, M.D. Axelsson, D. Malinovsky, D.C. Baxter, J. Anal. At. Spectrom. 17 (2002) 1231.
[105] S. Waheed, M. Wasim, A. Rahman, S. Ahmad, Geostand. Newsl. 25 (2001) 137.
[106] S. Bajo, L. Tobler, A. Wyttenbach, Fresenius' J. Anal. Chem. 347 (1993) 344.
[107] L.M. Bertini, I.M. Cohen, S.M. Resnizky, J. Radioanal. Nucl. Chem. 170 (1993) 225.
[108] M.A. Phedorin, V.A. Bobrov, E.P. Chebykin, E.L. Goldberg, M.S. Melgunov, S.V. Filippova, K.V. Zolotorev, Geostand. Newsl. 24 (2000) 205.
[109] Y. Zhang, P. Sun, Lihua-Jianyan-Huaxue-Fence 26 (1990) 275.
[110] K. Jiao, W. Jin, H. Metzer, Anal. Chim. Acta 260 (1992) 35.

Available online at www.sciencedirect.com
ScienceDirect
Talanta 71 (2007) 1144–1149
Talanta
www.elsevier.com/locate/talanta

Direct determination of cadmium in urine by tungsten-coil inductively coupled plasma atomic emission spectrometry using palladium as a permanent modifier

Amanda C. Davis, Clifton P. Calloway Jr. [1], Bradley T. Jones *

Department of Chemistry, Wake Forest University, Winston-Salem, NC 27109, USA

Received 17 April 2006; received in revised form 5 June 2006; accepted 5 June 2006
Available online 17 July 2006

Abstract

Cadmium is determined in urine samples collected from patients with age-related diseases. The urine is simply diluted 1:1 with water and placed on a tungsten coil electrothermal vaporizer treated with 200 μg of a permanent Pd modifier. A straightforward vaporization program is used to deliver the Cd vapor to an inductively coupled plasma atomic emission spectrometer. A high resolution spectrometer and a charge coupled device detector provide spectra across a 4.8 nm window encompassing two separate Cd emission lines: 226.5 and 228.8 nm. The limit of detection is 0.2 μg/L at each wavelength, and the linear dynamic range spans three orders of magnitude. The accuracy as measured with a urine standard reference material is 94%. The Pd modifier continues to be effective even after 150 vaporization cycles. Direct analysis of urine with the Pd modifier using simple aqueous calibration solutions provides results that are comparable to those observed after a much more complex method: chelation, extraction, and internal standardization without the modifier. The mean concentrations found by the two techniques differ by only 9%. The permanent Pd modifier allows direct analysis of limited sample volumes with decreased risks of contamination.
© 2006 Elsevier B.V. All rights reserved.

Keywords: Cadmium; Urine; Tungsten coil; Palladium; Permanent chemical modifier; Electrothermal vaporization; Inductively coupled plasma

1. Introduction

The determination of Cd in biological samples is of widespread interest. A recent review article on the subject cites 200 references from a 10-year period (1995–2005)[1]. The complicated matrices associated with blood, urine, and serum samples usually requires some form of sample pretreatment. Typical methods employed include acid digestion, extraction, and/or complexation reactions. Even with these methods, quantitation procedures often must compensate for the remaining sample matrix. The internal standard method, the method of standard additions, and/or matrix-matched standards are common approaches. Direct analysis of untreated biological samples with a simple aqueous calibration curve is seldom successful.

Matrix modifiers provide enhanced thermal separation of the analyte from concomitants by allowing increased pyrolysis temperatures. This is especially beneficial for volatile analytes such as Cd. Since the mid-1990s, several traditional matrix modifiers have been employed with tungsten coil (W-coil) atomizers: EDTA [2], $NH_4H_2PO_4$ with Triton X-100 and nitric acid [3], $NH_4H_2PO_4$, $(NH_4)_2HPO_4$ with $Pd(NO_3)_2$ [4] and a mix of ascorbic acid with NH_4NO_3, Pd, Mg, and their nitrated counterparts [5–7]. The use of platinum group metals (PGMs) as permanent chemical modifiers, and their mechanism of action, has been reviewed recently[8]. In a complimentary review, the efficacy of PGMs as modifiers on commonly determined volatile analytes was discussed at length [9]. In practice, Ir and Rh have been used as permanent modifiers for W-coil atomizers [10–14]. The advantages reported for using matrix modifiers in conjunction with metal atomizers are similar to those seen with the graphite furnace: a decrease in the apparent effects of concomitants, an increase in sensitivity for volatile analytes, and an increase the lifetime of the atomizer [7,15]. When 200 μg of Ir was used as a permanent modifier for the determination of Se by W-coil atomic absorption spectrometry (AAS), the

* Corresponding author. Fax: +1 336 758 3889.
E-mail address: jonesbt@wfu.edu (B.T. Jones).
[1] Present address: Department of Chemistry, Winthrop University, Rock Hill, SC 29733, USA.

0039-9140/$ – see front matter © 2006 Elsevier B.V. All rights reserved.
doi:10.1016/j.talanta.2006.06.005

coil lifetime was extended to over 1600 firings, and the relative standard deviation (R.S.D.) for 10 consecutive measurements was less than 7%. By increasing the pyrolysis temperatures, the sensitivity was increased by a factor of 3 [11]. Rhodium was used as a permanent modifier on the W-filament of an AAS system for the determination of Pb in blood and urine by Zhou et al. [12]. The W-filament endured 300 firings and required re-conditioning approximately every 30 firings with a run precision of 10% or better [12]. Rhodium-coated tungsten filaments have been used as electrothermal vaporization (ETV) sources and sample introduction devices for inductively coupled plasma mass spectrometry (ICP-MS). Again the Rh coating needed to be reapplied frequently due to loss during the vaporization cycle [13].

Modifiers have been employed much more frequently with graphite furnaces than with metal atomizers, so the mechanism of action with the metal devices is not as clearly understood [15]. Additionally, metal atomizers can vary in shape and size (i.e. W-tubes, coils, and filaments), thus the atomization environment is not constant and ultimately the modifier mechanism may vary. Tungsten coil atomizers have very fast heating rates and are considered open, non-isothermal environments which create a large temperature gradient between the surface and gas phase [4,15]. This further complicates the modifier's potential mechanism.

While debate concerning the mechanism for the permanent chemical modification of metal surfaces continues, recent literature supports the idea that a more thermally stable analyte is formed, analyte loss is minimized, and thermal separation from interfering matrix constituents is achieved. The present work explores the application of a permanent chemical modifier for the determination of Cd in urine by W-coil electrothermal vaporization inductively coupled plasma atomic emission spectrometry (ETV-ICP-AES). The modifiers described above (Ir, Pd, Rh, EDTA, ascorbic acid, and ammonium phosphates) were screened for this application, and Pd alone provided the most promising results. Electrodeposited palladium has been used previously as a means of permanent modification on a graphite surface for Cd determinations using electrothermal atomic absorption spectrometry [16,17]. Application of Pd to the W-coil vaporizer results in similar advantages for the determination of Cd in urine with the current study. The permanent modifier reduces the overall analysis time by eliminating the need to add modifier to every sample or after every vaporization cycle. Additionally, the W-coil ETV-ICP-AES system with a Pd permanent modifier allows direct analysis of urine samples with no pretreatment and straightforward calibration with aqueous standard solutions. Very small urine volumes may therefore be analyzed, so the technique is ideal for samples that are precious or limited in quantity.

2. Experimental

2.1. Instrumentation

The W-coil ETV-ICP-AES instrumentation has been described elsewhere [18]. Fig. 1 shows a schematic diagram of the system. A W-coil extracted from a 150 W light bulb (Orsam BRJ) is secured in an Al mount and housed in a glass vaporization cell (Ace Glass, product no. 5828-28) with three ports [19]. The first port is outfitted with a Teflon plug to provide an air tight seal during vaporization and provides a means of direct sample introduction onto the W-coil surface. The second port accepts the Al mount and sits perpendicular the first. The mount provides electrical connections to the laboratory-constructed power supply, as well as an inlet for the 5% H_2/Ar gas flow. The plasma was found to be unstable with a 10% H_2/Ar mixture (typical for W-coil analyses), but at 5% it was robust. The W-coil lifetime may have been slightly shortened in this less reducing atmosphere. The third port contains the junction between the vaporization cell and the axially oriented ICP. The junction is a 20 cm long, 0.25 in. o.d. straight glass tube with a glass joint socket (Ace Glass, part no. D119379). The 20 cm length is the shortest distance that allows the vaporization cell to be housed outside of the torch box. Minimizing the distance between the vaporization cell and the ICP minimizes peak broadening and increases sample transport efficiency [20], while placing the vaporization cell outside of the torch box allows for fast and simple sample introduction. The ICP was operated at 1.2 kW, with a coolant flow of 19 L/min, and an auxiliary flow of 1.3 LPM.

The laboratory-constructed, constant current power supply resistively heats the tungsten coil. An input signal of 1–5 V generates a corresponding output current in the range of 0–10 A. The temperature of the coil at a specific current can be approximated using a previously reported empirical equation: $T\ (\mathrm{K}) = 309(I) + 325$ [20]. A Visual Basic program allows the user to configure the vaporization cycle: pyroly-

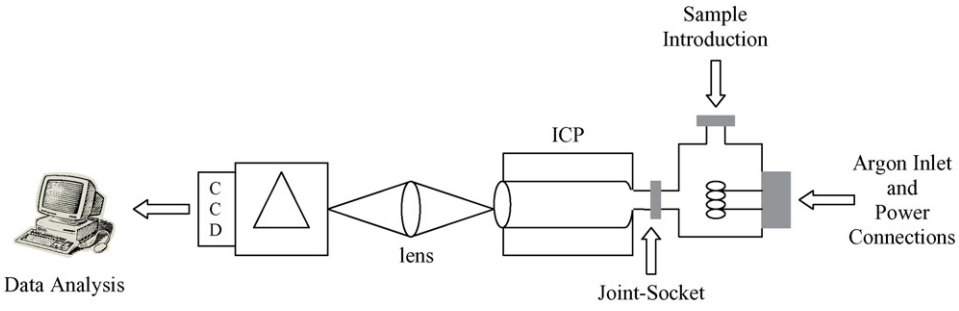


Fig. 1. Schematic diagram of the W-coil ETV-ICP-AES system.

sis time and current, atomization time and current, etc. The program also sends a detection trigger immediately prior to vaporization.

The sample vapor follows a linear path from the W-coil cell to the ICP. The emission from the plasma is focused 1:1 with a fused silica lens onto the entrance slit (10 μm) of a high resolution monochromator (McPherson Model 209 Czerny-Turner). The monochromator contains a 3600 grooves/mm grating that produces a typical spectral bandpass of 0.01 nm. A thermoelectrically cooled charged coupled device (Princeton Instruments Spec-10, Roper Scientific, Trenton, NJ) with an array of 1340 by 100 pixels, each approximately 20 μm × 20 μm in size, is used as the detection system. The FWHM is approximately 3 pixels while the entire spectral window spans approximately 4.8 nm. This enables simultaneous monitoring of Cd lines at 226.5 and 228.8 nm. The detector software has user-selectable parameters such as exposure time, the number of sequential spectra to be accumulated (or integrated), and the total number of spectra collected. Each of these may be altered by the user to ensure effective data collection. In most cases, the exposure time was set to 250 ms, and six successive exposures were accumulated, resulting in a single spectrum that integrated the emission signal collected during the 1.5 s period immediately following the onset of the vaporization step. Two such spectra were collected successively, so the first 3 s of the vaporization period were monitored. The Cd signal was negligible at times beyond 1.5 s at biologically relevant concentrations.

2.2. Standard and reagents

Aqueous Cd standard solutions were prepared by diluting a stock Cd solution (1000 μg/mL Spex, Assurance, Metuchen, NJ) with distilled-deionized water (Millipore Water System, Massachusetts, USA). A Pd stock solution (1000 μg/mL SPEX, Edison, NJ) was used for permanent modification of the W-coil. The standard reference material for trace metals in urine (SRM 2760 at elevated levels, NIST, Gaithersburg, MD) was used as a means of determining the accuracy of the method.

2.3. Optimization of the Pd modifier

A previous work using Ir as a permanent modifier for a W-coil found the optimum mass of modifier to be 200 μg [11]. Assuming a similar optimum for Pd, the performance of a 200 μg Pd modified W-coil was evaluated at increasing pyrolysis temperatures. A 20 μL aliquot of 10 μg/L Cd solution was pipetted directly onto the coil and the relative signal intensity was monitored at 226.5 and 228.8 nm. The vaporization cycle consisted of a pyrolysis time of 270 s at variable applied currents (1.5–3.5 A), a 10 s delay or cooling period with an applied current of 0 A, followed by a vaporization current of 7 A for 1 s. The 10 s cooling period assured that the W-coil was always at the same temperature (near room temperature) at the onset of the atomization step. This resulted in a sharper and more reproducible atomization profile. Variable sample composition and volume may result in slightly different coil temperatures after the 270 s pyrolysis time, so the cool step was added to correct for these small inconsistencies [21]. The change in the signal intensity as a function of increasing pyrolysis current was monitored. This experiment was repeated with a second, unmodified, W-coil. The pyrolysis curves for the modified (■) and unmodified (●) coils are shown in Fig. 2A (226.5 nm) and B (228.8 nm). Notice in both cases that the Cd signal is significantly higher at all pyrolysis currents with the modified coil. The pyrolysis curves at both wavelengths for the unmodified coil exhibit a sharp decrease in the Cd emission signal at pyrolysis currents is above 2.5 A. At 2.5 A the pyrolysis temperature is approximately 1098 K, which is slightly higher than the boiling point of Cd (1038 K). In contrast, the pyrolysis curves for the modified coil remain approximately unchanged up to a current of 3.5 A. At 4.0 A, however, the Cd signal for the modified coil dropped by 20%. A pyrolysis current of 3.5 A, therefore, produced the optimum amount of matrix degradation without loss of Cd signal. The final optimized vaporization cycle was therefore 270 s at 3.5 A (pyrolysis), 10 s at 0 A (cool), and 1 s at 7.0 A (vaporize).

With this vaporization cycle, the optimum amount of modifier was determined as follows. Four new W-coils were coated with increasing amounts of Pd (0, 60, 100 and 200 μg) by directly

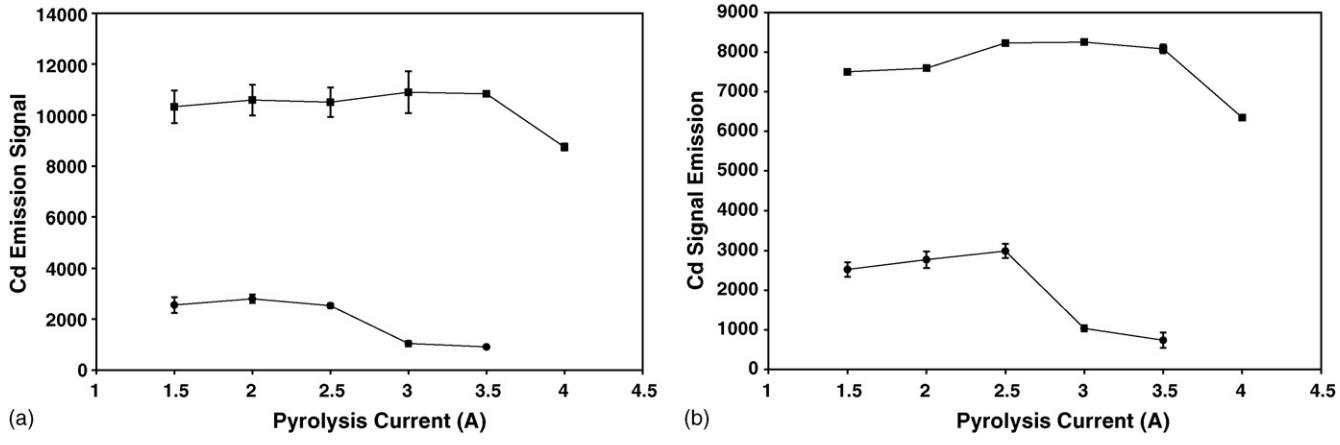


Fig. 2. (A) Pyrolysis curve for Cd monitored at 226.5 nm with (■) and without (●) 200 μg of Pd modifier added to the W-coil. (B) Pyrolysis curve for Cd monitored at 228.8 nm with (■) and without (●) 200 μg of Pd modifier added to the W-coil.

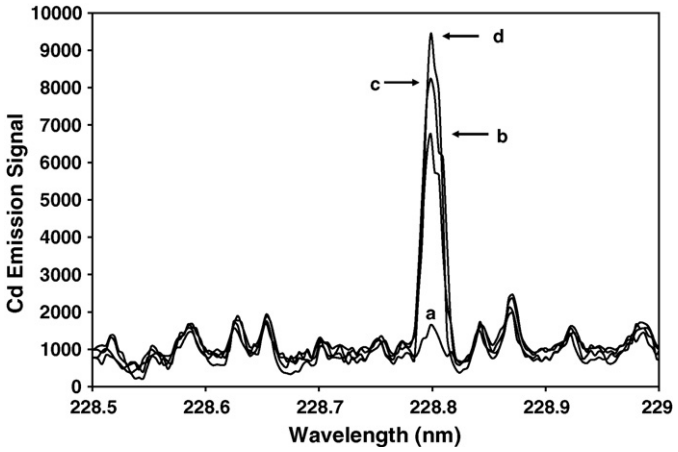


Fig. 3. Emission signals for 20 μL aliquots of 10 μg/L Cd vaporized from W-coils modified with 0, 60, 100, and 200 μg Pd; a, b, c, d, respectively.

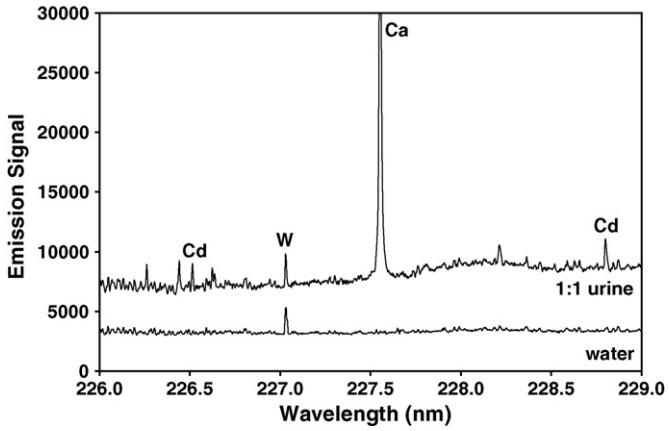


Fig. 4. W-coil ETV-ICP-AES spectrum for urine sample D (above) and an aqueous blank (below). The emission signal was accumulated during the 1.5 s immediately following the onset of vaporization.

depositing a different number of 20 μL aliquots of the Pd stock solution onto each coil (0, 3, 5, and 10 times, respectively). The vaporization cycle was performed after each 20 μL deposition. Once the coils were prepared, a 20 μL aliquot of 10 μg/L Cd standard solution was analyzed on each coil in triplicate. As described above, six successive exposure times of 250 ms were summed to produce a 1.5 s spectrum, and two of these adjacent spectra were saved, providing coverage of the 3 s immediately following the onset of vaporization. The first integrated spectrum (1.5 s) for each modifier amount is shown in Fig. 3. The Cd signal increases greatly with the addition of 60 μg Pd. This occurs because most of the Cd is lost during the pyrolysis step at the 3.5 A level (Fig. 2B). The signal continues to increase slightly with 100 and 200 μg Pd. Beyond 200 μg, the minute increase in emission intensity did not justify the time necessary to add additional modifier. Therefore, 200 μg Pd was chosen as the optimum amount of modifier. Calibration curves using these optimized conditions were prepared in biologically relevant range for Cd (1–10 μg/L).

3. Results and discussion

3.1. Analytical figures of merit

Fig. 4 is the W-coil ETV-ICP-AES emission spectrum collected during the vaporization of a real urine sample (sample D, above) and an aqueous blank (below). The signal was accumulated during the 1.5 s immediately following the onset of vaporization. Notice the intense Ca line which is present in all urine samples. Also note the two Cd emission lines. Each Cd line can be used for quantitation, thus, a single vaporization cycle produces two independent measures for Cd. Finally, the background emission signal is highly structured across this small wavelength window, and the absolute magnitude of the background signal (7000–9000 counts) is actually much larger than the Cd emission signal (2000–3000 counts). Nevertheless, the Cd emission lines are easily discernable atop the background, since the full spectrum is acquired. The analytical figures of merit are similar at each wavelength (Table 1). The limits of detection (3σ) are 0.2 μg/L with a linear dynamic range spanning three orders of magnitude in each case. Typically, the 226.5 nm line is more sensitive for Cd, but the current optical system drops in efficiency as wavelength is decreased, and the blank noise is higher at the lower wavelength for both water and urine samples (Fig. 4). The same optical system using a pneumatic nebulizer gives an LOD of approximately 1.0 μg/L using a 5 mL aliquot of aqueous standard solutions. Given the much smaller sample volume employed with the ETV and the direct analysis of the urine sample, the improvement factor of 200 reported previously for Cd ETV-ICP is observed in this case as well [20]. Analysis with pneumatic nebulization would require acid digestion and significant dilution of the sample. The accuracy of the method was determined by repetitively analyzing the standard reference material ($n = 5$). The certified value for Cd in the urine sample was 88 μg/L. At 226.5 nm, 71 ± 6 μg/L Cd was found, and at 228.8 nm 83 ± 3 μg/L was found. The percent recovery was therefore 81% and 94%, respectively. The precision of the technique using the reference material was 8.5% relative standard deviation at 226.5 nm, and 3.6% R.S.D. at 228.8 nm. The precision was also measured using an aqueous solution containing 10 μg/L Cd ($n = 10$), and the values were 4.2% R.S.D. at 226.5 nm and 3.1% R.S.D. at 228.8 nm.

The long-term stability of the Pd modifier was tested as follows. As explained above, 200 μg of Pd was applied to a fresh W-coil. The vaporization profile for a 20 μL aliquot of a solution containing 10 μg/L Cd was then obtained after 5, 50, 100, and 150 vaporization cycles following the original application of Pd (Fig. 5). Data points were collected at 100 ms intervals

Table 1
Analytical figures of merit

Wavelength (nm)	228.8	226.5
Limit of detection (μg/L)	0.2	0.2
Linear dynamic range (μg/L)	0.2–200	0.2–200
Precision (R.S.D., $n = 10$) (%)	3.1	4.2
Accuracy (recovery of Cd from SRM) (%)	94	81

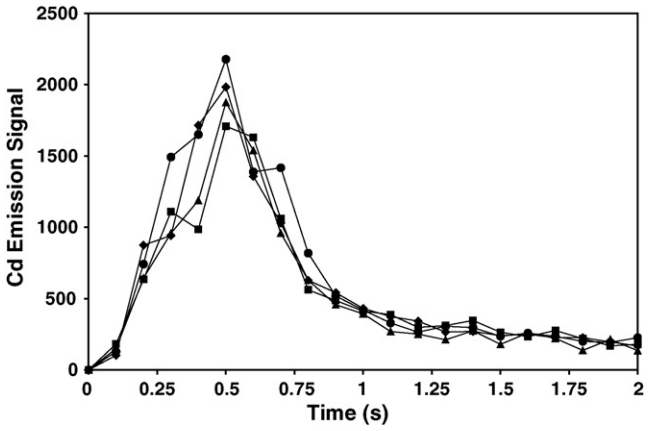


Fig. 5. Vaporization profiles for a 20 μL aliquot of 10 μg/L Cd collected 5 (▲), 50 (■), 100 (●), and 150 (♦) cycles after the application of 200 μg Pd to the W-coil.

(rather than 250 ms) so that any small changes in the profiles might be observed. In all cases the peak in the Cd emission signal appears at 0.50 s after the onset of vaporization. The peak shapes are almost identical, except for the noise associated with the measurement. The peak areas for the four measurements are quite similar, with only an 8.9% R.S.D.

3.2. Analysis of urine samples

Four urine samples (A–D) collected from patients with age-related disease were analyzed after simple 1:1 dilution with distilled deionized water: 500 μL urine combined with 500 μL water. A 20 μL aliquot of dilute urine was pipetted directly onto the Pd modified W-coil. The emission spectra were recorded (1.5 s) as described above (Fig. 4), and the urine-Cd concentrations were determined using the calibration curve prepared with aqueous standard solutions. This sample preparation procedure required no reagents or heating steps, and resulted in a dilution factor of only two.

The same four urine samples have been analyzed previously by the authors following a much more extensive sample preparation procedure involving a chelation/extraction step used in conjunction with the internal standard method [22]. In that procedure, a 1 mL urine sample was combined with 1 mL of trace metal grade nitric acid and the solution was placed in a heating block at 60 °C for 90 min. The sample was allowed to cool, and then neutralized with 1 mL trace metal grade ammonium hydroxide. The neutralized urine samples were then spiked with 2 μL of the internal standard solution (1000 μg/mL Bi). A 1 mL aliquot of the neutralized, spiked sample was then added to 1 mL of a 2% aqueous standard solution of the chelating agent APDC, and the solution was vortexed for 30 s. Two hundred microliters of an extracting agent (MIBK) was added to the mixture and vortexed for an additional 30 s. This mixture was then centrifuged at 1550 RPM for 2 min. Finally, a 20 μL aliquot of the organic supernatant was placed directly on the W-coil. This process resulted in a concentration factor of 5/3, and the analyte was effectively removed from the urine matrix prior to the analysis. GFAAS analyses of a large set of urine samples from patients with age-related disease have resulted in urine-Cd concentrations in the range 0.5–10 μg/L. A subset of these samples analyzed by W-coil ETV-ICP after organic extraction had urine-Cd concentrations in the range of 0.9–4.1 μg/L [22].

Table 2
Determination of Cd (μg/L) in real urine samples

Sample	Direct analysis with Pd permanent modifier	Combination of extraction and internal standard methods[a]
A	4.4 ± 0.3[b]	3.8 ± 0.2
B	2.7 ± 0.2	2.4 ± 0.1
C	2.6 ± 0.2	2.3 ± 0.1
D	4.2 ± 0.3	4.1 ± 0.1
Mean	3.5 ± 0.3	3.2 ± 0.1
Average % R.S.D.	10.4	6.2

[a] See Ref. [22].
[b] Mean ± 1 S.D. (n = 5).

A comparison of the results for the two methods is shown in Table 2. Each sample was analyzed five times, and the average concentration ± 1 S.D. is reported. The amount of Cd found in each sample is comparable for the two techniques, and the mean for the four concentrations differs by only 9%. The precision for the chelation/extraction method was 6.2% R.S.D., and for the direct analysis using the modifier the precision was only slightly higher (10.4% R.S.D.). Thus, the Pd permanent modifier allows accurate and precise urine-Cd determinations with a simple 1:1 dilution with water. The analysis of neat urine samples is clearly possible, however, at the expense of an increasing background signal. Fig. 4 shows that the background level approximately doubles when going from water to 1:1 diluted urine. Neat urine would be expected to cause a background at least three times higher than the blank level.

Time consuming sample preparation steps are avoided, and the Cd is determined directly in the urine matrix using a calibration curve prepared from aqueous solutions. Small sample volumes may thus be analyzed directly without the risk of contamination from multiple reagents. The permanent modifier also allows analysis of the complex urine sample without acid digestion steps. Finally, the W-coil ETV-ICP-AES method provides an additional level of confidence for the analyst, since the Cd emission line is clearly discernable atop the background emission level, and the level of Cd present may be determined at two different wavelengths simultaneously. By acquiring the full spectrum across a 4.8 nm window, the Cd emission signal is easily discriminated from the relatively high background emission signal. This technique is particularly valuable for samples that are precious or limited in volume.

Acknowledgements

This material is based upon work supported by the National Science Foundation and the Intelligence Technology Innovation Center through the joint "Approaches to Combat Terrorism" Program Solicitation NSF 03-569 (CHE-0346353).

References

[1] A.C. Davis, P. Wu, X. Zhang, X. Hou, B.T. Jones, Appl. Spectrosc. Rev. 41 (2006) 1–41.
[2] M.M. Silva, R.B. Silva, F.J. Krug, J.A. Nobrega, H. Berndt, J. Anal. Atom. Spectrom. 9 (1994) 861–865.
[3] P.J. Parsons, H. Qiao, K.M. Aldous, E. Mills, W. Slavin, Spectrochim. Acta Part B 50 (1995) 1475–1480.
[4] C.G. Bruhn, J.Y. Neira, G.D. Valenzuela, J.A. Nobrega, J. Anal. Atom. Spectrom. 13 (1998) 29–35.
[5] C.G. Bruhn, J.Y. Neira, M.I. Guzman, M.M. Darder, J.A. Nobrega, Fresenius' J. Anal. Chem. 364 (1999) 273–278.
[6] J.C.J. Silva, E.E. Garcia, A.R.A. Nogueira, J.A. Nobrega, Talanta 55 (2001) 847–854.
[7] C.G. Bruhn, N.A. San Francisco, J.Y. Neira, J.A. Nobrega, Talanta 50 (1999) 967–975.
[8] A.B. Volynsky, Spectrochim. Acta Part B: Atom. Spectrosc. 55 (2000) 103–150.
[9] A.B. Volynsky, Spectrochim. Acta Part B 59 (2004) 1799–1821.
[10] X. Hou, K.E. Levine, A. Salido, B.T. Jones, Anal. Sci. 17 (2001) 175–180.
[11] X. Hou, Y. Zhang, B.T. Jones, Spectrochim. Acta Part B 56 (2001) 203–214.
[12] Y. Zhou, P.J. Parsons, K.M. Aldous, P. Brockman, W. Slavin, Spectrochim. Acta Part B 57 (2002) 727–740.
[13] P.J. Parsons, Y. Zhou, C.D. Palmer, K.M. Aldous, P. Brockman, J. Anal. Atom. Spectrom. 18 (2003) 4–10.
[14] F. Barbosa Jr., S.S. Souza, F.J. Krug, J. Anal. Atom. Spectrom. 17 (2002) 382–388.
[15] J.A. Nobrega, J. Rust, C.P. Calloway, B.T. Jones, Spectrochim. Acta Part B: Atom. Spectrosc. 59 (2004) 1337–1345.
[16] M. Piascik, E. Bulska, Spectrochim. Acta Part B: Atom. Spectrosc. 56 (2001) 1615–1623.
[17] E. Bulska, K. Liebert-Ilkowska, A. Hulanicki, Spectrochim. Acta Part B: Atom. Spectrosc. 53 (1998) 1057–1062.
[18] A.C. Davis, B.W. Alligood, C.P. Calloway Jr., B.T. Jones, Appl. Spectrosc. 59 (2005) 1300–1303.
[19] A. Salido, B.T. Jones, Talanta 50 (1999) 649–659.
[20] K. Levine, K.A. Wagner, B.T. Jones, Appl. Spectrosc. 52 (1998) 1165–1171.
[21] A. Salido, C.L. Sanford, B.T. Jones, Spectrochim. Acta Part B 54 (1999) 1167–1176.
[22] A.C. Davis, C.P. Calloway Jr., B.T. Jones, Microchem. J. 83 (2006).

Available online at www.sciencedirect.com
ScienceDirect
Talanta 71 (2007) 1288–1293
Talanta
www.elsevier.com/locate/talanta

A monosegmented-flow Karl Fischer titrator

Emerson Vidal de Aquino, Jarbas José Rodrigues Rohwedder, Celio Pasquini *

Instituto de Química, Universidade Estadual de Campinas, Caixa Postal 6154, CEP 13084-971, Campinas, SP, Brazil

Received 30 May 2006; received in revised form 28 June 2006; accepted 28 June 2006
Available online 1 August 2006

Abstract

A monosegmented volumetric Karl Fischer titrator is described to mechanize the determination of water content in organic solvents. The system is based on the flow-batch characteristics of the monosegmented analysis concept and employs biamperometry to monitor the progress of the titration. The system shows accuracy and precision that are highly independent of the flow rate, does not require calibration, and is carried out in a closed system capable of minimizing contact of the sample and reagents with ambient moisture. Sample volumes in the range of 40–300 μL are employed, depending on the water concentration. An automatic dilution is provided to deal with concentrated samples. The consumption of Karl Fischer reagent depends on the water content of the sample but is not larger than 100 μL. The system was evaluated for determination of water in ethanol and methanol in the range 0.02–0.5% (w/w). The average relative precision estimated in that range (9–3%) is comparable to that obtained with a larger volume commercial system and no significant difference was observed between the results obtained for the two systems at the 95% confidence level. A complete titration can be performed in less than 5 min employing the proposed system.
© 2006 Elsevier B.V. All rights reserved.

Keywords: Water determination; Mechanized titration; Monosegmented analysis; Karl Fischer titration; Flow-batch analysis; Ethanol; Methanol

1. Introduction

The determination of water in several types of sample matrices using the Karl Fischer titration is one of the highest demand determinations of a single analyte determination. The number of daily determinations has been estimated to be above 500,000, in samples as diverse as food, isolating oil, pharmaceuticals, hydrocarbons and pure organic solvents such as alcohols [1].

There are many papers describing the mechanization of the Karl Fischer method with resulting improvements in sample throughput and reduction of sample and reagent consumption. Also, mechanization can provide analytical systems capable of manipulating hazardous substances employed in the composition of the Karl Fischer reagents, avoiding exposition of the operator and minimizing laboratory residues. Although the toxicity of this reagent has been reduced over the years [2] its composition and the residues it produces still require attention.

The Karl Fischer method has been automated by using the flow injection (FI) principle [3–9]. The main advantage of the FI-based method is sample throughput and the possibility of kinetic discrimination of interfering side-reactions. The greatest disadvantages of those systems are the need of analyte standards to calibrate the system and its critical dependence on flow rates.

Flow-batch systems have recently been proposed [10–12] based on multicommutation and the use of open chambers where titrations can be processed. They present an interesting option to automate the Karl Fischer titration, although they have not yet been described for this purpose. On the other hand, the system requires the use of a mixing chamber and the volume of sample, reagents and diluents are heavily dependent on the flow rate determined by the impelling devices, such as peristaltic pumps, affecting precision.

The monosegmented flow analysis concept [13] has been also applied to automate titration-based analytical methods [14–18]. However, the full exploitation of the concept as a flow-batch system, and its use to perform Karl Fischer titrations has not yet been described. The liquid monosegment, limited by the axial front and back air borders inside a tube, can be in fact visualized as a sample aliquot present in a vessel. The first titrator proposed, based on the monosegmented flow concept [17], employed the movement of the monosegment for a long distance inside a small bore tube in order to achieve homogenization after titrant addition, before spectrophotometric determination of the mixture.

* Corresponding author.
E-mail address: pasquini@iqm.unicamp.br (C. Pasquini).

0039-9140/$ – see front matter © 2006 Elsevier B.V. All rights reserved.
doi:10.1016/j.talanta.2006.06.034

This long tube approach forbids the use of electrochemical techniques, such as biamperometry and potentiomety, to monitor the progress of the titration because the monosegment has to be moved away from the detection cell. For a spectrochemical-based detection this operation is possible without causing serious trouble to measurement precision. However, for an electrochemical cell, the system becomes unstable due the alternating contact of air and liquid (titrated solution) with the electrodes.

This work describes a monosegmented flow-batch titrator system employing biamperometry to monitor the progress of Karl Fischer titrations. The system performs true titrations and precludes any calibration. The volume of the injected monosegment, the concentration of the Karl Fischer reagent and the volume required to achieve the end point of the titration are the only parameters necessary to perform the analysis. The system differs from those previously described [17,18] because part of the monosegment is always in contact with the detection cell and the homogenization is carried out by cycling between two points around the cell. This also contributes to a significant reduction in the size of the titrator.

The system has been evaluated for the determination of water in ethanol and methanol. The importance of determination of water in these two substances, and principally in the first, becomes evident if one considers that in Brazil, as in several other countries, the gasoline sold in fuel stations contains about 25% added absolute ethanol.

2. Experimental

2.1. Reagents and solutions

Analytical grade reagents and solvents and deionised water were employed throughout. Synthetic samples of methanol containing different amounts of water in the range 0.01–0.5% were prepared by addition of water to methanol previously dried for 24 h over activated molecular sieves (4A, Carlo Erba). Dried methanol was also used as diluent for highly concentrated samples. The water content of this dried methanol was estimated to be about 0.008% (w/w) by conventional Karl Fischer titration. When the dilution procedure was employed, a blank was run to account for the water content in the diluting solvent.

The Karl Fischer titrant solution was a commercial Combititrant 5 (Aquastar). A 1 μL of this solution reacts with 5.0 μg of water. The strength of this solution was checked by titrating methanol samples prepared to contain known amount of added water.

2.2. Equipment

The results of the titrations made with the proposed system were compared with those obtained by using a commercial batch titrator (Orion AF8). That system employs the biamperometric technique to locate the end point.

2.3. Monosegmented titrator

Fig. 1a shows a diagram of the proposed Karl Fischer monosegmented titrator, which is similar to the previously described titrators [17,18]. However, the titration procedure itself has been substantially altered. The syringe/step motor-based system employed for volumetric additions of the Karl Fischer reagent uses a gas-tight syringe of nominal volume equal to 500 μL and can deliver volumes with a precision of ±0.5 μL. A peristaltic pump (Ismatec IP8) was employed to impel the fluids in the system. The pump is controlled by the system microcomputer through a standard serial interface (RS-232). Besides controlling the peristaltic and syringe pumps, the microcomputer also controls three miniature three-way electromechanical valves (National Research, NR 161T031-12VDC) used to admit the washing solution (V_1), to allow for titrant refill of the syringe pump (V_2), and to avoid moisture entering the system through the waste tubing during the cycling operation of the monosegment (V_3). The microcomputer also monitors the logical state of three optical switches (PHCT 203) employed to locate the monosegment during the homogenization cycles. All these operations are made through a parallel interface (PCL 711S, Advantech) which contains a 12 bit analog-to-digital converter to allow for current measurement of the biamperometric detector, 16 digital outputs for valve control and 16 digital inputs for to access the logical state of opto-switches. The circuit for the detector is depicted in Fig. 1b. The potential difference applied to the electrodes was 250 mV.

The system has some points through which external moisture could enter, possibly altering the results of a titration. This is a constant source of concern even for automated batch systems. In the present system, moisture could find access through the air stream employed to carry the monosegment, through the washing solvent reservoir, through the titrant reservoir and through the air input from the tubing after the cell, when the cycling operation is moving the monosegment forward and backward. All these points have been protected against access of external moisture by using molecular sieve traps and by keeping (when possible) the solvents over molecular sieves.

Fig. 2a shows a detail of the sample introduction port. The device is made of Teflon® to allow working with organic solvents. The arrangement of the three loops, as shown, has been previously reported for the purpose of diluting a sample segment [19]. It is possible to note that, when the sample is injected using the device herein described, the contents of the three loops are simultaneously inserted into the system, carried by a dried gas stream while the central segment, containing the sample, is merged with the other two segments containing a diluent. The mixture is then passed to the next stage of the titrator.

Fig. 3 shows the flow-detection cell employed for biamperometric monitoring of the Karl Fischer titration. The cell was made of a 2 cm × 3 cm × 1 cm Teflon® block. The platinum electrodes were made of two metallic rods with 2 mm diameter, inserted perpendicularly to the cell body. Two optical-switches were placed 1 cm before and 1 cm after the flow cell to detect the location of the monosegment.

2.4. Titration processing

The titration of a sample starts when the user moves the injection port to the direction indicated in Fig. 2a (left). The

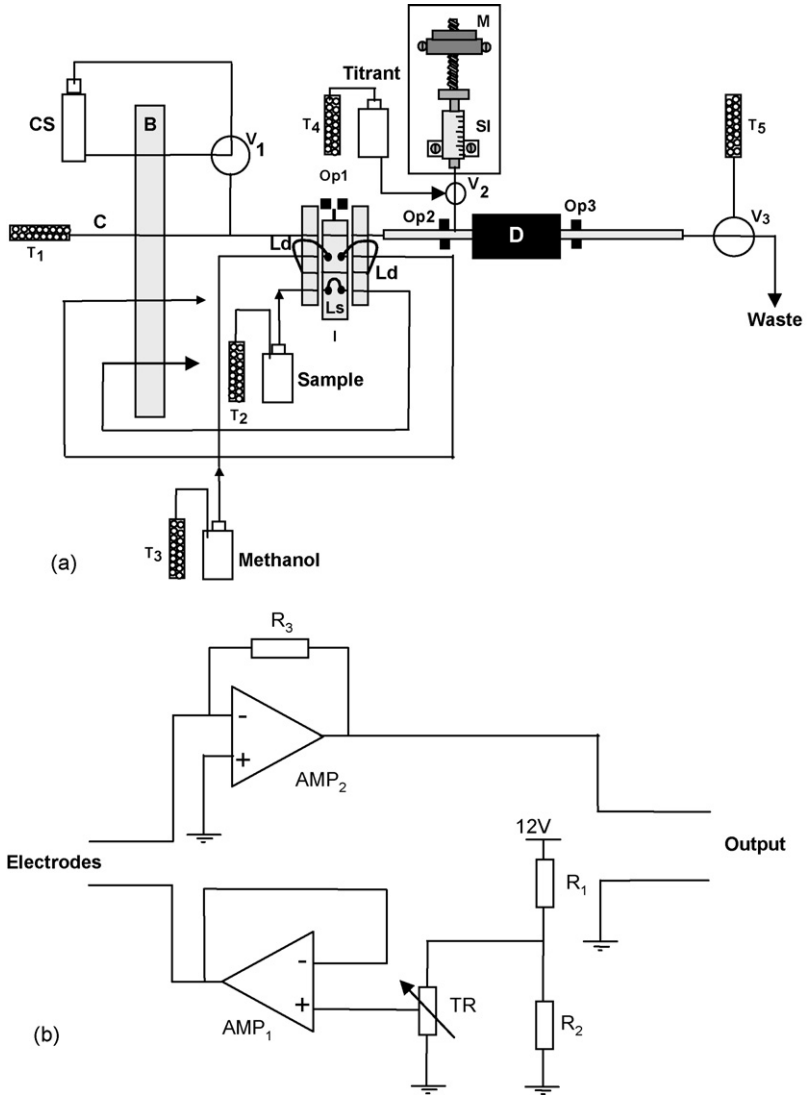


Fig. 1. (a) Schematic diagram of the Karl Fischer monosegmented titrator. CS, washing fluid (methanol dried over activated molecular sieve); C, dry air or dry nitrogen carrier gas; Ld, diluent loops; Ls, sample loop; I, injection port; $Op_{1–3}$, optical switches; D, biamperometric cell; $V_{1–3}$, three way electromechanical valves; SI, gas-tight syringe; M, stepper motor, $T_{1–5}$, traps containing activated molecular sieve. (b) Biamperometric detection circuit. TR, 10 kΩ trimpot; R_1, R_2 and R_3, resistors 10 kΩ, 2.2 kΩ and 1 MΩ, respectively; AMP_1 and AMP_2, 741 and 356 operational amplifiers, respectively.

sample introduction is detected by the microcomputer through OP1. The solutions contained in the three loops are simultaneously transported by an air carry stream to the titration cell. The segment formed by merging the loops volumes is stopped when its left air/liquid interface reaches the first opto-switch (OP_2). If a low concentration of water is present in the sample, all three loops are filled with the sample avoiding its dilution. If this is not the case, the monosegment is homogenized by cycling the monosegment position between the optical-switches surrounding the detection cell. The number of cycles is determined by the user. After homogenization (if necessary) the segment is stopped again with its right air/liquid interface at optical-switch (Op_3) also placed on the right side of the cell. The syringe pump delivers a pre-determined volume of titrant controlled by the number of steps sent to the motor. Typical volume increments vary from 5 to 20 μL. After titrant addition, the monosegment is again cycled to promote the reaction between titrant/titrand and the homogenization of the titrated mixture. Of course, the cycling operation, besides promoting the contact between the analyte and reagent, also gives the time for reaction to proceed to the equilibrium. The overall effect of the physical mixing and reaction kinetics (mainly near the titration end point, where lower excess of reagents are present) need to be considered when selecting the ideal number of cycles to be employed. The term "homogenization" refers, in this work, to the achievement of a stable measurement of the biamperometric current after both the physical mixing and chemical reaction have been processed. Each homogenization cycle requires about 3 s to be processed at the flow rate employed for the carrier air stream (5.0 mL min^{-1}). This time increases as the volume of the monosegment increases after each titrant addition. The titration proceeds until the programmed number of titrant increments has been attained. Alternatively, a pre-set value of current, measured by the biamperometric detector, can be employed as a fixed ref-

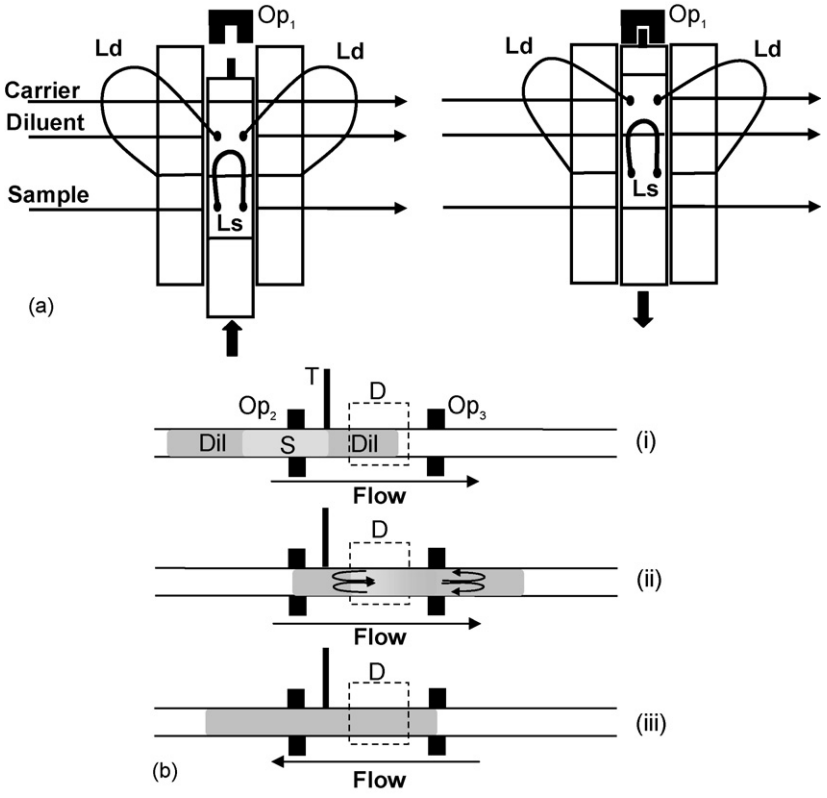


Fig. 2. (a) Arrangement of the reagent and sample loops in the monosegmented injection port (see Fig. 1 for other identifications); left, device in sampling mode; right, device in injection mode; Op_1, optical switch for identification of injector position. (b) Cycling operation for monosegment homogeneization. T, point of titrant addition; S, sample; Dil, diluent; D, biamperometric detection cell; Op_{2-3}, optical switches; i, ii and iii depict the three steps of one homogenization cycle.

erence value to stop titrant addition. A correction of the current value need to be performed before comparison with the pre-set value due the volumetric dilution caused by titrant addition. The corrected value is found multiplying the read value after each titrant addition by the ratio between the total volume of the segment (sample volume plus added titrant volume) and the initial sample volume. This is easily computed by the controlling software. The system is robust and does not show dependence of the flow rate established by the peristaltic pump. After finishing a titration, the system is washed by a segmented flow generated by turning the valve V_1 on for 10 s and pumping dried methanol to the confluence point with the gas carrier stream. Valve V_1 is then turned off and the methanol present in the system is flushed out by the air stream.

The resulting titration curves are stored and the end points are determined by the intercept obtained by extrapolating the two linear segments found before and after the titration end point.

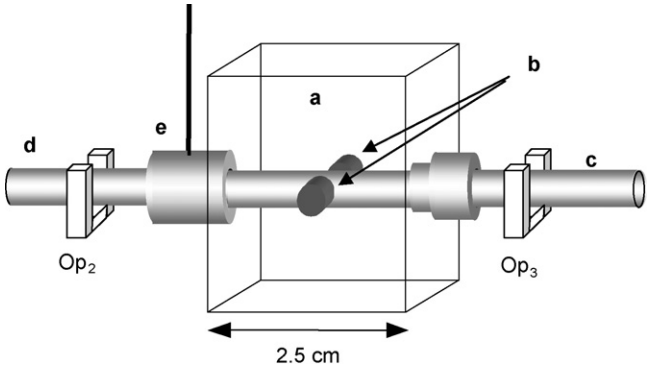


Fig. 3. Detection cell. (a) Teflon® block; (b) platinum electrodes for biamperometric detection; (d and c) Teflon® tubes; (e) point of titrant addition.

3. Results and discussion

The titration curve and, of course, end point location are affected by the number of cycles employed for monosegment homogenization. Fig. 4a shows the effect of the number of homogenization cycles on the biamperometric titration of a standard ethanol sample containing 0.76% (w/w) of water (sample loop = 40 μL, diluent loops = 2 × 85 μL, total monosegment volume = 210 μL). The effect of poor mixing and incompleteness of the reaction, mainly near the end point where the concentration of reagents (water and iodine) are lower, when using a number of cycles lower than 6 on the titration error is shown in Fig. 4b. The number of cycles necessary to achieve a homogeneous mixture of the titrated solution depends on the volume of the monosegment. This volume increases with the additions of titrant. Therefore, the number of cycles needs to be selected based on the prediction of the largest monosegment volume that will be produced up to the end of the titration. For an initial volume of 210 μL and titrant increments of 20 μL, necessary to titrate a sample containing up to 0.80% of water, eight homogenization cycles were required. This number drops to five cycles

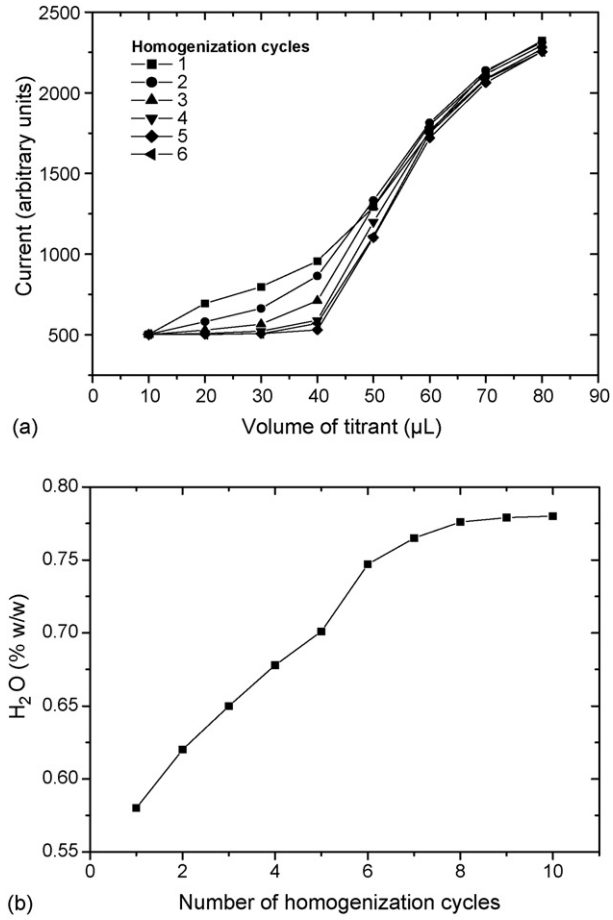


Fig. 4. Effect of the number of homogenization cycles after each titrant addition on the accuracy of the titration results. (a) Biamperometric titration curves of a 210 μL monosegment containing 0.76% (w/w) of water obtained with increasing numbers of homogenization cycles. (b) Effect of the number of homogenization cycles on the water concentration determined using the proposed system and the titration curves shown above.

for 5 μL increments when the titration involves water contents less than about 0.1%. The present system limits the minimum initial volume and the maximum final monosegment volume to 200 and 600 μL, respectively. The minimum volume is determined by twice the volume of the flow cell and the tubing path between the cell and the two optical-switches. The maximum volume is limited by the long time (excessive number of cycles) necessary to homogenize the monosegment composition and because larger monosegments are more prone to be disrupted during the cycling operation.

An upper limit of titratable water concentration can be increased by decreasing the volume of the sample loop (Ls) and diluting the sample using the two side loops (Ld) filled with a suitable diluent. By injecting 30 μL of sample and diluting it with two side loops of 135 μL to a final 300 μL volume, concentrations as high as 3% water can be titrated with the Karl Fischer solution employed in this work. If a higher concentrated titrant is available, higher water concentrations can be determined. Determinations at the lower concentration limit require that all three loops are filled with the sample to a total volume of 300 μL. The titrant syringe pump can deliver a minimum volume of 1 μL. Therefore, supposing that at least two points are necessary to define the linear segment before the end point in the biamperometric curve, the minimum titratable concentration, using the present Karl Fischer reagent solution, may be estimated as close to 0.005% (w/w).

Table 1 shows the results obtained for five replicate determinations of water in ethanol and methanol samples by the proposed titrator and by a commercial conventional batch titrator, employing the same Karl Fischer reagent. The results show a slightly better precision, expressed as the mean relative standard deviation, for the conventional (3.9%) system when compared with the proposed method (5.4%). The mean relative difference between the results is 5.4% with a predominance of somewhat lower results for the proposed titrator, that can be attributed to the higher risk of contamination of samples by external moisture in the conventional system, mainly for those samples presenting low water concentrations. Statistical analyses of the results showed that there are no significant differences between the results obtained by the two methods at the 95% confidence level.

Titrations, such as those shown in Table 1, can be performed in 3–5 min, depending on the number of titrant additions necessary. Of course, for routine determinations when concentration range of the sample can be anticipated, further optimization can reduce the titration time to the order of 2.5 min.

The presence of oxygen in the dried air carrier does not cause any significant effect on the determination of the end point of the Karl Fischer titrations. This was verified by using dried ambient air or dried nitrogen to carry the monosegment during the titration. Probably, it results from the small area of contact between the monosegment and the gas carrier stream.

Table 1
Results for determination of water in commercial samples of ethanol and methanol

Sample	Water content (%, w/w), proposed titrator (A)	Water content (%, w/w), conventional titrator (B)	Relative difference $[(A-B)\times 100/B]$ (%)
Ethanol 1	0.377 ± 0.014	0.409 ± 0.020	−7.8
Ethanol 2	0.514 ± 0.014	0.499 ± 0.017	3.0
Ethanol 3	0.538 ± 0.015	0.535 ± 0.008	0.6
Ethanol 4	0.268 ± 0.012	0.290 ± 0.006	−7.6
Methanol 1	0.0298 ± 0.0028	0.0329 ± 0.0021	−9.0
Methanol 2	0.0453 ± 0.0042	0.0473 ± 0.0025	−4.2

For ethanol: sample volume = 40 μL, volume of the monosegment after dilution = 270 μL. For methanol: sample volume = 270 μL (without dilution). The standard deviations refer to five determinations for each method and each sample.

The consumption of sample and reagents in the proposed system can be considered as its principal advantage over other automated Karl Fischer titrators. The average consumption of Karl Fischer reagent is typically lower than 100 μL and the sample volume is dictated by its water concentration being between 30 and 300 μL. This generates a lower quantity of residue and helps maintain environmental quality while lowering the cost per determination.

The system is isolated from its surroundings avoiding contact of the samples with external moisture and the samples are presented to the system without being exposed to ambient humidity. This certainly helps to improve the accuracy of the water determination.

The proposed titrator is an example of a flow-batch system in which the batch characteristic of the monosegmented concept is exploited to the extreme. The system presents reduced dimensions because homogenization, after titrant additions, is achieved by cycling instead of carrying the monosegment through a long manifold. Also, this approach permits the use of electrochemical monitoring of the monosegment titration because the cell can be maintained under stable conditions with the electrodes always in contact with the titrated solution.

4. Conclusions

The proposed system exploits the most important characteristic of the monosegmented concept to produce a mechanized titrator for water determination in organic solvents by the Karl Fischer method. The main advantages of this titrator are: its size; its ability to easily keep the sample and reagents free of contamination from ambient moisture; its independence of the precision of peristaltic pump flow rates; its capability to perform true titrations that preclude the use of analyte standards; its use of low volumes of sample (typically 30–300 μL) and Karl Fischer reagent (typically 100 μL), contributing to reduce both the cost of analysis and production of residue, and its use of electrochemical techniques to follow the titration progress and for end point location.

Acknowledgments

Authors are grateful to Dr. Carol H. Collins for critical manuscript revision. EVA thanks FAPESP for the PhD fellowship (Proc. 00/02190-1). CP is grateful to CNPq for the research grant and fellowship (Proc. 302708/88-0).

References

[1] U. Nordmark, A. Cedergren, Anal. Chem. 72 (2000) 172.
[2] E. Scholz, Analusis 10 (1982) 491.
[3] I. Kågevall, O. Åström, A. Cedergren, Anal. Chim. Acta 114 (1980) 199.
[4] H. Muller, G. Wallascheck, Z. Chem. 24 (1984) 75.
[5] R.E.A. Escott, A.F. Taylor, Analyst 110 (1985) 847.
[6] I. Nordin-Andersson, A. Cedergren, Anal. Chem. 57 (1985) 2571.
[7] H. Muller, J. Seelisch, D. Kirsch, Chem. Technol. 1 (1987) 25.
[8] C. Liang, P. Vacha, W.E. van der Linden, Talanta 35 (1988) 59.
[9] R. Chen, J. Ruzicka, G.D. Christian, Talanta 41 (1994) 949.
[10] E.P. Medeiros, E.C.L. Nascimento, A.C.D. Medeiros, J.G. Veras Neto, E.C. da Silva, M.C.U. Araújo, Anal. Chim. Acta 511 (2004) 113.
[11] R.S. Honorato, M.C.U. Araújo, R.A.C. Lima, E.A.G. Zagatto, R.A.S. Lapa, J.L.F.C. Lima, Anal. Chim. Acta 91 (1999) 396.
[12] F.R.P. Rocha, B.F. Reis, E.A.G. Zagatto, J.L.F.C. Lima, R.A.S. Lapa, J.L.M. Santos, Anal. Chim. Acta 119 (2002) 468.
[13] C. Pasquini, W.A. Oliveira, Anal. Chem. 57 (1985) 2575.
[14] E.M. Ganzarolli, A. Lehmkuhl, RR.R. Queiroz, I.G. Souza, Quim. Nova 22 (1999) 53.
[15] P.B. Martelli, B.F. Reis, M. Korn, J.L.F.C. Lima, Anal. Chim. Acta 387 (1999) 165.
[16] P.E. Borges, P.B. Martinelli, B.F. Reis, Microchim. Acta 135 (2000) 179.
[17] E.V. de Aquino, J.J.R. Rohwedder, C. Pasquini, Anal. Chim. Acta 438 (2001) 67.
[18] E.V. de Aquino, J.J.R. Rohwedder, C. Pasquini, ABC, 2006 (submmited for publication).
[19] V.O. Brito, I.M. Raimundo Jr., Anal. Chim. Acta 371 (1998) 317.

Available online at www.sciencedirect.com
ScienceDirect
Talanta 71 (2007) 1192–1197
Talanta
www.elsevier.com/locate/talanta

Characterization of solution-phase DNA hybridization by fluorescence correlation spectroscopy: Rapid genotyping of C677T from methylenetetrahydrofolate reductase gene

Chaoqing Dong, Pudun Zhang [1], Rui Bi, Jicun Ren *

College of Chemistry & Chemical Engineering, Shanghai Jiaotong University, 800 Dongchuan Road, Shanghai 200240, PR China

Received 12 March 2006; received in revised form 8 June 2006; accepted 9 June 2006
Available online 18 July 2006

Abstract

In this paper, fluorescence correlation spectroscopy (FCS) was applied to measure the hybridization fraction of the ssDNA probe with its perfectly matched 146 mer ssDNA and a base mismatched 146 mer ssDNA from human methylenetetrahydrofolate reductase (MTHFR) gene. The ssDNA fragments in this study were obtained by asymmetric PCR techniques. The measurements were performed on a laboratory-built FCS system based on the two components fitting procedure. The obtained results showed that FCS could discriminate the difference of thermal stability between perfectly matched and mismatched DNA duplex, and be used to characterize the genotype of C677T in MTHFR gene. Our data illustrated that FCS was a useful tool for rapid screening of single point genetic mutations/polymorphisms (SNP) combined with DNA hybridization.
© 2006 Elsevier B.V. All rights reserved.

Keywords: Genotyping; Fluorescence correlation spectroscopy; Solution-phase DNA hybridization; MTHFR gene

1. Introduction

Fluorescence correlation spectroscopy (FCS) is a single molecule detection technique using statistical analysis of the fluctuations of fluorescence emitted from a small observation volume. The autocorrelation function can provide us some important information, such as, the average number of independent fluorophores in the volume and the coefficient of diffusion. Since Magde et al. [1] and Elson and Webb [2] used fluorescence correlation spectroscopy technique to measure the diffusion and binding of ethidium bromide onto double-stranded DNA, FCS has become a powerful tool for detection and characterization of fluorophores in solution at the single molecule level. More detailed description of the theory and other possible applications can be found elsewhere [3,4].

The occurrence of oncogenesis is often the result of a single base mutation in DNA, especially when crucial genes are hit by strong irradiation and some chemicals. For example, some results showed that the C677T mutation of methylenetetrahydrofolate reductase (MTHFR) gene was associated with vascular disease, neural tube defects, preeclampsia and thrombosis. So, the determination of genotypes has become central to the characterization of disease-causing genes and the diagnosis of human genetic diseases. Various methods have been developed for genotyping or determination of point mutations, including allele-specific amplification (ASA) [5], amplification–refractory–mutation assay (ARMS) [6], polymerase chain reaction-restriction fragment length polymorphism (PCR-RFLP) [7], ligase chain reaction (LCR) [8] and short tandem repeat (STR) length polymorphism [9], single strand conformation polymorphism (SSCP) [10], heteroduplex polymorphism assay (HPA) [11], dideoxy fingerprinting [12], chemical or enzymatic cleavage of mismatches (CMC, EMC) [13,14], denaturing gradient gel electrophoresis (DGGE) [15] and capillary electrochromatography [16], etc. These methods require multiple steps, including size separation, and are time-consuming and labor intensive. Recently, many novel fluorescent oligonucleotide probes or PNA probes were developed and have been used for the SNP genotyping [17]. For example, combined with allele-specific amplification, two-color fluorescence cross-correlation spectroscopy (FCCS) can characterize the genotypes based on the correlation time by simultaneously

* Corresponding author. Tel.: +86 21 54746001; fax: +86 21 54741297.
E-mail address: jicunren@sjtu.edu.cn (J. Ren).
[1] Now he is at the School of Science, Beijing University of Chemical Technology.

0039-9140/$ – see front matter © 2006 Elsevier B.V. All rights reserved.
doi:10.1016/j.talanta.2006.06.019

attaching two PCR primers labeled with the two different colors dyes [18]. In order to lower the fluorescence background of unamplified two-color primers, Földes-Papp et al. recently probed direct genotyping unamplified genomic DNA from the whole blood by FCCS combined with DNA hybridization technique with the 'intelligent' probes [19]. This approach improved the detection of interacting fluorescent molecules compared to FCS, but the requirement of aligning two laser beams to the same spot made it experimentally challenging, i.e. the complicated instrumentation is necessitated, and cross-talk or chromatic aberrations sometime is generated.

To the best of our knowledge, although FCS technique is an effective tool to determine the number and size of DNA fragments at nano-molar concentrations, a few report on its application for mass screening of gene mutations. It has been reported that SNPs could be genotyped by the sequence-specific primer (SSP)-PCR method followed by fluorescence correlation spectroscopy [20,21]. In the present work, asymmetric PCR technique was first introduced to amplify the ssDNA fragment of target gene, and then FCS technique was used to monitor the hybridization process in solution between the ssDNA probe and the amplified ssDNA fragment. This approach was successfully used to characterize the C677T genotypes of the methylenetetrahydrofolate reductase gene. Our data show that FCS is a simple and reliable technique for genotyping of human genes.

2. Experimental

2.1. Apparatus and regents

Taq polymerase, PCR reaction buffer and dNTPs were purchased from Sangon Co. (Shanghai, China). Gene Amp PCR system 2400 was obtained from Applied Biosystems (CA, USA). Primers were synthesized by Sangon Co. The QIAamp DNA blood Mini kit was purchased from Qiagen (Hilden, Germany). All aqueous solutions were prepared with ultra-pure water from Milli Q System (Millipore, Bedford, MA, USA). The 20 mer gene-specific single strand DNA (ssDNA) probe was purchased in HPLC-pure quality from Sangon Co., which was labeled with 6-carboxy-fluorescein (6-FAM). The sequence was as following: 5′-(6-FAM)-ATGAAATCGACTCCCGCAGA-3′. The whole blood samples with EDTA were obtained from the students and staff in Shanghai Jiaotong University and were stored in a refrigerator at −20 °C until DNA extraction.

2.2. FCS setup

The laboratory-built FCS setup is shown in Fig. 1, which is similar to the previous design described elsewhere [22]. Briefly, the 488 nm laser beam from argon ion laser power source (43 Series, Melles Griot, CA, USA) was attenuated to 40 μW by a circular reflective neutral density filter, and then expanded to just fill the back aperture of the objective. The expanded laser beam was reflected into a water immersion objective (UplanApo, 60× NA1.2, Olympus, Japan) using a dichroic mirror (505DRLP, Omega Optical, USA). Then, the laser beam was focused into a droplet of sample solution on the cover glass by the objective and formed a small spot. The fluorescence was collected by the same objective and passed through the same dichroic mirror and a band pass filter (530DF30, Omega Optical). Finally, it was coupled into a 35 μm pinhole at the image plane in front of single photon counting module (SPCM-AQR16, Perkin-Elmer EG&G, Canada). The fluorescence fluctuations were correlated with a correlator card (ALV-5000/EPP, ALV-GmbH, Germany). The raw FCS data were nonlinearly fitted with Microcal Origin 6.0 software package based on the Levenberg–Marquardt algorithm.

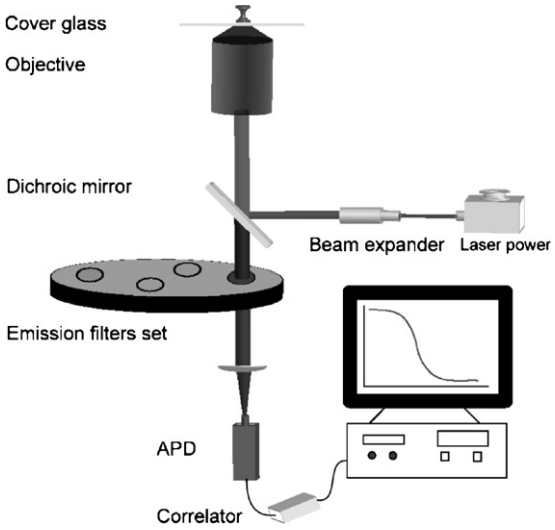


Fig. 1. Schematic FCS setup in our experiment.

2.3. DNA extraction and determination of the genotypes by capillary electrophoresis (CE)

Human genome DNA was extracted from whole blood using the DNA blood Mini Kit from QIAamp, following the instructions of the manufacture. DNA was dissolved in AE buffer (10 mmol/L of Tris containing 1 mmol/L EDTA, pH 7.5). The genotypes of samples were determined by PCR amplification, *Hin*fI digestion and capillary electrophoresis analysis as described in the reference [23]. The primers of PCR amplifications were 5′-TGAAGGAGAAGGTGTCTGCGGGA-3′ (forward) and 5′-AGGACGGTGCGGTGAGAGTG-3′ (reverse) which define a 198 bp PCR product that includes the C677T mutation. Capillary electrophoresis was performed on a P/ACE MDQ System (Beckman Instruments, Palo Alto, CA, USA). In the experiments of capillary electrophoresis, 80 mM TAPS buffer (pH 7.6) and 2.5% polyvinylpyrrolidone (PVP) (M_w 1000 kDa)–80 mM TAPS solution were used as separation buffer and sieving matrix of capillary electrophoresis. SYBR Gold (1:5000 final dilution of stock solution) was added to sieving matrix.

2.4. Preparation of 146 mer ssDNA fragments

2.4.1. Symmetric PCR

The PCR reaction mixture contained 10 mmol/L Tris–HCl, pH 8.3, 50 mmol/L KCl, 1.5 mmol/L $MgCl_2$, 0.1 g/L gelatin,

1 mL/L Trition X-100, 200 μmol/L each dNTP, 0.2 μmol/L each primer, 2 U Taq polymerase and −100 ng of template DNA in a final volume of 100 μL. The PCR reaction was performed on a Gene Amp PCR system 2400 (Applied Biosystems), using a three-step thermocycling profile with 36 cycles of 94 °C for 30 s (denaturation), 58 °C for 30 s (primer annealing) and 72 °C for 10 s (extension), preceded by 94 °C for 4 min and followed by 72 °C for 7 min.

The primers used were: 5′-GGAGCTTTGAGGCTGACC-TGAA-3′ (forward) and 5′-GACGATGGGGCAAGTGAT-3′ (reverse) which define a 146 bp PCR product that includes the C677T mutation. To confirm the fidelity of the reaction, PCR products were loaded in a 2% agarose gel prepared with 1× TBE buffer containing 0.5 μg/mL ethidium bromide and electrophoresed at 100 V for 30 min. Then, the sample was visualized by UV transillumination and its size was compared with a known DNA marker.

2.4.2. Asymmetric PCR

Four microliter templates prepared from the symmetric PCR and a negative control (water blank) was subjected to the asymmetric PCR. The asymmetric PCR reaction mixture is the same as the symmetric PCR, except for only 0.2 μmol/L forward primer in a final volume of 100 μL. The PCR reaction was performed on a Gene Amp PCR system 2400, using a three-step thermocycling profile with 25 cycles of 94 °C for 30 s, 58 °C for 30 s and 72 °C for 10 s, preceded by 94 °C for 5 min and followed by 72 °C for 7 min.

2.5. Hybridization experiments

Thirty microliter asymmetric PCR sample was transferred into a 200 μL Eppendorf tube, 2.5 μL single strand oligonucleotide probe (0.2 μmol/L) and 1 μL 5× SSC buffer was added and the total volume was adjusted to 50 μL with Milli Q water. Hybridization experiments were performed on Gene Amp PCR system 2400. The hybridization reaction mixture was kept at 95 °C for 5 min to ensure complete denaturation, and then maintained to the hybridization temperature over a 60 min period.

2.6. FCS measurements and data evaluation

Two microliter hybridization reaction mixtures were transferred quickly to 20 μL of ice-bath TE buffer in order to terminate the hybridization reaction [24]. Then, a 10 μL mixture was placed on the cover glass for FCS experiments. All FCS measurements were done at room temperature and the measurement time per sample was 30 s.

3. Results and discussion

3.1. ssDNA probe design

The DNA sequences and the external environments influence the thermal stability of DNA duplex. The most destabilizing effect during hybridization to the potential DNA duplex is the mismatched basepair. It was also found that a single base mismatch closer to the center of the oligonucleotide induced a larger T_m shift than a single base mismatch closer to the end of the oligonucleotide [25]. The ssDNA probe in this paper was designed to match with the mutated (T:T). Meanwhile, the ssDNA probe forms the unstable mismatch (C:A) structure with the normal (C:C). The designed probe is as following: 5′-(6-FAM)-ATGAAATCGACTCCCGCAGA-3′.

3.2. Characterization of solution-phase DNA hybridization

In an FCS experiment, the fluctuations of fluorescence ($\delta I(t)$) is recorded in real time and calculated as a function of time. Autocorrelation analysis of these fluctuations can be defined by the normalized autocorrelation function ($G(\tau)$):

$$G(\tau) = \frac{\langle \delta I(t) \delta I(t+\tau) \rangle}{\langle I(t) \rangle^2} \tag{1}$$

where the angular brackets represent a time average, $\delta I(t)$ the fluorescence intensity fluctuations at a given time t, $\delta I(t+\tau)$ the fluorescence intensity fluctuations at a given later time and τ is the time delay. The theory of FCS had been described elsewhere [3,4], If assuming the small observation volume as a three-dimensional Gaussian profile, the autocorrelation function has the following form:

$$G(\tau) = \frac{1}{N} \cdot \left(1 + \frac{T\, e^{-\tau/\tau_{triplet}}}{1-T}\right) \cdot \frac{1}{(1+(\tau/\tau_D))} \cdot \frac{1}{\sqrt{1+(\omega_0/z_0)^2 \cdot \tau/\tau_D}} \tag{2}$$

where N is the number of fluorescent molecules in the small observation volume, τ_D the characteristic diffusion time of fluorescent molecules, ω_0 and z_0 the lateral and axial radius of the volume and T is the fraction of fluorescent molecules in the triplet state with a lifetime $\tau_{triplet}$. ω_0 and z_0 were measured by using 1 nM Rhodamine Green solution, assuming its diffusion coefficient of $D = 2.8 \times 10^{-6}$ cm^2/s in water. The FCS curve of Rhodamine Green is shown in Fig. 2. The diffusion time τ_D of Rhodamine Green (∼43 μs) and the ratio of ω_0 to z_0 (∼0.25) can be obtained from Eq. (2), and τ_D is related to the diffusion coefficient, D.

$$\tau_D = \frac{\omega_0^2}{4D} \tag{3}$$

As a result, the obtained ω_0 and z_0 were about 0.22 and 0.88 μm, thus the detection volume ($V_0 = \pi^{3/2}\omega_0^2 z_0$) was calculated to be about 0.25 fL.

When ssDNA probe was hybridized to its ssDNA target, two fluorescent components coexisted in the volume element, including the free ssDNA probe and the formed dsDNA. The above autocorrelation function can be modified as the following two-component model when two components have the same fluorescence yield.

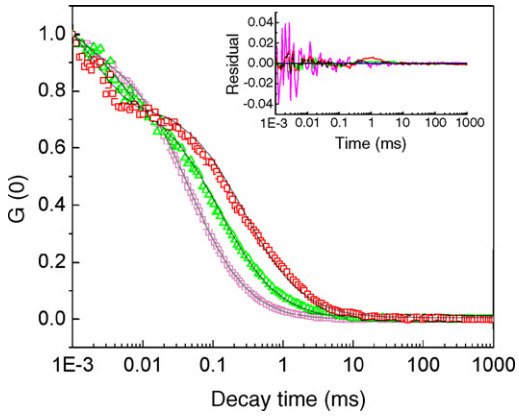


Fig. 2. Normalized fluorescence correlation function as decay time (symbols show experimental FCS curve, solid lines shows fit). The open pink circles (◯), open green triangles (△) and red squares (□) correspond to Rhodamine Green, 20 mer ssDNA probe and the hybridized dsDNA, respectively. The concentration of Rhodamine Green, ssDNA probe and dsDNA are 1, 10 and 10 nM. The inset shows the residuals for three samples with one-component fitting procedure. (For interpretation of the references to color in this figure legend, the reader is referred to the web version of the article.)

$$G(\tau) = \frac{1}{N} \cdot \left(1 + \frac{T\,\mathrm{e}^{-\tau/\tau_{\mathrm{triplet}}}}{1-T}\right) \cdot \left(\frac{y}{(1+(\tau/\tau_{\mathrm{D1}}))} \cdot \frac{1}{\sqrt{1+(\omega_0/z_0)^2 \cdot \tau/\tau_{\mathrm{D1}}}} + \frac{1-y}{(1+(\tau/\tau_{\mathrm{D2}}))} \cdot \frac{1}{\sqrt{1+(\omega_0/z_0)^2 \cdot \tau/\tau_{\mathrm{D2}}}}\right) \quad (4)$$

where y is the fraction of the free ssDNA probe in the solution and τ_{D1} and τ_{D2} are the diffusion time of the free ssDNA probe and the hybridized dsDNA, respectively. It was found in the following FCS experiment that there was a negligible difference of the brightness per molecule between the ssDNA probe and hybridized double-strand DNA (count rate per ssDNA probe was about 6.8 kHz, count rate per dsDNA was about 7.3 kHz and the background noise is 0.07 kHz). Therefore, according to Eq. (4), if τ_{D1} and τ_{D2} were known, y would be obtained with two-component fitting procedure. In order to determine τ_{D2} of the hybridized DNA duplex, it is essential to hybridize completely the ssDNA probe with asymmetric PCR product. Different volume (10–50 μL) of the asymmetric PCR product was directly added into the hybridization solution containing 0.0005 nmol ssDNA probe. The hybridization conditions were the following: 94 °C, 5 min; 80 °C, 10 min; 70 °C, 10 min; 60 °C, 10 min; 50 °C, 10 min; 40 °C, 10 min; 30 °C, 10 min; 20 °C, 10 min. One-component fitting procedure was applied to evaluate the yield of the hybridization. This procedure was feasible because the apparent FCS curve was actually a simple (weighted) sum of individual contribution of free and bound ssDNA probe. The apparent decay time could reflect the fraction of the hybridization. The fraction of hybridization increased with the increasing of the decay time. Fig. 3 gave the relationship of the diffusion time versus the volume of the asymmetric PCR product. It showed that 30 μL of the asymmetric PCR product was enough to hybridize with 0.0005 nmol ssDNA probe. The diffusion time of the hybridized double-strand DNA τ_{D2} was fitted to 232 ± 21 μs. The diffusion time τ_{D1} of the ssDNA probe is 125 ± 13 μs. The FCS curves of ssDNA probe and hybridized double-strand DNA are shown in Fig. 2. Note the shift in the decay time, indicating hybridization of ssDNA probe with the asymmetric PCR product. A triplet state can be seen at short correlation times with a lifetime of about 3 μs.

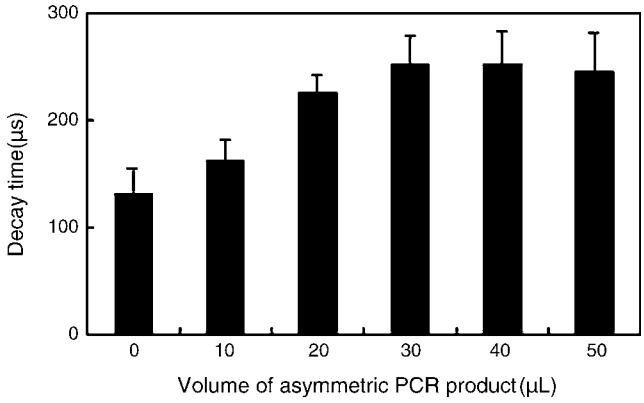


Fig. 3. The diffusion time was plotted vs. the volume (μL) of the asymmetric PCR product. The hybridization conditions: 94 °C, 5 min; 80 °C, 10 min; 70 °C, 10 min; 60 °C, 10 min; 50 °C, l0 min; 40 °C, 10 min; 30 °C, 10 min; 20 °C, 10 min. The hybridization solution contained 0.0005 nmol ssDNA probe.

The DNA hybridization is sensitive to temperature. The higher the hybridization temperature is, the shorter time to reach the hybridization equilibrium needs.

Hybridization reaction can be finished in minutes at 57 °C, but in several hours at room temperature. Besides, the DNA concentration also affects the equilibrium of hybridization. The time of hybridization will be delayed in the diluted solution. The relationship of the measured hybridization fraction under 57 °C was plotted versus the hybridization time (as shown in Fig. 4). At the hybridization experiments of ssDNA probe to the asymmetric PCR product, the hybridization fraction of ssDNA probe increases with the increase of time and the hybridization reaction and reach the equilibrium in about 25 min. Due to different diffusion times between the ssDNA probe and the hybridized ssDNA, hybridization fraction can be measured by

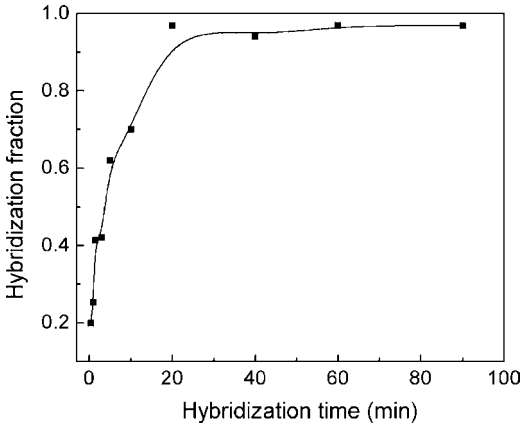


Fig. 4. The relationship of the measured hybridization fraction vs. the hybridization time. The hybridization temperature was at 57 °C. The hybridization solution contained 0.0005 nmol ssDNA probe and 30 μL asymmetric PCR products.

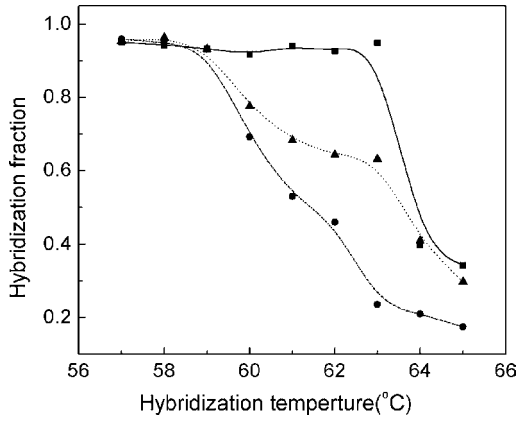


Fig. 5. The relationship of the measured hybridization fraction vs. the temperature. The solid squares (■), solid circles (●) and solid triangle (▲) were corresponded to the mutated (TT), the normal (CC) and the heterozygous (CT), respectively. The hybridization solution contained 0.0005 nmol ssDNA probe and 30 μL asymmetric PCR products. The hybridization time was 60 min.

two-component fitting procedure without separation of the free ssDNA and the hybridized ssDNA by fixing τ_{D1} and τ_{D2} as 125 and 232 μs, respectively.

As well-known, the thermal stability of a DNA duplex is determined by its internal structure, every percentage of mismatched bases lowers the melting temperature of the DNA duplex 1–1.5 °C [26]. For the hybridization between the 20 bases and complementary ssDNA, there is the 5% mismatched base, which remarkably affects the hybridization [25]. The relationship of the measured hybridization fraction versus the temperature is shown in Fig. 5. The rules and chemistry of DNA–DNA hybridization are classical Watson–Crick basepairing (A to T and G to C). At the same time, the denaturation and its reverse process always coexist. In our experiments when the hybridization temperature is in the range of 57–63 °C, the hybridization fraction of the ssDNA probe to the mutated changes hardly. But when at the higher temperature the denaturation process dominates the hybridization process and the hybridization fraction decreases. Single base mismatch between ssDNA probe and target ssDNA induces a more temperature-sensitive hybridization reaction than the perfectly matched, which results in that the hybridization fraction of the mismatched decreases markedly. A part of the heterozygous forms the single base mismatch structure with the ssDNA probe, so the hybridization fraction also decreases gradually. When the hybridization temperature is higher than 63 °C, the structure of dsDNA is destroyed and the hybridization fraction of the perfectly matched decreases gradually and the mismatched no longer hybridize with the ssDNA probe even. The measured hybridization fraction of the mutated (TT), the normal (CC) and the heterozygous (CT) at 63 °C is 94.9, 23.6 and 63.1%.

It is evident from the present results that hybridization fraction of ssDNA probe can be obtained directly from the autocorrelation function without physical separation of strands in conventional hybridization, based on the two-component fitting procedure. Hence, FCS technique can be used to monitor the hybridization process. Meanwhile, FCS can be used to study the influence of the single base mismatch on the thermal stability between perfectly matched and a point mismatched DNA duplex and discriminate the difference of hybridization fraction of ssDNA probe when the fluorescein-labeled ssDNA probe is hybridized to the different genotypes of MTHFR gene. The obtained hybridization fraction can distinguish the genotypes of MTHFR gene. In the conventional FCS experiment, in order to differentiate two components, the decay times should differ by at least a factor of 1.6, which limited the applications of FCS to the study of aggregation and binding. However, in the DNA hybridization, when the target ssDNA fragments are longer than 140 bases, FCS can be used to distinguish the free ssDNA probe and the hybridized DNA duplex using a 20 bases ssDNA probe. It is easily to amplify a larger target ssDNA fragment (>140 bases ssDNA) by PCR reaction.

4. Conclusion

Within this work, an approach has been developed to rapidly characterize the genotypes of genomic DNA samples by FCS. Although FCS is used to determine C677T genotypes of MTHFR gene in this paper, this method can be expendable to determine the genotypes of other genes including human, animals and plants, and maybe become a rapid and high throughput method for screening of genetic mutations and polymorphisms.

Acknowledgements

This work was financially supported by the National Natural Science Foundation of China (numbers 20271033 and 90408014), the key project of National Natural Science Foundation of China (number 20335020) and mega-projects of Science Research for the 10th Five-Year Plan of MSTPRC (2004BA720A04).

References

[1] D. Magde, E.L. Elson, W.W. Webb, Phys. Rev. Lett. 29 (1972) 705.
[2] E.L. Elson, D. Magde, Biopolymers 13 (1974) 1.
[3] S.T. Hess, S. Huang, A.A. Heikal, W.W. Webb, Biochemistry 3 (2002) 697.
[4] P. Schwille, Cell Biochem. Biophys. 34 (2001) 383.
[5] P. Prosser, Trends Biotechnol. 11 (1993) 238.
[6] K. Hayashi, Genet. Anal. Tech. Appl. 9 (1992) 73.
[7] E. Avaniss-Aghajani, K. Jones, D. Chapman, C. Brunk, Biotechniques 17 (1994) 144.
[8] J. Muth, P.M. Williams, S.J. Williams, M.D. Brown, D.C. Wallace, B.L. Karger, Electrophoresis 17 (1996) 1875.
[9] N. Zhang, E.S. Yeung, Anal. Chem. 68 (1996) 2927.
[10] J. Ren, A. Ulvik, P.M. Ueland, H. Refsum, Anal. Biochem. 245 (1997) 79.
[11] C. Gelfi, P.G. Righetti, V. Brancohni, L. Cremonesi, M. Ferrari, Clin. Chem. 40 (1994) 1603.
[12] G. Sarkar, H. Yoon, S.S. Sommer, Genomics 13 (1992) 441.
[13] R.G.H. Cotton, N.R. Rodrigues, R.D. Campbell, Proc. Natl. Acad. Sci. U. S. A. 85 (1988) 4397.
[14] J. Ren, A. Ulvik, H. Refsum, P.M. Ueland, Clin. Chem. 44 (1998) 2108.
[15] O. Khrapko, J.S. Hanekamp, W.G. Thilly, A. Belenkii, F. Foret, B.L. Karger, Nucleic Acids Res. 22 (1994) 364.
[16] J.M. Song, A. Asthana, D.P. Kim, Talanta 68 (2006) 940.
[17] C.M. Strohsahl, H. Du, B.L. Miller, T.D. Krauss, Talanta 67 (2005) 479.
[18] Z. Földes-Papp, J.M. Costa, U. Demel, G.P. Tilz, M. Kinjo, K. Saito, H. Kii, T. Takagi, M. Tamura, P. Thyberg, E. Birch-Hirschfeld, Exp. Mol. Pathol. 76 (2004) 212.

[19] Z. Földes-Papp, M. Kinjo, M. Tamura, E. Birch-Hirschfeld, U. Demel, G.P. Tilz, Exp. Mol. Pathol. 78 (2005) 177.
[20] M. Bannai, K. Higuchi, T. Akesaka, M. Furukawa, M. Yamaoka, K. Sato, K. Tokunaga, Anal. Biochem. 327 (2004) 215.
[21] K. Hori, W.S. Shin, C. Hemmi, T. Toyo-Oka, T. Makino, Curr. Pharm. Biotechnol. 4 (2003) 477.
[22] P. Zhang, L. Li, C. Dong, H. Qian, J. Ren, Anal. Chim. Acta 546 (2005) 46.
[23] A. Ulvik, J. Ren, H. Refsum, P.M. Ueland, Clin. Chem. 44 (1998) 264.
[24] M. Kinjo, R. Rigler, Nucleic Acids Res. 23 (1995) 1795.
[25] M.S. Chen, A. Laszlo, J.L. Roti, C.R. Hunt, Anal. Biochem. 239 (1996) 61.
[26] J. Sambrook, E.F. Fritsch, T. Maniatis, Molecular Cloning: A Laboratory Manual, second ed., Cold Spring Harbor Laboratory Press, Cold Spring Harbor, 1989, pp. 11.1–11.61.

Available online at www.sciencedirect.com
ScienceDirect
Talanta 71 (2007) 1252–1256
Talanta
www.elsevier.com/locate/talanta

Determination of manganese by flame atomic absorption spectrometry after its adsorption onto naphthalene modified with 1-(2-pyridylazo)-2-naphthol (PAN)

Aparecida P. dos Anjos, Lorena Cornejo-Ponce [1], Solange Cadore, Nivaldo Baccan *

Universidade Estadual de Campinas, Instituto de Química, Caixa Postal 6154, 13083-970 Campinas, SP, Brazil

Received 27 March 2006; received in revised form 6 June 2006; accepted 19 June 2006
Available online 25 July 2006

Abstract

A system for determination of manganese, after preconcentration with 3% (w/w) 1-(2-pyridylazo)-2-naphthol (PAN), adsorbed on microcrystalline naphthalene is proposed. An amount of 200 mg of this complexing mixture is placed in a glass column and conditioned with a NH_4Cl/NH_4OH buffer solution (pH 9.5). The aqueous sample, containing manganese, is treated with an ammonium tartrate solution, then with a hydroxylammonium chloride solution and, finally, with a buffer solution. The resulting solution is passed through the column containing microcrystalline naphthalene modified with 1-(2-pyridylazo)-2-naphthol (PAN) where Mn(II) is retained. The column is first washed with deionized water and then with 10.0 ml of dimethylformamide to dissolve the Mn(II)–PAN/naphthalene complex. Manganese is determined by air–acetylene flame atomic absorption spectrometry. About 1 μg of manganese can be concentrated from 200 ml of aqueous sample, allowing a preconcentration factor of 20, a limit of quantification of 5 ng ml^{-1} and R.S.D. of 3.8%. The accuracy was ascertained using certified reference materials, including samples of urine and glass. Water samples were also analysed and the results are in good agreement with those obtained by graphite furnace atomic absorption spectrometry.
© 2006 Elsevier B.V. All rights reserved.

Keywords: Manganese; Solid-phase extraction; PAN; Naphthalene; FAAS

1. Introduction

Manganese is an essential element to man, playing an important role in tissue and bone formation, in reproductive functions and in carbohydrate and lipid metabolisms. Its body load is about 10–20 mg [1]. The great diversity of methods concerning the determination of trace levels of manganese, in different matrices, demonstrates the importance of this element. One of the most common is that based on atomic absorption spectrometry, usually performed after a preconcentration step.

Liquid–liquid extraction [2,3] shows low efficiency when the distribution equilibrium between phases needs a long time to be established or the solubility of the formed complex is low in the organic solvent [4]. Fuginaga et al. [5], proposed a method based on liquid–liquid extraction at high temperature, followed by a liquid–solid separation at room temperature, but it cannot be applied in the extraction of metals that form thermally unstable complexes and, otherwise, is quite time consuming, mainly for the separation and drying of the solid phase. Satake et al. [6] modified this method—liquid–solid separation by adsorbing the metallic complex onto microcrystalline naphthalene. A naphthalene solution in acetone is added to the solution containing the metal and the complexing agent, under vigorous stirring. The precipitate, containing the complex adsorbed onto naphthalene, is filtered, the solid is dissolved in chloroform, the most appropriate organic solvent, and the concentration of the investigated metal is determined spectrophotometrically.

Other preconcentration techniques for trace metals have also been reported, using adsorption by organic reagents fixed on solid materials. The use of silica gel [7], bonded phases such as with silica C-18 [8], and resins like XAD-2 [9] and Amberlyst A-26 [10] is common.

One of the reagents that have been widely used for this type of concentration step is 1-(2-pyridylazo)-2-naphtol (PAN), which

* Corresponding author. Tel.: +55 19 3788 3125; fax: +55 19 3788 3023.
E-mail address: baccan@iqm.unicamp.br (N. Baccan).
[1] Present address: Departamento de Química, Facultad de Ciencias, Universidad de Tarapacá, Casilla 7D, Arica, Chile.

0039-9140/$ – see front matter © 2006 Elsevier B.V. All rights reserved.
doi:10.1016/j.talanta.2006.06.026

reacts with many metallic ions, producing coloured complexes that are usually insoluble in water but soluble in organic reagents, like chloroform, benzene and carbon tetrachloride [11]. Cheng and Bray [12] first utilised PAN as an analytical reagent and it has recently been immobilised on solid supports [13], ion exchange resins [9,14], polyurethane foam [15,16] and naphthalene [17–19]. In these cases, the determination is performed after elution of the metal by a suitable solvent.

Later, Satake et al. [20] proposed a method in which the system complexing reagent-naphthalene, previously prepared by coprecipitation, is placed in a glass column. The analyte solution is passed through the column and the metallic ion is totally retained. Instead of elution of the metal or metal-complex, there is then complete dissolution of the material (modified adsorbent plus metal) in an appropriate organic solvent and the concentration of the metal is determined by atomic absorption spectrometry. The system PAN–microcrystalline naphthalene has been used for the spectrometric [17,21–23] and differential pulse polarographic [24,25] determination of trace levels of metals.

In this paper, a procedure is proposed for the determination of manganese by flame atomic absorption after separation and preconcentration, using a glass column filled with microcrystalline naphthalene modified by 1-(2-pyridylazo)-2-naphthol (PAN). The applications of the proposed method for the analysis of waters, urine and glasses are also described.

2. Experimental

2.1. Reagents

The manganese standard solution (1000 mg l^{-1}) was prepared from metallic manganese (Riedel-de-Häen, 99.9%) treated with concentrated HCl. Appropriate dilutions were made from this solution, whenever necessary, with 0.2% (v/v) HNO_3.

The dimethylformamide (DMF, Nuclear) solution was prepared by mixing 5.0 ml of the amine and 100.0 ml of DMF.

1-(2-Pyridylazo)-2-naphthol (PAN, Carlo Erba), naphthalene (Carlo Erba) and other reagents were of analytical reagent grade. Deionised water (18.2 MΩ cm), obtained from a Milli-Q water system (Bedford, MA, USA), was used throughout.

2.2. Preparation of the extraction mixture (PAN–naphthalene)

Naphthalene (10.0 g) and 0.3 g of PAN were completely dissolved in 50 ml of acetone. This solution was rapidly transferred to 500 ml of deionized water, at 50 °C, with magnetic stirring. The microcrystalline naphthalene, coprecipitated along with PAN and was filtered by suction, washed with water and dried in air. In order to obtain a solid with homogeneous particles, the solid was passed through an appropriate nylon sieve (100–200 mesh) and then stored in a brown bottle.

2.3. Apparatus

A Procyon pH-meter equipped with a combined electrode and a Perkin-Elmer model 5000 atomic absorption spectrometer, equipped with a hollow cathode lamp for manganese as well as a deuterium lamp for background correction, were used. The AA spectrometer operated under the following conditions—wavelength: 279.5 nm; slit width: 0.2 nm; lamp current: 15 mA; flame: air–acetylene.

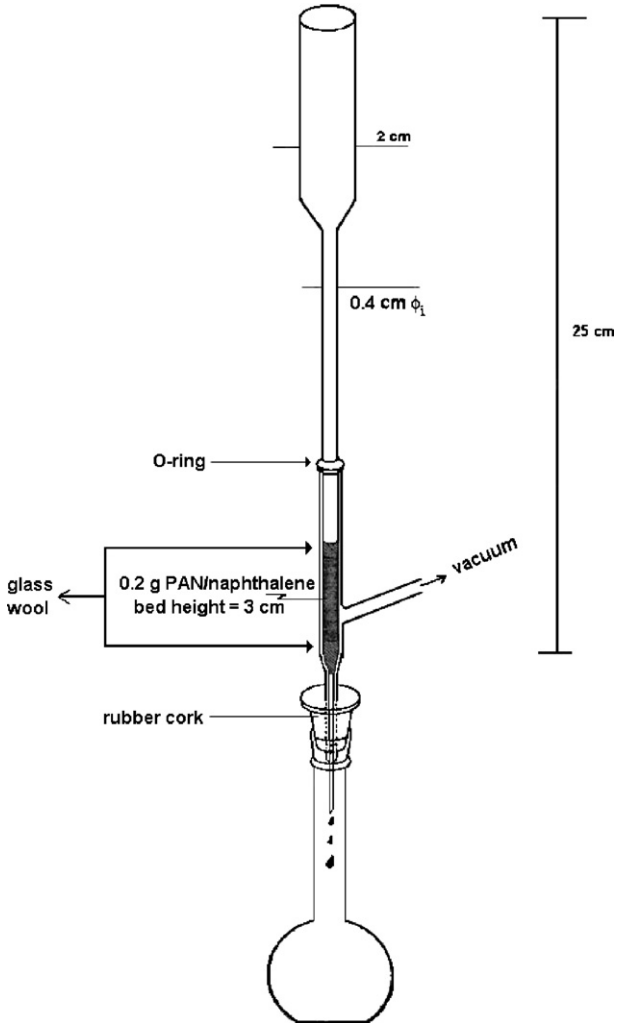


Fig. 1. Column system utilised for liquid–solid adsorption of manganese.

Fig. 1 shows the preconcentration system used throughout this work. The solution containing the analyte is passed through the column with the aid of a vacuum system. The experimental procedure was carried out with a set of 20 columns attached to a manifold and a typical water aspirator pump.

2.4. General procedure

An aliquot of sample solution containing 1–30 μg of manganese was taken into a 50 ml beaker and 5 ml of ammonia/ammonium chloride buffer (pH 9.5), 1 ml of 5% (w/v) ammonium tartrate solution, to avoid hydrolysis of other ions, and 2 ml of 10% (w/v) hydroxylammonium chloride, to prevent the oxidation of Mn(II) to Mn(III), were added. The solution was diluted to 50 ml with water and then passed through the column loaded with 200 mg of the PAN–naphthalene mixture, at a flow rate of 1 ml min^{-1}, using the vacuum system. The column was

washed with water and, after changing the collection flask, the solid material in the column, containing the coloured complex impregnated onto the naphthalene, was dissolved with 10.0 ml of DMF. This solution was aspirated into an air–acetylene flame and its absorbance was measured. The absorbance measurements obtained were corrected for the reagent blank signal, which varies between 0.02 and 0.04. To confirm the efficiency of retention on modified naphthalene, the solution, originally containing manganese that passed through the column was also analysed. After treatment with concentrated HNO_3 and heating until almost dryness, the resulting solution was transferred to a 10.0 ml volumetric flask, made up to volume and then also aspirated into an air–acetylene flame to measure the possible presence of residual manganese.

2.5. Samples

2.5.1. Determination of manganese in natural waters

The method was applied for the determination of manganese in lake (Taquaral Park and Unicamp Campus) water samples, after filtration with a cellulose membrane (0.45 μm). The results obtained by the proposed method were compared with those obtained by direct measurement using GFAAS, with magnesium nitrate as chemical modifier. The standard solutions were prepared in 0.2% (v/v) HNO_3.

2.5.2. Determination of manganese in a certified standard of urine

Certified urine standard (SRM 2670, National Institute of Standards & Technology) was reconstituted with 20.00 ml of deionized water and treated as described by Watanabe et al. [26]. The manganese concentration was determined by FAAS after the preconcentration step, using an analytical curve.

2.5.3. Determination of manganese in a certified standard of glass

Certified glass standards (SRM 610 and SRM 612, National Institute of Standards & Technology) were ground in an agate mortar and treated as described by Welz [27]. The final solution was passed through the column and the manganese concentration was determined by FAAS, using the analytical curve.

3. Results and discussion

3.1. Column system for liquid–solid adsorption

The column system shown in Fig. 1 was developed considering parameters such as speed, simplicity, efficiency and sensitivity. A 4 mm inner diameter for the column was established, taking into account the contact surface between the complexing mixture and the analyte, and considering that the adsorption efficiency diminished with larger inner diameters.

The PAN:naphthalene stoichiometric ratio was evaluated from 3 to 10% (w/w) and, since the results were very similar for Mn determination, the value of 3% was chosen. The particle size of the mixture was 100–200 mesh and a final volume of 10.0 ml of DMF was enough for complete dissolution of 200–400 mg of the sorption mixture. After definition of these parameters, a set of 20 columns was mounted, allowing a large number of extractions in a short time. Another advantage of the present system is that the dissolution of the column content does not need to be done right after the passage of the solution. The material containing the metal complex did not undergo any changes, even after 10 days of storage.

3.2. Study of adsorption efficiency of PAN on naphthalene

The adsorption of PAN on naphthalene is fast and simple, occurring upon contact between the PAN and naphthalene mixture in the acetone water solution. In this work, it was found that 99.6% of PAN adsorbs onto the naphthalene.

3.3. Choice of solvent for dissolving the PAN–Mn(II)–naphthalene system

The choice of an appropriate solvent is one of the factors of great importance when FAAS is used. This choice should consider both the dissolution of the content of the column and the efficiency of the burn processes taking place during the subsequent measurements. In the present work it was observed that DMF is quite adequate to obtain the desired conditions, with the advantage of being simpler and cheaper as well as burning better, without a residue in the flame.

3.4. Effect of complexation flow rate

The flow rate was investigated in the range varying from 0.5 to 2.5 ml min^{-1}. It was found that up to 2.0 ml min^{-1} the flow rate did not affect the adsorption while for higher values the efficiency of the extraction of manganese is reduced to about 90%. A flow rate of 1.0 ml min^{-1} was recommended for convenience.

3.5. Effect of pH

The pH of the aqueous phase is an important factor in solute distribution with accentuated acid–base properties. In liquid–liquid extraction, complete formation and extraction of the Mn(II)–PAN complex occurs between pH 8.8 and 9.7 [28]. The effect of the pH on solid-phase extraction during complex formation was investigated over the range 7.5–11.3. This system involves kinetic parameters that affect the contact time between metal and ligand. The complexing reaction is so fast that it is even possible to note the change in the colour of the mixture from orange (PAN) to violet [Mn(II)–PAN] immediately after contact with the solution. Fig. 2 shows the effect of pH on manganese sorption using the PAN/naphthalene/DMF system. The adsorption of manganese was quantitative in the pH range 8.8–10.8, which is similar to the results reported for liquid–liquid extraction [25].

3.6. Effect of aqueous phase volume

The effect of aqueous phase volume on the adsorption of manganese was studied. Sample volumes of 400 ml containing up to

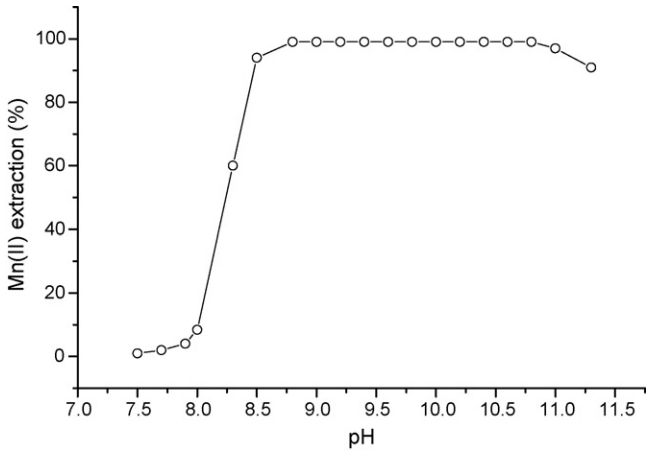


Fig. 2. Effect of pH on the adsorption of Mn(II)–PAN complex.

30.0 μg of manganese might pass through the column without reducing the total metal adsorption. However, volumes higher than 200 ml cause an excessive decrease in the flow rate because naphthalene becomes compacted under vacuum so 200 ml was chosen to obtain maximum effectiveness. A preconcentration factor of 20 is thus possible, considering the passage of 200 ml of sample through the column and its dissolution with 10 ml DMF, thus allowing the determination of manganese at low concentration levels.

3.7. Adsorption capacity of the adsorbent

Considering the stoichiometry of the PAN–naphthalene reaction as 1:2 [11], the amount of complexing reagent present in 200 mg of mixture should complex about 650 μg of the metal. Solutions containing 50–600 μg of manganese were passed through the system and it was observed that the adsorption capacity of the column is 1.5 mg of Mn per gram of adsorbent material, which means half of the stoichiometric quantity. This represents an advantage related to liquid–liquid extraction, which generally uses 10- or 20-fold excess of the complexing reagent.

3.8. Effect of diverse ions

It is well known that manganese determination is affected by some metallic ions when PAN is used as a colorimetric reagent in a liquid–liquid extraction, due to its high reactivity. Species such as Cd(II), Ni(II), Zn(II), Hg(II), Pb(II) and Co(II) could significantly influence the retention of manganese, reducing the retention capacity of the column.

Samples containing 30 μg of manganese and various amounts of different metal ions were prepared and the determination of Mn(II) was carried out by the described procedure. It was observed that only Zn(II) and Co(II) can affect the extraction of Mn(II) when they are present in an excess of more than 10 times that of the manganese. However, 30 μg of Mn(II) in the presence of a mixture containing 50 μg of each of the following ions, Cd(II), Hg(II), Ni(II), Co(II), Zn(II) and Pb(II), resulted in a recovery factor better than 99%.

Table 1
Results for manganese in urine (SRM 2670) and in glass (SRM 610 and 612)

Sample	Reference/certified value (μg ml^{-1})	Found values (μg ml^{-1})
SRM 2670	0.33	0.30; 0.31
SRM 610	485 ± 10	478; 480
SRM 612	39.6 ± 0.8	40.6; 41.6

Table 2
Manganese in waters from Unicamp Lake (100.0 ml) and Taquaral Lake (200.0 ml) using the proposed method, compared to results for GFAAS (n = 3)

Sample	Mn(II) (ng ml^{-1})	
	Proposed method, flame-AAS	GF-AAS
Unicamp Lake 1	45 ± 3	47.1 ± 2.1
Unicamp Lake 2	97 ± 4	99.5 ± 1.2
Taquaral	9.3 ± 0.5	9.5 ± 0.3

The presence of anions such as nitrate, sulphate, chloride, fluoride and cyanide did not affect the extraction of the manganese, even at a 300 times excess.

3.9. Accuracy and sensitivity

In order to evaluate the accuracy of the proposed method, manganese was determined in certified urine and glass materials. The results presented in Table 1 are in good agreement, showing that the proposed method might be used for Mn determination, even at low concentrations.

Considering that it is possible to retain 1 μg Mn from 200 ml of solution passing through the column, the dissolution with 10.00 ml DMF gives a limit of quantification of 5 ng ml^{-1}. A precision of 3.8% (R.S.D.) was calculated.

3.10. Determination of manganese in water

The method has been applied for determination of manganese in water. The results for the water of two lakes, Taquaral and Unicamp, are given in Table 2, and are comparable to the results obtained using GFAAS.

4. Conclusions

The proposed method for solid phase extraction is convenient, simple, sensitive and highly economic. An additional advantage is the fact that the complexing mixture does not need to be dissolved immediately after its formation, being stable for a significant time period. A preconcentration factor of 20 and a quantification limit of 5 ng ml^{-1} Mn were obtained with a precision of 3.8%. The percentage error between the values of certified samples and those obtained by the proposed method are of the order of 6%. In these conditions it was possible to determine manganese in different kind of samples at concentrations as low as 5 ng ml^{-1}.

Acknowledgements

The authors thank Carol H. Collins for assistance with the English manuscript. Fellowships from the Conselho Nacional de Desenvolvimento Científico e Tecnológico (CNPq) for A.P.A. and L.C.P. are also gratefully acknowledged.

References

[1] D.L. Tsalev, Z.K. Zaprianov, Atomic Absorption Spectrometry in Occupational and Environmental Health Practice, vol. 1, CRC Press Inc., Boca Raton, 1984, p. 153.
[2] J. Minczewski, J. Chwastowska, P. Dybczynski, Separation and Preconcentration Methods in Inorganic Trace Analysis, Ellis Horwood Ltd., New York, 1982, p. 97.
[3] M. Satake, B.K. Puri, S. Usami, Anal. Chim. Acta 199 (1987) 209.
[4] T. Nagahiro, K. Uesugi, M. Satake, Analusis 16 (1988) 120.
[5] T. Fujinaga, T. Kuwamoto, E. Nakayama, Talanta 16 (1969) 1225.
[6] M. Satake, Y. Matsumura, T. Fujinaga, Talanta 25 (1978) 718.
[7] G.G. Bortoleto, G.T. Macarovscha, S. Cadore, J. Braz. Chem. Soc. 15 (2004) 313.
[8] G. Giraudi, C. Pari, E. Mentasti, Ann. Chim. 74 (1984) 307.
[9] P. Bermejo-Barrera, M.A. Nancy, D.L. Cristina, B.B. Adela, Microchim. Acta 142 (2003) 101.
[10] S. Cadore, R.D. Goi, N. Baccan, J. Braz. Chem. Soc. 16 (5) (2005) 957–962.
[11] S. Shibata, 2-Pyridylazo compounds in analytical chemistry, in: H.A. Flaschka, A.J. Barnard (Eds.), Chelates in Analytical Chemistry, vol. 4, Marcel Dekker Inc., New York, 1972.
[12] K.L. Cheng, R.H. Bray, Anal. Chem. 27 (1975) 782.
[13] N. Bahramifar, Y. Yamini, Anal. Chim. Acta 540 (2005) 325.
[14] I. Narin, M. Soylak, Talanta 60 (2003) 215.
[15] M.P. Maloney, G.J. Moody, J.D.R. Thomas, Analyst 105 (1980) 1087.
[16] T. Braun, M.N. Abbas, Anal. Chim. Acta 119 (1980) 639.
[17] M.A. Taher, S. Puri, R.K. Bansal, B.K. Puri, Talanta 45 (1997) 411.
[18] M.A. Taher, Croat. Chem. Acta 76 (2003) 273.
[19] M. Behpour, S.M. Ghoreishi, S. Salehi, Acta Chim. Slov. 52 (2005) 323.
[20] M. Satake, B.K. Puri, S. Usami, Anal. Chem. 58 (1986) 2002.
[21] M.A. Taher, S. Puri, M.K. Gupta, B.K. Puri, Ind. J. Chem. Technol. 5 (1998) 321.
[22] M.A. Taher, Ann. Chim. 94 (2004) 437.
[23] M.A. Taher, S. Puri, A. Bhalotra, B.K. Puri, Quim. Anal. 18 (1999) 181.
[24] M.A. Taher, B.K. Puri, Iran J. Chem. Chem. Eng. 18 (1999) 6.
[25] A.K. Malik, V. Sharma, V.K. Sharma, J. Agric. Food Chem. 52 (2004) 7763.
[26] T. Watanabe, H. Nakatsuka, M. Ohashi, M. Ikeda, Sci. Tot. Environ. 79 (1989) 85.
[27] B. Welz, Atomic Absorption Spectrometry, 2nd ed., Wiley-VCH, Weinheim, 1985, p. 416.
[28] E.M. Donaldson, W.R. Inman, Talanta 13 (1966) 489.

Available online at www.sciencedirect.com
ScienceDirect
Talanta 71 (2007) 1257–1262
Talanta
www.elsevier.com/locate/talanta

Reagentless amperometric carbohydrate antigen 19-9 immunosensor based on direct electrochemistry of immobilized horseradish peroxidase

Du Dan [a,*], Xu Xiaoxing [b], Wang Shengfu [c], Zhang Aidong [a]

[a] *Key Laboratory of Pesticide & Chemical Biology of Ministry of Education, Central China Normal University, Wuhan 430079, PR China*
[b] *Department of Chemistry, Changshu Institute of Technology, Changshu 215500, PR China*
[c] *Ministry-of-Education Key Laboratory for the Synthesis and Application of Organic Functional Molecules, Wuhan 430062, PR China*

Received 8 May 2006; received in revised form 20 June 2006; accepted 20 June 2006
Available online 4 August 2006

Abstract

A reagentless immunosensor for rapid determination of carbohydrate antigen 19-9 (CA19-9) in human serum was proposed. This strategy was based on the immobilization of antibody in colloidal gold nanoparticle modified carbon paste electrode and the direct electrochemistry of horseradish peroxidase (HRP) that was labeled to a CA19-9 antibody. The nanoparticles were efficient for preserving the activity of immobilized biomolecules. Thus, the immobilized HRP displayed its direct electrochemistry with a rate constant of 1.02 s^{-1}. The incubation of the immunosensor in phosphate buffer solution (PBS) including CA19-9 antigen leading to the formation of antigen–antibody complex, which made the block of electron transfer of HRP toward electrode and resulted in significant peak current decrease of HRP. Under the optimal conditions, the current decrease was proportional to CA19-9 concentrations ranging from 2 to 30 U/ml with a detection limit of 1.37 U/ml at a current decrease by 10%. The immunosensor showed an acceptable accuracy compared with those obtained from immunoradiometric assays, with intra-assay coefficient of 7.3 and 6.9% at CA19-9 concentrations of 5 and 15 U/ml, respectively, and inter-assay coefficient of 9.6% at a CA19-9 concentration of 20 U/ml. The storage stability was acceptable in a pH 7.0 PBS at 4 °C for 10 days. This method avoids the addition of electron transfer mediator, thus simplifies the immunoassay procedure and decreases the analytical time. It provides a new promising platform for clinical immunoassay.
© 2006 Elsevier B.V. All rights reserved.

Keywords: Immunosensor; Electrochemical sensors; Enzyme labeled antibody; Carbohydrate antigen 19-9 (CA19-9); Colloidal gold nanoparticles

1. Introduction

In the management of cancer patients, tumor-associated antigens in serum have been used in clinical evaluations and non-invasive tests for relapse detection [1]. Carbohydrate antigen 19-9 (CA19-9) is one of the most important carbohydrate tumor markers, expressed in many malignancies. The determination of serum CA19-9 levels is of great importance for clinical diagnoses of pancreatic [2], colorectal [3], gastric [4] and hepatic carcinomas [5]. Although radioimmunoassay (RIA) and enzyme immunoassay (EIA) were successful for the determination of CA19-9, there involved complicated, tedious assay processes, time-consuming and specially equipped laboratories and/or skilful technology. Electrochemical immunosensors avoid these disadvantages and combine simple, portable, low-cost electrochemical measurement systems with specific and sensitive immunoassay procedures. This technique has attracted considerable interest and been applied to many fields such as clinical diagnosis [6,7], environmental pollutants detection [8] and biochemical analyses [9,10].

Generally, electrochemical immunosensors are prepared by immobilizing various kinds of antibody or antigen on the electrode surface, and the analytes are measured through the changes of potential, current, conductance or impedance caused by antigen-antibody immunoreaction. Many substrates or mediators such as horseradish peroxidase [11], alkaline phosphatase [12,13] and glucose oxidase [14] have been extensively used to improve the sensitivity of immunoassays. Correspondingly, some substrates such as H_2O_2 or O_2, naphthyl phosphate or *p*-aminophenol phosphate, O_2 or ferrocene and glucose or O_2 are needed in the test solutions for horseradish peroxidase (HRP), alkaline phosphatase, laccase and glucose oxidase, respectively. The addition of substrates or mediators to the analyte solution caused the immunoassay system more complex, and increased

* Corresponding author. Tel.: +86 27 67863 324.
E-mail address: dudan@mail.ccnu.edu.cn (D. Du).

0039-9140/$ – see front matter © 2006 Elsevier B.V. All rights reserved.
doi:10.1016/j.talanta.2006.06.028

the analysis time and reagents and sometimes even limited the immunoassay. Thus to get rid of mediators and reagents is highly desirable [15].

In the earlier study, some papers about developing mediatorless immunoassay have been reported [16–20]. Recently, one of the approaches of mediatorless immunoassay was to perform enzyme-channeling assays. Wright et al. [21] described a specific binding assay for biotin, Keay and McNeil [22] developed a separation-free electrochemical immunosensor for determination of atrazine. On the other hand, it has been proved that formation of a complex between the enzyme-labled antibody and antigen on the electrode surface resulted in a considerable shift in electrode potential due to the catalytic reduction of overvoltage. Application of this potential shift was also used to develop mediatorless immunoassay system [23].

The direct electrochemistry of the HRP has already been studied [24]. Recently, Dai et al. have reported a novel strategy for preparation of a reagentless carcinoma antigen-125 (CA125) immunosensor, which was actually based on the immobilization of antigen and the direct electrochemistry of HRP that was labeled to an antibody [25]. In addition, Chen et al. [26] have presented a reagentless immunoassay for chorionic gonadotrophin (hCG) based on the direct electron transfer of the immobilized HRP, which was labeled to hCG antibody. Since colloidal particles were used for immobilization of biomolecules [27], colloidal gold nanoparticles have been extensively used as a matrix and cytochemical label for the immobilization and study of cells [28,29] protein [30], enzyme [31] and antibodies [32]. This work proposed a simple and fast reagentless immunosensor for CA19-9 determination based on the immobilization of CA19-9 antibody in colloidal gold nanoparticle modified carbon paste electrode and the direct electrochemistry of HRP that was labeled to a CA19-9 antibody. The incubation of the immunosensor with CA19-9 solution resulted in the formation of an immunocomplex, which made the block of electron transfer of HRP toward electrode and resulted in significant peak current decrease of HRP. Due to the decrease of peak current, the detection of CA19-9 in serum samples obtained from clinically diagnosed patients with pancreatic carcinoma showed acceptable accuracy in comparison with the results obtained by immunoradiometric assay (IRMA). This presented method avoids the trouble of adding mediator to the sample solution and the pollution of some mediators to the electrode systems, which shows a potentially attractive for clinical immunoassay.

2. Experimental

2.1. Reagents

CA19-9 ELISA kits were purchased from Diagnostic Products (DPC, USA). The ELISA kits consisted of a series of CA19-9 standard solutions with different concentrations from 0 to 240 U/ml and a stock solution of HRP labeled CA19-9 specific antibody from goat. $AuCl_3HCl{\cdot}4H_2O$ (Au >48%) was obtained from Aldrich. Carbon graphite powder (<325 mesh, Johnson Matthey) and paraffin oil (from Fluka) were used for the preparation of carbon paste. Colloidal gold nanoparticles were prepared by adding 0.5 ml of 1% Na_3citrate solution to a boiling 50 ml solution of 0.01% $HAuCl_4$. Prior to use, $HAuCl_4$ and Na_3citrate aqueous solutions were filtered through a 22 μm microporous membrane filter and all glassware used in this procedure was cleaned in freshly prepared 3:1 HNO_3–HCl and then rinsed thoroughly in twice-distilled water. The mixture was maintained at boiling point for 15 min and stirred for another 15 min after removing the heating source to produce 24 nm-diameter colloidal gold particles. All other reagents were of analytical grade. All solutions were made up with double distilled water of 18 MΩ purified from a Milli-Q purification system. The serum samples were separated by centrifugation from blood, which was obtained from clinically diagnosed patients.

2.2. Apparatus

Electrochemical measurements were performed on a CHI 660 electrochemical analyzer (Co. CHI, USA) with a conventional three-electrode system comprising platinum wire as auxiliary electrode, saturated calomel electrode (SCE) as reference and HRP labeled CA19-9 antibody-colloidal gold modified carbon paste electrodes (HPR-CA19-9/Au–CPE) as working electrode. AC impedance experiments were carried out in 0.1 mM $K_3Fe(CN)_6{}^{3-}/K_4Fe(CN)_6{}^{4-}$ solution. The IRMA procedure was carried out with FMJ-182 Immunoradiometric Gramma Counter (China) according to the instructions in the operator's manual.

2.3. Preparation of CA19-9 immunosensor

The HPR–CA19-9/Au–CPE was prepared according to the following procedure. Prior to use, the graphite powder was treated at 700 °C for 30 s in a muffle furnace and then cooled to room temperature in a desiccator in the presence of activated silica gel. A 10 mg of graphite powder was mixed with 30 μl 24 nm colloidal gold solution and 30 μl HRP labeled CA19-9 antibody. After evaporation of water in a desiccator for 3 h, 3.6 μl paraffin oil was added to the mixture. A portion of the resulting paste was put into plastic syringe tube with the inner diameter of 0.60 mm to form a HPR–CA19-9/Au–CPE. Electrical contact to the paste was established by inserting a copper wire down the plastic syringe tube and into the back of mixture. The electrode was stored at 4 °C prior to use. After the electrode tip was gently rubbed on a fine paper to produce a flat surface, following experiments were carried out.

2.4. Measurement procedure

For the measurement of CA19-9, the HPR–CA19-9/Au–CPE was incubated in 1.0 ml CA19-9 antigen solution of different concentrations at 30 °C for 50 min to form HPR–CA19-9 complex/Au–CPE and then washed carefully with water. The formation of antigen–antibody complex made the block of electron transfer of HRP toward electrode and resulted in significant peak current decrease of HRP. The HPR–CA19-9/Au–CPE and HRP–CA19-9 complex/Au–CPE were immersed in the electrochemical cell to study the electrochemical response using cyclic

voltammetry (CV) and differential pulse voltammetry (DPV). All electrochemical measurements were done in an unstirred electrochemical cell. The DPV measurements were performed from +0.3 to −0.7 V with the pulse amplitude of 50 mV and the pulse width of 50 ms. AC frequency region was from 100 kHz to 0.01 Hz in 0.1 mM $Fe(CN)_6^{3-/4-}$ solution. The real area of the working electrode was determined by the slope of plot of the anodic peak current of 1.0 mM $K_3[Fe(CN)_6]$ in 0.1 M KCl versus the square root of scan rate to be 1.8×10^{-3} cm^2. All experimental solutions were deaerated by high purity nitrogen for 5 min and a nitrogen atmosphere was maintained over the solutions during the measurements.

3. Results and discussion

3.1. Cyclic voltammetric behavior of HPR–CA19-9/Au–CPE

Fig. 1 showed the cyclic voltammograms of Au–CPE (a), CPE (b), HPR–CA19-9/Au–CPE (c), HPR–CA19-9/CPE (d) and HPR–CA19-9 complex/Au–CPE (e) in the potential range from −0.7 to 0.3 V in pH 7.0 PBS. No peak was observed at both Au–CPE (curve a) and CPE (curve b). The presence of colloidal gold resulted in much lower background current. After immobilizing HRP labeled CA19-9 antibody, a pair of stable and well defined redox peaks was observed with regard to Fe (III) to Fe (II) conversion of the immobilized HRP. The anodic and cathodic peak potentials were −0.087 and −0.335 V (versus SCE) at 50 mV/s, respectively, with the formal potential of −0.211 V (curve c). Both the anodic and cathodic peak currents were proportional to the scan rate in the range from 5 to 300 mV/s (Fig. 2). From the peak-to-peak separations at different scare rates, an average electron transfer rate constant of 1.02 s^{-1} was obtained [33]. When HRP labeled CA19-9 antibody was mixed with carbon paste without the presence of colloidal gold nanoparticles, the HPR–CA19-9/CPE also showed the response of HRP (curve d in Fig. 1). Thus, carbon microparticle was an important factor for the direct electron transfer of HRP. However, the response of HPR–CA19-9/CPE was much smaller than that of HPR–CA19-9/Au–CPE, indicating that colloidal gold nanoparticles played an important role in making the active center of HRP to be exposed and facilitating the electron exchange between the HRP and electrode. After the obtained HPR–CA19-9/Au–CPE was immersed in 0.1 mM pH 7.0 PBS containing 15 U/ml CA19-9 antigen for incubation at 30 °C for 50 min, the cyclic voltammetric curve showed a couple of poor peaks with dramatically decreased peak current and increased peak-to-peak separation (curve e in Fig. 1). This was attributed to the formation of bulky antigen–antibody complex with high molar mass, which blocked the electron transfer of HRP towards the electrode. In order to obtain a high sensitivity, the decreased peak current recorded by DPV was used to detect the concentration of CA19-9 by this immunosensor.

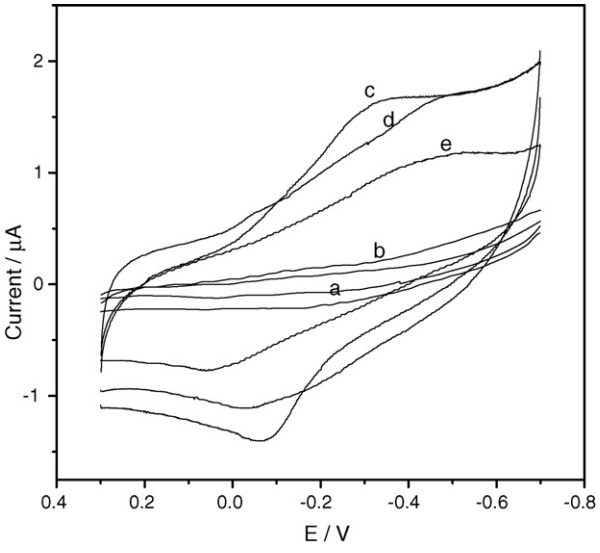


Fig. 1. Cyclic voltammograms of different electrodes in pH 7.0 PBS at 50 mV/s. (a) Au–CPE, (b) CPE, (c) HPR–CA19-9/Au–CPE, (d) HPR–CA19-9/CPE and (e) HPR–CA19-9 complex/Au–CPE.

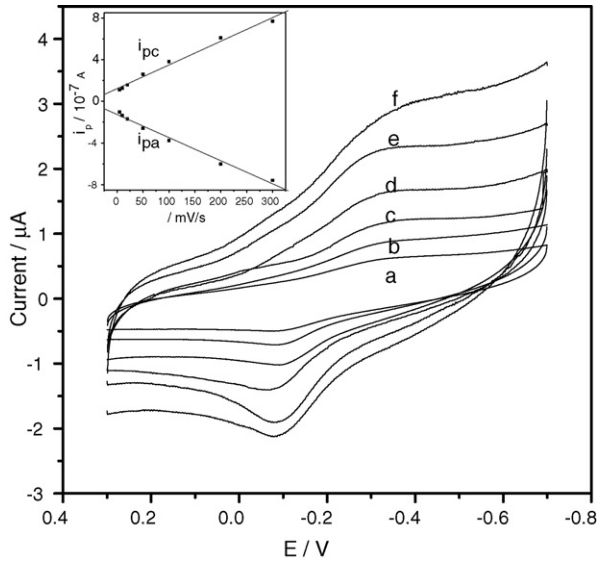


Fig. 2. Cyclic voltammograms of CA19-9 immunosensor at different scan rates in pH 7.0 PBS. The scan rates are (a) 5 mV/s, (b) 20 mV/s, (c) 50 mV/s, (d) 100 mV/s, (e) 200 mV/s and (f) 300 mV/s, respectively. *Inset*: plots of peak currents vs. scan rates.

3.2. AC impedance spectroscopy

The relationship between antigen concentration and the extent of the electrode insulation could also be shown in the charge-transfer resistance and the capacitance of AC impedance spectroscopy. Fig. 3 displayed the AC impedance spectroscopy on variable CA19-9 antigen concentrations. The association of antigen to the antibody resulted in the electrode insulation increasing towards the $Fe(CN)_6^{3-/4-}$ redox probe. The formation of stable antigen–antibody complex increased the charge-transfer resistance (R_{ct}). With the incubating CA19-9 concentrations at 0, 10, 20 and 30 U/ml, the R_{ct} of HPR–CA19-9/Au–CPE was induced to be 16578Ω, 20964Ω, 24118Ω and

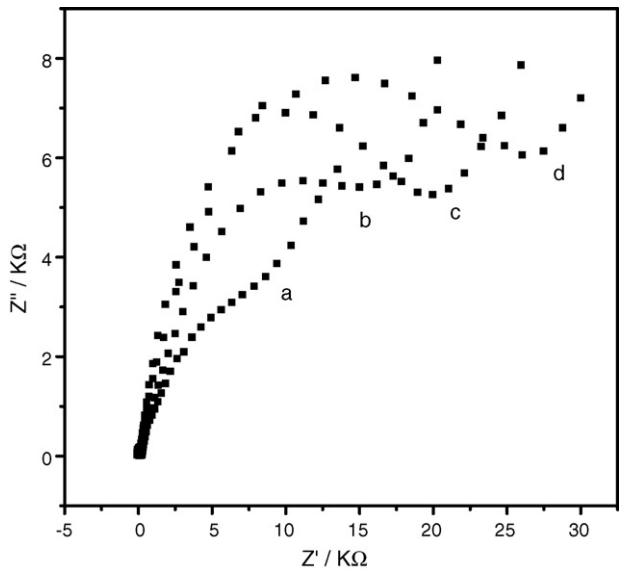


Fig. 3. The AC impedance spectroscopy of HPR–CA19-9/Au–CPE after incubated in CA19-9 solutions with variable concentrations. The CA19-9 concentrations in the incubation solution are (a) 0 U/ml, (b) 10 U/ml, (c) 20 U/ml and (d) 30 U/ml, respectively.

32477Ω, respectively. The further incubation resulted in much more increase in R_{ct}. This result implied the formation of antigen–antibody complex, which blocked the electron transfer of HRP due to the increase of the electrode interface resistance.

3.3. Optimization of immunosensor preparation

It was reported that small-sized colloidal gold (24 nm) provided more binding sites than large-sited colloidal gold (42 nm) and the optimal response occurred at the colloidal gold volume of 3 μl/mg carbon powder [34]. The amount of HRP labeled CA19-9 antibody immobilized in the colloidal gold carbon paste electrode greatly affected the direct electrochemistry of HRP and satisfactory preparation of the immunosensor. The effect of HRP labeled CA19-9 antibody content in carbon paste on the DPV peak current was shown in Fig. 4A. With increasing volumes of HRP labeled CA19-9 antibody solution added in the carbon paste, the HRP response increased, indicating that the colloidal gold particles facilitated the electron transfer between HRP and electrode. After the content was more than 3 μl in per milligram carbon powder, the HRP response decreased with the increasing of HRP labeled CA19-9 antibody solution. This phenomenon was attributed to the increase in the resistance and double layer capacitance of the electrode because of the decrease of ratio of carbon sensing sites in the paste. A maximum response occurred at the HRP labeled CA19-9 antibody solution of 3 μl in per milligram carbon powder.

3.4. Optimization of immunoassay conditions

The relationship between the DPV peak current of the HPR–CA19-9/Au–CPE and the pH indicated that the maximum response was at pH 7.0 (Fig. 4B). The same result was

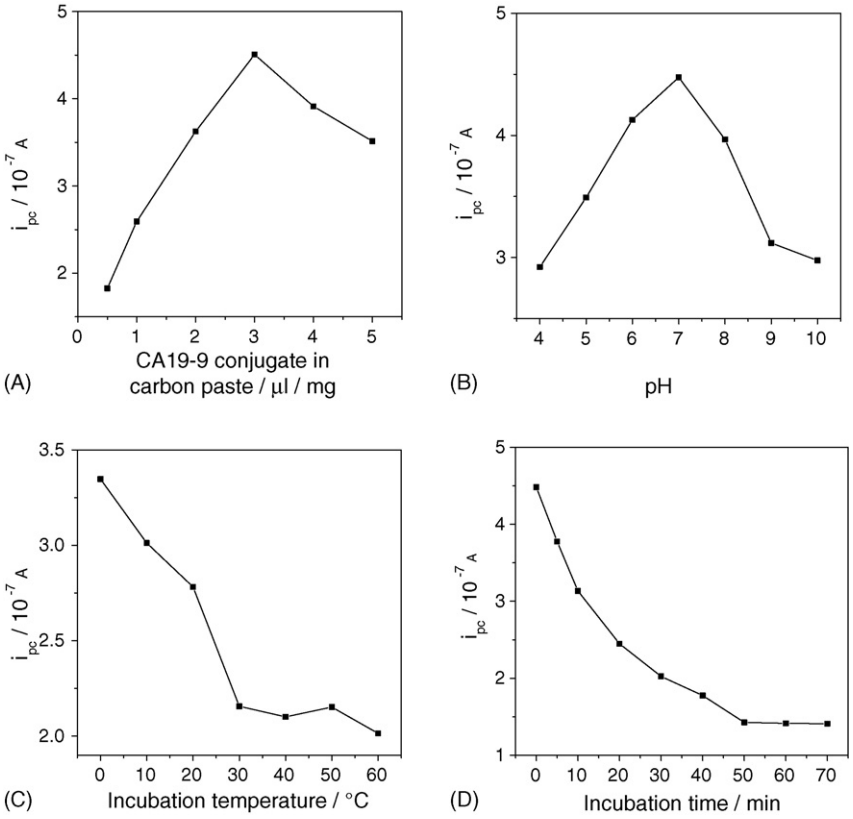


Fig. 4. (A) Effect of the content of HRP labeled CA19-9 antibody in carbon paste on the DPV peak current. (B) Effect of pH on the immunoassay. (C) Effect of incubation temperature on immunological reaction at immunosensor. (D) Effect of incubation time on immunological reaction at immunosensor.

also observed for soluble HRP [35], indicating that the Au–CPE matrix did not alter the optimal pH for electron transfer of immobilized HRP. Furthermore, this value was close to incubation pH usually used for the binding between antigen and antibody [6]. In order to provide uniform status, pH 7.0 PBS was selected for immunoassay and immunoreaction.

Other factors that influenced the immunoreaction between the immobilized HRP labeled CA19-9 antibody and CA19-9 in solution included the incubation temperature and incubation time. The effects of incubation temperature and incubation time on the DPV peak current were studied. Over a temperature range from 0 to 30 °C, the response of HPR–CA19-9 complex/Au–CPE decreased rapidly and did not change much more after 30 °C (Fig. 4C). The lower response at the incubation temperatures higher than 50 °C might be attributed to the low activity of the bound enzyme during incubation process [25]. Thus 30 °C was selected for incubation temperature. With increasing incubation time, the peak current decreased and tended to a steady state after 50 min (Fig. 4D). Longer incubation time was not necessary. Therefore, the optimal incubation conditions were 0.1 mM pH 7.0 PBS at 30 °C for 50 min.

3.5. Electrochemical detection of the immunosensor to CA19-9 concentration

The electrochemical detection of CA19-9 antigen was based on the block of electron transfer of immobilized HRP, which was controlled by the formation of antigen–antibody complex in the HPR–CA19-9/Au–CPE. The standard solution of CA19-9 at a known concentration or one serum sample was added to the incubation solution. The CA19-9 in the solution combined with the immobilized HPR–CA19-9/Au–CPE. The DPV cathodal peak current of the immobilized HRP showed a decrease with increasing CA19-9 concentrations in the incubation solution (Fig. 5A). The decrease in peak current was proportional to the CA19-9 concentration over the range of 2–30 U/ml with a correlation coefficient of 0.9911 and a linear slope of (0.0904 ± 0.017) μA U/ml (inset in Fig. 5A). The detection limit was calculated to be 1.37 U/ml taken as the concentration equivalent to a 10% decrease in signal [36]. Higher serum CA19-9 levels could be detected with an appropriate dilution.

Table 1
Comparison of serum CA19-9 levels determined using two methods[a]

Serum samples	Immunosensor (U/ml, %)	IRMA (U/ml, %)	Relative deviation (%)
1	5.0 ± 9	5.8 ± 8	−13.8
2	8.3 ± 7	8.9 ± 7	−6.7
3	14.7 ± 6	16.0 ± 6	−8.1
4	18.9 ± 6	17.7 ± 6	6.8
5	20.2 ± 6	19.3 ± 5	4.7
6	27.0 ± 5	30.2 ± 5	−10.6
7	28.1 ± 5	30.1 ± 4	−6.6
8	29.3 ± 5	27.4 ± 5	6.9
9	56.4 ± 4	62.2 ± 4	−9.3
10	153.2 ± 2	137.3 ± 3	11.6

[a] The reported data were based on six independent measurements. Uncertainties represent one standard deviation from the mean.

3.6. Selectivity and application of CA19-9 immunosensor

Because of the expression of other antigens such as CA125, carcinoembryonic antigen (CEA) in many gastrointestinal malignancies including pancreatic, colorectal, gastric and hepatic carcinomas, it was important to examine the selectivity of CA19-9 immunosensor. When the incubation solution contained 10 U/ml CA125, 10 U/ml CEA and 10 U/ml CA19-9, no obvious difference in current was observable in comparison with the result obtained in the presence of CA19-9 alone (Fig. 5B). An increase in CA125 and CEA concentration did not lead to a significant change in current. Thus, the immunosensor had a good selectivity to CA19-9.

After serum samples were diluted with the appropriate volumes of dilution solution, serum CA19-9 concentrations were detected from DPV peak currents of the CA19-9 immunosensor. In parallel, the CA19-9 concentrations were also detected with IRMA. The results were shown in Table 1. The relative deviations between the two methods were in the range

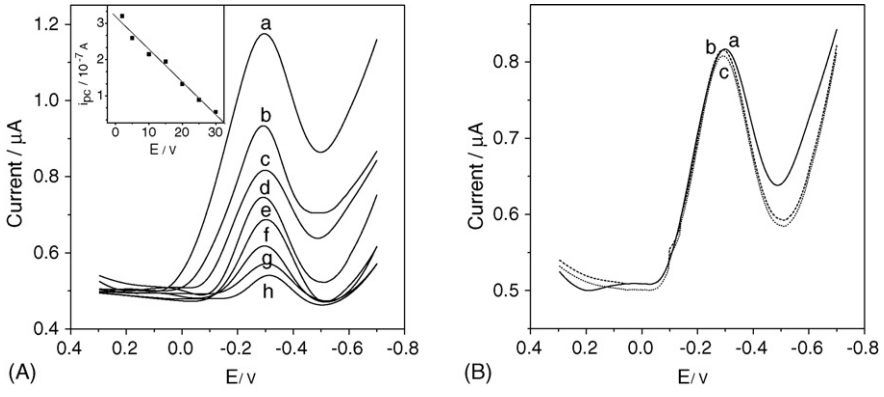


Fig. 5. Differential pulse voltammograms of CA19-9 immunosensors. (A) After incubated in CA19-9 solutions with variable concentrations of (a) 0 U/ml, (b) 2.0 U/ml, (c) 5.0 U/ml, (d) 8.0 U/ml, (e) 14.0 U/ml, (f) 20.0 U/ml, (g) 30.0 U/ml and (h) 40.0 U/ml, respectively, at 30 °C for 50 min in pH 7.0 PBS. *Inset*: Calibration for the CA19-9 determination. (B) After incubated in 10.0 U/ml CA19-9 solutions containing different other antigens. (a) 0 U/ml, (b) 10 U/ml CA125 and (c) 10 U/ml CEA.

of −13.8–11.6%, indicating an acceptable agreement. Thus, the immunosensor could be satisfactorily applied to the clinical determination of CA19-9 levels in pancreatic cancer samples.

3.7. Reproducibility and stability of the CA19-9 immunosensor

The intra-assay precision of the immunosensors was evaluated by assaying the CA19-9 levels of two sera for five replicate measurements in the same run. The intra-assay coefficients of variation with this method were 7.3 and 6.9% at CA19-9 concentrations of 5 and 15 U/ml, respectively. The inter-assay precision, or fabrication reproducibility, was estimated by determining in duplicate the CA19-9 level in one serum sample using five immunosensors made independently at the same electrode. The inter-assay precision was 9.6% at a CA19-9 concentration of 20 U/ml and indicating an acceptable reproducibility.

When the HPR–CA19-9/Au–CPE was not in use, it was stored in the refrigerator at 4 °C. The peak current of the HPR–CA19-9/Au–CPE was tested in pH 7.0 PBS everyday. It decreased gradually and retained 90% of its initial current after 10 days storage. The colloidal gold provided a biocompatible microenvironment around the biological molecule and essentially stabilized its biological activity. Furthermore, it was very efficient for facilitating the direct electron transfer between HRP and electrode.

4. Conclusions

The complex of antibody and antigen was a high molar mass entity and hence the block of electron transfer of redox probe toward electrode was enhanced. The extent of electrode insulation was controlled by the antigen concentration in the sample and the time of incubation. In this article, we studied the relationship between antigen concentration and the extent of the electrode insulation under a fixed time of incubation and proposed a novel reagentless immunosensor for CA19-9 determination based on the direct electrochemistry of HRP labeled on CA19-9 antibody. The immunosensor showed acceptable precision, reproducibility and storage stability. In comparison with the conventional IRMA approaches, this proposed method is simpler and rapid, thus provides a new promising platform for clinical immunoassay. This kind of bioelectrode could be applied as an electrochemical-sensing device for the antigen.

Acknowledgements

The authors are gratefully acknowledging the financial support of the Natural Science Foundation of Hubei Province (No. 2006ABA183), the Natural Science Foundation of Hubei Province Education Department (No. 2004D005) and the Key Laboratory of Pesticide & Chemical Biology of Ministry of Education, Central China Normal University.

References

[1] H. Magdelenat, J. Immunol. Methods 150 (1992) 133.
[2] N. Tanaka, S. Okada, H. Ueno, T. Okusaka, M. Ikeda, Pancreas 20 (2000) 378.
[3] T. Nakayama, M. Watanabe, T. Teramoto, M. Kitajima, Anticancer Res. 17 (1997) 1379.
[4] M. Kochi, M. Fujii, N. Kanamori, T. Kaiga, T. Kawakami, K. Aizaki, M. Kasahara, F. Mochizuki, Y. Kasakura, M. Yamagata, Gastric Cancer 3 (2000) 177.
[5] T. Uenishi, S. Kubo, K. Hirohashi, H. Tanaka, T. Shuto, T. Yamamoto, S. Nishiguch, Br. J. Cancer 88 (2003) 1894.
[6] D. Du, F. Yan, S.L. Liu, H.X. Ju, J. Immunol. Methods 283 (2003) 67.
[7] A. Clerico, S. Del Ry, D. Giannessi, Clin. Chem. 46 (2000) 1529.
[8] W. Vastarella, R. Nicastri, Talanta 66 (2005) 627.
[9] S.H. AlarcÃÃn, G. Palleschi, D. Compagnone, M. Pascale, A. Visconti, Talanta 69 (2006) 1031.
[10] F. Sellrie, J.A. Schenk, O. Behrsing, V. Böttger, B. Micheel, J. Immunol. Methods 261 (2002) 141.
[11] E. Salinas, A.A.J. Torriero, M.I. Sanz, F. Battaglini, J. Raba, Talanta 66 (2005) 92.
[12] M. Másson, Ö.V. Rúnarsson, F. Jóhannson, Talanta 64 (2004) 174.
[13] P. Fanjul-Bolado, M.B. González-García, A. Costa-García, Talanta 64 (2004) 452.
[14] T. Ruzgas, E. Csöregi, J. Emnéus, L. Gorton, G. Marko-Varga, Anal. Chim. Acta 330 (1996) 123.
[15] B.A. Kuznetsov, G.P. Shumakovich, O.V. Koroleva, A.I. Yaropolov, Biosens. Bioelectron. 16 (2001) 73.
[16] D.J. Litman, T.M. Hanlon, E.F. Ullman, Anal. Biochem. 106 (1980) 223.
[17] S.D. Varfolomeev, I.N. Kurochkin, A.I. Yaropolov, Biosens. Bioelectron. 11 (1996) 863.
[18] A.L. Ghindilis, O.V. Skorobogat'ko, V.P. Gavrilova, A.I. Yaropolov, Biosens. Bioelectron. 7 (1992) 301.
[19] C.A. Galán-Vidal, J. Muñoz, C. Domínguez, S. Alegret, Sens. Actuator B-Chem. 45 (1997) 55.
[20] T. Lötzbeyer, W. Schuhmann, Bioelectrochem. Bioenergy 42 (1997) 1.
[21] J.D. Wright, K.M. Rawson, W.O. Ho, D. Athey, C.J. McNeil, Biosens. Bioelectron. 10 (1995) 495.
[22] R.W. Keay, C.J. McNeil, Biosens. Bioelectron. 13 (1998) 963.
[23] A.L. Ghindilis, O.V. Skorobogat'ko, V.P. Gavrilova, A.I. Yaropolov, Biosens. Bioelectron. 7 (1992) 301.
[24] S.S. Rosatto, L.T. Kubota, G. Oliveira Neto, Anal. Chim. Acta 390 (1999) 65.
[25] Z. Dai, F. Yan, J. Chen, H.X. Ju, Anal. Chem. 75 (2003) 5429.
[26] J. Chen, J. Tang, F. Yan, H.X. Ju, Biomaterials 27 (2006) 2313.
[27] A. Rembaum, W.J. Dreyer, Science 208 (1980) 364.
[28] D. Du, H.X. Ju, X.J. Zhang, J. Chen, J. Cai, H.Y. Chen, Biochemistry 44 (2005) 11539.
[29] D. Du, S.L. Liu, J. Chen, H.X. Ju, H.Z. Lian, J.X. Li, Biomaterials 26 (2005) 6487.
[30] K.R. Brown, A.P. Fox, M.J. Natan, J Am. Chem. Soc. 118 (1996) 1154.
[31] S.Q. Hu, J.W. Xie, Q.H. Xu, K.T. Rong, G.L. Shen, R.Q. Yu, Talanta 61 (2003) 769.
[32] O.D. Velev, E.W. Kaler, Langmuir 15 (1999) 3693.
[33] E. Laviron, J. Electroanal. Chem. 101 (1979) 19.
[34] S.Q. Liu, H.X. Ju, Anal. Biochem. 307 (2002) 110.
[35] H.A. Harbury, J. Biol. Chem. 225 (1957) 1009.
[36] R.W. Keay, C.J. McNeil, Biosens. Bioelectron. 13 (1998) 963.

Available online at www.sciencedirect.com
ScienceDirect
Talanta 71 (2007) 1011–1015
Talanta
www.elsevier.com/locate/talanta

Particle isolation for analysis of uranium minor isotopes in individual particles by secondary ion mass spectrometry

F. Esaka *, K.T. Esaka, C.G. Lee, M. Magara, S. Sakurai, S. Usuda, K. Watanabe

Research Group for Analytical Science, Japan Atomic Energy Agency, Shirakata-Shirane 2-4, Tokai, Naka, Ibaraki 319-1195, Japan

Received 17 April 2006; received in revised form 9 May 2006; accepted 9 May 2006
Available online 10 July 2006

Abstract

A new technique to measure $^{234}U/^{238}U$ and $^{236}U/^{238}U$ isotope ratios for individual particles in environmental samples was developed, which was a combination of particle isolation under scanning electron microscope (SEM) and secondary ion mass spectrometry (SIMS). The technique was verified by measuring $^{234}U/^{238}U$ and $^{236}U/^{238}U$ isotope ratios in individual particles in a simulated environmental sample containing uranium standard (NBL CRM U010) and Pb metal particles. When the uranium particles were not isolated, the relative deviations of the measured isotope ratios from the reference values increased with increasing the signal intensity ratio of ^{208}Pb to ^{238}U, which was due to the molecular ion interferences by the Pb particles co-existing in the sputtered area. By the isolation of individual uranium particles, the interferences were eliminated and the measured isotope ratios were in good agreement with the reference values. The maximum relative deviations among 20 particles were 8.9% for $^{234}U/^{238}U$ and 13.1% for $^{236}U/^{238}U$ isotope ratios, respectively. The technique was also successfully applied to the analysis of a real swipe sample containing various kinds of elements.
© 2006 Elsevier B.V. All rights reserved.

Keywords: Uranium; Isotope ratio; Minor isotopes; Particles; SIMS; SEM; Isolation

1. Introduction

Natural uranium mainly consists of three isotopes: ^{234}U, ^{235}U and ^{238}U with relative isotopic abundances of 0.005, 0.72 and 99.27%, respectively [1]. Another isotope, ^{236}U, is produced by neutron capture of ^{235}U ($^{235}U + {}^{1}n \rightarrow {}^{236}U$) in nuclear reactors. During the process of nuclear fuel cycle, a small amount of particles containing uranium is formed and transported in the environment. The isotope ratios for the particle correspond to those of the material in the process. The determination of the isotope ratios for the particles is, therefore, recognized to be very important, from the viewpoint of nuclear safeguards, to verify the absence of undeclared activities [2,3]. The inspectors of International Atomic Energy Agency (IAEA) have been collecting environmental samples (swipe samples) on walls, floors and equipment in nuclear facilities all over the world and the analysis has been performed at IAEA Network of Analytical Laboratories (NWALs) [2–4].

Thermal ionization mass spectrometry (TIMS) combined with a fission track (FT) method is a promising technique to measure uranium isotopes for individual particles in swipe samples. In the technique, the uranium particles are identified by fission tracks created in a track detector by neutron irradiation [5–7]. The isotope ratios for the particles are then measured with TIMS. However, a neutron source such as a nuclear reactor is necessary for the FT method, which limits the availability. As an alternative method, secondary ion mass spectrometry (SIMS) has been applied to the analysis of uranium isotopes for individual particles [4,8–11]. Individual uranium particles are sputtered with primary ions and the secondary ions emitted are measured with a mass spectrometer. Although this method has high sample throughput and no need for a neutron source, a drawback remains regarding the analysis of uranium minor isotopes (^{234}U and ^{236}U). The accurate analysis of uranium minor isotopes as well as major isotopes (^{235}U and ^{238}U) in individual particles is essential for nuclear safeguards and non-proliferation. During the SIMS analysis, molecular ions are emitted from particles co-existing with the uranium particle in the sputtered area. Some of the molecular ions may give peaks on the uranium mass region and make it difficult to perform accurate isotope ratio analysis.

* Corresponding author. Tel.: +81 29 282 6165; fax: +81 29 282 6950.
E-mail address: esaka.fumitaka@jaea.go.jp (F. Esaka).

0039-9140/$ – see front matter © 2006 Elsevier B.V. All rights reserved.
doi:10.1016/j.talanta.2006.05.091

For example, $^{207}Pb^{27}Al^{+}$ molecular ions give interferences on a mass 234 [3]. There are two approaches to eliminate molecular ion interferences in SIMS analysis: high mass resolution and energy filtering techniques [12]. However, both the techniques significantly reduce ion signal intensities and make it difficult to conduct the analysis of uranium minor isotopes in trace levels in individual particles.

If individual uranium particles are isolated prior to the SIMS analysis, the isotope ratios will be measured without molecular ion interferences. The aim of this work is to develop such a method and to demonstrate its effectiveness with simulated and real environmental samples.

2. Experimental procedure

2.1. Samples

Swipe samples taken at nuclear facilities often contain Pb particles because Pb is widely used for radiation shielding [3]. Therefore, a simulated swipe sample was prepared from a mixture of Pb metal particles (Nilaco Co. Ltd., Japan) and uranium particles in a certified reference material (NBL CRM U010) using a 10 cm × 10 cm piece of high-purity cotton cloth (TX304, Texwipe Co. Ltd.) used for routine safeguards inspections. A real swipe sample was also taken at a laboratory in Japan Atomic Energy Agency (JAEA).

The particles in each sample were collected, by "Impaction method" [4,11], onto a glassy carbon planchet with a diameter of 25 mm and a thickness of 3 mm (Hitachi Chemical Co. Ltd., Japan). In this study, no grease coating was applied to the surface of the planchets, because the weak interaction between the collected particles and the surface of the planchet was suitable for particle isolation described below.

2.2. Isolation of individual particles

Both the planchet containing particles and a blank planchet were introduced into the main chamber of a scanning electron microscope (SEM) (JSM-6700F, JEOL Co. Ltd., Japan). For particle isolation, needles with a tip diameter of approximately 1 μm were fabricated [13], with a puller (PC-10, Narishige Co. Ltd., Japan), from glass rods with a diameter of 1 mm. The needle was then coated with gold in a sputtering instrument (SC-701AT, Sanyu Electron Co., Japan) and set to a manipulator attached to the main chamber of the SEM.

An example of particle isolation process for the simulated sample is shown in Fig. 1. A uranium particle is identified (Fig. 1(a)), picked up with the needle (Fig. 1(b)) and put onto another planchet (Fig. 1(c)). The isolation of the particle with a diameter from 0.5 to 20 μm was possible by using the needle. This particle isolation ability is sufficient for subsequent SIMS analysis because the uranium amounts of minor isotopes in the particle with the diameter of 0.5 μm are less than the detection limit in SIMS analysis [14].

2.3. Instruments

The planchet containing isolated uranium particles was removed from the chamber of the SEM instrument and introduced into the chamber of a secondary ion mass spectrometer (CAMECA IMS-6f) used for measuring uranium isotope ratios in individual particles. In SIMS analysis, an O_2^+ beam of 15 keV with current of 1–20 nA was used as the primary ion beam. The diameter of the beam was less than 10 μm. The positive secondary ions emitted from the particle were accelerated through 5 keV. An energy slit was adjusted for a band pass of 50 eV. The mass resolution was set at 300. The secondary ions at masses 234, 235, 236, 238 and 239 were counted in an automatic peak jumping mode. An electron multiplier was operated in the ion counting mode with a dead time of 25 ns. Mass calibration was performed each time before starting measurements of the particles. Mass bias corrections were conducted by comparing the measured isotope ratios for a certified uranium reference material (NBL CRM U050) with the reference values. The hydride formation rate of uranium ($^{238}UH/^{238}U$) was determined for each particle and used to correct the contribution of ^{235}UH to ^{236}U at a mass 236 [11,14].

3. Results and discussion

3.1. Analysis of simulated swipe sample

Twenty individual uranium particles, which were not isolated, in the simulated swipe sample containing CRM U010 and Pb metal particles were measured and the ^{208}Pb ions from the Pb particle co-existing in the sputtered area were also monitored. Fig. 2 shows the $^{234}U/^{238}U$ and $^{236}U/^{238}U$ isotope ratios plotted against the $^{208}Pb/^{238}U$ intensity ratios. When the $^{208}Pb/^{238}U$ intensity ratio is 0, i.e., no Pb particle exists in the sputtered area, the $^{234}U/^{238}U$ and $^{236}U/^{238}U$ isotope ratios are in good agree-

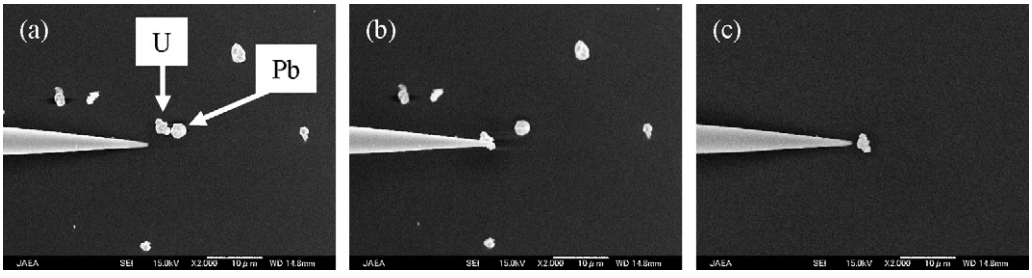


Fig. 1. The scanning electron microscopic images of particles in a simulated swipe sample containing CRM U010 and Pb metal particles. A uranium particle on a planchet was identified (a), picked up (b) and placed onto another planchet (c).

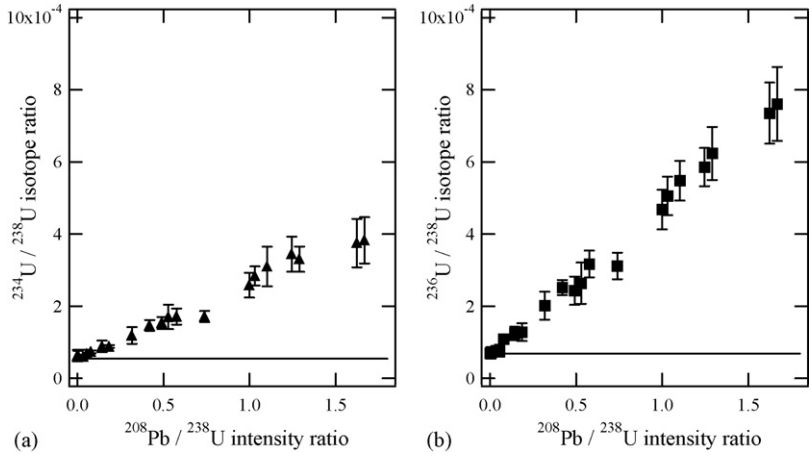


Fig. 2. The (a) $^{234}U/^{238}U$ and (b) $^{236}U/^{238}U$ isotope ratios measured for 20 individual uranium particles in a simulated swipe sample containing CRM U010 and Pb metal particles, plotted against the $^{208}Pb/^{238}U$ intensity ratios. The uranium particles were not isolated. The solid lines in (a) and (b) represent reference values of $^{234}U/^{238}U$ (5.46×10^{-5}) and $^{236}U/^{238}U$ (6.88×10^{-5}), respectively. The error bars represent one standard deviation.

ment with the reference values (5.46×10^{-5} for $^{234}U/^{238}U$ and 6.88×10^{-5} for $^{236}U/^{238}U$). However, both the isotope ratios increase with increasing the $^{208}Pb/^{238}U$ intensity ratio. When the $^{208}Pb/^{238}U$ intensity ratio is 1.00, the relative deviations of the $^{234}U/^{238}U$ and $^{236}U/^{238}U$ isotope ratios from the reference values are 374 and 581%, respectively. The increases in the $^{234}U/^{238}U$ and $^{236}U/^{238}U$ isotope ratios are presumably due to the contribution of $^{206}Pb^{12}C^{16}O^+$ and $^{208}Pb^{12}C^{16}O^+$ molecular ions. These results reveal that the presence of Pb particles in the sputtered area makes it impossible to measure the $^{234}U/^{238}U$ and $^{236}U/^{238}U$ isotope ratios accurately.

In addition to the Pb particles, we investigated the effects of molecular ions from Cr, Fe, Ni, Cu and Zn metal particles. As the results, it was found that the molecular ions produced from the Ni metal particles also gave interferences on the $^{234}U/^{238}U$ and $^{236}U/^{238}U$ isotope ratios, and those from the Zn metal particles on the $^{234}U/^{238}U$ isotope ratio. It is likely that there exist, in real samples, particles of other elements which induce the interferences like Pb, Ni and Zn. Furthermore, the contribution of molecular ions depends on the elemental composition of the particle. The use of other primary ions such as Ar^+ would give different contribution of molecular ions. Therefore, the estimation and correction of molecular ion interferences in the analysis of environmental samples is considerably difficult in practice.

Fig. 3 shows the results of the uranium isotope ratios for 20 individual particles, which were isolated prior to the SIMS analysis. As can be seen, the measured $^{234}U/^{238}U$ and $^{236}U/^{238}U$ isotope ratios for all particles are in good agreement with the reference values within experimental errors. The weighted (by the reciprocal of the square of the standard deviation) average values were $(5.50 \pm 0.18) \times 10^{-5}$ for $^{234}U/^{238}U$ and $(6.94 \pm 0.23) \times 10^{-5}$ for $^{236}U/^{238}U$ isotope ratios, corresponding to the reference values within experimental errors. The maximum relative deviations among 20 particles were 8.9% for $^{234}U/^{238}U$ and 13.1% for $^{236}U/^{238}U$ isotope ratios, respectively. Thus, the relative deviations are significantly improved, compared to those in the analysis of the particle without isolation.

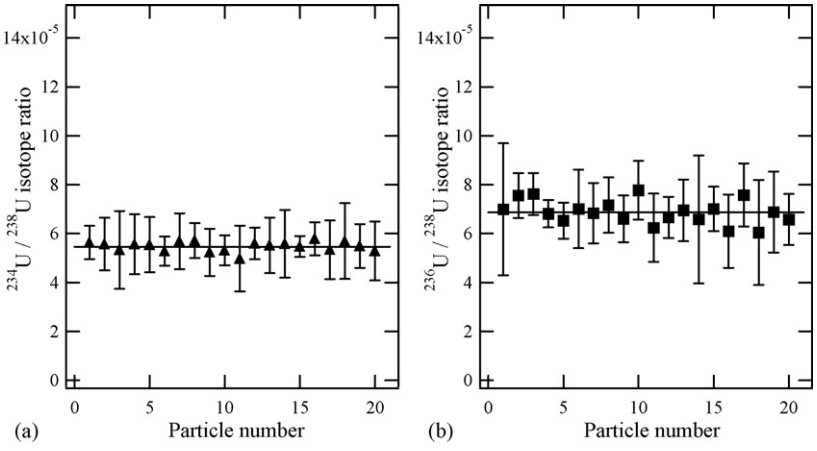


Fig. 3. The (a) $^{234}U/^{238}U$ and (b) $^{236}U/^{238}U$ isotope ratios measured for 20 individual uranium particles isolated from a simulated swipe sample containing CRM U010 and Pb metal particles. The solid lines in (a) and (b) represent reference values of $^{234}U/^{238}U$ (5.46×10^{-5}) and $^{236}U/^{238}U$ (6.88×10^{-5}), respectively. The error bars represent one standard deviation.

3.2. Analysis of real swipe sample

The technique was applied to the analysis of individual uranium particles in a real swipe sample taken at a laboratory in JAEA. Prior to the SIMS analysis, a part of the particles in the sample was collected on a Si planchet and the presence of Fe, Ca, S, Pb, Ti, Zn, Cu, Cr, Ni and U in the sample was confirmed with total-reflection X-ray fluorescence (TXRF) analysis as shown in Fig. 4. The elemental ratios of Pb, Zn and Ni to U were calculated to be 0.96, 0.60 and 0.20, respectively.

Fig. 5 shows the isotope ratios for 10 individual uranium particles, which were not isolated. The solid lines represent the isotope ratios of natural uranium (5.5×10^{-5} for $^{234}U/^{238}U$ [1] and 5.6×10^{-10} for $^{236}U/^{238}U$ isotope ratios [15]). Although the laboratory has handled only natural uranium, the measured $^{234}U/^{238}U$ isotope ratios for six particles are higher than that of natural uranium as shown in Fig. 5(a). Furthermore, the $^{236}U/^{238}U$ isotope ratios, which should be below the detection limit in SIMS analysis [14], were measured for six particles as shown in Fig. 5(b). The $^{236}U/^{238}U$ isotope ratios for four particles are not shown in Fig. 5(b) because the count rates of ^{236}U were the levels of background. These results indicate the presence of molecular ion interferences on the $^{234}U/^{238}U$ and $^{236}U/^{238}U$ isotope ratio analysis.

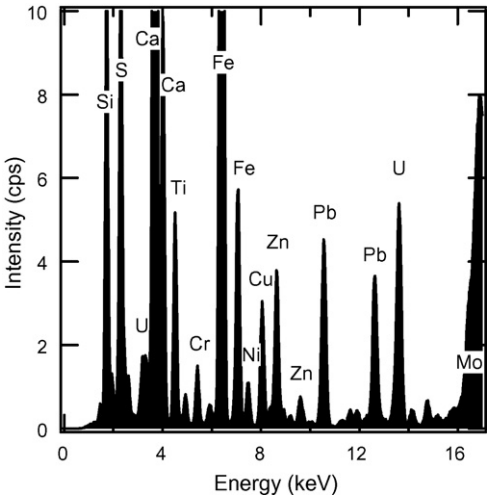


Fig. 4. The TXRF spectrum of the particles collected from a real swipe sample taken at a laboratory in JAEA onto a Si planchet. A Mo X-ray tube was operated at 40 kV and 40 mA and the acquisition time was chosen to be 300 s. The incident angle was set to 0.05°.

Fig. 6(a) shows a scanning electron microscopic image of 10 uranium particles isolated from the real swipe sample and placed onto a glassy carbon planchet. Fig. 6(b) shows the scanning electron image and the energy dispersive X-ray spectrum

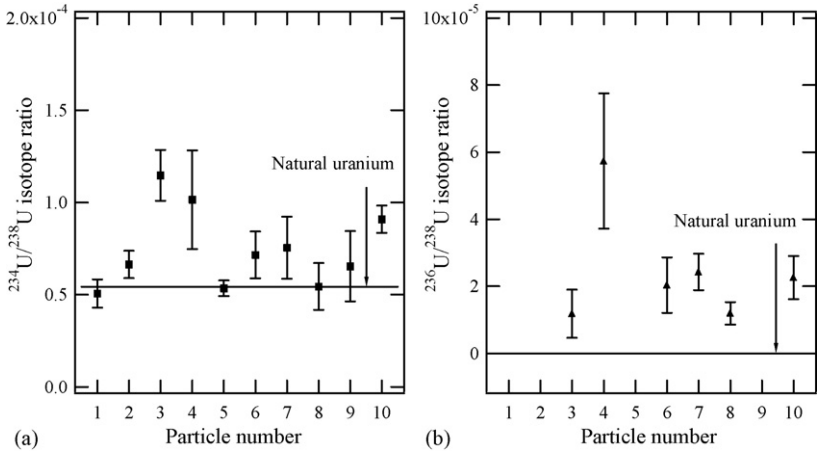


Fig. 5. (a) The $^{234}U/^{238}U$ and (b) $^{236}U/^{238}U$ isotope ratios measured for 10 uranium particles collected from a real swipe sample taken at a laboratory in JAEA. The uranium particles were not isolated. The solid lines in (a) and (b) represent the isotope ratios of natural uranium (5.5×10^{-5} for $^{234}U/^{238}U$ [1] and 5.6×10^{-10} for $^{236}U/^{238}U$ isotope ratios, respectively [13]). The error bars represent one standard deviation.

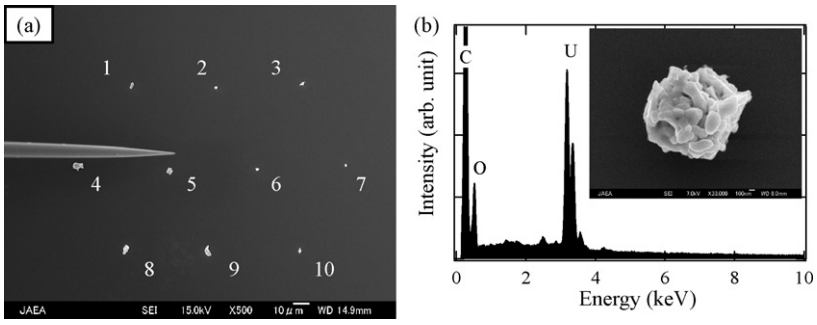


Fig. 6. (a) The scanning electron microscopic image of 10 uranium particles isolated from a real swipe sample taken at a laboratory in JAEA and (b) the scanning electron microscopic image of the uranium particle (no. 2 in (a)) and its energy dispersive X-ray (EDX) spectrum obtained with an acquisition time of 300 s.

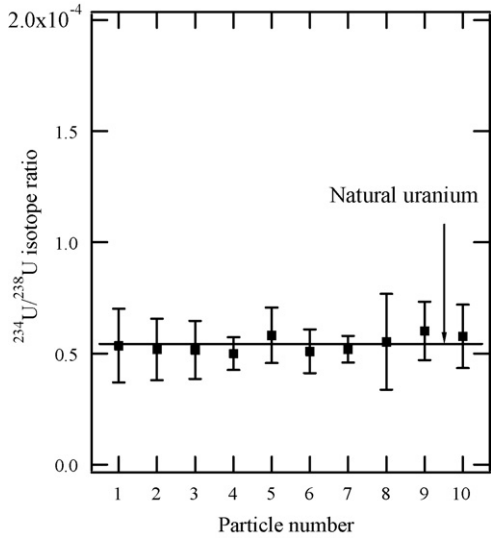


Fig. 7. The $^{234}U/^{238}U$ isotope ratios measured for 10 uranium particles in a real swipe sample taken at a laboratory in JAEA. The individual particles were isolated, prior to the isotope ratio analysis with SIMS. The solid line represents the $^{234}U/^{238}U$ isotope ratios of natural uranium (5.5×10^{-5}). The error bars represent one standard deviation.

of the uranium particle noted "2" in Fig. 6(a). The particle has a diameter of approximately 1.7 μm. The EDX spectrum indicates that the particle mainly consists of U and O. The C peak in the EDX spectrum is probably due to the planchet.

The $^{234}U/^{238}U$ isotope ratios measured for the isolated particles are shown in Fig. 7. The ratios for all particles correspond to that of natural uranium. The weighted average value of $(5.29 \pm 0.33) \times 10^{-5}$ is in good agreement with the ratio of natural uranium within experimental errors. The count rates of ^{236}U were less than 1 count/s, which are comparable to the levels of background. These results imply that the combination of particle isolation and SIMS analysis is effective for eliminating molecular ion interferences, which enables us to perform accurate analysis of minor isotopes in trace levels in environmental samples.

4. Conclusions

A combined method of particle isolation under scanning electron microscope and secondary ion mass spectrometry was developed to measure $^{234}U/^{238}U$ and $^{236}U/^{238}U$ isotope ratios for individual particles in environmental samples. When the $^{234}U/^{238}U$ and $^{236}U/^{238}U$ isotope ratios were measured for individual particles in a simulated swipe sample containing CRM U010 and Pb particles, inaccurate results were obtained due to the molecular ion interferences by the Pb particles co-existing in the sputtered area. When particle isolation was performed, the relative deviations of the $^{234}U/^{238}U$ and $^{236}U/^{238}U$ isotope ratios from the reference values were significantly improved. Furthermore, this method was successfully applied to the analysis of a real swipe sample containing various kinds of elements. From the results, the approach presented here was concluded to be effective for the analysis of minor uranium isotopes with trace levels in individual particles. By applying the technique to the analysis of the swipe samples collected by the IAEA inspectors, more valuable information would be obtained for nuclear safeguards. However, the molecular ion interferences by the elements, which originally exist in a uranium particle, are not eliminated by the proposed technique. In order to overcome the problem, a combination of particle isolation, particle dissolution, chemical separation and mass spectrometry such as TIMS and inductively coupled plasma mass spectrometry (ICP-MS) should be applied.

Acknowledgements

A portion of the paper is being performed under the auspices of Ministry of Education, Culture, Sports, Science and Technology of Japan. The authors wish to thank Dr. M. Betti and Dr. G. Tamborini, the Institute for Transuranium Elements (Karlsruhe, Germany), Joint Research Centre, European Commission, for valuable comments on SIMS analytical techniques for individual particles.

References

[1] P. De Bièvre, P.D.P. Taylor, Int. J. Mass Spectrom. Ion Processes 123 (1993) 149–166.
[2] D.L. Donohue, J. Alloys Compd. 271–273 (1998) 11–18.
[3] D.L. Donohue, Anal. Chem. 74 (2002) 28A–35A.
[4] P.M.L. Hedberg, K. Ingeneri, M. Watanabe, Y. Kuno, Proceedings of the 46th Institute of Nuclear Materials Management Annual Meeting, Phoenix, Arizona, July 10–14, 2005.
[5] O. Stetzer, M. Betti, J. van Geel, N. Erdmann, J.V. Kratz, R. Schenkel, N. Trautmann, Nucl. Instrum. Methods Phys. Res. A 525 (2004) 582–592.
[6] M.H. Lee, M. Douglas, S.B. Clark, Radiat. Meas. 40 (2005) 37–42.
[7] C.G. Lee, K. Iguchi, F. Esaka, M. Magara, S. Sakurai, K. Watanabe, S. Usuda, Jpn. J. Appl. Phys. 45 (2006) L294–L296.
[8] G. Tamborini, M. Betti, V. Forcina, T. Hiernaut, B. Giovannone, L. Koch, Spectrochim. Acta B 53 (1998) 1289–1302.
[9] D.S. Simons, G. Gillen, C.J. Zeissler, R.H. Fleming, P.J. McNitt, Secondary Ion Mass Spectrometry XI, John Wiley & Sons, New York, 1998, pp. 59–62.
[10] M. Betti, G. Tamborini, L. Koch, Anal. Chem. 71 (1999) 2616–2622.
[11] F. Esaka, K. Watanabe, H. Fukuyama, T. Onodera, K.T. Esaka, M. Magara, S. Sakurai, S. Usuda, J. Nucl. Sci. Technol. 41 (2004) 1027–1032.
[12] R.G. Wilson, F.A. Stevie, C.W. Magee, Secondary Ion Mass Spectrometry: A Practical Handbook for Depth Profiling and Bulk Impurity Analysis, John Wiley & Sons, New York, 1989.
[13] H.T. Miyazaki, Y. Tomizawa, S. Saito, T. Sato, N. Shinya, J. Appl. Phys. 88 (2000) 3330–3340.
[14] N. Erdmann, M. Betti, O. Stetzer, G. Tamborini, J.V. Kratz, N. Trautmann, J. van Geel, Spectrochim. Acta B 55 (2000) 1565–1575.
[15] X.L. Zhao, M.J. Nadeau, L.R. Kilius, A.E. Litherland, Nucl. Instrum. Methods Phys. Res. B 92 (1994) 249–253.

Available online at www.sciencedirect.com
ScienceDirect
Talanta 71 (2007) 1172–1179
Talanta
www.elsevier.com/locate/talanta

Development of an MSFIA-MPFS pre-treatment method for radium determination in water samples

Y. Fajardo [a], E. Gómez [a], F. Garcias [b], V. Cerdà [a], M. Casas [b,*]

[a] *Department of Chemistry, University of the Balearic Islands, E-07122 Palma, Spain*
[b] *Department of Physics, University of the Balearic Islands, E-07122 Palma, Spain*

Received 17 February 2006; received in revised form 24 May 2006; accepted 7 June 2006
Available online 13 July 2006

Abstract

A new automatic method for preconcentration and separation of radium in water samples has been developed. Such method combines both multisyringe (MSFIA) and multi-pumping (MPFS) flow analysis techniques allowing to analyze larger sample volumes with a higher throughput than other previous methodologies. Ra adsorbed on MnO_2, deposited on cotton fiber, is eluted with hydroxylamine and subsequently coprecipitated with $BaSO_4$. ^{226}Ra activity is determined off-line by using a low background proportional counter. The procedure yield is $(90 \pm 3)\%$ and its lower limit of detection 0.05 Bq L^{-1}. This method has been applied satisfactorily to different types of spiked water (tap, mineral and seawater).
© 2006 Elsevier B.V. All rights reserved.

Keywords: Radium; MSFIA; Water; MPFS; Automation; Preconcentration; Separation

1. Introduction

Radium is a naturally occurring element, found mainly in rocks, soil and some mineral and underground waters. Its isotopes, all being radioactive, are generated from the natural series of uranium ^{238}U, ^{235}U and ^{232}Th. Among them it is worthwhile mentioning ^{226}Ra, well known for its long half-life ($t_{1/2}$ = 1600 ± 7 years), widely spread in the environment and, therefore, considered one of the major contributors to the population internal dose [1,2]. Absorption of radium retained in soil or dissolved in water by plants and animals makes possible its incorporation into the trophic chain. Biologically, radium concentrates on human bones by replacing calcium [3], increasing in this way the internal radiation dose, which after a prolonged irradiation can cause serious health problems (anemia, cataracts, fractured teeth or cancer, especially bone cancer) [4].

On the other hand, radium content in natural waters has been used as a geochemical tracer to evaluate environmental and geophysical processes taking place on the Earth's crust or in the oceans [5–7]. Also, natural waters originating in areas near uranium mines, thermal waters, etc., usually present radium concentrations that ought to be controlled in order to determine their suitability for consumption and their effects in the population dose.

Also, as a result of some anthropogenic activities related mainly to energy production from coal power plants, ^{226}Ra levels have increased in atmosphere and on the Earth's surface. Thus, the development of analytical methodologies allowing the determination of Ra content at environmental levels in a simple and efficient way is required. In the case of drinking waters, European Union (EU) has established the limiting value of 0.1 Bq L^{-1} as a new guideline for total alpha activity [8].

Since the analyte concentration in water samples is usually very low, in addition to the use of large sample volumes, the performance of one or several preliminary stages of separation and preconcentration will be needed in order to eliminate the possible interferences present in the matrix of the analyzed sample. Most traditional methods of radium separation include precipitation and coprecipitation steps with sulfates, carbonates or insoluble phosphates [9–11].

The former methods involve a great consumption of reagents and are time-consuming, making the separation work tedious. Moreover, in the case of several Ra isotopes with $t_{1/2}$ of a few

* Corresponding author. Fax: +34 971173426.
E-mail address: montse.casas@uib.es (M. Casas).

0039-9140/$ – see front matter © 2006 Elsevier B.V. All rights reserved.
doi:10.1016/j.talanta.2006.06.012

days, time can become an inconvenience. Aiming to simplify the process, other methodologies are based on either chromatographic extraction [12], liquid–liquid extraction [13–15] or cationic exchange [16,17] techniques. However, occasionally and due to the low selectivity of the compounds or the resins used, these methodologies require either a combination of several exchange procedures [18] or the sequential elution of alkaline cations present in the matrix by using complex-forming organic solutions (EDTA, citric acid, etc.) involving a meticulous pH control.

Over several decades oceanographic researchers have used acrylic fibers impregnated with MnO_2 to extract radium and other trace elements from the ocean, which are subsequently analyzed by alpha or gamma spectroscopy [19–21].

The principle of this extraction technique, based on the adsorption of radium on MnO_2, has been applied by several authors to carry out separation and preconcentration of radium in different types of water [10,22–29]. Over the last years the great development of software and hardware has enabled the easy coupling of computers, by means of interfaces, to a great variety of equipment (measuring, sampling and sample injection, etc.), thus, automating a larger number of chemical analysis techniques, mainly those based on flow techniques.

The multisyringe flow injection analysis (MSFIA) developed in 1999 by Cerdà et al. [30] profits simultaneously from the advantages offered by the flow injection analysis (FIA) and sequential injection analysis (SIA) methodologies developed by Ruzicka et al. [31,32]. Subsequently, Lapa et al. [33] and Lima et al. [34] proposed a new way of impelling sample and reagents by using a multi-pumping flow system (MPFS).

In this work an MSFIA-MPFS combined method is proposed aiming to carry out the determination of radium at environmental levels in water samples. The described procedure allows obtaining, for large sample volumes, a higher throughput (4 samples/h).

2. Experimental

2.1. Reagents and standards

All solutions were prepared from analytical grade reagents with Millipore quality water.

$0.1\ mol\ L^{-1}$ potassium permanganate, Probus.
$0.1\ mol\ L^{-1}$ hydroxylamine, Prolabo in $0.2\ mol\ L^{-1}$ HCl, Scharlau.
$2\ mol\ L^{-1}$ acetic acid–acetate buffer of pH 3 with $0.25\ mg\ mL^{-1}$ Ba^{2+}.
$2\ mol\ L^{-1}$ sodium sulfate, Scharlau.
^{226}Ra standard of initial activity $(36.2 \pm 0.5)\ Bq\ mL^{-1}$ in $1\ mol\ L^{-1}$ HCl, prepared and certified by CIEMAT (Madrid, Spain).
Cotton fiber of pharmaceutical use.
Glass wool for chromatography.
Nitrocellulose filters of 47 mm diameter and 0.22 μm pore size, Millipore.

2.2. Samples

Samples employed to validate the proposed method are used directly without pre-treatment or dilution. When required, pH is adjusted to 7.

2.3. Equipment and software

The MSFIA-MPFS manifold used is shown in Fig. 1. MSFIA system is constituted basically by a multisyringe burette (BU4S, Crison Instruments, Alella, Barcelona, Spain) with programmable rate. This burette is equipped with four syringes (Hamilton, Switzerland) of 5 ml which are used as liquid drivers. Each syringe has a three-way solenoid valve (N-Research, Caldwell, NJ, USA) at the head, which facilitates the application of multicommutation schemes. The automatic control of the

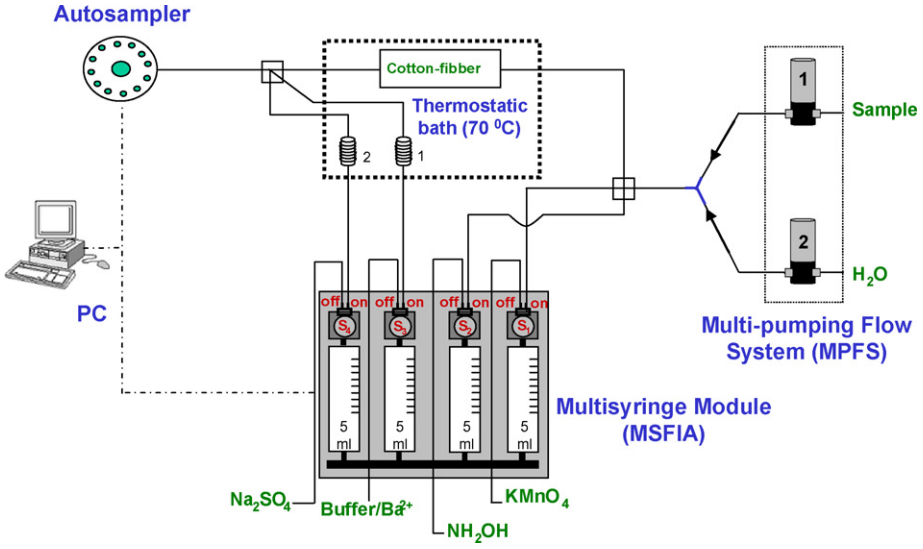


Fig. 1. MSFIA-MPFS manifold for the separation and preconcentration of Ra.

flow device is made via PC through an RS232C interface. Manifold is constructed with 0.8 and 1.5 mm internal diameter poly(tetrafluoroethylene) (PTFE) tubes. The loading coils are of 3.5 m long for coil 1, with which the acetate buffer/Ba^{2+} solution is loaded, and of 5.5 m long for coil 2 that contains the 2 mol L^{-1} sodium sulfate solution. The coils are placed in such a way so that the solutions are passed through a thermostatic bath (70 °C) in which the separation column is also found submerged. The remaining reagents are loaded and supplied directly with syringes. All connections are carried out by means of PVC connectors, except mixing tees, which were made with methacrilate.

The MPFS manifold consists of two solenoid micro-pumps (Bio-Chem Valve Inc., Boonton, New Jersey, USA) with a stroke volume of 20 μL. Each one allows the injection of a certain volume of reagent or sample varying the number of pulses. The flow rate is controlled according to the frequency and volume dispensed in each pulse. The solenoid pumps are computer controlled by means of an MSFIA/MPFS system (SCIWARE, Palma de Mallorca, Spain) which has eight digital 12 V output channels. This system is connected to a personal computer through an RS232 serial interface. Solenoid valves and micropumps are connected to the main module through an interface allowing to use solenoid protections in order to minimize heat generation (SCIWARE, Palma de Mallorca). These protections are only needed for valves [35].

The autosampler (Crison Microsampler) is used to collect the elutes from the column and reagents (Na_2SO_4 and acetate buffer/Ba^{2+}) from the MSFIA module. In addition, one of the positions was employed as waste.

A methacrylate column of 45 mm long and 3.5 mm internal diameter, with a capacity of 0.43 mL, constitutes the extraction system. The column is filled in with an adequate amount of cotton, to avoid compaction and, thus, possible overpressures which could affect the performance of the solenoid pumps.

Once the radiochemical separation has been concluded, determination of ^{226}Ra activity is carried out off-line with a Tennelec LB 4100 model low background proportional counter with an average efficiency of 23%. This equipment is provided with up to four series of four detectors each, which would permit the simultaneous alpha activity measurement for 16 samples.

In our procedure the proportional counter detection method has been selected instead of the alpha spectrometry option because it permits simultaneous alpha activity determination in a set of samples pre-treated with our MSFIA-MPFS system. This detection method is especially useful in laboratories where a large number of environmental samples must be analyzed. Nevertheless, ^{226}Ra activity determination using a proportional counter requires:

(a) the knowledge of the growth rate of ^{226}Ra alpha daughters;
(b) ensuring that only ^{226}Ra is retained in the chemical process, or alternatively the knowledge of the contribution of other alpha emitters retained in the process.

^{226}Ra separation from other alpha emitters and the growth of its daughters in our procedure have been tested by alpha spectrometry using a Canberra 7401 alpha spectrometer with an A450-18AM model passivated implanted planar silicon (PIPS) detector with 450 mm^2 of active area and 17 keV of energy resolution. The calibration has been carried out using a triple source of ^{233}U, ^{239}Pu and ^{241}Am obtained by electrodeposition. The detection efficiency depends on the detector-sample distance and its maximum value is 35%.

2.4. Procedure

The process of MnO_2 formation, extraction of radium, elution and coprecipitation with Ba^{2+} is controlled automatically with the *AutoAnalysis* computer package version 5.0 [36]. The process steps are described in Fig. 2. The flow rate and volume of the reagents for each step are depicted in Table 1. First, the 0.1 mol L^{-1} permanganate potassium solution is impelled towards the column, remaining in contact with the cotton fiber for 2 min to allow the formation of MnO_2. Then, permanganate solution excess is eluted with water. Simultaneously, pump 1 propels the sample towards the system at a flow rate of 5 mL min^{-1}. When the transportation of the sample has concluded, pump 2 supplies water to the column to separate possible interferences that have not been adsorbed on the MnO_2. Next, the multisyringe module dispenses 4 mL of 0.1 mol L^{-1} NH_2OH that reduces and dissolves completely the MnO_2 adsorbed onto

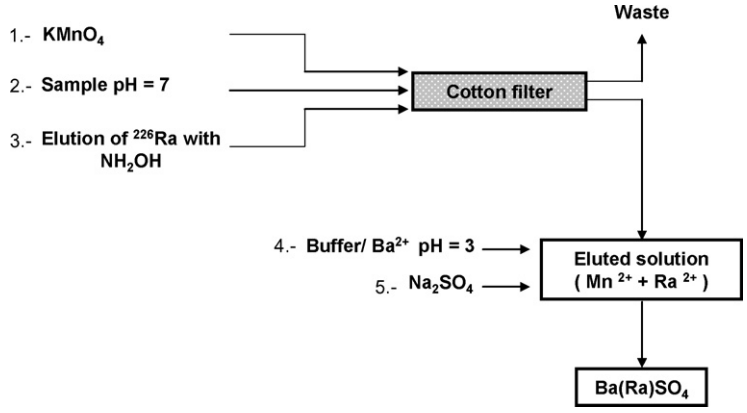


Fig. 2. Procedure for the separation and preconcentration of Ra.

Table 1
Main steps of the automated process for radium separation

Step	Performance	Flow rate (mL min^{-1})
1	Dispensation 4 mL of 0.1 mol L^{-1} $KMnO_4$. Preparation of the adsorbent	3
2	Dispensation of the sample fixed volume. Preconcentration	5
3	Elution of Ra with 0.1 mol L^{-1} NH_2OH.	5
4	Dispensation of 4 mL of Buffer/Ba^{2+}. Coprecipitant addition	5
5	Dispensation of 8 mL of 2 mol L^{-1} Na_2SO_4. Coprecipitation of Ra with $BaSO_4$	5

the cotton fiber and elutes jointly the deposited Ra towards the pre-assigned autosampler position. After this step has concluded, 4 mL of the acetate buffer/Ba^{2+} solution and 8 mL of 2 mol L^{-1} Na_2SO_4 are impelled simultaneously to the above autosampler position to coprecipitate radium as $Ba(Ra)SO_4$.

Once the automatic separation method has been applied, a slurry is formed in the autosampler. This is left for ageing off-line for 30 min aiming to assure the quantitative coprecipitation of Ra. Next, it is filtered through a Millipore filter of 0.22 μm pore size. The precipitate retained on the filter is dried over a stainless steel planchette, under an infrared lamp. Finally, the analyte alpha activity is measured with the low background proportional counter.

3. Results and discussion

Optimization of working conditions has been carried out using ^{226}Ra solutions prepared from a standard. In all cases, except otherwise stated, a sample volume of 40 mL has been used.

3.1. MnO_2 formation on cotton fiber

The capacity of MnO_2 to adsorb alkali-earthy metal cations, particularly radium, offers a convenient and effective method to implement automatic extraction techniques. Based on such properties, Caldés et al. [27] have reported that depending on the bath temperature, deposition time and chemical concentration of the $KMnO_4$ solution, the MnO_2 formation and retention process on the cotton fiber surface can be achieved in an effective way, without generating overpressures in the system.

3.1.1. Bath temperature

Within our manifold and for a temperature range between 70 °C and 80 °C the obtained ^{226}Ra recovery values are practically similar. However, at 80 °C the cotton fiber changes its physical properties, becoming more compact and causing overpressures, thus, the lifetime of the fiber being reduced drastically. Therefore, 70 °C was chosen as the working temperature value.

3.1.2. Deposition time

Morvan et al. [26] show that the efficiency of Ra retention process depends on the thickness of the MnO_2 coat, which is considerably related to the contact time between the $KMnO_4$ solution and the cotton fiber.

We have found that impelling a volume of 4 mL of 0.1 mol L^{-1} $KMnO_4$ through the column at a flow rate of 3 mL min^{-1} and, prior to the elimination of permanganate excess with water, leaving the solution in contact with the cotton fiber for 2 min is enough time to allow to form a MnO_2 coat with an adequate number of adsorption sites. The time corresponding to the MnO_2 deposition is used in the procedure to carry out the loading of the syringes.

3.2. Reuse of the cotton fiber

Inside the methacrylate column an adequate amount of cotton is placed in order to avoid overpressures within the manifold. Together with the cotton a small amount of glass wool for chromatography is placed to avoid clogging of the filling and to increase its lifetime. Fiber replacement takes place when after subsequent analyses the volume aspirated and impelled through the pumps diminishes successively. This volume variation can be explained in terms of the changes produced in the characteristics of the cotton, caused by the effect of temperature, $KMnO_4$ solution and the acid medium of hydroxylamine, creating compaction and deterioration of the filling. Consequently, cotton is replaced after carrying out 25 to 30 analyses.

3.3. pH of the sample

The amphoteric behavior of manganese dioxide enables to control and select the adsorption of radium on its surface by regulating the pH conditions [25,29]. The manganese oxide surface becomes positively charged by the presence of an excess of protons, thus, avoiding the adsorption of positive species such as Ra^{2+}. Besides, for pH values lower than 3, MnO_2 is dissolved. As pH increases a larger number of OH^- groups happen to occupy the MnO_2 surface, thus, facilitating the adsorption process. pH values higher than 9 enhance the precipitation of hydroxides and carbonates [37]. Eikenberg et al. [25] demonstrated that Ra and Po show a strong pH-dependence of their adsorption on the MnO_2 surface. Thus, whereas Po is better retained for pH values lower than 4, in the case of Ra higher retention occurs in a 6–8 pH range. Taking into account this behaviour and in order to avoid the Po interference, a pH value of 7 is selected to ensure an adequate adsorption of Ra.

3.4. Ionic concentration of the sample

The salt effect on the Ra adsorption was assessed by applying the analytical methodology to two ^{226}Ra solutions of 12.5 Bq L^{-1}. The first one was prepared with deionized water at pH 7, while the second one was made to simulate a syn-

thetic mineral water composed of 150 mg L^{-1} of bicarbonate, 20 mg L^{-1} of magnesium and 50 mg L^{-1} of calcium (these concentrations are similar to the ones of drinking waters). In the case of deionized water the ^{226}Ra recovery was of 84% with a relative standard deviation (R.S.D.) of 5.8% whereas for the synthetic mineral water the yield increased to 95% and its R.S.D. was also substantially enhanced (2.8%).

The worse results obtained for deionized water matrix may be explained by an analyte adsorption onto glass. This undesirable effect can be avoided if a synthetic mineral water matrix is used, as the presence of others cations (Ca^{2+}, Mg^{2+}, Na^{+}) would prevent the Ra adsorption. We must take into account that, according to thermodynamic values obtained by Langmuir et al. [38,39] in an ionic medium like the proposed above, Ra would only exist as Ra^{2+} form. As a result, a significative improvement for recovery and reproducibility was obtained. Therefore, determination of Ra was carried out accordingly with standards of the above-mentioned ionic concentration.

3.5. Sample volume and flow rate

The analysis time depends on the volume of the sample to be analyzed. In our particular case the use of solenoid pumps enables the optimization of such time, since a successive loading and unloading of coils and syringes is not required. The solenoid pump continuously impels to the manifold the sample volume defined *a priori*. It has been proved that the performance of the pumps is not altered during the execution time for a sample volume ranging from 40 mL to 200 mL. This permits to employ large sample volumes, a requirement to be fulfilled in any of the radioisotope analyses at environmental levels. Different sample flow rates (2mL min^{-1}, 3mL min^{-1} or 5 mL min^{-1}) have been studied. In all cases the retention process has been carried out quantitatively with a Ra recovery greater than 90%. In order to diminish the analysis time a flow rate of 5 mL min^{-1} was selected.

3.6. Elution with hydroxylamine

The MnO_2 coat is dissolved in the presence of a 0.1 mol L^{-1} hydroxylamine solution in hydrochloric medium sweeping jointly the Ra^{2+} ions retained on the surface. Caldés et al. [27] demonstrate that the complete dissolution of MnO_2 is carried out with 3 mL. In our manifold we used 4 mL and a flow rate of 5 mL min^{-1} in order to avoid carryover between samples.

3.7. Coprecipitation of Ba(Ra)SO_4

The low concentration of Ra^{2+} ions is responsible for the fact that when Na_2SO_4 is added the solubility product required for their isolation from the quantitative precipitation is not achieved. For this reason a coprecipitation with $BaSO_4$ is carried out. A Ba^{2+} solution of 0.25 mg mL^{-1} concentration is added together with an acetic acid/acetate buffer (pH 3); in this way the system is simplified and the analysis time reduced. The buffer and the Na_2SO_4 solution are added through channels that are different from the one of the elution fraction containing the dissolved Ra^{2+}. The best coprecipitation results are obtained when the resulting solution presents a temperature around 50 °C. Therefore, a reaction coil was placed for each solution and both coils were submerged in a thermostatic bath. Other aspects to be taken into account are the precipitate formation and ageing times. We have found that when the filtration is carried out immediately after having added the above-mentioned solutions the Ra recovery decreases up to 50%. However, when the precipitate is let to settle for approximately 30 min the recovery surpasses 90%.

In the determination of the alpha activity it is very important that the thickness of the sample remains small in order to reduce the phenomenon of self-absorption. Under the established working conditions the precipitate is distributed uniformly over the filter surface of 0.22 μm and in all cases the deposition mass is small enough so that the self-absorption factor remains practically negligible. Moreover, it must be considered that combination of the two separation processes enhances the selectivity of the analytical methodology and the ending deposition mass.

3.8. Variation of the activity with time

Once ^{226}Ra has been separated the isotope is disintegrated according to the $4n+2$ series until reaching the stable isotope ^{206}Pb. Alpha emitter isotopes generated from ^{226}Ra are the following:

$$^{226}Ra \xrightarrow[1.37\times10^{-11}\ s^{-1}]{\lambda_1} {}^{222}Rn \xrightarrow[2.10\times10^{-6}\ s^{-1}]{\lambda_2} {}^{218}Po \xrightarrow[3.78\times10^{-3}\ s^{-1}]{\lambda_3} \ldots {}^{214}Po$$

$$\xrightarrow[4.23\times10^{3}\ s^{-1}]{\lambda_4} \ldots {}^{210}Po \xrightarrow[5.70\times10^{-8}\ s^{-1}]{\lambda_5} {}^{206}Pb$$

Secular equilibrium of the radioactive chain, from ^{226}Ra to ^{214}Po, is achieved 20 days after ^{226}Ra is separated from the sample [25]. ^{210}Po must not be considered in this secular equilibrium due to the long half-live of its parent ^{210}Pb ($t_{1/2}$ = 22.2 years).

In order to corroborate the quantitative separation of ^{226}Ra reached by MSFIA-MPFS procedure, alpha spectrometry was used as detection method. By preparing a standard of 12.5 Bq L^{-1}, radium separation and coprecipitacion were developed and alpha spectrum of the filter with the analyte was adquired during 19 days, the detector chamber remaining closed all the time. We checked the ^{226}Ra presence immediately after the chemical separation and the growing of ^{222}Rn, ^{218}Po, and ^{214}Po. Taking into account the above mentioned ^{210}Pb half-live, early detection of ^{210}Po in the spectrum would imply that Po or Pb be retained during the chemical process. Fig. 3 shows the obtained alpha spectrum. The emission energies corresponding to ^{226}Ra (4.78 MeV) and its daughters are also depicted, i.e., ^{222}Rn (5.49 MeV), ^{218}Po (6.00 MeV), ^{214}Po (7.69 MeV). As it can be seen, the energy peak corresponding to ^{210}Po (5.30 MeV) is not present in the spectrum, confirming that neither Pb nor Po is absorbed on MnO_2 during the chemical process. The evolution of the alpha spectrum has been analyzed until the series reaches the secular equilibrium.

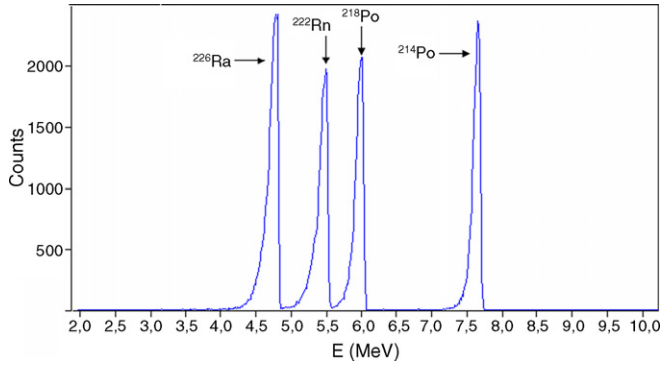


Fig. 3. Alpha emission spectrum for a synthetic mineral water sample. Measuring time was 19 days, starting immediately after separation process.

To validate the low background proportional counter detection method, the separation process was carried out with four different ^{226}Ra initial activities (0.13 Bq, 0.23 Bq, 0.38 Bq and 0.50 Bq, respectively). During 30 days the total alpha counting was attained for each filter by the counter. The measurement was carried out discontinuously (casual days) always using a counting time of 1000 min. Once this counting time finished, each sample was removed from the counter and stored in a closed container until the next measurement. The obtained results are shown in Fig. 4. In this way it was corroborated that 20 days later the total alpha activity was practically constant and four-fold the value obtained after the isolation of ^{226}Ra.

Since ^{226}Ra activity is measured with the proportional counter several hours after being separated, a correction is required because of generation of the above-mentioned daughters. This adjustment has been addressed in two ways:

(a) Linear fit: The growth curves of Fig. 4 for the four ^{226}Ra initial activities reveal that the total alpha activity variation during the first five days is approximately linear. Thus, the ordinate at the origin of the linear fit should correspond to the ^{226}Ra activity separated from the sample at $t = 0$. In Table 2 the linear equations obtained from values of Fig. 4 reveal that the corresponding ordinates at the origin are practically equal to the added ^{226}Ra activities.

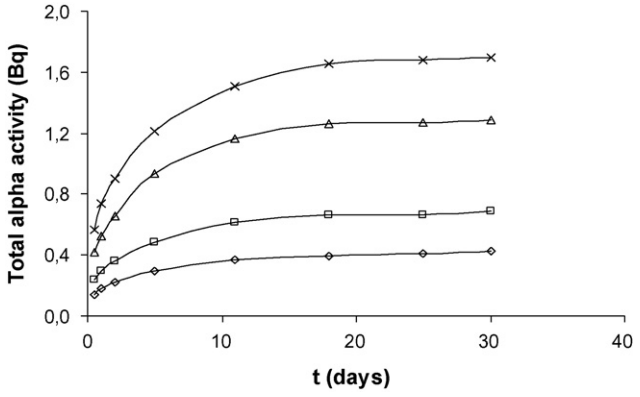


Fig. 4. Variation in time of the total alpha activity for four samples with different ^{226}Ra initial activities. (◊) M1 = 0.13 Bq; (□) M2 = 0.23 Bq; (△) M3 = 0.38 Bq; (×) M4 = 0.50 Bq.

Table 2
^{226}Ra activity determined from the total alpha activity values measured during the first 5 days

Added ^{226}Ra activity (Bq)	Fitted equation[a]	^{226}Ra activity (Bq) from fitted linear equation	^{226}Ra activity (Bq) from Bateman equations
0.13	$y = 0.0323x + 0.1377$	0.14	0.12
0.23	$y = 0.0514x + 0.2265$	0.23	0.21
0.38	$y = 0.1128x + 0.3741$	0.37	0.36
0.50	$y = 0.1396x + 0.5256$	0.53	0.50

[a] $y = ^{226}$Ra activity (Bq); x = time (days).

(b) By solving the Bateman equations system for the above radioactive series:

$$\begin{aligned} dN_1 &= -\lambda_1 N_1 dt \\ dN_i &= \lambda_{i-1} N_{i-1} dt - \lambda_i N_i dt \quad \text{for } i = 2 \text{ to } j, \end{aligned} \tag{1}$$

where j is the number of elements of the radioactive series, and $\lambda_i N_i$ their corresponding activities. According to the alpha spectrometry results, we assume that at $t = 0$, after the separation, only N_0 atoms of ^{226}Ra are present in the filter. The solution of this Bateman equations system provides the activity A_n of the nth member of the radioactive series in terms of the decay constants of all preceding members:

$$A_n = N_0 \sum_{i=1}^{n} c_i \, e^{-\lambda_i t} \quad \text{with} \quad c_m = \frac{\prod_{i=1}^{n} \lambda_i}{\prod_{i=1}^{n'} (\lambda_i - \lambda_m)}, \tag{2}$$

where the prime on the lower product means that the term $i = m$ is omitted. The sum of all A_n alpha activities is the total alpha activity A_T at time t, which we measure with the low background proportional counter. Therefore, from measured A_T and using equations (2), the number of existing ^{226}Ra atoms at $t = 0$ (N_0) and its initial activity (A_0) are calculated.

In Table 2 the results obtained from linear fit and from Bateman equations are shown, and in turn compared with the reference values. In both cases a good agreement with the expected value is obtained, thus, allowing a reasonable and quick calculation of ^{226}Ra initial activity in any of the two proposed ways.

3.9. Range of activities

The analytical method was applied to different activity values, taking 0.1 Bq L^{-1} as a reference value, which is the limiting value established for alpha emitters in drinking waters. For this analysis the injected sample volume was of 100 mL and the Ra recovery of 95%.

The study was also carried out for an activity value of 0.05 Bq L^{-1}, although in this case the sample volume was increased up to 200 mL in order to surpass adequately the background value. The obtained results were similar to those attained with a volume of 100 mL for an activity of 0.1 Bq L^{-1}, revealing that the method is applicable even when the radium activity is lower or equal to the legislated environmental value.

We have found that if the radium activity of the sample is higher than 50 Bq L^{-1} the process yield is reduced to 80%. For a sample volume of 40 mL the concentration range for which the method can be applied satisfactorily is comprised between 0.25 Bq L^{-1} and 50 Bq L^{-1} with a lower limit of detection (LLD) of 0.05 Bq L^{-1}. However, when greater sample volumes (200 mL) are involved the LLD can be decreased up to 0.01 Bq L^{-1}. In all cases the LLD is obtained by means of the Currie equation with a 95% of level confidence.

3.10. Reproducibility

Once all the experimental parameters were optimized the reproducibility of the method was checked using a ^{226}Ra standard solution of 12.5 Bq L^{-1}. The analysis in the same day of four samples sets was repeated for several times. In every case the total uncertainty (95% confidence level) was lower than 7.8%.

The R.S.D. obtained when four series of four experiments are developed in different days is 0.4% ($n = 16$ replicates), which demonstrates a good repeatability without replacing the cotton filling.

3.11. Analysis of real samples

The developed procedure has been applied to water samples. We have analyzed three different types of water samples (mineral, tap and sea waters) for which the Ra content is smaller than the LLD and, thus, experiments have been carried out with samples spiked with different ^{226}Ra concentrations.

Results, with their corresponding total uncertainties (95% confidence level), are shown in Table 3. As can be seen in all cases, the ^{226}Ra recovery, already corrected at $t = 0$, was over 90%. It should be noticed that matrix differences between samples are not a determining factor in the analyte recovery. Results reveal that the proposed method can be applied according to the legal requirements for total alpha activities in waters.

Table 3
Results obtained from the analysis of ^{226}Ra activity in different water samples

Sample	Origin	V (mL)	Added activity (Bq L^{-1})	Determined activity (Bq L^{-1})[a]
Tap water	Mallorca (Spain)	40	0.0	<LLD
		40	2.5	2.32 ± 0.21
		40	5.0	4.64 ± 0.38
		100	0.05	0.05 ± 0.01
		100	0.10	0.12 ± 0.02
Mineral water	Mallorca (Spain)	40	0.0	<LLD
		40	2.5	2.63 ± 0.23
		40	5.0	4.55 ± 0.38
		100	0.05	0.06 ± 0.01
		100	0.10	0.11 ± 0.02
Mineral water	Jaén (Spain)	40	0.0	<LLD
		40	2.5	2.54 ± 0.22
		40	5.0	4.60 ± 0.38
		100	0.05	0.06 ± 0.01
		100	0.10	0.11 ± 0.02
Seawater	Mallorca (Spain)	40	0.0	<LLD
		40	2.5	2.41 ± 0.22
		40	5.0	4.51 ± 0.37
		100	0.05	0.05 ± 0.01
		100	0.10	0.11 ± 0.02

[a] Mean value ± total uncertainty (number of samples = 3).

4. Conclusions

The combination of MSFIA-MPFS techniques offers several advantages, such as high throughput, versatility, flexibility and simplicity of the system. The incorporation of solenoid micro-pumps to MSFIA allows for the pre-treatment and preconcentration of large sample volumes in a short time avoiding a repetitive filling of the syringes. These facts are of special benefit in radioactivity environmental analysis where isotope concentrations are usually very low.

The adsorption of the analyte on MnO_2 is especially enhanced when the ionic content of the samples is within a similar range to that of drinking waters. It is possible to reuse the cotton filling up to 30 times without affecting the recovery of Radium.

The method presents a good reproducibility and can be applied to a wide range of concentrations of the analyte. The obtained LLD is smaller than the limiting value for the total alpha activity established by the European legislation for drinking waters.

Acknowledgements

This work has been partially supported by MEC (grants CTQ 2004-03256 and FIS 2005-02796). Y.F. thanks the Doctoral Program of Government of the Balearic Islands, through its department of R + D + I, for funding her research.

References

[1] M. Eisenbud, Environmental Radioactivity, second ed., Academic Press, New York, 1973.
[2] C.W. Sill, Nucl. Chem. Waste Manage. 7 (1987) 239.
[3] J.W. Stather, The environmental behaviour of Radium: The behaviour, effects and radiation dosimetry of radium in man. IAEA Technical Reports Series 310, vol. 2, 1990 (Chapter 3.1).
[4] Toxicological profile for radium, CAS # 7440-14-4, Agency for Toxic Substances and Disease Registry U.S. Public Health Service (ATSDR) in collaboration with U.S. Environmental Protection Agency (EPA), 1990.
[5] R.K. Blanchard, R.M. Hahne, B. Kahn, D. McCurdy, R.A. Mellor, M.S. Moore, J. Sedlet, Health Phys. 48 (1985) 587.
[6] W.S. Moore, Nature 380 (1996) 612.
[7] W.S. Rama, W.S. Moore, Geochim. Cosmochim. Acta 60 (1996) 4645.
[8] European Council Directive 98/83/EC on the quality of household water, Off. J. Eur. Communities L330 (1998) 32.
[9] A. Baeza, L.M. del Río, A. Jiménez, Radiochim. Acta 83 (1998) 53.
[10] J.C. Bayés, E. Gómez, F. Garcías, M. Casas, V. Cerdà, Appl. Radiat. Isot. 47 (1996) 849.
[11] D.A. Clifford, E.A. Higgins, Health Phys. 46 (1984) 503.
[12] W.C. Burnett, P.H. Cable, R. Moser, Radioact. Radiochem. 6 (1995) 36.
[13] A. Türler, F. Wegmüller, H.R. Von Gunten, K.E. Gregorich, D. Lee, D.C. Hoffman, M.M. Fowler, Radiochim. Acta 43 (1998) 149.
[14] P. Benzi, R. Righetti, P. Volpe, J. Radioanal. Nucl. Chem. 164 (1992) 211.

[15] C.M. Wai, Preconcentration of trace elements by solvent extraction, in: Z.B. Alfassi, C.M. Wai (Eds.), Preconcentration Techniques for Trace Elements, CRC Press, Boca Raton, 1992.
[16] V.M. Vdovenko, Y.V. Dubasov, Analytical Chemistry of Radium, John Wiley, New York, 1975.
[17] J. Korskisch, Handbook of Ion Exchange Resins: Their Application to Inorganic Analytical Chemistry, CRC Press, Boca Raton, 1989, p. 331.
[18] M. Yamamoto, H. Kawamura, Y.K. Igarashi, K. Ueno, Radiochim. Acta 55 (1991) 163.
[19] W.S. Moore, D.F. Reid, J. Geophys. Res. 78 (1973) 8880.
[20] W.S. Moore, R. Arnold, J. Geophys. Res. 101 (1996) 1321.
[21] W.S. Moore, Deep-Sea Res. 23 (1976) 647.
[22] W.S. Moore, L.M. Cook, Nature 253 (1975) 262.
[23] J. Michel, W.S. Moore, P.T. King, Anal. Chem. 53 (1981) 1885.
[24] J.L. Gascón, M.T. Crespo, M.L. Aceña, Anales de Física B 85 (1989) 360.
[25] J. Eikenberg, A. Tricca, G. Vezzu, S. Bajo, M. Ruethi, H. Surbeck, J. Environ. Radioact. 54 (2001) 109.
[26] K. Morvan, Y. Andres, B. Mokili, J.C. Abbe, Anal. Chem. 73 (2001) 4218.
[27] A. Caldés, E. Gómez, F. Garcías, M. Casas, V. Cerdà, Radioact. Radiochem. 10 (1999) 16.
[28] J.J. Mateos, E. Gómez, F. Garcías, M. Casas, V. Cerdà, Int. J. Environ. Anal. Chem. 83 (2003) 515.
[29] D.S. Moon, W.C. Burnett, S. Nour, P. Horwitz, A. Bond, Appl. Radiat. Isot. 59 (2003) 255.
[30] V. Cerdà, J.M. Estela, R. Forteza, A. Cladera, E. Becerra, P. Altamira, P. Sitjar, Talanta 50 (1999) 695.
[31] J. Ruzicka, E.H. Hansen, Anal. Chim. Acta 78 (1975) 145.
[32] J. Ruzicka, G.D. Marshall, Anal. Chim. Acta 237 (1990) 329.
[33] R.A.S. Lapa, J.L.F.C. Lima, F.R. Boaventura, J.L.M. Santos, E.A.G. Zagatto, Anal. Chim. Acta 466 (2002) 125.
[34] J.L.F.C. Lima, J.L.M. Santos, A.C.B. Dias, M.F.T. Ribeiro, E.A.G. Zagatto, Talanta 64 (2004) 1091.
[35] V. Cerdà, C. Pons, Trends Anal. Chem. 25 (2006) 236.
[36] E. Becerra, A. Caldera, V. Cerdà, Lab. Rob. Autom. 11 (1999) 131.
[37] J.A. Davis, D.B. Kent, Surface complexation modelling in aqueous geochemistry, in: M.F. Hochella, A.F. White (Eds.), Mineral–Water Interface Geochemistry, vol. 23, Mineralogical Society of America, Washington, DC, 1990, p. 177.
[38] D. Langmuir, A.C. Riese, Geochim. Cosmochim. Acta 49 (1985) 1593.
[39] D. Langmuir, D. Melchior, Geochim. Cosmochim. Acta 49 (1985) 2423.

Available online at www.sciencedirect.com
ScienceDirect
Talanta 71 (2007) 1118–1123
Talanta
www.elsevier.com/locate/talanta

Determination of vanadium in human hair slurries by electrothermal atomic absorption spectrometry

Kelly G. Fernandes [a,b], Ana Rita A. Nogueira [a,b], José A. Gomes Neto [c], Joaquim A. Nóbrega [a,*]

[a] *Grupo de Análise Instrumental Aplicada, Departamento de Química, Universidade Federal de São Carlos, Caixa Postal 676, São Carlos SP 13560-970, Brazil*
[b] *Embrapa Pecuária Sudeste, São Carlos SP, Brazil*
[c] *Departamento de Química Analítica, Universidade Estadual Paulista, Araraquara SP, Brazil*

Received 23 March 2006; received in revised form 2 June 2006; accepted 2 June 2006
Available online 14 July 2006

Abstract

This work describes an analytical procedure for vanadium determination in human hair slurries by electrothermal AAS using longitudinal heating (LHGA) and transversal heating (THGA) graphite furnace atomizers. The samples were powdered using cryogenic grinding and the hair slurries containing 0.2% (m/v) were prepared in three different media for determination of vanadium: 0.14 mol L^{-1} HNO_3, 0.1% (v/v) Triton X-100 and 0.1% (v/v) water soluble tertiary amines (CFA-C, pH 8). The limits of detection (LOD), limits of quantification (LOQ), and characteristic masses obtained were 0.28, 0.95 μg L^{-1} and 35 pg (LHGA) and 0.34, 1.13 μg L^{-1} and 78 pg (THGA), respectively. The accuracy of the analytical results obtained by the proposed procedure in both equipments was confirmed by a paired *t*-test at the 95% confidence level and compared with a conventional procedure based on acid digestion.
© 2006 Elsevier B.V. All rights reserved.

Keywords: Vanadium; Human hair; Slurry sampling; Graphite furnace AAS; LHGA; THGA

1. Introduction

Nowadays, hair analysis is requested mainly by doctors working with medicine orthomolecular to evaluate the nutritional state and the possible contaminations by heavy metals. Among the several elements of interest vanadium is an essential element to the organism. However, if present in excess it can cause several diseases or even the death. Vanadium is present in hair samples in concentrations from 90 to 160 μg kg^{-1} [1].

Hair is a solid material and its digestion is usually required before analysis. Usually, most of the methods proposed in the literature for determination of metals involve the acid digestion of hair samples. However, these procedures are time consuming and can cause contamination of the sample. The introduction of solid samples or slurries is an attractive alternative to circumvent these problems [2–6].

According to Kurfürst [7] there are advantages and limitations of slurry sampling in comparison to direct solid sampling. The main advantages of slurry sampling are the use of a higher representative sample mass for electrothermal atomization in graphite furnace atomic absorption spectrometry (GFAAS), easy introduction of the slurry into the atomizer, easy dilution, and possibility of analysis of refractory elements. The main limitations are the increased risk of contamination during grinding, reduced detection power due to the dilution of the pulverized sample, difficulties for too small samples, analyte distributions in biological structures cannot be studied due to the higher sample mass required and stringent homogeneity if no complete extraction occurs for the studied analytes.

Among the analytical techniques used for determination of metals in solid samples and slurries, the electrothermal atomic absorption spectrometry (ETAAS) has led to developments and relevant applications due to the advantages for the introduction of samples and other analytical parameters, such as reduced sample preparation time, decreased possibility of analyte losses by volatilization, reduced contamination by reagents, increased

* Corresponding author. Tel.: +55 16 3351 8088; fax: +55 16 3351 8350.
E-mail address: djan@power.ufscar.br (J.A. Nóbrega).

0039-9140/$ – see front matter © 2006 Elsevier B.V. All rights reserved.
doi:10.1016/j.talanta.2006.06.008

sensitivity and lower amount of concentrated acids [7–12]. The determination of metals in hair slurries is growing in the last years owing to its potential advantages compared to conventional procedures of sample digestion.

Bendicho and De Loos-Vollebregt [13] concluded in a review about direct analysis of solids by GFAAS that better analytical performance is obtained for sampling of slurries due to the facility of change concentrations and the mechanization of the sample introduction using the autosampler. Therefore, advantages of the analysis of solids and solutions can be matched.

The effectiveness of the analysis of slurries depends on several factors, such as homogeneity, density of the material, concentration of the slurry, diluents, characteristic of the homogenization system, and distribution of particle sizes [8,11,13].

The homogenization of slurries can be performed by using magnetic stirrers, vortex effect mixers, manual introduction of air bubbles, or ultrasonic probe [7–18,20–22]. Among these procedures, the ultrasonic agitation seems to be more efficient, because it can provide a partial extraction of the analyte from the solid phase to the solvent [8,10].

Another alternative to maintain the homogeneity of the slurry is using thickening agents as, for instance, Triton X-100, Viscalex, glicerol, non-ionic surfactants, organic solvents and a mixture of water soluble tertiary amines (CFA-C) [8,14,19]. These thickening agents are used with the purpose of avoiding the sedimentation of the suspended material.

The particle size distribution is one of the most important factors in the preparation of slurries, because it influences the stabilization, deposition, and atomization efficiency and, as consequence, it can affect both the precision and accuracy [8,13]. In ETAAS, the distribution of particles is a less critical factor compared to others analytical instrumental techniques, such as flame atomic absorption spectrometry (FAAS), inductively coupled plasma optical emission spectrometry (ICP OES), and inductively coupled plasma mass spectrometry (ICP-MS), due to the absence of a nebulization system and the largest residence time of solid particles in the atomizer [7].

The grinding of the sample is necessary to obtain smaller particle sizes. This procedure is prone to contamination, losses of volatile components, degradation, coagulation or melting of the sample due to the heating during the grinding process [20]. Several procedures of mechanical grinding have been used for the preparation of slurries. The choice of the procedure of mechanical grinding depends on the physical and chemical characteristics of the material to be pulverized and the required range size for final particles.

The procedure of cryogenic grinding was developed for the homogenization of biological materials. The cryogenic grinding is a process carried out at low temperatures with the frozen sample that allows a good homogenization of the sample and leads to accurate results for biological materials.

Santos Jr. et al. [20] demonstrated that using 5 min of precooling in liquid nitrogen and 2 min of grinding for deciduous teeth samples was possible to obtain homogeneous particle size distribution with 90% particles diameters lower than 150 μm.

Kamogawa et al. [18] investigated the use of cryogenic grinding for fast pulverization of hair samples. The particle size distribution obtained after 13 min of cryogenic grinding was determined by laser diffraction and the results showed that 90% of the particle was <95 μm. The particle size distribution obtained was suitable for slurry introduction using an autosampler.

In the last years, the preparation of slurries has been used in the determination of metals in hair samples for ETAAS [12–18,21–23]. However, at the best of our knowledge, any article was published in the literature about the determination of V in hair slurries by GFAAS with longitudinal or transversal heating atomizers. In the first configuration, the heating along the tube heating is less uniform, consequently the ambient inside of the graphite tube is not isothermal and smaller signals are expected. The maximum temperatures can reach around 3000 °C. In the latter one, the graphite tube heating is fast and uniform, leading to a more isothermal ambient inside of the graphite tube. However, the maximum temperature that can be reached is around 2600 °C.

A recent work was published by Hirano et al. [21] for determination of V in hair samples using solid sampling by GFAAS with a polarized Zeeman-effect background corrector. In this work it was demonstrated that the suppression of the analytical signal of vanadium during atomization was efficiently corrected when the heating program was used with the pyrolysis stage assisted by air in the graphite tube for a mass of 2 mg of hair introduced in the atomizer. The results obtained by the proposed procedure were in agreement with those obtained by applying a conventional procedure of acid digestion. According to these authors, a hair reference material (NIES No. 5) did not present a certified value for vanadium. The analytical results obtained for V in the reference material in nine laboratories using different techniques (GFAAS, molecular absorption spectrophotometry, ICP OES, and instrumental neutron activation analysis, INAA) varied from 0.2 to 1.2 mg kg^{-1}, which indicates the difficulty for vanadium determination in hair samples. The detection and quantification limits of the proposed procedure were not presented.

The aim of this study was to develop a simplified slurry procedure based on sample pulverization by cryogenic grinding and slurry preparation for determination of vanadium in hair samples by using two spectrometers with longitudinal or transversely heating atomizers.

2. Experimental

2.1. Instrumentation

Two graphite furnace atomic absorption spectrometers were used: a Varian Model 800 atomic absorption spectrometer (Varian, Mulgrave, Australia) and a Perkin-Elmer SIMAAS 6000 simultaneous multielement atomic absorption spectrometer (Shelton, CT, USA) equipped with an ultrasonic probe. Instrumental parameters for both instruments are detailed in Table 1. All signals were measured as integrated absorbance. The heating programs of the longitudinal and transversely heated atomizers are shown in Tables 2 and 3, respectively.

A SPEX CertiPrep Model 6750 freezer/mill (Metuchen, NJ, USA) was used to grind the hair samples. The particle size dis-

Table 1
Instrumental parameters for vanadium determination

Parameters	GFAAS with longitudinal heating	GFAAS with transversal heating
Instrument	Varian	Perkin-Elmer
Pyrolytic graphite tube	LHGA	THGA
Autosampler	GTA 100	AS-72
Background correction	Transversal Zeeman	Longitudinal Zeeman
Ar flow-rate (mL min^{-1})	3000	250
Radiation source	HCL*	HCL*
Applied current (mA)	20	40
Wavelength (nm)	318.5	318.5
Spectral resolution (nm)	0.2	0.7
Measurement mode	Integrated absorbance	Integrated absorbance
Integration time (s)	4.3	5.0

* Hollow cathode lamp.

Table 2
Heating program of LHGA for V determination in hair slurry*

Step	Temperature (°C)	Time (s) (ramp, hold)	Ar flow-rate (L min^{-1})
1	130	10, 30	3.0
2	300	5, 10	3.0
3	1400	5, 10	3.0
4	2800	0, 5	0 (Read)
5	2800	1, 3	3.0

* Injected volume of 15 μL.

tribution was determined by a CILAS 1064 Laser diffraction instrument (France).

The slurry homogenization in GFAAS with longitudinal heating was carried out using an ultrasonic bath Model USC 1400 (Unique, São Paulo, SP, Brazil). This step was performed automatically by a Ti ultrasonic probe (Model USS-100) available in the GFAAS with transversal heating.

A closed-vessel microwave-oven (Milestone Ethos 1600, Sorisole, Italy) was used for acid digestion of the hair samples.

A sub-boiling apparatus model subPUR (Milestone) was used to purify the concentrated nitric acid.

2.2. Reagents and materials

All dilutions were made using pure water (resistivity 18.2 MΩ cm) obtained in a Milli-Q water purification system (Millipore, Bedford, MA, USA). A stock standard solution containing 1000 mg L^{-1} V (Spex, Metuchen NJ, USA) was used. Double sub-boiling distilled HNO_3 was used throughout experiments to prepare the aqueous reference solutions. Triton X-100 (Merck, Darmstadt, Germany) and a mixture of water soluble tertiary amines brand named as CFA-C (Spectrasol, Warwick, NY, USA) were evaluated as additives to stabilize the slurries. Argon (99.999% purity, White Martins, Sertãozinho, SP, Brazil) was used as purge gas.

Table 3
Heating program of THGA for V determination in hair slurry*

Step	Temperature (°C)	Time (s) (ramp, hold)	Ar flow-rate (mL min^{-1})
1	110	5, 20	250
2	300	10, 20	250
3	1700	5, 20	250
4	2600	0, 5	0 (Read)
5	2600	1, 3	250

* Injected volume of 30 μL.

Two human hair powder samples were enriched with different concentrations of vanadium and used to verify the accuracy of the results obtained by acid digestion and the proposed procedure.

The vanadium reference solutions was prepared in 0.1% (v/v) Triton X-100, 0.1% (v/v) CFA-C or 0.14 mol L^{-1} HNO_3 media from a single stock standard solution (Spex Certiprep, Edison, NJ, USA). Acetone, 99.7% (v/v) (Mallinckrodt Baker, Mexico City, Mexico) was used to wash the hair samples.

All glassware, pipettes, autosampler cups, and polypropylene containers were acid washed with 1.4 mol L^{-1} HNO_3 for 24 h and thoroughly rinsed three times with ultrapure water before use.

2.3. Sample preparation

2.3.1. Hair washing

The hair samples were collected from the nape of the neck near to the scalp region and were cut with stainless steel scissors. The hair length varied between 0.5 and 1.0 cm. A hair washing step is needed to remove contamination exogenous trace elements from the hair surface. The washing procedure carried out in this work was proposed by the International Atomic Energy Agency as previously adopted by Kamogawa et al. [18]. The hair samples were firstly washed with pure water, then three times with acetone and again three times with pure water. Afterwards, the hair samples were oven-dried at 60 °C overnight.

2.3.2. Cryogenic grinding

Approximately 2.0 g of dried hair sample was inserted in a grinding vial, a polycarbonate cylinder supplied with two end plugs, immersed in liquid nitrogen and ground with a magnetically driven impactor. A time of 13 min was required to frozen and pulverize the hair sample and generate a powder with small particles. The grinding procedure was implemented with a first step of 5 min for sample freezing, followed by three cycles with two stages of pulverization and cooling with a total of 8 min. The particle size distribution obtained by cryogenic grinding was determined by laser diffraction. The results indicate that the particle size distribution obtained after 8 min of cryogenic grinding was composed by 90% of the particles <95 μm, 50% of the particles <50 μm and approximately 10% of the particles <7 μm. Most of particles presented sizes <95 μm that is suitable for slurry sampling in GFAAS.

2.3.3. Slurry preparation

A mass of 10–50 mg of powdered hair sample was accurately weighed, transferred to a volumetric flask and adjusted to a final volume of 10 mL by the addition of three different liquid media containing 0.14 mol L^{-1} HNO_3, 0.1% (v/v) Triton X-100 or 0.1% (v/v) CFA-C. The slurries were homogenized by ultrasonic batch or by ultrasonic probe during 15 s at 50 W power.

2.3.4. Microwave-assisted acid digestion

For comparative purposes, an acid decomposition was performed in a cavity microwave oven with closed-vessels. Previously, two samples were enriched with V according to the following procedure: masses of 0.8059 g of the sample 1 and 0.8041 g of the sample 2 were weighed in flasks of polyethylene. A volume of 10 mL of reference solutions containing 12.0 and 25.0 ng mL^{-1} V was added to samples 1 and 2, respectively. These samples were kept during 48 h. After, both samples were filtered and washed three times with pure water, and then dried at 60 °C overnight.

These samples enriched with V were acid digested in triplicate. A mass of 200 mg of dried powdered materials were accurately weight into the PFA digestion vessels, 2.0 mL of 50% (v/v) HNO_3 and 1.0 mL of 30% (m/m) H_2O_2 were added, and then the vessels were closed and placed on the microwave oven cavity. Thereafter, the following power/time program was run: step 1, 250 W/120 s; step 2, 0 W/90 s; step 3, 550 W/120 s; step 4, 600 W/180 s; step 5, 700 W/180 s; step 6 (ventilation), 0 W/300 s. After cooling, the digested samples were transferred to a 10 mL volumetric flask and diluted with pure water up to the mark. Vanadium in the digestates was determined by GFAAS with longitudinal heating and GFAAS with transversal heating.

2.3.5. Analytical procedure

The optimum pyrolysis and atomization temperatures were established with 30 μL of hair slurries spiked with 50 ng mL^{-1} V for GFAAS with longitudinal heating and 100 ng mL^{-1} V for GFAAS with transversal heating.

Analytical calibration curves of 1.0–5.0 ng mL^{-1} were performed using aqueous reference solutions prepared in 0.1% (v/v) CFA-C medium (pH 8) for V quantification in slurry samples. The injected volume into the atomizer was 15 μL for GFAAS with longitudinal heating and 30 μL for GFAAS with transversal heating, respectively. The volume introduced in THGA was higher to improve analytical signals obtained in this equipment.

3. Results and discussion

3.1. Electrothermal behavior of vanadium in GFAAS with longitudinal heating and GFAAS with transversal heating

The influence of the pyrolysis and atomization temperatures in the determination of vanadium in 0.2% (m/v) of hair slurry containing 50 ng mL^{-1} in 0.1% (v/v) Triton X-100 and 0.1% (v/v) CFA-C (pH 8) using GFAAS with longitudinal heating are shown in Fig. 1. The optimum pyrolysis and atomization temperatures obtained experimentally were 1600 and 2800 °C in 0.1% (v/v) Triton X-100 and 1400 and 2800 °C in 0.1% (v/v) CFA-C (Fig. 1). Background signals obtained in each condition are also shown.

The optimum pyrolysis and atomization temperatures for the determination of vanadium in 0.2% (m/v) of hair slurry containing 100 ng mL^{-1} in the media 0.1% (v/v) Triton X-100 and 0.1% (v/v) CFA-C (pH 8) using GFAAS with transversal heating are shown in Fig. 2. The pyrolysis and atomization temperatures determined were 1700 and 2600 °C for both media (Fig. 2).

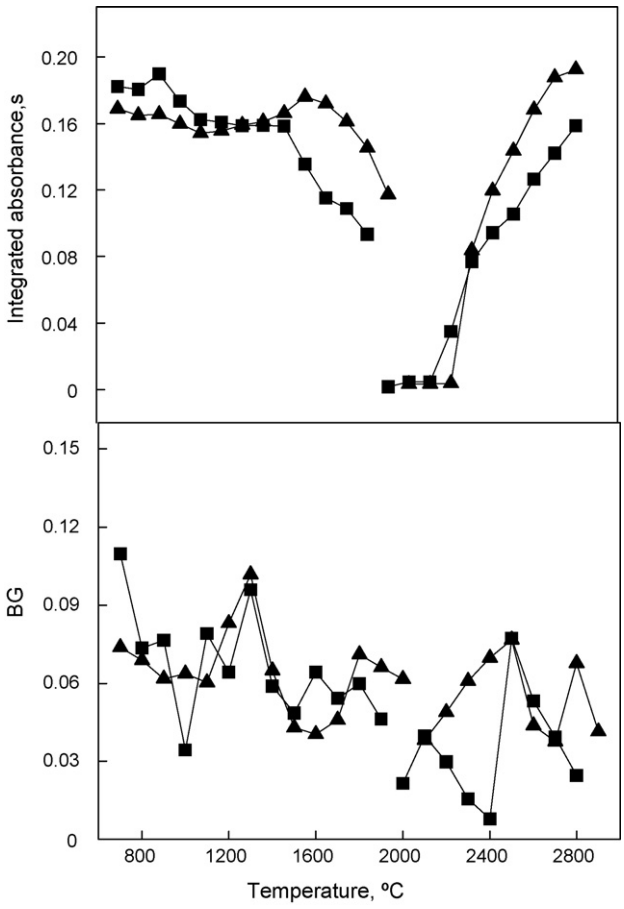


Fig. 1. (A) Pyrolysis and atomization curves in LHGA for 50 ng mL^{-1} V in 0.2% (m/v) hair slurry in 0.1% (v/v) Triton X-100 (▲) and 0.1% (v/v) CFA-C (pH 8) (■). (B) Background signals in LHGA for 50 ng mL^{-1} V in 0.2% (m/v) of hair slurry in 0.1% (v/v) Triton X-100 (▲) and 0.1% (v/v) CFA-C (pH 8) (■).

Background (BG) signals are also shown. Greater BG signals were obtained in both media in GFAAS with transversal heating. This can be due to the greater amount of mass added in GFAAS with transversal heating ($V = 30$ μL) in relation to the GFAAS with longitudinal heating ($V = 15$ μL).

3.2. Effect of the sample mass in the slurry

After establishing the pyrolysis and atomization temperatures, the effect of sample mass of the slurry on absorbance signals was evaluated for solutions containing 0.014 mol L^{-1} HNO_3, 0.1% (v/v) Triton X-100, and 0.1% (v/v) CFA-C (pH 8). The mass of hair was varied from 10 to 50 mg. Masses higher than 30 mg caused memory effects and accumulation of carbonaceous residues inside of the atomizer in both equipments. Smaller relative standard deviations in different media for both equipments were obtained with 20 mg hair. The effect of the medium in the integrated absorbance signals for V in 0.2% (m/v) of slurry is shown in Fig. 3A. The blank values obtained in Triton X-100 medium were five-fold larger than those obtained in CFA-C medium. On the other hand, memory effects were observed in HNO_3 medium mainly for deteriorated graphite tubes and this can explain the slightly better sensitivity observed in this

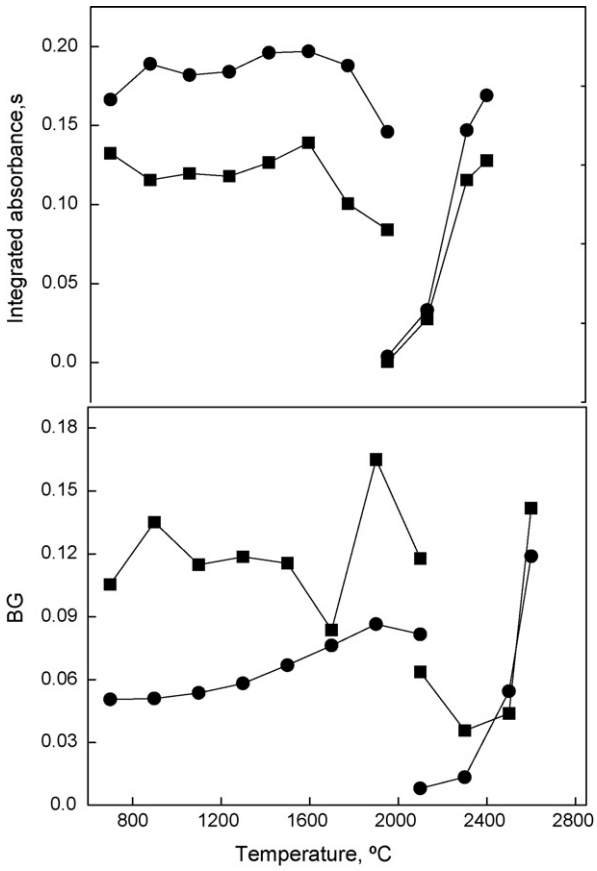


Fig. 2. (A) Pyrolysis and atomization curves in THGA for 100 ng mL^{-1} V in 0.2% (m/v) of hair slurry in 0.1% (v/v) Triton X-100 (●) and 0.1% (v/v) CFA-C (pH 8) (■). (B) Background (BG) signals in THGA for 100 ng mL^{-1} V in 0.2% (m/v) of hair slurry in 0.1% (v/v) Triton X-100 (●) and 0.1% (v/v) CFA-C (pH 8) (■).

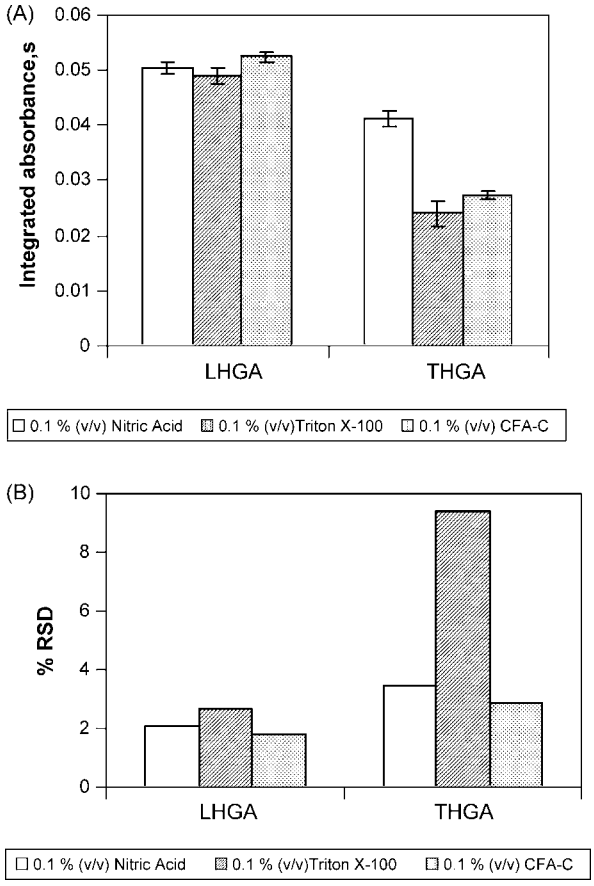


Fig. 3. (A) Mean integrated absorbances for V in 0.2% (m/v) of slurry in 0.014 mol L^{-1} HNO_3, 0.1% (v/v) Triton X-100 and 0.1% (v/v) CFA-C for LHGA and THGA. (B) Relative standard deviations ($n = 10$) for V in 0.014 mol L^{-1} HNO_3, 0.1% (v/v) Triton X-100 and 0.1% (v/v) CFA-C for LHGA and THGA.

medium. However, it should be emphasized that all these effects are critically dependent on graphite tube surface conditions. The relative standard deviations in each medium for slurries containing 0.2% (m/v) are also shown in Fig. 3B for both equipments. For GFAAS with longitudinal heating and GFAAS with transversal heating, a greater absorbance signal and smaller deviation relative standard deviations were obtained in 0.1% (v/v) CFA-C medium.

3.3. Calibration and analytical performance

The matrix effects were evaluated by comparing the slopes between analytical calibration curves built up using reference solutions prepared in CFA-C medium and based on standard additions technique. The slopes of the analytical calibration curves obtained by both strategies were similar independent on the atomizer employed. Therefore, calibration based on reference solutions prepared in CFA-C was adopted owing to its simplicity. The accuracy of the proposed method was evaluated using enriched hair samples. Vanadium determination in slurries and digests were carried out using two atomizer configurations. The analytical calibration curves were built up from 5.0 to 30.0 ng mL^{-1} V in 0.1% (v/v) CFA-C (pH 8) and 1.0% (v/v) HNO_3 medium. The equations of the analytical curves of calibration obtained in 0.1% (v/v) CFA-C for LHGA ($Q_A = 0.0003 + 0.00188c$, $r = 0.9996$) and in 1.0% (v/v) HNO_3 ($Q_A = 0.001 + 0.00161c$, $r = 0.9981$) were similar, where Q_A is the integrated absorbance and c is the vanadium concentration. For THGA, the equations of the analytical curves obtained in 0.1% (v/v) CFA-C ($Q_A = -0.00017 + 0.00171c$, $r = 0.9996$) and in 1.0% (v/v) HNO_3 ($Q_A = -0.00005 + 0.00264c$, $r = 0.9998$) were also shown similar. The analytical curves obtained experimentally in GFAAS with longitudinal heating and GFAAS with transversal heating presented similar angular coefficients.

The results obtained in the determination of V in digested samples and hair slurries by LHGA and THGA are similar (Table 4). Accuracy of analytical results obtained by the proposed procedure in both equipments was confirmed by the paired t-test at the 95% confidence level compared with the conventional acid digestion procedure. Results obtained for five hair samples are shown in Table 5. All slurries were prepared in CFA-C medium. The results obtained in both atomizers for vanadium in hair slurries were similar. It can be seen that larger relative standard deviations were obtained for THGA compared with LHGA. This can be related to memory effects or graphite tube lifetime. It should also be pointed out that all five samples are female hair samples submitted to treatment with color dyes.

Table 4
Mean and standard deviation values ($n = 3$) for V in slurries and digests of hair enriched samples obtained by LHGA and THGA

Sample	LHGA (C/μg g^{-1} V)[a]		THGA (C/μg g^{-1} V)[b]	
	Digest	Slurry[c]	Digest	Slurry[c]
1	0.60 ± 0.04	0.67 ± 0.05	0.58 ± 0.05	0.69 ± 0.02
2	0.85 ± 0.05	0.86 ± 0.03	0.68 ± 0.06	0.59 ± 0.03

[a] Injected volume of 15 μL.
[b] Injected volume of 30 μL.
[c] Injected volume of 20 mg in 10 mL.

Table 5
Mean and standard deviation values ($n = 3$) for V determination in human hair slurries by LHGA and THGA

Sample	LHGA[a] slurry[c] (C/μg g^{-1} V)	THGA[b] slurry[c] (C/μg g^{-1} V)
1	0.92 ± 0.07	1.09 ± 0.16
2	0.87 ± 0.05	1.02 ± 0.37
3	1.07 ± 0.06	1.33 ± 0.27
4	1.05 ± 0.09	0.94 ± 0.32
5	0.90 ± 0.07	0.91 ± 0.18

[a] Injected volume of 15 μL.
[b] Injected volume of 30 μL.
[c] Injected volume of 20 mg in 10 mL.

This indicates the feasibility of the analytical procedure proposed for the determination of V in hair slurries in 0.1% (v/v) CFA-C for both atomizers.

The detection and quantification limits obtained for the proposed procedure by LHGA were 0.28 and 0.95 μg L^{-1}. The characteristic concentration and characteristic mass obtained were 2.3 ng mL^{-1} and 35 pg, respectively. For THGA, the detection and quantification limits obtained for the proposed procedure were of 0.34 and 1.13 μg L^{-1}. The characteristic concentration and characteristic mass obtained were 2.6 ng mL^{-1} and 78 pg, respectively.

4. Conclusions

Owing to the refractory character of the vanadium, high temperatures of atomization are required to obtain suitable signal profiles in GFAAS. A limiting factor in the vanadium determination was the maximum temperature reached in THGA configuration. However, even using atomization temperature lower than the optimum for V, good results were obtained for vanadium determination in slurries and acid digests of hair.

The procedure developed for vanadium determination in hair slurries can be applied using both equipments. The developed procedure is simple, rapid and fast and it can be applied for the routine determination of vanadium in human hair samples.

Acknowledgements

The authors gratefully acknowledge the financial support provided by Fundação de Amparo à Pesquisa do Estado de São Paulo (FAPESP, Process 03/00326-1). The authors also would like to thank the Conselho Nacional de Desenvolvimento Científico e Tecnológico (CNPq) for fellowships and grants.

References

[1] D. Pozebon, V.L. Dressler, A.J. Curtius, Quim. Nova 22 (1999) 838.
[2] N.J. Miller-Ihli, J. Anal. At. Spectrom. 12 (1997) 205.
[3] V. Terzieva, S. Arpadjan, J. Anal. At. Spectrom. 13 (1998) 815.
[4] P. Viñas, N. Campillo, I. López-Garcia, M. Hernández-Córdoba, Fresenius J. Anal. Chem. 349 (1994) 306.
[5] A. Carlosena, M. Gallego, M. Valcárcel, J. Anal. At. Spectrom. 12 (1997) 479.
[6] R.A. Conte, M.T.C. De-Loos-Vollebregt, Fresenius J. Anal. Chem. 367 (2000) 722.
[7] U. Kurfürst (Ed.), Solid Sample Analysis. Direct and Slurry Sampling Using GF-AAS and ETV-ICP, Springer, Berlin, 1998, p. 279.
[8] M.J. Cal-Prieto, M. Felipe-Sotelo, A. Carlosena, J.M. Andrade, P. López-Mahía, S. Muniategui, D. Prada, Talanta 56 (2002) 1.
[9] C.E.C. Magalhães, M.A.Z. Arruda, Quim. Nova 21 (1998) 1.
[10] N.J. Miller-Ihli, Fresenius J. Anal. Chem. 337 (1990) 271.
[11] N.J. Miller-Ihli, Anal. Chem. 64 (1992) 964.
[12] N.J. Miller-Ihli, J. Anal. At. Spectrom. 9 (1994) 1129.
[13] C. Bendicho, M.T.C. De Loos-Vollebregt, J. Anal. At. Spectrom. 6 (1991) 353.
[14] P. Bermejo-Barrera, A. Moreda-Piñeiro, T. Romero-Barbeito, J. Moreda-Piñeiro, A. Bermejo-Barrera, Talanta 43 (1996) 1099.
[15] J. Stupar, F. Dolinsek, Spectrochim. Acta Part B 51 (1996) 665.
[16] P. Bermejo-Barrera, A. Moreda-Piñeiro, J. Moreda-Piñeiro, A. Bermejo-Barrera, Anal. Chim. Acta 349 (1997) 319.
[17] P. Bermejo-Barrera, A. Moreda-Piñeiro, J. Moreda-Piñero, A. Bermejo-Barrera, Talanta 45 (1998) 1147.
[18] M.Y. Kamogawa, A.R.A. Nogueira, L.M. Costa, E.E. Garcia, J.A. Nóbrega, Spectrochim. Acta Part B 56 (2001) 1973.
[19] M.C. Santos, A.R.A. Nogueira, J.A. Nóbrega, J. Braz. Chem. Soc. 16 (2005) 372.
[20] D. Santos Jr., F. Barbosa Jr., S.S. Souza, F.J. Krug, J. Anal. At. Spectrom. 18 (2003) 939.
[21] Y. Hirano, K. Yamamura, K. Oguma, K. Harada, Anal. Sci. 17 (2001) 351.
[22] P. Bermejo-Barrera, E.M. Verdura-Constenla, A. Moreda-Piñeiro, A. Bermejo-Barrera, Anal. Chim. Acta 398 (1999) 263.
[23] P. Bermejo-Barrera, E.M. Verdura-Constenla, J. Moreda-Piñeiro, A. Bermejo-Barrera, Fresenius J. Anal. Chem. 360 (1998) 712.

Available online at www.sciencedirect.com
ScienceDirect
Talanta 71 (2007) 1001–1010
Talanta
www.elsevier.com/locate/talanta

Development of a simple extraction procedure for chlorpyrifos determination in food samples by immunoassay

J.A. Gabaldón [a], A. Maquieira [b], R. Puchades [b,*]

[a] Centro Tecnológico Nacional de la Conserva (CTC), C/Concordia s/n, 30500 Molina de Segura, Murcia, Spain
[b] Departamento de Química, Universidad Politécnica de Valencia, Camino de Vera s/n, 46071 Valencia, Spain

Received 10 November 2004; received in revised form 24 March 2006; accepted 6 April 2006
Available online 4 August 2006

Abstract

The suitability of immunoassay methodology for rapid and accurate determination of chlorpyrifos in vegetables was tested. The optimised ELISA detection limit was 0.32 ng/ml, with a working range from 0.69 to 6.21 ng/ml and an immunoassay test-mid point (IC_{50}) of 2.08 ng/ml. A rapid sample preparation procedure considering different parameters such as the amount of sample, volume of extractant, extraction time and dilution factor was optimised. The developed direct extraction (DE) and multiresidue (ME) standard procedures were performed in different fortified fresh and processed vegetable samples (tomato, bonnet pepper, bean, pea, asparagus, broccoli, watermelon, melon, lettuce, cucumber, celery and red pepper). Recoveries were in all cases in the whole range 85.2–108.9% for both DE and ME extracts. Also, the comparison of the results obtained by both immunochemical and chromatographic methods for spiked fruits and vegetables were good with a correlation coefficient (r) of 0.97.
© 2006 Elsevier B.V. All rights reserved.

Keywords: Immunoassay; Rapid extraction procedure; Fruits; Vegetables; Organophosphorous; Pesticides; Chlorpyrifos

1. Introduction

Chlorpyrifos, was first introduced and patented by Dow Chemical Company in 1965 [1] and commercially available as formulated Dursban® for indoor use and Lorsban® for crop protection. Chlorpyrifos is a broadly active, non-systemic insecticide used to control a variety of soil insects and arthropods on a wide range of crops including citrus fruits, peaches, nectarines, vegetables, cereals, maize and tobacco. In addition, post-harvest application prior to storage is indicated for pest protection. Non-crops uses of chlorpyrifos include application to soil surrounding building structures as barriers to termites and control of household insects such as ants and cockroaches.

It is moderately toxic to mammalian species [2] but extremely toxic to a wide range of non-target aquatic biota [3]. It's effective by ingestion and contact, being absorbed through skin, gut and pulmonary membranes. Chlorpyrifos acts by phosphorylating acetylcolinesterase both at the synapse of neurones and in the plasma [4,5].

Chlorpyrifos is actually one of the most widely used insecticides in the world at the rate of over 50,000 kg/year in Europe [6] and in amounts exceeding 5 million kg/year in US agriculture and 4 million kg/year for non-agricultural uses [7]. Due to its widespread use, persistency and toxicity, chlorpyrifos has been included in priority lists of pesticides within the EU [8]. Also, high chlorpyrifos residue occurrence in food [9,10] and environmental compartments [11] have been reported.

Since fruits and vegetables are an important part of the human diet, organophosphorous insecticides are used to obtain high yields. As a result, pesticide residue determination is very important in this type of foods because of government regulations and human health.

Different chromatographic methods for the determination of chlorpyrifos residues and its main metabolites in food and environmental samples have been developed [12–18]. For example, limits of detection (LOD) between 0.05 and 0.5 ng/ml were reached using tin layer chromatography (TLC) [19]; also high pressure liquid chromatography (HPLC)—with LOD of 16 ng/l—for the analysis of chlorpyrifos in water [20], or reverse phase HPLC for simultaneous determination of chlorpyrifos and their degradation products, have been reported [21]. In addition, gas chromatography (GC) coupled to nitrogen/phosphorous (NPD) [22,23], atomic emission (AED) [24], electron capture

* Corresponding author. Tel.: +34 963 877342; fax: +34 963 877349.
E-mail address: rpuchade@qim.upv.es (R. Puchades).

0039-9140/$ – see front matter © 2006 Elsevier B.V. All rights reserved.
doi:10.1016/j.talanta.2006.04.041

(ECD) [25] or flame photometric detectors (FPD) [26], have also been applied for the determination of chlorpyrifos.

The limited specificity of the described detectors encourages the application of mass spectrometry (MS) techniques that have been coupled to liquid (LC–MS) [27] or gas (GC–MS) [28] chromatographs for the single, and unequivocal, identification of chlorpyrifos in environmental compartments. For the determination of organophosphate pesticide in fruits and vegetables both (LC–MS) or (GC–MS) have also been applied, showing LODs between 0.001 and 0.004 mg/kg [29] and 0.005 mg/kg [30], respectively.

Although chromatographic techniques provide low limits of detection, preliminary treatment (extraction, cleanup, preconcentration, etc.) of the sample typically remains a mandatory requirement, which makes the procedure laborious.

As alternative—or complement—to conventional techniques, sensitive and specific immunochemical methods [31], based on ELISA format, have previously been described and applied to the detection of chlorpyrifos [32–34]; mainly in water samples—using mAbs coated to microtiter plates [35] or linked to magnetic particles [36]—with LOD of 6.0 and 0.1 ng/ml, respectively; soils at concentrations ranging from 50 to 500 ng/g [37]; olive oil—using pAbs on an indirect coated plate immunoassay—show limits of detection of 0.3 and 0.07 ng/g [38], or fruits and vegetables with recoveries in the range 82–123% [39].

Whereas water samples can be analysed directly, identification and removal of matrix effects are the major drawbacks for the application of pesticide immunoassay in foods [40]. In this sense, methods need to be developed to provide reliable data, using minimum sample processing, or otherwise many of the potential advantages of the immunoassays, such as low cost, speed, and simplicity, would be lost [41].

Determination of chlorpyrifos in environmental and food samples by immunoassay is difficult due to its hydrophobicity. Some authors have reported plastic adsorption of chlorpyrifos, resulting in low recoveries and inaccurate results [32,33]. Therefore, a careful use of the equipment (pipettes, tips, ELISA plates) is necessary to minimize analyte losses.

This paper reports the development of a rapid preparation procedure—cost effective and simple—to adapt the immunoassay to the analysis of chlorpyrifos in foods. A preparation scheme considering the sample amount, volume of extractant, extraction time and dilution factor was optimised. For this purpose, both direct extraction (DE) and multiresidue (ME) standard procedures were performed in different fortified fresh and processed vegetable samples. Analytical parameters such as sensitivity, accuracy and reproducibility were evaluated and the results discussed in comparison with those achieved using a well-established GC/MS method.

2. Experimental

2.1. Materials and instrumentation

The monoclonal anti-chlorpyrifos antibody (mAb) and the hapten PNC [*O*-ethyl-*O*-(2,4,5-trichlorophenyl)-*N*-(2-carboxyethyl) phosphoramidothioate], used to prepare the enzymatic tracer PNC–HRP through a modification of the anhydride mixed method [42] were a gift from Laboratorio Integrado of Bioingeniería (LIB) [35].

Poly(oxyethylensorbitan)monolaurate (Tween 20) and *O*-phenylenediamine (OPD) were purchased from Sigma Chemical Co., (St. Louis, MO). Horseradish peroxidase (HRP) was purchased from Boehringer (Mannheim, Germany). *N*-Hidroxisuccinimide (NHS) and diciclohexilcarbodiimide (DCC), used to obtain hapten protein conjugate were from Fluka–Aldrich (Madrid, Spain). Sodium azide, ammonium sulphate and *N*,*N*-dimethylformamide (DMF) were purchased from Panreac (Barcelona, Spain), and chromatographic gel Sephadex G-25 was from Pharmacia (Lund, Suecia). All other reagents used were analytical or biochemical grade. Analytical standards of chlorpyrifos, chlorpyrifos-methyl, chlorpyrifos-oxon, fenchlorphos, bromophos, trichloronate, diazinon and the chlorpyrifos metabolite 3,5,6-trichloro-2-pyridinol (TCP) were purchased from Dr. Ehrenstorfer (Augsburg, Germany) and Riedel de Häen (Seelze-Hannover, Germany). Stock solutions of pesticides were prepared in *N*,*N*-dimethylformamide (DMF) and kept at −20 °C. Standards were daily prepared in PBS by serial dilutions from the stock using borosilicate glass tubes, since we found that plastic material adsorbs chlorpyrifos, as also reported by different authors [32,33,43].

The coating buffer (CB) was 50 mM sodium carbonate–bicarbonate buffer pH 9.6. Phosphate buffered saline (PBS) was a solution of 10 mM phosphate, 137 mM NaCl, 2.7 mM KCl, pH 7.4. PBS-T was PBS with 0.05% Tween-20. Citrate–phosphate buffer was 25 mM sodium citrate, 62 mM sodium phosphate buffer, pH 5.4. The enzymatic substrate solution was OPD (2 mg/ml) and H_2O_2 (0.012%) in citrate–phosphate buffer.

Polystyrene microtiter plates were purchased from Costar (Cambridge, MA, USA). Washing steps were carried out using a 12-channel microplate washer from Nunc (Roskilde, Denmark). Absorbances were read with a Multilabel Counter 1420 microplate reader from Wallac (Turku, Finland) at dual wavelength mode. Data processing was performed using Sigmaplot software package (Jandel Scientific, Erkrath, Germany).

For GC analysis a 6890 Hewlett-Packard device—automatic sampler—provided with a 5% phenyl-methyl siloxane capillary column (HP-5MS) model 19091S-433 (30 m length × 250 μm diameter × 0.25 μm film thickness) and flame-ion detector (FID) was used. Also, a 5973 mass selective detector (MS) operated in a selected ion monitoring (SIM) mode was employed for peak identification.

2.2. ELISA procedure using antibody-coated format

Working concentrations were determined by titration assays using different concentrations of mAb (from 5 to 20 mg/l) and tracer (from 0.4 to 1 mg/l). Optimal concentrations for mAb and PNC–HRP were chosen to give absorbance values in the range 0.7–1.0 units in absence of analyte in 1 h.

For competitive assays flat bottom polystyrene ELISA plates were coated overnight at 4 °C with 5 mg/l (0.1 ml/well) of

mAb in coating buffer (CB). Plates were washed four times with PBS-T. Then, 0.05 ml/well of chlorpyrifos standards (0.02–2000 ng/ml) or samples—by quadruplicate,—followed by 0.05 ml/well of a 0.8 mg/l solution of the tracer PNC–HRP, were added to the coated plates and incubated for 1 h at room temperature in the dark. Once washed, the HRP tracer activity was measured by adding 0.1 ml/well of substrate solution (2 mg/ml OPD and 0.012% H_2O_2 in 25 mM citrate, 62 mM sodium phosphate buffer, pH 5.4). After 10 min, the enzymatic reaction was stopped (adding 0.1 ml/well of 2.5 M sulphuric acid), and the absorbance was read at 490 nm as test wavelength and 650 nm as reference wavelength.

To evaluate the specificity of the mAb, different chemically related and unrelated compounds were assayed. Four calibration curves for each compound were obtained in optimised ELISA conditions. The cross-reactivity (CR) values were calculated according to the following equation:

$$\mathrm{CR}\,(\%) = \frac{(\mathrm{IC}_{50})\,\text{chlorpyrifos}}{(\mathrm{IC}_{50})\,\text{chemically related compound}} \times 100$$

2.3. GC/MS operating conditions

Previous to GC/MS analysis, vegetable extracts (see Section 2.5) were conditioned with ethylacetate/hexane (1/1). Helium was used as carrier gas with a flow rate of 1.2 ml/min and samples were injected in the splitless mode by an autoinjector. The column temperature was held at 90 °C for 1 min, then increased 10 °C/min to 210 °C, 5 °C/min to 240 °C, 30 °C/min to 270 °C and held at this temperature for 10 min. Injector temperature was 250 °C. Peak identification was carried out by selected ion monitoring of three characteristic fragment ions (*m/z* 258, 286, 314) and chlorpyrifos concentration was calculated by the equation:

$$[\text{chlorpyrifos}] = \frac{A_\mathrm{m} C_\mathrm{p} V_\mathrm{r}}{A_\mathrm{p} P}$$

where A_m is the sample peak area, C_p the stock concentration in ng/g, V_r volume of the reconstituted extract in l, A_p the stock peak area and P is the weight of sample in kg.

2.4. Optimisation of a direct extraction protocol (DE)

Tacking into account the polarity (octanol/water partition coefficient) of the analyte, acetone was used as solvent for extraction of chlorpyrifos in vegetable samples.

Weight of sample, volume of solvent, extraction time—by shacking—to achieve high yields and optimal dilution of the extracts in assay buffer, in order to provide accurate and sensitive determinations, were previously evaluated.

Canned tomato sample—selected as model matrix—was fortified with chlorpyrifos at 500 ng/g and homogenised overnight. Then, 10, 20, 30, and 40 ml of acetone were respectively added to 5, 10, 15 and 20 g of spiked/homogenised sample and sacked for 5, 10, 15 and 20 min. Afterwards, samples were extracted following the rapid extraction protocol described in Section 2.5.

Acetone direct extraction (ADE)—as rapid sample treatment method,—was evaluated using as reference the multiresidue Luke method (ME) [44].

Recovery studies were carried out by spiking homogenised canned tomato samples with a known amount of chlorpyrifos, in the range 96–780 ng/g. The samples were then extracted by both ADE and ME methods and analysed by ELISA.

In order to determine the precision of ADE method, tomato and pepper samples fortified at 400 ng/g were tested. Four spikes of each level were allowed to set for 1 h before extracting. Samples were extracted and analysed as described in Section 2.5.

To study the reproducibility and accuracy of extraction method 1 kg of canned tomato sample was fortified at 500 ng/g. Twelve aliquots of 5 g and 12 of 15 g (see Section 2.5), were respectively extracted using ADE and ME, and analysed by ELISA once a day for six different days.

Canned pepper and tomato samples were fortified with chlorpyrifos by a lab technician, and provided as blind samples. Vegetable samples were previously checked by GC–MS method for free chlorpyrifos contamination. Samples (six of each one) were extracted by both ADE and ME methods and the chlorpyrifos concentration in the extract determinate by ELISA.

2.5. Sample preparation and extraction

Fresh and processed vegetables (asparagus, bean, broccoli, bonnet pepper, celery, cucumber, lettuce, melon, pea, red pepper, tomato and watermelon) were collected from a local market of Valencia (Spain) and checked for chlorpyrifos by GC–MS. Before extraction procedure, samples were chopped and homogenised in a blender Osterizer (Milwaukee, WI). After this, chlorpyrifos-free samples were fortified at different levels (0—as control,—400, and 600 ng/g) with a 1000 mg/l chlorpyrifos standard, mixed, homogenised overnight and extracted according to the procedure described below. Briefly, vegetable samples (5 g) and 10 ml of acetone were blended for 10 min, and the supernatant vacuum filtered through 0.45 μm nylon filters (Durapore® membrane filters) using a Millipore extraction device. The extracts were then conditioned by diluting 1/25 (v/v) in PBS 2× and checked for chlorpyrifos with both ELISA and GC–MS methods. In order to assess assay reproducibility, triplicates of each fortification level were performed.

The results obtained by rapid extraction (ADE) coupled to ELISA assay were compared with that obtained by GC–MS.

On the other hand, samples were also extracted using the method described by Luke et al. [44] with slight modifications. Briefly, fortified samples (15 g) were homogenised for 30 s with 30 ml of acetone using an Ultra-turrax T-25 apparatus mixer (Hanke and Junkle, Germany). A 30 ml of dichloromethane and 30 ml of light petroleum were subsequently added, and the mixture was homogenised again for 60 s. After centrifugation for 5 min at 4000 rpm, a portion of 25 ml of the organic layer was transferred to a conical-bottom flask, the solvent evaporated to dryness and reconstituted with 5 ml of an ethyl acetate–hexane mixture (1/1, v/v). Finally, 0.002 ml of each sample was injected by pulsed splitless, on the GC column for chlorpyrifos quantification. For ELISA determination, the extract was

reconstituted in 2 ml of acetone and conditioned in the assay buffer.

2.6. Statistical study

With the aim to achieve information about the effect of several factors—type of sample, insecticide concentration, extraction and determination methods,—in the chlorpyrifos recovery, an analysis of variance (ANOVA) using Startgraphics Plus 5.0 statistical software package were carried out. In all cases, a multiple comparison of mean values was done using LSD test.

For all statistical analyses, the significance level was set at 0.05. The significance level is the probability of incorrectly rejecting the null hypothesis in a given statistical test; it is set *a priori* to running a test to ensure correctness. To determine the statistical significance of the analyses performed, a *p*-value was generated with each statistic. The *p*-value is the lowest level at which the significance level can be rejected; in this case, any *p*-value less than 0.05 would show that the test is statistically significant.

A factorial design by triplicate ($n = 3$), with four factors at different levels was used:

(a) Type of matrix
Twelve levels qualitative factor: (1) tomato; (2) pea; (3) bean; (4) asparagus; (5) bonnet pepper; (6) broccoli; (7) celery; (8) watermelon; (9) cucumber; (10) melon; (11) lettuce; (12) red pepper.
(b) Chlorpyrifos concentration
Two levels qualitative factor: (1) low fortification level (400 ng/g) and (2) high fortification level (600 ng/g).
(c) Extraction method
Two levels qualitative factor: (1) acetone direct extraction (ADE) and (2) multiresidue extraction (ME).
(d) Determination method
Two levels qualitative factor: (1) ELISA and (2) GC–MS.

3. Results and discussion

The highest maximum absorbance (B_0) to IC_{50} chlorpyrifos ratio (concentration giving 50% of B_0) was obtained by using 5 mg/l mAb PO4 as coating immunoreagent and 0.8 mg/l of PNC–HRP enzyme tracer. These were selected as optimal to carry out competitive assays, achieving an IC_{50} value of 1.8 mg/l in aqueous media.

Matrix effect in food samples frequently occur due to the coloured extracts or the content of lipids, proteins, polyphenols that may be coextracted throughout sample preparation [41]. As food samples usually have to be extracted prior to immunochemical analysis, the method of analyte extraction is of great importance. Usually, water-soluble analytes can be efficiently extracted in aqueous buffer. However, many pesticides—like chlorpyrifos—are not readily water soluble [45] and must be extracted with an organic solvent.

For the extraction of pesticides from solid foods, a variety of solvents such as acetone, ether, petroleum ether, methanol, acetonitrile or hexane have been tested [46]. Direct analysis of extracts by IA requires the use of solvents that are miscible with water and (at low concentrations) non-denaturating to proteins such as Ab. IA are to a certain degree tolerant to a variety of solvents, but each system must be tested to determine which solvent can be accepted and to what extent [47].

Consequently, tolerance level of the immunoreagents to acetone solvent was studied. The optimal percentage was estimated tacking into account two approaches: (i) no practical effects on the Ab–Ag interactions and (ii) minimal dilution of the extracts. Competitive assays were carried out with different acetone percentages from 2 to 20. As can be seen in Fig. 1, adverse effects appears at acetone concentrations higher than 8% with a reduction of B_0 close to 80%. Thus, selecting 4% acetone as optimum, the values obtained for the more representative parameters—B_0 and IC_{50}—were 0.89 and 2.08 ng/ml, respectively.

Tacking into account the previously selected conditions, a set of individual curves ($n = 50$) were normalised by expressing the absorbance as the percentage of the maximum response to obtain the standard curve (Fig. 2). The errors bars—each point represents the mean ± standard deviation—at each calibration point show the assay to assay variability expected from small differences in timing, temperature, or reagent age over the 50 assays.

The error bars demonstrate the good reproducibility achieved, with coefficients of variation (CV) lower than 5.6% for all chlorpyrifos concentrations tested.

Working in acetone medium (4%), the linear range for the chlorpyrifos ELISA assay was from 0.69 to 6.21 ng/ml with an IC_{50} value of 2.13 ng/ml.

The limit of detection or least detectable dose (LOD) is the smallest concentration of the analyte that produced a signal significantly different from zero with a stated degree of confidence. There is a general consensus in favour of selecting the analyte dose that provides a reduction of B_0 of 10 % (IC_{10}), or the dose providing three times the standard deviation (S.D.) from the mean measurement of the blank dose signal.

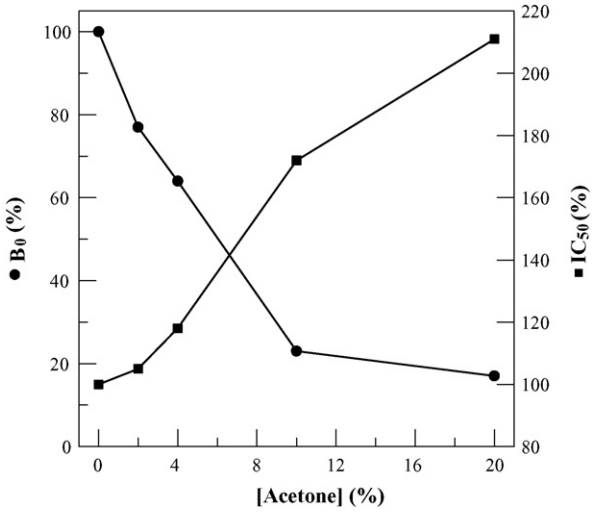


Fig. 1. Influence of acetone percentage in the ELISA assay. Maximum absorbance (●) and IC_{50} value (■) are expressed relative to the control inhibition curve, performed without organic solvent.

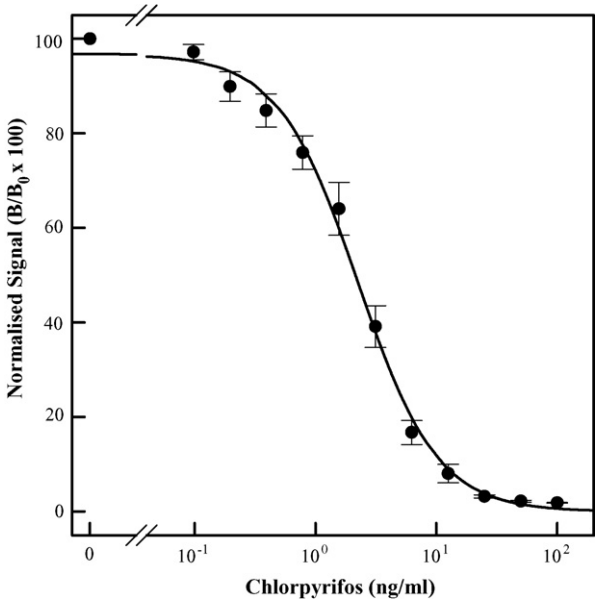


Fig. 2. Normalised standard curve for chlorpyrifos using optimised assay conditions in acetone medium. Each point represents the mean of 50 determinations.

The limit of detection (LOD) was estimated by analysis of five sets of 12 replicates of the zero standard. The mean absorbance value minus three-fold S.D. was equivalent to a $0.9B_0$ concentration [48], which corresponded to an estimated limit of detection of 0.32 ng/ml.

The limit of quantification (LQ) is the smallest concentration of analyte that can be measured in samples so as to yield a predicted concentration with a stated relative precision and accuracy [49]. Commonly, the selected LQ is defined by the upper limit of the linear range of the dose–response curve ($0.8B_0$), or by the mean absorbance value minus 10-fold S.D.

The limit of quantification (LQ) was calculated on the basis of the analysis of 20 tomato samples fortified with 70 ng/g of chlorpyrifos (data not shown); representing the estimated LQ of the method. Chlorpyrifos concentration was calculated by the equation:

$$[\text{chlorpyrifos}] = \frac{CfV}{P}$$

where C is the concentration in ng/g obtained (0.7 ng/g, in theory) interpolating, in the dose–response curve, the signal values, f the diluting factor, V the volume of the extract in l and P is the weight of sample in kg.

The mean concentration determined for the 20 samples was 73 ng/g with a S.D. of 5 ng/g. For residue that are above the LOD but below the validated LQ, numerical values should be reported as less than the LQ (73 ng/g) because the residue levels cannot be reliably quantified.

3.1. Specificity studies

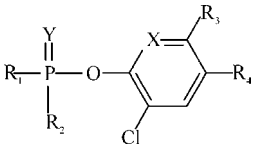
Specificity for chlorpyrifos assay was evaluated by means of competitive curves obtained with other related or unrelated organophosphorous insecticides (chlorpyrifos-methyl, chlorpyrifos-oxon, fenchlorphos (F), bromophos (B), trichloronate (T), diazinon, the chlorpyrifos metabolite 3,5,6-trichloro-2-pyridinol (TCP) and a standard containing a mix of F, B and T). The structure and cross-reactivity (CR) data for each compound is given in Table 1.

As can be seen, chlorpyrifos-methyl is recognised to the same extent (CR 102%) as chlorpyrifos, as it had been previously reported in other works [32,35,50]; presumably because the methyl groups were better accommodated by the antibody binding sites. Only the immunoassay described by Lawruk et al. [36] showed a lower CR (26%) for this compound, probably because the hapten used for immunization maintains both ethoxyl groups in the phosphate ester. Although the quantification would not be reliable for samples containing both pesticides, the occurrence of such samples is unlikely since the simultaneous application of both pesticides to the same crop makes no sense, provided that a good agricultural practice is observed.

Nevertheless, the antibody shows poor affinity for other compounds tested (CR < 15%). The lack of reactivity was related with the loss of nitrogen atom in the aromatic ring. Bromophos was poor recognised, probably due the presence of bromide in R_4 position.

Chlorpyrifos-oxon—the biologically active phosphate ester analogue of chlorpyrifos,—had poor reactivity in the immunoassay (1.3%), lower than CR values given by other authors [32,38].

Table 1
Structure and cross-reactivity values (CR) obtained for chlorpyrifos and related compounds tested

Structure	Compound	R_1	R_2	X	R_3	R_4	Y	IC_{50} (ng/ml)	CR (%)
	Chlorpyrifos	EtO	EtO	N	Cl	Cl	S	2.13	100
	Chlorpyrifos-methyl	MeO	MeO	N	Cl	Cl	S	2.08	102
	Fenchlorphos (F)	MeO	MeO	C	Cl	Cl	S	14.91	14.3
	Trichloronate (T)	EtO	Et	C	Br	Cl	S	22.75	9.4
	Bromophos (B)	EtO	EtO	C	Cl	Br	S	46.33	4.6
	Mix of F, B, T							9.73	22.0
	Chlorpyrifos-oxon	EtO	EtO	N	Cl	Cl	O	164	1.3

	Unrelated compounds	IC_{50} (ng/ml)	CR (%)
(TCP) metabolite	3,5,6-Trichloro-2-pyridinol	$>10^3$	5×10^{-2}
Other organophosphate insecticide	Diazinon	$>10^3$	3×10^{-2}

This fact illustrates the affinity of the monoclonal antibody for the thiophosphte ester substituent.

A cross-reactivity of 14.3% for fenchlorphos was obtained. Reported immunoassays for chlorpyrifos showed variable cross-reactivity for this compound (6% and 75%) [32,33]. The assay described by Brun et al. [38] showed negligible CR with assay A, but 15% was displayed for assay B.

On the other hand, the immunoassays for chlorpyrifos showed negligible CR for both diazinon and TCP. Since TCP is the main chlorpyrifos metabolite, it is possible to determine chlorpyrifos without TCP interferences.

Finally, CR of the fenchlorphos, bromophos and trichloronate mix was higher than those obtained for each compound, but lower than the addition of their individual values.

3.2. Extraction conditions

Optimal extraction conditions were selected according to the accuracy (percent recovery) and precision (percent coefficient of variation) parameters, using the recovery values and the coefficients of variation (CVs), respectively.

Whereas the assayed amounts of sample had no influence in the chlorpyrifos determination, it was indeed the extraction time of sample with acetone solvent. Thus, 5 or 10 min were successfully to obtain recoveries close to 100% (CV < 8.3%). Higher contact times—15 and 20 min—gave poor recoveries of chlorpyrifos (82% and 77%, respectively), probably due to extraction process.

Based on the length of extraction protocol and acetone consumption—toxic waste—the optimal conditions selected were 5 g of sample, 10 ml of solvent and 10 min as extraction time.

3.3. Analysis of vegetable samples

Firstly, acetone direct extraction (ADE) was evaluated as rapid method of sample preparation. Taking into account the dilution factor of the acetone extracts and MRL for chlorpyrifos in tomato (500 ng/g), recovery studies were carried out in fortified canned tomato samples at concentrations from 96 to 780 ng/g. Chlorpyrifos concentration in the extracts, was determined by ELISA and the results are presented in Table 2. All values are the mean of three extractions for sample and four measures for extract.

The method accuracy and method precision are derived from 144 determinations performed on tomato sample across the concentration range. The average percent recoveries ranged from 95% to 122% (ADE) and 93% to 133% (ME) across the fortification range. The coefficient of variation in percentage (%CV) ranged from 8% to 18% (ADE) and 3% to 16% (ME) across the 12 fortification levels. Based on mean recovery values obtained—105% ADE and 104% ME—and CV, we can remark that both extraction methods are suitable for chlorpyrifos determination in canned tomato samples.

Subsequently, the study was extend to other matrices such as fresh and canned pepper samples fortified at 400 ng/g, using canned tomato as internal control.

As can be seen in Table 3, the recoveries achieved using ADE (mean 94%) were higher than those obtained by ME (mean 80%). This fact may be explained by the higher extractant strength of the solvents used in multiresidue method, able to extract pigments and other sample colorants that could interfere in the ELISA (matrix effects), since the extracts are directly analysed by simple dilution [32].

3.4. Reproducibility studies

In order to study the reproducibility of the results, 1 kg of canned tomato was fortified with chlorpyrifos at 500 ng/g. Twelve aliquots of 5 g were extracted using ADE, another twelve aliquots of 15 g extracted using ME (see Section 2.5), and all extracts were analysed by ELISA. The average recovery (Table 4) of the fortified tomato sample was 97% ADE and 96.3% ME, with all samples within the whole range of recoveries 88–105%. Also, the overall reproducibility for six different days looks excellent, with an average CV lower than 5%.

Table 2
Recovery of chlorpyrifos in canned tomato samples using ELISA and both extraction procedures

Acetone direct extraction (ADE)			Multiresidue extraction (ME)		
Chlorpyrifos added (ng/g)	Chlorpyrifos determined (ng/g)	Recovery (%)	Chlorpyrifos added (ng/g)	Chlorpyrifos determined (ng/g)	Recovery (%)
0	n.d.	–	0	n.d.	–
96	109 ± 15	113	96	128 ± 5	133
144	155 ± 12	108	144	152 ± 3	105
200	189 ± 10	95	200	208 ± 12	104
260	249 ± 13	96	260	253 ± 7	97
300	360 ± 18	120	300	295 ± 10	98
350	428 ± 9	122	350	334 ± 16	93
400	422 ± 12	105	400	463 ± 12	116
450	454 ± 10	101	450	465 ± 7	103
500	526 ± 12	105	500	518 ± 8	104
550	562 ± 16	102	550	538 ± 9	98
600	570 ± 8	95	600	613 ± 8	102
780	752 ± 10	96	780	746 ± 14	96

Values as mean ± S.D. ($n = 12$). n.d., non-detected.

Table 3
Recovery study of chlorpyrifos in natural and tinned vegetable samples using ELISA and both extraction protocols

Sample	Chlorpyrifos added (ng/g)	Acetone direct extraction (ADE)		Multiresidue extraction (ME)	
		Chlorpyrifos determined (ng/g)	*R* (%)	Chlorpyrifos determined (ng/g)	*R* (%)
Red pepper[a]	0	n.d.		n.d.	
	400	436 ± 16	109	340 ± 19	85
Red pepper[a]	0	n.d.		n.d.	
	400	364 ± 6	91	248 ± 22	62
Green pepper[a]	0	n.d.		n.d.	
	400	320 ± 18	80	296 ± 17	74
Padrón pepper[a]	0	n.d.		n.d.	
	400	388 ± 10	97	356 ± 10	89
Tomato[b]	0	n.d.		n.d.	
	400	364 ± 7	91	362 ± 19	90

Values as mean ± S.D. ($n = 12$). *R*, recovery; n.d., non-detected.
[a] Natural.
[b] Tinned.

3.5. Analysis of blind samples

Once optimised both ELISA method and the sample treatment, the accuracy of the proposed methodology for the determination of chlorpyrifos in vegetables was studied using blind samples. Before addition step, samples were checked by GC–MS for incurred chlorpyrifos residues. Different tomato and pepper samples were extracted by both methods and the chlorpyrifos concentration in the extract determined by ELISA. Each sample was evaluated in four separate assays, by triplicate, on the same day to verify reproducibility and minimize chlorpyrifos degradation. Table 5 summarizes the accuracy of the chlorpyrifos immunoassay in vegetable samples.

In all cases, the amount of chlorpyrifos added was completely recovered, with average percentage of recovery ranging from 94% to 120% for ADE and 107% to 128% for ME, across the fortification range.

The accurate recovery of the fortified vegetable samples suggests that no matrix effects or interferences were present in the samples analysed, and the method ADE/ELISA was accurate across the chlorpyrifos concentrations tested.

Table 4
Reproducibility studies of extraction protocol in tomato samples fortified with chlorpyrifos at 500 ng/g

Sample	Acetone direct extraction (ADE)		Multiresidue extraction (ME)	
	Chlorpyrifos (ng/g)	Recovery (%)	Chlorpyrifos (ng/g)	Recovery (%)
1	492.0	98.4	488.5	97.7
2	498.0	99.6	501.0	100.2
3	479.0	95.8	488.5	97.7
4	448.5	89.7	525.0	105.0
5	523.0	104.6	477.5	95.5
6	482.5	96.5	482.5	96.5
7	475.0	95.0	473.0	94.6
8	467.0	93.4	461.5	92.3
9	486.0	97.2	455.0	91.0
10	480.0	96.0	476.0	95.2
11	483.0	96.7	440.0	88.0
12	502.5	100.5	510.0	102.0
Mean value	485 ± 4	97.0	482 ± 5	96.3

Values as mean ± S.D. ($n = 12$).

3.6. Evaluation of both analytical methods

The validation of results given by IAs is usually carried out by comparison with chromatographic methods. When possible, validation of IAs is better performed using real samples contaminated by the analyte [51]. Correlation studies between ADE/ELISA and ME/GC–MS methods were performed. Twelve canned, fresh and frozen vegetable samples fortified at two levels (400 and 600 ng/g) were analysed, in triplicate, for chlorpyrifos by GC–MS in the SIM mode and by ELISA, as described in Section 2.5. In all cases a non-fortified sample was checked by GC–MS for incurred chlorpyrifos residues and used as control.

Recovery results for the spiked vegetable samples measured by ELISA and GC–MS methods are given in Table 6. For example, in the case of asparagus we recovered almost 100% of chlorpyrifos—ELISA data,—with independence of the extraction protocol employed. Similar results were achieved when vegetable extracts were analysed by chromatography.

Both spiking levels performed for the ELISA test were in the linear range of IA. The average immunoassay recovery was 95% and 100.7% for ME and ADE, respectively, with CV ranging from 0.1% to 8% with most below 4. Such results are considered very well for residue methods [52], especially considering that the application of any immunoassay in complex matrices such as food and crops is more difficult than to water samples [53].

For GC–MS the average recovery was in the range 99% (ME)–96% (ADE) with higher coefficients of variation in percentage (1–10.3%).

Correlation obtained by established ME/GC–MS method and proposed ADE/ELISA method for both fortification levels seem to be satisfactory. The regression analysis for the lower fortification level (400 ng/g) yields the equation $y = 10.3 + 0.95x$ and a correlation coefficient (r) of 0.974 between methods. The equation obtained for the high fortification level (600 ng/g) was $y = 20.6 + 0.96x$, with $r = 0.967$.

Table 5
ELISA determination of chlorpyrifos concentration in blind samples extracted by ADE and ME methods

Sample	Chlorpyrifos added (ng/g)	Acetone direct extraction (ADE)		Multiresidue extraction (ME)	
		Chlorpyrifos determined (ng/g)	Recovery (%)	Chlorpyrifos determined (ng/g)	Recovery (%)
1[a]	0	n.d.		n.d.	
2[a]	0	n.d.		n.d.	
3[a]	470	473 ± 7	101	526 ± 9	112
4[a]	520	491 ± 57	94	558 ± 49	107
5[a]	0	n.d.		n.d.	
6[a]	500	602 ± 28	120	641 ± 91	128
7[b]	0	n.d.		n.d.	
8[b]	450	531 ± 17	118	480 ± 17	107

Values as mean ± S.D. ($n = 12$). n.d., non-detected.
[a] Canned tomato.
[b] Canned pepper.

Results obtained demonstrated the potential of the proposed methodology for quantitative analysis of chlorpyrifos in vegetable samples in a rapid, sensitive and cost-effective way, with recoveries close to those obtained by reference method.

In addition, results of the variance multifactor analysis (Table 7) show that individual matrix factor and the interactions between type of matrix-extraction method, type of matrix-determination method and extraction-determination methods were significant.

The interaction matrix-determination method (see Fig. 3a) gave no divergences, although for watermelon (8) we obtained higher recoveries using reference method (GC–MS).

As can be seen in Fig. 3b the interaction type of matrix-extraction method does not show significant differences with

Table 6
Recovery values obtained for chlorpyrifos in vegetables using ELISA and GC–MS techniques (comparison of extraction methods)

Sample	Chlorpyrifos added (ng/g)	ELISA						CG–MS					
		Multiresidue extraction (ME)			Acetone direct extraction (ADE)			Multiresidue extraction (ME)			Acetone direct extraction (ADE)		
		Mean value[a]	CV (%)	*R* (%)	Mean value	CV (%)	*R* (%)	Mean value	CV (%)	*R* (%)	Mean value	CV (%)	*R* (%)
Tomato[b]	400	402.2	3.2	100.5	426.6	6.5	106.6	412.9	2.9	103.8	390.6	1.5	97.6
	600	607.7	1.1	101.3	613.6	2.4	102.3	649.5	4.3	108.2	564.5	1.5	94.0
Bonnet pepper[b]	400	352.0	1.7	88.0	422.7	1.5	105.7	418.4	4.2	104.6	378.2	2.7	94.5
	600	527.6	1.4	87.9	625.9	1.1	104.3	601.6	3.6	100.3	545.3	1.0	90.8
Bean[b]	400	368.5	4.8	92.1	425.4	1.4	106.3	410.3	1.0	102.6	359.5	6.8	89.9
	600	593.6	5.9	98.9	597.0	8.0	99.5	598.5	2.2	99.7	546.0	1.5	91.0
Pea[b]	400	350.9	3.1	87.7	383.4	5.6	95.8	399.2	3.4	99.8	343.0	10.3	85.7
	600	514.3	4.1	85.7	547.8	1.8	91.3	613.3	2.4	102.2	548.2	2.1	91.4
Asparagus[b]	400	413.2	2.2	103.3	409.8	4.0	102.4	378.5	2.0	94.6	385.5	1.5	96.3
	600	641.0	4.6	106.8	622.0	2.6	103.7	594.0	3.0	99.0	559.6	3.9	93.3
Broccoli[c]	400	351.5	4.0	87.9	408.0	2.4	102.0	384.2	6.6	96.0	422.5	3.5	105.6
	600	544.6	2.2	90.8	547.3	2.5	91.2	590.2	4.3	98.4	615.0	2.0	102.5
Watermelon[d]	400	385.0	2.6	96.3	366.3	5.9	91.6	395.1	8.2	98.8	413.9	3.7	103.5
	600	528.6	1.8	88.1	598.1	2.9	99.7	610.0	4.5	101.7	602.9	1.9	100.5
Melon[d]	400	401.4	4.6	100.3	397.3	4.4	99.4	402.0	1.7	100.5	383.8	3.6	95.9
	600	565.7	1.9	94.3	586.2	3.7	97.7	573.0	7.4	95.5	563.3	4.7	93.9
Lettuce[d]	400	418.6	3.0	104.6	411.3	2.7	102.8	412.1	1.0	103.0	411.4	2.8	102.8
	600	543.5	2.0	90.6	641.3	2.9	106.8	555.9	2.9	92.6	583.7	3.2	97.3
Cucumber[d]	400	385.5	2.9	96.4	383.5	0.1	95.9	415.0	6.3	103.7	370.6	2.2	92.7
	600	637.0	1.7	106.2	544.3	5.5	92.4	567.1	5.1	94.5	587.2	3.0	97.9
Celery[d]	400	367.0	6.6	91.7	435.7	5.2	108.9	387.8	1.3	96.9	398.8	7.1	99.7
	600	586.0	4.7	97.6	591.8	2.3	98.6	601.7	2.3	100.2	553.6	1.1	92.3
Red pepper[d]	400	340.6	1.2	85.2	405.5	1.3	101.4	356.0	1.8	89.0	388.5	4.2	97.1
	600	582.0	6.7	97.0	615.0	3.4	102.5	544.1	2.8	90.7	590.2	3.2	98.4

CV, coefficient of variation; *R*, recovery.
[a] $n = 3$.
[b] Canned.
[c] Freezed.
[d] Natural samples.

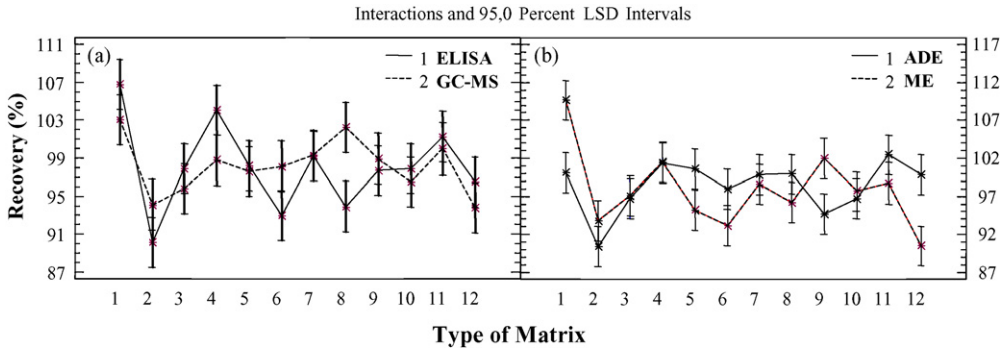


Fig. 3. Interaction graphs type of matrix-determination method (a) and type of matrix-extraction method (b). (1) Tomato, (2) pea, (3) bean, (4) asparagus, (5) bonnet pepper, (6) broccoli, (7) celery, (8) watermelon, (9) cucumber, (10) melon, (11) lettuce, and (12) red pepper.

Table 7
Results of the analysis of variance (ANOVA)

Source	Sum of squares[a]	d.f.[b]	Mean square[c]	*F*-ratio[d]	*p*-Value[e]
Main effect					
Type of matrix (A)	2833.35	11	257.577	5.98	0.0000
[Chlorpyrifos] (B)	166.345	1	166.345	3.85	0.0506
Extraction method (C)	21.1948	1	21.1948	0.49	0.4838
Analysis method (D)	1.4273	1	1.4273	0.03	0.8557
Interactions					
AC	1923.69	11	174.881	4.05	0.0000
AD	1025.35	11	93.2133	2.16	0.0170
CD	1564.15	1	1564.1	36.29	0.0000
Residual value	10731.8	249	43.0995		
Sum	18274.7	286			

[a] Mean sum of squared deviations of each group.
[b] Number of degrees of freedom.
[c] (Sum of squares)/(number of degrees of freedom).
[d] (Found variation of the group averages)/(expected variation of the group averages).
[e] Statistical significance.

the exception of tomato (1) and watermelon (8) with higher recoveries using ME. For cucumber (9) and red pepper (12) ADE gave a higher recovery values.

In resume, the chlorpyrifos concentration in vegetable extracts—from ADE or ME—determined by ELISA or GC–MS was well correlated. Also, chlorpyrifos recoveries obtained by ADE/ELISA (average 100.7%) or by reference method ME/GC–MS (average 99%) do not shown significant differences. However, variance analysis data suggest the use of ADE/ELISA or ME/GC–MS to improve chlorpyrifos recovery.

4. Conclusions

The performance characteristics of a rapid ADE-ELISA method for the quantitative determination of chlorpyrifos in vegetable samples have been summarised.

Highly sensitive and selective immunoassay, for the determination of chlorpyrifos residues—in organic canned and fresh vegetable extracts,—has been developed.

Also, a direct extraction procedure using low amount of organic solvent was optimised. Studies have shown that the pesticide recoveries using ADE (average 96–100.7%) were higher or equal than those obtained by multiresidue extraction (average 95–99%). This fact demonstrated the potential of ADE as rapid, reproducible and high throughput extraction method of chlorpyrifos in vegetable samples, suitable for screening purposes.

In relation to previous extraction methods, the direct extraction procedure here developed show potential advantages since they provide reliable data, low cost, speed, and simplicity, require minimum sample processing, low amount of organic solvent and enhance chlorpyrifos analysis by immunoassay.

The ELISA performances (accuracy and precision) were comparable to those obtained by instrumental techniques. The immunoassay compares favourably to gas chromatographic methods for the analysis of vegetable samples ($r = 0.97$) and exhibits within and between assay variability <5% with results obtained in 2 h.

Although chlorpyrifos concentration in vegetable extracts—from ADE or ME—determined by ELISA or GC–MS was well correlated, variance analysis data suggest the use of ADE/ELISA or ME/GC–MS to enhance chlorpyrifos recovery.

In addition, the proposed method (ADE/ELISA) have allowed the direct analysis of vegetable extracts without preconcentration or clean-up steps, to obtain fast responses in a short time with a minimum consumption of reagents an of potentially pollutant organic solvents.

Acknowledgements

This work was supported by project 4I01SICT002 (CTIC-Murcia, Spain). The author J.A. Gabaldón acknowledges a grant from Instituto de Fomento de la Región de Murcia by means of the Séneca Program. The authors wish to thank LIB for providing the immunoreagents.

References

[1] C.R. Worthing, THE PESTICIDE Manual, 6th ed., The British Crop Protection Council, Croydon, 1979.
[2] K.D. Racke, Rev. Environ. Contam. Toxicol. 131 (1993) 1.
[3] S. Ward, A.H. Arthington, B.J. Pusey, Ecotoxicol. Environ. Saf. 30 (1995) 2.
[4] A. Goldstein, L. Aronow, S.M. Kalman, Principles of Drug Action: The Basis of Pharmacology, Wiley, New York, 1974.

[5] D. Grob, J.C. Harvey, J. Clin. Invest. 37 (1958) 350.
[6] D. Barceló, J. Chromatogr. 643 (1993) 117.
[7] US EPA, Pesticide Industry Sales and Usage: 1992 and 1993 Market Estimates, Office of Pesticide Programs, Washington, DC, 1994.
[8] S. Lacorte, S.B. Lartiges, P. Garrigues, D. Barceló, Environ. Sci. Technol. 29 (1995) 431.
[9] E. Neidert, R.B. Trotman, P.W. Saschenbrecker, J. AOAC Int. 77 (1994) 18.
[10] US Food and Drug Administration, J. AOAC Int. 77 (1994) 161A.
[11] L.G. Nico, D.J. Schaeffer, D.C. Taphorn, A. Barbarino-Duque, Fresen. Environ. Bull. 3 (1994) 685.
[12] US Food and Drug Administration, Pesticide Analytical Manual, vol. I, FDA, Rockville, MD, 1979.
[13] Association Official Analytical Chemists, Official Methods of Analysis, AOAC, Arlington, VA, 1995.
[14] D. Simon, S. Helliwell, K. Robards, Anal. Chim. Acta 360 (1998) 1.
[15] H. Jin, G.R. Webster, N.J. Holliday, P. Pines, A. Westwood, J. Environ. Sci. Health B 31 (1996) 751.
[16] J. Oliva, S. Navarro, A. Barba, G. Navarro, J. Chromatogr. A 833 (1999) 43.
[17] R. Carabias-Martínez, E. Rodriguez-Gonzalo, P.H. Paniagua-Marcos, J. Hernández-Méndez, J. Chromatogr. A 869 (2000) 427.
[18] P. López-Roldán, M.J. López de Alda, D. Barceló, Anal. Bioanal. Chem. 378 (2004) 599.
[19] A. Pasha, Y.N. Vijayashankar, N.G.K. Karanth, J. AOAC Int. 79 (1996) 1009.
[20] A. Di Corcia, M. Marchetti, Anal. Chem. 63 (1991) 580.
[21] H.B. Wang, M.K. Wong, C.Y. Mok, J. Agric. Food Chem. 42 (1994) 2625.
[22] S. Magdic, A. Boyd-Boland, K. Jinno, J.B. Pawliszyn, J. Chromatogr. A 736 (1996) 219.
[23] P.L. Wylie, K. Uchiyama, J. AOAC Int. 79 (1996) 571.
[24] B.F. Scott, J. Struger, H. Tse, J. Environ. Anal. Chem. 61 (1995) 129.
[25] N.K. Wilson, J.C. Chuang, C. Lyu, J. Expo. Anal. Environ. Epidemiol. 11 (2001) 449.
[26] D.E. Glotfelty, M.S. Majewski, J.N. Seiber, Environ. Sci. Technol. 24 (1990) 353.
[27] S. Lacorte, D. Barceló, J. Chromatogr. A 712 (1995) 103.
[28] J.A. Noblet, L.A. Smith, I.H. Suffet, J. Agric. Food Chem. 44 (1996) 3685.
[29] H.G. Mol, R.C. van Dam, O.M. Steijger, J. Chromatogr. A 1015 (2003) 119.
[30] K. Adou, W.R. Bontoyan, P.J. Sweeney, J. AOAC Int. 87 (2004) 1224.
[31] B.D. Hammock, R.O. Mumma, in: J. Harvey, G. Zweig (Eds.), Recent Advances in Pesticide Analytical Methodology, American Chemical Society, Washington, DC, 1980, pp. 321–352.
[32] A.S. Hill, J.H. Skerritt, R.J. Bushway, W. Pask, K.A. Larkin, M. Thomas, W. Korth, K. Bowner, J. Agric. Food Chem. 42 (1994) 2051.
[33] J.J. Manclús, J. Primo, A. Montoya, J. Agric. Food Chem. 42 (1994) 1257.
[34] K.S. Nam, J.W. King, J. Agric. Food Chem. 42 (1994) 1469.
[35] J.J. Manclús, A. Montoya, J. Agric. Food Chem. 44 (1996) 4063.
[36] T.S. Lawruk, A.M. Gueco, C.A. Mihaliak, S.C. Dolder, G.E. Dial, D.P. Herzog, F.M. Rubio, J. Agric. Food Chem. 44 (1996) 2913.
[37] A. Oubiña, J. Gascón, I. Ferrer, D. Barceló, Environ. Sci. Technol. 30 (1996) 509.
[38] E.M. Brun, M. Garcés-García, R. Puchades, A. Maquieira, J. Agric. Food Chem. 53 (2005) 9352.
[39] R.J. Bushway, Z. Fan, J. Food Protect. 61 (1998) 708.
[40] D.P. Herzog, C.A. Mihaliak, S.W. Jourdan, T.S. Lawruk, J. Clin. Ligand Assay 18 (1995) 150.
[41] J.H. Skerritt, B.E. Amita-Rani, in: R.C. Beiev, H.L. Stanker (Eds.), Agrochemical Immunoassay of Insecticides, Fungicides, Pesticides, (ACS Symposium Series No. 621), American Chemical Society, Washington, DC, 1995, p. 29.
[42] K.M. Rajskowsky, N. Cittanova, B. Desfosses, M.F. Jayle, Steroids 29 (1997) 701.
[43] K.D. Racke, Rev. Environ. Contam. Toxicol. 131 (1993) 1.
[44] M.A. Luke, J.E. Froberg, H.T. Masumoto, J. Assoc. Off. Anal. Chem. 58 (1975) 1020.
[45] J.A. Noblet, L.A. Smith, I.H. Suffet, J. Agric. Food Chem. 44 (1996) 3685.
[46] A.S. Hill, J.V. Mei, C. Yin, B.S. Ferguson, J.H. Skerrit, J. Agric. Food Chem. 39 (1991) 1882.
[47] P. Nugent, in: T. Cairns, J. Sherma (Eds.), Emerging Strategies for Pesticide Analysis, CRC Press, Boca Raton, FL, 1992, p. 247.
[48] A.R. Midgely, G.D. Niswender, R.W. Rebar, Acta Endocrinol. 63 (1969) 163.
[49] C.A. Mihaliak, S.A. Berberich, in: J.O. Nelson, A.E. Karu, R. Wong (Eds.), Immunoanalysis of Agrochemicals: Emerging Technologies, (ACS Symposium Series No. 586), American Chemical Society, Washington, DC, 1995, pp. 228–300.
[50] Y.A. Cho, H.S. Lee, E.Y. Park, Y.T. Lee, B.D. Hammock, K.C. Ahn, J.K. Lee, Bull. Korean Chem. Soc. 23 (2002) 481.
[51] M.C. Hennion, 26 (1998) M149.
[52] G.A. Parker, J. Assoc. Off. Anal. Chem. 74 (1991) 868.
[53] D. Barceló, M.C. Hennion (Eds.), Techniques and Instrumentation in Analytical Chemistry, Elsevier, Amsterdam, 1997, p. 542.

Available online at www.sciencedirect.com
ScienceDirect
Talanta 71 (2007) 1339–1344
Talanta
www.elsevier.com/locate/talanta

Uncertainty due to the quantification step in analytical methods

Javier Galbán [a,*], Carlos Ubide [b]

[a] Analytical Biosensors Group, INA, Analytical Chemistry Department, Faculty of Sciences, University of Zaragoza, Pedro Cerbuna 12, Zaragoza 50009, Spain
[b] Applied Chemistry Department, Chemistry Faculty, University of Pais Vasco, P.O. Box 1072, 20080 San Sebastián, Spain

Received 27 December 2005; received in revised form 19 June 2006; accepted 6 July 2006
Available online 28 August 2006

Abstract

The quantification step is an important source of uncertainty in analytical methods, but it is frequently misunderstood and disregarded. In this paper, it is shown how this uncertainty is closely related to the linear response range of a method, and to the Pearson correlation coefficient of the calibration line. So, if there is a need for a pre-fixed quantification uncertainty, the linear response range will be affected. Some practical cases are given showing the quantification uncertainty significance. The theoretical equation giving the value of the quantification uncertainty is deduced from which new conclusions can be taken out. Because of that, the quantification uncertainty can easily be calculated and the parameters that really affect its value are shown along the paper. Some final considerations about detection limits and two-point calibration lines are also given. The paper can also be considered a reflection on uncertainty owed to calibration and on their consequences on the analytical methodology.
© 2006 Elsevier B.V. All rights reserved.

Keywords: Uncertainty; Calibration; Correlation coefficient

1. Introduction

Because uncertainty (u) clouds analytical results, it is one of the most critical parameters characterizing an analytical determination. During the last few years, and with the introduction of qualimetrics, a large number of efforts have been done in order to provide general rules to improve the uncertainty evaluation. Three general strategies [1] have been proposed, namely:

(a) The "bottom-up" strategy, in which the combined uncertainty is calculated from the individual uncertainty of each operation of the analytical process; these individual values can be theoretically estimated or experimentally obtained from nested experimental designs [2]. This methodology was proposed by the ISO and lately adopted by the Eurachem; both have provided detailed guides to be used [3].
(b) The "top-down" approach proposed by the Analytical Methods Committee [4]. Here the total uncertainty of a method is calculated as a whole from the results obtained in an interlaboratory study.
(c) Obviously the "top-down" methodology can not be applied in every case, then "mixed strategies", which make use of results obtained during the validation process [see for example 5,6], are used for obtaining the combined uncertainty of a part of the procedure.

Unfortunately these methodologies have not taken roots in the normal practice; in the most of research papers the uncertainty is calculated by using the classical approach (which usually gives the repeatability or the intermediate uncertainty). In our opinion, it would be very useful to offer critical studies of the uncertainty due to the different operations of the analytical procedure and to provide tools that allow a quick and simple evaluation of the most relevant ones.

As it is well known a usual analytical procedure consists of the main following steps: sampling, sub-sampling, sample treatment, measurement and quantification. In general sampling is considered by researchers as the most uncertain step in the analytical process and many mathematical models have been proposed to evaluate how sampling should to be done, depending on the highest uncertainty allowed. However, sampling is usually performed out of laboratory and it is not easy to calculate the uncertainty that affects it, so it is not specifically considered. The sub-sampling, sample treatment and measurement uncertainties are usually obtained as a whole during reproducibility studies.

* Corresponding author. Tel.: +34 976761292; fax: +34 976761292.
E-mail address: jgalban@unizar.es (J. Galbán).

0039-9140/$ – see front matter © 2006 Elsevier B.V. All rights reserved.
doi:10.1016/j.talanta.2006.07.031

The quantification step, made frequently by interpolation in the calibration graph, is intuitively considered as a low-uncertainty step and its effect is consequently disregarded. However, its incidence cannot be neglected prior to confirmation and, for instance, it is known to be the main source of uncertainty in some situations [7]; the higher the uncertainty of the calibration standards signal (due to the pre-treatment, or chemical reactions involved in the method, or the nature of the signal obtained) the higher the uncertainty in the quantification step (i.e. many biochemical methods).

This paper deals with this kind of uncertainty. Three aspects are considered: (a) calculation; a method is discussed for simple calculation; (b) minimization; the real parameters affecting uncertainty are faced; (c) effect on the method validation; the magnitude of the uncertainty due to this step is considered.

2. A model for quantifiying uncertainty due to a calibration line

2.1. General model

It is usual in the literature to find equations to calculate this kind of uncertainty; however it seems necessary to consider its deduction in order to know which uncertainty sources are really included. Let's consider the signals ($y_1, \ldots, y_n$) obtained from several standards of analyte ($x_1, \ldots, x_n$ being their concentrations). After applying the least squares model, the following line is obtained:

$$y = b_0 + b_1 x \tag{1}$$

with

$$r = \frac{\sum_{i=1}^{n}(x_i - \bar{x})(y_i - \bar{y})}{\sqrt{\sum_{i=1}^{n}(x_i - \bar{x})^2 \sum_{i=1}^{n}(y_i - \bar{y})^2}} \tag{2}$$

being

$$b_1 = \frac{\sum_{i=1}^{n}(x_i - \bar{x})(y_i - \bar{y})}{\sum_{i=1}^{n}(x_i - \bar{x})^2} \tag{3}$$

$$b_0 = \bar{y} - b_1\bar{x} \tag{4}$$

From the analytical signal obtained from the sample to be analysed (y_s), the concentration of the analyte (x_s) can be calculated as

$$x_s = \frac{y_s - b_0}{b_1} \tag{5}$$

Eq. (4) shows how b_0 and b_1 are not independent from each other and Eq. (5) says that the uncertainty in x_s depends on the uncertainty of y_s, b_0 and b_1. As it is known, when a magnitude (x) depends on several individual magnitudes $z_1, z_2, \ldots, z_n$ according to a function (f), the combined standard uncertainty of x ($s_{(x)}$) will be given by

$$s_{(x)} = \sqrt{\sum_{i=1}^{n}\left(\frac{\partial f}{\partial z_i}\right)^2 s^2_{(z_i)} + 2\sum_{i=1}^{n-1}\sum_{j=i+1}^{n}\left(\frac{\partial f}{\partial z_i}\right)\left(\frac{\partial f}{\partial z_j}\right) s_{(z_i,z_j)}}$$

$s_{(z_i,z_j)}$ being the covariance between the i and j parameters. In this particular case and considering (5):

$$s_{(x_s)} = \sqrt{\left(\frac{\partial x_s}{\partial y_s}\right)^2 s^2_{(y_s)} + \left(\frac{\partial x_s}{\partial b_0}\right)^2 s^2_{(b_0)} + \left(\frac{\partial x_s}{\partial b_1}\right)^2 s^2_{(b_1)} + 2\left(\frac{\partial x_s}{\partial y_s}\right)\left(\frac{\partial x_s}{\partial b_1}\right) s_{(y_s,b_1)} + 2\left(\frac{\partial x_s}{\partial y_s}\right)\left(\frac{\partial x_s}{\partial b_0}\right) s_{(y_s,b_0)} + 2\left(\frac{\partial x_s}{\partial b_0}\right)\left(\frac{\partial x_s}{\partial b_1}\right) s_{(b_0,b_1)}}$$

For estimating the uncertainty due to the interpolation in a calibration line, the previous this equation can be simplified to:

$$s_{(x_s)} = \sqrt{\left(\frac{\partial x_s}{\partial b_1}\right)^2 s^2_{(b_1)} + \left(\frac{\partial x_s}{\partial b_0}\right)^2 s^2_{(b_0)} + 2\left(\frac{\partial x_s}{\partial b_0}\right)\left(\frac{\partial x_s}{\partial b_1}\right) s_{(b_0,b_1)}} \tag{6}$$

This simplification is based on two considerations. First of all, the b_0 and/or b_1 parameters are independent on y_s so their covariances are null. Secondly, the $s^2_{(y_s)}$ term refers to the uncertainty in obtaining the y_s value and it compiles the uncertainty due to the rest of the analytical method (sampling, sub-sampling, sample pre-treatment and measurement). Because in this paper we are only interested in the uncertainty due to the quantification step, the $s^2_{y_s}$ term will not be taken into account. The values of the partial derivatives can be deduced from (5):

$$\left(\frac{\partial x_s}{\partial y_s}\right) = \frac{1}{b_1}; \qquad \left(\frac{\partial x_s}{\partial b_0}\right) = -\frac{1}{b_1};$$
$$\left(\frac{\partial x_s}{\partial b_1}\right) = -\frac{1}{b_1^2}(y_s - b_0) = -\frac{x_s}{b_1} \tag{7}$$

the values of $s^2_{(b_1)}$ and $s^2_{(b_0)}$ can be obtained from the literatures [8,9], but the value of $s_{(b_0,b_1)}$ is not easily found and it has been deduced here:

$$s^2_{(b_1)} = s^2_{y/x}\frac{1}{\sum_i (x_i - \bar{x})^2}, \qquad s^2_{(b_0)} = s^2_{y/x}\frac{\sum_i x_i^2}{n\sum_i (x_i - \bar{x})^2},$$
$$s_{(b_0,b_1)} = -s^2_{y/x}\frac{\bar{x}}{\sum_i (x_i - \bar{x})^2} \tag{8}$$

being [8,9]:

$$s^2_{y/x} = \frac{\sum_i (y_i - \hat{y})^2}{n-2} = \frac{1}{n-2}\left(\sum_i (y_i - \bar{y})^2 - b_1^2\sum_i (x_i - \bar{x})^2\right) \tag{9}$$

where the $\hat{y}$ values are the estimated y values calculated from the regression line corresponding to the individual x-values. Taking Eqs. (7) and (8) to (6), and considering the summation identity:

$$\sum_i (x_i - \bar{x})^2 = \sum_i x_i^2 - n\bar{x}^2$$

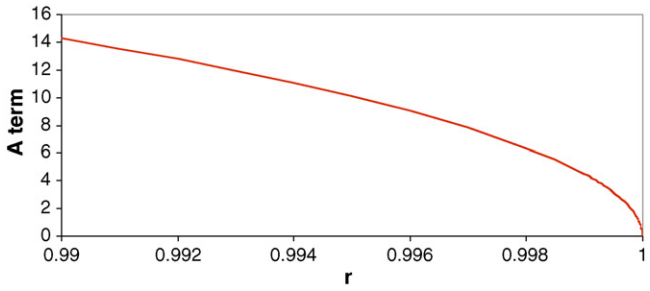


Fig. 1. Variation of the A term as a function of the r value.

the following well-known equation is obtained:

$$s^2_{(x_s)} = \frac{s^2_{y/x}}{b_1^2}\left(\frac{1}{n} + \frac{(x_s - \bar{x})^2}{\sum (x_i - \bar{x})^2}\right)$$

This expression gains significance if the correlation coefficient (2) of the calibration line and the $s_{y/x}$ values (9) are included:

$$s_{(x_s)} = \sqrt{\left(\frac{1}{n-2}\right)\left(\frac{1-r^2}{r^2}\right)\left(\frac{\sum (x_i - \bar{x})^2}{n} + (x_s - \bar{x})^2\right)}$$

More often the uncertainty is expressed as the relative standard deviation (R.S.D.) because it does not depend on the absolute vale of the mean:

$$\text{R.S.D.} = 100\frac{s_{(x_s)}}{x_s} = 100\frac{\bar{x}}{x_s}\sqrt{\left(\frac{1}{n-2}\right)\left(\frac{1-r^2}{r^2}\right)\left(\frac{1}{n}\sum\left(\frac{x_i}{\bar{x}} - 1\right)^2 + \left(\frac{x_s}{\bar{x}} - 1\right)^2\right)} \quad (10)$$

Eq. (10) shows the uncertainty expression in a non-frequent way (as a function of r) what may help to tackle the problem from a different point of view. The statistics r is frequently calculated in analytical methods and used as an indicator of linearity, but it is not a useful indicator of it. On the contrary, in Eq. (10) a different use of r can be given by relating it to uncertainty rather than to linearity. For a better discussion, Eq. (10) can be expressed as

$$\text{R.S.D.} = \frac{A}{\sqrt{(n-2)}}(C^2 B + (1 - C)^2)^{1/2} \quad (11)$$

$$A = 100\sqrt{\left(\frac{1-r^2}{r^2}\right)} \quad (12a)$$

$$B = \frac{1}{n}\sum_{i=1}^{n}\left(\frac{x_i}{\bar{x}} - 1\right)^2 \quad (12b)$$

$$C = \frac{\bar{x}}{x_s} \quad (12c)$$

In addition to n, the importance of the A, B and C terms in (12) comes from the fact that each of them contains one of the parameters affecting to the uncertainty due to quantification: (a) the correlation coefficient (r) (A term); Fig. 1 shows how the A term changes for r ranging from 0.99 to 1; (b) the number of the calibration standards used and their relative concentrations (B term); (c) the relation between the sample concentration and that of (the) centroid of the calibration line, i.e., if the interpolation is performed close to or far away from the centroid (C term). Let's begin the discussion taking the B term as the starting point. The concentrations of the standards used for the calibration line can be chosen according to different criteria, so a large number of situations is possible; however most of the analytical calibration lines can be included in one of the following two cases: the equally spaced standards (EES) and the several order of magnitude (SOM) situations. Both cases will be now considered.

2.2. The equally spaces standards (ESS) case

In techniques showing a linear response range of about one order of magnitude (molecular absorption spectrometry, atomic absorption spectrometry, amperometry, ...) it is very usual that the standards are prepared in such a way that their concentrations are equally spaced (for example if five standards are to be prepared from 0 up to 10 mg L^{-1}, the analyst will probably choose 0, 2.5, 5, 7.5 and 10 mg L^{-1} approximately). This is a very good choice for two reasons: (a) from the point of view of Eq. (10) this correspond to a situation in which, for a given number of points, n, the B term takes one of the most low values; (b) it can be demonstrated that, in this case, the B value is independent of the absolute values of the standard concentrations, and it only depends on the number of standards. The following expression is fulfilled [10]:

$$B = \frac{1}{n}\sum_{i=1}^{n}\left(\frac{2i - n - 1}{n - 1}\right)^2 \quad (13)$$

In general the number of standards used ranges between 3 and 10; for these case the application of (13) gives the B values (B_{ESS}) indicated in Table 1.

For discussion purposes the concentration range from 0k to 10k will be used, k being a number which can takes any value. Under the ESS condition, the centroid of the concentration range is 5k. Theoretically, it is possible to interpolate any value falling into the linear response range, from the quantification limit on. In this case, it would be acceptable for the quantification limit a value of about 0.5k, so the higher value of the C term would be around 10; on the other side, the higher concentration is 10k so the lower value of C will be 0.5. Fig. 2A shows how the R.S.D./A ratio (used instead of R.S.D. to avoid the correlation coefficient effect) changes with C; in Fig. 2B the part of Fig. 1 corresponding to C values between 0.5 and 1.5 is highlighted.

As it can be seen in Fig. 2, low values of R.S.D./A are originated when interpolation is made around the centroid or for low C values (concentrations higher than $\bar{x}$). However, when the interpolation is performed below the centroid, the R.S.D./A quickly increases, and interpolations close to the quantification limit produce a very high uncertainty. Oddly enough, and contrary to what it is generally considered, the centroid is not the point at which the lower uncertainty is obtained, but it

Table 1
B values for representative ESS and SOM cases

	n							
	3	4	5	6	7	8	9	10
B_{ESS}	0.667	0.556	0.501	0.468	0.445	0.426	0.413	0.408
B_{SOM}	1.50	2.28	3.09	3.91	4.73	5.54	6.36	7.18

shifts to lower C values as the number of calibration points diminishes.

To obtain the overall R.S.D. value the parameters shown in Figs. 1 and 2 must be multiplied. For example, lets suppose a calibration graph made with five standards ($n=5$) under ESS condition with concentrations ranging between 0 and 1 mg L^{-1} ($k=0.1$ mg L^{-1}) and $r=0.995$; in this case Fig. 1 gives a $A=10.0$. Different samples are interpolated giving concentrations of 0.5 mg L^{-1} ($C=1$, centroid), 0.1 mg L^{-1} ($C=5$) and 0.05 mg L^{-1} ($C=10$), about the quantification limit); Fig. 2 gives R.S.D./A values of 0.408, 3.08 and 6.61 respectively, then the R.S.D. value due to interpolation is 4.1%, 31% and 66%, respectively, which are probably higher than the uncertainty due to the rest of the method (including sampling, sub-sampling, sample treatment and instrumental noise).

2.3. The several order of magnitude (SOM) case

For those techniques showing a linear response range along several orders of magnitude (some methods in molecular fluorescence spectrometry, ICP emission spectrometry, MS spectrometry, several detectors in gas chromatography, ion selective electrodes, . . .) one standard is usually prepared for each order of magnitude. For example, if the linearity is thought to be obeyed from 0.1 to 10^{-5} M, standards of 0, 10^{-5}, 10^{-4}, 10^{-3}, 10^{-2} and 10^{-1} are prepared. Again, the B value (B_{SOM}) is independent of the absolute standards concentration and it only depends on the number of standards. A simple representative expression such as Eq. (13) cannot be obtained, but it is possible to calculate it from Eq. (12b). Table 1 gives B_{SOM} values for n ranging from 3 to 10.

As in the previous case, the interpolation could be done in any part of the calibration line (any C value). Fig. 3 shows a plot of log(R.S.D./A) *versus* log(C) for $n=5$ (similar representations for other values of n are included as Supplementary material); the logarithmic scale is used because of the broad range of values for both parameters.For R.S.D. calculation the value in Fig. 1 has to be multiplied by the corresponding value derived from Fig. 3. As an example, suppose a calibration line from 0 to 1000 μg/l (calibration points 0, 1, 10, 100, 1000; $\bar{x}=222.2$), showing a correlation coefficient $r=0.9998$, in which a sample is interpolated such as $X_s=2$ ($C=111$); from the Fig. 3 (log $C=2.046$), log(R.S.D./A) = 2.302 → R.S.D./A = 200.7, and from Fig. 1 $A=2$, and then the R.S.D. value due to quantification will be:

R.S.D. ≈ 400%

What does this mean? The least squares method is based in two suppositions:

(1) The y values are independent from each other; that is, the signal value corresponding to a concentration is independent of the signal value that corresponds to a different concentration. This is quite usual in the analytical practice.
(2) The uncertainty of a signal is independent of the size of the signal, i.e. the same uncertainty of the y value will be obtained for a concentration k than for another 1000k; this value is given by $s_{y/x}$ (9). This is a valuable approximation for short concentration ranges, but unrealistic in instrumental analysis, and especially in the SOM case because the uncertainty (noise, etc.) is frequently proportional to the analytical signal. As a result the conventional least squares method should not be applied in the SOM case because

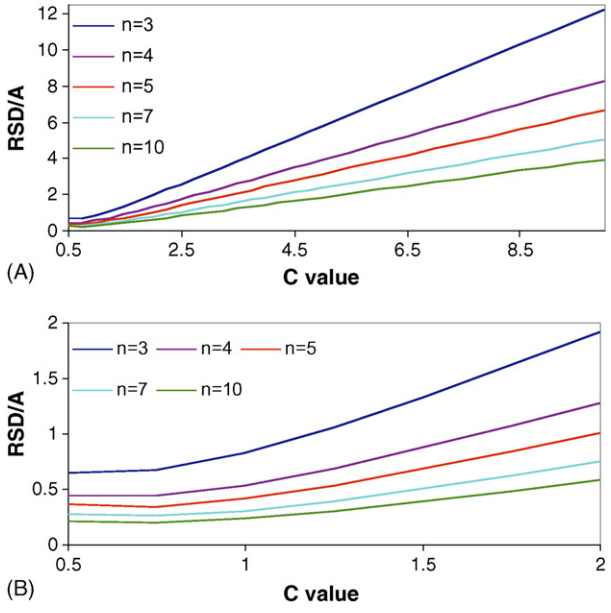


Fig. 2. (A) Variation of the R.S.D./A value as a function of C for the ESS case. (B) Expanded view of the (A).

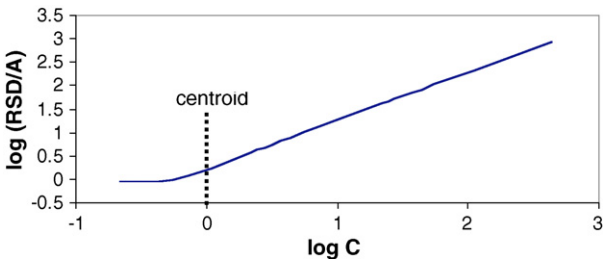


Fig. 3. Variation of the log(R.S.D./A) value as a function of log C for the SOM case ($n=5$).

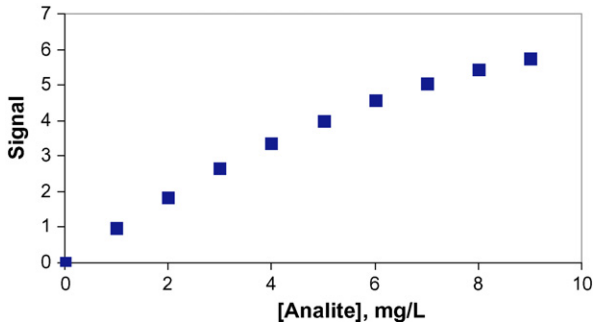


Fig. 4. Example of a calibration study in a ESS case.

the uncertainty obtained will be far from real; in fact, the usual error theory cannot be applied when the axes scale is not linear (log, etc.). In these cases, the Weighted Least Squares Method should probably be applied. A similar problem happens for the EES case, but the signals obtained for the calibration line are not so different (one order of magnitude) and the difference between uncertainties will not be too large. In these circumstances the experimenter will have to decide according to the particular situation. Obviously if the least squares method cannot be used, either for calibration or uncertainty, the correlation coefficient will not be a proper estimation of linearity. In general, it must be concluded that Eqs. (11) and (12) are an easy way to evaluate R.S.D. due to quantification.

3. Analytical consequences

3.1. Uncertainty due to the quantification step

The previously developed model permits to calculate the R.S.D. due to quantification in an easy way. Figures and examples shown here stress two important aspects: (a) the R.S.D. due to quantification only depends on how the calibration line is built; (b) the R.S.D. is specially high when interpolation is done under the centroid of the calibration line, and for that reason it should be considered as an important part of the total uncertainty (see Supplementary Data); (c) in general the centroid is considered the most precise point for interpolation; this is true in absolute terms (s_x) but not in relative terms (R.S.D.) which is more useful in many cases.

3.2. Which is the linear response range for a method?

Fig. 4 shows an example of a typical calibration curve for an ESS case. In this usual case we normally establish a subjective r value under which the curve can not be considered straight (for example 0.995 or 0.999).

The model proposed here (Section 2) can help to establish an objective criterion. It must be kept in mind that the r value changes with the linear range chosen and, consequently, so does the R.S.D. due to quantification. Table 2 gives the R.S.D. value depending on the amplitude of the linear range considered, and supposing that the interpolation is performed for $C = 1.5$ in all cases.

A possible practice could be to obtain the value of $s_c(x)$ apart from the interpolation step; then, the highest response range would be chosen as that which produces an uncertainty that can be neglected when compared with $s_c(x)$.

3.3. Other models for the quantification of uncertainty

Some other models can be found in the literature for the calculation of the uncertainty including quantification. For example a very usual model [11] is represented by Eq. (14) m being the number of replicates on the same sample. Eq. (14) reduces to Eq. (15) when the sample is measured only once:

$$s^2_{x_{\text{sam}}} = \frac{s^2_{y/x}}{b_1^2}\left(\frac{1}{m} + \frac{1}{n} + \frac{(x_{\text{sam}} - \bar{x})^2}{\sum (x_i - \bar{x})^2}\right) \tag{14}$$

$$s^2_{x_{\text{sam}}} = \frac{s^2_{y/x}}{b_1^2}\left(1 + \frac{1}{n} + \frac{(x_{\text{sam}} - \bar{x})^2}{\sum (x_i - \bar{x})^2}\right) \tag{15}$$

We have been unable to find the mathematical deduction of Eqs. (14) and (15), but they are based on the fact that uncertainty sources for standards are the same as for the sample. However in the vast majority of the analytical problems, the sample is affected by a number of uncertainty sources which are not present in the standards: sampling and sub-sampling uncertainty, sample dissolution or extraction, interferences elimination, . . .; all these steps contribute to the combined uncertainty, so, the use of both equations in a blind manner could bring on confusion and this is the reason why we recommend to calculate the uncertainty due to quantification as a separate source of uncertainty using Eq. (14), whenever necessary.

3.4. On the two-point ("one-point") calibration lines

In the last few years it is sometimes proposed in the analytical literature (especially when dealing with atomic or chromatographic methods) the use of so called two-point calibration lines. The "one-point" calibration method also uses the origin of the calibration plot (0, 0), so in practise it is a two-point calibration line. A straight line defined with two points has obviously no

Table 2
Values of %R.S.D. for different concentration ranges in the calibration line (a value $C = 1.5$ is supposed in all the cases)

n	3	4	5	6	7	8	9	10
r	0.9997	0.9992	0.998	0.997	0.996	0.994	0.991	0.988
Upper limit (mg/L)	2	3	4	5	6	7	8	9
%R.S.D.	3.3	3.4	3.7	4.0	4.3	4.6	5.0	5.4

"mathematical" uncertainty that could be assigned to slope and intercept, but it has chemical uncertainty. However, the model described when applied to a two-point calibration line gives a mathematical indetermination (R.S.D. = $0 \times \infty$).

For this reason the two-point method should be used just to confirm some previous and habitual calibration line still in use. A significance test can be done to check whether slope and intercept from the two-point calibration line differ significantly from those belonging to the old calibration line, for the confidence level desired. Because of the strong correlation between slope and intercept when linear regression analysis is done, independent tests cannot be recommended, but the joint confidence ellipse test can be tried instead [12]. In this test a joint confidence ellipse is defined for slope and intercept of the original calibration plot. In this space a point defined by the slope and intercept of the two points calibration line should lie inside the ellipse if the old calibration line is still to be valid; on the contrary the old calibration plot will have to be checked.

3.5. The limit of detection

The limit of detection (LOD) is considered as the minimum concentration (x_{LOD}) or amount of analyte that originates an analytical signal that differs significantly from the background, according to the confidence level desired. To interpret the term "differs significantly", the IUPAC recommendations are usually followed [13,14] and the criterion $3s_{blank}$ is applied, where s_{blank} is the standard deviation of the experimental signal for analyte absent. So the x_{LOD} is given by

$$x_{LOD} = \frac{3s_{blank}}{b_1} \quad (16)$$

Eq. (16) has the advantage that it easily allows straightforward LODs that can be compared with any other obtained under the same premises. Nonetheless, whenever x_{LOD} is experimentally obtained there is a feeling that Eq. (16) gives some underestimation of this parameter; or in other words, the x_{LOD} is useful for comparison but, apparently, the absolute value seems to be too low and not very real. The reason is, probably, that s_{blank} has been considered the only source of uncertainty. Obviously there is some extra uncertainty associated to the quantification process, and only when b_0 is essentially 0 and b_1 is well-defined, s_{blank} will be a good estimation of the total uncertainty, but, unfortunately, this does not usually happen in the daily practice. Winefordner and Long [15] already stressed this problem. They compared the LOD values obtained after of using Eq. (16) and those obtained after considering the uncertainty in b_0 and b_1 (they did not take into account the covariance between them) and showed examples (corresponding to the SOM case) in which the difference between both values of LOD were about 1000 times.

Actually, the signal $y_{blank} + 3s_{blank}$ corresponding to the X_{LOD} is very low, so C will be large and the uncertainty will be extreme. For example, consider a calibration graph according to the following equation (y is in relative units and x in mg L^{-1}):

$$y = 3.48x + 0.32, \qquad r = 0.9990,$$

$$n = 5 \text{ (ESS) (up to 20 mg L}^{-1}\text{, } \bar{x} = 10)$$

and suppose a value for $s_{blank} = 0.35$. The value for x_{LOD} will be:

$$x_{LOD} = \frac{3 \times 0.35}{3.48} = 0.30 \text{ mg L}^{-1}$$

Using Eq. (12), $A = 4.5$, $B = 0.50$, $C = 28.6$ and then the %R.S.D. of the x_{LOD} due to the use of the calibration line will be: 87.3%, which obviously represent a very low reliability.

Acknowledgements

Financial support from MEC, Spain (projects PPQ2003-07318-C02-02 and CTQ 2005-05761) is here acknowledged. The authors want to thank Dr. Fernando Plo (Departamento de Métodos Estadísticos, Facultad de Ciencias, Universidad de Zaragoza) for his technical advice.

Appendix A. Supplementary data

Supplementary data associated with this article can be found, in the online version, at 10.1016/j.talanta.2006.07.031.

References

[1] A. Maroto, R. Boqué, J. Riu, F.X. Rius, Trends Anal. Chem. 18 (1999) 577.
[2] D. Harvey, J. Chem. Ed. 79 (2002) 360.
[3] These guides can be downloaded free of charge from NIST and Eurachem websites http://www.physics.nist.gov/cuu/Uncertainty/ and http://www.eurachem.ul.pt/guides/, respectively.
[4] Analytical Methods Committee, Analyst 20 (1995) 2303.
[5] A. Maroto, R. Boqué, J. Riu, F.X. Rius, Anal. Chim. Acta 440 (2001) 171.
[6] R. Romero, G. Bagur, D. Gázquez, M. Sánchez-Viñas, L. Cuadros-Rodríquez, M. Ortega, LC&GC 22 (2004) 150.
[7] G. Bagur, M. Sánchez-Viñas, D. Gázquez, M. Ortega, R. Romero, Talanta 66 (2005) 1168.
[8] J.C. Miller, J.N. Miller, Statistics for Analytical Chemistry, 4th ed., Prentice Hall, 2000, Chapter 5.
[9] R. Caulcutt, R. Boddy, Statistics for Analytical Chemistry, Chapman and Hall, 1983, Chapter 5.
[10] J. Galbán, J. Chem. Ed. 81 (2004) 1053.
[11] J.N. Miller, in: A. Townshend (Ed.), Encyclopaedia of Analytical Science, Academia Press, London, 1995, p. 4798.
[12] D.L. Massart, B.G.M. Vandeginste, L.M.C. Buydens, S. De Jong, P.J. Lewi, J. Seyers-Verbeke, Handbook of Chemometrics and Qualimetrics: Part A, Elsevier, Amsterdam, 1997, pp. 193–194.
[13] L.A. Currie, Pure Appl. Chem. 67 (1995) 1699.
[14] L.A. Currie, Anal. Chim. Acta 391 (1999) 127.
[15] J.D. Winefordner, G.L. Long, Anal. Chem. 55 (1983) 712A.

Available online at www.sciencedirect.com
ScienceDirect
Talanta 71 (2007) 1393–1398
Talanta
www.elsevier.com/locate/talanta

Sequential injection analysis with second-order treatment for the determination of dyes in the exhaustion process of tanning effluents

V. Gómez [a], J. Font [b], M.P. Callao [a,*]

[a] *Analytical and Organic Chemistry Department, Rovira i Virgili University, Marcel·lí Domingo, s/n. Campus Sescelades, 43007 Tarragona, Spain*
[b] *Escola Universitària d'Enginyeria Tècnica Industrial d'Igualada, Pl. del Rei 15, 08700, Igualada, Spain*

Received 3 April 2006; received in revised form 15 June 2006; accepted 6 July 2006
Available online 23 August 2006

Abstract

A sequential injection (SI)-DAD spectrophotometric method to control the exhaustion of dyes in a mixture of three dyes from a tanning industry process has been developed. It is based on an interdiffusion process of the sample and reagents which leads to a gradual fall in pH through the channel to the detector recording a data matrix. The aim of this paper is to develop a second-order calibration model that is unaffected by interferents by applying multivariate curve resolution with alternating least squares (MCR-ALS). We obtained a linear calibration in the 5–30 mg l^{-1} range with a correlation coefficient of 0.999 for each dye with detection limits of 2.6, 3.9 and 2.1 mg l^{-1} for Acid Red, Acid Brown and Acid Orange, respectively. The simultaneous determination of the three dyes from tanning samples showed a satisfactory precision for the three analytes. The method has been validated comparing the concentration of some spiked samples with the expected concentration using a *t*-paired test. When we used this method to study the exhaustion of dyes, we found that there were several stages in this process. These data may be the key to optimising the exhaustion process.
© 2006 Elsevier B.V. All rights reserved.

Keywords: Dyes determination; Tanning effluents; Multivariate curve resolution; Sequential injection analysis

1. Introduction

Large quantities of dyes are used in a wide range of applications. These include textiles, paint pigments, printing inks and food colouring. The textile industry is the largest consumer of dyes, accounting for two-thirds of the dyestuff market. Interest in determining dyes are both technological (to determine the proportions of base dyes needed to achieve a certain tone) and environmental (their synthetic precursors, intermediates and degradation products are potential health hazards [1–5]).

Several analytical procedures, e.g., spectrophotometry [6], solid-phase spectrophotometry [7], voltammetry [8], polarography [9–10], capillary electrophoresis [11–13] and chromatography, have been used to determine dyes [14–16]. Spectrophotometric methods have been used for the routine quantitative determination of synthetic dyes [17]. Binary dye mixtures showing a strong spectral overlap have easily been resolved by derivative and bivariate techniques [18–19]. As the colour normally comprises a mixture of two or more colorant dyes, a method that is able to determine multiple components is needed. Preference is therefore given to chromatographic methods over spectrophotometry since spectrophotometry sometimes suffers spectral interference that cannot be solved by the derivative ratio spectra methods[20].

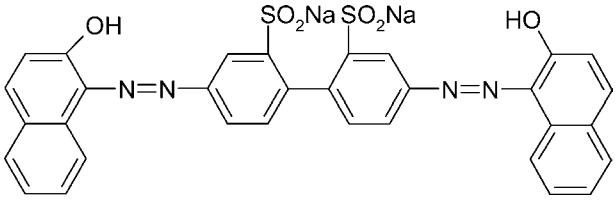
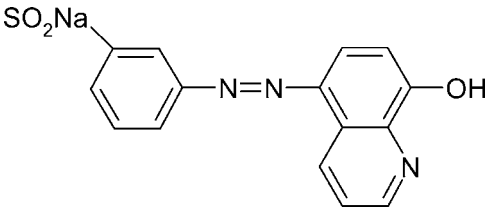
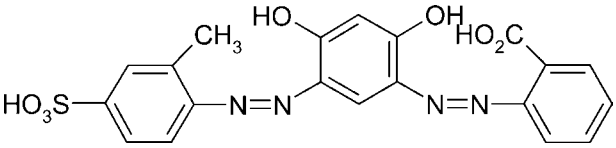
Chemometric techniques such as multiple linear regression (MLR), principal component regression (PCR), partial least squares (PLS) and bilinear least squares (BLLS) have already been applied for analysing mixtures of several dyes [21–24].

The aim of this paper is to develop an analytical method for studying the exhaustion of dyes in the standard dyeing process of the leather industry. The colour obtained in the process depends on how the dyes enter into the leather, i.e., on factors such as bath volume, the surface area of the leather, and total turning time. In this paper, we hope to obtain information that will help to optimise the dyeing process and to determine the amount of dye that remains in the wastewaters once at the end of the process. We studied three dyes. Table 1 shows the structure, name and chemical index of these dyes.

* Corresponding author. Tel.: +34 977558299; fax: +34 977558446.
E-mail address: mariapilar.callao@urv.cat (M.P. Callao).

0039-9140/$ – see front matter © 2006 Elsevier B.V. All rights reserved.
doi:10.1016/j.talanta.2006.07.019

Table 1
Structure, name, chemical index and colour of the dyes used in the tanning industry

Structure	CI[a], number and name	Colour
	Acid Red 97	Bright yellowish red
	Acid Orange 61	Orange
	Acid Brown 425	Dull reddish brown

[a] Colour index.

Our method is based on combined sequential injection analysis and multivariate curve resolution with alternating least squares (SIA-MCR-ALS)[25]. This SIA system does not use hazardous reagents and the amount of chemical waste generated during the analysis is minimal. Multi-way analysis is becoming popular due to the availability of high-order instrumental data and the proliferation of chemometric algorithms for data processing [26–29]. Unlike other techniques like PARAFAC or Tucker, MCR-ALS is highly flexible when defining the type of data because it enables us to work with trilinear data when two modes are in common (spectra and time) and with non-trilinear data when only one mode (the spectra) is in common. A particularly appealing property of multi-way data is second-order advantage [30], a term which was coined to describe analysis in the presence of unsuspected interferents.

We have found no references in the literature that use this method to treat such complex mixtures as those in this study.

2. SIA-MCR-ALS

Sequential injection analysis (SIA), known as the second generation of flow systems [31], enables the sample and the reagents to be introduced sequentially into the system. Fig. 1 shows a scheme for a SIA system. First, the sample and the reagents are aspirated towards the syringe and stored into the waiting coil (A). They are then pumped to the reaction coil (B), where the reagents mix with the sample via an interdiffusion process.

The analytical process involved sequential aspiration of first: about 4500 μl of the carrier (water), second: reagents (sodium hydroxide and/or sulphuric acid) and third: sample (mixtures containing the three dyes). The interdiffusion process of the sample and reactants lead to a gradual fall in pH through the channel to the detector. The synthetic dyes are polyprotic species, so when the sample reaches the detector, the most acid species appears first, followed by the mixture of this species with its conjugate base. The working conditions (volume and concentrations of reagents and sample volume) for obtaining a suitable response (sequential appearance of the acid and basic species of each dye) were determined using several dyes standards.

The obtained signal is a data matrix, $D(m \times n)$ and corresponds to a set of spectra at different pH. m are the times and n are the wavelengths at which the absorbance is recorded. As an example, Fig. 2 shows the data matrix obtained when the process is applied to one of the dyes studied.

The aim of second-order data treatment techniques such as MCR-ALS is to decompose the raw matrix D into the product of two matrices according to Eq. (1):

$$\boldsymbol{D} = \boldsymbol{C}\boldsymbol{S}^{\mathrm{T}} + \boldsymbol{E} \quad (1)$$

where matrix C $(m \times p)$ has column vectors corresponding to the profiles of concentration of the p pure components that are

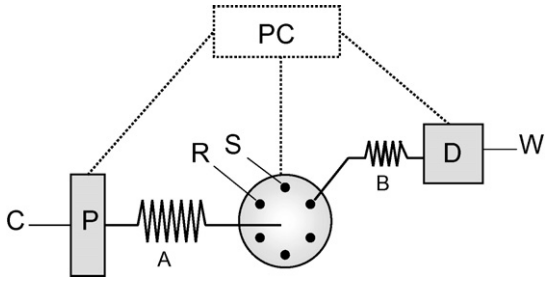


Fig. 1. Scheme of the proposed sequential injection system. C: carrier; S: sample; R: reagents; P: pump; V: multi-position valve; D: detector; PC: computer; A: holding coil; B: reaction coil; W: waste.

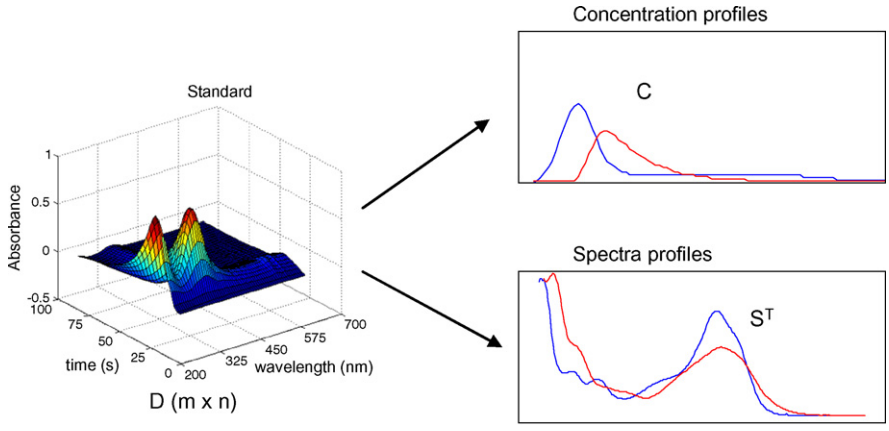


Fig. 2. MCR-ALS procedure working with a matrix of a single dye (Acid Red).

present in matrix $\boldsymbol{D}$. The row vectors of matrix $\boldsymbol{S}^{\mathrm{T}}$ ($p \times n$) correspond to the spectra of the p pure components, and $\boldsymbol{E}$ is the matrix of the residuals. A scheme of this process is given in Fig. 2. The spectral profiles can be used to identify the substances that provide a signal and the concentration profiles can be used to obtain the areas of each species, which are directly related to the concentration. A set of constraints [32] and working with augmented matrices [33–35] is introduced in the resolution process.

To establish a calibration model, augmented matrices are obtained from a matrix corresponding to a calibration standard, a matrix corresponding to a standard solution of constant composition, which we call the reference standard and the vectors corresponding to the spectra of the dyes. From the concentration profiles we obtained the relative area r_{p} (2).

$$r_{\mathrm{p}} = \frac{a_{\mathrm{p}}}{a_{\mathrm{rst,p}}} \tag{2}$$

where a_{p} and $a_{\mathrm{rst,p}}$ are the areas of the calibration standard and of the reference standard, respectively and we established a univariate linear regression as (3):

$$r_{\mathrm{p}} = b_0 + b_1 \cdot c_{\mathrm{p}} \tag{3}$$

where c_{p} is $c_{\mathrm{st}}/c_{\mathrm{rst,p}}$, in which c_{st} is the concentration of the standards and $c_{\mathrm{rst,p}}$ is the concentration of the reference standard, and b_1 and b_0 are the parameters of the regression line. The samples were analysed by the same procedure and the value of the concentration of each analyte in the sample, was obtained from its corresponding r_p value and the calibration parameters.

3. Experimental

3.1. Reagents and samples

In all analyses, we used analytical grade chemicals. These were NaOH and H_2SO_4 from PROLABO and purified water from a Milli-Q water system from MILLIPORE, USA.

Standard buffer solutions of pH 4 7 (Hamilton) were used to calibrate the pH meter.

Dyes were obtained from Trumpler Española, S.A. (Barberà del Vallès, Barcelona, Spain).

Standard solutions of Acid Red 97, of Acid Brown 425 and of Acid Orange 61 were prepared in Ultrapure Milli-Q water and diluted as required. Acid Orange 61 and Acid Brown 425 correspond to a chromium complex whose ligand has the structure shown in Table 1.

The carrier stream is Ultrapure Milli-Q water.

In Table 2 we can see the steps of the whole tanning process. The seven samples in the study belong to the fourth step, *Greas-*

Table 2
Tanning process

First step: remoisturizing
Add acetic acid and moisturizing tensoactive agent
Turn for 10 min
Empty bath
Second step: retanning
Add acrylic lubricant resin
Turn for 20 min
Add organic chromium
Turn for 90 min
Empty bath
Add formic acid
Turn for 15 min
Empty bath
Third step: neutralizing
Add sodium formiate
Turn for 15 min
Add sodium hydrogen carbonate
Turn for 90–100 min
Empty bath
Add water
Turn for 10 min
Empty bath
Fourth step: greasing and dyeing
Add sulphated triolein and phosphoric ester
Turn for 40 min
Add dyes (6.96 g of each)
Turn for 60 min Samples 1–6
Add formic acid
Turn for 30 min Samples 7–8
Empty bath
Add water
Turn for 5 min
Empty bath and wring out

ing and dyeing. We can divide these samples into two groups: samples 1–6, which are taken every 10 min during the first turning process after the addition of dyes, and samples 7 and 8, which are taken after 15 min in the second turning process when formic acid is added.

3.2. Instrumental and software

This system comprised a Cavro XL 3000 stepper motor-driven syringe pump of 5 ml equipped with a six-port multiposition automatic selection valve (Eurosas EPS 1306 BPB), and a Hewlett-Packard 8452A spectrophotometer with a Hellma 178.713QS flow-through cell. All tubes to connect the various components of the flow system were made of Omnifit PTFE with 0.8 mm (i.d.). The lengths of the holding and reaction coils were 2 and 0.7 m, respectively. The syringe pump, the automatic valve and the data acquisition provided by the spectrophotometer were controlled by a personal computer (PC) via an RS-232 interface, a PCL-711S PC- Lab-Card and an HP-IB IEEE488 interface for communications, respectively.

The spectra were recorded from 220 to 720 nm in 2 nm steps. As each sample passed through the detector, 100 measurements, one every 0.7 s, were taken. The data were acquired and monitored by the spectrophotometer using the HP89531A software. The instrumentation was controlled by customised software.

A Crison pH meter was used to measure the pH of the samples.

All calculations for multivariate curve resolution with alternating least squares (MCR-ALS) were performed with laboratory-written software under a MATLAB 5.3 computer environment [36] available from http://www.ub.es/gesq/mcr/mcr.htm [37].

4. Results and discussion

First we studied the spectral characteristics of each dye at different pHs in static mode. We measured the absorbance in solutions ranging from pH 1 to 14 in increments of 1 unit of pH. The spectra obtained for each dye are shown in Fig. 3. For Acid Red, we obtained spectrum *a* up to pH 11, between pH 11 and 12 the dye evolved, and at higher pHs we obtained spectrum *b*. For Acid Orange, we obtained spectrum *d* up to pH 2, between pH 2 and 3 the dye evolved, and at higher pHs we obtained spectrum *c*. Finally, for Acid Brown we obtained spectrum *e* up to pH 8, between pH 8 and 9 the dye evolved, and at higher pHs we obtained spectrum *f*. Acid Red was the most sensitive dye, followed by Acid Brown and Acid Orange, in ratios of approximately 3:1.5:1.

By studying each dye individually, we checked that the two species for each dye could be resolved by applying a pH gradient (with NaOH for Acid Red and Acid Brown and with H_2SO_4 for Acid Orange). The linearity of the response of each dye was also studied in these conditions. Acid Red was lineal between 1 and 50 mg l^{-1}, Acid Brown was lineal between 5 and 100 mg l^{-1} and Acid Orange was lineal between 5 and 150 mg l^{-1}.

We then prepared an analytical sequence to resolve the six species in a mixture of three dyes. Because of the pHs at which

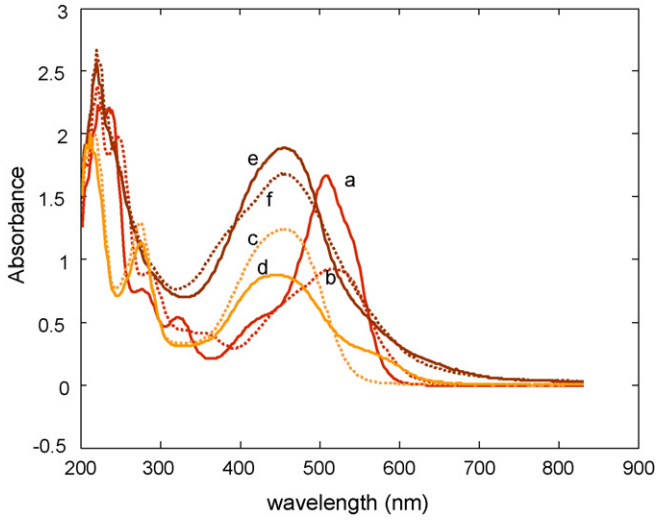


Fig. 3. Spectra of each dye obtained using a stopped-flow mode. Acid Red was measured at 50 mg l^{-1} while Acid Brown and Acid Orange were measured at 100 mg l^{-1}. Continuous lines are the acid forms and the dotted lines are the alkaline forms. (a and b) correspond to Acid Red, (b and c) correspond to Acid Orange and *d* and *f* correspond to Acid Brown.

the three dyes evolve (2–3 for Acid Orange, 10–11 for Acid Brown and 11–12 for Acid Red), we studied an analytical sequence in which we first aspirated NaOH of concentrations between 0.01 and 0.1 M, then the sample and finally H_2SO_4 of the same concentrations. The studied NaOH and H_2SO_4 volumes ranged between 0.042 and 0.083 ml, and the sample volume was 0.25 ml. Flow rate was 1.5 ml min^{-1}. We did not consider this variable, because lower values lengthens the residence time too much and leads to concentration profiles that are too wide and the areas are less reproducible.

The species reached the detector in the following order: first the three acid species, then the basic species of Acid Orange, followed by the basic species of Acid Brown and the basic species of Acid Red. Although we modified the concentrations and volumes of the reagents, this sequence did not produce satisfactory results because we were not able to resolve all the species.

Although the concentration and spectra profiles of Acid Orange could not be obtained after the resolution, we decided to work with an alkaline analytical sequence rather than a complete gradient. In this way, the system contained five components: Acid Red, Basic Red, Acid Brown, Basic Brown and Basic Orange (a–c, e, f following the notation in Fig. 3). The experimental conditions were selected by changing the NaOH concentration in the 0.01–0.1 M range and the NaOH volume in the 0.042 to 0.25 ml range. NaOH concentrations were those used in the batch mode. NaOH and sample volumes were selected taking into account the dimensions of the reactors of the system and the carrier volume necessary to avoid that the reagents and the sample enter into the syringe. The optimal conditions for analysing mixtures containing the three dyes were: a NaOH concentration of 0.025 M, a NaOH volume of 0.083 ml, a sample volume of 0.25 ml.

Fig. 4 shows the concentration profiles and the spectra of the five species of interest obtained using MCR-ALS of an aug-

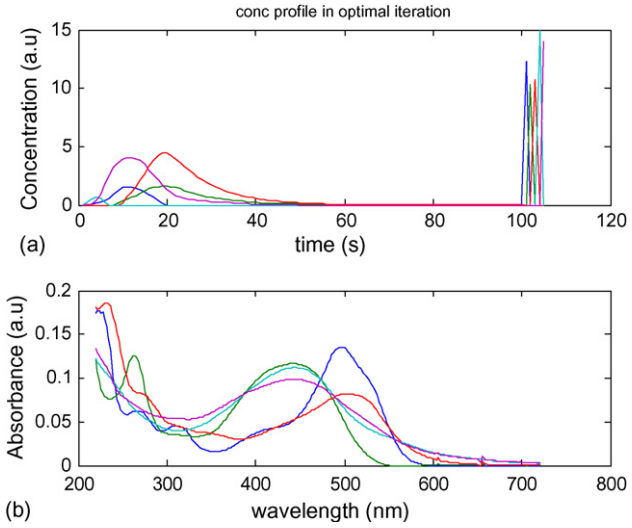


Fig. 4. Normalized concentration profiles (a) and pure spectra (b) obtained by multivariate curve resolution of the analysis of an augmented data matrix formed with Sample 1 (sample taken after one minute of turning in the tanning process) and the standard vectors of each dye considered (species a–c, e and f). a is in blue, b in red, c in green, e in turquoise and f in purple. (For interpretation of the references to colour in this figure legend, the reader is referred to the web version of the article.)

mented matrix from a mixture of the three dyes and the individual spectra of each species. Spectra obtained in the resolution show similar sensitivities because of the normalisation of the ALS algorithm.

To establish calibration models for each dye, we prepared a set of calibration standards containing the three studied dyes of known concentrations in the 5–30 mg l^{-1} range (5–10–15–20–30). Each of these standards contained the same concentration of dye at each level. To avoid working with solutions that were too absorbent, the working interval was lower than the maximum for each dye.

To determine the value of r_p in Eq. (2), the sum of the areas of both the acid and the basic species of Acid Red and Acid Brown had to be taken into account because this increases the reproducibility of the results. This is because a change in the pH gradient in the reactor increases the area of one of the species and decreases the area of the other.

Figures of merit for each calibration line are shown in Table 3. As calibration was modelled with relative values of both the signal (quotient of areas) and the concentration (quotient of concentrations), ideally the regression line should have a slope of 1 and an ordinate at the origin of 0. To check whether the regressions lines satisfy this condition, we compared the slope and ordinates at the origin of each line with those of the ideal line. This was done using a joint test of ordinate and slope [38]. The F values obtained for 95% of confidence are shown in the table. Limits of detection (LOD), calculated taking into account the uncertainty in the regression line [38] with 95% confidence, are also shown in this table.

The concentrations of each dye in the samples were calculated from Eq. (3), and applying the corresponding dilution factors. Samples had to be diluted to be analysed in the concentration range of the regression line. The standard deviation of the results

Table 3
Figures of merit for calibrations of the three dyes: Acid Red, Acid Brown and Acid Yellow

	Dye		
	Acid Red	Acid Brown	Acid Orange
b_1	0.9744	1.0451	0.9675
b_0	0.0197	−0.0291	0.0474
R	0.9995	0.9980	0.9996
S_{b1}	0.0169	0.0387	0.0166
S_{b0}	0.0102	0.0234	0.0101
S_e	0.0108	0.0248	0.0107
n	5	5	5
X_d (mg l^{-1})	2.6	3.9	2.12
F_{cal}	1.29	1.03	8.22
F_{critic} (0.05, 2, 3)		16.04	

b_1 and b_0 are the slope and the intercept of the calibration curve, R the correlation coefficient, s_{b1} and s_{b0} are the standard deviation of the slope and the intercept, s_e the standard error, n the number of points, x_d the limit of detection, F_{cal} is the calculated value and F_{critic} is the stadistic value.

was calculated from the calibration line parameters [39]. These results are shown in Table 4. Although the standard deviation of the analysed samples was mostly the same, when we applied the corresponding dilution factors it can be seen that this value increases as the concentration of the sample is bigger.

The accuracy of the method is checked calculating the dyes concentration in spiked samples where known concentrations of standards were added. The difference between each pair of results (concentrations of the spiked samples and concentrations of the samples without spiking) should ideally be the concentration of the added standard. With these data (differences of concentration/concentration of standards) we applied a paired t-test [39], adopting the null hypothesis in which the differences between both paired series of data correspond to a population with $\mu_d = 0$. After applying the corresponding t-test, we have concluded that there is no significant difference at 90% confidence.

The evolution of the dyes concentration in front of the time of turning is shown in Fig. 5. Error bars show the uncertainty of each value calculated at 95% confidence. We can see that there were four stages in the exhaustion of the dyes. In the first stage (up to 20 min), there was a sharp drop in the concentration. Between minute 20 and 60, the decline was more gradual. Between minute 60 and 75, there was another sharp drop in

Table 4
Concentrations of the dyes

Sample no.	Time of turning (min)	Concentration ± $s(5)$[a] (mg l^{-1})		
		Acid Red	Acid Brown	Acid Orange
1	1	4100 ± 140	4200 ± 300	4220 ± 140
2	10	2180 ± 40	2630 ± 90	3230 ± 40
3	20	1160 ± 24	2170 ± 60	1773 ± 24
4	30	1020 ± 24	1690 ± 50	1665 ± 24
5	45	808 ± 18	1060 ± 40	1437 ± 19
6	60	687 ± 18	880 ± 40	873 ± 18
7	75	316 ± 7	50 ± 20	235 ± 7
8	90	191 ± 8	30 ± 20	0 ± 10

[a] s evaluated from the regression line parameters.

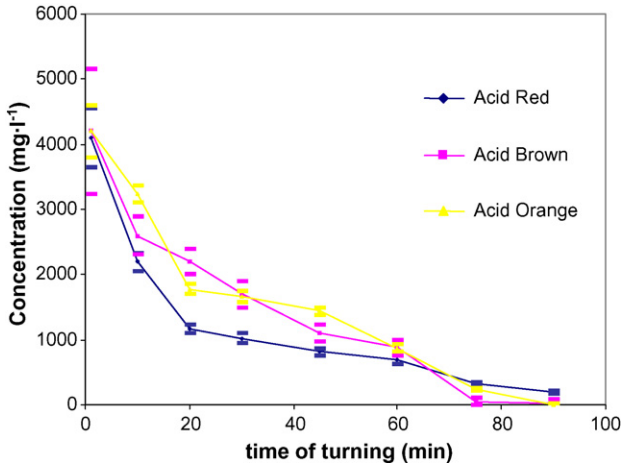


Fig. 5. Exhaustion of the dyes expressed in mg l^{-1}. Error bars have been calculated from the linear calibration parameters.

concentration due to the addition of formic acid. After minute 75 there were practically no more changes in concentration. In sample 7 (75 min of turning), the concentrations were 300, 40 and 240 mg l^{-1} for Acid Red, Acid Brown and Acid Orange, respectively. This means that the percentage dye fixation in all cases was over 93% and over 99% in the case of Acid Brown.

5. Conclusions

SIA-DAD with MCR-ALS is a good method for studying the evolution of a mixture of three dyes in the dyeing process of the tanning process.

This system is simple and fast, uses common reagents and has a high frequency of analysis (12 samples h^{-1} including all steps in a SIA process, i.e., cleaning, preparing and analyzing).

The main advantage of this system is that three analytes can be quantified satisfactorily in a single analysis. Also, it may be possible to optimise the dye exhaustion process in order to reduce the exhaustion time by adding formic acid earlier.

Acknowledgements

The authors would like to thank the Spanish Ministry of Education, Culture and Sports (Project BQQ2003-01142) for economic support, the Departament d'Universitats, Recerca i Societat de la Informació de la Generalitat de Catalunya (DURSI) and the Fons Social Europeu of the Catalan Government for providing Verónica Gómez with a doctoral fellowship.

References

[1] R.D. Combes, R.B. Haveland-Smith, Mutat. Res. 98 (1982) 101.
[2] C.C. Sigman, P.A. Papa, M.K. Doeltz, L.R. Perry, A.M. Twhigg, C.T. Helmes, Environ. Sci. Health 20 (1985) 427.
[3] J.R. Dipalma, Am. Farm. Physician 42 (1990) 1347.
[4] M.S. Bathia, Indian J. Med. Sci. 50 (1996) 285.
[5] L. Koutsogeorgopoulou, C. Maravelias, G. Methenitou, A. Koutselinis, Vet. Hum. Toxicol. 40 (1998) 1.
[6] J.J.B. Nevado, J.R. Flores, C.G. Cabanillas, M.J.V. Llerena, A.C. Salcedo, Talanta 46 (1998) 933.
[7] L.F. Capitán-Vallvey, M.D. Fernández, I. de Orbe, R. Avidad, Talanta 47 (1998) 861.
[8] A.G. Fogg, A.M. Summan, Analyst (1983) 891.
[9] P.L. López de Alba, L. López-Martínez, L.M. De León-Rodríguez, Electroanalysis 14 (2002) 197.
[10] S. Combeau, M. Chatelut, O. Vittori, Talanta 56 (2002) 115.
[11] Y. Masukawa, J. Chromaogr. B 1108 (2006) 140.
[12] H. Borwitzky, W.E. Haefeli, J. Bruhenne, J. Chromatogr. B 826 (2005) 244.
[13] H.Y. Huang, C.W. Chiu, S.L. Sue, C.F. Cheng, J. Chromatogr. A 995 (2003) 29.
[14] M.C. Genaro, E. Gioannini, S. Angelino, R. Aigotti, D. Giacosa, J. Chromatogr. A 767 (1997) 87.
[15] C.S. Eskilsson, R. Davidsson, L. Mathiasson, J. Chromatogr. A 955 (2002) 215.
[16] M.C. Garrigós, F. Reche, M.L. Marín, K. Pernas, A. Jiménez, J. Chromatogr. A 963 (2002) 427.
[17] J.J. Berzas, J. Rodriguez Flores, M.J. Villaseñor Llerena, N. Rodríguez Fariñas, Anal. Chim. Acta 391 (1999) 353.
[18] P.L. López-de-Alba, L. López-Martínez, K. Wróbel-Kaczmarczyk, K. Wróbel, J. Amador-Hernández, Anal. Lett. 29 (1996) 487.
[19] P.L. López-de-Alba, L. López-Martínez, M. González-Leal, Y. Estrada-Hernández, Quim. Anal. 18 (1999) 291.
[20] E.C. Vidotti, W.F. Costa, C.C. Oliveira, Talanta 68 (2006) 516.
[21] M. Blanco, T. Canals, J. Coello, et al., Anal. Chim. Acta 419 (2000) 209.
[22] J.J. Berzas-Nevado, C. Guiberteau-Cabanillas, A.M. Contento-Salcedo, Anal. Lett. 32 (1999) 1879.
[23] J.J. Berzas-Nevado, J.R. Flores, M.J.V. Llerena, Talanta 48 (1999) 895.
[24] N.R. Marsili, A. Lista, B.S. Fernández-Band, H.C. Goicoechea, A.C. Olivieri, Analyst 130 (2005) 1291.
[25] A. Pasamanotes, M.P. Callao, Trends Anal Chem. 25 (2006) 77.
[26] N.M. Faber, R. Bro, P.K. Hopke, Chemom. Intell. Lab. Syst. 65 (2003) 119.
[27] R. Bro, Chemom. Intell. Lab. Syst. 38 (1997) 149.
[28] M. Linder, R. Sundberg, Chemom. Intell. Lab. Syst. 42 (1998) 159.
[29] R. Tauler, A. Smilde, R. Kowalsky, J. Chemometrics 9 (1995) 31.
[30] K.S. Booksh, B.R. Kowalski, Anal. Chem. 66 (1994) 782A.
[31] J. Ruzicka, G.D. Marshall, G.D. Christian, Anal. Chem. 62 (1990) 1861.
[32] R. Tauler, A. Izquierdo-Ridorsa, E. Cassasas, Chemom. Intell. Lab. Syst. 18 (1993) 293.
[33] A. de Juan, E. Casassas, R. Tauler, in: R.A. Meyers (Ed.), Encyclopedia of Analytical Chemistry, John Wiley and Sons Ltd, Chichester, 2000, pp. 9800–9837.
[34] A. Izquierdo-Ridorsa, J. Saurina, S. Hernández-Cassou, R. Tauler, Chemom. Intell. Lab. Syst. 38 (1997) 183.
[35] C. Ruckebusch, L. Duponchel, J.P. Huvenne, J. Saurina, Anal. Chim. Acta 515 (2004) 183.
[36] Matlab, The Mathworks, South Natick, MA, USA.
[37] R. Tauler, A. de Juan, Multivariate Curve Resolution homepage, http://www.ub.es/gesq/mcr/mcr.htm.
[38] D.L. Massart, B.G.M. Vandeginste, et al., Handbook of Chemometrics and Qualimetrics Part A, Elsevier, Amsterdam, 1997.
[39] J.N. Miller, J.C. Miller, Statistics and Chemometrics for Analytical Chemistry, 4th ed., Prentice-Hall, Madrid, 2002.

Available online at www.sciencedirect.com
ScienceDirect
Talanta 71 (2007) 1110–1117
Talanta
www.elsevier.com/locate/talanta

Voltammetric determination of adenosine and guanosine using fullerene-C_{60}-modified glassy carbon electrode

Rajendra N. Goyal [a,*], Vinod K. Gupta [a], Munetaka Oyama [b], Neeta Bachheti [a]

[a] *Department of Chemistry, Indian Institute of Technology Roorkee, Roorkee 247667, India*
[b] *Kyoto University, Katsura, Nishikyo-ku, Kyoto 615-8520, Japan*

Received 4 May 2006; received in revised form 1 June 2006; accepted 1 June 2006
Available online 7 July 2006

Abstract

A fullerene-C_{60}-modified glassy carbon electrode (GCE) is used for the simultaneous determination of adenosine and guanosine by differential pulse voltammetry. Compared to a bare glassy carbon electrode, the modified electrode exhibits an apparent shift of the oxidation potentials in the cathodic direction and a marked enhancement in the voltammetric peak current response for both the biomolecules. Linear calibration curves are obtained over the concentration range 0.5 μM–1.0 mM in 0.1 M phosphate buffer solution at pH 7.2 with a detection limit of 3.02×10^{-7} M and 1.45×10^{-7} M for individual determination of adenosine and guanosine, respectively. The interference studies showed that the fullerene-C_{60}-modified glassy carbon electrode exhibited excellent selectivity in the presence of hypoxanthine, xanthine, uric acid and ascorbic acid. The proposed procedure was successfully applied to detect adenosine and guanosine in human blood plasma and urine, without any preliminary pre-treatment.
© 2006 Elsevier B.V. All rights reserved.

Keywords: Fullerene-C_{60}-modified glassy carbon electrode; Adenosine; Guanosine; Blood plasma; Urine

1. Introduction

Purine nucleosides are well-known for their metabolic and biological effects in human system. Their detection and determination has become increasingly important in the field of biomedical research owing to their importance in normal cellular functions. The importance of such a determination stems from the fact that changes in the concentration of these nucleosides in body fluids have been used to indicate the presence of various diseases [1,2] and hence, their analysis is highly desirable. Guanosine and adenosine are two important nucleosides found in nucleic acids, which are vital in various biological processes. Adenosine modulates physiological functions in heart and brain, and regulates oxygen supply during cell stress [3] and has also been suggested to be useful in the regulation of renal function [4]. Guanosine plays a protective role during brain ischemia [5] and, mediates the process of RNA splicing [6]. Excretion of elevated levels of nucleosides, including adenosine and guanosine, in urine has been shown to be related to carcinoma [7,8]. The measurement of adenosine and guanosine levels in plasma has been suggested to be a new diagnostic marker to investigate various liver diseases [9].

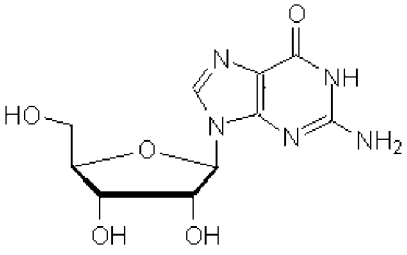
In view of the importance of adenosine and guanosine in human physiology, attempts have been made to determine them simultaneously in body fluids, since both occur together in biological system, by various techniques. In the recent years, several analytical methods have been developed for the determination of adenosine and guanosine in the presence of each other [10–17]. Although the chromatographic methods are sensitive, they require sample pre-treatment and time-consuming extraction steps. Also, many of the proposed methods have low column efficiencies and long analysis time. Electrochemical determination has shown to be a powerful method for the detection of a wide range of analytes including several purine compounds. However, electrooxidation of these compounds requires a relatively high oxidation potential, which limits the selectivity. Use of chemically modified electrodes could be beneficial since they render certain advantages such as decrease of the potential required for the electrochemical reaction to occur and enhancement of the sensitivity due to catalytic activity. Literature survey reveals that there are only a few reports for the simultaneous determination of adenosine and guanosine voltammetrically.

* Corresponding author. Tel.: +91 1332 285794; fax: +91 1332 273560.
E-mail address: rngcyfcy@iitr.ernet.in (R.N. Goyal).

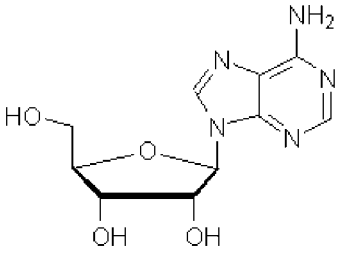
0039-9140/$ – see front matter © 2006 Elsevier B.V. All rights reserved.
doi:10.1016/j.talanta.2006.06.002

Chen and co-workers achieved the simultaneous determination of purine bases, ribonucleosides and ribonucleotides by capillary electrophoresis-electrochemistry with a copper electrode [18]. Boron doped diamond electrodes have recently been used to study the direct oxidation of adenosine and guanosine [19], however, the anodic peak potentials were observed at relatively high potentials. Yao et al. have reported the simultaneous determination of purine bases and their nucleosides at glassy carbon electrode (GCE) [20]. However, the studies were carried out in Britton–Robinson buffer at pH 2–4, which probably give little useful information concerning the biological system.

The aim of the present work is to develop a simple and reliable voltammetric procedure that could be adopted for the detection of adenosine and guanosine simultaneously in body fluids such as blood plasma and urine. Since differential pulse voltammetry is one of the popular techniques for carrying out trace analysis in various samples due to its high sensitivity and multianalysis capability, it has been utilized in the present investigation. The determination has been carried out at physiological pH utilizing the voltammetric oxidation peaks of both the nucleosides at fullerene-C_{60}-modified glassy carbon electrode, which could offer a promising way to reduce overpotential effects because the determination is based on a electrocatalytic oxidation mechanism. The catalytic activity of this electrode for various applications has recently been demonstrated [21,22].



Guanosine



Adenosine

2. Experimental

2.1. Apparatus

The electrochemical experiments were carried out using a computerized BAS (Bioanalytical Systems, West Lafayette, USA) CV-50W voltammetric analyzer. Electrochemical studies were performed using a conventional three-electrode glass cell with a platinum wire as an auxillary electrode and Ag/AgCl electrode (3 M NaCl) as reference (Model MF-2052 RB-5B). The working electrode was bare or C_{60}-modified glassy carbon electrode having a diameter ~3 mm. Phosphate buffers of appropriate pH and ionic strength (0.1 M) were prepared according to the method of Christian and Purdy [23]. The pH of the buffers was measured using a Century India Ltd. digital pH meter (Model CP-901) after proper standardization with 0.05 M potassium hydrogen phthalate (pH 4.0 at 5 °C) and 0.01 M borax (pH 9.2 at 25 °C) buffers. All potentials reported in the text are referred to Ag/AgCl electrode.

2.2. Reagents

Adenosine, guanosine, uric acid, ascorbic acid, hypoxanthine and xanthine were acquired from Merck and used as received. Fullerene-C_{60} of purity 98% and 99.5% were purchased from Aldrich, USA. All other chemicals used in this investigation were of analytical grade and were used without further purification. Fresh solutions of adenosine and guanosine solutions were prepared just prior to use.

2.3. Procedure

The stock solutions of adenosine and guanosine (each 2 mM) were prepared in doubly distilled water. For voltammetric experiments, 2.0 mL of the stock solution of adenosine/guanosine was mixed with 2.0 mL of phosphate buffer (0.1 M) of desired pH. The solutions were deoxygenated by bubbling high-purity nitrogen for 8–10 min before recording the voltammograms. For studying the effect of concentration, different sets of solution in the concentration range 0.5 μM–1.0 mM were prepared at pH 7.2 by appropriately diluting stock solution and differential pulse voltammograms (DPVs) were recorded employing the following parameters: pulse amplitude, 50 mV; sample width, 20 ms; pulse width, 50 ms; pulse period, 200 ms; sweep rate, 20 mV/s; sensitivity, 100 μA/V.

2.4. Sample preparation

Blood samples from three volunteers were obtained from the local hospital. The blood with EDTA as anti-coagulant was ultracentrifuged and the blood plasma obtained was used to determine adenosine and guanosine by the method reported.

Urine samples received from laboratory personnel were used after dilution with water by 100 times.

2.5. Fabrication of fullerene-C_{60}-modified glassy carbon electrode

The bare glassy carbon electrode was polished with alumina (BAS, USA) and then zinc oxide (Aldrich) using the BAS polishing kit before modification. It was then dipped in a beaker containing H_3PO_4 solution (0.2 M) to remove the adhered powder, and rinsed with distilled water after which the electrode was dried. Stock solution of C_{60} (150 μM) was prepared by dissolving in CH_2Cl_2. A known volume (40 μL) of this solution

was coated onto the surface of the clean and dried GCE using a microsyringe and dried in a stream of hot air (45 °C). The working electrode surface with a well-coated layer of fullerene was then pretreated according to the procedure described by Szucs and co-workers [24], partially reducing the C_{60} film formed on GCE surface in 1.0 M KOH in the potential range 0.0 to −1.5 V with a 10 mV/s scan rate. On partially reducing a fullerene film, it becomes conducting and hence can be used as an electrode material having special electrocatalytic properties. Subsequently, the electrode is placed in phosphate buffer solution (pH 7.2), which was previously de-oxygenated with high purity nitrogen for atleast 10 min. The electrode was then equilibrated in it by cyclic scanning in the potential range of 550 to −50 mV under a nitrogen atmosphere. The fullerene-C_{60}-modified glassy carbon electrode was then ready for use. As reported earlier, the surface coverage of C_{60} on GCE has been calculated as ∼85% [22].

3. Results and discussion

3.1. Voltammetric behavior of adenosine and guanosine

The cyclic voltammograms recorded for a binary mixture of 1.0 mM guanosine and 1.0 mM adenosine at the bare and fullerene-C_{60}-modified glassy carbon electrode in 0.1 M phosphate buffer solution at pH 7.2 are illustrated in Fig. 1. At the modified electrode, guanosine and adenosine gave two well-defined oxidation peaks in the first anodic sweep at about 990 mV (peak G) and 1290 mV (peak A), while the response at the bare GCE is very poor with a relatively small peak at 1030 mV and a small bump at 1390 mV. The peak potential of both the biomolecules was slightly less positive at the modified electrode than those obtained at the bare GCE. The enhancement of the oxidation peak current response appeared to be little. Therefore, it was decided to record differential pulse voltammograms.

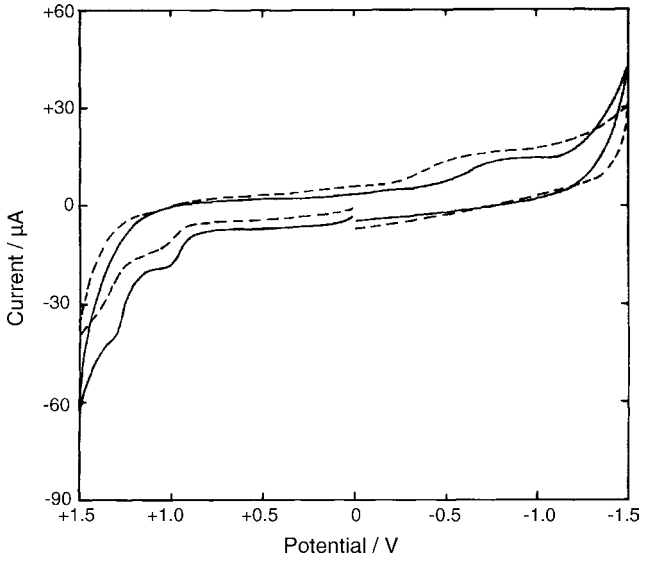


Fig. 1. Cyclic voltammograms obtained for solution containing both guanosine (1.0 mM) and adenosine (1.0 mM) at pH 7.2 at bare (- - -) and fullerene-C_{60}-modified (—) glassy carbon electrode.

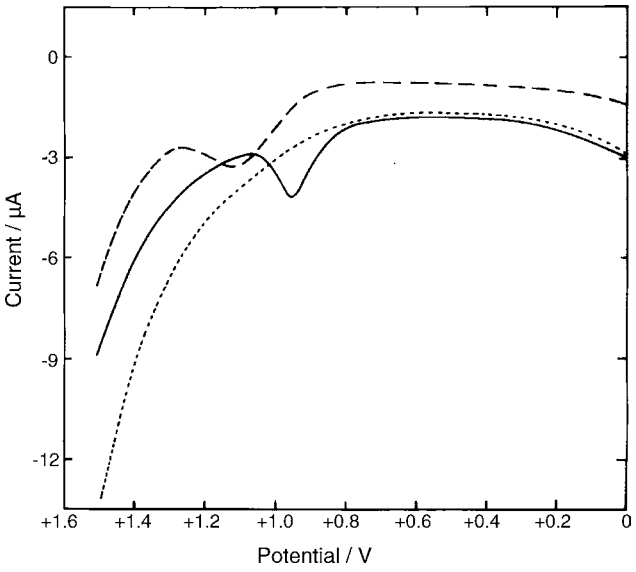


Fig. 2. Differential pulse voltammograms observed for (a) 0.1 mM guanosine at pH 7.2 at bare (- - -) and fullerene-C_{60}-modified (—) glassy carbon electrode (b) PBS (pH 7.2) at fullerene-C_{60}-modified glassy carbon electrode (. . .).

3.2. Individual determination of guanosine and adenosine

Fig. 2 shows the differential pulse voltammograms (DPVs) obtained at the bare and fullerene-C_{60}-modified glassy carbon electrode for 0.1 mM guanosine at 0.1 M phosphate buffer solution of pH 7.2. At the surface of the bare GCE, guanosine produces a broad anodic peak at E_p 1128 mV, a relative high positive potential. However, a sharp anodic peak at a lower positive potential, E_p 960 mV was obtained at the fullerene-C_{60}-modified glassy carbon electrode surface. A significant increase in the peak current in conjunction with the reduction of the oxidation potential of the process at the modified electrode revealed that fullerene-C_{60}-modified glassy carbon electrode act as a very efficient promoter to enhance the kinetics of the electrochemical process. DPV measurements were performed for guanosine oxidation at the modified electrode over the entire pH range at a sweep rate of 20 mV/s. It was found that the E_p decreases linearly with increasing pH as shown in Fig. 3(a). The plot of E_p versus pH (in the pH range 2.0–10.1) was a straight line with a slope of 34.2 mV per pH unit. The dependence of E_p versus pH using linear regression analysis can be expressed by the relation:

E_p (pH 2.0 − 10.1) = [1215 − 34.19 pH] mV versus Ag/AgCl having correlation coefficient ∼0.9930.

With increasing concentration of guanosine, the peak current (i_p) was found to increase in the range 0.5 μM–1.0 mM at pH 7.2 and practically became constant at higher concentrations. The plot between i_p and concentration of guanosine from the data generated during DPV studies was linear and passed through the origin as shown in Fig. 3(b). The dependence of peak current (after background current correction in peak current) can be expressed by the equation.

$$i_p\,(\mu A) = 10.337C$$

where C is in mM having a correlation coefficient of 0.9933 and a sensitivity of 0.010 μA μM^{-1}. This behavior indicated that

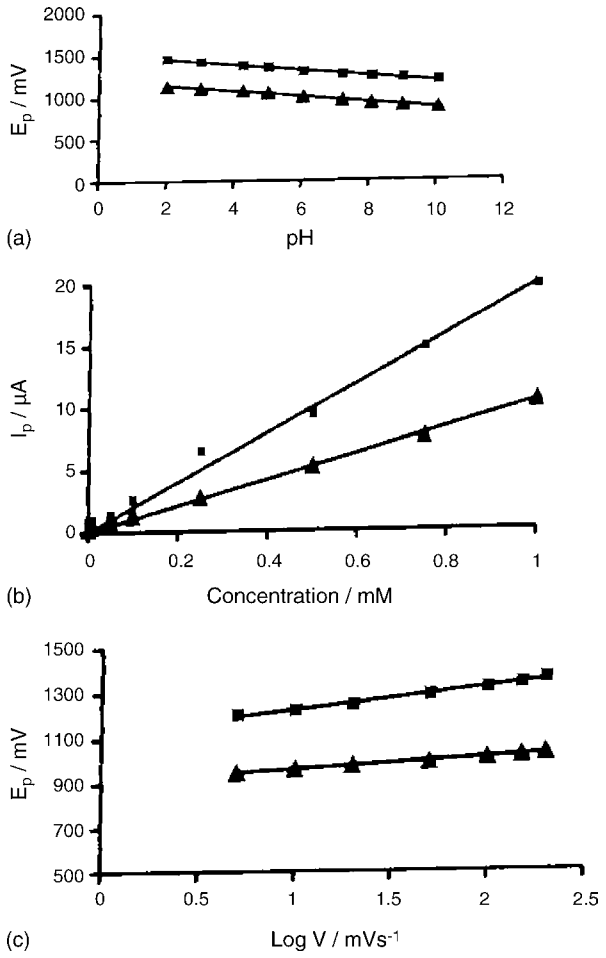


Fig. 3. (a) Observed dependence of peak potential (E_p) on pH for 0.5 mM guanosine (▲) and 0.5 mM adenosine (■) at fullerene-C_{60}-modified glassy carbon electrode. (b) Calibration plot observed for guanosine (▲) and adenosine (■) at fullerene-C_{60}-modified glassy carbon electrode at pH 7.2. (c) Plot of E_p vs. logarithm of sweep rate of 0.5 mM guanosine (▲) and 0.5 mM adenosine (■) at pH 7.2.

guanosine can be safely estimated in the concentration range 0.5 μM–1.0 mM at fullerene-C_{60}-modified glassy carbon electrode. The detection limit (3σ) of guanosine is found to be 1.45×10^{-7} M.

The effect of sweep rate (v) on peak potential and peak current was studied in the sweep range 5–200 mV/s at pH 7.2. It was found that the peak current increased and the peak potential shifted towards more positive potential with an increase in sweep rate. The nature of the plot of E_p versus log v was linear (Fig. 3(c)) suggesting the nature of the electrode reaction as EC in which charge transfer is followed by irreversible chemical reactions. The dependence of E_p on log v can be expressed by the equation:

$$E_p\,(\text{mV}) = 48.396 \log v + 914.3$$

The DPV response of 0.1 mM adenosine in 0.1 M, pH 7.2 phosphate buffer solution on bare and modified GCE is illustrated in Fig. 4. As can be seen, the oxidation signal of adenosine at bare electrode is weak yielding a small peak at 1350 mV,

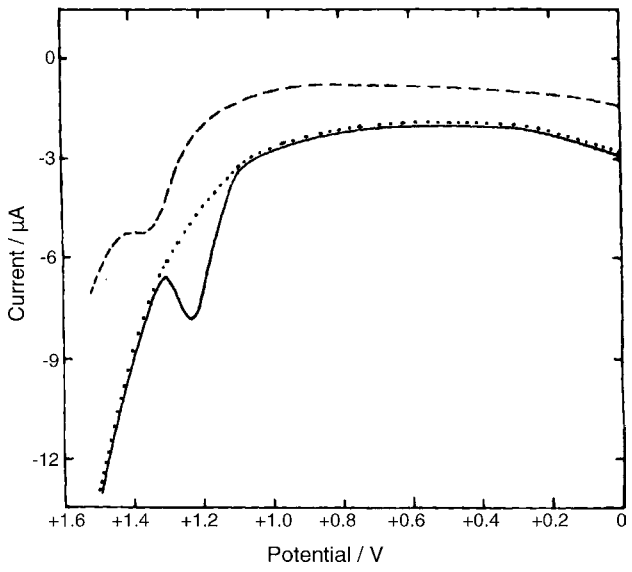


Fig. 4. Differential pulse voltammograms for (a) 0.1 mM adenosine at pH 7.2 at bare (- - -) and fullerene-C_{60}-modified (—) glassy carbon electrode (b) PBS (pH 7.2) at fullerene-C_{60}-modified glassy carbon electrode (. . .).

whereas, the modified electrode yields a well-defined peak at 1224 mV with enhanced peak current. The lowered oxidation potential and the increased peak current response again indicate that the C_{60} film is able to accelerate the rate of adenosine electron transfer.

The pH dependence of peak potential (E_p) obtained for 0.5 mM adenosine was studied in the pH range between 2.0 and 10.1 (Fig. 3(a)). A linear dependence over the entire pH range studied was found. The E_p–pH relationship can be expressed by the relation:

E_p (pH 2.0 − 10.1) = [1526 − 33.57 pH] mV versus Ag/AgCl having correlation coefficient of 0.9904.

The linear range existing between the analytical signal and adenosine concentration was studied for solutions of increasing adenosine concentration. The dependence of peak current response (after correction of background current) on the concentration of adenosine at pH 7.2 is depicted in Fig. 3(b). The results showed that the peak current increased linearly with increase in adenosine concentration in the range 0.5 μM–1.0 mM. The dependence of peak current on concentration can be expressed by the relation:

$$i_p\,(\mu\text{A}) = 19.851C$$

where C is in mM, with a correlation coefficient of 0.9880 and a sensitivity of 0.020 μA μM^{-1}. The detection limit of adenosine was found to be 3.02×10^{-7} M.

The effect of sweep rate on peak current and peak potential of adenosine was studied in the range 5–200 mV/s. The peak current increased with increase in sweep rate (v) and the peak potential shifted to more positive values with increasing v. The plot of E_p versus log v (Fig. 3(c)) was linear with a correlation coefficient of 0.9940 and this behavior was consistent with the EC nature of the reaction in which the electrode reaction is coupled with an irreversible follow-up chemical reactions.

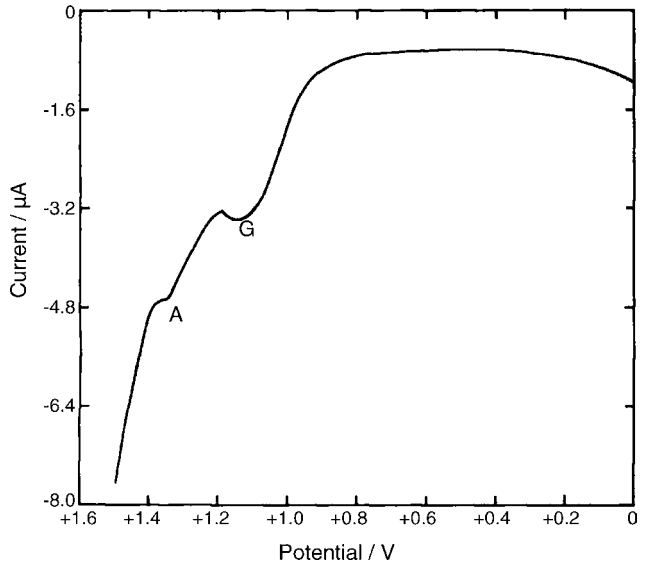


Fig. 5. Differential pulse voltammogram for solution containing both guanosine (0.05 mM) and adenosine (0.05 mM) at pH 7.2 at bare glassy carbon electrode.

The relationship expressing the linear dependence of E_p on $\log v$ is:

$$E_p(\text{mV}) = 95.528 \log v + 1130.7$$

3.3. Simultaneous determination of adenosine and guanosine

The main objective of the present investigation is to simultaneously determine the concentration of both adenosine and guanosine using the fullerene-C_{60}-modified glassy carbon electrode. Fig. 5 shows the differential pulse voltammogram obtained at the bare electrode in 0.1 M phosphate buffer containing 0.05 mM adenosine and 0.05 mM guanosine. Rather

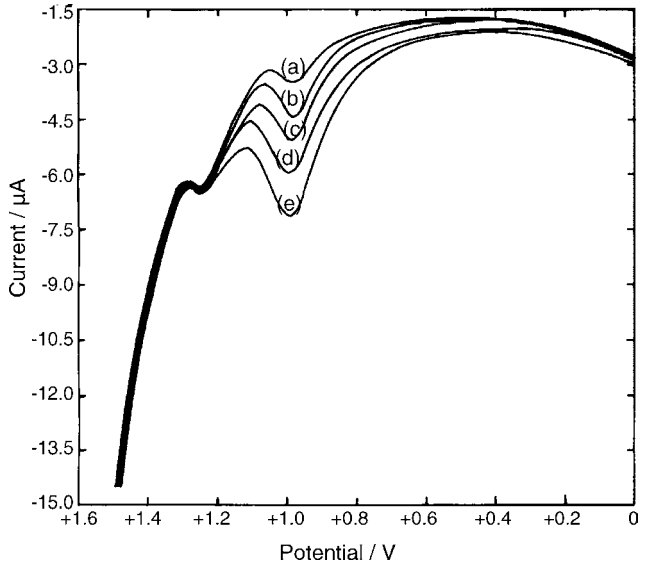


Fig. 6. DPVs of a mixture of adenosine and guanosine at the fullerene-C_{60}-modified glassy carbon electrode at pH 7.2. Concentration of guanosine was changed keeping the concentration of adenosine constant (i.e. [adenosine] = 0.05 mM; [guanosine]: (a) 0.01 (b) 0.10 (c) 0.20 (d) 0.30 (e) 0.40 mM).

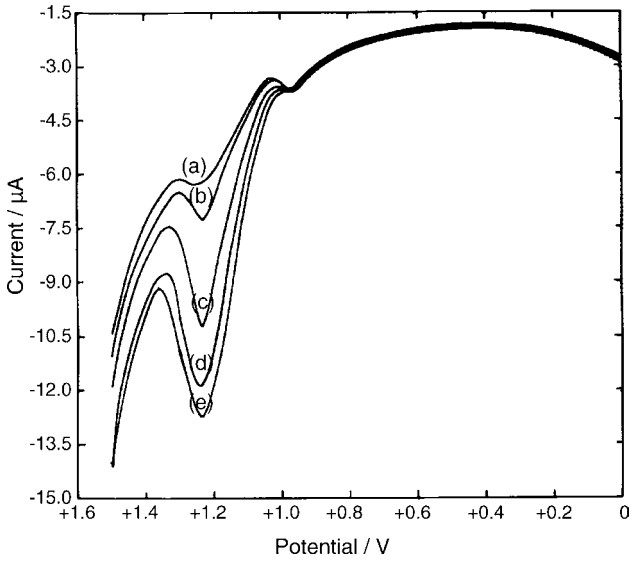


Fig. 7. DPVs of a mixture of adenosine and guanosine at the fullerene-C_{60}-modified glassy carbon electrode at pH 7.2. Concentration of adenosine was changed keeping the concentration of guanosine constant (i.e. [guanosine] = 0.05 mM; [adenosine]: (a) 0.01 (b) 0.10 (c) 0.20 (d) 0.30 (e) 0.40 mM).

broad oxidation peaks for both the analytes are obtained at relatively high oxidation potentials. On the other hand, the modified electrode electrocatalytically oxidises adenosine and guanosine resulting in two well-defined and well-separated peaks. Fig. 6 shows the differential pulse voltammograms for different concentration of guanosine in the presence of a fixed concentration of adenosine (0.05 mM). As can be seen, the voltammetric peak of adenosine was unaltered by the addition of guanosine and the voltammetric signal of guanosine increased with increase in its concentration. Similarly, while varying the concentration of adenosine (keeping the concentration of guanosine constant, i.e. 0.05 mM), the oxidation peak current of adenosine increased (Fig. 7). The calibration curves for both adenosine and guanosine were linear for a wide range of concentration (0.01–0.40 mM). Thus, electrochemical signals of adenosine and guanosine are independent of each other at fullerene-C_{60}-modified glassy carbon electrode and hence simultaneous determination of both the analytes at the modified electrode was realized.

3.4. Stability and reproducibility of the modified electrode

Since the method for the preparation of the modified electrode is easy, the long-term stability of the electrode is not so important. However, the stability of the modified electrode was evaluated. After the modified electrode was stored for approximately 1 week, only a small decrease of current sensitivity with a relative standard deviation (R.S.D.) of about 4.53% for 0.10 mM adenosine and 4.28% for 0.10 mM guanosine was observed which can be attributed to the excellent stability of the modified electrode. Furthermore, the reproducibility of the modified electrode has been investigated. A series of six successive scans in the solution containing 0.5 mM adenosine and 0.5 mM guanosine were performed separately at the same fullerene-C_{60}-modified glassy carbon electrode. The R.S.D. was found to be 1.97 and 0.85% for the analytes, respectively

indicating excellent reproducibility of the modified electrode. To ascertain the reproducibility of the results further, four different modified electrodes, independently constructed based on the same electrode, shows an acceptable reproducibility with a relative standard deviation of 1.59 and 2.15% for 0.5 mM adenosine and 0.5 mM guanosine, respectively.

3.5. Effect of the amount of C_{60}

The influence of immobilised C_{60} quantities onto the peak current response of adenosine and guanosine was investigated. For this purpose different volumes of the C_{60} solution in dichloromethane were cast on the electrode surface. When the surface was dried more amount of C_{60} was added. Thus, 5, 20, 40, 60 and 80 μL of C_{60} solution were deposited. It was observed that the increase in C_{60} deposition at the electrode surface from 5 to 40 μL led to an increment in the peak current response of 0.5 mM of both the nucleosides. At C_{60} amount more than 40 μL, the peak currents of both the analytes became almost constant. Thus, it is concluded that the optimum amount of C_{60} required to catalyze the oxidation of these nucleosides is 40 μL.

3.6. Interference study

The major sources of interference in adenosine and guanosine determination can be few common coexisting substances in biological fluids. These species could lead to either new voltammetric peaks or to an overlap with the existing ones, influencing their peak potential and peak current response. The effects of hypoxanthine, xanthine, uric acid and ascorbic acid on the voltammetric peak response of 0.05 mM adenosine and 0.05 mM guanosine was examined. In all the cases, no substantial change in peak current response of both the analytes was observed upto four-fold excess of each of the interferents. The data is summarized in Table 1. The voltammetric response of 0.05 mM guanosine in presence of the interferents (ascorbic acid, uric acid and xanthine) is demonstrated in Fig. 8.

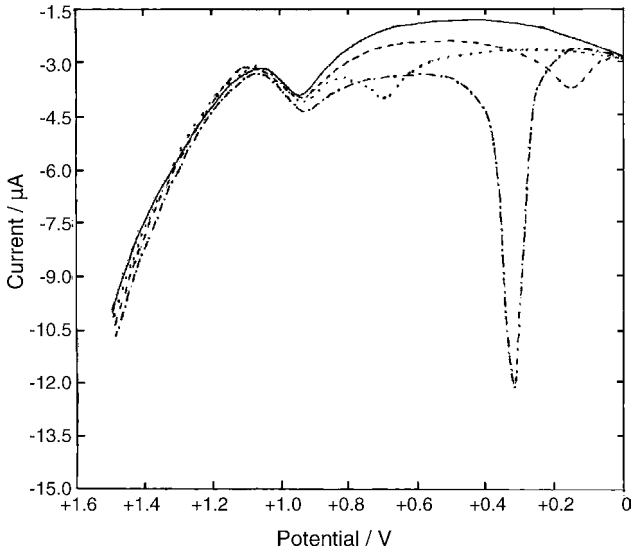


Fig. 8. DPVs of 0.05 mM guanosine at the modified electrode in the absence (—) and in the presence of 0.75 mM of each of the interferents, i.e. ascorbic acid (- - -), uric acid (- - - -) and xanthine (. . . . . .).

3.7. Analytical applications:

3.7.1. Human blood plasma

The fullerene-C_{60}-modified glassy carbon electrode has been utilized to detect the adenosine and guanosine content in three

Table 1
Influence of interferents on the voltammetric response of 0.05 mM adenosine and 0.05 mM guanosine at the fullerene-C_{60}-modified glassy carbon electrode

Interferent	Concentration of interferents (mM)	Change in i_p of adenosine		Change in i_p of guanosine	
		(μA)	(%)	(μA)	(%)
Ascorbic acid	0.05	−0.030	0.44	0.000	0.00
	0.10	−0.030	0.44	0.000	0.00
	0.25	−0.090	1.31	0.076	1.95
	0.50	0.090	1.31	0.036	0.92
	0.75	0.480	6.97	0.114	2.92
Hypoxanthine	0.05	0.034	0.49	−0.069	1.77
	0.10	−0.056	0.81	−0.069	1.77
	0.25	0.004	0.06	−0.069	1.77
	0.50	−0.006	0.09	−0.075	1.92
	0.75	0.114	1.65	−0.605	15.50
Uric acid	0.05	0.000	0.00	0.045	1.15
	0.10	0.060	0.87	−0.069	1.77
	0.25	0.060	0.87	0.000	0.00
	0.50	0.070	1.02	0.069	1.77
	0.75	0.960	13.93	0.454	6.59
Xanthine	0.05	−0.020	0.29	0.000	0.00
	0.10	−0.090	1.31	0.000	0.00
	0.25	−0.030	0.44	0.069	1.77
	0.50	−0.090	1.31	0.076	1.95
	0.75	0.760	11.03	0.138	3.54

Table 2
Recovery of adenosine and guanosine added to human blood plasma

Added (μM)	Adenosine		Guanosine	
	Observed (μM)	Recovery (%)	Observed (μM)	Recovery (%)
Sample 1				
10	10.17	101.70	9.80	98.00
50	50.50	101.00	52.80	105.60
100	100.52	100.52	103.03	103.03
Sample 2				
10	9.91	99.10	10.25	102.50
50	50.09	100.18	50.13	100.26
100	101.98	101.98	100.05	100.05
Sample 3				
10	9.99	99.90	9.91	99.10
50	50.69	101.37	49.97	99.94
100	102.16	102.16	103.75	103.75

Table 3
Analytical recovery of adenosine and guanosine added to urine samples

Sample no.	Added (μM)		Found (μM)		Recovery (%)	
	Adenosine	Guanosine	Adenosine	Guanosine	Adenosine	Guanosine
1	10	10	9.50	9.64	95.00	96.40
	25	25	24.42	25.03	97.68	100.12
	50	50	51.10	51.60	102.02	103.20
2	10	10	9.53	9.95	95.30	99.50
	25	25	24.76	25.23	99.04	100.92
	50	50	49.15	48.96	98.30	97.92

human blood plasma samples. The determination of their concentration was performed by standard addition method. Prior to their analysis, the samples were diluted with pH 7.2 phosphate buffer solution. The results are presented in Table 2. The recoveries, determined by spiking the samples with a measured amount of standard solutions of adenosine and guanosine, were found to be 99.10–102.16% for adenosine and 98.00–105.60% for guanosine.

3.7.2. Human urine

The practical analytical application of the method was further established by the selective measurement of adenosine and guanosine in human urine without any preliminary treatment. Two human urine samples obtained from laboratory personnel were determined with the method presented above. Before analysis, the samples used for detection were diluted 100 times. Then, the samples were spiked with certain amounts of adenosine and guanosine, separately. The results of the determination are listed in Table 3. The recovery rates of the spiked samples were determined and ranged from 95.0 to 102.0% for adenosine and 96.4 to 103.2% for guanosine, respectively.

4. Conclusions

The present study, reports an efficient method to determine adenosine and guanosine in the presence of each other utilizing fullerene-C_{60}-modified glassy carbon electrode. Yao et al. suggested the determination of adenosine and guanosine using linear sweep voltammetry [20]. However, the pH and non-linear relationship between i_p versus concentration at pH values around neutrality limited the range for their determination as 0.05–0.5 mM only. Adenosine and guanosine were detected electrochemically by Fortin et al. with a relatively high detection limit of 10 and 50 μM, respectively [19]. The present investigation demonstrates the simultaneous determination of both the biomolecules using the modified electrode in the concentration range 0.5 μM to 1.0 mM with a detection limit of 3.02×10^{-7} M for adenosine and 1.45×10^{-7} M for guanosine, which is lower than reported in earlier voltammetric studies. The reduced fullerene-C_{60} film exhibits interesting electrocatalytic properties by catalyzing the electrooxidation of adenosine and guanosine. The method described above is not only easy to perform, but also requires less time, financial input and sample amount than reported for other approaches. Hence, it is an attractive alternative to HPLC analysis in both routine and research laboratories. The proposed method was satisfactorily applied to the detection of adenosine and guanosine in human blood plasma and urine samples.

Recently, Compton and co-workers reported that C_{60} itself provides no electrocatalysis and the electrocatalytic activity of fullerene-C_{60}-modified glassy carbon electrode is due to graphite impurities present in the C_{60} material [25]. However, when voltammetric experiments were carried out in our laboratory employing highly pure C_{60} (purity 99.5%), we observed shift in peak potential with enhancement in peak current at partially reduced C_{60} modified glassy carbon electrode.

Thus, fullerene-C_{60}-modified glassy carbon electrode appears to exhibit electrocatalytic activity towards the oxidation of adenosine and guanosine.

Acknowledgements

One of the authors (N.B.) is thankful to the Council of Scientific and Industrial Research, Delhi for awarding Senior Research Fellowship. Financial assistance for this work was provided by C.S.I.R., New Delhi vide grant no. 01(2045)/02/EMR-II.

References

[1] R.A. Hartwick, P.R. Brown, J. Chromatogr. 143 (1997) 383–389.
[2] R. Sheng, F. Ni, Anal. Chem. 63 (1991) 437–442.
[3] J. Zhang, L. Belardinelli, K.A. Jacobson, D.H. Otero, S.P. Baker, Mol. Pharm. 52 (1997) 491–498.
[4] D. Kloor, K. Yao, U. Delabar, H. Osswald, Clin. Chem. 46 (2000) 537–542.
[5] M.E.D.S. Frizzo, D.R. Lara, A.D.S. Prokopiuk, C.R. Vargas, C.Z. Salbego, M. Wajner, D.O. Souza, Cell. Mol. Neurobiol. 22 (2002) 353–363.
[6] R. Malathi, I.M. Johnson, J. Biomol. Struct. Dyn. 18 (2001) 709–712.
[7] Y. Chen, Y. Zheng, N. Wang, S. Lu, T. Pang, Q. Yang, G. Xu, Aizheng 22 (2003) 537–540.
[8] J. Yang, G. Xu, H. Kong, Y. Zheng, T. Pang, Q. Yang, J. Chromatogr. B 780 (2002) 27–33.
[9] M. Inomata, Iwate Igaku Zasshi 42 (1990) 793–810.
[10] S. Giannattasio, S. Gagliadi, M. Samaja, E. Marra, Br. Res. Prot. 10 (2003) 168–174.
[11] J.D.Z. Feng, P.K.F. Yeung, Therap. Drug Monit. 22 (2000) 177–183.
[12] K. Nakano, T. Yasaka, K.H. Schram, M.L.J. Reimer, T.D. Mc Clure, T. Nakao, H. Yamanoto, J. Chromatogr. 515 (1990) 537–546.
[13] I.N. Duvaz, N. Voiculetz, Chromatogram 10 (1989) 7–9.
[14] A.P. Halfpenny, R.P. Brown, Chromatographia 21 (1986) 317–320.
[15] G. Sander, J. Wieland, D. Topp, Clin. Chim. Acta 152 (1985) 355–361.
[16] C.W. Gehrke, R.W. Zumwalt, K.C. Kuo, Clin. Liq. Chromatogr. 2 (1984) 139–154.
[17] G. Schoech, J. Thomale, H. Lorenz, H. Suberg, U. Karsten, Clin. Chim. Acta 108 (1980) 247–257.
[18] H. Lin, D.K. Xu, H.Y. Chen, J. Chromatogr. A 760 (1997) 227–233.
[19] E. Fortin, J.C. Tune, P. Mailley, S. Szunerits, B. Marcus, J.P. Petit, M. Mermoux, E. Vieil, Bioelectrochemistry 63 (2004) 303–306.
[20] T. Yao, T. Wasa, S. Musha, Bull. Chem. Soc. Jap. 50 (1977) 2917–2920.
[21] R.N. Goyal, V.K. Gupta, A. Sangal, N. Bachheti, Electroanalysis 17 (2005) 2217–2223.
[22] R.N. Goyal, S.P. Singh, Talanta 69 (2006) 932–937.
[23] G.D. Christian, W.C. Purdy, J. Electroanal. Chem. 3 (1962) 363–367.
[24] M. Csiszar, A. Szucs, M. Tolgyesi, A. Mechler, J.B. Nagy, M. Novak, J. Electroanal. Chem. 497 (2001) 69.
[25] R.T. Kachoosangi, C.E. Banks, R.G. Compton, Anal. Chim. Acta 566 (2006) 1–4.

Available online at www.sciencedirect.com
ScienceDirect
Talanta 71 (2007) 1039–1046
Talanta
www.elsevier.com/locate/talanta

Optimization of experimental parameters in single-drop microextraction–gas chromatography–mass spectrometry for the determination of periodate by the Malaprade reaction, and its application to ethylene glycol

Manju Gupta, Archana Jain, Krishna K. Verma *

Department of Chemistry, Rani Durgavati University, Jabalpur 482001, Madhya Pradesh, India

Received 7 April 2006; received in revised form 28 May 2006; accepted 28 May 2006
Available online 10 July 2006

Abstract

The aim of present work was to optimize the experimental parameters in single drop microextraction under solution immersion (SDME) and headspace (HS-SDME) extraction modes for the determination of periodate using guaifenesine [3-(2′-methoxyphenoxy)-1,2-propane diol] and norephedrine (phenylpropanolamine) as new and alternative reagents for the Malaprade reaction. The reactions were complete within 5 min resulting in the formation of 2-(2′-methoxyphenoxy)-acetaldehyde and benzaldehyde, respectively. SDME/HS-SDME of oxidation products with 2 μl of anisole or 1 μl of toluene, respectively, has permitted the determination of periodate at $\mu g\,l^{-1}$ concentration levels. The results indicated that HS-SDME (range 0.01–10 $mg\,l^{-1}$, $r^2 = 0.9990$; limit of detection 1.55 $\mu g\,l^{-1}$) was more sensitive than SDME (range 0.05–50 $mg\,l^{-1}$, $r^2 = 0.9984$; limit of detection 3.42 $\mu g\,l^{-1}$), and was inexpensive, rapid and convenient. Tolerance of excess of iodate has permitted the application of this method in the determination of ethylene glycol in motor oil; the average recovery on spiked sample was 98.6% with R.S.D. of 4.2%.
© 2006 Elsevier B.V. All rights reserved.

Keywords: Single-drop microextraction; Immersion; Headspace; Periodate; Ethylene glycol; GC–MS

1. Introduction

Periodate is an important oxidant which can oxidize many inorganic and organic compounds. Most of the oxidizable organic compounds have groups amino, imino, carboxyl or diol on adjacent carbons. The reaction between periodate and the above mentioned groups is well known as the Malaprade reaction, and was used for the indirect determination of 1,2-diols and related compounds [1–3]. Periodate is exclusively associated with the oxidation of metal ions, polyhydroxy compounds and in catalytic applications at trace level. Determination of periodate is important in organic chemistry, biology and life sciences [4,5].

Several methods have been reported for the determination of periodate. Ion-selective liquid membrane electrode has been used for the direct determination of periodate [6]. Generally used spectrophotometric methods which employed a colour reaction of periodate with amodiaquine dihydrochloride, pyrogallol red and salicylaldehyde guanylhydrazone [3,7,8] but the concentration of reagents affects the colour development and these methods are pH dependent [7,8]. Other methods include flow injection analysis [9,10], photometry [11], fluorimetry [12], thin layer chromatography [13] and capillary electrophoresis [14]. Some of these methods have high limit of detection [3,9,10], suffer from many interference [12] and/or have narrow dynamic range [3,8].

There has been growing interest in trace enrichment techniques using solid phase extraction (SPE) [15–17] that was developed as an alternative to liquid–liquid extraction (LLE) since the latter is time consuming and makes use of large volumes of solvents that constitute a risk for the environment and the analysts. In off-line SPE, a part of the final extract is injected into the column while the major part remains unutilized. This results in reduction in sensitivity of the overall method. To overcome this problem, SPE is performed in on-line mini-columns and the whole extract is transferred to the analytical column. Such couplings are often cumbersome and require elaborated instrumentation [18,19].

Solid phase microextraction (SPME) have been developed in order to reduce extraction time, solvent consumption and

* Corresponding author.
E-mail address: arichna@sancharnet.in (K.K. Verma).

0039-9140/$ – see front matter © 2006 Elsevier B.V. All rights reserved.
doi:10.1016/j.talanta.2006.05.083

waste formation [20]. SPME is solvent-free, simple and rapid technique, and features simultaneous extraction and preconcentration of analytes directly from an aqueous sample or from its headspace. Here, the whole portion of extract is transferred to the column. The main drawbacks with SPME are that its fibres are expensive and there is likelihood for analytes carry over between the runs, which could invalidate the results [21]. Also the lifetime of fibres is limited because the solid-phase materials degrade with usage. Moreover, the partial loss of SPME fibre coating could result in additional peaks [22].

More recently, efforts have been placed on miniaturizing the LLE extraction procedure by greatly reducing the extracting solvent to aqueous phase ratio. Single drop microextraction (SDME), using typically 1–3 μl of an organic solvent at the tip of a microsyringe, has evolved from this novel approach [23–25]. After extraction, the microdrop is retracted back into the syringe and transferred to the GC for analysis. SDME has the advantages of high extraction speed and extreme simplicity. It uses inexpensive apparatus and virtually eliminates solvent consumption. The range of application of SDME has been demonstrated by the determination of trihalomethanes [26], nitroaromatics [27], antifouling agents [28], BTEX [20,29], PAHs [30], phenols [31,32], bisphenol A [33], chlorobenzenes [34,35], pesticides [36,37], carbonyl compounds [38], chemical warfare agents [39], iodine [40], organotin compounds [41] and selenium [42]. There have been reported many variations of SDME, such as drop-to-drop microextraction [43], directly suspended solvent microextraction [44], dispersive liquid–liquid microextraction, [45] and nanolitre size droplet microextraction in a microfluidic system [46].

The aim of the present work was to optimize the experimental conditions of single drop microextraction in immersion (SDME) and headspace (HS-SDME) modes and to examine the feasibility of this method in the determination of $\mu g\,l^{-1}$ concentration level of periodate in aqueous sample using guaifenesine [3-(2′-methoxyphenoxy)-1,2-propanediol] and norephedrine (phenylpropanolamine) as alternative reagents in the so-called Malaprade reaction and measuring the oxidation products 2-(2′-methoxyphenoxy)-acetaldehyde and benzaldehyde, respectively, by GC. As an application of this method, determination of ethylene glycol in motor oil has been demonstrated.

2. Experimental

2.1. Instrumentation

The chromatographic studies were performed on Agilent G1800B GCD system (HP 5890 series II with a quadrupole mass detector) with a HP-5 (5% phenyl substituted methylpolysiloxane) 30 m × 0.25 mm i.d.; 0.25 μm film thickness capillary column and helium (99.999%) carrier gas at a flow rate of $1\,ml\,min^{-1}$; and Agilent system (HP 5890 series II with a flame ionization detector) with a HP-5 (5% phenyl substituted methylpolysiloxane) 30 m × 0.32 mm i.d.; 0.25 μm film thickness capillary column and nitrogen (99.999%) carrier gas at a flow rate of $3\,ml\,min^{-1}$. The injector temperature was maintained at 250 °C and all injections were made in splitless mode. The GC–MS transfer line was maintained at 300 °C, electron ionization at 70 eV and the mass spectrum scanned from *m/z* 45–450. Chromatographic data were acquired using a HP ChemStation software G1074B version A.01.00 (GC–MS) and Rev.A.06.03 (GC-FID). A 5 μl microsyringe was used for extraction/injection. Extraction vials, 4 ml, with PTFE silicon septum and screw cap with a hole (Supelco, Bellefonte, PA, USA), 8 mm × 1.5 mm magnetic stir bars and a magnetic stirrer were used.

2.2. Reagents, standards and samples

Guaifenesine was obtained from Torque Pharmaceuticals Pvt. Ltd., Issapur, India, and a solution of it, 100 mg in 50 ml, was prepared in deionized water. Norephedrine was obtained from Sigma, St. Louis, MO, USA, and its reagent solution contained 50 mg of substance in 50 ml of deionized water. The internal standard solutions, prepared separately, of 4-methoxyacetophenone (Merck, Mumbai, India) and 4-nitrobenzaldehyde (Merck, Mumbai, India), 20 mg each in 10 ml of methanol, or of acetophenone (Merck, Mumbai, India), 10 mg in 10 ml of methanol.

Analytical reagent grade potassium periodate (BDH, Mumbai, India) was oven-dried and a stock solution of $1000\,mg\,l^{-1}$ periodate was made by dissolving 120.4 mg of potassium periodate in 100 ml of water. The stock solution of ethylene glycol, about $1000\,mg\,l^{-1}$, was prepared in deionized water and standardized [3]. Less concentrated solution of periodate and ethylene glycol were made by sequential dilution and stored in a cool place.

GC grade or high purity solvents cyclohexane, isooctane, benzene, toluene, anisole and 1-butanol were obtained from Merck, India.

2.3. Extraction process

A 5 μl microsyringe containing 1–3 μl of the appropriate extracting solvent was penetrated through the septum of the vial containing the sample solution until the tip protruded 1 cm below the meniscus of sample solution (4 ml) or placed in the headspace of the sample solution (2 ml). The syringe was clamped and the plunger depressed to cause the solvent to form a drop suspended at the tip. After 15 min of equilibration (stir rate 400 rpm), the plunger was withdrawn to retract the microdrop into the microsyringe and immediately transferred into the GC injection port for analysis.

2.4. General method of periodate determination

A 40–500 μl aliquot of periodate solution was mixed with 100 μl of 1% sodium hydrogencarbonate solution, and 200 μl of guaifenesine or norephedrine. The solution was mixed well by swirling and kept for 5 min at ambient temperature. Thereafter, 10 or 20 μl of 4-methoxyacetophenone or 4-nitrobenzaldehyde as internal standard was spiked, the solution diluted to 4 ml with deionized water and subjected to SDME (drop immersion). In the alternate method, after the reaction of periodate with

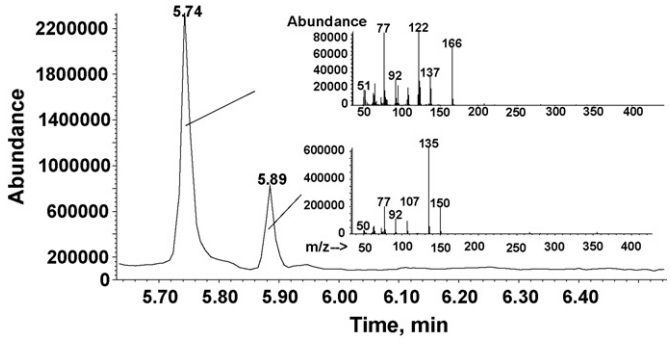


Fig. 1. Single drop microextraction of 10 mg l^{-1} periodate after reaction with guaifenesine using 2 μl of anisole as extracting solvent. The GC oven temperature was held at 100 °C for 2 min and then ramped to 190 °C at 20° min^{-1} and held for 0.2 min. Peaks designation, 2-(2′-methoxyphenoxy)acetaldehyde (5.74 min) and 4-methoxyacetophenone (5.89 min), internal standard. Insert: mass spectra of corresponding peaks.

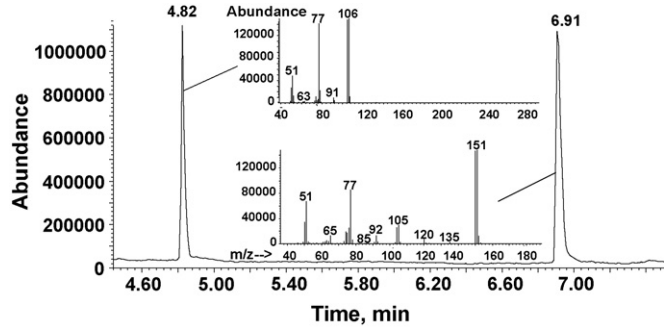


Fig. 2. Single drop microextraction of 1 mg l^{-1} periodate after reaction with norephedrine using 1.5 μl of toluene as extracting solvent. The GC oven temperature was held at 60 °C for 2 min, ramped linearly to 120 °C at 20°C min^{-1}, then to 260 °C at 70 °C and held for 0.5 min. Peaks designation, benzaldehyde (4.82 min) and 4-nitrobenzaldehyde (6.91 min), internal standard. Insert, mass spectra of corresponding peaks.

norephedrine, the solution was mixed with 1 g of sodium chloride, spiked with 5 μl of acetophenone internal standard, diluted to 2 ml with deionized water and subjected to HS-SDME. The GC oven temperature program is given Figs. 1–3.

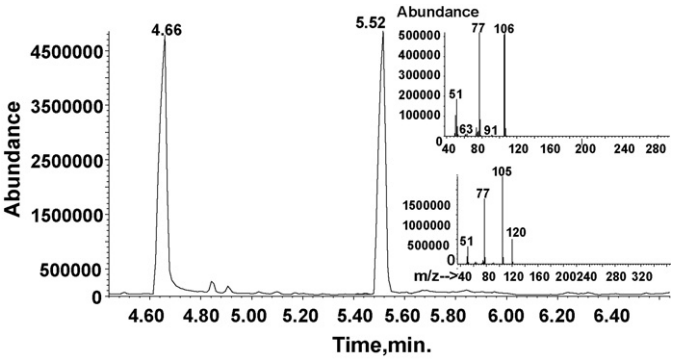


Fig. 3. Headspace single drop microextraction of 1 mg l^{-1} periodate after reaction with norephedrine using 1.5 μl of toluene as extracting solvent. The GC oven temperature was held at 60 °C for 2 min ramped linearly to 120 °C at 20 °C min^{-1}, then to 200 °C at 70 °C and held for 0.5 min. Peaks designation, benzaldehyde (4.66 min) and acetophenone (5.52 min), internal standard. Insert: mass spectra of peak at 4.66 min (upper trace) and at 5.52 min (lower trace).

3. Results and discussion

3.1. The chemistry

1,2-Diols and 1,2-aminoalcohols are oxidized to carbonyl compounds by periodate; the overall reaction being occurring through a cyclic intermediate [47]. The reactions complete within 5 min at room temperature in neutral solutions. The products have been identified by their GC and comparison with the mass spectra of authentic compounds. A plausible fragmentation pattern for 2-(2′-methoxyphenoxy)acetaldehyde, formed by the reaction of guaifenesine with periodate, is given in Scheme 1.

3.2. Optimization of extraction conditions

Three phases are involved during HS-SDME, the sample, its headspace, and the extracting phase. There are two interfaces involved, between the sample and headspace, and the headspace and extracting solvent. The rate-determining step can be either the analyte evaporation from the sample to its headspace or the analyte diffusion into the extracting drop. Mass transfer in the headspace is considered as a faster process because diffusion coefficients of the analytes in the gas phase are usually 10^4–10^5 times larger than those in the liquid phase [30].

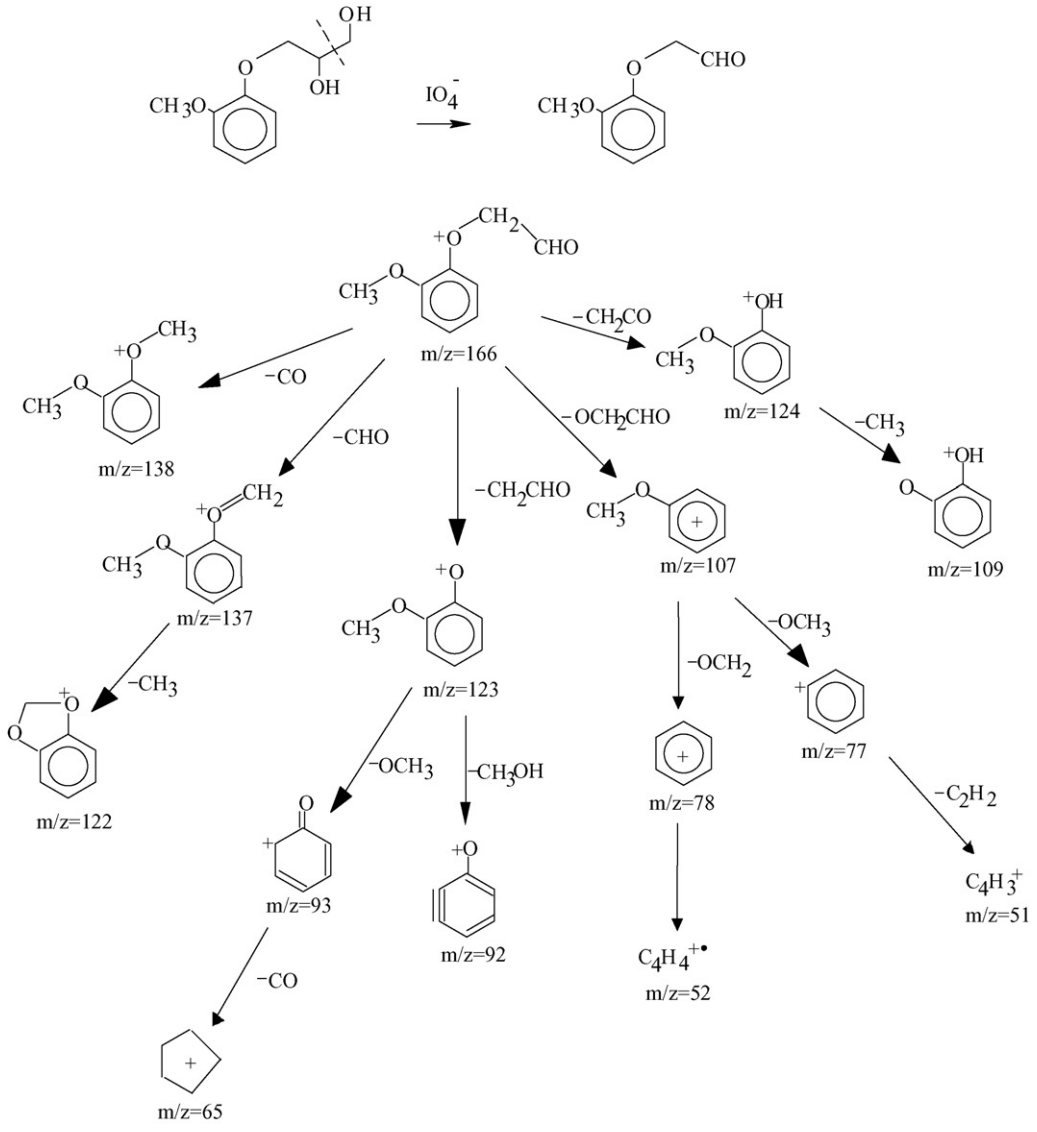
Different parameters that influence the SDME/HS-SDME efficiency were optimized independently and include the nature of solvent used as extractant, temperature of sample solution, stirring rate, ionic strength, volume of microdrop and aqueous sample, and extraction time.

3.3. Selection of organic solvent

The choice of an appropriate solvent is essential for the SDME/HS-SDME method. The extraction solvent has to meet certain requirements, viz., low volatility (HS-SDME); optimum immiscibility in the aqueous medium (SDME), high partition ratio for analytes; and separated from the analyte peaks in the chromatogram [22]. For the SDME of 2-(2′-methoxyphenoxy)acetaldehyde, formed by periodate upon reaction with guaifenesine, among the solvents examined benzene, isooctane, hexane, cyclohexane, anisole and toluene, the extraction was better in aromatic solvents, and anisole gave the optimum extraction efficiency (Fig. 4). This observation was ostensibly due to relatively high polarity of anisole.

In order to determine the organic solvent that would give optimum extraction yield for the SDME of benzaldehyde, formed by reaction of periodate with norephedrine, benzene, isooctane, cyclohexane, toluene, and hexane were examined. Among these, toluene gave the best extraction efficiency (Fig. 4). Anisole could not be used here since benzaldehyde eluted on the tailing portion of anisole. Out of two solvents, toluene and 1-butanol, that were examined for the HS-SDME of benzaldehyde, toluene was found better since using this solvent the correlation coefficient and limit of detection were 0.9990 of 1.55 μg l^{-1} of periodate, respectively; the corresponding values in extraction with 1-butanol were 0.9773, and 50 μg l^{-1} of periodate.

m/z	abundance, %	m/z	abundance, %	m/z	abundance, %
51	16.26	92	3.22	123	32.48
52	17.31	93	0.69	124	21.45
65	21.28	107	6.42	137	39.27
77	88.99	109	10.39	138	22.40
78	12.00	122	99.99	166	86.14



Scheme 1. Proposed mass fragmentation pathways of 2-(2′-methoxyphenoxy)acetaldehyde formed by reaction of guaifenesine with periodate.

3.4. Optimization of microdrop volume

In SDME the volume of the organic drop does not remain constant during the extraction because no solvent is completely immiscible with water. However, a slight decrease in drop volume is acceptable because it will occur to the same extent for standard and the sample [48]. A test volume of 4 ml of 10 mg l^{-1} periodate was reacted with guaifenesine in deionized water and extracted with 1–3 μl of solvent. The results indicated that increasing the microdrop volume (Fig. 5) enhanced the extraction efficiency. However, large drop volumes such as 3 μl could be prone to accidental dislodgement. Drop volume of 2 μl was used in subsequent experiments. Fig. 5 also indicated

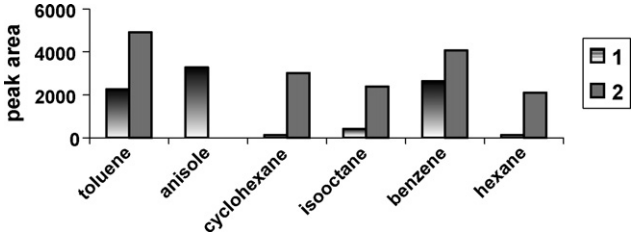


Fig. 4. Study of organic solvents for SDME of aldehyde product of guaifenesine (label 1, drop volume, 2 μl) and of norephedrine (label 2, drop volume, 1 μl) formed on reaction with 10 mg l^{-1} of periodate.

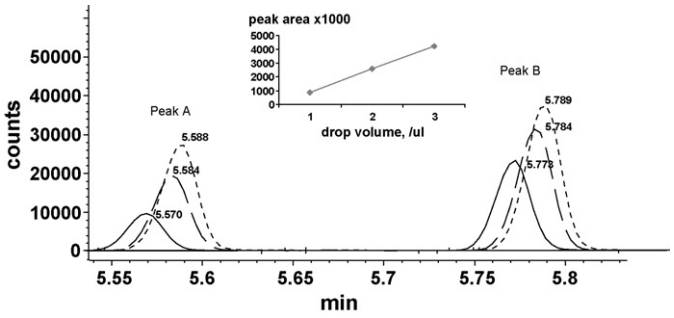


Fig. 5. Effect of drop volume, 1–3 μl, of anisole on the peak retention time and peak area, inset, as used in the SDME of aldehyde product of guaifenesine formed on reaction with 10 mg l^{-1} periodate. Peak designation: A, 2-(2′-methoxyphenoxy)acetaldehyde and B, 4-methoxyacetophenone.

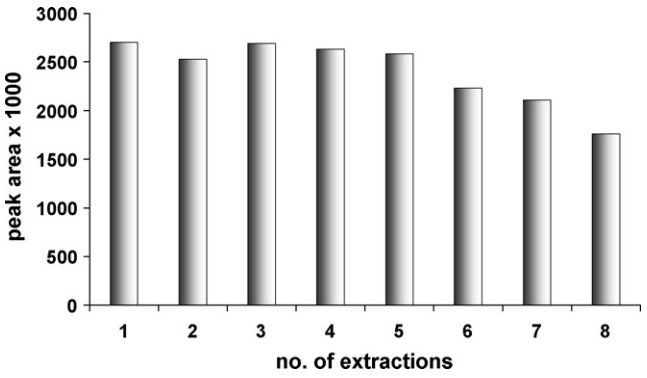


Fig. 6. Multiple single drop microextraction of 50 mg l^{-1} periodate treated with guaifenesine using 2 μl of anisole; equilibration time 15 min.

that the retention time for peaks also increased slightly with drop volume; this may be due to the increase of the injected volume.

The effect of microdrop volume on the analytical signal of 20 mg l^{-1} of periodate reacted with norephedrine was determined. The extraction increases by increasing the microdrop volume, however, beyond 1.5 μl of toluene, splitting of peaks of benzaldehyde and 4-nitrobenzaldehyde (IS) was noticed. An aliquot of 1.5 μl of toluene was used in subsequent work.

3.5. Optimization of extraction time

Extraction time is one of important factors in SDME method and it is necessary to determine the time when the amount of analyte in organic solvent drop is optimum [22,49]. A profile of the extraction of the 2-(2′-methoxyphenoxy)-acetaldehyde into the anisole microdrop versus time was determined in order to assess the optimum extraction time. Test solutions of 4 ml of 20 mg l^{-1} periodate were reacted with guaifenesine and extracted for the period 5–60 min. A 15 min extraction time was found optimum.

Test solutions of 4 ml of 10 mg l^{-1} periodate were reacted with norephedrine and the benzaldehye thus formed was extracted with 1.5 μl of toluene for the period 5–60 min. Optimum extraction was obtained in 15 min. In HS-SDME, optimum extraction was found in 15 min using a series of aqueous samples spiked with 1 mg l^{-1} of periodate and treated with norephedrine.

3.6. Optimization of reaction time

The effect of time on the reaction of 20 mg l^{-1} of periodate with guaifenesine was studied by comparing the peak areas obtained for acetaldehyde derivative. Optimum peak areas were observed when the reaction mixture was kept for 5 min. The reaction with norepridine was also complete within 5 min.

3.7. Multiple microextraction with single drop

In typical SDME analyses, the sample solution is extracted only once and then discarded. But, after one sampling, most of the analyte was remaining in the sample solution and on performing SDME again in the same sample gave the result as in previous run. The reason was a fresh and identical equilibrium that occurred between the analyte of sample solution and in the organic drop. Periodate, 20 mg l^{-1}, reacted with guaifenesine was subjected to a repeated SDME in the same sample and the observed peak area in each extraction is shown in Fig. 6. If an infinite number of extractions are carried out, the analytes will be completely removed from the sample. The total area counts of the peaks corresponding to the analyte should be equal to the sum of the areas from each individual extraction. In this respect SDME differs from most other analytical techniques in that the recovery is sometimes well under 4%, however, it is possible to obtain extremely reproducible and accurate results [50].

3.8. Effect of sample and headspace volume

At fixed analyte mass, the effect of volume of aqueous sample and its headspace, a set of extraction experiments were performed on 1 ml of 50 μg l^{-1} of periodate diluted up to 4 ml with deionized water in a 4 ml vial. Fig. 7 shows that increasing sample dilution resulted in decrease in extraction. A sample volume of 2 ml was used in HS-SDME.

3.9. Effect of salt addition

Addition of salt (sodium chloride) increases the ionic strength of the solution and decreases the solubility of organic analytes, and this effect has been used extensively in classical solvent extraction. The effect of sodium chloride concentration was investigated for periodate–norephedrine reaction, and SDME

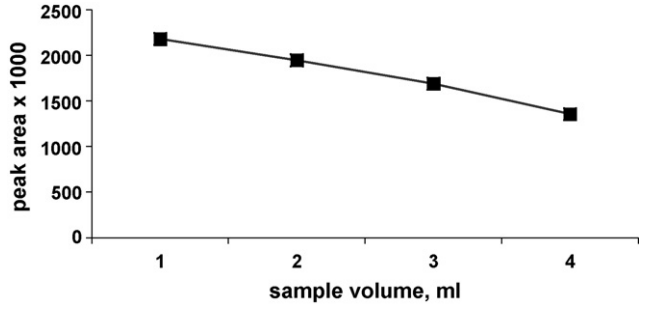


Fig. 7. Effect of sample/headspace volume on HS-SDME of 1 ml of 50 μg l^{-1} periodate diluted with different volumes of water and treated with norephedrine; equilibration time 15 min; extracting solvent 1.5 μl of toluene.

efficiency was monitored. The results showed decrease in extraction, in a given period, with increase in ionic strength for the targeted analyte. The reason for this is probably due to kinetics, the equilibrium is attained more quickly when the salt concentration is lower [39].

In HS-SDME, addition of salt reduces the solubility of hydrophobic compounds and increases the sensitivity of headspace analysis [50]. For this purpose, the ionic strength of solutions was modified by addition of 0–1 g of sodium chloride in the sample spiked with 1 mg l^{-1} of periodate, and treated with norephedrine. Water molecules preferably form hydration sphere around the salt ions and this situation weakens the analyte–water interaction that will drive additional analytes into the headspace [51]. Accordingly, addition of salt promotes the transport of analytes to the headspace and hence to the extracting drop. The sample solution must be saturated with salt, and 1 g of sodium chloride was sufficient for this purpose.

3.10. Calibration graph and detection limit

The dependence of the chromatographic signal on the concentration of periodate was determined under optimum conditions of SDME and GC–MS. A rectilinear calibration graph was obtained for periodate, reacted with guifenesine, in the range 0.05–50 mg l^{-1} with slope, intercept and correlation coefficient of 0.0522, 0.126 and 0.9984, respectively, for total ion chromatography (TIC), and 0.0155, 0.035 and 0.9992, respectively, for extracted ion chromatography. The limit of detection (LOD) in TIC was 3.42 μg l^{-1} (S/N = 3) and the R.S.D. was in the range 2–4%.

Using norephedrine as reagent and SDME of the benzaldehyde, calibration graph was linear in the range 0.05–10 mg l^{-1} periodate, the value of slope, intercept and correlation coefficient was 0.4754, 0.6484 and 0.9984 in TIC. The LOD was 4.48 μg l^{-1} and the R.S.D. was in the range 2–4%. In the headspace mode (HS-SDME), the calibration graph was rectilinear in the range 0.01–10 mg l^{-1}; the value of slope, intercept and correlation coefficient was 0.6850, 0.2142 and 0.9990, respectively, in TIC. The LOD was 1.55 μg l^{-1} and the R.S.D. was in the range 4–7%. The HS-SDME was also performed (above range) with GC-FID when the slope, intercept and correlation coefficient were 0.9495, 0.1037 and 0.9992, respectively; the limit of detection was 2.25 μg l^{-1}.

3.11. The indirect determination of ethylene glycol

Polar compounds, such as ethylene glycol, produce tailing peaks in GC and it makes necessary to derivatize them before injection. Phase transfer would be additional step for analyzing aqueous samples. Application of the Malaprade reaction is an attractive alternative for diols. Ethylene glycol is used as a coolant and antifreeze, and it is often necessary to determine it in oil.

The most widely used methods for the determination of 1,2-diols and related compounds are based on the Malaprade reaction. The applicability of the present method to the determination of μg l^{-1} level of periodate in the presence of large amounts of iodate suggested its possible use for the indirect determination of 1,2-diols via the Malaprade reaction. Motor engine oil samples were spiked with known amounts of ethy-

Table 1
Comparison of diverse procedures for the determination of periodate

Reagent/chemistry	Linear range (mg l^{-1})	LOD (μg l^{-1})	Reference
Spectrophotometry			
Amodiaquine dihydrochloride/redox reaction	10–60	400	[3]
Pyrogallol red/redox reaction	0.1–14	?	[7]
Salicylaldehyde guanylhydazone/redox reaction	10–45	?	[8]
Gallocyanine/redox reaction	0.02–2.2	?	[11]
Amiloride hydrochloride/ion-pair formation	0.01–10	10	[52]
Ferroin/redox reaction	0.4–5	250	[53]
Iodidemethylene blue/redox reaction	0.1–3.5	70	[54]
Iodide/redox reaction	0.1–1.2	10	[55]
Flow injection-spectrophotometry			
Iodide/redox reaction	0.05–5	30	[9]
Salicylaldehyde guanylhydazone/redox reaction	5–50	350	[10]
Pyrogallol red/redox reaction	0.15–14	134	[56]
Me_3N^+ iodide/redox reaction	0.05–10	16	[57]
Fluorimetry			
Thiamine/fluorescent product formation	0.1–3.4	50	[12]
Paracetamol/fluorescent product formation	0.1–1	7.6	[58]
Tetraiodofluorescein/fluorescence quenching	0.076–2	19	[59]
Capillary electrophoresis			
Molybdate/complex formation	0.38–38.2	?	[14]
Gas chromatography			
Guifenesine/Malaprade reaction (SDME)	0.05–50	3.42	This work
Norephedrine/Malaprade reaction (SDME)	0.05–10	4.46	This work
Norephedrine/Malaprade reaction (HS-SDME)	0.01–10	1.55	This work

lene glycol, diluted with hexane and extracted with water. The aqueous phase from the separation was further extracted with chloroform and then analysed for ethylene glycol. A portion of aqueous extract was treated with a measured excess of periodate and after completion of reaction, the remaining amount of periodate was determined by its reaction with norephedrine (HS-SDME). A blank determination on periodate without the organic compound was carried out simultaneously. The difference in peak area ratios was related to the amount of periodate consumed and thus to glycol present when referred to the calibration graph. In the analysis of a sample the recoveries of ethylene glycol from oil were between 98% and 102%, average 98.6%, with R.S.D. of 4.2% ($n = 6$).

3.12. Interferences

The Malaprade reaction is specific cleavage of 1,2-diol group (as present in guaifenesine) and 1-amino-2-ol group (as present in norephedrine) by periodate, and since the carbonyl products formed in the reaction are determined in the present work, a number of other oxidizing agents such as iodate, bromate, chlorate and dichromate when also present do not interfere in the determination of periodate.

Similar to ethylene glycol, polyhydroxy compounds such as glycerol and carbohydrates also react with periodate and indeed the interference of these compounds is quantitative. However, such compounds are less likely to be present in motor engine oil when ethylene glycol is determined.

4. Conclusions

The proposed reaction schemes are straightforward conversion of periodate into 2-(2′-methoxyphenoxy) acetaldehyde or benzaldehyde that are rapid and unaffected by the presence of large amounts of iodate. In this study SDME and HS-SDME have been demonstrated as viable means of quantifying trace level of periodate in real samples. SDME/HS-SDME methods integrate sampling, extraction, cleanup, and sample introduction in a single step. This method has advantage of high sensitivity, simplicity, short preconcentration time, renewability of drop for extraction and low consumption of solvent. It is an attractive alternative when compared to SPME and to other labour intensive methods such as LLE or SPE. For the determination of periodate, norephedrine could be used in both SDME and HS-SDME, the HS-SDME was found to be about three times more sensitive.

A comparison of present method with previously reported methods of periodate determination in given in Table 1. The present method has distinct advantages in terms of wide linear dynamic range and low limit of detection (LOD).

Acknowledgements

We are grateful to the Torque Pharmaceuticals Pvt. Ltd., Issapur, India, for gratis sample of guaifenesine. A.J. thanks the Department of Science & Technology, New Delhi, for the award of a grant under Women Scientist Scheme (SR/WOS-A/CS/2004).

References

[1] Z.A.K. Haree, Microchem. J. 31 (1985) 375.
[2] D.H. Rammler, R. Bilton, R. Haugland, C. Parkinson, Anal. Biochem. 52 (1973) 198.
[3] K.K. Verma, D.S. Gupta, S.K. Sanghi, A. Jain, Analyst 112 (1987) 1519.
[4] M.S. El-Shahawi, A.B. Farag, Anal. Chim. Acta 307 (1995) 139.
[5] A.M. El-Wakil, A.B. Farag, M.S. El-Nahas, Talanta 40 (1993) 841.
[6] A.K. Jain, M. Jahan, V. Tyagi, Analyst 114 (1989) 1155.
[7] J. Ghasemi, S. Saaidpour, A.A. Ensafi, Anal. Chim. Acta 508 (2004) 119.
[8] J.J.B. Nevado, P.V. Gonzalez, Analyst 114 (1989) 243.
[9] A.A. Ensafi, M.A. Chamjangali, Spectrochim. Acta Part A 59 (2003) 2897.
[10] J.J.B. Nevado, P.V. Gonzalez, Analyst 114 (1989) 989.
[11] A.A. Ensafi, S. Zakei, Anal. Lett. 32 (1999) 1643.
[12] N. Jie, D. Yang, Q. Zhang, J. Yang, Z. Song, Anal. Chim. Acta 359 (1998) 87.
[13] A. Mohammad, J.P.S. Chahar, E. Iraqi, V. Agrawal, J. Plan. Chromatogr. Mod. TLC 13 (2000) 12.
[14] Y. Nakashima, H. Shen, K. Kusuyama, S. Himeno, Anal. Sci. 15 (1999) 725.
[15] I. Liška, J. Chromatogr. A 885 (2000) 3.
[16] V. Pichon, J. Chromatogr. A 885 (2000) 195.
[17] J. Pawliszyn (Ed.), Sampling and Sample preparation for Field and Laboratory: Fundamentals and New Directions in Sample Preparation, Elsevier, Amsterdam, 2002.
[18] K.K. Verma, A.J.H. Louter, A. Jain, E. Pocurull, J.J. Vreuls, U.A.Th. Brinkman, Chromatographia 44 (1997) 372.
[19] R.B. Geerdink, W.M.A. Niessen, U.A.Th. Brinkman, J. Chromatogr. A 970 (2002) 65.
[20] J. Pawliszyn (Ed.), Application of Solid Phase Microextraction, Royal Society of Chemistry, Cambridge, 1999.
[21] P. Helena, I.K. Locita, Trends Anal. Chem. 18 (1999) 272.
[22] A. Tankeviciute, R. Kazlauskna, V. Vickackaite, Analyst 126 (2001) 1674.
[23] M.A. Jeannot, F.F. Cantwell, Anal. Chem. 68 (1997) 2935.
[24] M.A. Jeannot, F.F. Cantwell, Anal. Chem. 69 (1997) 235.
[25] M.H. Ma, F.F. Cantwell, Anal. Chem. 71 (1999) 388.
[26] R. Zhao, W. Lao, X. Xu, Talanta 62 (2004) 751.
[27] E. Psillakis, N. Kalogerakis, J. Chromatogr. A 907 (2001) 211.
[28] D.A. Lambropoulou, T.A. Albanis, J. Chromatogr. A 1094 (2004) 17.
[29] J.M. Kokosa, A. Przyjazny, J. Chromatogr. A 983 (2003) 205.
[30] S. Shariati-Feizabadi, Y. Yamini, N. Bahramifar, Anal. Chim Acta 489 (2003) 21.
[31] H. Bagheri, A. Saber, S.R. Mousavi, J. Chromatogr. A 1046 (2004) 27.
[32] M. Saraji, M. Bakhshi, J. Chromatogr. A 1098 (2005) 30.
[33] M. Kawaguchi, R. Ito, N. Endo, N. Okanouchi, N. Sakui, K. Saito, H. Nakazawa, J. Chromatogr. A 1110 (2006) 1.
[34] L. Vidal, A. Canals, N. Kalogerakis, E. Psillakis, J. Chromatogr. A 1089 (2005) 25.
[35] M. Khajeh, Y. Yamini, J. Hassan, Talanta 69 (2006) 1088.
[36] D.A. Lambropoulou, E. Psillakis, T.A. Albanis, N. Kalogerakis, Anal. Chim. Acta 516 (2004) 205.
[37] P. Liang, L. Guo, Y. Liu, S. Liu, T. Zhang, Microchem. J. 80 (2005) 19.
[38] N. Li, C. Deng, N. Yao, X. Shen, X. Zhang, Anal. Chim. Acta 540 (2005) 317.
[39] M. Palit, D. Pardasani, A.K. Gupta, D.K. Dubey, Anal. Chem. 77 (2005) 711.
[40] P. Das, M. Gupta, A. Jain, K.K. Verma, J. Chromatogr. A 1023 (2004) 33.

[41] V. Colombini, C. Bancon-Montigny, L. Yang, P. Maxwell, R.E. Sturgeon, Z. Mester, Talanta 63 (2004) 555.
[42] S. Fragueiro, I. Lavilla, C. Bendicho, Talanta 68 (2006) 1096.
[43] H.-F. Wu, J.-H. Yen, C.-C. Chin, Anal. Chem. 78 (2006) 1707.
[44] L. Yangcheng, K. Quan, L. Guangsheng, D. Youyuan, Anal. Chim. Acta 566 (2006) 259.
[45] M. Rezaee, Y. Assadi, M.-R.M. Hosseini, E. Aghaee, F. Ahmadi, S. Berijani, J. Chromatogr. A 1116 (2006) 1.
[46] M. Kumemura, T. Korenaga, Anal. Chim. Acta 558 (2006) 75.
[47] P.Y. Bruice, Organic Chemistry, Pearson Education, New Delhi, 2001, p. 805.
[48] F.F. Canwell, M. Losier, in: J. Pawliszyn, D. Barcelo (Eds.), Wilson & Wilson's Comprehensive Analytical Chemistry, vol. 37, Elsevier, Amsterdam, 2002, pp. 297–340.
[49] S.A. Barshick, W.H. Griest, Anal. Chem. 70 (1998) 3015.
[50] Z.E. Penton, J. Pawliszyn, D. Barcelo (Eds.), Wilson & Wilson's Comprehensive Analytical Chemistry, vol. 37, Elsevier, Amsterdam, 2002, pp. 279–296.
[51] H. Lord, J. Pawliszyn, J. Chromatogr. A 902 (2000) 17.
[52] M.S. El-Shahawi, Anal. Chim. Acta 356 (1997) 85.
[53] A. Afkhami, F. Mosaed, Microchem. J. 68 (2001) 35.
[54] A. Afkhami, A.R. Zarei, Talanta 53 (2001) 815.
[55] A. Afkhami, A.R. Zarei, Talanta 60 (2003) 63.
[56] A.A. Ensafi, M.A. Chamjangali, Spectrochim. Acta 58 (2002) 2835.
[57] M.S. El-Shahawi, F.A. Al-Hashemi, Talanta 43 (1996) 2037.
[58] N. Jie, X. Sun, J. Yang, Q. Zhang, Z. Liu, Z. Song, Anal. Lett. 30 (1997) 2441.
[59] N. Jie, Q. Zhang, N. Li, G. Eao, Q. Zhang, Mikrochim. Acta 140 (2002) 45.

Available online at www.sciencedirect.com
ScienceDirect
Talanta 71 (2007) 1239–1245
Talanta
www.elsevier.com/locate/talanta

Simultaneous on-line preconcentration and determination of trace metals in environmental samples using a modified nanometer-sized alumina packed micro-column by flow injection combined with ICP-OES

Chaozhang Hang, Bin Hu *, Zucheng Jiang, Nan Zhang

Department of Chemistry, Wuhan University, Wuhan 430072, PR China

Received 12 April 2006; received in revised form 16 June 2006; accepted 18 June 2006
Available online 4 August 2006

Abstract

A novel organic reagent 3-(8-quinolinylazo)-4-hydroxybenzoic acid (QAHBA) was synthesized for chemically modified nanometer-sized alumina, and it was characterized with infrared spectrum and ^{1}H NMR spectra. By using modified nanometer-sized alumina as micro-column packing material, a new method of flow injection (FI) on-line preconcentration coupled to ICP-OES was developed for simultaneous determination of trace metals (Ag, Pd, Au, Ga, In and Nb) in geological and environmental samples. The effects of pH, sample flow rate, sample volume, elution and interfering ions on the recovery of the analytes have been investigated. Under the optimized operating conditions, the adsorption capacity of the modified nanometer-sized alumina for Ag, Pd, Au, Ga, In and Nb were found to be 5.1, 7.6, 17.7, 15.6, 8.1 and 12.3 mg g^{-1}, respectively. With 4 min preconcentration time and 24 s elution time, the enrichment factor was 10 and the sample frequency was 10 h^{-1}. The detection limits of this method for Ag, Pd, Au, Ga, In and Nb were 0.12, 0.44, 0.27, 0.19, 0.54 and 0.18 μg l^{-1}, respectively, while the R.S.D.s were 1.6, 2.3, 4.5, 1.6, 1.9 and 1.7% ($n = 7$, $c = 50$ ng ml^{-1}), respectively. The proposed method has been applied to the determination of these trace metals in geological-certified reference materials and natural water samples with satisfactory results.
© 2006 Elsevier B.V. All rights reserved.

Keywords: Modified nanometer-sized alumina; Flow injection; On-line micro-column; Preconcentration; QAHBA; ICP-OES

1. Introduction

In recent years, some rare metals including gallium, indium, niobium, silver, gold and palladium receiving worldwide attention due to their industrial application. They are commonly used in the automobile, nuclear technique, electronic, and chemical industries. Hence, they can easily get into the environment. Therefore, more and more interest was focused on their resulting consequences on environment. In view of that, there is need to develop a monitoring technique for Ag, Pd, Au, Ga, In and Nb in environmental assessment.

The direct determination of extremely low concentrations of the target trace elements by modern analytical techniques is often difficult and it is necessary to employ some preconcentration steps. In recent years, the coupling of flow injection (FI) on-line micro-column separation and preconcentration techniques to ICP-OES/MS has been proved to be powerful for the determination of ultratrace levels of elements [1,2]. This combination not only provides an improvement in detection limits but also reduces the interference from matrix.

Most studies have used micro- or mini-column packed with various sorbents to meet all the analytical needs for extraction as well as separation of the analyte of interest [3,4]. Nowadays, many adsorption materials, such as organic chelate resin [5–7], modified silica gel [8,9], activated alumina [10] and PTFE materials such as the KR and PTFE beads [11–13] were used in this technology. More recently, nanometer-sized materials [14–18], C60–C70 fullerene and its derivative [19,20], were also explored for this purpose.

Nanometer-sized material is a new solid material that gained importance due to its special properties [21,22]. The regime of nanoparticle is from 1 to almost 100 nm, which falls between the classic fields of chemistry and solid-state physics. One of its properties is that most of the atoms of the nanoparticle are on

* Corresponding author. Tel.: +86 27 87218764; fax: +86 27 68754067.
E-mail address: binhu@whu.edu.cn (B. Hu).

0039-9140/$ – see front matter © 2006 Elsevier B.V. All rights reserved.
doi:10.1016/j.talanta.2006.06.033

the surface. The surface atoms are unsaturated and can therefore bind with other atoms, possessing a highly chemical activity. In our previous studies [15–18], we have systematically studied adsorption behaviors of metal ions on nanometer-sized TiO_2 and nanometer-sized Al_2O_3. However, it should be pointed out that these nanometer-sized metal oxides are not selective enough and not suitable for samples with complicated matrices. In order to improve the selectivity of the sorbent, the modification of the adsorption material is usually required. The most often used method is to load a kind of specific chelate reagent by physical or chemical procedure on the surface of this material. The former method is simple but the loaded reagent is prone to leaking out from the sorbent, while the chemical-bonded material is more stable and can be used repeatedly. Recently, we also succeed in speciation of dissolved iron(II) and iron(III) in environmental water samples by gallic acid-modified nanometer-sized alumina through interactions between surface hydroxyls of alumina and carboxy group of gallic acid [17].

Heterocyclic compounds with N, O and S atoms are effective ligands for metal ions [23,24]. Functional resin and heterocyclic compound that include N functional group had been used for preconcentration of Ga, In and noble metals [25,26]. As reagents commonly used in spectrophotometry, derivatives of 8-aminoquinoline can form stable and tinctorial compound with metal ions under special condition due to azo and other functional group can act as conjugate atoms of metal ions [27,28]. Heterocyclic compounds with carboxylic group, can be used as modifiers. Their carboxylic group can react with the hydroxyl group on the surface of nanometer-sized alumina.

The aim of this work was to develop a simple and sensitive method for the determination of some trace elements including gallium, indium, niobium, argentine, aurum and palladium by ICP-OES using a micro-column packed with nanometer-sized alumina modified by a novel organic reagent 3-(8-quinolinylazo)-4-hydroxybenzoic acid (QAHBA). The experimental conditions for retention and elution conditions of the target elements have been optimized. Finally, the proposed method was applied to the determination of these metals in geological-certified reference materials and natural water samples.

2. Experimental

2.1. Apparatus

Intrepid XSP Rasial ICP-OES (Thermo, USA) with a concentric model nebulizer and a cinnabar model spray chamber was used for the determination. The optimum operation conditions were summarized in Table 1. The modified nanometer-sized alumina was characterized by 170SX FT-IR (NICOL ET, USA); Varian Mercury 300 model HNMR (Varian, USA). The pH values were controlled with a Mettler Toledo 320-S pH meter (Mettler Toledo Instruments Co. Ltd., Shanghai, China) supplied with a combined electrode. A WX-3000 microwave accelerated digestion system (EU Chemical Instruments Co. Ltd., Shanghai, China) was used for sample digestion. An IFIS-C flow injection system (Ruimai Tech. Co. Ltd., Xi'an, China) and a self-made PTFE micro-column (20 mm × 2.0 mm i.d.) packed with modified nanometer-sized alumina were used in the on-line separation/preconcentration process.

Table 1
Operation parameters of Intrepid XSP Rasial ICP-OES

RF generator power (W)	1150
Frequency of RF generator (MHz)	27.12
Coolant gas flow rate ($l\,min^{-1}$)	14
Auxiliary gas ($l\,min^{-1}$)	0.5
Solution uptake rate ($ml\,min^{-1}$)	1.6
Maximum integration times (s)	30
Analytical wavelength (nm)	Ag, 328.068; Ga, 294.364; Au, 242.795; In, 303.936; Pd, 324.270; Nb, 309.418

2.2. Standard solution and reagents

Sodium nitrite and *p*-hydroxybenzoic acid are of chemical reagent grade; 8-aminoquinoline was obtained from New Jersey (98%, New Jersey, USA); Ga and In standard solutions ($1\,g\,l^{-1}$) were obtained, respectively from spec pure Ga_2O_3 and In_2O_3 dissolved in 5% nitric acid. Au, Ag and Pd standard solutions ($1\,g\,l^{-1}$) were obtained respectively from highly pure $AuCl_3$, $AgNO_3$, $PdCl_2$ dissolved in 2% nitric acid, respectively. Solution of Nb ($1\,g\,l^{-1}$) was prepared from spec pure Nb_2O_5. The digestion of Nb_2O_5 based on the procedure reported in Ref. [29].

Working solutions were prepared daily by appropriate dilutions of stock solutions. The standard stock solutions (1 or $10\,g\,l^{-1}$) of other elements were prepared from their salts by a conventional method. $HClO_4$, HCl, HF and HNO_3 were of a highly pure grade and all other reagents used were of analytical reagent grade. High purity deionized water was used throughout. Nanometer-sized Al_2O_3 was prepared in our laboratory, and the details on its synthesis and characterization were described in Ref. [16].

2.3. Synthesis of 3-(8-quinolinylazo)-4-hydroxybenzoic acid

The synthesis was carried out by dissolving equal molar amounts of 8-aminoquinoline and *p*-hydroxybenzoic acid (2 mmol) in 10 ml ethanol mixed with 10 ml of water containing 2 mmol of HCl in a 100 ml round-bottom flask. This mixture was magnetically stirred for 2 h at room temperature to bring both molecules into solution; the final solution exhibits a slight yellow color. After everything had dissolved, the flask was placed in an ice bath to cool for 2 h with continued stirring. Then, 0.3 mmol of sodium nitrite was added to the mixture, and the resulting suspension was stirred and cooled on ice for 12 h. There was clear indication that the reaction has proceeded apparently due to the change in solution color to light red after ~2 h [30]. The azo compound was filtered off, washed with water, air dried and recrystallized from ethanol.

2.4. Synthesis of modified nanometer-sized Al_2O_3

Portions of nanometer-sized Al_2O_3 were taken into 5 mol l^{-1} HNO_3 and refluxed for 6 h at 60 °C with stirring by a magnetic stirrer. Then, it was filtered through a 0.45 μm membrane, washed with high purity deionized water and ethanol several times and dried in vacuum. QAHBA-modified nanometer-sized Al_2O_3 was prepared by taking 5 g of activated nanometer-sized Al_2O_3 powder and placing into 100 ml of ethanol solution containing 1% (m/v) QAHBA and refluxed for 2 h under the protection of N_2. The modified nanometer-sized alumina powder was washed by ethanol in order to eliminate the redundant QAHBA on the surface of the alumina. The resulting powder was dried in vacuum for future use.

2.5. Micro-column preparation

A total of 50 mg of QAHBA-modified nanometer-sized Al_2O_3 was filled into a PTFE micro-column (20 mm × 2.0 mm i.d.) plugged with a small portion of glass-wool at both ends. Before use, methanol and high purity deionized water were passed through the column in sequence in order to clean it. Then, the column was conditioned to the desired pH with 0.1 mol l^{-1} NH_4NO_3 buffer solution.

2.6. General procedure

The operation sequence of the FI on-line column preconcentration and determination is shown in Fig. 1. In preconcentration step, pump P1 was activated, so that the sample was drawn through the column. And in elution step, pump P2 was activated, so that the eluent was propelled through the column reversedly. In this instance, the continuous impact on the sorbent could be avoided. Then, the elution solution was introduced into the ICP-OES for determination.

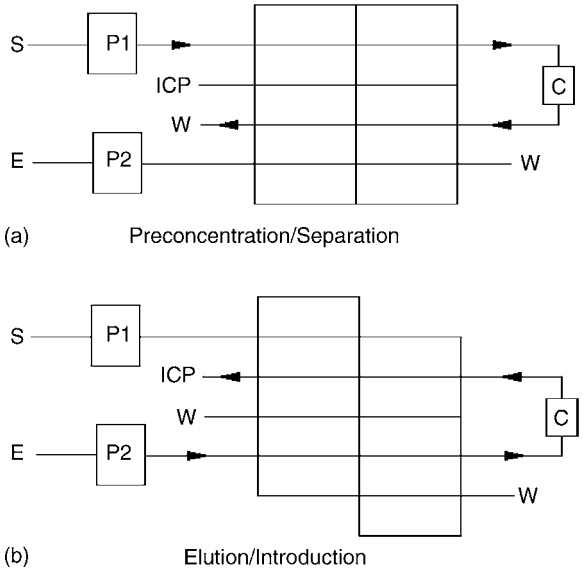


Fig. 1. FI manifold and operation for on-line preconcentration/separation and ICP-OES determination: (a) preconcentration/separation step; (b) elution/introduction step. For details see text. S, sample; E, elution; W, waste; C, micro-column packed with modified nanometer Al_2O_3; P1, P2, peristaltic pumps; ICP, ICP torch.

2.7. Sample preparation

(i) For the geological-certified reference material of soil (provided by the Institute of Geophysical and Geochemical prospecting, Langfang, China), 0.1000 g of GBW07401 (GSS-1) were weighed and put into PTFE digestion vessel. After adding 4 ml of HNO_3, 1 ml of $HClO_4$ and 1 ml of HF, the vessel was capped and shaken for 3 min to allow thorough mixing of the sample and acids. The vessel was then place on the turntable. The microwave system was operated as follow: 2 min at 8 atm and 600 W; 3 min at 12 atm and 800 W; 8 min at 16 atm and 800 W [31]. The blank solution was prepared under the same condition of mixed acids and microwave program. After digestion, the vessel was cooled in air to room temperature. And then, the digest was filtered and transferred into 25 ml of flask, adjusted to pH 4.5 and diluted to calibration with high purity distilled water for analysis.

(ii) For the geological-certified reference material of platinpalladium ore (provided by the Institute of Geophysical and Geochemical Prospecting, Langfang, China), 1.0000 g of GBW07293 (dried at 100 °C for 4 h) and 1.000 g of sodium peroxide were weighed in nickel crucibles and placed in a muffle furnace for 15 min at 700 °C [32]. The residues were dissolved in hot water in a beaker and solutions obtained were heated to near dryness. Then, the residues dissolved in dilute hydrochloric acid and the dissolved salts were then centrifuged. Before use, the pH value was adjusted to 4.5 with 0.1 mol l^{-1} HNO_3 and 0.1 mol l^{-1} $NH_3{\cdot}H_2O$.

(iii) Lake water sample, collected from East Lake, Wuhan, China, was filtered through a 0.45 μm membrane filter (Tianjing Jinteng Instrument Factory, Tianjin, China), acidified to pH of about 1 with concentrated HNO_3 prior to storage for use. Before use, the pH value was adjusted to 4.5 with 0.1 mol l^{-1} HNO_3 and 0.1 mol l^{-1} $NH_3{\cdot}H_2O$.

3. Results and discussion

3.1. Characterization of 3-(8-quinolinylazo)-4-hydroxybenzoic acid

3.1.1. FT-IR spectra

From the spectra (Fig. 2), it can be seen that the spectral band at 3451 and 3360 cm^{-1} correspond to N–H stretching frequency of 8-AQ were invisible in the QAHBA spectra, which indicates N–H has reacted. The QAHBA also has absorption bands at 1676 cm^{-1} typical of stretching of C=O that appeared at 1675 cm^{-1} in the *p*-HBA spectra. The band corresponding to the asymmetrical N=N mode of stretching mode, near 1600 cm^{-1}, was not detected as it merged with strong C=C ring vibration [33]. The other characteristic functional groups such as ν_{C-O-C} at 1162 cm^{-1} and ν_{OH} at 3376 cm^{-1} were confirmed from the IR spectrum of QAHAB.

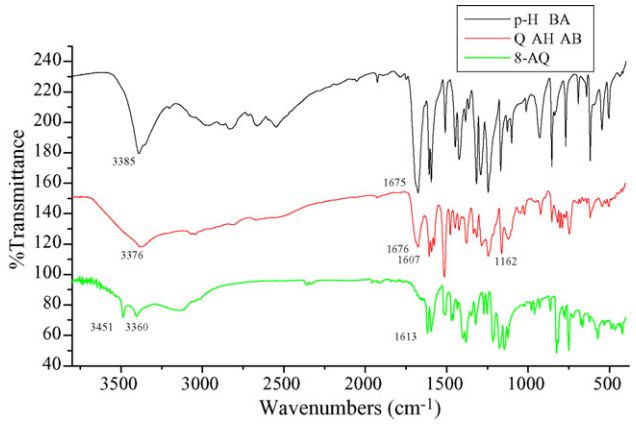


Fig. 2. FT-IR spectra of *p*-HBA, QAHBA and 8-AQ.

3.1.2. ^1H NMR

^{1}H nuclear magnetic resonance spectra were recorded with a Varian Mercury 300 model ^{1}H NMR (Fig. 3). The sample was dissolved in $CDCl_3$ and transferred into sample tube. As can be seen, there are nine peaks in the ^{1}H nuclear magnetic resonance spectra. The highest peak belongs to $CDCl_3$ and the other peaks stand for eight kinds of H. The result shows the height of the peak d is about two times greater than other peaks (a, b, c, e, g, h, i). Hence, the spectra indicated that the target compound has nine kinds of H. In the spectra, the values of δ are beside 7.3, which imply the H of target compound is belong to Ar–H($\delta \approx 7.30$). The differences are due to the effect of the electron-withdrawing group and the electron-donating group. The analysis result of the peaks was listed as follows: δ8.68 (s, 1H(7), $J = 3.6$ Hz), δ8.11(d, 1H(1), $J = 8.7$ Hz), δ7.87 (d, 1H(6), $J = 6.6$ Hz), δ7.5 (t, 2H(3, 4), $J = 6.6$ Hz), δ7.43 (t, 1H(8), $J = 7.8$ Hz), δ7.2 (t, 1H(5), $J = 8.7$ Hz), δ7.07 (d, 1H(2), $J = 9.6$ Hz), δ6.3 (d, 1H(9), $J = 9.6$ Hz). Base on the results, we found that the spectra is corresponding to the structure of the target compound.

3.2. Selectivity and probable mode of chelation of modified nanometer-sized alumina to metal ions

The adsorption behavior of various metal ions on QAHBA-modified nanometer-sized alumina was operated according to the general procedure. Fig. 4 shows the dependence of adsorption percentage of tested metal ions on the pH. As can be seen, the adsorption percentage of Ag, Au are higher than 80% and Pd can be completely adsorbed by the modified alumina at pH < 4, while other metals are adsorbed poorly. This is due to the strong chelation between the noble metal ions and azo functional group. It was found that within a pH range of 4.5–6.5, all the metal ions are adsorbed quantitatively on QAHBA-modified nanometer-sized alumina. When pH > 7, all the target analytes were quantitatively adsorbed with the exception of Pd. This could be attributed to the hydroxylation of the metal ions at higher pH. As we know, the surface of modified alumina shows electronegative character under basic condition, while Pd^{2+} may form an anionic compound of $[Pd(NH_3)_2Cl_4]^{2-}$ with negative charge. Therefore, the electrostatic repulsion may result in decrease of the recovery of Pd^{2+} at pH > 6.5.

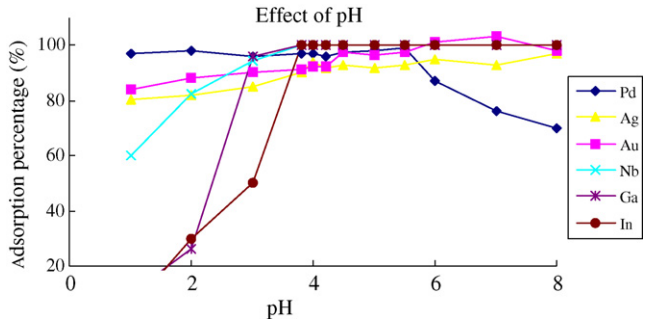


Fig. 4. The dependence of adsorption percentage of tested metal ions on pH.

The stability of metal complexes generally depends on the size and number of rings they form. The hexa-member and penta-member rings are the most stable among the ring compound, and the larger the number of rings, the higher the stability of the ring compound. The possible modes of chelation between the functional groups on the surface of modified alumina and metal ions are shown in Fig. 5. It can be seen that the studied metal ions and the functional groups on the surface of modified alumina can form a complex with a hexa-member and a penta-member rings.

3.3. The optimization of elution conditions

It was found that Ag, Au and Pd could not be eluted without thiourea. Hence, a mixed solution of HNO_3 and thiourea was used for fast and quantitative recovery of the retained analytes from the column.

3.3.1. Concentration of thiourea

By keeping the concentration of HNO_3 at 1.5 mol l^{-1}, the effect of thiourea concentration on the recovery of the studied ions was investigated with the thiourea concentration varying among 1–5% (m/v). The results showed the recovery of Ag, Au and Pd increased with the increase in concentration of thiourea first and then remain constant with further increase in thiourea concentration, while the recovery of Ga, In and Nb remain unchanged with the increase in concentration of thiourea. Considering the possible effect of thiourea on the subsequent

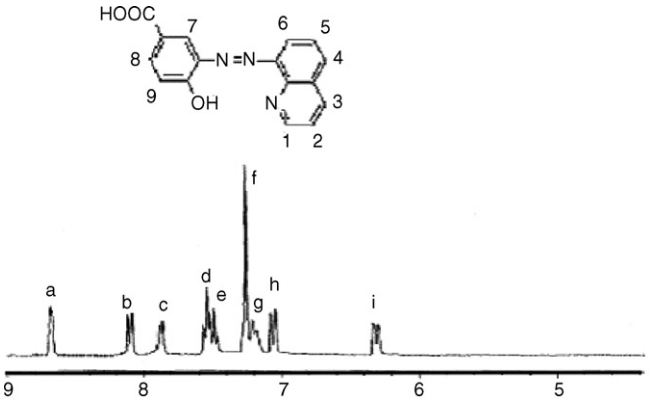


Fig. 3. ^{1}H NMR spectra of QAHBA.

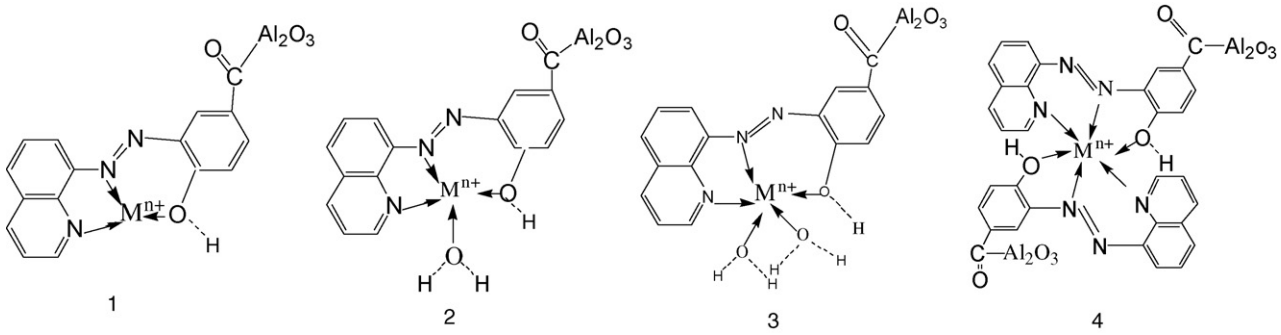


Fig. 5. Probable modes of chelation of the adsorbent QAHBA with the investigated metal ions.

ICP-OES determination, 3% (m/v) thiourea was chosen in this work.

3.3.2. Concentration of HNO_3

By keeping the thiourea concentration at 3%, the effect of HNO_3 concentration on the recovery of analytes was explored. Ag, Au and Pd can be easily eluted with the HNO_3 concentration of 0.1 mol l^{-1}. However, Ga, In and Nb can only be recovered quantitatively with the HNO_3 concentration higher than 1 mol l^{-1}. In this work, 1 mol l^{-1} HNO_3 was selected.

3.3.3. Elution volume and elution flow rate

The effect of elution volume for quantitative elution of the studied ions was investigated. We found that 0.6 ml of elution solution containing 1 mol l^{-1} HNO_3 and 3% (m/v) thiourea was sufficient to recover analytes quantitatively.

The effect of elution flow rate on recovery of analytes was investigated by keeping the elution volume of 0.6 ml containing 1 mol l^{-1} HNO_3 and 3% (m/v) thiourea. The result indicates that the analytes can be recovered quantitatively at flow rate range of 0.5–1.5 ml min^{-1}. Hence, elution flow rate of 1.5 ml min^{-1} was selected in this experiment.

3.4. Sample flow rate and sample volume

The sample flow rate should be optimized to ensure quantitative retention along with minimization of the time required for sample processing. It was found that, with the increase in flow rate, the analyte recoveries decrease slowly, but still over 90% recovery could be obtained with the flow rate up to 1.5 ml min^{-1}. In this work, sample flow rate of 1.5 ml min^{-1} was selected.

In order to investigate the breakthrough volume, the sample solutions of 10, 25, 50, 100, 150 and 200 ml containing 5 g of analytes, respectively, and then operated according to the general procedure. It was found that the analytes could be quantitatively retained when sample volumes were less than 75 ml. To trade off the enrichment factor and analytical speed, a sample volume of 6 ml and an elution volume of 0.6 ml were used, so that an enrichment factor of 10 and a sampling frequency of 10 h^{-1} were obtained in this work.

3.5. Coexisting ions interference

For the study of interference by other coexisting ions, such as K^+, Na^+, Ca^{2+}, Mg^{2+}, Al^{3+}, Fe^{3+}, Zn^{2+} and Cu^{2+}, on the preconcentration and determination of analytes were examined under the optimum conditions described above using the FI–ICP-OES set up shown in Fig. 1. The results show that in the presence of 10,000 mg/l K^+, 8000 mg/l Na^+, 5000 mg/l Ca^{2+} and Mg^{2+}, 1000 mg/l Al^{3+}, Zn^{2+} and Cu^{2+}, 50 mg/l Fe^{3+}, the recoveries of the analytes are still above 90%.

3.6. Analytical performance

With 4 min preconcentration time and 24 s elution time, the sampling frequency was 10 h^{-1} and the enrichment factor was 10. The detection limits (evaluated as the concentration corresponding to three times the standard deviation of 11 runs of the blank solution) and relative standard deviations ($n = 7$,

Table 2
Comparison of LOD and R.S.D. of methods

	Modified nano-sized Al_2O_3		Results from conventional nebulization		Modified silica gel [6]		Nano-sized TiO_2 [18]		Resin [8]		High-surface-area ZrO_2 [2]		Tannic cotton [35]	
	LOD ($\mu g\,l^{-1}$)	R.S.D. (%)	LOD ($\mu g\,l^{-1}$)	R.S.D. (%)	LOD ($\mu g\,l^{-1}$)	R.S.D. (%)	LOD ($\mu g\,l^{-1}$)	R.S.D. (%)	LOD ($\mu g\,l^{-1}$)	R.S.D. (%)	LOD ($\mu g\,l^{-1}$)	R.S.D. (%)	LOD ($\mu g\,l^{-1}$)	R.S.D. (%)
Ag	0.12	1.6	1.1	5.7	4	0.5	6	4.5	–	–	–	–	–	–
Au	0.27	4.5	2.5	4.5	22	0.9	16	8.7	0.5	4.2	–	–	–	–
Pd	0.44	2.3	4.1	6.4	19	1.7	12	7.4	1.0	4.1	–	–	–	–
Ga	0.19	1.6	1.7	4.2	–	–	–	–	–	–	0.01	<8	–	–
In	0.54	1.9	5.2	5.4	–	–	–	–	–	–	0.009	5.5	–	–
Nb	0.18	1.7	1.6	4.3	–	–	–	–	–	–	–	–	0.8	2.6

$c = 50\ ng\ ml^{-1}$) of this method with other works reported and the compared results from conventional nebulization were listed in Table 2. As can be seen, the LOD and R.S.D.s of this method are almost better than other reported adsorbents (determination by ICP-OES). Although Ref. [2] reported good LOD and R.S.D.s for Ga and In, the major drawback of the work is the time-consuming enrichment procedure (33 min for a 100 ml sample).

Regeneration is one of the key factors in evaluating the performance of the adsorption material. When the concentration of HNO_3 in the eluting agent is $1\ mol\ l^{-1}$, the column packed with modified nanometer-sized alumina can be re-used more than 30 times. However, when concentration of HNO_3 in the eluting agent is greater than $2.5\ mol\ l^{-1}$, the column cannot be re-used. This could be due to the bond breakage between the $–CO_2–Al$ bonding in the modified nanometer-sized alumina.

The adsorption capacity is another important factor in evaluating the adsorption material, because it determines how much modified nanometer-sized alumina is required to quantitatively concentrate the analytes from a given solution. The capacity study used was adapted from the method recommended by Maquieira et al. [34], and the maximal adsorption capacities for Ag, Pd, Au, Ga, In and Nb were found to be 5.1, 7.6, 17.7, 15.6, 8.1 and $12.3\ mg\ g^{-1}$, respectively.

3.7. Sample analysis

The proposed method was applied to the determination of analytes in natural lake water sample (East Lake, Wuhan, China), and the results along with the recoveries for the spiked samples are given in Table 3.

In order to establish the validity of the proposed procedure, the method has been applied to the determination of the content of target metals in certified reference materials (GBW07401 geological samples, GBW07293 geological samples). The results are listed in Table 4. As can be seen, a good agreement between determined values and the certified values could be obtained.

Table 3
Analytical results of Ag, Pd, Au, Ga, In and Nb in synthetic water and lake water (mean ± S.D., $n = 3$)

Element	Added ($ng\ ml^{-1}$)	Founded ($ng\ ml^{-1}$)	Recovery (%)
Ag	0	n.d[a]	–
	10	9.3 ± 1.3	93
	20	17.8 ± 0.8	89
Au	0	n.d[a]	–
	10	9.8 ± 1.1	98
	20	19.2 ± 0.6	96
Pd	0	n.d[a]	–
	10	10.8 ± 1.0	108
	20	21.1 ± 0.9	106
Ga	0	n.d[a]	–
	10	10.5 ± 1.6	105
	20	19.1 ± 1.5	96
In	0	n.d[a]	–
	10	10.4 ± 0.6	104
	20	17.8 ± 0.8	89
Nb	0	1.02 ± 0.7	–
	10	9.5 ± 0.5	86
	20	20.9 ± 0.5	98

[a] n.d., not detected.

Table 4
Determination of certified reference materials (mean ± S.D., $n = 3$)

Sample	Element	Certified ($\mu g\ g^{-1}$)	Added ($\mu g\ g^{-1}$)	Found ($\mu g\ g^{-1}$)	Recovery (%)
GBW07401	Ag	0.35 ± 0.007	0	0.32 ± 0.04	–
			1	1.22 ± 0.13	90.4
	Ga	19.3 ± 1.7	0	18.6 ± 2.1	–
			10	33.1 ± 2.2	113
	Nb	16.6 ± 2.2	0	17.1 ± 1.6	–
			10	26.3 ± 1.2	98.8
	In	0.08 ± 0.02	0	n.d.[a]	–
			1	1.06 ± 0.11	106
GBW07293	Au	0.045	0	0.04 ± 0.01	–
			1	0.88 ± 0.06	88.0
	Pd	0.568	0	0.54 ± 0.04	–
			1	1.50 ± 0.09	95.7
	Ag	–	0	n.d.[a]	–
			1	0.95 ± 0.04	95.2
	Ga	–	0	1.37 ± 0.12	–
			1	2.16 ± 0.23	91.1
	In	–	0	n.d.[a]	–
			1	0.89 ± 0.05	89.0
	Nb	–	0	27.29 ± 2.3	–
			10	34.69 ± 2.7	93.2

[a] n.d., not detected.

4. Conclusion

A novel organic reagent 3-(8-quinolinylazo)-4-hydroxybenzoic acid (QAHBA) was synthesized and characterized with infrared spectrum and ^1H NMR spectra. It was found that, the nanometer-sized alumina modified with QAHBA in this study is chemically stable and has efficient analytical performance in an on-line preconcentration system. The methodology was employed to real samples and it gave good accuracy, low limits of detection, excellent precision and relatively high kinetic adsorption on the target analytes, which show its potentiality in trace and even ultratrace analysis in various samples with complicated matrix.

Acknowledgment

Financial support from NCET, MOE of China is gratefully acknowledged.

References

[1] H. Karami, M.Z. Mousavi, Y. Yamini, M. Shamsipur, Anal. Chim. Acta 509 (2004) 89.
[2] E. Vassileva, N. Furuta, Fresen. J. Anal. Chem. 370 (2001) 52.
[3] J. Chen, C.Z. Huang, B. Hu, Z.C. Jiang, J. Agric. Food Chem. 52 (2004) 6843.
[4] L. Abranko, Z. Stefanka, P. Fodor, Anal. Chim. Acta 493 (2003) 13.
[5] Y.W. Wu, Z.C. Jiang, B. Hu, Geostand. Geoanal. Res. 28 (2004) 383.
[6] P. Pohl, B. Prusisz, W. Zyrnicki, Talanta 67 (2005) 155.
[7] B.L. Gong, X.Q. Li, F.G. Wang, X.J. Chang, Talanta 52 (2000) 217.
[8] P. Liu, Q.S. Pu, Q.Y. Sun, Z.X. Su, Fresen. J. Anal. Chem. 366 (2000) 816.
[9] R. Vlas'a'nkova, V. Otruba, J. Bendl, M. Fis'era, V. Kanicky, Talanta 48 (1999) 839.
[10] T. Alexandra, K. Vassilis, Anal. Bioanal. Chem. 374 (2002) 66.
[11] Z.L. Fang, S.K. Xu, L.P. Dong, W.Q. Li, Talanta 41 (1994) 2165.
[12] J.H. Wang, E.H. Hansen, J. Anal. Atom. Spectrom. 17 (2002) 248.
[13] J.H. Wang, E.H. Hansen, J. Anal. Atom. Spectrom. 17 (2002) 1278.
[14] P. Liang, B. Hu, Z.C. Jiang, Y.C. Qin, T.Y. Peng, J. Anal. Atom. Spectrom. 16 (2001) 863.
[15] P. Liang, Y.C. Qin, B. Hu, T.Y. Peng, Z.C. Jiang, Anal. Chim. Acta 440 (2001) 207.
[16] J. Yin, Z.C. Jiang, G. Chang, B. Hu, Anal. Chim. Acta 540 (2005) 333.
[17] X.L. Pu, B. Hu, Z.C. Jiang, C.Z. Huang, Analyst 130 (2005) 1175.
[18] Y.C. Q, Y.P. Hang, R. Wanjanul, Z.C. Jiang, B. Hu, Anal. Sci. 19 (2003) 1417.
[19] J. Mun˜oz, J.R. Baena, M. Gallego, M. Valca'rcel, J. Anal. Atom. Spectrom. 17 (2002) 716.
[20] M.G. Pereira, E.R. Pereira-Filho, H. Berndt, M.A.Z. Arruda, Spectrochim. Acta Part B 59 (2004) 515.
[21] A. Henglein, Chem. Rev. 89 (1989) 1861.
[22] Q.J. Xue, K. Xu, Prog. Chem. (Chinese) 12 (2000) 431.
[23] H. Filik, K.I. Berker, N. Balkis, R. Apak, Anal. Chim. Acta 518 (2004) 173.
[24] M.M. Omar, G.G. Mohamed, Spectrochim. Acta A 61 (2005) 929.
[25] S.V. Vartak, V.M. Shinde, Talanta 45 (1998) 925.
[26] V.K. Singh, N.K. Agnihotri, H.B. Singh, R.L. Sharma, Talanta 55 (2001) 799.
[27] P. Nagaraja, H.S. Yathirajan, K.R. Sunitha, R.A. Vasantha, Anal. Lett. 35 (2002) 1531.
[28] L. Wang, Z.B. Yuan, Q.F. Hu, J.Y. Yin, G.Y. Yang, Chin. J. Anal. Chem. 33 (2005) 371.
[29] S.Q. Li, B. Hu, Z.C. Jiang, J. Anal. Atom. Spectrom. 19 (2004) 387.
[30] R.H. Uibel, J.M. Harris, Anal. Chem. 77 (2005) 991.
[31] L. Moberg, K. Pettersson, I. Gustavssonb, J. Anal. Atom. Spectrom. 14 (1999) 1055.
[32] E.K. Shibuyaa, J.E.S. Sarkis, J. Enzweilerb, J. Anal. Atom. Spectrom. 13 (1998) 941.
[33] M.E. Mahmoud, E.M. Soliman, Talanta 44 (1997) 1063.
[34] A. Maquieira, H.A.M. Elmahadi, R. Puchades, Anal. Chem. 66 (1994) 3632.
[35] L.N. Li, J.T. Ma, Z.F. Sa, S.J. Zhao, YanKuang CeShi 20 (2001) 27.

Available online at www.sciencedirect.com
ScienceDirect
Talanta 71 (2007) 1088–1095
Talanta
www.elsevier.com/locate/talanta

A novel spectrophotometric method for batch and flow injection determination of cyanide in electroplating wastewater

Saad S.M. Hassan *, Mohamed S.A. Hamza, Ali E. Kelany

Department of Chemistry, Faculty of Science, Ain Shams University, Cairo, Egypt

Received 1 April 2006; received in revised form 30 May 2006; accepted 1 June 2006
Available online 24 July 2006

Abstract

A sensitive and highly selective spectrophotometric method is described for the determination of cyanide. It is based on a reaction of cyanide with aquacyanocobyrinic acid heptamethyl ester (ACCbs) reagent (orange color) at pH 9.5 to give dicyanocobester (DCCbs) (violet color). The increase of the absorption bands of the reaction product at 368 and 580 nm and the decrease of the reagent band at 353 nm are linearly proportional to the cyanide concentration. The method is used in static mode for determining cyanide over the concentration range 0.04–1.20 $\mu g\,ml^{-1}$ with a detection limit of 0.02 $\mu g\,ml^{-1}$ and for hydrodynamic analysis of 0.4–5.2 $\mu g\,ml^{-1}$ cyanide. Application for batch and flow injection monitoring of cyanide in electroplating wastewater samples gives results agree within ± 1.2% with those obtained by the standard potentiometry using the cyanide ion selective electrode. The method is practically free from interferences by PO_4^{3-}, NO_3^-, NO_2^-, SO_4^{2-}, F^-, Cl^-, Br^-, I^-, S^{2-} and SCN^- ions and gives results with average recoveries of 97.6–99.2%. Advantages offered by using ACCbs as a chromogen for cyanide assay are: (i) high selectivity and sensitivity of the coordination site of the reagent towards cyanide ion; (ii) fast reaction, since legation takes place at the axial position of the reagent; (iii) good solubility and stability of the reagent in aqueous solutions over a wide pH range; (iv) high stability of the reagent (ACCbs) and the colored complex product (DCCbs) and (v) possible absorbance measurements at three different wavelengths.
© 2006 Elsevier B.V. All rights reserved.

Keywords: Spectrophotometry; Aquacyanocobyrinic acid heptamethylester (aquacyanocobester); Cyanide determination; Flow injection analysis; Electroplating wastewater

1. Introduction

Monitoring of cyanide in industrial wastes is highly demanded for environmental control, especially in electroplating, precious metal refining and metal cleaning industries. Methods in current use for determination of total, free and complexed cyanide, include separation of hydrogen cyanide gas from the acidified sample solution by the standard distillation method, collection in alkaline solution followed by assessment using spectrophotometry [1–26], fluorimetry [27,28], indirect atomic absorption spectrometry [29–33], polarography [34,35], potentiometry [36–41] and chromatography [42–44]. The spectrophotometry is by far the most superior to other methods.

Spectrophotometric methods for cyanide assessment are based on direct, indirect and enzymatic reactions. Conversion of cyanide into cyanogen chloride or cyanogen bromide followed by chromogenic reactions with pyridine solutions of barbituric acid [1,5], pyrazolone [20], isonicotinic acid-barbiturates [2,3], 1,4-phenylenediamine [4] and benzidine [6] have been suggested. Direct reaction of cyanide with 2,2-dihydroxy-1,3-indanedione in alkaline media [17] or ninhydrine to form hydrindantin which decompose in alkaline media to give colored products has been repoted [19].

Determination of cyanide by indirect methods is based on decoloration of some colored complexes such as triiodide [7], iodine/starch [8], Ag^+/codion 2B [10], Ag^+/porphyrin derivatives [11], Ag^+/*N*-(2-thiozolyl-2-hydroxybenzamide) [12], Cu^{2+}/*N*,*N*-diethyl-1,4-phenylenediamine [14] and Ni^{2+}/2-(5-bromopyridylazol)-5-diethylaminephenol [15]. Reaction of cyanide with a known excess of formaldehyde to form hydroxylacetonitrile followed by condensation of the unreacted reagent with 3-methyl-2-methyl-2-benzolenone hydrazone gives azine derivative which upon oxidation with Fe^{3+} gives a blue cationic dye [9].

* Corresponding author. Fax: +20 2 682 2991.
E-mail address: saadsmhassan@yahoo.com (S.S.M. Hassan).

0039-9140/$ – see front matter © 2006 Elsevier B.V. All rights reserved.
doi:10.1016/j.talanta.2006.06.010

Enzymatic spectrophotometric determination of cyanide involves catalytic oxidation of L-tyrosine using tyrosinase enzyme. The dark colour developed due to the formation of melanin is suppressed by cyanide ion [16]. Thiosulfate sulfurtransferase enzyme has been also used to convert CN^- in the presence of $S_2O_3^{2-}$ into SCN^- which is measured as Fe^{3+}/thiocyanate complex [18]. Most of these methods, however, have the drawbacks of several time-consuming derivatization reactions [1–6,9,16,18,19], slow colour development [3,4,7–9,13,15,17,19], reagent instability or carcinogenity [4,6] and interference by most common ions [4,7–10,19,23].

In the present work, microgram quantities of cyanide ion are spectrophotometrically determined under static (batch) and hydrodynamic (FIA) mode of operations by a chromogenic reaction at pH 9.5 with aquacyanocobyrinic acid heptamethyl ester known as aquacyanocobester (ACCbs). Absorbance changes of aquacyanocobester reagent and dicyanocobester (DCCbs) reaction product are measured at different wavelengths as a function of cyanide concentrations. The method is satisfactorily applied to monitor cyanide in electroplating wastewater.

2. Experimental

2.1. Equipment

All absorbance measurements were made using Shimadzu UV–vis spectrophotometer (model UV-1601) with 1.00 cm light path length matched quartz cells (~4 ml total volume). The pH measurements were made using an Orion digital pH/mV meter (model SA 720) and an Orion combined glass pH electrode (model 80-02). A solid state Orion cyanide ion selective electrode (model 9406 BN) was used for potentiometric measurements of cyanide ion. The components of the flow injection setup were a peristaltic pump (Ismatec MS Reglo) and an injection valve (Ominfit, Cambridge, UK) with 100 μl sample loop. The flow Tygon tubes (P/N A00349 and P/N A00355) and the pump tubes (red/red 2 mm internal diameters) were obtained from ALKEM, USA. The distance between the injection valve and spectrophotometric cell was 75 cm including a 50-cm reaction coil. The data were obtained using Shimadzu spectrophotometer (model UV-1601) equipped with a 1.00 cm light path length flow cell. The out put signals were recorded using UVPC v3.9 software (Fig. 1).

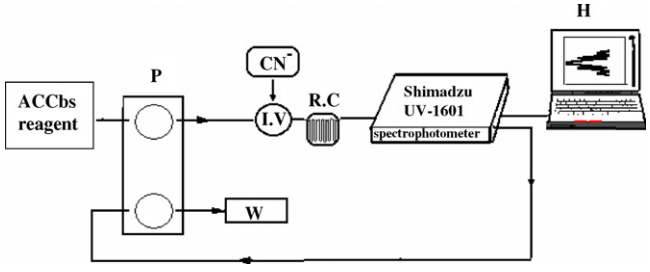


Fig. 1. Flow injection manifold for spectrophotometric determination of cyanide, I.V., injection valve; P, peristaltic pump; R.C., reaction coil; W, waste; H, laptop computer.

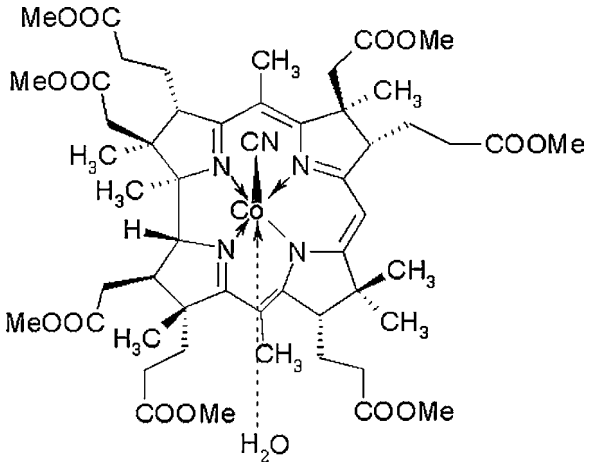


Fig. 2. Chemical structure of aquacyanocobester (ACCbs) reagent, [molecular formula $C_{53}H_{76}CoN_5O_{14}$, molecular mass 1066.15].

2.2. Reagents and chemicals

All chemicals were of analytical grade and deionized double-distilled water was used throughout. Potassium cyanide was purchased from M & B Chemicals (Dagenham, England). Potassium hydroxide was obtained from Riedel-de Haen (Germany), acetic acid (99.5%) was supplied by Prolabo (Italy). All the tested interfering anions were potassium salts of analytical grade. Aquacyanocobester (ACCbs) (Fig. 2) was prepared from Vitamin B_{12}, as described previously [45,46]. The purity of the reagent was checked with HPLC using 4.6 mm × 256 mm column filled with TSK-Gel silica-60 stationary phase, dichloromethane (97.3%) as a mobile phase and a 1 ml min^{-1} elution rate. Formation of ACCbs was detected by the appearance of a characteristic absorption band at 353 nm.

2.3. Analytical procedure

Aliquots (2 ml) of 2×10^{-4} mol l^{-1} working ACCbs reagent solution of pH 9.5 were transferred into 1.0 path light length spectrophotometer quartz cell (4 ml total capacity) and the absorbance was measured at 353, 368 and 580 nm, against a blank containing deionized water adjusted to the same pH. Different cyanide solutions (2, 5, 10, 20, 100, 125, 150 μl, of 1.0×10^{-3} mol l^{-1}) were added, the volume was completed to 3 ml using deionized water, the mixtures were shaken and the absorbancies were measured at 353, 368 and 580 nm after 20 s. Calibration curves constructed by plotting the absorbance change at each wavelength against the cyanide concentration give linear relationships. A calibration plot connecting cyanide concentration against the most sensitive absorption at 368 nm was used for all subsequent measurements of unknown cyanide test solutions. The spectrophotometric measurements were measured in triplicate.

2.4. Flow injection analysis of cyanide

A flow through spectrophotometric cell was used in a single-stream flow injection system. The carrier solution containing

8×10^{-4} mol l^{-1} (ACCbs) reagent adjusted to pH 9.5 was propelled through the cell, by means of a peristaltic pump and PTFE tubing, at a flow rate of 1.75 ml min^{-1}. An Omnfit injection valve was used for successive injection of 100 μl aliquots of cyanide sample solutions (0.4–5.2 μg ml^{-1}) into the flowing stream. The cyanide and ACCbs reagent were allowed to mix before reaching the flow-through spectrophotometric cell. The distance between the injection valve and the spectrophotometric cell was 75 cm. The cell was placed in a Shimadzu spectrophotometer (model UV-1601) attached to a computer system to record absorbance signals at 368 nm.

2.5. Determination of cyanide in electroplating wastewater

Cyanide distillation apparatus [1] consisting of a 1-l boiling flask, air inlet, condenser, gas scrubber, suction flask trap and aspirator was fit connected. A 50.0 ml aliquot of the cyanide test sample was added and diluted to 500 ml with deionized distilled water. A 10 ml portion of 1 mol l^{-1} NaOH solution was transferred to the gas scrubber. About 50 mg of $PbCO_3$ was added to the scrubber to precipitate S^{2-} ions, if present [1,9,15]. A flow of air (~1 bubble s^{-1}) was allowed to enter the boiling flask to carry out HCN gas from flask to the gas scrubber. About 2 g sulfamic acid was added through the inlet tube, followed by 50 ml of 11 mol l^{-1} H_2SO_4 through the inlet tube. The contents were mixed for 3 min and 20 ml of 50% $MgCl_2 \cdot 6H_2O$ reagent was added. The mixture was refluxed for 1 h. Heating was discontinued and airflow was continued for 15 min. After cooling the absorption solution in the scrubber was quantitatively transferred to a 250 ml volumetric flask. The gas scrubber was rinsed with distilled water and the collected solution was adjusted to pH 9.5, diluted to volume with distilled water and mixed thoroughly. The cyanide ion concentration was determined as described above.

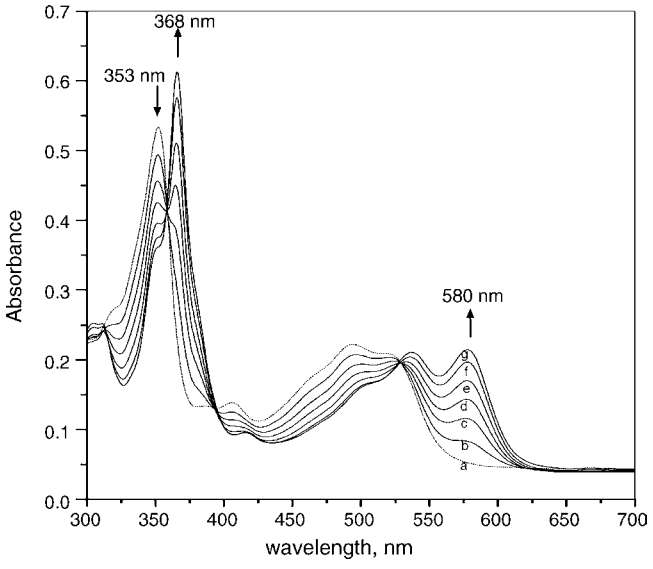
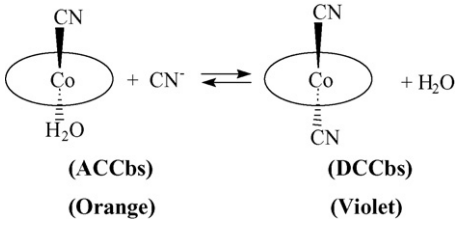


Fig. 3. Absorption spectra of: (a) aquacyanocobester (ACCbs) reagent and its reaction product with: (b) 80, (c) 170, (d) 260, (e) 350, (f) 435 and (g) 520 ng ml^{-1} cyanide.

3. Results and discussion

3.1. Characteristics of the absorption spectra

The orange color of aqueous aquacyanocobester (ACCbs) solution exhibited three characteristic absorption bands, with absorption maxima at 353, 495 and 525 nm. On the addition of cyanide to aquacyanocobester, a significant intense violet color of dicyanocobester complex (DCCbs) was instantaneously developed and four isobestic points at 313, 358, 395 and 529 nm were observed. New absorption bands at 368, 540 and 580 nm were also appeared (Fig. 3). This indicated a strong interaction between CN^- ion and (ACCbs) and revealed that the reaction proceeded without any side reactions or equilibrium overlapping anomalies. Equilibrium and kinetic studies on the reactions of similarly related compounds (e.g., alkylcobalamins and deoxyadenosylcobinamide) with cyanide ion have been previously described [47,48] .The equilibrium established between CN^- ion and (ACCbs) can be simplified and represented by Eq. (1):



(1)

Absorption bands at 353, 368 and 580 nm displayed intensity variations linearly proportional to the change of cyanide ion concentration. With the increase of cyanide level, the intensities of 368 and 580 nm bands increased and the intensity of 353 nm band decreased. The most sensitive band was that at 368 nm which was selected for flow injection analysis. No significant effect was noticed due to the interaction of the reagent with high concentrations of most common ions. In the presence of SO_3^{2-} ions at pH > 9.5, however, slight variations of the absorbances at 353, 368 and 580 nm were noticed.

3.2. Influence of pH

The influence of pH on the reaction of aquacyanocobester and cyanide ions can be predicted from the relation: $HCN/CN^- = 10^{9.2}/10^{pH}$ where availability of free cyanide ion increased with the increase of pH. The effect of pH on ACCbs reagent in the absence and the presence of 0.4 μg ml^{-1} cyanide was investigated at 353, 368 and 580 nm (Fig. 4). It is evident that the optimum range for the reaction is pH 8.5–10.0. Above pH 10.5, a slight interference due to HO^- takes place. All subsequent measurements were made at pH 9.5.

3.3. Effect of foreign anions

The effect of foreign anions on the reaction of ACCbs reagent with cyanide ion was studied at 353, 368 and 580 nm using a fixed cyanide concentration (2×10^{-5} mol $l^{-1} \equiv 0.52$ μg ml^{-1}) and varied concentrations (1.0×10^{-5}–1.0×10^{-1} mol l^{-1}) of

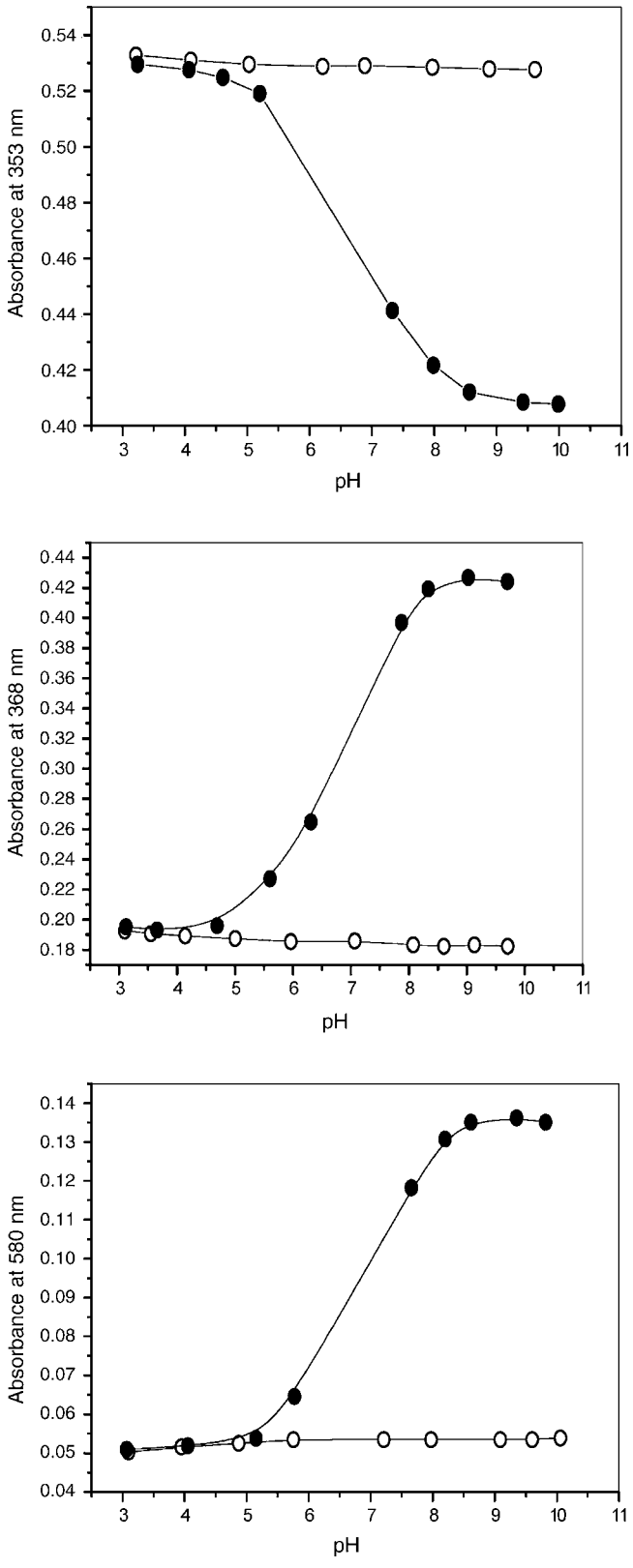


Fig. 4. Effect of pH on the absorbance of: (-◯-◯-) (ACCbs) and (-●-●-) (DCCbs) at 353, 368 and 580 nm.

Table 1
Tolerance limits (change in absorbance $\leq \pm 5\%$) of some diverse ions on the reaction of aquacyanocobester with cyanide [cyanide = 0.52 μg ml^{-1}]

Diverse ion (DI)	Tolerance ratio [DI:CN^-], w/w		
	353 (nm)	368 (nm)	580 (nm)
NO_2^-	160	175	197
NO_3^-	180	195	225
F^-	186	189	215
Cl^-	263	236	338
I^-	530	520	615
SO_3^{2-}	7	35	75
Br^-	610	650	770
SCN^-	168	190	195
SO_4^{2-}	600	650	810
Citrate	535	610	735
Tartrate	510	550	670
Oxalate	580	630	650
PO_4^{3-}	520	550	620

some foreign ions such as SCN^-, I^-, F^-, Br^-, Cl^-, NO_3^-, NO_2^-, SO_3^{2-}, SO_4^{2-}, PO_4^{3-}, oxalate, citrate and tartrate. These species are potential interferents with cyanide ion and commonly present in some electroplating baths. Since prior distillation step was utilized, gas releasing ions such as NO_2^- and SO_3^{2-} ions were also tested. The foreign species was considered as interferent if it caused an error of $\pm$ 5% of the analytical signal of the DCCbs complex. The ratio of CN^-:interferant was varied and the tolerated concentrations were obtained. Table 1 summarizes the tolerance limits of various tested foreign ions. The results revealed that most of the common ions have no interfering effect on the proposed spectrophotometric method for determination of cyanide. The interference of SO_3^{2-} ion as well as many heavy metal ions on the determination of cyanide ions was circumvented through acid distillation of the cyanide test solutions in presence of $PbCO_3$ [1,9,15].

3.4. Effect of reagent concentration

Portions of ACCbs reagent (1.0×10^{-5} mol l^{-1}) at pH 9.5 were allowed to react with a series of varied cyanide concentrations (3.8×10^{-7}–4.6×10^{-5} mol l^{-1}) and the absorbances were measured at 353 nm, 368 and 580 nm. It was found that maximum absorbance appeared at the stoichiometry of 1:1 ACCbs:CN^- molar ratio. A reagent solution (2.0×10^{-4} mol l^{-1}) was used for all subsequent measurements of 7.7×10^{-7}–4.6×10^{-5} mol l^{-1} ($\equiv$ 0.02–1.2 μg ml^{-1}) cyanide ion.

3.5. Determination of cyanide

Under optimized conditions, the proposed assay method was validated according to the standard quality control/quality assurance standards [49]. The linear response range, lower detection limit, accuracy (recovery), precision or repeatability (CV_w), between-day variability (CV_b) and sensitivity (slope) were measured. Six batches (six determinations each) with standard 0.5 μg ml^{-1} cyanide solution were spectrophotometrically

Table 2
Performance characteristics of aquacyanocobester based spectrophotometric batch method for the determination of cyanide

Parameter	λ_{max} = 353 nm[a]	λ_{max} = 368 nm[a]	λ_{max} = 580 nm[a]
Linear range (μg ml^{-1})	0.04–1.20	0.04–1.20	0.02–1.20
Detection limit (μg ml^{-1})	0.02	0.02	0.02
Slope	0.301	0.664	0.325
Correlation coefficient (r^2)	0.9999	0.9995	0.9997
Standard deviation (σ)	0.13	0.37	0.17
Between-day variability (CW_b) (%)	0.5	0.8	0.7
Within-day repeatability (CV_w) (%)	0.3	0.5	0.2
Accuracy (%)	99.2	96.8	97.6
Molar absorptivity (ε)	0.78×10^4	1.72×10^4	0.84×10^4
Optimum (pH)	8.5–10.0	8.5–10.0	8.5–10.0

[a] Average of six measurements.

measured using ACCbs reagent and monitoring the increase of the absorbances at 368 and 580 nm and the decrease of the absorbance at 353 nm. The results obtained are presented in Table 2. At pH 9.5, Beer's law was obeyed over the concentration ranges of 0.04–1.20, 0.04–1.20 and 0.02–1.20 μg ml^{-1} with a detection limit of 0.02 μg ml^{-1} cyanide at 353, 368 and 580 nm, respectively (Fig. 5). The relative standard deviations were 0.13, 0.37 and 0.17% (n = 6) and the slopes of the calibration curves were 0.301, 0.664 and 0.325 at 353, 368 and 580 nm, respectively. The lower limit of detection was calculated according to IUPAC recommendations [50]: lower limit of detection = $K\,S_0/S$ where S_0 is the standard deviation of the blank measurements

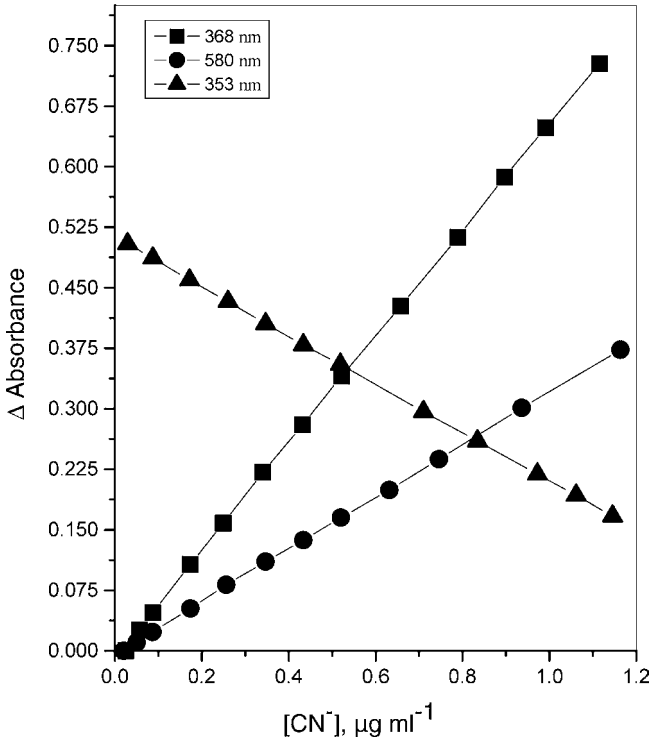


Fig. 5. Calibration plots of cyanide at different wavelengths.

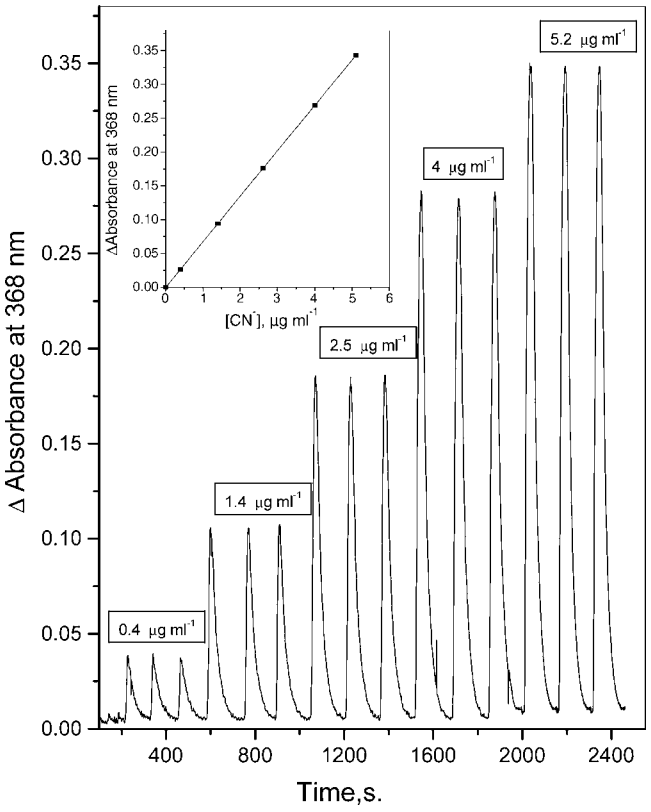


Fig. 6. Flow chart for spectrophotometric determination of cyanide based on (ACCbs) reagent at 368 nm.

(n = 6), S is the slope of the calibration curve and K is a numerical factor depending on the degree of confidence level needed. With K = 3 (i.e. 3 S_0) the detection limit was 20 ng ml^{-1}.

3.6. Flow injection analysis

The flow injection variables were studied, including sample injection volume, rate of flow, length of the flow Tygon tubes and the distance between the injection valve and spectrophotometric cell.

Flow injection measurements of cyanide using ACCbs were examined, by using a carrier solution consisting of 8.0×10^{-4} mol l^{-1} ACCbs at pH 9.5. Portions (100 μl) of the standard and test cyanide solutions were injected in a low-dispersion flow injection manifold. Typical representative out put signals of 0.4–5.2 μg ml^{-1} cyanide are shown in Fig. 6. The lower limit of detection is 0.25 μg ml^{-1} which is higher than that obtained by batch measurements, probably due to sample dilution. The measurements were made at the most sensitive 368 nm band, using a flow rate of 1.75 ml min^{-1}. The sampling rate was approximately 26–30 determinations per hour. The return time (recovery time), defined as the period between the appearance of the maximum signal of cyanide concentration ($\leq$ 2 μg ml^{-1}) and the return to the base line, was less than 1.7 min. With high cyanide concentrations ($\geq$ 4 μg ml^{-1}), the recovery time was less than 2.5 min. No base line shift or absorbance drift was observed throughout a 1 h run.

Table 3
Batch and flow injection spectrophotometric determination of cyanide in some industrial electroplating wastewater using aquacyanocobester chromogen

Wastewater	Cyanide ($\mu g\,ml^{-1}$)[a]		
	Spectrophotometry		Potentiometry [34,40]
	Batch	FIA	
Electroplating silver bath	225.3	223.1	222.4
Electroplating gold bath	323.5	322.8	325.7
Reins silver bath	105.7	108.4	103.6
Reins gold bath	118.2	119.1	115.4
Electroplating main out fall	42.9	41.7	43.6
The main out fall	5.3	4.6	3.9

[a] Average of six determinations.

Previously described on-line methods for determining CN^- involved different approaches. One approach is the use of on-line columns packed with either silica gel beads embedded by solid $CdCO_3$ [51] or CuS [52] to allow conversion of CN^- into soluble cadmium and copper cyano complexes followed by atomic absorption spectrometric measurement of cadmium and copper, respectively. However, these heterogeneous conversion reactions are influenced by many kinetic factors. Whereas the pH influenced the solubility of $CdCO_3$ and other side reactions with the carrier solution yielding variable background values [51], the mole ratio of Cu:CN reaction was found to be ~1:15 compared to a predicted 1:5 ratio revealing one-third conversion efficiency [52].

Table 4
Analytical features of some spectrometric methods used for batch and flow injection (on-line) determination of cyanide

Reagent	λ_{max} nm	pH	Range of detection, $\mu g\,ml^{-1}$	Lower detection limit, $\mu g\,ml^{-1}$	Interferents	Reaction time, or sample rate	Ref.
1,3-Dimethyl barbituric acid	600	5.3	0.005–0.5	0.005	Ni^{2+}, Co^{2+}, Mn^{2+}, Hg^{2+}, S^{2-}, SCN^-	5 min	[2]
1,4-Phenylenediamine[a]	515	–	0.005–100	0.005	Fe^{2+}, Ni^{2+}, Cu^{2+}, SCN^-	25 min	[4]
Benzidine[a]	522	–	0.2–20	0.2	SCN^-	10 min	[6]
KIO_3/I^-/cetyltrimethyl ammonium bromide/emulsifier	365	7	0–0.48	–	S^{2-}, SO_3^{2-}, $S_2O_3^{2-}$	10 min	[7]
Iodine/iodide/starch	570	7	0.02–0.80	0.02	S^{2-}, SO_3^{2-}, $S_2O_3^{2-}$	10 min	[8]
Formaldehyde/3-methyl -2-benzo-thiazolinone hydrazone	635	8.5–9.5	0.01–0.20	0.01	Hg^{2+}, Fe^{3+}, Fe^{2+}, S^{2-}, SCN^-	45 min	[9]
Br_2/PADAP/Ni^{2+}	560	8	0.50–15.0	0.02	S^{2-}, heavy metal ions	20 min	[15]
Tyrosinase/L-tyrosine	475	7.4	0.26 –7.8	0.26	–	5 min	[16]
2,2-Dihydroxy-1,3-indanedione	510	10	0.01–1.0	0.01	SCN^-, heavy metal ions	15 min	[17]
Ninhydrin	590	12–12.8	0.04–0.24	0.018	Fe^{2+}, Cu^{2+}, V^{5+}	30 min	[19]
2,6-Dihydroxy3-(4′,5″-dimethyl-2′-thiazolylazo)/Ni^{2+}	550	8.2	0.30–10.4	0.30	NR	25 min	[21]
N-(2′-Thiazolyl)-2-hydroxybenzamide/Ag^+	445	8	0.096–0.90	0.09	NR	Few minutes	[22]
Phenolphthalein	552	10.3	0.60–4.30	0.10	S^{2-}, oxidizig agents, halogens, aldehydes	Few seconds	[23]
CNBr/pyridinium chloride/sulfanilic acid	460	–	0.50–3.00	0.50	NR	–	[24]
5-(4-Sulfophenylazol)-8-aminoquinoline	600	9	Up to 0.20	–	Cu^{2+}, Co^{2+}, Ag^+, Zn^{2+}, Hg^{2+}, Pb^{2+}	15 min	[25]
Antipyridyldiazoamino-2,4-dinitrobezene/Ag^+	546	–	0.28–8.0	0.20	Cd^{2+}, Ni^{2+}, Hg^{2+}, Zn^{2+}, Cu^{2+}, SO_3^{2-}	–	[26]
Cadmium carbonate	228.8AAS	10	Up to 15	0.20	Cl^-, I^-, F^-, SCN^-, SO_4^{2-}	FIA (1 line) 72 sample h^{-1}	[51]
Cupric sulfide	324.7 AAS	11	1.0–50	1.0	Citrate	FIA (1 line) 40–50 sample h^{-1}	[52]
Chloramine-T/pyridine/barbituric acid[a]	578	6–8	0.3–5.0	0.1	Br^-, I^-, SCN^-, Ag^+, Cu^{2+}, Ni^{2+}	FIA (4 lines) 20 ample h^{-1}	[53]
1,3-Dimethyl barbituric acid[a]	600	12	0.001–0.250	0.006	SCN^-, NO_3^-, NO_2^-, SO_3^{2-}, CO_3^{2-}	FIA (5 lines) 22 sample h^{-1}	[54]
Phenolphthalin/cupric sulfide	552	10.3	0.6–4.30	0.6	Ferricyanide, halogens, aldehydes	FIA (3 lines) 70 sample h^{-1}	[55]
2,2′-Dipyridyl-2-quinolylhydrazone/Cu^{2+}	540	5.8	Up to 3.0	0.004	SCN^-	FIA (4 lines) 60 sample h^{-1}	[56]
Aquacyanocobester	353	9.5	0.04–1.20	0.02	SO_3^{2-}	20 s (batch)	Present work
	368		0.04–1.20				
	580		0.02–1.20	0.25			
	368		0.40–5.20			FIA (1 line) 30 sample h^{-1}	

NR: not reported, AAS: atomic absorption spectrometry, FIA: flow injection (on-line) analysis.
[a] Carcinogenic reagent.

The second FI approach involved a conversion of CN^- into CNCl by reaction with chloramine-T, followed by a second reaction with either pyridine-barbituric acid [53] or 1:3-dimethylbarbituric acid [54] at 35–40 °C. Both methods involved the use of several buffers and reagents and utilized a multi channel FI setup. Since, CNS^- and CN^- ions responded to the same reaction, measurement of CN^- was carried out by assessment of the total $CN^- + CNS^-$ in one run, masking of CN^-, measurement of CNS^- in a second run and calculation of CN^- concentration by difference [54].

The third approach was based on a reaction of CN^- with either phenolphthalin/copper sulfide,in a packed column, [55] or with copper(II)/2,2′-dipyridyl-2-quinolylhydrazone [56] followed by spectrophotometric measurement of the reaction products. Whereas the first reagent is not stable, the second method involved solvent extraction and two runs for measurement of CN^- in the presence of CNS^-. The proposed FI method, however, has the advantages of the use of only one sensitive and selective reagent at room temperature in a single channel manifold for direct determination of CN^- without any significant interference from CNS^- and many other common anions.

3.7. Determination of cyanide in industrial wastewater

Flow injection spectrophotometric determination of cyanide in industrial wastewater samples of electroplating baths was made after prior distillation with acid to decompose the metal cyanide complexes and to liberate and absorb HCN in alkaline solution. This permitted elimination of most interferents and measurements of as low as 0.04 μg ml^{-1} cyanide at 368 nm. The mean recovery obtained for determining 1.0 μg ml^{-1} (six measurements) at the most sensitive 368 nm absorption band was 98.7% with a relative standard deviation of ± 0.5%. These results (Table 3) were compared with data obtained with potentiometry using a solid state cyanide ion selective electrode [40]. The data obtained by both methods were in good agreement.

At 95% confidence limit, the calculated Student's *t*-value (0.73) did not exceed the theoretical value (1.94). An *F*-test, revealed no significant difference between the means and variances of the two set of results. A comparison of the main analytical features of the proposed method was made with many of the previously published batch and on-line spectrophotometric and atomic absorption spectrometric methods (Table 4). Some of these methods exhibited higher detection limit (100–500 μg ml^{-1}) [4,6,21–24,27], longer reaction time (5–30 min) [2,4,8,10,15,17,19,21,25] and serious interferences by F^-, Cl^-, Br^-, I^-, S^{2-}, $SO_3{}^{2-}$ $SO_4{}^{2-}$, $NO_3{}^-$, $NO_2{}^-$, $CO_3{}^{2-}$, citrate and SCN^- ions [17,19,23,26,51–56]. Nature of the reactions, linear range, lower detection limits, interferents, number of sample output and number of manifold channels used in the published FIA of cyanide are also shown in Table 4. The present method, however, displayed lower detection limit (0.02 μg ml^{-1}), shorter reaction time (~20 s for batch and 2 min for FIA) and tolerance of high concentrations of many interfering common ions including CNS^-.

4. Conclusions

The reaction of aquacyanocobyrinic acid heptamethyl ester (aquacyanocobester, ACCbs) with cyanide ion at pH 9.5 develops an intense violet color due to the formation of dicyanocobester (1:1 ACCbas:CN complex). The reaction is highly selective for cyanide in the presence of many common ions. The spectrum of the reaction product shows a decrease of the absorption band at 353 nm. Variations of the absorbancies at 353,368 and 580 nm are linearly related to cyanide concentrations over the range 0.04–1.2 μg ml^{-1}. The method is used for manual and flow injection analysis of low cyanide concentrations down to 20 ng ml^{-1} and allows monitoring of cyanide at three different wavelengths by the same reaction in one run. The relative standard deviation is 0.3–0.9% and the accuracy is 97.6–99.2%. Application for the determination of cyanide in electroplating wastewaters gives results agree fairly well with data obtained by potentiometric methods using the solid state cyanide ion selective electrode.

References

[1] M.A. Franson (Ed.), Standard Methods for the Examination of Water and Wastewater, 15th ed., American Public Health Association, Washington, DC, 1980.
[2] S. Bianting, N.N. Barry, Water Res. 32 (1998) 3698.
[3] E. Nakamura, M. Yagi, Bunseki-Kagaku 49 (2000) 55.
[4] L.S. Bark, H.G. Higson, Talanta 11 (1964) 621.
[5] G.V.L.N. Murty, T.S. Viswanhan, Anal. Chim. Acta 25 (1961) 293.
[6] W.N. Aldridge, Analyst 69 (1944) 262.
[7] M. Wang, D.L. Luo, Fenxi-Huaxue 28 (2000) 519.
[8] M. Wang, D.L. Luo, Y. Gong, L. Jianyan, Huaxue Fence 37 (2001) 25.
[9] K. Geetha, N. Balasubramanian, Anal. Lett. 34 (2001) 2507.
[10] H. Ishii, K. Kohata, Talanta 38 (1991) 511.
[11] Y.R. Zhu, F.S. Wei, F. Yin, Talanta 30 (1983) 795.
[12] B.S. Garg, N. Bhojak, P. Dwivedi, J.S. Bist, M.B. Aggarwal, Indian. J. Chem, (Sect. A): Inorg. Bioinorg. Phys. Theor. Anal. Chem. 38 (1999) 395.
[13] A. Velasco, M. Silva, M. Valcarcel, Talanta 38 (1991) 303.
[14] M. Hoshino, K. Nagashima, M. Kamaya, N. Nakano, Bunseki-Kagaku 52 (2003) 481.
[15] F.S. Wei, Y.Q. Liu, F. Yin, N.K. Shen, Talanta 28 (1981) 694.
[16] T. Tatsuma, K. Komori, H.-H. Yeoh, N. Oyama, Anal. Chim. Acta 408 (2000) 233.
[17] G. Drochioiu, Talanta 56 (2002) 1163.
[18] T. Fonong, Analyst 112 (1987) 1033.
[19] N. Padmarajaiah, S.H.K. Mattighatta, S.Y. Hemmige, S.P. Jainara, Anal. Sci. 18 (2002) 1027.
[20] J. Epstein, Anal. Chem. 19 (1947) 272.
[21] M.F. Garcia, M.J. Sanchez, M.A. Rodriguez, Mikrochim. Acta II (1989) 259.
[22] B.S. Garg, N. Bhojak, P. Dwivedi, J.S. Bist, M.B. Aggarwal, Indian. J. Chem, (Sect. A): Inorg. Bioinorg. Phys. Theor. Anal. Chem. 38 (1999) 395.
[23] H.A.T. Hussein, Talanta 44 (1997) 545.
[24] C.C. Chien, F.C. Chang, S.C. Wu, Mikrochim. Acta II (1980) 9.
[25] Z.J. Huang, E. Tang, J.Y. Yin, Q.H. Xu, Fenxi-Shiyanshi 18 (1999) 83.
[26] H.W. Goa, Asian J. Chem. 11 (1999) 122.
[27] C.Q. Jiang, X.Q. Li, S.M. Jiang, Fenxi Huaxue 22 (1994) 1190.
[28] F.S. Goksel, A. Aydin, A.S. Saracoglu, Chim. Acta-Turc 14 (1986) 321.
[29] F.T. Esmadi, M. Kharoaf, A.S. Attiyat, Anal. Lett. 23 (1990) 1069.
[30] B.X. Xu, T.M. Xu, Y.Z. Fang, Talanta 31 (1984) 141.
[31] S. Chattaraj, A.K. Das, Analyst 116 (1991) 739.
[32] S.S.M. Hassan, Fresenius Z. Anal. Chem. 312 (1982) 354.

[33] S.S.M. Hassan, Organic Analysis Using Atomic Absorption Spectrometry, Ellis Horwood, Chichester, England, 1984.
[34] P.C. Do-Nascimento, D. Bohrer, L.M. De-Carvalho, Analyst 123 (1998) 1151.
[35] D. Bohrer, P.C. Do-Nascimento, S.G. Pomblum, E. Seibert, L.M. de-Carvalho, Fresenius J. Anal. Chem. 361 (1998) 780.
[36] M.S. Frant, J.W. Ross, J.H. Riseman, Anal. Chem. 44 (1972) 2227.
[37] V.M. Jovanoic, M.S. Jovanavic, Analyst 113 (1988) 27.
[38] M.T. Neshkova, E.M. Pancheva, Anal. Chim. Acta 242 (1991) 73.
[39] S.S.M. Hassan, S.A.M. Marazouk, A.H.K. Mohamed, N.M. Badawy, Electroanalysis 16 (2004) 298.
[40] T.S. Ma, S.S.M. Hassan, Organic Analysis Using Ion Selective Electrodes, 1–2, Academic Press, London, 1982.
[41] S.S.M. Hassan, Anal. Chem. 49 (1977) 45.
[42] M. Nonomura, Anal. Chem. 59 (1987) 2073.
[43] G. Esposito, Anal. Chem. 57 (1985) 1168.
[44] A. Kito, K. Komatsu, Bunseki Kagaku 32 (1983) 201.
[45] R.A. Firth, H.A.O. Hill, B.E. Mann, J.M. Pratt, R.G. Thorp, R.J.P. Williams, J. Chem. Soc. (1968) 2419.
[46] A.J. Markwell, J.M. Pratt, M.S. Shaikjee, J.G. Toerien, J. Chem. Soc. Dalton Trans. (1987) 1349.
[47] M.S.A. Hamza, X. Zou, K.L. Brown, R. van Eldik, Inorg. Chem. 40 (2001) 5440.
[48] N.E. Brasch, A.G. Cregan, M.E. Vanselow, J. Chem. Soc., Dalton Trans. (2002) 1287.
[49] J.K. Tylor, Quality Assurance of Chemical Measurements, CRC Press, Boca Raton, Florida, 1987.
[50] H.M.N.H. Irving, H. Freiser, T.-S. West (Eds.), IUPAC compendium of Analytical Nomenclature, Definitive Rules, Pergamon Press, Oxford, 1981.
[51] M. Noroozifar, M. Khorasani-Motlagh, S.-N. Hosseini, Anal. Chim. Acta 528 (2005) 269.
[52] A.T. Haj-Hussein, G.D. Christian, J. Ruzicka, Anal. Chem. 58 (1986) 38.
[53] A. Rios, M.D. Luque de Castro, M. Valcarcel, Talanta 31 (1984) 673.
[54] J.C.L. Meeussen, E.J.M. Temminghoff, M.G. Keizer, I. Novozamsky, Analyst 114 (1989) 959.
[55] A.T. Haj-Hussein, Talanta 44 (1997) 545.
[56] D.G. Themelis, P.D. Tzanavaras, Anal. Chim. Acta 452 (2002) 295.

Available online at www.sciencedirect.com
ScienceDirect
Talanta 71 (2007) 1068–1074
Talanta
www.elsevier.com/locate/talanta

Microwave-assisted steam distillation for the determination of organochlorine pesticides and pyrethroids in Chinese teas

Jie Ji, Chunhui Deng, Huiqin Zhang, Yunyun Wu, Xiangmin Zhang *

Department of Chemistry, Fudan University, Shanghai 200433, China

Received 10 April 2006; received in revised form 27 May 2006; accepted 30 May 2006
Available online 7 July 2006

Abstract

In this work, microwave-assisted steam distillation (MASD) extraction method followed by gas chromatography/electron capture detection (GC/ECD) was developed for the determination of organochlorine pesticides (OCPs) and pyrethroids in the Chinese teas. MASD is a combination of microwave-assisted extraction (MAE) and steam distillation techniques. Water vapor generated by microwave irradiation is used to accelerate desorption of the analytes from the sample, and the nonpolar organic solvent used for trapping the analytes is kept from direct contact with the sample by the water. Therefore, relatively clean extracts were obtained compared to the method directly using organic solvent as extraction solvent, such as ultrasonic extraction (USE). Microwave power of 200 W and irradiation time of 2 min was found to be the optimum conditions for the MASD process, and *n*-heptane was chosen as the analyte-trapping solvent in the study. Five OCPs (α-HCH, γ-HCH, dicofol, *p*,*p*′-DDE, *p*,*p*′-DDT) and two pyrethroids (bifenthrin, fenvalate) were determined using this extraction method in the tea samples. The relative standard deviation (R.S.D.) of the analytes varied from 2.2 to 8.4%, and the method detection limits (MDLs) found were lower than 0.23 μg/kg. The recoveries of the seven compounds in the Jasmine tea sample were between 84.04 and 110.1%. Comparative results obtained by MASD and USE were also discussed in the study.
© 2006 Elsevier B.V. All rights reserved.

Keywords: Microwave-assisted steam distillation; Organochlorine pesticides; Pyrethroids; Analyte-trapping solvent; Chinese teas

1. Introduction

Organic pollutants have been shown to exhibit potentially harmful effects to the environment and human beings. As an example pesticides used in agricultural as well as industrial should be considered as hazardous chemicals with great concern for the general population. Organochlorine pesticides (OCPs) and pyrethroids are two kinds of the most widely used pesticides, for they have been effective in the control of pests and diseases. Due to their low biodegradability and high persistence, they are ubiquitous among environmental samples, such as food, air, water, soil, sediments and biological tissues [1–4]. Moreover, these chemicals are known to induce cancer and be endocrine disrupters in several organisms for their toxic characteristic. Although the use of most OCPs and pyrethroids has been banned or restricted in industrialized countries, they are still detected in the environment [5–8].

OCPs and pyrethroids, like dicofol and fenvalate, are widely used in the teas, mainly for the purpose of eliminating the mite and other pests. Tea has been the most favourite drink since thousands of years ago in China, and nowadays it is also very popular in the other countries of the world for its characteristic aroma, flavor and health benefits [9]. But only a few studies were published in the area of pesticides research for the Chinese teas [10,11]. The complexity of the matrix made the identification and quantification of pesticides in Chinese teas difficult. Soxhlet extraction and ultrasonic extraction (USE), followed by a complicated clean-up process, are the conventional sample preparation method before gas chromatography/electron capture detection (GC/ECD) for the determination of OCPs and pyrethroids in the tea.

Microwave-assisted extraction (MAE) of organic pollutants was first introduced in 1986 by Ganzler et al. [12]. Since that time, this extraction technique has been successfully applied to extract organic compounds, such as PAHs, pesticides, PCBs and phenols, from various solid and liquid matrices, such as sediments, soils, plant materials and water samples [13–17]. MAE was more effective and reduced the sample preparation time and

* Corresponding author. Fax: +86 21 65641740.
E-mail address: xmzhang@fudan.edu.cn (X. Zhang).

0039-9140/$ – see front matter © 2006 Elsevier B.V. All rights reserved.
doi:10.1016/j.talanta.2006.05.087

solvent volumes substantially in comparison with conventional extraction techniques, as the heating during MAE is based on the direct effect of microwaves on molecules by ionic conduction and dipole rotation. MAE solvents for the extraction of organic pollutant are usually *iso*-octane, acetonitrile, dichloromethane (DCM) [18–20], acetone [21,22] and mixtures of low relative permittivity solvents with acetone, as *n*-hexane–acetone [21–26]. Water also acts as an efficient extraction solvent of MAE process, because water molecules with a high dielectric constant were characterized by a high ability to absorb microwave energy [27]. But other extraction methods, like solid phase microextraction (SPME) and liquid phase microextraction (LPME), are usually combined with MAE as a further preparation for the sample, when the extraction solvent is water [28–30].

In this work, a novel microwave-assisted steam distillation (MASD) extraction method was applied for the determination of OCPs and pyrethroids in Chinese teas. MASD technique, which uses water as the extraction solvent, is a combination of MAE and steam distillation method. The samples of Chinese teas, which were immersed in the water solvent, were heated by microwave irradiation. Under this condition, the analytes (OCPs and pyrethroids) were desorbed from the matrix with water vapor, and absorbed by the nonpolar organic solvent covered on the water. Then the extracts with very little clean-up were analyzed by GC/ECD. This method gives relatively clean extracts in comparison with conventional MAE using organic solvent. In MAE, direct contact between organic solvent and sample matrix often causes low selectivity for the extracts, but mainly hydrophobic and volatile or semi-volatile compounds are recovered by the combination with steam distillation [32–34], in some cases, even clean-up is unnecessary for GC analysis [31]. In addition, MAE and steam distillation are the coinstantaneous process in MASD, so the total extraction time of MASD is relatively short compared to the MAE–SPME [35–37] or MAE–LPME technique. Jasmine tea, Longjing tea and Maofeng tea were analyzed by MASD–GC/ECD in this report, and the effects of the extraction conditions on efficiency and a comparison between this method and USE are also presented.

2. Experimental

2.1. Reagent and samples

Distilled water was purified by a Milli-Q system (Milford, MA, USA). Analytical grade acetone, *n*-hexane, *n*-heptane, *n*-octane, cyclohexane, Florisil and activated carbon were from Guoyao (Shanghai, China). Pesticide standards of OCPs (α-HCH, γ-HCH, dicofol, *p*,*p*′-DDE, *p*,*p*′-DDT) and pyrethroids (bifenthrin, fenvalate) were obtained from Supelco (Bellefonte, PA, USA). Stock solutions were prepared for each compound respectively in hexane with a concentration of 100 μg/ml. Heptachlor, also obtained from Supelco, was used as internal standard (IS) in the study, for it was not detected in the samples of Chinese teas. Prepared stock solution of IS was 10 μg/ml. All the stock solutions were stored in a refrigerator at 4 °C. Standard solutions of analytes at the concentration level of interest were prepared daily from the stock solution, and 100 ng of IS was added in each solution.

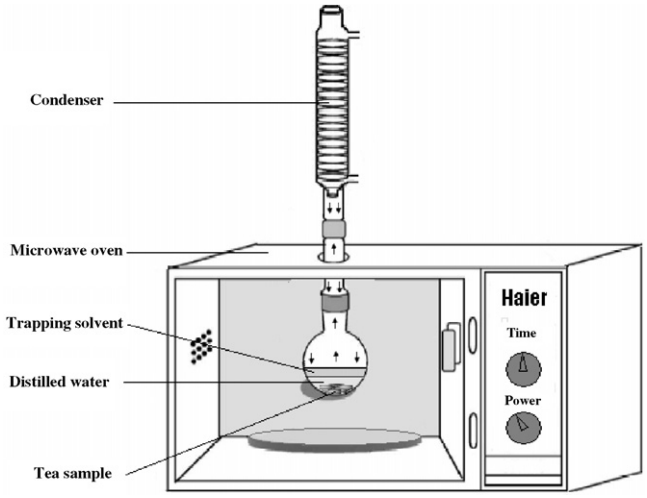


Fig. 1. Extraction apparatus of the microwave-assisted steam distillation.

Three kinds of Chinese teas, Jasmine tea, Longjing tea and Maofeng tea, were purchased from local supermarket (Shanghai, China). All of them are classified into green tea according to the degree of fermentation (unfermented).

2.2. Microwave-assisted steam distillation procedure

The apparatus of MASD used in this study is shown in Fig. 1. After addition of 200 ng heptachlor, 2 g Jasmine tea sample was put into a 100 ml round-bottom flask containing 25 ml distilled water. After the sample soaked up the water in a few minutes, 20 ml of nonpolar organic solvent used for analyte-trapping solvent, such as *n*-hexane, *n*-heptane, *n*-octane and cyclohexane, was added to the flask to cover the distilled water. Then the flask was put into a MO-2270M1 model microwave oven (Haier, Qingdao, China). The flask with the tea sample was heated by a microwave at the power of 100–400 W for 2–6 min, and a condenser with a continuous flow of freezing water was used to condense the water vapour, so that the water could take part in the extraction process repeatedly. Upon the termination of the microwave irradiation, the flask was cooled in the air. After cooling, the organic solvent was removed and concentrated to 1 ml using a rotary evaporator without heating. Then, the concentrated extract was passed through a glass extraction cartridge (8 mm i.d.) packed with 1.0 g anhydrous sodium sulfate, 0.4 g activated carbon and 0.5 g activated Florisil, which was rinsed with *n*-hexane after packing. The analytes were eluted from the column with 10 ml acetone–*n*-hexane solvent (1:1, v/v) and collected in a 50 ml pear-shaped flask. And the eluate was concentrated to 1 ml by a rotary evaporator.

2.3. Ultrasonic extraction procedure

An ultrasonator model DS-5510 (Shangchao, Shanghai, China) was used in USE procedure. After addition of 200 ng heptachlor, 2 g Jasmine tea sample was put into a 50 ml vial

(Chromacol, Herts, UK), and the vial was sealed with an aluminum cap with PTFE-silicon septa. About 20 ml acetone–*n*-hexane (1:1, v/v) was then put into the vial. One hour latter, the vial with sample completely immersed in the solvent was sonicated with continuous power for 30 min. After a 15 min cooling step, the raw extract was transferred to a pear-shaped flask. The remained teas were washed three times with 1 ml portions of *n*-hexane. The combined solution of raw extract and wash solution was filtered and concentrated to 1 ml using a rotary evaporator without heating. Then the concentrated extract was passed through a solid phase extraction (SPE) cartridge (15 mm i.d.) packed with 1.0 g anhydrous sodium sulfate, 3.0 g activated carbon and 4.0 g activated Florisil, which was rinsed with *n*-hexane after packing. The analytes were eluted from the column with 20 ml acetone–*n*-hexane solvent (1:1, v/v) and collected in a 50 ml pear-shaped flask. And the eluate was concentrated to 1 ml by a rotary evaporator.

2.4. Instruments

Analyses of OCPs and pyrethroids in the extracts were performed using a gas chromatograph system CP-3800 (Varian, Palo Alto, USA) with electron capture detector. The GC/ECD system was equipped with a CP-Sil 5 CB fused silica capillary column (15 m × 0.25 mm i.d., 0.25 μm film thickness), and nitrogen (99.999%, purity) was used as the carrier gas at 1 ml/min flow rate. The injection port temperature was set at 280 °C, and detector temperature was 330 °C. The injector was operated in splitless mode, and an amount of 1 μl concentrated extract was injected. Analytes were separated an oven temperature program built as follows: initial temperature 75 °C (hold at 2 min), increased at 25–200 °C/min (hold 2 min) and finally increased at 6–280 °C/min (hold 8 min).

2.5. Analytical data

Linear range for the analytes was studied by replicate analysis of the standard solutions (from 0.1 to 2000 ng/ml) spiked with 100.0 ng/ml heptachlor (IS), and 1 μl standard solution was directly injected and analyzed by GC/ECD system. The linear regression values were calculated with the average peak areas of three replicate injections for each analyte. Recoveries of the analytes were studied with Jasmine tea spiked with 63.4 ng α-HCH, 80.2 ng γ-HCH, 913.6 ng dicofol, 78.0 ng *p*,*p*′-DDE, 649.2 ng *p*,*p*′-DDT, 861.0 ng bifenthrin, 739.2 ng fenvalate and 200.0 ng heptachlor (IS). And apparent recoveries of all the analytes using MASD were compared with the recoveries obtained by USE. Relative standard deviation (R.S.D.) was studied by the analysis of spiked Jasmine tea sample. Also, the peak height of each compound of the spiked Jasmine tea sample was used to calculate the detection limit (S/N = 3) of this work.

3. Results and discussion

3.1. The extraction device

Fig. 1 shows the extraction device of MASD used in this study. Because microwave was not absorbed by the nonpolar organic solvent, it penetrated the nonpolar solvent and directly heated the water solvent with the tea sample immersed in. Then, the analytes (OCPs and pyrethroids) in the sample were desorbed from the matrix, and absorbed by the nonpolar organic solvent covered on the water. It was supposed that the water vapor accelerated vaporization of the volatile and semi-volatile solvent, including OCPs and pyrethroids. Then the water was condensed on the inner face of the condenser and took part in the extraction repeatedly. Through this process, OCPs and pyrethroid molecules carried by water vapor were trapped in the nonpolar organic solvent without direct contact between the organic solvent and the tea sample. After extraction, the green color of the organic solvent was much lighter than that obtained by the extraction with direct contact between organic solvent and the sample, such as USE and MAE. And the distilled water used as extraction solvent was dark yellow and turbid, with small sediment and particles in it. So the MASD is a relatively selective extraction method, and mainly hydrophobic and volatile or semi-volatile compounds are recovered by the extraction process.

Enough amount of water was supposed to be used in this MASD procedure in order to keep the tea sample from direct contact with the organic solvent. And a comparatively short microwave irradiation time was used to prevent the excessive vaporization of water for the same reason. In this work, 25 ml water was used and it proved to be a proper amount to the extraction in the subsequent experiment, for it reached the equilibrium between vaporization and condensation during the extraction process. The extraction time used in MASD was from 2 to 6 min, and the effect of extraction time will be discussed later.

The vaporization of a part of nonpolar organic solvent covered on the water was also accelerated by the water vapor during the extraction process, and it resulted in poor extraction efficiency if the ratio of vaporized solvent was too high. In the work, 20 ml nonpolar organic solvent, a relatively large amount of solvent, was used to avoid this influence. Also, a continuous flow of freezing water was used for the condenser to accelerate the speed of condensation.

3.2. Optimization of MASD procedure

The effects of organic extraction solvent, microwave power and microwave extraction time of MASD were investigated in the study. Jasmine tea sample spiked with 200.0 ng heptachlor (IS) were treated through MASD method described above. The extraction efficiency of dicofol, *p*,*p*′-DDE, bifenthrin and fenvalate in the sample were investigated and the analytical results obtained by GC/ECD measurement under different conditions were compared to obtain the optimum extraction conditions.

3.2.1. Selection of extraction solvent

In the proposed method, the extraction solvent should have little capacity of microwave absorption, and good extraction efficiencies for the analytes. Nonpolar solvent can absorb less microwave energy than polar solvent, so, the nonpolar organic solvent was considered. Effects of the organic extraction solvent on dicofol, *p*,*p*′-DDE (OCPs) and bifenthrin, fenvalate

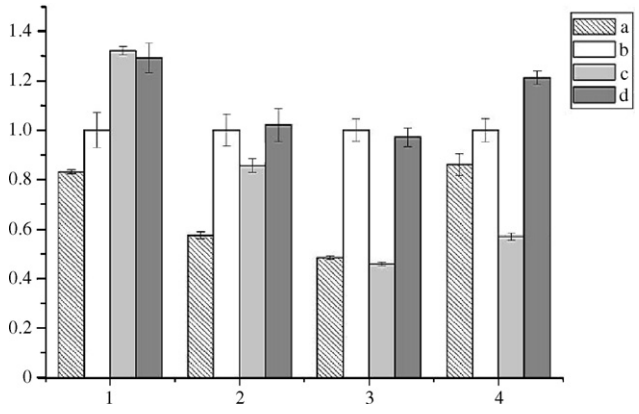


Fig. 2. Effect of different analyte-trapping solvent for the MASD process of the Jasmine tea. Solvent: cyclohexane (a), *n*-hexane (b), *n*-octane (c), *n*-heptane (d). Compounds: dicofol (1), *p*,*p*′-DDE (2), bifenthrin (3), fenvalate (4). Microwave power: 230 W, microwave extraction time: 2 min.

(pyrethroids) analysis in Jasmine tea are shown in Fig. 2. Four kinds of different nonpolar organic solvent (cyclohexane, *n*-hexane, *n*-octane and *n*-heptane) were used as the analyte-trapping solvent of the MASD (microwave power: 230 W, microwave extraction time: 2 min). Results obtained by the USE–GC/ECD measurement were compared, and the solvent that gave the best extraction efficiencies of the four pesticides was select. Aromatic hydrocarbon such as toluene was not investigated in this study because of the low recovery yields. It might be caused by the absorption of microwave irradiation [31]. Observed concentrations in Fig. 2 are the mean values of triplicate measurements (error bars, S.D.), and they are shown as the relative value normalized to the values obtained by *n*-hexane. Although it gave the best extraction efficiency of dicofol while *n*-octane was used as the trapping solvent, the extraction efficiency of pyrethroids was poor compared to the other solvents. Among the four solvents, *n*-heptane was selected as the organic trapping solvent for the further study, because it relatively gave the best extraction efficiency of the four analytes studied. But the reason for the difference in the extraction efficiency of the organic solvent tested was not clear yet.

3.2.2. Microwave extraction time and power

The effects of microwave extraction time and microwave power on the analytical results are shown in Fig. 3. *n*-Heptane was used for MASD, and the analytical results (peak areas normalized to the IS) of dicofol, *p*,*p*′-DDE, bifenthrin and fenvalate in Jasmine tea obtained by GC/ECD measurement depending

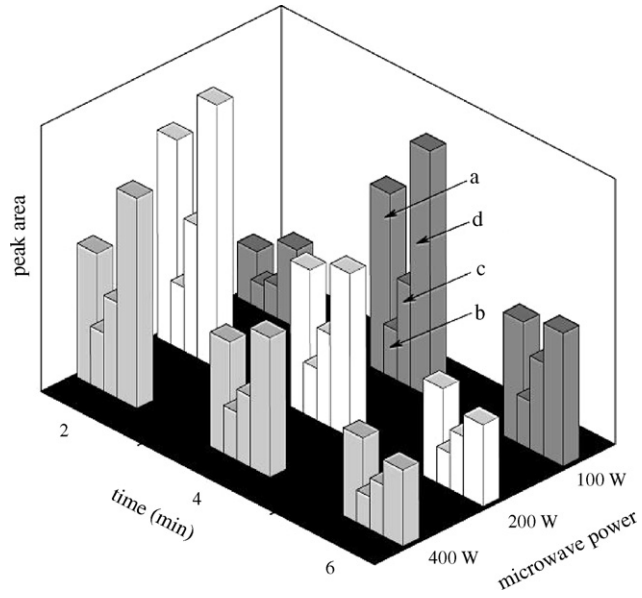


Fig. 3. Effect of microwave power and irradiation time on detector response area for the MASD process of the Jasmine tea. Compounds: dicofol (a), *p*,*p*′-DDE (b), bifenthrin (c), fenvalate (d). Analyte-trapping solvent: *n*-heptane.

on microwave extraction time and microwave power were compared. When the microwave power was 100 W, extraction time of 4 min gave the best extraction efficiency. But the peak areas would reach a relative maximum at the extraction time of 2 min when the microwave power was 200 and 400 W. Then a decrease was observed for longer exposure times, possibly due to degradation of the compounds resulting from higher temperature. Meanwhile, response signals observed mostly decreased when the microwave power increased at the same irradiation time, also for reasons of the degradation of the analytes. As seen from Fig. 3, the best extraction efficiency was obtained at microwave power of 200 W and extraction time of 2 min. The MASD conditions were then used for the followed study.

3.3. Method validation

Several levels of standard solutions (from 0.1 to 2000 ng/ml) spiked with 100.0 ng/ml heptachlor (IS) were directly analyzed by GC/ECD system. The linear range and linear regression values were obtained by the analytical results of GC/ECD measurement. The accuracy of the determination of OCPs and pyrethroids was quantified by the recovery of 2 g Jasmine tea sample spiked with standard analytes and IS. The precision

Table 1
Analytical performance characteristics of combined MASD–GC/ECD measurement for OCPs and pyrethroids determinations in Jasmine tea sample

Analytes	R^2	Intraday R.S.D. (%)	Interday R.S.D. (%)	LOD (μg/kg)	Linear range (ng/ml)	Recovery yields (%)
α-HCH	0.9921	8.4	10.9	0.025	0.1–100	96.84
γ-HCH	0.9974	6.9	9.7	0.049	0.2–200	84.04
Dicofol	0.9939	4.7	6.6	0.21	1–2000	110.1
p,*p*′-DDE	0.9922	6.5	8.6	0.039	0.2–100	88.20
p,*p*′-DDT	0.9960	5.1	7.1	0.19	1–1000	98.80
Bifenthrin	0.9948	3.9	5.9	0.17	1–1000	97.47
Fenvalate	0.9988	2.2	3.7	0.23	1–1600	97.79

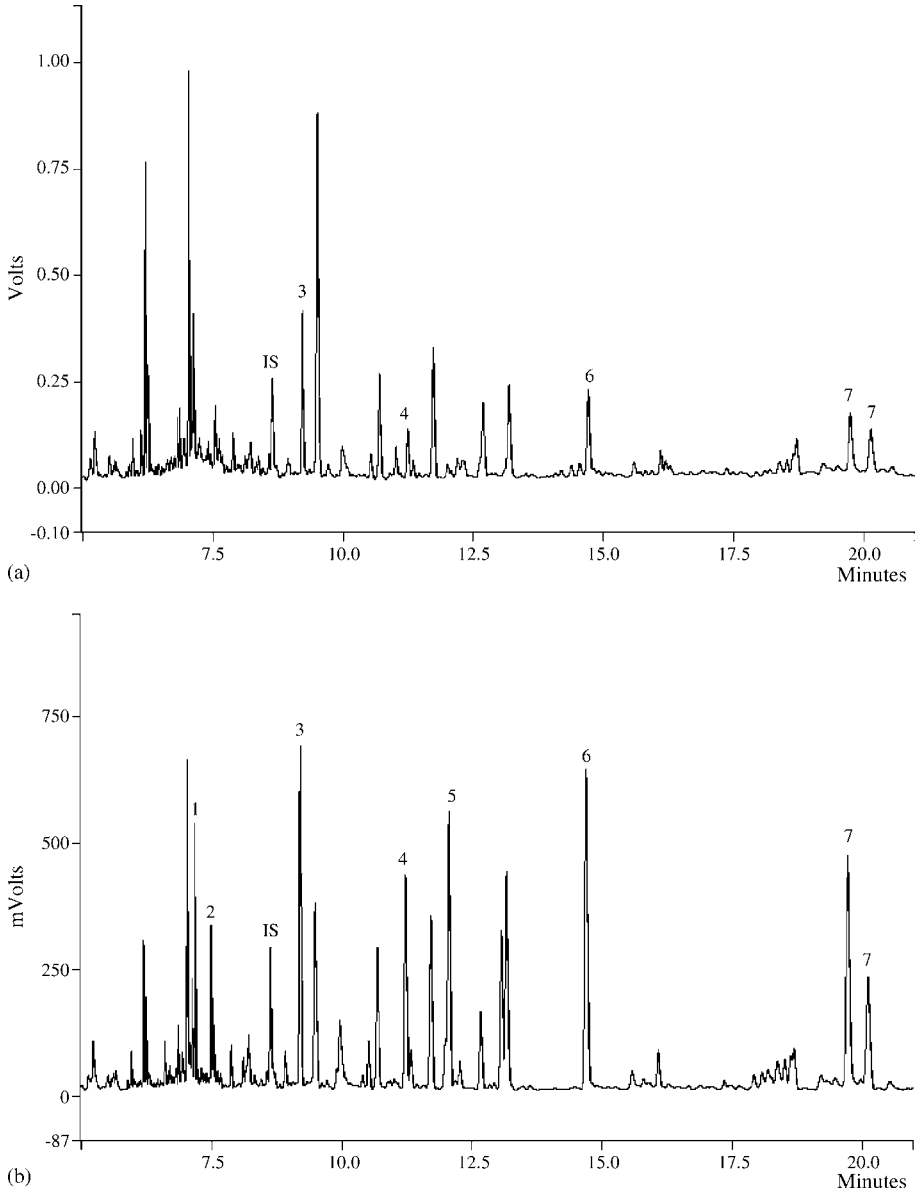


Fig. 4. GC/ECD chromatograms of the Jasmine tea sample. (a) The Jasmine tea sample using MASD extraction. (b) The Jasmine tea sample spiked with standard analytes using MASD extraction. Peaks: α-HCH (1), γ-HCH (2), dicofol (3), *p*,*p*′-DDE (4), *p*,*p*′-DDT (5), bifenthrin (6), fenvalate (7), heptachlor (IS). Chromatographic conditions: microwave power: 230 W, microwave extraction time: 2 min. Analyte-trapping solvent: *n*-heptane.

was expressed by the relative standard deviation (R.S.D.) values for both interday and intraday, and the R.S.D. values were given in Table 1. LOD was also calculated from the analytical results (Table 1). The correlation coefficients of the linear calibration curves for all the analytes were above 0.9921. The precision of the method evaluated by three replicated determinations was less than 9%, and the limits of detection (LODs) calculated via three times the background noise level were below 0.23 μg/kg.

Fig. 4a and b are the chromatograms of Jasmine tea sample and Jasmine tea sample spiked with standard analytes (as discussed in Section 2.5) respectively obtained by MASD–GC/ECD measurement. Fenvalate has four isomers, and gives two peaks on a CP-Sil 5 CB fused silica capillary column, and the peak area sum of the two peaks was used to calculate the fenvalate concentration. The method was then applied to the determination of OCPs and pyrethroids in Longjing tea and Maofeng tea separately. The concentrations of OCPs and pyrethroids determined in the three kinds of Chinese tea samples are summarized in Table 2. The existences of these compounds were identified by the retention time. Dicofol, bifenthrin and fenvalate were the three compounds detected in all the tea samples, and they were proved to be three kinds of the most widely used pesticides in the teas, for the purpose of eliminating the mite and other pests. On the other hand, HCHs that used to be the OCPs often used in the vegetables and fruits were not found in either tea sample. The concentrations of dicofol, *p*,*p*′-DDE, bifenthrin and fenvalate in the Jasmine tea sample were the highest in the three kinds of teas, and it could be seen that the Jasmine tea sample was seriously polluted.

Table 2
The concentration of OCPs and pyrethroids in three kinds of Chinese tea sample

Analytes	Retention time[a] (min)	Jasmine tea (μg/kg)	Longjing tea (μg/kg)	Maofeng tea (μg/kg)
α-HCH	7.156	nd[b]	nd	nd
γ-HCH	7.469	nd	nd	nd
Dicofol	9.170	991.8 ± 22.4	53.4 ± 2.4	157.3 ± 6.9
p,p′-DDE	11.186	11.1 ± 0.9	nd	nd
p,p′-DDT	12.022	nd	4.1 ± 0.2	nd
Bifenthrin	14.662	203.0 ± 6.4	17.6 ± 1.1	86.8 ± 4.3
Fenvalate	19.675, 20.063[c]	316.8 ± 10.7	73.8 ± 2.7	8.2 ± 0.3

[a] As retention time of IS was 8.597 min.
[b] nd, lower than detection limits (S/N = 3).
[c] Fenvalate has four isomers, and gives two peaks on a CP-Sil 5 CB fused silica capillary column.

Table 3
Comparative study of OCPs and pyrethroids concentrations and recoveries using different extraction methods (Jasmine tea sample)

Analytes	MASD		USE	
	Concentrations (μg/kg)	Recovery yields (%)	Concentrations (μg/kg)	Recovery yields (%)
α-HCH	nd[a]	96.84	1.5	75.39
γ-HCH	nd	84.04	nd	63.84
Dicofol	991.8	110.1	846.0	81.15
p,p′-DDE	11.1	88.20	12.6	44.36
p,p′-DDT	nd	98.80	nd	63.37
Bifenthrin	203.0	97.47	114.7	75.35
Fenvalate	316.8	97.79	76.0	49.12

[a] nd, lower than detection limits (S/N = 3).

3.4. Comparison with ultrasonic extraction

The chromatogram of Jasmine tea sample obtained by the USE–GC/ECD measurement was also studied. Response signals decreased obviously compared to the chromatogram obtained by the MASD for the relatively poor extraction efficiency. The comparison of OCPs and pyrethroids concentrations and recoveries between MASD and USE is in Table 3. Although the concentrations of OCPs showed nearly no difference between the two extraction methods, it resulted in comparatively low concentrations of pyrethroids when the USE was used as the extraction method. The recovery yields of all the analytes by the USE were also lower than the yields by the MASD as described in Table 3.

4. Conclusions

In the study, the MASD technique followed by GC/ECD measurement had been successfully applied to the determination of OCPs and pyrethroids in the Chinese teas. Because of the relatively greater sample throughput, lower method detection limit, less extraction time and simplification of the clean-up process (the lack of necessity of solid–liquid separation and small amounts of sorbents required for clean-up), the MASD technique has the advantage of the conventional extraction methods directly using organic solvent as extraction solvent, such as the USE. Therefore, a simple technique for determination of pesticides like OCPs and pyrethroids can be performed by the MASD method.

Acknowledgement

This work was supported by Shanghai Research Project of Science and Technology on Scientific Instrument, Natural Science Foundation of China (Project No. 39870451) and National Basic Research Priorities Programme (Project No. 2001CB510202).

References

[1] S. Tanabe, H. Iwata, R. Tatsukawa, Sci. Total Environ. 154 (1994) 163.
[2] F. Wania, D. Mackay, Environ. Sci. Technol. 30 (1996) 390A.
[3] Q.X. Zhou, J.P. Xiao, W.D. Wang, G.G. Liu, Q.Z. Shi, J.H. Wang, Talanta 68 (2006) 1309.
[4] E. Porazzi, M.P. Martinez, R. Fanelli, E. Benfenati, Talanta 68 (2005) 146.
[5] A.D. Leone, E.M. Ulrich, C.E. Bodnar, R.L. Falconer, R.A. Hites, Atmos. Environ. 34 (2000) 4131.
[6] C. Gonçalves, M.F. Alpendurada, J. Chromatogr. A 968 (2002) 177.
[7] F.G. Ye, Z.G. Xie, X.P. Wu, X.C. Lin, Talanta 69 (2006) 97.
[8] C.Z. Dong, Z.R. Zeng, X.J. Li, Talanta 66 (2005) 721.
[9] C.S. Yang, J.Y. Chung, G. Yang, S.K. Chhabra, M.J. Lee, J. Nutr. 130 (2000) 472S.
[10] H.W. Hsiung, H.S. Jin, Anal. Chim. Acta 428 (2000) 111.
[11] L.S. Cai, J. Xing, L. Dong, C.Y. Wu, J. Chromatogr. A 1015 (2003) 11.
[12] K. Ganzler, A. Salgo, K. Valko, J. Chromatogr. 371 (1986) 299.
[13] K.K. Chee, M.K. Wong, H.K. Lee, J. Chromatogr. A 736 (1996) 211.
[14] J. Parera, F.J. Santos, M.T. Galceran, J. Chromatogr. A 1046 (2004) 19.
[15] C.H. Deng, N. Yao, B. Wang, X.M. Zhang, J. Chromatogr. A 1103 (2006) 15.
[16] C.H. Deng, X.Q. Xu, N. Yao, N. Li, X.M. Zhang, Anal. Chim. Acta 556 (2006) 289.

[17] J.G. Wilkes, E.D. Conte, Y. Kim, M. Holcomb, J.B. Sutherland, D.W. Miller, J. Chromatogr. A 880 (2000) 3.
[18] L.E. García-Ayuso, M. Sánchez, A. Fernández de Alba, M.D. Luquede Castro, Anal. Chem. 70 (1998) 2426.
[19] J.R. Dean, I.J. Barnabas, I.A. Fowlis, Anal. Incl. Anal. Commun. 32 (1995) 305.
[20] O.S. Fatoki, R.O. Awofolu, J. Chromatogr. A 983 (2003) 225.
[21] A. Egizabal, O. Zuloaga, N. Etxebarria, L.A. Fernĭandez, J.M. Madariaga, Analyst 123 (1998) 1679.
[22] J.R. Dean, G. Xiong, Trends Anal. Chem. 19 (9) (2000) 553.
[23] V. Lopez-Avila, J. Benedicto, C. Charan, R. Young, W.F. Beckert, Environ. Sci. Technol. 29 (1995) 2709.
[24] V. Lopez-Avila, R. Young, W.F. Beckert, Anal. Chem. 66 (1994) 1097.
[25] V. Lopez-Avila, R. Young, J. Benedicto, P. Ho, R. Kim, W.F. Beckert, Anal. Chem. 67 (1995) 2096.
[26] S. Jayaraman, R.J. Pruell, R. McKinney, Chemosphere 44 (2001) 181.
[27] A. Pastor, E. Vazquez, R. Ciscar, M. de la Guardia, Anal. Chim. Acta 344 (1997) 241.
[28] B. Albero, C. Sanchez-Brunete, J.L. Tadeo, Talanta 66 (2005) 917.
[29] A. Latorre, S. Lacorteb, D. Barceló, M. Montury, J. Chromatogr. A 1065 (2005) 251.
[30] H.P. Li, G.C. Li, J.F. Jen, J. Chromatogr. A 1012 (2003) 129.
[31] M. Numata, T. Yarita, Y. Aoyagi, A. Takatsu, Anal. Chem. 75 (2003) 1450.
[32] L. Ramos, G.P. Blanch, L. Hernández, M.J. González, J. Chromatogr. A 690 (1995) 243.
[33] V. Seidel, W. Lindner, Anal. Chem. 65 (1993) 3677.
[34] L. Ramos, J. Tabera, L.M. Hernández, M.J. González, Anal. Chim. Acta 376 (1998) 313.
[35] Y. Wang, M. Bonilla, H.M. McNair, J. High Resolut. Chromatogr. 20 (1997) 213.
[36] W.H. Ho, S.J. Hsieh, Anal. Chim. Acta 428 (2001) 111.
[37] M. Zhu, F.J. Aviles, E.D. Conte, D.W. Miller, P.W. Perschbacher, J. Chromatogr. A 833 (1999) 223.

Available online at www.sciencedirect.com
ScienceDirect
Talanta 71 (2007) 1186–1191
Talanta
www.elsevier.com/locate/talanta

Bioconjugation of functionalized fluorescent YVO_4:Eu nanocrystals with BSA for immunoassay

Juan Kang [a], Xin-Yue Zhang [b], Ling-Dong Sun [a,*], Xin-Xiang Zhang [a,*]

[a] *College of Chemistry, Peking University, 100871 Beijing, China*
[b] *College of Life Science, Peking University, 100871 Beijing, China*

Received 27 December 2005; received in revised form 6 June 2006; accepted 9 June 2006
Available online 14 December 2006

Abstract

Novel fluorescent YVO_4:Eu nanocrystals were ~15 nm in diameter and had been functionalized with phosphorous polyacrylic acids at the surface during the synthesis, which illuminated their potential in bioassays. In this paper, bovine serum albumin (BSA) was covalently coupled to activated nanocrystals from primary amine groups by EDC and sulfo-NHS chemistry successfully. Reaction condition, including concentration, pH value and separation methods, were carefully chosen and well discussed. Binding site number was determined simply by measuring BSA concentration using optimized microplate bicinchonic acid (BCA) assay and nanocrystals concentration according to their fluorescence emission in the monodisperse bioconjugate suspension. Transmission electron microscopy (TEM) imaging showed the monodispersity of the bioconjugates. Fluorescent characteristics were also retained. Immunoblots verified that BSA was covalently coupled to nanocrystals and remained immunoreactive. Finally, the two-step heterogeneous time-resolved fluoroimmunoassay (TR-FIA) of rabbit anti-BSA polyclonal antibody (PcAb) was operated to further validate the bioconjugates.
© 2006 Elsevier B.V. All rights reserved.

Keywords: Nanocrystal; Bioconjugation; BSA; Fluorescence; Immunoassay

1. Introduction

Immunoassay has become one of the most sensitive and specific methods for quantification in clinical diagnosis with the development of various labels. Many efforts have been devoted to develop fluorescent labels for their high sensitivity and convenience in detection based on fluorescence excitation, emission, lifetime and polarization. Different types of fluorescent labels, such as organic fluorescers, green fluorescent protein (GFP) and lanthanide chelates, have been reported. Organic fluorescent molecules like fluorescein have been widely used because of their high quantum yield. But they are easy to bleach and self-quench in multiple labeling [1,2]. GFP can emit strong and stable light, but is susceptive to the environment and bulk in volume to multiple labeling [3]. The fluorescence of lanthanide chelates have specific advantages. They have been successfully used in multianalyte assays because of their large stokes shift, narrow and differential emission band and excitation band dependent on chelates. Time-resolved fluorescence assays based on their long lifetime almost avoid the interferences of scattering light and autofluorescence from biological samples [4,5]. Several effective signal amplifying methods, including enzyme catalyze magnifying [6], streptavidin–biotin system [7] and nano or microparticles containing many lanthanide ions [10], have been developed to enhance the sensitivity of lanthanide chelates.

Fluorescent nanoparticles as labels become popular for their potential to realize ultrahigh sensitive immunoassays in recent two decades [8–22]. Their uppermost advantage lies in increasing the ratio of fluorescent dyes to proteins (i.e., the F/P ratio) greatly while minimizing dye self-quenching effects and decreasing the loss of protein activities. What's more, lanthanide chelates nanoparticles possess narrow and stable fluorescence emission. However, most of nanoparticles reported in past immunoassays are >30 nm in diameter, most at sub-micrometer scale, which are proven to bring obvious prolonged equilibration time and enhanced nonspecific adsorption [11]. Novel YVO_4:Eu nanocrystals were synthesized (unpublished). They have a preferable diameter of 15 nm. On one side, the kinetic

* Corresponding authors. Tel.: +86 10 62754680; fax: +86 10 62751708.
E-mail address: zxx@pku.edu.cn (X.-X. Zhang).

0039-9140/$ – see front matter © 2006 Elsevier B.V. All rights reserved.
doi:10.1016/j.talanta.2006.06.022

properties of the nanocrystals could be improved and non-specific adsorption decreased meanwhile; on the other side, the nanocrystals are big enough to bind several proteins on the surface, which is expected to increase the immunological affinity [22]. Since the bioconjugation of nanoparticles with biomolecules is still a delicate and complex process which restricts their wide applications, here we tried to bind a layer of BSA around the nanocrystal surface using EDC and sulfo-NHS. The bioconjugates were purified by repeated ultracentrifugation. And we determined the binding site number accurately and simply with BCA assay and fluorescence measurement. Both the monodispersity and fluorescence of nanocrystals, and the immunoactivity of BSA retained after bioconjugation. Finally, the nanocrystal-BSA bioconjugates were used in the heterogeneous immunoassay for anti-BSA PcAb successfully. The results indicated that the bioconjugation method was effective and set the foundation for the real application of nanocrystals in future.

2. Experimental

2.1. Materials and instruments

YVO_4:Eu nanocrystals were synthesized in an aqueous solution (to be published). In brief, europium ions were coordinated first with phosphorous polyacrylic acids, then sodium orthovanadate was added. The mixture reacted for 3 days at 180 °C and resulted in colloidal solution of nanocrystals. As shown in Fig. 1, the diameter of nanocrystals was 15 ± 2 nm statistically. According to the nanocrystal cell parameters from X-ray diffraction analysis (XRD), its density was calculated, the single nanocrystal mass estimated, then the nanocrystal molar concentration determined. In our experiments, we found that nanocrystals did not become monodisperse until they were diluted to 6×10^{-9} M. In the thermal gravimetric analysis, phosphorous polyacrylic acids at the surface of nanocrystals were pyrolyzed and vaporized. Calculated from the mass loss, a nanocrystal contained ~2000 carboxyl groups.

BSA (Fraction V) was purchased from Sigma (USA). *N*-(3-dimethylaminopropyl)-*N*′ethylcarbodiimide hydrochloride (EDC) and *N*-hydroxysulfosuccinimide sodium salt (sulfo-NHS) were from Fluka (Switzerland). Glycine was obtained from Promega (USA) and BCA (>98.0%) was from Bio Basic Inc. (Canada). Rabbit normal IgG and anti-BSA PcAb were purified from rabbit normal serum and anti-BSA serum, respectively, with Protein A column (Pharmacia, Sweden). Horseradish peroxidase conjugated goat anti-rabbit IgG antibody (Go a Rb IgG/HRP) and diaminobenzidine (DAB) were purchased from Sino-American Biotechnology Co. (China). Other reagents were of analytical grade without further purification. Deionized water was used throughout.

Nitrocellulose (NC) membrane was from Millipore (USA). White and high binding 96-well microtiter plate was from Corning (USA).

The fluorescence excitation band, emission band and lifetime of nanocrystals in 2 mM Tris–HCl (pH 8.0, containing 0.05% Tween 20) and europium ions in the enhancement solution [23], were measured with FLS920 fluorometer (Edinburgh Instruments, Britain). The time-resolved fluorescence emission of nanocrystals at 615 nm in the microtiter well was detected with Gemini XS/EM (Molecular Devices, USA). Ultracentrifugation was operated on Optima^{TM} L-80XP (Beckman, USA). Monodispersity of nanocrystals was evaluated under TEM JEM-1010 (JEOL, Japan). The absorbance at 560 nm was read on the Tecan Genius plate reader (Austria) in the microplate BCA assay. Electrophoresis and electroblotting were carried out in horizontal electrophoresis cell and Trans-Blot SD Semi-Dry Transfer Cell (Bio-Rad, USA), respectively.

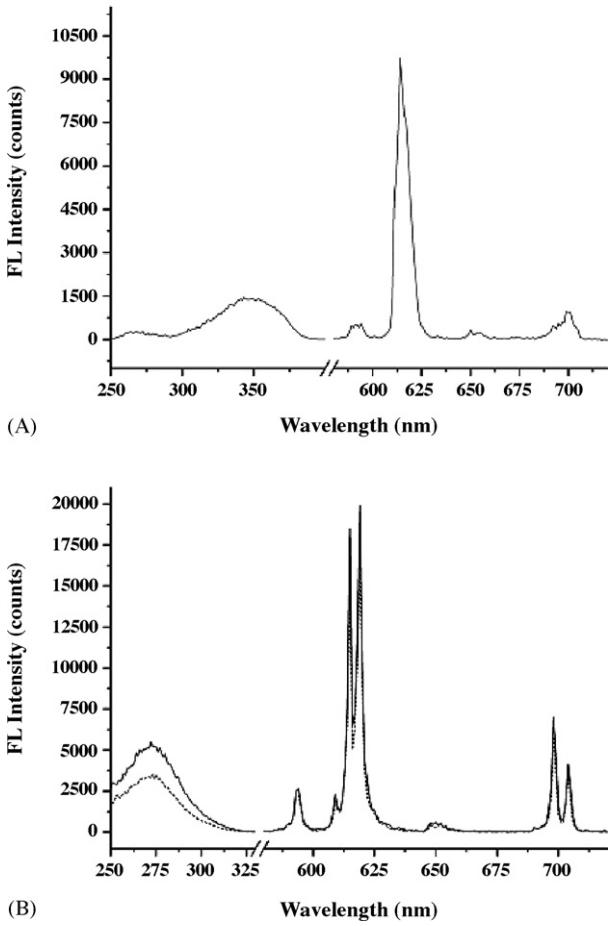


Fig. 1. TEM images of nanocrystals before (A) and after (B) coupled with BSA at 100,000-fold magnification. The inset shows the higher resolution images of a single nanocrystal at 8,300,000-fold magnification.

2.2. Detection limit of nanocrystals in solution

Nanocrystal stock solution (0.1%, w/v) was serially diluted into the 1 mL/L Triton X-100 solution, and a 200 μL aliquot of the solutions were monitored. Lower limit of detection (LLD) was calculated from 3 S.D. of the signals of diluents containing no nanocrystals.

2.3. Binding of nanocrystals with BSA

Nanocrystal stock solution (0.1%, w/v) was diluted 40 times in 20 mM phosphate buffer (pH 6.0) and sonicated 5 s at a power

level of 80 W before bioconjugation. Carboxyl groups were first activated with 0.15 mg/mL EDC and 1.6 μg/mL sulfo-NHS for 15 min. Then 0.4 mg BSA was added. After slow shaking at 4 °C for 24 h, 10 mg glycine was added to block the remaining active groups for 3 h at room temperature. Nanocrystal-BSA bioconjugates were ultracentrifuged and washed 5 times with 0.01 M PBST, and finally resuspensed in 2 mM Tris–HCl (pH 8.0, containing 0.05% Tween 20). The suspension was centrifuged at 2500 rpm for 35 min to remove noncolloidal aggregates from monodisperse suspension and stored at 4 °C. Noncovalent adsorption control was carried out simultaneously, following the same steps except that neither EDC nor sulfo-NHS was added.

2.4. Binding site number

Fluorescence emission–concentration correlation curve was recorded in nanocrystal solutions from 1.75×10^{-10} to 1.12×10^{-8} M, diluted with 2 mM Tris–HCl (pH 8.0, containing 0.05% Tween 20), to determine the nanocrystal concentration of the bioconjugate solution. Quantification of the coupled BSA was carried out using the optimized microplate BCA assay protocol. Reagent A: 205 mg Na_2CO_3, 405 mg sodium tartrate in 30 mL water and adjusted to pH 11.25 with 10 M NaOH; reagent B: 400 mg BCA in 10 mL water; reagent C: 80 mg $CuSO_4 \cdot 5H_2O$ in 2 mL water; working solution: 1 vol reagent C mixed with 25 vol reagent B, then 26 vol reagent A added to the C/B mixture. The monodisperse bioconjugate suspension or BSA standard solution (150 μL) was mixed with 150 μL working reagent in a microplate well, incubated for 2 h at 37 °C. The absorbance at 560 nm was plotted versus the concentration of BSA standard solutions. BSA amount in the bioconjugate solution was determined using interpolation. The number of covalently coupled BSA per nanocrystal was obtained comparing the BSA and nanocrystal concentration in the bioconjugate.

2.5. Immunoblots

To further testify that BSA was covalently conjugated to nanocrystals, 30 μL bioconjugates and its controls (free nanocrystals and noncovalent adsorption control) were electrophoresed on a 1.2% agarose gel at 100 V for 60 min, photographed under ultraviolet illumination, then transferred onto a 0.45 μm NC membrane at 15 V for 60 min. The membrane was incubated with 5% (w/v) nonfat milk (NFM), and then 50 μg/mL anti-BSA PcAb. Go a Rb IgG/HRP was chosen as secondary antibody and DAB as substrate.

2.6. Immunoassay

Fifty microlitre of anti-BSA PcAb solution serially diluted to 0.4–100 μg/mL with 0.01 M PBS was coated on the wells of a 96-well microtiter plate by physical adsorption at 4 °C for 16 h. Simultaneously 5 μg/mL rabbit normal IgG was coated as the negative calibrator. After washed thrice with 300 μL 0.01 M PBST, 100 μL of 5% (w/v) NFM was added to each well. The plate was incubated at 37 °C for 0.5 h and washed. Then 1×10^{-9} M nanoparticle-BSA solution containing 5% (w/v) NFM and 0.05% (w/v) NaN_3 was added in the 50 μL volume. After incubating at 37 °C for 2 h and washing, the fluorescence emission at 615 nm was read directly from the well bottom at the time-resolved mode. LLD was calculated from 3 S.D. of the signals of the zero calibrator.

3. Results and discussion

3.1. Nanocrystals

Excitation and emission spectra of nanocrystals and europium ions were shown in Fig. 2. Lifetimes of them were the same at 1 ms. The emission peak at 615 nm of europium ions was split into two narrow peaks at 615 and 619 nm because of the change of ligand field. In our experiment, we found that 1.75×10^{-10} M nanocrystals in the 2 mM Tris–HCl solution (pH 8.0, containing 0.05% Tween 20) was equivalent to 1.5×10^{-5} M europium ions in the enhancement solution in the fluorescence intensity at 615 nm, i.e., a single nanocrystal comprising about ~1700 chelated europium ions (concluded from its stoichiometric formula and the single mass) was comparable to ~50,000 europium ions. The protection of europium ions in the nanocrystal from water quenching was key to this increase of fluorescence efficiency presumptively.

The loss of signal attributable to the temporally resolved emission of lanthanide ions was effectively compensated for by use of the nanocrystals. As shown in Fig. 3. LLD of nanocrystals in 200 μL solution reached 3.76×10^6 pcs, corresponding to 6.25×10^{-18} M nanocrystals.

Fifteen nanometer nanocrystals in this study offer a 7-fold reduction in radius and an ~350-fold reduction in particle volume compared with 107 nm nanoparticles containing many Eu(III) chelates reported [10–12]. This could help to increase the kinetics and sensitivity of nanoparticle labeled immunoassays. First, according to the Einstein–Stokes equation $D = kT/6\pi r\mu$ (where D is Brownian diffusivity, k the Boltzmann's constant,

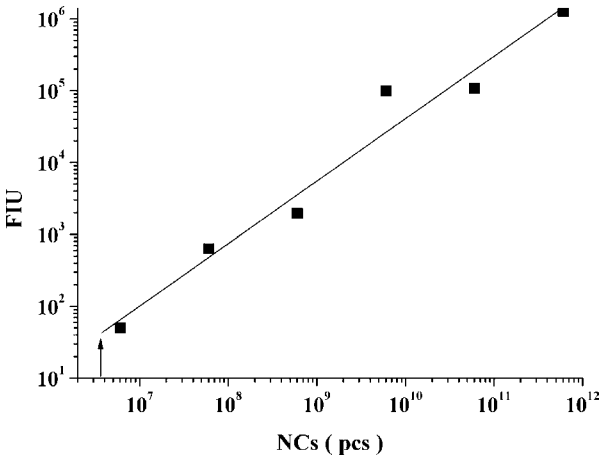


Fig. 2. Fluorescence excitation and emission spectra of europium ions (A) in the enhancement solution and nanocrystals (B) in the 2 mM Tris–HCl (pH 8.0, containing 0.05% Tween 20) before (solid line) and after (dash line) coupled with BSA. ex slit 0.15 nm; em slit 0.20 nm.

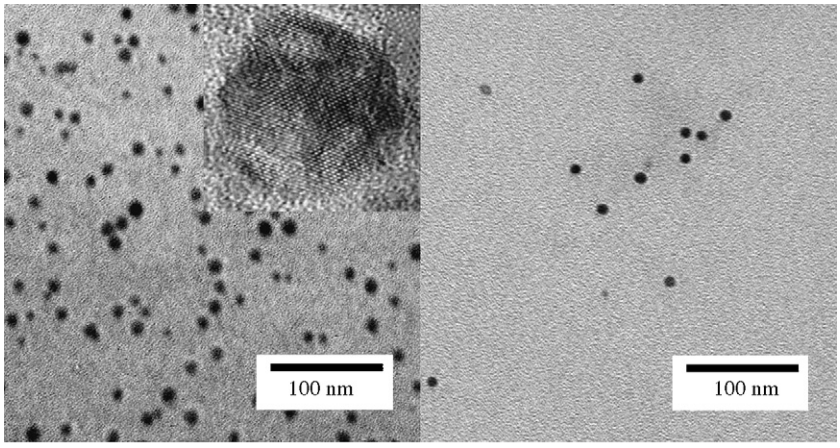


Fig. 3. Dilution curve of nanocrystals in the 1 mL/L Triton X-100 solution (200 μL) measured with a time-resolved plate fluorometer. ex 272 nm, em 614 nm; start time 250 μs, stop time 850 μs; the arrow indicates the lower limit of detection.

T the absolute temperature, r the radius and μ is viscosity of the medium), the size reduction achieved should improve the kinetic properties of nanocrystals. Second, the access of smaller nanocrystals to complex target molecules could be easier because of decreased steric hindrance in heterogeneous immunoassays [12]. Finally, in homogeneous nanoparticle label-based energy-transfer assays, diminished particle volume favors the specific signal of the label by lowering the fractional proportion of the nanoparticle core volume that is generating only background signal [16].

Based on calculations, the density of carboxylic groups at the surface was 2–3 μm^{-2} for the nanocrystals while 1–2 μm^{-2} for reported nanoparticles [10–12]. This is expected to improve the stability of nanocrystal colloidal solution and lower its nonspecific adsorption in immunoassays [11].

3.2. Bioconjugation

Monodispersity of nanocrystal-BSA conjugates is essential in maintaining the particle number and diminishing NSB in immunoassays. Because nanocrystals have many carboxylic acids and BSA has about 60 amine groups on the surface, aggregation could result in EDC and sulfo-NHS coupling chemistry [24]. Several strategies were taken. First, nanocrystals were activated by EDC and sulfo-NHS before excessive BSA was added. Second, the pH value of the reaction medium was a little above the isoelectric point of proteins (pI), because severe aggregates will result from electrostatic adsorption of positive proteins with negative nanocrystals below the pI, whereas EDC will hydrolyze quickly and protein reactivity would diminish when the pH value is too high. The pI of BSA is about 5, so the pH of reaction medium was controlled to 6. More alkaline medium was needed for binding antibodies whose pI is 7–8. Third, adequate glycine was added to deactivate the reactants completely when the reaction was finished. Thus, in the ultracentrifugation step, no severe aggregates would result. Finally, another centrifugation step was performed to remove noncolloidal aggregates from end products. TEM imaging showed that the end bioconjugates were well monodisperse (Fig. 1).

It is important to separate nanocrystal-protein bioconjugates from free proteins in the sensitivity of immunoassays. Different separation methods, including ultrafiltration, centrifugation and gel filtration, could be used. Because the nanocrystals have a diameter of the similar scale to biomolecules, separation mehods based on size difference, like ultrafiltration and gel filtration, is somewhat difficult. What's more, severe adsorption on the ultrafiltration membrane decreased the bioconjugate recovery greatly. Gel filtration cannot suppress noncovalent adsorption completely even with the eluent buffer containing surfactants, though it is moderate and can keep biomolecular conformation. Those noncovalently adsorbed biomolecules could easily depart from the nanocrystals and influence the sensitivity. Repeated ultracentrifugations were expected to wipe off noncovalent adsorption, but could bring mechanical damage to proteins and nanocrystals. In the experiments, we found that free nanocrystal control was prone to break down and supernatant, whereas bioconjugated nanocrystals were more stable in ultracentrifugation. So ultracentrifugation might remove free nanocrystals selectively from the products to some extent.

The result showed that excitation band, emission band and lifetime of nanocrystals were not changed after bioconjugation (Fig. 2B).

3.3. Binding site number

The volume of a protein molecule can be estimated very simply and reliably from its molecular weight and an average protein partial specific volume (partial specific volume = volume/molecular weight) [25]. The average value of experimentally determined partial specific volumes is ~0.73 cm^3/g for soluble globular proteins. This value varies from protein to protein, but the range is rather narrow. According to this theory the radius of BSA molecule was about 2.7 nm, so a packed monolayer of BSA on the surface of each nanocrystal would correspond to 33 molecules given that there was at least 2 nm distance between two BSA molecules needed to retain the protein activity. According to the standard curve of BCA

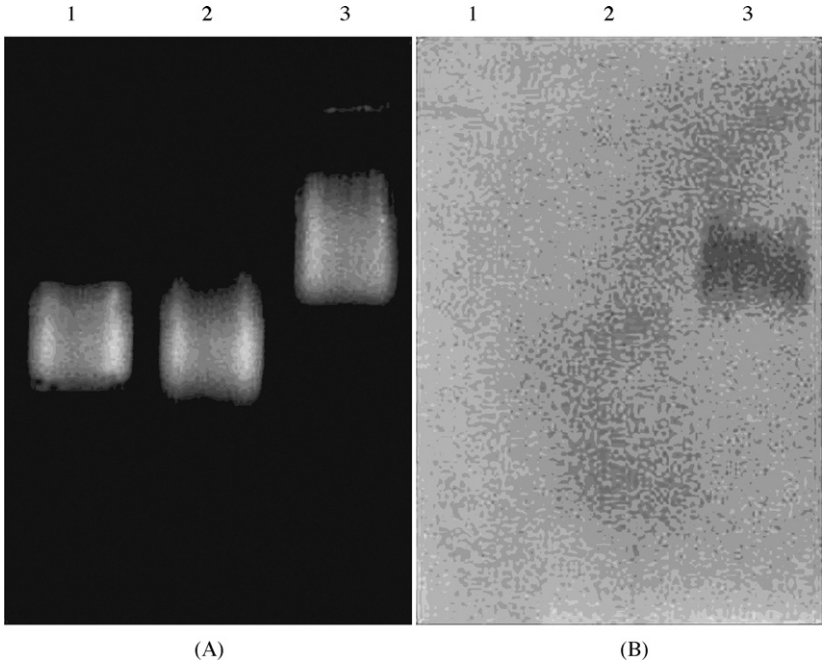


Fig. 4. Electrophoresis (A) and immunological blots (B) of nanocrystals. Lanes 1–3 are free nanocrystals control, noncovalent adsorption control and nanocrystal-BSA bioconjugates, respectively.

assay, the concentration of BSA was 3.1 μg/mL in the bioconjugate solution. From the fluorescence–concentration correlation curve of nanocrystals, there was 5.17×10^{-9} M nanocrystals in the same solution. And the number of BSA bound to each nanocrystal was 9 which was not above the maximum 33.

3.4. Immunoblots of the bioconjugate

The tests showed that agarose gel is the suitable support for electrophoresis of nanocrystals. Nanocrystal-BSA bioconjugates moved more slowly than free ones because of their increased volume and decreased surface charges (Fig. 4A). At the same time, gel imaging showed that noncovalent adsorption control migrated at the same speed as free nanocrystals control. This indicated that noncovalent adsorption was totally suppressed. Sequent semidry electro-transfer and immunological detection supported the above conclusions and implied that the immunoreactivity of BSA was retained after coupling (Fig. 4B).

3.5. Immunoassay for anti-BSA PcAb

The potential of the novel fluorescent nanocrystal as labels was demonstrated in a two-step heterogeneous immunoassay for anti-BSA PcAb. The calibration curve, based on three replicates of calibrators, was presented in Fig. 5. The LLD was 1.3 μg/mL, which should relate to the purifying method and low affinity of anti-BSA PcAb in this immnunoassay to a great extent [26]. Higher sensitivity would be expected in choice of high affinitive antibody and optimized immunoassay. However, this was comparable to or a little lower than the LLD (2.2 μg/mL) reported [9], which used the similar two-step immunoassay and IgG prepared by salting out method. The dynamic detection range covered two orders of magnitude, and good linearity was

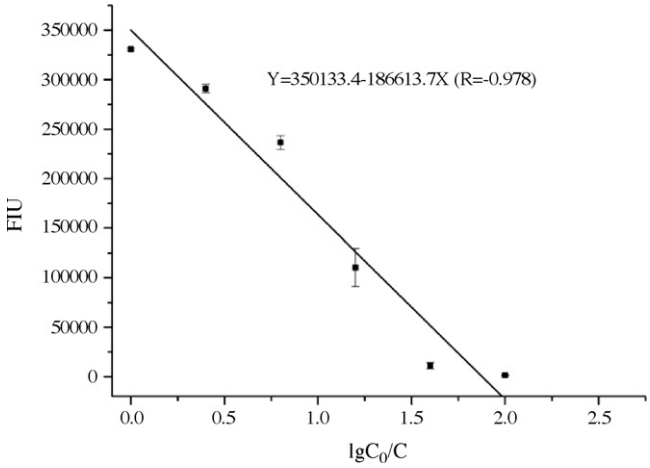


Fig. 5. Calibration curve of TR-FIA by using the novel nanocrystal-labeled BSA for anti-BSA PcAb. Error bars correspond to ±3 S.D.

achieved. The concentrations CVs were from 0.4 to 22.9%. It was found, that in the case of zero calibrator and negative calibrator, the mean value of fluorescence intensity was lower as compared with the value for 0.4–100 μg/mL BSA-specific PcAb, which undoubtedly confirmed the specificity of the nanoparticle labeled fluoroimmunoassay.

4. Conclusions

Novel fluorescent YVO_4:Eu nanocrystals functionalized with phosphorous polyacrylic acids were used in the bioconjugation with BSA. In this experiment, ~9 BSA molecules were covalently coupled to a nanocrystal. The monodispersity and fluorescent properties of nanocrystals and the immunoreactivity of BSA were retained after bioconjugation. Moreover,

LLD of nanocrystals in solution was very low. The preliminary immunoassay using nanoparticle-labeled BSA presented enabled possibilities of this novel nanocrystal and the bioconjugation method for bioassay applications.

Acknowledgement

The authors thank the financial support from National Natural Science Foundation of China.

References

[1] I.C. McKay, D. Forman, R.G. White, Immunology 43 (1981) 591–602.
[2] A. Benchaib, R. Delorme, M. Pluvinage, et al., Histochem. Cell Biol. 106 (1996) 253–256.
[3] H. Morise, O. Shimomura, F.H. Johonson, et al., Biochemsitry-US 13 (1974) 2656–2662.
[4] E. Soini, T. Lovgren, CRC Crit. Rev. Anal. Chem. 18 (1987) 105.
[5] E.P. Diamandis, R.C. Morton, E. Reichstein, et al., Anal. Chem. 61 (1989) 48.
[6] M. Petrovas, S. Spiros, Evriklia, et al., Clin. Biochem. 32 (1999) 241–247.
[7] Q.P. Qin, T. Lolvgren, K. Pettersson, Anal. Chem. 73 (2001) 1521–1529.
[8] M. Hall, I. Kazakova, Y.M. Yao, Anal. Biochem. 272 (1999) 165–170.
[9] A. Kamyshny, S. Magdassi, Colloid Surf. B 18 (2000) 13–17.
[10] H. Härmä, T. Soukka, T. Lövgren, Clin. Chem. 47 (2001) 561–568.
[11] T. Soukka, J. Paukkunen, H. Härmä, et al., Clin. Chem. 47 (2001) 1269–1278.
[12] P. Huhtinen, T. Soukka, H. Härmä, et al., J. Immunol. Methods 294 (2004) 111–122.
[13] P. Huhtinen, O. Kuronen, H. Härmä, Anal. Chem. 77 (2005) 2643–2648.
[14] W. Yang, D. Trau, R. Renneberg, et al., J. Colloid Interface Sci. 234 (2001) 356–362.
[15] Y. Bruemmel, C.P. Chan, R. Renneberg, Langmuir 20 (2004) 9371–9379.
[16] J. Feng, G. Shan, A. Maquieira, et al., Anal. Chem. 75 (2003) 5282–5286.
[17] J.O. Koskinen, J. Vaarno, A.E. Soinib, et al., Anal. Biochem. 328 (2004) 210–218.
[18] Z. Ye, M. Tan, J. Yuan, et al., Anal. Chem. 76 (2004) 513–518.
[19] M. Tan, G. Wang, J. Yuan, et al., J. Mater. Chem. 14 (2004) 2896–2901.
[20] Z. Ye, M. Tan, J. Yuan, et al., Talanta 65 (2005) 206–210.
[21] W.O. Gordon, J.A. Carter, B.M. Tissue, J. Lumin. 108 (2004) 339–342.
[22] T. Soukka, H. Härmä, J. Paukkunen, et al., Anal. Chem. 73 (2001) 2254–2260.
[23] D. Ba, W. He, Contemporary Immunological Technology and Application, Peking University Health Center & Peking Union Medical College Press, Beijing, China, 1998.
[24] G.T. Hermanson, Bioconjugate Techniques, Academic Press, CA, USA, 1995.
[25] Y. Harpaz, M. Gerstein, C. Chothia, Structure 2 (1994) 641–649.
[26] R.P. Ekins, in: C.P. Price, D.J. Newman (Eds.), Principles and Practise of Immunoassay, Macmillan, London, UK, 1997.

Available online at www.sciencedirect.com
ScienceDirect
Talanta 71 (2007) 1382–1386
Talanta
www.elsevier.com/locate/talanta

Analysis and stability of polymorphs in tablets: The case of Risperidone

I. Karabas [a,b], M.G. Orkoula [a,b], C.G. Kontoyannis [a,b,*]

[a] *Department of Pharmacy, University of Patras, Patras, Greece*
[b] *Institute of Chemical Engineering and High Temperature Chemical Processes, FORTH, P.O. Box 1414, Patras GR-26500, Greece*

Received 23 March 2006; received in revised form 13 June 2006; accepted 6 July 2006
Available online 5 September 2006

Abstract

Identification of the crystal phase of an active pharmaceutical ingredient (API) in a pharmaceutical tablet is of outmost importance since different polymorphs exhibit different physicochemical properties. Furthermore, some of the crystal phases are protected by patents. Identification of Risperidone polymorph A in film coated commercial tablets was attempted using IR spectroscopy, Raman spectroscopy and X-ray powder diffraction (XRPD). The stability of this polymorph through time and during the manufacturing process was also examined. The inability of IR and Raman techniques to identify the presence of polymorph A in the tablets, despite their lower detection limits for Risperidone, left the XRPD as the only technique that could be used for identifying the presence of Risperidone A against the other crystal phases in the presence of the excipients. Polymorph A was proved to be stable during the manufacturing process and after a storage period of 2 years.
© 2006 Elsevier B.V. All rights reserved.

Keywords: X-ray powder diffraction; FT-IR; Raman; Risperidone; Polymorphs; Tablets

1. Introduction

Many pharmaceutical solids exhibit polymorphism, which is frequently defined as the ability of a substance to exist as two or more crystalline phases that have different arrangements and/or conformations of the molecules in the crystal lattice [1]. Polymorphism may also include solvation or hydration products (also known as pseudopolymorphs) and amorphous forms [2]. Polymorphs and/or solvates of an active pharmaceutical ingredient (API) can have different chemical and physical properties such as melting point, chemical reactivity, apparent solubility, dissolution rate, optical and electrical properties, vapor pressure and density. These properties can have a direct impact on the process-ability of drug substances and the quality/performance of drug products, such as stability, dissolution and bioavailability.

One polymorph may convert to another during manufacturing and storage, particularly when a metastable form is used. Since an amorphous form is thermodynamically less stable than any crystalline form, inadvertent crystallization from an amorphous drug substance may occur. As a consequence of the higher mobility and ability to interact with moisture, amorphous drug substances are also more likely to undergo solid-state reactions. In addition, phase conversions of some drug substances are possible when exposed to a range of manufacturing processes [3]. Milling/micronization operations may result in polymorphic form conversion of a drug substance. In the case of wet granulation processes, where the usual solvents are aqueous, one may encounter a variety of interconversions between anhydrates and hydrates, or between different hydrates. Spray-drying processes have been shown to produce amorphous drug substances. The most stable polymorphic form of a drug substance is often used because it has the lowest potential for conversion from one polymorphic form to another while the metastable form may be used to enhance the bioavailability. Therefore, it is essential to ensure that polymorphic differences are addressed via design and control of formulation and process conditions to physical and chemical stability of the product over the intended shelf-life.

Based on these, some regulatory agents may refuse to approve an application for a new dug referencing a listed drug if the

* Corresponding author at: Institute of Chemical Engineering and High Temperature Chemical Processes, FORTH, P.O. Box 1414, Patras GR-26500, Greece. Tel.: +30 2610 997727/969328; fax: +30 2610 997658.
E-mail address: cgk@iceht.forth.gr (C.G. Kontoyannis).

0039-9140/$ – see front matter © 2006 Elsevier B.V. All rights reserved.
doi:10.1016/j.talanta.2006.07.009

application contains insufficient information to show that the drug substance is the "same" and remains the "same" as that of the reference listed drug during the expected shelf-life. Even in the cases where the regulatory agent accepts the crystal phases as equivalent, an additional complication stems from the patented protection of some metastable polymorphs.

Physicochemical measurements and techniques that are commonly used to determine the crystal phases are [4]: melting point (including hot-stage microscopy), solid-state IR, X-ray powder diffraction, thermal analysis procedures (DSC, TGA and DTA), Raman spectroscopy, optical microscopy and solid-state NMR. Microscopy, thermal analysis methodology and solid-state NMR are generally considered as sources of supporting information. The definite criterion for the existence of polymorphism is via demonstration of a non-equivalent crystal structure, usually by comparison of the X-ray diffraction patterns. Although most of these techniques can be easily applied to pure crystal phases it is mostly Raman spectroscopy and X-ray powder diffraction (XRPD) that have been used for rapid screening and identification of new crystal phases in high-throughput crystallization [5]. Despite the large array of available techniques the identification of an active ingredient in a formulation in the presence of numerous excipients is neither easy nor straightforward.

In this work, an attempt was made to identify the presence of the crystal phases of the active ingredient Risperidone, a benzisoxazole derivative that is used as an antipsychotic drug, in commercially available film coated tablets, using Raman and IR spectroscopy as well as XRPD. Furthermore, the possibility of the transformation of the API from one crystal phase to another with time or due to the manufacturing process was examined, through these techniques. There are three known polymorphs of Risperidone (A, B and E) for which only the XRPD spectra are available [6].

2. Experimental

2.1. Materials used

Risperidone is commercially available in film-coated tablets containing 0.5, 1, 2, 4, 6 and 8 mg of the active ingredient. Film coated Risperidone A tablets with 8 mg strength as well as placebo tablets and pure Risperidone form A were kindly provided by Specifar Pharmaceuticals SA, Athens, Greece. The tablets contained the following excipients: lactose, maize starch, microcrystalline cellulose, Hypromellose 2910, magnesium stearate, colloidal anhydrous silica, sodium lauryl sulphate and propylene glycol. Each tablet weighted 185 mg. The film coating was carefully removed from the tablets with a scalpel.

Attempts were made to prepare Risperidone B and E following the recipes given in the relevant patent [4]. One recipe yielded the form B while several others yielded mixtures of A and B. Polymorph E could not be obtained.

2.2. Characterization of the samples

The X-ray powder diffraction analysis was performed (Philips 1830/40) on finely powdered samples using the Cu Kα (40 kV and 30 mA) radiation and Ni filter with a scanning speed of 0.005° $2\theta\,s^{-1}$. Time constant was set at 2 s. XRPD spectra of the pure A and B Risperidone polymorphs are shown in Fig. 1.

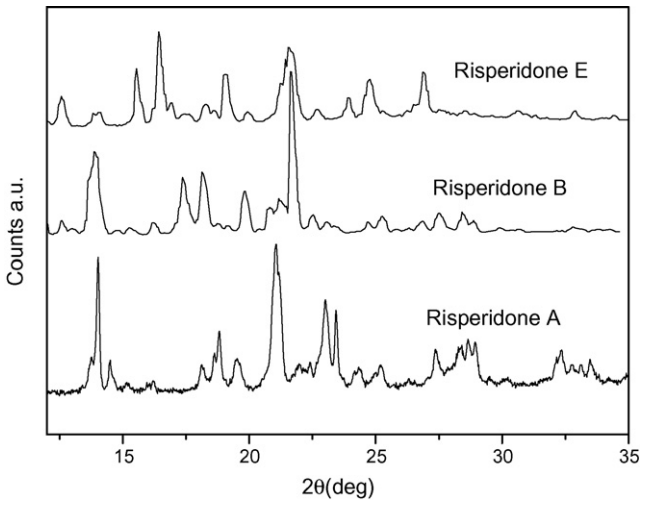


Fig. 1. XRPD spectra of the three known Risperidone polymorphs (A, B and E).

The Raman spectra were recorded using a FRA-106/S FT-Raman (Bruker) with the following characteristics: the laser excitation line used, was the 1064 nm of a Nd:YAG laser. A secondary filter was used to remove the Rayleigh line. The scattered light was collected at an angle of 180°. The system was equipped with a liquid N_2 cooled Ge detector (D 418). The power of the incident laser beam was about 370 mW on the sample's surface. Typical spectral line width was 0.5 cm^{-1} while the recorded spectra were the average of 300 scans. Raman spectra from the samples that were in the form of powders, e.g. raw Risperidone, were recorded by placing in aluminum cylindrical cups with 10 mm diameter and 4 mm height having a cavity in the center of 2 mm diameter and 1 mm depth. Homogeneity of the powders was verified by obtaining five Raman spectra for each mixture, focusing the laser beam at randomly selected spots of the surface. Spectra of uncoated and the as-received intact film coated tablets were recorded by placing directly into laser's beam path. Raman spectra of the pure A and B Risperidone polymorphs are shown in Fig. 3A and B, respectively.

All infrared spectra were recorded from 4000–400 cm^{-1}, using the EQUINOX 55 (Bruker) FT-IR spectrometer. Each spectrum was the average of 200 scans using a spectral resolution of 4 cm^{-1}. The IR spectra were recorded and stored using a spectroscopic software (OPUS, Version 2.0). FT-IR spectra of the pure substances and tablets were obtained by grounding and mixing 2 mg in an agate mortar with 200 mg of desiccated IR grade potassium bromide (Merck) in a dry box. Pellets were obtained by compression of the powdered mixtures in a stainless-steel die at 8 MPa for 5 min. IR spectra of the pure A and B Risperidone polymorphs are shown in Fig. 5A and B, respectively.

3. Results and discussion

3.1. Comparison of spectra of Risperidone polymorphs

3.1.1. X-ray powder diffraction spectra

The XRPD spectra of the synthetically prepared A and B crystal phases of Risperidone can be seen in Fig. 1 and are in accordance with the spectra quoted in the relevant patent [4]. In Fig. 1, the XRPD spectrum of polymorph E, from ref. [4], can also be seen. It is apparent that there are significant differences in the spectra which can be used to identify their appearance in the sample. For example, Risperidone A exhibits a major reflection at 21.05° 2θ while Risperidone B and E at 21.6° 2θ. Furthermore, the peak at 18.83° and the double peak at 23.03° and 23.43° 2θ can differentiate A polymorph against B and E. The presence of the other two crystal phases (B and E) can be verified by existence of peaks 17.4° and the double peak at 15.5° and 16.4°, respectively. Purity of A crystal form can be ascertained by absence of any peak at the area of 17.5° and 27° 2θ.

Though differentiation between the two polymorphs in a mixture of two appears to be feasible, the discrimination should also be checked in the case of a formulation where a number of other substances are present. An XRPD spectrum of the placebo of the commercial tablet is quoted in Fig. 2 as well as the spectrum of a powdered tablet containing 8 mg Risperidone in a total amount of 185 mg of the tablet. It is noted that the API cannot be detected in the spectrum of the tablet which is overwhelmed by the presence of placebo, indicating that XRPD detection limit in the case of Risperidone is higher than 8 mg/tablet.

3.1.2. Raman spectra

The Raman spectra of the synthetically prepared A and B crystal phases of Risperidone can be seen in Fig. 3. There are numerous differences between Risperidone A and B such as the double peak at 3051 and 3069 cm^{-1} for Risperidone A, having the 3069 cm^{-1} vibration stronger than the former, while Risperidone B exhibits a single peak at 3055 cm^{-1} with a shoulder at 3069 cm^{-1}. An additional strong peak for polymorph B can be seen at 2963 cm^{-1}. Details of some of the additional differences between Risperidone A and B can be seen in Fig. 4. Polymorph A exhibits a double peak at 432 and 440 cm^{-1}, a double peak at 1260 and 1271 cm^{-1} and a single peak at 1397 cm^{-1} as opposed to polymorph B whereas single peaks appear at 434 cm^{-1}, 1266 cm^{-1} and a double peak at 1390 and 1402 cm^{-1}. The Raman spectra that were excited from 8 mg intact commercial tablets, after the removal of the coating, as well as from tablets of placebo, can also be seen in Fig. 3. It can be seen that though the concentration of the API is only 4.3% (w/w) in the commercial tablet, its presence can be certified easily as the spectra (Fig. 3T and P) differ in three regions, marked with arrows. These differences are probably sufficient to identify the presence of API in the tablet though, as shown earlier, it is not possible to distinguish between A and B crystal forms. At this point it is worth noting that although the detection limit of Raman spectroscopy for Risperidone is lower than the

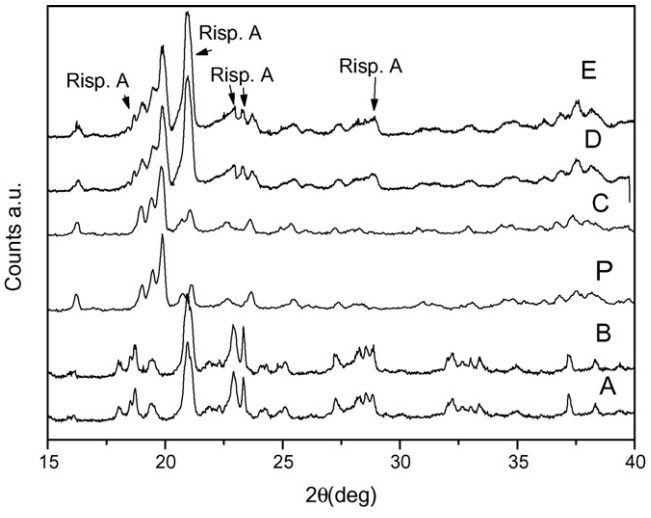


Fig. 2. XRPD spectra of: (A) Risperidone A; (B) Risperidone A recorded from the same powder 2 years after obtaining spectrum A; (P) placebo of Risperidone; (C) powdered tablet of commercial 8 mg Risperidone; (D) powdered tablet with 25% (w/w) Risperidone A; (E) powdered tablet with 25% (w/w) Risperidone A recorded from the same powdered tablet 2 years after obtaining spectrum D.

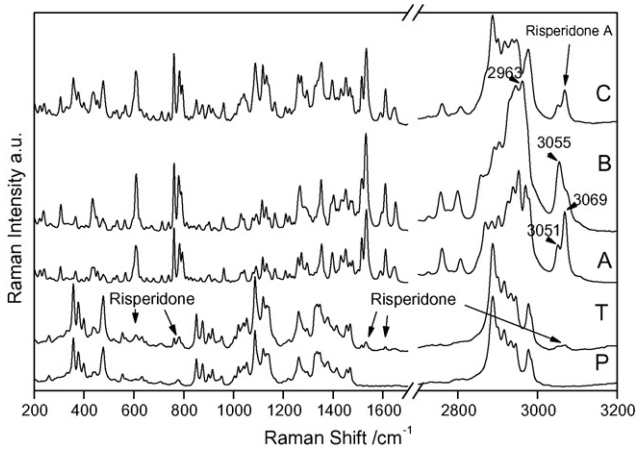


Fig. 3. FT-Raman spectra of: (A) Risperidone A; (B) Risperidone B; (C) tablet with 25% (w/w) Risperidone; (P) Risperidone placebo; (T) commercial tablet with 8 mg Risperidone (uncoated).

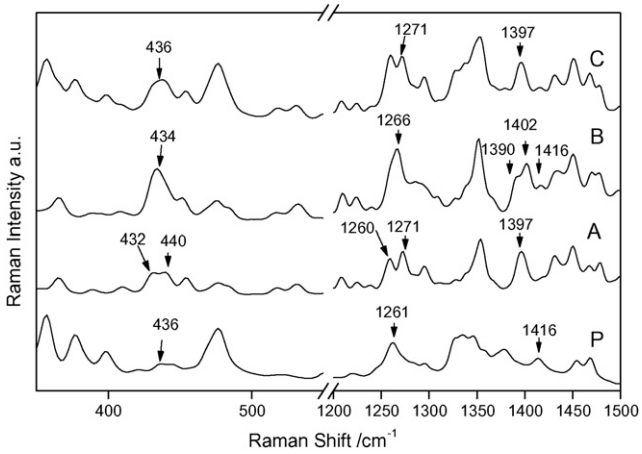


Fig. 4. FT-Raman spectra of: (A) Risperidone A; (B) Risperidone B; (C) tablet with 25% (w/w) Risperidone; (P) Risperidone placebo.

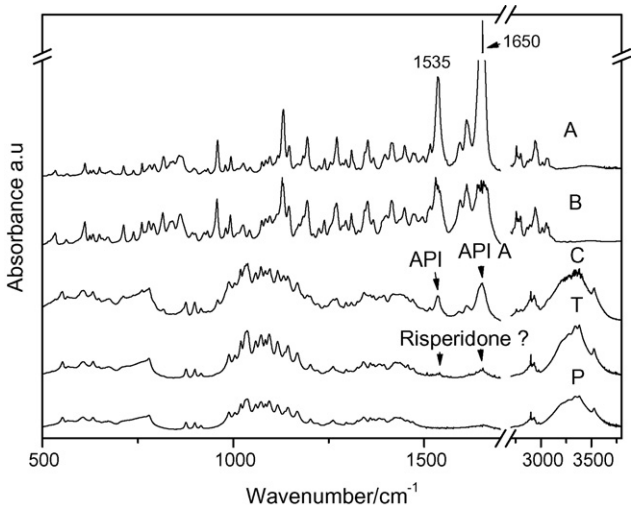


Fig. 5. FT-IR spectra of: (A) Risperidone A; (B) Risperidone B; (C) powdered tablet with 25% (w/w) Risperidone; (T) powdered commercial tablet with 8 mg Risperidone (uncoated); (P) Risperidone placebo.

respective for XRPD this advantage is not useful for the task at hand.

3.1.3. IR spectra

The IR spectra of the synthetically prepared A and B crystal phases of Risperidone, the placebo and the uncoated powdered commercial tablet with 8 mg API can be seen in Fig. 5. The major bands for both polymorphs appear at 1535 and 1650 cm^{-1}, but the major difference between them is that the vibration at 1650 cm^{-1} appears as single peak in polymorph A whereas in polymorph B multiple peaks can be observed. In the spectrum obtained from the powdered tablet (Fig. 5T) the presence of the API could not be detected with the exception of two minor noise-like wide bands, marked with arrows, which appear at around 1535 and 1650 cm^{-1}. Unfortunately, these bands cannot be used for identification of the API.

3.2. Polymorph A stability tests

3.2.1. Twenty-five percent Risperidone tablets

Among the targets of this work was to verify if Risperidone A in tablets transforms with time or through the manufacturing process to a different crystal phase. Since neither the FT-IR nor the Raman was capable of differentiating between the crystal phases, despite their better detection limits than the XRPD, a different approach was followed. A labscale batch of Risperidone tablets with 25% (w/w) Risperidone was manufactured by the pharmaceutical company following the same manufacturing process as with the commercially available concentrations. Working with a 25% (w/w) of Risperidone was chosen after testing mixtures of 10 and 15% (w/w). In the XRPD spectra obtained from the 10 and 15% (w/w) mixtures (not shown) only the main reflection of Risperidone A could be barely observed at 21.0° 2θ on the top of a placebo reflection indicating that the XRPD detection limit for Risperidone A was approximately 10% (w/w). The Raman and IR spectra recorded from the same mixtures (not shown) were not more helpful than those recorded from the tablet with 8 mg API. Although a 10% (w/w) mixture could have been used for testing the stability of A polymorph based on XRPD data, a 25% (w/w) was thought to be more helpful for the analysis due to the appearance of additional Risperidone reflections, as well as to have Raman and IR spectra that might permit the identification of Risperidone A.

The Raman spectrum obtained from the tablet with 25% (w/w) Risperidone A can be seen in Fig. 3C. The increased quantity of the active ingredient allows the positive identification of Risperidone A in these tablets. The wide band at 436 cm^{-1} (Fig. 4C) stems from the addition of polymorph A double peak at 432 and 440 cm^{-1} and the placebo vibration at 436 cm^{-1} (Fig. 4P). The polymorph A vibrations at 1271 and 1397 cm^{-1} (Fig. 4C) as well as at 3051 and 3069 cm^{-1} (Fig. 3C) are unaltered due to the absence of the respective placebo vibrations. It should be noted though that the presence of these vibrations does not rule out the possibility of the simultaneous presence of small quantity of B crystal phase.

The FT-IR spectrum obtained from the tablet with 25% (w/w) Risperidone A can be seen in Fig. 5C. The presence of a single peak at 1650 cm^{-1} indicates the presence of Risperidone A but this does not also exclude the possibility of the simultaneous presence of small amounts of B crystal phase since the multiple peaks of B at 1650 cm^{-1} can be hidden under the apparently single peak at 1650 cm^{-1}.

3.2.2. Manufacturing process stability test

In the sample with 25% (w/w) Risperidone (Fig. 2D) the characteristic reflections of Risperidone polymorph A (Fig. 2A), as well as the diffraction peaks of the compounds consisting the placebo (Fig. 2P), were detected. Furthermore, no additional reflections were detected including the most prominent diffraction peaks at 21.6° 2θ of polymorphs B and E. This indicates that during the manufacturing process no transformation of Risperidone A took place. Therefore, in the case of Risperidone, XRPD proved to be the only reliable technique for identifying the presence of A polymorph and simultaneously exclude the possibility of the presence of the other two polymorphs.

3.2.3. Stability tests with time

In order to test the stability of Risperidone A with time, the XRPD spectra of raw Risperidone A in powder form were recorded with a time interval of 2 years (Fig. 2A and B). The XRPD spectra of tablets with 25% (w/w) Risperidone A were also recorded shortly after their manufacture (Fig. 2D) and after 2 years (Fig. 2E). In both cases, and in order to simulate real-life scenario, in the interim period the powders were placed in a laboratory cabinet for protection against the light but neither the temperature nor the humidity was controlled. No difference was observed indicating there is no transformation or degradation of the active ingredient after a storage period of 2 years.

4. Conclusions

From the application of X-ray powder diffraction, FT-IR and FT-Raman spectroscopy on the above mentioned specimens and

raw materials as well as on tablets, it is apparent that there is no straightforward process that can be applied in order: (a) to identify the presence of different crystal phases of the active ingredient and/or (b) to test their stability. Product oriented methodologies should be devised using all available techniques depending on a number of factors including the percentage of the active ingredient in the formulation, the problems arising from the presence of the excipients, the detection limits of the different techniques for the active substance in question and the availability of all crystal forms, including the patented.

For Risperidone A, the case study of this work, it can be safely concluded that no transformation takes places during the manufacturing process or during a storage period of 2 years. None of the techniques used could positively identify the presence of polymorph A in the commercial tablets with 8 mg API. In tablets with increased API strength IR and Raman proved to be incapable of excluding the simultaneous presence of other crystal phases although positive identification of polymorph A was accomplished. Only the information obtained from XRPD could be used for the identification of form A and the exclusion of forms B and E.

Acknowledgments

Authors would like to thank Specifar Pharmaceuticals SA for its help and in particular Ms. Eirini Vasilopoulos from the Department of Product Development.

References

[1] D.J. Grant, in: H.G. Brittain (Ed.), Polymorphism in Pharmaceutical Solids, Marcel Dekker, Inc., New York, 1999, pp. 1–31 (Chapter 1).
[2] International Conference on Harmonization Q6A Guideline: Specifications for New Drug Substances and Products: Chemical Substances, October 1999.
[3] H.G. Brittain, E.F. Fiese, in: H.G. Brittain (Ed.), Polymorphism in Pharmaceutical Solids, Marcel Dekker, Inc., New York, 1999, pp. 279–330 (Chapter 8).
[4] H.G. Brittain, in: H.G. Brittain (Ed.), Polymorphism in Pharmaceutical Solids, Marcel Dekker, Inc., New York, 1999, pp. 227–271 (Chapter 6).
[5] S. Morissette, O. Almarsson, M. Peterson, J. Remenar, M. Read, A. Lemmo, S. Ellis, M. Cima, C. Gardner, Adv. Drug Deliv. Rev. 56 (2004) 275.
[6] B. Krochmal, D. Diller, B.-Z. Dolitzky, J. Aronhime, Preparation of Risperidone, U.S. Patent No. 6,750,341 and PCT/WO 02/12200 A1, Feb 14, 2002.

Available online at www.sciencedirect.com
ScienceDirect
Talanta 71 (2007) 1405–1410
Talanta
www.elsevier.com/locate/talanta

Selective stopped-flow sequential injection method for the spectrophotometric determination of titanium in dental implant and natural Moroccan phosphate rock

Fotini S. Kika, Demetrius G. Themelis *

Laboratory of Analytical Chemistry, Department of Chemistry, Aristotle University of Thessaloniki, 541 24 Thessaloniki, Greece

Received 4 April 2006; received in revised form 12 June 2006; accepted 6 July 2006
Available online 1 September 2006

Abstract

The present work reports the first sequential injection (SI) method for the spectrophotometric determination of Ti(IV). The method is based upon the reaction of Ti(IV) with chromotropic acid (CA) in acidic medium to form a water-soluble complex ($\lambda_{max} = 420$ nm). The chemical and instrumental variables of the system that affected the reaction were studied. Selectivity was greatly enhanced using ascorbic acid. A linear calibration graph was obtained in the range 0.2–10.0 mg l^{-1} Ti(IV) at a sampling frequency of 24 h^{-1}. The precision was satisfactory ($s_r = 1.5\%$ at 5.0 mg l^{-1} Ti(IV), $n = 12$) and the 3σ limit of detection, c_L, was 0.7 mg l^{-1} ($n = 10$). The developed method proved to be adequately selective and was applied successfully to the analysis of real samples (dental implant and natural Moroccan phosphate rock) giving accurate results based on recovery studies (98–105%).
© 2006 Elsevier Ireland Ltd. All rights reserved.

Keywords: Sequential injection; Titanium; Spectrophotometry; Chromotropic acid; Rocks; Dental implant

1. Introduction

Metallic titanium is well known for its excellent corrosion resistance, being able to withstand attack by dilute sulphuric and hydrochloric acid, most organic acids, moist chlorine gas and chloride solutions. It is as strong as steel, but much lighter and it is heavier than aluminum, but twice as strong. These properties make titanium very resistant to the usual kinds of metal fatigue [1].

Approximately 95% of titanium production is consumed in the form of titanium dioxide, TiO_2, an intensely white permanent pigment with good covering power in paints, paper, toothpaste and plastics. Titanium alloys are principally used for aircrafts and missiles where lightweight strength and ability to withstand extremes of temperature are important. It also has potential use in desalination plants for converting sea water in fresh water.

Being judged completely inert and immune to corrosion by all body fluids and tissue and thus totally bio-compatible, titanium is one of the few materials that naturally match the requirements for implantation in the human body. Its capacity for joining with bone and other tissue—osseo integration makes it suitable for medical applications, such as total replacement of arthritis hips, knee joints, facial treatments and dental implants [2].

Therefore, the need for the routine determination of titanium either in geological samples, such as silicate rocks or in dental implants have been receiving increasing attention. As regards the automated methods of analysis, flow injection (FI) is an important technique for this purpose as it involves low consumption of reagents and sample, exhibits rapid response and is easy to manipulate. Several methods for the determination of titanium(IV) by FI have been reported using various detection systems, such as spectrophotometry [3–9], chemiluminescence [10,11], inductively coupled plasma atomic emission spectrometry [12], inductively coupled plasma–mass spectrometry [13,14] and isotope dilution high resolution inductively coupled plasma–mass spectrometry [15]. The majority of the above methods were applied to the determination of Ti(IV) in silicate rocks [3–7,15], while some of them were applied to the determination of Ti(IV) in water [8,14], brines [8], aluminum alloy [9] and microalloyds [13].

* Corresponding author. Tel.: +30 2310 997804; fax: +30 2310 997719.
E-mail address: themelis@chem.auth.gr (D.G. Themelis).

0039-9140/$ – see front matter © 2006 Elsevier Ireland Ltd. All rights reserved.
doi:10.1016/j.talanta.2006.07.018

However, FI has some inherent drawbacks that have been addressed by the development of sequential injection analysis, SI [16]. Briefly, the advantages of SI over FI are the simpler flow manifold, the reduced consumption of samples and reagents, the easier and move convenient variation of the experimental parameters and the greater potential for fluidic handling. To the best of our knowledge, no SI method has been reported so far for the spectrophotometric determination of Ti(IV).

The present work reports the first SI method for the spectrophotometric determination of Ti(IV) and it is based upon the reaction of Ti(IV) with chromotropic acid, CA, in acidic medium to form a water-soluble complex ($\lambda = 420$ nm). The proposed method is simple, rapid, cost-effective, adequately selective and was applied successfully to the accurate and precise analysis of dental implant and natural Moroccan phosphate rock.

2. Experimental

2.1. Apparatus

A schematic diagram of the SI setup is depicted in Fig. 1. The SI manifold consists of a micro-electrically actuated 10-port selection valve (Valco, Switzerland), a double-beam spectrophotometer (Tecator 5023 FI star, Sweden) with a 1 cm path length flow cell, a detector controller (Tecator 5032 FI star, Sweden), and a peristaltic pump (Gilson Minipuls3, Villiers-le-Bel, France) [17]. The absorbance was monitored at 420 nm. The flow system used 0.7 mm i.d. Teflon tubing throughout. Tygon pump tubes were used for aspirating-delivering the solutions.

The hardware was interfaced to the controlling PC through a multi function I/O card (6025 E, National Instrument, Austin, TX). The control of the system and the data acquisition from the detector were performed through a special program developed in house using the LabVIEW 5.1.1 instrumentation software package (National Instrument). The response signal of the detector was acquired digitally and the data were saved in ASCII format for further manipulation (peak height measurement, digital filtering, etc.).

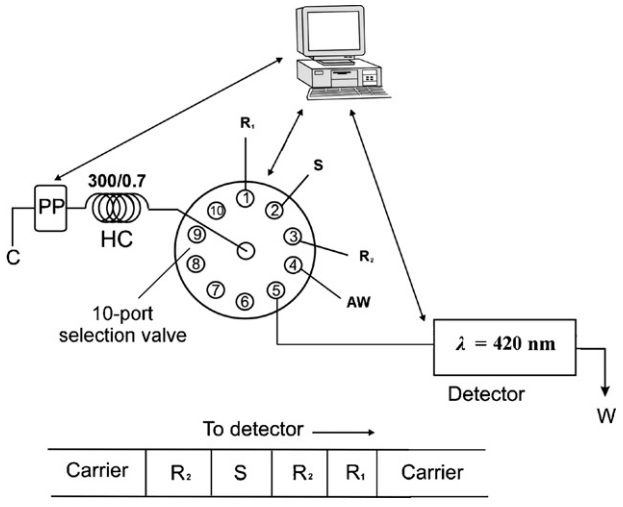


Fig. 1. SI manifold for the determination of titanium. S: sample; R_1: buffered 3500 mg l^{-1} chromotropic acid (pH 4.8); R_2: 4000 mg l^{-1} ascorbic acid; C: carrier (H_2O); PP: peristaltic pump; W: waste; AW: auxiliary waste; HC: holding coil; numbers above coils denote length/i.d. (cm/mm) ratio.

2.2. Chemicals and reagents

All chemicals were of analytical-reagent grade and were provided by Merck (Darmstadt, Germany), unless stated otherwise, and all the solutions were made up by doubly de-ionized water.

The standard solution of CA [γ(CA) = 8000 mg l^{-1}] was prepared daily by dissolving 0.2 g of chromotropic acid disodium salt dehydrate in 25 ml of water. All the CA solutions were covered with aluminum foil during storage and measurements as CA is sensitive to light.

The standard solution of ascorbic acid (AsA) (γ = 5000 mg l^{-1}) was prepared daily by dissolving 1 g of solid AsA in 200 ml doubly de-ionized water.

Working solutions of CA were prepared by dilution with buffer solution, while the AsA working solutions were prepared by dilution with double de-ionized water immediately before use.

Working Ti(IV) solutions were made daily by appropriate dilutions of the stock Ti(IV) solution ($\gamma = 1000 \pm 2$ mg l^{-1} in 5 mol l^{-1} HCl, Merck) and appropriate amounts of HCl solution were added in order all the resulted solutions have a final amount concentration of 0.05 mol l^{-1}. The addition of the HCl solution both prevents the hydrolysis of the Ti(IV) solutions and the standard solutions have the acidity that the real samples have after their pretreatment (see Section 2.4).

Constant ionic strength ($I = 0.2$ mol l^{-1}) acetate buffer solution (pH 4.80) was prepared from CH_3COOH and NaOH (1 mol l^{-1} each). For buffers with higher ionic strength values in the optimization procedure, the ionic strength was adjusted by the addition of appropriate amounts of solid KCl.

Appropriate concentration of H_3BO_3 ($w = 4\%$) was used for the pretreatment of the dental implant sample.

All solutions were degassed with purified nitrogen before use. All stock solutions were stored in polyethylene containers. All the polyethylene containers and glassware used for aqueous solutions containing metal ions were cleaned in (1 + 1) HNO_3, while the rest of the glassware was cleaned in $w = 3\%$ Decon 90. All were rinsed with de-ionized water before use.

2.3. Procedure for aqueous solutions

The sequence for the determination of Ti(IV) by the proposed method is shown in Table 1. Fifty microlitres of 4000 mg l^{-1} AsA solution, 100 μl of the standard/sample, 50 μl of 4000 mg l^{-1} AsA solution and 150 μl of 3500 mg l^{-1} CA solution in buffer pH 4.8 were aspirated in this order in the holding coil (HC), through ports 1, 2 and 3 of the selection valve, respectively. The four zones were propelled to the detector through port 5 at a flow rate of 1.0 ml min^{-1}. When the reaction mixture entered the flow cell of the detector, the flow was stopped and the reaction was allowed to proceed for 40 s, in order to gain maximum sensitivity. The cycle time was 150 s (24 determinations per hour). When changing between different solutions of samples, standards or reagents an additional wash-

Table 1
Sequence steps of a complete SI measurement cycle for the UV method

Time (s)	Pump action	Flow rate (ml min^{-1})	Valve position	Action description
0	Off	–	1	Selection of AsA port
5	Aspirate	0.6	1	Aspiration of AsA in holding coil
1	Off	–	2	Selection of sample port
10	Aspirate	0.6	2	Aspiration of sample in holding coil
1	Off	–	1	Selection of AsA port
5	Aspirate	0.6	1	Aspiration of AsA in holding coil
1	Off	–	3	Selection of CA, buffer port
15	Aspirate	0.6	3	Aspiration of CA, buffer in holding coil
1	Off	–	5	Selection of detector port
22	Deliver	1.0	5	Propulsion of reaction mixture to detector
40	Off	–	5	Stopped-flow step
49	Deliver	1.2	5	Propulsion of reaction mixture to waste
0	Off	–	5	End of measuring cycle

ing step was performed in order to avoid carryover effects; the new solution was aspirated to the HC for 10 s at 2.0 ml min^{-1}, and then flushed through port 4 to the auxiliary waste (AW) for 20 s at 2.0 ml min^{-1}. Note that in order to avoid overpressure and/or bubble formation in the valve, the pump was stopped for 1 s between changing ports.

The transient signal from the detector was recorded as a peak, the height of which was proportional to Ti(IV) concentration in the samples, and was used for all measurements. The recorded peaks were sharp and the base-line stable. The blank signal was recorded by replacing the sample/standard solution with 0.05 mol l^{-1} HCl solution. Five replicates per sample or standard were made in all instances.

2.4. Pretreatment and determination of titanium in dental implant and natural Moroccan phosphate rock

An accurately weighed 0.1 g dental implant was transferred to a beaker. Four and a half microlitres of doubly de-ionized water were added and the sample was dissolved with 0.5 ml of 40% mass fraction of HF. When the sample was completely dissolved, 0.5 ml concentrated HNO_3 was added drop wise until the titanium was completely oxidized. When the oxidation of titanium was complete, decoloration of the solution was observed. Afterwards, 2.6 ml of 4% mass fraction of H_3BO_3 solution were added and the solution was transferred to a 100-ml volumetric flask with 2 mol l^{-1} HCl [18]. Then, 0.25 ml of the resulted solution was further diluted with doubly de-ionized water to 100 ml and final amount concentration of 0.05 mol l^{-1} HCl and analyzed using the above-described SI procedure for aqueous solutions. Five replicates were made in all instances.

The analysis of Moroccan rock was carried out by fusing 1 g of rock [Community Bureau of Reference (BCR) No. 32] with a mixture of Na_2CO_3 and K_2CO_3 of mass fraction ratio of 6:1 for 3 h at 800–1000 °C. The melted mass was cooled and treated with 1% volume fraction of HCl and evaporated to dryness. The residue was dissolved in 10% volume fraction of HCl and filtered. The filtrate was diluted to 100 ml and analyzed using the above-described SI procedure for aqueous solutions [6]. The resulted solution was analyzed using the above-described SI procedure for aqueous solutions. Five replicates were made in all instances.

3. Results and discussion

3.1. Preliminary studies

Preliminary experiments showed that the reaction product could be formed under SI conditions, having an absorbance maximum at 420 nm. The SI setup consisted of two zones, the sample and the buffered reagent zone. The initial values of the chemical and SI variables were: γ(CA) = 5000 mg l^{-1} in acetate buffer pH 5.2, γ(Ti(IV)) = 5 mg l^{-1} in 0.05 mol l^{-1} HCl, I = 0.1 mol l^{-1}, V(sample) = 100 μl, V(CA in acetate buffer) = 100 μl (10 s aspiration time at 0.6 ml min^{-1}), while the reaction mixture was propelled to the detector at a flow rate of 1.2 ml min^{-1}. The order of the aspiration of the sample and the reagent solution proved not to be critical. The almost negligible differences in the signals were caused by slightly different dispersion effects on the sample zone according to the order of its aspiration. In addition, stopped-flow experiments showed that the reaction was completed in 40 s.

3.2. Study of chemical and SI variables

The chemical and SI variables were studied using an assay which comprises of the sample and the buffered reagent zone. In all cases, calibration curves for Ti(IV) were constructed in the range of 1.0–10.0 mg l^{-1} in order to study the sensitivity, the determination range and the linearity of the method. The starting SI variables were: V(sample) = 100 μl, V(CA in acetate buffer) = 100 μl, l(RC) = 0 cm and qv = 1.2 ml min^{-1}.

The influence of pH on the reaction was studied in the range 4.2–5.6, using a series of standard acetate buffers. The results showed that the reaction pH has a marked effect on the linearity for pH values varying between 4.2 and 4.8 without affecting significantly the sensitivity of the method. The best linearity was achieved at a pH value of 4.8 and this value was selected for the subsequent experiments.

The effect of the ionic strength was studied in the range 0.1–0.7 mol l^{-1}. The results showed that the reaction was not influenced by the increase of the ionic strength. Therefore, the value of 0.2 mol l^{-1} was selected for the following experiments for simplicity reasons.

The effect of the CA mass concentration was investigated in the range 1000–5000 mg l^{-1}. The signal intensity increased by increasing the CA mass concentration in the range of 1000–3500 mg l^{-1} and then decreased. The maximum signal intensity was achieved for CA mass concentration of 3500 mg l^{-1}. Additionally, at this value, the maximum working range and linearity of the calibration curve were achieved. Thus, a CA mass concentration of 3500 mg l^{-1} was chosen for subsequent work.

The influence of the HCl amount concentration in the sample solution was studied in the range 0.05–0.2 mol l^{-1}. At HCl amount concentrations of 0.1 and 0.2 mol l^{-1} there was a significant decrease in signal intensity due to pH change. Therefore, HCl amount concentration of 0.05 mol l^{-1} was selected for further experiments.

The effect of the stop-flow period was investigated from 20 to 60 s. The results showed that the stop-flow period has a noticeable influence on the sensitivity of the method. For time period lower than 40 s, the signal intensity was increased linearly, leveled off up to 50 s and then decreased. Thus, the stop-flow period of 40 s was selected as higher sensitivity was achieved while the working range and the linearity did not differ in both cases.

Using the preferred chemical parameters mentioned above, the SI variables were studied. Experiments were carried out to determine the optimum volumes of the aspirated sample and reagent solution. The effect of the buffered CA solution volume was studied in the range 50–200 μl. In this case, the peak heights increased up to 100 μl and then leveled off. Maximum linearity was achieved for CA solution volumes above 150 μl. Additionally, the signal of the blank solution increased linearly with increasing buffered CA solution volume and therefore the volume of 150 μl was selected. The effect of the aspirated sample volume was studied in the range 50–200 μl. The peak heights increased non-linearly with increasing sample volume and a volume of 100 μl was selected for subsequent experiments as it is preferable the volume of the aspirated acidic sample solution to be lesser than the volume of the aspirated reagent solution in order the buffer to maintain its capacity and the pH of the reaction not to be altered.

With the selected sample and buffered reagent volumes and at a propulsion flow rate of 1.2 ml min^{-1}, the influence of the reaction coil length was examined in the range 0–100 cm. The length of the reaction coil determined both the degree of overlapping of the sample and reagent zones and the period of time that the reaction was allowed to proceed. The results showed that using the necessary PTFE connection tubes between the selection valve and the detector produced adequate overlapping of the sample and reagent zones. Since the stopped-flow step was adopted, no additional reaction coil was used prior to the detector.

Table 2
Maximum tolerance mole ratio of various ions on the determination of 1.0 mg l^{-1} Ti(IV) under the selected chemical and SI conditions for aqueous solutions

Ion added	Tolerable ratio of mass concentrations[a]
Cd(II), Ca(II)	1000
SO_4^{2-}	600
PO_4^{3-}, CO_3^{2-}	400
Cu(II), Mg(II)	150
Co(II), Ni(II), Mn(II)	100
B(III)	50
Zn(II), V(V), Al(III)	20
Fe(III)	5
Cr(VI)	2

[a] The tolerable ratio is calculated for a ±5% relative error in the absorbance.

3.3. Study of interferences

The effect of foreign ions on the absorbance signal was studied under the selected conditions described above. The criterion for interference was fixed at a relative error, e_r, of less than ±5% of the average absorbance signal at a Ti(IV) mass concentration of 1.0 mg l^{-1}. The results are summarized in Table 2.

As can be seen, the only serious interferences were found to be Fe(III) and Cr(VI) as they caused a positive error (increase of the absorbance intensity). However, Cr(VI) could not interfere in the samples analyzed in this work. NaF, hydroxylammonium chloride and ascorbic acid (AsA) were used in order to counter the Fe(III) interference. The masking reagents were added in the buffered reagent solution and calibration curves were recorded in each case while the masking of Fe(III) was also checked. When AsA was used the linearity and the dynamic working range were retained and simultaneously the best masking efficiency was obtained. Subsequently, this reagent was selected in order to study and improve further the selectivity of the method.

3.4. Selectivity of the method

Several SI manifolds were tested at AsA mass concentrations namely 1000, 2000 and 4000 mg l^{-1} in order to improve the masking efficiency of AsA. The most effective SI manifold was consisted of three zones by punctuating the zone of AsA solution (100 μl) by the zone of the sample solution, having in this way a system with a "sandwich" look. The sequence steps are described in Table 1.

Using this manifold calibration curves were recorded at three AsA mass concentrations of 1000, 2000 and 4000 mg l^{-1}. The results proved that the linearity and the working range were independent of the AsA mass concentration. In addition, the masking efficiency of the AsA reagent at the above three mass concentrations of AsA was checked. The results showed that an AsA mass concentration of 4000 mg l^{-1} gave the best results. Apart from eliminating the interference of Fe(III) the use of the "sandwich" manifold and of AsA as masking reagent improved significantly the tolerance of the assay against all the ions that were tested for interference effects in Section 3.3, except for Ni(II), Mn(II) and PO_4^{3-}.

Table 3
Recovery experiments

SI method	Ti(IV) added (mg l^{-1})	Ti(IV) found[a] (mg l^{-1})	Recovery (%)
Natural Moroccan phosphate rock [(BCR) No. 32]	–	1.80 ± 0.06[b]	
	1.00	2.85 ± 0.09	105
	2.00	3.8 ± 0.1	100
	5.00	7.0 ± 0.1	104
Dental implant [3*i* (IOSS515)]	–	2.30 ± 0.07	
	1.00	3.35 ± 0.06	105
	2.00	4.4 ± 0.1	105
	5.00	7.2 ± 0.2	98

[a] Mean of five results.
[b] Standard deviation.

Table 4
Accuracy of the proposed method

SI method	Ti(IV) found g^{-1} sample[a] (μg)		
	Proposed method	Reference value[b]	e_r[c] (%)
Natural Moroccan phosphate rock [(BCR) No. 32]	180[d] ± 6[e]	171[d]	−5.3
Dental implant [3*i* (IOSS515)]	92[f] ± 2[e]	89[f]	+3.4

[a] Mean of five results.
[b] Value of the certified reference materials.
[c] Relative error.
[d] μg g^{-1}.
[e] Standard deviation.
[f] Mass fraction (%).

3.5. Features of the proposed method

Under the selected chemical and SI variables and using the SI setup shown in Fig. 1, a calibration curve for Ti(IV) was recorded. The calibration curve was linear in the range 0.2–10.0 mg l^{-1} and was described by the regression equation,

$$A = [(67.9 \pm 0.2) \times 10^{-3}] \times \gamma(\mathrm{Ti(IV)}) + [(28.1 \pm 3.0) \times 10^{-3}]$$

where A is the absorbance and γ(Ti(IV)) is the mass concentration of the analyte, with a relative standard deviation, s_r, of 1.5% at 5 mg l^{-1} Ti(IV) ($n = 12$), a correlation coefficient, r, of 0.9999, and a 3σ detection limit of 0.7 mg l^{-1} ($n = 10$). All the standards were run in 5 replicate injections, while for the detection limit calculation the blank was run in 10 replicate injections.

3.6. Determination of titanium in natural Moroccan phosphate rock and dental implant

The proposed SI assay was applied to the determination of titanium in natural Moroccan phosphate rock [(BCR) No. 32] and dental implant [3*i* (IOSS515)]. In the natural Moroccan phosphate rock, the titanium was calculated as 180 μg g^{-1} and in the dental implant 92% (Table 4). Both values were in good agreement with the theoretical value of the certified reference materials. The accuracy of the SI method was checked with recovery experiments by spiking the samples solutions with known amounts of Ti(IV). The experimental results were satisfactory in all cases, with recoveries ranging between 100 and 105% for the natural Moroccan phosphate rock and 98–105% for the dental implant (Table 3).

4. Conclusions

This article describes the first SI spectrophotometric method for the selective determination of Ti(IV) with application in dental implant and natural Moroccan phosphate rock. The developed method is simple, rapid, uses commercially available reagents and its recovery results for the determined samples are satisfactory.

Acknowledgement

The project was partially funded by "Herakleitos", EPEAEK, Greek Ministry of Education.

References

[1] http://en.wikipedia.org/wiki/Titanium.
[2] http://www.titaniuminfogroup.co.uk/.
[3] T. Mochizuki, R. Kuroda, Analyst 107 (1982) 1255.
[4] S. Kozuka, K. Saito, K. Oguma, R. Kuroda, Analyst 115 (1990) 431.
[5] M.G.M. Andrade, S.L.C. Ferreira, B.F. Santos, A.C.S. Costa, Talanta 39 (1992) 1229.
[6] R. Purohit, S. Devit, Analyst 117 (1992) 1175.

[7] R.E. Santelli, R.C. dos Santos Araujo, Analyst 117 (1992) 1519.
[8] M. Munoz, J. Alonso, J. Bartroli, M. Valiente, Analyst 115 (1990) 315.
[9] J. Wang, R. He, Anal. Chim. Acta 276 (1993) 419.
[10] A.A. Alwarthan, A. Townshend, Anal. Chim. Acta 196 (1987) 135.
[11] A.A. Alwarthan, A. Almuaibed, A. Townshend, Anal. Sci. 7 (1991) 623.
[12] S. Hirata, Y. Umezaki, M. Ikeda, Anal. Chem. 58 (1986) 2602.
[13] A.G. Coedo, M.T. Dorado, Appl. Spectrosc. 49 (1995) 115.
[14] K.L. Yang, S.J. Jiang, T.J. Hwang, J. Anal. At. Spectrom. 11 (1996) 139.
[15] A. Makishima, E. Nakamura, J. Anal. At. Spectrom. 15 (2000) 263.
[16] C.E. Lenehan, N.W. Barnett, S.W. Lewis, Analyst 127 (2002) 997.
[17] A. Ivaska, J. Ruzicka, Analyst 118 (1993) 885.
[18] D. Myers, At. Absirp. Newsl. 6 (1967) 89.

Available online at www.sciencedirect.com
ScienceDirect
Talanta 71 (2007) 1294–1297
Talanta
www.elsevier.com/locate/talanta

Transition metal ion selective *ortho*-ester diazophenylcalix[4]arene

Tae Hyun Kim [a], Su Ho Kim [b], Le Van Tan [a], Yu Jin Seo [a], Sun Young Park [b], Hasuck Kim [a,*], Jong Seung Kim [b,*]

[a] *School of Chemistry, Seoul National University, Seoul 151-747, Republic of Korea*
[b] *Department of Chemistry, Institute of Nanosensor & Biotechnology, Dankook University, Seoul 140-714, Republic of Korea*

Received 5 June 2006; received in revised form 28 June 2006; accepted 28 June 2006
Available online 4 August 2006

Abstract

New chromogenic dizophenylcalix[4]arene **1** showing selective color change to transition metal ions over other alkaline and alkaline earth metal ions has been prepared in the cone conformation and tested for its usefulness.
© 2006 Elsevier B.V. All rights reserved.

Keywords: Calix[4]arene; Chromoionophore; Complexation; Transition metal ions

1. Introduction

The development of chromoionophores has been a very active research area in supramolecular chemistry, since these can be applied to many useful chemical sensor technologies [1]. The chromoionophore is constructed from two functionally different parts: (a) an ionophore part, which recognizes ions and functions to a particular ionophore; and (b) a chromophore part, which transforms a chemical information produced by ionophore–ion interaction to an optical signal [2].

Calixarenes [3] have been extensively used as hosts for a wide range of metal ions in selective transport, potentiometric, optical, and chromoionophoric system [4–9]. In particular, calixarene chromoionophores have long been studied as specific metal ion indicators since Shinkai and co-workers reported that calix[4]arene having one 4-(4-nitrophenyl)azophenol unit with three ethyl ester groups shows especially Li^+ ion selectivity with respect to the UV–vis band shift [10]. Many interesting aspects of complexation of alkali and alkaline earth metal ions were disclosed by studying the absorption behavior of chromophoric groups [2,11]. However, there are relatively few reports on the design of sensor for transition metal ions [12]. Although, a variety of effective chromogenic sensors for alkali metal and alkaline-earth metal cation such as K^+ [13], Ca^{2+}[13], and Cs^+[14] have already been developed, those for Ba^{2+} and Cr^{3+} has been rarely reported.

Azophenol groups are one of the most frequently employed functions as a signaling device for the design of chromogenic ionophores, and many derivatives based on the crown ethers and calixarenes exhibit a pronounced chromogenic behavior towards a variety of cations, and even chiral amines [15]. Among them azocalixarenes are particularly attractive for their efficient ionophoric properties towards some of important guest ions such as Ca^{2+} or K^+ ion [16].

We have been also interested in the designing selective coloring sensor (calixarene chromophores) towards specific metal cations [9,14]. In this work, we are reporting a promising result that **1** is able to selectively discriminate transition metal ions with Pb^{2+} ion selectivity over alkali- and alkaline earth metal cations (Fig. 1).

2. Experimental

2.1. Synthesis

2.1.1. 5,11,17,23-tetra[(2-Ethyl acetoethoxyphenyl) (azo)phenyl]calix[4]arene (*1*)

A solution of 2-aminobenzoate (3.10 g, 18.7 mmol), $NaNO_2$ (1.46 g, 21.1 mmol) and conc. HCl (5 mL) in water (10 mL) was added dropwise over a period of about 15 min into a solution of calix[4]arene (2.00 g, 4.70 mmol) in THF:pyridine (5:2) (25 mL) at 0 °C. The solution was allowed to be stirred for

* Corresponding authors. Tel.: +82 2 799 1351; fax: +82 2 797 3277.
E-mail addresses: hasuckim@snu.ac.kr (H. Kim), jongskim@dankook.ac.kr (J.S. Kim).

0039-9140/$ – see front matter © 2006 Elsevier B.V. All rights reserved.
doi:10.1016/j.talanta.2006.06.035

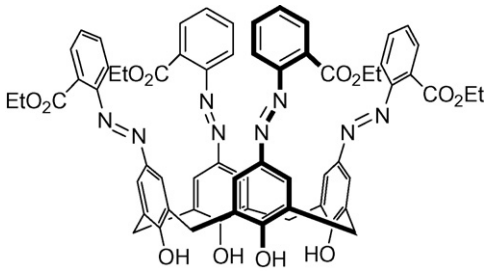
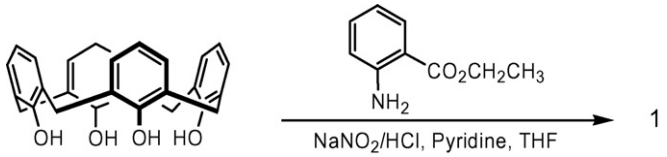


Fig. 1. Structure of diazo-coupled calix[4]arene **1**.

15 min and then additional 24 h at room temperature. After removal of the solvent *in vacuo*, the resulting solid was dissolved in EtOAc (100 mL) and the organic layer was washed three times with water. The organic layer was dried over anhydrous $MgSO_4$ and the solvent was removed *in vacuo* to give a reddish oil. Column chromatography using EtOAc:hexane (2:1) provided 2.4 g (45%) of **1** as a yellow orange solid. m.p.: 158–162 °C. IR (KBr pellet, cm^{-1}): 3220, 1735. ^1H NMR (200 MHz, $CDCl_3$): δ 7.43–7.22 (m, 24 H, Ar–H), 4.24 (d, 4 H, Ar–C*H*$_2$–Ar), 3.97–3.86 (m, 8 H, $COCH_2CH_3$, $J = 6.9$, 7.3, and 6.7 Hz), 3.42 (d, 4 H, Ar–C*H*$_2$–Ar), 0.82–0.75 (t, 12 H, $COCH_2CH_3$, $J = 6.9$ Hz). ^{13}C NMR (DMSO-d_6): δ 168.1, 159.2, 151.5, 145.3, 132.3, 130.8, 129.7, 129.6, 129.0, 124.5, 119.7, 61.5, 32.3, and 14.8. FAB MS *m/z* (m^+): Calcd., 1129.18. Found, 1129.0. Anal. Calcd. for $C_{64}H_{56}N_8O_{12}$: C, 68.07; H, 5.00. Found: C, 68.05; H, 5.02.

2.2. Analytical procedures

Absorption spectra were measured with Sinco-S3130 UV–visible recording spectrophotometer (Korea). UV stock solutions of iononphore **1** (2×10^{-4} M, in CH_3CN) and metal perchlorate (2×10^{-2} M, in CH_3CN) were prepared. The metal solution was diluted 10 and 100 times to give 2×10^{-3} and 2×10^{-4} M solutions. Aliquots of metal solution were added to the ionophore solution, and the final concentration and composition of the solution were adjusted to the desired value by adding extra CH_3CN. The stability constants (K_a) for complexation between ionophore **1** and metal cations were determined on the basis of the nonlinear curve fitting procedure for a 1:1



Scheme 1. Synthetic route of compound **1**.

complex:

$$r = \frac{A - A_f^0}{A_c - A_f^0} + \frac{A - A_f^0}{C_f^0 \times K_a \times (A_c^0 - A)}$$

where r is the added equivalents of cations, A_f^0, A and A_c^0 are absorbance of the free ligand, the ligand plus r equivalents of cations and the ligand plus large excess cation solutions, C_f^0 the concentration of the free ligand and K_a is the stability constant [17,18].

3. Results and discussion

Cone-5,11,17,23-*tetra*[(2-ethylacetoethoxyphenyl)(azo)-phenyl]calix[4]arene (**1**) was synthesized by adaptation of synthetic methods reported earlier (Scheme 1) [19,20]. Diazo coupling reaction of calix[4]arene with ethyl 2-aminobenzoate, sodium nitrite and concentrated HCl in pyridine with THF (5:2) gave desired product **1** in moderate yield. The cone conformation of **1** is confirmed by its NMR spectra: (a) two doublets at 4.24 and 3.42 ppm with an AB pattern for methylenic protons of $ArCH_2Ar$ in the ^1H NMR spectra and (b) singlet at 32.3 ppm for the $ArCH_2Ar$ bridge carbons in the ^{13}C NMR spectra.

The chromogenic ionophore properties of **1** upon alkali and alkaline earth metal cation complexation were investigated by examining the UV–vis absorption behaviors of the host in CH_3CN solution (Fig. 2). **1** showed characteristic UV spectral behaviors of azocalix[4]arene derivatives and their absorption maxima are located at 345 and 487 nm corresponding to π–π^* and n–π^* transitions, respectively, which are in accordance with typical diazo spectra. These observations suggest that **1** exist as a mixture of the two tautomeric forms, namely an azophenol form and quinone-hydrazone form in CH_3CN solution [19,20]. This can be explained by the assumption that an azophenol form of **1** gets stabilized through a six-membered hydrogen bonded

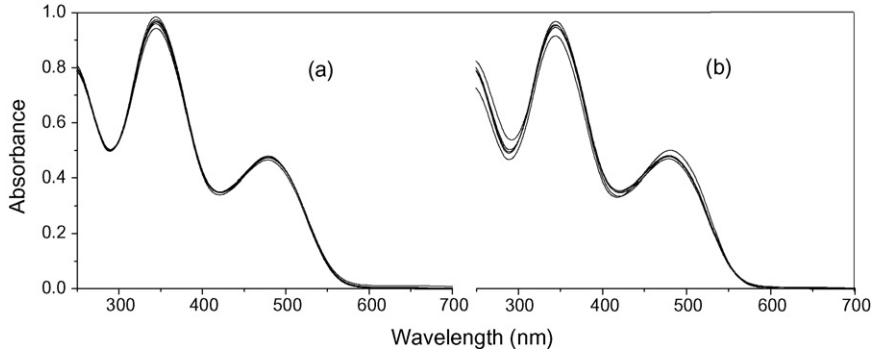


Fig. 2. Absorption spectra of **1** with various alkali metal ions (a) and alkaline earth metal ions and (b) both ligand and metal cations are 2×10^{-5} M in CH_3CN.

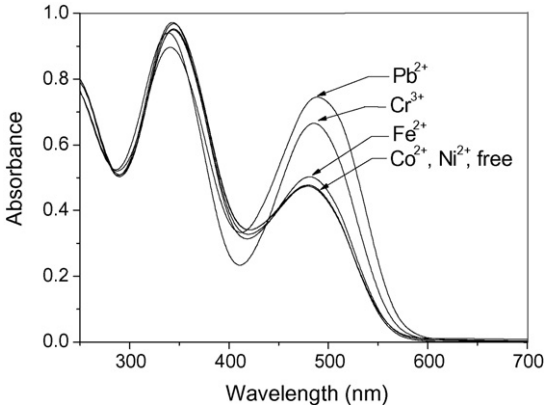


Fig. 3. Absorption spectra of **1** (2×10^{-5} M) with various transition metal ions (2×10^{-5} M) in CH_3CN.

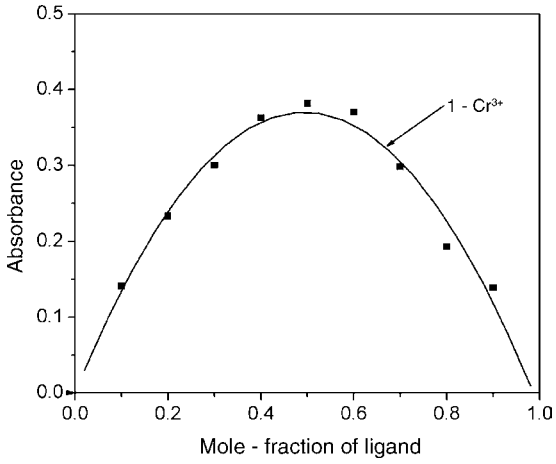


Fig. 4. Job's continuous variation plot for **1**-Cr^{3+} at 487 nm ([Ligand] + $[M^{n+}] = 2 \times 10^{-5}$ mol L^{-1}).

structure between azo unit and *ortho*-ester group represented by a quinone-hydrazone form (vide infra) [20].

We next investigated the affinity of **1** for a series of alkali, alkaline earth and transition metal ions. Absorption spectra of 0.02 mM **1** in the presence of one equivalent of metal ions are shown in Figs. 2 and 3. No significant changes in absorption spectra were seen when alkali and alkaline earth metal ions were added to **1** (Fig. 2), whereas marked bathochromic shifts were observed for transition metal ions (Fig. 3). Among the tested transition metal ions, the Pb^{2+} ion showed the most pronounced response and the induced absorbance intensity at 487 nm increased in order of $Pb^{2+} > Cr^{3+} > Fe^{2+} > Co^{2+} \approx Ni^{2+}$. This result implies that there is a subtle balance between metal complexation-induced release of protons from the azophenols to the quinone-hydrazone tautomer [3], and the *ortho*-ester groups of **1** can stabilize the quinone-hydrazone form in azocalix[4]arene after adding transition metal ions. Concerning complexation between hosts and metal ions, metal cation is able to interact with the phenol unit of the lower rim and azo group in the medium cavity. However, due to the intramolecular hydrogen bonding of lower rim, metal ions may be accommodated within the region of the medium cavity of the calixarene [21,22]. This arrangement could facilitate simultaneously π–π interactions between metal ions and the negative change center of **1** [21].

For the complexation ratio between ligand and metal ion, the Job's plot experiment was conducted by varying the concentration of both **1** and Cr^{3+}. The maximum point at the mole fraction was about 0.5 which refers to a typical ligand–metal complex ratio of 1:1 as shown in Fig. 4.

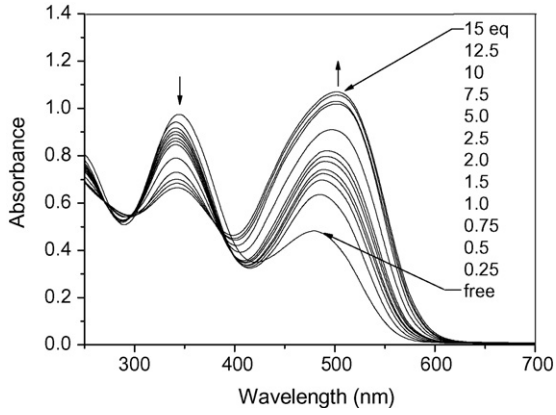


Fig. 5. Changes in absorption spectra as a function of $[Pb^{2+}]$ [**1**] = 2×10^{-5} M in CH_3CN.

To have a further insight into the chromogenic behavior of **1**, the absorption profile as a function of metal ion concentration was obtained (Fig. 5). **1** exhibited a gradual increase in absorption intensity at the λ_{max} of 487 nm and a decrease at the λ_{max} of 345 nm upon the addition of incremental lead ions. From the plot of the absorbance changes of **1**-Pb^{2+} system, the stability constant was determined by nonlinear curve fitting procedure and found to be 5.5×10^3 M^{-1} in CH_3CN. The stability constants for other transition metal ions are summarized in Table 1.

The visible color changes of **1** upon various metal cations was also observed and depicted in Fig. 6 where only transition metal ions change the color of the **1** from yellow to deep orange. From

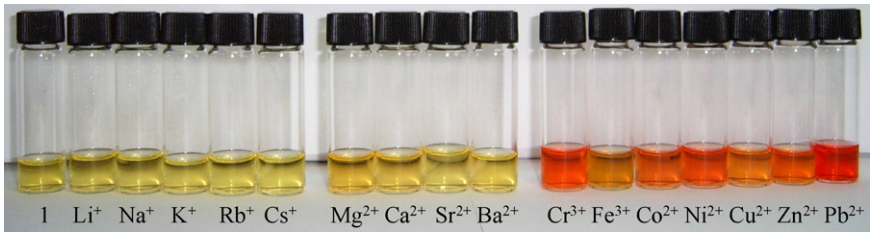


Fig. 6. Color change of **1** (2×10^{-5} M) in various metal cation (2×10^{-3} M) solutions.

Table 1
Stability constants for the complexation of **1** with transition metal ion perchlorates in CH_3CN at room temperature

Metal ions	Stability constants (K_a)
Cr^{3+}	4.4×10^3
Fe^{2+}	1.4×10^3
Pb^{2+}	5.5×10^3

Stability constants were determined by nonlinear fitting curve procedure [17,18].

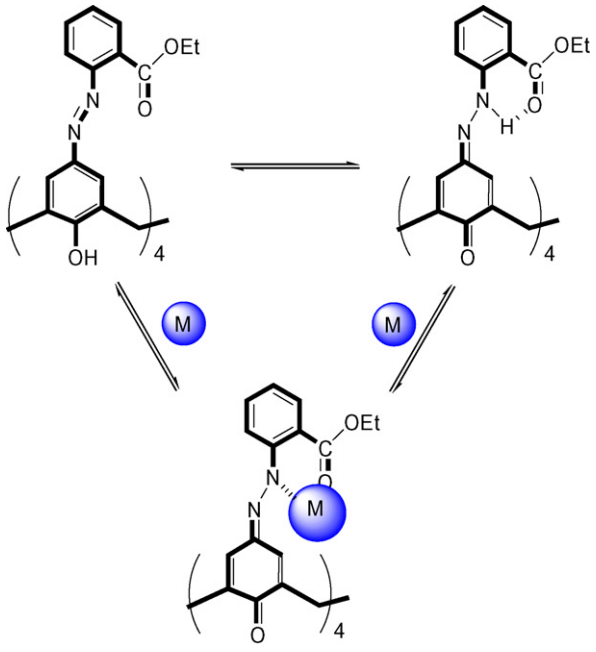


Fig. 7. Plausible complexation mechanism of **1** with transition metal ions.

the results of complexation study, the plausible complexation mechanism based on the 1:1 complexation is proposed as Fig. 7.

In conclusion, cone-*tetra*azocalix[4]arene (**1**) has been prepared and its color change upon the addition of alkali, alkaline earth, and transition metal ions were investigated. Compound **1** shows selective color changes to transition metal ions over other metal ions from yellow to orange, which is mainly due to metal ion complexation-induced release of protons from the azophenols to the quinone-hydrazone tautomer followed by internal complexation of the metal ion with aid of nitrogen atoms and *ortho*-ester carbonyl groups by 1:1 complexation event.

Acknowledgment

This research was fully supported by grant from cooperative research of KRF (2005-C00101) and BK21.

References

[1] L.L. Lu, S.F. Zhu, X.Z. Liu, Z.Z. Xie, X. Yan, Anal. Chim. Acta. 535 (2005) 183.
[2] Y. Inoue, G.W. Gokel, Cation Binding by Macrocycles: Complexation of Cationic Species by Crown Ethers, M. Dekker, New York, 1990.
[3] (a) C.D. Gutsche, in: J.F. Stoddart (Ed.), Calixarenes, Monographs in Supramolecular Chemistry, vol. 1, Royal Society of Chemistry, Cambridge, UK, 1989;
(b) J. Vicens, V. Böhmer (Eds.), Calixarenes: A Versatile Class of Macrocyclic Compounds, Kluwer, Dordrecht, 1991;
(c) V. Böhmer, Angew. Chem. Int. Ed. Engl. 34 (1995) 713;
(d) C.D. Gutsche, in: J.L. Atwood, J.E.D. Davies, D.D. MacNicol (Eds.), Inclusion Compounds, vol. 4, Oxford University Press, New York, 1991, pp. 27–63;
(e) J.-D. Van Loon, W. Verboom, D.N. Reinhoudt, Org. Prep. Proceed. Int. 24 (1992) 437–462;
(f) R. Ungaro, A. Pochini, in: H.-J. Schneider (Ed.), Frontiers in Supramolecular Organic Chemistry and Photochemistry, VCH, Weinheim, Germany, 1991, pp. 57–81;
(g) G.D. Andreetti, F. Ugozzoli, R. Ungaro, A. Pochini, in: J.L. Atwood, J.E.D. Davies, D.D. MacNicol (Eds.), Inclusion Compounds, vol. 4, Oxford University Press, New York, 1991, pp. 64–125.
[4] W.F. Nijenhuis, E.G. Buitenhuis, F. de Jong, E.J.R. Sudhölter, D.N. Reinhoudt, J. Am. Chem. Soc. 113 (1991) 7963.
[5] P.L.H.M. Cobben, R.J.M. Egberink, J.R. Bomer, P. Bergveld, W. Verboom, D.N. Reinhoudt, J. Am. Chem. Soc. 114 (1992) 10573.
[6] B. Bühlmann, E. Pretsch, E. Bakker, Chem. Rev. 98 (1998) 1593.
[7] J.S. Kim, O.J. Shon, J.A. Rim, S.K. Kim, J. Yoon, J. Org. Chem. 67 (2002) 2348.
[8] J.S. Kim, O.J. Shon, J.K. Lee, S.H. Lee, J.Y. Kim, K.M. Park, S.S. Lee, J. Org. Chem. 67 (2002) 1372.
[9] J.S. Kim, O.J. Shon, S.H. Yang, J.Y. Kim, M.J. Kim, J. Org. Chem. 67 (2002) 3165.
[10] H. Shimizu, K. Iwamoto, K. Fujimoto, S. Shinkai, Chem. Lett. (1991) 2147.
[11] A.P. deSilva, H.Q.N. Gunaratne, T. Gunnlaugsson, A.J.M. Huxley, C.P. McCoy, J.T. Rademacher, T.E. Rice, Chem. Rev. 97 (1997) 1515.
[12] Q.L. Ma, H.M. Ma, Z.H. Wang, M.H. Su, H.Z. Xiao, S.C. Liang, Chem. Lett. (2001) 100.
[13] N.Y. Kim, S.K. Chang, J. Org. Chem. 63 (1998) 2362.
[14] (a) S.H. Lee, J.Y. Kim, J. Ko, J.Y. Lee, J.S. Kim, J. Org. Chem. 69 (2004) 2902;
(b) S.H. Lee, S.K. Kim, J.H. Bok, S.H. Lee, J. Yoon, K. Lee, J.S. Kim, Tetrahedron Lett. 46 (2005) 8163.
[15] T. Hayashita, M. Takagi, Comprehensive Supramolecular Chemistry, vol. 1, Pergamon, Oxford, 1996.
[16] Z. Asfari, V. Böhmer, J. Harrowfield, J. Vicens (Eds.), Calixarenes 2001, Kluwer Academic Publishers, Dordrecht, The Netherlands, Boston, 2001.
[17] C.D. Chriswell, A.A. Schilt, Anal. Chem. 47 (1975) 1623.
[18] S.K. Kang, PhD Dissertation, Seoul National University, 1999, pp. 156–157.
[19] H.M. Chawla, M. Nanda, Arkivoc (2003) 171.
[20] F. Karci, I. Sener, H. Deligoz, Dyes Pigments 59 (2003) 53.
[21] T. Kao, C. Wang, Y. Pan, Y. Shiao, J. Yen, C. Shu, G. Lee, S. Peng, W. Chung, J. Org. Chem. 70 (2005) 2912.
[22] J. Lu, R. Chen, X. He, J. Electroanal. Chem. 528 (2002) 33.

Available online at www.sciencedirect.com
ScienceDirect
Talanta 71 (2007) 1438–1440
Talanta
www.elsevier.com/locate/talanta

Short communication

Sunlight-induced covalent immobilization of proteins

Saroj Kumar, Pradip Nahar *

Institute of Genomics and Integrative Biology (CSIR), Mall Road, Delhi 110007, India

Received 24 May 2006; received in revised form 21 June 2006; accepted 21 June 2006
Available online 25 July 2006

Abstract

Horseradish peroxidase (HRP) and glucose oxidase (GOD) were immobilized by sunlight onto the photoreactive cellulose membrane prepared by the reaction of cellulose membrane with 1-fluoro-2-nitro-4-azidobenzene (FNAB). A correlation between sunlight intensity and immobilization was studied. Sunlight intensity required for optimum immobilization was found to be 21,625 lux beyond which no appreciable increase in immobilization was observed. Around 2.5-fold increase in absorbance value was observed when HRP immobilization was carried out by sunlight than in dark or on untreated surface. Sunlight exposure gave better immobilization compared to 365 nm UV light. Thus, sunlight could be used as a potential alternative to UV light for immobilization of biomolecules such as carbohydrate, DNA or protein.
© 2006 Elsevier B.V. All rights reserved.

Keywords: Sunlight; Photoimmobilization; 1-Fluoro-2-nitro-4-azidobenzene; Photoreactive polymer

1. Introduction

In recent years photochemical immobilization has become a useful technique for covalently fixing proteins, DNA or carbohydrates required for different applications [1–3]. Photochemical immobilization on solid surface offer unique advantage over thermochemical immobilization such as (i) any biomolecule irrespective of their functional group can be immobilized by photochemical method, (ii) it is non-invasive method and there is no need of any harsh reaction conditions, and (iii) micro patterning can be carried out easily for microarray technique by controlling light exposure. In the last couple of years, 1-fluoro-2-nitro-4-azidobenzene (FNAB) has been widely used for photochemical activation of solid supports for different applications [4–7]. One of the reasons for use of FNAB is its simple and single step method of preparation with high yield.

Recently, we have prepared photoreactive polymers using FNAB and found them efficient in binding a protein molecule without any additional reagent through UV light in an UV Stratalinker 2400 (Stratagene, USA) [8,9]. However, such instrument is not available in most of the laboratory. Nahar et al. have recently reported an easily accessible sunlight method for photochemical activation of a polymer surface [10].

In this communication, we have explored sunlight for photochemical immobilization of enzymes. Horseradish peroxidase (HRP) and glucose oxidase (GOD) showed efficient immobilization when placed on the photoreactive cellulose membranes and exposed to sunlight.

2. Materials and methods

Horseradish peroxidase (HRP) and *o*-phenylenediamine (OPD) were purchased from Sigma, USA. Glucose oxidase (GOD) was purchased from Boehringer, Mannheim (Germany). Cellulose microporous membrane (MWCO, 3.5 KD) was purchased from Spectrum, TX, USA. Other reagents and solvents were of analytical grade. FNAB was prepared from 4-fluoro-3-nitroaniline through the diazotization reaction as reported earlier [8].

Phosphate-buffered saline (PBS) was prepared by adding 0.85% NaCl to phosphate buffer (0.01 M, pH 7.2). Substrate dye buffer was prepared by mixing 12 ml of citrate buffer (0.025 M citric acid and 0.05 M $Na_2HPO_4{\cdot}2H_2O$, pH 5), 5 μl of H_2O_2 (30%, w/v), and 5 mg of OPD. All the experiments were carried out in triplicates.

Abbreviations: FNAB, 1-fluoro-2-nitro-4-azidobenzene; HRP, horseradish peroxidase; GOD, glucose oxidase

* Corresponding author. Tel.: +91 11 27667439; fax: +91 11 27667471.
E-mail addresses: p_nahar@hotmail.com, pnahar@igib.res.in (P. Nahar).

0039-9140/$ – see front matter © 2006 Elsevier B.V. All rights reserved.
doi:10.1016/j.talanta.2006.06.029

2.1. Preparation of photoreactive cellulose membrane

Cellulose membrane was cut into 1-cm^2 discs and washed with distilled water and methanol. FNAB (60 mg/10 ml of toluene/10 cellulose discs) solution together with discs were taken in a conical flask and sonicated for 10 min in a sonicator bath. During this period, 50 μl of 30% KOH was added dropwise into the flask. The mixture was further stirred slowly on a magnetic stirrer for 45 min at 45 °C. Discs were washed with ethanol three times, dried and kept in a dark bottle, in a dark place. These photoreactive cellulose discs were used for further experiments.

2.2. Immobilization of enzymes by sunlight and UV light irradiation in different time periods

Photoreactive cellulose discs were put on glass petri plates and HRP (1 μg/100 μl PBS/disc) was spread onto the activated discs. Petri plates were placed in sunlight for 10, 20, 30, 40 and 50 min, respectively. Intensity of sunlight was 22,957 lux as measured by a digital luxmeter and temperature recorded was 22 °C. After the stipulated time cellulose discs were washed four times with washing buffer (0.05% Tween-20 in PBS) to remove the unbound enzyme. Cellulose discs having immobilized enzyme were put into the wells of a microtiter plate and substrate dye buffer (300 μl/well) was added. After 5 min of color development, reaction was stopped by adding 20 μl/well of stop solution (5% of H_2SO_4) and absorbance was recorded at 490 nm.

GOD was immobilized similarly using 6 μg of GOD/100 μl of 0.01 M phosphate buffer, pH 7/disc. Immobilized GOD was assayed by adding 300 μl/well of substrate solution having 200 μl of 9% glucose solution, 50 μl of HRP (1 mg/ml dilution) and 50 μl of OPD (3 mg/ml of PB). After 12 min, 20 μl/well of stop solution was added and absorbance was recorded at 490 nm.

Control experiment was carried out similarly except that the immobilization reaction was carried out in dark (0 lux). In another control experiment, enzyme was immobilized onto an untreated cellulose membrane.

Comparison between sunlight and UV light-mediated immobilization was carried out by doing photoimmobilization by UV light at 365 nm in an UV Strataliker (Model 2400; Stratagene, USA).

2.3. Optimization of sunlight intensity

Photoreactive cellulose discs were put on glass petri plates and HRP (1 μg/100 μl PBS/disc) was spread onto the activated discs. Petri plates were then placed in sunlight for 30 min at 7, 8, 9, 10, 11 a.m. and 12 noon, respectively. Sunlight intensity was measured by a luxmeter. After the exposure the discs were washed by washing buffer and the activity of the enzyme was assayed.

3. Results and discussion

Recently, we have reported sunlight-mediated activation of inert polymer for thermochemical immobilization of a protein [10]. Our study was aimed to find out whether in the reverse procedure, biomolecule could be immobilized by sunlight without loosing its activity. In this procedure photoreactive cellulose membrane was prepared in a thermochemical reaction with 1-fluoro-2-nitro-4-azidobenzene in presence of a basic catalyst. The reaction occurred by displacing fluoro group by hydroxyl group of cellulose. Photoreactive cellulose membrane thus prepared had a photolabile azido group, which in presence of light formed a reactive nitrene. Later inserted into the C–H bond of the enzymes forming an immobilized enzyme.

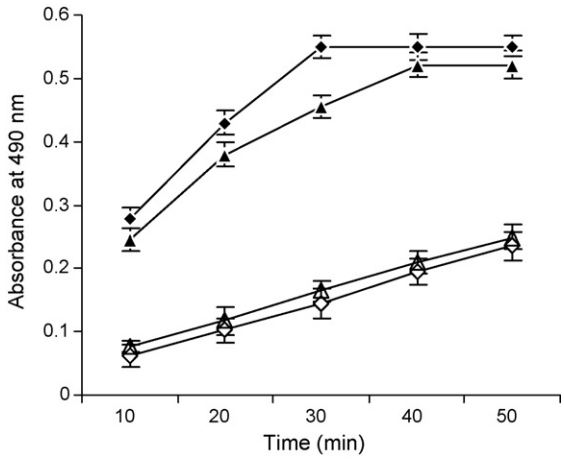


Fig. 1. Immobilization of HRP by sunlight (♦, ◊) and UV light (▲, △) irradiation in 10, 20, 30, 40 and 50 min, respectively, onto activated (♦, ▲) and untreated (◊, △) cellulose membrane.

The study was carried out in Delhi (latitude 28.38 °C N longitude 77.12E), India, in winter. The temperature during the course of the experiments was recorded in between 21 and 25 °C.

HRP was immobilized onto the photoreactive cellulose by sunlight (22,957 lux) in 10, 20, 30, 40 and 50 min, respectively. Sunlight irradiation for 30 min was found as optimum time for HRP immobilization. The results were very much similar to that obtained by UV light-mediated immobilization except that the maximum immobilization in later case occurred in 40 min (Fig. 1). As was expected, very little immobilization in 30 min was observed when it was carried out either by sunlight or UV light onto untreated cellulose membrane (Fig. 1). Similar results were obtained when immobilization was carried out onto photoreactive cellulose membrane in dark (0 lux) (results not shown). In both these cases immobilization was through adsorption, which increased with increase in time. Similar results were obtained when GOD was immobilized by sunlight instead of HRP (Fig. 2).

Finally, we have studied the effect of sunlight intensity on immobilization. This was important as immobilization depends on light, which in turn depends on its intensity. As intensity of the sunlight varies from place to place and from time to time it was necessary to find an optimum intensity for immobilization of a biomolecule. To determine the effect of sunlight intensity photoreactive cellulose together with the enzyme was placed under sunlight for 30 min at different times of the day. In the morning (8 a.m.), sunlight intensity was very less (10,222 lux); however, it increased gradually to 61,247 lux at 12 noon. As seen

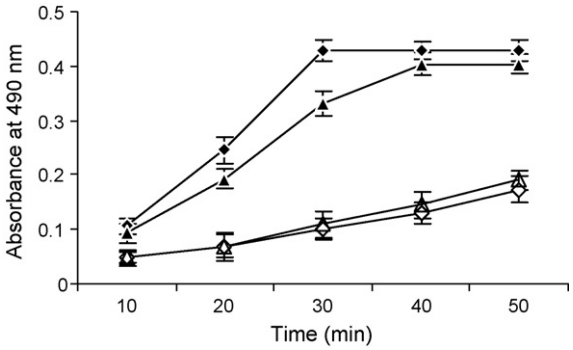


Fig. 2. Immobilization of GOD by sunlight (♦, ◊) and UV light (▲, △) irradiation in 10, 20, 30, 40 and 50 min, respectively, onto activated (♦, ▲) and untreated (◊, △) cellulose membrane.

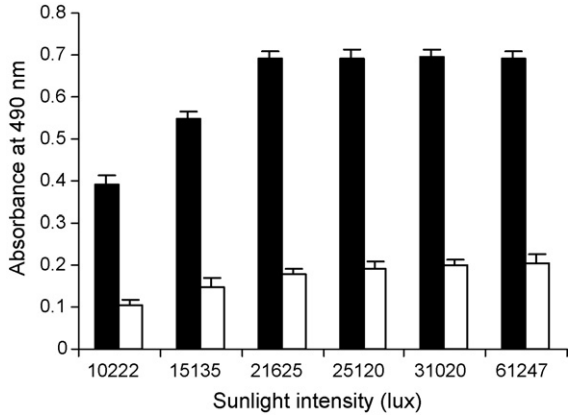


Fig. 3. Immobilization of HRP in 30 min by sunlight at 10,222, 15,135, 21,625, 25,120, 31,020 and 61,247 lux intensity respectively onto activated (■) and (□) untreated cellulose membrane at 21–23 °C.

from Fig. 3, immobilization of HRP increased till the intensity of 21,625 lux beyond which it remained unchanged indicating that the reaction can be carried out in a wide range of intensity. It demonstrates that immobilization reaction can be efficiently achieved in 21,625 lux, which is not very bright sunlight and may be available in most part of the world.

The optimum sunlight intensity of 21,625 lux for immobilization of biomolecule is very much akin to the optimum sunlight intensity of 26,300 lux for activation of the surface as reported in our earlier work [10]. The results were as per our expectations, as in both the cases light transforms the azido group of FNAB or photoreactive polymer into highly reactive nitrene, which instantly binds to the polymer surface or biomolecule.

Temperature raised by UV lights either in an UV Strataliker or other closed system may have a detrimental effect on the biomolecule during immobilization, especially if UV irradiation has to be continued for longer time, which might be required while using other photolinker. In such case, the reaction has to be carried out by cooling the reaction vessel. However, sunlight mediated immobilization, being carried out in an open space, has no such problem.

Besides temperature, intensity of sunlight is uniform for a particular time and space whereas the same is not true for UV light. Even in UV Strataliker about 10% variations in intensity was observed when it was measured in different places inside the Strataliker. The maximum intensity was found in the center but decreased at the corners of the Strataliker.

Thus, sunlight could be a very good alternative to UV light for photoimmobilization. The method does not require any equipment and is suitable for large scale as well as small-scale immobilization. The method may also find potential applications for photoimmobilization using other photolinkers or biomolecules. Besides, the method may be potentially useful for preparation of protein or DNA micoarray.

References

[1] H. Hasuda, O.H. Kwon, I.-K. Kang, Y. Ito, Synthesis of photoreactive pullulan for surface modification, Biomaterials 26 (2005) 2401–2406.
[2] N. Barie, M. Rapp, H. Sigrist, H.J. Ache, Biosens. Bioelectr. 13 (1998) 855–860.
[3] R. Barner, W. Huber, J. Hubscher, J. Hurst, D. Schlatter. Biosensors layers. US patent 5,986,066 (1999).
[4] A. Naqvi, P. Nahar, R.P. Gandhi, Anal. Biochem. 306 (2002) 74–78.
[5] U. Bora, L. Chug, P. Nahar, J. Immunol. Meth. 268 (2002) 171–177.
[6] U. Bora, K. Kannan, P. Nahar, J. Immunol. Meth. 293 (2004) 43–50.
[7] P. Nahar, U. Bora, Anal. Biochem. 328 (2004) 81–83.
[8] A. Naqvi, P. Nahar, Anal. Biochem. 327 (2004) 68–73.
[9] U. Bora, P. Sharma, K. Kannan, P. Nahar, J. Biotechnol. 126 (2006) 220–229.
[10] P. Nahar, A. Naqvi, S.F. Basir, Anal. Biochem. 327 (2004) 162–164.

Available online at www.sciencedirect.com
ScienceDirect
Talanta 71 (2007) 1441–1443
Talanta
www.elsevier.com/locate/talanta

Short communication

Voltammetric determination of hafnium with calconcarboxylic acid

Halyna Levytska, Oksana Orshuliak *

Department of Analytical Chemistry, Faculty of Chemistry, Ivan Franko National University, Kyryla and Mefodia Str., 6, 79005 Lviv, Ukraine

Received 20 February 2006; received in revised form 2 June 2006; accepted 30 June 2006
Available online 8 August 2006

Abstract

The interaction of Hf(IV) with calconcarboxylic acid (1-(2-hydroxy-4-sulfo-1-naphtylazo)-3-naphtolic acid) was investigated by cyclic voltammetry varying various factors (pH, ionic strength, contents of ethanol and scan rate). Optimal conditions of Hf(IV) determination in the presence of calconcarboxylic acid were found: acetic buffer solution pH 2.6, scan rate 0.5 Vs^{-1}. The detection limit of Hf(IV) concentration was 2.46×10^{-7} mol L^{-1}. The influence of foreign ions on the Hf(IV) determination was studied. It was established that some metals like cadmium, nickel, zinc, copper and titanium could be determined with Hf(IV) simultaneously. The method of voltammetric determination of hafnium was tested on model solutions and used in the determination of Hf(IV) in terbium-base alloy.
© 2006 Elsevier B.V. All rights reserved.

Keywords: Hafnium; Calconcarboxylic acid (CCA); Cyclic voltammetry

Calconcarboxylic acid (1-(2-hydroxy-4-sulfo-1-naphtylazo)-3-naphtolic acid) is a good complexant which early was used for voltammetric determination of Co(II) [1], Ni(II) [2] and spectrophotometric determination of Ca(II) [3] and Cu(II) [4]. Complexation of hafnium with calconcarboxylic acid has not been studied before. Not many methods for the determination of hafnium are known. However, some of these methods have low sensitivity and low selectivity. The complex of hafnium with 4-(2-pyridylazo)resorcinol [5], biacetylmonoxime nicotinylhydrazone [6] and 3-hydroxychromone [7] have been proposed for spectrophotometric determination of hafnium. Quercetin [8] and myricetin [9] have previously been reported as reagents of the fluorometric determination of hafnium. The methods of voltammetric determination of hafnium are not numerous. Only the polarographic determination of hafnium with 4-(2-pyridylazo)resorcinol and 4-(2-pyridylazo)-2-naphtol [10] is known.

This paper describes the determination of hafnium with calconcarboxylic acid by the cyclic voltammetry.

1. Experimental

1.1. Apparatus

All voltammetric curves were obtained on digital voltammetric equipment which combines a personal computer with a three electrode system consisting of the dropping mercury as the working electrode (DME), $Hg/HgCl_2$ (saturated KCl) reference electrode and a platinum-wire counter electrode. The pH-meter model MV 870 DIGITAL-pH-MESSEGERÄT was used for the pH measurements.

1.2. Reagents

All reagents were of analytical grade and the solutions were prepared with bi-distilled water.

A stock standard solution of 1×10^{-2} mol L^{-1} Hf(IV) was prepared by dissolving 0.1855 g hafnium sulfate in 50 mL volumetric flask with 2 mol L^{-1} H_2SO_4. The solution was standardized titrimetrically with $EDTANa_2H_2$.

Stock standard solution of 1×10^{-3} mol L^{-1} calconcarboxylic acid was prepared by dissolving a precise amount of dye in aqueous-ethanol solution (15 vol%).

* Corresponding author.
E-mail address: bilyk_oksana@mail.ru (O. Orshuliak).

0039-9140/$ – see front matter © 2006 Elsevier B.V. All rights reserved.
doi:10.1016/j.talanta.2006.06.036

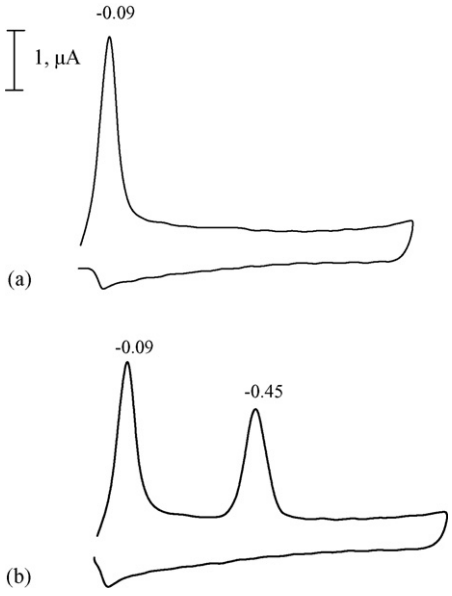


Fig. 1. Cyclic voltammograms of CCA in the absence (a) and presence (b) of Hf(IV) ions; $\upsilon = 0.5\,V\,s^{-1}$. $C_{CCA} = 5 \times 10^{-5}\,mol\,L^{-1}$; $C_{Hf(IV)} = 6 \times 10^{-6}\,mol\,L^{-1}$; pH 2.6.

The necessary stabilization of pH was achieved by $HCl + NH_4Cl$ and acetic buffer solutions.

1.3. Procedure

A 10.0 mL volume of solution containing Hf(IV) $4 \times 10^{-6}\,mol\,L^{-1}$, CCA $5 \times 10^{-5}\,mol\,L^{-1}$, ethanol 12 vol% and acetic buffer solution (pH 2.6) was transferred into a voltammetric cell. Dissolved oxygen was removed from the solutions by argon purging. The voltammogram was recorded by applying a linear scan ($0.5\,V\,s^{-1}$) in the range of 0.0 to -1.0 V. The peak of the complex was observed at -0.45 V (Fig. 1).

1.4. Analysis of terbium-base alloy

A weight of 0.0876 g sample was dissolved in 3 mL concentrated hydrochloric acid and 1ml concentrated nitric acid with heating. The solution was evaporated to solid residue. After addition of 2 mL of concentrated sulfuric acid it was evaporated again to appearance of fume. The solution was cooled and transferred to a 50 mL standard flask, diluted to the mark with $2\,mol\,L^{-1}$ H_2SO_4. Transfer an aliquot of 0.1 mL into a 25 mL flask and analyse as already described.

2. Results and discussion

No peak was found on the voltammogram in a solution containing acetic buffer solution (pH 2.6) and $6 \times 10^{-6}\,mol\,L^{-1}$. The cyclic voltammogram of calconcarboxylic acid at the pH 2.6 is shown in Fig. 1a. It shows one cathodic peak at -0.09 V. In the presence of Hf(IV) ions, the appearance of the addition peak at -0.45 V is observed on the voltammogram CCA (Fig. 1b). It has more negative potential than the reduction peak of the free reagent. This peak has the form of isosceles triangle. The absence of anodic peaks testifies that the reduction of the complex compound is an irreversible process. The current of the CCA reduction peak decreases, and that of the additional peak raises by increasing Hf(IV) concentration. This indicates that the additional peak is caused by the reduction of hafnium complex.

2.1. Optimum conditions for hafnium determination

The influence of pH on voltammetric characteristics of hafnium complex with CCA was studied. It was determined that stable and maximal currents are observed when the pH is between 2.4 and 2.9.

The influence of the ionic strength (0.1–1.2) on the reduction peak of complex was studied. The current of additional peak is stable and shows a maximum value when the ionic strength >0.8. The ionic strength of 1.0 was found to be optimal.

The addition of ethanol causes an increase of the current of the complex Hf(IV)–CCA up to the content of 12 vol% of ethanol, where current begins to decrease with increasing ethanol content. Such increase of the current of the complex with increasing ethanol content is connected to the poor solubility of CCA at pH 2.6. The addition of ethanol improves the solubility of CCA and therefore increases the current of the complex. Therefore, all feature experiments were carried out with 12 vol% of ethanol.

The effect of variation of the CCA concentration on the peak of the complex was studied. The peak increases with the CCA concentration up to $5.0 \times 10^{-5}\,mol\,L^{-1}$, and at higher concentration of CCA, the peak decreases. A concentration of $5.0 \times 10^{-5}\,mol\,L^{-1}$ was found to be optimal.

The increase of scan rate causes a shift of the reduction peak of the complex in the negative region of potential and increases the height of the peak. The scan rate (υ) was performed in the range of 0.14–6.00 $V\,s^{-1}$. Since the most legible and high peaks were obtained at $\upsilon = 0.5\,V\,s^{-1}$, all the following investigations were carried out at this scan rate.

2.2. Composition of the complex

The composition of the complex was established by the Job's method (voltammetric version) and modified method of DeFord and Hume [11].The ratio of the hafnium ion to reagent was found to be 1:2.

2.3. Linear range and detection limit

The hafnium complex shows a linear relationship in the range 2×10^{-7} to $8 \times 10^{-6}\,mol\,L^{-1}$ when $5.0 \times 10^{-5}\,mol\,L^{-1}$ CCA was used. The calibration graph can be described with the expression $I = 0.11 + 2.22 \times 10^5\,C$ with $r = 0.999$. Detection limit was estimated to be $2.46 \times 10^{-7}\,mol\,L^{-1}$.

2.4. Effect of foreign ions

Under the chosen conditions, the effect foreign ions on the determination of $8 \times 10^{-6}\,mol\,L^{-1}$ Hf(IV) was studied. The experimental results show that $1.2 \times 10^{-5}\,mol\,L^{-1}$ Pb(II);

Table 1
Determination of Hf(IV) in model solution

Dye	Added $C_{Hf(IV)}$ (mol L^{-1})	Found $C_{Hf(IV)}$ (mol L^{-1})	R.S.D. (%)
Calconcarboxylic acid	4.0×10^{-7}	$(4.06 \pm 0.13) \times 10^{-7}$	3.20
	1.0×10^{-6}	$(0.99 \pm 0.06) \times 10^{-6}$	2.53
	4.0×10^{-6}	$(3.99 \pm 0.02) \times 10^{-6}$	0.25

$C_{CCA} = 5 \times 10^{-5}$ mol L^{-1}; pH 2.6; $\varphi = 12$ vol%.

1.6×10^{-5} mol L^{-1} Ti(IV) and Pd(II); 2.4×10^{-5} mol L^{-1} Cu(II); 3.2×10^{-5} mol L^{-1} Fe(III); 1.6×10^{-4} mol L^{-1} Pt(IV), Mn(II), Cd(II) and Tb(III); 2.0×10^{-4} mol L^{-1} Al(III) and Fe(II); 2.4×10^{-4} mol L^{-1} Ni(II); 3.2×10^{-4} mol L^{-1} Co(II); 6.4×10^{-4} mol L^{-1} Mg(II); $>2 \times 10^{-3}$ mol L^{-1} Zn(II) do not affect determination of Hf(IV) with an error of $\leq$5%. It was observed that Hf(IV) could not be determined in the presence of EDTA and SCN^-. Accordingly, the above reagents could not be used as masking agents. Under the experimental conditions used, zirconium behaves similarly to hafnium, but the height of peak is lower. The addition of Ti(IV) at 1.6×10^{-5} mol L^{-1} gives rise to a new peak (that has less negative potential than the Hf(IV)–CCA peak), associated with reduction of the Ti–CCA complex. This peak separation is sufficient to allow simultaneous measurement of the two metals. A similar pattern is observed by addition of Cu(II) at 8×10^{-6} mol L^{-1}. Also some metals like cadmium, nickel and zinc could be determined with Hf(IV) simultaneously, because they are reduced at more negative potentials than the Hf(IV)–CCA complex.

2.5. Applications

For the determination of low-content of hafnium, the proposed method is highly sensitive and has good selectivity. This fact is further confirmed by analysing different samples of varying compositions. The proposed method was tested on model solutions. The results are presented in Table 1. The relative standard deviation is less than 5%. Therefore, the obtained results are reproducible and satisfactory. Also, the proposed method was successfully applied to the determination hafnium in the terbium-base alloy (72% Tb(III), 9.5% Hf(IV) and 18.5% Al(III)). The result obtained was 9.42 ± 0.07% (R.S.D. 0.28%), which confirms the validity of the procedure.

References

[1] G. Levytska, S. Tymoshuk, Ann. Pol. Chem. Soc. 3 (2004) 326.
[2] M.K. Amini, M. Kabiri, J. Irantan Chem. Soc. 2 (2005) 32.
[3] K. Jayanta, Anal. Sci. 21 (2005) 1491.
[4] H.W. Gao, Can. J. Appl. Spectrosc. 39 (5) (1994) 132.
[5] S. Kayanaraman, T. Fukasawa, Anal. Chem. 55 (1983) 2239.
[6] M.A. Cejas, Anal. Chim. Acta 158 (1984) 287.
[7] I. Takushi, M. Akira, Anal. Chim. Acta 125 (1981) 155.
[8] T. Kouimtzis, A. Townshend, Analyst 98 (1973) 40.
[9] S. Talipov, L. Zel'tser, Chem. Abstr. 89 (1978) 225547.
[10] V.Ph. Toropova, G.K. Budnikov, Z. Neorg. Khim. 12 (1975) 3269.
[11] D.D. DeFord, D.N. Hume, J. Am. Chem. Soc. 73 (1951) 5321.

Available online at www.sciencedirect.com
ScienceDirect
Talanta 71 (2007) 1130–1135
Talanta
www.elsevier.com/locate/talanta

In-channel indirect amperometric detection of heavy metal ions for electrophoresis on a poly(dimethylsiloxane) microchip

Xin-Ai Li [a,b], Dong-Mei Zhou [a], Jing-Juan Xu [b,*], Hong-Yuan Chen [b]

[a] *State Key laboratory of Soil and Sustainable Agriculture, Institute of Soil Science, Chinese Academy of Sciences, Nanjing 210008, China*
[b] *Key Lab of Analytical Chemistry for Life Science (MOE), School of Chemistry and Chemical Engineering, Nanjing University, Nanjing 210093, China*

Received 30 March 2006; received in revised form 1 June 2006; accepted 3 June 2006
Available online 7 July 2006

Abstract

In-channel indirect amperometric detection mode for microchip capillary electrophoresis with positive separation electric field is successfully applied to some heavy metal ions. The influences of separation voltage, detection potential, the concentration and pH value of running buffer on the response of the detector have been investigated. An optimized condition of 1200 V separation voltage, −0.1 V detection potential, 20 mM (pH 4.46) running buffer of 2-(*N*-morpholino)ethanesulfonic acid (MES) + L-histidine (L-His) was selected. The results clearly showed that Pb^{2+}, Cd^{2+}, and Cu^{2+} were efficiently separated within 80 s in a 3.7 cm long native separation PDMS/PDMS channel and successfully detected at a single carbon fibre electrode. The theoretical plate numbers of Pb^{2+}, Cd^{2+}, and Cu^{2+} were 1.2×10^5, 2.5×10^5, and 1.9×10^5 m^{-1}, respectively. The detection limits for Pb^{2+}, Cd^{2+}, and Cu^{2+} were 1.3, 3.3 and 7.4 μM (S/N = 3).
© 2006 Elsevier B.V. All rights reserved.

Keywords: Indirect amperometric detection mode; Heavy metal ions; Poly(dimethylsiloxane); Microchip capillary electrophoresis; Carbon fibre electrode

1. Introduction

Metal ions are essential components of biological systems; however, they may have toxic or even carcinogenic properties at high concentrations. The contamination of our environment (such as water and soil) due to the heavy metal ions is a very serious and challenging problem. Therefore, it is very important to analyze the presence of heavy metal ions in the environment. The most commonly used method for the determination of heavy metals is atomic absorption spectrometry (AAS) [1,2], including flame AAS and cold vapour AAS, which usually needs costly instruments. Electrochemical techniques such as stripping voltametry and potentiometry (ion selective electrodes) are potentially the cheapest method for the determination of trace metals [3–7]. However this method is usually used to detect only one or few kinds of metal ions except that based on mercury or mercury film electrodes. For many years, capillary electrophoresis (CE) has been used for metal ions, which is supposed to be a good technique [8–11] for its universality and sensitivity. Still there is a need of fast and inexpensive analysis for metal ions. For this purpose microfluidic chips has attracted significant attention, as microchips offer a number of advantages including speed of analysis, portability, ability to multiplex, and compatibility with integration allowing development of "micro-total-analysis systems (μTAS)" [10,12,13].

Detection of metal ions in CE system is usually performed with indirect or direct ultraviolet–vis absorption spectrometry, but this detection mode suffers from lack of sensitivity when miniaturized for the use in micro-CE [14,15]. Electrochemical detection is an alternative method. It includes three electrochemical detection techniques, i.e., amperometric, potentiometric, and conductometric detection techniques. Unlike optical detection techniques, excellent sensitivity is obtained when electrochemical detection is miniaturized [16–18]. However, for these commonly used electrochemical detection techniques, problems arise from the need to isolate the small detection potential from the CE voltage and current, and from the requirement for precise alignment of the separation microchannel and working electrodes. Various configurations of microchip and detectors have been developed to decrease the negative effect of these problems [19–25]. Unlike these researches, our group established a new in-channel indirect amperometric detection mode for microchip

* Corresponding author. Tel.: +86 25 83597294; fax: +86 25 83594862.
E-mail address: xujj@nju.edu.cn (J.-J. Xu).

0039-9140/$ – see front matter © 2006 Elsevier B.V. All rights reserved.
doi:10.1016/j.talanta.2006.06.009

CE, in which the negative effect of separation electric field has been transferred into a new universal detection approach [26]. The detection method has been successfully used to detect alkali metal ions, inorganic anions and native amino acids, as well as EOF rates [26–29].

As well known, in order to amperometrically detecting multi-heavy metal ions, a mercury or mercury impregnated electrode is usually needed. Because of its toxicity and the difficulty in miniaturization, mercury or mercury impregnated electrodes are infrequently used in micro-CE, especially in in-channel detection mode. In this work, using our previously developed method, a single carbon fibre electrode was successfully used as an amperometric detector for the detection of heavy metal ions Pb^{2+}, Cd^{2+}, and Cu^{2+} with a detection limit of micro-molar level. It may give a good example for the detection of heavy metal ions using a mercury-free detector.

2. Experimental

2.1. Materials

All chemicals were of reagent grade and doubly distilled water was used throughout. Sylgard 184 (PDMS) was from Dow Corning (Midland, MI, USA). Histidine (His) and 2-(*N*-morpholino)ethanesulfonic acid (MES) were purchased from Sigma (St. Louis, MO, USA). $Pb(NO_3)_2$, $CuCl_2{\cdot}2H_2O$, $CdCl_2$, and CH_3COOH with analytical grade were purchased from Shanghai Chemical Reagents Factory (Shanghai, China). The electrolyte solutions were prepared from stock solutions of 40 mM 2-(*N*-morpholino)ethanesulfonic acid (MES) and 40 mM L-histidine (L-His). The pH of all electrolytes was adjusted with 4% (v/v) acetic acid (Shanghai, China). Stock solutions (10 mM) of Pb^{2+}, Cu^{2+} and Cd^{2+} were prepared from their salts. Before use, the analytes were diluted with corresponding running buffer solutions. In addition, all solutions were degassed in an ultrasonic bath for 5 min and passed through a 0.22 μm cellulose acetate filter (Xinya Purification Factory, Shanghai, China). Hypodermic needles were used to introduce the buffer and solutions into the microchip reservoirs.

2.2. Instrumentation

The integrated CE-EC PDMS microchip system was similar to that described previously [28]. It comprised a homemade HV power, which provided an adjustable voltage range between 0 and 5000 V. Parameters such as sampling voltage, sampling time, separation voltage, and separation time could be set up and automatically switched via an RS232 communication port of PC through a homemade computer program. The separation current could be monitored graphically in real time.

The simple-cross single-separation channel PDMS microchip was made based on a master composed of a positive relief structure of GaAs made in No. 55 Electronic Institute (Nanjing, China) by using standard microphotolithographic technology and reaction ion etching. The chip had a 40 mm long separation channel (from injection cross to the channel outlet) and a 5 mm long injection channel (between the sample reservoir and injection cross). The channels had a maximum depth of 18 mm and a width of 50 mm. The microchip had a four-way injection cross that was connected to the three reservoirs and the separation. Before use, the PDMS layer with microchannel and the PDMS flat were ultrasonically cleaned subsequently with acetone, methanol and water for 20 min each and were then dried under infrared lamp. Then they were sealed together to form a reversible PDMS microchip.

The PDMS microchip was fixed on a plexiglass holder that integrated a precisely three-dimensional system (Shanghai Lian Yi Instrument Factory of Optical Fibre and Laser, China). A clip of optical fiber that can be fastened in the three-dimensional system was used to closely clip the carbon fiber microelectrode. Platinum wires, inserted into the individual reservoirs on the holder, served as contacts to the HV power supply.

A computer-controlled potentiostat-function generator system Model CHI-660B from CH Instruments, Shanghai, China, was used in all the electrochemical tests. The working microelectrodes were single carbon fibre cylinders with diameter of 8 μm. All the microelectrodes were homemade. Firstly, a glass capillary with an inner diameter of 0.5 mm was pulled to form a fine tip. And then a single carbon fiber was carefully mounted onto the tip and fixed with epoxy. A copper wire was connected with the carbon fiber through carbon powder on the other end of capillary and then fastened with epoxy. Before use, the tip of the protruded carbon fiber was cut with a clean scalpel to form a 1 mm cylinder electrode under a microscope.

2.3. Procedure

A three-electrode configuration was used in all electrochemical tests, with a single carbon fiber cylinder working electrode, an Ag/AgCl reference and a Pt wire auxiliary electrode. After the microchip was held on a plexiglass holder, a working electrode was inserted into the electrode hole on the platform and then pegged on the three-dimensional system, then the electrode tip was carefully inserted into the separation channel with ca. 30 μm. The electropherograms were recorded at a fixed detection potential. The working electrode was treated at +1.5 V for 200 s and then −1.0 V for 200 s before use and once the baseline current obviously changed. Then the running buffer reservoir was filled with the buffer and the sample reservoir with the sample mixture. The injections were performed by applying a desired potential for 3 s to the sample reservoir with the detection reservoir grounded while all other reservoirs floating. Separations were performed by switching the HV contacts and applying the corresponding separation voltages to the running buffer reservoir with the detection reservoir grounded and all other reservoirs floating. All experiments were performed at room temperature.

3. Results and discussion

Since the detection response is resulted from the difference of coupling degree of CE voltage to the oxidation potential of oxygen when the sample plug and the running buffer through the working electrode, the difference of conductivity between the

sample plug and the running buffer is an essential factor to influence the detection signal. It is well known that carrier electrolytes with a low-mobility co-ion are preferred for analysis of small ions. 2-(*N*-Morpholino)ethanesulfonic acid (MES) + histidine is a typical carrier electrolyte with a low-mobility co-ion used for the separation of small ions. In the following sections the influence of some experimental parameters such as the buffer pH, concentration, the separation voltage and the detection potential on the separation efficiency and detection sensitivity were studied in detail.

3.1. Effect of the buffer pH

Microchip capillary electrophoresis was the same as traditional capillary electrophoresis, in which the separation medium pH influenced the ξ potential of the interior of capillary, EOF rate, the migration time and separation efficiency of analytes. Therefore, we studied the effect of the buffer pH on the separation efficiency. Fig. 1 is the dependence of the resolutions (R_s) between Cd^{2+} and Pb^{2+}, Pb^{2+} and Cu^{2+}on the pH of running buffer. R_s gradually increase from 0.2 to 2.2 for Cd^{2+} and Pb^{2+} and 2.4 to 4.1 for Pb^{2+} and Cu^{2+} with the buffer pH decrease from 5.52 to 3.87 and the cations could be well separated as pH below 5.03 (R_s between Cd^{2+} and $Pb^{2+} > 1.3$). While, the peak currents increased with pH changing from 5.52 to 4.46, further reducing the buffer pH, the peak currents decreased (not shown). Synthetically considering the two factors of separation efficiency and detection sensitivity, pH 4.46 was the best choice.

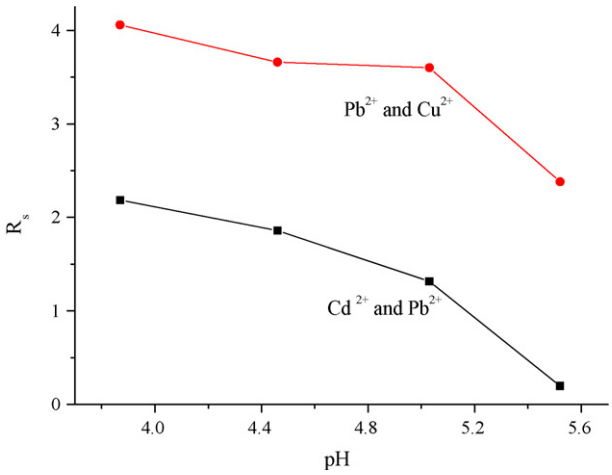


Fig. 1. The dependence of the resolutions between Cd^{2+} and Pb^{2+}, Pb^{2+} and Cu^{2+} on the buffer pH. Experimental parameters: sample, 1.0 mM lead, cadmium and copper cations, running buffer, 20 mM MES + L-His; sampling voltage, 800 V; sampling time, 3 s; separation voltage, 1200 V; detection potential, 0 V.

3.2. Effect of the buffer concentration

The influence of the buffer concentration on the separation efficiency and detection sensitivity was also investigated. Electropherograms of 1.0 mM Pb^{2+}, Cd^{2+} and Cu^{2+} in pH 4.46 running buffer with different concentration were carried out. It was found that the buffer concentration hardly influenced the migration time of the analytes. The half-peak widths of the three cations decreased with the increase of the buffer concentration from 10 to 30 mM, while the theoretical plate numbers increased (Fig. 2a). Generally, in order to minimize electromigrative dispersion and to obtain high separation efficiencies the mobilities of analyte ions and carrier electrolyte co-ions should be similar. For the carrier electrolytes with a low-mobility co-ion such as MES + histidine, high concentrations make for electrostacking, which helps to suppress peak dispersion. Thus the higher the buffer concentration is, the smaller the half-peak widths and the larger the theoretical plate numbers are. However, the peak currents of the three cations increased with the increase of the buffer concentration from 10 to 20 mM, and then decreased with the further increase of the buffer concentration (Fig. 2b). It may be due to the following reasons. On one hand, higher concentration of the running buffer makes for electrostacking, which results in relatively higher concentration of the sample plug and then a relatively high signal. On the other hand, higher concentration of running buffer will result in high ionic strength, which will decrease the difference of conductivity between the running

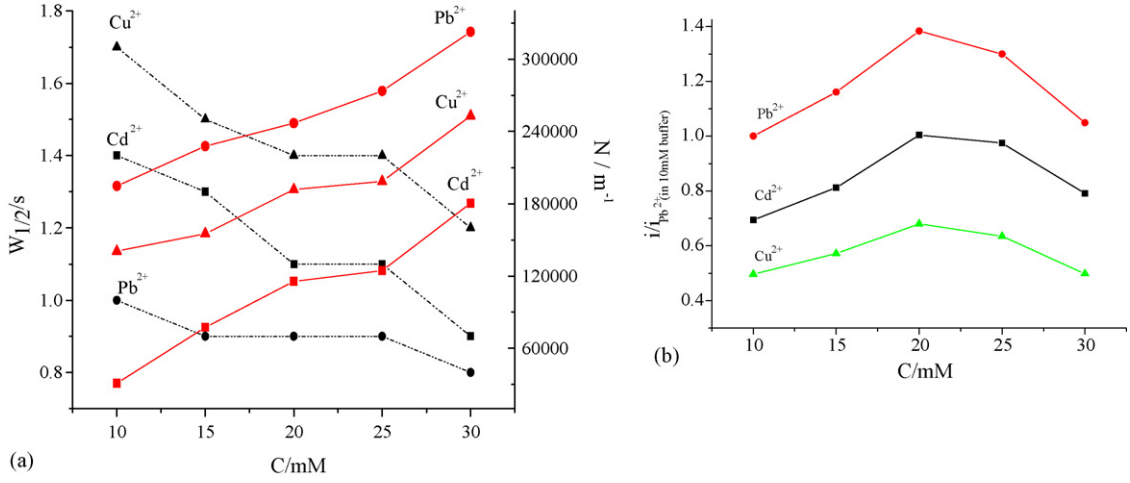


Fig. 2. The effects of the buffer concentration on the half-peak widths (dot) and the theortical plate numbers (line) (a) and the peak currents (standardized by the peak current of Pb^{2+} in 10 mM buffer) (b). Experimental parameters: running buffer, pH 4.46 MES + L-His; other parameters same as in Fig. 1.

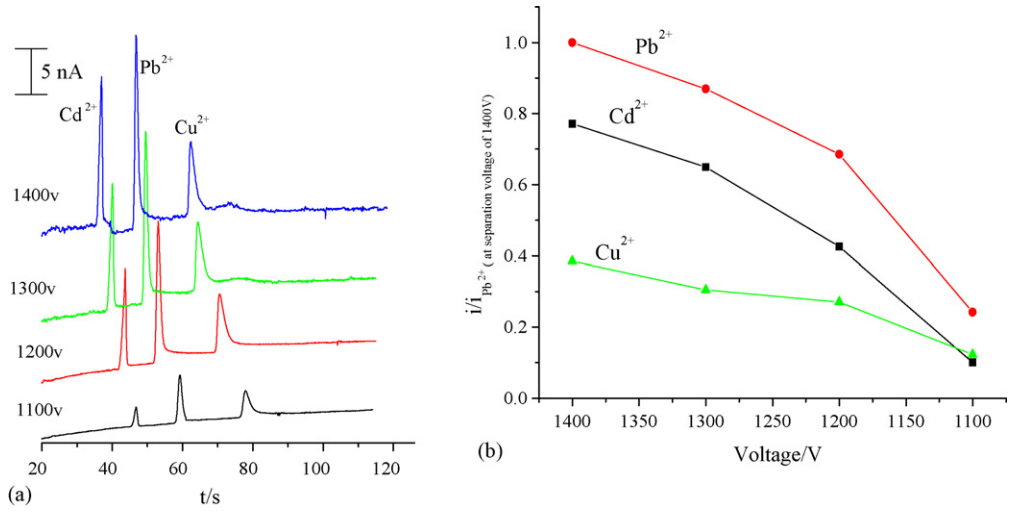


Fig. 3. (a) Electropherograms of 1.0 mM lead, cadmium and copper cations at different separation voltages. (b) The relationship between the peak currents (standardized by the peak current of Pb^{2+} at the separation voltage of 1400 V) and the separation voltage. Experimental parameters: running buffer, 20 mM MES + L-His, pH 4.46; other parameters same as in Fig. 1.

buffer and the sample plug and result in a low signal. At lower concentrations of the running buffer (from 10 to 20 mM), the former factor is dominant and results in the increase of the peak currents. With the further increase of the concentration of the running buffer, the later factor is dominant and the peak currents decreased.

3.3. Effect of separation voltage

Since the electrochemical detection principle is based on the coupling of separation electric field on the electrochemical detector, the influence of separation voltage on detection is a major factor in improving detection sensitivity. The electropherograms of 1.0 mM Pb^{2+}, Cd^{2+} and Cu^{2+} under different separation voltage was shown in Fig. 3a. By enhancing the separation voltage, the migration times of the three cations obviously shorten due to the EOF and electrophoretic flow in same direction, which simultaneously increase with the increase of separation electric field. In addition, a relative ascent of the amperometric signal was observed with the voltage increasing in that the coupling effect on amperometric detection potential is also strengthened with the enhancement of the separation electric field, thus resulting in larger peak current corresponding to accelerated electrochemical response. The sensitivity of the signal with the change of separation voltage is different for the three cations. From Fig. 3b, we can see that the Cd^{2+} and Pb^{2+} have the similar change rate of the peak currents, while the peak current of Cu^{2+} has a relatively lower change rate with the change of separation voltage. This phenomenon may be due to the different complexation degrees of the three cations with the running buffer and ionic mobilities. It also make for that the separation order does not follow the sequence of the mobilities (the ionic mobilities in water of Pb^{2+}, Cd^{2+}, Cu^{2+} ions are 7.36, 5.60, 5.56 ($\times 10^{-8}$ m^2 s^{-1} V^{-1}), respectively [9]). When separation voltage was higher than 1300 V, the baseline went more and more unsteady. It was that high separation voltage would produce air bubble and consequently result in clogging of the channel. In conclusion, the separation voltage of 1200 V was a good choice for the detection of these metal cations.

3.4. Effect of detection potential

The influence of the detection potential applied to the carbon fiber electrode was studied for Pb^{2+}, Cd^{2+} and Cu^{2+} at separation voltage of 1200 V in this work (Fig. 4). It was observed in Fig. 4a that the peak current decreased clearly with the increase of detection potential from −0.2 to 0.4 V. However, the baseline becomes unsteady with the decrease of detection potential because of a large noise in the negative potential. The sensitivity of the signal with the change of detection potential is also different for the three cations (Fig. 4b). From Fig. 4b, we can see that the Cd^{2+} and Pb^{2+} have the similar change rate of the peak currents, while the peak current of Cu^{2+} has a relatively lower change rate with the change of detection potential. This phenomenon is similar to the effect of separation voltage on the signal.

3.5. Linear range and detection limit

According to the above studies on separation voltage, detection potential, the concentration and pH value of running buffer, an optimized condition of 1200 V separation voltage, −0.1 V detection potential, 20 mM (pH 4.46) of MES + L-His as running buffer was selected. Under this condition, the in-channel indirect amperometric microchip detector displays well-defined concentration dependence for these heavy metal cationic species. Linear ranges of peak current from 5.0 μM to 1.0 mM (correlation coefficients, 0.9987), from 5.0 μM to 2.0 mM (correlation coefficients, 0.9979), and from 10 μM to 2.0 mM (correlation coefficients, 0.9949) were obtained for Pb^{2+}, Cd^{2+}, and Cu^{2+} with a 10 s of sampling time, respectively (Fig. 5). The detection limits for Pb^{2+}, Cd^{2+}, and Cu^{2+} were estimated to be 1.3, 3.3

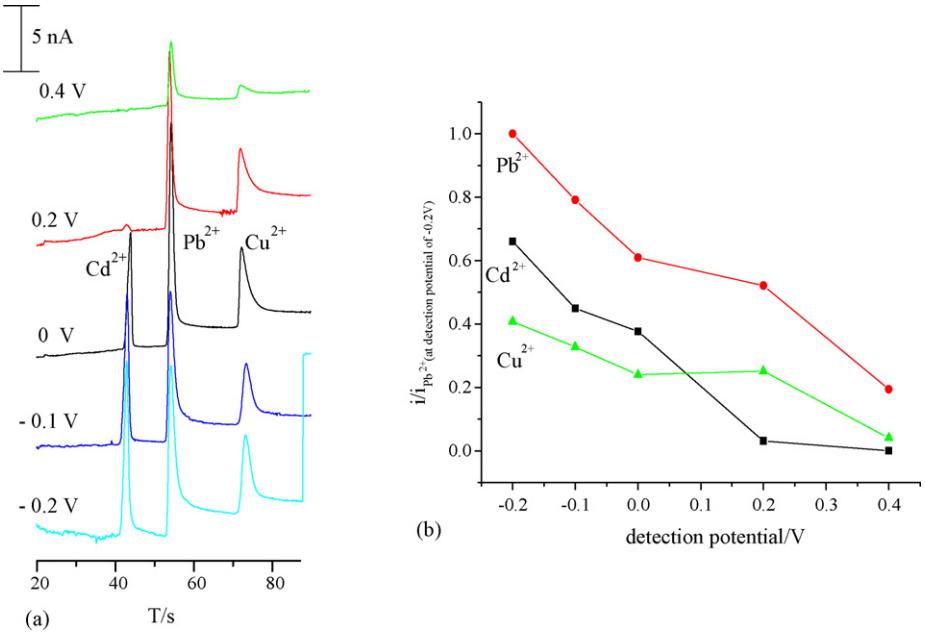


Fig. 4. (a) Electropherograms of 1.0 mM lead, cadmium and copper cations at different detection potentials. (b) The relationship between the peak currents (standardized by the peak current of Pb^{2+} at the detection potential of −0.2 V) and the detection potential. Experimental parameters: separation voltage, 1200 V; other parameters same as in Fig. 3.

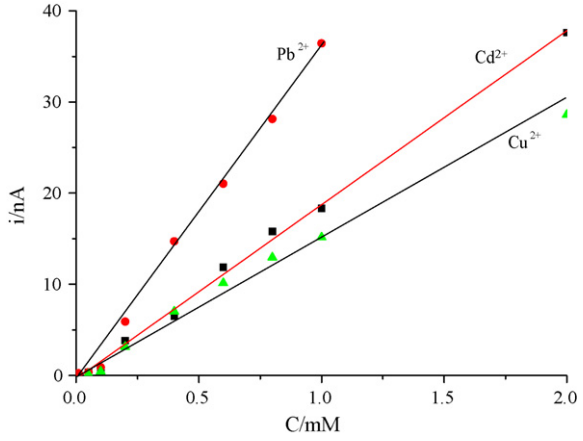


Fig. 5. The linear relationship between the detection signal of the three cations and different concentrations. Experimental parameters: sampling time, 10 s; separation voltage, 1200 V; detection potential, −0.1 V; other parameters same as in Fig. 3.

and 7.4 μM (S/N = 3), respectively. Furthermore, we can obtain the theoretical plate numbers for 1.0 mM Pb^{2+}, Cd^{2+}, and Cu^{2+} were 1.2×10^5, 2.5×10^5, and 1.9×10^5 m^{-1} with a 3 s of sampling time, respectively.

4. Concluding remarks

In conclusion, a single carbon fiber cylinder working electrode has been successfully used in the determination of heavy metal ions with a simple indirect amperometric detection mode in a PDMS microchip. It provides the advantage of avoiding the use of toxic mercury or mercury impregnated electrode in the amperometric detection of heavy metal ions. The results presented here combined with our previous reports demonstrated that this in-channel indirect amperometric detection mode for microchip CE was well universal and was expected to find a wide range of applications.

Acknowledgements

This work was supported by the National Natural Science Foundation of China (Nos. 20575029, 20475025, 20521503, 20635020) and the key project of the Science and Technology Research of MOE.

References

[1] M. Soylaka, S. Saracoglub, U. Divriklic, L. Elcic, Talanta 66 (2005) 1098.
[2] J.L. Capelo, G.M. Rivas, L.G. Oliveira, C. Vilhena, A.C. Santos, T. Valada, M. Galesio, P. Oliveira, M.D.R. Gomes da Silva, E.M. Gaspar, S. Alves, C. Fernandez, C. Vazc, Talanta 68 (2006) 813.
[3] M.A. Rahman, M.S. Won, Y.B. Shim, Anal. Chem. 75 (2003) 1123.
[4] T. Jeong, H.K. Lee, D.C. Jeong, S. Jeon, Talanta 65 (2005) 543.
[5] S.C.C. Monterroso, H.M. Carapuc, A.C. Duarte, Talanta 65 (2005) 644.
[6] T. Kappes, P.C. Hauser, Analyst 124 (1999) 1035.
[7] C.N. Yarnitzky, Rev. Anal. Chem. 19 (2000) 319.
[8] J. Tanyanyiwa, P.C. Hauser, Anal. Chem. 74 (2002) 6378.
[9] J. Tanyanyiwa, P.C. Hauser, Electrophoresis 23 (2002) 3781.
[10] H.D. Willauer, G.E. Collins, Electrophoresis 24 (2003) 2193.
[11] A. Padarauskas, Anal. Bioanal. Chem. 384 (2005) 132.
[12] P. Kubáň, P. Kubáň, V. Kubáň, Electrophoresis 23 (2002) 3725.
[13] C.J. Evenhuis, R.M. Guijt, M. Macka, P.R. Haddad, Electrophoresis 25 (2004) 3602.
[14] C. Vogt, G.L. Klunder, Fresenius J. Anal. Chem. 370 (2001) 316.
[15] I. Ali, V.K. Gupta, H.Y. Aboul-Enein, Electrophoresis 26 (2005) 3988.
[16] I. Poels, L.J. Nagels, Anal. Chim. Acta 385 (1999) 417.
[17] J. Wang, Talanta 56 (2002) 223.
[18] J. Wang, Electroanalysis 17 (2005) 1133.
[19] J.S. Rossier, R. Ferrigno, H.H. Girault, J. Electroanal. Chem. 492 (2000) 15.

[20] D.C. Chen, F.L. Hsu, D.Z. Zhan, C.H. Chen, Anal. Chem. 73 (2001) 758.
[21] D.M. Osbourn, C.E. Lunte, Anal. Chem. 75 (2003) 2710.
[22] N.A. Lacher, S.M. Lunte, Anal. Chem. 76 (2004) 2482.
[23] R.S. Martin, K.L. Ratzlaff, B.H. Huynh, S.M. Lunte, Anal. Chem. 74 (2002) 1136.
[24] J. Wang, B. Tian, E. Sahlin, Anal. Chem. 71 (1999) 3901.
[25] J. Wang, G. Chen, M.P. Cheatrathi, A. Fujishima, D.A. Tryk, D. Shin, Anal. Chem. 75 (2003) 935.
[26] J.J. Xu, N. Bao, X.H. Xia, Y. Peng, H.Y. Chen, Anal. Chem. 76 (2004) 6902.
[27] J.J. Xu, Y. Peng, N. Bao, X.H. Xia, H.Y. Chen, Electrophoresis 26 (2005) 3615.
[28] J.J. Xu, Y. Peng, N. Bao, X.H. Xia, H.Y. Chen, J. Chromatogr. A 1095 (2005) 193.
[29] N. Bao, J.J. Xu, Q. Zhang, J.L. Hang, H.Y. Chen, J. Chromatogr. A 1099 (2005) 203.

Available online at www.sciencedirect.com
ScienceDirect
Talanta 71 (2007) 1124–1129
Talanta
www.elsevier.com/locate/talanta

Sensitive determination of phenothiazines in pharmaceutical preparation and biological fluid by flow injection chemiluminescence method using luminol–$KMnO_4$ system

Yinhuan Li [a,b], Weifen Niu [a], Jiuru Lu [a,*]

[a] *School of Chemistry and Materials Science, Shaanxi Normal University, Xi'an 710062, China*
[b] *School of Science, Xi'an Jiaotong University, Xi'an 710049, China*

Received 23 March 2006; received in revised form 2 June 2006; accepted 3 June 2006
Available online 17 July 2006

Abstract

A flow injection chemiluminescence method was described for the determination of four phenothiazine drugs, namely, chlorpromazine hydrochloride, perphenazine hydrochloride, fluphenazine hydrochloride and thioridazine hydrochloride. Strong Chemiluminescence (CL) signal was produced when above-mentioned drug was injected into the mixed stream of luminol with $KMnO_4$. The linear ranges of the method were 0.0020–1.0 μg/mL chlorpromazine hydrochloride, 0.0040–3.0 μg/mL perphenazine hydrochloride, 0.0020–5.0 μg/mL fluphenazine hydrochloride and 0.0050–1.0 μg/mL thioridazine hydrochloride. The detection limits were 0.4 ng/mL chlorpromazine hydrochloride, 0.7 ng/mL perphenazine hydrochloride, 2 ng/mL fluphenazine hydrochloride and 0.7 ng/mL thioridazine hydrochloride. The proposed method was applied to the determination of chlorpromazine hydrochloride in injections and in mental patient's urine samples and the satisfactory results were achieved. The possible CL reaction mechanism was also discussed briefly.
© 2006 Elsevier B.V. All rights reserved.

Keywords: Chemiluminescence; Flow injection; Phenothiazines

1. Introduction

Phenothiazine derivatives are a large group of tricyclic antidepressants which are commonly used for the treatment of psychiatric patients suffering depressions [1]. The monitoring of these compounds is important for quality assurance in pharmaceutical industry and for obtaining optimum therapeutic concentrations in body fluids to minimize the risk of toxicity. Therefore, it is important to develop simple and sensitive methods for the determination of these drugs. A wide variety of analytical techniques are available for the determination of phenothiazine drugs in pharmaceutical preparations and biological samples, such as spectrophotometry [2–4], electrochemical methods [5–7], chromatography [8] and capillary electrophoresis [9].

Chemiluminescence (CL) method has been frequently used for the analysis of pharmaceutical compounds in recent years [10–14] because of its promising advantages of low detection limit, wide linear dynamic range and relatively simple and inexpensive instrumentation. Several CL systems have been reported for the determination of phenothiazine drugs [15–23]. They were based on the acidic $KMnO_4$ reaction [15–17], Ce(IV) reaction sensitized by rhodamine B [18], luminol–H_2O_2–Cr^{3+} reaction [19], luminol–Fe^{2+} reaction [20], luminol reaction in micelles [21] and electrogenerated $Ru(bpy)_3^{2+}$ reaction [22,23]. The analytical parameters of the previous reported CL methods for the determination of phenothiazine drugs were summarized in Table 1.

We here proposed a simple and sensitive flow injection CL method for the determination of four phenothiazine drugs, including chlorpromazine hydrochloride, perphenazine hydrochloride, fluphenazine hydrochloride and thioridazine hydrochloride. It was based on the fact that strong CL signal could be produced when above-mentioned drug was injected into the reaction mixture of luminol with $KMnO_4$. The method

* Corresponding author. Tel.: +86 29 85303911; fax: +86 29 85307774.
E-mail address: ljr@snnu.edu.cn (J. Lu).

0039-9140/$ – see front matter © 2006 Elsevier B.V. All rights reserved.
doi:10.1016/j.talanta.2006.06.007

Table 1
Analytical parameters of the previous CL methods for the determination of phenothiazine drugs (unit: μg/mL)

Species	CL reactions	Linear ranges	Detection limits	References
Chlorpromazine	Acidic $KMnO_4$ reaction		7.1	[15]
Thioridazine	Acidic $KMnO_4$ reaction	1.0–30.0	0.5	[17]
Fluphenazine	Ce(IV) reaction sensitized by rhodamine B	0.5–90	0.01	[18]
Chlorpromazine	Luminol–H_2O_2–Cr^{3+} reaction	3.6–355	13	[19]
Chlorpromazine	Luminol–Fe^{2+} reaction	0.7–7.1		[20]
Chlorpromazine	Luminol reaction in reverse micelles	0.05–10	0.006	[21]
Chlorpromazine	Electrogenerated $Ru(bpy)_3^{2+}$ reaction	0.3–6.4	0.24	[22]
Chlorpromazine	Electrogenerated $Ru(bpy)_3^{2+}$ reaction	0.004–1.1	0.001	[23]

was successfully applied to the determination of chlorpromazine hydrochloride in injections and in mental patient's urine samples.

2. Experimental

2.1. Apparatus

The schematic diagram of the CL flow system used was shown in Fig. 1. PTFE tubing (0.8 mm i.d.) was used as the connect material in the flow system. A peristaltic pump was used to deliver all solutions; each at a flow rate of 2.1 mL/min. Sample injection (50 μL) was automated operated by means of a six-way valve. The CL signal produced in the flow cell was measured using an IFFS-A multifunction CL analyzer (Xi'an Remax Electronic Science-Tech Ltd. Co., China). The CL data acquisition and treatment were performed by using an MCDR-A multifunction data processing system (Xi'an Remax). CL spectra and fluorescence spectra were taken on CRT-970 fluorescence spectrophotometer (Shanghai Third Analytical Instrumental Plant).

2.2. Reagents and solutions

All chemicals were of analytical reagent grade except luminol, which was synthesized by the Institute of Analytical Science of Shaanxi Normal University (Xi'an, China). Doubly distilled water was used throughout the experiments. Chlorpromazine hydrochloride, perphenazine hydrochloride, fluphenazine hydrochloride and thioridazine hydrochloride were obtained from the Chinese Pharmaceutical and Biological Test Institute (Beijing, China). Potassium permanganate was purchased from Xi'an Chemical Plant (Xi'an, China). Stock solutions (500.0 μg/mL) of each drug were prepared by dissolving 50.0 mg of the drug in 100 mL of water. They were stored in a refrigerator and protected from light. Working solutions were prepared by appropriately diluting the stock solution when used. Stock solution (0.01 mol/L) of luminol was prepared by dissolving 1.771 g luminol in 50 mL of 1 mol/L sodium hydroxide and diluting to 1 L with water. Stock solution (0.02 mol/L) of potassium permanganate was prepared by dissolving 3.16 g of $KMnO_4$ in 1 L of boiled water, filtering through glass wool and protecting from light.

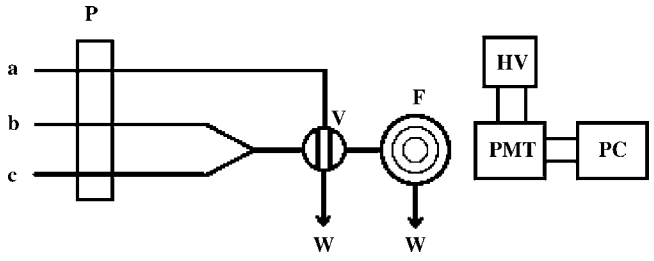


Fig. 1. Schematic diagram of CL flow system. (a) Phenothiazines solution; (b) luminol solution; (c) potassium permanganate solution; P, peristaltic pump; V, injection valve; F, flow cell; PMT, photomultiplier tube; HV, high voltage; PC, personal computer; W, waste.

2.3. Procedure

As shown in Fig. 1, flow lines were connected with phenothiazine solution, luminol solution and $KMnO_4$ solution, respectively. Luminol solution was firstly mixed with $KMnO_4$ solution via a Y-piece to give a stable baseline. Then 50 μL solution of phenothiazine was injected into the merged stream of luminol with $KMnO_4$ by means of a six-way valve to produce CL. The concentration of phenothiazine was quantified by the CL intensity.

3. Results and discussion

3.1. Kinetic characteristic of the CL reaction

The CL kinetic characteristic of the reaction was investigated using the static system of the IFFS-A multifunction CL analyzer. Fig. 2 shows the typical CL intensity-time profile. A strong CL was recorded when 1.0 mL solution of 20 μmol/L $KMnO_4$ was injected into 1.0 mL solution of 10 μmol/L luminol (peak a). After CL signal declined about 45s, subsequently injecting 1.0 mL 0.5 μg/mL chlorpromazine hydrochloride resulted in a new CL reaction (peak b). About 80s later, the CL reaction terminated and the CL signal declined to baseline.

3.2. Optimization of experimental conditions

The experimental conditions were optimized using 0.05 μg/mL chlorpromazine hydrochloride solution as a model. The optimized parameters were of reaction medium, luminol concentration and $KMnO_4$ concentration.

It was observed that higher CL signal and better repeatability could be obtained when sodium hydroxide was added into sample solution than into luminol solution. The effect of sodium

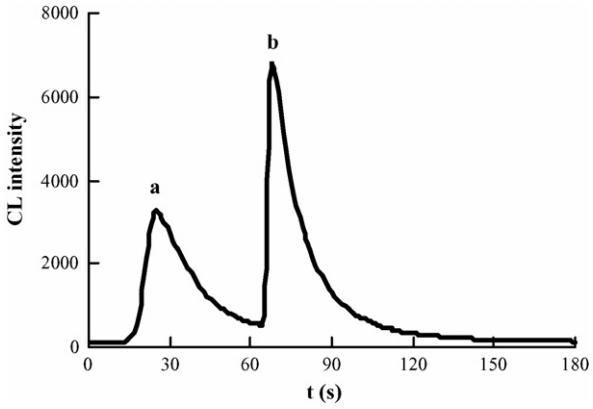


Fig. 2. The CL intensity-time profile. (a) injecting 1.0 mL 20 μmol/L $KMnO_4$ into 1.0 mL 10 μmol/L luminol; (b) injecting 1.0 mL 0.5 μg/mL chlorpromazine hydrochloride into above reaction mixture.

hydroxide concentration on the CL reaction was examined in the 0.02–0.1 mol/L. Finally, 0.05 mol/L of sodium hydroxide was employed because it gave larger signal-to-blank ratio and higher CL signal.

The concentrations of luminol and $KMnO_4$ were important parameters in the experiments. The effect of different concentrations combination of luminol (1–100 μmol/L) and $KMnO_4$ (1–500 μmol/L) was studied. The experimental results showed that the maximum CL signal and signal-to-blank ratio was obtained when 10 μmol/L of luminol and 20 μmol/L of $KMnO_4$ were used.

The effect of flow rate on the reaction was examined in the range 0.7–3.5 mL/min. The CL signal increased with increase in flow rate from 0.7 to 2.1 mL/min. When the flow rate was higher than 2.1 mL/min, the CL signal changed slightly. Therefore, 2.1 mL/min of flow rate was employed.

3.3. Analytical performance

Under the selected experimental conditions, the calibration graphs for four phenothiazine drugs were prepared. The parameters of calibration graphs and the detection limits ($3s_b$) were summarized in Table 2. The relative standard deviations for 0.01 and 0.1 μg/mL solutions of phenothiazine drugs in 11 repeated measurements were also showed in Table 2. A complete analysis, including sampling and injecting, could be performed in 30 s, giving a sample throughput of 120/h.

3.4. Interference

In order to assess the possibility of applying the proposed method, the effect of foreign species was examined by analyzing synthetic sample solutions containing 0.050 μg/mL of chlorpromazine hydrochloride and various amount of each potential interferent. A foreign species was considered not to interfere if it caused a relative error less than 5% in the determination of chlorpromazine hydrochloride. No interference has been found when including up to a 1000-fold Na^+, K^+, Al^{3+}, Fe^{3+}, Fe^{2+}, NO_3^-, SO_4^{2-}, CO_3^{2-}, PO_4^{3-}, starch, glucose, lactose, leucine, 500-fold Ca^{2+}, tryptophan, 200-fold urea, 100-fold Mg^{2+}, Cl^-, 10-fold Mn^{2+}, Pb^{2+}, 1-fold fluphenazine hydrochloride, 0.2-fold ascorbic acid, epinephrine and 0.02-fold uric acid.

3.5. Application

3.5.1. Determination of chlorpromazine hydrochloride in pharmaceutical preparations

Ascorbic acid is commonly used as the anti-oxidant for chlorpromazine hydrochloride injection [24]. The experimental results indicated that the effect of ascorbic acid could be eliminated by the addition of Fe^{3+}. Experimental result indicated that 50-fold amount of ascorbic acid did not interfere with the determination of 0.05 μg/mL of chlorpromazine hydrochloride when 50 μg/mL Fe^{3+} was present in sample solution.

Five injections were homogenized. A portion of sample was transferred into a 50 mL beaker, to which 2.5 mL of 1 mg/mL Fe^{3+} solution was added. The solution was stood for 1 min and then 5 mL of 0.5 mol/L NaOH solution were added. The resultant solution was diluted with water to 50 mL and filtered. The filtrate was then analyzed according to the procedure described in Section 2. The results were summarized in Table 3. The *t*-test assured that there were no significant differences between the results obtained by the proposed method and those obtained by the Chinese Pharmacopoeia method [25] at the confidence level of 95%.

3.5.2. Determination of chlorpromazine hydrochloride in mental patient's urine

In order to apply the proposed method to the determination of chlorpromazine hydrochloride in mental patient's urine, a chlorpromazine-imprinted polymer was employed to eliminate the interferents existed in urine. The chlorpromazine-imprinted polymer was synthesized by using batch method with chlorpro-

Table 2
Analytical performances

Phenothiazines	Linear range (μg/mL)	Regression equation (ng/mL)	Correlation coefficient (r^2)	Detection limit ($3s_b$) (ng/mL)	R.S.D. (%) ($n = 11$)	
					0.01 μg/mL	0.1 μg/mL
Chlorpromazine hydrochloride	0.002–1.0	$I = 4.62C + 92.0$	0.9938	0.4	1.2	0.4
Perphenizine hydrochloride	0.004–3.0	$I = 2.33C - 38.8$	0.9972	0.7	1.5	0.3
Fluphenazine hydrochloride	0.002–5.0	$I = 0.76C + 30.0$	0.9972	2	1.6	0.5
Thioridazine hydrochloride	0.005–1.0	$I = 3.20C - 40.0$	0.9959	0.7	2.0	0.6

Table 3
Determination of chlorpromazine hydrochloride in injections

Sample	Nominal content	Proposed method[a]	R.S.D. (%) ($n=5$)	Pharmacopoeia method[b]	R.S.D. (%) ($n=3$)
040912	25 mg/1 mL	24.9 ± 0.5 (mg/1 mL)	2.1	24.5 ± 0.2 (mg/1 mL)	0.8
041110	50 mg/2 mL	49.9 ± 1.0 (mg/2 mL)	1.9	49.2 ± 0.4 (mg/2 mL)	0.9

[a] Average of five determinations ± S.D.
[b] Average of three determinations ± S.D.

mazine as the template molecule and the procedure was similar to that reported previously [26]. The procedure of molecular imprinting-chemiluminescence method (MI-CL) consisted of four steps: adsorption of chlorpromazine, removing the other substances except chlorpromazine, CL detection and cleaning the MIP column. The flow system and procedure has been described in detail in elsewhere [27]. The experimental conditions corresponding to the four steps of MI-CL method were examined. The optimum conditions were 180 s of adsorption time, 120 s of washing time, 80 s of detection time and 80 s of cleaning time. When chlorpromazine-imprinted polymer was used, the tolerance limits were 1000-fold urea, 200-fold uric acid, 100-fold ascorbic acid, 50-fold fluphenazine hydrochloride and 2-fold epinephrine.

Blank urine samples were collected from the healthy volunteers and the urine samples from the mental patients were collected after taking chlorpromazine hydrochloride for 8 h. After centrifuging at 3000 rpm for 15 min, 1 mL of the supernatant was transferred into a 100 mL volumetric flask, diluted with water to the mark and used as the sample solution. The results for the determination of chlorpromazine hydrochloride in urine samples were summarized in Table 4. Recovery tests were also carried out by adding a known amount of chlorpromazine hydrochloride in samples and the results were also summarized in Table 4. The *t*-test assumed that there were no significant differences between recoveries and 100% at confidence level of 95%.

3.6. Discussion on the reaction mechanism

To elucidate the reaction mechanism, the following experiments were performed using chlorpromazine hydrochloride as a model.

Table 4
Determination of chlorpromazine hydrochloride in urine samples

Urine samples	Determined[a] (μg/mL)	R.S.D. (%, $n=3$)	Added (μg/mL)	Found (μg/mL)	Recovery (%)
Volunteer 1	0		1.00	0.96	96
			2.00	2.04	102
Volunteer 2	0		1.00	1.03	103
			2.00	1.95	98
Mental patient 1	0.42 ± 0.01	3.3	1.00	1.37	95
			2.00	2.36	97
Mental patient 2	0.78 ± 0.02	3.1	1.00	1.74	96
			2.00	2.71	97

[a] Average of three determinations ± S.D.

Firstly, weak CL was recorded when alkaline chlorpromazine hydrochloride solution was injected into $KMnO_4$. Strong CL was detected when chlorpromazine hydrochloride solution was injected into the mixed solution of luminol and $KMnO_4$.

Secondly, the CL spectra of luminol–$KMnO_4$ reaction and luminol–$KMnO_4$–chlorpromazine hydrochloride reaction were drawn by means of a refitted CRT 970 fluorescence spectrophotometer (Fig. 3). Both spectra had same maximum emission wavelength at 425 nm. This indicated that the CL spectra were independent of chlorpromazine hydrochloride, the emitter of luminol–$KMnO_4$–chlorpromazine hydrochloride reaction was still the excited state of 3-aminophthalate ions (3-AP*) [28], the oxidation product of luminol [29].

Thirdly, when luminol was mixed with $KMnO_4$ solution, the purple of $KMnO_4$ solution changed gradually into green. This result indicated $KMnO_4$ was firstly reduced to K_2MnO_4 [30] and luminol was oxidized to 3-aminophthalate ions (3-AP) [29].

Fourthly, no CL signal was observed when injecting chlorpromazine hydrochloride into the mixed solution of luminol and K_2MnO_4. This experiment indicated that K_2MnO_4 was irrelevant to the CL reaction.

Fifthly, the alkaline mixed solutions of luminol and $KMnO_4$ with different concentration ratio were prepared remaining luminol concentration at 1.0×10^{-5} mol/L. The concentration ratios of luminol to $KMnO_4$ were 1:0.5 for solution A and 1:5 for solution B. When chlorpromazine hydrochloride was injected into above solution, the CL signal from solution B was much higher than that from solution A. This experiment suggested that $KMnO_4$ was indispensable to the CL reaction.

Sixthly, the fluorescent spectra of the reaction mixtures of luminol–$KMnO_4$ (a), $KMnO_4$–chlorpromazine hydrochloride (b) and luminol–$KMnO_4$–chlorpromazine hydrochloride

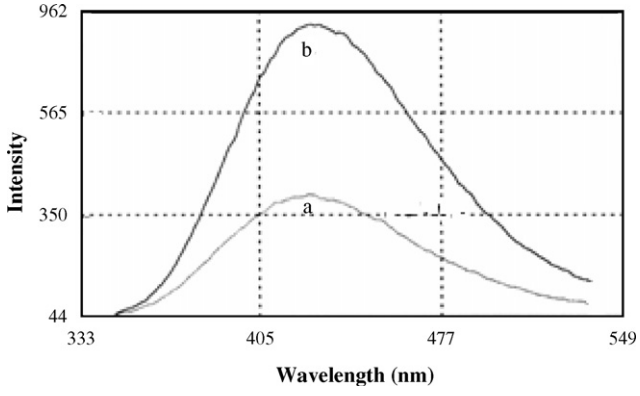


Fig. 3. CL spectra. The CL spectra of the reaction of (a) 10 μmol/L luminol + 20 μmol/L $KMnO_4$; (b) 10 μmol/L luminol + 20 μmol/L $KMnO_4$ + 2.0 μg/mL chlorpromazine hydrochloride.

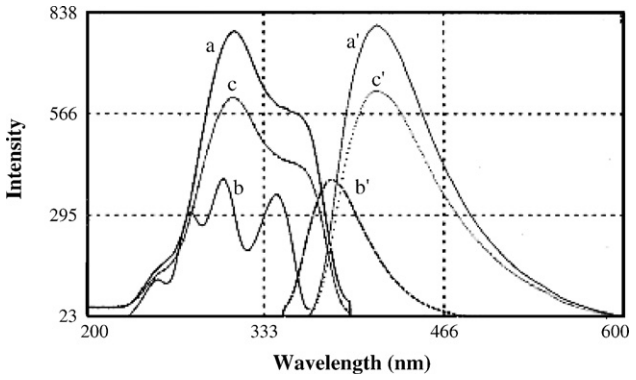


Fig. 4. The fluorescent spectra. The excitation and emission spectra of the reaction mixtures of (a, a′): 10 μmol/L luminol + 20 μmol/L $KMnO_4$; (b, b′): 20 μmol/L $KMnO_4$ + 2.0 μg/mL chlorpromazine hydrochloride; (c, c′): 10 μmol/L luminol + 20 μmol/L $KMnO_4$ + 2.0 μg/mL chlorpromazine hydrochloride.

(c) were scanned using a CRT 970 fluorescence spectrophotometer (Fig. 4). The excitation spectra and emission spectra were similar for the reaction mixtures (a, c), the excitation wavelength and emission wavelength were within the range of 240–400 nm (λ_{ex} = 314 nm) and 370–600 nm (λ_{em} = 425 nm), respectively. They were identical with the excitation spectrum and emission spectrum of 3-AP [28]. The excitation wavelength and emission wavelength for reaction mixture (b) were 240–370 nm (λ_{ex} = 306 nm) and 350–470 nm (λ_{em} = 386 nm), respectively. It was identical with the spectrum of the oxidation product of chlorpromazine hydrochloride [31], sulphone compound [32]. It was also interestingly found that the excitation spectrum of sulphone compound (b) largely overlapped with that of 3-AP (a, c), which suggested that the energy released by reaction between $KMnO_4$ and chlorpromazine hydrochloride could be absorbed not only by sulphone compound to form excited state of sulphone compound but also by 3-AP to form 3-AP*, respectively.

Based on the above discussion, the following possible reaction mechanism was suggested: Chlorpromazine hydrochloride reacted with $KMnO_4$ and the energy was released. The released energy was absorbed by 3-AP to form 3-AP*. The 3-AP* returned to ground state and generated CL.

$$\text{Luminol} + KMnO_4 \rightarrow \text{3-AP} + K_2MnO_4 + h\nu \quad (425\,\text{nm})$$

$$KMnO_4 + \text{chlorpromazinehydrochloride} + \text{3-AP} \rightarrow \text{sulphonecompound} + K_2MnO_4 + \text{3-AP}^*$$

$$\text{3-AP}^* \rightarrow \text{3-AP} + h\nu \quad (425\,\text{nm})$$

The same phenomenon was also found when chlorpromazine hydrochloride was replaced by other three phenothiazine drugs. This may be attributed to their similar molecular structure and fluorescence characteristics [31]. Therefore, the CL reaction mechanism for other three phenothiazine drugs should be identical with that of chlorpromazine hydrochloride.

4. Conclusion

Four phenothiazine drugs including chlorpromazine hydrochloride, perphenazine hydrochloride, fluphenazine hydrochloride and thioridazine hydrochloride were found to produce strong CL in $KMnO_4$–luminol reaction. The proposed method has wider linear ranges (The linear range extended 2–3 magnitudes) and lower detection limit (The detection limit was two magnitudes lower than that of most reported CL methods). The proposed method was successfully applied to the determination of chlorpromazine hydrochloride in injections and in mental patient's urines. The possible CL reaction mechanism was investigated.

Acknowledgement

The authors gratefully acknowledge the financial support from Shaanxi Normal University for Doctoral Fund.

References

[1] J. Karpinska, B. Starczweska, H. Puzanowska-tarasiewicz, Anal. Sci. 12 (1996) 161–170.
[2] M.A. El-Maaboud Ismail, Talanta 44 (1997) 1173–1182.
[3] T. Aman, J. Anwar, A. Ahmad, L. Latif, Anal. Lett. 36 (2003) 2961–2974.
[4] K. Basavaiah, J.M. Swamy, Chem. Anal. 47 (2002) 139–146.
[5] A. Ferancová, E. Korgová, T. Buzinkaiová, W. Kutner, I. Štepánek, J. Labuda, Anal. Chim. Acta 447 (2001) 47–54.
[6] Z. Yang, J. Kauffmann, M.A. Valenzuela, S. Özkan, Mikrochim. Acta 131 (1999) 85–90.
[7] I. Nemcova, K. Nesmerak, D. Rychlovsky, J. Koutnikova, Talanta 65 (2005) 632–637.
[8] M.C. Quintana, M.H. Blanco, J. Kacal, L. Hernandez, Talanta 59 (2003) 417–422.
[9] F.J. Lara, A.M. Garcia-Campana, F. Ales-Barrero, J.M. Bosque-Sendra, Anal. Chim. Acta. 535 (2005) 101–108.
[10] Y. Fuster Mestre, L. Lahuerata Zamora, J. Martinez Calatayud, Luminescence 16 (2001) 213–235.
[11] A. Townshend, W. Ruengsitagoon, C. Thongpoon, S. Liawruangrath, Anal. Chim. Acta 541 (2005) 105–111.
[12] N. Anastos, N.W. Barnett, S.W. Lewis, N. Gathergood, P.J. Scammells, D.N. Sims, Talanta 67 (2005) 354–359.
[13] Y.D. Liang, J.F. Song, T. Tian, Anal. Bioanal. Chem. 380 (2004) 918–923.
[14] X.F. Yang, H. Li, Talanta 64 (2005) 478–483.
[15] P.J.L. Lopez, A. Townshend, Anal. Commun. 33 (1996) 31–33.
[16] L. Wang, W.R.G. Baeyens, G. Van der Weken, A.M. Garcia-Campana, X.R. Zhang, E. Smet, Luminescence 15 (2000) 128–129.
[17] A. Kojlo, J. Michalowski, E. Wolyniec, J. Pharm. Biomed. Anal. 22 (2000) 85–91.
[18] F.A. Aly, A.A. Alwarthan, N.A. Alarfaj, Anal. Chim. Acta 358 (1998) 255–262.
[19] L. Wang, W.R.G. Baeyens, G. Van der Weken, A.M. Garcia-Campana, X.R. Zhang, E. Smet, Luminescence 15 (2000) 81–83.
[20] T. Perez-Ruiz, C. Martinez-Lozano, A. Sanz, M.T.S. Mignel, Lab. Autom. Inf. Manage. 34 (1999) 149–158.
[21] W. Shi, J. Yang, Y. Huang, J. Pharm. Biomed. Anal. 36 (2004) 197–203.
[22] G.M. Greenway, S.J.L. Dolman, Analyst 124 (1999) 759–762.
[23] G. Xu, S. Dong, Anal. Chem. 72 (2000) 5308–5312.
[24] W. Liu, Pharmaceutical Analysis, People's Medical Publishing House, Beijing, 1999, p. 151.
[25] Society of Pharmacopoeia of Hygiene Department. Part II. Chemical Industry Press, Beijing, 2000, p. 574.

[26] F. Nie, J.R. Lu, Y.H. He, J.X. Du, Talanta 66 (2005) 728–733.
[27] Y.H. He, J.R. Lu, M. Liu, J.X. Du, Analyst 130 (2005) 1032–1037.
[28] E.H. White, M.M. Bursey, J. Am. Chem. Soc. 86 (1964) 941–942.
[29] E.H. White, O. Zafiriou, H.H. Kagi, J.H.M. Hill, J. Am. Chem. Soc. 86 (1964) 940–941.
[30] J. Du, W. Liu, J. Lu, Acta Chim. Sinica 62 (2004) 1323–1326.
[31] T.J. Mellinger, C.E. Keeler, Anal. Chem. 35 (1963) 554–558.
[32] J.E. Wallace, J.D. Biggs, J. Pharm. Sci. 60 (1971) 1346–1352.

Available online at www.sciencedirect.com
ScienceDirect
Talanta 71 (2007) 1205–1210
Talanta
www.elsevier.com/locate/talanta

Uniform-sized molecularly imprinted polymer for metsulfuron-methyl by one-step swelling and polymerization method

Xiangjun Liu, Zhiyong Chen, Rui Zhao *, Dihua Shangguan, Guoquan Liu, Yi Chen

Beijing National Laboratory for Molecular Sciences, Laboratory of Analytical Chemistry for Life Science, Institute of Chemistry, Chinese Academy of Sciences, Beijing 100080, China

Received 24 January 2006; received in revised form 10 June 2006; accepted 11 June 2006
Available online 18 July 2006

Abstract

Uniform-sized molecularly imprinted polymer (MIP) beads for metsulfuron-methyl (MSM) were firstly prepared by one-step swelling and polymerization method using 4-vinylpyridine (4-VPY) and ethylene glycol dimethacrylate (EDMA) as functional monomer and cross-linker, respectively. The preparation was optimized by varying the ratio of MSM to 4-VPY. The chromatographic behaviors of MSM and other structurally related sulfonylureas (SUs) on the resultant MIP column were evaluated. The imprinted polymer revealed specific affinity to the template and the fair resolution of SUs was also obtained. Furthermore, the uniform-sized MSM-MIP was used as the solid phase extraction (SPE) material to enrich MSM in real water samples before reversed-phase HPLC (RP-HPLC) analysis. The recovery of MSM from 100 mL of drinking water at a 50 ng/L spike level was 99.59% with R.S.D. of 1.13%. The detection limit was about 6.0 ng/L of MSM when enriching a 100 mL water sample.
© 2006 Elsevier B.V. All rights reserved.

Keywords: Molecularly imprinted polymer; One-step swelling and polymerization method; Metsulfuron-methyl; Solid phase extraction; Water sample

1. Introduction

Metsulfuron-methyl (MSM) is one of the sulfonylureas herbicides (SUs), which have been widely used for controlling weeds in crops due to their high herbicidal activity and selectivity, as well as low mammalian toxicity ($LD_{50} > 4000$ mg/kg) [1]. Compared to other herbicides, SUs have much lower dosage rate (4–20 g of active ingredient per hectare). As a widely used herbicide, its persistence in real samples such as soil, river, especially drinking water, must to be evaluated. The maximum allowed concentration level for herbicides and pesticides in drinking water within Europe is 100 ng/L [2]. It is a challenge for determining MSM in water samples at such low concentration. Up to now, some methods such as gas chromatography [3], capillary electrophoresis [4], immunoassay [5] and liquid chromatography [6] have been used for analysis of sulfonylureas in various matrices. Because of the low level of sulfonylureas presented, an enrichment step before quantitative determination is necessary and also become a crucial step in analytical process. Liquid–liquid extraction (LLE) [7], solid phase extraction (SPE) [8,9] and supported liquid membrane extraction (SLME) [1,6] have been used to enrich sulfonylureas herbicides. However, some methods suffered from relatively low enrichment factor. So, developing a new effective enrichment material is absolutely necessary.

Molecular imprinting technique is an increasingly applied method for preparing polymers with predetermined molecular recognition properties. The obtained molecularly imprinted polymers (MIPs) possess many advantages, for instance, easy preparation, chemical stability and pre-determined selectivity. The most widely used method for preparing MIPs is bulk polymerization. To produce particles with a desired size, the block MIPs must be crushed, ground and sieved. The particles obtained by this way are highly irregular, causing a loss of their chromatographic performance. Spherical MIPs packed in columns gave better flow properties and low backpressures. Some elegant methods have thus been developed for preparing MIP beads such as suspension polymerization in a perfluorocarbon solvent, which simplified the process but kept the recognition ability of MIPs [10]. Moreover, multi-step swelling and polymerization method was explored for preparing uniform-sized MIPs, which showed better separation ability [11,12]. Recently uniform-sized MIPs for sulfamethazine (SMZ) were prepared by one-step swelling and polymerization method in our lab,

* Corresponding author. Tel.: +86 10 62557910; fax: +86 10 62559373.
E-mail address: zhaorui@iccas.ac.cn (R. Zhao).

0039-9140/$ – see front matter © 2006 Elsevier B.V. All rights reserved.
doi:10.1016/j.talanta.2006.06.021

which is a simpler method in the preparation of monodisperse polymer beads and the good separation of SMZ and its analogs on the MIPs stationary phase was obtained [13]. Since Sellergren [14] firstly utilized the MIPs as SPE material for enrichment and analysis of pentamidine from the urine sample, molecularly imprinted solid phase extraction (MISPE) has been applied in some areas, such as biological and pharmaceutical samples analysis [15–17], environmental samples analysis [18–21].

The bulk MIPs for MSM have been prepared and showed the selectivity for the template molecule [22,23], however, the resultant material was not characterized as the HPLC stationary phase. In this paper, a new uniform-sized MIPs for MSM were prepared by one-step swelling and polymerization method. 4-Vinylpyridine (4-VPY) and EDMA were selected as functional monomer and cross-linker, respectively. The ratio of monomer to template was optimized. The chromatographic behaviors of SUs on the column packed with the spherical MIPs were investigated and the recognition mechanism was discussed. Furthermore, the MIP beads were used as sorbents in SPE and applied to the enrichment of trace MSM at low ng/L level in real drinking water samples. The washing step in the SPE process was optimized. A RP-HPLC procedure was used for the determination of MSM after extraction.

2. Experimental

2.1. Materials and instruments

Metsulfuron-methyl (MSM), thifensulfuron-methyl (TSM), bensulfuron-methyl (BSM) and tribenuron-methyl (TBM) (Fig. 1) were gifts from Jiangsu Changlong Chemical Ltd. (Changzhou, China). Styrene was purchased from Beijing Zhonglian Chemical Ltd. (Beijing, China). Methacrylic acid (MAA) and 2,2′-azobis(2-isobutyronitrile) (AIBN) were purchased from Beijing Chemical Plant (Beijing, China). Ethylene glycol dimethacrylate (EDMA) was purchased from Suzhou Anli Chemical Plant (Suzhou, China). 4-VPY was purchased from Acros Organics (USA). Trifluoroacetic acid (TFA, protein sequencing grade) was purchased from Sigma Chemical CO. (USA). Poly (vinyl alcohol) (PVA) 17-88 was purchased from Beijing Organic Chemical Plant (Beijing, China). Sodium dodecyl sulphate (SDS) was purchased from Shanghai No.1 Chemical Reagent Factory (Shanghai, China). Ethylenedinitrilotetraacetic acid disodium salt (EDTA) was purchased from Guangdong Xilong Chemical Plant (Shantou, China). Acetonitrile and methanol (HPLC grade) was purchased from Fisher (USA). Tetrahydrofuran (AR grade) was purchased from Tongguang Chemicals Company (Beijing, China). Chloroform (AR grade) was purchased from Beijing Chemical Plant. Styrene, 4-VPY and MAA were distilled under vacuum to remove stabilizers prior to use. AIBN was re-crystallized from ethanol before use.

The HPLC system consisted of a Hitachi L-7100 Pump (Japan), a Hitachi L-7420 UV–vis Detector (Japan), a Hitachi L-7610 Degasser (Japan), a Hitachi D-7000 Interface (Japan), a L-7300 Column Oven (Japan) and a Rheodyne 7725i sample injector (USA). Ultrasonic homogenizer containing a microtip probe (Ultrasonic homogenizer 4710 series, Ti-horn 20 kHz) was from Cole-Parmer (USA). Scanning electron microscope (S-4300) was from Hitachi (Japan). Column slurry-packer was from Chemco (Japan).

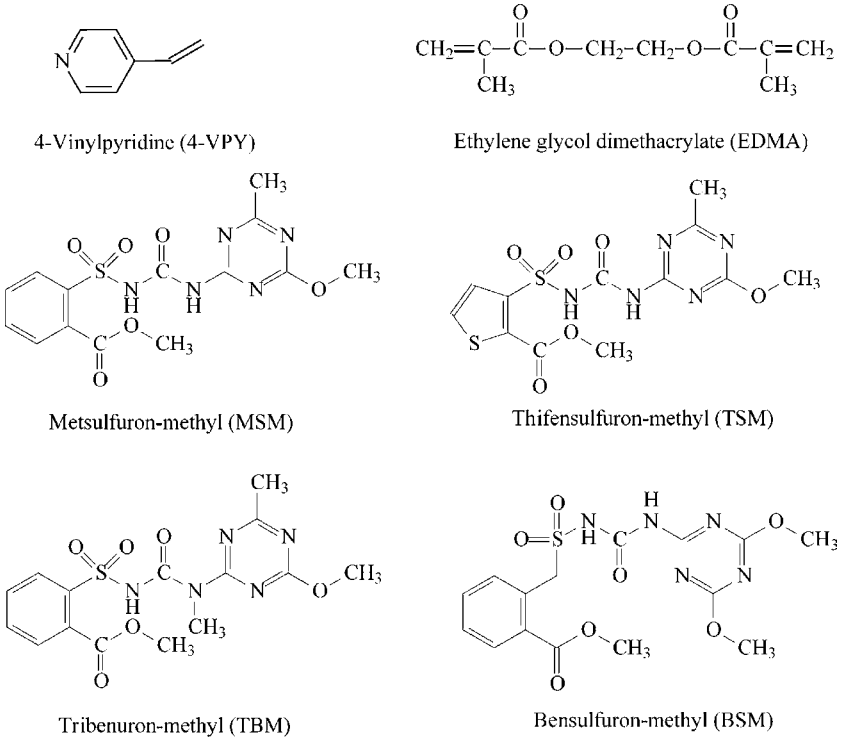


Fig. 1. Molecular structures of sulfonylurea herbicides, monomer and cross-linker used in this study.

2.2. Preparation of uniform-sized spherical molecularly imprinted polymers for MSM

2.2.1. Preparation of monodisperse polystyrene seeds by dispersion polymerization

Monodisperse polystyrene (PS) seeds were synthesized using dispersion polymerization [24]. Styrene, AIBN and PVP were used as monomer, initiator and steric stabilizer, respectively. Styrene (5 mL), AIBN (0.15 g), PVP (0.5 g) and ethanol (50 mL) were weighed into a 100 mL volumetric flask. After purged with nitrogen for 10 min to remove the dissolved oxygen, the flask was sealed and the reaction was carried out at 70 °C for 24 h. The resultant microspheres (PS seeds) were washed with ethanol and water, and then redispersed into an aqueous solution of 1% PVA with a particle content of 0.1 g/mL. The suspension of PS seeds was used in the following step in order to get the final products.

2.2.2. Preparation of uniform-sized spherical MIPs by one-step swelling and polymerization method

The preparation of uniform-sized MIPs using one-step swelling and polymerization method [13] was carried out as follows: 5 mL of the above obtained suspension including 0.5 g of PS seeds was suspended into 100 mL of homogeneous distilled water solution containing 1 g of PVA and 0.1 g of SDS. The mixture containing MSM (template), MAA or 4-VPY (molar amounts are shown in Table 1), 25 mmol of EDMA, 0.1 g of BPO, 7 mL of chloroform and 5 mL of acetonitrile was combined together with a solution of PVA, SDS and distilled water, and then was emulsified by sonication for about 2 min. The emulsified mixture was added dropwise to the mixture of PS seeds via stirring at a speed of 100 rpm within 2.5 h. After swelling 12 h at ambient temperature, the polymerization was carried out at 60 °C on an oil bath for 24 h. The obtained polymer beads were washed with water three times to remove the stabilizer (PVA) and emulsifier (SDS). Then the polymer particles were washed with methanol and tetrahydrofuran, respectively, followed by vacuum-dryness at room temperature. The blank MIP beads for control experiments were prepared identically to the process described above, except the addition of imprinted molecule.

2.3. Evaluation of the uniform-sized spherical MIPs

The micrographics of the molecularly imprinted polymer particles for MSM were characterized by scanning electron microscope (SEM).

In order to evaluate the chromatographic properties, the prepared MSM-MIP and blank MIP beads were slurry-packed into the stainless-steel columns (70 mm × 5.0 mm i.d.) using methanol as the slurry solvent, respectively. For HPLC analysis, the flow rate was maintained at 0.5 mL/min. Detection was performed at 220 nm. The retention factor was calculated from the equation $k = (t_R - t_0)/t_0$, where t_R and t_0 are the retention time of retained and unretained solutes. The retention time of the unretained solute t_0, was measured by injecting acetone. The imprinting factor (IF) was calculated from the equation $IF = k_{imprinted}/k_{non\text{-}imprinted}$.

2.4. MISPE process

The established MIPs column was used as the MISPE device directly for enriching the MSM in real drinking water samples. The samples used for optimizing the MISPE process were prepared by spiking MSM in the redistilled water at a 100 ng/L concentration level. Drinking water sample was collected from the tap in the laboratory. To eliminate sediments and gas pockets in the pipes, the water was collected after flushing for about 10 min. The tap water sample was spiked with MSM at a 50 ng/L concentration level, and then was disposed with EDTA at a 10 g/L level to eliminate the effect of Ca^{2+} and Mg^{2+} existed in the tap water [20]. All of the water samples were filtrated with 0.22 μm membrane before analysis.

The MISPE procedure was carried on the HPLC pump of Hitachi L-7100. Prior to extraction, the MIP column was washed with elution solvent of CH_3CN/H_2O (95:5, v/v) for 10 min and equilibrated with redistilled water for 15 min (1.0 mL/min). After enriching 100 mL of water sample (2.0 mL/min, 50 min), the washing solvent of CH_3CN/H_2O (10:90, v/v) was pumped through the MIPs column to elute certain level of interference. Then the elution solvent was switched to the column at a flow rate of 1.0 mL/min in order to elute the enriched MSM from the MISPE column. The collected eluted fraction (4 mL) was

Table 1
The optimization of the preparation conditions for uniform-sized MSM-MIPs stationary phase[a,b,c]

MIP	Amount of MSM (mmol)	Amount of 4-VPY (mmol)	Amount of MAA (mmol)	k			
				MSM	TBM	BSM	TSM
P1	1.5	0	6	0.03	–	–	–
P2	1.5	6	0	3.04	0.11	0.34	2.19
P3	0	6	0	2.71	0.12	0.44	2.00
P4	2	7	0	5.35	0.20	0.54	3.95
P5	4	7	0	7.40	0.28	0.84	5.38
P6	0	7	0	2.74	0.13	0.45	2.02

[a] Quantity of PS seeds: 0.5 g; amount of EDMA: 25 mmol; initrator: BPO, 0.1 g; porogen mixture: chloroform/acetonitrile (mL), 7/5; polymerization temperature: 60 °C.
[b] HPLC conditions: column, 70 mm × 5.0 mm i.d.; mobile phase, 100% acetonitrile (0.1% acetic acid, v/v); flow rate, 0.5 mL/min; detection, 220 nm.
[c] (–) means no any retention.

dried using a stream of nitrogen. The residues were dissolved in 110 μL of mobile phase and analyzed by RP-HPLC.

2.5. RP-HPLC analysis

RP-HPLC analysis for MSM quantification was performed on the Hitachi HPLC system as described in Section 2.1. An Ultimate C_{18} column (250 mm × 4.6 mm i.d., 5 μm, Shanghai, China) was used for the chromatographic separation. The detection wavelength was 220 nm. The mobile phase was CH_3CN (0.1% CF_3COOH)–H_2O (40:60, v/v) with a flow rate of 1.0 mL/min. Peak areas were used for quantification.

The calibration curve (amount of MSM versus peak area) was prepared using pure MSM as the standard. The different concentrations of pure MSM were prepared as 0.10, 0.25, 0.50, 1.0, 2.5 and 5.0 μg/mL. The absorbance was detected at 220 nm. The correlation coefficient (r) of the standard curve was equal to 0.9995 ($n = 4$). From this curve, the recovery of MSM from MISPE could be determined.

3. Results and discussion

3.1. Preparation and characterization of the uniform-sized spherical MIPs

One-step swelling and polymerization method is a simpler and more convenient technique to prepare monodisperse spherical particles, which was firstly used to prepare MSM-imprinted polymer beads with uniform size in this study.

It is known that the specific interaction between template and functional monomer is an important factor for molecular recognition. In order to find out the suitable functional monomer for the template MSM, 4-VPY and MAA were chosen as the basic and acidic monomer to prepare the MSM-MIPs (Table 1). Clearly, the retention factor for MSM on the MAA-MIPs (P1) was only 0.03 while that on 4-VPY MIPs (P2) was 3.04. The reason may be explained that MSM is an acidic molecule (pK_a 3.2), resulting in the acidic monomer MAA cannot form a stable complex with MSM through the non-covalent interaction. In general, the basic functional monomers are preferably chosen for preparing MIPs towards the template containing acid groups and vice versa [25], so 4-VPY was chosen as functional monomer in the following studies.

In order to obtain the MIPs with good recognition ability for MSM, the molar amounts of the functional monomer and the template were optimized and the retention factors of MSM and other structurally related SUs on each MSM-MIPs column were summarized in Table 1. Namely, when the amount of MSM and 4-VPY were 1.5 and 6 mmol, the retention factor of MSM was 3.04 on MSM-MIP (P2) and 2.71 on blank MIP (P3), and then the corresponding IF of MSM was only 1.12. When the amounts of MSM and 4-VPY were 4 and 7 mmol, MSM expressed the largest retention factor ($k = 7.40$) on the MSM-MIP column (P5) while only 2.74 on the blank MIP column (P6), so the IF of MSM was up to 2.70. Moreover, the retention factors became bigger along with the increase of the amount of template. The most possible reason is that the amount of PS particles was definite during the MIP preparation, the more template was added, the more template-monomer complex formed and distributed into PS particles. So the density of imprinted sites increased and the efficiency of MIP column was improved.

The scanning electron micrographs of the uniform-sized MIPs beads for MSM were shown in Fig. 2. It can be clearly found that the diameter of the beads is about 7.5 μm. When the magnification was 12,000, a lot of holes in the MIPs beads could be seen, which will be in favor of kinetics in chromatographic process. Furthermore, the MIPs beads exhibited good mechanical intensity and permeability. The backpressure of the column (70 mm × 5.0 mm i.d.) was as low as 3.0 MPa at the flow rate of 1.0 mL/min. When the flow rate was up to 5.0 mL/min, the column backpressure was 14.1 MPa and there was no evidence that the MIPs were compressed, indicating that the MIPs beads could be used in fast flow when necessary, for example as SPE material to enrich trace compound existed in real samples.

3.2. Binding specificity of MSM imprinted polymers

In order to verify the selectivity of the resultant MIPs, MSM and other three related sulfonylureas herbicides was evaluated. The chromatogram on P5 imprinted stationary phase was shown in Fig. 3. As expected, MSM, the template, had the biggest retention factor over all the solutes (as shown in Table 1 and Fig. 3). Tribenuron-methyl (TBM) and bensulfuron-methyl (BSM) have almost no retention on every MSM-MIPs column. The structural difference between MSM and TBM molecules is that TBM is a methylation product of MSM at –NH– group bound to tri-

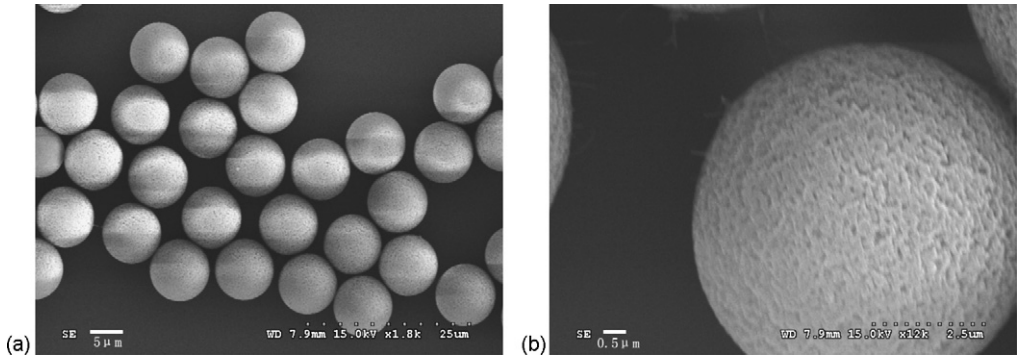


Fig. 2. Scanning electron micrograph of the uniform-sized MIPs for MSM. Magnification: (a)1800×; (b)12,000×.

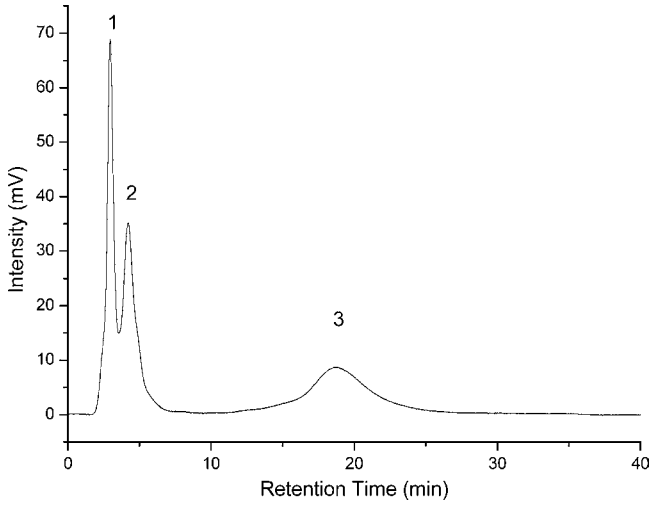


Fig. 3. Chromatogram of MSM and other selected SUs on the MSM-MIPs (P5). 1: TBM, 2: BSM, 3: MSM. HPLC condition was the same as that in Table 1.

azine ring. It suggested that the hydrogen of the sulfonylurea group of the MSM was an important imprinting site for forming hydrogen bond as a proton donor with the nitrogen atom of pyridine ring in 4-VPY molecule as a proton acceptor during the imprinted process. Because TBM cannot form this hydrogen bond, it is hardly retentive in all the MIPs. And this also indicated that the hydrogen bond is very important in molecular recognition. Although bensulfuron-methyl (BSM) molecule has the same proton donor as MSM, it has very short retention time on each MIPs stationary phase. The reason may be that BSM has one more methylene group than MSM and the methyl group of the triazine ring is replaced by methoxyl group, so the molecular dimension and spatial structure of BSM are very different from MSM, which resulted in the BSM cannot enter the imprinting cavities of MIPs and also cannot interact with the pyridyl group of the MIPs. Moreover, thifensulfuron-methyl (TSM) molecule has almost the same structure with template MSM and the only difference is that the phenyl group of MSM is replaced by the thiazole group, so TSM molecule can easily enter the cavities of MIPs and form hydrogen bond with nitrogen atom of pyridine ring in 4-VPY. This led to TSM had a bigger retention factor than TBM and BSM and the MSM-MIPs showed some cross-reactivity to the TSM. The results demonstrated that the specific affinity and selectivity of the resultant MIPs was contributed by a combination of hydrogen bond interaction and shape recognition.

3.3. Optimization of the conditions for the MISPE procedure

In order to validate the reliability and the applicability of this MIP column for real samples, an off-line SPE procedure was selected for MSM analysis at trace concentration level (ng/L). Because the resultant uniform-sized MIPs beads for MSM showed low backpressure and high penetrability, the MIPs column (P5) was used as SPE device directly.

Washing step as an important factor in MISPE was optimized by selecting a CH_3CN–H_2O ratio and washing time.

Table 2
Recovery of the MSM with different washing solvent and washing time ($n = 3$)[a]

Washing solvent[b]	Recovery (R.S.D., %)	Washing time (min)[c]	Recovery (R.S.D., %)
90%H_2O + 10%CH_3CN	97.40 (1.26)	5	97.40 (1.26)
80%H_2O + 20%CH_3CN	44.30 (4.38)	7	101.73 (4.38)
70%H_2O + 30%CH_3CN	8.81 (17.98)	10	63.25 (0.79)
100%CH_3CN	–[d]		

[a] The RP-HPLC analytical conditions used for the determination of the recovery were in Section 2.5.
[b] 5 mL of washing solvent with a flow rate of 1.0 mL/min was used in the washing step.
[c] 90% H_2O + 10% CH_3CN (v/v) was used as the washing solvent with a flow rate of 1.0 mL/min.
[d] (–) means not detected.

The aqueous solution of pure MSM at 100ng/L was used in the optimization process. The recovery of MSM after washing with different washing solvents and different washing time was shown in Table 2. It can be clearly seen that the recovery of MSM becomes lower along with increasing the acetonitrile proportion. When the acetonitrile content was 30%, almost all the enriched MSM on the MISPE column was eluted due to the high elution power of the washing solvent. And when acetonitrile content was 20%, the average recovery was 44.30% with a R.S.D. of 3.59%. However, when 10% acetonitrile was selected, the recovery of MSM was up to 97.40%.

Obviously, long-term washing can remove more interference from the MISPE column but the enriched MSM can also be partially eluted. When the washing time was lasted to 10 min, the recovery of MSM decreased to 63.25% with a R.S.D. of 0.79%. A satisfactory recovery of 101.73% was obtained at washing time of 7 min. In a word, a combination of 10% acetonitrile + 90% H_2O was used as the washing solvent and 7 min was chosen as the washing time in the following study.

3.4. Detection limit and reproducibility of the MISPE-RP-HPLC method

The solutions spiked with MSM at different concentration were analyzed using the MISPE-RP-HPLC procedure for three times to determine the detection limit and reproducibility of this method. The results were shown in Table 3. The recoveries of MSM spiked at 20, 50 and 100 ng/L level were in the range of 92.66–101.73% with R.S.D. of 3.13–4.91%. The data indicated that the MISPE-RP-HPLC method had good recovery and reproducibility for analyzing MSM at low concentration

Table 3
Recovery and reproducibility of the MSM at different concentration by the MISPE-RP-HPLC method ($n = 3$)

MSM concentration (ng/L)	Recovery (%)	Reproducibility (R.S.D., %)
100	101.73	4.38
50	101.11	3.13
20	92.66	4.91

The RP-HPLC analytical conditions were shown in Section 2.5.

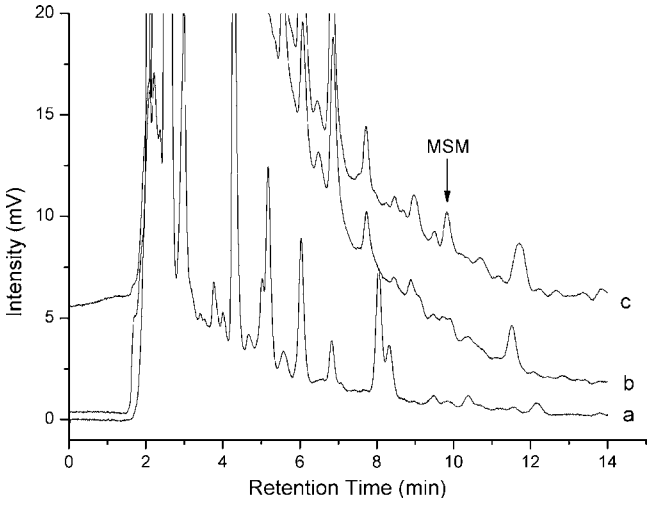


Fig. 4. Chromatograms of drinking water samples obtained after molecularly imprinted solid phase extraction. (a) Drinking water sample spiked with MSM, but not disposed with EDTA; (b) drinking water sample disposed with EDTA, but not spiked with MSM; (c) drinking water sample spiked with MSM, and disposed with EDTA. The RP-HPLC conditions are shown in Section 2.5.

ng/L level. The detection limit estimated by utilizing the signal/noise of 3 was 6.0 ng/L when enriching a 100 mL water sample.

3.5. Analysis of drinking water samples

The performance of the MIP beads in the extraction of MSM from real drinking water samples was investigated. The tap water from our lab was chosen as the real drinking water sample, which was spiked with MSM at a concentration level of 50 ng/L. Firstly, 100 mL of the drinking water sample was directly extracted by MISPE, and then analyzed by RP-HPLC. Unfortunately, no MSM was detected from the spiked drinking water sample (Fig. 4a). This may be due to the interference of Ca^{2+} or Mg^{2+} presented in the sample matrix. It is well known that the organic amine and the compound containing –NH– group is efficient ligand for divalent metal ions such as the Ca^{2+} or Mg^{2+}. As a result, Ca^{2+} or Mg^{2+} existed in the drinking water samples may form a complex with MSM through secondary amino group of MSM and with 4-VPY through nitrogen atom so as to MSM cannot be eluted from the MIP column [20]. Therefore the drinking water sample spiked with MSM must be dealt with in advance to eliminate the effect of Ca^{2+} and Mg^{2+}. EDTA was selected as the metal ion chelating agent. After disposed with EDTA, the Ca^{2+} or Mg^{2+} ions formed the coordinate bonds with EDTA, so the free MSM in water sample was adsorbed on the MIPs column and analyzed by RP-HPLC. Fig. 4b and c showed the chromatograms of EDTA treated drinking water samples with and without spiked MSM and a peak of MSM could be clearly founded in Fig. 4c. The recovery of MSM was 99.59% with a R.S.D. of 1.13% ($n = 3$). The high recovery and the good reproducibility of this process demonstrated that the MISPE-RP-HPLC method revealed good accuracy and precision for analysis of trace concentration of MSM in the drinking water samples.

4. Conclusion

One-step swelling and polymerization method, a rather simple procedure, was used for preparing the uniform-sized molecularly imprinted polymer beads for MSM. The resultant MIPs showed highest affinity and selectivity toward MSM over other SUs. The hydrogen bond formed between MSM and 4-VPY and the cavity shape played the crucial roles in the molecular recognition. Furthermore, the MIPs beads have also been successfully applied to determine trace MSM in real water samples. The good recovery and reproducibility were successfully achieved.

Acknowledgements

This work was financially supported by National Natural Science Foundation of China (20435030, 20575072) and Chinese Academy of Sciences (KJCX2-SW-H06).

References

[1] J.F. Liu, J.B. Chao, G.B. Jiang, Y.Q. Cai, J.M. Liu, J. Chromatogr. A 995 (2003) 21.
[2] Economic Commission for Europe, Drinking Water Directive, 80/778/EEC, 1980.
[3] E.G. Cotterill, Pestic. Sci. 34 (1992) 291.
[4] A.J. Krynitsky, J. AOAC Int. 80 (1997) 392.
[5] A. Knopp, D. Knopp, R. Niessner, Environ. Sci. Technol. 33 (1999) 358.
[6] J.B. Chao, J.F. Liu, M.J. Wen, J.M. Liu, Y.Q. Cai, G.B. Jiang, J. Chromatogr. A 955 (2002) 183.
[7] I. Ahmad, J. Assoc. Off. Anal. Chem. 70 (1987) 745.
[8] M. Rodriguez, D.B. Orescan, Anal. Chem. 70 (1998) 2710.
[9] B. Koppen, N.H. Spliid, J. Chromatogr. A 803 (1998) 157.
[10] A.G. Mayes, K. Mosbach, Anal. Chem. 63 (1996) 3769.
[11] K. Hosoya, Y. Kishii, K. Kimata, T. Arati, N. Tanaka, F. Sevc, J.M.J. Frechet, J. Chromatogr. A 690 (1995) 21.
[12] J. Haginaka, H. Sanbe, H. Takehira, J. Chromatogr. A 857 (1999) 117.
[13] Z.Y. Chen, R. Zhao, D.H. Shangguan, G.Q. Liu, Biomed. Chromatogr. 19 (2005) 533.
[14] B. Sellergren, Anal. Chem. 66 (1994) 1578.
[15] W. Chen, F. Liu, X.M. Zhang, K.A. Li, S.Y. Tong, Talanta 55 (2001) 29.
[16] D. Stevenson, Trends Anal. Chem. 18 (1999) 154.
[17] F. Nie, J. Lu, Y. He, J. Du, Talanta 66 (2005) 728.
[18] X.C. Dong, N. Wang, S.L. Wang, X.W. Zhang, Z.J. Fan, J. Chromatogr. A 1057 (2004) 13.
[19] J.J. Ou, L.H. Hu, L.G. Hu, X. Li, H.F. Zou, Talanta 69 (2006) 1001.
[20] Q.Z. Zhu, P. Degelmann, R. Niessner, D. Knopp, Environ. Sci. Technol. 36 (2002) 5411.
[21] S. Buyuktiryaki, R. Say, A. Ersoz, E. Birlik, A. Denizli, Talanta 67 (2005) 640.
[22] Q.Z. Zhu, K. Haupt, D. Knopp, N. Niessner, Anal. Chim. Acta 468 (2002) 217.
[23] J. Bastide, J.P. Cambon, F. Breton, S.A. Piletsky, R. Rouillon, Anal. Chim. Acta 542 (2005) 97.
[24] K.P. Lok, C.K. Oberr, Can. J. Chem. 63 (1985) 209.
[25] A.J. Paine, W. Luymes, J. McNulty, Macromolecules 23 (1990) 3104.

Available online at www.sciencedirect.com
ScienceDirect
Talanta 71 (2007) 1369–1374
Talanta
www.elsevier.com/locate/talanta

Use of membrane micropumps for introducing the sample solution in flame atomic absorption spectrometry

Ignacio López-García [a], Joanna Kozak [b], Manuel Hernández-Córdoba [a,*]

[a] Department of Analytical Chemistry, Faculty of Chemistry, University of Murcia, E-30071 Murcia, Spain
[b] Department of Analytical Chemistry, Jagiellonian University, 30-060 Kraków, Poland

Received 2 March 2006; received in revised form 14 June 2006; accepted 6 July 2006
Available online 21 August 2006

Abstract

The advantages of using membrane micropumps to introduce sample or standard solutions in flame atomic absorption spectrometry are discussed, using two entirely computer-controlled manifolds which allow a wide range of dispersion coefficients to be obtained. Coupling micropumps to the manifold facilitates calibration graphs to be obtained using a single standard solution. Other advantages include a handy on-line dilution stage for excessively concentrated samples as well as the possibility of obtaining pulsed absorbance–time profiles that once submitted to the Fourier transformation, provide amplitude–frequency plots representing an innovative, not yet fully exploited vision of atomic absorption analytical data.
© 2006 Elsevier B.V. All rights reserved.

Keywords: FAAS; Calibration; Automation; On-line dilution; Micropumps; MPFS; Pulsed signals

1. Introduction

The usual way to introduce sample solutions in flame atomic absorption spectrometry (FAAS) is by direct aspiration using the suction effect produced in a pneumatic nebulizer. There is no clear reason for such a commonly accepted way of operation, since the ongoing development of continuous flow methodologies offers more versatile and interesting ways for the same purpose. Thus, as Welz accurately pointed out several years ago [1], flow injection (FI) can be considered revolutionary in almost all aspects of AAS and it has been shown repeatedly that FI is far more than an elegant way for sample handling and introduction. Although peristaltic pumps are the most frequently used propelling devices for the purpose here discussed, the sample solution can be introduced in multiple ways [2,3], including the use of pulse-free devices [4,5]. Sometimes, the drawback posed by the pulse due to the rollers of peristaltic pumps has been turned into a benefit by taking advantage of the fact that the action of the rollers is periodical and highly reproducible [6,7], whereas other approaches take advantage of pulsed flows to obtain turbulent regimes and then high dispersion degrees useful in some detectors [8,9].

The purpose of this study was to assess the possibility of using solenoid-based micropumps (MPs), instead of peristaltic pumps, for both continuous and pulsed introduction of the sample solution in FAAS, thus facilitating on-line dilution and, consequently, the obtaining of calibration graphs with a single solution, as well as the measurement of solutions too concentrated to be measured by direct aspiration. These low-cost, versatile, easily computer-controlled propelling devices can be easily implemented into flow systems due to their small size, resulting in a multipumping flow system (MPFS), which has recently proven advantageous in molecular UV–vis absorption detection [10,11].

2. Experimental

2.1. Instrumentation and reagents

All the measurements were obtained using a Perkin-Elmer (Norwalk, CT, USA) Model 1100B atomic absorption spectrometer. Air-acetylene flames were used exclusively. The nebulizer uptake rate was measured to be 15.5 ml min^{-1}. Measurements were carried out at 324.8 nm using an ordinary hollow cathode lamp as the radiation source. A stock standard solution of

* Corresponding author. Fax: +34 968364148.
E-mail address: hcordoba@um.es (M. Hernández-Córdoba).

0039-9140/$ – see front matter © 2006 Elsevier B.V. All rights reserved.
doi:10.1016/j.talanta.2006.07.007

copper (1000 μg ml^{-1}) was obtained from Panreac (Spain). To study solutions with very high concentration, a 10 mg ml^{-1} copper solution was prepared by dissolving metallic copper in nitric acid. Appropriate dilutions were made to obtain working standard solutions.

To obtain a complete control of the system, a Windows®-based software was developed specifically in collaboration with the Central Unit for Supporting Research (CUSR) of the University of Murcia. To this purpose, the signal was obtained directly from the motherboard of the instrument before digitalization. The software allowed direct plotting on the computer screen, in real time, of the analytical signal and the saving of the data in ASCII format, as well as the later treatment of the signal, including digital filtering and quantification using both peak height and peak area. This software, together with a home-made data acquisition card and an analogical–digital interface entirely designed at the Department of Analytical Chemistry of the University of Murcia, also allowed the easy remote control of the micropumps.

Commercial micropumps (Bio-Chem Valve Inc., Bonton, USA) that dispense nominal volumes of 8, 25, 50 and 125 μl (references 090SP12-8, 120SP12-25, 120SP12-50 and 150SP12-125, respectively) were used. These micropumps are solenoid-operated membrane pumps that work in the following way. The diaphragm of the pump is held closed with an internal spring mechanism. When voltage is applied, the solenoid coil becomes energized and pulls the diaphragm open. This opening action causes fluid to be drawn into the pump chamber. The fluid is dispensed from the pump when the voltage is dropped sufficiently to de-energize the coil allowing the internal spring to force the diaphragm back to the closed position. For this, a square wave signal (12 V for the amplitude) is required. The frequency of operation can be adjusted up to 250 strokes per minute (120 strokes in 150SP12-125 model), which means maximum flow rates of 2, 6.25, 12.5 and 15 ml min^{-1}, respectively, if used as propelling devices. The volumes spent to refill the MPs were experimentally measured using tubing of 10 cm length and 0.6 mm internal diameter for both the inlet and outlet of the 8, 25, 50 and 125 μl micropumps, and were found to be 230, 290, 380 and 525 μl, respectively. For the specific case of controlling the micropumps, the analogical interface was provided with three channels that can be programmed independently and which work in a simultaneous way. The main parameters used for programming the operation of the micropumps are schematized in Fig. 1, in which V is the voltage applied to the pump. The duration of each pulse (e.g. the injection stage) is constant and depends on the particular pump used. The system controlled the time elapsed between pulses (t_i), the number of pulses within a cycle (n) and the time elapsed between cycles (t_w). The software also included an initial time (t_0) that can be used to carry out an autozero of the detector.

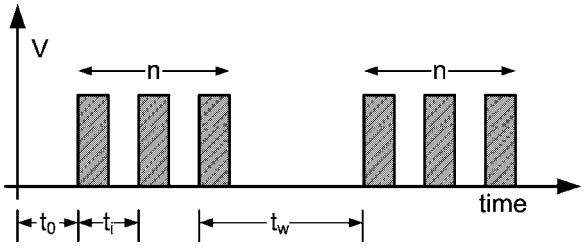


Fig. 1. Timing diagram for MPs operation. See the text for details.

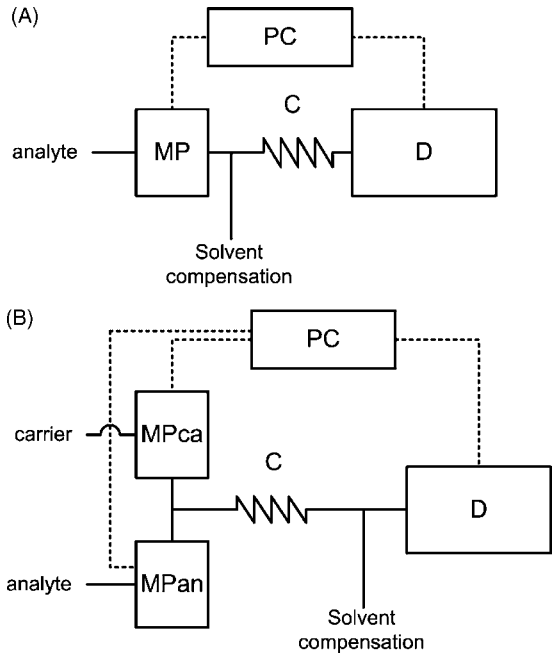


Fig. 2. Manifolds studied. MPs, micropumps; PC, personal computer with an input/output interface; D, FAAS detector; C, dispersion device (coil or gradient tube).

2.2. Manifolds

A great number of manifolds were considered, those shown in Fig. 2 being finally selected due to their versatility. In all cases, the flow manifold comprised a set of solenoid micropumps, flow lines made of 0.5 mm i.d. PTFE tubing and dispersion coils made of both 0.8 mm i.d. PTFE tubing and 2 mm i.d. silicone tubing. Mixing points and end-fittings were obtained from Omnifit (Cambridge, UK).

3. Results and discussion

3.1. Manifold A

This simple manifold with a single micropump allows a wide variety of dilution degrees to be achieved, enabling a calibration line to be obtained using a single standard solution and, if necessary, the on-line dilution of samples too concentrated to be measured by means of the conventional aspiration mode.

Using this manifold with the different pumps available, MP1, MP2, MP3 and MP4, that deliver 8, 25, 50 and 125 μl per stroke, respectively, the dispersion coefficients obtained were 32, 8, 6 and 1.6, respectively. The inclusion of simple gradient tubes allowed, in accordance with flow methodology, higher dilution degrees to be obtained. Thus, for example, the dispersion obtained after a simple injection of analyte solution delivered

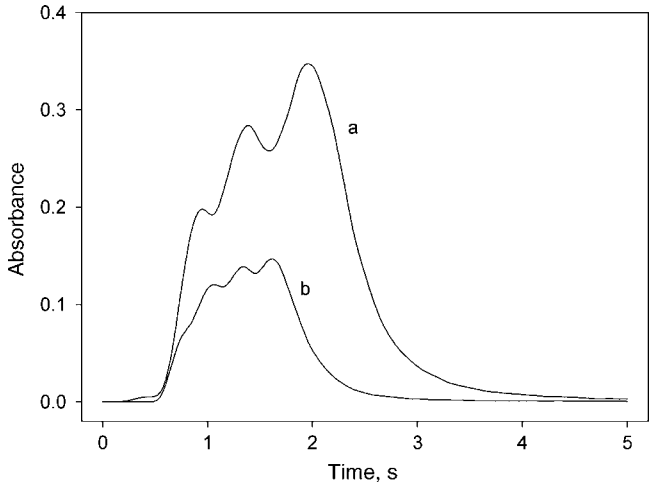


Fig. 3. Curve a: signal obtained of a 10 μg ml^{-1} copper solution injected by MP4 (125 μl internal volume, $n = 3$ and $t_i = 0.5$ s). Curve b: signal obtained of a 50 μg ml^{-1} copper solution injected by MP1 (8 μl internal volume, $n = 4$ and $t_i = 0.3$ s). In both cases a 500 μl dispersion coil was included in the manifolds.

by MP1 (8 μl) was as high as 395. There is nothing new in these results that are predictable by the theory and similar data would be obtained if the sample solutions were introduced by means of a peristaltic pump equipped with a loop. However, the use of MPs provide better versatility because several consecutive injections of analyte solution can be carried out in a faster and easier way than when using the classical peristaltic pump-loop combination.

It should be noted that the time necessary to refill the MPs is short (0.25 s for MP1, MP2 and MP3, and 0.5 s for MP4), which means that several consecutive injections can be carried out in a short time, thus introducing different amounts of analyte into the flow system. In this way, the absorbance–time profile would not be a set of narrow, well-differentiated peaks, but that resulting from the partial mixing of the analyte plugs propelled at each stroke. Fig. 3 shows two of these profiles obtained when successive injections were carried out using two different pumps and solutions. In these cases, the area of the absorbance–time profile, which is related to the amount of analyte reaching the detector, must be used as the analytical signal. This fact is not a drawback in practice because, since the system is computer-controlled, the task of obtaining the area is assumed by the software with no waste of time by the operator. The only obvious limitation is that the response of the detector must be within the linear response range of the spectrometer.

From the above, the versatility of the system is clear. The influence of the time (t_i) elapsing between injections was studied. It was experimentally found that, to obtain reproducibility when several successive injections were carried out, the minimum t_i value was 0.3 s for MP1, MP2 or MP3 and 0.5 s when using the 125 μl pump (MP4). The effect of the number of successive injections on the analytical signal was also studied using the four MPs available separately and in the presence or absence of gradient tubes. In this way, it was thoroughly verified that there was always a linear relationship between the number of injections carried out with an MP and a given solution and the analytical signal (area), provided that the essential condition of being in the linear response range of the spectrometer was fulfilled.

It is important to note that there is a physical effect which is inherent to the characteristics of the manifolds used, and which could affect the reproducibility of the results, depending on the volume released in each stroke and the time elapsed between one pulse and the next one. In fact, after an MP has carried out a given stroke, the pump is closed but the continuous flow of solvent through the compensation channel leads to depletion of the analyte in the first layers of the small plug of solution, which remains static at this point. The extension of this depletion effect is dependent on the time elapsing between injections and on the exact geometry of the connection used for the compensation channel. To study this effect, a number of experiments were made by carrying out sets of four successive injections with $t_i = 1$ and using different intervals of time between each set, thus evaluating the extent of the depletion effect from the decrease in the signal. The experiments were made using different pieces for the connection and tubes of different internal diameters. In this way, it was verified that the use of a 120° three-way connector together with 0.8 mm i.d. connecting tubes rendered the depletion effect negligible even after 1 min of continuous flow of solvent through the connecting piece. Using this configuration, only when the time elapsing between strokes exceeded 90 s was a 0.3% decrease in the signal observed.

The analytical signal (area) was verified to be related to the concentration of the sample solution by the simple equation

$$\text{area} = K \times V_p \times n \times C$$

where V_p is the internal volume of the particular MP used, n the number of injections and C represents the analyte concentration. The proportionality factor, K, includes the detector response and can be evaluated from the introduction of a standard solution.

The versatility of the system is given by the number of injections carried out, the pump to be used being selected in accordance with the concentration of the analyte solution, so that a signal within the linear response range is obtained. In any case, if necessary, two pumps, one of them with a relatively high inner volume (125 μl) and the other with a smaller volume (8 μl) together with the variability provided by the change in the number of injections should cover the entire range of concentrations that are normally found in FAAS practice.

One additional feature of the manifold is the easy periodical generation of concentration profiles which, as discussed elsewhere [6,7] for the case of using peristaltic pumps as the propelling devices, allows analytical signals to be obtained in a non-conventional, suggesting way. As shown in Fig. 4A, when consecutive injections of the same solution were carried out using appropriate experimental conditions, the absorbance–time profile, which should be periodical, is hidden by the noise associated with the experimental measurement. However, if the absorbance–time pair data are treated by means of the Fourier transformation (FFT), a frequency spectrum, such as that shown in Fig. 4B, is obtained. Because these data were obtained using a time interval of 5 s between one injection and the next, the

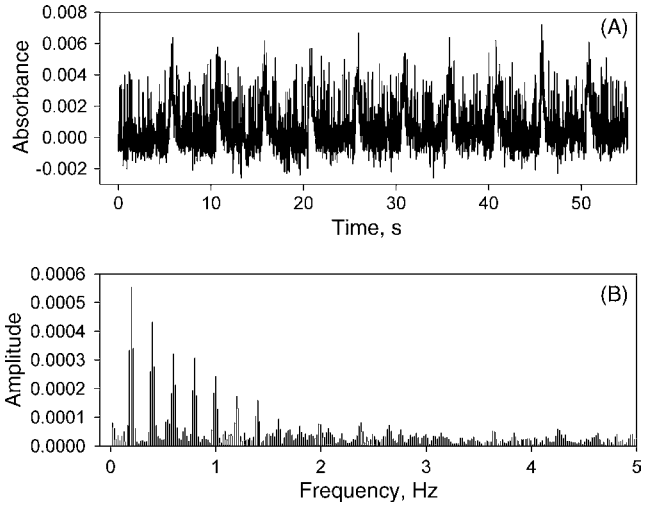


Fig. 4. Graph A: signal obtained of a 2 μg ml^{-1} copper solution injected by using MP1 (8 μl internal volume, $n = 10$ and $t_i = 5$ s) without a dispersion coil. Graph B: Amplitude vs. frequency plot.

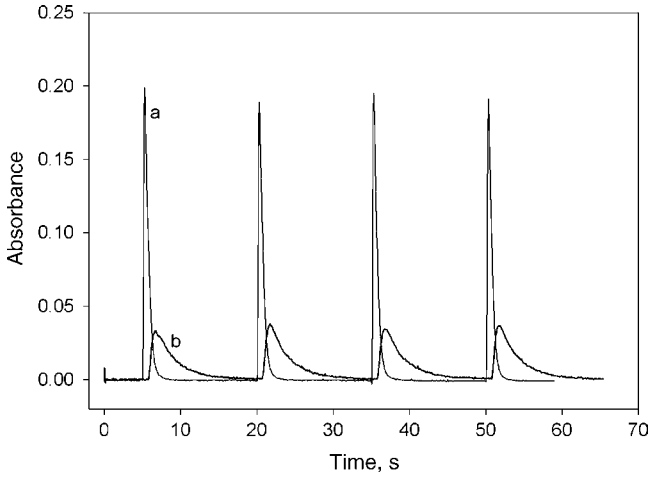


Fig. 5. Signals obtained of several injections of a 200 μg ml^{-1} copper solution. Lines *a* and *b* correspond to the use of manifolds A and B, respectively. See the text for details.

frequency spectrum shows a maximum at 0.2 Hz, the harmonics also being clearly appreciated. The information provided by the frequency domain can be plotted in a variety of ways. The amplitude can be calculated as

$$2\left(\frac{\mathrm{Re}^2 + \mathrm{Im}^2}{N}\right)^{0.5}$$

where Re is the real component of the FFT at a given frequency, Im the imaginary component and N is the data set size. It was experimentally verified that the signal (amplitude) obtained in this way was proportional to the concentration of the analyte used.

The effect of the number of injections on the amplitude of the periodical signal was also studied, the results showing that five injections sufficed to obtain a constant, maximum amplitude, which means that only 40 μl of sample solution are required for a reliable measurement when using MP1. Working with this micropump, a linear calibration graph was verified in the 0.2–20 μg ml^{-1} copper concentration range. To improve sensitivity MP4 (125 μl per stroke) can be used. In this case, the calibration graph was linear in the 0.05–10 μg ml^{-1} copper range. In both cases, RSD values below ±3% were obtained (five measurements for each experimental point).

3.2. Manifold B

This manifold allows high dispersions to be obtained without an excessive deterioration of the sampling frequency, demonstrating the versatility of using MPs. In this case, a small sample plug is introduced into the system by means of a micropump, MP_{an}, while another pump, MP_{ca}, of a high internal volume, is operated at a high frequency so that it propels solvent at a flow rate, FR_{ca}, lower than the nebulizer uptake rate, FR_n, in such a way that the difference between both flow rates is compensated by aspirating solvent through a compensation channel. The high dispersion in this way obtained can be further increased by including a small gradient tube into the system. This arrangement is more versatile for obtaining variable dispersion degrees than similar manifolds based on the use of peristaltic pumps. The FR_{ca} can be modified by varying the time between pulses t_i. Fig. 5 shows the signals obtained when 8 μl aliquots of a 200 μg ml^{-1} copper solution were injected into the manifold using a 500 μl gradient tube and operating MP_{ca} (50 μl micropump) at 3.3 Hz (line b). The signals obtained from the same solution injected into manifold A are also included for comparison purposes (line a). The dispersion coefficient changed from 32 to 230, while the theoretical sampling frequency still remained as high as 240 samples per hour. A decrease in the FR_{ca} value led to a substantial change in the dispersion coefficient. Thus, when MP_{ca} (8 μl micropump) was used for propelling the carrier at 3.3 Hz, the dispersion coefficient increased up to 900, although the sampling frequency decreased to 30 samples h^{-1}.

As Fig. 6A shows, a linear relationship between the analytical signal and the FR_{ca} value was verified for FR_{ca}/FR_n ratios in the 0.1–0.9 range. Fig. 6A also shows the variation of the dispersion coefficient when gradient tubes of different volumes were included in the manifold. It is noteworthy that, despite the significant increase in the dispersion coefficient, the sampling frequency only decreased to 120 samples h^{-1} for 1500 μl gradient tubes using a 50 μl pump operated at 3.3 Hz as MP_{ca}.

Some of the results obtained when varying the number of injections are given in Fig. 6B. This possibility permits a wide range of dispersion coefficients to be obtained without excessive deterioration of the sampling frequency. Thus, for example, using a value corresponding to 10% of the nebulizer uptake rate for FR_{ca}, the analytical signals (both peak area and peak height) were found to be proportional to the number of injections in the 1–10 range. While the sampling frequency only decreased from 60 to 40 samples h^{-1}, the dispersion coefficient changed to 940 and 93 for $n = 1$ and 10, respectively. Consequently, by selecting suitable experimental conditions, the calibration range can be extended by three orders of magnitude when compared with the conventional aspiration mode used in FAAS.

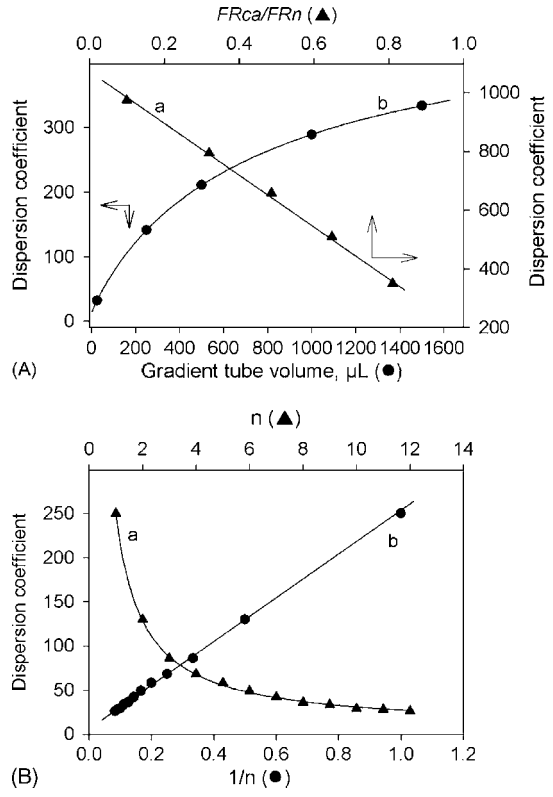


Fig. 6. Graph A: influence of the flow rate ratio and the volume of the dispersion device on the dispersion coefficient. Graph B: effect of the number of injections on the dispersion coefficient. Manifold B was used in all cases.

Manifold B can also use air, instead of solvent, as the fluid through the compensation channel. To study this possibility, MP_{ca} was used for washing purposes and no coil dispersion was inserted. The sample was introduced into the system by means of several consecutive injections carried out by MP_{an} (25 μl micropump). For these experiments, the channel compensation was open to air and MP_{ca} was programmed to carry out a single injection when the analytical signal reached to baseline, which allowed tubing and spray chamber to be washed. Fig. 7 shows a comparison of the results obtained when using air (curve b) or water compensation (curve a). In both cases, different injections of a 10 μg ml^{-1} copper solution were made, the micropump working at 3.3 Hz. As can be seen, there was a six-fold increase in sensitivity when using air compensation. When the frequency at which MP_{an} was operated decreased to 0.5 Hz, the nebulization efficiency increased even more and a nine-fold increase in sensitivity was obtained.

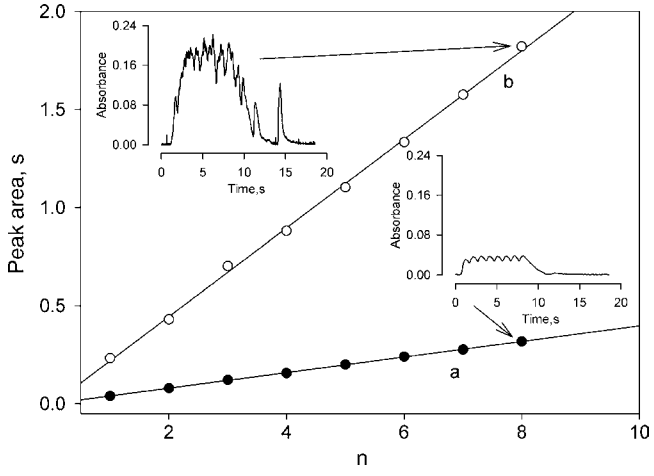


Fig. 7. Effect of water or air compensation (curves a and b, respectively) in the peak area obtained of several consecutive injections of a 10 μg ml^{-1} copper solution using MP2 (25 μl internal volume, n = variable and t_i = 1 s) as MP_{an} and MP4 (125 μl internal volume, n = 1 and t_i = 15 s) as MP_{ca}. No dispersion device was used. The inserted graphs correspond to the particular experiment marked by the arrow.

The slopes of calibration graphs obtained when flow compensation was made with air or water clearly showed the advantage of using air. Thus, introducing the sample solution by means of only two 25 μl injections with t_i = 2 s and using a single 125 μl water injection with MP_{ca} 15 s before sample injection, the slopes of the calibration graphs were 0.0078 and 0.0592 s ml μg^{-1} for water and air compensation, respectively. The RSDs of these measurements were always below 2.6% (five measurements for each experimental point).

4. Conclusion

The use of solenoid micropumps with different internal volumes represents an interesting way for the discrete and periodical introduction of the sample solution in FAAS. Such a way is more versatile than the conventional aspiration mode and presents interesting features and differences compared with the use of peristaltic pumps for the same purpose, the reduced size, easy operation and maintenance of MPs being a clear advantage. A suitable selection of the experimental manifold provides similar or better sensitivities than those achieved by means of conventional FAAS. In addition, the easy and handy on-line dilution process facilitates calibration graphs by using a single standard solution as well as the measurement of samples too concentrated to be measured directly by the aspiration mode. The manifolds here studied, which follow the basic principles of the MPFS, could be useful for analytical detection systems other than FAAS.

Acknowledgements

The authors are grateful to the Spanish MEC (Project BQU2003-01731) for financial support. J. Kozak also acknowledges a fellowship in the framework of the NATO Science Fellowships Programme.

References

[1] B. Welz, Spectrochim. Acta Part B 54 (1999) 2081.
[2] R.C. Prados-Rosales, J.L. Luque-García, M.D. Luque de Castro, Anal. Chim. Acta 461 (2002) 169.
[3] R.C. Prados-Rosales, J.L. Luque-García, M.D. Luque de Castro, Anal. Chim. Acta 480 (2003) 181.
[4] G. Tao, Z. Fang, J. Baasner, B. Welz, Anal. Chim. Acta 481 (2003) 273.
[5] A. Ratka, H. Berndt, Anal. Bioanal. Chem. 375 (2003) 275.

[6] I. López-García, M. Sánchez-Merlos, M. Hernández-Córdoba, Spectrochim. Acta Part B 51 (1996) 1761.
[7] I. López-García, M. Sánchez-Merlos, P. Viñas, M. Hernández-Córdoba, J. Anal. At. Spectrom. 16 (2001) 1185.
[8] X.D. Wang, T.J. Cardwell, R.W. Cattrall, G.E. Jenkins, Anal. Commun. 35 (1998) 97.
[9] J.A.V. Prior, J.L.M. Santos, J.L.F.C. Lima, Anal. Bioanal. Chem. 375 (2003) 1234.
[10] R.A.S. Lapa, J.L.F.C. Lima, B.F. Reis, J.L.M. Santos, E.A.G. Zagatto, Anal. Chim. Acta 466 (2002) 125.
[11] J.L.F.C. Lima, J.L.M. Santos, A.C.B. Dias, M.F.T. Ribeiro, E.A.G. Zagatto, Talanta 64 (2004) 1091.

Available online at www.sciencedirect.com
ScienceDirect
Talanta 71 (2007) 1282–1287
Talanta
www.elsevier.com/locate/talanta

Electrochemical sensor for amino acids and albumin based on composites containing carbon nanotubes and copper microparticles

Guillermina L. Luque, Nancy F. Ferreyra, Gustavo A. Rivas *

INFIQC, Departamento de Físico Química, Facultad de Ciencias Químicas, Universidad Nacional de Córdoba, Ciudad Universitaria, 5000 Córdoba, Argentina

Received 16 May 2006; received in revised form 28 June 2006; accepted 28 June 2006
Available online 14 August 2006

Abstract

This work reports on the analytical performance of composites obtained by dispersing copper microparticles and multi-wall carbon nanotubes within a mineral oil binder (CNTPE-Cu) for the determination of amino acids and albumin. The strong complexing activity of amino acids towards copper makes possible an important improvement in the sensitivity for the determination of amino acids and albumin. This new electrode permits the highly sensitive amperometric detection of amino acids, even the non-electroactive ones, at very low potentials (0.000 V) and physiological pH (phosphate buffer solution pH 7.40). The response of the electrode is highly dependent on the amount of copper, demonstrating the crucial role of the metal in the analytical performance of the sensor. The best analytical performance is obtained for the electrode containing 6.0% (w/w) copper. The resulting sensor shows a fast response (7 s) and a sensitivity that depends on the nature of the amino acid. The electrode surface demonstrates an excellent resistance to surface fouling, with R.S.D. of 4% for the sensitivities of 10 successive calibration plots. Albumin is determined with CNTPE-Cu using a protocol based on the accumulation of the protein for 10 min at −0.100 V, followed by the square-wave voltammetric analysis. The quantification of albumin concentration in lyophilized control serum gives excellent agreement with the classical spectrophotometric methodology and with the value informed for the supplier.
© 2006 Elsevier B.V. All rights reserved.

Keywords: Carbon nanotubes; Composite; Copper; Amino acids; Albumin

1. Introduction

Since their discovery in 1991 [1], carbon nanotubes (CNTs) have been widely used in different fields. Due to their uniqueness, CNTs have received enormous attention for the preparation of electrochemical sensors, as it was widely reviewed [2–7].

One of the main problems when preparing sensors based on CNTs is their low solubility in usual media. Different strategies for dispersing CNTs and immobilizing them on the surface of electrodes have been proposed. They have been dispersed in acidic solutions [8,9], *N*,*N*′-dimethylformamide [10] and polymeric matrices like Nafion [11,12], chitosan [13,14] and polyethylenimine [15]. Another attractive avenue was the incorporation of CNTs in composite matrices using different binders like Teflon [16] and bromoform [17]. We have proposed a new composite electrode based on the dispersion of multi-wall carbon nanotubes (MWCNT) within mineral oil [18]. The resulting electrode, so-called carbon nanotubes paste electrode (CNTPE), combines the ability of CNTs to promote electron-transfer reactions with the attractive advantages of composite materials. We have demonstrated the excellent catalytic properties of CNTs on the electrochemical behavior of different bioanalytes as well as the usefulness of CNTPE as a matrix for the immobilization of redox enzymes for further development of sensitive glucose [18]; lactate, ethanol, phenols, catechols [19]; nucleic acids [20]; pesticides [21] and neurotransmitters [22] sensors. We have also reported the advantages of the incorporation of copper microparticles into the CNTPE for glucose biosensing due to the excellent catalytic properties of copper on the reduction of hydrogen peroxide [23].

We are reporting here a sensor for the quantification of amino acids and albumin based on the incorporation of copper microparticles within a carbon nanotubes paste electrode (CNTPE-Cu) prepared with multi-wall carbon nanotubes.

* Corresponding author. Tel.: +54 351 4334169/80; fax: +54 351 4334188.
E-mail address: grivas@mail.fcq.unc.edu.ar (G.A. Rivas).

0039-9140/$ – see front matter © 2006 Elsevier B.V. All rights reserved.
doi:10.1016/j.talanta.2006.06.041

The development of efficient analytical methodologies for the quantification of amino acids is very important due to the significance of these compounds in several fields. Different spectroscopic methods have been proposed such as chemiluminescence, fluorescence, spectrometry [24]. In general, one of the main problems of these methodologies is the need for previous derivatization of the amino acids. Electrochemical methods have been also proposed, some ones based on the oxidation of electroactive amino acids like tyrosine, tryptophan and cysteine [25]. Other methodologies have proposed the direct detection of underivatized amino acids and peptides through the catalytic oxidation of amino acids in 0.1 M NaOH at Cu [26] or Ni surfaces [27] as well as at carbon electrodes modified with these metals [28,29]. Wang and co-workers [28] have reported the sensitive amperometric quantification of non-electroactive amino acids in alkaline solutions at 0.55 V at glassy carbon electrodes modified with single-wall carbon nanotubes (SWCNTs) and nickel hydroxide film deposited on the top of the CNTs layer. Wang et al. [29] has also reported the use of CNTPE containing copper powder in a weight ratio 1:1:2 (carbon/oil/Cu) as a capillary electrophoresis detector for the determination of carbohydrates. In the same contribution, they have also shown one electropherogram for the separation of glycine, histidine and arginine in NaOH pH 13.0 at 0.55 V. Zen et al. [30] have proposed the use of a screen printed electrode modified with copper nanoparticles obtained by photo-electrochemical deposition, for the sensitive amino acids quantification at pH 8.

In this work we propose the determination of amino acids, electroactive or non-electroactive, at low potentials and physiological pHs using a multi-wall carbon nanotubes composite containing copper microparticles. The influence of the electrode composition on the analytical performance of the resulting amino acids sensor is discussed in the following sections. The usefulness of the CNTPE-Cu for the quantification of albumin in pure solutions and in human serum control samples, as well as a comparison with the usual spectrophotometric determination is included.

2. Experimental

2.1. Reagents

Copper (99% purity) microparticles (−325 mesh, 10% max, +325 mesh, 99%) were acquired from Alfa Aesar. Multi-wall carbon nanotubes 15–45 nm diameter, 1–5 μm length, and 95% purity were purchased from NanoLab, U.S.A. and used without any additional treatment. The mineral oil was from Aldrich. Bovin seric albumin (A-4503) and all amino acids were purchased from Sigma. The kit for spectrophotometric determination of albumin was obtained from Wiener lab (Proti 2). Lyophilized control serum (Standatrol S-E) for albumin determinations was obtained from Wiener lab. Other chemicals were reagent grade and used without further purification.

All solutions were prepared with ultrapure water ($\rho = 18\,M\Omega\,cm$) from a Millipore-MilliQ system. The amino acids were dissolved in water to obtain the stock solutions. A 0.050 M phosphate buffer solution pH 7.40 was employed as supporting electrolyte.

2.2. Apparatus

Electrochemical measurements were performed with a TEQ_02 and Epsilon (BAS) potentiostats. The electrodes were inserted into the cell (BAS, Model MF-1084) through holes in its Teflon cover. A platinum wire and Ag/AgCl, 3 M KCl (CH Instruments) were used as counter and reference electrodes, respectively. All potentials are referred to the latter. A magnetic stirrer provided the convective transport during the amperometric measurements. Copper electrode 99.9% purity was used for voltammetric experiments.

Carbon nanotubes paste electrodes (CNTPE) were prepared by mixing in an agate mortar MWCNTs powder (60.0%, w/w) and mineral oil (40.0%, w/w) for 30 min. CNTPEs containing copper (CNTPE-Cu) were prepared in a similar way, mixing first the copper microparticles with the mineral oil for 1 min, followed by the incorporation of the carbon nanotubes powder and additional mixing for 30 min. A portion of the resulting composite was packed firmly into a Teflon tube cavity of 3 mm diameter. The electric contact was established through a stainless steel screw. The composite was packed before performing every new experiment and the surface was smoothed onto a weighing paper, with exception of the stability studies performed using the same surface.

Scanning electronic microscopy (SEM) pictures were obtained with a Hitachi S3000N microscope equipped with secondary and backscattered electron detectors, as well as with a X-rays detector.

A UV-1601 Shimadzu spectrophotometer was used for the spectrophotometric determinations.

2.3. Procedure

2.3.1. Amino acids determination

Amperometric measurements were conducted in a stirred 0.050 M phosphate buffer solution pH 7.40 by applying a potential of 0.000 V and allowing the transient currents to decay to a steady-state value prior to the addition of the analyte and subsequent current monitoring. All measurements were performed at room temperature.

2.3.2. Albumin determination

2.3.2.1. Electrochemical quantification. A square wave voltammogram between −0.200 and 1.000 V was obtained after holding the CNTPE-Cu at −0.100 V for 10 min in a stirred solution of albumin. The voltammetric parameters are the following: frequency of 25 Hz, pulse amplitude of 25 mV, staircase step 10 mV and scan rate of $0.250\,V\,s^{-1}$.

2.3.2.2. Spectrophotometric quantification. Albumin reacts specifically (without previous separation) with the anionic form of 3,3′,5,5′-tetrabromo cresolsulfonftaleina (BCF) at pH 3.8. The analytical signal was obtained from the absorbance at 625 nm.

3. Results and discussion

3.1. Amino acids detection

Fig. 1 depicts a typical amperometric response at 0.000 V for successive additions of 5.0×10^{-4} M L-histidine at CNTPE (dotted line) and at CNTPE-Cu (6.0%, w/w) (solid line). Since L-histidine is not electroactive, the CNTPE does not respond to successive additions of the amino acid. In contrast, a sensitive and fast (steady-state signal reached within 7 s) response is obtained at CNTPE-Cu, evidencing the formation of a complex between Cu(II) produced at the applied potential and L-histidine [30]. Similar results were obtained with other amino acids. Cyclic voltammetric experiments using a copper electrode were also performed (not shown). In agreement with previous results [26,30], an increase in the current at 0.000 V was observed due to the oxidation of Cu_2O to CuO in the presence of L-histidine in 0.010 M NaOH. This increase in the current is a consequence of the complex formation between Cu(II) and the amino acid-ligand that facilitates the copper dissolution. The electrocatalytic oxidation of the amino acids at 0.660 V was also observed. Similar experiments in a 0.050 M phosphate buffer solution at 0.020 V s^{-1} showed a broad peak current due to the oxidation of Cu to CuO at 0.000 V. This current also increased in the presence of the L-histidine, although the electrocatalytic oxidation of the amino acid did not occur under these conditions, in agreement with the results obtained by Warner and Weber [31].

Fig. 2 shows a hydrodynamic voltammogram for 3.34×10^{-4} M L-histidine prepared in a 0.050 M phosphate buffer solution pH 7.40 at CNTPE-Cu (6.0%, w/w). The current rapidly rises from −0.200 to 0.000 V due to the oxidation of copper to CuO favored by the formation of the complex with the amino acid, and then it levels off. In consequence, 0.000 V was selected as the working potential for further amperometric determinations.

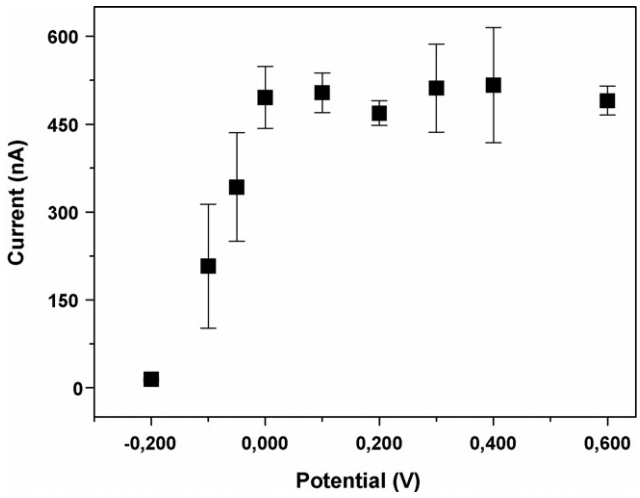


Fig. 2. Hydrodynamic voltammogram for 3.34×10^{-4} M L-histidine at CNTPE-Cu (6.0%, w/w). Supporting electrolyte: 0.050 M phosphate buffer solution pH 7.40.

Fig. 3 shows the effect of copper content within the CNTPE-Cu on the sensitivity towards L-histidine obtained from amperometric recordings at 0.000 V using CNTPE containing different amounts of the metal. The sensitivity increases within the studied range of copper percentages (from 0.0 to 18.0%, w/w) showing an almost linear relationship up to 12.0% (w/w), demonstrating the crucial role of copper in the response of the biosensor. However, despite this enhance in sensitivity when the amount of copper increases, the response becomes less reproducible. The best compromise between sensitivity and reproducibility was attained with 6.0% (w/w) of copper. X-rays determination of the percentage of surface copper using a detector assembled to the scanning electron microscope indicates that the surface copper increases with the amount of copper within the composite being 1.21%, 1.86% and 4.48% for 6.0%, 12.0%, and 18.0% (w/w) copper, respectively.

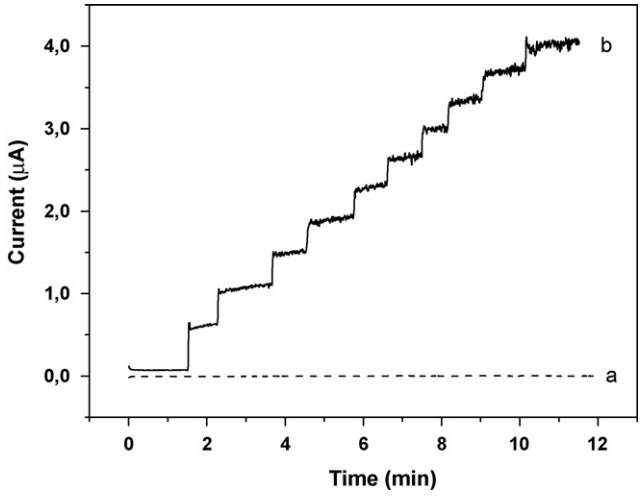


Fig. 1. Amperometric recordings for successive additions of 5.00×10^{-4} M L-histidine at CNTPE [60.0% (w/w) MWCNT and 40.0% (w/w) oil] (a) and at CNTPE-Cu (6.0%, w/w) (b). Working potential 0.000 V. Supporting electrolyte: 0.050 M phosphate buffer solution pH 7.40.

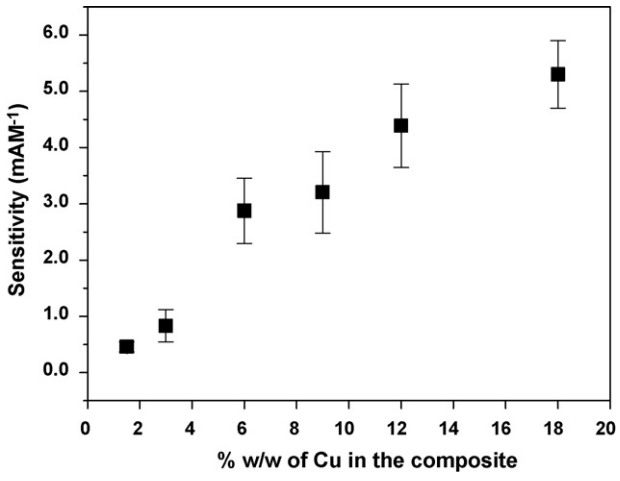


Fig. 3. Dependence of the sensitivity of the electrode towards L-histidine on the copper content in the composite obtained from amperometric recordings at 0.000 V for successive additions of 5.0×10^{-6} M L-histidine. Supporting electrolyte: 0.050 M phosphate buffer solution pH 7.40.

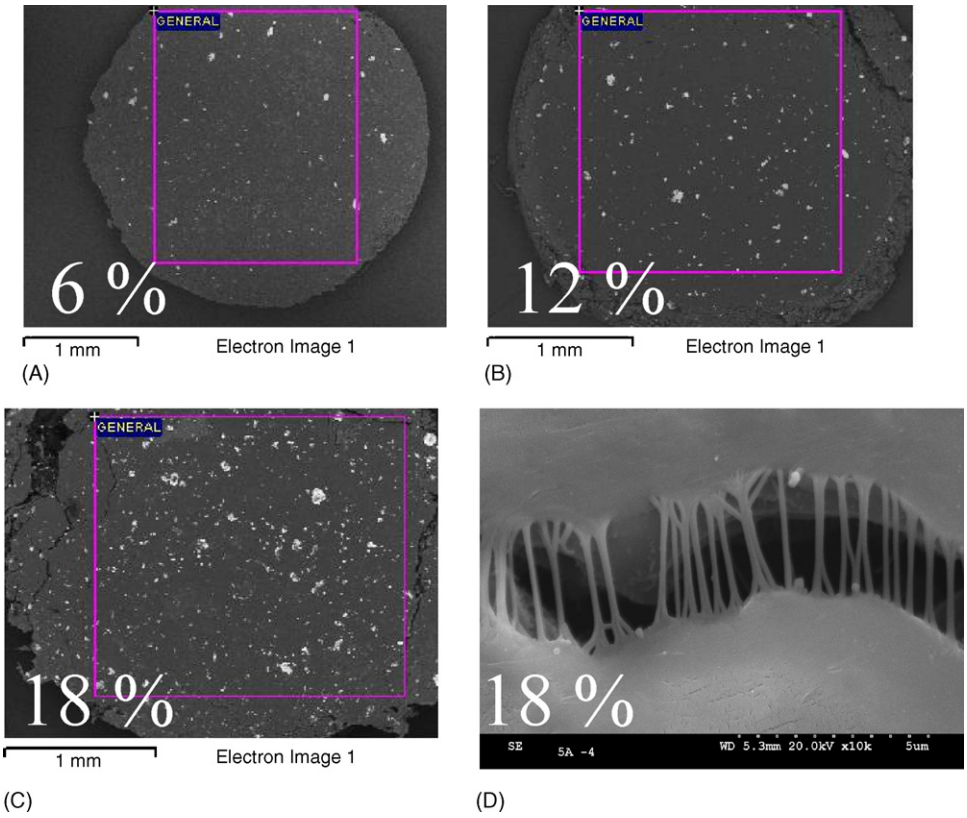


Fig. 4. SEM pictures for CNTPE containing 6.0% (A), 12.0% (B) and 18.0% (C and D) (w/w) copper. Magnifications: 35× (A–C); 10,000× (D).

Fig. 4 shows SEM pictures for CNTPEs prepared with 6.0% (A), 12.0% (B) and 18.0% (C, D) (w/w) copper.

As expected, according to the previous discussion, the copper microparticles are distributed in the whole surface as islands immersed within the composite material. Fig. 4D shows more details about the border between copper microparticles and CNTs within the dispersion, demonstrating the intimate contact between them. This fact facilitate the charge transfer between copper and CNTs.

Table 1
Analytical parameters for L-amino acids taken from calibration plots obtained from amperometric recordings at 0.000 V

Aminoacids	Sensitivity (μA M^{-1})	r	DL (M)	QL (M)
Histidine	$(29 \pm 6) \times 10^2$	0.9998	2×10^{-6}	7×10^{-6}
Cystine	$(28.8 \pm 0.1) \times 10^2$	0.9994	3×10^{-6}	1×10^{-5}
Tyrosine	522 ± 7	0.998	2×10^{-5}	6×10^{-5}
Serine	353 ± 2	0.9996	1×10^{-4}	3×10^{-4}
Asparagine	270 ± 1	0.9996	3×10^{-4}	8×10^{-4}
Glycine	175 ± 1	0.9998	5×10^{-5}	1×10^{-4}
Glutamine	168.4 ± 0.3	0.99993	5×10^{-5}	2×10^{-4}
Phenylalanine	166 ± 4	0.9991	5×10^{-5}	2×10^{-4}
Threonine	134 ± 1	0.9994	1×10^{-4}	4×10^{-4}
Alanine	134 ± 1	0.99991	1×10^{-4}	4×10^{-4}
Arginine	126 ± 2	0.9990	4×10^{-4}	1×10^{-3}
Aspartic acid	111 ± 4	0.998	4×10^{-5}	1×10^{-4}
Leucine	104 ± 2	0.9997	8×10^{-5}	3×10^{-4}
Tryptophan	91 ± 2	0.9992	5×10^{-5}	1×10^{-4}
Valine	83 ± 1	0.9991	5×10^{-5}	2×10^{-4}
Lysine	83 ± 3	0.993	1×10^{-4}	3×10^{-4}
Proline	19.8 ± 0.4	0.998	2×10^{-4}	7×10^{-4}

Other conditions as in Fig. 2. QL, quantification limit; DL, detection limit.

Table 1 displays the analytical parameters for the determination of different amino acids obtained from amperometric recordings at 0.000 V. L-Histidine, that presents the largest complex formation constant in solution [32], shows the highest sensitivity. In general, a correlation between sensitivity and complex formation constants in solution is observed in all cases. The detection limits (calculated as 3.3 times the ratio between the standard deviation of the blank and sensitivity), are in the range of 10^{-6} or 10^{-5} M. Therefore, this sensor offers the possibility to perform the electrochemical determination of electroactive and non-electroactive amino acids at 0.000 V at physiological pHs, representing a good alternative to most of the traditional methods.

One important parameter, especially considering the use of this electrode for determinations in flow systems, is the short-term stability of the surface. Fig. 5 depicts the effect of successive calibration plots using the same surface on the resulting sensitivities for L-histidine (performed under the experimental conditions previously described). The results demonstrate that the stability of the sensor is excellent, with R.S.D. of 4.0% for 10 successive calibrations (implying more than 2 h of continuous use).

3.2. Albumin determination

Proteins are usually determined in clinical applications by spectrophotometric methods based on the Biuret reaction [33].

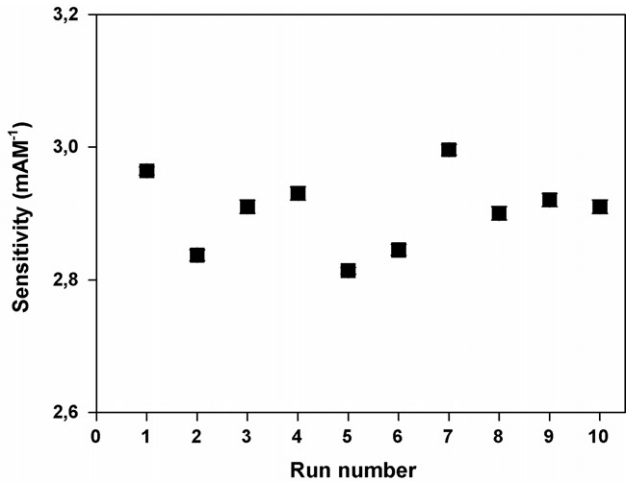


Fig. 5. Sensitivity for L-histidine obtained from successive amperometric experiments at 0.000 V as a function of the run number. Other conditions as in Fig. 2.

Electrochemical methods have been also used for the determination of proteins like myoglobin, hemoglobin and insulin in connection with chronopotentiometric stripping analysis [34]. Insulin quantification was also reported by using a glassy carbon electrode modified with CNTs [35]. The electrochemical determination of albumin was also performed using an enzymatic electrode based on the use of tyrosinase [36]. Here, we are proposing the detection of albumin at physiological pHs and low-potential.

In order to obtain the most reproducible and sensitive detection of albumin, the protocol for the detection of amino acids was modified. Albumin was first accumulated at the electrode surface for 10 min at −0.100 V followed by the quantification using square wave voltammetry (SWV). Fig. 6 shows square-wave voltammograms obtained at CNTPE (A) and at CNTPE-Cu (18.0%, w/w) (B) for a 0.050 M phosphate buffer solution pH 7.40 (dotted line) and for a 20 mg/mL albumin solution (solid line). In the case of CNTPE, there is a small oxidation peak at 0.700 V corresponding to the direct electrooxidation of the tyrosine and tryptophan residues [37]. When copper is present (B),

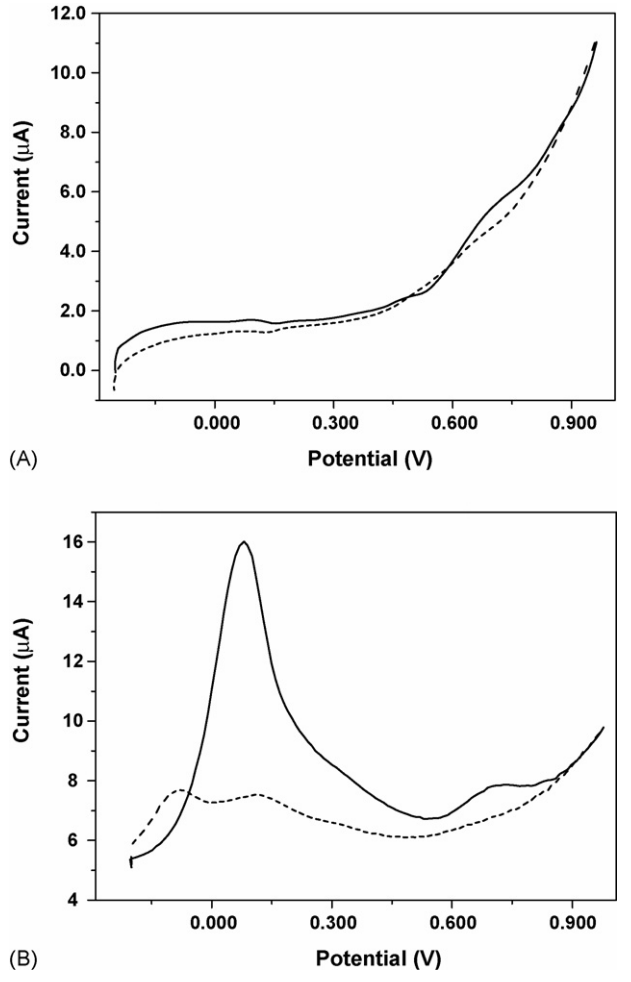


Fig. 6. Square wave voltammograms for 0.0 (dotted line) and 20.0 (solid line) mg/mL albumin at CNTPE (A) and at CNTPE-Cu (18.0%, w/w) (B). Conditions: protein accumulation at −0.100 V for 10 min followed by a square wave voltammogram between −0.200 and 1.000 V. Frequency of 25 Hz, pulse amplitude of 25 mV, staircase step 10 mV and scan rate of 0.250 V s^{-1}.

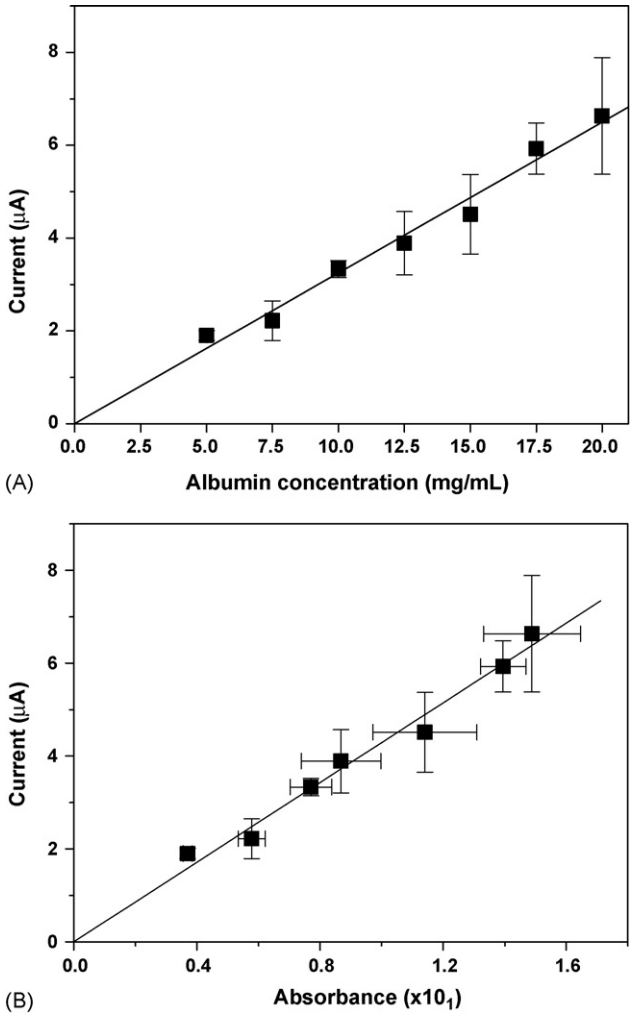


Fig. 7. (A) Calibration plot for albumin using CNTPE-Cu (18.0%, w/w). Conditions as in Fig. 6. (B) Comparison between the electrochemical and spectrophotometric determination of albumin. Electrochemical working conditions: as in Fig. 6; spectrophotometric conditions: wavelength 625 nm.

two typical peaks for copper oxidation appears at −0.080 V (Cu to Cu_2O) and 0.110 V (Cu_2O to CuO) in the phosphate solution. In the presence of the protein, an important increase in the signal at 0.100 V is obtained due to the oxidation of copper(II) facilitated by formation of the complex with the amino acids residues. At 0.700 V the direct oxidation of the electroactive amino acids is also observed. It is important to remark the huge difference between the direct oxidation signal and that signal obtained in the presence of copper as a consequence of the formation of the complex. These significant differences make this methodology very useful.

Fig. 7A depicts a linear relationship ($r = 0.993$) between the oxidation current at 0.100 V and albumin concentration from 5.0 up to 25.0 mg/mL albumin. The detection limit was 5.0 mg/L, taken as the ratio between 3.3 times the standard deviation of the blank and the sensitivity.

The analytical performance of the proposed sensor was validated by spectrophotometry. Fig. 7B compares the response obtained with both techniques, with a good correlation ($r = 0.989$).

The proposed methodology was also used for the determination of albumin in a lyophilized control serum. The value obtained by spectrophotometry was 7.2 ± 0.3 g/dL, while the one determined by our methodology was 6.9 ± 0.7 g/dL, indicating an excellent agreement with the value of 6.9 g/dL informed by the supplier. These results are clear evidence that the different compounds present in the serum do not interfere with our determination.

4. Conclusions

In summary, we have demonstrated that the incorporation of copper microparticles within the CNTPE offers a highly sensitive and stable constant-potential amperometric detection of all amino acids even the non-electroactive ones at very low potentials and at physiological pH. The sensitivity demonstrated to be highly dependent on the amino acid nature and on the copper amount within the composite. The CNTPE-Cu also represents an interesting strategy for the sensitive and fast determination of albumin at low potentials and physiological pH. This excellent analytical performance makes the CNTPE-Cu a very good alternative as detector for the quantification of amino acids in flow measurements like flow injection analysis and capillary electrophoresis. Our group is currently working in this direction with very promising results.

Acknowledgements

The authors thank Fundación Antorchas, Consejo Nacional de Investigaciones Científicas y Técnicas de Argentina (CONICET), Secretaría de Ciencia y Tecnología de la Universidad Nacional de Córdoba (SECyT-UNC), Agencia Nacional de Promoción Científica y Tecnológica (ANPCyT) and Asociación de Bioquímicos de la Provincia de Córdoba (ABC) for the financial support. G.L.L. thanks ANPCyT for the fellowships received. The authors acknowledge Autonoma University of Madrid, Dr. Esperanza Bermejo and Dr. Manuel Chicharro for the SEM pictures.

References

[1] S. Iijima, Nature 354 (1991) 56.
[2] M. Trojanowicz, Trends Anal. Chem. 25 (2006) 480.
[3] Q. Zhao, Z. Gan, Q. Zhuang, Electroanalysis 14 (2002) 23.
[4] J. Wang, Electroanalysis 17 (2005) 7.
[5] J. Wang, Analyst 130 (2005) 421.
[6] M. Valcarcel, B.M. Simonet, S. Cardenas, E.B. Suarez, Anal. Bioanal. Chem. 382 (2005) 1783.
[7] C.E. Banks, R.G. Compton, Analyst 131 (2006) 15.
[8] M. Musameh, J. Wang, A. Merkoci, Y. Lin, Electrochem. Commun. 4 (2002) 743.
[9] J. Wang, A.-N. Kawde, M. Musameh, Analyst 128 (2003) 912.
[10] X.X. Yan, D.-W. Pang, Z.-X. Lu, J.-Q. Li, H.J. Tong, Electroanal. Chem. (2004) 47.
[11] J. Wang, M. Musameh, Y. Lin, J. Am. Chem. Soc. 125 (2003) 2408.
[12] S.A. Miscoria, J. Desbrieres, G. Barrera, G. Rivas, Talanta, in press.
[13] M. Zhang, A. Smith, W. Gorski, Anal. Chem. 76 (2004) 5045.
[14] L. Qian, X. Yang, Talanta 68 (2006) 721.
[15] M.D. Rubianes, G.A. Rivas, submitted for publication.
[16] J. Wang, M. Musameh, Anal. Chem. 75 (2003) 2075.
[17] P.J. Britto, K.S.V. Santhanam, P.M. Ajayan, Bioelectrochem. Bioenerg. 41 (1996) 121.
[18] M.D. Rubianes, G.A. Rivas, Electrochem. Commun. 5 (2003) 689.
[19] M.D. Rubianes, G.A. Rivas, Electroanalysis 17 (2005) 73.
[20] M.L. Pedano, G.A. Rivas, Electrochem. Commun. 6 (2004) 10.
[21] M. Chicharro, E. Bermejo, M. Moreno, A. Sánchez, A. Zapardiel, G.A. Rivas, Electroanalysis 17 (2005) 476.
[22] M. Chicharro, A. Sánchez, E. Bermejo, A. Zapardiel, M.D. Rubianes, G.A. Rivas, Anal. Chim. Acta 543 (2005) 84.
[23] G. Luque, N.F. Ferreyra, G.A. Rivas, Microchim. Acta 152 (2006) 277.
[24] M.A. Schwarz, P.C. Hauser, Lab on a Chip 1 (2001) 1.
[25] X. Jiming, W. Yanping, X. Yuezchong, J. Litong, K. Tanaka, Talanta 60 (2003) 1123.
[26] P. Luo, Z. Fuzhen, R.P. Baldwin, Anal. Chem. 63 (1991) 1702.
[27] K. Sato, J.-Y. Jin, T. Takeuchi, T. Miwa, Y. Takekoshi, S. Kanno, S. Kawase, Talanta 53 (2000) 1037.
[28] R.P. Deo, N.S. Lawrence, J. Wang, Analyst 129 (2004) 1076.
[29] J. Wang, G. Chen, M. Wang, M.P. Chatrathi, Analyst 129 (2004) 512.
[30] J.-M. Zen, C.-T. Hsu, A.S. Kumar, H.-J. Lyu, K.-Y. Lin, Analyst 129 (2004) 841.
[31] A.M. Warner, S.G. Weber, Anal. Chem. 61 (1989) 2664.
[32] http://www.coldcure.com/html/stability_constants.html.
[33] A.G. Gornall, C.J. Bardawill, M.M. David, J. Biol. Chem. 177 (1949) 751.
[34] J. Wang, G.A. Rivas, X. Cai, M. Chicharro, P.A.M. Farias, E. Palecek, Electroanalysis 8 (1996) 902.
[35] J. Wang, M. Musameh, Anal. Chim. Acta 511 (2004) 33.
[36] M.Ch. Chuang, C. Liu, C. Yang, Sens. Actuators B 114 (2006) 357.
[37] C.G. Nam, Z.Z. Feng, W.X. Li, D.J. Ping, C.H. Qin, Anal. Chim. Acta 452 (2002) 245.

Available online at www.sciencedirect.com
ScienceDirect
Talanta 71 (2007) 1150–1154
Talanta
www.elsevier.com/locate/talanta

Silica modified with zirconium oxide for on-line determination of inorganic arsenic using a hydride generation-atomic absorption system

Greice T. Macarovscha, Gisele G. Bortoleto, Solange Cadore *

Instituto de Química, Universidade Estadual de Campinas, CP 6154, 13083-970, Campinas, SP, Brazil

Received 14 March 2006; received in revised form 5 June 2006; accepted 6 June 2006
Available online 14 July 2006

Abstract

In the present work, an on-line pre-concentration system, using SiO_2/ZrO_2 as solid phase adsorbent, for the determination of low concentrations of arsenic was developed.

In this procedure, total inorganic arsenic present in the sample is reduced to As (III) with L-cysteine and the solution is passed into a glass column ($\phi_i = 3$ mm; $h = 35$ mm) containing 70 mg of SiO_2/ZrO_2 (100–230 mesh) to retain the As (III), with the solution flowing at 3.2 mL min^{-1}. After 2 min, the concentrated species are eluted with 3 mol L^{-1} HCl (3.2 mL min^{-1}) loading a 150 μL loop while a 1.0% (m/v) sodium borohydride solution loads the other loop of a FI–HG AAS system. The elution step is carried out during 7 s and, at the same time, the SiO_2/ZrO_2 phase is regenerated for the next concentration cycle. The arsine generated is carried with N_2 (flow rate = 90 mL min^{-1}) to a quartz cell where the electrothermal atomization process occurs.

Under these conditions, a 20-fold enrichment factor is obtained considering the increase of sensitivity in the analytical curve after the concentration step. The limits of detection and quantification were 0.05 and 0.35 μg L^{-1}, respectively, with an injection frequency of about 28 h^{-1} and relative standard deviation lower than 8%. Four metallurgical reference materials were analyzed with the proposed method after their acid dissolution. The results obtained were in good agreement with certified values.
© 2006 Elsevier B.V. All rights reserved.

Keywords: Arsenic; Liquid–solid extraction; Zirconium oxide; FI–HG AAS

1. Introduction

Since the metallurgical properties of steel can be affected by the presence of even trace amounts of many elements, a suitable method for a sensitive, fast and simple routine determination of these elements is therefore highly desirable. The magnitude of any such effect depends on the concentration of the elements present, the composition of the steel, the metallurgical condition of the steel and its final application. Arsenic, similar to phosphorus, reduces the ductility of steel the and, at the same time, increases its brightness. These influences on the quality of the steel are already observable at very low concentrations (0.0002–0.02%) [1,2].

Since its introduction 50 years ago, atomic absorption spectrometry (AAS) has been developed into a well-established and well-known instrumental technique for the determination of many elements. The first experiments with AAS, using a flame as atomizer were described by Walsh [3] in 1955. The concept of electrothermal atomization (ETA) was introduced by L'vov [4] and allows the atomisation of sample in a single step. The sample placed onto a graphite electrode was dried and this electrode was introduced into a graphite tube that was heated by resistance heating and the sample was atomized using a direct current arc.

In 1969, Holak [5] used the concept of hydride generation to determine arsenic. When the acidified sample, containing arsenic, was put in contact with a reducing reagent there was the generation of the volatile hydride, AsH_3. Some advantages of the generation of volatile hydrides are: the analyte is separated from the matrix, minimizing the interferences; the selectivity is enhanced due to the reduced quantities of interfering species; using a batch system it may be possible to have enrichment of the analyte; the limits of detection (LOD) are improved, allowing the determination of trace levels of the appropriate elements, espe-

* Corresponding author.
E-mail address: cadore@iqm.unicamp.br (S. Cadore).

0039-9140/$ – see front matter © 2006 Elsevier B.V. All rights reserved.
doi:10.1016/j.talanta.2006.06.006

cially in environmental studies; the systems can be automated, reducing the amount of reagents and increasing the transport efficiency of the analyte to the atomizer [6,7].

Considering the benefit obtained with this technique, the development of new analytical methods employing flow injection with hydride generation (FI–HG) AAS is of great interest. Sometimes, however, the concentration of the analyte is very low and a pre-concentration step is necessary.

Pre-concentration techniques for trace metals, like analyte sorption on solid materials, modified or not with organic reagents, have been frequently used. The metal or metal-complex is eluted from the solid material by a suitable solvent and afterwards determination of the metal is performed.

The usual reactions for arsenic pre-concentration make use of organic reagents which are able to separate As (III) from As (V), such as dithiocarbamates [8–10] and dithiophosphate [11–13] sorbed on solid materials. Some inorganic materials such as ion exchange resins [14], zeolites [15] and alumina [16] have also been used as sorbent material for ions from aqueous solutions.

Chemically modified silica has been widely used as a stationary phase for HPLC and as support for enzyme immobilizations as well as for a sorbent of metallic ions from aqueous and non-aqueous solutions. Its wide application is due to the great number of surface modification reactions the silica undergoes. This results in a solid with different chemical properties on its surface, while preserving the important mechanical properties of silica, like rigidity, porosity, particle size and defined pores, high surface area, resistance to swelling in the presence of solvents and thermal and chemical stability [17].

In the present work, a pre-concentration method using silica modified with zirconium oxide as a solid phase sorbent, coupled to a FI–HG AAS system that allows the determination of total inorganic arsenic present in steel samples, is described.

2. Experimental

2.1. Reagents

Analytical reagent grade materials were used for all the experiments. Deionized water (18.2 MΩ cm) obtained from a Milli-Q water system (Bedford, MA, USA) was used throughout.

The arsenic standard solution was prepared by dissolving 1.0000 g As_2O_3 (Carlo Erba) in 20% (w/v) NaOH (Carlo Erba) with the addition of two drops of phenolphthalein. This solution was neutralized with 20% HCl (v/v), diluted to a final volume of 1000 mL with 1 mol L^{-1} HCl solution and stored in a polyethylene bottle, under refrigeration.

Solutions of sodium tetrahydroborate were prepared by dissolving $NaBH_4$ powder (Nuclear) in 0.05 mol L^{-1} KOH (Merck) and stored in plastic bottles, under refrigeration. The solution is stable for about 2 weeks, with no loss of the observed absorption signal.

The L-cysteine used is from Synth.

Silica modified with zirconium oxide was synthesized according to the procedure described by Gushikem et al. [18].

2.2. Sample preparation

Four certified reference metallurgical materials (steels) from the National Institute of Standards and Technology (NIST, Gaithersburg, MD, USA) were analyzed: SRM 361, 362, 363 and 364 were accurately weighed (20–60 mg) into a 100 mL beaker. Concentrated nitric acid (15 mL) was added and the mixture was carefully heated on a hot plate until close to dryness. After cooling, the samples were transferred to appropriate volumetric flasks and diluted with deionized water. A 2 mL aliquot was transferred to a 100 mL beaker, treated with 0.1 g of L-cysteine and the pH was adjusted to 3.5 with dilute NaOH. The solution was transferred to a 100 mL volumetric flask and the volume was completed with deionized water. The arsenic content was determined after a pre-concentration step.

2.3. Apparatus

The pre-concentration system coupled to the FI–HG AAS system is shown in Fig. 1. In the FI–HG system an eight-channel peristaltic pump (Ismatec®, ICP High Precision Multichannel Dispenser) introduced the sample and the reducing reagent ($NaBH_4$) into a merging-zones manifold through Tygon tubes (Technicon) at appropriate flow rates for each solution. Sample loop, reaction coils and transmission lines were made from Teflon tubing (CPL, 0.8 mm i.d.). Prior to introduction into the system, the total inorganic arsenic present in the sample is reduced to As (III) with 0.1% (w/v) L-cysteine. The solution was then passed into a column (i.d. = 3 mm; h = 35 mm) containing 70 mg of silica modified with zirconium oxide (100–230 mesh) at 3.2 mL min^{-1}, where As (III) was retained. After 2 min, the concentrated species were eluted with 3 mol L^{-1} HCl (3.2 mL min^{-1}), loading a 150 μL sample loop while a 1.0% (m/v) sodium borohydride solution was loaded into a second loop of the system. The elution time was 7 s and, at the same time, the sorbent material was regenerated for the next pre-concentration cycle. The excess acid in the elution solution assures that all arsenic was eluted. The arsine generated by reaction with the borohydride in the reaction coil was carried with N_2 (flow rate = 90 mL min^{-1}) to a quartz cell wound with Ni–Cr wire, where the atomization process occurred. The temperature of the quartz cell needed for AsH_3 atomization was obtained and controlled with a Varivolt regulator, connected to the Ni–Cr coil. The electrothermal cell was aligned in the optical path of an atomic absorption spectrometer (Varian, Model Gemini AA 12/1475) equipped with a hollow cathode lamp for arsenic as well as a deuterium lamp for background correction, under the following conditions: wavelength: 193.7 nm; slit width: 0.5 nm; lamp current: 10 mA. For the pH adjustment of the samples a Hanna Instruments pH meter was utilized.

3. Results and discussion

3.1. Effect of eluent

Chemical properties of the eluent may significantly influence the determination of arsenic. The literature cites KOH

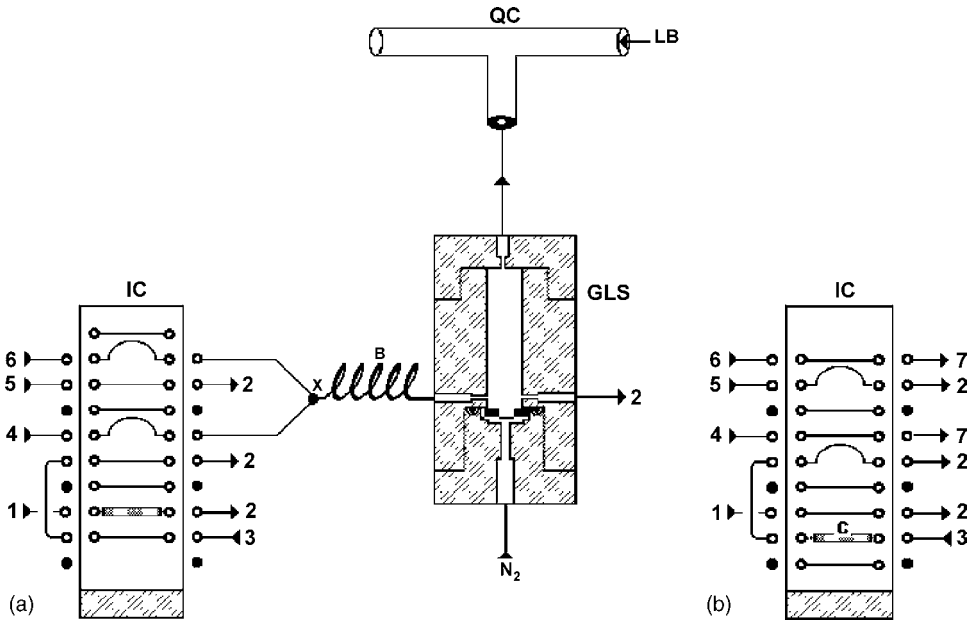


Fig. 1. (a) FI–HG AAS pre-concentration system in the sorption position for the determination of As : (1) sample (2.8 mL min^{-1}); (2) waste; (3) 3 mol L^{-1} HCl (eluent) (3.2 mL min^{-1}); (4) 1 mol L^{-1} HCl (2.8 mL min^{-1}); (5) 1% (w/v) $NaBH_4$ (2.8 mL min^{-1}); (6) H_2O (2.8 mL min^{-1}); HG AAS system; (IC) injector; (B) reaction coil (30 cm); (X) confluence point; GLS gas–liquid separator; (QC) atomizer; (LB) optical path; (C) glass mini-column with sorbent material. (b) Injector–commutator in the elution position.

[19], HNO_3 [20], HCl and NaOH [21] as eluents for arsenic using solid supports modified with zirconium oxide. The effect of diluted base and acid were verified for the proposed pre-concentration system and diluted KOH and HCl were tested. The experimental results obtained with HCl showed to be the more adequate. Varying the concentration of acid solution from 0.1 to 5.0 mol L^{-1}, the best results were obtained with concentrations above 1.0 mol L^{-1} HCl. To ensure sufficient acidity, 3.0 mol L^{-1} HCl was used for the remaining studies.

3.2. *pre-concentration and elution flow/pre-concentration and elution time—a chemometric study*

A screening study was carried out to determine an adequate condition for the flow rate and time for the pre-concentration and elution steps. For this purpose the 2^4 factorial design was employed resulting in sixteen experiments, the levels of which are shown in Table 1.

The experimental data were obtained and the variable effects were calculated using the program *Chemomatrix* [22]. It was observed that the factors A–C have significant statistical values. The best signal from the system in these experiments was reached using the conditions shown in the third column of Table 1.

Table 1
Factors and level employed in the multivariate study

Factor	Level (−)	Level (+)	Best values
(A) Pre-concentration time (s)	90	120	120
(B) Elution time (s)	7	9	7
(C) Pre-concentration flow (mL min^{-1})	2.8	3.2	2.8
(D) Elution flow (mL min^{-1})	2.8	3.2	3.2

3.3. *Effect of the amount of solid sorbent*

In order to evaluate the optimum amount of solid sorbent to be used, different lengths of a 0.3 cm diameter of glass minicolumns were evaluated. Using a 2.0 cm long column resulted in low amounts of analyte being retained. This is due to lesser amount of the sorbent material packed in the column. On the other hand, a longer column proved to be inconvenient to couple into the injector. A 3.5 cm long column which contains approximately 70 mg of sorbent material, gave the highest analytical signals.

3.4. *Effect of pH on the adsorption*

The pH of the aqueous phase is an important factor in solute distribution with accentuated acid–base properties. Silica modified with zirconium oxide is a material with an amphotheric character, acquiring positive charge in acidic medium and negative charge in basic medium and without an established charge zero point (PZC) [17]. As a result, the interaction between As (III) and zirconium oxide may be affected, considering different surface modifications that take place as the pH changes. The effect of pH on the liquid–solid extraction (adsorption) was investigated and Fig. 2 shows that the adsorption of arsenic was quantitative in the range from pH 3.0 to 10.0.

3.5. *Interferences*

Dedina [23] classified the interferences of the hydride generation technique into two groups, the liquid phase interferences and the gaseous phase interferences, while Hershey and Keliher [24] described that arsenic is one of the hydride-forming elements least susceptible to interference. In order to identify

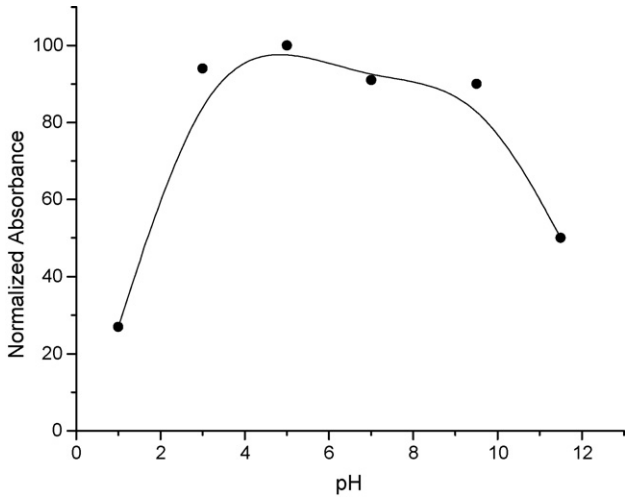


Fig. 2. Effect of pH on the sorption of As with silica modified with zirconium oxide.

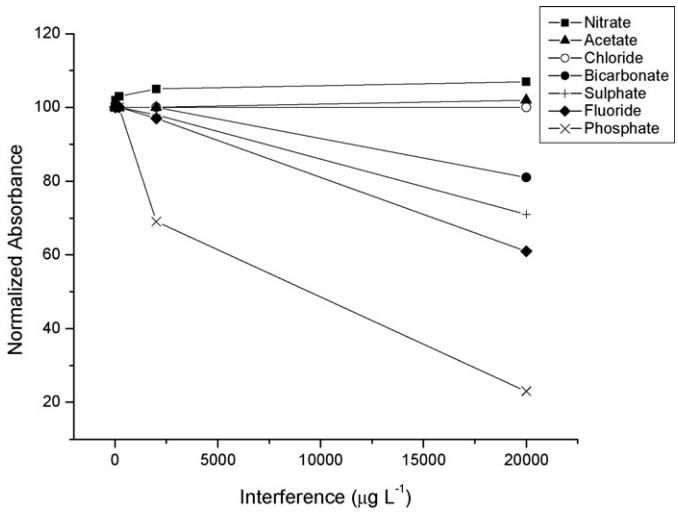


Fig. 4. Interference effects of anions on the determination of As using silica modified with zirconium oxide.

species that could interfere in the determination of arsenic using the proposed system a study was carried out, evaluating both the liquid (considering cations and anions) and gaseous phases.

The concentration of arsenic was fixed at 2 μg L^{-1} and the probable interferents were evaluated in the following concentrations: Cd (8 μg L^{-1}), V (16 μg L^{-1}), Co (14 μg L^{-1}), Cr (20 μg L^{-1}), Cu (20 μg L^{-1}), Ba (36 μg L^{-1}), Mo (16 μg L^{-1}), Ni (20 μg L^{-1}), Zn (26 μg L^{-1}), Al (160 μg L^{-1}), Fe (300 μg L^{-1}), K (2000 μg L^{-1}), Mg (4800 μg L^{-1}), Na (7000 μg L^{-1}) and Ca (18,000 μg L^{-1}). The interference effect was evaluated considering the difference between the absorbance for arsenic in the presence and in the absence of the element studied. Fig. 3 shows that aluminium and iron interfered significantly in the arsenic determination, but this effect may be associated with the hydride generation system, not to the pre-concentration step [25,26] and it may be efficiently overcome in the presence of L-cysteine.

Moretto and Cadore [27] used a mixture of KI/Ascorbic acid as masking reagent in the on-line determination of As, however in the present work the use of this mixture is not appropriate for the adsorbent material used for arsenic pre-concentration (SiO_2/ZrO_2).

Hydride forming elements that can intervene more easily with the system, competing for the $NaBH_4$, better than the competition for the active sites of the adsorbent, were tested in two concentrations: 15 and 30 μg L^{-1} for Pb (II) and 1 and 2 μg L^{-1} for the other elements: Sb (III), Sb (V), Se (IV), Se (VI), Bi (III) and Sn (IV).

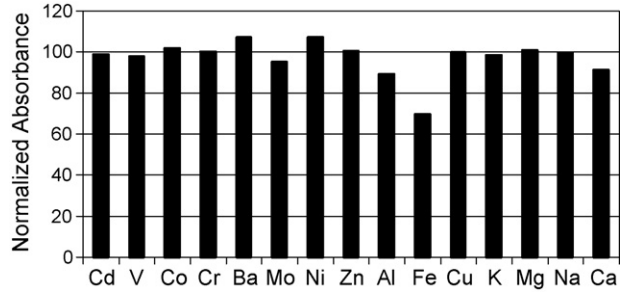


Fig. 3. Interference effects of cations on the determination of As using silica modified with zirconium oxide.

The effects of some anionic species (NO_3^-, HCO_3^-, Cl^-, $CH_3CHO_2^-$, F^-, SO_4^{2-} and PO_4^{3-}) were studied at four different concentrations, representing an excess of 10, 100, 1000 and 10,000 times related to the arsenic concentration, which was maintained at 2 μg L^{-1}. Fig. 4 shows that bicarbonate, fluoride, sulphate and phosphate interfered in the arsenic determination. Phosphate drastically decreased the analytical signal even at low concentrations. Paräniemi and Ahlgrén also observed the interference of phosphate and fluoride, using zirconium-loaded activated charcoal and attributed it as due to competition for the active sites of the material [28]. The higher interference effect of phosphate is probably due to the low solubility product ($K_{So}[Zr_3(PO)_4] = 1.0 \times 10^{-132}$) leading to an intense competition between phosphate and arsenate anions by the adsorbent material [29].

A more detailed study with phosphate showed that in concentrations above 100 μg the interference of phosphate limits the applicability of this system.

3.6. Effect of pH on phosphate interference

Fig. 5 shows the pH effect on phosphate interference, evaluated by varying the phosphate concentration from 200 to 20,000 μg L^{-1} for a 2 μg L^{-1} arsenic level. As can be seen the phosphate interference occurs over the entire pH range, but most significantly at low pH, due to the amphotheric character of the pre-concentration material.

3.7. Figures of merit and the determination of As steel samples

In order to calculate the enhancement factor for the system using silica modified with zirconium oxide as sorbent material, analytical curves with and without the pre-concentration step

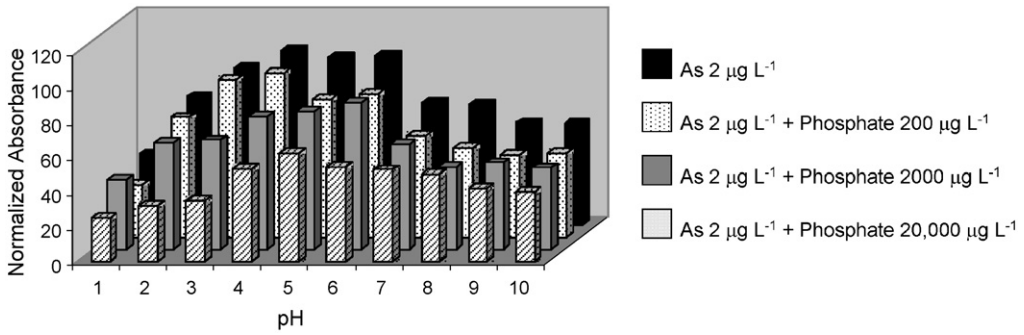


Fig. 5. Effect of pH on phosphate interference.

Table 2
Arsenic content in steel samples

SRM	Arsenic concentration certified (% m/m)	Arsenic concentration found (% m/m)	R.S.D. (%)
361	0.017 ± 0.001	0.019 ± 0.001	6.07
362	0.092 ± 0.005	0.094 ± 0.006	5.97
363	0.010 ± 0.001	0.011 ± 0.001	7.85
364	0.052 ± 0.005	0.055 ± 0.001	1.20

were obtained. It is possible to note an increase in the sensitivity. An enhancement factor of 20 was calculated taking into account the increase in the analytical signal. The efficiency of the minicolumn was not affected even after 200 pre-concentration runs.

The limit of detection (3σ) and the limit of quantification (10σ) were calculated as 0.05 $\mu g\,L^{-1}$ of As and 0.35 $\mu g\,L^{-1}$ of As, respectively, after pre-concentration. Relative standard deviations less than 8% were obtained for different concentrations of arsenic.

Four steel samples were analysed: SRM 361 (AISI Steel), SRM 362 (94B17 Steel Modified), SRM 363 (Chromium–Vanadium Steel) and SRM 364 (High-Carbon Steel Modified). The results obtained, described in Table 2, agree with the certified values within the 95% confidence level and showed the adequacy of the system studied, considering the limit of concentration due to possible interfering species. The recovery values show that the system was not affected by the presence of interferents within the specified ranges.

4. Conclusion

The procedure for on-line pre-concentration of inorganic arsenic using silica modified with zirconium oxide as sorbent material, coupled to hydride generation, showed to be fast (28 determinations h^{-1}) and of low cost (one column may be used for more than 200 pre-concentration cycles, without loss of efficiency). The enrichment factor of 20-fold is adequate for the determination of low levels of arsenic. The limit of detection of 0.05 $\mu g\,L^{-1}$ allowed the determination of arsenic in steel.

Because the proposed system is highly affected by phosphate and sulphate it is not recommended for water analyses. On the other hand it is adequate for arsenic determination in metallurgical samples.

Acknowledgements

The authors gratefully acknowledge Dr. Carol H. Collins for assistance with English in this manuscript and the Fundação de Amparo à Pesquisa do Estado de São Paulo (FAPESP) and the Coordenação de Aperfeiçoamento de Pessoal de Nível Superior (CAPES) for financial support of this work and fellowships.

References

[1] H.D. Fleming, R.G. Ide, Anal. Chim. Acta 83 (1976) 76.
[2] B. Welz, M. Melcher, Spectrochim. Acta 36 B (1981) 439.
[3] A. Walsh, Spectrochim. Acta 7 (1955) 108.
[4] B.V. L'vov, Spectrochim. Acta 17 (1961) 761.
[5] W. Holak, Anal. Chem. 41 (1969) 1712.
[6] S. Cadore, N. Baccan, J. Anal. At. Spectrom. 12 (1997) 637.
[7] S. Cadore, A.P. dos Anjos, N. Baccan, Analyst 123 (1998) 1717.
[8] T.I. Tikhomirova, V.I. Fadeeva, J. Anal. Chem. 52 (1997) 230.
[9] A.R.K. Dapaah, A. Ayame, Anal. Sci. 13 (1997) 405.
[10] Q. Zhang, H. Minami, S. Inoue, I. Atsuya, Fresenius J. Anal. Chem. 370 (2001) 860.
[11] G.I. Malofeeva, E.M. Sedykh, L.S. Rozhkova, L.N. Bannykh, J. Anal. Chem. 54 (1999) 162.
[12] V. Arancibia, A. Lopes, M.C. Zúñiga, R. Segura, Talanta 68 (2006) 1567.
[13] J.A.G. Gomes Neto, R. Montes, A.A. Cardoso, Talanta 50 (1999) 959.
[14] C.I.S. Narcise, L.D. Coo, F.R. del Mundo, Talanta 68 (2005) 298.
[15] M.P. Elizalde-Gonzalez, J. Mattusch, R. Wennrich, J. Environ. Monit. 3 (2001) 22.
[16] G.G. Bortoleto, S. Cadore, Talanta 67 (2005) 169.
[17] Y. Gushikem, S.S. Rosatto, J. Braz. Chem. Soc. 12 (2001) 695.
[18] Y. Gushikem, C.R.M. Peixoto, U.P. Rodrigues Filho, L.T. Kubota, E. Stadler, J. Colloid Interface Sci. 184 (1996) 236.
[19] A. Yuchi, A. Ogiso, S. Muranaka, T. Niwa, Anal. Chim. Acta 494 (2003) 81.
[20] E. Vassileva, N. Furuta, Fresenius J. Anal. Chem. 370 (2001) 52.
[21] D.Q. Trung, C.X. Anh, N.X. Trung, Y. Yasaka, M. Fujita, M. Tanaka, Anal. Sci. 17 (2001) 1219.
[22] Software Chemomatrix. http://cevada.iqm.unicamp.br.
[23] J. Dedina, Anal. Chem. 54 (1982) 2097.
[24] J.W. Hershey, P.N. Keliher, Spectrochim. Acta 41B (1986) 713.
[25] P.K. Dasgupta, H. Huang, G. Zhang, G.P. Cobb, Talanta 58 (2002) 153.
[26] B. Daus, J. Mattusch, R. Wenrich, H. Weiss, Talanta 58 (2002) 57.
[27] A.L. Moretto, S. Cadore, Microchim. Acta 146 (2004) 239.
[28] S. Peräniemi, M. Ahlgrén, Anal. Chim. Acta 302 (1995) 89.
[29] L. Meites, Handbook of Analytical Chemistry, MacGraw-Hill Book Company, New York, 1963.

Available online at www.sciencedirect.com
ScienceDirect
Talanta 71 (2007) 1352–1363
Talanta
www.elsevier.com/locate/talanta

Challenges in modelling and optimisation of stability constants in the study of Cu–$(TAPS)_x$–$(OH)_y$ system by polarography

Carina M.M. Machado, Helena M.V.M. Soares *

REQUIMTE, Department of Chemical Engineering, Faculty of Engineering, University of Porto, Rua Dr. Roberto Frias, 4200-465 Porto, Portugal

Received 22 February 2006; received in revised form 28 June 2006; accepted 6 July 2006
Available online 17 August 2006

Abstract

This work describes the application of polarography, a technique scarcely used for modelling and optimisation of stability constants, in the study of copper complexes with [(2-hydroxy-1,1-bis(hydroxymethyl)ethyl)amino]-1-propanesulfonic acid (TAPS). Direct current polarography (DCP), using low total copper ion and large total ligand to total copper concentration, enabled the full characterization of Cu–$(TAPS)_x$–$(OH)_y$ system, whose complexation occurs in the pH range of copper hydrolysis and $Cu(OH)_2$ precipitation. Cu–$(TAPS)_x$–$(OH)_y$ system was studied by DCP and glass electrode potentiometry (GEP) in aqueous solution at fixed total ligand to total metal concentrations ratios and varied pH values (25.0 °C; $I = 0.1$ M, KNO_3). The predicted model, as well as the overall stability constants values, are (as log β): $CuL^+ = 4.2$, $CuL_2 = 7.8$, $CuL_2(OH)^- = 13.9$ and $CuL_2(OH)_2^{2-} = 18.94$. GEP only allowed confirming the stability constants for CuL^+ and CuL_2 and was used to determine the pK_a of TAPS, 8.342.

Finally, a briefly comparative analysis between TAPS and other structural related buffers was done. Evaluation based on $\log \beta_{CuL}$ versus pK_a revealed that TES, TRIS, TAPS and AMPSO coordinated via amino and hydroxymethylgroups forming a five-membered chelate ring. For BIS-TRIS and TAPSO, and possibly DIPSO, one or more five-membered chelate rings involving additional hydroxyl groups are also likely formed.
© 2006 Elsevier B.V. All rights reserved.

Keywords: TAPS; [(2-Hydroxy-1,1-bis(hydroxymethyl)ethyl)amino]-1-propanesulfonic acid; Biological buffers; Copper; Stability constants; Electrochemical techniques

1. Introduction

Hydrogen buffers are used to maintain a constant concentration of hydrogen ions in solution. The hydrogen donor/acceptor can be oxygen, as is the case of phosphate; however, for many biological buffers nitrogen acts as a donor/acceptor since a variety of substituents can tailor the amine pK_a to neutral pH. Nowadays, several chemical suppliers devote a special section of their catalogues, where a long list of popular amine-based buffers is available [1,2].

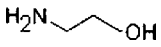
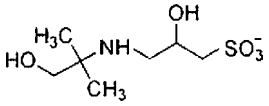
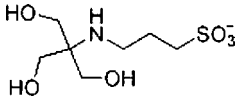
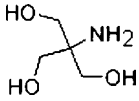
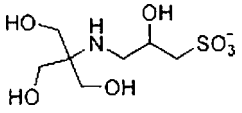
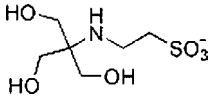
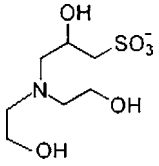
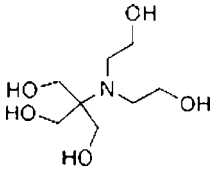
When researchers consult these long lists of commercial available pH buffers, they are faced with several buffers for the same pH buffering range; these pH buffers have different metal complexation strength. To exemplify this statement, for buffering solutions at pH 7.5, we can choose one of these pH buffers among others: DIPSO, HEPES, MOPS, PIPES, TAPSO, TES and TRIS. In what concerns copper complexation, we can divide these buffers in three different groups: DIPSO [3], TAPSO [4], TES [5] and TRIS [5] are strong copper complexing agents, whereas MOPS [6] and PIPES [7] do not complex copper and HEPES [8] complexes incipiently.

Usually researchers obtain buffer conditions from previous publications. The primary concern is that buffers do not participate in the reaction system through inhibition, activation or complexation. It is usually assumed that initial investigations for buffer controls have been performed and that reported results are free of buffer artefacts. However, in most of the cases, these studies were not performed and several interferences are described in the literature where metal ions complexation by these biological buffers occurs. To exemplify this statement, two cases are presented: (i) the enzymatic activity of acetylcholinesterase (AChE) is inhibited when Tris is used to prepare the Ellman's reaction solution [9] and (ii) the generation of fluorescence, browning and polymerization of lysozyme, when using the TAPSO buffer,

* Corresponding author. Tel.: +351 225 081 650; fax: +351 225 081 449.
E-mail address: hsoares@fe.up.pt (H.M.V.M. Soares).

0039-9140/$ – see front matter © 2006 Elsevier B.V. All rights reserved.
doi:10.1016/j.talanta.2006.07.011

Table 1
Comparison between CuL^+ complex stability constants and basicity for some biological buffers and other amines

Ligand	Structures	pK_a	Log β_{CuL}	References
Methylamine		10.65	4.11	[5]
Ethanolamine		9.52	4.50	[5]
Ammonia	NH_3	9.28	4.12	[5]
N-(1,1-Dimethyl-2-hydroxyethyl)-3-amino-2-hydroxypropanesulfonic acid (AMPSO)		9.05	4.62	[13]
[(2-Hydroxy-1, 1-bis(hydroxymethy)-ethyl)amino]-1-propanesulfonic acid (TAPS)		8.34	4.2	This work
2-Amino-2-hydroxymethyl-1,3-propanediol (THAM or TRIS)		8.10	4.05	[5]
2-Hydroxy-3-[tris(hydroxymethyl)methylamino]-1-propanesulfonic acid (TAPSO)		7.55	4.41	[4]
2-[(2-Hydroxy-1,1-bis(hydroxymethyl)ethyl)-amino]ethanesulfonic acid (TES)		7.5	3.9	[5]
3-(*N,N*-bis[2-hydroxyethyl]amino)-2-hydroxypropanesulfonic acid (DIPSO)		7.47	4.2	[3]
2-bis(2-hydroxyethyl)amino-2-(hydroxymethyl)-1,3-propanediol (BIS-TRIS)		6.54	5.27	[5]

were markedly inhibited under both aerobic and non-aerobic conditions [10]; these interferences are probably due to their (TRIS or TAPSO) metal complexation.

Common buffers used in various analytical, biochemical and other applications involving metal ions [10–12] include zwitterionic buffers such as *N*-(1,1-dimethyl-2-hydroxyethyl)-3-amino-2-hydroxypropanesulfonic acid (AMPSO), 2-bis(2-hydroxyethyl)amino-2-(hydroxymethyl)-1,3-propanediol (BIS-TRIS), 3-(*N,N*-bis[2-hydroxyethyl]amino)-2-hydroxypropanesulfonic acid (DIPSO), 2-hydroxy-3-[tris(hydroxymethyl)-methylamino]-1-propanesulfonic acid (TAPSO), 2-[(2-hydroxy-1,1-bis(hydroxymethyl)ethyl)amino]ethanesulfonic acid (TES) or 2-amino-2-hydroxymethyl-1,3-propanediol (TRIS). These buffer anions possess a primary (TRIS), secondary (AMPSO, TAPSO or TES) or a tertiary (DIPSO and BIS-TRIS) amine function, and also β-alcohol groups (structures were included in Table 1), which can all potentially coordinate to metals. In fact, it has been shown that all of these buffers complex with copper ions in solutions especially at theirs buffering pH range [3–5,13].

The [(2-hydroxy-1,1-bis(hydroxymethyl)ethyl)amino]-1-propanesulfonic acid, usually known as TAPS, is also a zwitterionic buffer widely used in various applications [14–17]. This buffer is structural related with the biological buffers described above. Thus, it is expected that TAPS also complexes copper and therefore it is fundamental the knowledge of the stability constants values for taking into account when complexation of the buffer with copper ion takes place.

In the present work, we report the overall stability constants for the species formed between TAPS and Cu^{2+}, at 0.1 M KNO_3 ionic strength and 25.0 ± 0.1 °C. The full characterization of the system was done with the employment of direct current polarography (DCP). Some complementary information was obtained by glass electrode potentiometry (GEP). Experiments by alternating current polarography (ACP) were also carried out to check if this buffer adsorbs at the mercury working electrode surface, under the experimental conditions used. TAPS' protonation constant was also determined by GEP.

2. Experimental

2.1. Materials and reagents

The ligand TAPS (99.5%) was purchased from Sigma–Aldrich (St. Louis, MO, USA) and was used as received. The copper standard solution, 3.1×10^{-2} M, was purchased from Merck.

Additional information about the remaining reagents and experimental conditions was described previously [4].

2.2. Apparatus

All experiments were carried out in a Metrohm (Herisau, Switzerland) jacketed glass vessel, equipped with a magnetic stirrer, and thermostatted at 25.0 ± 0.1 °C using a water bath.

2.2.1. Polarography

Polarographic measurements were performed using a Model 663 VA stand (Metrohm) equipped with a multimode electrode (Metrohm, Model 6.1246.020), as a working electrode, used in the dropping mercury electrode mode. A silver/silver chloride (3 M KCl) and a glassy carbon were used as reference and counter electrodes (both from Metrohm), respectively. The VA stand was attached to a microAutolab (Eco Chemie, Utrecht, The Netherlands) system controlled by a personal computer. The pH measurements were conducted with a GLP 22 pH meter Crison (Barcelona, Spain) with a sensitivity of ±0.1 mV (±0.001 pH units) with a silver/silver chloride reference electrode (Metrohm) and a glass electrode (Metrohm).

2.2.2. Potentiometry

The potentiometric titrations were performed with a PC-controlled system assembled with a Crison MicropH 2002 meter, a Crison MicroBU 2030 microburette, a Philips GAH 110 glass electrode and an Orion 90-02-00 (double junction) reference electrode with the outer chamber filled with 0.1 M KNO_3. Automatic acquisition of data was done using a homemade program, COPOTISY.

2.3. Procedure

2.3.1. Calibration of the glass electrode

For all techniques used, the calibration of the glass electrode (pH measured as $-\log [H^+]$) was accomplished as previously described [13].

2.3.2. Alternating current polarography

Adsorption studies of TAPS were performed by ACP. Experiments were run, in the absence of copper, for buffer concentrations ranging from 8.0×10^{-4} to 1.4×10^{-2} M at three different pH values: 6.34, 8.34 and 10.34. These pH values were chosen because they correspond to experimental conditions where TAPS occurs as HL (100%), HL and L^- (50% of each) and L^- (100%), respectively, and thus, allows analysing the adsorption effects in all forms of the ligand.

The experimental conditions used were: an amplitude of sinusoidal alternating current of 5 mV, a frequency of 75 Hz and a scan rate of 2.5 mV/s; the capacitive current (i_{ac}) was measured at a phase angle of 90°. The potential range scanned was from 0.2 to −1.2 V versus Ag/AgCl(s), 3 M KCl.

2.3.3. Glass electrode potentimetry

Firstly, GEP was used to determine the protonation constants of the buffer at 25.0 ± 0.1 °C and 0.1 M KNO_3 ionic strength. Six titrations were performed using a total of three different TAPS solutions containing 6.0×10^{-3} or 1.0×10^{-2} M in 0.1 M KNO_3. For each titration, about 300 points were collected between pH 4.9 and 11.9.

For Cu–$(TAPS)_x$–$(OH)_y$ system, four titrations (two independent solutions) were carried out, between pH 3.4 and 7.0 (for each titration, about 40 points were collected), with a total ligand to total copper concentration ($[L_T]$:$[Cu_T]$) ratio set to 10.0, $[Cu_T] = 1.0 \times 10^{-3}$ M. For these experiments, a stock solution was prepared with the addition of all the reagents. The addition of KNO_3 was calculated in a way of keeping the final ionic strength at 0.1 M.

For both cases, monotonic additions of standardized KOH 0.1 M were done.

2.3.4. Direct current polarography

The study of the electrochemical behaviour of Cu–$(TAPS)_x$–$(OH)_y$ system was performed by DCP. A step potential of 4 mV and a drop time of 1 and 2 s (for the lower copper concentration), were used. Two $[L_T]$:$[Cu_T]$ ratios were run. The total copper concentration was 7.0×10^{-6} M for 151.6 $[L_T]$:$[Cu_T]$ ratio and 4.0×10^{-5} M for 97.5 $[L_T]$:$[Cu_T]$ ratio. Polarographic titrations were performed between pH 3.9 and 10.5; in this way, for each titration, about 50 polarograms were obtained. The procedure used to collect the data points was identical to the one described elsewhere [4].

2.4. Data treatment

The modelling and optimization procedures of polarographic data were done using the Cukrowski method; the support theory of the method was described elsewhere [18]. This method has several advantages when compared with the DeFord and Hume method. DeFord and Hume method only allows to evaluate stability constants of several ML_n complexes formed consecutively under the following experimental conditions: titration of a metal ion solution with increasing concentration of the ligand at fixed pH with the requirement of full reversibility of the electrochemical signal recorded for a labile metal/ligand sys-

Table 2
Dissociation constant for water, protonation constant for the ligand TAPS and overall stability constants for Cu(II) complexes with OH^-, at 25.0 °C

	Equilibrium	Log β	μ	References
Water	$H^+ + OH^- \Leftrightarrow H_2O$	13.78	0.1	[5]
TAPS	$L^- + H^+ \Leftrightarrow HL$	8.342 ± 0.001	0.1	This work
Copper	$Cu^{2+} + OH^- \Leftrightarrow Cu(OH)^+$	6.1	0.1	[5]
	$Cu^{2+} + 2OH^- \Leftrightarrow Cu(OH)_2$	11.8	0.1	[5]
	$2Cu^{2+} + 2OH^- \Leftrightarrow Cu_2(OH)_2{}^{2+}$	16.8	0.1	[5]
	$3Cu^{2+} + 4OH^- \Leftrightarrow Cu_3(OH)_4{}^{2+}$	33.5	0.1	[5]
	$Cu(OH)_2$ (s) $\Leftrightarrow Cu^{2+} + 2OH^-$	−18.3	0.1	[22]

tem. The main limitation of this method is that it is based on simple data interpretation without involving mass-balance equations. The new methodology developed by Cukrowski describes a polarographic speciation method applied to fully labile, inert, or mixed metal/ligand systems on the polarographic time scale, investigated at fixed total ligand to total metal concentrations ratio and varied pH. The resolution of mass-balance equations for total metal and total ligand concentrations allowed the successful use of polarography in the study of $M_zL_x(OH)_y$ species. The model is refined by comparing experimental and calculated complex formation curves (ECFC and CCFC, respectively) [18,19].

The simulation and optimization of the models and complex formation constants from potentiometric titrations data were performed using ESTA program [20,21]. The refinement operations involve solving mass-balance equations, including equation for the total proton concentration, in such a way that the computed free proton concentration reproduces the experimental recorded potential of the glass electrode.

The protonation constants for water [5] and for TAPS and the metal hydroxide formation constants, $Cu_x(OH)_y{}^{(2x-y)}$ [5] (Table 2) were kept fixed during the refinement operations.

3. Results and discussion

3.1. Calculation of TAPS protonation constants

TAPS is a zwitterionic buffer, which has two acidic sites, the sulphonic (pK_{a_1}) and the amino (pK_{a_2}) groups (see insert in Fig. 1). The first protonation constant is released from the sulphonic group at a rather low pH (pK_a value less than 3.0 [4]), which is not relevant for the present study since it was not expected that TAPS complexes copper at pH values lower than 5.0. Potentiometric data were refined using ESTA program and the refinement of pK_{a_2} performed, between pH 7.4 and 9.4 using 483 points, gave a value of 8.342 ± 0.001 with a Hamilton R-factor [21] of 0.0153.

3.2. Ligand adsorption and reversibility studies

ACP at a phase angle of 90° was used to test if there was adsorption of TAPS at the mercury electrode surface. Under these experimental conditions, because the capacitive current is maxima and a non-faradaic process is expected, the current is mainly capacitive in nature and proportional to the double layer capacity. Fig. 1 shows the variation in the capacitive current

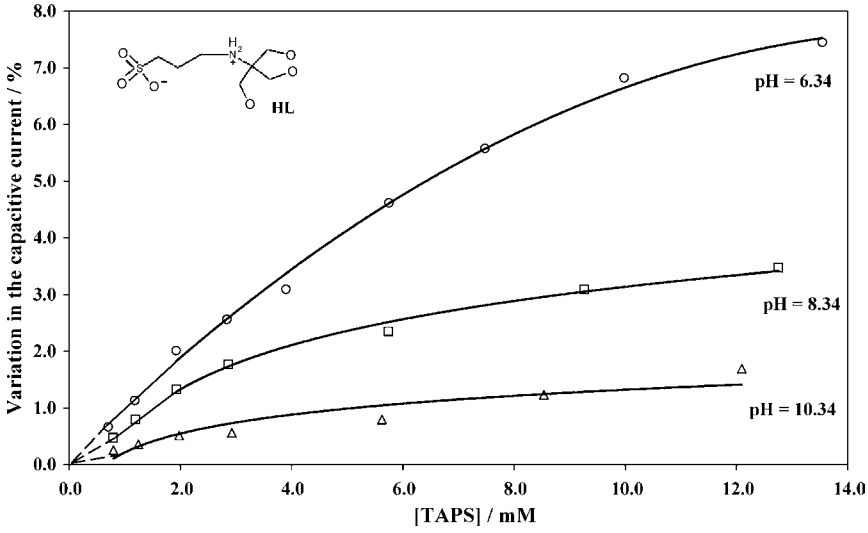


Fig. 1. Variation in the capacitive current recorded by ACP with the increase of TAPS concentration at three pH values, 6.34, 8.34 and 10.34. The values, expressed in percentage, were calculated from the difference between the capacitive current recorded in the presence and in the absence of the buffer, at −0.2 V, from ACP curves with a phase angle of 90° in 0.1 M KNO_3.

(expressed in percentage) obtained with the increase of ligand concentration relatively to the background solution (0.1 M KNO_3), at a reduction potential typical for Cu^{2+} (−0.2 V [23]), for three pH values, pH 6.34, 8.34 and 10.34.

For pH 10.34, where the ligand is totally in the L^- form, the variation in the capacitive current with the increase of the ligand concentration was less than 2% for all the TAPS concentration range tested. At pH 6.34, the variation in the capacitive current was slightly pronounced than for other pH values, being recorded a variation of about 7.5% for the highest TAPS concentration tested, 1.4×10^{-2} M. For pH = pK_a (where the ligand exists half in the protonated form, HL, and half in the deprotonated form, L^-), a halfway situation between the other ones was recorded (Fig. 1). In a previous work, similar adsorption interference was obtained with TAPSO [4], which is a structural related pH buffer. However, no significant influence in the recorded polarograms or in the refined stability constants was verified [4]. Thus, it was decided to use 3.9×10^{-3} M TAPS as the highest ligand concentration for the polarographic study of Cu–$(TAPS)_x$–$(OH)_y$ system.

To characterize the Cu–$(TAPS)_x$–$(OH)_y$ system, two polarographic titrations were performed, $[L_T]$:$[Cu_T]$ = 151.6 and 97.5 with total copper concentrations of 7.0×10^{-6} and 4.0×10^{-5} M, respectively. After the addition of the ligand, the recorded diffusion current of DC wave decreased by about 20% and the position of the polarographic signal has changed by about 6 mV towards more negative values for the lowest $[L_T]$:$[Cu_T]$ ratio. For the highest $[L_T]$:$[Cu_T]$ ratio, a decrease of 13% in the diffusion current and a shift of less than one mV towards more cathodic values was observed. This was probably due to adsorption of the ligand into the mercury electrode surface. To correct for this phenomenon, the values for the diffusion current and half-wave potential for metal in the presence of the ligand were used has reference point for both titrations, since these values were recorded at a pH where no complexation was expected (pH value below 5.0, Fig. 2A).

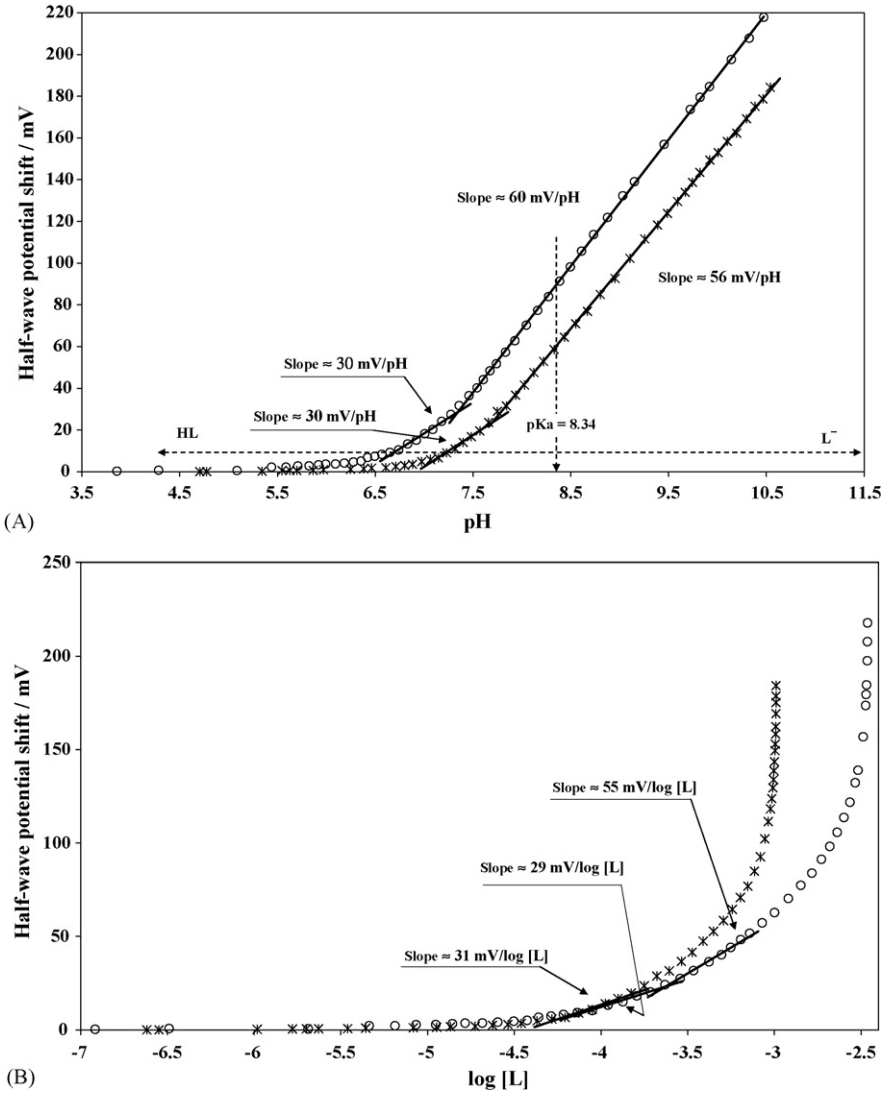


Fig. 2. Prediction of species from DCP data: $[L_T]$:$[Cu_T]$ = 97.5 (points), $[L_T]$:$[Cu_T]$ = 151.6 (asterisks) with $[Cu_T] = 4.0 \times 10^{-5}$ and 7.0×10^{-6} M, respectively. Observed half-wave potential shift as a function of pH (A) and as a function of the logarithm of the free ligand concentration (B).

The analysis of the DC polarograms collected for both $[L_T]$:$[Cu_T]$ ratios, in the pH range between 3.9 and 10.5, showed that Cu–$(TAPS)_x$–$(OH)_y$ system behaved as labile and/or quasi-labile on the polarographic time scale; only one peak corresponding to all labile species present in solution, which shifted to more cathodic potential values (data not shown). For the performed titrations, it was also verified that the system was fully reversible; the steepness of the waves varied between 0.9 and 1.0.

3.3. Prediction of species formed from DCP titrations

The prediction of the species present in solution was accomplished by graphical analysis of the slopes drawn from the observed half-wave potential shift as a function of pH (Fig. 2A) and as a function of the logarithm of the free ligand concentration (Fig. 2B). The results of the two polarographic titrations, $[L_T]$:$[Cu_T] = 151.6$ (asterisks) and 97.5 (points) with total copper concentrations of 7.0×10^{-6} and 4.0×10^{-5} M, respectively, were included in Fig. 2, as well as the protonation constant value and the respective forms of the ligand.

The prediction of the species and the pH ranges where they are formed and exist as predominant metal containing species can be made from the slopes of the straight lines defined in the curve half-wave potential shift as a function of pH and as a function of the logaritm of the free ligand concentration. When only one metal species is reduced in the pH range where one form of a ligand is predominant, a slope of $59.16/n$ mV/pH unit and proton involved, and a slope of $59.16/n$ mV/log[L] and ligand involved in the electrochemical reaction at 25 °C (n is the number of electrons involved in the reaction) should be obtained. The support theory of the method was described elsewhere [18,19].

For the lowest $[L_T]$:$[Cu_T]$ ratio, the analysis of the data shows that no complexation occurs until pH 5.5 and for $[L_T]$:$[Cu_T] = 151.6$, the complexation only starts at pH 6.5 (lower metal concentration). For $[L_T]$:$[Cu_T] = 97.5$, three slopes were identified. Between pH 6.8 and 7.3, a slope of about 30 mV/pH was observed indicating the presence of CuL^+ and/or $Cu(OH)^+$; one proton is involved to generate HL and/or H_2O in the electrochemical reaction at the dropping mercury electrode:

$$CuL^+ + H^+ + 2e^- \Leftrightarrow Cu(Hg) + HL$$

$$Cu(OH)^+ + H^+ + 2e^- \Leftrightarrow Cu(Hg) + H_2O$$

From pH 7.4 up to 10.5 a slope of 60 mV/pH was drawn. Between pH 7.4 and 8.4, the ligand exists mainly in the protonated form and the slope of 60 mV/pH indicates that up to three species can be present in solution; CuL_2 and/or CuL(OH) and/or $Cu(OH)_2$ develop a theoretical slope of 59 mV/pH due to the involvement of two protons in the reaction at the DME:

$$CuL_2 + 2H^+ + 2e^- \Leftrightarrow Cu(Hg) + 2HL$$

$$CuL(OH) + 2H^+ + 2e^- \Leftrightarrow Cu(Hg) + HL + H_2O$$

$$Cu(OH)_2 + 2H^+ + 2e^- \Leftrightarrow Cu(Hg) + 2H_2O$$

The formation of $Cu(OH)_2$, as major species, is very unlikely since no precipitation was observed up to pH 10.5, which shows that copper–TAPS complexes must be formed.

From pH 8.5 to 10.5, a slope of 60 mV/pH, as that obtained in the pH range between pH 7.4 and 8.4, was obtained. Above the pK_a, the main form of the ligand is L^-, which indicates the formation of $CuL_x(OH)_2$ species. The electrochemical reaction at the DME involves two protons:

$$CuL_x(OH)_2{}^{x-} + 2H^+ + 2e^- \Leftrightarrow Cu(Hg) + xL^- + 2H_2O$$

Apparently, the $CuL_2(OH)^-$ species does not exist in appreciable amount, under the experimental conditions tested, since no slope indicative of its predominance was obtained. If this species was formed below the pK_a, the theoretical slope should be 88.5 mV/pH, three protons involved in the reduction reaction at the DME:

$$CuL_2(OH)^- + 3H^+ + 2e^- \Leftrightarrow Cu(Hg) + 2HL + H_2O$$

and the observed slope was just about 60 mV/pH. But if one considers that this species should exist in higher amount above the pK_a, where the ligand is mainly in the deprotonated form, the slope should decrease to a value of 29.5 mV/pH, only one proton involved in the DME reaction:

$$CuL_2(OH)^- + H^+ + 2e^- \Leftrightarrow Cu(Hg) + 2L^- + H_2O$$

So, two possibilities can be considered: (1) this species does not exist in appreciable amount in the pH region analysed or (2) is exactly formed in the deprotonation region, which would result in a slope value between 88.5 and 29.5, i.e. a slope characteristic of a reduction reaction involving two protons, 59 mV/pH.

For $[L_T]$:$[Cu_T] = 151.6$, a similar slope profile to that recorded for $[L_T]$:$[Cu_T] = 97.5$ was drawn (Fig. 2A), being about 0.5 units shifted to higher pH values, which evidences a slight decrease of complexation for this ratio.

The graphical analysis of half-wave potential shift versus log[L] (Fig. 2B) shows characteristic slopes of CuL and CuL_2, for $[L_T]$:$[Cu_T] = 97.5$, in the pH range 6.5–7.3 and 7.4–8.0, respectively. For $[L_T]$:$[Cu_T] = 151.6$, a slope characteristic of CuL was possible to draw in the pH range between 7.1 and 7.6. These slopes indicate that these species should be major species in the pH range where the slopes were drawn.

From the considerations described above, the proposed model for Cu–$(TAPS)_x$–$(OH)_y$ system should include the following species: CuL^+, CuL_2, CuL(OH) and $CuL_x(OH)_2{}^{x-}$. In order to form a logical sequence of species, the $CuL_2(OH)^-$ species should also be considered, as a minor species, resulting in the model: CuL^+, CuL(OH), $CuL(OH)_2{}^-$, CuL_2, $CuL_2(OH)^-$ and $CuL_2(OH)_2{}^{2-}$.

3.4. Modelling procedures and refinement of stability constants

3.4.1. DCP results

The adopted strategy for the refinement of the stability constants from DCP data from both titrations performed is summarized in Table 3.

Table 3
Overall stability constants for Cu–$(TAPS)_x$–$(OH)_y$ system determined by DCP: $[L_T]:[Cu_T] = 97.5$ (49 points between pH 3.9 and 10.5) and 151.6 (52 points between pH 4.7 and 10.5), with $[Cu_T] = 4.0 \times 10^{-5}$ and 7.0×10^{-6} M, respectively; and GEP: $[L_T]:[Cu_T] = 10.0$, $[Cu_T] = 1.0 \times 10^{-3}$ M (four titrations, 118 points between pH 3.4 and 6.6)

Complexes	DCP				GEP	
	$[L_T]:[Cu_T] = 97.5$		$[L_T]:[Cu_T] = 151.6$		$[L_T]:[Cu_T] = 10.0$	
	Model 1	Model 2	Model 1	Model 2	Model 1	Model 2
CuL^+ $Cu^{2+} + L^- \Leftrightarrow CuL^+$	4.07 ± 0.03	4.10 ± 0.03	4.09 ± 0.05	4.22 ± 0.05	4.10 ± 0.02	4.09 ± 0.02
$CuL(OH)$ $Cu^{2+} + L^- + OH^- \Leftrightarrow CuL(OH)$	10.66 ± 0.03	NI	10.60 ± 0.03	NI	11.05 ± 0.02	NI
$CuL(OH)_2{}^-$ $Cu^{2+} + L^- + 2OH^- \Leftrightarrow CuL(OH)_2{}^-$	16.47 ± 0.01	NI	16.00 ± 0.01	NI	NI	NI
CuL_2 $Cu^{2+} + 2L^- \Leftrightarrow CuL2$	R	7.58 ± 0.06	R	7.9 ± 0.1	R	7.67 ± 0.02
$CuL_2(OH)^-$ $Cu^{2+} + 2L^- + OH^- \Leftrightarrow CuL_2(OH)^-$	NI	13.70 ± 0.03	NI	14.01 ± 0.03	NI	NI
$CuL_2(OH)_2{}^{2-}$ $Cu^{2+} + 2L^- + 2OH^- \Leftrightarrow CuL_2(OH)_2{}^{2-}$	NI	18.91 ± 0.01	NI	18.97 ± 0.01	NI	NI
SD/mV	0.5841	0.5211	0.5866	0.3326		
Hamilton R-factor					0.06694	0.06882

For DCP, SD represents an overall fit of complex formation curves, the computed curve in the objective experimental function [4]. For GEP, Hamilton R-factor stands for a statistical Hamilton R-factor generated by the program ESTA [21]. R, rejected; NI, not included.

For both $[L_T]:[Cu_T]$ ratios, the refinement operations started with the fitting of two simpler models: Model 1: CuL^+, CuL_2, $CuL(OH)$ and $CuL(OH)_2{}^-$ and Model 2: CuL^+, CuL_2, $CuL_2(OH)^-$ and $CuL_2(OH)_2{}^{2-}$. Because graphical analysis (Fig. 2B) has confirmed the presence of CuL_2, for $[L_T]:[Cu_T] = 97.5$, it was decided to include this species in both models, for both $[L_T]:[Cu_T]$ ratios. For both ratios, the fit of Model 1 resulted in the rejection of CuL_2 and the fit of Model 2 improved significantly the standard deviation (Table 3), indicating that CuL^+, CuL_2, $CuL_2(OH)^-$ and $CuL_2(OH)_2{}^{2-}$ species should exist in considerable amount in the pH range tested. From a statistical point of view, no other species are necessary to explain the experimental data obtained. Given that CuL_2 exists in significant amount, as it is indicated for the lower $[L_T]:[Cu_T]$ ratio (see Fig. 2B), it is reasonable to consider that the hydroxides species formed in solution result from the hydrolyses of CuL_2 species, explaining the preference for Model 2.

3.4.2. GEP results

In previous works [3,4], the formation of $CuL(OH)_y{}^{(1-y)}$ for Cu–$(TAPSO)_x$–$(OH)_y$ and Cu–$(DIPSO)_x$–$(OH)_y$ systems was evidenced particularly when low $[L_T]:[Cu_T]$ ratios were used.

In order to design the best experimental conditions to obtain further information about the final model of Cu–$(TAPS)_x$–$(OH)_y$ system, several species distribution diagrams (SDD) were simulated for a wide range of $[L_T]:[Cu_T]$ ratios (between 1 and 20) (data not shown), using Model 2 refined from DCP data (Table 3). We were particularly interested on designing experimental conditions for running potentiometric titrations with lower $[L_T]:[Cu_T]$ ratios using high copper concentrations (about 1.0×10^{-3} M). These conditions would favor the formation of $CuL(OH)_y{}^{(1-y)}$ species [3,4] and, if they were formed, would allow us to confirm their presence. For $[L_T]:[Cu_T]$ ratios lower than 17 ($[Cu^{2+}] = 1.0 \times 10^{-3}$ M), $Cu(OH)_2$ precipitation was predicted at about pH 8. For $[L_T]:[Cu_T]$ ratios higher than 18, no precipitation was predicted but $[L^-]/[\sum_{x,y=0}^{2} CuL_x(OH)_y{}^{(2-x-y)}]$ ratios higher than 6 were predicted; thus, under these experimental conditions, erroneous stability constants should be obtained because all the titration goes towards the deprotonation of the ligand and not to neutralise protons liberated from the copper complexation. The main reason why for TAPSO and DIPSO was possible to run potentiometric titrations using low $[L_T]:[Cu_T]$ ratios is due to the fact that the amino group of these buffers [3,4] is more acidic than TAPS' amino group (for TAPSO and DIPSO, the pK_a values are around 7.5, which is about one log unit lower than TAPS (Table 2)), which gave, for the same experimental conditions, a large amount of free ligand concentration available in the pH range of copper hydrolysis and $Cu(OH)_2$ precipitation to complex copper and thus avoids its precipitation.

In order to confirm some of the stability constants values (CuL^+ and CuL_2) refined by DCP, it was decided to run potentiometric titrations for $[L_T]:[Cu_T]$ ratio set to 10.0 ($[Cu_T] = 1.0 \times 10^{-3}$ M). Due to the early precipitation, experimental data were only possible to be collected up to pH 6.6. This fact disabled the refinement of $CuL_x(OH)_2{}^{x-}$ species, which should start to be formed at about pH 7.0–7.5. The obtained results are summarized in Table 3. Thus, we started with two models: Model 1 constituted by CuL^+, $CuL(OH)$ and CuL_2 and Model 2 constituted by CuL^+ and CuL_2. Other species ($CuL_2(OH)^-$ and $CuL_x(OH)_2{}^{x-}$) were not included due to the

narrow titration pH range used in the refinement. For Model 1, ESTA rejected CuL_2. However, this cannot really mean that this species was not formed. One must not forget that the formation of CuL_2 and CuL(OH) uses the same amount of protons:

$$Cu^{2+} + 2HL \Leftrightarrow CuL_2 + 2H^+$$

$$Cu^{2+} + HL + H_2O \Leftrightarrow CuL(OH) + 2H^+$$

which makes it difficult for ESTA to distinguish between these two species.

Table 3 evidences that both final models (Model 1: CuL^+ and CuL(OH) and Model 2: CuL^+ and CuL_2) fitted the experimental results with similar Hamilton R-factors. Additionally, the stability constants values for CuL^+ and CuL_2 species refined by GEP (Model 2) were in perfect agreement with the values refined by DCP data (Model 2, Table 3).

3.4.3. Final model and overall stability constants values for $Cu–(TAPS)_x–(OH)_y$ system

The analysis of refinement DCP data evidenced that Model 2 (CuL^+, CuL_2, $CuL_2(OH)^-$ and $CuL_2(OH)_2{}^{2-}$) is the model that better explains the experimental data. Additionally, the analysis of GEP data raised the possibility of formation of CuL(OH) species. Considering this, SDD were generated for DCP and GEP experiments using the model constituted by: CuL^+, CuL(OH), CuL_2, $CuL_2(OH)^-$ and $CuL_2(OH)_2{}^{2-}$, for which stability constants values were calculated as the average stability constant values, as log β ($CuL^+ = 4.2$, $CuL_2 = 7.8$, $CuL_2(OH)^- = 13.9$ and $CuL_2(OH)_2{}^{2-} = 18.9$) obtained from all the experiments (two DCP and four GEP experiments) plus the CuL(OH) species refined from GEP (CuL(OH) = 11.05). In Fig. 3A, the SDD for $[L_T]:[Cu_T]$ ratio 97.5 was included.

The species distribution shown in this figure does not corroborate the slopes analysis, hence the major species between 7.0 and 8.0 is CuL(OH) and not CuL_2, as it was evidenced from Fig. 2B.

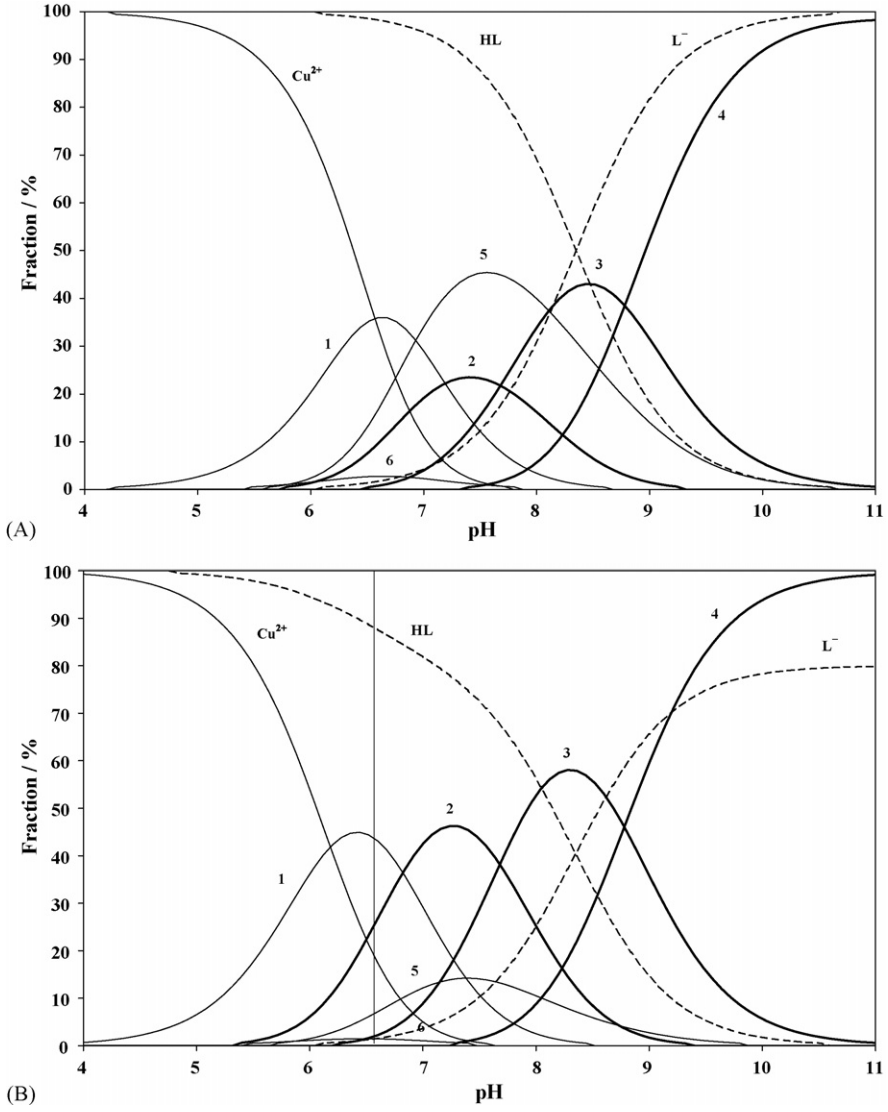


Fig. 3. Species distribution diagram for $Cu–(TAPS)_x–(OH)_y$ system. (A) $[L_T]:[Cu_T] = 97.5$, $[Cu_T] = 4.0 \times 10^{-5}$ M; (B) $[L_T]:[Cu_T] = 10$, $[Cu_T] = 1.0 \times 10^{-3}$ M. The species present in the figure are: (1) CuL^+, (2) CuL_2, (3) $CuL_2(OH)^-$, (4) $CuL_2(OH)_2{}^{2-}$, (5) CuL(OH), and (6) $Cu(OH)^+$, with stability constants set to (as log β): 4.2, 7.8, 13.9, 18.9, 11.05 (A) or 10.6 (B), and 6.1, respectively. The vertical line indicates the pH at which precipitation was observed.

Thus, if CuL(OH) exists must have a lower log β. Decreasing $\log \beta_{ML(OH)}$ to 10.6 and maintaining all the other stability constant values ($CuL^+ = 4.2$, $CuL_2 = 7.8$, $CuL_2(OH)^- = 13.9$ and $CuL_2(OH)_2^{2-} = 18.9$), SDD generated for GEP experimental conditions (Fig. 3B) indicates that up to pH 6.6, besides the formation of CuL, CuL_2 predominates against CuL(OH) species and even if it was formed there was no sufficient amount to be determined by the GEP tested conditions. Therefore, it is clear that CuL(OH) species is not formed and should not be included in the final model for Cu–$(TAPS)_x$–$(OH)_y$ system.

Thus, the final model should be CuL^+, CuL_2, $CuL_2(OH)^-$ and $CuL_2(OH)_2^{2-}$, for which the average stability constant values ($CuL^+ = 4.2$; $CuL_2 = 7.8$, $CuL_2(OH)^- = 13.9$ and $CuL_2(OH)_2^{2-} = 18.94$) were calculated. SDD were generated for both DCP $[L_T]$:$[Cu_T]$ ratios, as well as for GEP conditions (Fig. 4).

The analysis of SDD for $[L_T]$:$[Cu_T]$ ratio 10.0 (Fig. 4A) predicts the formation of CuL^+ and CuL_2 prior the precipitation predicted to occur at pH 6.6, and this precipitation was just observed experimentally. Fig. 4B and C evidences that CuL^+, CuL_2, $CuL_2(OH)^-$ and $CuL_2(OH)_2^{2-}$ and CuL^+, $CuL_2(OH)^-$ and $CuL_2(OH)_2^{2-}$ are the major species for $[L_T]$:$[Cu_T]$ ratios 97.5 and 151.6, respectively, whose predominance is in perfect agreement with the graphical analysis slopes (Fig. 2). As suspected by the prediction of species (Fig. 2), $CuL_2(OH)^-$ is formed exactly in the region of the deprotonation of the ligand and this is why no characteristic slope for this species was found in the graphical analysis (Fig. 2B); the obtained slope resulted from the average of the predicted theoretical slopes prior and after deprotonation (see Section 3.3). Above pH 9.0 $CuL_2(OH)_2^{2-}$ is the major species present in solution. These SDD (Fig. 4) also show that, in the buffering pH range (between 7.34 and 9.34), $CuL_2(OH)^-$ and $CuL_2(OH)_2^{2-}$ are the main species present in solution.

It is very important to emphasize that the characterization of Cu–$(TAPS)_x$–$(OH)_y$ system was based in the analysis of a wide-ranging experimental conditions: $[L_T]$:$[Cu_T]$ varied from 10 up to 151.6, with $7.0 \times 10^{-6} < [Cu^{2+}] < 1.0 \times 10^{-3}$ M and $1.1 \times 10^{-3} < [TAPS] < 1.0 \times 10^{-2}$ M. Results described above have shown that no other $[L_T]$:$[Cu_T]$ ratios were possible to be tested and provide additional information about the final model.

SDD (Fig. 4) evidence that, in the buffering pH range, TAPS is a strong copper complexing agent. Specifically, Fig. 4C shows that for $[L_T]$:$[Cu_T]$ 151.6, free copper ion concentration decreases in the presence of 1.0×10^{-3} M of TAPS from initial $[Cu_T] = 7.0 \times 10^{-6}$ M to 1.8×10^{-6} and 5.0×10^{-10} M at pH 7.34 and 9.34, respectively. These results evidence that for in vitro studies of metal toxicity, where biologists usually use a pH buffer plus a metallic buffer, TAPS can be used simultaneously as pH and pCu buffer considering the stability constants values determined in this work.

3.5. Comparative analysis of several Cu–$(L)_x$–$(OH)_y$ systems with structural proposal

As mentioned before, TAPS is a zwitterionic buffer structurally related with others biological buffers, namely, AMPSO, BISTRIS, DIPSO, TAPSO, TES and TRIS, whose structures can be found in Table 1. Protonation constants, as well as values for the CuL^+ complex stability constant (as log β) for all these Cu–$(L)_x$–$(OH)_y$ systems, are also summarized in Table 1. Additionally, protonation constants and log β for CuL^+ for Methylamine, Ethanolamine and Ammonia were also included (Table 1).

Regarding the basicity of the amino group, it is possible to verify that the substitution of hydroxyl groups in the ligand leads to a systematic decrease of pK_a values; for instance AMPSO, TAPS and TAPSO, which are structural related, have two, three and four hydroxyl groups, respectively, and a decrease of the protonation constant of about 0.7 and 0.8 log units was observed (Table 1). In contrast, the extent of the carbon chain increases the pK_a values. While TES has an ethanesulfonic acid chain, TAPS has a propanesulfonic acid and its pK_a value is about 0.8 log units higher than for TES (Table 1).

A simple evaluation based on the basicity of the ligands' amino groups, points out to enlargement in the stability constants values with the increase of the pK_a [24], which was observed for TES, TAPS and AMPSO, but for other buffers, this was not the case. To account for the different basicity of these ligands, a graphical representation of the $\log \beta_{ML}$ versus pK_a values was drawn (Fig. 5); with increasing ligand basicity, complex stability should also increase and for structurally related ligands straight lines should result [25].

Fig. 5 shows that TES, TRIS, TAPS, AMPSO fitted rather well to a straight line, indicating that with the increase of theirs pK_a values a linear increase of the stability constant was observed. Bellow that straight line, it is possible to find the stability constants for Ammonia, Ethanolamine and Methylamine. From these three ligands, Ethanolamine is closer to the straight line (Fig. 5), which is a hint that one hydroxyl group of TES, TRIS, TAPS, AMPSO and Ethanolamine, participate in the complex formation, forming a five-membered chelate ring. This is in agreement with the fact that crystal structures of copper(II) complexes with TRIS, determined by single-cristal X-ray data, evidenced that TRIS ligand coordinated via amino and hydroxymethylgroups forming a five-membered chelate ring [26,27]. Fig. 5 also evidenced that BISTRIS, DIPSO and TAPSO are above the straight line, indicating that the steric hindrance is diminished, by a stronger chelating effect. It is also possible to draw a second straight line with a negative slope with BISTRIS, DIPSO and TAPSO, as it is shown in Fig. 5. This line represents an increase of the chelating effect hence with the increase of pK_a the $\log \beta_{CuL}$ diminished (Fig. 5). This fact is probably due to additional formation of one or more five-membered chelate rings involving additional hydroxyl groups. Recently, the analysis of crystal Cu^{2+}-BIS-TRIS, by single crystal X-ray diffraction analysis, evidenced that BIS-TRIS acted as a neutral pentadentate ligand: four hydroxyl oxygen atoms and one nitrogen atom [28].

The comparative analysis of the strength of $Cu(TAPSO)^+$ and $Cu(TAPS)^+$ (Fig. 5) with the structures of the ligands (Table 1) suggests that the TAPSO's hydroxyl group near the sulfonic group is also involved in the coordination, forming the second additional five-membered chelate ring and increasing the

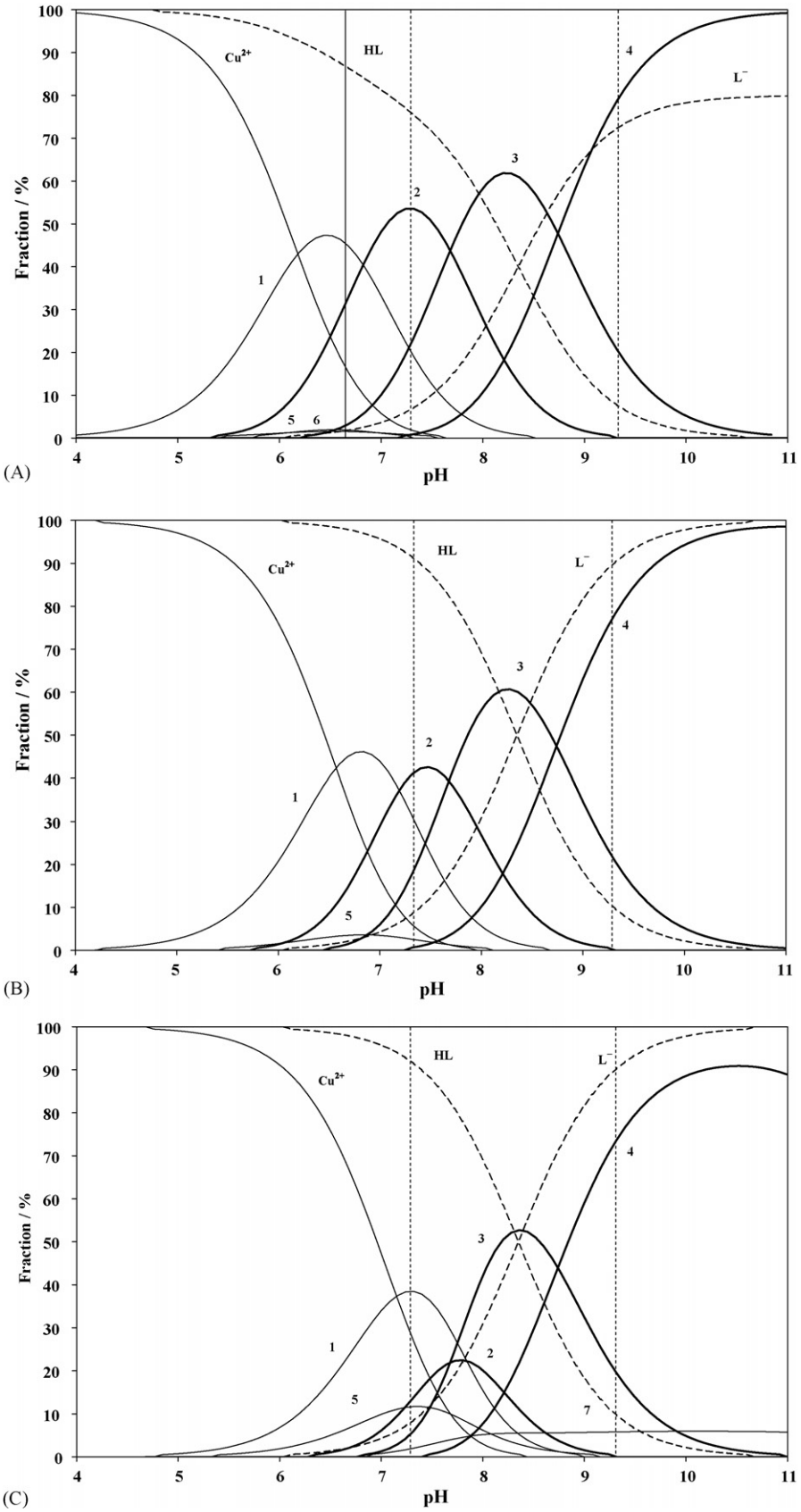


Fig. 4. Species distribution diagram for the final model of Cu–$(TAPS)_x$–$(OH)_y$ system. (A) $[L_T]:[Cu_T] = 10$, $[Cu_T] = 1.0 \times 10^{-3}$ M; (B) $[L_T]:[Cu_T] = 97.5$, $[Cu_T] = 4.0 \times 10^{-5}$ M; (C) $[L_T]:[Cu_T] = 151.6$, $[Cu_T] = 7.0 \times 10^{-6}$ M. The species present in the figure are: (1) CuL^+, (2) CuL_2, (3) $CuL_2(OH)^-$, (4) $CuL_2(OH)_2{}^{2-}$, (5) $Cu(OH)^+$ and (6) $Cu_2(OH)_2{}^{2+}$, (7) $Cu(OH)_2$, with stability constants set to, as $\log \beta$, 4.2, 7.8 13.9, 18.94, 6.1, 16.8 and 11.8, respectively. The vertical line indicates the pH at which precipitation was observed.

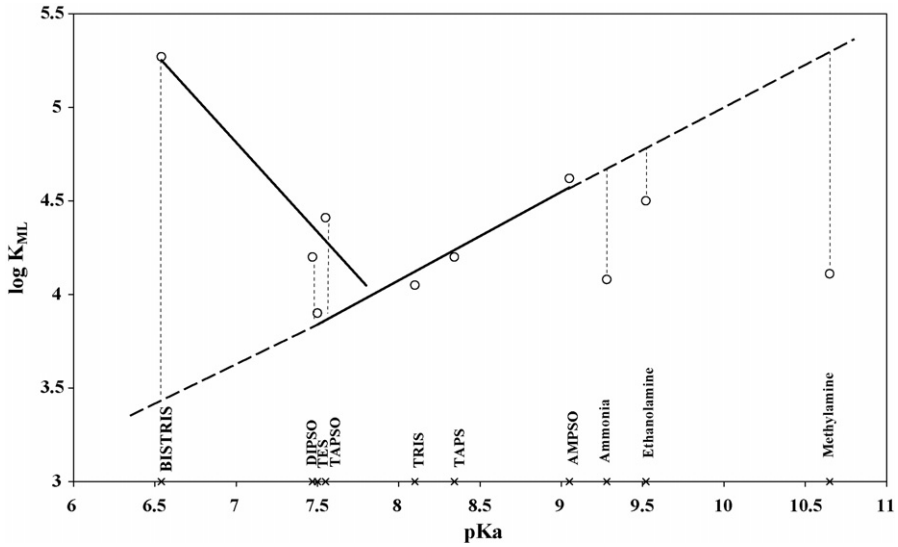


Fig. 5. Relationship between log β_{CuL} and pK_a for Cu^{2+} and several biological buffers and other amines.

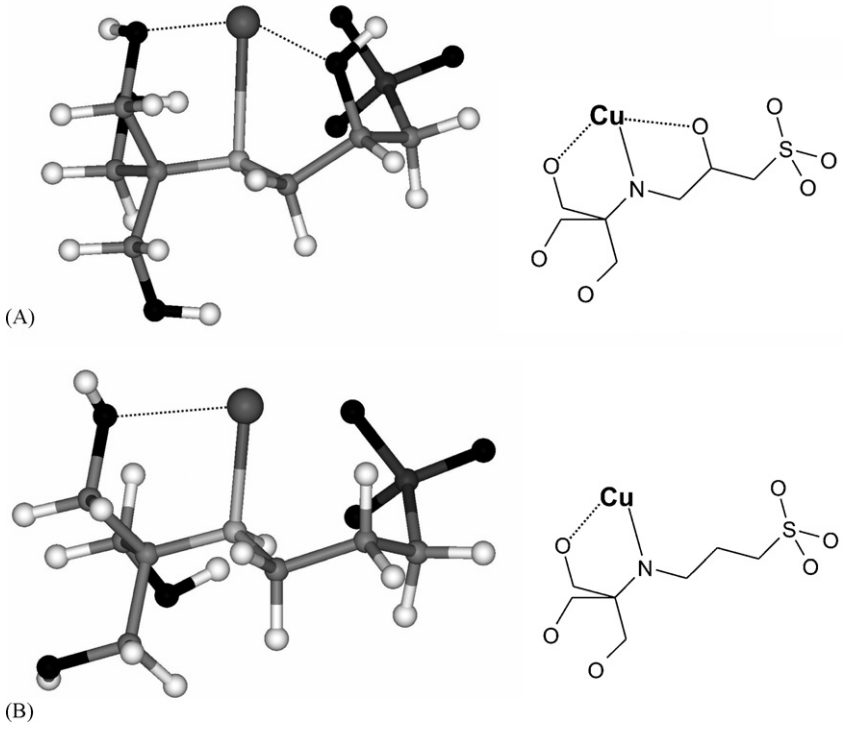


Fig. 6. Proposed structures for $Cu(TAPSO)^+$ (A) and $Cu(TAPS)^+$ (B) complexes. For $Cu(TAPSO)^+$ complex, copper coordination to TAPSO' amino group and two hydroxyl groups forming two five-membered chelate rings is shown (A). For $Cu(TAPS)^+$ complex, the coordination via amino and one of the β-hydroxy groups of TAPS forming only one five-membered chelate ring (B) is shown.

stability of the CuL complex. Thus, TAPSO is most likely a tridentate ligand, coordinating by the amino group and by two hydroxyl groups, forming two five-membered chelate rings. On the other hand, TAPS is most likely a bidentate ligand coordinating via amino and one of the β-hydroxy groups forming one five-membered chelate ring. The proposed structures for $Cu(TAPSO)^+$ and $Cu(TAPS)^+$ complexes are illustrated in Fig. 6.

4. Conclusions

Results present herein demonstrated that the polarographic technique of speciation and refinement of stability constants for reversible (and quasi-reversible) metal ions, employed in this work, gave a significative contribute on the characterization of metal-ligand systems for which other available techniques were unable to. The use of DCP became determinant for full and

adequate characterization of the systems due to the following reasons: (i) complexation occurs in the region of copper hydrolysis and $Cu(OH)_2$ precipitation and (ii) ligands are very simple with no double bonds, which disabled the use of fluorescence and UV–vis for which low concentration of ligands (between 10^{-7} and 10^{-4} M) could be applied if ligands absorbed.

Acknowledgements

The authors thank the "Fundação para a Ciência e a Tecnologia" from Portuguese Government for the financial support of this work with FEDER funds, by the project POCTI/39950/QUI/2001. One of us (Carina Machado) is also gratefully acknowledged for a grant scholarship financed under the project POCTI/39950/QUI/2001. We also thank Professor Ignacy Cukrowski from University of Pretoria, South Africa for polarographic modelling software (3D-CFC program) and Professor Carlos Gomes from the Faculty of Sciences/Porto University for the COPOTISY program. A special thanks to Rute Fonseca for drawing the structures of the complexes.

References

[1] Fluka and Riedel-de-Haen, Laboratory Chemicals and Analytical Reagents, 2005/2006.
[2] Sigma, Biochemicals and Reagents for Life Science Research, 2005.
[3] C.M.M. Machado, S. Scheerlinck, I. Cukrowski, H.M.V.M. Soares, Anal. Chim. Acta 518 (2004) 117.
[4] C.M.M. Machado, I. Cukrowski, P. Gameiro, H.M.V.M. Soares, Anal. Chim. Acta 493 (2003) 105.
[5] R.M. Smith, A.E. Martell, NIST Standard Reference Database 46 NIST Critically Selected Stability Constants of Metal Complexes Database. Version 3. 0, US Department of Commerce, National Institute of Standards and Technology, 1997.
[6] H.M.V.M. Soares, S.C. Pinho, G.R.T.M. Barros, Electroanalysis 11 (1999) 1312.
[7] Q.Y. Yu, A. Kandegedara, Y.P. Xu, D.B. Rorabacher, Anal. Biochem. 253 (1997) 50.
[8] M. Sokolowska, W. Bal, J. Inorg. Biochem. 99 (2005) 1653.
[9] M.F. Frasco, D. Fournier, F. Carvalho, L. Guilhermino, Biomarkers 10 (2005) 360.
[10] F. Hayase, T. Shibuya, J. Sato, M. Yamamoto, Biosci. Biotechnol. Biochem. 60 (1996) 1820.
[11] J.L. Westrup, M.B. Fritzen, A.J. Souza, G.C. Bedendo, F. Nome, H.D. Fiedler, J. Braz. Chem. Soc. 16 (2005) 982.
[12] E. Fischer, C.M.G. Van Den Berg, Anal. Chim. Acta 432 (2001) 11.
[13] C.M.M. Machado, I. Cukrowski, H.M.V.M. Soares, Helvetica Chim. Acta 86 (2003) 3288.
[14] J.J. Lee, W.T. Ford, J. Am. Chem. Soc. 116 (1994) 3753.
[15] D. Nurok, M.C. Frost, D.M. Chenoweth, J. Chromatogr. 903 (2000) 211.
[16] H. Choi, Y. Kim, Bull. Korean Chem. Soc. 24 (2003) 943.
[17] T.N. Chiesl, W. Shi, A.E. Barron, Anal. Chem. 77 (2005) 772.
[18] I. Cukrowski, Anal. Chim. Acta 336 (1996) 23.
[19] I. Cukrowski, M. Adsetts, J. Electroanal. Chem. 429 (1997) 129.
[20] P.M. May, K. Murray, D.R. Williams, Talanta 32 (1985) 483.
[21] P.M. May, K. Murray, D.R. Williams, Talanta 35 (1988) 825.
[22] E. Hogfeldt, Stability Constants of Metal–Ion Complexes. Part A. Inorganic Ligands, Pergamon Press, 1982.
[23] Metrohm Application–Bulletin no 36, Herisau, Switzerland, 1975.
[24] A.E. Martell, R.D. Hancock, Metal Complexes in Aqueous Solutions, Plenum Press, New York and London, 1996.
[25] K.H. Scheller, T.H.J. Abel, P.K. Polanyi, B.E. Fischer, H. Sigel, Eur. J. Biochem. 107 (1980) 455.
[26] S. Kotila, J. Valkonen, Acta Chemica Scandinavica 47 (1993) 957.
[27] S. Kotila, J. Valkonen, Acta Chemica Scandinavica 48 (1994) 200.
[28] Y. Inomata, Y. Gochou, M. Nogami, F.S. Howell, T. Takeuchi, J. Mol. Struct. 702 (2004) 61.

Available online at www.sciencedirect.com
ScienceDirect
Talanta 71 (2007) 1326–1332
Talanta
www.elsevier.com/locate/talanta

Modelling of Pb–$(TAPS)_x$–$(OH)_y$ system and refinement of stability constants in the region of lead hydrolysis and lead hydroxide precipitation

Carina M.M. Machado [a], Olle Victoor [a,b], Helena M.V.M. Soares [a,*]

[a] *REQUIMTE, Department of Chemical Engineering, Faculty of Engineering, University of Porto, Rua Dr. Roberto Frias, 4200-465 Porto, Portugal*
[b] *KaHo St.-Lieven, Industrial Engineering, Department Biochemistry-Microbiology, Gebroeders Desmetstraat 1, B-9000 Gent, Belgium*

Received 7 October 2005; received in revised form 28 June 2006; accepted 6 July 2006
Available online 27 September 2006

Abstract

The influence of [(2-hydroxy-1,1-bis(hydroxymethyl)ethyl)amino]-1-propanesulfonic acid (TAPS) on solutions containing lead(II) was studied by direct current polarography (DCP) and glass electrode potentiometry (GEP). The readings were taken at fixed total TAPS to total lead(II) concentration ratios and various pH values, at 25.0 ± 0.1 °C and ionic strength 0.1 M KNO_3.

Due to the basic pK_a of the ligand, which occurs in the pH range where large amount of lead polynuclear species are formed, and the occurrence of ligand adsorption, that disabled the use of high concentrations of TAPS on DCP experiments, GEP and DCP experimental conditions were put to the limit in order to provide the correct Pb–TAPS–OH model and reliable stability constants.

The proposed final model is: PbL, PbL_2, $PbL_2(OH)$ and $PbL_2(OH)_2$ with overall stability constants values, as $\log \beta$, 3.27 ± 0.06, 6.5 ± 0.1, 12.7 ± 0.1 and 17.27 ± 0.06, respectively.

A comparative analysis of the strength of complexation of TAPS and a structural related buffer, 2-hydroxy-3-[tris(hydroxymethyl)methylamino]-1-propanesulfonic acid (TAPSO), with lead is also discussed.
© 2006 Elsevier B.V. All rights reserved.

Keywords: TAPS; [(2-Hydroxy-1,1-bis(hydroxymethyl)ethyl)amino]-1-propanesulfonic acid; Biological buffers; Lead; Stability constants; Electrochemical techniques

1. Introduction

Hydrogen ion concentration plays an important role in the chemistry of aqueous solutions because it competes with metallic cations in solution for ligand binding sites. Therefore, metal ion speciation studies are usually carried out at a constant pH to simplify the interpretation of the results. For this purpose, it is frequently necessary to add a pH buffer. However, the choice of a pH buffer may constitute an important problem since many of them (inorganic or organic ones) traditionally used are also complexing agents and may disturb the equilibrium state. For example, 2-amino-2-(hydroxymethyl)-1,3-propanediol (TRIS) is a pH buffer currently used for speciation studies [1–4], even though it complexes metal ions [5].

The biological buffer [(2-hydroxy-1,1-bis(hydroxymethyl) ethyl)amino]-1-propanesulfonic acid (TAPS) is chemically related with TRIS and has a pK_{a2} value that allows buffering the pH in the range between 7.3 and 9.3, which covers the range of pH that occurs in the environmental systems. So, TAPS can be an alternative choice when heavy metal speciation studies are undertaken.

TAPS is now commercially available at least by two major chemical suppliers [6,7]. However, because TAPS contains hydroxyl groups in addition to amine nitrogen, as it happens with TRIS, metal complexes of TAPS is expected to be formed in environmental systems containing metal ions when this compound is used to control the pH.

As far as we know, no reports regarding studies of the interaction between TAPS and lead are described in the literature. Thus, we think that the knowledge of the stability constants for Pb–$(TAPS)_x$–$(OH)_y$ system will upgrade the information about the stability constants of ions complexation with biological buffers commercially available.

In the present work, we report the overall stability constants for the species formed between TAPS and lead ion, which is an important environmental metal ion, at 0.1 M KNO_3

* Corresponding author. Tel.: +351 225081650; fax: +351 225081449.
E-mail address: hsoares@fe.up.pt (H.M.V.M. Soares).

0039-9140/$ – see front matter © 2006 Elsevier B.V. All rights reserved.
doi:10.1016/j.talanta.2006.07.016

ionic strength and 25.0 ± 0.1 °C. The characterization of the Pb–$(TAPS)_x$–$(OH)_y$ system was done by direct current polarography (DCP) using total ligand to total metal concentration ($[L_T]$:$[Pb_T]$) ratios of various orders of magnitude. Glass electrode potentiometry (GEP) only allowed confirming the stability constant value of PbL and $PbL_2(OH)$ complexes. Experiments by alternating current polarography (ACP) were also carried out to check if TAPS adsorbs at the mercury working electrode surface, under the experimental conditions used.

2. Experimental

2.1. Materials and reagents

The ligand TAPS (99.4%) was purchased from Sigma–Aldrich (St. Louis, MO, USA) and used as received. The standard lead solution, 9.6×10^{-3} M, was purchased from Merck.

Additional information about the remaining reagents and experimental conditions were described previously [8].

2.2. Apparatus

All experiments were carried out in a Metrohm (Herisau, Switzerland) jacketed glass vessel, equipped with a magnetic stirrer, and thermostatted at 25.0 ± 0.1 °C using a water bath.

2.2.1. Polarography

Polarographic measurements were performed using a Model 663 VA stand (Metrohm) equipped with a multimode electrode (Metrohm, Model 6.1246.020) as a working electrode, used in the dropping mercury electrode mode. A silver/silver chloride (3 M KCl) and a glassy carbon were used as reference and counter electrodes, respectively (both from Metrohm). The VA stand was attached to a microAutolab (Eco Chemie, Utrecht, The Netherlands) system controlled by a personal computer. A drop time of 1 s and a step potential of 4 mV were used.

The pH measurements were conducted with a GLP 22 pH meter Crison (Barcelona, Spain) with a sensitivity of ±0.1 mV (±0.001 pH units), with a silver/silver chloride reference electrode (Metrohm) and a glass electrode (Metrohm).

2.2.2. Potentiometry

The potentiometric titrations were performed with a PC-controlled system assembled with a Crison MicropH 2002 meter, a Crison MicroBU 2030 micro burette, a Philips GAH 110 glass electrode and an Orion 90-02-00 (double junction) reference electrode with the outer chamber filled with 0.1 M KNO_3. Automatic acquisition of data was done using a home-made program, COPOTISY.

2.3. Procedure

2.3.1. Calibration of the glass electrode

For both techniques used, the calibration of the glass electrode (pH measured as $-\log[H^+]$) was accomplished as previously described [9].

2.3.2. Alternating current polarography

In order to evaluate the adsorption of the ligand TAPS on the surface of the mercury of the working electrode, ACP polarograms were run in the absence of the metal ion. The experimental conditions used were described elsewhere [10].

2.3.3. Direct current polarography

The study of the electrochemical behaviour of Pb–$(TAPS)_x$–$(OH)_y$ system was performed by direct current polarography. The procedure used to run the polarographic titrations was described previously [8]. Three $[L_T]$:$[Pb_T]$ ratios were used, 41.5, 88.7 and 124.3, with $[Pb_T]$ of 9.9×10^{-5}, 9.6×10^{-6} and 2.4×10^{-5} M, respectively. The scanned pH range varied between 4.8 and 10.4. About 70 points were obtained for each ratio.

2.3.4. Glass electrode potentiometry

For studying potentiometrically the Pb–$(TAPS)_x$–$(OH)_y$ system, one $[L_T]$:$[Pb_T]$ ratio was performed: $[L_T]$:$[Pb_T] = 6.2$ with $[Pb_T] = 9.7 \times 10^{-4}$ M (five titrations were performed using two independent solutions; for each titration, about 70 points were collected between pH 5.0 and 9.5) Monotonic additions of standardized KOH 0.1 M were done.

2.4. Data treatment

The refinement of polarographic data was done using the Cukrowski method; all the equations that support theoretically the method were defined elsewhere [11]. This method uses mass-balance equations written for a labile (on the polarographic time scale) and reversible metal–ligand system studied at a fixed total ligand to total metal concentration ratio and varied pH. The refinement operations were performed using the polarographic program 3D-CFC [12] and are based on the comparative analysis of the experimental and calculated complex formation curves (ECFC and CCFC, respectively) (Eqs. (1) and (2), respectively) [11,13]:

$$(E(\mathrm{M}) - E(\mathrm{comp}))_{\mathrm{pH}(i)} - \frac{RT}{nF} \ln \left(\frac{I(\mathrm{comp})}{I(\mathrm{M})} \right)_{\mathrm{pH}(i)} = f(\mathrm{pH}) \quad (1)$$

$$\frac{RT}{nF} \ln \left(\frac{[\mathrm{M_T}]}{[\mathrm{M}]} \right)_{\mathrm{pH}(i)} = f(\mathrm{pH}) \quad (2)$$

where E(M), I(M) and E(comp), I(comp) stand for the potential (half-wave $E_{1/2}$) and current (limiting diffusion I_d) in the absence and the presence of metal complexes, respectively. The total metal ion $[M_T]$ and ligand $[L_T]$ concentrations are known at any stage of the experiment, calculated from mass-balance equations. The refinement of stability constants is achieved by the computation of the free metal ion concentration [M] from mass-balance equations written for the assumed model. The computed [M] is used by Eq. (2). During the iterative operation, the values of refined stability constants are varied. The refinement operation is completed when the CCFC fits best the experimental objective function, e.g., the ECFC.

Table 1
Protonation constants for water, TAPS and overall stability constants for Pb(II) complexes with OH^-, at 25.0 °C

	Equilibrium	log β	μ	References
Water	$H^+ + OH^- \Leftrightarrow H_2O$	13.78	0.1	[5]
TAPS	$L^- + H^+ \Leftrightarrow HL$	8.342	0.1	[10]
Lead	$Pb^{2+} + OH^- \Leftrightarrow Pb(OH)^+$	6.0	0.1	[5]
	$Pb^{2+} + 2OH^- \Leftrightarrow Pb(OH)_2$	10.3	0.5	[5]
	$Pb^{2+} + 3OH^- \Leftrightarrow Pb(OH)_3^-$	13.3	0.5	[5]
	$3Pb^{2+} + 4OH^- \Leftrightarrow Pb_3(OH)_4^{2+}$	31.7	0.5	[5]
	$4Pb^{2+} + 4OH^- \Leftrightarrow Pb_4(OH)_4^{4+}$	35.5	0.1	[5]
	$6Pb^{2+} + 8OH^- \Leftrightarrow Pb_6(OH)_8^{4+}$	67.4	0.5	[5]
	$Pb(OH)_2$ (s) $\Leftrightarrow Pb^{2+} + 2OH^-$	−16.1	0.0	[16]

The simulation and optimization of model and complex formation constants from potentiometric titrations data were performed using ESTA program [14,15]. The refinement operations used in potentiometry involve solving mass-balance equations, including equation for the total proton concentration, in such a way that the computed free proton concentration reproduces the experimental recorded potential of the glass electrode.

During the refinement operations of the different systems, the water [5] and ligand [10] protonation constants, as well as all known formation constants for lead hydroxide species, $Pb_x(OH)_y$ [5], were kept fixed (Table 1).

3. Results and discussion

3.1. TAPS adsorption and lead reversibility studies

Because metal stability constants calculated by polarographic techniques can be influenced by the ligand adsorption, the best experimental conditions would be in the absence of adsorption of the ligand. ACP at a phase angle of 90° was used to test if there was adsorption of TAPS at the mercury electrode surface. This phase angle was chosen because the capacitive current is maxima and a non-Faradaic process is expected; thus, under these experimental conditions, the current is mainly capacitive in nature and proportional to the double layer capacity.

The adsorption effect can be quantified by comparing the AC polarograms for the background solution with the polarograms obtained with increasing ligand additions. Fig. 1 shows the variation in the capacitive current (expressed in percentage) obtained with the increase of ligand concentration relatively to the background solution (0.1 M KNO_3), at a reduction potential typical for Pb^{2+} (−0.35 V [17]), for three pH values, pH 6.34, 8.34 and 10.34.

For pH 6.34, where the ligand is totally in the HL form, the variation in the capacitive current with the increase of the ligand concentration was less than 5% for all the TAPS concentration range tested. At pH 10.34, the variation in the capacitive current was slightly pronounced than for other pH values, being recorded a variation of 19% for the highest TAPS concentration tested, 1.2×10^{-2} M; for 3.0×10^{-3} M of TAPS, about 9% variation in the capacitive current was observed. This increase of the adsorption effect in the region of zero charge potential (about −0.4 V), i.e., the region where the surface of mercury electrode has no charge, suggests that, at this potential, the adsorption of TAPS is mainly due to the uncharged part of the ligand. For pH = pK_a (where the ligand exists one-half in the protonated form, HL, and one-half in the deprotonated form, L^-), a midway situation between the other ones was recorded (Fig. 1). The results described above point out that a maximum TAPS concentration of 3.0×10^{-3} M should be used for studying Pb–$(TAPS)_x$–$(OH)_y$ system by DCP.

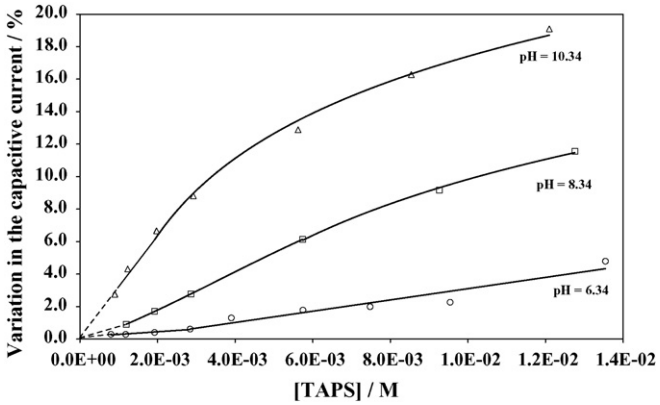


Fig. 1. Variation in the capacitive current recorded by ACP with the increase of TAPS concentration at three pH values, 6.34, 8.34 and 10.34. The values, expressed in percentage, were calculated from the difference between the capacitive current recorded in the presence and in the absence of the buffer, at −0.35 V, from ACP curves with a phase angle of 90° in 0.1 M KNO_3.

The analysis of polarographic titrations for Pb–$(TAPS)_x$–$(OH)_y$ system showed that the addition of the ligand caused a decrease in the recorded DC wave of the metal of about 20% and the position of the polarographic signal has changed by about 3 mV towards more positive values for both ratios. This could be due to some minor adsorption effect. To correct for that phenomenon, the half-wave potential and the diffusion current of the metal ion in the presence of the ligand (values recorded in a pH region where no complexation occurs) was used, as a reference point, for computing the shift in the peak potential. In addition, the wave steepness values did not change significantly (values varied between 0.9 and 1.0) for all the titrations performed, indicating that lead reduction process at the mercury electrode surface was fully reversible.

3.2. DCP graphical prediction of species present in solution

The analysis of DC polarographic data in all the pH range tested showed that Pb–$(TAPS)_x$–$(OH)_y$ system behaved as labile and dynamic on the polarographic time scale; only one peak corresponding to all labile species present in solution, which shifted to more cathodic potential values, was observed (Fig. 2). This figure shows a decrease of the limiting current of the polarograms recorded along the polarographic titration with the increase of pH. This fact can be explained by several reasons: (i) a dilution effect (which is a minor effect), (ii) coefficient diffusion of the complexes lower than the coefficient diffusion of the lead ion and probably (iii) formation of quasi-labile complexes.

For DCP data, species prediction present in solution was accomplished by graphical analysis and interpretation of the

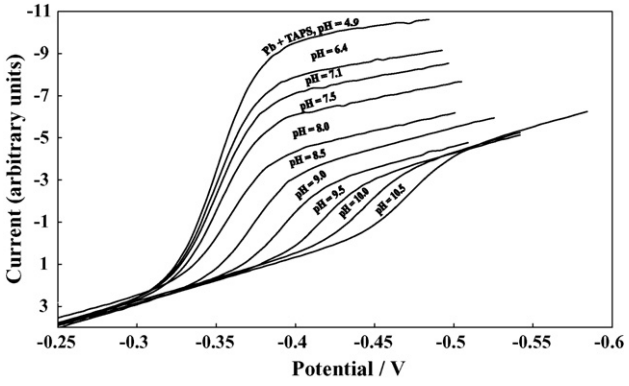


Fig. 2. Typical DC polarograms of lead in the presence of TAPS with the increase of the pH. No correction for dilution was made (curves are seen as recorded).

slopes of the variation of the observed half-wave potential shift as a function of the pH (Fig. 3A) and of the logarithm of the free ligand concentration (Fig. 3B). As an example, the results obtained for $[L_T]$:$[Pb_T] = 41.5$ will be analyzed below. Similar results were obtained for the other $[L_T]$:$[Pb_T]$ ratios (data not shown).

From Fig. 3A, three regions and two slopes were identified in all the pH region analyzed. The value of the protonation constant and the respective forms of the ligand were also marked in the figure. The possible reactions at the dropping mercury electrode (DME), according to the pH of the solution, are also marked in the figure (charges were omitted for sake of simplicity). The first slope, drawn between pH 7.1 and 7.7, has a value of 30 mV/pH. This value indicates some interaction between lead and TAPS, as PbL species; when one proton is involved in the reaction at the DME electrode (formation of PbL) a theoretical slope of 29.5 mV/pH should be obtained, as it is indicated in Fig. 3A. Additionally, the reduction of Pb(OH) species also develops a slope of similar magnitude (Fig. 3A). Between pH 7.7 and 10.4, a slope of 51 mV/pH was recorded (Fig. 3A). In this wide pH region, one must pay attention to the predominate form of the ligand present in solution, as is indicated in the figure. Up to pH 8.34, the possible species present in solution are: PbL(OH) and PbL_2 species and $Pb(OH)_2$ metal hydroxide species. The presence in solution of PbL(OH) and PbL_2 species would result in a theoretical slope of 59 mV/pH, and the recorded slope is very close to this value (51 mV/pH). Probably it still exists in solution some PbL species, causing the little drop in the theoretical slope from 59 to 51 mV/pH. The reduction of the metal hydroxide, $Pb(OH)_2$, should also be considered (slope = 59 mV/pH, see reactions in Fig. 3A). However, the formation of this metal hydroxide species, as a major one, should be excluded since no precipitation was observed up to pH 10.4; this clearly indicates that the ligand must be involved in the complex formation with lead. Above the pK_a, from 8.34 up to 10.4, the occurrence of a non-Nernstian slope, 51.0 mV/pH, is explained if the coexistence of all the hydroxide species, $PbL_x(OH)_y$ (x and $y = 1$ and 2), in solution at this pH range is considered (see reactions in Fig. 3A). The presence of $PbL_x(OH)_2$ species in solution, with a theoretical slope to 59 mV/pH, is probably the major species present in solution in this last pH region (Fig. 3A), resulting a slope closer to 59 mV/pH than to 29.5 mV/pH.

The formation of PbL_n species was evaluated by the graphical analysis of the observed half-wave potential shift versus log[L] (Fig. 3B). The presence of PbL and PbL_2 in solution was clearly evidenced since slopes of 29 and 60 mV/log[L], respectively, were obtained.

From the graphical analysis described above, the proposed model for Pb–$(TAPS)_x$–$(OH)_y$ system should include PbL, PbL_2 and $PbL_x(OH)_2$ species. In order to have a sequence of complexes, the species $PbL_x(OH)$, should also be tested in the fitting procedures.

3.3. Modelling and optimization of the stability constants: DCP and GEP

The modelling procedures and the optimization of the stability constants were performed using the ECF and CCF curves assuming different models shown in Table 2 and Fig. 4.

In this figure, the corrected shift in half-wave potential (ECFC curve), calculated according to Eq. (1), was plotted in function of pH. The CCF curve for lead hydroxide species (dashed line) was also included in the figure. The comparison between the former curve (dashed line) and the ECFC clearly shows the occurrence of complexation between lead and TAPS; in the absence of TAPS complexation, precipitation would occur around pH 8.0 and that

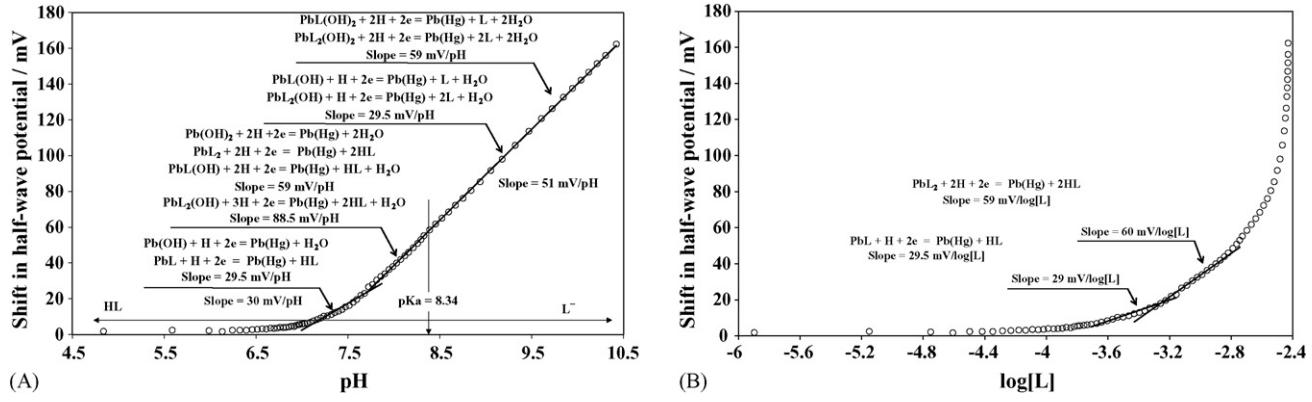


Fig. 3. Interpretation of the DCP experimental data for Pb–$(TAPS)_x$–$(OH)_y$ system involving the corresponding slopes and electrochemical reactions at the DME electrode surface for $[L_T]$:$[Pb_T] = 41.5$, $[Pb_T] = 9.9 \times 10^{-5}$ M, 0.1 M KNO_3 at 25.0 °C. Variation in the half-wave potential shift with the pH (A) and log[L] (B).

Table 2
Refinement of the stability constants (as log β) obtained for Pb–$(TAPS)_x$–$(OH)_y$ system by polarography ($[L_T]:[Pb_T] = 88.7$, $[Pb_T] = 9.6 \times 10^{-6}$ M, 58 points collected between pH 7.4 and 10.0; $[L_T]:[Pb_T] = 41.5$, $[Pb_T] = 9.9 \times 10^{-5}$ M, 78 points collected between pH 4.8 and 10.4) and by potentiometry ($[L_T]:[M_T] = 6.2$, $[Pb_T] = 9.7 \times 10^{-4}$ M, two titrations, 59 points collected between pH 4.4 and 7.6)

Complexes	DCP experiments				GEP experiments	
	$[L_T]:[Pb_T] = 41.5$		$[L_T]:[Pb_T] = 88.7$		$[L_T]:[Pb_T] = 6.2$	
	Model 1	Model 2	Model 1	Model 2	Model 1	Model 2
PbL, $Pb + L \Leftrightarrow PbL$	3.0 (F)	3.28 ± 0.05	3.0 (F)	3.0 ± 0.1	3.14 ± 0.06	3.25 ± 0.04
PbL(OH), $Pb + L + OH \Leftrightarrow PbL(OH)$	9.99 ± 0.01	NI	9.11 ± 0.03	NI	9.51 ± 0.06	NI
$PbL(OH)_2$, $Pb + L + 2OH \Leftrightarrow PbL(OH)_2$	14.89 ± 0.01	NI	14.25 ± 0.08	NI	R	NI
PbL_2, $Pb + 2L \Leftrightarrow PbL_2$	R	6.5 ± 0.1	R	R	R	R
$PbL_2(OH)$, $Pb + 2L + OH \Leftrightarrow PbL_2(OH)$	NI	12.83 ± 0.02	NI	12.56 ± 0.03	NI	12.47 ± 0.05
$PbL_2(OH)_2$, $Pb + 2L + 2OH \Leftrightarrow PbL_2(OH)_2$	NI	17.22 ± 0.01	NI	17.31 ± 0.01	NI	R
SD (mV)	3.21	0.764	0.977	0.549		
Hamilton R-factor					0.0723	0.0616

For DCP, SD represents an overall fit of complex formation curves, the computed curve in the objective experimental function [8]; for GEP, Hamilton R-factor stands for a statistical Hamilton R-factor generated by the program ESTA [15]; NI, not included; R, rejected; F, fixed value.

was not observed. It is also possible to see that the gap between the calculated curve for the lead hydroxide species and the experimental data has a maximum difference of about 52 mV, which indicates without any doubt that complexes between lead and TAPS are formed, besides the metal hydroxide complexes.

In order to have a sequence of formed species, the refinement procedures started with two simple models: Model 1, $PbL + PbL(OH) + PbL(OH)_2 + PbL_2$, and Model 2, $PbL + PbL_2 + PbL_2(OH) + PbL_2(OH)_2$. The results obtained for two $[L_T]:[Pb_T]$ ratios are summarized in Table 2.

For Model 1, for all DCP ratios analyzed, PbL_2 was always rejected; this fact is in disagreement with the graphical analysis of Fig. 3B. Also for this model, PbL is systematically rejected. These facts suggest that this model does not explain the experimental results. The refinement of Model 2 for all DCP ratios proved to be the model that better fitted the experimental results, with lower standard deviation. For the $[L_T]:[Pb_T]$ ratio 88.7, PbL_2 was also rejected and PbL was refined to a low value (Model 2; Table 2). This fact just evidences that probably Pb(OH) is the major species becoming complicated the refinement of other species present in solution at lower quantity. For the $[L_T]:[Pb_T]$ ratio 41.5, it was possible to refine all species. The CCFC for this ratio and for Model 2 was included in Fig. 4. From a statistical point of view, Model 2, $PbL + PbL_2 + PbL_2(OH) + PbL_2(OH)_2$, fitted the experimental results, for all $[L_T]:[Pb_T]$ ratios, with lower standard deviation than Model 1, suggesting that Model 2 reproduces better the experimental data.

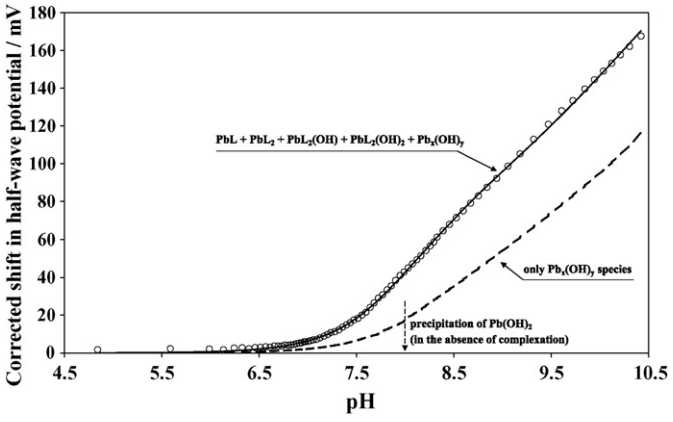


Fig. 4. Experimental (circles) and calculated (lines) complex formation curves obtained for the models indicated in the figure for DCP data: $[L_T]:[Pb_T] = 41.5$, $[Pb_T] = 9.9 \times 10^{-5}$ M, at 25.0 °C and 0.1 M KNO_3. Values of the stability constants used for the models are summarized in Table 2. CCFC for $Pb_x(OH)_y$ complexes was also included (dashed line).

In order to provide more information, we decided to run GEP titrations. This technique, which works at much lower $[L_T]:[M_T]$ ratios, can provide important information for the characterization of the system under study. $[L_T]:[Pb_T]$ ratios 6.2 was tested, with $[Pb_T] = 9.7 \times 10^{-4}$ M. Due to the precipitation of the metal hydroxide species, GEP titration was only possible to run up to pH 7.8. The adopted strategy for refinement of data is synthesized in Table 2. The refinement of the Model 1 ($PbL + PbL(OH) + PbL(OH)_2 + PbL_2$) and Model 2 ($PbL + PbL_2 + PbL_2(OH) + PbL_2(OH)_2$), resulted in the rejection of $PbL_x(OH)_2$ species, due to the lack of data points at high pH values. Even though, there were no experimental evidences of the formation of PbL_2 species, attempts to include it were made; the refinement operations always resulted in its rejection (Models 1 and 2; Table 2). Also, for $[L_T]:[Pb_T]$ ratio 6.2, the model constituted by $PbL + PbL_2(OH)$ fitted better the experimental data than model constituted by $PbL + PbL(OH)$ (Hamilton R-factor lower for Model 2; Table 2).

It is important to emphasize the good agreement for PbL and $PbL_2(OH)$ overall stability constants refined from DCP and GEP data (Table 2). This fact evidenced that even though a slight adsorption of the ligand (less than 3% at pH 8.34) was predicted from ACP experiments (Fig. 1), the values of stability constants obtained from DCP and GEP are very similar. In addition, these results also evidence that no significant induced adsorption of complexes have occurred.

Gathering the information obtained from GEP and DCP data just described above, it is possible to say that the model for Pb–$(TAPS)_x$–$(OH)_y$ system should include the species:

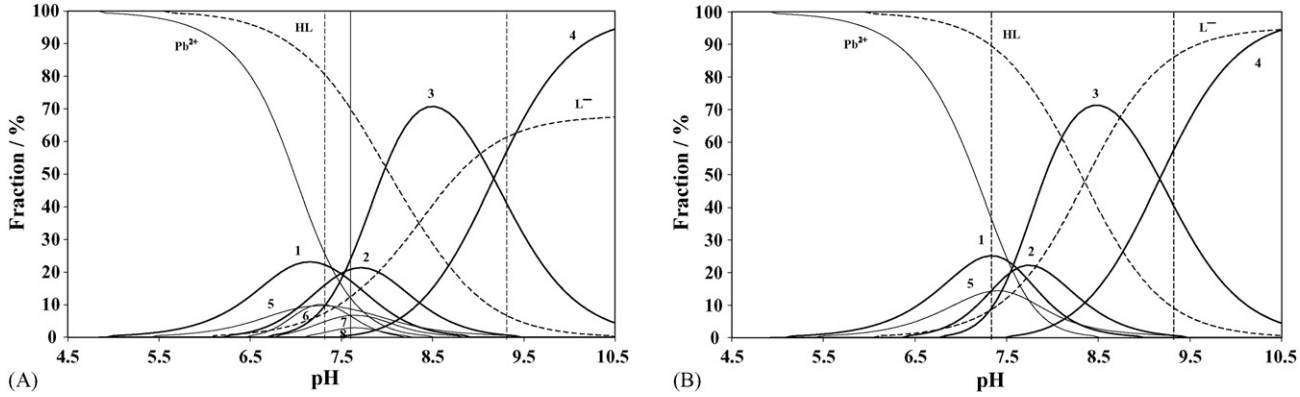


Fig. 5. Species distribution diagrams computed for Pb–$(TAPS)_x$–$(OH)_y$ system. GEP experimental conditions: $[L_T]:[Pb_T] = 6.2$ (A), with $[Pb_T] = 9.7 \times 10^{-4}$ M. DCP experimental conditions: $[L_T]:[Pb_T] = 41.5$ (B), with $[Pb_T] = 9.9 \times 10^{-5}$ M. The metal–ligand model consisted of PbL (1), PbL_2 (2), $PbL_2(OH)$ (3), $PbL_2(OH)_2$ (4), Pb(OH) (5), $Pb_4(OH)_4$ (6), $Pb_3(OH)_4$ (7) and $Pb_6(OH)_8$ (8) for which stability constants, as $\log \beta$, were set to 3.27, 6.5, 12.7, 17.27, 6.0, 35.5, 31.7 and 67.4, respectively. The solid vertical line indicates the pH at which precipitation is predicted.

PbL, PbL_2, $PbL_2(OH)$ and $PbL_2(OH)_2$. In a first attempt, the following overall stability constants values for PbL, PbL_2, $PbL_2(OH)$ and $PbL_2(OH)_2$ could be proposed: 3.1 ± 0.2, 6.5 ± 0.1, 12.6 ± 0.2 and 17.3 ± 0.1, respectively. Note that standard deviations indicate here the ranges in stability constants refined from Model 2 of all ratios tested by DCP and GEP (Table 2).

To test the proposed model, species distribution diagrams (SDD) were generated for $[L_T]:[Pb_T]$ ratios 6.2 (GEP experimental conditions) and for the $[L_T]:[Pb_T]$ ratios 41.5 (DCP experimental conditions) (Fig. 5). For $[L_T]:[Pb_T]$ ratio 6.2, the first analysis of the SDD shows the existence of several polynuclear lead species (Pb(OH), $Pb_3(OH)_4$, $Pb_4(OH)_4$ and $Pb_6(OH)_8$) prior the precipitation predicted to occur at about 7.8 and this was just observed (Fig. 5A); thus, only PbL species was possible to refine accurately. For $[L_T]:[Pb_T] = 88.7$ (data not shown), SDD evidenced that, PbL is a minor species, since it is completely covered by Pb(OH); almost 50% of Pb(OH) is formed and only 9% of PbL in the same pH range. For $[L_T]:[Pb_T] = 41.5$ (Fig. 5B), SDD shows that even though Pb(OH) exists in high amount (about 18%), PbL predominates and therefore, it was possible to refine this species (Table 2). Based on the amount of the PbL complex formed in the various $[L_T]:[Pb_T]$ tested, only the refined values coming from Model 2 of GEP and from DCP ($[L_T]:[Pb_T] = 41.5$) were considered for calculating the final overall stability constant value $\log \beta_{PbL} = 3.27 \pm 0.06$.

For $[L_T]:[Pb_T]$ ratio 88.7, SDD predicts, besides the formation of PbL and Pb(OH), the formation of PbL_2 (6%), $PbL_2(OH)$ (49%) and $PbL_2(OH)_2$ (79%) (data not shown). This clearly shows that, for this ratio, no appropriate conditions were available to refine accurately other species besides $PbL_2(OH)$ and $PbL_2(OH)_2$. Therefore, the final overall stability constant for PbL_2 species was only possible to be refined from $[L_T]:[Pb_T]$ ratio 41.5, being the value 6.5 ± 0.1. The final stability constant value for $PbL_2(OH)$ was calculated considering the values coming from $[L_T]:[Pb_T]$ ratios 41.5 (see also Fig. 5B) and 88.7, which resulted in the final value (as $\log \beta$) 12.7 ± 0.1. Generated SDD unequivocally shows that the stability constant for $PbL_2(OH)_2$ was possible to be refined from DCP conditions, with a final value of 17.27 ± 0.06.

In conclusion, the final proposed model is PbL, PbL_2, $PbL_2(OH)$ and $PbL_2(OH)_2$ for which the following overall stability constants values, as $\log \beta$, are 3.27 ± 0.06, 6.5 ± 0.1, 12.7 ± 0.1 and 17.27 ± 0.06, respectively. In Fig. 5, SDD for the final model for two ratios $[L_T]:[Pb_T]$ 6.2 (GEP conditions, Fig. 5A) and 41.5 (DCP conditions, Fig. 5B) are shown.

The analysis of Fig. 5A and B confirms that the use of different $[L_T]:[Pb_T]$ was fundamental to define completely the model in the buffering pH region. As it was mentioned above, GEP conditions, in the case of this system, only allowed determining with high certainty PbL species. On the other hand, DCP conditions allowed to define other species and to determine their overall stability constant values, as was the case of PbL_2, $PbL_2(OH)$ and $PbL_2(OH)_2$ species. The refined stability constant value for $PbL_2(OH)_y$ species suggests that the formation of these species resulted from the hydrolysis of PbL_2, according to the following reaction:

$$PbL_2(H_2O)_x^{n+}\,(aq) + H_2O\,(l) \leftrightarrow H_3O^+\,(aq) + PbL_2(OH)_y(H_2O)_{x-1}^{(n-y)+}\,(aq) \quad (3)$$

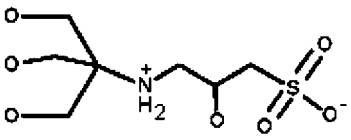
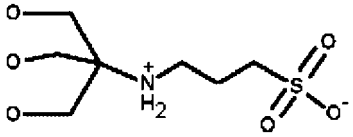
since the stability constant value of $PbL_2(OH)$ species is just the sum of: $\log \beta_{PbL_2(OH)} = \log \beta_{PbL_2} + \log \beta_{Pb(OH)} = 6.5 + 6.0 = 12.5$ (0.2 log difference) and $\log \beta_{PbL_2(OH)_2} = \log \beta_{PbL_2} + \log \beta_{Pb(OH)_2} = 6.5 + 10.3 = 16.7$ (0.57 log difference).

Fig. 5 also shows that, in the buffering pH range (7.32–9.32), $PbL_2(OH)$ and $PbL_2(OH)_2$ are the most important species to be considered and PbL and PbL_2 in a smaller extent.

3.4. Comparative evaluation of Pb^{2+}–$(L)_x$–$(OH)_y$ systems

TAPSO and TAPS are two biological buffers currently commercialised at least by two major chemical suppliers [6,7] and for which metal complexation properties we have been studying in the last years [8,10,18–20]. They are structural related and contain at least two hydroxyl groups in β carbons nearby

Table 3
Protonation and stability constants (as log β) for Pb^{2+}–$(L)_x$–$(OH^-)_y$ systems

Ligand	TAPSO	TAPS
Structure		
pK_a	7.55	8.342
$\log \beta_{ML}$	3.7 ± 0.1	3.27 ± 0.06
$\log \beta_{ML2}$	6.6 ± 0.1	6.5 ± 0.1
$\log \beta_{ML2(OH)}$	12.9 ± 0.1	12.7 ± 0.1
$\log \beta_{ML2(OH)2}$	17.8 ± 0.1	17.27 ± 0.06
References	[8,18]	[10], this work

to a secondary amino group (Table 3). Specifically, in the case of TAPSO and TAPS, the only difference between these two buffers is the fact that TAPSO has one more hydroxyl group than TAPS in the β carbon nearby the sulfonic group (Table 3).

The comparison of the lead complexation properties observed with TAPSO [18] and TAPS shows that lead binds stronger with TAPSO (Table 3). A simple evaluation based on the basicity of the two ligands points out to an enlargement in the stability constant values with the increase of the pK_a [21], which was not observed (Table 3). The fact that PbL stability constants, for Pb–$(TAPSO)_x$–$(OH)_y$ system, is 0.4 log unit higher than for Pb–$(TAPS)_x$–$(OH)_y$ system, though the basicity of TAPSO is about 0.8 smaller than for TAPS, suggests that the TAPSO's hydroxyl group near the sulfonic group is involved in the coordination, forming a five-membered chelate ring and increasing the stability of the PbL complex.

Acknowledgements

The authors thank the "Fundação para a Ciência e a Tecnologia" from Portuguese Government for the financial support of this work with FEDER funds, by the project POCTI/39950/QUI/2001. One of us (Carina Machado) is also gratefully acknowledged for a grant scholarship financed under the same project. We also thank Professor Ignacy Cukrowski from University of Pretoria (South Africa) for polarographic modelling software (3D-CFC program) and Professor Carlos Gomes from University of Porto (Portugal) for the COPOTISY program.

References

[1] D.M. Anderson, F.M.M. Morel, Limnol. Oceonogr. 23 (1978) 283–295.
[2] P.R. Hawkins, D.J. Griffiths, Bot. Mar. 25 (1982) 31–33.
[3] J.M. Díaz-Cruz, J.H.A.M. Wonders, H.G. Jong, H.P. Van Leeuwen, J. Electroanal. Chem. 375 (1994) 127–139.
[4] C.M.G. Van Den Berg, Mar. Chem. 50 (1995) 139–157.
[5] R.M. Smith, A.E. Martell, NIST Standard Reference Database 46, NIST Critically Selected Stability Constants of Metal Complexes Database, Version 3.0, US Department of Commerce, National Institute of Standards and Technology, 1997.
[6] Sigma, Biochemicals and Reagents for Life Science Research, 2005.
[7] Fluka, Riedel-de-Haen, Laboratory Chemicals and Analytical Reagents, 2005/2006.
[8] C.M.M. Machado, I. Cukrowski, P. Gameiro, H.M.V.M. Soares, Anal. Chim. Acta 493 (2003) 105–119.
[9] C.M.M. Machado, I. Cukrowski, H.M.V.M. Soares, Helv. Chim. Acta 86 (2003) 3288–3304.
[10] C.M.M. Machado, H.M.V.M. Soares, Talanta 71 (2007) 1352–1363.
[11] I. Cukrowski, Anal. Chim. Acta 336 (1996) 23–36.
[12] I. Cukrowski, Dedicated to polarography program 3D-CFC unpublished work.
[13] I. Cukrowski, M. Adsetts, J. Electroanal. Chem. 429 (1997) 129–137.
[14] P.M. May, K. Murray, D.R. Williams, Talanta 32 (1985) 483–489.
[15] P.M. May, K. Murray, D.R. Williams, Talanta 35 (1988) 825–830.
[16] E. Hogfeldt, Stability Constants of Metal–Ion Complexes—Part A: Inorganic Ligands, Pergamon Press, 1982, p. 49.
[17] Metrohm Application—Bulletin No. 36, Herisau, Switzerland, 1975.
[18] C.M.M. Machado, I. Cukrowski, H.M.V.M. Soares, Electroanalysis 17 (2005) 1291–1301.
[19] C.M.M. Machado, I. Cukrowski, H.M.V.M. Soares, Talanta 68 (2006) 819–830.
[20] C.M.M. Machado, H.M.V.M. Soares, submitted for publication.
[21] A.E. Martell, R.D. Hancock, Metal Complexes in Aqueous Solutions, Plenum Press, New York/London, 1996.

Available online at www.sciencedirect.com
ScienceDirect
Talanta 71 (2007) 1312–1318
Talanta
www.elsevier.com/locate/talanta

Protein microarrays enhanced performance using nanobeads arraying and polymer coating

C.A. Marquette [a,*], M. Cretich [b], L.J. Blum [a], M. Chiari [b]

[a] *Laboratoire de Génie Enzymatique et Biomoléculaire, UMR CNRS 5013 Bat. CPE, Université Claude Bernard Lyon 1, 43 Bd. du 11 Nov. 1918, 69622 Villeurbanne Cedex, France*
[b] *Istituto di Chimica del Riconoscimento Molecolare, CNR, Via Mario Bianco 9, 20131 Milano, Italy*

Received 8 March 2006; received in revised form 8 June 2006; accepted 30 June 2006
Available online 14 August 2006

Abstract

A nanosize material composed of 330 nm glass beads coated with a copolymer of *N*,*N*-dimethylacrylamide (DMA), *N*,*N*-acryloyloxysuccinimide (NAS) and [3-(methacryloyl-oxy)propyl]trimethoxysilane (MAPS) was developed to improve the protein immobilization on biochips. The developed material, bearing rabbit-IgG proteins, was arrayed as 150 μm spots trapped at the surface of a poly(dimethylsiloxane) elastomer (PDMS), and compared to copoly(DMA-NAS-MAPS)-coated glass slides and latex beads based biochips. Evidences were made through scanning electron microscopy that the newly developed material based microarray exhibited surface irregularities at the submicron level leading to high specific area.

The combination of such large immobilization area with the highly efficient protein immobilization of the copoly(DMA-NAS-MAPS) polymer, enabled the achievement of microarrays exhibiting good performances both in pure media and complex samples (human sera). Indeed, high specific/non-specific signal ratio was found using this optimized immobilization procedure.

Chemiluminescent detection of anti-rabbit-IgG was obtained through peroxidase labeled antibodies in the 5 μg/l to 10 mg/l range. Application of the developed system to real samples was achieved for the detection of rheumatoid factor (RF) through a capture assay. Interesting results were obtained, with a RF detection over the 5.3–485 IU/ml range and without measurable matrix effect or non-specific signal.
© 2006 Elsevier B.V. All rights reserved.

Keywords: Biochip; Chemiluminescence; Microarray; PDMS; Rheumatoid factor

1. Introduction

Protein microarrays are becoming important tools in proteomics [1,2], drug discovery programs [3], and diagnostics [4,5]. The amount of information obtained from small quantities of biological samples is significantly increased in the microarray format. This feature is extremely valuable in protein profiling, where samples are often limited in supply and unlike DNA, cannot be amplified [6]. However, protein microarrays are more challenging to prepare than are DNA chips [5] because several technical hurdles hamper their application. The surfaces typically used with DNA [7–10] are not easily adaptable to proteins, owing to the biophysical differences between the two classes of bio-molecules [11–14]. Arrayed proteins must be immobilized in a native conformation to maintain their biological functions. Unfortunately, proteins tend to unfold when immobilized onto a support so as to allow internal hydrophobic side chains to form hydrophobic bonds with the solid surface [15]. The accessibility of the protein is also of crucial importance to achieve proper recognition since the interactions between proteins and the immobilization support reduce the accessibility of the target, leading to false negative results [11].

The present study was aimed at evaluating the analytical performances of protein microarrays produced through different immobilization procedures. The proteins probes were grafted either to: (i) polymer-coated glass slides [16,17], (ii) latex microbeads immobilized at the surface of a PDMS (poly(dimethylsiloxane)) elastomer [18–20] or (iii) polymer-coated glass nanobeads entrapped at the surface of a PDMS substrate (Fig. 1).

The polymer coating was achieved by combining the adsorptive properties of poly(dimethylacrylamide) onto glass

* Corresponding author. Tel.: +33 4 72 44 82 14; fax: +33 4 72 44 79 70.
E-mail address: christophe.marquette@univ-lyon1.fr (C.A. Marquette).

0039-9140/$ – see front matter © 2006 Elsevier B.V. All rights reserved.
doi:10.1016/j.talanta.2006.06.039

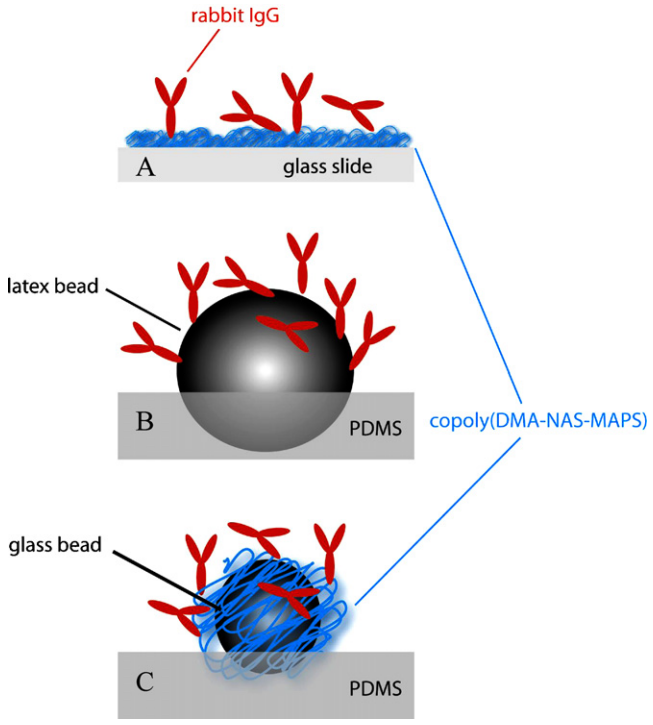


Fig. 1. Graphical representation of the three immobilization systems. (A) Copoly(DMA-NAS-MAPS)-coated glass slide; (B) latex based PDMS biochip; (C) copoly(DMA-NAS-MAPS)-coated glass nanobeads based PDMS biochip.

with a reaction between the silanol groups and electrophilic groups, pending from the polymer backbone. The copolymer of *N*,*N*-dimethylacrylamide (DMA), *N*,*N*-acryloyloxysuccinimide (NAS) and [3-(methacryloyl-oxy)propyl]trimethoxysilane (MAPS) formed then a highly hydrophilic coating with accessible functionalities to which modified DNA [21], proteins [17] or peptides can be covalently grafted. In all cases copoly(DMA-NAS-MAPS)-coated surfaces were shown to immobilize probes in a random conformation and to create an aqueous micro-environment in which linear epitopes or Fc and Fab domains of a capture antibody are freely exposed.

Protein immobilization on latex microbeads was obtained through the formation of covalent bonds between carboxylate residues present on the surface of the beads and protein amino residues. Those modified beads were trapped at the surface of a PDMS elastomer and generated spots of high specific surface [18]. Such system was previously shown to enable the successful "on chip" immobilization of various biological molecules such as inactive proteins (antigen), enzymes [20] and DNA strands [18]. However, a lack of protein accessibility was found in a particular case (P24 capside protein from HIV-1) [19] leading to poor biochip performances.

As an original solution to this problem, the present study proposes a new hybrid immobilization technique taking advantages of both the high quality grafting of proteins onto copoly(DMA-NAS-MAPS) and the high specific surface generated by bead spotting.

The above immobilization systems will be herein used as a microarray support for protein–protein interaction experiments and compared regarding their performances in the assessment of rheumatoid factor (RF) in human serum samples.

2. Experimental

2.1. Reagents

Ammonium sulfate, goat anti-rabbit-IgG peroxidase labeled (whole molecule), *N*,*N*-dimethylacrylamide (DMA), 3-(trimethoxysilane) propyl methacrylate (MAPS) were obtained from Sigma (France). *N*-Acryloyloxysuccinimide was supplied by Polysciences (Warrington, PA). Immunoglobulins from rabbit serum (rabbit-IgG) were obtained from Life Line Lab (Pomezia, Italy). Goat anti-human Ig(G + A + M) peroxidase labeled antibodies were purchased from Jackson ImmunoResearch Laboratories (West Grove, PA, USA).

PDMS precursor and curing agent (Sylgard 184) were supplied by Dow Corning. All buffers and aqueous solutions were made with distilled, demineralised water.

2.2. Synthesis of copoly(DMA-NAS-MAPS)

The monomers (20.17 mmol DMA, 0.42 mmol NAS, 0.21 mmol MAPS) were dissolved in dried tetrahydrofuran (THF) in a 50-ml, round-bottomed flask, equipped with condenser, magnetic stirrer, and nitrogen connection. The solution was degassed by alternating a nitrogen purge with a vacuum connection over a 30-min period. Azoisobutyronitrile (AIBN) was added to the solution, which was then warmed to 50 °C and maintained at this temperature under a slightly positive pressure of nitrogen for 24 h. After the polymerization was completed, the solution was precipitated by adding petroleum ether. The supernatant was eliminated, and the whole procedure was repeated two times. The polymer was dried under vacuum for 4 h at room temperature.

2.3. Glass slide coating and protein immobilization

Untreated microscope glass slides (Sigma) were pretreated with 1 M NaOH for 30 min and 1 M HCl for 1 h, washed with water, and dried. After the pre-treatment, glass slides were immersed for 30 min in a copoly(DMA-NAS-MAPS) solution (1%, w/v in water solution of ammonium sulfate at 20% saturation level), then rinsed with water and dried under vacuum at 80 °C.

Rabbit-IgG were dissolved in a PBS buffer (100 mM phosphate, 150 mM NaCl, 100 mM KCl, pH 7.4) at a 1 mg/ml concentration and spotted as 1.2 nl drop with a BioChip Arrayer BCA1 (Perkin-Elmer) on the copoly(DMA-NAS-MAPS) slides. Each array was composed of eight spots (four specifics and four non-specifics) where the non-specific ones were obtained by spotting bovine serum albumin.

After an overnight binding in a 30 °C thermostated water saturated chamber, the obtained microarrays were rinsed and blocked with BSA (1%, w/v) in PBS for 1 h.

2.4. Coating of silica nanospheres and protein immobilization

Silica nanospheres were coated with a copolymer of *N*,*N*-dimethylacrylamide (DMA), *N*,*N*-acryloyloxysuccinimide (NAS) and [3-(methacryloyl-oxy)propyl]trimethoxysilane (MAPS) using a fast, inexpensive and robust procedure consisting in simply dispersing nanobeads in a dilute aqueous polymer solution. Coating of nanospheres required then only two steps: pre-treatment and adsorption of polymer.

Silica nanospheres (non-porous, 330 nm from Bangs Laboratories Inc.) were pretreated with 1 M NaOH for 15 min, washed with water, treated with HCl 1 M for 1 h and extensively rinsed with water. In the second step, pretreated nanospheres were dispersed for 30 min in a solution of copoly(DMA-NAS-MAPS) (1%, w/v in a water solution of ammonium sulfate at a 20% saturation level). The nanobeads were then washed extensively with water and dried under vacuum at 80 °C for 30 min.

For protein immobilization, 45 mg of polymer-coated nanobeads were dissolved in 400 μl of a 10 mg/ml Rabbit-IgG solution in PBS (optimized concentration), sonicated for 2 min and stand to react under stirring during 2 h. At that time the reaction was completed and the non-grafted protein was washed out through four cycles of centrifugation/re-suspension in 500 μl of PBS and stored at 4 °C.

A similar protocol was applied to bovine serum albumin (BSA) to obtain non-specific beads used as negative control during the biochip experiments.

2.5. Protein immobilization onto latex microbeads

About 100 μl of commercialized latex beads suspension in water (1 μm of diameter from Polyscience, Inc. (France)) were mixed with 100 μl of 0.1 M 1-ethyl-3-(3-dimethyl-aminopropyl)carbodiimide and 100 μl of 0.1 M *N*-hydroxysuccinimide and incubated under stirring for 1 h. The excess of reagents was then removed by centrifugation, and the activated beads were re-suspended in 400 μl of a 5 mg/ml rabbit-IgG solution in PBS (optimized concentration). The latex beads were incubated under stirring for 2 h, then washed in distilled water by successive centrifugation/re-suspension cycles and stored at 4 °C.

A similar protocol was applied to bovine serum albumin (BSA) to obtain non-specific beads used as negative control during the biochip experiments.

2.6. Micro- and nano-beads based biochip preparation

The biochips were prepared by arraying 1.2-nl drops of spotting solutions with a BioChip Arrayer BCA1 (Perkin-Elmer). The spotting solutions were prepared by mixing 100 μl of either spotting buffer A (glycerol 2.5%, NaCl 0.05 M in water) or spotting buffer B (30 mM Veronal buffer, pH 8.5 containing 30 mM KCl, 0.2 M NaCl, 0.1% Tween and 1% BSA) with 10 μl of an aqueous suspension (1%, w/v) of micro- or nano-beads bearing rabbit-IgG, respectively.

Each array was composed of 8 spots (4 specifics and 4 non-specifics) that were spotted on the surface of a 3D PVC master composed of 24 rectangular structures ($w = 5$ mm, $l = 5$ mm, $h = 1$ mm). After spotting, the spots were dried and the arrays were transferred to a PDMS interface, by pouring a mixture of precursor and curing agent (10:1) onto the PVC substrate, and cured for 5 min at 90 °C. Peeling off the PDMS polymer then terminated the biochip preparation.

The 3D structure resulting from this process was then a 24-well PDMS microarray (inner volume 25 μl), with 16-spot arrays at the bottom of each well. All incubation or washing steps for a particular array were then performed by depositing a 20 μl solution volume into each well.

Before performing immunoassays, the micro- and nano-beads based biochips were saturated with PBSA (PBS containing BSA 1%, w/v), for 20 min.

2.7. Polyclonal anti-rabbit antibody-binding tests

The different systems – glass slide microarrays, microbeads and nanobeads biochips – already saturated with BSA were incubated at 37 °C for 1 h in the presence of increasing concentrations (from 5 ng/ml to 10 μg/ml) of peroxidase labeled anti-rabbit-IgG antibodies in PBSA. The biochips and microarrays were then washed 20 min with VBS (30 mM Veronal, 0.2 M NaCl, pH 8.5) and were ready to be measured.

2.8. Rheumatoid factor (RF) detection in human sera

The different systems – glass slide microarrays, microbeads and nanobeads biochips – already saturated were incubated at 37 °C for 1 h with standardized human serum samples (a gift from Life Line Lab) containing different amounts of RF (0–485 IU/ml, determined by RF ELISA Auraflex, Alfa Biotech, Pomezia, Italy). For glass slide microarrays, the sera were diluted 1:100 in PBSA, whereas they were diluted 1:10 in PBSA for microbeads biochips and 1:100 in PBSTA (PBS containing BSA 1%, w/v and Tween-20 0.1%, v/v) for nanobeads biochips.

The glass microarrays and the biochips were then washed 10 min with PBS, saturated with PBSA for 20 min and incubated for 1 h at 37 °C in the presence of peroxidase labeled anti-human IgG antibodies at a concentration of 26.6 μg/ml in PBSA for glass slide microarrays and microbeads biochips and at a concentration of 8 μg/ml in PBSTA for nanobeads biochips. The biochips and microarrays were then washed 20 min with VBS and were ready to be measured.

2.9. Microarrays and biochips measurements

The ready-to-measure biochips and microarrays were covered with VBS containing 200 μM of luminol, 500 μM of hydrogen peroxide and 20 μM of *p*-iodophenol. The arrays were introduced into the CCD light measurement system (Intelligent Dark Box II, Fuji Film) and the emitted light integrated for 10 min for binding tests and RF detection, respectively. The obtained biochip pictures were quantified with a FUJIFILM image analysis program (Image Gauge 3.12).

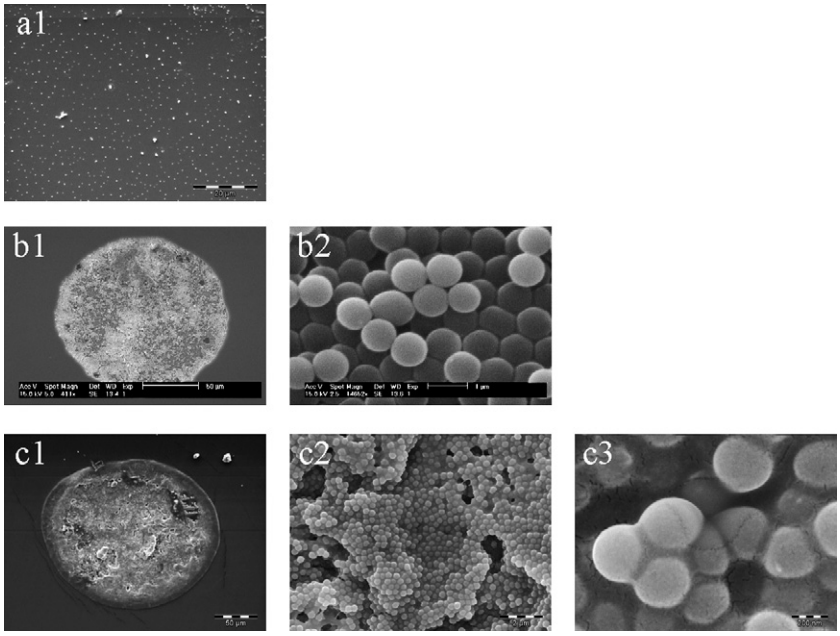


Fig. 2. Scanning electron microscopy images (15 kV) of the three developed systems based on: (a) coated glass slide; (b) 1 μm latex beads; (c) 330 nm coated glass beads.

3. Results and discussion

Surface irregularity is an important factor in sensing layer development since for equivalent geometrical surfaces, really different specific surfaces – i.e. real developed surfaces – could be obtained. Thus, using equivalent area of the microarray, different amounts of bio-molecules could be immobilized depending on the "roughness" of the surface.

The present study aims at evaluating the analytical performances of protein microarrays produced by three different immobilization procedures generating different levels of local specific surface and different protein immobilization efficiencies. These procedures are based on the grafting of protein probes to: (i) polymer-coated glass slides, (ii) latex microbeads immobilized at the surface of a PDMS (poly(dimethylsiloxane)) elastomer and (iii) polymer-coated glass nanobeads entrapped at the surface of a PDMS substrate.

These three different surfaces were first imaged through scanning electron microscopy (SEM). Fig. 2a1, b1 and c1 show the 150 μm spots obtained on copoly(DMA-NAS-MAPS)-coated glass slide, latex biochip and copoly(DMA-NAS-MAPS)-coated glass beads biochip, respectively. As expected, no irregularity at all could be observed from the coated glass slide spot, evidencing a low specific area. On the contrary, both latex and coated glass beads based spots exhibit nicely defined 150 μm spots with irregular surface.

Higher resolution images (Fig. 2b2 and c2) revealed differences between latex and coated glass beads based spots. The use of 330 nm glass beads instead of 1 μm latex beads generated the higher specific surface accompanied of a clear entrapment of the glass beads in the copoly(DMA-NAS-MAPS). This last point is made obvious with the highest resolution image (Fig. 2c3) where the nanobeads appeared to be entrapped together in polymer shells.

These morphological characterizations suggest differences in the organization of the microarrays surface, leading to increasing specific surfaces from coated glass slides to latex beads and finally coated glass beads based microarrays. Differences in the microarrays performances are then expected since more biological material will be immobilized onto highly irregular surfaces.

The present analytical system – RF detection – is an interesting model for studying protein immobilization on novel

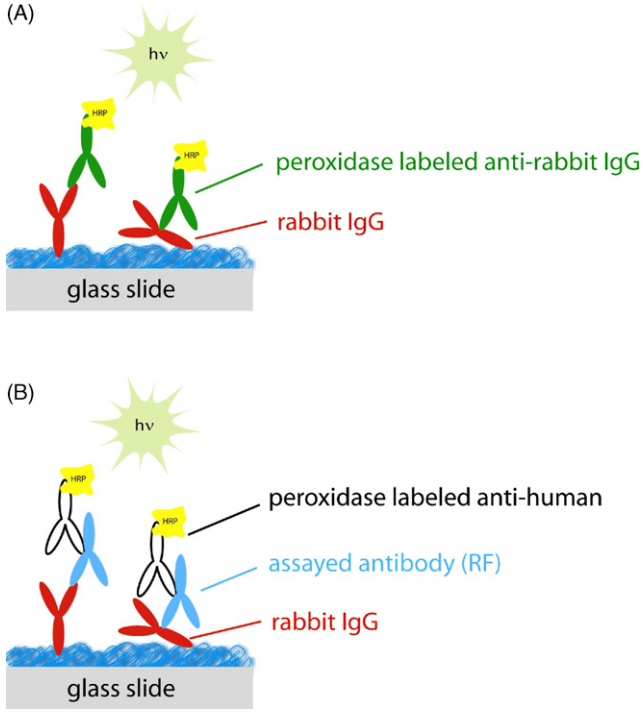


Fig. 3. Schematic view of the different immunoassays performed. Only the coated glass slide is shown. (A) Polyclonal anti-rabbit antibody-binding tests; (B) RF detection in human sera.

supports since it requires immobilizing the antigen within a highly accessible conformation. Indeed, because this test is based upon the recognition of rabbit-IgG by polyclonal antibodies from human serum [22–24], the sensitivity of the test depends on the number of available epitopes on the immobilized probe.

The three different immobilization procedures studied herein were first tested through their ability to generate sensing elements (spots of immobilized protein) on which polyclonal antibodies could bind specifically and extensively (Fig. 3A). For this purpose, glass slide microarrays, microbeads biochips and nanobeads biochips were incubated with peroxidase labeled anti-rabbit polyclonal antibodies from goat at different concentrations and the chemiluminescent signals obtained in each condition were quantified and plot to build the binding diagrams of Fig. 4.

As shown by Fig. 4 micrographs, the three systems are highly specific to polyclonal anti-IgG antibodies from purified solution, with no measurable non-specific binding on the immobilized BSA spots (negative control). Nevertheless, interesting differences in the three binding diagrams could be observed. As expected from previous studies [17] the copoly(DMA-NAS-MAPS)-coated glass slide provided a relatively good response to the presence of polyclonal anti-rabbit-IgG antibodies through the entire range of concentration tested (from 5 μg/l to 5 mg/l) whereas a saturation plateau was found for concentrations higher than 5 mg/l with a maximum chemiluminescent signal of 30 000 a.u. As expected [19], the latex microbeads based biochip exhibited a shifted detection range (from 50 μg/l to 10 mg/l). Two important observations must be pointed out. The first is that, no saturation of the binding sites at high antibody concentrations was observed with the latex microbeads biochip. The second is that, the maximum signal obtained with this system (50 000 a.u.) was higher than that provided by the coated microarray slides. This suggests that using latex beads enabled the immobilization of a higher amount of rabbit-IgG in the sensing layer. However, the detection limit of the slides was 10 times lower than that obtained with the latex microchip. This difference reveals a lack of accessibility of one or more epitopes of the protein directly immobilized on latex beads, which could lead to an underestimated titration.

Finally, a mixed behavior could be found in the diagram of the coated beads biochip. Indeed, it could be seen that this last system produced no saturation at high concentrations, a maximum chemiluminescent signal of 35 000 a.u. and a detection range from 10 μg/l to 10 mg/l.

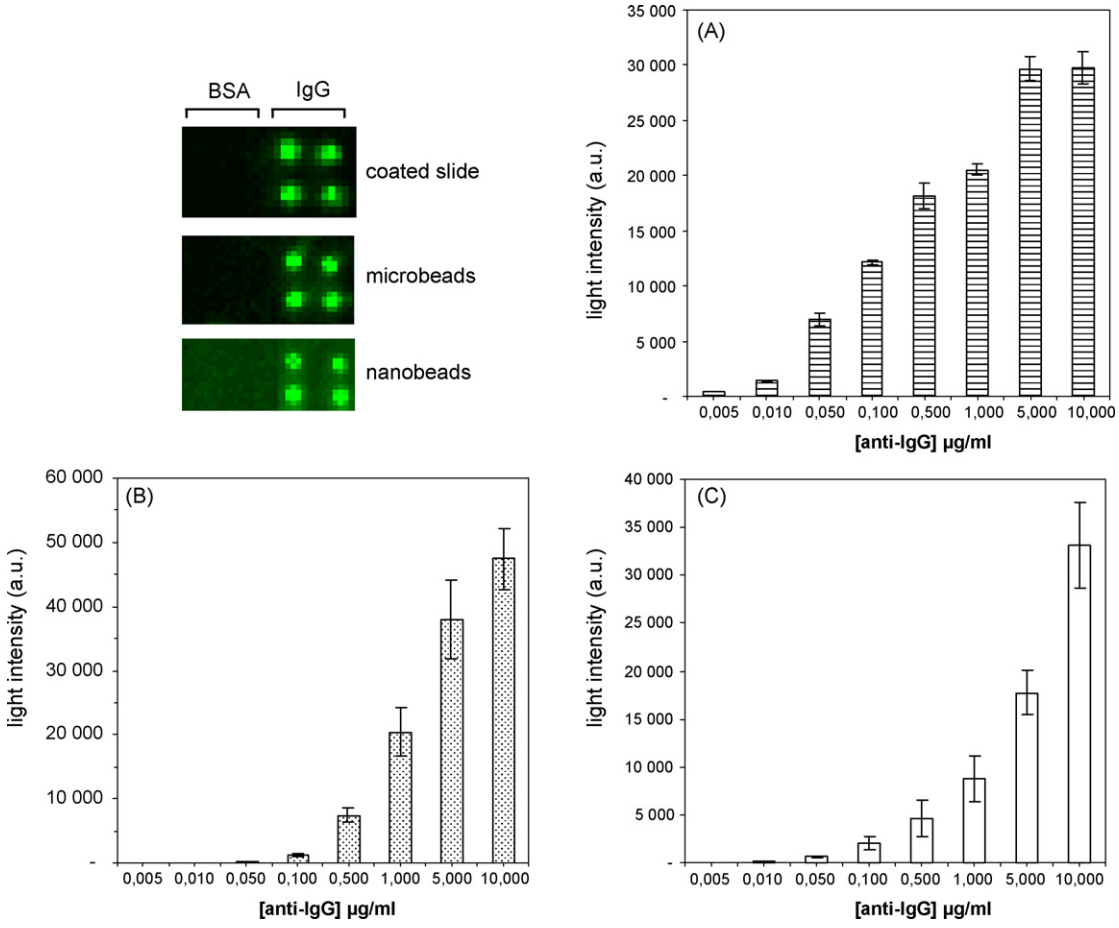


Fig. 4. Polyclonal anti-rabbit antibody-binding tests on the different analytical systems. The micrograph shows typical chemiluminescent images from each system. (A) Binding diagram from the copoly(DMA-NAS-MAPS)-coated glass slide microarray; (B) binding diagram from the latex beads based biochip; (C) binding diagram from the copoly(DMA-NAS-MAPS)-coated nanobeads based biochip. Error bars are the S.D. of three replicates.

Coating 330 nm beads with copoly(DMA-NAS-MAPS), grafting rabbit-IgG on it and using these hybrid beads to generate high specific surface spots at the surface of a PDMS elastomer combines then the advantages of polymer-coated glass slides with those of beads use, providing both high sensitivity and linearity in a broad range of concentrations.

As shown above, the three systems exhibit a different behavior against polyclonal anti-IgG antibodies from purified solution in which no interfering proteins or antibodies are present. The aim of this second study was to test the performances of each system in real micro-analytical experiments in the presence of high concentrations of background proteins (e.g., albumin, fibrinogen, antibodies).

RFs are immunoglobulins of any isotype with activity directed against the antigenic sites on the Fc region of human or animal IgG (Fig. 3B). Seventy to eighty percent of patients with confirmed rheumatoid arthritis show an increase in the RF [22]; therefore, RF assay is a serological test widely used for the diagnosis of rheumatoid arthritis. Conventional serological tests for the measurement of RF rely on enzyme-linked immunoassay (EIA) or enzyme-linked immunosorbent assay (ELISA). Testing the present systems according to their ability to detect RF imply the use of human sera.

Thus, standardized human serum samples containing different amounts of RF (0–485 IU/ml) were incubated on the different microarrays and biochips. Fig. 5 presents the results obtained from each analytical system and each sample, with dataset standardized regarding the maximum chemiluminescent signal of each plot:

$$I = \frac{I_i}{I_{\max}}; \quad i = 0\text{–}485$$

For each particular system, the RF detection conditions were optimized in order to obtain the best analytical performances. Glass slide based microarrays and nanobeads biochips were incubated with sera diluted 1:100 whereas latex bead biochips were used on 10 times less diluted samples (1:10).

This first remark points out one of the major problems of the latex beads biochips (Fig. 5B), the lack of reactivity of the immobilized antigen against a multiple epitope binding antibody solution, which could be due to a non-adapted immobilization chemistry. In order to detect RF on a large concentration range,

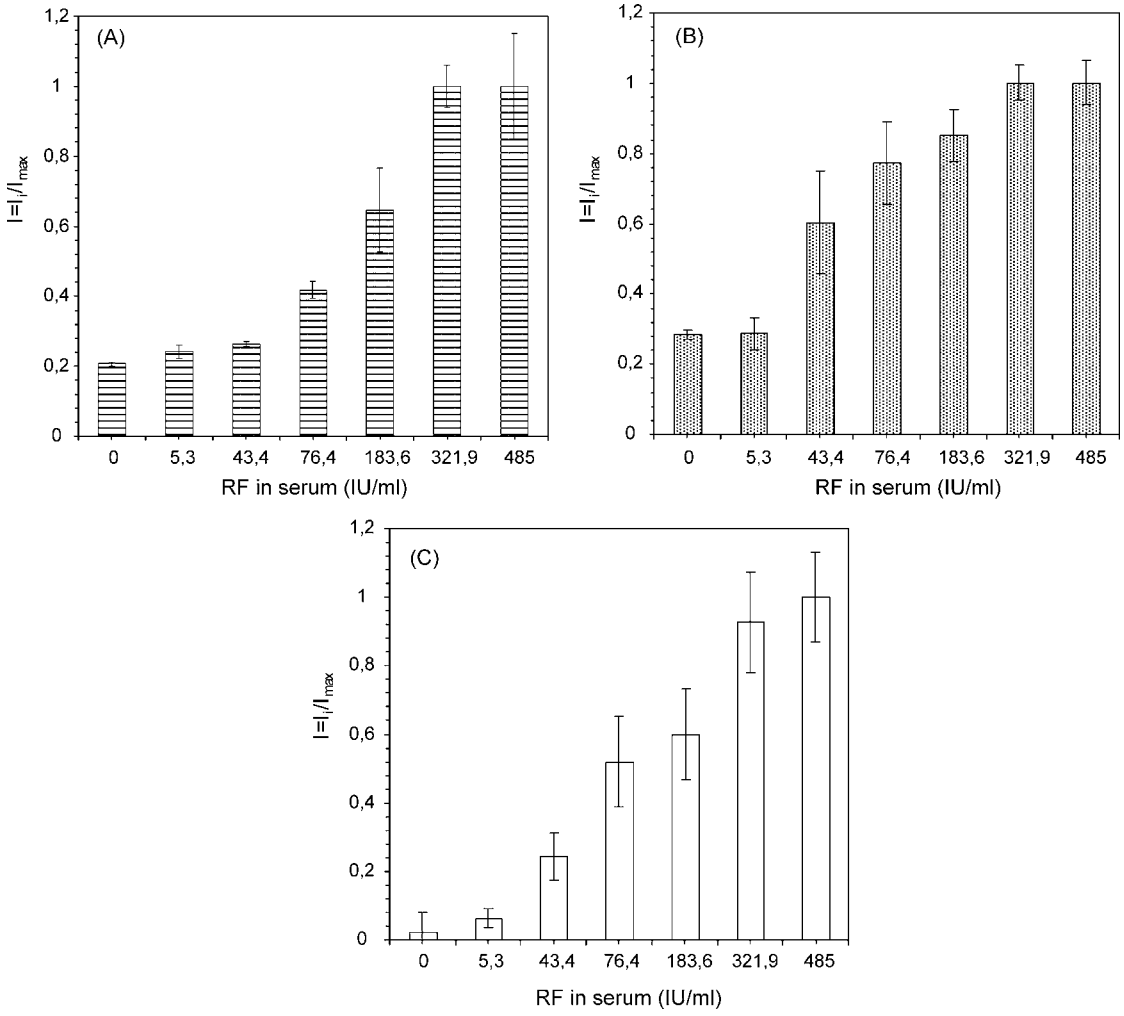


Fig. 5. RF detection in human sera using: (A) the copoly(DMA-NAS-MAPS)-coated glass slide microarray; (B) the latex beads based biochip; (C) the copoly(DMA-NAS-MAPS)-coated nanobeads based biochip. Error bars are the S.D. of three replicates.

the biochip requires highly concentrated samples, leading to significant non-specific signals at low RF values (0 and 5.3 IU/ml). The direct consequence of the presence of a strong background signal is a significant limitation in the detection range obtained.

For glass slide system, the copoly(DMA-NAS-MAPS) coating enables, as discussed before, the immobilization of freely accessible IgG which appeared to be a good sensing element for RF detection in diluted samples (Fig. 5A). Indeed, the entire range of tested RF was detected, except for the 321.9 IU/ml value which was not distinguished from the 485 IU/ml. Moreover, this system generated a non-specific signal for the 0 IU/ml sample, resulting in a poor reliability for the analytical results obtained at low RF concentrations.

Finally, coated nanobeads biochips provides the most interesting results. Indeed, the full range of RF concentrations tested in complex samples could be detected with no doubt and on diluted samples. Moreover, as shown in Fig. 5C, a very low signal was recorded from the sensing layers incubated with the 0 IU/ml sample, contrary to what was obtained with microbeads or glass slide biochips. This latter point evidences an interesting low non-specific binding of the hybrid sensing layer made of inorganic nanobeads coated with copoly(DMA-NAS-MAPS).

4. Conclusions

In this study we investigated the suitability, as a protein immobilization, of a new submicron material composed of glass nanometric beads coated with a copolymer of *N*,*N*-dimethylacrylamide (DMA), *N*,*N*-acryloyloxysuccinimide (NAS) and [3-(methacryloyl-oxy)propyl]trimethoxysilane (MAPS) [16]. Coating of glass nanobeads with copoly(DMA-NAS-MAPS) was produced using a fast, inexpensive and robust procedure consisting in simply dispersing nanospheres in a dilute aqueous polymer solution.

The new material, obtained as a suspension, was subsequently derivatized with an antigen (rabbit-IgG) and used to produce PDMS elastomer based biochips according to a well established previously described procedure [18–20]. The analytical performances of the novel biochip were compared to those obtained, either with copoly(DMA-NAS-MAPS)-coated glass slides or with a latex microbeads based systems. Scanning electron microscopy was used to characterize the surface of the different systems. An increasing surface irregularity was found from coated glass slides to latex beads and finally coated glass beads based microarrays.

Evidences were made that the new material exhibited interesting characteristics in term of protein immobilization, accessibility and specific/non-specific signal ratio. The immobilized protein, used as antigen, was shown to enable the specific binding of large amount of polyclonal antibodies either in pure media or complex matrices. Thus, microarrays were developed, displaying mixed behavior combining the highly efficient protein immobilization of the copoly(DMA-NAS-MAPS) and the high specific surface of the beads based spotting procedure. Such novel nanosized structures could help increasing the performances of analytical microsystems.

Acknowledgment

Published with the support of the European Commission, Sixth Framework Program, Information Society Technologies. NANOSPAD (no. 016610).

References

[1] J.M. Boutell, D.J. Hart, B.L.J. Godber, R.Z. Kozlowski, J.M. Blackburn, Proteomics 4 (2004) 1950.
[2] R.B. Jones, A. Gordus, J.A. Krall, G. MacBeath, Nature 439 (2006) 168.
[3] S. Bodovitz, T. Joos, J. Bachmann, Drug Discov. Today 10 (2005) 283.
[4] Y.-S. Lee, M. Mrksich, Trends Biotechnol. 20 (2002) s14.
[5] H. Zhu, M. Snyder, Curr. Opin. Chem. Biol. 7 (2003) 55.
[6] D.S. Wilson, S. Nock, Angew. Chem. Int. Ed. 42 (2003) 494.
[7] H. Salin, T. Vujasinovic, A. Mazurie, S. Maitrejean, C. Menini, J. Mallet, S. Dumas, Nucl. Acids Res. 30 (2002) e17.
[8] H.T. Ng, A. Fang, L. Huang, S.F.Y. Li, Langmuir 18 (2002) 6324.
[9] O. Melnyk, X. Duburcq, C. Olivier, F. Urbès, C. Auriault, H. Gras-Masse, Bioconjugate Chem. 13 (2002) 713.
[10] S. Venkatasubbarao, Trends Biotechnol. 22 (2004) 630.
[11] W. Kusnezow, J.D. Hoheisel, J. Mol. Recognit. 16 (2003) 165.
[12] D. Stoll, M.F. Templin, J. Bachmann, T.O. Joos, Curr. Opin. Drug Discov. Dev. 8 (2005) 239.
[13] J. LaBaer, N. Ramachandran, Curr. Opin. Chem. Biol. 9 (2005) 14.
[14] K.Y. Tomizaki, K. Usui, H. Mihara, ChemBioChem 6 (2005) 782.
[15] J.E. Butler, Methods 22 (2000) 4.
[16] M. Chiari, M. Cretich, A. Corti, F. Damin, G. Pirri, R. Longhi, Proteomics 5 (2005) 3600.
[17] M. Cretich, G. Pirri, F. Damin, I. Solinas, M. Chiari, Anal. Biochem. 332 (2004) 67.
[18] C.A. Marquette, L.J. Blum, Anal. Chim. Acta 506 (2004) 127.
[19] C.A. Marquette, A. Degiuli, E. Imbert-Laurenceau, F. Mallet, C. Chaix, B. Mandrand, L.J. Blum, Anal. Bioanal. Chem. 381 (2005) 1019.
[20] C.A. Marquette, L.J. Blum, Biosens. Bioelectron. 20 (2004) 197.
[21] G. Pirri, F. Damin, M. Chiari, E. Bontempi, L.E. Depero, Anal. Chem. 76 (2004) 1352.
[22] E.S. Cathcart, Rheumatoid Factors Laboratory Diagnostics Procedure in the Rheumatic Diseases, 2nd ed., Little Brown, Boston, 1975.
[23] T.L. Moore, R.W. Dorner, Clin. Biochem. 26 (1993) 75.
[24] T. Ota, Rinsho Byori: Jpn. J. Clin. Pathol. 51 (2003) 649.

Available online at www.sciencedirect.com
ScienceDirect
Talanta 71 (2007) 1399–1404
Talanta
www.elsevier.com/locate/talanta

Direct determination of major elements in solid plant materials by electrothermal vaporization inductively coupled plasma atomic emission spectrometry

Pierre Masson *

USRAVE, Centre de Recherches INRA de Bordeaux, B.P. 81, 33883 Villenave d'Ornon Cedex, France

Received 3 April 2006; received in revised form 13 June 2006; accepted 6 July 2006
Available online 11 September 2006

Abstract

The present work demonstrates the capability of electrothermal vaporization (ETV) to become an important tool of solid sample introduction in ICP-AES for plant sample analysis. Direct determination of Al, Ca, Fe, K, Mg, Mn, Na and Zn was investigated in powdered plant samples. Obtaining good results for major elements in plant samples was governed by some special operating conditions. The sensitivity of the method necessitated the use of ICP in radial view configuration. The behavior of elements during vaporization was studied between 500 and 2600 °C. External calibration was carried out using solid external (cellulose) spiked with aqueous standard solutions. However, performances of the analytical method were found dependent of argon flow rates. Analytical accuracy of the method was tested in three reference materials. Analytical results agreed with certified values when cellulose was used in calibration. However, K could not be determined because of excessive sensitivity. Without cellulose, it was found that Fe results were underestimated and Zn results overestimated. Relative standard deviations varied from 3 to 23%. Limits of detection varied from 1 to 80 ng g^{-1} from one element to the other for a typical mass sample of 2 mg.
© 2006 Elsevier B.V. All rights reserved.

Keywords: Electrothermal vaporization; Inductively coupled plasma; Plant sample; Major elements

1. Introduction

Electrothermal vaporization (ETV) is now a well established sample introduction device for inductively coupled plasma atomic emission spectrometry (ICP-AES) and inductively coupled plasma mass spectrometry (ICP-MS) [1]. As the vaporization and the atomization/ionization/excitation of elements were realized in two separate steps, the ETV and ICP operating parameters can be optimized independently. Concerning ICP-AES, robust conditions are generally defined as high RF power and wide internal diameter of the torch injector [2,3]. Concerning ETV working conditions, direct analysis of solid samples requires a specific study of analyte behavior in sample matrix used. The main goal in developing solid sample introduction technique is to separate in time the vaporization of analytes from the vaporization of matrix components but also to achieve efficient transport of volatilized elements to ionization source [4].

However, working directly with solid samples involves some operational problems. Sample manipulation [4] and calibration [4–9] were considered problematic. Today, recent developments gave us tools to minimize these drawbacks. Different systems, specifically dedicated for this purpose, are now commercially available and make possible multi-element analysis on environmental or biological samples [10–21]. Accurate method for multi-element analysis of some trace elements in plant matrices has been reported recently [10] using ETV and axial view ICP-AES. In this study, cellulose was chosen as support for calibration. In these conditions, transport efficiency did not depend on element in sample matrix or on cellulose.

Now, the intention of the present work was to demonstrate the capability of solid sampling ETV–ICP to accomplish the simultaneous determination of major elements (Al, Ca, Fe, K, Mg, Mn, Na and Zn) in plant materials. These elements are essential in plant development. Creating a rapid method to measure those in plant samples will be welcome for agronomic

* Tel.: +33 5 57 12 24 05; fax: +33 5 57 12 23 99.
E-mail address: masson@bordeaux.inra.fr.

0039-9140/$ – see front matter © 2006 Elsevier B.V. All rights reserved.
doi:10.1016/j.talanta.2006.07.013

studies. Determination of some major elements (Cu, Fe Mn) in plant samples using ETV was rarely reported. Therefore, literature on this subject concerns especially atomic absorption spectrometry [16,22–25]. However, in the case of ICP analysis, the concentrations of these elements encountered in plant samples (at the $g\,kg^{-1}$ level) required some adaptations in comparison with trace elements analysis. Sensitivity of the method becomes a drawback for these analytes because it is difficult to dilute the samples with ETV. The problem is usually solved by using less sensitive lines. Here, the sensitivity of the method was also decreased with the use of ICP in radial view configuration.

A short study of vaporization temperatures was first carried out. Next, the influence of argon flow rates were studied on signal intensities of analytical elements on cellulose spiked with standard solution and a true plant sample (maize). Finally, accuracy and precision of the whole procedure were controlled on various certified reference materials presenting different properties in terms of origin, matrix composition and concentration range of elements.

2. Experimental

2.1. Apparatus and conditions

An ETV 4000 (Spectral systems, Fürstenfeldbruck, Germany) electrothermal vaporizer was used. The ETV 4000 unit is a commercially available system containing graphite-tube furnace, power supply, gas supply, water cooler and autosampler. Graphite sample holders (in boat shape) can be easily and reproducibly loaded into the cylindrical graphite furnace with the aid of a pair of tweezers. After loading the sample, one end of the furnace is closed using a shutter. Operation of the ETV was completely computer controlled. The temperature of various steps of heating program and the time period can be selected. The temperature ranges from room temperature up to about 3000 °C. During the temperature program, argon gas flow rates originating from both end of the graphite tube remove all vapors. Metal ions are transformed into volatile metal halogenides by addition of halogen containing reaction gas ($CHClF_2$) which was active ($2.3\,ml\,min^{-1}$) before starting the vaporization step and improve the volatilization of elements [26–30]. In fact, several elements studied form fluoride or chloride compounds which have boiling points at lower temperatures than the corresponding oxide or carbide. For example, the boiling points of Al, AlF_3 and Al_2O_3 are, respectively, 2519 °C, 1276 °C (sublimation) and 3000 °C. The influence of this gaseous modifier was not studied here. Construction designs of the ETV 4000 were reported by Hassler et al. [31].

The simultaneous ICP instrument was a Thermo Elemental (Franklin, MA, USA) dual view IRIS INTREPID ICP-AES spectrometer with CCD detector and equipped with a standard extended torch and a quartz injector tube (2.4 mm i.d.). For this study, the instrument was used with radial view. However, in this configuration, height of measurement was fixed. Operating parameters of the ICP for multi-element measurement were selected in a previous work [10]. They were remained constant in this work and summarized in Table 1 as well as spectral lines chosen for this study. ETV–ICP produces a transient signal as a consequence of pulsed heating of the ETV. Peak area of the transient signal was integrated over time and was used for data handling. For background correction, intensities were also measured to the sides of each peak. ETV unit was interfaced to the ICP via a 30 cm long and 6 mm internal diameters PTFE tubing. The sample vapors were injected directly into the plasma.

Table 1
Operating parameters of the ETV atomizer and ICP spectrometer

ETV	
Carrier argon flow rate ($l\,min^{-1}$)	0.3
Bypass argon flow rate ($l\,min^{-1}$)	0.1
Freon flow rate ($ml\,min^{-1}$)	2.3
Sample mass analyzed (mg)	1–5
Plasma	
Power (kW)	1.35
Argon flow rate ($l\,min^{-1}$)	15
Auxilliary argon flow rate ($l\,min^{-1}$)	1.5
Measured wavelength (nm)	
Al	396.1
Ca	318.1
Cu	324.7
Fe	238.2
K	766.4
Mg	279.0
Mn	259.3
Na	589.5
Zn	213.8

2.2. Reagents and samples

All reagents used were analytical grade. Five multi-element standard solutions containing, respectively, Al (0, 5, 10, 20 and $40\,mg\,l^{-1}$), Ca (0, 12.5, 25, 50 and $100\,mg\,l^{-1}$), Fe (0, 2, 4, 8 and $16\,mg\,l^{-1}$), K (0, 50, 100, 200 and $400\,mg\,l^{-1}$), Mg (0, 10, 20, 40 and $80\,mg\,l^{-1}$), Mn (0, 2, 4, 8 and $16\,mg\,l^{-1}$), Na (0, 5, 10, 20 and $40\,mg\,l^{-1}$) and Zn (0, 2, 4, 8 and $16\,mg\,l^{-1}$) were prepared by diluting appropriate volumes of $1000\,mg\,l^{-1}$ commercially available stock solutions (Merck, Darmstadt, Germany) with distilled water. These solutions were acidified by 5% (v/v) of concentrated HNO_3 (Baker analyzed, Phillipsburg, NJ, USA).

Acid washed cellulose (Baker analyzed, Phillipsburg, NJ, USA) and maize sample (entire plant) were the two solid materials used in the investigation. The maize sample is an internal reference material produced in our laboratory. This sample is composed of various maize samples dried, crushed, mixed and stabilized using gamma radiation. This sample is also used to adapt or develop analytical methods for plant samples because it is less expensive that true certified reference materials. Cellulose was used to study the vaporization of elements. Cellulose and maize were used in the investigation of the dependence of the analyte transport efficiencies with the different argon gas flows. The accuracy of the method was ultimately controlled using three types of NIST (National Institute of Standard and Technology, Gaithersburg, MD, USA) standard reference materials

(SRMs): SRM 1568 (rice flour), SRM 1573a (tomato leaves), and SRM 1575a (pine needles).

2.3. Measurements

Before performing measurements, a purification process involving halocarbon assisted thermal purification at 2600 °C was performed on graphite boats. Next, samples were introduced manually into purified graphite boat on a Metler microbalance with a precision of 0.01 mg. The amount of cellulose weighed was typically 2 mg. Aliquots of the standard solutions (10 μl) had been introduced manually on the cellulose powder by means of a micropipette. For other samples, obtained results were divided by corresponding sample mass weighed in order to have comparable values (reported to the mass unit).

During the optimization of the ETV parameters, three replicate measurements of spiked cellulose and maize sample were carried out for each condition investigated. Result was taken to be the mean. Concerning reference materials, every determination consisted of five replicate measurements of samples and results were, in this case, taken to be the mean and standard deviation values to appreciate the precision of the method. Purified cellulose with additions of standard solutions was used to determine calibration curves.

3. Results and discussion

3.1. Vaporization temperatures

Plant materials are largely organic. Pyrolysis step facilitates the removal of matrix prior to the vaporization of analytes. From a chemical point of view, plant samples can be regarded as mixtures of cellulose, hemicelluloses, lignin and several minor components [32]. Optimization of the pyrolysis of plant samples step have been investigated in a previous work [10]. On the contrary, vaporization temperatures established for trace elements analysis were not necessary adapted to the determination of major elements. Elements such as alkali metals or alkaline earth metals could have different behaviors from transition metals ones.

Vaporization involves processes in the solid phase and in the gaseous phase. In any case, it is essential to control the process of vaporization efficiently. The vaporization step of the heating cycle was optimized by measuring element signal intensities generated by cellulose spiked with the medium standard solution as a function of the temperatures. Fig. 1 shows for Al, Ca and Fe the effect of the vaporization temperature on signal intensities. The others elements showed exactly the same behavior. All target elements were vaporized under halocarbon vapors at approximately the same time, in the temperature range of 1400–2000 °C. Temperature above 2300 °C guarantees complete evaporation of elements from the sample. No vaporization temperature below 1400 °C must be used.

No shift of the peak signals appears, suggesting that no compound of lower volatility is formed in the condensed phase. Because the final aim of this investigation was to determine simultaneously all elements, thermal cycle previously optimized

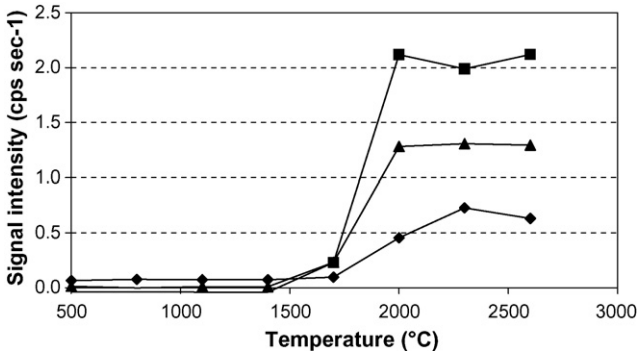


Fig. 1. Effect of the vaporization temperature on signal intensities for Al (♦), Ca (■) and Fe (▲). Matrix = cellulose spiked with 100 ng Al, 250 ng Ca and 40 ng Fe.

for trace elements [10] could be used. The vaporization temperatures selected (1900 and 2400 °C) were high enough for the least volatile analyte. However, direct insertion of more than 5 mg solid sample posed sometimes problems on the stability of the plasma. The presence of significantly larger amounts of matrix constituents could lead to extinguish the plasma. In these conditions, a new step in the heating cycle was introduced at 600 °C to remove the most resistant organic compounds of plant samples [19,33]. The final heating program is given in Table 2.

3.2. Argon gas flow rates

Before and during evaporation process, a mixture of carrier gas (argon) and reaction gas (Freon) is guided through the heating tube and over the sample. Additionally, at the end of the heating-tube and at the front of the transport tube a second argon flow is added named bypass flow [34]. This gas leads to the rapid condensation of the sample vapors. Several works demonstrated the utility of this second argon flow [34–37]. Therefore, the formation of aerosol was explained by Kantor [38] with physical considerations. Next, the total flow of gas carries the aerosol particles into the plasma. It has been demonstrated that the formation of a stable aerosol is required to guarantee transport efficiency of the volatilized analytes from the ETV unit to the ICP torch [38–40]. Therefore, the observation zone was fixed in the radial view ICP used. Position of analytical zone in the plasma was then related to gaseous conditions. From the point of view of maximum available efficiency, the variation of the two argon flow rates must be studied simultaneously to reach the best compromise conditions for multi-element measurement.

For this study, the two mentioned argon flow rates were optimized together with an experimental design. The element signal

Table 2
Thermal cycle of the ETV

Program step	Temperature (°C)	Ramp (s)	Hold time (s)
Pyrolysis I	270	30	60
Pyrolysis II	600	30	30
Vaporization	1900	15	15
Cleaning	2400	2	15
Cooling	20	60	10

Table 3
Effect of carrier and bypass gas flow rates on the emission signal intensities (cps s^{-1}) of some elements (Al, Ca and Fe)

Carrier flow rate (l min^{-1})	Bypass gas flow rate (l min^{-1})				
	0.1	0.2	0.3	0.4	0.5
Al					
0.00			0.22		
0.05		4.14		5.20	
0.10	4.65		8.00		5.87
0.15		6.47		7.37	
0.20			5.96		
Ca					
0.00			0.01		
0.05		2.41		3.45	
0.10	2.27		4.26		1.90
0.15		4.57		3.61	
0.20			3.43		
Fe					
0.00			0.02		
0.05		0.92		0.98	
0.10	0.93		0.90		0.56
0.15		1.07		0.64	
0.20			0.79		

Matrix = cullose spiked with 100 ng Al, 250 ng Ca and 40 ng Fe.

Table 4
Effect of carrier and bypass gas flow rates on the emission signal intensities (cps s^{-1}) of some elements (Al, Ca and Fe)

Carrier flow rate (l min^{-1})	Bypass gas flow rate (l min^{-1})				
	0.1	0.2	0.3	0.4	0.5
Al					
0.00			2.83		
0.05		3.33		5.49	
0.10	4.90		5.17		5.79
0.15		7.20		5.09	
0.20			5.78		
Ca					
0.00			2.30		
0.05		8.78		9.38	
0.10	7.04		10.66		6.65
0.15		9.91		6.37	
0.20			7.56		
Fe					
0.00			1.33		
0.05		2.40		2.22	
0.10	2.53		2.49		2.01
0.15		2.46		1.87	
0.20			2.43		

Matrix = maize sample.

intensities generated by cellulose spiked with the medium standard solution were presented in function of the two argon flow rates. The response surfaces obtained for Al, Ca and Fe were illustrated in Table 3. Thus, it is possible to visualize the transport efficiency of element in relation with the gaseous conditions of ETV. Comparable plots were obtained for others elements. The relative standard deviations obtained on measurements for each element varied between 5 and 20%. It can be then noted that signal intensities showed no significant changes for each individual element for bypass gas flow rate included between 0.4 and 0.2 l min^{-1} and carrier gas flow rate included between 0.05 and 0.20 l min^{-1}. Decay of emission intensities were especially observed only without carrier gas flow rate and, to a certain extent, for the extreme values of bypass argon gas flow rate.

Concerning the carrier gas, it can be expected that without gas flow, no argon was available to transport elements to the exit of the furnace. Increasing carrier gas flow corresponded to significant change in the amount of hot vapor of the sample components mixed with the cold gas behind the vaporization cell and then transported in the ICP torch. For a 0.10 l min^{-1} bypass flow rate, gravitational settling of aerosol particles can occur along the length of the transfer tube [39,40] and a fraction of analytes did not reach the plasma. For the highest bypass flow rate (0.50 l min^{-1}), the depressive effect observed on spectral line intensities could be assigned to the residence time of the analyte species which decreased in the plasma zone used for observation.

However, for accurate results, experimental domain for optimum signal intensities must be the same for sample and calibration. Transport efficiency of volatilized elements was verified by measuring element signal intensities per mass unit sample on maize sample as a function of the two argon gas flow rates. Response surfaces obtained for Al, Ca and Fe were illustrated in Table 4. It appeared that, in comparison with spiked cellulose, decay of the emission signals were not significant for the extreme flow rates of bypass argon (0.10 and 0.50 l min^{-1}). This tendency was verified for all elements. It could perhaps be explained by the nature of the sample matrix. In the case of maize sample, aerosol generated was probably transported more easily from ETV unit to the plasma. From analytical point of view, 0.30 and 0.10 l min^{-1} were chosen for bypass gas flow rate and carrier gas flow rate, respectively, in the next experiments. These values appeared as the best compromise conditions for multi-element measurement.

3.3. Analyze of certified reference materials

On the base of the previous observations obtained with the cellulose sample and the maize powder sample, the analytical method created was employed for plant samples with certified values. For this purpose, the standard reference materials NIST 1568 (rice flour), NIST 1573a (tomato leaves) and NIST 1575a (pine needles) were used. The results obtained were presented in Table 5 and show good agreement between the found values and the certified ones. The calibration with cellulose produced then accurate results, showing that this calibration form was very effective for major elements and trace elements in plant samples [10]. The linearity of the standards was satisfactory for all species ($r^2 > 0.99$).

However, K was not determined in samples. In fact, K is very concentrated in plant samples. Here, the concentration of K is high enough to saturate the optical detector at 766 nm. Usually, the problem can be solved by using another wavelength but the only other wavelength available for K (404 nm) on this spectrometer lacked of sensitivity. This situation was the same for the determination of Ca in NIST 1573a which has very

Table 5
Results ($\mu g\ g^{-1}$) for elements in certified plant samples NIST 1575a (pine needles), NIST 1568a (rice flour) and NIST 1573a (tomato leaves)

	Al	Ca	Cu	Fe	Mg	Mn	Na	Zn
NIST 1575a								
Mean ($n=5$)	535	2375	2.8	43	1026	485	70	38
S.D.	22	68	0.1	4	21	30	2	2
R.S.D.	4.1	2.9	4.6	8.4	2.0	6.1	3.2	3.9
Certified value	580 ± 30	2500 ± 100	2.8 ± 0.2	46 ± 2	1060 ± 170	488 ± 12	63 ± 1	38 ± 2
NIST 1568a								
Mean ($n=5$)	3.9	150	1.4	3.2	730	22.1	7.5	19.4
S.D.	0.9	17	0.8	1.5	112	1.5	1.5	2.3
R.S.D.	23.0	11.3	57.1	47.7	15.3	6.9	20.0	11.9
Certified value	4.4 ± 1.0	118 ± 6	2.4 ± 0.3	7.4 ± 0.9	560 ± 20	20 ± 1.6	6.6 ± 0.8	19.4 ± 0.5
NIST 1573a								
Mean ($n=5$)	557		5.46	350	11757	242	146	29.8
S.D.	45		0.54	33		19	5	1.2
R.S.D.	8.1		9.9	9.6		7.9	3.7	4.1
Certified value	598 ± 12		4.70 ± 0.14	368 ± 7	(12000)	246 ± 8	136 ± 4	30.9 ± 0.7

The value in the parentheses is not certified but only indicative. The calibration was carried out with standard solutions on cellulose.

Table 6
Results ($\mu g\ g^{-1}$) for elements in the NIST 1575a (pine needles) certified plant sample

	Al	Ca	Cu	Fe	Mg	Mn	Na	Zn
NIST 1575a								
Mean ($n=5$)	567	2680	2.9	27	1088	517	67	47
S.D.	42	128	0.2	4	68	32	5	3
R.S.D.	7.4	4.8	6.9	12.8	6.2	6.1	7.1	6.7
Certified value	580 ± 30	2500 ± 100	2.8 ± 0.2	46 ± 2	1060 ± 170	488 ± 12	63 ± 1	38 ± 2

Calibration was carried out against aqueous standard solutions without cellulose. The calibration was carried out with standard solutions without cellulose.

high concentration of Ca ($50.5\ mg\ g^{-1}$). The relative standard deviations obtained were below 10% for NIST 1573a and NIST 1575a. They appeared sometimes enough high (50%) for the less mineralized sample (NIST 1568a). Obtaining repeatable results in the determination of elements by ICP-AES with ETV as introduction device depends on the homogeneity of samples [41] especially in consideration of the mass weighed (1–3 mg). The rice flour sample was the less mineralized sample. In this case, the results can indicate that the distribution of elements was non-homogeneous through the various particles constituting the sample. However, the precisions obtained for majors elements were better than those obtained for trace elements [10]. No signal suppression was observed indicating that matrix effects are absent under the experimental conditions defined. No obvious memory effect was noticed during the analysis.

When calibration against aqueous standards was used without cellulose the results appeared also good in NIST 1575a (Table 6) except for Fe and Zn. Concerning Zn, overestimated concentration was observed. An explanation was that without cellulose, less organic matter was vaporized at the same time of metal. It results a decrease in the concentration of stable particles formed at the end of the furnace. The concentration of particles in the vapor is insufficient to promote good condensation of Zn atoms on these nuclei transported to the plasma. Concerning Fe, the obtained concentration appeared underestimated. An explanation of this phenomenon was difficult to find. However, the calibration with cellulose produced accurate results, showing that this calibration form was very effective.

3.4. Detection limits

The detection limits of studied elements are given in Table 7. They were obtained from the peak area and three times the standard deviation of the background noise measured with ten replicates of the platform alone empty. The sensitivities attained with ETV–ICP-AES were better than those obtained on solutions with radial ICP equipped with pneumatic nebulization [42].

Table 7
Detection limits ($ng\ g^{-1}$) for 2 mg of sample

Element	Detection limit
Al	20
Ca	80
Cu	1
Fe	20
Mg	40
Mn	1
Na	40
Zn	4

4. Conclusions

The determination of major elements with ETV–ICP-AES in plant sample is fairly simple. ETV offers the possibility of in situ sample preparation by selective vaporization of different sample components, using appropriate heating programs. A multi-step furnace temperature program, consisting of a drying step, a pyrolysis step, a vaporization step and finally a high temperature cleaning step is enough to fulfill this requirement. Calibration with cellulose and aqueous standards produced accurate results in good agreement with certified values. The calibration mode suggested that the addition of cellulose as simulated plant matrix has beneficial effect on the similarity between sensitivities established for solid samples and aqueous standard solutions.

However, it was clear that metals contained within the plant must behave not differently than they would have as metals salts present on the outside of cellulose. For this, the two argon flow rates were of vital importance to obtain the best signal intensities for elements. They were responsible of three competitive effects, efficiency of formation of dry aerosol, transport efficiency of analytes between ETV unit and ICP-AES and residence time of the species in the plasma.

To date, the analysis of plant powder samples by electrothermal vaporization is a good alternative to major element detection in digested plant samples. Compared to routine liquid analysis with digestion procedures, the present approach was extremely easy and fast. However, ETV remains an appropriated sample introduction system when the speed with which results are obtained is considered more important than precision. Therefore, elements present in high concentration in the plant sample (K, and sometimes Ca) can produce signal intensities too high for measurement. This last aspect can be considered as the more important limitation of the method.

Acknowledgment

This research was supported by the regional council of Aquitaine with the agreement 20040309007A.

References

[1] T. Kantor, Spectrochim. Acta B 56 (2001) 1523.
[2] J.M. Mermet, Anal. Chim. Acta 250 (1991) 85.
[3] C. Dubuisson, E. Poussel, J.M. Mermet, J. Anal. At. Spectrom. 12 (1997) 281.
[4] M.A. Belarra, M. Resano, F. Vanhaecke, L. Moens, Trends Anal. Chem. 12 (2002) 828.
[5] F. Vanhaecke, M. Resano, L. Moens, Anal. Bioanal. Chem. 374 (2002) 188.
[6] R.W. Fonseca, N.J. Miller-Ihli, Spectrochim. Acta B 51 (1996) 1591.
[7] L. Moens, P. Verrept, S. Boonen, F. Vanhaecke, R. Dams, Spectrochim. Acta B 50 (1995) 463.
[8] M. Berglund, D.C. Baxter, Spectrochim. Acta B 47 (1992) 1567.
[9] S. Boonen, F. Vanhaecke, L. Moens, R. Dams, Spectrochim. Acta B 51 (1996) 271.
[10] P. Masson, Can. J. Anal. Sci. Spectsc. 50 (2005) 268.
[11] T. Buchkamp, G. Hermann, Spectrochim. Acta B 54 (1999) 657.
[12] M. Resano, E. Garcia-Ruiz, F. Vanhaecke, C. Crespo, M.A. Belarra, J. Anal. At. Spectrom. 19 (2004) 958.
[13] F. Vanhaecke, S. Boonen, L. Moens, R. Dams, J. Anal. At. Spectrom. 12 (1997) 125.
[14] Y.-C. Li, S.-J. Jiang, S.-F. Chen, Anal. Chim. Acta 372 (1998) 365.
[15] S. Boonen, F. Vanhaecke, L. Moens, R. Dams, Spectrochim. Acta B 51 (1996) 271.
[16] J. Bernhardt, T. Buchkamp, G. Herman, G. Lasnitschka, Spectrochim. Acta B 55 (2000) 449.
[17] Y. Okamoto, Fresenius J. Anal. Chem. 367 (2000) 300.
[18] P.-C. Li, S.-J. Jiang, Anal. Chem. Acta 495 (2003) 143.
[19] G. Galbacs, F. Vanhaecke, L. Moens, R. Dams, Microchem. J. 54 (1996) 272.
[20] K.C. Friese, K.-H. Grobecker, U. Wätjen, Fresenius J. Anal. Chem. 370 (2001) 499.
[21] M. Ovari, G. Zaray, J. Hassler, Microchem. J. 73 (2002) 125.
[22] M.A. Belarra, C. Crespo, M.P. Martinez-Garbayo, J.R. Castillo, Spectrochim. Acta B 52 (1997) 1855.
[23] M.A. Belarra, M. Resano, J.R. Castillo, J. Anal. At. Spectrom. 13 (1998) 489.
[24] T. Buchkamp, G. Herman, Spectrochim. Acta B 54 (1999) 657.
[25] J. Bernhardt, T. Buchkamp, G. Herman, G. Lasnitschka, Spectrochim. Acta B 54 (1999) 1821.
[26] J.M. Ren, E.D. Salin, Spectrochim. Acta B 49 (1994) 555.
[27] J.M. Ren, E.D. Salin, Spectrochim. Acta B 49 (1994) 567.
[28] D.M. Goltz, D.C. Grégoire, C.L. Chakrabarti, Spectrochim. Acta B 50 (1995) 1365.
[29] D.R. Lide, Handbook of Chemistry and Physics, 71st ed., CRC Press, Boca Raton, 2004–2005.
[30] T. Kantor, Spectrochim. Acta B 55 (2000) 431.
[31] J. Hassler, A. Detcheva, O. Forster, P.R. Prezl, K. Florian, Ann. Chim. 89 (1999) 827.
[32] G. Varhegyi, M.J. Antal Jr., E. Jakab, P. Szabo, J. Anal. Appl. Pyrol. 42 (1997) 73.
[33] P. Mader, V. Haber, J. Zelinka, Analusis 25 (1997) 175.
[34] T. Kantor, M.T.C. de Loos-Vollebregt, Spectrochim. Acta B 58 (2003) 1901.
[35] U. Schäffer, V. Krivan, Anal. Chem. 70 (1998) 482.
[36] T. Kantor, S. Güçer, Spectrochim. Acta B 54 (1999) 763.
[37] N.G. Berrymann, T.U. Probst, Fresenius J. Anal. Chem. 355 (1996) 783.
[38] T. Kantor, Spectrochim. Acta B 143 (1988) 1299.
[39] C.M. Sparks, J. Holocombe, T.L. Pinkston, Spectrochim. Acta B 48 (1993) 1607.
[40] D.C. Grégoire, R.E. Sturgeon, Spectrochim. Acta B 54 (1999) 773–786.
[41] M.A. Belarra, M. Resano, J.R. Castillo, J. Anal. At. Spectrom. 14 (1999) 547.
[42] P. Masson, J.M. Esvan, Analusis 23 (1995) 437.

Available online at www.sciencedirect.com
ScienceDirect
Talanta 71 (2007) 1180–1185
Talanta
www.elsevier.com/locate/talanta

Autonomous microfluidic system for phosphate detection

Christina M. McGraw, Shannon E. Stitzel, John Cleary, Conor Slater, Dermot Diamond *

Adaptive Sensors Group, National Centre for Sensor Research, School of Chemical Sciences, Dublin City University, Dublin 9, Ireland

Received 23 February 2006; received in revised form 30 May 2006; accepted 7 June 2006
Available online 18 July 2006

Abstract

Miniaturization of analytical devices through the advent of microfluidics and micro total analysis systems is an important step forward for applications such as medical diagnostics and environmental monitoring. The development of field-deployable instruments requires that the entire system, including all necessary peripheral components, be miniaturized and packaged in a portable device. A sensor for long-term monitoring of phosphate levels has been developed that incorporates sampling, reagent and waste storage, detection, and wireless communication into a complete, miniaturized system. The device employs a low-power detection and communication system, so the entire instrument can operate autonomously for 7 days on a single rechargeable, 12 V battery. In addition, integration of a wireless communication device allows the instrument to be controlled and results to be downloaded remotely. This autonomous system has a limit of detection of 0.3 mg/L and a linear dynamic range between 0 and 20 mg/L.
© 2006 Elsevier B.V. All rights reserved.

Keywords: Wireless; Sensor; Network; Environment; Phosphate

1. Introduction

Eutrophication is a process in which the overabundance of nutrients in a water system stimulates excessive plant growth (algae, weeds, etc.). This process deteriorates the health of an aquatic ecosystem [1,2] by decreasing the amount of dissolved oxygen available for other organisms and is one of the most common water quality issues for many regions [1,3]. Phosphorus, in the form of phosphate, is a limiting nutrient in natural waters and a key component in the eutrophication process. Therefore the monitoring of phosphate levels is a crucial step in the protection of vulnerable areas.

Phosphate measurements are typically made by manual collection and filtering of samples. Manual sample collection is not only labor intensive and costly, but provides limited information about the spatial and temporal distribution of phosphate throughout a water system. The need for high-frequency phosphate measurements was highlighted by Donohue et al. [4] who, through biweekly and monthly sampling, monitored distributions of nitrogen and phosphorus in 11 rivers over a 2-year period. River flow rates were obtained for each sample and the relationship between river flow and nutrient concentration was studied. Their results indicated that the transfer of nutrients to rivers can occur on the order of hours. In addition, significant seasonal differences in phosphate concentration were measured, highlighting the need for an autonomous sensor capable of making high frequency measurements over an extended period of time.

Different types of monitoring systems have been developed over the years. 'Snapshots' of water quality throughout a marine system have been obtained through shipboard measurements using portable instrumentation [5]. While this method led to fine-scale spatial resolution of water quality, it provided limited temporal resolution since measurements required transects of the water by boat. The development of autonomous, field-based sensors has allowed long-term environmental monitoring of natural waters. Martz et al. [6] demonstrated a submersible sensor capable of continuous monitoring of pH in a river. Measurements, made every 15 min, allowed small daily fluctuations in pH to be resolved. Although this system was capable of autonomous data acquisition, data transfer required manual download at the site. Blain et al. [7] used a MAREL data buoy to monitor tempera-

* Corresponding author. Tel.: +353 1 700 5404; fax: +353 1 700 7995.
E-mail address: dermot.diamond@dcu.ie (D. Diamond).

0039-9140/$ – see front matter © 2006 Elsevier B.V. All rights reserved.
doi:10.1016/j.talanta.2006.06.011

ture, salinity, dissolved oxygen, and fluorescence in the Irish Sea over a 29-month period. Data was collected every 20 min and measurements were transferred to a land-based data center twice daily using a GSM modem. Frequent sampling led to monitoring of daily cycles and allowed the detection of rapid events, such as a fast phytoplankton bloom. While the value of high frequency, autonomous measurements was demonstrated, the system was too large (4 m diameter, 10 t weight) for deployment in remote areas or small water bodies, such as streams.

The development of portable, field-deployable devices requires that all the components of the analysis system be compact, protected from the environment, and capable of operating autonomously for long periods of time. In this work, a system for the detection of phosphate in natural waters has been miniaturized and packaged into a compact and portable system. This completely autonomous device incorporates sampling, reagent handling, mixing of reaction products, colorimetric detection, waste containment, wireless communication, and a power supply. The system employs a low-power detection and communication system, so the entire instrument can operate autonomously for 7 days on a 12 V battery. Integration of a wireless communication device allows acquisition parameters to be controlled remotely and adjusted according to individual needs, in addition to enabling data transfer.

The autonomous system is based on the yellow vanadomolybdophosphoric acid method for phosphate detection. The yellow method is a simple colorimetric technique which involves the formation of vanadomolybdophosphoric acid when a phosphate-containing sample is mixed in a 1:1 ratio with an acidic reagent containing ammonium molybdate and ammonium metavanadate. The resulting solution absorbs strongly below 400 nm. The measured absorbance of the yellow solution is used to determine the concentration of phosphate in the original sample. Previous studies have shown that this method is easily adapted to a microfluidic manifold [8]. In addition, the long-term stability of the reagent makes the technique well suited for autonomous, field-deployable devices [9]. Using a microfluidic manifold in combination with a bench top pump and spectrophotometer, the yellow method was used for analysis of phosphate in river water [10]. Although phosphate concentrations as low as 0.1 mg/L were detected with the microfluidic system, the samples required on-site collection and filtration before being brought back to the laboratory for analysis. The current system extends this previous work by packaging the entire analysis system into a portable and autonomous device.

2. Experimental

2.1. Materials

All solutions are prepared with Milli-Q deionized water (Milli-Ro Plus 30 System, Millipore, Billerica, MA). A 50 mg/L stock solution of *ortho*-phosphate is made by dissolving 0.2195 g of anhydrous potassium dihydrogen phosphate (60218, Fluka, Buchs, Switzerland) in 1 L of deionized water. A 2.25 mL of sulphuric acid (S/9200/PB17, Fisher Chemicals, Leicestershire, England) is added to preserve the stock solution. 0–20 mg/L P–PO_4^{3-} standard solutions are prepared from dilutions of the stock solution with deionized water. The reagent is prepared by dissolving 7.1431 g of ammonium molybdate (A-7302, Sigma, Dorset, England) and 0.3580 g of ammonium metavanadate (20555-9, Aldrich, Dorset, England) in 95 mL of concentrated hydrochloric acid (37 wt.% in water) (926, BDH Laboratory Supplies, Dorset, England) and 905 mL of water.

2.2. Microfluidic chip design

In the first phosphate sensor, colorimetric detection in the microfluidic chip was based on a microcuvette with a 400 μm path length [10]. The sample and reagent were introduced into the chip through separate inlets and mixed in a 1:1 ratio at a T-junction. The resulting yellow solution passed into the microchip's optical cuvette where detection of phosphate was possible by aligning an LED and photodiode detector on opposite sides of the microcuvette. However, when a bubble entered or was formed in the microcuvette, the miniature pump did not provide enough energy to deform the bubble and push into the waste channel. The bubble would remain in the optical cuvette, preventing accurate absorbance measurements, until the chip was flushed by hand. This trapping of bubbles limited the lifetime of the sensor to about 12 h of autonomous operation.

In response, a new microfluidic chip was designed which eliminates the microcuvette and replaces it with a serpentine channel (Fig. 1a). The smooth dimensions of the serpentine channel allow bubbles which enter the microfluidic chip to pass through without becoming trapped. The chip is fabricated in a 2 mm × 16 mm × 32 mm piece of clear polymethyl methacrylate (PMMA) using micromilling techniques. Before milling, the top surface of the PMMA is coated with black ink in order to minimize the amount of background light reaching the detector. After milling, the chip is sealed with a second layer of PMMA using pressure sensitive adhesive. The sample and reagent are

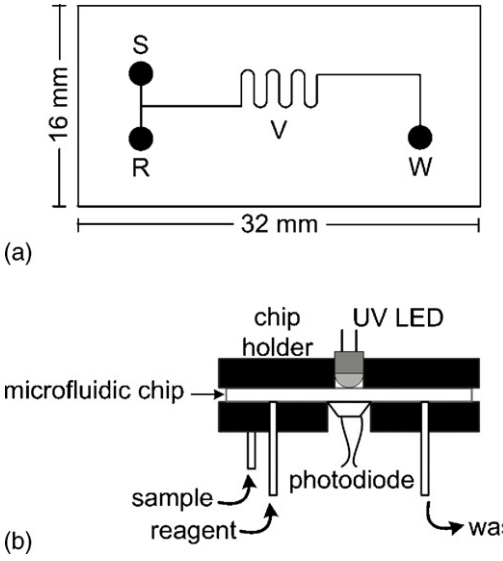


Fig. 1. (a) Microfluidic chip layout with sample (S) and reagent (R) inlets, a serpentine reaction channel and viewing area (V), and waste outlet (W); (b) cross-sectional view of the microfluidic chip holder and detection components.

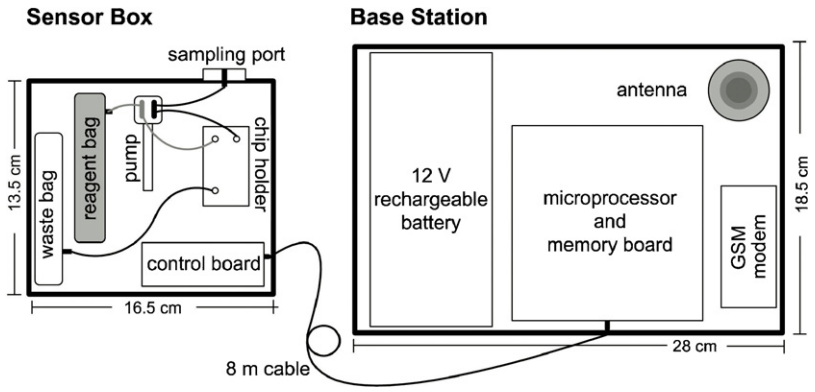


Fig. 2. Diagram of the phosphate sensor and base station.

introduced into the chip through separate inlets and mixed at a T-junction. The solution flows through the 22 mm long serpentine channel, designed to cover the entire active area of a photodiode detector, before exiting the chip through a waste outlet. Channels of 200 μm width and 200 μm depth ensure that mixing of the reagent and sample occurs through diffusion on the time scale of the experiment.

2.3. Experimental setup

The microfluidic chip is integrated into a portable analytical system that incorporates all sampling, detection, and communication components. Polyetheretherketone (PEEK) tubing (175 μm inner diameter), is used for the introduction and removal of the sample, reagent, and waste into the chip inlets and outlet. Epoxy resin adhesive provides leak-free connections between the PEEK tubing and the microfluidic chip. The detection components and the microfluidic chip are held in place with a Perspex chip holder. The chip is secured between the two plates of the chip holder, while a hole in the top plate houses a photodiode (S1227-33BR, Hamamatsu Photonics UK Limited, Hertfordshire, UK) and a hole in the bottom plate holds a 370 nm LED (NSHU550E model, Nichia Corporation, Tokushima, Japan). The photodiode detector and LED are aligned on opposite sides of the chip's serpentine channel, so absorbance measurements of the yellow complex can be made [8] (Fig. 1b).

A miniature dual-channel peristaltic pump (2PP10.S, Eurolink Associates, Tyne & Wear, UK) controls the flow of the phosphate solution and reagent into the microfluidic chip. With Teflon tubing of 0.19 mm inner diameter (116-0549-020, Anachem Ltd., Luton, UK), the flow rate is 2 μL/min. The reagent is stored in a leak-free plastic bag with a PEEK tubing outlet. The reagent storage bag is attached to the tubing of one channel of the peristaltic pump; the tubing of the second channel of the pump is attached to the water sampling port, which is described further below. The fluid from the waste outlet is contained in a second plastic waste bag. The volume of the chip and all sampling tubing is 8 μL.

Development of a field-deployable device requires that the system be protected from the environment, while still allowing sampling and communication. This is done by packaging the entire system into two waterproof polycarbonate boxes (Fig. 2). A 28.0 cm × 18.5 cm × 13 cm box contains the power supply, hardware, and communication components; a 16.5 cm × 13.5 cm × 9.5 cm box houses the peristaltic pump, microfluidic chip, thermistor, light source, detector, and reagent and waste containment bags. These boxes are connected by an 8 m communication cable, although radio communication between the two boxes has been demonstrated in a similar system [11].

The sampling port consists of a 13 mm piece of 0.50 mm inner diameter PEEK tubing placed through the wall of the sensor box. One end of the PEEK tubing is flush with the outer wall of the box and sealed by a polyethersulfone filter membrane with 0.45 μm micropores (Supor 450, Pall Corporation, East Hills, NY); the other end of the PEEK tubing is attached to the pump tubing. The pump must pull the water through the membrane, filtering out large particulate matter, before the fluid can enter the microfluidic chip.

The base station (Whistonbrook Technologies Ltd., Luton, UK) consists of electronic control, data acquisition, and communication components powered by a 12 V, 7 Ah lead acid battery and sealed in the larger waterproof box. The system parameters can be changed via a laptop computer, which communicates with the base station through either a GSM modem or a serial port. Customized software allows the user to set the pumping time, define a measurement delay to ensure completion of the reaction, choose the number of measurements to be made, and decide whether communication with the system is done through the serial port or the GSM modem. Individual measurements can be performed manually or a series of measurements can be made automatically at user-defined intervals. The system is capable of storing the values of up to 40 measurements before download of the data to the computer is necessary. In the following experiments, all communication with the sensor base station is done wirelessly from a laptop computer using the GSM modem.

2.4. Measurements

The sensitivity of the system was determined from the 0, 0.5, 1.0, 5.0, 10, and 20 mg/L P–PO_4^{3-} standards. The minimum measurement time needed for each measurement is 15 min; 10 min for sample and reagent pumping (to ensure that a new

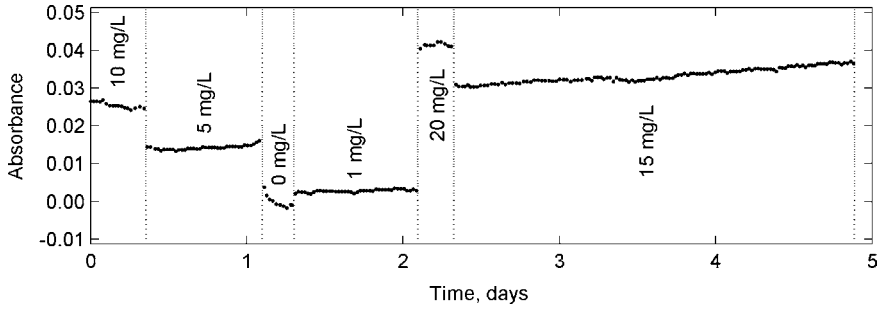


Fig. 3. System response to varying P–PO_4^{3-} concentrations during a 5-day continuous run in the laboratory.

water sample is filtered and introduced to the sampling chamber) and 5 min for the reaction of the phosphate and reagent to go to completion. At the end of the reaction time, the LED is pulsed for 1 ms while the photodiode measures the intensity. In order to obtain an estimate of the variation of the measurement, each measurement was repeated four times. Intensity values were converted to absorbance using the 0 mg/L P–PO_4^{3-} standard as the reference sample.

The ability of the system to operate autonomously was evaluated in the laboratory over a 5-day period. Using the acquisition parameters given above, measurements of the phosphate standards were made every 30 min for 117 h. For each concentration, a series of 10–136 intensity measurements were made.

A field trial of the phosphate sensor was carried out in the Towns River, Co., Offaly, Ireland during a 36-h period between 27 and 29 March, 2006. Due to a decrease in the reaction time caused by the cold environment, it was necessary to increase the time between measurements to 45 min. The final concentration was calculated from the average of two consecutive measurements. On-site calibration was possible by alternating measurements of phosphate in the river with 0 and 5 mg/L P–PO_4^{3-} standards brought to the field. During the river measurements, the sensor was submerged in the water and the base station left on the nearby bank. Data was downloaded remotely to a laptop computer using the base station's GSM modem.

During the field trial, three water samples were collected for analysis back in the laboratory. After collection, each sample was immediately filtered with the polyethersulfone membrane filter, stored in an acid-washed sample bottle, and frozen within 30 min of collection. In the laboratory, aliquots of each thawed sample were mixed with the yellow reagent and the absorbance of the solution was measured in a bench-top spectrophotometer (Cary 50, Varian, Inc., Palo Alto, CA).

3. Results and discussion

Calibration results show a linear relationship between absorbance and P–PO_4^{3-} concentration. The linear fit of the calibration data is described by $A = 1.98 \times 10^{-3} \times C + 1.01 \times 10^{-3}$ where A is the absorbance of the solution and C is the concentration of phosphate in the original sample (mg/L). The R^2 value is 0.998 and the standard errors of the slope and intercept estimates are 2.0×10^{-5} and 2.0×10^{-4}, respectively. The limit of detection (LOD) of the system, defined as the concentration equal to three times the standard deviation of the measurement above the background absorbance, is 0.3 mg/L.

The ability of the sensor to operate autonomously over 5 days is shown in Fig. 3. During the test period, 241 measurements were collected and analyzed. Although this experiment was performed in the laboratory, the system was not disturbed during this time period and the device was controlled and data collected remotely using the GSM modem.

The laboratory results in Fig. 3 indicate that the system is capable of operating autonomously on a single, rechargeable, 12 V battery for extended periods of time. As expected, the absorbance changes linearly with P–PO_4^{3-} concentration. However, the system shows a drift in intensity of approximately 0.01%/h over the time course of the experiment. This drift is likely caused by staining of the viewing window by the vanadomolybdophosphoric acid. The effect of the observed drift is minimized by applying a constant correction factor to the intensity measurements. A linear fit of the concentration versus absorbance data for the long-term run is described by $A = 2.08 \times 10^{-3} \times C + 1.88 \times 10^{-3}$. $R^2 = 0.985$ and the standard errors of the slope and intercept estimates are 2.4×10^{-5} and 2.0×10^{-4}, respectively. These values agree with the calibration results and show that the sensor response is still linear over the longer time period.

The system LOD over the 5-day laboratory trial is 1.5 mg/L P–PO_4^{3-}, five times higher than the LOD of the initial calibration experiment. The significant increase in LOD during this 5-day laboratory trial is caused partly by changes in temperature, as the brightness of the LED varies with temperature and leads to small changes in measured intensity. The temperature-induced intensity changes are most clearly observable in the 0 mg/L series of data in Fig. 3. A 5 °C change in temperature inside the sensor box at time = 1.1 days led to the spike in absorbance seen in the 0 mg/L data. This resulted in a relatively large standard deviation for the 0 mg/L data and increased the LOD of the sensor during the 5-day laboratory trial.

The system's intensity drift of approximately 0.01%/h also led to a higher LOD for the 5-day laboratory trial. The calibration experiment was done over a 7 h time period, while the laboratory-based long-term run lasted for 117 h. The expected changes in intensity due to drift for these experiments are 0.1% and 2%, respectively. While the drift correction minimizes the long-term increase in absorbance, Fig. 3 shows it does not fully correct the upward trend. This drift increases the measurement error, leading to a further increase in the LOD.

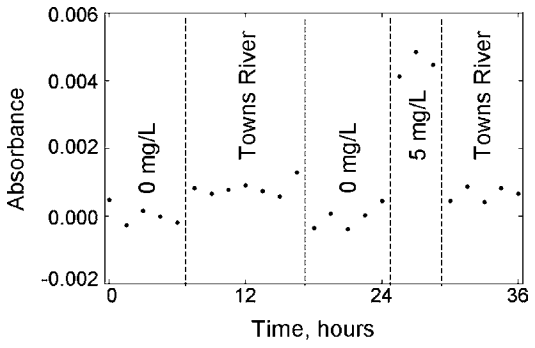


Fig. 4. Field measurements of P–PO_4^{3-} in the Towns River, Co., Offaly, Ireland.

The drift-corrected results from the Towns River measurements are shown in Fig. 4. During the 36-h field trial, the water temperature varied between 7 and 9 °C. Using the 0 and 5 mg/L data for on-site calibration, the measured concentrations of P–PO_4^{3-} in the river were 0.9 ± 0.5 mg/L ($n = 7$) and 0.7 ± 0.5 mg/L ($n = 5$) for the two series of measurements. The LOD of the sensor in the field was 1.0 mg/L P–PO_4^{3-}. River samples taken during the trial were analyzed in the laboratory and gave phosphate levels of 0.4 ± 0.1 mg/L ($n = 3$). These laboratory results are lower than the average field test results, but fall well within the 95% confidence intervals of the Towns River measurements given above and reflect the fact that phosphate levels vary with time. In addition, the field results in Fig. 4 clearly show that the instrument is sufficiently sensitive to distinguish between the blank standard (i.e. 0 mg/L P–PO_4^{3-}) and the measured river concentrations of phosphate.

The LOD of the phosphate sensor over long time periods could be improved if the effects of temperature and drift were reduced. The addition of a heater to the sensor box would help stabilize the internal temperature of the sensor and minimize the temperature-induced intensity changes of the LED, although it would also increase the overall energy consumption of the system. In addition, occasional blank measurements would significantly improve the drift correction. Further improvements may be seen if the system was redesigned to offer a broader range of absorbance measurement techniques. Currently, the system is configured to make one intensity measurement per experiment. Improvements in the signal to noise ratio, and therefore LOD, could be achieved through techniques such as signal averaging.

Long-term deployment of the sensor is limited by the lifetime of the sensor's battery and the reagent and waste storage capabilities. At current sampling rates, it is possible to make 32 measurements a day, with a reagent consumption of less than 1 mL each day. Reagent consumption, and waste containment, could be reduced further if the sampling rate was decreased. For example, six samples per day would still allow daily events to be monitored, but would also lead to an eight-fold reduction in reagent consumption. At this reduced sampling rate, less than 50 mL of reagent would be consumed annually, a volume easily contained in the waste storage bags. Further reduction in reagent consumption could be achieved by minimizing the dead volume of the system through more efficient use of the system's tubing.

In addition to minimizing the amount of reagent consumed, reducing the sampling frequency would extend the lifetime of the sensor. At current sampling rates of 48 measurements and 2–6 GSM downloads per day, the sensor can operate for 7 days off a single, rechargeable 12 V battery. Since operation of the pump is the most significant drain on the battery, the sensor's lifetime would increase significantly if the sampling rate were decreased. Minimization of the system's dead volume would allow shorter pumping times and a subsequent decrease in power consumption. Alternatively, incorporation of a solar powered device could be used to significantly extend the battery life.

A second limitation to long-term deployment of the sensor is fouling of the filtration membrane. The fouling may be due to colloidal clogging of the membrane pores or the formation of a biofilm on the membrane surface. Biofouling is caused by the growth of biological organisms on submerged surfaces and limits deployment periods of environmental sensors [12]. In eutrophic water systems, where this sensor is designed to be deployed, the effects of biofouling are especially significant. In response, the sampling port is designed for fast and easy on-site replacement of the filtering membrane. More work is needed to determine how often the membranes should be replaced for long-term deployment of the sensor in natural waters.

Common interferences associated with this detection method are arsenate and silicate, which can react with the reagent to form colored acid complexes [13]. In natural waters, where these ions may be present, this reaction can interfere with the measurement of phosphate. Methods have been developed to minimize the effect of these interferences [13,14], although none have been incorporated into this sensor. However, this sensor is designed for deployment in areas with high phosphate levels, where the effect of interferences is less significant [15]. In addition, compared with high-temperature techniques used in the laboratory to decrease reaction times, the low river temperatures should minimize the effect of the silicate interference [14]. If, in the future, a heater is incorporated into the sensor to minimize the temperature-induced intensity changes of the LED, care must be taken to keep the reaction temperature low so the effect of the silicate interference is minimized.

The LOD for laboratory-based experiments done on a short time scale was 0.3 mg/L P–PO_4^{3-}. For longer trials and field measurements, the LOD increased to 1.0–1.5 mg/L P–PO_4^{3-}. While this is greater than the 0.1 mg/L P–PO_4^{3-} level defined by the European Union's environmental directives as an indicator for excessive algal growth [16], higher concentrations of phosphate have been measured in agricultural, industrial, and densely populated areas. For example, a study of phosphate in Dublin's Broadmeadow River used the yellow method to detect an average concentration of 1.5 mg/L P–PO_4^{3-} [10]. The autonomous sensor results indicate that the device is sufficiently sensitive for *in situ* measurements of phosphate in these regions.

4. Conclusions

A portable system for long-term monitoring of phosphate has been developed. This completely autonomous device incorporates sampling, reagent and waste storage, colorimetric detection, wireless communication, and a power supply into a complete, miniaturized system. Integration of a wireless

communication device allows acquisition parameters to be controlled remotely and adjusted according to individual needs. In addition, wireless communication capabilities allow the results to be downloaded remotely and displayed in real time. The autonomous capabilities of the system, combined with the portability and wireless communication, provide the flexibility needed for on-site phosphate monitoring. This system demonstrates the potential of truly autonomous microfluidic platforms for use in long-term environmental monitoring.

Acknowledgements

The authors thank Nigel Kent for his assistance with experimental aspects of this project. This research was supported by the Environmental Protection Agency (Grant 2004-RS-AIC-M4) and Science Foundation Ireland Adaptive Information Cluster award (Grant 03/IN.3/1361).

References

[1] V.H. Smith, G.D. Tilman, J.C. Nekola, Environ. Pollut. 100 (1999) 179.
[2] C.P. Mainstone, W. Parr, Sci. Total Environ. 282–283 (2002) 25.
[3] S.R. Carpenter, N.F. Caraco, D.L. Correll, R.W. Howarth, A.N. Sharpley, V.H. Smith, Ecol. Appl. 8 (1998) 559.
[4] I. Donohue, D. Styles, C. Coxon, K. Irvine, J. Hydrol. 304 (2005) 183.
[5] J. Hodge, B. Longstaff, A. Steven, P. Thornton, P. Ellis, I. McKelvie, Mar. Pollut. Bull. 51 (2005) 113.
[6] T.R. Martz, J.J. Carr, C.R. French, M.D. DeGrandpre, Anal. Chem. 75 (2003) 1844.
[7] S. Blain, J. Guillou, P. Treguer, P. Woerther, L. Delauney, E. Follenfant, O. Gontier, M. Hamon, B. Leilde, A. Masson, C. Tartu, R. Vuillemin, J. Environ. Monit. 6 (2004) 569.
[8] M. Bowden, M. Sequeira, J.P. Krog, P. Gravesen, D. Diamond, Analyst 127 (2002) 1.
[9] M. Bowden, D. Diamond, Sens. Actuators B: Chem. 90 (2003) 170.
[10] M. Bowden, M. Sequiera, J.P. Krog, P. Gravesen, D. Diamond, J. Environ. Monitor. 4 (2002) 767.
[11] K. Crowley, J. Frisby, S. Murphy, M. Roantree, D. Diamond, Sens. Actuators A 122 (2005) 222.
[12] A. Kerr, M.J. Smith, M.J. Cowling, Mater. Des. 24 (2003) 247.
[13] C.Z. Katsaounos, D.L. Giokas, A.G. Vlessidis, E.K. Paleologos, M.I. Karayannis, Sci. Total Environ. 305 (2003) 157.
[14] C. Neal, M. Neal, H. Wickham, Sci. Total Environ. 251/252 (2000) 511.
[15] H.P. Jarvie, P.J.A. Withers, C. Neal, Hydrol. Earth Syst. Sci. 6 (2002) 113.
[16] I.P.A. Morais, I.V. Toth, A.O.S.S. Rangel, Talanta 66 (2005) 341.

Available online at www.sciencedirect.com
ScienceDirect
Talanta 71 (2007) 1430–1433
Talanta
www.elsevier.com/locate/talanta

Short communication

Porous silicon as functionalized material for immunosensor application

O. Meskini [a], A. Abdelghani [b,*], A. Tlili [b], R. Mgaieth [a], N. Jaffrezic-Renault [c], C. Martelet [c]

[a] *LPSCM, Faculté des Sciences de Monastir, Route de kairouan, 5000 Monastir, Tunisia*
[b] *Unité de Recherche de Physique des Semiconducteurs et Capteurs, IPEST, La Marsa, 2070 Tunis, Tunisia*
[c] *CEGELY, ECL, 36 Avenue Guy de Collongue, 69134 Ecully Cedex, France*

Received 19 December 2005; received in revised form 25 April 2006; accepted 12 May 2006
Available online 14 July 2006

Abstract

Recently, for sensor application, porous silicon has received a great deal of attention due to the high specific surface area and the easy fabrication using some established processes of the usual silicon technology. We herein, report the development of a novel immunosensors based on porous silicon for antigen detection. The multilayer immunosensor structure was fabricated following the successive steps: APTS self-assembled monolayer (SAM) layer, glutaaldehyde linker, anti-rabbit IgG binding. The insulating properties of the aminopropyl-triethoxysilane (APTS) monolayer were studied with cyclic voltammetry and the molecular structure was characterized with Fourier-transform infrared (FTIR) technique. The binding between antibody and different antigen concentration (rabbit IgG) was monitored by measuring the capacitance–voltage curve of the antibody functionalized EIS structure. A detection limit of 10 ng/ml of antigen can be detected.
© 2006 Elsevier B.V. All rights reserved.

Keywords: Biosensors; EIS structure; *C*(*V*); FTIR; Antibody; Antigen

1. Introduction

Recently, porous silicon has been used as an optical interferometric transducer for detecting small organic molecules (biotin and digoxigenin) and 16-nucleotide DNA oligomers, at pico- and femtomolar analyte concentrations [1,2]. Moreover, microcavity resonators made of porous silicon have been used for biosensor applications. These resonators possess the unique characteristics of line narrowing and luminescence enhancement. Chan et al. [3] fabricated a DNA biosensor based on a porous silicon microcavity structure. The microcavity structure was highly sensitive and any slight change in the effective optical thickness modified its reflectivity spectrum, causing a spectral shift in the interference peaks. Potentiometric biosensors based on porous silicon have been described [4]. The enzymes penicillinase and lipase were separately immobilized on the surface of porous silicon to detect penicillin and triglycerides [5–7]. The hydrolysis reactions caused a local change in the pH of the solution. The enzyme oxidized porous silicon-crystalline structure was used to detect the changes in pH during hydrolysis as a shift in the capacitance–voltage (*C–V*) characteristics.

This paper deals with a new method to biofunctionalize porous silicon surface for immunosensor application. The functionalization of the porous silicon surface can be achieved by the formation of a self-assembled monolayer (SAM) of aminopropyl-triethoxysilane (APTS). The amino groups on the surface can be used for Schiff base formation with glutaaldehyde, then covalent binding of the antibody (anti-IgG) can be easily achieved. Different antigen concentration can be detected with a good reproducibility. Each step can be controlled by high sensitive capacitance–voltage measurements on the functionalized EIS structure.

2. Experimental set-up

2.1. Materials

Unless otherwise specified, all materials were used as received. The 3-aminopropyl-triethoxysilane (minimum 98%), glutaaldehyde, anti-rabbit IgG and the rabbit IgG were from Sigma. Antibodies and antigen were kept frozen until use and were made with 100 mM phosphate buffer saline. A Millipore

* Corresponding author. Tel.: +216 71 74 00 48; fax: +216 71 74 65 51.
E-mail address: aabdelghani@mailcity.com (A. Abdelghani).

0039-9140/$ – see front matter © 2006 Elsevier B.V. All rights reserved.
doi:10.1016/j.talanta.2006.05.089

grade water with a specific resistance of 18.2 MΩ cm^2, was used throughout the experiments.

2.2. Porous silicon preparation

Devices were manufactured in silicon substrate p-type, weakly boron-doped (≈10^{15} at cm^3) and oriented according to the crystalline direction ⟨1 0 0⟩. Before electrochemical anodization of silicon, the samples were firstly cleaned with a solution of acetone and then were rinsed with desionised water (18 MΩ). Porous silicon layers were made by the anodic etching in a 1:2.5 mixture of 48 wt.% HF solution and ethanol at a constant current density of 50 mA/cm^2 for 2–5 s. The anodization process was carried out in an electrolytic cell made of teflon. Concerning the effect of porosity (depending upon initial material resistivity, HF concentration and anodic current) on the sensitivity of the sensor, it was previously shown that the porosity close to 65% is the optimum value [17].

2.3. Silanization

The activation of the porous silicon surfaces was performed by thermally activated method with the 3-aminopropyltriethoxysilane. The porous silicon substrates were kept in a vial containing one drop of the amino-silane and heated for 4–5 h at 100 °C. The vapour of amino-silane condensed with the hydroxyl groups on the surface of porous silicon and provided reactive amino groups. Finally, the substrates were thoroughly rinsed with ethanol and dried with nitrogen.

2.4. Immobilization of glutaaldehyde cross-linker

The substrates were immersed into a solution of glutaaldehyde (2.5%) adjusted to pH 7 using sodium hydroxide. The wafers were kept in the solution for 1 h at room temperature. It was important to rinse successively with water in order to remove all excess of glutaaldehyde.

2.5. Covalent binding of antibody and blocking layer

The antibody (5 μg/ml in acetic/acetate buffers, pH 5) was dropped onto the treated substrates at 37 °C for 1 h. Under these conditions, the glutaaldehyde groups react with the amino groups of the antibody. After the immobilization, the substrate was cleaned with 0.05% Tween 20 in phosphate buffered saline (PBS) and with water. In order to prevent non-specific adsorption, the substrates were dipped for 30 min at room temperature into a 0.1% bovine serum albumin (BSA) solution.

2.6. Antigen–antibody binding

The substrates were put in contact with antigen (rabbit IgG, 5 μg/ml) in acetic/acetate buffer pH 5 for 1 h, then, rinsed with 0.05% Tween 20 in PBS and finally with distilled water.

2.7. Electrochemical measurement

The cyclic voltammetry was performed using the Voltalab 40 (Radiometer Analytical, Lyon, France) impedance analyser. The electrolyte was 1 mM PBS solution at pH 7.4. The voltage range from −0.8 to 0.8 V with a scan rate of 25 mV/s.

The capacitance–voltage measurement were performed with the same Voltalab 40 impedance analyser with applied potential (versus reference electrode) between −0.8 and 0.8 V with a step of 50 mV. A dc bias (V) and an exciting alternative signal were applied to the working electrode. The amplitude of the alternative signal was 5 mV and the working frequency was fixed to 10 kHz.

In all our experiments, we used an Ag/AgCl reference electrode. The surface area of the platinum counter-electrode was 0.385 cm^2 and that of the working electrode, about 0.19 cm^2. All connections were made with coaxial cables to minimize any external electrical noise. All measurements were carried out at room temperature in the dark, and in a faradaic box. The electrolyte was degassed before use, to prevent any formation of air bubbles. More details about this technique can be found in references [8–15].

2.8. Fourier-transformed infrared spectroscopy

Fourier-transformed infrared (FTIR) spectra were obtained in reflection mode with a Brucker IFS 66/S spectrometer equipped with a Middle Infrared (MIR) source, a DTGS detector and a KBr separating mirror. All spectra were collected with 64 scans for the reference and the sample, with 4 cm^{-1} resolution. For porous silicon, first we record the spectrum of mirror as a reference, and then that of porous silicon. The ratio of the second one to the first one gave the spectrum of the porous silicon. For the silane monolayer, first we record the spectrum of the porous silicon as a reference, and then of the APTS treated porous silicon. The ratio of the second one to the first one gave the spectrum of the silane monolayer.

3. Results and discussion

3.1. FTIR on APTS treated porous silicon

Fig. 1a and b shows the FTIR spectrum of the porous silicon and of the silane monolayer between 500 and 3500 cm^{-1}. The spectrum of the porous silicon is identified with the bands at 1080 and 1100 cm^{-1} which correspond to the Si–O vibration mode.

The formation of siloxane bands on porous silicon is proven by the presence of two bands at 1080 and 1180 cm^{-1}. These bands are assigned to the symmetric stretch mode of (Si–O) [16]. These bands indicate that the siloxane bond formation has occurred between the silane and the porous silicone surface. Another peaks appears at 745 and 537 cm^{-1}, these band correspond to N–H deformation out of plane mode and symmetric stretch mode of Si–C, respectively. Finally, main band is clearly observed in the high frequency region. These are assigned to the symmetric vibration mode of CH_2, the antisymmetric vibration mode of CH_2 and the antisymmetric vibration mode of the alkyl silane chains.

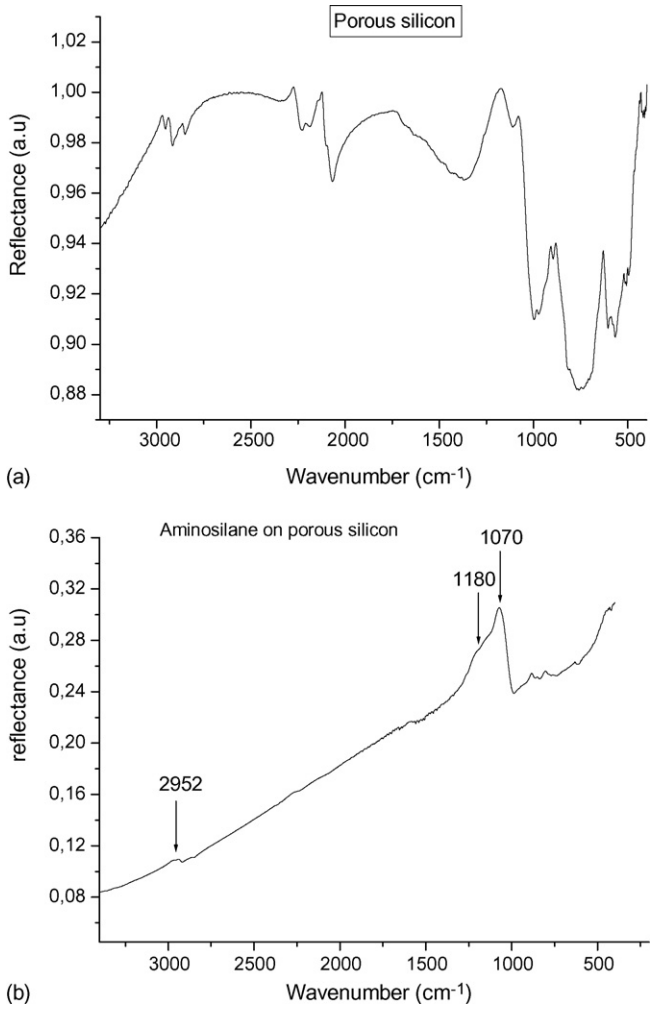


Fig. 1. FTIR spectrum of: (a) the porous silicon between 500 and 3500 cm^{-1} and (b) the silane layer between 500 and 3500 cm^{-1}.

3.2. Porous silicon/SAM/electrolyte interface

Cyclic voltammograms of the porous silicon electrode were registered before and after the self-assembled monolayer deposition in PBS buffer and the results are presented in Fig. 2. As shown in the figure, the pretreated porous silicon electrode presents, a reversible cyclic voltammogram, indicating a clean porous surface. The two peaks (negative current and positive current) indicating that the oxydo-reduction reactions on porous silicon can be observed. The formation of the APTS self-assembled monolayer on porous silicon electrode (Fig. 2) resulted in the decrease of the faradaic current. Then, the SAM monolayer act as a blocking layer for any faradaic process which indicating a high insulating properties.

3.3. Capacitance of the porous silicon/SAM/antibody/electrolyte interface

The capacity measurements of the porous silicon electrode before (with silane) and after the deposition of the antibody layer are presented in Fig. 3. The deposition of the antibody layer leads to a significant decrease in the total capacitance

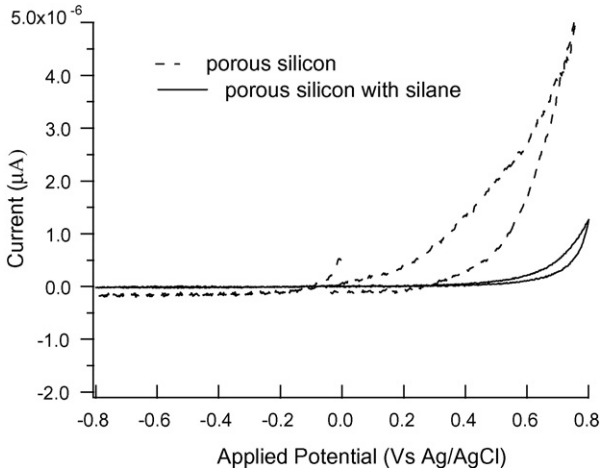


Fig. 2. Cyclic voltammograms of the porous silicon electrode before and after the self-assembled monolayer deposition in PBS buffer.

at accumulation regime range ($V > 0.2$ V). This decrease in the accumulation regime, is attributed to a change in dielectric constant and in the thickness of the studied structure (the capacitance of an equivalent plane condensator is equal to $C = \varepsilon\varepsilon_0 s/e$). The relative variation of the capacitance is 37% compared to 30% obtained with flat silicon [18].

3.4. Antigen detection

Fig. 4 shows the capacitance measurements of the biofunctionalized porous silicon (after the deposition of the BSA blocking molecules) electrode after equilibrium with different antigen concentrations. The total capacitance in accumulation regime decreased after adding antigen. This decrease is attributed to an increase in the thickness and to a rearrangement in the structure of the antibody which induces a variation of the dielectric constant.

By fixing the applied potential in the accumulation regime (for example, 0.4 V), the sensitivity of the biosensor

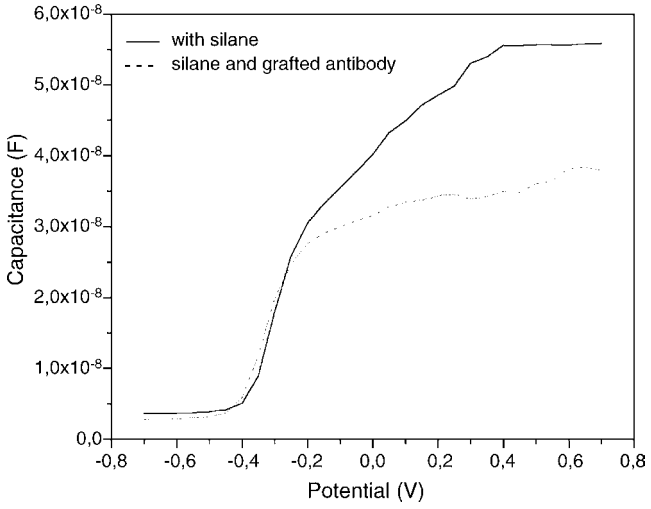


Fig. 3. The capacitance measurements of the porous silicon electrode before (with silane layer straight line) and after the deposition of the antibody (layer in PBS solution at pH 7.4).

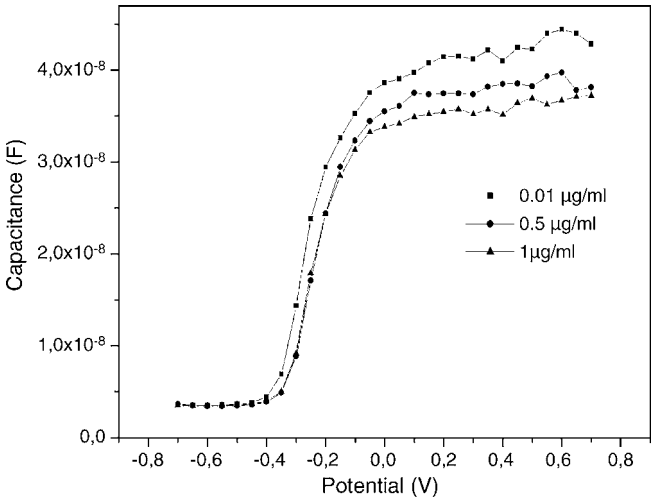


Fig. 4. The capacitance measurements of the biofunctionalized porous silicon electrode after different antigen concentrations (straight line: 0.01 μg/ml; dashed line: 0.5 μg/ml; dotted line: 1 μg/ml).

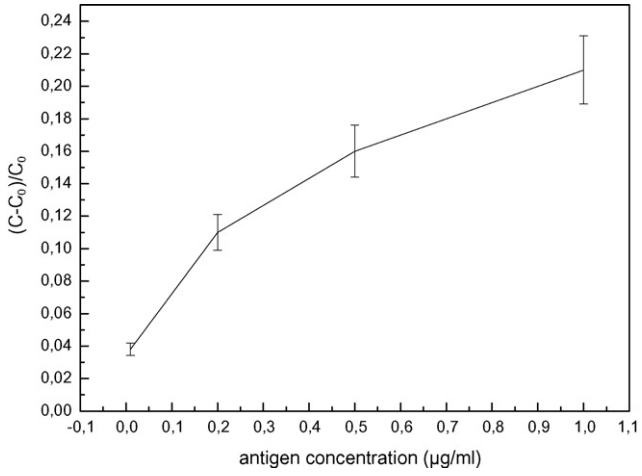


Fig. 5. The sensitivity of the biosensor vs. the antigen concentration.

$((C - C_0)/C_0)$ for each antigen concentration can be obtained (cf. Fig. 5). The capacitance C_0 corresponds to the capacitance without antigen, and C corresponds to the capacitance for each antigen concentration. For a concentration of antigen of 1 μg/ml, the relative variation of capacitance is equal to 20%, compared to 4% for flat silicon [18]. The lowest detection limit that induces a measurable capacitance variation is about 10 ng/ml antigen.

4. Conclusion

Porous silicon substrates have been used for antibody–antigen interaction. Electrochemical methods and optical methods are combined to exhibit the formation of the silane monolayer and to show its insulating properties. The capacitance measurement technique provides a sensitive tool to monitor the specific interaction between antibody and antigen. Comparing the sensitivity obtained with flat silicon and porous silicon, this later material shows a quite higher sensitivity for the antigen detection (multiplied by five). The lowest antigen concentration (10 ng/ml) detected by porous silicon opens the possibility of using this biofunctionalized material for future biosensing devices.

Acknowledgements

The author (Dr. A. Abdelghani) thanks the Alexander Von Humboldt Foundation for the material donation. The electrochemical and FTIR measurement was performed in the Unité de Recherche de Physique des Semiconducteurs et Capteurs (La Marsa).

References

[1] V.S. Lin, K. Motesharei, K.P. Dancil, M.R. Ghadiri, Science 278 (1997) 840.
[2] G. Di Francia, L. Quercia, S. La Ferrara, S. Manzo, S. Chiavarini, F. Cerullo, F. De Filippo, V. La Ferrara, P. Maddalena, R. Vitiello, Second Workshop on Chemical Sensors and Biosensors, Rome, Italy, March 18–19, 1999.
[3] S. Chan, P.M. Fauchet, Y. Li, L.J. Rothberg, B.L. Miller, Phys. Status Solidi, A. Appl. Res. 182 (2000) 541.
[4] M. Thust, M.J. Schöning, S. Frohnhoff, R. Arens-Fischer, P. Kordos, H. Lüth, Meas. Sci. Technol. 7 (1996) 26.
[5] M.J. Schöning, A. Kurowski, M. Thust, P. Kordos, J.W. Schultze, H. Lüth, Sens. Actuators B 64 (2000) 59.
[6] R.R. Reddy, A. Chadha, E. Bhattacharya, Biosens. Bioelectron. 16 (2001) 313.
[7] R.R.K. Reddy, I. Basu, E. Bhattacharya, A. Chadha, Curr. Appl. Phys. 3 (2003) 155.
[8] A. Tlili, S. Hleli, A. Abdelghani, Sensors 4 (2004) 104.
[9] H. Hillebrandt, G. Wiegand, M. Tanaka, E. Sackmann, Langmuir 15 (1999) 8451.
[10] J.R. MacDonald, Impedance Spectroscopy, Wiley, New York, 1987.
[11] M. Herlem, B. Fahys, S. Zairi, N. Jaffrezic-Renault, Electrochim. Acta 47 (2002) 2597.
[12] A. Kaminsky, J. Willner, D. Mandler, J. Electrochem. Soc. 40 (1993) 215.
[13] S. Wawzonek, T.W. McIntyre, J. Electrochem. Soc. 114 (1967) 1025.
[14] A. Abdelghani, C. Jacquin, E. Sackmann, Mater. Chem. Phys. 70 (2001) 187.
[15] A. Abdelghani, S. Hleli, K. Cherif, Mater. Lett. 6 (2002) 1064.
[16] M. Cai, M. Ho, E. Pemberton, Langmuir 16 (2000) 3446.
[17] S. Zairi, C. Martelet, N. Jaffrezic-Renault, Talanta 55 (2001) 951.
[18] P. Bataillard, F. Gardies, N. Jaffrezic-Renaukt, C. Martelet, Anal. Chem. 60 (1988) 2374.

Available online at www.sciencedirect.com
ScienceDirect
Talanta 71 (2007) 1211–1218
Talanta
www.elsevier.com/locate/talanta

Effect of hydrophobic chain length of the chiral surfactant on enantiomeric separations by electrokinetic chromatography: Comparison between micellar and vesicular pseudo-stationary phases

Ashok Mohanty, Joykrishna Dey *

Department of Chemistry, Indian Institute of Technology, Kharagpur 721302, India

Received 2 April 2006; received in revised form 11 June 2006; accepted 11 June 2006
Available online 18 July 2006

Abstract

Two novel amino acid based surfactants sodium *N*-(4-*n*-decyloxybenzoyl)-L-valinate (SDeBV) and sodium *N*-(4-*n*-octyloxybenzoyl)-L-valinate (SOBV) have been synthesized and used as chiral selectors for enantiomeric separations by micellar electrokinetic chromatography (MEKC). The aggregation behavior of the surfactants was studied in buffered aqueous solution using surface tension and fluorescence probe techniques. The microenvironment of the aggregates was studied using pyrene, and 1,6-diphenyl-1,3,5-hexatriene (DPH) as probe molecules. Results of these studies indicate that these two surfactants form micelles in buffered aqueous solution. Successful enentioseparation has been achieved for 1,1′-bi-2-naphthol (BOH), 1,1′-binaphthyl-2,2′-diylhydrogenphosphate (BNP), 2,8-dimethyl-6H-5,11-methanodibenzo[*b*,*f*] [1,5]diazocine (Tröger's base, TB), and benzoin (BZN) using the two chiral selectors SDeBV and SOBV. The separations were optimized with respect to surfactant concentration, pH, and buffer concentration. The results are discussed in light of the aggregation behavior of the surfactants. A comparison of the results of this study has been made with the data from literature to investigate the effect of self-assembly morphology on enantiomeric separations.
© 2006 Elsevier B.V. All rights reserved.

Keywords: Capillary electrophoresis; MEKC; Enantiomeric separation; Hydrophobic chain length

1. Introduction

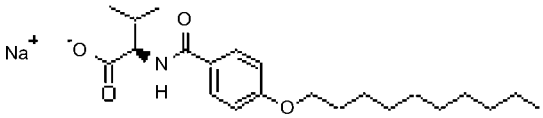
Enantiomeric separation of chiral molecules is important to environment and biological fields as well as to synthetic chemists and pharmaceutical industry. This is primarily because of the need for pure enantiomers in biomedical studies, asymmetric synthesis, catalysis, and medicines. Micellar electrokinetic chromatography (MEKC), the mode of capillary electrophoresis (CE) introduced by Terabe et al. [1] for analysis of neutral analytes, is an extensively used analytical technique for enantiomeric separations in recent years [2,3]. The technique involves use of a surfactant at a concentration above its critical micellar concentration (cmc) in the background electrolyte (BGE). The surfactant molecules self-assemble to form micelles that act as the pseudo-stationary phase. Chiral separation in MEKC is achieved by use of a chiral selector in the BGE in combination with an achiral surfactant like sodium dodecyl sulfate (SDS). Different chiral selectors used in MEKC include but not limited to cyclodextrins, macrocyclic antibiotics, crown ethers, and calixarenes, etc. [4–7]. An alternative way is to use a chiral surfactant above its cmc in the background electrolyte. The chiral surfactant form micelles with stereogenic centers at the surface and it acts as the chiral selector. A variety of chiral surfactants have been used in MEKC to achieve enantiomeric separation of a wide spectrum of compounds like chiral drugs, pesticides, atropisomeric compounds, and derivatized amino acids [8–25]. The chiral surfactants utilized are naturally occurring surfactants digitonin [8], saponin [9], and bile salts [10], glucopyranoside based sulfate and phosphate surfactants [11], amino acid based surfactants [12–19] and polymeric surfactants [20–25]. Among all the chiral surfactants, amino acid based monomeric and polymeric surfactants are most widely used. This is because of the advantages associated with the amino acid based surfactants. The advantages are (i) surfactants with a variety of chiral

* Corresponding author. Tel.: +91 3222 283308; fax: +91 3222 255303.
E-mail address: joydey@chem.iitkgp.ernet.in (J. Dey).

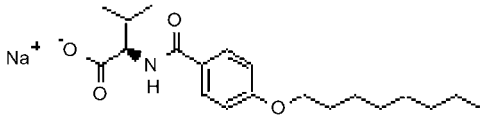
0039-9140/$ – see front matter © 2006 Elsevier B.V. All rights reserved.
doi:10.1016/j.talanta.2006.06.020

headgroups and chemical compositions can be synthesized to manipulate the chiral selectivities, and (ii) both D and L optical configurations of amino acid-based surfactants are available to determine enantiomeric impurities more accurately by reversal of migration order of the two enantiomers. In fact, a number of reports have appeared in the literature in which authors have used surfactants and polymers having different amino acids as headgroups to investigate the mechanism of chiral recognition [26–30]. The results of these studies indicate that chiral recognition occurs due to interaction of the analytes with the chiral selector near the stereogenic center, i.e. at the micellar surface. However, the effect of length of the hydrophobic tail of the surfactant on enantiomeric separations has not been reported so far. The change in length of the hydrophobic tail of the surfactant can lead to formation of different kind of aggregates by the surfactant molecules when dissolved in the BGE. This is because, hydrophobic interaction between the hydrocarbon tails of the surfactant molecules is one of the driving forces for aggregate formation and in most cases, it determines the extent of close packing of the surfactant molecules during aggregate formation. Therefore, difference in hydrophobic chain length will result in difference in shape, size, and physical properties like microviscosity, micropolarity of the self-assemblies formed. All these factors will have direct influence on the partitioning of the analyetes with the pseudo-stationary phase, which is the essential condition to obtain separation in electrokinetic chromatography (EKC).

In our recent works reported earlier [17–19], we have used the vesicle-forming amino acid based surfactants sodium *N*-(4-*n*-dodecyloxybenzoyl)-L-amino acidates having L-valine, L-leucine, and L-isoleucine (SDBV, SDBL, and SDBIL, respectively) as the headgroups for enantiomeric separations of 1,1′-bi-2-naphthol (BOH), 1,1′-binaphthyl-2,2′-diylhydrogenphosphate (BNP), 2,8-dimethyl-6H-5,11-methanodibenzo[*b*,*f*][1,5]diazocine (Tröger's base, TB), and benzoin (BZN) using EKC. The vesicular pseudo-stationary phase has been shown to provide very large migration window, good chiral selectivity, and resolution for the above compounds. We have also shown that the structure of the surfactant headgroup has significant effect on enantiomeric separations [19]. In this work, two new surfactants sodium *N*-(4-*n*-decyloxybenzoyl)-L-valinate (SDeBV), and sodium *N*-(4-*n*-octyloxybenzoyl)-L-valinate (SOBV) have been synthesized and used as chiral selectors for enantiomeric separation of BOH, BNP, BZN, and TB (see Chart 1 for molecular structures). The surfactants SDeBV and SOBV have ten and eight carbon atoms, respectively, in the hydrocarbon chain and both have L-valine as the hydrophilic headgroup. The purpose of this study is to evaluate the effect hydrophobic chain length of the surfactants on enantiomeric separations. Before using in EKC, the aggregation behavior of the surfactants was studied in borate buffer to know the type of aggregates formed by these surfactants. It was found that unlike SDBV, which form vesicles, both SDeBV and SOBV form micelles in borate buffer. Nevertheless, successful enantiomeric separations were obtained for the said analytes using both SDeBV and SOBV. The chromatographic results obtained for the micellar and vesicular systems have been compared.



Sodium N-(4-n- decyloxybenzoyl)- L-valinate (SDeBV)



Sodium N-(4-n-octyloxybenzoyl)- L-valinate (SOBV)

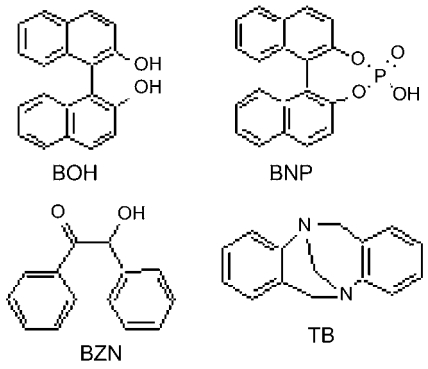


Chart 1. Molecular structures of the surfactants and analytes.

2. Experimental

2.1. Materials

The racemic mixtures and pure enantiomers of 1,1′-bi-2-naphthol, 1,1′-binaphthyl-2,2′-diylhydrogenphosphate, 2,8-dimethyl-6H-5,11-methanodibenzo[*b*,*f*] [1,5]diazocine (Tröger's base), and benzoin were purchased from Sigma (St. Louis, MO, USA) and Aldrich (Milwaukee, WI, USA). The fluorescence probes pyrene and 1,6-diphenyl-1,3,5-hexatriene (DPH) were obtained from Aldrich and recrystallized thrice from acetone–ethanol mixture before use. Dodecanophenone was obtained from Aldrich and sodium tetraborate was purchased from SRL (Mumbai, India). Fused silica capillary was obtained from Polymicro Technologies (Phoenix, AZ, USA). The surfactants SDeBV and SOBV were synthesized and purified in the laboratory using reported procedure [17,18,31].

2.2. Instrumentation

The Prince CE system (Prince Technologies, The Netherlands) equipped with an autosampler, Lambda 1010 variable wavelength UV–vis detector (Bischoff, Leonberg, Germany), and inbuilt temperature control system was utilized in this study. Uncoated fused silica capillary having 50 μm internal diameter and 87 cm total length (31.5 cm from inlet to detector) was used for all the separations. Data was collected and processed on a personal computer using Dax 7.0 data acquisition and analysis software. A digital pH meter model

pH5652 (Electronics corporation of India limited, Calcutta, India) with a glass electrode was used for pH measurements. Surface tension measurements were performed using a Du Nüoy ring tensiometer (S.D. Hudson & Co., Kolkata). A Perkin Elmer LS-55 luminescence spectrometer equipped with a filter polarizer and thermostated cell holder was used for fluorescence measurements. Temperature was controlled by use of a Neslab RTE 7 circulating bath (Thermo Neslab, USA).

2.3. Methods

Stock borate buffer solutions (100 ml) of desired concentration and pH were prepared by dissolving appropriate amount of solid sodium tetraborate decahydrate in Milli-Q water (18 MΩ resistivity) and adjusting the pH by addition of either dilute HCl or dilute NaOH. The surfactant solutions employed for separations were made by mixing weighed amount of solid surfactant in the appropriate buffer solution. The pH of the surfactant solutions in buffer was again measured and adjusted if required. The surfactant solutions were then filtered through a membrane filter of 0.45 μm pore size (Millipore, Bedfold, MA, USA) and degassed in a Bandelin Sonorex (Model RK 100 H) ultrasonic bath for 5 min prior to use. All sample solutions were prepared by dissolving 4 mg of solute in 2 ml methanol for stock solution and diluting this to a concentration of 0.4–0.6 mg/ml with buffer solution for analysis. The final sample contained 20–30% (v/v) methanol. For fluorescence measurements, stock solutions (1×10^{-3} M) of pyrene and DPH were made in methanol. Aliquots of this solution was added to 5 ml of the surfactant solution of desired concentration to make the final pyrene and DPH concentrations 1×10^{-6} and 5×10^{-6} M, respectively. Pyrene was excited at 335 nm and emission spectrum was recorded in the range of 350–500 nm. DPH was excited at 350 nm and the emission intensity was followed at 450 nm.

2.4. Electrophoretic procedure

The untreated fused silica capillary was first activated by purging with 1 M NaOH for 30 min followed by 0.1 M NaOH for additional 60 min. At the beginning of each day the capillary was first rinsed with 0.1 M NaOH for 30 min and with water for 30 min. For MEKC separations, the capillary was treated successively with 0.1 M NaOH, water, buffer and run buffer (surfactant solution in buffer) for 5 min each using 1000 mbar pressure before injection of a new sample. Between two successive runs of the same sample, the capillary was rinsed only with water and run buffer for 5 min each. The injection of the sample was done using a pressure of 20 mbar for 0.02 min. Separations were carried out by applying a constant voltage of 15–25 kV. Detection was performed at a wavelength of 230 nm. The surfactants has absorption maximum at 255 nm. At 230 nm the molar absorptivity of the surfactants is relatively low (4500 l mol^{-1} cm^{-1}) compared to that of the analytes (1,05,000 l mol^{-1} cm^{-1} for BOH). Due to the use of low concentration of surfactants, no difficulty was faced while detecting the analytes.

2.5. Calculations

Resolution (R_s) was calculated using the method involving peak width at half-height [18].

$$R_s = \frac{(2.35/2)(t_{r2} - t_{r1})}{W_{50(1)} + W_{50(2)}} \quad (1)$$

where t_{r1} and t_{r2} are the migration time and $W_{50(1)}$ and $W_{50(2)}$ are the peak width at 50% height of the 1st and 2nd isomer, respectively. The selectivity (α) was calculated from the ratio of the migration time of the two enantiomers. The t_{mc} values were measured using dodecanophenone as the micelle marker. The t_{mc} was measured to be 72.3 min for SDeBV and 43.6 min for SOBV in 50 mM borate buffer pH 9.7 with an applied voltage of 15 kV.

3. Results and discussion

3.1. Aggregation behavior of the surfactants in buffer solution

The aggregation behavior of the surfactants SDeBV and SOBV were investigated in buffered aqueous solution prior to their use in MEKC. The objective was to know the nature of the self-assemblies formed by these surfactants. The studies were performed in 50 mM borate buffer, pH 9.7. The critical aggregation concentration (cac) was determined by surface tension measurement method. Surface tension (γ) of a series of surfactant solutions made in borate buffer solution was measured and plotted against the surfactant concentration. The breakpoint in the plot of γ versus log (concentration) gave the cac value. The cac value thus obtained for SDeBV and SOBV are listed in Table 1. The cac value of SDBV in same buffer solution reported earlier [18] is also included in the table for comparison purpose. As expected, the cac value increases with the decrease of hydrophobic chain length. To investigate the microenvironment of the self-assemblies, fluorescence probe studies were performed using pyrene and DPH as extrinsic probe molecules. The ratio of intensities of first and third vibronic bands in the emission spectrum of pyrene (I_1/I_3) is known to be highly sensitive to the polarity of the region in which pyrene molecule is solubilized [32]. Due to highly hydrophobic nature, pyrene has very low solubility in water and gets solubilized inside the surfactant aggregates when dissolved in surfactant solutions above their cac. Thus, measurement of I_1/I_3 gives an indication about the micropolarity of the self-assemblies. The I_1/I_3 value of pyrene was measured in presence of 2 mM SDeBV and SOBV. The values are included in Table 1. The data presented in Table 1 reveal that the microenvironment of the self-assemblies

Table 1
Critical aggregation concentration (cac), polarity ratio (I_1/I_3), and fluorescence anisotropy (r) of DPH in SDeBV, SOBV, and SDBV surfactants

Surfactant	cac × 10^5 (M)	I_1/I_3	r
SDeBV	6.1	1.07	0.072
SOBV	50.2	1.09	0.064
SDBV	2.4	1.05	0.112

of SDeBV and SOBV is relatively more polar compared to that of SDBV. This may be due to the loose packing of the SDeBV and SOBV monomers in the self-assemblies, which allow the penetration of water molecules into the aggregate core resulting in an increase of micropolarity. The loose packing of the surfactant monomers in the self-assemblies of SDeBV and SOBV is further indicated by the low fluorescence anisotropy value (r) of DPH molecule measured in presence of these surfactants above their cac. DPH is a well-known microviscosity or more appropriately microfluidity probe and has been used for studying many surfactant self-assembly systems [33–35]. The r is an index of equivalent microviscosity in the surfactant aggregate core. The r-value measured in presence of 2 mM SDeBV and SOBV are tabulated in Table 1. Comparison of the r-values of the three surfactants indicates that the microenvironment of SDeBV and SOBV aggregates is less rigid compared to that of SDBV. In fact, the r-values obtained for SDeBV and SOBV are similar to the r-value measured for micelle forming surfactants sodium dodecyl sulfate (0.054) and sodium dodecylbenzene sulfonate (0.061). The low r-value and high I_1/I_3 ratio obtained for the self-assemblies of SDeBV and SOBV indicate that unlike SDBV, which form vesicles, these two surfactants form micelles in buffered aqueous solution. The formation of micellar structures by SDeBV and SOBV in buffer solution was further confirmed by the transmission electron microscopic study. No recognizable structures could be observed in the samples made from the solutions of SDeBV and SOBV. The shortening of the hydrophobic chain length in these surfactants results in weakening of the hydrophobic interactions among the surfactant tails during aggregate formation. This hinders the tight packing of the surfactant monomers and does not favor vesicle formation.

3.2. Enantiomeric separations

After characterizing the nature of self-assemblies formed by the surfactants SDeBV and SOBV in borate buffer solution, both the surfactants were used as chiral selectors for enantiomeric separation of the chiral compounds BOH, BNP, BZN, and TB. The method development procedure involves optimization of resolution (R_s) with respect to the analytical parameters like pH, buffer concentration, and surfactant concentration. The surfactants SDeBV and SOBV being sodium salts of carboxylic acids, get precipitated out of the solution at pH < 7.0. Therefore, all the separations were carried out in the alkaline pH range. Borate buffer was used as the background electrolyte as it has low conductivity and high buffer capacity in the studied alkaline pH range (8.5–10.3). First, the pH was optimized for enantiomeric separation of all the four analytes BOH, BNP, BZN, and TB using both SDeBV and SOBV as chiral selectors. A series of experiments were performed using 50 mM borate buffers having pH 8.5, 9.0, 9.3, 9.7, and 10.3 with either 2 mM SDeBV or 4 mM SOBV. The applied voltage was 15 kV for all the cases. From the pH optimization study (results not shown here) it was found that the optimum pH for enantiomeric separation of BOH is 9.7 and the optimum pH for all other three analytes BNP, BZN, and TB is 10.3. In order to find the optimum buffer concentration, separations were carried out individually for all the four analytes in the buffer concentration range of 30–70 mM using both SDeBV and SOBV. The pH of the borate buffer was 9.7 for BOH and 10.3 for BNP, BZN, and TB. The results of buffer concentration optimization study show that 50 mM borate buffer provides optimum resolution for BOH, BNP, and TB and 60 mM borate buffer gives the optimum separation for BZN using both SDeBV and SOBV. The optimized conditions of pH and buffer concentration obtained for enantiomeric separation of BOH, BNP, BZN, and TB are same as reported in the literature [18] for separation of these analytes using SDBV as chiral selector. This is expected because the molecular structures of the chiral selectors are same except the length of the hydrophobic tail. The difference in hydrophobic chain length, however, results in difference in cmc of the surfactants as shown by aggregation behavior study. Therefore, one expects the optimum surfactant concentration needed for separation of any particular analyte to be different for the three surfactants SDBV, SDeBV, and SOBV. The optimization of surfactant concentration for enantiomeric separation of each individual analyte is discussed below. The previously optimized conditions of pH and buffer concentration, i.e. 50 mM borate buffer pH 9.7 for BOH, 50 mM borate buffer pH 10.3 for BNP and TB, and 60 mM borate buffer pH 10.3 was used for this study.

3.2.1. Optimization of SDeBV concentration

The concentration of SDeBV was varied in the range 0.5–7.0 mM. The representative electropherograms showing the effect of SDeBV concentration on enantiomeric separation of BOH are shown in Fig. 1. The applied voltage was 25 kV. Similar

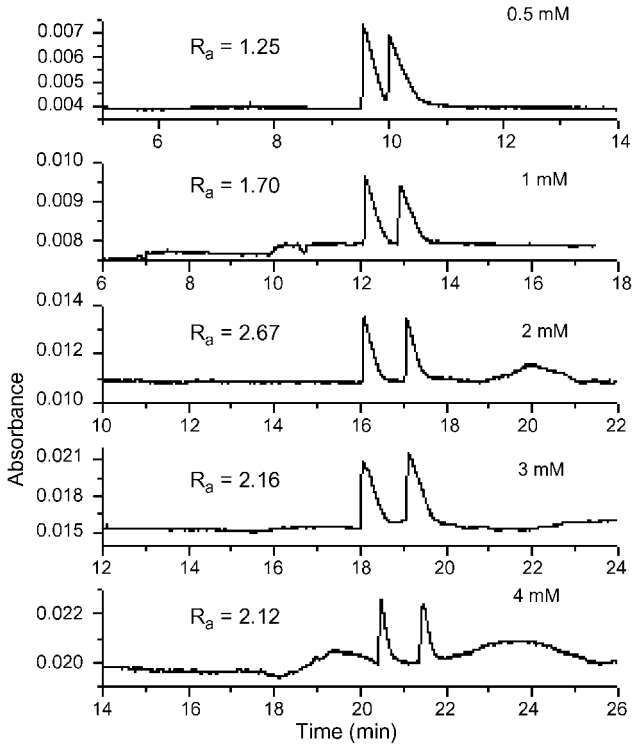


Fig. 1. Electropherograms showing effect of SDeBV concentration on enantiomeric separation of BOH. Separation condition: 50 mM borate buffer, pH 9.7 and the applied voltage is 25 kV.

Table 2
EOF migration time (t_o), migration time of first and second enantiomer (t_1 and t_2), selectivity (α), and resolution (R_s) values for enantiomeric separation of BOH, BNP, and BZN at different SDeBV concentrations

Analyte	[SDeBV] (mM)							
	0.5	1.0	2.0	3.0	4.0	5.0	6.0	7.0
BOH[a]								
t_o	4.42	4.42	4.40	4.38	4.40	4.26	–	–
t_1	9.55	12.12	16.09	18.10	20.47	21.10	–	–
t_2	10.01	12.93	17.09	19.14	21.46	21.84	–	–
α	1.05	1.06	1.06	1.06	1.05	1.04	–	–
R_s	1.25	1.70	2.67	2.16	2.12	2.05	–	–
BNP[b]								
t_o	–	–	6.23	6.08	6.41	6.39	6.41	6.27
t_1	–	–	15.32	15.45	18.59	20.48	21.90	21.91
t_2	–	–	15.64	15.85	19.22	21.32	22.84	22.91
α	NS	NS	1.02	1.02	1.03	1.04	1.04	1.04
R_s	NS	NS	1.25	1.47	1.89	2.46	2.51	2.73
BZN[c]								
t_o	–	–	–	10.07	10.11	10.10	10.02	9.89
t_1	–	–	–	14.06	15.31	15.48	16.41	16.95
t_2	–	–	–	14.31	15.66	15.81	16.85	17.42
α	NS	NS	NS	1.01	1.02	1.02	1.02	1.03
R_s	NS	NS	NS	1.17	1.58	1.60	1.60	1.78

NS, no separation.
[a] Separation condition: 50 mM borate buffer pH 9.7, 25 kV.
[b] Separation condition: 50 mM borate buffer pH 10.3, 20 kV.
[c] Separation condition: 60 mM borate buffer pH 10.3, 15 kV.

concentration optimization studies were performed for all other analytes BNP, BZN, and TB. The applied voltage was 20 kV for the separations of BNP, and 15 kV for BZN and TB. The R_s values and other chromatographic parameters are included in Table 2. Values for TB are not included in the table because baseline separation could not be obtained using SDeBV. From Table 2 it can be observed that R_s value for BOH increases with the increase of surfactant concentration, reaches a maximum at 2 mM, and then starts falling again. Thus, the optimum SDeBV concentration for the separation of BOH is 2 mM. In case of BNP and BZN, R_s value increases with the increase of surfactant concentration up to 7 mM. SDeBV concentration higher than 7 mM could not be employed due to the detection problem caused by the significant absorbance of the surfactant. A minimum of 2 mM and 3 mM SDeBV is required for the enantiomeric separation of BNP and BZN, respectively. TB could not be baseline separated using SDeBV. The highest R_s value obtained is 1.26 using 4 mM SDeBV. The migration order of the two enantiomers was determined using spiking technique. The (*S*)-BOH migrates faster and hence interacts weakly with the SDeBV micelles compared to the (*R*) enantiomer. The migration order for BNP enantiomers was opposite. The (*R*)-BNP migrates faster compared to the (*S*)-BNP.

3.2.2. Optimization of SOBV concentration

The cmc of SOBV is 0.5 mM. For SOBV concentration optimization studies, concentration of SOBV was varied in the range of 1–7 mM. The representative electropherograms showing effect of SOBV concentration on enantiomeric separation

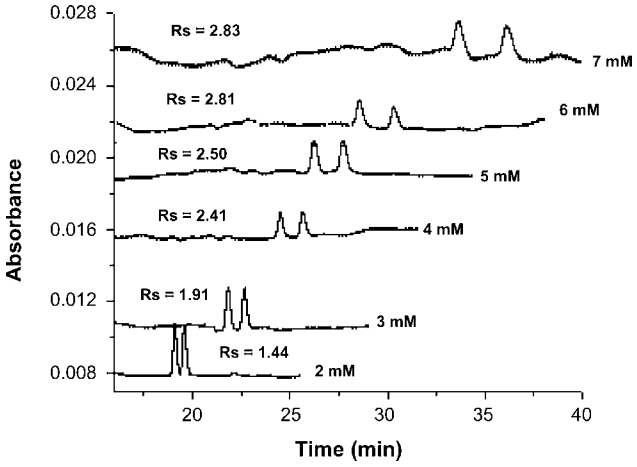


Fig. 2. Effect of SOBV concentration on enantiomeric separations of BNP. Separation condition: 50 mM borate buffer, pH 10.3. The applied voltage was 20 kV.

of BNP are presented in Fig. 2. The applied voltage was 20 kV. Similar studies were performed for all other analytes BNP, BZN, and TB. The applied voltage was 20 kV for BNP, and 15 kV for BZN and TB. The R_s values and other chromatographic parameters thus obtained in each case are included in Table 3. Due to lack of baseline separation, values for TB are not included in the table. The optimum SOBV concentration for separation of BOH is 3 mM, which is slightly higher than the optimum SDBV and SDeBV concentration required for separation of the said analyte. As expected, no separation could be achieved for BOH using 0.5 mM SOBV and only partial separation could

Table 3
EOF migration time (t_o), migration time of first and second enantiomer (t_1 and t_2), selectivity (α), and resolution (R_s) values for enantiomeric separation of BOH, BNP, and BZN at different SOBV concentrations

Analyte	[SOBV] (mM)						
	1.0	2.0	3.0	4.0	5.0	6.0	7.0
BOH[a]							
t_o	5.97	6.11	5.98	5.95	–	–	–
t_1	10.45	18.72	22.37	29.02	–	–	–
t_2	10.80	20.39	24.53	31.78	–	–	–
α	1.03	1.08	1.09	1.09	–	–	–
R_s	1.17	3.70	3.43	3.30	–	–	–
BNP[b]							
t_o	–	6.88	6.84	6.81	6.85	6.81	6.93
t_1	–	19.09	21.83	24.51	26.22	28.47	33.63
t_2	–	19.58	22.66	25.68	27.71	30.24	36.11
α	NS	1.02	1.04	1.05	1.05	1.06	1.07
R_s	NS	1.44	1.91	2.41	2.50	2.81	2.83
BZN[c]							
t_o	–	–	–	10.23	10.19	10.38	10.12
t_1	–	–	–	14.28	15.34	16.41	17.07
t_2	–	–	–	14.52	15.68	16.82	17.58
α	NS	NS	NS	1.02	1.02	1.02	1.03
R_s	NS	NS	NS	0.97	1.28	1.46	1.81

NS, no separation.
[a] Separation condition: 50 mM borate buffer pH 9.7, 20 kV.
[b] Separation condition: 50 mM borate buffer pH 10.3, 20 kV.
[c] Separation condition: 60 mM borate buffer pH 10.3, 15 kV.

be achieved using 1 mM SOBV owing to its higher cmc value. Resolution improved drastically when SOBV concentration was raised from 1 to 3 mM. Upon further increase of surfactant concentration R_s value decreases slightly due to broadening of the peaks. The minimum SOBV concentration required for separation of BNP and BZN are 2 and 4 mM, respectively. The R_s values increase continuously for both of these analytes with the increase of SOBV concentration up to 7 mM after which separations could not be carried out due to detection problem as discussed earlier. Therefore, 7 mM SOBV was considered to be the optimum surfactant concentration for these two analytes. The migration order of the two enantiomers was determined by spiking technique. As expected, the migration order does not change with the change in length of hydrophobic tail of the surfactants.

3.2.3. *Effect of hydrophobic chain length of surfactants on chiral separation*

In order to evaluate the effect of change of hydrophobic chain length on enantiomeric separations, the results obtained from the separations of BOH, BNP, BZN, and TB using SDBV, SDeBV, and SOBV were compared. It is to be noted that the change in the length of hydrophobic tail of the surfactants results in formation of different types of aggregates by these surfactants. SDBV forms vesicles [17,18] whereas both SDeBV and SOBV form micelles. Therefore, comparison of the results will help to gain knowledge about the effect of aggregate morphology on chiral selectivity of the chiral surfactants. For comparison, results obtained for any particular analyte using the same separation conditions (pH, buffer concentration, voltage, and optimum surfactant concentration) are considered. The conditions considered are 50 mM borate buffer, pH 9.7 containing 2 mM surfactant for BOH, 50 mM borate buffer, pH 10.3 containing 6 mM surfactant for BNP, 60 mM borate buffer, pH 10.3 with 6 mM surfactant for BZN, and 50 mM borate buffer, pH 10.3 with 4 mM surfactant for TB. The applied voltage was 15 kV in all the cases. The electropherograms for BOH, BNP, BZN, and TB using SDBV, SDeBV, and SOBV as chiral selectors are shown in Figs. 3 and 4. The chromatographic parameters

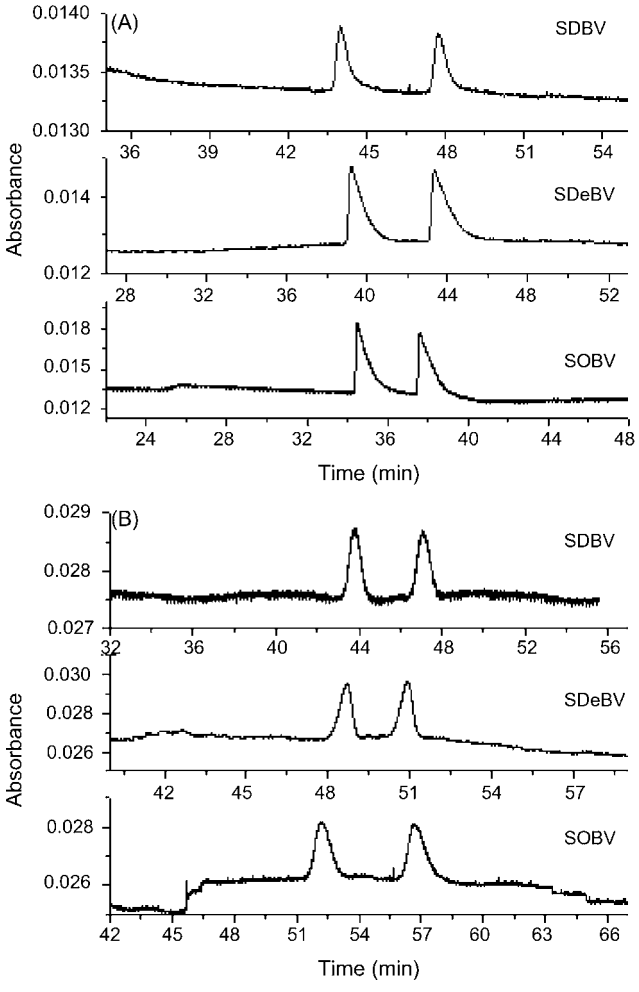


Fig. 3. Electropherograms obtained for enantiomeric separation of BOH (A) and BNP (B) using SDBV, SDeBV, and SOBV as chiral selectors. Separation conditions: 50 mM borate buffer, pH 9.7 with 2 mM surfactant for BOH and 50 mM borate buffer, pH 10.3 with 7 mM surfactant for BNP. The applied voltage is 15 kV.

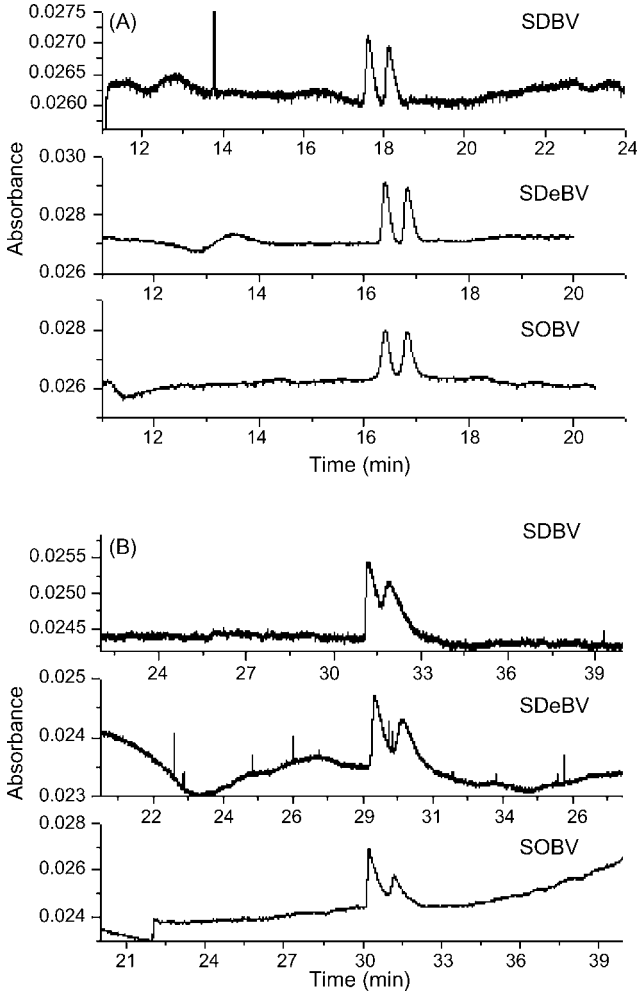


Fig. 4. Electropherograms obtained for enantiomeric separation of BZN (A) and TB (B) using SDBV, SDeBV, and SOBV as chiral selectors. Separation conditions: 60 mM borate buffer, pH 10.3 with 6 mM surfactant for BZN and 50 mM borate buffer, pH 10.3 with 4 mM surfactant for TB. The applied voltage is 15 kV.

Table 4
EOF migration time (t_o), migration time of first enantiomer (t_1), selectivity (α), and resolution (R_s) values for enantiomeric separation of BOH, BNP, BZN, and TB using three chiral selectors SDBV, SDeBV, and SOBV

Analyte	SDBV	SDeBV	SOBV
BOH			
t_o	7.86	7.87	7.92
t_1	43.95	39.22	34.52
α	1.09	1.10	1.09
R_s	5.23	3.70	3.65
BNP			
t_o	9.93	10.05	10.11
t_1	43.77	48.64	52.20
α	1.07	1.06	1.08
R_s	3.04	2.73	3.10
BZN			
t_o	10.14	10.02	10.38
t_1	15.92	16.41	16.41
α	1.03	1.02	1.02
R_s	1.61	1.60	1.50
TB			
t_o	10.14	9.22	9.36
t_1	30.68	29.72	30.24
α	1.02	1.03	1.03
R_s	1.06	1.26	1.67

For separation conditions, see text.

migration time of EOF (t_o), migration time of first enantiomer (t_1), α, and R_s in each case are listed in Table 4. Some of the salient features of the data presented in Table 4 are (i) the t_1 values obtained for BOH using the three surfactants decreases in the order SDBV > SDeBV > SOBV and for BNP the order is reversed, (ii) the α value for any particular analyte (BOH, BNP, BZN, or TB) using the three different chiral selectors are practically same, and (iii) the R_s value obtained for the analytes using the three chiral selectors are comparable except for BOH for which a slight higher resolution can be obtained using SDBV. The above results can be explained taking into account the type of aggregates formed by the surfactants in buffer solution, i.e. vesicles or micelles and the physical properties like micropolarity of the aggregates. Vesicles are larger in size compared to micelles and pose more solubilizing ability for the hydrophobic compounds. So the analytes are expected to interact more strongly with the vesicles compared to micelles. This is reflected in the larger t_1 values for BOH using SDBV compared to the other two surfactants. BZN, and TB being relatively small molecules and less hydrophobic, get almost equally partitioned between the vesicular and miceller phase. The low t_1 value obtained for BNP using SDBV is due to the high charge density of the vesicles. BNP is negatively charged in the working pH range and the electrostatic repulsion at the vesicle surface decreases it's partitioning with the vesicles. It is well known that chiral recognition occurs because of interaction of the analyte with the chiral selector near the stereogenic center. The chiral head group of SDBV, SDeBV and SOBV is same. Therefore, the α values obtained for the analytes using the three surfactants are nearly same. However, the R_s values obtained for each analyte using the three chiral selectors are slightly different owing to the difference in retention times.

4. Conclusion

In summary, two micelle-forming amino acid based surfactants SDeBV and SOBV having different hydrophobic chain length were used as chiral selectors for enantiomeric separation of chiral compounds BOH, BNP, BZN, and TB. The results of this study were compared with our earlier published results of vesicle-forming surfactant SDBV to evaluate the effect of hydrophobic chain length on enantioselectivity. The results obtained from the above studies indicate that the morphology of the self-assemblies formed by the surfactants has no significant effect on enantioselectivity of the surfactants when used as chiral selectors in MEKC. The type of aggregate formed, however, have effect on other chromatographic parameters like analysis time, retention factor, and resolution.

Acknowledgements

This work is supported by a grant (No. SP/S1/G-36/99) from Department of Science and Technology (DST), New Delhi. A.M. thanks CSIR, New Delhi for providing a fellowship.

References

[1] S. Terabe, K. Otsuka, K. Ichikawa, A. Tsuchiya, T. Ando, Anal. Chem. 56 (1984) 111.
[2] T.J. Pappas, M. Gayton-Ely, L.A. Holland, Electrophoresis 26 (2005) 719.
[3] S. Terabe, Anal. Chem. 77 (2004) 240A.
[4] R. Vespalec, P. Bocek, Chem. Rev. 100 (2000) 3715.
[5] D.W. Amstrong, K.L. Rundlet, J.R. Chen, Anal. Chem. 66 (1994) 1690.
[6] R. Kuhn, F. Enri, T. Bereuter, J. Hausler, Anal. Chem. 64 (1992) 2815.
[7] M. Sanchez Pena, Y. Zhang, I.M. Warner, Anal. Chem. 69 (1997) 3239.
[8] K. Otsuka, S. Terabe, J. Chromatogr. 515 (1990) 221.
[9] Y. Ishihama, S. Tertabe, J. Liq. Chromatogr. 16 (1993) 933.
[10] S.E. Lucangioli, C.N. Carducci, S.L. Scioscia, A. Carlucci, C. Bregni, E. Kenndler, Electrophoresis 24 (2003) 984.
[11] D.C. Tickle, G.N. Okafo, P. Camillari, R.F.D. Jones, A.J. Kirby, Anal. Chem. 66 (1994) 4121.
[12] K. Otsuka, J. Kawahara, K. Tatekawa, S. Terabe, J. Chromatogr. 559 (1991) 209.
[13] K. Otsuka, K. Karuhaka, M. Higashimori, S. Terabe, J. Chromatogr. A 680 (1994) 317.
[14] A. Daboshi, T. Ono, S. Hara, Y. Yamaguchi, J. Chromatogr. 480 (1989) 413.
[15] A.G. Peterson, E.S. Ahuja, J.P. Foley, J. Chromatogr. B 683 (1996) 15.
[16] J.R. Mazzeo, E.R. Grover, M.E. Swartz, J.S. Peterson, J. Chromatogr. A 680 (1994) 125.
[17] A. Mohanty, J. Dey, Chem. Commun. 12 (2003) 1384.
[18] A. Mohanty, J. Dey, J. Chromatogr. A 1070 (2005) 185.
[19] A. Mohanty, J. Dey, J. Chromatogr. A, in press.
[20] C.P. Palmer, J.P. McCarney, Electrophoresis 25 (2004) 4086.
[21] S.A. Shamshi, C.P. Palmer, I.M. Warner, Anal. Chem. 73 (2001) 140A.
[23] F.H. Billiot, E.J. Billiot, I.M. Warner, J. Chromatogr. A 922 (2001) 329.
[24] J. Tarus, T. Jernigan, K. Morris, I.M. Warner, Electrophoresis 25 (2004) 2720.
[25] S.A.A. Rizvi, D.N. Simons, S.A. Shamsi, Electrophoresis 25 (2004) 712.
[26] S.J. Thibodeaux, E. Billiot, E. Torres, B.C. Valle, I.M. Warner, Electrophoresis 24 (2003) 1077.

[27] H. Yarabe, E.J. Billiot, I.M. Warner, J. Chromatogr. A 875 (2000) 179.
[28] S.A.A. Rizvi, D.N. Simons, S.A. Shamsi, Electrophoresis 25 (2004) 712.
[29] E. Billiot, I.M. Warner, Anal. Chem. 72 (2000) 1740.
[30] S.J. Thibodeaux, E. Billiot, I.M. Warner, J. Chromatogr. A 966 (2002) 179.
[31] A. Mohanty, J. Dey, Langmuir 20 (2004) 8452.
[32] K. Kalyansundaram, J.K. Thomas, J. Am. Chem. Soc. 99 (1977) 2039.
[33] S. Roy, A. Mohanty, J. Dey, Chem. Phys. Lett. 414 (2005) 23.
[34] S. Roy, J. Dey, Langmuir 21 (2005) 10362.
[35] M. Shinitzky, A.C. Dianoux, C. Itler, G. Weber, Biochemistry 10 (1971) 2106.

Available online at www.sciencedirect.com
ScienceDirect
Talanta 71 (2007) 1075–1082
Talanta
www.elsevier.com/locate/talanta

Chemically modified silica gel with aminothioamidoanthraquinone for solid phase extraction and preconcentration of Pb(II), Cu(II), Ni(II), Co(II) and Cd(II)

Wittaya Ngeontae, Wanlapa Aeungmaitrepirom *, Thawatchai Tuntulani

Department of Chemistry, Faculty of Science, Chulalongkorn University, Bangkok 10330, Thailand

Received 27 April 2006; received in revised form 31 May 2006; accepted 31 May 2006
Available online 20 July 2006

Abstract

Silica gel chemically bonded with aminothioamidoanthraquinone was synthesized and characterized. The metal sorption properties of modified silica were studied towards Pb(II), Cu(II), Ni(II), Co(II) and Cd(II). The determination of metal ions was carried out on FAAS. For batch method, the optimum pH ranges for Pb(II), Cu(II) and Cd(II) extraction were ≥3 but for Ni(II) and Co(II) extraction were ≥4. The contact times to reach the equilibrium were less than 10 min. The adsorption isotherm fitted the Langmuir's model showed the maximum sorption capacities of 0.56, 0.30, 0.15, 0.12 and 0.067 mmol/g for Pb(II), Cu(II), Ni(II), Co(II) and Cd(II), respectively. In the flow system, a column packed modified silica at 20 mg for Pb(II) and Cu(II), 50 mg for Cd(II), 60 mg for Co(II), Ni(II) was studied at a flow rate of 4 and 2.5 mL/min for Ni(II). The sorbed metals were quantitatively eluted by 1% HNO_3. No interference from Na^+, K^+, Mg^{2+}, Ca^{2+}, Cl^- and SO_4^{2-} at 10, 100 and 1000 mg/L was observed. The application of this modified silica gel to preconcentration of pond water, tap water and drinking water gave high accuracy and precision (%R.S.D. ≤ 9). The method detection limits were 22.5, 1.0, 2.9, 0.95, 1.1 μg/L for Pb(II), Cu(II), Ni(II), Co(II) and Cd(II), respectively.
© 2006 Elsevier B.V. All rights reserved.

Keywords: Silica; Anthraquinone; Preconcentration; Heavy metal

1. Introduction

Flame atomic absorption spectrometry (FAAS) is one among common techniques for heavy metals determination because it offers many advantages, for example, high sample throughput, low cost operation, high precision and specificity. On the other hand, this technique has some drawbacks such as chemical interference from the sample matrix and its high detection limit. So the trace concentration level cannot be determined by this technique. However, these problems can be resolved by the preconcentration technique because this technique can simultaneously remove the sample matrix and enrichment concentration.

There are many techniques available for metal preconcentration such as liquid–liquid extraction (LLE) [1] and solid phase extraction (SPE) [2–14]. The advantages of SPE over LLE are the easy of use, the high preconcentration factor and flexibility to choose the solid phase for optimum results. However, the main drawback of SPE is the lack of selectivity [2], which leads to high interference of the other existing species with the target metal ion. Increasing selectivity of the sorbent is thus an interesting area of research.

Among many types of solid phase use in SPE, silica gel immobilized with various organic compounds as metal chelating agent has received great attention. The selectivity of the immobilized surface towards metal ions depends on various factors such as size of the modifier, activity of the loaded group and characteristic of the hard-soft acid-base. The modified silica gel generally exhibits higher sorption capacities than those of organic polymer-based resins. Reactive sites of silica gel exist in large number, and therefore the number of organic molecules immobilized is high which results in good sorption capacity for metal ions.

There are several recent reports on the use of functionalized silica gel for metal enrichment. The synthetic pathway of modified silica gel were similar to the reaction of organosilane with silanol groups on silica gel but the difference was the type of chelating molecules which selectively chelate to metal

* Corresponding author. Tel.: +662 218 7607; fax: +662 254 1309.
E-mail address: wanlapa@sc.chula.ac.th (W. Aeungmaitrepirom).

0039-9140/$ – see front matter © 2006 Elsevier B.V. All rights reserved.
doi:10.1016/j.talanta.2006.05.094

ions, for example, 2-aminothiazole [3], 2,5-dimercapto-1,3,4-thiadazole [4], 2-mercapto-5-phenylamino-1,3,4-thiadazole [5], formylsalicylic acid [6], 2,4-dichlorophenoxyacetic acid [7], 2-pyridinecarboxaldehyde phenylhydrazone [8], 4-amino-3,5,6-trichloropicolinic acid [9] and 2-mercaptobenzothiazole [10].

In this work, aminothioamidoanthraquinone chemically modified silica was synthesized and characterized. The solid phase extraction of Pb(II), Cu(II), Ni(II), Co(II) and Cd(II) in batch and column modes was studied. Parameters that can affect the sorption and elution efficiency of the metal ions were studied. Then, the method was applied to preconcentrate metal ions from natural water samples.

2. Experimental

2.1. Reagents

The reagents used in the synthesis were 2-aminothiophenol (Merck), 2-aminoanthraquinone (Fulka), aminopropyl triethoxy silane (Acros Organic), chloroacetyl chloride (Merck). All chemicals were used without further purification. Commercial grade solvents such as dichloromethane, hexane, methanol and ethyl acetate were purified by distillation. Acetonitrile and toluene were dried over CaH_2 and freshly distilled under nitrogen atmosphere prior to use. Standard metal solutions (BDH Laboratory Supplies) were prepared by stepwise dilution of 1000 ppm stock standard solution. The working metal solutions were freshly prepared by stepwise dilution from stock solutions. The pH of solution was adjusted with 1% HNO_3 and 1% KOH. All solutions were prepared by using Milli-Q water with 18 $M\Omega\,cm^{-2}$. All reagents were of analytical grade.

2.2. Apparatus and instrument

The pH measurements were carried out with Hanna Instrument pH 211. The pH meter was calibrated against two standard buffer solutions of pH 4.0 and 7.0. The determination of metal ion concentrations was performed on a Perkin-Elmer PE100 Flame atomic absorption spectrometry by using air-acetylene flame. Other instrumental parameters were used as recommended by manufacturers. The centrifuge Centaur2 (Sanyo®) was used at 3500 rpm for 5 min to separate modified silica and extracted metal solution in batch experiments. In column modes, the flow was induced by peristaltic pump ISMATEC with a Tygon® tube i.d. 2.79 mm.

2.3. Synthesis of aminothioamidoanthraquinone silica (phase Q)

2.3.1. Synthesis of 3-aminopropylsilica **(1)**

Silica gel (50 g) suspended in 200 mL of dried toluene was refluxed and mechanically stirred under nitrogen atmosphere for 2 h. To this suspension, 20 mL of aminopropyl triethoxysilane was added dropwise and the mixture was kept under reflux for 24 h. The solid was filtered, washed with ethanol. The immobilized silica gel, named Amino-SiO_2, was dried in vacuum at room temperature [11].

2.3.2. Synthesis of chloroamidoanthraquinone **(2)**

Into a 250 mL two-necked round bottom flask equipped with a reflux condenser, 2-aminoanthraquinone (1.0 g, 4.5 mmol), pyridine (0.5 mL, 6.2 mmol) and dichloromethane (60 mL) were mixed and stirred under nitrogen atmosphere at 0 °C. Chloroacetyl chloride (0.4 mL, 5.4 mmol) in dichloromethane (20 mL) was then added dropwise. After stirring for 4 h, the solution was transferred to a separatory funnel and extracted with 3 M HCl. The dichloromethane layer was washed with saturated sodium chloride solution. The organic layer was then dried over anhydrous sodium sulfate, filtered and evaporated to dryness to obtain a dark green residue. The residue was further dissolved in dichloromethane and hexane was then slowly added. The chloroamidoanthraquinone was precipitated as dark green solid (1.2 g, 85%). The product was dried in vacuum and kept in desiccator.

^{1}H NMR spectrum ($CDCl_3$, 400 MHz.): δ (in ppm) 10.32 (s, 1H, *H*NCO), 8.10 (m, 4H, H_a), 7.64 (m, 2H, H_b), 7.30 (s, 1H, H_c), 4.03 (s, 2H, OCCH_2Cl)

2.3.3. Synthesis of aminothioamidoanthraquinone **(3)**

Into a 100 mL two-necked round bottom flask equipped with a reflux condenser, 2-aminothiophenol (0.1 g, 0.9 mmol), sodium carbonate (0.2 g, 2.0 mmol) and acetonitrile (30 mL) were mixed and stirred under nitrogen atmosphere at room temperature for 30 min. Chloroamidoanthraquinone (0.25 g, 0.8 mmol) in acetonitrile (20 mL) was then added dropwise. The solution was refluxed for 12 h. Sodium carbonate was filtered off and acetonitrile was evaporated to obtain a dark yellow solid. The residue was dissolved in dichloromethane and hexane was then slowly added. The aminothioamidoanthraquinone was precipitated as dark yellow solid (0.3 g, 91%). The product was dried in vacuum and kept in desiccator.

^{1}H NMR spectrum (DMSO-d_6, 400 MHz.): δ (in ppm) 10.72 (b, 1H, *H*NCO), 8.41 (s, 1H, H_d), 8.18 (m, 3H, H_e), 8.01 (d, J = 8.8 Hz, 1H, H_f), 7.90 (m, 2H, H_g), 7.26 (d, J = 8 Hz, 1H, H_h), 7.03 (t, J = 8 Hz, 1H, H_i), 6.69 (d, J = 8 Hz, 1H, H_k), 6.47 (t, J = 8 Hz, 1H, H_j), 3.62 (s, 1H, COCH_2S). Mass spectrometry: ESI-MS m/z = 389.3 [$C_{22}H_{16}N_2O_3S + H^+$] Elemental analysis: Anal. Cal. $C_{22}H_{16}N_2O_3S$; C 68.02, H 4.15, N 7.21. Found C 68.06, H 4.07, N 7.10.

2.3.4. Synthesis of aminothioamidoanthraquinone silica **(4)**

Into a 250 mL two-necked round bottom flask containing a suspension of 25 g of amino-SiO_2 **(1)** in 150 mL of dried toluene, 0.25 g of aminothioamidoanthraquinone was added. The mixture was stirred and heated at 100 °C under nitrogen atmosphere for 24 h. The suspension was allowed to cool to room temperature. The silica was filtered and washed with dichloromethane (2× 200 mL), methanol (2× 200 mL) and dichloromethane (2× 200 mL), respectively, to give an orange solid aminothioamidoanthraquinone silica named phase

Q. The product was dried in vacuum and kept in a desiccator.

2.4. Characterization

The functional group on modified silica gel was characterized by FTIR-Spectroscopy (Nicollet Impact410) using KBr pellet. The specific surface area was obtained by using the BET equation on a Thermofinnigan Sorptomatic1990. The organic moieties were characterized by nuclear magnetic resonance spectrometer (DPX-300 Brucker Biospin for solid state NMR; Varian 400 MHz for solution state), mass spectrometer and elemental analysis.

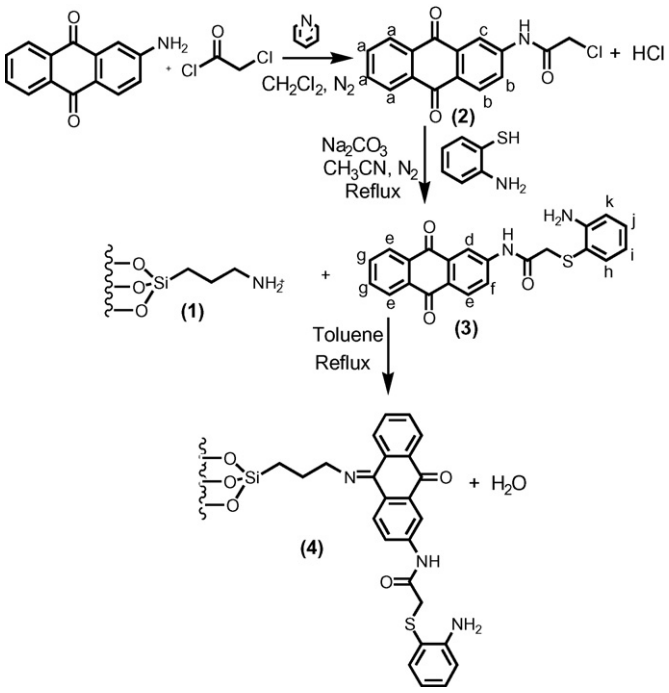
2.5. Extraction study of the modified silica

2.5.1. Batch method

The effects of solution pH and contact time on the sorption of metal ions were evaluated on batch method. A suspension of 20 mg of phase Q in 5 mL of metal solution at a concentration of 10 ppm for Pb(II), 5 ppm for Cu(II), Ni(II), Co(II) and 2 ppm for Cd(II), was mechanically stirred at room temperature. The adsorption isotherm experiment, the temperature was controlled at 298 ± 1 K. After extraction, the solid phase was separated by centrifugation at 3500 rpm for 5 min. Residual metal concentration of the supernatant was determined by a flame atomic absorption spectrometer. All experiments were performed in triplicate.

2.5.2. Column method

The column method was investigated to obtain the optimum conditions for sorption and desorption of each metal. The effect of solution flow rate, eluent, sample volume and interfering ions were evaluated in triplicate. A mini-column was prepared by using homemade columns. The metal ion solutions were adjusted to appropriate pH before passing through the mini-column at a controlled flow rate. The sorbed ions were desorbed by passing 5 mL of 1% HNO_3 at a flow rate of 0.5 mL/min.



Scheme 1. Synthesis of aminothioanthraquinone silica (phase Q).

3. Results and discussion

3.1. Preparation of aminothioamidoanthraquinone

The silanol group of silica gel is very inert for chemical reactions but it can react easily with 3-aminopropyltriethoxysilane to yield the siloxane bond and amino groups attached to the silica surface. This group is capable to react with ketone or aldehyde to yield the Schiff's base compound. Following this concept, described in previous research [12,13], the aminothioamidoanthraquinone silica was synthesized by the reaction of aminopropyl silica and aminothioamidoanthraquinone via Schiff's base linkage. The synthesis procedure is shown in Scheme 1.

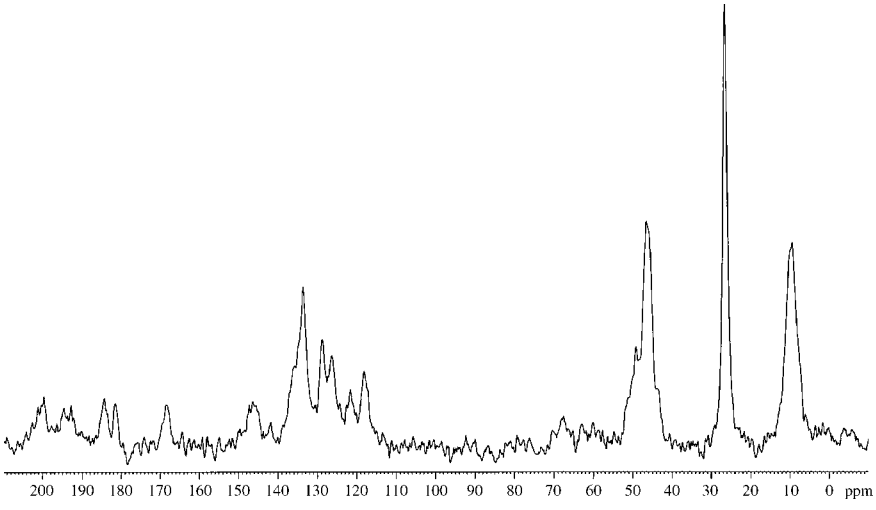


Fig. 1. ^{13}C NMR spectrum of aminothioanthraquinone modified silica gel.

The IR spectrum confirms the presence of aminothioamidoanthraquinone bonded to the silica surface. The absorption peaks at 1649 and 1552 cm^{-1} are due to C=C and C=N stretching, respectively. A large and broad band near 3600 cm^{-1}, is corresponding to the silanol group stretching and the adsorbed water molecule [14]. A broad and intense band at 1100 cm^{-1} is the siloxane vibration (Si–O–Si) and a less intense band at 900 cm^{-1}.

The specific surface area (S_{BET}) [15] of phase Q was obtained by nitrogen adsorption at several pressures. The S_{BET} of phase Q being 308.4 $m^2\ g^{-1}$ is smaller than that of non-functionalized silica gel, $S_{BET} = 484.2 \pm 6.4\ m^2\ g^{-1}$ reported by Arakaki et al. [14]. A decrease in S_{BET} is probably due to the presence of the organic moieties that can block the access nitrogen to the silica base [16–18]. The BJH average pore diameter of phase Q is 55.6 Å.

The solid state ^{13}C NMR spectrum is shown in Fig. 1. The signals observed at $\delta = 9.5$, 26.5 and 46.5 ppm have been assigned to the linkage carbons between aminothioamidoanthraquinone and silica gel; Si–CH_2, –CH_2 and –CH_2–N, respectively. Other signals at 110–200 ppm are corresponding to specific carbons of aminothioamidoanthraquinone moiety [19].

3.2. Effect of solution pH

The acidity of a solution has two effects on metal sorption. Firstly, proton in acid solution can protonate binding sites of the chelating molecules. Secondly, hydroxide in basic solution may complex and precipitate many metals. Therefore, pH of a solution is the first parameter to be optimized.

The sorption capacity of each metal ion, determined by Eq. (1), as a function of pH is shown in Fig. 2.

$$N_f = \frac{n_i - n_f}{m} \quad (1)$$

where N_f is the sorption capacity (mg metal/g phase Q); n_i is initial amount of metal ion (mg); n_f is amount of metal ion in supernatant (mg) and m is the amount of phase Q (g).

The optimum pH for maximum sorption of Pb(II), Cu(II) and Cd(II) have occurred at pH ≥3, Co(II) and Ni(II) at pH ≥4. This can be explained by the different binding affinity of the binding sites, which was attributed to the deprotonation

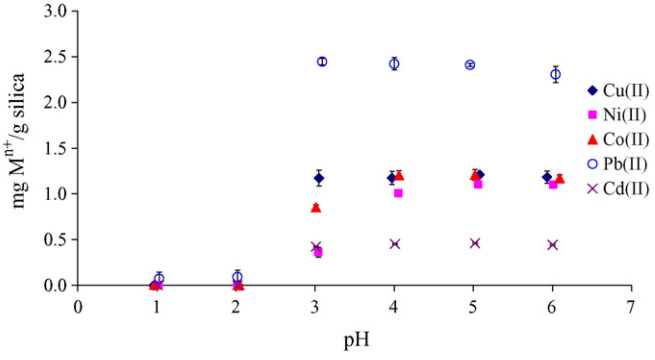


Fig. 2. Effect of solution pH on sorption of Pb(II) 10 ppm; Cu(II), Ni(II), Co(II) 5 ppm and Cd(II) 2 ppm.

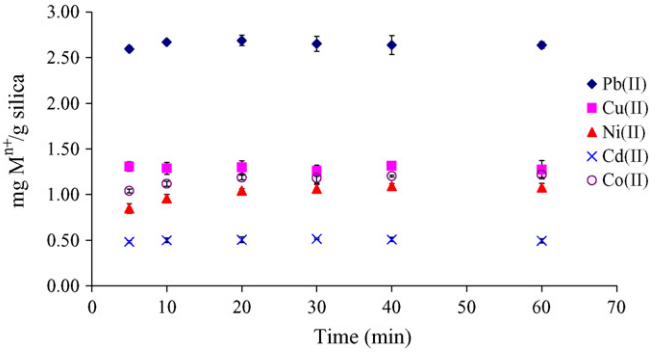


Fig. 3. Effect of contact time of metal ions sorption on phase Q at 298 ± 1 K [10 ppm Pb(II), 5 ppm Cu(II), 2 ppm Cd(II) at pH 3.5 and 5 ppm Ni(II), Co(II) at pH 4.5; 20 mg phase Q].

of aromatic amino group on aminothioamidoanthraquinone of sorbent.

3.3. Effect of contact time

The contact time was varied from 5 to 60 min and the results are shown in Fig. 3. It took only 5 min for Pb(II), Cu(II) and Cd(II) and only 10 min in the case of Ni(II) and Co(II). The results indicate that phase Q has a rapid adsorption kinetics, therefore, it is suitable for an application in flow system or using in the preconcentration of trace metal ions.

3.4. Adsorption isotherm

The adsorption phenomena at the solid–liquid interface were commonly described by the adsorption isotherm model, for example, Langmuir isotherm equation (Eq. (2)) [20].

$$\frac{C}{N_f} = \frac{1}{bN_f^s} + \frac{C}{N_f^s} \quad (2)$$

where N_f is the amount of metal ion per gram of sorbent (sorption capacity), C the equilibrium concentration of the metal ion, $b = K_{eq}/a$, where a represents the activity of the solvent in solution and N_f^s is the maximum sorption capacity of the sorbent.

The experiments were carried out at 298 ± 1 K using batch method. The results are shown in Fig. 4. All of the least square fitted with Eq. (2) (corresponding to Fig. 4(1B and 2B) giving a correlation coefficient (r) higher than 0.99 indicated that the adsorption of all metal ions on phase Q was a Langmuir type adsorption mechanism. The monolayer coverage of metal ions on the silica surface occurred and other mechanisms such as precipitation and second adsorption on the first layer did not occur. The b values obtained are in high level (Table 1). These results indicate that the metal ions are directly coordinated on phase Q, probably by using nitrogen, sulfur and oxygen donor atoms, without other transfer mechanism [21,22]. According to the size of metal ions and hard-soft acid base rule, we propose that Pb(II), Cu(II) and Cd(II) would bind to the N_2S moiety of the aminothioamidoanthraquinone while Co(II) and Ni(II) would bind to the OS moiety of the host compartment as shown in Fig. 5. Moreover, maximum sorption capacity order obtained is Pb(II) > Cu(II) > Ni(II) > Co(II) > Cd(II).

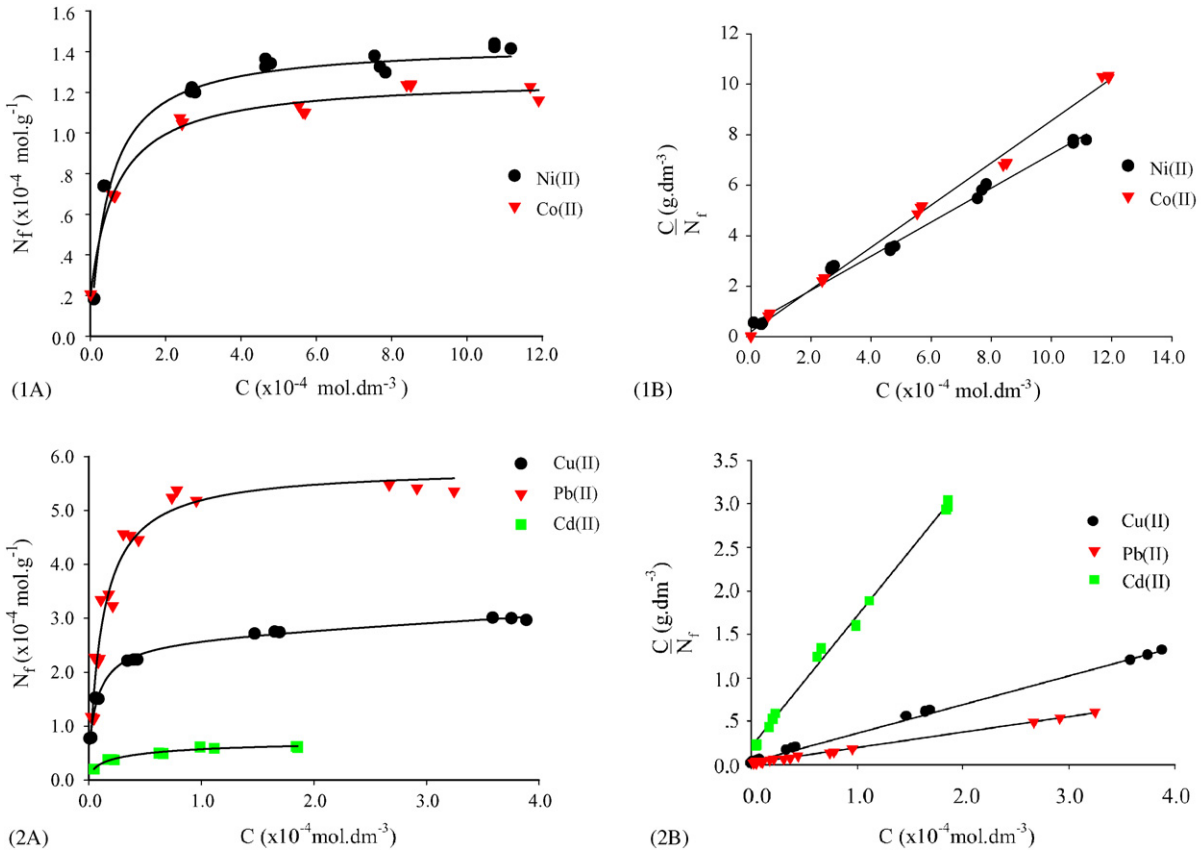


Fig. 4. Adsorption isotherm of Ni(II) and Co(II) at pH 4.5 (1A), Pb(II), Cu(II) and Cd(II) at pH 3.5 (2A) and Langmuir adsorption model fit of Ni(II) and Co(II) (1B), Pb(II), Cu(II) and Cd(II) (2B) on phase Q at 298 ± 1 K.

Table 1
Thermodynamic parameters of Langmuir's adsorption isotherm at 298 ± 1 K

Elements	Equation	b (L/mol) $\times 10^4$	N_f^s (mol/g) $\times 10^{-4}$	r
Pb(II)	$y = 1778.6x + 0.0187$	9.5	5.6	0.9992
Cu(II)	$y = 3317.1x + 0.2440$	13.6	3.0	0.9990
Ni(II)	$y = 6745.4x + 0.4949$	1.4	1.5	0.9961
Co(II)	$y = 8355.5x + 0.2031$	4.1	1.2	0.9978
Cd(II)	$y = 15006x + 0.2120$	7.1	0.7	0.9975

3.5. Effect of solution flow rate

The sorption on phase Q packed mini-column was studied at varying flow rate controlled with a peristaltic pump. Test solutions were prepared by using 5 mL of each metal solution with concentration 10 ppm for Pb(II), 5 ppm for Cu(II), Ni(II), Co(II) and 2 ppm for Cd(II). Test solutions were passed through the mini-column at varying solution flow rate between 0.5 and 6 mL/min. The results present in Fig. 6 show that the sorption of Pb(II), Cu(II) and Cd(II) were not affected by flow rate. On the other hand, there were decrease in sorption of Ni(II) and Co(II) with increasing flow rate. This behavior was undesirable for the flow system because a little change of flow rate would cause significant change in extraction efficiency. However, sorption efficiencies were improved by increasing the amount of phase Q to 60 and 40 mg for Ni(II) and Co(II), respectively, without the effect of flow rate.

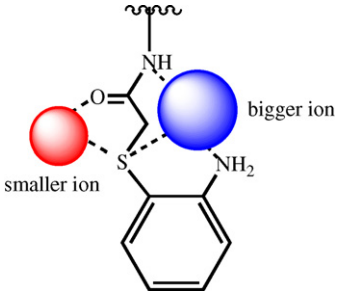


Fig. 5. Proposed mode of chelation for adsorption of investigated metal ions onto aminothioamido moieties.

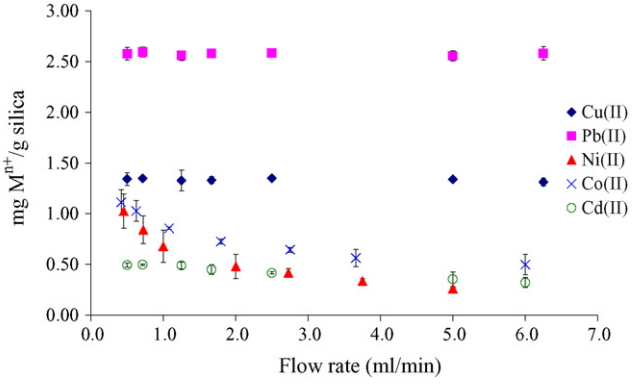


Fig. 6. Effect of solution flow rates on column packed with 20 mg of phase Q at 298 ± 1 K [pH 3.5 for Pb(II), Cu(II) and Cd(II), pH 4.5 for Ni(II) and Co(II)].

3.6. Effect of stripping concentration

Nitric acid was chosen for stripping sorbed metal ions because it was a suitable matrix for determination by FAAS. The acid concentration was an important factor because at lower concentration of proton may be not enough to protonate the chelation site. On the other hand, high acid concentration may affect to the determination step due to the contamination from acid used. Therefore, concentration of nitric acid used must be optimized.

The solutions were prepared by using Pb(II), Cu(II) and Cd(II) 25, 10, 5 μg at pH 3.5 and Ni(II), Co(II) 10 μg at pH 4.5. The silica weight used for Pb(II), Cu(II) and Cd(II) were 20 mg and 40 and 60 mg for Co(II) and Ni(II), respectively. The individual sorbed metal ion was eluted from the column with 5 mL of 1–7 % (v/v) HNO_3 with stripping flow rate of 0.5 mL/min at 298 ± 1 K. It was found that the %recovery of each metal ion using different concentrations of eluent was not significantly different (Table 2). The 1% HNO_3 was sufficient for highest recovery of each metal ion.

3.7. Effect of sample volume

In order to achieve a high preconcentration factor, metal ions in the large sample volume has been quantitatively sorbed and desorbed by a small stripping volume. However, incomplete retention of metal ions will occur probably due to the sample itself act as eluent or less contact of analyte on sorbent. The effect of sample volume on metal sorption was studied by passing 25–100 mL through the column packed with 20–60 mg of phase Q at an optimum flow rate. The adsorption of Cu(II) and Pb(II) with 20 mg of phase Q were not affect by sample volume (Table 3). High recovery of Ni(II) was obtained when the sample volume of 50 mL was used. The increases in amount of phase Q to 50 and 60 mg could improve the recovery percentages of Cd(II) and Co(II), respectively, for 100 mL of sample volume solution.

3.8. Effect of interfering ion

The cations and anions used in this study were chosen from their major abundance in nature, for example, Na^+, K^+, Mg^{2+}, Ca^{2+}, Cl^- and $SO_4{}^{2-}$. The salts used were chloride salt and sodium salt for cation and anion interfering studies, respectively. The experiments were performed in three levels of the interfering ion concentrations under the optimum conditions of each

Table 2
Effect of stripping concentration

HNO_3 (%, v/v)	Recovery* (%)				
	Cu(II)	Pb(II)	Cd(II)	Co(II)	Ni(II)
1	95 ± 8	92 ± 4	92 ± 5	95 ± 2	94 ± 6
3	97 ± 2	94 ± 7	93 ± 5	91 ± 1	96 ± 2
5	96 ± 1	92 ± 4	89 ± 6	93 ± 2	95 ± 1
7	96 ± 5	91 ± 1	89 ± 11	91 ± 1	94 ± 2

* Mean value ± $\frac{t_{0.05}s}{\sqrt{n}}$, $n = 3$.

Table 3
Effect of sample volume on recovery of metal ions

	Phase Q (mg)	Recovery* (%)		
		25 mL	50 mL	100 mL
Cu(II)	20	105 ± 2	106 ± 5	104 ± 3
Pb(II)	20	89 ± 6	82 ± 3	82 ± 6
Ni(II)	60	97 ± 3	92 ± 3	57 ± 7
Co(II)	40	97 ± 2	88 ± 4	62 ± 3
Co(II)	60	94 ± 4	92 ± 6	87 ± 4
Cd(II)	20	95 ± 1	83 ± 2	48 ± 4
Cd(II)	50	96 ± 1	97 ± 2	94 ± 1

* Mean value ± $\frac{t_{0.05}s}{\sqrt{n}}$, $n = 3$ [add 10, 5, 2 μg at pH 3.5 for Pb(II), Cu(II) and Cd(II), respectively; 5 μg at pH 4.5 for Ni(II) and Co(II)].

Table 4
Effect of the interfering ions to %recovery

Elements	No interfering ion	Recovery* (%)		
		10 ppm	100 ppm	1000 ppm
Cu(II)	94 (4)	–	–	–
Na^+		101 (3)	107 (1)	104 (6)
K^+		105 (1)	108 (2)	105 (1)
Mg^{2+}		103 (1)	108 (4)	107 (1)
Ca^{2+}		100 (3)	106 (2)	105 (1)
Cl^-		100 (1)	107 (1)	109 (3)
$SO_4{}^{2-}$		103 (2)	106 (1)	107 (1)
Pb(II)	89 (1)	–	–	–
Na^+		89 (3)	95 (1)	97 (3)
K^+		87 (3)	95 (1)	97 (3)
Mg^{2+}		93 (4)	89 (6)	93 (4)
Ca^{2+}		89 (7)	96 (3)	98 (1)
Cl^-		89 (6)	89 (3)	93 (3)
$SO_4{}^{2-}$		94 (3)	89 (3)	101 (3)
Cd(II)	97 (2)	–	–	–
Na^+		102 (1)	106 (1)	102 (2)
K^+		102 (1)	101 (1)	104 (1)
Mg^{2+}		101 (1)	100 (1)	97 (2)
Ca^{2+}		103 (1)	101 (2)	103 (1)
Cl^-		99 (1)	104 (1)	106 (1)
$SO_4{}^{2-}$		94 (2)	103 (1)	106 (1)
Co(II)	91 (1)	–	–	–
Na^+		92 (1)	96 (1)	92 (1)
K^+		90 (3)	92 (1)	91 (1)
Mg^{2+}		90 (1)	89 (1)	91 (1)
Ca^{2+}		99 (1)	99 (1)	94 (4)
Cl^-		96 (1)	99 (1)	98 (2)
$SO_4{}^{2-}$		96 (1)	99 (1)	98 (2)
Ni(II)	94 (4)	–	–	–
Na^+		100 (3)	100 (3)	96 (1)
K^+		98 (6)	100 (2)	95 (2)
Mg^{2+}		98 (1)	97 (1)	93 (2)
Ca^{2+}		98 (1)	98 (1)	90 (2)
Cl^-		97 (2)	97 (2)	92 (2)
$SO_4{}^{2-}$		100 (2)	104 (2)	99 (2)

* Mean value (S.D.), $n = 3$ [10, 5, 2 μg at pH 3.5 for Pb(II), Cu(II) and Cd(II), respectively; 5 μg at pH 4.5 for Ni(II) and Co(II); sample volume = 100 mL (50 mL for Ni(II); sorbent = 20 mg for Pb(II) and Cu(II), 50 mg for Cd(II), 60 mg for Ni(II) and Co(II)].

Table 5
Pb(II), Cu(II), Ni(II), Co(II) and Cd(II) in Chulalongkorn University pond water by phase Q column preconcentration[**]

Element	Add (μg)	Found[*] (μg)	Recovery[*] (%)	R.S.D. (%)
Pb(II)	0	nd	–	–
	50	40.2 ± 2.2	80 ± 4	5
Cu(II)	0	nd	–	–
	5	4.1 ± 0.4	85 ± 8	9
Ni(II)	0	nd	–	–
	5	5.0 ± 0.1	100 ± 2	2
Co(II)	0	nd	–	–
	5	4.9 ± 0.09	98 ± 1	1
Cd(II)	0	nd	–	–
	2.5	2.4 ± 0.06	97 ± 2	2

[*] Mean value ± $\frac{t_{0.05}s}{\sqrt{n}}$, $n = 6$, nd = not detectable.

[**] [pH 3.5 for Pb(II), Cu(II) and Cd(II); pH 4.5 for Ni(II) and Co(II); sample volume = 100 mL (50 mL for Ni(II)); sorbent = 20 mg for Pb(II) and Cu(II), 50 mg for Cd(II), 60 mg for Ni(II) and Co(II); 5 mL of 1% HNO_3 as stripping solution at flow rate 0.5 mL/min].

Table 6
Pb(II), Cu(II), Ni(II), Co(II) and Cd(II) in tap water by phase Q column preconcentration[**]

Element	Add (μg)	Found[*] (μg)	Recovery[*] (%)	R.S.D. (%)
Pb(II)	0	nd	–	–
	50	41.4 ± 2.2	83 ± 4	5
Cu(II)	0	nd	–	–
	5	4.5 ± 0.1	91 ± 2	2
Ni(II)	0	nd	–	–
	5	5.1 ± 0.08	101 ± 1	1
Co(II)	0	nd	–	–
	5	4.8 ± 0.07	97 ± 1	1
Cd(II)	0	nd	–	–
	2.5	2.6 ± 0.05	102 ± 2	2

[*] Mean value ± $\frac{t_{0.05}s}{\sqrt{n}}$, $n = 6$, nd = not detectable.

[**] [pH 3.5 for Pb(II), Cu(II) and Cd(II); pH 4.5 for Ni(II) and Co(II); sample volume = 100 mL (50 mL for Ni(II)); sorbent = 20 mg for Pb(II) and Cu(II), 50 mg for Cd(II), 60 mg for Ni(II) and Co(II); 5 mL of 1% HNO_3 as stripping solution at flow rate 0.5 mL/min].

metal. The interference was apparent if the recovery of metal ion decreases in the presence of interfering ions.

The experiments were constructed at 298 ± 1 K. The results represent in Table 4 show that all of interfering ions did not interfere. The recoveries were not less than those in the absence of analyte at all three levels of interfering ion concentrations. These results indicate that phase Q have a high selectivity towards soft metals and have a potential to apply to real sample that contains diverse ions.

3.9. Application to natural real water samples

All of the optimized parameters were used for real samples. The objective is to test the method in the real condition. The pond water is a representative of natural water sample. In the real situation the heavy metals are present in trace amount among the various substances, for example, alkali and alkali earth metals, organic matters, humic acid, etc. These matters are obstacles in the determination of heavy metal. The accuracy and precision of the method were evaluated using spiked samples.

The purpose method was applied to the determination of Pb(II), Cu(II), Ni(II), Co(II) and Cd(II) in real water samples: (i) Chulalongkorn University's pond water, (ii) tap water and (iii) drinking water. All samples were collected with polyethylene bottle and used without storage. The Chulalongkorn University's pond water was filtered through the nylon 0.45 μm membrane; tap water and drinking water were used without other pretreatment. The results are shown in Tables 5–7.

For Pb(II), Cu(II), Ni(II), Co(II) and Cd(II) in Chulalongkorn University pond water, the recoveries were 80, 85, 100, 98 and 97, respectively. All the recoveries were in the acceptable range. These results indicated good accuracy of the method. In the precision point of view, the %R.S.D. of six replicates were less than 9%. These results showed that the proposed method gave a high precision and could be used with high repeatability.

The application of phase Q to tap water and drinking water gave the similar result. The recoveries of Pb(II), Cu(II), Ni(II), Co(II) and Cd(II) in tap water were 83, 91, 101, 97 and 102%, respectively, and in drinking water were 75, 101, 94, 97 and 103%. All of the recoveries of each metal were in the acceptable range, which indicated a good accuracy of the method. The exception was the recovery of Pb(II) in drinking water which was only at 75%. This may be due to the presence of Cu(II) 13.6 μg in drinking water. Cu(II) may compete with Pb(II) in the extraction. In the precision point of view, the %R.S.D. of six replicates were less than 5% in tap water sample, and in drinking water were less than 9%. Consequently, the method detection limits were 22.5, 1.0, 2.9, 0.95 and 1.1 μg/L for Pb(II), Cu(II), Ni(II), Co(II) and Cd(II), respectively, which are comparable to sensitivity of standard method (solvent extraction) [23].

Table 7
Pb(II), Cu(II), Ni(II), Co(II) and Cd(II) in drinking water by phase Q column preconcentration[**]

Element	Add (μg)	Found[*] (μg)	Recovery[*] (%)	R.S.D. (%)
Pb(II)	0	nd	–	–
	50	37.5 ± 2.6	75 ± 5	7
Cu(II)	0	13.6 ± 0.3	–	–
	2.5	16.1 ± 0.2	101 ± 9	9
Ni(II)	0	nd	–	–
	5	4.7 ± 0.09	94 ± 2	2
Co(II)	0	nd	–	–
	5	4.9 ± 0.2	97 ± 3	4
Cd(II)	0	nd	–	–
	2.5	2.6 ± 0.1	103 ± 4	4

[*] Mean value ± $\frac{t_{0.05}s}{\sqrt{n}}$, $n = 6$, nd = not detectable.

[**] [pH 3.5 for Pb(II), Cu(II) and Cd(II); pH 4.5 for Ni(II) and Co(II); sample volume = 100 mL (50 mL for Ni(II)); sorbent = 20 mg for Pb(II) and Cu(II), 50 mg for Cd(II), 60 mg for Ni(II) and Co(II); 5 mL of 1% HNO_3 as stripping solution at flow rate 0.5 mL/min].

Table 8
Comparison of sorption capacities (μmol g^{-1}) on some modified silica gel and weight of sorbent for column method (mg)

Ligand	Weight (mg)	Metal ions				
		Pb(II)	Cu(II)	Ni(II)	Co(II)	Cd(II)
Aminothioamido-anthraquinone	20–60	560	300	150	120	70
2,4-Dichlorophenoxy-acetic acid [7]	200	–	440	320	–	140
1,8-Dihydroxyanthra-quinone [12]	1000	76.4	–	–	–	70.2
N-[3-(trimethoxysilyl)propyl]-ethylenediamine [24]	–	–	184	261	–	–
5-Formyl-8-hydroxy-quinoline [25]	1000	158	448	255	205	92
o-Dihydroxybenzene [26]	1000	82	348	178	175	32

4. Comparison of sorption capacities

The sorption capacity on phase Q and the weight of sorbent used in column method are compared with those of other modified silica gel represent in Table 8. Phase Q shows comparable capacity level to several sorbents presented in previous reports, especially the sorption capacity for Pb(II) (560 μmol g^{-1}). Considering a very small amount of phase Q in column method was used in comparison with the previous reports.

5. Conclusions

We have successfully synthesized a novel chemically modified silica gel containing aminothioamidoantraquinone and applied to solid phase extraction and preconcentration of some heavy metal ions. This phase was found to adsorb for Pb(II) over Cu(II), Co(II), Ni(II) and Cd(II). The method detection limits have been improved under the optimal conditions on mini-column. In the application of the proposed method to preconcentration of natural sample such as pond water, tap water and drinking water gave high accuracy and precision without the interference ion effect.

Acknowledgements

The authors thank the Development and Promotion of Science and Technology Talents Project for scholarship. This work was sponsored by Graduate School of Chulalongkorn University.

References

[1] A.N. Anthemidis, G.A. Zachariadis, C.G. Farastelis, J.A. Stratis, Talanta 62 (2004) 437.
[2] P.K. Jal, S. Patel, B.K. Mishra, Talanta 62 (2003) 1005.
[3] P.S. Roldan, I.L. Alcantara, G.R. Rocha, C.C.F. Padilha, P.M. Padilha, Anal. Bioanal. Chem. 375 (2003) 574.
[4] K. Terada, K. Matsumoto, Y. Nanao, Anal. Sci. (1985) 1145.
[5] L. Roman, E. Florean, R. Safndulescu, S. Mirel, J. Pharm. Biomed. Anal. 14 (1996) 1003.
[6] M.E. Mahmoud, E.M. Soliman, Talanta 44 (1997) 15.
[7] A.G.S. Prado, C. Airoldi, Anal. Chim. Acta 432 (2001) 201.
[8] S. Watanesk, A.A. Schilt, Talanta 33 (1986) 895.
[9] A.G.S. Prado, A.H. Tosta, C. Airoldi, J. Colloid Interface Sci. 269 (2004) 259.
[10] A. Safavi, N. Iranpoor, N. Saghir, Sep. Purif. Technol. 40 (2004) 303.
[11] L.T. Kubota, J.C. Moreira, Analyst 114 (1989) 13.
[12] A. Goswami, A.K. Singh, Talanta 58 (2002) 669.
[13] R.K. Sharma, A. Goel, Anal. Chim. Acta 534 (2004) 137.
[14] L. Arakaki, J. Espinola, S. Oliveira, J. Freitas, A. Gouveia, C. Airoldi, Colloid Surf. A 203 (2002) 129.
[15] S. Brunauer, P. Emett, E. Teller, J. Am. Chem. Soc. 60 (1994) 309.
[16] C. Airoldi, M.R.M.C. Santos, J. Matter Chem. 4 (1994) 1979.
[17] M.R.M.C. Santos, C. Airoldi, J. Colloid Interface Sci. 183 (1996) 416.
[18] E.F.S. Vieira, J.A. Simoni, C. Airoldi, J. Matter Chem. 7 (1997) 2249.
[19] M.M. Hassanien, K.A. Abou-El-Sherbini, Talanta 68 (2005) 1550.
[20] A.S. Erses, M.A. Fazal, T.T. Onaya, W.H. Craig, J. Hazard. Mater. B121 (2005) 223.
[21] N.L.D. Filho, Y. Gushikem, W.L. Polito, J. Moreira, E.O. Ehirim, Talanta 42 (1995) 1625.
[22] M. Santos, C. Airoldi, J. Colloid Interface Sci. 183 (1996) 416.
[23] S.L. Sachdev, P.W. West, Environ. Sci. Technol. 4 (1970) 749.
[24] N. Chiron, R. Guilet, E. Deydier, Water Res. 37 (2003) 3079.
[25] A. Goswami, A.K. Singh, B. Venkataramani, Talanta 60 (2003) 1141.
[26] G. Venkatesh, A.K. Singh, B. Venkataramani, Microchim. Acta 114 (2004) 233.

Available online at www.sciencedirect.com
ScienceDirect
Talanta 71 (2007) 1233–1238
Talanta
www.elsevier.com/locate/talanta

Quantification of cephalexin as residue levels in bovine milk by high-performance liquid chromatography with on-line sample cleanup

Regina V. Oliveira, Angela C. De Pietro, Quezia B. Cass *

Departamento de Química, Universidade Federal de São Carlos, Caixa Postal 676, São Carlos, 13565-905 SP, Brazil

Received 20 April 2006; received in revised form 15 June 2006; accepted 16 June 2006
Available online 25 July 2006

Abstract

A multidimensional, selective and precise high performance liquid chromatography (HPLC) method based on direct injection of biological samples has been developed for the determination of cephalexin in skimmed and whole bovine milk. The cephalosporin antibiotic was extracted from bovine milk using an octyl restricted access medium bovine serum albumin column (C_8-RAM-BSA) and analyzed on an octadecyl column using phosphate buffer (pH 7.5, 0.01 M): ACN (92:8, v/v) and ultraviolet detection at 260 nm. The calibration graph was linear in the concentration range of 25–1600 ng/mL and this is in accordance with the tolerance level of 100 ng/mL set by the FDA (Food and Drug Administration) and EU (European Union) for cephalexin as residue in bovine milk. The intra- and inter-day coefficients of variation for the replicate analysis at the quality control levels were less than 15% while the transfer efficiency was in the range of 90.2–92.3%. The limits of detection and quantification were 10 and 20 ng/mL, respectively.
© 2006 Elsevier B.V. All rights reserved.

Keywords: Restricted access medium (RAM); Column switching; Direct injection; Cephalosporins; Bovine milk

1. Introduction

Worldwide milk productivity has important economic contribution. Nowadays, many efforts have been made to improve high quality milk production, such as genetic research of bovine animals, improvements in nutrition quality and close monitoring of animal health [1]. Besides its economic importance, milk also has an essential nutritional aspect, being considered a critical nutrient source for children and adults [2].

The most important concern related to milk and dairy product production is the improper administration of antibiotics to dairy cows to fight infections such as mastitis and to promote growth and maintain good animal health [3,4]. The excessive use of antibiotics may lead to residual levels in milk, meat and tissues and it could cause serious human health consequences, evolution of antibiotic-resistant bacteria as well as technological problems in dairy products [5,6]. For these reasons, the presence of antibiotics in milk is regulated by the Food and Drug Administration (FDA) and European Council Regulation (ECC) 2377/90 and maximum residues limits (MRLs) have been set for veterinary drug residues in tissues and milk [7,8]. For example, in bovine milk, MRLs for cephalexin has been set at 100 ng/mL.

Cephalexin (Fig. 1), a cephalosporin antibiotic, is an effective broad spectrum antibiotic that targets both Gram positive and Gram negative bacteria [9] and has therefore become a widely administrated antibiotic for treating and preventing bacterial infections in lactating cows.

Routinely, microbial assays are used to perform testing of milk. However, they fail to identify and to quantify the residual antibiotics. Thus, sensitive and specific confirmatory tests are still needed. As an analytical approach, high performance liquid chromatography is recognized as the technique of choice for analyzing drugs and metabolites in challenging biomatrices [10,11]. Sample preparation is usually necessary to remove interfering matrix components. In this field, continued efforts are made to develop faster analytical methods.

Several chromatographic methods, using various stationary phases and mobile phases have been described for determination of cephalosporins antibiotics in diverse biological fluids [10–15] but only a few methods are reported for bovine milk [13–19].

* Corresponding author. Tel.: +55 16 33518087; fax: +55 16 33518350.
E-mail address: quezia@pesquisador.cnpq.br (Q.B. Cass).

0039-9140/$ – see front matter © 2006 Elsevier B.V. All rights reserved.
doi:10.1016/j.talanta.2006.06.024

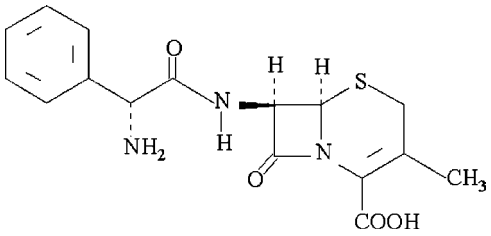


Fig. 1. Chemical structure of cephalexin.

All of them used different off-line sample clean-up procedures prior to analysis such as liquid–liquid extraction, ultrafiltration, protein precipitation and solid-phase extraction. However, these traditional methods increase the total analysis time and reduce the recovery of the analytes of interest.

Milk is a very challenging sample matrix and only a reduced number of methods deals with direct injection of milk samples [20,21–27]. The success obtained for quantification of cefoperazone by micro sample deproteinization [25] prompt us to develop a completely automated HPLC method by coupling a C_8-RAM-BSA column to an octadecyl column for quantification of cephalexin as a residue in bovine raw milk.

2. Experimental

2.1. General

Acetonitrile (HPLC grade) was purchased from Mallinckrodt Baker (St. Louis, MO), and water was purified by a Milli-Q purification system (Millipore, São Paulo, Brazil). Dihydrogen potassium phosphate was obtained from Cinética Química (São Paulo, SP, Brazil); bovine serum albumin (fraction V powder minimum 98%) and tetrabutylammonium hydrogen phosphate from Sigma (St. Louis, MO); glutaraldehyde and sodium borohydride were from Merck (Darmstadt, Germany). The 47 mm diameter, 0.45 μm Nylon membranes used to filter all of the mobile phases were also from Millipore. Cephalexin was generously donated from Pfizer (São Paulo, SP, Brazil). Natural pasteurized whole milk and skimmed milk were obtained from different bakeries in São Carlos (SP, Brazil).

2.2. Instrumentation and chromatographic conditions

The HPLC system consisted of two Shimadzu LC-10ATVP pumps (Kyoto, Japan), with one of the pumps containing a valve FCV-10AL for selecting solvent, an autoinjector model SIL 10AVP, a degasser model DGU-14A, a column oven CTO-10A (at 30 °C), a SPD-6AV UV–vis detector (at 260 nm), and an SCL 10AVP interface. A sample valve HPLC 7000 Nitronic EA (Supelco, St. Louis, MO) was used for the automated column switching. Data acquisition was done on Shimadzu Class-VP software.

Analysis was performed on an octadecyl Hypersil analytical column (150 mm × 4.6 mm i.d.) (5 μm; 120 Å) and a restricted access medium Hypersil C_8 BSA column (100 mm × 4.6 mm i.d.) (10 μm; 120 Å). Both columns were packed by ascending slurry method at 7500 psi, using methanol. After, the columns were conditioned for 12 h using methanol at flow rate of 1.0 mL/min [28,29]. The restricted access media C_8-BSA column was prepared as previously described [29].

2.3. Standard solutions and spiked sample preparation

Stock solutions of cephalexin (200 μg/mL) was prepared in water. From this stock solution eight standards solutions were prepared in water at the following concentrations: 16.0, 8.00, 4.00, 2.00, 1.00, 0.750, 0.500, and 0.250 μg/mL. Quality control solutions were prepared at 0.300, 6.40, and 12.0 μg/mL. Stock, standard and quality control solutions were prepared fresh weekly.

Calibration standard, quality control and milk unknown solutions were prepared by aliquoting 20 μL of the appropriate standard solution into a series of culture tubes and reconstituting using 200 μL of milk (skimmed or whole) that was previously centrifuged at 15,000 × *g* at 20 °C for 10 min, or water (for the extraction efficiency evaluations), and then 20 μL of a 1.3 mM solution of tetrabutylammonium hydrogen phosphate prepared in 0.01 M phosphate buffer (pH 7.5) was added to each tube. After, the solutions were vortex-mixed for 15 s, aliquots of 180 μL were transferred to auto-sampler vials and 120 μL was injected into the column-switching HPLC system. For the stability assay, the spiked milk samples were thawed to room temperature and 20 μL of 1.3 mM tetrabutylammonium hydrogen phosphate was added to each tube just before analysis. For method development and validation skimmed milk type A was used.

2.4. Method validation

Eight calibration-spiked skimmed milk standards (1.60, 0.800, 0.400, 0.200, 0.100, 0.075, 0.050, and 0.025 μg/mL) were prepared in triplicate using blank skimmed milk. The calibration curve was constructed by plotting the peak area ratio against the concentration of cephalexin.

For selectivity purposes, analyses of drug-free skimmed milk and skimmed milk spiked with cephalexin were assessed daily.

The extraction efficiency of cephalexin from spiked skimmed milk by the C_8-RAM-BSA column was determined by analyzing quality control samples at three different concentrations: 0.030, 0.640, and 1.20 μg/mL. The peak area ratios of five extracted samples at each concentration were compared with those of five injections of standard solutions in water at the same concentrations to derive a percent extraction.

Inter- and intra-day variability of the method was evaluated by replicate analysis at the same three concentrations (0.030, 0.640, and 1.20 μg/mL). Five samples of each concentration were prepared in milk on 3 nonconsecutive days.

The accuracy of the method was evaluated by back-calculation; it was also tested using blinded unknowns, at two different concentrations, which were prepared by a different analyst.

The acceptance criterion for the limit of quantification was that the precision and accuracy for three extracted samples were under 20% variability [28]. The limit of detection was deter-

mined by the lowest concentration of analyte, which resulted in a signal-to-noise ratio of three.

The stability of cephalexin in milk samples was assessed by comparing assay results in fortified samples at the three quality control concentrations (0.030, 0.640, and 1.20 μg/mL) and by analyzing aliquots of the samples after storage in different conditions. All stability determinations were carried out by comparing the analysis of a set of freshly prepared samples in skimmed milk to a set of samples in skimmed milk, which had been stored. The stability of the quality control milk samples containing cephalexin and drug-free milk samples (matrix) were evaluated in the following conditions: (a) sitting at room temperature for 4 h (bench-top stability) and 24 h (auto-sampler stability), respectively; (b) stored at −20 °C and exposed to three freeze–thaw cycles; (c) stored at 4 and at −20 °C for 15 days. Variation less than 15% in the concentration of the samples between assays and the initial response were the criteria for the stability evaluation [30].

2.5. Application of the method

The developed method was applied to quantify cephalexin in whole pasteurized milk samples in 10 different unknown concentrations. All samples were prepared by a different analyst (blind test) in duplicate. Besides this, six different brands of pasteurized milk obtained from different bakeries in São Carlos, SP, Brazil, were evaluated for monitoring cephalexin residues.

3. Results and discussion

To perform HPLC analysis in a biological matrix, composed of proteins and lipids, a sample cleanup is always required. The sample preparation process can be time consuming. To minimize sample handling time and the number of sample preparation steps a RAM column coupled to the analytical column by a column switching system was chosen for the cephalexin analysis in bovine milk.

The use of restricted access media bovine serum albumin (RAM-BSA) for milk sample cleanup has been described by our group [21,25] and the retention of a series of five cephalosporin antibiotics in the different mobile phases were evaluated.

Based on previous published results [25], a C_8-RAM-BSA column was selected for the on-line sample cleanup. In order to determine the elution profile and retention times of the analyte in the milk matrix, the RAM column was directly connected to the UV detector.

Successive injections of whole milk samples (40 injections of 100 μL) into the C_8-RAM-BSA column resulted in lost of precision on the cephalexin retention factor. This was probably due to lipid adsorption by the RAM column. Thus, in order to minimize this effect and increase the lifetime of the RAM column, skimmed milk was adopted for the method development. This modification allowed good column performance and a lifetime for the RAM column of about 40 mL of milk (400 samples).

Addition of an ion-pair reagent, tetrabutylammonium hydrogen phosphate, during sample preparation had been explored with success for extracting amoxicillin human plasma samples [28] and for extracting cefoperazone from milk samples [25] and was used again, this time to promote a higher retention factor for cephalexin on both columns, thus leading to satisfactory separation of co-eluents on the analytical column.

The pH of the buffer solution was important for cephalexin retention and also for the milk protein's exclusion. Different protein exclusion and retention profiles were observed by varying the pH of the buffer. Phosphate buffer at pH 6.0 as mobile phase provided efficient removal of the milk proteins and matrix interferents by increasing the ionic strength and also allowed a good retention time for the cephalexin antibiotic on the RAM-BSA. The composition of the analytical mobile phase was investigated considering pH buffer solutions (pH 5.0–7.5) and percentage of acetonitrile (5.00–10.0%). Optimal chromatographic conditions were obtained using 0.01 M phosphate buffer (pH 7.5): acetonitrile (92:8, v/v) at flow-rate of 1.0 mL/min.

The employed column-switching system used is illustrated in Fig. 2. The milk samples were directly injected onto the RAM column (position 1) and milk proteins were excluded by the C_8 RAM using 0.01 M phosphate buffer (pH 6.0): acetonitrile (95:5, v/v). The six-port valve remained in this position for 8.0 min and then the valve changed to position 2, redirecting the flow to the C_{18} analytical column. Cephalexin was transferred from 8.0 to 13.0 min using the same mobile phase as for protein exclusion. After this time, the valve was switched back to position 1 for cleaning and conditioning the RAM column. The C_8 RAM column was cleaned with a mixture of acetonitrile:water:isopropanol (75:20:5, v/v/v). In mean time, cephalexin was analyzed on the C_{18} column using 0.01 M phosphate buffer (pH 7.5): acetonitrile (92:8, v/v). The flow-rate 1.0 mL/min was used during the entire analysis sequence and

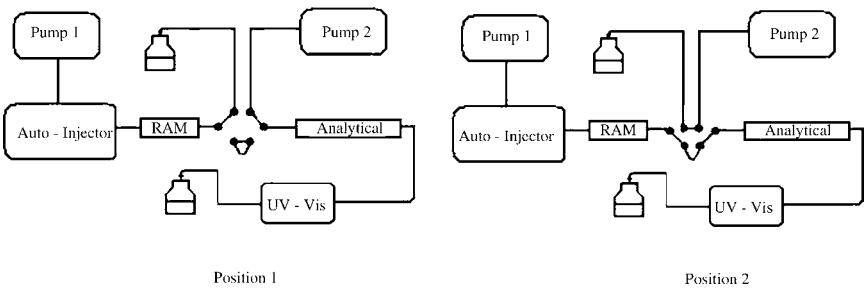


Fig. 2. Schematic diagram of the column-switching system.

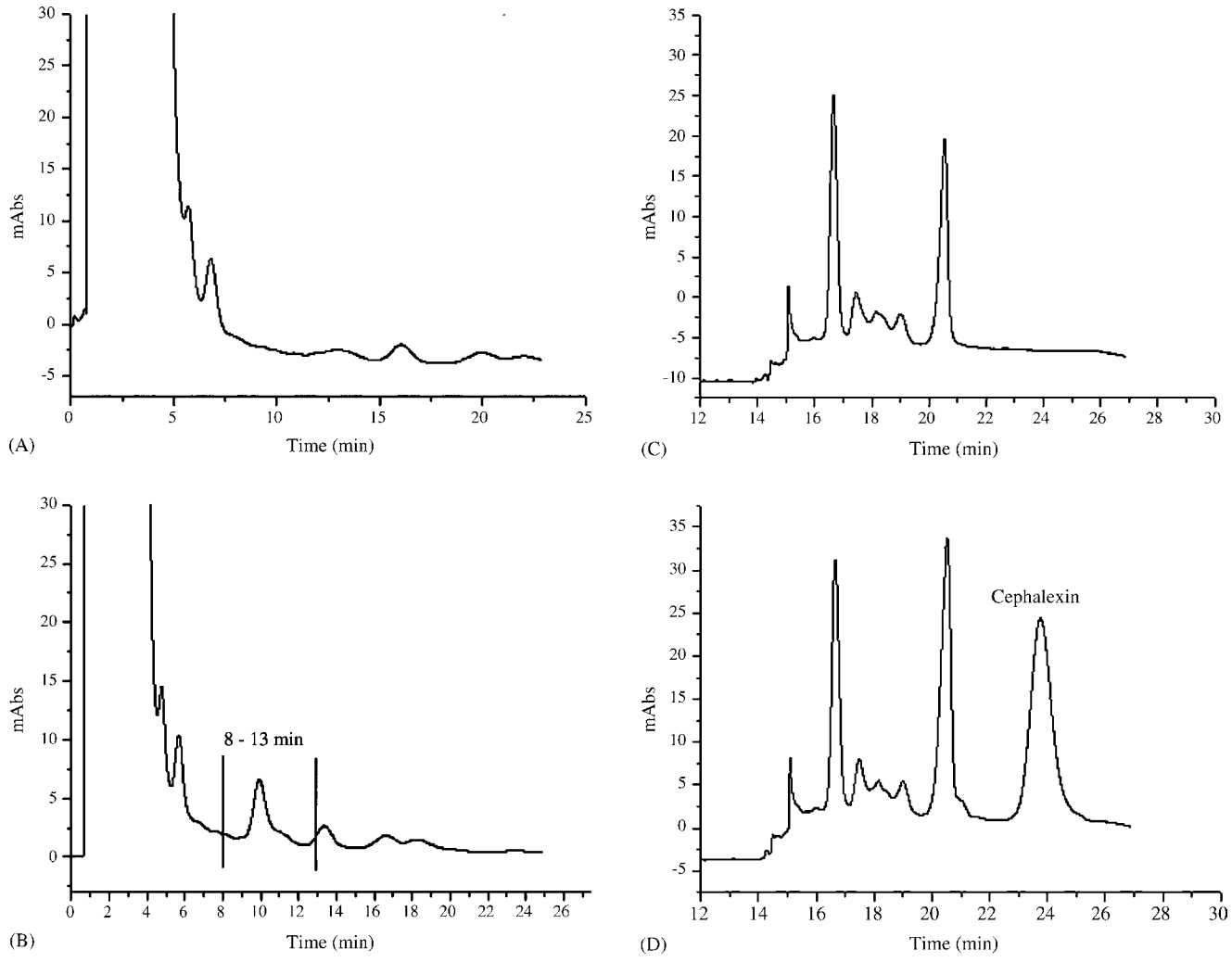


Fig. 3. Representative chromatograms of milk free drug (A) and milk spiked with cephalexin 2000 ng/mL (B) at the RAM column alone and milk free drug (C) and spiked milk with cephalexin 1200 ng/mL (D) using the HPLC multidimensional system.

the absorbance was measured at 260 nm. The total analysis was 26 min and, to achieve the necessary sensitivity, an injection volume of 120 μL was used.

Representative chromatograms of milk free drug and milk spiked at 2000 ng/mL samples using the RAM column alone are shown at Fig. 3 (Fig. 3A and B) while the chromatograms at Fig. 3C and D were obtained using the HPLC column switching system at the optimized chromatographic conditions for milk free drug sample and milk sample spiked at 1200 ng/mL. In the chromatograms shown in Fig. 3A and B, it can be noticed that the exclusion of milk proteins are accomplished before the established time of transferring cephalexin to the analytical column. The comparison of the chromatogram given at Fig. 3C with the one at 3D highlights that no interferences are observed in the region of interest where the cephalexin elutes.

The method validation was carried out according to internationally accepted criteria [30]. The calibration curve was linear from 0.025 to 1.60 μg/mL. The following regression equation and correlation coefficient was obtained: $y = 9.87 \times 10^{-6}x - 0.002$; $r^2 = 0.999$. Inter- and intra-day precision and accuracy were established at three quality control samples (high, medium, and low concentrations) prepared in five replicates and analyzed on 3 nonconsecutive days. The precision was expressed as coefficient of variation (CV%) and the accuracy was evaluated by back-calculation and expressed as the percent deviation between amount found and amount added at the three concentrations examined. All precision and accuracy results led to satisfactory intra- and inter-day precision, with coefficient of variation ≤15%. These results obtained are presented in Table 1.

The extraction and transfer efficiencies (Table 1) were determined at the same three quality control concentration levels. The results were calculated based on comparison to an aqueous cephalexin solution at corresponding concentrations. High recoveries were obtained at the three concentrations examined.

The limit of quantification (LOQ) was 20 ng/mL while the limit of detection (LOD) was 10 ng/mL. Two blind samples containing unknown concentrations to the analyst produced accuracies in the range of 101–104% at concentration levels of 64 and 960 ng/mL with CV% at the range of 1.63–8.69 for the duplicate analysis of the samples.

The long-term storage, short-term storage (bench-top), freeze–thaw stability and autosampler stability were all evalu-

Table 1
Accuracy and intra- and inter-day variability for the assay of cephalexin in bovine milk

Concentration (ng/mL)	1st Day[a]		2nd Day[a]		3rd Day[a]		Pooled[b]		Recovery[a]
	Accuracy (%)	CV (%)	Accuracy (%)	CV (%)	Accuracy (%)	CV (%)	Accuracy (%)	CV (%)	Mean ± S.D.
30.00	85.6	6.56	99.3	9.68	96.6	7.58	93.8	7.94	92.3 ± 8.8
640.00	107	1.19	96.7	3.55	97.7	2.26	100	2.33	91.1 ± 1.6
1200	105	1.52	95.6	3.25	97.7	1.77	99.4	2.18	90.2 ± 2.3

[a] $n = 5$.
[b] $n = 15$.

Table 2
Accuracy and intra- and inter-day variability for the 10-blinded spiked-milk samples of cephalexin in whole bovine milk

Concentration (ng/mL)	Accuracy (%)	CV (%)	Concentration (ng/mL)	Accuracy (%)	CV (%)
32.00	107	2.11	234.0	89.2	4.53
66.00	90.0	2.08	460.0	98.5	2.63
88.00	98.9	3.44	620.0	97.2	1.54
148.0	94.0	6.56	1060	95.2	2.01
190.0	94.8	0.50	1360	99.0	2.90

ated. Analytical standard solutions were stable for 15 days when stored at 4 or −20 °C. Milk samples spiked with cephalexin were stable for 24 h when kept at 4 or −20 °C. For short-term storage (bench-top) the samples were prepared and kept at room temperature for 4 h before analysis and all of them proved to be stable. Autosampler stability was also determined and all samples were stable over the 24 h period evaluated. The stability of cephalexin in spiked-milk samples during three freeze–thaw cycles was evaluated and the antibiotic was stable for one cycle. The assay for evaluation of matrix stability showed that the matrix was stable for a 3-day period when stored at 4 or −20 °C. Different batches of milk were also evaluated and no significant difference was observed between them.

The developed method was applied for quantification of 10-blinded spiked-milk samples (whole milk) with unknown concentrations of cephalexin to the analyst. The samples were prepared in duplicate and in different concentrations simulating a pharmacological profile. The analysis of these samples was carried out jointly with the analyses of quality control samples. The accuracy and precision obtained met the acceptance criteria in all samples evaluated. The results are described in Table 2.

The validated method has been successfully applied to monitor residues in eight different types of whole pasteurized milk (grades A–C) samples. The analyzed milks were purchased at local bakeries in São Carlos, Brazil. Cephalexin or other interfering compounds with the same retention time as the antibiotic were not found in any of these batches of whole milk.

4. Conclusions

The goal of this work was to develop an HPLC-UV method using on-line sample cleanup restricted access medium (RAM) column for monitoring residues of cephalexin antibiotic in bovine milk. The column-switching method described herein was proved to be simple, sensitive, selective, precise and accurate. Further, the total analysis time, was only 26 min and the sample treatment involved only a centrifugation for 10 min at 15,000 × *g* making it an attractive alternative to the laborious traditional employed methods. The method can be efficiently used to establish the withdrawal time after cephalexin administrations.

Acknowledgments

The authors acknowledge the financial support from Fundacão de Amparo a Pesquisa do Estado de Sao Paulo (FAPESP). The grants from Conselho Nacional de Desenvolvimento Científico e Tecnológico (CNPq) and Coordenação de Aperfeiçoamento de Nível Superior (CAPES) are also acknowledged.

References

[1] J.J. Kennelly, D.R. Glimm, Can. J. Anim. Sci. 78 (1998) 23.
[2] L. Hambraeus, Bibl. Nutr. Diet. 53 (1996) 37.
[3] S.A. McEwen, W.D. Black, A.H. Meek, J. Dairy Sci. 74 (1991) 2128.
[4] J. Turnidge, J. Antimicrob. Chemoth. 53 (2004) 26.
[5] A. Romano, M.J. Torres, F. Namour, C. Mayorga, M.C. Artesani, A. Venuti, J.L. Gueant, M. Blanca, Allergy 57 (72) (2002) 52.
[6] L. Grunwald, M. Petz, Anal. Chim. Acta 483 (1/2) (2003) 73.
[7] U.S. Food and Drug Administration. Code of Federal Regulations, Title 21, 1999. Section 556.
[8] Council Regulation (EEC) 2377/90 June 26, 1990 (OJ No. L 224, 18.8.1990).
[9] L.S. Goodman, A. Gilman, Antimicrobial agents, in: J.G. Hardnab, L.L. Limbird, A.G. Gilman (Eds.), The Pharmacological Basis of Therapeutics, 10th ed., McGraw-Hill, New York, 2001, pp. 1189–1218.
[10] A. Marzo, L. Dal Bo, J. Chromatogr. A 812 (1998) 17.
[11] F. Péhourcq, C. Jarry, J. Chromatogr. A 812 (1998) 159.
[12] P. Meltz, S.J. Kohlhepp, D.N. Gilbert, J. Chromatogr. B 773 (2) (2002) 159.
[13] L.K. Sørensen, L.K. Snor, J. Chromatogr. A 882 (2000) 145.
[14] M. Becker, E. Zittlau, M. Petz, Anal. Chim. Acta 520 (1/2) (2004) 19.
[15] D.M. Holstege, B. Puschner, G. Whitehead, F.D. Galey, J. Agric. Food Chem. 50 (2002) 406.
[16] J. Keever, R.D. Voyksner, K.L. Tyezkowska, J. Chromatogr. A 794 (1998) 57.
[17] W.A. Moats, R.D. Romanowski, J. Chromatogr. A 812 (1/2) (1998) 237.
[18] F.J. Schenck, P.S. Callery, J. Chromatogr. A 812 (1998) 99.

[19] J. Jordan, B. Ludwig, J. Chromatogr. 362 (1986) 263.
[20] N.M. Cassiano, V.V. Lima, R.V. Oliveira, A.C. de Pietro, Q.B. Cass, Anal. Bioanal. Chem. 384 (2006) 1462.
[21] A.V. Pereira, Q.B. Cass, J. Chromatogr. B 826 (2005) 139.
[22] M.L. Menezes, G. Felix, J. Liq. Chromatogr. Relat. Technol. 19 (19) (1998) 3221.
[23] M.L. Menezes, G. Felix, J. Liq. Chromatogr. Relat. Technol. 21 (18) (1998) 2863.
[24] M.L. Menezes, G. Felix, A.C.C.O. Demarchi, Chromatographia 47 (1/2) (1998) 81.
[25] R.V. Oliveira, Q.B. Cass, J. Agric. Food Chem. 54 (2006) 1180.
[26] V.K. Agarwal, J. Liq. Chromatogr. 13 (12) (1990) 2475.
[27] M.J. Gonzalez, B. Jiménez, L.M. Hernández, C. Vidal-Madjar, H. Place, J. High Resolut. Chromatogr. Chromatogr. Commun. 16 (2) (1993) 129–130.
[28] Q.B. Cass, R.F. Gomes, S.A. Calafatti, J. Pedrazolli Jr., J. Chromatogr. A 987 (2003) 235.
[29] N.M. Cassiano, Q.B. Cass, A.L.G Degani, I.W. Wainer, Chirality 14 (9) (2002) 731.
[30] U.S. Food and Drug Administration, Bioanalytical method validation, in: Guindance for Industry, U.S. GPO, Washington, DC, 2001, p. 1–22.

Available online at www.sciencedirect.com
ScienceDirect
Talanta 71 (2007) 1155–1165
Talanta
www.elsevier.com/locate/talanta

Determination of total antioxidant capacity by a new spectrophotometric method based on Ce(IV) reducing capacity measurement

Dilek Ozyurt [a], Birsen Demirata [a], Resat Apak [b,*]

[a] *Department of Chemistry, Faculty of Science & Letters, Istanbul Technical University, Maslak, Istanbul, Turkey*
[b] *Department of Chemistry, Faculty of Engineering, Istanbul University, Avcilar, Istanbul, Turkey*

Received 9 September 2005; received in revised form 5 June 2006; accepted 7 June 2006
Available online 17 July 2006

Abstract

Dietary antioxidants widely found in fruits and vegetables may serve the task of reducing oxidative damage in humans induced by free radicals and reactive oxygen species under 'oxidative stress' conditions. The aim of this work is to develop a simple, low-cost, sensitive, and diversely applicable indirect spectrophotometric method for the determination of total antioxidant capacity of several plants. The method is based on the oxidation of antioxidants with cerium(IV) sulfate in dilute sulfuric acid at room temperature. The Ce(IV) reducing capacity of the sample is measured under carefully adjusted conditions of oxidant concentration and pH such that only antioxidants and not other organic compounds would be oxidized. The spectrophotometric determination of the remaining Ce(IV) was performed after completion of reaction with antioxidants. Quercetin and gallic acid were used as standards for flavonoids and phenolic acids, respectively, and results of antioxidant measurements were reported as trolox equivalents. The developed procedure was successfully applied to the assay of total antioxidant capacity due to simple compounds such as trolox, quercetin, gallic acid, ascorbic acid, catechin, naringin, naringenin, caffeic acid, chlorogenic acid, ferulic acid, and *p*-coumaric acid, and due to phenolic acids and flavonoids in the arieal parts of nettle (*Urtica Dioica* L.). Blank correction of significantly absorbing plant extracts at 320 nm could be made with the aid of spectrophotometric titration. Plant selection was made in respect to high antioxidant content, and extraction was made with water. The proposed method was reproducible, and the trolox equivalent antioxidant capacities (TEAC coefficients) of the tested antioxidant compounds were correlated to those found by reference methods such as ABTS and CUPRAC. Since the TEAC coefficients found with the proposed method of naringin–naringenin and rutin–catechin pairs were close to each other, this Ce(IV)-based assay probably caused the simultaneous hydrolysis of flavonoid glycosides to the corresponding aglycones and their subsequent oxidation such that the hydrolysis products exhibed antioxidant capacities roughly proportional the number of –OH groups contained in a molecule.
© 2006 Elsevier B.V. All rights reserved.

Keywords: Total antioxidant capacity assay; Flavonoids; Phenolic antioxidants; Cerium(IV) sulfate; Spectrophotometry

1. Introduction

Antioxidants are vital in combating the free radicals, which damage human cells under 'oxidative stress' conditions and an imbalance of free radicals may cause grave disturbances in cell metabolism. Free radicals are instable species because they have unpaired electrons and seek stability through electron pairing with biological macromolecules. The proteins, lipids, and DNA of healthy human cells are good sources for these pairing electrons. Thus oxidative stress conditions can cause DNA and protein damage, lipid peroxidation, cancer, atherosclerosis, ageing, and inflammatory diseases [1,2]. Sources of free radicals include metabolism by-products, neutrophiles, UV radiation, air and water pollutants, fatty foods, hazardous chemicals, and cigarette smoke.

Natural antioxidants such as dietary plant flavonoids are increasingly attracting attention. They are natural disease-preventing, health-promoting, and anti-ageing substances. Flavonoids are essentially ingested through food rather than being metabolically synthesized.

Reports that contradict the putative role of flavonoids as antioxidant and anti-cancer agents have also taken place in literature [3]. Flavonoids are plant secondary metabolites widely distributed in the plant kingdom. More than 6000 flavonoids have been identified in plants [4]. They can be subdivided into six classes; flavone, flavanone, flavanol, flavonol, isoflavone and

* Corresponding author. Tel.: +90 212 4737028.
E-mail address: rapak@istanbul.edu.tr (R. Apak).

0039-9140/$ – see front matter © 2006 Elsevier B.V. All rights reserved.
doi:10.1016/j.talanta.2006.06.015

anthyocyanidin with respect to the structure and conformation of heterocylic oxygen ring (C ring) of the core molecule [5].

Antioxidant capacity/activity assay methods existing in literature based on the measurement of radical scavenging activity of antioxidant compounds suffer from the difficulties encountered in the formation and stability of colored radicals [6], such as ABTS (2,2′-azinobis-(3-ethylbenzothiazoline-6-sulfonic acid)) [7], and DPPH (2,2′-diphenyl-1-picrylhydrazyl) [8], the former being more dependent on the type of reaction used for radical generation, i.e., enzymatic or chemical. The evaluation of antioxidant activity by the changes of DPPH absorbance should be carefully interpreted since the absorbance of DPPH at 517 nm is decreased by light, oxygen, pH, and type of solvent in addition to the antioxidant [9]. In some kinetic-based assays, the inhibition of accumulation of colored radical reagents in the presence of antioxidants is expressed in the units of "lag time" (i.e., the time period required for the colored radical to emerge in the reaction medium), constituting a rather unobjective approach for antioxidant assay, because "lag time" is not always linearly correlated to antioxidant concentration. Measurement of oxygen radical scavengers with methods such as the ORAC test of antioxidant capacity [10] may be interfered by hydroxyl radical scavengers like benzoate, which are not true antioxidants. On the other hand, the ferric reducing ability (FRAP) assay of antioxidants [11], which is based on ferric-to-ferrous reduction in the presence of a Fe(II)-stabilizing ligand such as tripyridyltriazine, is non-responsive to thiol-type antioxidants like glutathione. The common drawback of the existing antioxidant activity assays for foodstuffs is that the measured variable is either the quantity or reactivity (or both) of antioxidant compounds, thereby posing a debate to the objectivity of such procedures as high- and low-reactivity compounds produce a wide range of stoichiometric factors compared to that of a reference compound such as trolox. The range of tests used for antioxidant activity measurement is also a testimony to the uncertainty surrounding the chemistry of phenolic compounds. Thus for example, in tests where free radical oxidation is induced by a metal ion like Cu(II) or Fe(III), it is uncertain whether the test measures the ability of the phenolic to interact with a free radical or its ability to bind the metal ion [12]. Current literature taking a philosophical look at antioxidant indexes clearly states that there is no "total antioxidant" as a nutritional index available for food labeling because of the lack of standard quantitation methods [13]. As a result, the antioxidant activities of common vegetables (total sample size: 927) collected from the US market, analyzed using the ORAC and FRAP procedures, did not correlate well [13], which may partly be attributed to the different mechanisms of these assays as being hydrogen atom-transfer or electron-transfer [14]. To briefly summarize the current situation, there is no single, widely acceptable assay method applicable to a reasonable variety of compounds and food matrices. Due to this difficulty, various food products containing flavonoids as the main antioxidant components may not be classified with respect to their antioxidant capacity, and therefore, the public cannot easily understand and compare the antioxidant content of various food plants (e.g., like the total hardness of potable water products, from which everybody understands the same meaning). In this regard, Apak et al. have recently developed the CUPRAC (cupric ion reducing antioxidant capacity) method of total antioxidant assay in foodstuffs [15] and human plasma [16] to overcome the aforementioned difficulties. Easily adaptable and low-cost methods equating the total antioxidant capacity of flavonoids in complex samples to the total reducing capability by flavonoids of simple chromogenic oxidants are continuously searched in antioxidant research to replace the high-cost and relatively instable radical chromogen reagents like ABTS and DPPH.

Nettle: *Urtica dioica* L. has become a source of folk medicine for the treatment of many diseases. The aqueous methanolic extract of nettle's roots has been used in clinics for the treatment of prostatic hyperplasia in Europe [17]. The seeds and the aqueous extract of the aerial parts of *U. dioica* L. have been occasionally used as a herbal medicine by cancer patients in Turkey [17]. The leaf is used as a diuretic, for arthritis, prostatitis, rheumatism, rheumatoid arthritis, high blood pressure and allergic rhinitis [18].

In the present study, a simple and inexpensive spectrophotometric method was developed for the determination of total antioxidant capacity of simple antioxidant compounds, their synthetic mixtures, and plant extracts. This method is based on the oxidation of antioxidant compounds with Ce(IV) sulfate at room temperature under controlled conditions of reagent concentration and pH such that only true antioxidants and not other organic compounds would be oxidized, and the absorbance of unreacted Ce(IV) is measured at 320 nm. The developed procedure was successfully applied to the assay of total antioxidant capacity due to simple compounds such as trolox, quercetin, gallic acid, ascorbic acid, catechin, rutin, naringin, naringenin, caffeic acid, chlorogenic acid, ferulic acid, and *p*-coumaric acid, and due to phenolic antioxidants in the arieal parts of *U. Dioica* L., a real sample. Plant selection was made in respect to high antioxidant content, and extraction was made with water since the efficiency of water extraction of nettle was shown to be significantly higher than that of 70% ethanol and pure methanol [19]. In accord with Wagner's work on water extraction of biologically active compounds from *U. dioica* [20], Gulcin et al. extracted the air-dried plant with water to demonstrate the antioxidant, antimicrobial, and analgesic activities of nettle [21]. The total antioxidant capacity and reducing phenolics content of the test samples were recorded as trolox-, gallic acid-, and quercetin-equivalents. The obtained results of antioxidant assay were correlated to those obtained by reference methods such as ABTS [7,22] and CUPRAC [15,16].

2. Materials and methods

2.1. Chemicals, herbal samples, and instrumentation

Quercetin dihydrate (abbreviated as QR) and neocuproine (2,9-dimethyl-1,10-phenanthroline), were supplied from Sigma Chemical Co., trolox (6-hydroxy-2,5,7,8-tetramethylchroman-2-carboxylic acid, abbreviated as TR) from Aldrich Chemicals Co., ABTS (2,2′-azinobis(3-ethylbenzothiazoline-6-sulfonic acid) diammonium salt) radical reagent from Fluka (kept at +4 °C); ethyl alcohol (containing 96% EtOH) from Riedel;

Ce(IV) sulfate tetrahydrate, Ce(III) nitrate hexahydrate, sulfuric acid (mass percentage: 98%), potassium dichromate, iodine, KI, starch, ammonium acetate, copper(II) chloride, and the rest of the chemicals including individual antioxidants (gallic acid, ascorbic acid, rutin, catechin, naringin, naringenin, caffeic acid, chlorogenic acid, ferulic acid, and *p*-coumaric acid) were purchased from E. Merck. Herbs used in the preparation of 'herbal tea' infusions (common sage: *salvia officinalis*, green tea: *camellia sinensis*, sweet basil: *ocimum basilicum*, and thyme: *thymus vulgaris*) were donated by Malatya Pazari, Istanbul. Nettle: *U. dioica* L. was collected from various parts of the Black Sea Coast of Turkey, and dried accordingly.

A cerium(IV) sulfate solution containing 2×10^{-3} M Ce(IV) was prepared by dissolving 0.0809 g $Ce(SO_4)_2{\cdot}4H_2O$ in 25 mL distilled water, adding 17 mL concentrated H_2SO_4, and thoroughly mixing by the aid of a magnetic stirrer until total dissolution at room temperature. This solution was totally transfered to a 100 mL-flask, and diluted to the mark with distilled water. The Ce(IV) stock solution was standardized iodometrically by adding excess KI, and titrating the liberated iodine (triiodide complex) with a standard solution of sodium thiosulfate (which was previously standardized against potassium dichromate) using starch as indicator.

All absorbance measurements were made at the prespecified wavelength of the selected spectrophotometric method using a Philips 3700 UV–vis spectrophotometer using a pair of matched quartz cuvettes of 1-cm thickness (light path). All fluorophotometric measurements were carried out with a Perkin-Elmer 204 fluorescence spectrophotometer equipped with a 150 W xenon arc lamp.

2.2. Plant material and extraction

The herbal samples (weighing 1.50 g) wrapped in a purse of standard membrane filter material (inert polymeric material) were dipped into and pulled out of beakers containing 250 mL of freshly boiled water for the first 2 min, and let to steep for the remaining 3 min in the covered beakers (total steeping time was 5 min). The purses containing extracted herbal samples were removed, and the partly turbid solutions were filtered through a black band Whatman quantitative filter paper after cooling to room temperature. The clear extract was properly diluted for cerium(IV), CUPRAC and ABTS assays of total antioxidant capacity. All infusions were analyzed as fresh as possible for reliability of the results; however, the assay results did not change even after 48 h storage of the tea extracts at +4 °C. For the purpose of comparison of extraction efficiencies, dried nettle was also extracted with pure methanol and 1:1 (v/v) $MeOH + H_2O$ mixture.

The dried nettle sample (weighing 1.00 g) was pounded into small parts with a porcelain mortar. The dried powdered aerial parts of the plants were extracted with boiling distilled water and were mixed with magnetic stirrer for 15 min. The extract was filtered through a Whatman filter paper into a 25 mL-flask, and diluted to the mark with distilled water. The aqueous extract of nettle was prepared just before the experiments so as to prevent any undesired degradation reactions.

2.3. Recommended spectrophotometric total antioxidant assay based on Ce(IV) oxidation

One milliliter of 2.0×10^{-3} M Ce(IV) solution was added to 1 mL of quercetin solution of approximate concentration 1.0×10^{-5} M, and the mixture was diluted to 10 mL with distilled water. After shaking for a few minutes, the solution was let to stand for 30 min at room temperature. The absorbance of the reaction mixture was measured at 320 nm against a blank composed of distilled water. Similarly, 1 mL aqueous extract of nettle was reacted with 1.0 mL of 2.0×10^{-3} M Ce(IV) solution, and diluted to 10 mL with water for the antioxidant assay due to phenolics content as described above. The difference in absorption (ΔA) arising from Ce(IV) between the blank (containing the same amount of Ce(IV)) and phenolics—reacted solutions was recorded. Since the difference in absorbances of reagent and sample solutions (ΔA) is measured, a slight initial absorbance of the sample at 320 nm could be tolerated as long as the Ce(IV)-oxidized products did not strongly absorb at the same wavelength. Dilution of sample or spectrophotometric titration (as described in Section 3.4.) is recommended for plant extracts of initial absorbance: $A_{320} \geq 0.2$ absorbance units. The most precise results of antioxidant capacity measurements via Ce(IV) reducing power were obtained for an absorbance difference (ΔA) range of 0.2–0.8. A small absorbance correction for the reagent blank may be necessary when the quercetin equivalent concentration of the sample exceeded 1.0×10^{-5} M.

2.4. ABTS spectrophotometric assay of total antioxidant capacity

An ABTS chromogenic radical reagent solution at 7 mM concentration was prepared in water. To this solution was added $K_2S_2O_8$ (as an oxidant for conversion of ABTS into a radical cation) to yield a final persulfate concentration of 2.45 mM. The colour of the resulting solution was blue-green. This radical solution was kept in a stoppered flask in the dark at room temperature for 12–16 h before use in actual measurements. The kept solution was diluted with 96% ethanol at a ratio of 1:10. The absorbance of the 1:10 diluted $ABTS^{\bullet+}$ radical cation solution was 1.28 ± 0.04 at 734 nm. To (x) mL of the sample solution (herbal extract) were added 1 mL of final $ABTS^{\bullet+}$ solution, and $(4 - x)$ mL 96% EtOH, and the change of absorbance during 6 min was recorded (usually the absorbance decrease at the sixth minute was used for calculations).

2.5. CUPRAC spectrophotometric assay of total antioxidant capacity

To a test tube were added 1 mL of $CuCl_2$ solution (1.0×10^{-2} M), 1 mL of neocuproine alcoholic solution (7.5×10^{-3} M), and 1 mL NH_4Ac buffer solution, and mixed; (x) mL of herbal extract followed by $(1.1 - x)$ mL of water were added (total volume = 4.1 mL), and mixed well. Absorbance against a reagent blank was measured at 450 nm after 30 min. Since the molar absorptivity of trolox in the CUPRAC method is $\varepsilon = 1.67 \times 10^4$ L mol^{-1} cm^{-1}, and the calibration curve for

trolox is a line passing through the origin, the trolox equivalent molar concentration of the herbal extract sample in final solution may be found by dividing the observed absorbance to the ε for trolox. The trolox equivalent antioxidant capacity may be traced back to the original extract considering all dilutions, and proportionated to the initial mass of herbal material taken to find a capacity in the units of mmol TR/g dry matter.

2.6. Calculation of total antioxidant capacity of herbal material

The molar absorptivity of trolox in the above reference methods were as follows: $\varepsilon_{TR} = 1.67 \times 10^4$ L mol^{-1} cm^{-1} (CUPRAC method); $\varepsilon_{TR} = 2.6 \times 10^4$ L mol^{-1} cm^{-1} (ABTS method).

If a herbal infusion (initial volume = V_{cup}) prepared from (m) grams of dried plant was diluted (r) times prior to analysis, and a sample volume of V_s was taken for analysis from the diluted extract, and colour development (after addition of reagents) was made in a final volume of (V_f) to yield an absorbance of (A_f), then the trolox equivalent antioxidant capacity of the herb (in mmol TR per gram of dried plant, or simply mmol TR/g) was found using the equation:

$$\text{Capacity(in mmol TR/g)} = (A_f/\varepsilon_{TR})(V_f/V_s)r(V_{cup}/m)$$

2.7. Optimizing recommended methods

For optimizing the maximum absorption wavelength of Ce(IV) as a function of sulfuric acid concentration (so that this wavelength would not shift with pH), absorption spectra of 2×10^{-4} M Ce(IV) solutions containing a varying final hydrogen ion concentration of 0.008–0.914 M were recorded against water in the range 200–400 nm. The spectral change of Ce(IV) as a result of reaction with quercetin was observed by adding quercetin to 2 μmol Ce(IV) solution containing an optimal sulfuric acid concentration of 0.3 M such that the final quercetin concentration in the mixture would be between 4×10^{-6} and 1×10^{-5} M, diluting to 10 mL total volume with water, letting to stand at room temperature for 30 min, and recording absorption spectra against water between 200 and 400 nm. Any possible interference due to antioxidant compounds themselves at the optimal wavelength of 320 nm (selected for determination of remaining Ce(IV) in solution) was checked by recording the spectra of trolox, ascorbic acid, catechin, gallic acid, quercetin, naringin, and naringenin in the same wavelength range at the concentration order of 10^{-5} M.

Since the proposed method for indirect antioxidant capacity assay is based on Ce(IV) determinations after reaction with antioxidants, the calibration curve of cerium was drawn at 0.3 M sulfuric acid concentration and 320 nm wavelength in the concentration range of 4.0×10^{-5} to 5.0×10^{-4} M of Ce(IV). The calibration curve for quercetin was constructed by adding increasing amounts of quercetin to 1 mL of 2.0×10^{-3} M Ce(IV) dissolved in 0.3 M sulfuric acid, and measuring the absorbances of the diluted (total volume = 10 mL) solutions after 30 min such that the curve would exhibit a negative slope for quercetin concentration.

For determining the stoichiometry of the redox reaction between Ce(IV) and flavonoids, spectrophotometric titration was carried out. To a series of 10 mL-flasks, 1 mL aliquots of 2.0×10^{-3} M Ce(IV) dissolved in 0.3 M sulfuric acid, followed by varying amounts of quercetin were added such that the final (analytical) concentration of quercetin in the mixtures would lie in the range 2.12×10^{-6} to 8.48×10^{-6} M. After dilution with water to 10 mL, absorbances at 320 nm were read after 30 min against water. The absorbance readings were plotted against quercetin concentrations. Spectrophotometric titrations were repeated for fixed initial concentrations of Ce(IV) of 5×10^{-4}, 3.3×10^{-4}, 2.55×10^{-4}, and 1.85×10^{-4} M. The intersection point of the sloped arms of these plots with the horizontal axis yielded the quercetin concentrations stoichiometrically equivalent to the initial Ce(IV). Spectrophotometric titrations were further extended to ascorbic acid and trolox by plotting absorbance *versus* [Ce(IV)]/[antioxidant] molar ratio.

To check whether the Ce(IV) reagent – under the given reaction conditions – attacks aromatic double bonds and side chains of substances which are not listed under the common name of 'antioxidants' acting as electron-transfer agents, varying amounts of benzoic acid and acetyl salicylic acid were added to a fixed amount of acidic Ce(IV), and any absorbance change was noted. For this purpose, 0.1–1.0 mL of 3.35×10^{-4} M acetyl salicylic acid and 1.0–2.5 mL of 4.72×10^{-3} M benzoic acid were added separately to 1.5 mL of 2×10^{-3} M Ce(IV) solution prepared in 0.3 M sulfuric acid; the mixtures were diluted to 10 mL with water, well mixed, and absorbances at 320 nm were recorded after 30 min. Similar measurements were made with glucose, saccarose, and citric acid to test reagent selectivity.

The validity of the proposed method for evaluating synthetic ternary mixtures of antioxidants (containing each at μM levels) was tested by maintaining a final Ce(IV) concentration of 2.0×10^{-4} M in ternary antioxidant mixtures, and measuring the absorbance (A_{found}) after the reaction was completed. Since the molar absorptivity (ε) of each individual antioxidant compound in the proposed method is known, the expected absorbance ($A_{expected}$) of the ternary mixture can be found by applying the principle of the additivity of absorbances (i.e., the (εC) product is additive) according to Beer's law:

$$A_{expected} = \varepsilon_1 C_1 + \varepsilon_2 C_2 + \varepsilon_3 C_3,$$

$$A_{found} = A_{Ce(IV)} - A_{measured}$$

and the $A_{expected}$ values were compared with A_{found}.

The possibility of interaction of a given flavonoid (quercetin) with the antioxidants of a real complex sample (nettle extract) to produce apparent deviations from Beer's law was tested by redrawing the calibration curve of quercetin (for final concentrations varying between 5.08×10^{-6} and 1.97×10^{-5} M) in a solution containing 5.18×10^{-4} M Ce(IV) in 0.3 M sulfuric acid and 0.1 mL of nettle extract (prepared from 1 g nettle in 25 mL water), and comparing the slope of the line obtained (abs. *versus* quercetin concn.) with that of pure quercetin.

The quercetin-equivalent flavonoid content of nettle was found by spectrophotometric titration: varying volumes (1.2–4.0 mL) of the nettle extract (prepared from 1 g dried nettle

in 250 mL water) were added to a solution containing a fixed Ce(IV) concentration of 4×10^{-4} M using the standard procedure, and that volume of nettle extract equivalent to initial cerium was recorded (i.e., from the intersection point of the two arms of absorbance *versus* extract volume curve). The flavonoid content was given as:

flavonoid content(mass%)

= (quercetin equivalent concn. of test sample(g/L)

×total volume of water extract(L)/sample weight(g))

×100

3. Results and discussion

3.1. Spectrophotometric method development

The developed indirect spectrophotometric method of total antioxidant capacity due to flavonoids is based on the redox reaction between flavonoids and Ce(IV) at room temperature, and the concentration of remaining Ce(IV) is measured as an indication of initial antioxidant concentration. Therefore the maximum absorption wavelength selection for Ce(IV) is important, and solution acidity should be properly adjusted such that this wavelength should not shift with pH. Considering the hydrolytic equilibria of Ce(IV);

$$Ce^{4+} + H_2O \rightleftarrows Ce(OH)^{3+} + H^+, \quad K_1 = 0.2$$

$$Ce(OH)^{3+} + H_2O \rightleftarrows Ce(OH)_2{}^{2+} + H^+, \quad K_2 = 0.16$$

Table 1 shows that the maximal absorption wavelength for Ce(IV) remains unchanged at 320 nm when the relative abundance of Ce(IV) cation as the parent diprotic acid, i.e., $\alpha_{Ce(IV)}$, reaches 0.5. This requires that the final sulfuric acid molarity of the analyte (antioxidant) solutions be adjusted to 0.3 M. Lower acidities cause a wavelength shift due to the relative abundance of mono- and di-hydroxo species of cerium(IV) as the conjugate bases. Thus optimal acidity and measurement wavelength were kept at these values throughout the experiments.

Table 1
The effect of H^+ ion molarity on the maximum absorption wavelength and relative abundance of Ce(IV)

$[H^+]$	Wavelength, λ_{max} (nm)	Absorbance	$\alpha_{Ce(IV)}$
0.008	274.0	0.750	0.020
0.020	296.0	0.757	0.011
0.031	304.0	0.769	0.024
0.052	307.0	0.784	0.060
0.073	311.0	0.808	0.103
0.093	312.5	0.845	0.146
0.114	314.0	0.873	0.192
0.214	318.5	0.987	0.380
0.314	320.0	0.996	0.510
0.414	320.1	1.001	0.600
0.514	319.9	1.027	0.662
0.714	320.0	1.021	0.745
0.914	319.9	1.012	0.800

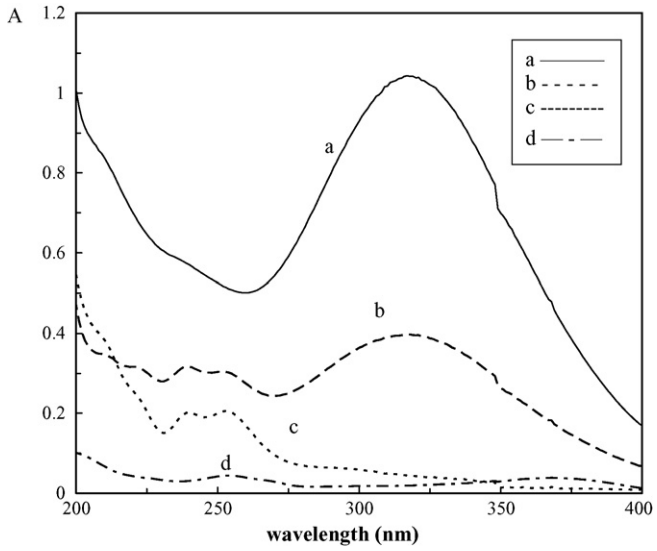


Fig. 1. Absorption spectra of Ce(IV), quercetin, and binary mixtures of Ce(IV) + quercetin against water; (a) —, 2×10^{-4} M Ce(IV); (b) – – –, 2×10^{-4} M Ce(IV) + 4×10^{-6} M quercetin; (c) - - - -, 2×10^{-4} M Ce(IV) + 1×10^{-5} M quercetin; (d) – – –, 1×10^{-5} M quercetin.

The spectra of 2×10^{-4} M Ce(IV) alone and of mixtures composed of Ce(IV) + varying concentrations of quercetin in 0.3 M sulfuric acid solution are shown in Fig. 1. The intensity of the 320 nm-band due to Ce(IV) decreases proportionally with increasing quercetin concentrations as a result of the redox reaction involved, and new bands between 230 and 260 nm appear as a result of Ce(III) formation. It may be seen from Fig. 1 that at a quercetin concentration of 1×10^{-5} M (i.e., 19.6-fold cerium), the 320 nm-band due to cerium(IV) completely disappears due to the favourable stoichiometry of the redox components (i.e., quercetin is completely oxidized with Ce(IV) within the 30 min-reaction time), and the formed Ce(III) neither absorbs at this wavelength nor gives a complex with the oxidation product of quercetin. Thus the 320 nm-band may be safely used for quercetin quantitation. Either quercetin (Fig. 1) or other selected antioxidants (trolox, ascorbic asid, catechin, and gallic acid) do not appreciably absorb at this wavelength (figure not shown) at concentrations $\leq 1 \times 10^{-5}$ M, but a small correction for self absorption may be necessary for the flavonoids of quercetin, naringin, and naringenin, and phenolic acids of caffeic, ferulic, chlorogenic and *p*-coumaric acids at higher concentrations when the reference cell in absorbance measurements is water instead of a reagent blank. However it is safe to use distilled water as blank in the optimal concentration range, and therefore, higher concentrations of phenolic antioxidants may be diluted. A sulfuric acid concentration of 0.3 M and a measurement wavelength of 320 nm (against water) were kept throughout.

3.2. Calibration lines and reaction stoichiometry

The equation for the calibration line of Ce(IV) in the cerium concentration range 4.0×10^{-5} to 5.0×10^{-4} M was:

$$A_{320} = 5.21 \times 10^3 C_{Ce(IV)} - 0.044, \quad (R^2 = 0.9981)$$

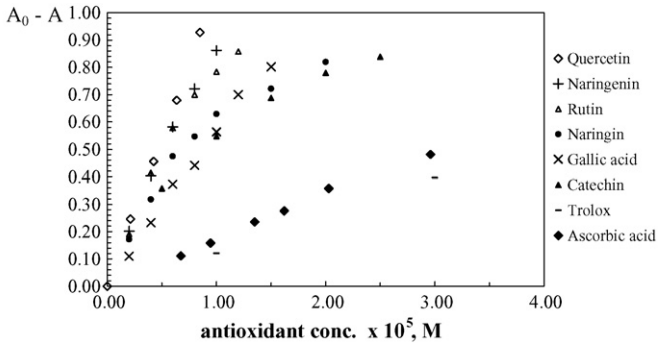


Fig. 2. Calibration curves of antioxidants with the indirect Ce(IV)-based method; $\Delta A = (A_0 - A)$ vs. antioxidant molar concentration.

yielding a molar absorptivity of 5.21×10^3 L mol^{-1} cm^{-1} for cerium. Flavonoids and phenolics were quantified indirectly through their ability to reduce a fixed initial concentration of Ce(IV). In indirect spectrophotometric determinations, the equation for the calibration line of quercetin (QR) in the concentration range $\approx(0.2–0.9) \times 10^{-5}$ M was:

$$A_{320} = 0.985 - 1.035 \times 10^5 C_{QR}, \quad (R^2 = 0.9987);$$

and for gallic acid (GA) in the concentration range $\approx(0.2–1.5) \times 10^{-5}$ M was:

$$A_{320} = 0.987 - 5.48 \times 10^4 C_{GA}, \quad (R^2 = 0.994)$$

yielding a molar absorptivity of 1.035×10^5 L mol^{-1} cm^{-1} for quercetin and 5.48×10^4 L mol^{-1} cm^{-1} for gallic acid. Naturally the equations for antioxidants have negative slopes, because measurements were made in solutions containing an initial fixed (2×10^{-4} M) concentration of Ce(IV). If decrease in absorbance (ΔA) was plotted against quercetin concentration, then the calibration line would have a positive slope (see Fig. 2). The ideal linear ranges of antioxidants used for constructing the calibration curves are depicted in Table 2.

The aqueous solubility of quercetin 4′-ß-glycoside was determined to be >300 μM, or 3.0×10^{-4} M in the literature [23]. The highest concentration of quercetin tested in our work was 1.0×10^{-5} M, without posing any problem of aqueous solubility.

Table 2
The ideal linear ranges of antioxidant compounds used for constructing the calibration curves ($r \geq 0.999$)

Antioxidant compound	Concentration range ($\times 10^5$ M) for ideal linearity
Quercetin	0.21–0.85
Rutin	0.20–1.20
Catechin	0.50–2.50
Trolox	1.00–7.00
Ascorbic acid	0.68–6.80
Gallic acid	0.20–1.50
Naringenin	0.20–1.00
Naringin	0.20–1.00
Caffeic acid	0.50–2.50
Ferulic acid	0.50–2.50

It should be noted here that total phenolics assay is also possible simply by measuring the fluorescence of the Ce(III) produced as a result of the redox reaction concerned. The fluorescent species have excitation and emission maxima at 260 and 360 nm, respectively. Quercetin solutions in the concentration range 2.61×10^{-6} and 2.61×10^{-5} M gave a roughly linear relationship of fluorescence *versus* concentration, where R^2 was 0.9989. However the aim of this work is to report the spectrophotometric and not the spectrofluorometric method, and therefore, fluorometric measurements were reported only as preliminary experiments.

The calibration lines of quercetin was redrawn for varying initial Ce(IV) concentrations of 5×10^{-4}, 3.3×10^{-4}, 2.55×10^{-4}, and 1.85×10^{-4} M, and the found slopes were averaged ($N = 5$) for reporting the mean molar absorptivity of $(1.033 \pm 0.010) \times 10^5$ for quercetin. This value, divided by the molar absorptivity for Ce(IV), yields a coefficient of 19.8, revealing the stoichiometric ratio of quercetin oxidation by tetravalent cerium. Here it was also shown that the molar absorptivity for quercetin in this indirect method is independent from the initial concentration of Ce(IV) taken for analysis. Spectrophotometric titration of quercetin, trolox, and ascorbic acid solutions (individually) with Ce(IV) (see Fig. 3A) yielded at the inflection points of these curves stoichiometric coefficients of 19.6, 2.5, and 2.9 for the mentioned antioxidant compounds, respec-

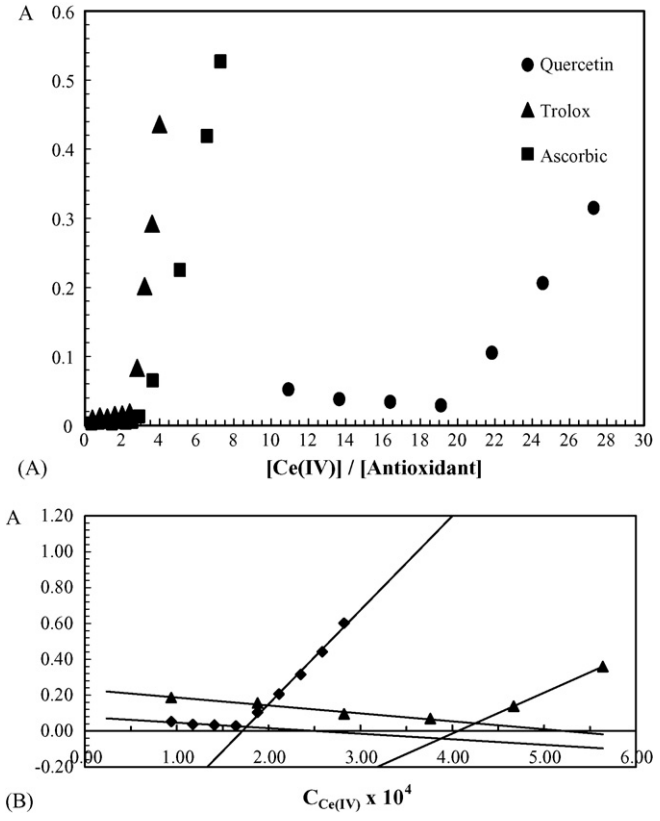


Fig. 3. (A) Spectrophotometric titration of (●) 8.61×10^{-6} M quercetin, (▲) 5.0×10^{-5} M trolox, (■) 2.75×10^{-5} M ascorbic acid solutions with standard Ce(IV) solution (blank: water); (B) spectrophotometric titration (absorbance vs. Ce(IV) molar concentration) of 8.61×10^{-6} M (■) and 2.15×10^{-5} M (▲) quercetin solutions with standard Ce(IV) solution (reference: water).

tively. The stoichiometric ratio of Ce(IV)–QR reaction was further confirmed from spectrophotometric titration data presented in Fig. 3B, where 4.2×10^{-4} M Ce(IV) corresponded to 2.15×10^{-5} M QR, or 1.70×10^{-4} M Ce(IV) corresponded to 8.61×10^{-6} M QR, yielding Ce(IV)/QR ratios of 19.5 and 19.7, respectively, for these two distinct concentration levels. The UV spectrum of an equivalent mixture of Ce(IV) + QR overlapped with that of pure Ce(III) at the same concentration (figure not shown). The production of Ce(III) from the redox reaction with QR was also confirmed by fluorescence spectroscopy (results not shown), because only Ce(III) but neither Ce(IV) nor QR showed a fluorescence under the experimental conditions. Thus the trolox-equivalent antioxidant capacities, or TEAC values – first introduced conceptionally by the ABTS/TEAC method of total antioxidant capacity assay [7] – of quercetin and ascorbic acid can be calculated with respect to the proposed method as approximately 8 and 1.1, respectively. The TEAC coefficient of a given antioxidant compound is defined as the mM trolox-equivalent concentration of 1 mM solution of the tested compound with respect to the selected assay, or simply as the ratio of the molar absorptivity of the tested compound to that of trolox [15], using the selected spectrophotometric method.

The calibration lines of selected antioxidants (i.e., trolox, ascorbic acid, gallic asid, catechin, rutin, naringin, naringenin, caffeic acid, chlorogenic acid, ferulic acid, and *p*-coumaric acid) with respect to the proposed method were drawn; the molar absorptivities and the corresponding TEAC coefficients were calculated, and depicted in Table 3. The proposed method generally performed well for trolox, ascorbic acid, gallic acid, and other phenolic (hydroxycinnamic) acids. The TEAC coefficients do not show high variations compared to those of reference methods except for rutin, quercetin, naringin, and naringenin (the developed method rated higher TEAC coefficients than other methods for the latter four compounds). It may be inferred from the experimental findings that quercetin oxidation probably proceeded further with Ce(IV) – compared to other redox-based assays – but the results were reproducible. Nevertheless, the high antioxidant capability of quercetin is an expected behaviour, because the antioxidant potency of flavonoids of similar conjugation level is roughly proportional to the total number of –OH groups, and is positively affected by the presence of *o*-dihydroxy moiety in the B-ring [12]. Quercetin, a flavonoid having all of these favourable properties as prerequisites for high antioxidant power, exhibited the highest capacity in the proposed method. Also the relatively high TEAC coefficients of naringin and naringenin obtained using the proposed method (see Table 3) may be attributed to the fact that naringin, the glycoside of naringenin, was probably both hydrolyzed (under the highly acidic conditions of the proposed method) to the aglycone, i.e., the –*O*-neohesperidase substituent on the aromatic ring was converted to –OH, and simultaneously oxidized by Ce(IV), thereby exerting full antioxidant power close to that of the aglycone, naringenin. Since the proposed method of this work makes use of acidic hydrolysis (analogic to enzymatic hydrolysis at physiological pH *in vivo*) and Ce(IV) oxidation of the formed polyphenol simultaneously, the flavonoid glycosides like naringin and rutin approach in trolox equivalent antioxidant capacity to naringenin and quercetin, respectively (see Table 3). It has been established that flavonoid glycosides may exert their full antioxidant power in the organism as a result of enzymatic hydrolysis to the corresponding aglycones (i.e., polyhydroxy phenolic compounds) for which newly introduced –OH groups contribute to antioxidant power [15]. The rutin/quercetin pair showed TEAC coefficients of 7.5/7.9 in the proposed method, while the naringin/naringenin pair exhibited TEAC values of 5.3/6.6. These values were never so close with ABTS/TEAC, CUPRAC or FRAP. Thus it may be considered as an advantage of the proposed method that the sugar bond is broken so that the parent flavonoid may exert full antioxidant potency, nearly approaching that of the corresponding aglycon. By making hydrolysis and oxidation reactions simultaneously feasible, the developed method may give a higher rating to flavonoid glycosides than other antioxidant assays. One of the authors had witnessed a similar (double-fold) increase in the antioxidant capacity of naringenin using the CUPRAC method [15], when a preliminary acidic hydrolysis was performed before oxidation with the copper(II)–neocuproine reagent.

Table 3
The molar absorptivities and TEAC coefficients of various antioxidant compounds with respect to the proposed method, in comparison to the findings of ABTS/TEAC and CUPRAC reference methods

Antioxidant compound	ε (L mol^{-1} cm^{-1})	TEAC coefficient		
		Proposed method	Reference methods	
		$\varepsilon_{Antioxidant}/\varepsilon_{Trolox}$	ABTS	CUPRAC
Trolox	1.31×10^4	–	–	
Quercetin	1.04×10^5	7.90	4.7	4.4
Rutin	8.94×10^4	7.50	2.4	(2.6)
Gallic acid	5.48×10^4	4.20	3.0	2.6
Ascorbic acid	1.42×10^4	1.08	1.0	1.0
Catechin	4.50×10^4	3.44	2.4	3.1
Naringenin	8.59×10^4	6.56	1.5	(2.3)
Naringin	6.97×10^4	5.32	0.2	0.2
Caffeic acid	2.55×10^4	1.94	1.4	2.9
Chlorogenic acid	3.12×10^4	2.38	1.2	2.5
Ferulic acid	3.54×10^4	2.70	2.1	1.2
p-Coumaric acid	2.94×10^4	2.22	1.8	0.6

Repeatability (as R.S.D.) was approximately 5% for hydroxycinnamic acids and 3% for other antioxidants. The values in parantheses in the CUPRAC column were obtained under incubation at 50 °C of samples with the CUPRAC reagent (Apak et al., 2004).

Linear correlation (for binary combinations of the findings of Ce(IV), ABTS, and CUPRAC methods) of TEAC coefficients of nine antioxidant compounds (excluding rutin and naringin, since they are not hydrolyzed and oxidized at the same time with reagents other than Ce(IV)), gave the following equations:

$$AC_{Ce(IV)} = 1.44AC_{ABTS} + 0.541, \quad (r = 0.731);$$

$$AC_{Ce(IV)} = 1.27AC_{CUPRAC} + 0.689, \quad (r = 0.666);$$

$AC_{ABTS} = 0.645\ AC_{CUPRAC} + 0.645$ ($r = 0.667$) (AC_i: total antioxidant capacity found with method *i*). In terms of TEAC coefficients of antioxidant compounds found with electron transfer-based assays [14], the developed Ce(IV)-based method

is comparable to ABTS and CUPRAC in the same manner as CUPRAC is to ABTS.

3.3. Interferences, analytical performance, and applicability to synthetic and real mixtures

Since the developed method was based on Ce(IV) oxidation of antioxidants, common anions and cations did not interfere with the proposed method except reducing agents capable of reacting with tetravalent cerium. Also transition and heavy metal cations like Fe(III) and Al(III) capable of forming complexes with flavonoids (via Ar–OH and Ar=O groups) did not interfere, because the redox reaction of flavonoids with Ce(IV) had a much higher equilibrium constant than those of simple or chelating complexation reactions with donor oxygen atoms. Since cerium(IV) is a strong oxidant, it may be speculated whether such a powerful oxidizing agent may oxidize compounds other than those listed under the common name of 'antioxidants'. To test this speculation, benzoic acid up to 10^{-3} M and acetylsalicylic acid up to 0.5×10^{-4} M concentrations were added separately to 3×10^{-4} M Ce(IV) solutions, but the observed absorbances with the proposed method remained at 1.55 ± 0.05, showing that the cerium reagent at the optimized concentration and acidity levels did not attack benzoic and acetyl salicylic acids, which are not true reducing agents in the 0.2–0.6 V standard potential range of interest in physiological reactions with antioxidants. The results obtained with these and other organic compounds not categorized under the title of 'antioxidants' were listed in Table 4, as original Ce(IV) recovery (%) *versus* molar concentration of possible interferent. Consequently, it was found that simple sugars widely found in food plants, e.g., glucose and saccarose, remained intact and did not appreciably change the recovery of Ce(IV) in the recommended method (with a maximum error of 3.5% in Ce(IV) recovery), similar to the behaviour of benzoic or acetylsalicylic acid. Citric acid, used as a food preservative, affected the recovery, and the critical citric acid concentration causing 10% relative error was 2.0×10^{-6} M. Here, it should be indicated that, given sufficient time, all Fe(III)-based assays including FRAP are affected by citric acid due to the favourable redox potential [24]. Actually, very few antioxidant assays like CUPRAC are not interfered by citric acid [15]. Therefore, the proposed method is considerably selective toward true antioxidants.

A study of theoretical redox chemistry of Ce(IV) shows that Ce(IV) sulfate solutions are remarkably stable over prolonged periods (may even be boiled for a short time without appreciable change in concentration). A solution of Ce(IV) sulfate surpasses a permanganate(VI) solution in stability [25]. Formal potential measurements show that the redox potential of the Ce(IV)–Ce(III) system is greatly dependent upon the nature and concentration of mineral acid present, and takes the smallest value in sulfuric acid due to the complexation effect of SO_4^{2-} on Ce(IV) [26]. Vladescu et al. [27] measured the Ce(IV)–Ce(III) conditional potential for $(0.5–1.0) \times 10^{-2}$ M Ce(IV)–sulfate solutions in (0.2–1.0) M H_2SO_4 (conditions somewhat similar to our experimental values) as $E^0 = 1.175 \pm 0.175$ V, much less than the standard potential of 1.87 V in 8 M $HClO_4$. Czappa [26] showed that the presence of complexing inorganic anions like sulfate may reduce the complexing ability of Ce(IV) with organic substrates, and may therefore retard the oxidation of organic compounds by Ce(IV), since Ce(IV)–organic substrate complexation is a prerequisite of fast inner-sphere electron transfer [28]. Therefore we assume that in H_2SO_4 solutions of low acidity, both hydrolysis and sulfato-complexes of Ce(IV) may coexist, decreasing the effective concentration of Ce^{4+}, and therefore the redox potential and oxidation rate of tetravalent cerium. Thus, due to unfavourable thermodynamics and kinetics for dilute Ce(IV) sulfate solutions of moderate acidity, the

Table 4
Study of potential interferents, i.e., organic substances not listed under the common name of antioxidants, depicted as Ce(IV) recovery (%) vs. interferent concentration (M)

[Benzoic acid] × 10^4	Recovery (%)
0	100
1.43	99.3
2.86	98.6
4.72	98.3
7.08	97.3
9.44	96.8

[Glucose] × 10^5	Recovery (%)
0	100
2	100
5	100
7	100
10	99.5
15	98

[Acetylsalicylic acid] × 10^6	Recovery (%)
0	100
3.35	99.1
10	98.7
16.8	98.2
23.4	97.5
33.5	96.6

[Citric acid] × 10^6	Recovery (%)
0	100
0.05	98.9
0.07	97.6
0.2	94
0.5	93
0.7	94
1	94
2	91
5	88
7	84
10	84
15	76

[Saccarose] × 10^5	Recovery (%)
0	100
2	97
5	95.4
7	95
10	97
15	96.5

Table 5
Evaluation of synthetic mixtures of antioxidant compounds with the proposed method

Composition of mixture	$A_{expected}$	A_{found}	Agreement (%)
2.50×10^{-3} mM quercetin 2.50×10^{-3} mM trolox 2.68×10^{-3} mM ascorbic acid	0.331	0.359	+8.5
4.0×10^{-3} mM quercetin 4.0×10^{-3} mM ferulic acid 4.28×10^{-3} mM ascorbic acid	0.618	0.584	−5.5
2.4×10^{-3} mM gallic acid 4.0×10^{-3} mM chlorogenic acid 4.0×10^{-3} mM ascorbic acid	0.314	0.311	−1.0
2.0×10^{-3} mM trolox 1.2×10^{-3} mM gallic acid 2.0×10^{-3} mM ascorbic acid	0.121	0.109	−9.9
2.0×10^{-3} mM quercetin 1.2×10^{-3} mM gallic acid 1.0×10^{-3} mM caffeic acid	0.300	0.285	−5.0

Ce(IV) oxidizing reagent of the proposed assay selectively oxidizes antioxidant compounds but not all organic substrates. This may be closely related to the redox chemistry of biologically important antioxidants mostly in the potential range of 0.2–0.6 V.

By using a Ce(IV) initial concentration of 2×10^{-4} M, the standard deviation in determining 4.25×10^{-6} M quercetin with the proposed method was 1.4×10^{-8} M, RSD being 0.33% ($N = 10$). The LOD (defined by IUPAC as 'three times the standard deviation of a blank divided by the molar absorptivity, or the slope of the calibration line') and LOQ in quercetin determination were 0.2 and 0.7 μM, respectively.

In evaluation of synthetic ternary mixtures of antioxidants with the aid of the proposed method, the $A_{expected}$ values were compared with A_{found} (see Section 2), and the results are depicted in Table 5. The results were generally additive within at most ± 10% agreement (of expected and found absorbances), meaning that the total antioxidant capacity of a synthetic mixture was equal to the sum of its constituents. Had there been an apparent deviation from Beer's law in the measured absorbances of antioxidant compounds with respect to the developed spectrophotometric method, the principle of additivity of absorbances would not have been valid. Likewise, the same behaviour was observed in a real mixture such as nettle extract (see Fig. 4). The calibration lines (i.e., abs. *versus* concn.) of quercetin drawn in water and in nettle extract were parallel, meaning that the various antioxidants in nettle extract did not interact with quercetin so as to quench or intensify the absorbances expected from quercetin, and therefore there were no chemical deviations from Beer's law, as demonstrated earlier for other systems of total antioxidant assay [11,15]. Ascorbic acid and trolox exhibited the same behaviour in nettle extract (figures not shown).

As regards the practisability of the reagent to antioxidant media other than food extracts, Ce(IV), being a water-soluble reagent, would be expected to function for hydrophilic plasma antioxidants. As a comparison, the CUPRAC reagent may quantitate lipophilic antioxidants only in hexane-dichloromethane extract [16]. The reduction product of the CUPRAC reagent – bis(neocuproine) copper(I) chloride – is a chelate, and therefore is soluble in dichloromethane, but the Ce(IV) reagent is not (because of the hydration energy barrier). Thus the developed Ce(IV)-based assay is expected to be useful for hydrophilic but not lipophilic plasma antioxidants.

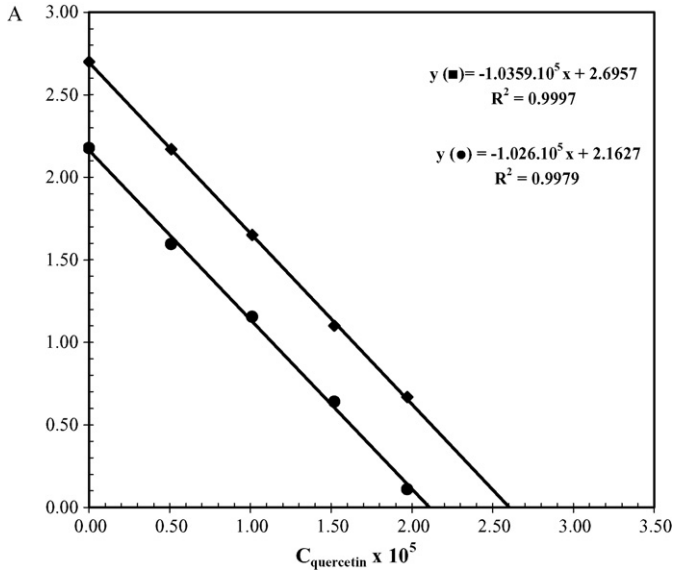


Fig. 4. The calibration curve of quercetin alone and in nettle extract; (A) ■, initial solution: 5.3×10^{-4} M Ce(IV) + quercetin solutions of varying concentration (5.08×10^{-6} to 1.971×10^{-5} M). (B) ●, initial solution: 5.3×10^{-4} M Ce(IV) + 0.1 mL nettle extract (prepared from 1 g plant material in 25 mL water) + Quercetin solutions of varying concentration (5.08×10^{-6} to 1.971×10^{-5} M).

3.4. Analysis of herbal samples, precision, and comparison of results

Spectrophotometric titration of 4.0×10^{-4} M Ce(IV) solution with varying volumes (1.2–4.0 mL) of nettle extract (prepared from 1 g plant material in 250 mL water) gave the curve in Fig. 5, from which 10 mL of 4.0×10^{-4} M Ce(IV) was shown to be equivalent to 2.7 mL of the extract. In spectropho-

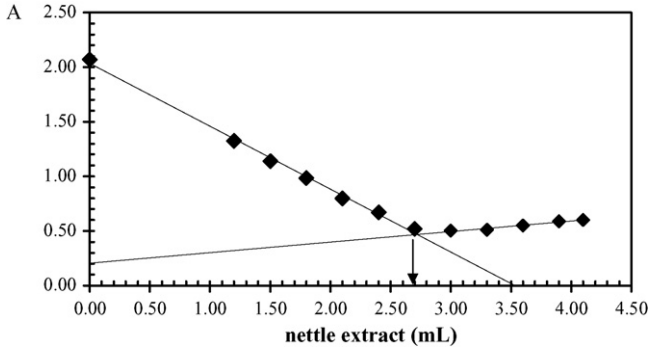


Fig. 5. Determination of quercetin-equivalent flavonoid concentration of nettle extract (prepared from 1 g plant material in 250 mL water) by spectrophotometric titration of 4.0×10^{-4} M initial Ce(IV) solution with varying volumes of the extract.

tometric titration, an initial fixed Ce(IV) solution – in excess of the analyte – is titrated with the plant extract (absorbance recorded as a function of titrant volume), and the steadily decreasing left arm of the curve (due to decreasing Ce(IV)) is intersected by the monotonously increasing right arm (due to A_{320} of the plant extract) at the equivalence point, from which the trolox or gallic acid equivalent antioxidant capacity of the extract can be calculated. Since the stoichiometric coefficient for Ce(IV)/quercetin redox reaction is 20:1, nettle was calculated to contain 0.018 ± 0.001 mmol quercetin-equivalent (or 0.033 ± 0.001 mmol gallic acid-equivalent) antioxidant capacity per gram. In accord with the recommendation of Osinska et al. (2003), the extraction efficiency with hot water was highest, e.g., phenolic antioxidants content of nettle, as expressed in the units of mmol gallic acid (GA) per gram dry plant, were found as 0.033, 0.019, and 0.007 mmol GA/g for water, 1:1 water-MeOH, and pure MeOH extractions, respectively. Water was the most successful solvent of antioxidant extraction specifically for nettle probably because of the composition of phenolics in the plant, e.g., phenolic acids of caffeic acid, chlorogenic acid, *p*-coumaric acid, hydroxybenzoic and elagic acids might have played a higher role in the observed antioxidant capacity than flavonoids of kaemferol-3-*O*-rutinoside, isorhammetin-3-*O*-glycoside, and quercetin-3-*O*-rutinoside [29].

The findings of the developed method were compared to those of ABTS/persulfate reference assay applied on nettle extract (see Table 6; five different runs). The *F*-test confirmed that the 'null hypothesis' was valid at 95% confidence level, and that there were no significant differences between the precisions (variances) of the two methods while the mean antioxidant capacities were similar. The trolox-equivalent antioxidant capacities of four herbal samples (basil, thyme, green tea, and sage) measured on five different runs with the proposed method were comparable to those found by ABTS/persulfate and CUPRAC reference methods (Table 7). It is natural that the results obtained with a variety of electron-transfer based antioxidant assays would give comparable but not identical results for real samples due to the diversity of reaction conditions (pH, redox potential, etc.) of these assays [14].

Table 6
Comparison of the findings of the proposed method and ABTS/persulfate radical assay (sample: nettle extract)

Sample run	Proposed method (mmol quercetin/g nettle)	ABTS/persulfate method (mmol quercetin/g nettle)
X_1	0.0165	0.0150
X_2	0.0158	0.0154
X_3	0.0160	0.0149
X_4	0.0162	0.0155
X_5	0.0185	0.0161
Mean x	0.0166	0.0154
Standard deviation (s)	0.0011	0.0005
Relative standard deviation (%)	6.62	3.24
Variance (s^2)	1.21×10^{-6}	2.5×10^{-7}
F-test	$F_e < F_t(S_1^2/S_2^2 = F_e) \rightarrow 4.84 < 6.39$	

The mean total antioxidant capacity of nettle was 0.017 mmol QR/g, or 0.032 mmol GA/g.

Table 7
Comparison of results obtained with the proposed method with the findings of ABTS/persulfate and CUPRAC assays for four herbal samples

Herbal sample	Total antioxidant content (mmol trolox equivalent/g plant material)		
	Developed method	$ABTS^+$/persulfate	CUPRAC
Sweet basil	1.05	0.77	1.18
Thyme	0.94	0.52	0.54
Green tea	0.88	0.76	1.07
Sage	0.09[a]	0.41[b]	0.56[b]

[a] Wet sample.
[b] Dry sample (dried sample approximately reaches 1/5 of its original weight).

4. Conclusions

This work reports the development a simple, low-cost, sensitive, and diversely applicable indirect spectrophotometric method for the determination of total antioxidant capacity due to total phenolics content of several plants. The method is based on the oxidation of phenolics with tetravalent cerium at room temperature. The Ce(IV) reducing capacity of the sample is measured under carefully adjusted conditions of oxidant concentration and pH such that only antioxidants and not other organic compounds (such as benzoic acid, acetyl salicylic acid, and simple sugars, which do not act as reducing agents) would be oxidized. The advantage of the method is its simplicity, and applicability to conventional laboratories (without high-level instrumentation), added to the possibility of measuring the fluorescence of the Ce(III) produced as a result of the redox reaction concerned, besides absorptimetric measurement of the remaining Ce(IV). The findings of the proposed method were compared to those of ABTS/persulfate assay, and applied to total antioxidant capacity assays of a number of herbal extracts. The precisions of the Ce(IV) and ABTS methods were alike, and the TEAC coefficients of antioxidants found with the proposed method correlated to those of ABTS and CUPRAC. Flavonoid glycosides were simultaneously hydrolyzed (to the corresponding aglycones) and oxidized with the acidic Ce(IV) reagent, exerting full antioxidant power in the assay such that the observed antioxidant capacity would be roughly proportional to the number of hydroxyl groups in the aglycone molecule. In principle, plant pigments absorbing at 320 nm should not interfere with the proposed method as long as they do not involve in a redox reaction with Ce(IV) salts, as difference absorptimetric measurements of the original and redox-reacted sample solutions were recorded, the difference corresponding to the consumed Ce(IV) concentration, and consequently to the total phenolics content of the sample. Spectrophotometric titration is recommended for plant extracts highly absorbing at the analytical wavelength, $\lambda_{max} = 320$ nm. However, other reducing agents capable of reacting with Ce(IV) – if present in a complex mixture – may interfere. The oxidizing reagent (of reduced strength) is simply a Ce(IV) solution in dilute sulfuric acid, and the required instrument is a spectrophotometer. There are no hardly available

radicalic reagents, which also pose stability problems during storage and application. This is the first documentation of a cerium(IV)-based total antioxidant assay for a wide variety of antioxidant compounds individually and in mixtures. For potential researchers who wish to practise and improve the developed method, we propose the name 'CERAC' to be further used for the assay, meaning 'ceric ion reducing antioxidant capacity'.

Acknowledgements

This work was supported by Istanbul Technical University Research Foundation under the M.Sc. Thesis (D. Ozyurt) Project; grant number 30820. The authors wish to thank Ulker Food Research & Development Division for the supply of certain antioxidant compounds. The authors are also grateful to the State Planning Organization of Turkey for the support given to the Advanced Research Project of Istanbul University 2005K120430. One of the authors (R. Apak) is thankful to Istanbul University Research Fund for their support to the Project YOP-4/27052004, and to Istanbul University Bilimsel Arastirma Projeleri (BAP) Yurutucu Sekreterligi for the support enabling the presentation of part of this work in the Aegean Analytical Chemistry Days (5th AACD) International Meeting, Thessaloniki, Greece, 5–8 October, 2006.

References

[1] A. Braca, C. Sortino, M. Politi, I. Morelli, J. Mendez, J. Ethnopharmacol. 79 (2002) 379.
[2] S.J. Maxwell, Drugs 49 (1995) 345.
[3] W.F. Hadnick, S. Ahmad, R.S. Pardini, Adv. Exp. Med. Biol. 439 (1998) 131.
[4] J.B. Harborne, C.A. Williams, Phytochemistry 55 (2000) 481.
[5] C.A. Rice-Evans, N. Miller, Free Radical Biol. Med. 20 (1996) 933.
[6] M.B. Arnao, Trends Food Sci. Technol. 11 (2000) 419.
[7] N.J. Miller, C.A. Rice-Evans, M.J. Davies, V. Gopinathan, A. Milner, Clin. Sci. 84 (1993) 407.
[8] C. Sanchez-Moreno, J.A. Larrauri, F. Saura-Calixto, J. Sci. Food Agric. 76 (1998) 270.
[9] B. Ozcelik, J.H. Lee, D.B. Min, J. Food Sci. 68 (2003) 487.
[10] G. Cao, C.P. Verdon, A.H.B. Wu, H. Wang, R.L. Prior, Clin. Chem. 41 (1995) 1738.
[11] I.F.F. Benzie, J.J. Strain, Anal. Biochem. 239 (1996) 70.
[12] K. Robards, P.D. Prenzler, G. Tucker, P. Swatsitang, W. Glover, Food Chem. 66 (1999) 401.
[13] B. Ou, D. Huang, M. Hampsch-Woodill, J.A. Flanagan, E.K. Deemer, J. Agric. Food Chem. 50 (2002) 3122.
[14] D. Huang, B. Ou, R.L. Prior, J. Agric. Food Chem. 53 (2005) 1841.
[15] R. Apak, K. Guclu, M. Ozyurek, S.E. Karademir, J. Agric. Food Chem. 52 (2004) 7970.
[16] R. Apak, K. Guclu, M. Ozyurek, S.E. Karademir, M. Altun, Free Radical Res. 39 (2005) 949.
[17] P. Akbay, A.A. Basaran, U. Undeger, N. Basaran, Phytother. Res. 17 (2003) 34.
[18] H. Wetherit, Dev. Food Sci. 29 (1992) 15.
[19] E. Osinska, R. Wieslawa, A. Wojciechowska, Lithuanian Institute of Horticulture, Scientific Works 2003m. T22(4), web: http://www.lsdi.lt/mokslo_darbai_eng.htm.
[20] H. Wagner, F. Willer, B. Kreher, Planta Med. 55 (1989) 452–454.
[21] I. Gulcin, O.I. Kufrevioglu, M. Oktay, M.E. Buyukokuroglu, J. Ethnopharmacol. 90 (2004) 205–215.
[22] R. Re, N. Pellegrini, A. Proteggente, A. Pannala, M. Yang, C. Rice-Evans, Free Radical Biol. Med. 26 (1999) 1231.
[23] R.A. Walgren, K.J. Karnaky Jr., G.E. Lindenmayer, T. Walle, Pharmacol. Exp. Ther. 294 (2000) 830.
[24] K. Guclu, K. Sozgen, E. Tutem, M. Ozyurek, R. Apak, Talanta 65 (2005) 1226.
[25] J. Bassett, R.C. Denney, G.H. Jeffery, J. Mendham (Eds.), Vogel's Textbook of Quantitative Inorganic Analysis, 4th ed., Longman, Beccles and London, 1978, pp. 363–367.
[26] D.J. Czappa, Doctor's Dissertion, The Institute of Paper Chemistry, Appleton, Wisconsin, 1974.
[27] L. Vladescu, I. Badea, D. Moja, Roum. Biotechnol. Lett. 7 (2002) 655.
[28] L.Y. Cho, J.M. Madurro, J.R. Romero, J. Catal. 186 (1999) 31.
[29] W. Roslon, Z. Weglarz, Acta Hort. (ISHS) 597 (2003) 101.

Available online at www.sciencedirect.com
ScienceDirect
Talanta 71 (2007) 1219–1225
Talanta
www.elsevier.com/locate/talanta

Amperometric detection of hydrazine by cyclic voltammetry and flow injection analysis using ruthenium modified glassy carbon electrodes

Jill S. Pinter*, Kenneth L. Brown, Paul A. DeYoung, Graham F. Peaslee

Departments of Chemistry and Physics, Hope College, Holland, MI 49422-9000, United States

Received 5 August 2005; received in revised form 2 June 2006; accepted 12 June 2006
Available online 28 July 2006

Abstract

Glassy carbon electrodes modified with (5-amino-1,10-phenanthroline)bis(bipyridine)ruthium(II) chloride hydrate, $[(bpy)_2Ru(5\text{-}phenNH_2)]Cl_2\cdot H_2O$, are shown to oxidize hydrazine with excellent sensitivity. The presence of an amine group on the ruthenium complex facilitates electropolymerization onto the electrode surface. Using cyclic voltammetry, a large catalytic current is observed upon oxidation of hydrazine in phosphate buffer (pH 5.0), compared to the current obtained from the ruthenium-modified electrode with no hydrazine present. The sensitivity of cyclic voltammetry is sufficient for obtaining a linear calibration curve for hydrazine over the range of 10^{-5} to 10^{-2} M. Hydrodynamic amperometry was used to determine the working potential for flow injection analysis. The limit of detection for hydrazine was determined to be 8.5 μM using FIA. The thickness of these films was shown to increase linearly with the number of electropolymerization cycles, in the range of 1000–2500 nm for 5–20 cycles, respectively, using Rutherford backscattering spectrometry (RBS). RBS analysis also suggests that the film is multilayered with the outermost layers containing a high ruthenium concentration, followed by layers where the concentration of ruthenium decreases linearly and approaches zero at the electrode surface.
© 2006 Elsevier B.V. All rights reserved.

Keywords: Cyclic voltammetry; Chemically modified electrodes; Ruthenium; Rutherford backscattering spectrometry (RBS); Film thickness; Flow injection analysis

1. Introduction

The motivation for the development of better sensors for the detection of hydrazine comes from the many commercial applications of hydrazine and its environmental and health hazards. The practical applications of hydrazine include its use in agricultural chemicals (pesticides), pharmaceutical intermediates, photographic chemicals, corrosion protection treatments for boilers, and as rocket fuel [3–6]. However, the Environmental Protection Agency (EPA) has classified hydrazine as a probable human carcinogen after studies of increased incidences of lung and liver tumors in mice exposed to hydrazine [3]. Since hydrazine is highly soluble in water, there are serious concerns about ground and surface water contamination, and several ongoing research efforts are underway to determine better ways to monitor hydrazine in the environment. Previously published work includes hydrazine detection methods based on amperometry/electrochemistry [7–11], flow injection analysis (FIA) [16,17], ion chromatography [12], chemiluminescence (CL), and various types of spectroscopy [13–15]. However, the chemistry involved in many of these methods is extremely complex, and the current sensor designs are not compact or mobile. The advantage of a sensor based on the work described here is that it is easy to use, and has the potential of being a very portable sensor.

In this work, hydrazine detection is accomplished through the combination of amperometry and flow injection analysis, as would be applied to the analysis of ground-water contamination. The presence of a ruthenium complex thin film on an electrode surface allows for the oxidation of hydrazine, and a catalytic current is obtained. Previous work [18,19] has explored other ruthenium complex polymer modified electrodes, such as $[Ru\text{-}(4\text{-methyl-}4'\text{-vinylbipyridine})_3](PF_6)_2$ and $[Ru^{II}(tpy)(bpy)(OH_2)]^{2+}$, but neither were applied to the detection of hydrazine. The current work introduces a new coordinate group on ruthenium, 5-amino-1,10-phenanthroline (5-$phenNH_2$), which initiates the polymerization process through

* Corresponding author. Present address: Michigan State University, NSCL 1 Cyclotron, East Lansing, MI 48824-1321, United States.
E-mail address: pinter@nscl.msu.edu (J.S. Pinter).

0039-9140/$ – see front matter © 2006 Elsevier B.V. All rights reserved.
doi:10.1016/j.talanta.2006.06.017

the oxidation of the amine group to form radical cations. These radical cations couple to each other to form the polymer film on the electrode surface so that detection of hydrazine may be accomplished. The application of flow injection analysis allows for the continuous monitoring of hydrazine. With the exceptional stability of the ruthenium electrodes described below, and the extremely sensitive FIA system, potential applications for continuous monitoring of ground water based on this electrode design are possible.

The ruthenium films were characterized for thickness using Rutherford backscattering spectrometry (RBS). While RBS has been used previously for thin film characterization [20–22], there has not been much work involving organic polymer films, as discussed here. In RBS, accelerated alpha particles are directed on the electrode surface at 4.5 MeV of total energy, and energy is lost due to the Coulomb interaction between the alpha particle and surrounding electrons of the target as the particle travels through the film. This loss in energy is material specific, dependent on the atomic number and density of species within the film. Upon collision with a specific nucleus, a new alpha-particle energy can be determined from the angle of deflection and mass of target atom. From the conservation of momentum, a collision with a large atom causes the alpha particle to scatter with most of its incident energy, while the large atom has little recoil. On the other hand, a collision with a small atom results in greater recoil of the atom and less energy for the scattered alpha particle. The final energy loss comes from Coulomb interactions as the scattered alpha particle exits the film. A substrate produces an edge, while a thick film forms a rectangular step, with the front edge corresponding to the energy of deflection off of the surface of the film. The width of the rectangular step is dependent on the energy loss as the particle travels into and out of the film. A thin film produces a peak, again with the front edge corresponding to the energy of deflection off of the surface, but the energy loss is much less as the particle does not have as far to travel within the film, thus the narrow peak shape.

2. Experimental

2.1. Apparatus

Electrochemical measurements were carried out with a CH Instruments 601A electrochemical analyzer (CH Instruments, Inc., Austin, TX). The electrochemical cell was a three-electrode system consisting of a glassy carbon working electrode (diameter of 3 mm), a platinum auxiliary electrode, and an Ag/AgCl (3 M NaCl) reference electrode. The flow injection analysis system consisted of a Hitachi Intelligent pump (model L-6200A from Delta Technical Products Company), an Alcott autosampler (model 728), and a detector. An Electrochemical Detector (Coulochem III, ESA, Inc., Chelmsford, MA) contains an analytical cell (model 5040), as well as a guard cell (model 5020). The analytical cell includes a glassy carbon target working electrode, a counter electrode made of stainless steel, and a solid-state reference electrode. The guard cell, composed of stainless steel, palladium, and graphite, is used to oxidize electroactive species that may be present as trace impurities in the mobile phase, and was placed between the pump and the injector. A flow rate of 0.5 mL/min was used in the FIA system. Data acquisition was provided by TotalChrom software (Perkin-Elmer). All pH measurements were done on a Jenco digital pH meter. Rutherford Backscattering Spectrometry measurements were performed on a 1.7 MV Pelletron tandem particle accelerator with a nuclear microprobe at the Hope Ion Beam Analysis Laboratory (HIBAL). Subsequent RBS analyses were performed offline with RUMP software [23,24].

2.2. Chemicals and reagents

The details pertaining to the synthesis of the ruthenium complex have been reported elsewhere [1,2] with some modifications as reported here. The reagents used in the preparation of the crude product, *cis*-$(bpy)_2RuCl_2{\cdot}xH_2O$, include $RuCl_3{\cdot}xH_2O$ (Aldrich Chemical Company, Milwaukee, WI), 2,2′-bipyridine (Sigma Chemical Company, St. Louis, MO), lithium chloride (Aldrich), and *N*,*N*-dimethylformamide (DMF, Sigma–Aldrich Co., St. Louis, MO). In preparation of the final product of (5-amino-1,10-phenanthroline)bis(bipyridine)ruthium(II) chloride hydrate, $[(bpy)_2Ru(5\text{-}phenNH_2)]Cl_2{\cdot}H_2O$, the reagents used include: 5-amino-1,10-phenanthroline (Polysciences, Inc., Warrington, PA), ammonium chloride (NH_4Cl, Fisher Chemicals, Fairlawn, NJ), and acetonitrile (Aldrich). All solvents used were of analytical reagent grade, and any water used was distilled. Hydrazine solutions were made from hydrazine sulfate ($(NH_2)_2{\cdot}H_2SO_4$, J.T. Baker Chemical Co., Phillipsburg, NJ), and a phosphate buffer of pH 5.00. The phosphate buffer was prepared using sodium hydrogenphosphate (0.10 M Na_2HPO_4, Aldrich), and sodium phosphate (0.1 M NaH_2PO_4, Allied Chemical Company, New York, NY). The pH 8.00 buffer was made from NH_4Cl and NH_4OH (Aldrich).

In all electropolymerizations, the concentration of the ruthenium complex was 5.00×10^{-3} M, and tetraethylammonium perchlorate (TEAP) was used as a supporting electrolyte (0.10 M, from GSF Chemicals, Columbus, OH), with acetonitrile as the solvent. During characterization using cyclic voltammetry, the concentration of hydrazine varied from 1.00×10^{-5} to 1.00×10^{-2} M in the phosphate buffer. Measurements of hydrazine using FIA used concentrations from 10 to 90 μM.

2.3. Preparation of ruthenium complex

The end product used in electropolymerization was $[(bpy)_2Ru(5\text{-}phenNH_2)]Cl_2{\cdot}H_2O$ (bpy is 2,2′-bipyridine, phen is 1,10-phenanthroline) [1]. Before this product was made, the crude product *cis*-$(bpy)_2RuCl_2{\cdot}xH_2O$ [2] was synthesized as an intermediate step. These complexes were made as reported previously, with slight modifications.

2.3.1. *cis*-$(bpy)_2RuCl_2{\cdot}xH_2O$

Reagent grade DMF (25 mL) was added to commercial $RuCl_3{\cdot}xH_2O$ (4.70 mmol), bipyridine (7.49 mmol), and LiCl (2.48 mmol). This dark brown solution was heated at reflux for 8 h. The mixture was cooled to room temperature, and 40 mL of acetone were added. The solution was placed in a constant tem-

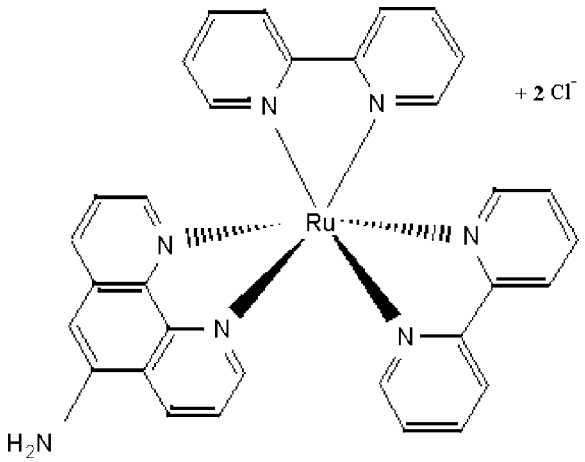


Fig. 1. Molecular structure of $[(bpy)_2Ru(5\text{-}phenNH_2)]Cl_2{\cdot}H_2O$.

perature bath of water and ethylene glycol at 0 °C, and remained there overnight. Vacuum filtration gave a black crystalline solid, and a dark red-violet solution. The solid was washed with equal volumes of distilled water and diethyl ether, and then dried overnight.

2.3.2. *[(bpy)2Ru(5-phenNH2)]$Cl_2{\cdot}H_2O$*

The crude product, *cis*-$(bpy)_2RuCl_2{\cdot}xH_2O$ (1.73 mmol) was dissolved in 90 mL of hot H_2O. This solution was combined with another solution of 5-amino-1,10-phenanthroline (1.94 mmol) dissolved in 180 mL of hot ethanol. The combined solution was deoxygenated with argon for 20 min, and then heated at reflux for 3 h, under the blanket of argon. Upon addition of a five-fold molar excess of NH_4Cl dissolved in water, a bright orange precipitate resulted. The bright orange product was collected by vacuum filtration, and is shown in Fig. 1. Proton NMR spectra were obtained using a 400 MHz spectrophotometer. Dimethylsulfoxide (d_6-DMSO) was used as the solvent in all NMR characterization measurements. Integration of signals in the ^1H NMR spectrum for characterization of the complex revealed the presence of 25 protons in the range of 3.5–8.9 ppm. Protons associated with the bipyridine organic moiety showed doublet peaks (8.30–8.50 and 7.50–7.70 ppm) and triplet peaks (7.30–7.50 and 8.00–8.20 ppm). Signals related to the 5-amino-1,10-phenanthroline ligand, showed chemical shifts and singlet peaks at 3.5 ppm ($-NH_2$) and 7.06 ppm. Doublet peaks (8.83, 8.27, 8.08, and 8.03 ppm) and triplet peaks (7.55 and 7.99) were also present in the spectrum.

2.4. Procedure for electropolymerization and characterization

The glassy carbon working electrodes were polished by placing several drops of polishing alumina suspension (0.05 μm particle size, Bioanalytical Systems) on a wetted polishing pad (Bioanalytical Systems). The electrode was moved in a circular motion, both clockwise and counterclockwise across the surface of the pad. A figure-of-eight motion was also performed. Polishing was done for approximately 5 min, upon which the electrode was rinsed with distilled water. The electrode was also placed in an ultrasonic cleaner for ten minutes to remove adsorbed alumina particles on the electrode surface. It was rinsed once again with distilled water, and allowed to dry.

Electropolymerization of the ruthenium complex on the electrode surface was accomplished by cycling the potential between +1.600 and +0.200 V, at a scan rate of 50 mV/s. The peak currents increased as the number of cycles of electropolymerization increased, until 50 cycles, after which the peak currents stayed relatively constant. Each film was characterized in the presence and absence of hydrazine in 0.10 M phosphate buffer (pH 5.0), at a scan rate of 5 mV/s. An electrode with no ruthenium film was also characterized in the presence of hydrazine for comparison. Each film was characterized in hydrazine solutions varying in concentration from 1.00×10^{-5} to 1.00×10^{-2} M. A calibration curve was established from the oxidation peak currents.

3. Results and discussion

3.1. Ru-complex films on glassy carbon electrodes: electropolymerization

Fig. 2 shows cyclic voltammograms corresponding to 50 cycles of electropolymerization. Two quasireversible redox couples and one irreversible oxidation peak were identified within the potential window of 1.6–0.20 V. Peaks 1 and 2 have a formal redox potential, $E^{\circ\prime}$, of 1.4 V corresponding to the Ru(III)/Ru(II) couple. Peak 3 situated at 1.1 V represents the irreversible oxidation of the amine group. The other redox couple identified as Peaks 4 and 5 with an $E^{\circ\prime}$ ca. 0.38 V is due to further electrochemical processes of the 5-amino-1,10phenanthroline ligand. The formal reduction potential is taken as the average of the cathodic and anodic peak potentials. The peak assignments are consistent with what is known about the electrochemical behavior of ruthenium bound to the bipyridine and 5-amino-1,10phenanthroline ligands. To verify the potential for the oxidation of the amine group several drops of concentrated H_2SO_4 were added to the electropolymerization monomer solu-

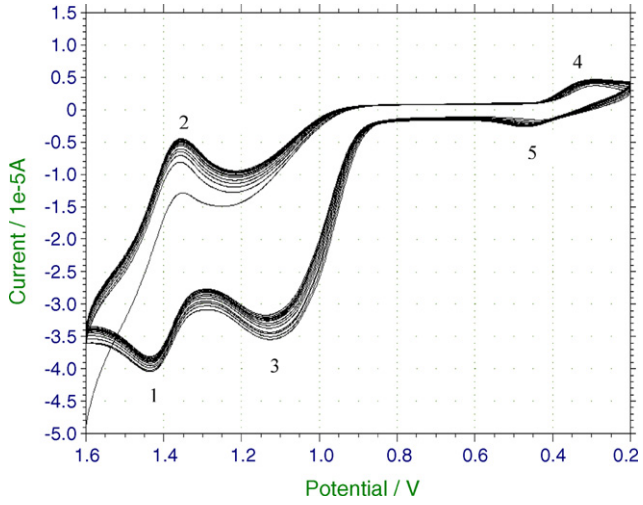


Fig. 2. Cyclic voltammogram of the electropolymerization of $[(bpy)_2Ru(5\text{-}phenNH_2)]Cl_2{\cdot}H_2O$ onto glassy carbon electrode. Concentration of monomer in solution is 5.00×10^{-3} M in 0.10 M TEAP and acetonitrile as solvent.

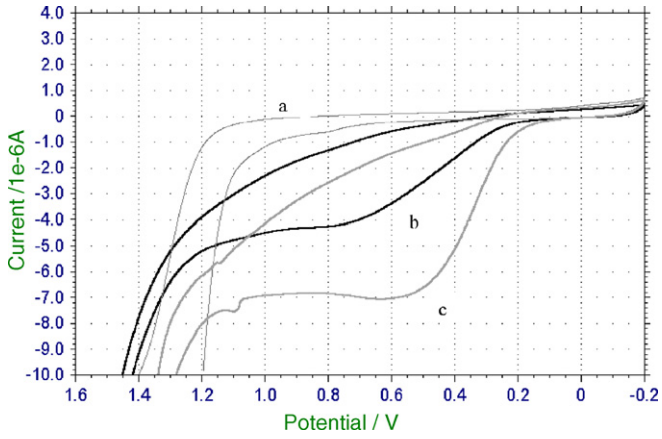


Fig. 3. Characterization of chemically modified glassy carbon electrode by cyclic voltammetry. Phosphate buffer serves as the supporting electrolyte solution. Curve a: 0.01 M hydrazine and a bare glassy carbon electrode. Curve b: electropolymerized ruthenium film with no hydrazine present. Curve c: electropolymerized ruthenium film in the presence of 0.01 M hydrazine.

tion. Upon addition of concentrated H_2SO_4, the strong peak at 1.1 V disappeared. Subsequent cyclic voltammetric scans in this environment did not produce a polymeric thin film. This indicates that the oxidation of the amine group is responsible for the peak at 1.1 V. The mechanism of electropolymerization of aromatic amines which involves several steps has been well-established and well-documented in the literature [25–29]. The initiation step is the oxidation of the amine group which occurs by the removable an electron from the lone pair of electrons of the amine nitrogen to form radical cations. This is followed by chemical reactions involving the loss of a proton and coupling of monomer units to form the polymer film on the electrode surface. The electropolymerization scan also shows that the peaks increase upon increasing cycle number, which signifies the formation and growth of film on the electrode surface with each cycle.

3.2. Ru-complex films on glassy carbon electrodes: cyclic voltammetric characterization

Characterizations of the films in the presence and absence of hydrazine in an aqueous buffer solution by cyclic voltammetry are shown in Fig. 3. With a bare electrode (curve a), in a hydrazine solution, there is an oxidation peak that is off scale at a high potential greater than 1.2 V. When the modified electrode was placed in the buffer solution with no hydrazine present, an anodic peak (curve b) was present at ca. 0.75 V and is related to the oxidation of Ru^{2+} to Ru^{3+} as shown in Eq. (1). After the addition of hydrazine with the ruthenium film present, a strong oxidation peak (curve c) appears at ca. 0.58 V, at a similar peak potential where the $Ru^{2+} \rightarrow Ru^{3+}$ process occurs. This suggests that the Ru(III/II) redox couple is responsible for the oxidation of the hydrazine as shown in Eqs. (2) and (3). After diffusion of the substrate, $N_2H_{4(bulk,\,red)}$, from the bulk solution to the electrode, the substrate at the electrode surface, $N_2H_{4(elec,\,red)}$, undergoes a mediated charge transfer reaction with the ruthenium-based film. The increase in peak current shown in cyclic voltammogram curve *c*, relative to curve *b*, in addition to the decrease in overpotential, is evidence of an excellent catalytic process for the oxidation of hydrazine at the modified electrode surface. The equations related to the electrochemical response of hydrazine towards the modified electrode surface are described by Eqs. (1)–(3),

$$\text{Ru(II)-5phenNH}_2 \leftrightarrow \text{Ru(III)-5phenNH}_2 + e^- \quad (1)$$

$$\text{Ru(III)-5phenNH}_2 + N_2H_{4(bulk,red)} \leftrightarrow [\text{Ru(III)-5phenNH}_2]\cdots N_2H_{4(elec,red)} \quad (2)$$

$$[(\text{Ru(III)-5phenNH}_2]\cdots N_2H_{4(elec,red)} \rightarrow \text{Ru(II)-5phenNH}_2 + N_2H_{4(ox)} \quad (3)$$

A calibration equation for hydrazine using a concentration range of 1.00×10^{-5} to 1.00×10^{-2} M was obtained using cyclic voltammetry and was determined to be:

$$\text{peak height} = 9.60 \times 10^{-6}(\text{A/mM})\,[H_2NNH_2] - 9.22 \times 10^{-8}(\text{A}) \quad (4)$$

3.3. Flow injection analysis approach

The same electropolymerization process was used to place the ruthenium film on the surface of a different glassy carbon electrode, designed specifically for the FIA system. Upon characterization of the film, the anodic peak was observed at the same potential, confirming the presence of the same film used in the cyclic voltammetry studies. Hydrodynamic amperometry experiments in Fig. 4A were used to determine the best operating potential for the detection of hydrazine in FIA. The potential was varied in 0.10 V increments from −0.100 to 1.200 V. Based on the hydrodynamic amperogram, a suitable signal was prevalent in the range of 0.700–0.900 V. Fig. 4B shows FIA signals based on repetitive injections of 5 μL injections of hydrazine corresponding to 0.01 and 0.02 M concentrations. The calibration curve shown in Fig. 5 was obtained using concentrations of hydrazine ranging from 10 to 90 μM is given by the following equation:

$$\text{peak height} = 646.41\,(\mu\text{V}/\mu\text{M})\,[H_2NNH_2] - 2195.7\,(\mu\text{V}) \quad (5)$$

The detection limit of 8.5 μM for this system is based on FIA measurements using 5 μL injections and is reported as the concentration that provided a signal-to-noise ratio of 3.

3.4. Determination of film thickness

The films were characterized for thickness using Rutherford backscattering spectrometry. Spectra were obtained for a blank electrode (Fig. 6a), as well as electrodes with films of 5, 10, and 20 cycles of electropolymerization (at 50 mV/s scan rate). A sapphire substrate and a gold film standard were used in the energy calibration, with the gold standard also used to determine the resolution of the detector. The spectrum for 20 cycles of electropolymerization is shown in Fig. 6b, which includes a

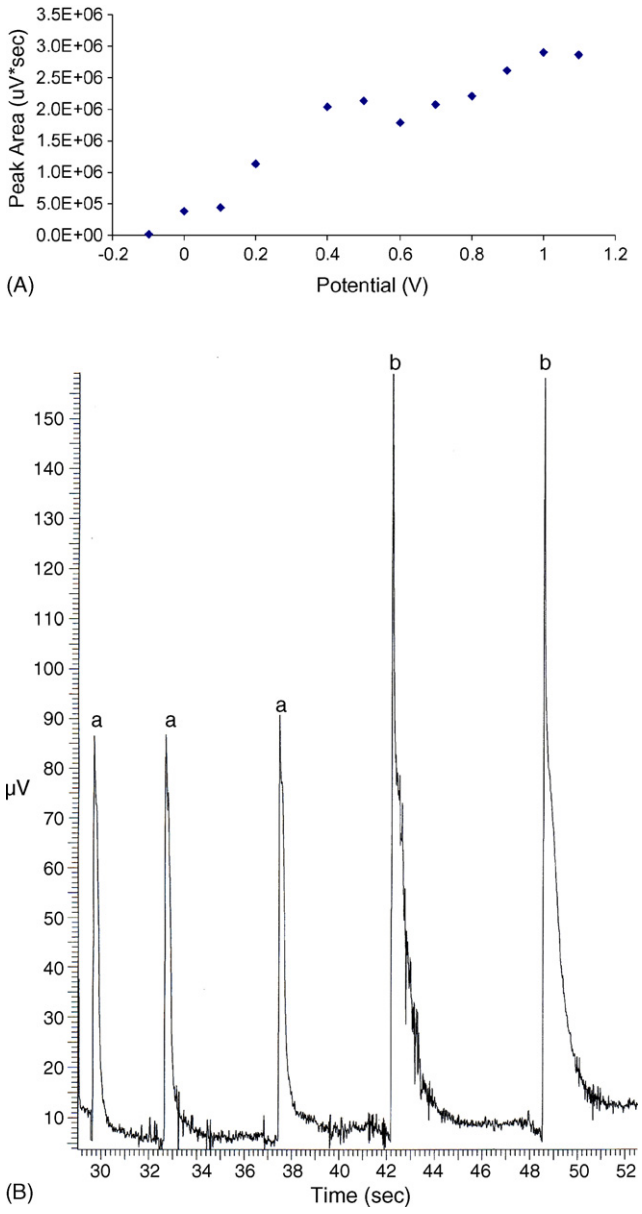


Fig. 4. (A) Hydrodynamic amperogram using 0.01 M hydrazine in phosphate buffer. (B) Typical 5 μL injections of 0.01 M (a) and 0.02 M (b) solutions of hydrazine.

large carbon edge, and smaller peaks for the elements nitrogen, oxygen, chlorine, and ruthenium, all of which are present in the film. The RUMP software package [23,24] was used to create theoretical models that could be compared to experimental data, based on known beam parameters, geometry, and elemental compositions. Table 1 shows the simulation for 20 cycles of electropolymerization, and an expanded spectrum of the region of interest around the heavy elements can be found in Fig. 6b.

In Table 1, the electrode surface corresponds to the thick glassy carbon substrate, on top of which the ruthenium film is placed. This peak profile shown as the smooth solid line fit to the data in Fig. 7a indicates that the electropolymerization film itself can be reasonably modeled assuming that it is divided into two parts: an outer layer and inner layer. The outer layer is farthest

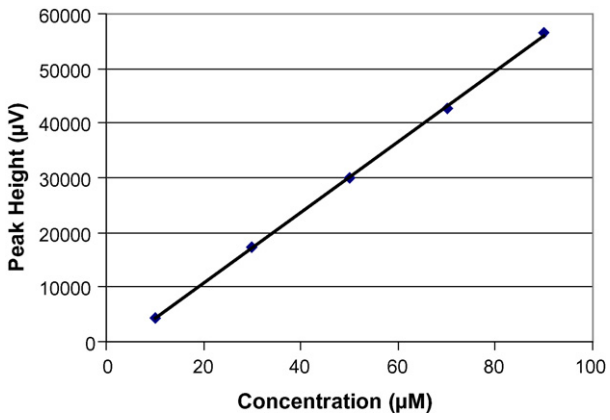


Fig. 5. Calibration curve for hydrazine using FIA. Concentrations of hydrazine range from 10 to 90 μM. The correlation coefficient is 0.998.

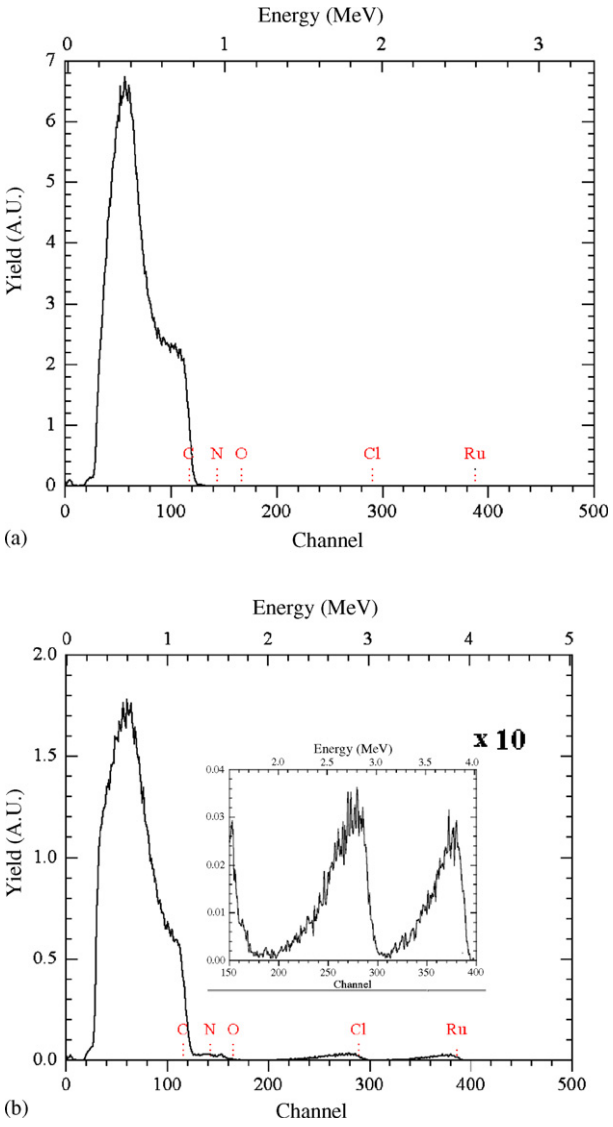


Fig. 6. Experimental RBS spectra of (a) blank glassy carbon electrode and (b) electrode with ruthenium film, 100 cycles of electropolymerization. Spectra generated using RUMP software package.

Table 1
Simulation generated in RUMP for 20 cycles of electropolymerization

Film profile	Thickness (nm)	Elemental composition
Outermost layer	2,500	C (6.813), O (0.100), N (0.039), H (4.257), Ru (0.002), Cl (0.028)
Inner layer	2,000	C (6.813), O (0.100), N (0.039), H (4.257), Ru and Cl are diffusant
Electrode surface	700,000	C (1)

from the electrode surface, and has a uniform (constant) distribution of all species within the film. This is represented by the flat portion of the fit curve in Fig. 7a. The inner layer closest to the electrode surface has a nonuniform distribution of ruthenium and chlorine sites throughout this portion of the film. In this case, it is modeled to have the same uniform concentration as the outer

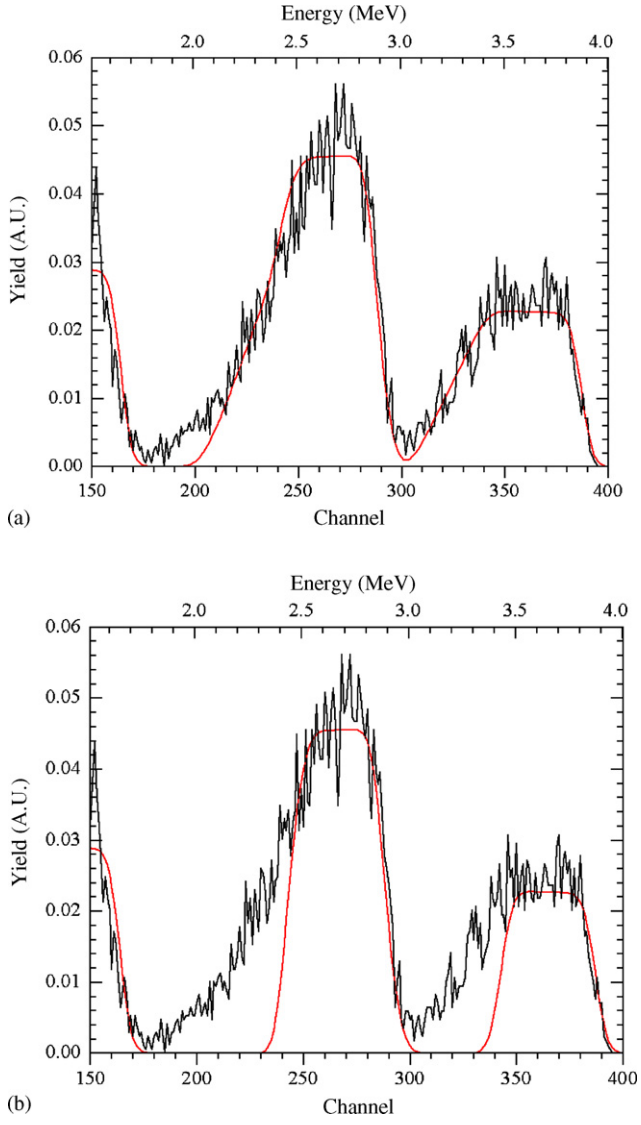


Fig. 7. Expanded RBS spectrum of glassy carbon electrode with ruthenium film, 20 cycles of electropolymerization. The smooth curve is a theoretical model of the spectrum with (a) linear diffusion of ruthenium and chlorine sites and (b) uniform sites throughout the film.

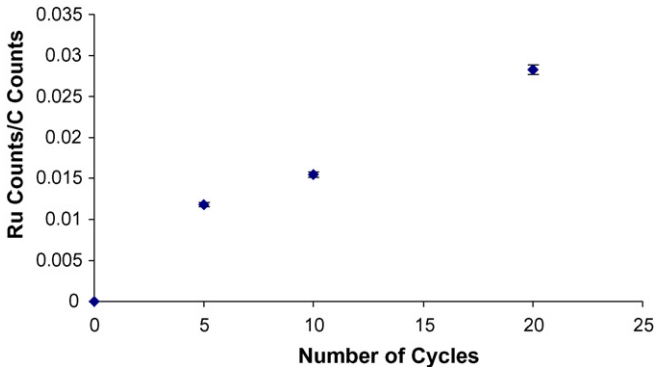


Fig. 8. Amount of ruthenium present in films of varying cycles of electropolymerization. Integration of ruthenium peak is normalized with respect to carbon peak.

layer on the surface, and it decreases linearly to zero concentration at the electrode surface. This nonuniform distribution of ruthenium sites confirms that the ruthenium must be mobile during the electropolymerization process, since more of it is found on the surface layer than on the interior layers of the polymer film. In the characterization voltammetric scan, the oxidation peak of curve b in Fig. 3 is broad and has a peak width greater than 90.6 mV at half the peak height maximum, indicating the presence of non-equivalent redox centers or attractive/repulsive-type forces present within the film [25–28]. This observation of non-uniform ruthenium and chlorine distribution found for all samples studied by RBS, parallels the observation of the possible non-equivalent redox centers or attractive/repulsive-type forces present within the film obtained by cyclic voltammetry. The RBS spectrum (Fig. 7a) confirms that there is indeed an inner layer of the film which is nonuniform in redox centers, and a uniform outer layer. Fig. 7b shows the same spectrum modeled with uniform ruthenium and chlorine concentrations throughout the film. This provides information about the mobility of the redox sites during the electropolymerization process.

The amount of ruthenium present in the film was determined by integration of the number of counts over the ruthenium peak. Fluctuation in beam current was accounted for by dividing the total ruthenium counts by the total carbon counts, thus normalizing with respect to the carbon substrate. The amount of ruthenium present in the film was determined to increase roughly linearly as the number of cycles of electropolymerization increased (at least below 50 cycles), as shown in Fig. 8.

The same model was used to fit the other spectra, with the thickness of the layers on the electrode surface being the only variable that changed significantly. While there appeared to be no apparent trend in the thickness of the nonuniform inner layer, the uniform outer layer increased in thickness with increasing number of cycles of electropolymerization, as shown in Fig. 9. The thickness is shown to saturate at the higher number of cycles, also confirming the electropolymerization in Fig. 2, which shows a stabilizing reduction peak current. A set of electrodes with a higher number of cycles of electropolymerization was tested multiple times in the accelerator during beam conditioning (while the data reported here was the result of only one beam irradiation). The repeated exposure to beam was observed

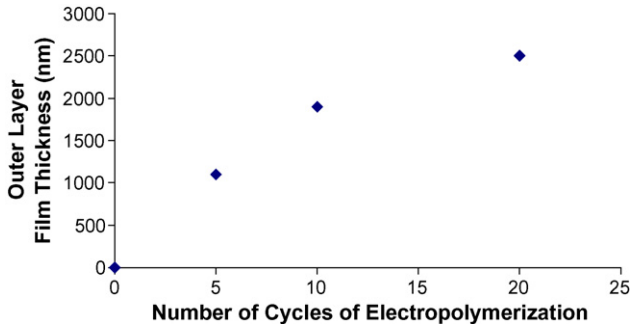


Fig. 9. Thickness of ruthenium films at varying number of cycles of electropolymerization. RBS spectra were used to generate this plot, each fit to a theoretical simulation to determine film thickness. The thickness is shown to increase linearly with the number of cycles of electropolymerization.

to cause physical damage to the films. While the films were shown to always display the same increasing trend in thickness for the outer uniform layer, the films which were irradiated repeatedly were overall much thinner. This was due to local heating and ablation of the surface by the incident beam of alpha particles.

4. Conclusion

The ruthenium complex, $[(bpy)_2Ru(5\text{-}phenNH_2)]Cl_2 \cdot H_2O$, electropolymerized onto a glassy carbon electrode surface allows for oxidation of hydrazine in solution, and thus detection of the compound. Detection of hydrazine is accomplished through cyclic voltammetry and FIA. Rutherford Backscattering studies show that the film is composed of an outer layer, uniform in concentration of ruthenium, as well as an inner layer that is nonuniform with respect to ruthenium. The nonuniform layer decreases linearly in concentration from the uniform layer, until the concentration of ruthenium reaches approximately zero at the electrode surface. The thickness of films with 5–25 cycles of electropolymerization fall in the region of 1000–2500 nm, becoming saturated in thickness at the higher number of cycles.

Acknowledgements

We would like to thank the Hope Ion Beam Analysis Laboratory (HIBAL) at Hope College for use of the accelerator, and Dave Daugherty for his technical support as well as the NSF MRI-0319523 for funding. We also wish to thank Dr. Elizabeth Sanford and Dr. Steven Taylor for use of their organic synthesis equipment. Financial support from the Arnold and Mabel Beckman Foundation is gratefully acknowledged.

References

[1] B.P. Sullivan, D.J. Salmon, Inorg. Chem. 17 (1978) 3334–3341.
[2] C.D. Ellis, L.D. Margerum, Inorg. Chem. 22 (1983) 1283–1291.
[3] U.S. Environmental Protection Agency, Integrated Risk Information System (IRIS) on Hydrazine/Hydrazine Sulfate, National Center for Environmental Assessment, Office of Research and Development, Washington, DC, 1999.
[4] U.S. Environmental Protection Agency, Health and Environmental Effects profile for Hydrazine and Hydrazine Sulfate, Environmental Criteria and Assessment Office, Office of Health and Environmental Assessment, Office of Research and Development, Cincinnati, OH, 1984 (EPA/600/x-84/332).
[5] E.S. Budavari, The Merck Index, in: An Encyclopedia of Chemicals, Drugs, and Biologicals, 11th ed., Merck and Co. Inc., Rahway, NJ, 1989.
[6] Agency for Toxic Substances and Disease Registry (ATSDR), Toxicological Profile for Hydrazines, Public Health Service, U.S. Department of Health and Human Services, Atlanta, GA, 1997.
[7] I.G. Casella, M.R. Guascito, A.M. Salvi, E. Desimoni, Anal. Chim. Acta 354 (1997) 333–341.
[8] K. Ozoemena, T. Nyokong, Talanta 67 (2005) 162–168.
[9] A. Salimi, K. Abdi, Talanta 63 (2004) 475–483.
[10] S.V. Guerra, L.T. Kubota, C.R. Xavier, S. Nakagaki, Anal. Sci. 15 (1999) 1231–1234.
[11] J. Wang, T. Golden, R. Li, Anal. Chem. 60 (1988) 1642–1645.
[12] R. Gilbert, R. Rioux, Anal. Chem. 56 (1984) 106–109.
[13] A. Safavi, A.A. Ensafi, Anal. Chim. Acta 300 (1995) 307–311.
[14] S.M. Golabi, H.R. Zare, Electroanalysis 11 (1999) 1293–1300.
[15] S.V. Guerra, L.T. Kubota, C.L. Xavier, S. Nakagaki, Anal. Sci. 15 (1999) 1231–1234.
[16] J. Wang, Z. Lu, Electroanalysis 1 (1989) 517–521.
[17] M. Ebadi, Can. J. Chem. 81 (2003) 161–168.
[18] C. Felcmann, R. Alt, G. Greiner, H. Rau, M. Worner, Phys. Chem. Chem. Phys. 2 (2000) 3483–3489.
[19] F. Geneste, C. Moinet, S. Ababou-Girard, F. Solal, Inorg. Chem. 44 (2005) 4366–4371.
[20] M.E. Makgae, C.C. Theron, W.J. Przybylowicz, A.M. Crouch, Mater. Chem. Phys. 92 (2005) 559–564.
[21] S. Nakao, K. Saitoh, M. Ikeyama, H. Niwa, S. Tanemura, Y. Miyagawa, S. Miyagawa, M. Tazawa, P. Jin, Nucl. Instrum. Methods Phys. Res., Sect. B 141 (1998) 246–251.
[22] C.E. Vallet, B.V. Tilak, R.A. Zuhr, C.P. Chen, J. Electrochem. Soc. 144 (1997) 1289–1295.
[23] J.W. Mayer, L.R. Doolittle, M.O. Thompson, E.J. Kramer, RUMP, Cornell University, 1989.
[24] L.R. Doolittle, Nucl. Instrum. Methods Phys. Res., Sect. B 15 (1986) 227–231.
[25] K.L. Brown, H.A. Mottola, Langmuir 14 (1998) 3411–3417.
[26] K.L. Brown, J. Shaw, M. Ambrose, H.A. Mottola, Microchem. J. 72 (2002) 285–298.
[27] K.L. Brown, J.S. Pinter, K.L. Ewing, T.R. Ruch, M. Ambrose, I. Hesslesweet, Anal. Lett. 38 (2005) 769–780.
[28] F.W.M. Nyasulu, H.A. Mottola, J. Electroanal. Chem. 239 (1988) 175–186.
[29] C.D. Ellis, L.D. Margerum, R.W. Murray, T.J. Meyer, Inorg. Chem 22 (1983) 1283–1291.

Available online at www.sciencedirect.com
ScienceDirect
Talanta 71 (2007) 1364–1368
Talanta
www.elsevier.com/locate/talanta

Interferences elimination in ion chromatography by inclusion of the interfering ion into the mobile phase—Analysis of fluoride in chloride rich dietary samples

Bartlomiej Prusisz *, Katarzyna Grymuza, Pawel Pohl

Wroclaw University of Technology, Analytical Chemistry Group, Faculty of Chemistry, Smoluchowskiego 23, 50-372 Wroclaw, Poland

Received 24 February 2006; received in revised form 29 June 2006; accepted 6 July 2006
Available online 22 August 2006

Abstract

New approach to the chloride interferences elimination by addition of the interfering ion to the mobile phase is proposed and evaluated. Different eluents for the non-suppressed ion chromatographic analysis of fluorides in chlorides rich samples were tested and compared with eluent recommended by the column manufacturer. The limit of detection, linearity range and resistance to matrix effects caused by chlorides were the comparison criteria. The applicability of the selected eluent was demonstrated through the analysis of the edible salts and various tea samples. The employment of the proposed eluent shorten the time of the analysis since the only required preparation steps for edible salts were the dissolution and appropriate dilution of the samples. The recovery test was employed to verify the obtained results.
© 2006 Elsevier B.V. All rights reserved.

Keywords: Ion chromatography; Interferences elimination; Fluoride; Edible salt; Tea

1. Introduction

Impact of fluoride on human health is still a controversial issue. Besides its widely recognized beneficial effect of decreasing risk of dental caries [1], the recent studies implies that fluoride ions have significant impact on children's intelligence [2] causing in higher concentrations mental retardation (IQ < 70) and borderline intelligence (IQ 70–79). The increase in fluoride concentration in drinking water can increase cases of arthopathy and arthresis [3], as well as bone tumor (osteosarcoma) occurrence among young boys [4]. Allergy and hypersensitivity to fluoride were also reported [5]. Precise measurements of fluoride content in food allows assessment of fluoride daily intake and, as a consequence, avoid fluoridation.

Thus, measurements of fluoride concentration in edible salts is of a primary importance as it is currently estimated that more people in the world are exposed to fluoridated salt than fluoridated water. Countries with extensive salt fluoridation programs include: Austria, Bolivia, Columbia, Costa Rica, Dominican Republic, France, Germany, Honduras, Nicaragua, Panama, Switzerland, and Venezuela, so far similar programs are not undertaken in USA or Canada.

A high performance ion chromatography (HPIC) is often a method of choice in the analysis of fluoride content in dietary samples due to satisfactory sensitivity, wide linearity range and usually short time of a single run. Applications of HPIC to the analysis of fluoride in coffee, tea, spinach, fruits [6,7] as well as alcoholic beverages [8] are known. However, the method still offers a lot of challenges when applied to complex matrix samples. Fluoride ions in biological samples and food are usually accompanied by considerably larger amount of chlorides. In such cases, the overloading of the column is a common encounter, while the necessary dilution or reduction of the sample volume lead to serious decrease in the sensitivity. Therefore, to allow the analyte detection, certain minimum sample size must be injected. Consequently, the chloride ions present at high concentrations overwhelm and saturate the column and disturb its equilibrium. In such cases, the fluoride peak is either totally masked or distorted due to the loss of the resolution [9]. Moreover, in case of fast eluting anions, negative dips or deviations from baseline can interfere with fluoride analysis [10]. As a

* Corresponding author. Tel.: +48 71 3203445; fax: +48 71 3284330.
E-mail address: bartlomiej.prusisz@pwr.wroc.pl (B. Prusisz).

0039-9140/$ – see front matter © 2006 Elsevier B.V. All rights reserved.
doi:10.1016/j.talanta.2006.07.010

result, in chlorides rich samples, the quantification of fluorides is demanding task prone to inaccuracy.

Various sample preparation steps allowing matrix removal prior to the HPIC analysis were proposed over the years. Chlorides can be precipitated with counterions from the sulfonated resin [11], adsorbed on silver oxide [12], or removed using online IC–IC or ICE–IC mode [11]. The application of the preconcentration of analytes on a chelating resin enabling determination of Ca and Mg ions in 30% sodium chloride solution [13] was reported. The column switching and concentration system was successfully applied to the analysis of ammonium in seawater [14]. Pretreatment for the removal of large excess of chloride from the sample matrix with on-guard silver cartridges were employed prior to the iodate and sulphate analysis of the iodized salt [15]. Still, every preparation step increases time and complexity of the analysis as well as the risk of contamination.

The objective of this study was to propose and evaluate the applicability of a new mobile phases for the ion chromatographic analysis of fluorides in the chloride rich samples. Interferences reduction was accomplished by the addition of the interfering ion to the eluents. Considering the above described problems, the desired eluent should elute fluoride anions within reasonably short time but simultaneously far enough from the water dip to avoid possible interferences. Further, it has to be, as much as possible, resistant to matrix effects caused by chloride ions, even when measuring fluoride in such complex samples as aqueous solutions of edible salts.

The optimized procedure applying chosen eluent was used for the analysis of fluoride content in sea salt, fluoridated salt and in addition, in various teas. The results obtained were verified by the recovery test of spiked sea salt.

2. Experimental

2.1. Equipment

High performance ion chromatography system employed in this study consisted of a Knauer (Berlin, Germany) solvent pump WellChrom Mini-Star K-500, a Knauer column thermostat Jetstream 2, a Knauer six-port valve A0258 and a conductivity detector model 550 Alltech (Deerfield, IL, USA). The detector was interfaced with a data acquisition unit Knauer WellChrom v7566 working with a personal computer equipped with Knauer EuroChrom 2000 software Version 1.2. The HPLC column used was an anion-exchange Hamilton (Reno, NV, USA) PRP-X100 (4.1 × 150 mm) with a PRP-X100 guard column (2.3 × 25 mm). Sample loop of 100 μL was used throughout the experiments.

Ultrasonic bath model Ultrasons-H, Selecta (Abrera, Spain) was used in the ultrasonic assisted sample extraction procedure. For sample solutions filtration, Knauer Minisart-RC 25 cellulose membrane filters (pore size of 0.45 μm) in polypropylene housing were used throughout the experiments.

2.2. Chemicals

De-ionized water (18.3 MΩ cm resistivity) obtained from Barnstead (Dubuque, IA, USA) EASYpure^{TM} model D7033 water system was used for preparation of all solutions and eluents. HPLC grade methyl alcohol (99.93% pure; Aldrich, USA), 4-hydroxybenzoic acid (99% pure; Aldrich), sodium hydroxide (analytical grade; POCh, Poland) and sodium chloride (spectral grade; POCh, Poland) were employed for the preparation of the eluents. Working standard solutions of fluorides and chlorides were prepared from ion chromatography stock standard solutions (1000 mg L^{-1}; Fluka, Switzerland) by the appropriate dilutions.

2.3. Eluents and conditions

The mobile phases were 4.0 mmol L^{-1} *p*-hydroxybenzoic acid in 97.5% water and 2.5% methyl alcohol solution (pH 8.5) and solutions of sodium chloride at concentrations correspondent to 10 and 20 mmol L^{-1}. For the pH adjustment, a solution of 1.0 mol L^{-1} sodium hydroxide was used.

All measurements were carried out with upper conductivity range set to 1.0 μS and a time constant of 0.5 s. The flow rate of the mobile phase was 2.0 mL min^{-1}. The temperatures of the column thermostat and the conductivity cell were 30 °C.

An isocratic elution mode by non-suppressed ion chromatography was employed in all the experiments. The identification of each ion was performed by the injection of the solutions containing a single ion. The instrument was calibrated with blank and standards of F^- and Cl^- ions at concentrations of 0.1, 0.2, 1.0, 5.0 and 10 mg L^{-1}.

2.4. Sample preparation

The sea and fluoridated salts samples solutions were prepared by simple dissolution of exactly weighed salt amounts in de-ionized water. The resulting solutions were quantitatively transferred into the volumetric flasks and then brought up to the volume. Before injection onto the column, the samples were filtered through syringe filters (0.45 μm).

For the preparation of the tea samples, often used ultrasonic facilitated extraction was applied [13]. The exactly weighted tea leaves (around 1 g) were mixed with 10 mL of de-ionized water in glass tubes and placed in the ultrasonic bath for 30 min at the 30 °C. After extraction, the resulting solutions were filtered, and injected onto the column. Routinely, the fresh tea and salt solutions were prepared few hours before measurements.

3. Results and discussion

3.1. Eluents characteristic

Since any eluent constituent present in the sample is invisible to the detection system [16], an attempt was made to eliminate chloride peak from the analyzed solutions by usage of the mobile phases containing chloride anions. For that purpose, four sodium chloride solutions differ in NaCl concentration and acidity were chosen as eluents. For the evaluation purposes, the eluent recommended by the column manufacturer was also examined (4.0 mmol L^{-1} *p*-hydroxybenzoic acid, pH 8.5). Chromatographic figures of merit for the examined eluents were

Table 1
Chromatographic characteristic of fluoride anions on different mobile phases

	Detection limit ($mg\,L^{-1}$)	Upper linearity limit ($mg\,L^{-1}$)	Regression coefficient (R^2)	Retention time (min)	Asymmetry factor
4 $mmol\,L^{-1}$ *p*-hydroxybenzoic acid, pH 8.5	0.087	120	0.9987	2.033	1.514
10 $mmol\,L^{-1}$ NaCl, pH 7	0.029	40	0.9927	3.450	2.081
20 $mmol\,L^{-1}$ NaCl, pH 7	0.020	30	0.9995	3.350	1.931
10 $mmol\,L^{-1}$ NaCl, pH 8.5	0.033	50	0.9995	3.103	2.294
20 $mmol\,L^{-1}$ NaCl, pH 8.5	0.030	50	0.9988	2.889	1.709

assessed measuring the standard solutions of fluoride ions at concentrations of 0.1, 0.2, 1.0, 5.0 and 10 $mg\,L^{-1}$. Detection limit, was evaluated by measuring ten successive signals of fluoride in the solution containing traces of F^-. This figure was calculated as the concentration equivalent to the signal being three-folded standard deviation of the measured fluoride peaks. Comparison of chromatographic characteristics of fluoride anions obtained using different mobile phases is shown in Table 1.

As can be seen, sodium chloride solutions as eluents exhibit about two-fold lower detection limits in comparison to that obtained for the eluent recommended by the column manufacturer, but the linearity range in case of those eluents is also about two to three-fold shorter. Lower detection limits provide accuracy needed for the sensitive measurements of usually low concentrations of the ions of interest and the drawback of shorter linearity range can be easily overcome by simple dilution. Fluorides retention time of 3 min can be regarded as far enough from the water dip to minimize its interference, on the other hand, not extending the time of analysis beyond necessity.

The most important parameter of the investigated eluents is their resistance to the matrix effect caused by chlorides. To examine that property, the solutions with the same fluoride content (0.1, 0.2, 1.0, 5.0 and 10 $mg\,L^{-1}$) and various concentrations of chlorides were measured. Next, the detection limits of fluorides, obtained for the solutions of different chloride ions content were calculated using the method described earlier in the chapter. The results are shown in Fig. 1. In case of mobile phase containing *p*-hydroxybenzoic acid, chloride ions present at concentration of 500 $mg\,L^{-1}$ obstruct fluoride measurements in all standards solutions but the one with the highest F^- concentration (10.0 $mg\,L^{-1}$). For all eluents used, besides fluoride peak, the peak of chlorides is present proving that although the signal from chlorides is decreased, it can not be completely eliminated by the described approach.

3.2. Measurements of edible salts samples

Samples of three different edible sea salts and one edible fluoridated salt were dissolved in de-ionizated water and filtered through 0.45 μm filters. It was found that too extensive dilution of salt samples resulted in low chloride concentration, but simultaneously the concentrations of fluorides was considerably lowered and, as a consequence, were below the detection limit. On the contrary, high salt concentrations resulted in severe increase in matrix effects and column overloading caused by chloride ions. The best found compromise of those opposing trends were the sample solutions containing 2500 $mg\,L^{-1}$ of Cl^- ions. Comparison of the separations accomplished using the investigated eluents allowed the selection of the most suitable one for the task, that is 20 $mmol\,L^{-1}$ NaCl solution, pH 7. The chromatogram of the 'Sea salt 1' sample solution obtained after the optimization procedure is presented in Fig. 2. After the selection of the mobile phase and the dilution factor, the samples of edible salts were measured in three replicates and the found concentrations are given in Table 2. As can be seen from Table 2, the relative standard deviations of the obtained results are within a range between 20 and 25%. Concerning a challenging sample composition, this precision can be regarded as satisfactory. Measured fluoride concentrations were around

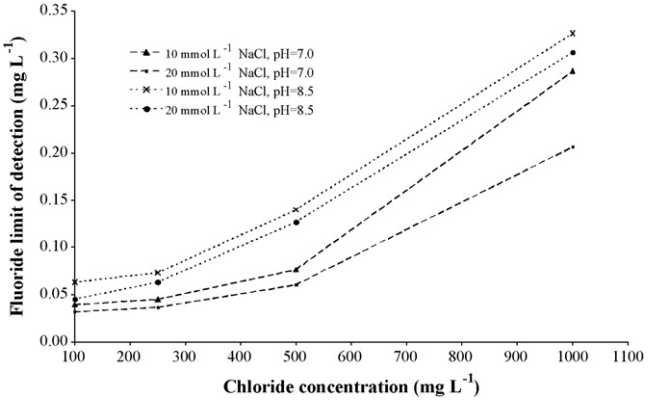


Fig. 1. Influence of chloride concentration on the sensitivity of fluoride measurement.

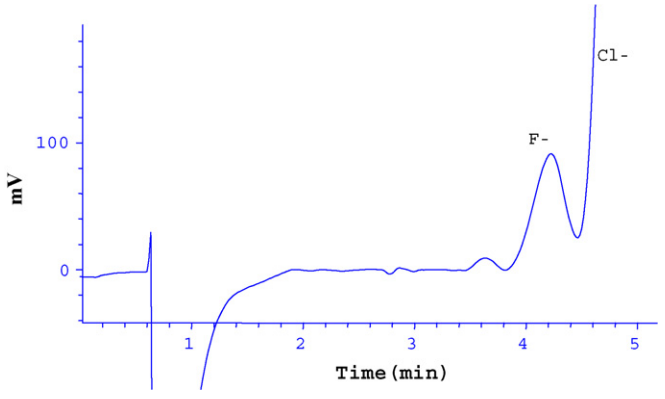


Fig. 2. Chromatogram of the sea salt sample solution obtained using 20 $mmol\,L^{-1}$ NaCl, pH 7 eluent.

Table 2
Determined fluoride concentrations (μg g^{-1}) in edible salt samples ($N = 3$)

Sample	Mean	S.D.
Sea salt 1	142	36
Sea salt 2	130	28
Sea salt 3	99	21
Fluoridated salt	209	41

0.8 mg L^{-1} in the presence of the chloride ions of concentration of 2500 mg L^{-1}. Thus, the application of the proposed eluent allows the measurements of fluorides in the presence of three orders of magnitude bigger chloride concentration and the avoidance of time consuming and cumbersome sample preparation steps usually performed to separate or remove the interfering chloride ions.

3.3. Recovery test

To verify the accuracy of the results, the recovery test was performed to measure the fluoride concentration in one of the examined edible sea salts (Sea salt 1). For that purpose, the solution of fluoride standard was added to three samples of the analyzed sea salt in quantity adequate to approximately double the fluoride concentration in the final sample solutions. Then, the solutions were appropriately diluted and filtered. Final concentration of fluoride ions in original sample solution was 0.586 mg L^{-1}, and the standard added increased this concentration to 1.09 mg L^{-1}. Next, the samples were measured and the fluoride ions recovery was calculated. Typical chromatograms are presented in Fig. 3. Find recovery of 96.6 ± 10.9% proves accuracy of the measurements.

3.4. Analysis of tea samples

To check the applicability of the described procedure to the analysis of other dietary samples, tea as one of the main sources of fluorides in human diet was chosen. Five different tea kinds were prepared as described in Section 2.4 and measured using 20 mmol L^{-1} NaCl solution (pH 7) as eluent. The results are

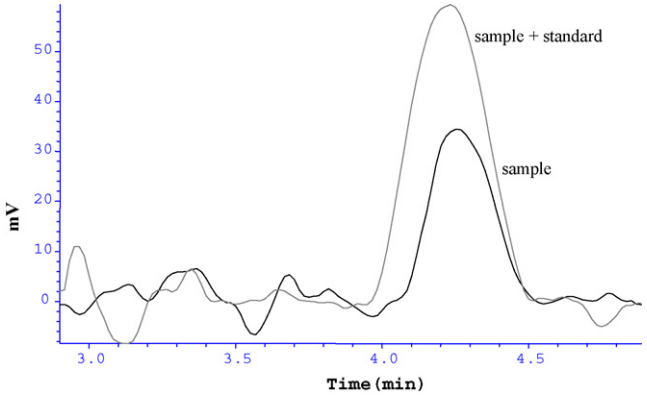


Fig. 3. Peaks of fluoride ions in the sea salt solutions without fluoride standard and with added 0.500 mg L^{-1} F$^-$. Eluent: 20 mmol L^{-1} NaCl, pH 7. Chromatograms after baseline correction.

Table 3
Fluoride and chloride anions content (μg g^{-1}) in various tea kinds ($N = 3$)

	Fluoride		Chloride	
	Mean	S.D.	Mean	S.D.
Shanghai green	574	58	407	35
Yunnan green	689	51	373	32
Yunnan black	858	69	393	29
Madras black	597	39	434	31
Assam black	379	31	798	62

shown in Table 3. It has been ascertained that even 10 mmol L^{-1} NaCl solutions are suitable for the quantification of fluoride ions in analyzed tea samples. Lower concentrations of chlorides allow usage of eluent with lower chloride concentration and assure better measurement precision. In case of tea samples, the precision of the measurements in terms of relative standard deviation is not exceeding 10%. It is noteworthy that although the concentrations of measured ions vary significantly, the sum of the fluoride and chloride concentrations in all tested tea kinds is compellingly stable within the range of 981–1251 μg g^{-1}.

4. Conclusions

The applicability of aqueous solutions of sodium chloride as eluents in the analysis of fluorides was tested and compared with the eluent recommended by the column manufacturer using limits of detections, linearity range and resistance to matrix effects caused by chlorides as comparison criteria.

The chosen eluent, that is 20 mmol L^{-1} NaCl solution, pH 7, enables quantification of fluorides accompanied by high chloride concentrations. The eluent of 4.0 mmol L^{-1} *p*-hydroxybenzoic acid in 97.5% water and 2.5% methyl alcohol solution (pH 8.5) is suitable for the analysis of fluorides in the presence of chloride concentrations not bigger then two orders of magnitude, whereas the selected NaCl solution can be used for quantification of fluorides in samples containing over three orders of magnitude bigger chloride concentrations. That feature, together with reasonably low fluoride detection limit allow measurements of fluorides content in edible sea and fluoridated salts after simple sample dissolution and avoiding fluoride preconcentration or separation steps. The accuracy of the method was verified by the recovery test.

The same proposed eluent was successfully applied to the analysis of various tea samples with possible applications in the analysis of fluorides in isotonic beverages, brines, estuarine and sea waters.

The presented approach to the elimination of interferences caused by interfering ion can be adopted to the wide range of analytical procedures e.g. analysis of rubidium ions in the presence of large amounts of potassium ions.

References

[1] R.P. Ellwood, D.M. O'Mullane, Community Dent. Oral Epidemiol. 24 (1996) 1.

[2] Q. Xiang, Y. Liang, L. Chen, C. Wang, B. Chen, X. Chen, M. Zhouc, Fluoride 36 (2003) 84.
[3] B. Spittle, Fluoride 26 (1993) 267.
[4] E.B. Bassin, Association between fluoride in drinking water during growth and development and the incidence of osteosarcoma for children and adolescents, Ph.D. Thesis, Harvard School of Dental Medicine, Boston, Massachusetts, 2001.
[5] M. Lamberg, H. Hausen, T. Vartiainen, Community Dent. Oral Epidemiol. 25 (1997) 291.
[6] P.L. Buldini, S. Cavalli, A. Trifiro, J. Chromatogr. A 789 (1997) 529.
[7] S.S. Goyal, J. Chromatogr. A 789 (1997) 519.
[8] S. Warnakulasuriya, C. Harris, S. Gelbier, J. Keating, T. Peters, Clin. Chim. Acta 320 (2002) 1.
[9] J.S. Fritz, D.T. Gjerde, C. Pohlandt, Ion Chromatography, Hüthing, Heidelberg, 1982.
[10] R. Slingsby, R. Kiser, Trends Anal. Chem. 20 (2001) 288.
[11] M. Laikhtman, J. Riviello, J.S. Rohrer, J. Chromatogr. A 816 (1998) 282.
[12] M.C. Quintana, M.H. Blanco, L. Hernandez, J. Liq. Chromatogr. Related Technol. 26 (2003) 763.
[13] M. Zhou, D. Guo, Microchem. J. 65 (2000) 221.
[14] Y. Huang, S.-f. Mou, J.M. Riviello, J. Chromatogr. A 868 (2000) 209.
[15] S.D. Kumar, B. Maiti, P.K. Mathur, Talanta 53 (2001) 701.
[16] B.M. De Borba, C.M. Kinchin, D. Sherman, T.K. Cook, P.K. Dasgupta, Anal. Chem. 72 (2000) 96.

Available online at www.sciencedirect.com
ScienceDirect
Talanta 71 (2007) 1096–1102
Talanta
www.elsevier.com/locate/talanta

Magnetic loading of carbon nanotube/nano-Fe_3O_4 composite for electrochemical sensing

Song Qu [a], Joseph Wang [b], Jilie Kong [a], Pengyuan Yang [a], Gang Chen [a,*]

[a] *Department of Chemistry, Fudan University, Shanghai 200433, China*
[b] *Departments of Chemical & Materials Engineering and Chemistry, Arizona State University, Tempe, AZ 85287-5001, USA*

Received 19 April 2006; received in revised form 31 May 2006; accepted 1 June 2006
Available online 10 July 2006

Abstract

An electrochemical sensing platform was developed based on the magnetic loading of carbon nanotube (CNT)/nano-Fe_3O_4 composite on electrodes. To demonstrate the concept, nano-Fe_3O_4 was deposited by the chemical coprecipitation of Fe^{2+} and Fe^{3+} in the presence of CNTs in an alkaline solution. The resulting magnetic nanocomposite brings new capabilities for electrochemical devices by combining the advantages of CNT and nano-Fe_3O_4 and provides an alternative way for loading CNT on electrodes. The fabrication and the performances of the magnetic nanocomposite modified electrodes have been described. Cyclic voltammetry (CV) and constant potential measurement indicated that the incorporated CNT exhibited higher electrocatalytic activity toward the redox processes of hydrogen peroxide. In addition, chitosan (CTS) has also been introduced into the bulk of the CNT/nano-Fe_3O_4 composite by coprecipitation to immobilize glucose oxidase (GOx) for sensing glucose. The marked electrocatalytic activity toward hydrogen peroxide permits effective low-potential amperometric biosensing of glucose, in connection with the incorporation of GOx into CNT/Fe_3O_4/CTS composite. The accelerated electron transfer is coupled with surface renewability. TEM images and XRDs offer insights into the nature of the magnetic composites. The concept of the magnetic loading of CNT nanocomposites indicates great promise for creating CNT-based biosensing devices and expands the scope of CNT-based electrochemical devices.
© 2006 Elsevier B.V. All rights reserved.

Keywords: Carbon nanotube; Magnetic loading; Electrochemical sensing; Composite; Magnetite; Hydrogen peroxide; Glucose

1. Introduction

Since Iijima reported the existence of carbon nanotubes in 1991 [1], they have attracted much attention because of their high electrical conductivity, mechanical strength and chemical stability [2,3]. The unique properties of carbon nanotube (CNT) make them extremely attractive for electrochemical sensors and biosensors [4–6]. Recent investigations demonstrated that CNT shows strong electrocatalytic activity and the minimization of surface fouling when it was employed to improve the electrochemical response of some important bioactive substances [7–10]. A variety of carbon nanotube electrodes have been fabricated for sensing different redox compounds, including CNT modified screen-printed carbon electrode [11], CNT powder microelectrode [12], CNT/Teflon composite electrode [13], CNT screen-printed electrode [14], CNT/epoxy composite electrode [15], CNT/copper composite electrode [16], etc.

To modify CNT on the surface of electrodes, CNTs were usually dispersed in solvents [17,18] or polymer solutions (such as Nafion [19] and chitosan (CTS) [20] solutions) that were cast on the electrodes because CNTs were insoluble in most solvents. Recently, methods based on electrochemical deposition [21] and electrochemical polymerization [22,23] have been employed for loading CNT on electrodes. CNT-based electrodes have been demonstrated to reduce the overpotential of hydrogen peroxide significantly [4,21]. The ability of carbon nanotubes to promote the electron-transfer reactions of hydrogen peroxide suggests great promise for oxidase-based amperometric biosensors [4]. However, the selectivity and stability of the electrochemical determination of hydrogen peroxide were usually inadequate at conventional electrodes because there is a large overpotential for the direct oxidation of hydrogen peroxide. A traditional

* Corresponding author. Tel.: +86 21 6466 1130; fax: +86 21 6564 1740.
E-mail address: gangchen@fudan.edu.cn (G. Chen).

0039-9140/$ – see front matter © 2006 Elsevier B.V. All rights reserved.
doi:10.1016/j.talanta.2006.06.003

approach to lowering the oxidation potential of hydrogen peroxide has relied on the use of redox mediators with low formal potentials [24].

Magnetic loading provides an alternative approach to load various materials on electrodes. Willner et al. have reported the magnetic control of enzymatic reactions using magnetic particles functionalized with redox relay units [25,26]. Ferrocene-functionalized magnetic particles were thus used for electrically contacting glucose oxidase (GOx) and the electrode. The use of magnetic fields to align CNT [27] and to self-assemble CNT devices [28] has been reported. Recently, Musameh and Wang have demonstrated that the magnetic and catalytic properties of CNT can be exploited for the magnetoswitchable control of electron-transfer reactions [29]. Herein, we report on a novel electrochemical-sensing platform for the detection of hydrogen peroxide based on the magnetic loading of carbon nanotube/nano-Fe_3O_4 (CNT/Fe_3O_4) composite on electrodes. The magnetic nanocomposite dispersed in water could be loaded onto the surface of magnetic electrode with the aid of the Fe_3O_4 nanoparticles. Although CNT/Fe_3O_4 nanocomposites have been synthesized to adsorb heavy metal ions [30] and to minimize the sedimentation of Fe_3O_4 particles [31], there is no earlier report on the magnetic loading of CNT/Fe_3O_4 composite on electrodes for electrochemical sensing.

In the present work, it has been demonstrated that magnetic CNT/nano-Fe_3O_4 composite prepared by coprecipitation exhibited excellent electrocatalytic ability in the reduction and oxidation of hydrogen peroxide. In addition, CNT/nano-Fe_3O_4/chitosan composite has also been prepared by coprecipitation to immobilize glucose oxidase covalently for sensing glucose. The attractive analytical performances of the magnetic nanocomposite modified electrodes, along with the characterization of the nanocomposites, are illustrated in the following sections.

2. Experimental

2.1. Reagent and solutions

β-D-Glucose and glucose oxidase (EC 1.1.3.4, from Aspergillus niger, 158 units/mg) were obtained from Sigma (St. Louis, MO, USA). Glutaraldehyde (25 wt.% solution in water) was the product of Merck (Germany). Chitosan (CTS, 75–85% deacetaylation) was purchased from Aldrich (Milwaukee, WI, USA). Multiwall carbon nanotubes (MWCNT, 30–60 nm diameter, 5–15 μm long), with a purity of 95%, were provided by Shenzhen Nanoport Company (Shenzhen, China). Ammonium ferrous sulfate and ammonium ferric sulfate were both purchased from SinoPharm (Shanghai, China). Other chemicals were all analytical grade.

The supporting electrolyte for the electrochemical investigations was 50 mM phosphate buffer (pH 7.4). Stock solutions of 1 M glucose were allowed to mutarotate for 24 h before use and subsequently kept in a 4 °C refrigerator, while solutions of hydrogen peroxide (1 M) were prepared by diluting a 30 wt.% a stocking solution with doubly distilled water. CTS solution (0.2 wt.%) was prepared by dissolving 0.4 g of CTS in 10 mg/mL acetic acid while GOx solution was made by dissolving 50 mg GOx in 10 mL of 50 mM phosphate buffer (pH 7.4). 5 mg/mL of glutaraldehyde solution was prepared by the appropriate dilution of 25 wt.% solution of glutaraldehyde using 50 mM phosphate buffer (pH 7.4).

2.2. Apparatus

Cyclic voltammetry (CV) and constant potential measurements were performed with a CHI 830B electrochemical analyzer (Shanghai Chen-Hua Instruments Co., Shanghai, China) in a three-electrode system consisted of a 2.2 mm diameter graphite-epoxy composite electrode with small magnets accommodated inside, a platinum auxiliary electrode, and a saturated calomel electrode (SCE) as the reference electrode. XRD measurements were carried out using a Rigaku D/max-rB diffractometer (Rigaku, Tokyo, Japan) with Cu Kα1 radiation (40 kV, 60 mA). The size and morphology of magnetic nanoparticles were observed by TEM using a JEOL model JEM-2011(HR) at 200 kV. The sample for TEM analysis was obtained by dipping a holy grid to nanoparticles-dispersed ethanol solution and evaporated in air at room temperature.

2.3. Preparation of CNT/Nano-Fe_3O_4 composites

Further purification of the multiwalled carbon nanotubes was accomplished by stirring the CNT in concentrated nitric acid at 60 °C for 12 h. Subsequently, the obtained CNT was dried at 110 °C for 4 h. The CNT/Fe_3O_4 nanoparticle composite was prepared by the *in situ* chemical coprecipitation of Fe^{2+} and Fe^{3+} in alkaline solution in the presence of CNTs. The molar ratio of Fe^{2+}:Fe^{3+} was 1:2. The magnetic composite was prepared by suspending 1.0 g purified CNT in 200 mL of solution containing 1.7 g (4.33 mmol) $(NH_4)_2Fe(SO_4)\cdot 6H_2O$ and 2.51 g (8.66 mmol) $NH_4Fe(SO_4)_2\cdot 12H_2O$ at 50 °C under N_2 atmosphere. After the solution was sonicated (30 W, 40 kHz) for 10 min, 10 mL of 8 M NH_4OH aqueous solution was added dropwise to precipitate the iron oxides while the mixture solution was sonicated. The pH of the final mixture should be in the range of 11–12. To promote the complete growth of the nanoparticle crystals, the reaction was carried out at 50 °C for 30 min under constant mechanical stirring. The precipitate was isolated in the magnetic field, and the supernatant was separated from the precipitate by decantation. Impurities (such as sulfate and ammonia) in the CNT/Fe_3O_4 samples were removed by washing with copious amounts of doubly distilled water and the precipitate was isolated by a permanent magnet. The obtained CNT/Fe_3O_4 nanocomposite was then washed with 150 mL of absolute alcohol for three times. Subsequently, the composite was dried under vacuum. The content of CNT in the composite was approximately 50 wt.%. If no CNT was added to the coprecipitation solution of Fe^{2+}:Fe^{3+}, pure Fe_3O_4 nanoparticles could be obtained for the control experiments. The chemical reaction of the Fe_3O_4 precipitation occurring in the container is as follows:

$$2Fe^{3+} + Fe^{2+} + 8NH_3\cdot H_2O = Fe_3O_4 + 4H_2O + 8NH_4^+$$

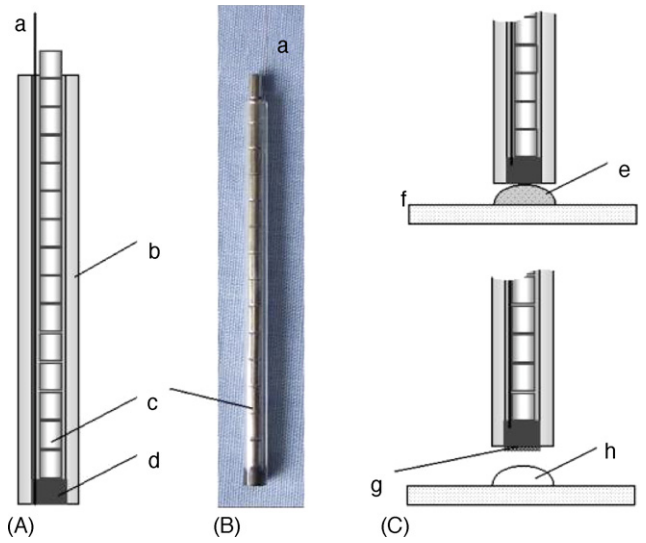


Fig. 1. Schematic diagram (A) and photograph (B) of the magnetic electrode and (C) schematic of the magnetic loading process on the CNT–Fe_3O_4 composite. (a) Copper wire, (b) glass tube, (c) NdFeB magnet, (d) graphite-epoxy composite electrode, (e) water drop with CNT/Fe_3O_4 composite dispersed inside, (f) Plexiglas plate, (g) CNT/Fe_3O_4 composite loaded on the electrode and (h) water drop.

When the CNT, ammonium ferrous sulfate and ammonium ferric sulfate involved in the above procedures were dissolved in 200 mL CTS solution (0.1 wt.%) instead of water, the obtained precipitate was CNT/Fe_3O_4/CTS composite. The primary amino groups of CTS in the composite can facilitate the immobilization of enzymes such as GOx. A 20 mg of the CNT/Fe_3O_4/CTS composite was dispersed in 2 mL of 5 mg/ml GOx solution by 1 min sonication and the mixture was kept in a 4 °C refrigerator for 2 h. And then, the supernatant was removed from the precipitate by decanting with the aid of a magnet. The precipitate was dispersed in 2 mL of 5 mg/mL of glutaraldehyde for 15 min to cross-link the primary amino groups of chitosan and GOx. The magnetic enzyme material was washed with water and immersed in 50 mM phosphate buffer (pH 7.4) at 4 °C overnight to remove the reagents and the excess nonimmobilized GOx from the composite. The obtained magnetic biosensing composite, CNT/Fe_3O_4/CTS/GOx, was dispersed in 10 mL of 50 mM phosphate buffer (pH 7.4) and was kept in a 4 °C refrigerator for future use.

2.4. Magnetic electrode fabrication

Fig. 1 illustrated schematic diagrams of the magnetic electrode. Epoxy resin and hardener (Zhejian Cixi Tiandong Adhesive Co. Ltd., Ningbo, China) were mixed thoroughly at a weight ratio of 2:1. Graphite powder (Aldrich, Wilwaukee, WI, USA) and epoxy resin/hardener were hand-mixed at a ratio of 1:1 (w/w). The graphite-epoxy composite was subsequently packed into a glass tube (Fig. 1(b), 2.2 mm i.d., 5 mm o.d., 60 mm long) by pressing the end into a sample of the composite to a depth of ~3 mm. A stainless-steel rod (1.5 mm diameter) was employed to press the graphite-epoxy composite (Fig. 1(d)) inside the tube to acquire a flat inner surface. A piece of copper wire (Fig. 1(a), 15 cm long, 50 μm diameter) was inserted into the glass tube with the aid of the stainless-steel rod until the twisted end of the copper wire was buried into the graphite-epoxy composite inside the glass tube. Subsequently, the composite was allowed to cure at room temperature for at least 12 h. Note that the copper wire should be immobilized just beside the inner wall of the glass tube so that NdFeB permanent magnets (Fig. 1(c), 1.5 mm diameter, 4 mm height, Shanghai Heng-qiang Magnetic Material Co. Ltd., Shanghai, China) could be taken out from the tube. Prior to use, the magnetic microdisc electrode was successively polished with emery paper and alumina powder, sonicated in doubly distilled water. Fig. 1B is the photograph of the magnetic electrode.

2.5. Magnetic loading

Before loading, 15 pieces of NdFeB permanent magnets mentioned above were inserted into the glass tube of the electrode until the magnet touched the inner surface of the graphite-epoxy composite electrode. 20 mg of the magnetic composites was dispersed in 10 mL of water with the aid of sonication and will be referred to as the loading solution. And then, 10 μL aliquots of this loading solution containing 20 μg CNT were taken out with a pipette under sonication and were dropped on the surface of a piece of clean Plexiglas plate. Glass plate could not work well because it is hydrophilic. The amount of the composite loaded on the magnetic electrode can be changed by controlling the volume of the loading solution on the Plexiglas plate. As shown in Fig. 1C, the carbon disc part of the magnetic electrode was allowed to touch the top of the water drop (Fig. 1(e)). The CNT/nano-Fe_3O_4 composite would move toward the surface of the electrode and aggregated there to form a modification layer (Fig. 1(g)). The magnets inside the electrode tube can prevent the magnetic particles from escaping. When the magnets inside tube were taken out, the magnetic modification layer could be removed by flushing with water or sonicating in water. Pure magnetite nanoparticles and CNT/Fe_3O_4/CTS/GOx could be loaded on the surface of the electrode in the same procedures. Based on the CVs before and after loading CNT/nano-Fe_3O_4 composite (not shown), the modification layer can be removed completely by sonication when the magnets were taken out.

2.6. Procedures

The cyclic voltammetry measurements were carried out in the desired potential range at a scan rate of 100 mV/s and no solution agitation was necessary during the run. Measurements of the amperometric response to the sample solution were performed at a desired potential while the solution was being magnetically stirred at 300 rpm continuously. Because the supporting electrolytes were magnetically stirred, the magnetic electrode should be inserted into the electrolyte through a hole inside the rubber plug on a cylinder electrochemical cell (20 mm i.d., 50 mm height) to prevent it from vibrating. The surface of the magnetic electrode was downwards and should be immersed into the solution for no more than 5 mm so that the influence of the magnetic stirrer could be minimized.

3. Results and discussion

In order to load the magnetic nanocomposite on the electrode, a specially designed magnetic electrode has been prepared by using NdFeB permanent magnets (Fig. 1). The magnets facilitate the magnetic loading of the nanocomposite and can prevent the composite from falling off in the solution. The magnetic electrode can carry a 0.5 g iron screw on its surface. When the magnets were taken away or put back, the magnetic composite loaded on the electrode would fall off or could be reloaded, allowing a simple and fast method for renewing the modification layer on the electrodes. Transmission electron microscopy (TEM) was performed to observe the microstructure of the magnetic composite powders. Fig. 2A illustrates the TEM image of the CNT/nano-Fe_3O_4 composite. The diameter of Fe_3O_4 nanoparticles in Fig. 2A is in the range of 10–30 nm. A higher resolution TEM image of the CNT/nano-Fe_3O_4 composite as shown in Fig. 2B illustrates the nature of the composite material. Although the composites had been sonicated in ethanol before TEM measurements, a great amount of Fe_3O_4 nanoparticles were found on the surface of CNTs, indicating the strong interaction between CNT and nano-Fe_3O_4. It could be concluded that the CNTs in the composite were coated with nano-Fe_3O_4 that facilitated the magnetic loading of CNT on the surface of the electrodes.

Fig. 2C displays the X-ray diffraction (XRD) patterns of CNT and the CNT/nano-Fe_3O_4 composite. Diffraction peaks assigned to CNTs at $2\theta = 26.5^\circ$ [32] can be clearly seen for both pure CNT and CNT/nano-Fe_3O_4 composite, indicating that the CNTs structure was not destroyed after the chemical coprecipitation of Fe_3O_4. As shown in Fig. 2C, the other two weak peak of CNT merged with that of Fe_3O_4. Six characteristic peaks for Fe_3O_4 ($2\theta = 30.2^\circ$, 35.6°, 43.3°, 53.7°, 57.3° and 62.8°), marked by their indices ((2 2 0), (3 1 1), (4 0 0), (4 2 2), (5 1 1) and (4 4 0)) [33], were observed for the CNT/nano-Fe_3O_4 composite, indicating that the resultant Fe_3O_4 particles in the composite were pure Fe_3O_4 with a spinel structure.

The magnetic lodging of magnetic CNT composite permits a variety of manipulations, including the modification of electrode surfaces and the fabrication of biosensors. The CNT/Fe_3O_4 association does not impair the electrocatalytic properties of CNT. Such behavior has been demonstrated for the redox processes of hydrogen peroxide that are of considerable interest for the operation of oxidase-based amperometric biosensors.

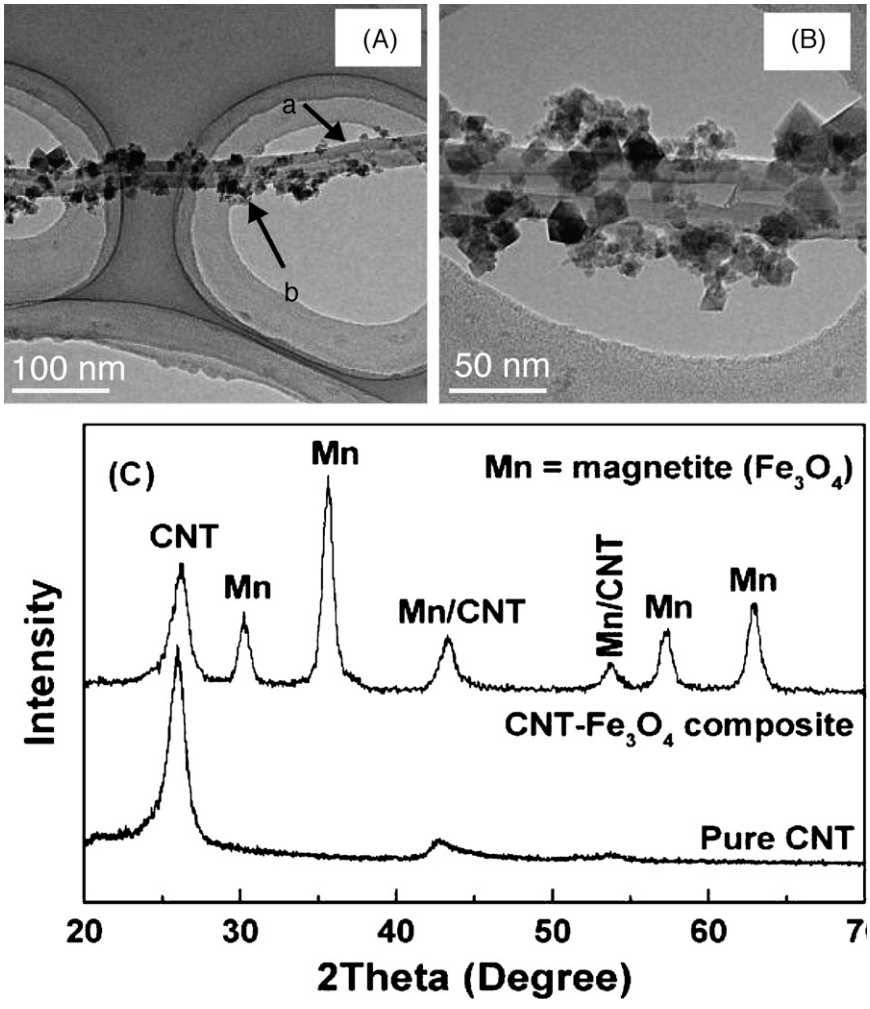


Fig. 2. (A and B) Typical transmission electron micrographs (TEMs) of the MWCNT/nano-Fe_3O_4 composite and (C) XRD pattern of CNTs and the CNT/Fe_3O_4 composites. (a) MWCNT and (b) Fe_3O_4 nanoparticles.

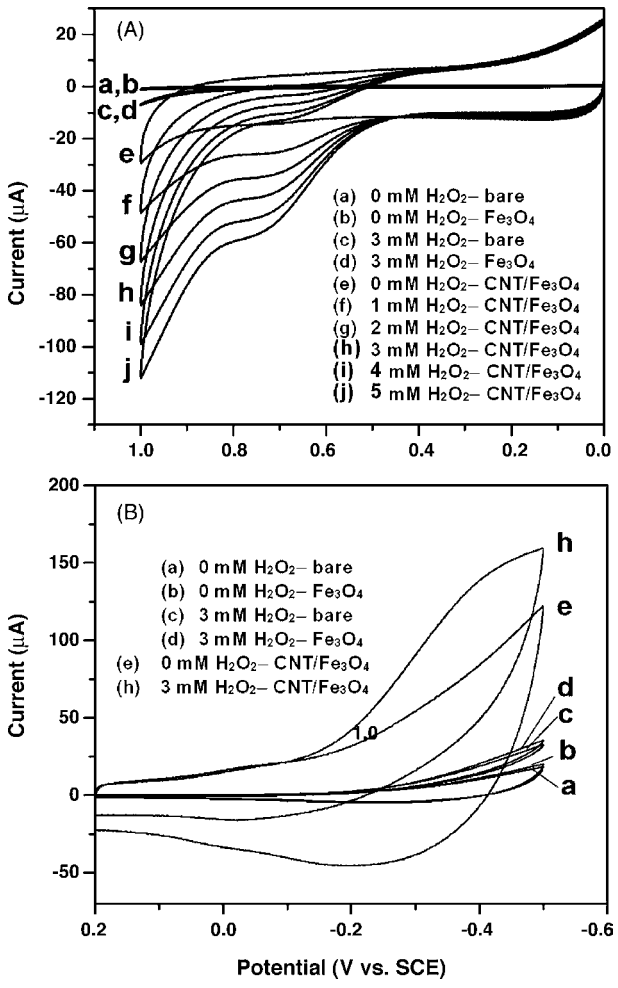


Fig. 3. Cyclic voltammograms of (a, b and e) 0, (f) 1, (g) 2, (c, d and h) 3, (i) 4, (j) 5 mM hydrogen peroxide in 0.05 M phosphate buffer solution (pH 7.4) at the bare (a and c), Fe_3O_4 nanopartile modified (b and d) and CNT/Fe_3O_4 composite modified (e–j) electrodes in the potential range of 0 to 1.0 (A) and 0.3 to −0.5 V (B). The amount of the loaded magnetic materials, 20 μg; scan rate, 100 mV/s.

Fig. 3 compares the cyclic voltammograms (CVs) of 0.05 M phosphate buffer solution (pH 7.4) containing (a, b, e) 0, (f) 1, (g) 2, (c, d, h) 3, (i) 4 and (j) 5 mM hydrogen peroxide at bare (a, c), Fe_3O_4 nanoparticle modified (b, d) and CNT/nano-Fe_3O_4 composite modified (e–j) electrodes at a scan rate of 100 mV/s. The electrode loaded with CNT/nano-Fe_3O_4 composite exhibits significantly enhanced currents for the oxidation and reduction of hydrogen peroxide starting around +0.45 and −0.1 V (versus SCE), respectively. Thus, the CNT/Fe_3O_4 modified electrode not only improves the redox currents but also decreases the overvoltage potential for the oxidation and reduction of hydrogen peroxide, allowing convenient low-potential amperometric detection. The catalytic activity can be demonstrated by the well-defined peaks at +0.7 V (A) and −0.36 V (B). Fig. 3A(e–j) illustrates that the addition of hydrogen peroxide to the supporting solution in the steps of 1 mM results in a nearly linear increase in the peak currents for the oxidation of hydrogen peroxide. In contrast, poor electrochemical response was obtained at the surface of both the bare (c) and the Fe_3O_4 (d) modified electrodes over the commonly used potential range. The oxidation current of hydrogen peroxide starts to increase at potentials that are higher than +0.85 V while the reduction currents increase at potentials that are lower than −0.3 V at both CNT-free electrodes. It can be concluded that Fe_3O_4 loaded on the magnetic electrodes does not exhibit electrocatalytic activity toward the redox processes of hydrogen peroxide and the elctrocatalytic activity of CNT/Fe_3O_4 loaded on the electrode mainly comes from CNT. The equations for the electrooxidation and electroreduction of H_2O_2 over CNT can be illustrated as follow:

$$H_2O_2 + 2H_2O - 2e \rightarrow 2H_3O^+ + O_2$$

$$H_2O_2 + 2H_3O^+ + 2e \rightarrow 4H_2O$$

The amount of CNT/Fe_3O_4 plays a crucial role in the electrocatalytic reduction of hydrogen peroxide. Fig. 4A shows the effect of the amount of CNT/nano-Fe_3O_4 composite on the amper-

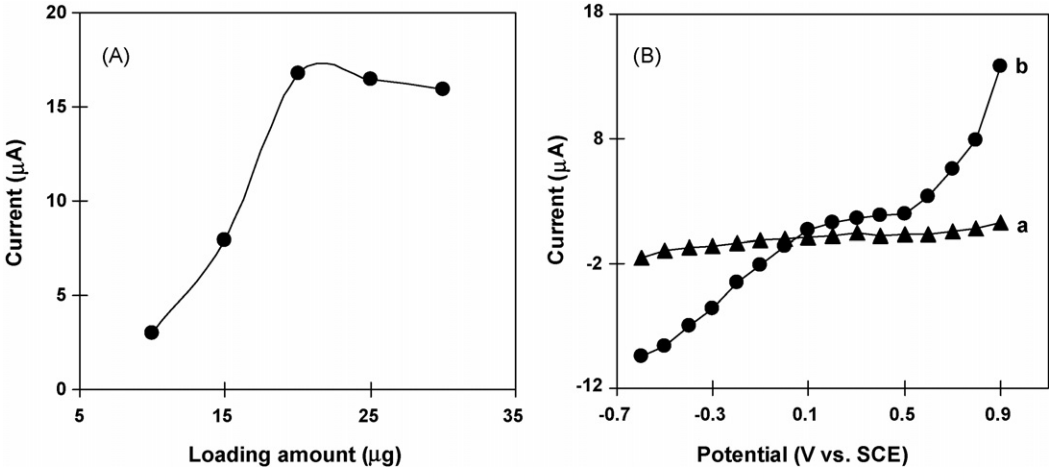


Fig. 4. (A) Effect of the amount of CNT/nano-Fe_3O_4 composite on the current response of 5 mM hydrogen peroxiode at potential of −0.1 V (vs. SCE) and (B) hydrodynamic voltammograms (HDVs) for 1 mM hydrogen peroxide at a bare (a) and a CNT/nano-Fe_3O_4 composite (b) electrode. The amount of the loaded composite, 20 μg; electrolyte, 50 mM phosphate buffer (pH 7.4); stirring rate, 300 rpm.

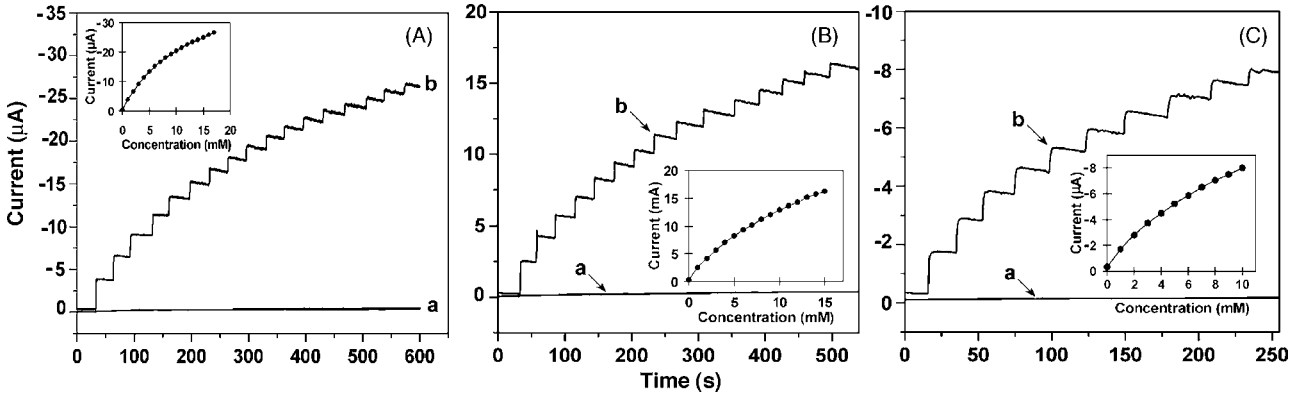


Fig. 5. Amperometric response of the bare (a) and the CNT/Fe_3O_4 composite modified (b) electrodes to the successive addition of 1 mM hydrogen peroxide at the potential of (A) −0.1 and (B) +0.4 V (vs. SCE). (C) Amperometric response of the bare (a) and the magnetic electrode loaded with Fe_3O_4/CNT/CTS–GOx composite (b) to the successive addition of 1 mM glucose at the potential of −0.1 V (vs. SCE). Also shown (in the insets) are the plots of amperometric currents versus the concentrations of hydrogen peroxide (A and B) and glucose (C) at the electrodes modified with magnetic CNT composite. Other conditions, as in Fig. 4.

ometric current response of 5 mM hydrogen peroxide at the constant potential of −0.1 V (versus SCE). The current increases to a value of 16.8 μA, upon raising the nanocomposite amount between 10 and 20 μg, and decreases gradually to 15.9 μA upon increasing the amount to 30 μg. The dropping of the current implies that the excess composite may disturb the mass transformation on the surface of the electrode. Fig. 4B compares the hydrodynamic voltammograms (HDVs) for 1 mM hydrogen peroxide at the bare electrode (a) and the CNT/Fe_3O_4 composite modified electrode (b). It is obvious that the current response for the oxidation and the reduction of hydrogen peroxide at the bare electrode was poor. A small response was observed at more positive or more negative potentials for the oxidation or reduction of hydrogen peroxide, respectively. In contrast, the CNT/Fe_3O_4 composite modified electrode exhibited enhanced current response with significant decrease in the overvoltages.

Such electrocatalytic activities facilitate the low-potential amperometric measurements of hydrogen peroxide. Fig. 5A compares the amperometric response (at −0.1 V) of the bare (a) and the CNT/Fe_3O_4 modified (b) electrodes to the successive additions of 1 mM hydrogen peroxide, along with the resulting calibration plots (insets). As expected from the voltammetric data, the bare and the Fe_3O_4 modified electrodes are not responsive to these concentration changes using this low detection potential. However, well-defined and fast amperometric signals are observed for these 1 mM-H_2O_2 additions at the CNT/Fe_3O_4 modified electrode, generating steady-state signals within 2–3 s. The CNT-based magnetic electrode offers substantially larger signals, reflecting the electrocatalytic activity of CNT (b). In addition, the hydrogen peroxide response was not affected by regenerating the surface of the electrode. Such renewability was indicated from a series of seven successive measurements each recorded on a freshly loaded surface, yielding satisfactory reproducible signals with relative standard derivation (R.S.D.) of 5.3% (not shown).

The CNT/nano-Fe_3O_4 coated electrodes exhibit highly electrocatalytic activity toward not only the reduction but also the oxidation of hydrogen peroxide. Fig. 5B illustrates the current-time recordings obtained by increasing the hydrogen peroxide concentration in the steps of 1 mM at the bare (a) and the CNT/Fe_3O_4 coated (b) electrodes at the detection potential of +0.4 V. The greatly enhanced amperometric response and the short response time (2–3 s) at the CNT-based device reflects the accelerated oxidation of hydrogen peroxide, in accordance with the HDV data illustrated in Fig. 4B. Although the oxidation potential has been significantly reduced to 0.3–0.5 V by the CNT/nano-Fe_3O_4 composite, some coexistent substances (such as dopamine, ascorbic acid, uric acid, etc.) in the body fluids at physiological levels may interfere with the determination because they are electroactive at the potentials above 0.2 V. So the glucose biosensor based on the magnetic loading of the CNT/Fe_3O_4/CTS/GOx composite on the base electrode was allowed to run at potential of −0.1 V in reduction mode so that the interferences of dopamine, ascorbic acid and uric acid were minimized. Fig. 5C illustrates the amperometric response of the magnetic electrode loaded with Fe_3O_4/CNT/CTS/GOx composite to the successive addition of 1 mM glucose. Well-defined current responses for glucose were obtained at the magnetic biosensor. The reaction occurring at the biosensor is very fast to reach a dynamic equilibrium upon each addition of the sample solution, generating a steady-state current signal within 5–6 s. The high sensitivity is accompanied by a low noise level (despite the large voltammetric background current). In order to test the selectivity of the magnetic biosensor, amperometric responses were obtained by a batch addition of interfering species (0.2 mM ascorbic acid, 0.2 mM uric acid and 0.2 mM dopamine) after the addition of 5 mM glucose. The interferences of dopamine, ascorbic acid and uric acid, have not been found because they are not electroactive at the detection potential of −0.1 V. Because chitosan dissolved in the acidic solution can be precipitated in alkaline solution, CTS was coprecipapted with Fe^{3+} and Fe^{2+} in the presence of CNT to form magnetic CNT/Fe_3O_4/CTS composite, a versatile biosensing material. The CNTs inside the composite form a conductive network that can accommodate Fe_3O_4, CTS and other functional components. The primary amino groups in CTS facilitate the further immobilization of enzyme, DNA or proteins, while the magnetic moiety of the composite provides conveniences for magnetic loading and magnetic isolation.

4. Conclusions

It has been demonstrated that CNT/nano-Fe_3O_4 composite can be magnetically loaded on electrodes for electrochemical sensing, providing an alternative rapid way for creating CNT-based devices for electrochemical sensing by combining the advantages of CNT and nano-Fe_3O_4. Various chemical and biological components could be readily incorporated into the bulk of the magnetic nanocomposite by coprecipitation and cross-linking. It has been demonstrated that the CNT/nano-Fe_3O_4 composite loaded on the electrode with the aid of magnets offered an electrocatalytic platform for electrochemical sensing. The magetic nanocomposite can be removed upon taking away the magnets inside the electrodes, providing a useful avenue for preparing renewable CNT-based biosensors and CNT modified electrodes. The biosensor fabrication technology demonstrated in this work is readily applicable to the fabrication of other biosensors based on oxidases, such as biosensors for cholesterol, alcohol, lactate, acetylcholine, choline, hypoxanthine, xanthine, etc. In addition, other carbon materials such as graphite powder, activated carbon or carbon black can also be coated with magnetic nanoparticles by the procedures developed in this work for electrochemical sensing, solid-phase microextraction, etc.

Acknowledgments

This work was supported by Shanghai Science Committee (051107089 and 2004ZR140150212), NSFC (20405002), State Education Ministry of China and the 863 program of China.

References

[1] S. Iijima, Nature 354 (1991) 56–58.
[2] R.H. Baughman, A. Zakhidov, W.A. de Heer, Science 297 (2002) 787–792.
[3] P.M. Ajayan, Chem. Rev. 99 (1999) 1787–1799.
[4] J. Wang, Electroanalysis 17 (2005) 7–14.
[5] R.S. Chen, W.H. Huang, H. Tong, Z.L. Wang, J.K. Cheng, Anal. Chem. 75 (2003) 6341–6345.
[6] J. Wang, M. Musameh, Anal. Chem. 75 (2003) 2075–2079.
[7] Z.H. Wang, J. Liu, Q.L. Liang, Y.M. Wang, G. Luo, Analyst 127 (2002) 653–658.
[8] G. Zhao, S.Q. Zang, K.Z. Liu, S. Lin, J. Liang, X.Y. Guo, Z.J. Zhang, Anal. Lett. 35 (2002) 2233–2244.
[9] J. Wang, M. Musameh, Analyst 128 (2003) 1382–1385.
[10] M. Musameh, J. Wang, A. Merkoci, Y.H. Lin, Electrochem. Commun. 4 (2002) 743–746.
[11] J. Wang, G. Chen, M.P. Chatrathi, M. Musameh, Anal. Chem. 76 (2004) 298–302.
[12] Y.D. Zhao, W.D. Zhang, H. Chen, Q.M. Luo, Talanta 58 (2002) 529–534.
[13] J. Wang, M. Musameh, Anal. Chem. 75 (2003) 2075–2079.
[14] J. Wang, M. Musameh, Analyst 129 (2004) 1–2.
[15] G. Chen, L.Y. Zhang, W. Wang, Talanta 64 (2004) 1018–1023.
[16] J. Wang, G. Chen, M. Wang, M.P. Chatrathi, Analyst 129 (2004) 512–515.
[17] H. Luo, Z. Shi, N. Li, Z. Gu, Q. Zhuang, Anal. Chem. 73 (2001) 915–920.
[18] F.H. Wu, G.C. Zhao, X.W. Wei, Electrochem. Commun. 4 (2002) 690–694.
[19] J. Wang, M. Musameh, Y. Lin, J. Am. Chem. Soc. 125 (2003) 2408–2409.
[20] M. Zhang, A. Smith, W. Gorski, Anal. Chem. 76 (2004) 5045–5050.
[21] X.L. Luo, J.J. Xu, J.L. Wang, H.Y. Chen, Chem. Commun. 16 (2005) 2169–2171.
[22] M.L. Guo, J.H. Chen, J. Li, B. Tao, S.Z. Yao, Anal. Chim. Acta 532 (2005) 71–77.
[23] M. Gao, S. Huang, L. Dai, G. Wallace, R. Gao, Z. Wang, Angew. Chem. Int. Ed. 39 (2000) 3664–3667.
[24] J. Wang, Electroanalysis 13 (2001) 983–988.
[25] R. Hirsch, E. Katz, J. Wasserman, I. Willner, J. Am. Chem. Soc. 122 (2000) 12053–12054.
[26] E. Katz, I. Willner, Electrochem. Commun. 4 (2001) 201–204.
[27] M. Fujiwara, E. Oki, M. Hamada, Y. Tanimoto, I. Mukouda, Y. Shimomura, J. Phys. Chem. A 105 (2001) 4383–4386.
[28] D. Long, J. Lazorcik, R. Shahidhar, Adv. Mater. 16 (2004) 814–819.
[29] M. Musameh, J. Wang, Langmuir 21 (2005) 8565–8568.
[30] X.J. Peng, Z.K. Luan, Z.C. Di, Z.G. Zhang, C.L. Zhu, Carbon 43 (2005) 855–894.
[31] H.T. Pu, F.J. Jiang, Nanotechnology 16 (2005) 1486–1489.
[32] W.Z. Zhu, D.E. Miser, W.G. Chan, M.R. Hajaligol, Mater. Chem. Phys. 82 (2003) 638–647.
[33] D.H. Chen, M.H. Liao, J. Mol. Catal. B Enzyme 16 (2002) 283–291.

Available online at www.sciencedirect.com
ScienceDirect
Talanta 71 (2007) 1054–1060
Talanta
www.elsevier.com/locate/talanta

Role of Ion exchange in permeation processes

Jayshree Ramkumar [a], Tulsi Mukherjee [b,*]

[a] *Analytical Chemistry Division, Bhabha Atomic Research Centre, Trombay, Mumbai 400085, India*
[b] *Chemistry Group, Bhabha Atomic Research Centre, Trombay, Mumbai 400085, India*

Received 1 May 2006; received in revised form 29 May 2006; accepted 29 May 2006
Available online 13 July 2006

Abstract

The single ion transport of transition metal ions like Cu^{2+}, Co^{2+}, Ni^{2+} and Zn^{2+} were carried out through the H^+ and alkali metal ion forms of Nafion membrane. These studies showed that the ion exchange selectivity coefficient of the permeating ion had an effect on its transport process. It was found that the diffusion coefficient values (D) were directly proportional to the selectivity coefficient (K). This shows that the initial stage of permeation is governed by ion exchange process (effect of K on D).
© 2006 Elsevier B.V. All rights reserved.

Keywords: Single ion transport; Pre-treatment; Correlation between diffusion coefficient and ion exchange selectivity

1. Introduction

Study of transport process in membranes is of recent origin but it has been pursued with great vigour ever since a number of synthetic ion exchange resins of high selectivity were synthesized [1–3]. The separation of a metal ion from a multi-ionic mixture by selective transport through membrane processes was of importance from both fundamental and practical viewpoints. For the selective permeation, the desired metal ion in a mixture has to be preferentially sorbed into the membrane phase and then be transported across the membrane phase. Subsequently, such membranes were used for desalination purposes. An appropriate driving force was essential for an uphill transport (building up of the concentration of the permeating ion across the concentration gradient). The driving force could be due to difference in pH of the solutions, concentration difference of the permeating species or an electrical potential. The pH difference was generally responsible for the transport in liquid membrane systems, whereas the electrical potential difference was the driving force for the transport across ion exchange membranes. Donnan dialysis was essentially the transport of the charged species across a membrane due to concentration difference. The combined effect of electrical potential difference and concentration gradient results in the process of electro-dialysis. Ion exchange membranes, used in electro-dialysis permit the separation of the species, without any change in the phase. Depending on the type of the driving ion used, Donnan dialysis can be applied to the recovery of metal ions from wastewater. There were many studies on the use of ion exchange membranes for Donnan dialysis [4]. Electro-dialysis was principally used for the production of brine from seawater. For this specific application, special cation exchange membranes were often used to reduce the permeability of alkaline earth metal ions with respect to sodium ions [5]. Since ion exchange membranes were used for various purposes, requirements for membranes with specific properties have increased.

Ion exchange membranes find many industrial applications primarily due to their property of perm-selectivity. The term perms-electivity denotes the difference in permeability between the ions of opposite charges. It is to be mentioned that the perm-selectivity of a membrane is a function of various external parameters. The ion exchange between two solutions separated by a perm-selective cation exchange membrane [6] or an anion exchange membrane [7] has been studied in detail and a few possible analytical applications have been pointed out. There were several reports on the permeation of neutral substances [8], heterocyclic bases [9] and cations [10,11]. Knowledge of the basic transport phenomena of ions in ion exchange membranes was important for the applications of these membranes. Several studies on the development of mathematical models for predicting and correlating the rates were found in literature [12].

* Corresponding author. Tel.: +91 22 25595234; fax: +91 22 25505331.
E-mail address: mukherji@barc.gov.in (T. Mukherjee).

0039-9140/$ – see front matter © 2006 Elsevier B.V. All rights reserved.
doi:10.1016/j.talanta.2006.05.082

The transport behaviour of various transition metal ions like Cu^{2+}, Co^{2+}, Ni^{2+} and Zn^{2+} through the H^+ and alkali metal ion forms of Nafion membrane has been studied in detail. It was expected that there would be a possible effect of the ion exchange selectivity coefficient of the permeating ion on its transport process.

2. Experimental

2.1. Reagents

i Circular pieces of Nafion membranes (35 mm diameter approximately) were pre-treated in different ways as follows:
- N: Nafion was immersed in cold 2 M HCl for 3 h.
- AT: Nafion was refluxed with 1:1 HNO_3 for 1 h, and then boiled with distilled water (∼60 °C) for 0.5 h.
- WT: Nafion was boiled with distilled water for 1 h, and then immersed in cold 2 M HCl for 3 h.

It was then washed well and stored under distilled water till further use.

ii EDTA solution: 18.6 g of disodium salt of ethylene diammine tetraacetic acid (BDH AnalaR) and dissolved in 500 ml of distilled water to give a stock solution of 0.1 M. A suitable volume of this stock solution was added when required.

iii Sodium acetate solution: 6.8 g of the salt (E. Merck GR) was dissolved in 500 ml of distilled water to give a stock solution of 0.1 M. This solution was used along with acetic acid for pH adjustments.

iv Metal ion solutions: the alkali metal ion solutions were prepared by dissolving the appropriate amounts of their chloride salts in distilled water. The transition metal ion solutions were prepared by dissolving suitable amounts of their salts in dilute acid. And these solutions were standardized by EDTA titrations using suitable metallochromic indicators.

2.2. Procedure

The experimental set-up is given in Fig. 1. The permeation experiments were carried out in a U type cell specially designed for this purpose. Two flat ground ends of standard flanged joints FG 15 (Quick Fit, UK) were each connected to a glass tube bent at an angle of 90°. Circular pieces of clean swollen membrane (pre-treated differently) were equilibrated with metal ion solutions for three hours to convert them into desired alkali metal ionic form. These membranes (designated as M^{n+}–N, M^{n+}–AT and M^{n+}–WT where M refers to the alkali metal ion and N, AT, WT refer to the type of pre-treatment carried out), with an effective area of permeation of 254 mm^2, were held tightly in between the joints clamped mechanically to provide a leak proof system. The two compartments on either side of the membrane are designated as the feed (F) and receiving (R) compartments. The feed compartment was filled with a definite volume (20 ml) of solution of the particular transition metal ion of 0.01 M at a pH of 4. The receiving compartment contained an equal volume of solution of EDTA or NaOH of known concentration at a suitable pH. The solutions in both the compartments were continuously stirred using magnetic stirrers (s) to reduce concentration polarization.

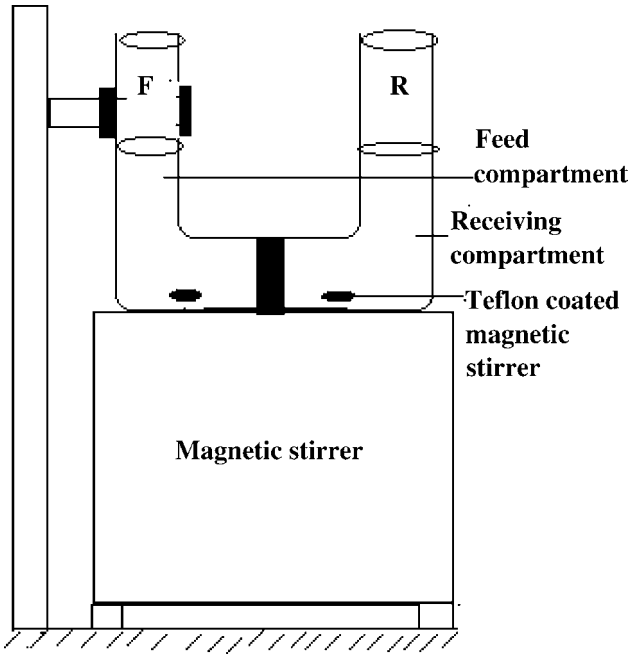


Fig. 1. Permeation Cell.

The concentrations of Cu^{2+} and Ni^{2+} in the receiving compartment were determined spectrophotometrically [13] by measuring the absorbance of the EDTA complexes directly. The concentration of cobalt as its EDTA complex was determined by using phosphomolybdic acid [14]. For the permeation of Zn^{2+} the receiving compartment contained 0.1 M NaOH. The concentration of Zn^{2+} permeated was monitored at regular intervals by withdrawing 1ml of the receiving solution and treating it with Zincon reagent at pH of 9–10 using ammonia and measuring the absorbance at 580 nm [15].

The absorbance measurements were carried out using a Shimadzu 210 A UV–vis spectrophotometer using a 1 cm quartz cell. The pH measurements were carried out using EIL 7030 pH meter equipped with a combination electrode.

About 0.25 g of Nafion in the H^+ forms were equilibrated with 25ml of mixture of metal chloride and HCl (MCl_2 + HCl) (where M = Cu^{2+}, Ni^{2+}, Co^{2+}, Zn^{2+}) solutions overnight. The concentrations of both MCl_2 and HCl were 0.1 M but the volumes of MCl_2 and HCl in the mixture were varied to give different equivalent fraction in the resin phase. The composition of the metal ions left behind in the aqueous phase was estimated by complexometric titrations with EDTA (sodium salt of ethylenediammine tetraaceticacid) using suitable metallochromic indicators [13]. The equilibrium compositions of the exchanger and solution phases were obtained from the initial composition of the solution, the amount of exchanger used, its capacity and the transition metal ion at equilibrium.

3. Results and discussion

The pendant $-SO_3H$ groups in the perfluorinated ionomer form clusters of 40 Å diameter separated by a distance of 50 Å

Table 1
Concentration profiles in permeation cell compartments Cu^{2+}–AT after 3 h

Feed compartment		Receiving compartment	
Initial $[Cu^{2+}]$ (mol l^{-1})	Decrease in $[Cu^{2+}]$ (mol l^{-1})	[EDTA] (mol l^{-1})	Increase in $[Cu^{2+}]$ (mol l^{-1})
NIL	NIL	NIL	$<10^{-5}$
NIL	NIL	5×10^{-2}	1.0×10^{-4}
3×10^{-3}	2.1×10^{-3}	5×10^{-2}	2.0×10^{-3}
1×10^{-2}	4.5×10^{-3}	5×10^{-2}	4.6×10^{-3}

and inter-connected through channels of 10 Å when swollen in water [16,17]. The high acidity of the SO_3H group was responsible for a quantitative neutralization of the membrane by other metal ions. When a cation exchange membrane separates two solutions of a given electrolyte of different concentrations, the cation will permeate from the concentrated to the dilute solution as a result of the concentration gradient.

Since Nafion is a cation exchange membrane, it was thought that the pH of the external solution would affect the affinity of the membrane towards different metal ions. However a high degree of selectivity in the uptake of these metal ions cannot be obtained by controlling the pH alone. The only way to bring about selectivity is to ensure that only the metal ion of interest is present as cationic species. As the permeation of co-ions (anions) across a cation exchange membrane was low (because of the perm-selectivity), the use of complexing agents, which form anionic metal complexes, can prevent the permeation of other cations. Similarly, the complexing agents could be used to prevent the back permeation of metal ion from the receiving phase and thus enhanced the permeation process. Hence, in all the studies, EDTA was used in the receiving side to form anionic metal complexes. The role of EDTA in enhancing the permeation process can be understood from the nature of equilibrium involved in the receiving compartment. This can be represented by the following equation:

$$2Na + \overline{Cu} \leftrightarrow Cu + 2\overline{Na}$$

Addition of EDTA to this compartment results in the complexation of Cu^{2+} in the solution and so the equilibrium is shifted towards the right. The deficiency of Cu^{2+} concentration in the membrane phase was compensated by further uptake of the metal ion from the feed compartment. This continued till equilibrium was reached. If it is assumed that the cations are transported across the membrane only due to ion exchange process, the permeation of Cu^{2+} would involve the transport of other cations (Na^+) from the receiving to the feed compartment. The excess of Na^+ is available from the buffer and also that released due to complexation of Cu^{2+} with EDTA.

The transport behaviour of transition metal ions through Nafion membranes equilibrated with alkali metal ions were carried out to understand the role of ion exchange selectivity on permeation process. It was thought that if permeation were influenced by ion exchange selectivity, there would be a definite correlation between the diffusion coefficients of transition metal ion with respect to its ion exchange selectivity coefficient.

In order to understand the various aspects of permeation, initial experiments were carried out on the permeation of Cu^{2+} across the Nafion membrane in Cu^{2+} form. The results of this experiment are given in Table 1. In this experiment, it was observed that the leaching of Cu^{2+} from the membrane on equilibration with de-ionized water for more than 3 h was negligible while the amount leached with EDTA was quite small but measurable. These observations were quantified from the leaching experiments. The results of mass balance experiments with Cu^{2+} ion in the feed show that the loss in concentration in the feed compartment was equivalent to the gain in the receiving compartment. Any leaching from the membrane phase was automatically compensated by the permeation from the feed. These results show that the self-leaching of Cu^{2+} ion was negligible. Experiments show that the number of moles of Cu^{2+} ion permeated in a given time (after 5 h) was dependant on the initial concentration of the feed solution. These results are given in Table 2. The decrease in permeation could be due to the deviation of the system from Donnan distribution law at high ionic concentration. Moreover, the high cation concentration was likely to block the diffusion pathway and lower the permeation rate.

It was seen that the permeation rate was affected by factors like pH, reagent and buffer concentrations. It was observed that the permeation rate was independent of pH between 3 and 5.5. There was a marginal increase with increase in the concentration of EDTA in the narrow range of 0.025–0.05 M. Since a high EDTA concentration in the receiving compartment results in a simultaneous increase in the Na^+ concentration, the permeation decreases. Therefore, all the permeation studies were carried out using 0.05 M EDTA as the receiving solution. The concentration of the pure salt solution in the feed was around 0.05 M because the ion exchange studies were carried out under these conditions.

The concentration profiles for the transport of transition metal ions through Nafion equilibrated with alkali metal ions are given in Figs. 2–4. Most of the studies used the Nernst–Planck equation to describe the relation between transfer rates of permeating species and forces acting on the system [18]. The following assumptions were made to arrive at the equation that describe the transport process: (i) system was diffusion-controlled; (ii) under conditions of no current flow, the sum of the fluxes of the

Table 2
Dependence of the amount of permeate on the feed concentration

$[Cu^{2+}]$ (M)	% Permeated
2.5×10^{-3}	75
5.0×10^{-3}	68
7.5×10^{-3}	56
1.0×10^{-2}	51

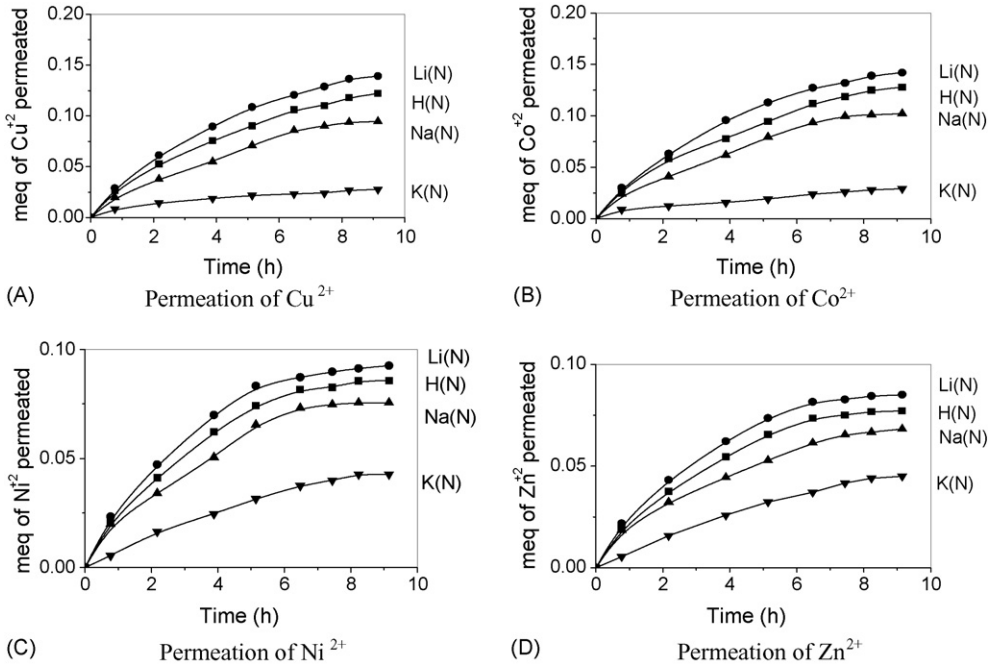


Fig. 2. Concentration profiles of transition metal ions through Nafion sample N.

two ions (in opposite directions) was zero; (iii) amount of co-ions in the membrane was smaller compared to the ion exchange capacity and no co-ions permeate; (iv) thermodynamic equilibrium exists at the membrane-solution interface; (v) osmotic water flow across the membrane can be ignored; (vi) overall electro-neutrality was maintained, i.e. the total concentration of counter ions in the membrane phase was equal to that of fixed ions, which was denoted by the exchange capacity (Q). Eqs. (1) and (2) mathematically represent the conditions (ii) and (vi), respectively.

$$z_A C_{AM} + z_B C_{BM} = Q \tag{1}$$

$$z_A J_A + z_B J_B = 0 \tag{2}$$

where z_A, C_{AM} and J_A refer to the charge, concentration of the ion in the membrane phase and molar flux of the species A, respectively. Fick's first law can describe the molar flux J of the solute through the membrane [19]. Integration between the

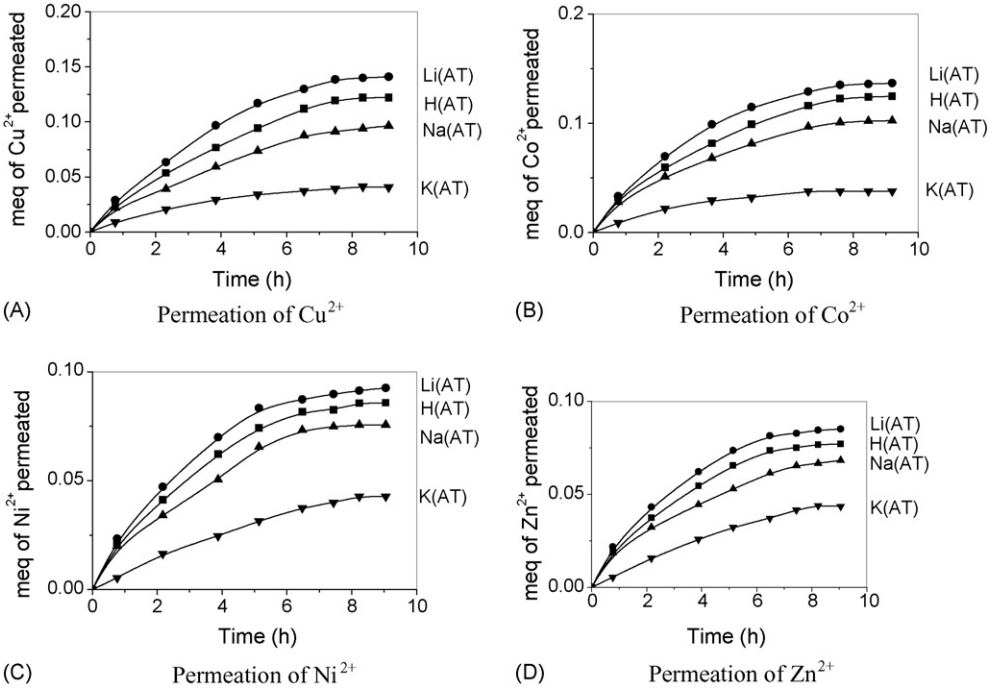


Fig. 3. Concentration profiles of transition metal ions through Nafion sample AT.

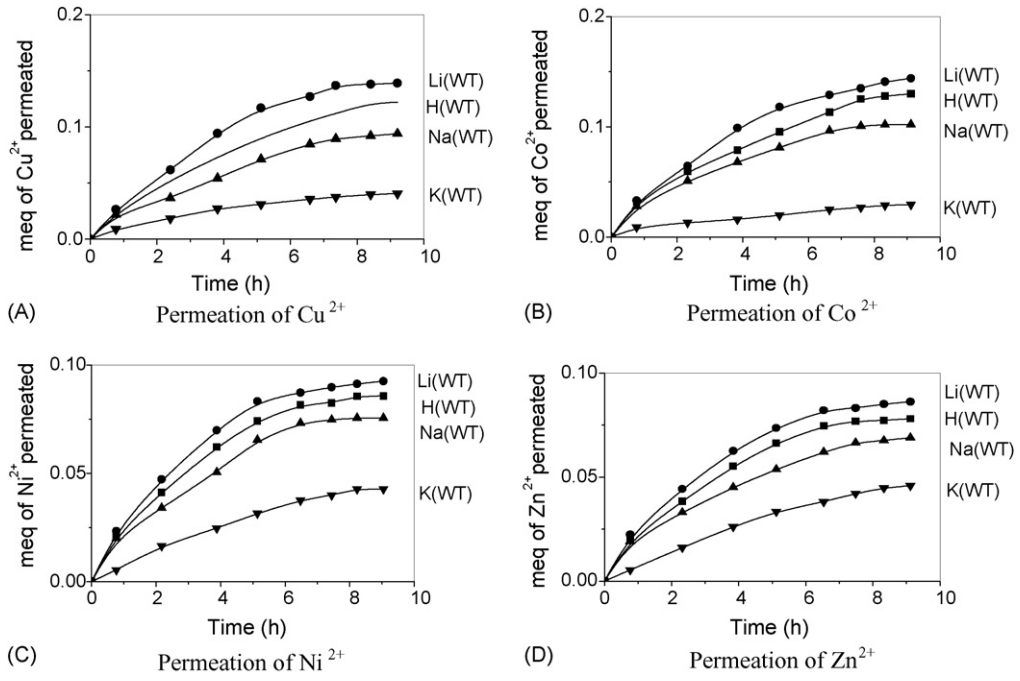


Fig. 4. Concentration profiles of different transition metal ions through Nafion sample WT.

membrane surfaces in contact with the feed and the receiving solutions gives:

$$J = \frac{D(C_{FM} - C_{RM})}{\delta} \tag{3}$$

where D was the diffusion coefficient of the permeating solute, δ was the thickness of the membrane, C_{FM} and C_{RM} denote the concentrations of the permeating species at the membrane surfaces in contact with the feed and receiving solutions. The flux was also correlated to the change in the concentration of the solute in the receiving phase using the mass balance equation where, V_R and C_R were the volume and solute concentration of the receiving solution and A was the effective area available for permeation.

$$J = \left(\frac{V_R}{A}\right) \times \left(\frac{\delta C_R}{\delta t}\right) \tag{4}$$

Since the C_{FM} and C_{RM} were not easily measured, an equilibrium relationship between the concentration of the solute in the membrane phase and that in the bulk solution was required. It was seen that there exists ion exchange equilibrium on either side of the membrane interface. Taking this into account can help us to calculate the C_{FM} and C_{RM}.

Consider the two sides of the membrane in contact with the ions in solutions.

Feed			**Receiving**	
$A + \overline{B} \leftrightarrow B + \overline{A}$			$B + \overline{A} \leftrightarrow A + \overline{B}$	
$K_B^{A_F} = [\overline{A}]_F^{zB}[B]_F^{zA} / [A]_F^{zB}[\overline{B}]_F^{zA}$	(5)	**M E M B R**	$K_B^{A_R} = [A]_R^{zB}[\overline{B}]_R^{zA} / [\overline{A}]_R^{zB}[B]_R^{zA}$	(7)
$K_B^{A_F} = [\overline{A}]_F[B]_F^2 / [A]_F[\overline{B}]_F^2$	(6)		$K_B^{A_R} = [A]_R[\overline{B}]_R^2 / [\overline{A}]_R[B]_R^2$	(8)

Here the bars represent the metal ion in the membrane phase.

It was seen that the ion exchange equilibrium operating on the two sides of the membrane were represented by their respective selectivity coefficients, K. If A and B were the same, the effect of these ion exchange reactions will be the same and will not be very obvious. The effect of K will be more pronounced when A and B on the two sides were different. In the experiments carried out in the present permeation study, A was di-valent and B was mono-valent, i.e. zA = 2 and zB = 1.

If a system consists of two solutions of different compositions separated by a cation exchange membrane, there exists a thermodynamic equilibrium [6]. Therefore, the exchange of ions follows a stoichiometric ratio. Using this principle, it was easy to calculate the concentration of Na^+ permeated into the feed compartment. The concentrations of Cu^{2+} on the membrane surface, near the feed and receiving solutions were calculated using Eqs. (6) and (8), respectively, as follows: If the feed contains a solution of Cu^{2+} of known concentration, membrane was in the Na^+ form, and the receiving phase contained Na^+ ion (as EDTA used was in its di sodium form), then the following ion exchange equilibrium would operate at the two sides of the membrane.

Feed compartment:

$$Cu + 2\overline{Na} \Leftrightarrow \overline{Cu} + 2Na \tag{9}$$

$$K_{Na}^{Cu_F} = \frac{[\overline{Cu}]_F[Na]_F^2}{[Cu]_F[\overline{Na}]_F^2} \tag{10}$$

The initial concentrations of Cu^{2+} and Na^+ in the feed and receiving compartments were known. From the transport experiments, the concentration of Cu^{2+} in the receiving phase was determined and therefore it is possible to calculate the values of $[Na]_F$ and also of $[\overline{Cu}]_F$.

Table 3
Diffusion coefficients (D X 10^8) cm^2/s of permeating transition metal ions

	Cu^{2+}			Co^{2+}			Ni^{2+}			Zn^{2+}		
	N	AT	WT	N	AT	WT	N	AT	WT	N	AT	WT
Li^+	1.87	1.48	9.98	2.44	3.23	7.37	1.47	1.39	2.34	1.24	1.40	2.60
H^+	1.16	1.05	4.59	1.28	2.38	3.38	1.11	1.12	1.37	0.92	1.07	1.85
Na^+	1.13	0.98	4.51	1.43	1.99	3.46	1.40	1.41	1.57	0.75	0.99	1.59
K^+	0.05	0.27	0.59	0.03	0.17	0.19	0.34	0.42	0.24	0.40	0.57	0.95

Receiving compartment:

$$\overline{Cu} + 2Na \Leftrightarrow Cu + 2\overline{Na} \tag{11}$$

$$K_{Cu}^{Na_R} = \frac{[Cu]_R[\overline{Na}]_R^2}{[\overline{Cu}]_R[Na]_R^2} \tag{12}$$

The concentrations of Cu^{2+} (determined experimentally) and Na^+ in the receiving phase were known. The concentration of Na^+ in the membrane phase was represented as:

$$\overline{Na}_R = \overline{Na}_F - \overline{Cu}_R \tag{13}$$

Therefore, Eq. (12) can be rewritten as:

$$K_{Cu}^{Na_R} = [Cu]_R \frac{(\overline{[Na]}_F[\overline{Cu}]_R)^2}{[\overline{Cu}]_R[Na]_R^2} \tag{14}$$

Using the above equation, the concentration of Cu^{2+} on the membrane surface adjacent to the receiving solution can be calculated.

Combining the Eqs. (3) and (4), we get

$$\left(\frac{\delta C_R}{\delta t}\right) = D \times A \frac{(C_{FM} - C_{RM})}{(V_R \times \delta)} \tag{15}$$

Since all the parameters except D were known, we can use Eq. (15) to calculate D for each transport experiment. The values of D calculated for each of the single ion transport were given in Table 3.

It is seen that when a transition metal ion say Cu^{2+} permeates through Nafion incorporated with alkali metal say Na^+, then from Eqs. (9) and (10), it is clear that the ion exchange reaction between Cu^{2+} in solution and Na^+ in the resin phase will

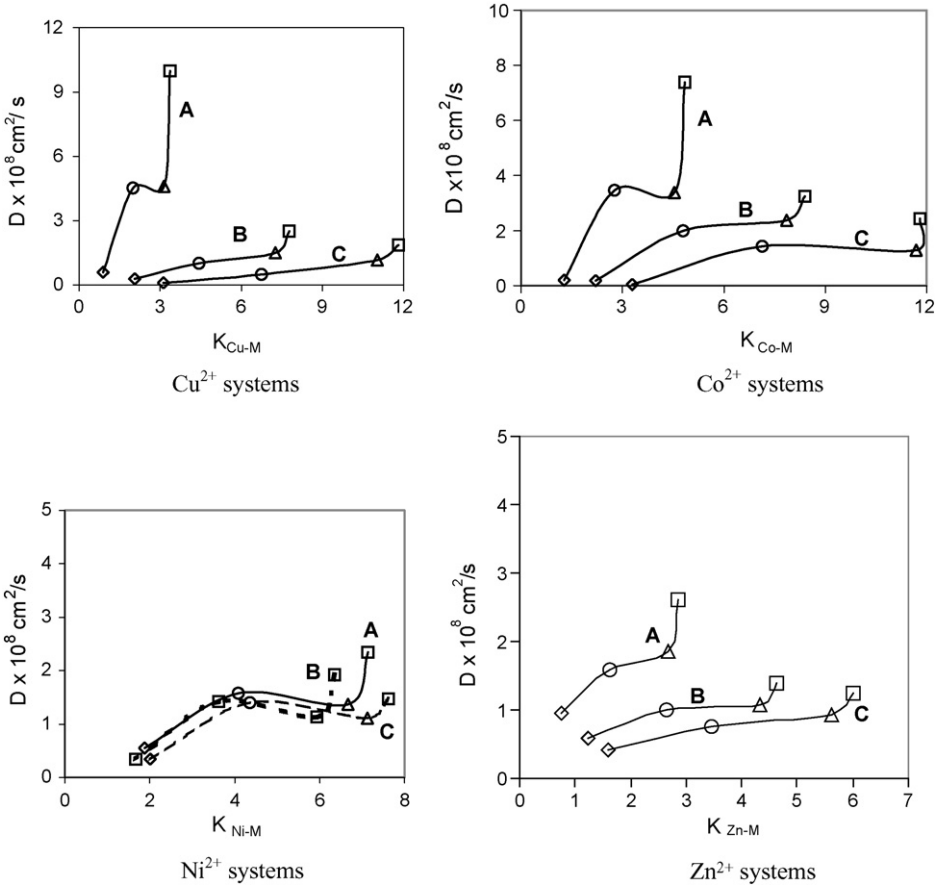


Fig. 5. Plots of D vs. K for different transition metal ions using Nafion. A, B and C refer to the curves for the samples WT, AT and N, respectively. (□) denotes Li^+, (△) denotes H^+, (◯) denotes Na^+ and (◇) denotes K^+.

definitely affect the transport rate. Hence the ion exchange selectivity of this reaction is expected to affect the D value. It is known that cation exchangers have lower selectivity for Li^+ than that of H^+. Therefore the ion exchange selectivity K for Cu^{2+}–Li^+ is higher than that of Cu^{2+}–H^+. Fig. 5 gives the plots of diffusion coefficient (D) versus selectivity coefficient (K). It was seen that the D values were dependent on the K value. As K increases, D also increases. This shows that the initial ion exchange was an important factor, which affects the permeation rate (as given by D). The nature of pre-treatment of Nafion has an effect on its K value and therefore on D. It was seen from that the WT samples have the maximum value for D. This can be understood as follows. After the initial ion exchange with the counter-ion in the membrane phase, the permeating ion was stripped in the receiving phase. Hence if the affinity for the particular ion of the membrane was high, the stripping will be low and therefore the diffusion coefficient value will also be low.

4. Conclusions

It is seen from the above studies that the ion exchange plays a key role in the permeation of ions across cation exchange membrane like Nafion. The pre-treatment of these membranes also affects the ion exchange and therefore the permeation processes as reflected in the D values.

References

[1] K.W. Sollner, The Encyclopaedia of Electrochemistry, C.A. Hampel (Ed.), Reinhold, New York.
[2] F.A. Williams, A. Dyer, Advances in Ion Exchange for Industry and Research, Royal society of chemistry, 1999.
[3] J.A. Marinsky, Ion Exchange, Marcel Dekker Inc., New York, 1966.
[4] R.W. Wallace, J. Phys. Chem. 68 (1964) 2418.
[5] Y. Mizutani, J. Membr. Sci. 54 (1990) 223.
[6] W.J. Blacdel, T.J. Hampert, Anal. Chem. 38 (1966) 1305.
[7] W.J. Blacdel, T.J. Hampert, Anal. Chem. 39 (1967) 1262.
[8] D.L. Feldhem, C.M. Elbott, J. Membr. Sci. 70 (1992) 9.
[9] T.T.B. To, R.D. Noble, C.A. Koval, J. Membr. Sci. 75 (1992) 293.
[10] A.T. Chariff, A. Elmidaoin, C. Gavach, J. Membr. Sci. 76 (1993) 39.
[11] A. Chapotot, G. Pourcelly, C. Gavach, J. Membr. Sci. 96 (1994) 167.
[12] H. Miyoshi, J. Membr. Sci. 141 (1998) 101.
[13] A.L. Vogel, A Textbook of Quantitative Inorganic Analysis, third ed., ELBS, 1968.
[14] R. Parkash, R. Bansal, S.K. Rehani, S. Dixit, Talanta 46 (1998) 1573.
[15] G. Lewis, Handbook of Analytical Chemistry, MIR, Moscow, 1975.
[16] A. Eisenberg, H.L. Yeager (Eds.), "Perfluorinated Ionomers", ACS Symp. Ser. 180 (1982).
[17] A. Eisenberg, M. King (Eds.), Ion Containing Polymers, Academic Press, New York, 1977.
[18] N. Lakshminarayaniah, Transport Phenomena in Membranes, Academic Press, New York, 1969.
[19] M.S. Kang, K.S. Yoo, S.J. Oh, S.H. Moon, J. Membr. Sci. 188 (2001) 61.

Available online at www.sciencedirect.com
ScienceDirect
Talanta 71 (2007) 1319–1325
Talanta
www.elsevier.com/locate/talanta

Determination of total and methyl mercury in human permanent healthy teeth by electrothermal atomic absorption spectrometry after extraction in organic phase

M. Saber-Tehrani *, M.H. Givianrad, H. Hashemi-Moghaddam

Department of Chemistry, Science and Research Branch, Islamic Azad University, P.O. Box 1415-775, Tehran, Iran

Received 17 April 2006; received in revised form 11 June 2006; accepted 5 July 2006
Available online 5 September 2006

Abstract

A simple and sensitive method has been developed for determination of inorganic and methyl mercury in biological samples by ETAAS. For determination of methyl mercury; it was transferred to toluene phase by acid leaching extraction method. For total mercury after digestion of samples; it was extracted to toluene phase by means of the chelating agent diethyldithiocarbamate. Formation of complex between MeHg and diethyldithiocarbamate enhance the MeHg signal and increases the reproducibility. Furthermore, Pd–DDC was used as modifier for both mercury and methyl mercury determinations. The optimization performance was independently carried out by modifying the parameters such as temperature of mineralization, atomization and gas flow rate for methylmercury and inorganic mercury in ETAAS. The limits of detection were 0.15 and 0.12 $\mu g\, g^{-1}$ for methyl mercury and total mercury, respectively. The repeatability of the measurements of whole procedure were 15.8% for methyl mercury and 16.9% for total mercury determination. The accuracy of the method has been investigated by means of spiking different amounts of methylmercury and inorganic mercury to the samples. The recoveries were found within the range of 88–95% for methyl mercury and 85–92% for total mercury. For determination of total mercury, the method was validated by CVAAS. The obtained results by the present procedure were in good agreement with those of the CVAAS. The proposed method was applied for 30 human permanent healthy teeth (without filling) which significant positive correlations were found among number of amalgam filling and total mercury and MeHg.
© 2006 Elsevier B.V. All rights reserved.

Keywords: Methyl mercury; Mercury; Teeth; Acid leaching; Correlation; ETAAS

1. Introduction

Mercury exists in the environment in a variety of compounds with different properties in terms of mobility, toxicity, bioavailability and volatility [1]. It is well known that organomercury compounds are much more toxic than mercury in its inorganic or elemental form. Mercury has been found to accumulate in vital organs and tissue, such as liver, heart muscle, and brain. Further, its affect on the body's immune system is potentially harmful, possibly contributing to diseases such as leukemia. The release of some trace elements especially mercury from metallic amalgam filling and its long-term exposure on human health has been controversially matter of concern for several decades. It has been found that considerable amount of mercury vapor are released from dental amalgam to chewing gum after chewing, just for 10 min [2]. The American dental association has recently supported a statement that "getting rid of amalgam would be like getting rid of aspirin", whereas several European government have banned use of amalgams in children, women of childbearing age and renal patients [3]. Based on a number of studies in Sweden, the World Health Organization review of inorganic mercury, determined that mercury absorption is estimated to be roughly four times higher from amalgam fillings than from fish consumption. The absorbed amount can vary notably from person to person. Some experts believe "there is no safe level of mercury exposure" [4,5].

The best bio-indicator for tracing the elements is tooth, because metals deposit in the tooth material during lifetime.

* Corresponding author. Tel.: +98 21 44817142 5; fax: +98 21 44817146.
E-mail address: drmsabertehrani@yahoo.com (M. Saber-Tehrani).

0039-9140/$ – see front matter © 2006 Elsevier B.V. All rights reserved.
doi:10.1016/j.talanta.2006.07.005

Also human permanent healthy teeth may be used as biosensor or trap of toxic metals for long-term exposure during the whole life [6].

One of the most critical steps for determination of mercury compounds in biological samples is the extraction of mercury compounds to the appropriate phase. The most common techniques are steam distillation [7] supercritical fluid extraction [8] and acid or basic liquid extraction either at room temperature [9] or using different heating source such as sonication [10] or microwave [11]. However, the more popular procedures used to separate mercury species from solid biological materials are based on the method developed by Westöö [12], which uses a solvent extraction process combined with an acid pretreatment with hydrochloric acid. Acid could liberate mercury species from protein thiol groups. Only organic species, such as methyl-mercury, are extracted after the treatment as has been shown by Kratzer et al. [13]. Also, the presence of chelating agent should be mandatory for extraction of total mercury in organic solvent. The most conventional technique used in mercury speciation studies is gas chromatography followed by electron capture detection (ECD) [14,15], The low sensitivity associated with this detector for organomercury species is improved by replacing the ECD with the other elemental detectors such as atomic absorption spectrometry (AAS) [16], atomic fluorescence spectrometry (AFS) [17] and inductively coupled plasma mass spectrometry (ICP-MS) [18,19]. Moreover, high performance liquid chromatography (HPLC) technique, which used widely for speciation analysis of mercury compounds [20], has also been coupled to different detection techniques such as AAS [21], AFS [22,23] or ICP-MS [24,25].

The disadvantages of the above-mentioned techniques are due to difficulty of the procedure, low efficiency, loss of mercury, expensive and sophisticated instruments. Furthermore, the problems with atomic absorption techniques like CVAAS could be related to the mercury cold vapour generation from an organic solution. Therefore, the direct determination of methylmercury in organic phase without any pre-treatment process like back extraction might eliminate these problems.

In this work, a sensitive and efficient method was developed for determination of methylmercury in organic phase by ETAAS after acid leaching extraction. In addition, for determination of total mercury, the samples were digested and the mercury contents of samples transferred to minimum amount of toluene phase by formation of complex between Hg and diethyldithiocarbamate. Consequently, in comparison to other methods, a less expensive and uncomplicated analytical method for total mercury and methylmercury determinations is presented. In addition, new treatment step of the samples and also low amount of sample for analysis by this method is offered.

Accordingly, from an analytical point of view, determination of mercury in human permanent healthy teeth is very important [26,27]. Thus, investigation the influence of number of the amalgam fillings in the mouth, on the concentration of mercury and methyl mercury in human permanent healthy teeth was performed.

2. Experimental

2.1. Instrumentation

A Varian model Spectra AA-220 atomic absorption spectrometer equipped with a GTA-100 graphite furnace atomizer, deuterium lamp as a background corrector, a Varian programmable sample dispenser and 1 nm spectral bandwidth of the monochromator were used for determination of total mercury and methylmercury. The measurements were performed at 253.7 nm, using a Varian Hg hollow cathodic lamp operated at 4 W which connected to a Varian power supply and Pyrolytic coated partitioned tubes were used throughout analysis. A chromium-steel micromill was used to pulverize and grind the teeth samples. An adjustable rocker shaker (Cole-parmer®-60 Hz) was used to shake the samples.

Also, total mercury was analyzed by cold-vapor AAS on a Varian Spectra AA-220, VGA 77 Vapor Generator Accessory that equipped with deuterium lamp background correction.

2.2. Reagents and standards

The reagents used for the preparation of all solutions were of the highest obtainable purity using deionized water, Nanopure water system with specific resistivity of 18.3 $M\Omega\,cm^{-1}$ (Millipore). Inorganic mercury (Hg^{2+}) stock standard solution (1000 $mg\,l^{-1}$) was prepared from mercury chloride (Merck 99.5%). Stock standard solution of 1000 $mg\,l^{-1}$ of methylmercury chloride pestanal®, analytical standard (Riedel-de Haën® 98.4%), prepared in methanol gradient grade. Sodium diethyldithiocarbamate trihydrate, analytical grade (Merck 99%), palladium(II) chloride (59%Pd Merck), nitric acid, suprapur (Merck 65%), hydrochloric acid, extra pure (Merck 32%), sodium chloride, Suprapur®(Merck 99.5%), copper(II) sulphate pentahydrate (Merck 99%), toluene, extra pure (Merck 99%), methanol, gradient grade (Merck), sodium borohydride (Merck 95%), as the reducing agent during mercury analysis, sodium hydroxide (Merck 99%), argon 99.999% purity as sheathing gas for atomizer.

2.3. Sample preparation

The teeth were collected from Legal Medicine Organization of Iran from 30 adults who died on June to July 2004 less than 48 h after death. Adults aged from 18 to 78 years including 24 males and 6 females belonging to an urban area in Tehran province. All of the teeth were healthy without any restoration with metallic amalgam or filling. Types of teeth and quality of teeth from carious or non-carious point of view were recorded by visual inspection of a dentist which 18 out of 30 were carious. For each tooth the number of amalgam fillings present in the mouth of individuals were carefully noted from zero to six but no information were taken regarding date of restoration.

After pulling out, the teeth were rinsed with distilled water for eliminating traces of blood and saliva and then have been cut sagittally in the buccolingual direction with a low speed

diamond saw microtome [28]. Carious substance was removed with a tungsten carbide bur from each tooth. One half of each tooth was put away for future study. The other half of teeth were rinsed in 0.1N HCl solution, then washed with deionized water, allowed to dry and stored at −20 °C until the end of sampling process.

Afterward, to simplify the crushing and grinding process, each tooth wrapped in plastic film and was introduced into liquid nitrogen. It was ground in a chromium-steel micromill. After grinding of each tooth, the mill was cleaned and brushed. Each tooth powder sample was placed in polyethylene vial and lyophilized overnight. The samples weighted again to determine the water content of each tooth that varied depending on each tooth group: for molars 12.73 ± 3.12%, for canines 10.21 ± 1.94% and for incisors 8.87 ± 1.23%.

2.4. Digestion of samples for determination of total mercury

The certain amounts of powder samples not exceeding 0.1 g were dissolved in 2 ml of 2N HCl and stored at 50 °C for 6 days in closed and sealed polypropylene test tubes [29]. The digested samples transferred and diluted to 10 ml and stored at 4 °C for next step.

2.5. Extraction of total mercury in toluene phase by DDC for ETAAS

4 ml of digested samples, which prepared in previous step, were transferred into separatory funnel and then 1 ml of a 2% (m/v) DDC solution in methanol as well as 4 ml of ultra pure water were added to the funnel. Subsequently, the mercury diethyldithicarbamate complex formed was quantitatively extracted with 3 ml of toluene after 5 min shaking by rocker shaker [30].

2.6. Extraction of methylmercury in toluene phase for ETAAS

A 0.1 g portion of each sample was transferred into polytetrafluoroethylene vial (20 ml) and 4 ml of deionized water, 1 ml of HCl 32%, 1 g of NaCl, 0.4 ml of $CuSO_4$ 5%(m/v) and after all 4 ml of toluene were added, shaking for 2 h by rocker shaker and centrifuged for 5 min (2000 rpm) [12]. Finally, 3 ml of toluene phase was taken and kept at 4 °C for next step.

2.7. Preparation of the palladium modifier in toluene

A 1 ml of a 3000 μg ml^{-1} palladium solution, prepared as describe by Welz et al. [31], was transferred into a separatory funnel and then 1 ml of a 2% (m/v) DDC solution as well as 5 ml of ultra pure water were added to the funnel. Subsequently, the palladium diethyldithicarbamate complex formed was quantitatively extracted with 10 ml of toluene after 1 min shaking. Thus, the concentration of palladium in the extract was 300 μg ml^{-1}.

2.8. Preparation of extracts for determination of methylmercury and total mercury by ETAAS

A 30 μl of Pd–DDC in toluene, which was already made, was added to methyl mercury and total mercury extracts, respectively. In addition, 50 μl of 0.2%(m/v) DDC solution in methanol was added only to methyl mercury extracts. Consequently, the overall concentration of Pd–DDC in solutions would be 2.92 and 2.97 μg ml^{-1} for methyl mercury and total mercury extracts, respectively. Finally, the samples were mixed, then transferred to an autosampler cup and subjected to ETAAS.

2.9. Determination of total mercury by CVAAS

In addition, the digested samples of step 2.4 were applied for determination of total mercury by conventional CVAAS method. The solution consists of 0.3% (w/v) sodium borohydride and 0.5% (w/v) of sodium hydroxide was used as the reducing agent during the mercury analysis [29].

3. Result and discussion

The aim of this work was the extraction of total mercury and methyl mercury in minimum amount of organic phase, individually. Then, the determination of these compounds should be accomplished by the appropriate technique. However, primarily a number of digestion methods were applied for digestion of samples. The presence of oxidizing acids or agents could interfere in the next extraction process. Hence, digestion with HCl was chosen [29], because no amount of oxidizing agent and minimum amount of acid was used.

The chelating agent DDC, was applied for extraction of total mercury in toluene [30]. This matter is because of high efficiency of extraction for mercury–DDC complexes. Also, a method based on Westöö extraction was used for selective extraction of the organomercury from teeth samples. In this method after the acid digestion, successive extraction with toluene was applied to separate the inorganic from the organic mercury species.

Various optimization experiments were carried out to obtain the best condition for determination of mercury species in the toluene phase by ETAAS.

3.1. The influence of different concentration of Pd–DDC modifier on absorbance

In order to realize the adequate concentration of chemical modifier for methyl mercury determination, a series of standard solutions consist of methyl mercury (500 μg l^{-1}), DDC (3.2×10^{-3}% (m/v)) and different amount of Pd–DDC modifier were prepared. Also, for total mercury, an extract containing Hg–DDC with the overall concentration of 250 μg l^{-1} in toluene was prepared. The obtained results either for mercury or for methyl mercury by ETAAS are shown in Fig. 1, which indicated that for methyl mercury and total mercury determinations, in modifier concentrations above 2.50 μg ml^{-1}, the absorbance is high and the variation of absorbance is negligible. On the other hand, the background absorbance would be highly promoted

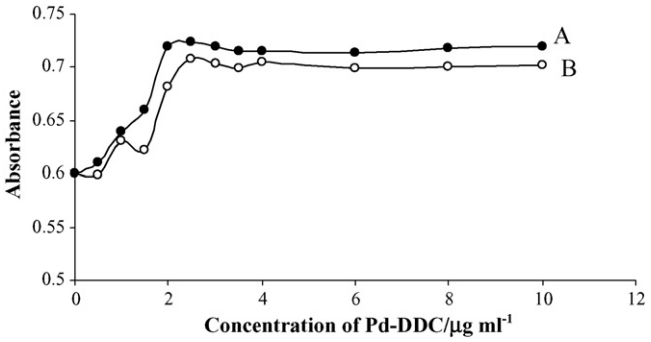


Fig. 1. The influence of different concentration of Pd–DDC modifier on absorbance of total and methyl mercury (curve A for total mercury and curve B for methyl mercury).

in the modifier concentration above 4 μg ml^{-1}. Therefore, in view of these results, the concentration between 2.5 and 4 μg ml^{-1} was chosen as the optimal concentration of modifier (Fig. 1).

3.2. Graphite furnace temperature programs

3.2.1. Total mercury determination

Study of the best condition for graphite furnace steps was carried out by optimization of hold time, temperature of mineralization, temperature of atomization and gas flow rate. For this purpose, an extract with 3 ml of toluene, was prepared from an aqueous solution containing 150 μl of 5 μg ml^{-1} Hg^{2+}, 1 ml of a 2% (m/v) DDC solution and ultra pure water to give a total volume of 9 ml. Suitable amounts of Pd–DDC modifier were added to the extracts to give 2.97 μg ml^{-1} palladium in the solution injected into the atomizer. In addition, for obtaining the most suitable times, temperatures and flow rates, the common way of working with graphite furnace AAS was followed.

With regard to the toluene boiling point (112 °C), the drying temperature was selected and applied to the two individual steps, one at 90 °C and another at 100 °C, with hold times of 15 and 10 s, respectively. This temperature could be sufficient to take out the solvent completely.

From mineralization and atomization curves, optimum temperatures 260 and 900 °C were achieved for the mineralization and atomization stages, respectively. In addition, the hold times of 5 s selected for mineralization and 8s for atomization step.

Moreover, the obtained atomization temperatures for standards and samples were not different, then the temperature of 900 °C was considered for both.

After all, a temperature of 1800 °C as a cleaning step was added to program to remove any residue from the tube before performing the next injection. The holding time of 3 s was selected for this step. In Figs. 2 and 3, the obtained mineralization and atomization curves are shown. These curves obtained in presence of Pd–DDC modifier.

The gas flow rate of argon was also studied in each step and the optimal flow rate of 300 ml min^{-1} obtained for all steps except for the atomization step, which required no amount of argon flow to achieve adequate signal (Fig. 4).

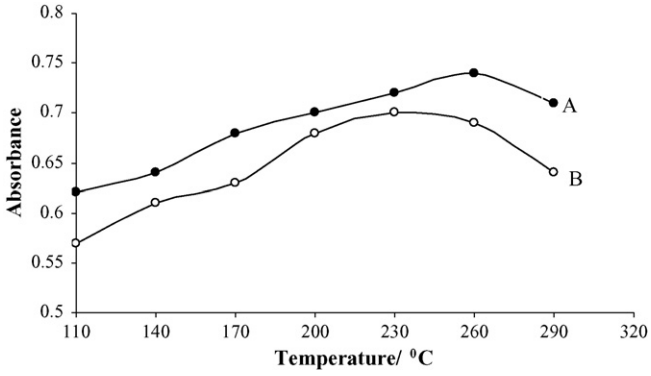


Fig. 2. The mineralization temperature curves for total and methyl mercury in presence of Pd–DDC modifier (curve A for total mercury and curve B for methyl mercury).

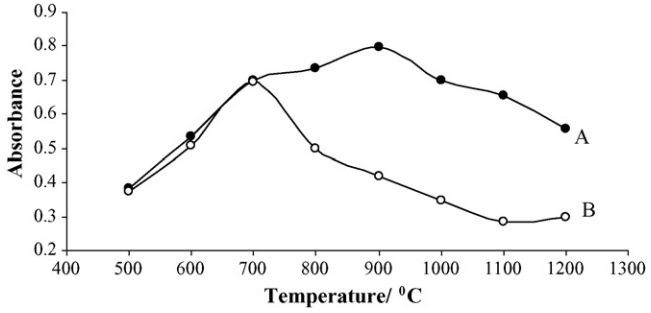


Fig. 3. The atomization temperature curves for total and methyl mercury in presence of Pd–DDC modifier (curve A for total mercury and curve B for methyl mercury).

3.2.2. Methyl mercury determination

To obtain the optimal temperature program for methyl mercury, a solution consists of 500 μg l^{-1} of methylmercury, 3.2×10^{-3}% (m/v) DDC and 2.92 μg ml^{-1} Pd–DDC in toluene was prepared.

The drying temperatures and hold times considered the same, as already mentioned for total mercury determination, because the similar solvent applied in both cases. The optimal mineralization temperature was 230 °C; however, 260 °C was more practicable. Because at 260 °C the background signal was lower and the results were more reproducible, then 260 °C selected

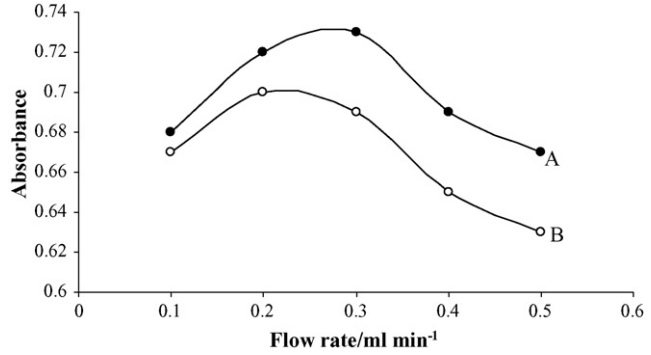


Fig. 4. The argon flow rate curves in presence of Pd–DDC modifier (curve A for total mercury and curve B for methyl mercury).

Table 1
Graphite furnace temperature program for determination of total mercury and methyl mercury, wavelength 253.7 nm, spectral bandwidth 1 nm, mercury hollow cathodic lamp 4 W, injected volume 20 μl, matrix modifier, Pd–DDC in toluene 2.97 and 2.92 μg ml^{-1} for total and methyl mercury, respectively, deuterium lamp background correction, pyrolytic coated partitioned tubes, peak area measurement mode

Step	Temperature (°C)	Hold (s)	Ar flow (ml min^{-1})
Total mercury			
Dry 1	90	15	300
Dry 2	100	10	300
Mineralization	260	5	300
Atomization	900	8	0(read)
Clean	1800	3	3000
Methyl mercury			
Dry 1	90	15	200
Dry 2	100	10	200
Mineralization	260	5	200
Atomization	700	8	0(read)
Clean	1800	3	3000

as the best mineralization temperature. At higher mineralization temperatures, the analyte losses are considerable which cause to generate non-desirable signal in this step. Also, the hold time of 5 s was selected for this step.

Studying the atomization step was carried out in the range of 500–1200 °C. The optimum atomization temperature was selected 700 °C within the temperature interval studied. In addition, the hold time of 8 s was obtained for this step. At this temperature, no tailed peaks were observed which indicates lack of analyte losses. Besides, the obtained atomization temperatures for standards and samples were not different, then the temperature of 700 °C was considered for both.

The temperature of 1800 °C and hold time of 3 s was selected for cleaning step. In Figs. 2 and 3, the obtained mineralization and atomization curves are shown, in presence of Pd–DDC modifier. Furthermore, gas flow rate of 200 ml min^{-1} was also selected in each step except for the atomization step (Fig. 4). Because of applying the organic solvent, the role of flow rate is much important. Then, in the case of methyl mercury determination due to high volatility of methyl mercury than inorganic mercury, lower flow rate was presented better results.

It is worthwhile to express that the background correction was used throughout the analysis.

The lifetime of graphite tubes, which used in this temperature program, was so considerable. This might be because of the application of mild temperature program. This is important from economic point of view. Table 1 summarizes the proposed graphite furnace temperature program for total and methyl mercury.

3.3. Standard calibration and standard addition curves

Calibration and standard addition graphs were obtained using ETAAS program reported in Table 1. The following standard calibration and standard addition curves were obtained from the analysis of standards and teeth samples by procedure described. The regression lines ($A = b + mC$) were calculated as follows:

standard calibration for total mercury :

$$A = 1.15 \times 10^{-3} + 2.78 \times 10^{-3}C, \quad r = 0.999$$

standard addition for total mercury :

$$A = 1.35 \times 10^{-2} + 2.58 \times 10^{-3}C, \quad r = 0.998$$

standard calibration for methyl mercury :

$$A = -8.21 \times 10^{-3} + 1.40 \times 10^{-3}C, \quad r = 0.999$$

standard addition for methyl mercury :

$$A = 0.85 \times 10^{-2} + 1.37 \times 10^{-3}C, \quad r = 0.997$$

where "A" is the absorbance, "m" the slope of the line, constant term of regression "b" the intercept with the y-axis and "C" the concentration of total mercury or methyl mercury, in μg l^{-1}.

The differences of slopes between standard calibration and standard addition for total mercury and also methyl mercury were not significant based on Student's t-test at a confidence level of 95%. With respect to similarity of the slopes of standard calibration and standard addition curves and also atomization temperatures which considered the same for samples and standards it was concluded that either standard calibration or standard addition methods might be regarded for the measurements. Thus, for ease of use the standard calibration applied throughout the analysis.

3.4. Analytical figures of merit

Sensitivity of the procedure based on the slope of the standard calibration line are 2.78×10^{-3} and 1.40×10^{-3} l μg^{-1} for total and methyl mercury, respectively. Furthermore, sensitivity was studied by means of the limit of detection (LOD), the limit of quantification (LOQ) and the characteristic mass (m_0), defined as follows:

$$\mathrm{LOD} = \frac{3s}{\mathrm{slope}}, \qquad \mathrm{LOQ} = \frac{10s}{\mathrm{slope}}$$

$$m_0 = \frac{VC0.0044}{\text{mean absorbance}}$$

where s is the standard deviation of eight successive measurements of a blank; slope means the slope of the standard calibration curve; V the volume of solution injected into the graphite furnace and C the standard concentration, in μg l^{-1}.

According to these equations: the LOD and LOQ for total mercury are 1.60 and 5.30 μg l^{-1} (0.12 and 0.40 μg g^{-1}) and also for methyl mercury 3.86 and 12.85 μg l^{-1} (0.15 and 0.50 μg g^{-1}), respectively. Ultimately, the characteristic mass (m_0), 24 and 68 pg were obtained for total and methyl mercury, correspondingly.

Precision, which is a measure of reproducibility, expressed as percent relative standard deviation (RSD) within the linear range, was obtained by:

$$\mathrm{RSD} = 100\frac{\sigma}{\bar{X}}$$

The repeatability of the measurements, as the mean RSD was 2.1% for total mercury and 0.8% for methyl mercury for eight successive individual measurements of the same sample. In addition, RSD of the whole procedure, expressed as the RSD of the concentration measured for three replicated analysis of the same sample, were 16.9% for total mercury and 15.8% for methyl mercury.

The accuracy of method has been investigated by means of spiking different amounts of methyl mercury and inorganic mercury to the samples. The recoveries were found within the range of 85–92% for total mercury and 89–95% for methyl mercury, which are tabulated in Table 2. Also, the validity of the proposed method was confirmed for determination of total mercury, by comparing the data obtained from the mentioned method with results obtained by a well-known method, namely CVAAS. The results are listed in Table 3, which is expressed as $\bar{x} \pm ((t\,\mathrm{S.D.})/\sqrt{N})$, where S.D. is the standard deviation regarding to three measurements, N is three determinations and t the t'Student parameter for $N-1=2$ grades of freedom at the confidence level of 95%. The obtained results by this procedure were in good agreement with proposed method.

Table 2
Recoveries corresponding to total and methyl mercury determination by means of spiking different amounts of mercury and methyl mercury to the teeth samples

Mercury content ($\mu g\,l^{-1}$)	Hg^{2+} spiked ($\mu g\,l^{-1}$)	Recovery (%)	Methyl mercury spiked ($\mu g\,l^{-1}$)	Recovery (%)
5.6	25	90.2	25	94.4
	50	92.0	50	89.5
	100	85.4	100	93.2

3.5. Application

The proposed method was applied for determination of total and methyl mercury in human permanent healthy teeth. According to the procedure, which mentioned before, 30 human permanent healthy teeth (without filling) were analyzed, in order to investigate the influence of the number of amalgam fillings on mercury compounds in teeth. The ETAAS determinations were carried out in triplicate, so the mean concentrations of methyl mercury are listed in Table 3.

Moreover, correlation analysis base on Pearson correlation coefficient was performed. Significant positive correlation is the

Table 3
Total mercury and methyl mercury concentrations in human permanent healthy teeth, expressed as $\bar{X} \pm ((t\,\mathrm{S.D.})/\sqrt{N})$, for $N=3$ measurements and $t_{(N-1=2)} = 4.30$

Code	Proposed method			CVAAS
	Number of amalgam filling	Total mercury ($\mu g\,g^{-1}$)	Methyl mercury ($\mu g\,g^{-1}$)	Total mercury ($\mu g\,g^{-1}$)
T_1	3	1.57 ± 0.08	0.95 ± 0.07	1.54 ± 0.07
T_2	2	3.41 ± 0.07	2.21 ± 0.09	3.36 ± 0.09
T_3	4	2.18 ± 0.10	1.19 ± 0.16	2.13 ± 0.07
T_4	2	2.73 ± 0.05	1.67 ± 0.03	2.80 ± 0.06
T_5	3	6.84 ± 0.06	4.29 ± 0.07	6.77 ± 0.05
T_6	1	2.74 ± 0.05	1.02 ± 0.05	2.68 ± 0.03
T_7	3	1.62 ± 0.09	0.80 ± 0.03	1.54 ± 0.05
T_8	4	4.59 ± 0.03	2.64 ± 0.01	4.55 ± 0.07
T_9	1	0.50 ± 0.04	0.25 ± 0.01	0.55 ± 0.04
T_{10}	6	8.51 ± 0.08	4.04 ± 0.11	8.44 ± 0.06
T_{11}	4	9.22 ± 0.07	5.71 ± 0.15	9.15 ± 0.07
T_{12}	4	5.58 ± 0.06	1.98 ± 0.06	5.52 ± 0.09
T_{13}	2	4.85 ± 0.04	2.75 ± 0.03	4.95 ± 0.06
T_{14}	0	0.49 ± 0.09	0.25 ± 0.04	0.53 ± 0.04
T_{15}	6	6.99 ± 0.10	4.02 ± 0.10	6.90 ± 0.05
T_{16}	3	1.43 ± 0.07	0.79 ± 0.08	1.33 ± 0.09
T_{17}	3	2.73 ± 0.08	0.76 ± 0.04	2.80 ± 0.03
T_{18}	3	3.59 ± 0.11	2.02 ± 0.11	3.67 ± 0.06
T_{19}	3	5.26 ± 0.08	2.95 ± 0.03	5.19 ± 0.09
T_{20}	3	3.28 ± 0.06	1.95 ± 0.09	3.36 ± 0.07
T_{21}	1	1.97 ± 0.06	0.20 ± 0.06	1.90 ± 0.08
T_{22}	3	4.11 ± 0.04	2.55 ± 0.08	4.05 ± 0.06
T_{23}	3	6.83 ± 0.12	4.11 ± 0.15	6.74 ± 0.04
T_{24}	2	2.90 ± 0.02	1.45 ± 0.06	2.81 ± 0.05
T_{25}	4	1.02 ± 0.03	0.50 ± 0.07	0.98 ± 0.07
T_{26}	0	1.89 ± 0.08	0.78 ± 0.02	1.83 ± 0.03
T_{27}	0	0.76 ± 0.07	0.40 ± 0.05	0.81 ± 0.10
T_{28}	3	4.53 ± 0.06	1.15 ± 0.09	4.47 ± 0.06
T_{29}	2	3.17 ± 0.05	2.01 ± 0.06	3.12 ± 0.08
T_{30}	2	4.91 ± 0.03	3.55 ± 0.07	4.86 ± 0.05

Table 4
Pearson correlation matrix for total mercury, methyl mercury and number of amalgam filling in human permanent healthy teeth

	Number of amalgam filling	Total mercury	Methyl mercury
Number of amalgam filling	1.0000	0.6344	0.5603
Total mercury		1.0000	0.9426
Methyl mercury			1.0000

relationship between two sets of data in which the values of two variables increase or decrease together, significantly [32]. In this study, positive correlations were found among number of amalgam filling, mercury and methyl mercury ($r > 0.4490$, $n = 30$) at a confidence level of 99% (Table 4). Therefore, based on the correlations, increase or decrease of mercury species content in healthy teeth would be affected by number of amalgam filling.

4. Conclusion

A suitable and sensitive method was developed for determination of total and methyl mercury in biological samples by ETAAS. The simplicity and effortlessness of the procedure is due to the direct determination of total and methyl mercury in organic phase, which could offer the new treatment step of the samples with minimum amount of sample for analysis. By formation of complex between mercury and methyl mercury with DDC, the analytical signal and the reproducibility typically improved which was accomplished by adding the chemical modifier. Based on the obtained figures of merit, the quality of the results was acceptable in comparison to other conventional methods like CVAAS. Therefore, this is a convenient and economical method, which could be considered as an alternative for total and methyl mercury determination in biological samples. Thus, the applicability of the method to real samples was proved for teeth samples.

Therefore, based on the correlations, increase or decrease of mercury in teeth would be followed by increase or decrease of amalgam filling. Accordingly, with respect to these correlations, it is concluded that the considerable amounts of mercury could be released from dental amalgam in long period and would accumulate in permanent healthy teeth.

Acknowledgment

The authors are so grateful to the Legal medicine Organization of Iran for providing the samples and Laboratory Complex of I.A.U. for valuable technical assistance.

References

[1] M.S. Hosseini, H. Hashemi-Moghaddam, Talanta 67 (2005) 555.
[2] G. Sallsten, J. Thoren, L. Barregard, A. Schutz, G. Skarping, J. Dent. Res. 75 (1996) 594.
[3] G. Honsen, R. Victor, E. Engeldinger, C. Schweitzer, Occup. Environ. Med. 61 (2004) 535.
[4] WHO, Trace Elements in Human Nutrition and Health, World Health Organization, Geneva, 1996.
[5] S. Caroli, N. Violante, A. Alimonti, O. Senofeonte, L. Fornarelli, E. Coni, E. Sabbioni, R. Pietra, E. Cristallini, G.B. Bolis, in: B.b. Ribas, P. Schramel (Eds.), Falconieri, in Trace Element Analytical Chemistry in Medicine and Biology, vol. 6, CSIC, Madrid, Espana, 1994, pp. 173–250.
[6] B. Nowak, Biol. Trace Elem. Res. 52 (1996) 11.
[7] M. Horvat, N.S. Bloom, L. Liang, Anal. Chim. Acta 281 (1992) 135.
[8] H. Emteborg, E. Börjklund, F. Ödman, L. Karlsson, L. Mathiasson, W. Frech, D. Baxter, Analyst 121 (1996) 19.
[9] L. Liang, M. Horvat, E. Cernichiari, B. Gelein, S. Balogh, Talanta 43 (1996) 1883.
[10] A.I. Cabañero, Y. Madrid, C. Cámara, J. Anal. At. Spectrom. 17 (2002) 1595.
[11] C.M. Tseng, A. De Diego, F. Martin, D. Amouroux, O.F.X. Donard, J. Anal. At. Spectrom. 12 (1997) 743.
[12] G. Westöö, Acta Chem. Scand. 20 (1966) 2131.
[13] K. Kratzer, P. Benes, V. Speváckova, D. Kolihová, J. Zilková, J. Anal. At. Spectrom. 9 (1994) 303.
[14] M.J. Vazquez, A.M. Carro, R.A. Lorenzo, R. Cela, Anal. Chem. 69 (1997) 221.
[15] M. Hovart, A.R. Byrne, K. May, Talanta 37 (1990) 207.
[16] C.M. Tseng, A.D. Diego, F.M. Martin, D. Amouroux, O.F.X. Donard, J. Anal. At. Spectrom. 12 (1997) 629.
[17] L. Liang, M. Horvat, E. Cernichiari, B. Gelein, S. Balogh, Talanta 43 (1996) 1883.
[18] J. Holz, J. Kreutzmann, R.D. Wilken, R. Falter, Appl. Organomet. Chem. 13 (1999) 789.
[19] L. Yang, Z. Mester, R.E. Sturgeon, J. Anal. At. Spectrom. 18 (2003) 431.
[20] H. Hintelmann, R.D. Evans, J.Y. Villeneuve, J. Anal. At. Spectrom. 10 (1995) 619.
[21] R. Eiden, R. Falter, B. Agustin-Castro, H.F. Scholer, Fresenius J. Anal. Chem. 357 (1997) 439.
[22] R. Falter, G. Ilgen, Fresenius J. Anal. Chem. 358 (1997) 407.
[23] E. Ramalhosa, S. Rio-Segade, E. Pereira, C. Vale, A. Duarte, J. Anal. At. Spectrom. 16 (2001) 643.
[24] R. Falter, G. Ilgen, Fresenius J. Anal. Chem. 358 (1997) 401.
[25] R. Rai, W. Maher, F. Kirkowa, J. Anal. At. Spectrom. 12 (2002) 1560.
[26] L. Pszonicki, J. Dudek, J. Anal. At. Spectrom. 14 (1999) 1755.
[27] O. Acar, A.R. Turker, Z. Kilic, Talanta 49 (1999) 135.
[28] B. Jalevic, H. Odelius, W. Dietz, J.G. Noren, Arch. Oral Biol. 46 (2001) 239.
[29] H.M. Tvinnereim, R. Eide, T. Riise, Sci. Total Environ. 255 (2000) 21.
[30] E. Bulska, H. Emteborg, D.C. Baxter, W. Frech, D. Ellingsen, Y. Thomassen, Analyst 117 (1992) 657.
[31] B. Weltz, G. Schlemmer, J.R. Mudakavi, J. Anal. At. Spectrom. 3 (1988) 695.
[32] J.C. Miller, J.N. Miller, Statistics for Analytical Chemists, 3rd ed., Ellis Horwood Pub, London, U.K, 1993.

Available online at www.sciencedirect.com
ScienceDirect
Talanta 71 (2007) 1411–1416
Talanta
www.elsevier.com/locate/talanta

Development and characterisation of an immunoaffinity chromatographic column for the on-line determination of the pesticide triclopyr

F.G. Sanchez*, A.N. Diaz, R.G. Herrera, L.P. San Jose

Department of Analytical Chemistry, University of Malaga, 29071 Malaga, Spain

Received 10 February 2006; received in revised form 30 June 2006; accepted 7 July 2006
Available online 23 August 2006

Abstract

An immunoaffinity column for the selective extraction and concentration of the herbicide triclopyr from water samples and quantification on line by HPLC has been developed. The immunoaffinity device was prepared by immobilising triclopyr antibodies to hydrazide derivatized azlactona beds. Efficient desorption of bound triclopyr was achieved with 70% ethanol/water solution. The column was evaluated regarding selectivity, recovery, capacity, saturation volume and reusability. Obtained results show that immunoaffinity chromatography (IAC) can be used for quantitative extraction, concentration and determination of triclopyr from water samples.
© 2006 Elsevier B.V. All rights reserved.

Keywords: Immunoaffinity chromatography; Pesticide triclopyr; Determination

1. Introduction

The potential chemical complexity of environmental matrices leads to lengthily sample preparation procedures in order to eliminate interferences that may hinder the quantification of the analyte of interest.

Pesticides applied for crop protection and conservation, are usually included in a wide range of polarities and solubilities. The polar nature of several pesticides and the low levels in surface waters and other environmental systems make them difficult to analyze without previous steps including clean-up and pre-concentration. Sample preparation methods usually rely on partition in organic solvents (liquid–liquid extraction (LLE)), or on the use of adsorbents that retain the percolated compound based on hydrophobic interactions or polarity characteristics (solid phase extraction (SPE)). These methods often fail to remove interfering compounds from complex sample matrices due to lack of specificity and work poorly for polar compounds.

Immunoaffinity chromatography offers many advantages over traditional pesticide clean-up and pre-concentration methods. It is based on molecular recognition by exploiting the specific interactions of antibody against specific target analytes. The main advantages are the exquisite selectivity, the simplified handling technique and little or no use of organic solvents. The main drawback is that no readily commercially available immunoaffinity columns for pesticides exist because antibodies against a particular pesticide must be previously obtained in this study.

Antibodies raised against a specific target pesticide can be immobilised on a solid phase and will selectively retain the pesticide, but not the other constituents of the sample matrix because the specific nature of molecular recognition. Antigens captured in the affinity column are eluted with the adequate mobile phase and the components retained can be determined by a further analytical technique or on line with a photometric detector.

In recent years, antibody-based immunoaffinity columns (IA column) have been applied in a variety of samples as a high specific means for isolating and concentrating compounds [1–9]. The first immunosorbents developed for pesticides were directed against triazine and phenylurea herbicides [10], fipronyl [11], diazinon [12], imazalil [13], avermectin [14] and propanil [8]. Several reviews [15–24] have been published reporting and discussing the basic properties and applications of immunosorbent cartridges in trace analysis.

Triclopyr is a systemic herbicide, chemical name 3,5,6-trichloro-2-pyridyloxyacetic acid, is used as herbicide for control of woody plants and broad leaved weeds in grasslands and rice field. Triclopyr analysis is mainly carried out by using

* Corresponding author. Tel.: +34 952 131972; fax: +34 952 131884.
E-mail address: f_garcia@uma.es (F.G. Sanchez).

0039-9140/$ – see front matter © 2006 Elsevier B.V. All rights reserved.
doi:10.1016/j.talanta.2006.07.015

gas chromatography (GC) with electron capture detector after derivatization [25–27], direct GC [28–31] or liquid chromatography [32,33]. These chromatographic methods require clean-up steps and the use of large amounts of organic solvents. Some advantages can be obtained by using immunoassay methods such as fluorescence polarization [34] and ELISA [35]. The objective of this study was to optimize an on-line immunoextraction and quantitation of triclopyr in a single step with a selective IA column. In this paper we report and discuss the development and evaluation of an immunoaffinity chromatography column for the extraction and determination of the herbicide triclopyr.

2. Experimental

2.1. Materials

Triclopyr (99.9%) and MCPA (99.9%) were supplied by Dr. Ehrenstorfer (Germany) and 2,4-D (99%) by Riedel-de-Haën (Seelze, Germany) and 2,4,5-T (95%) by Sigma (St. Louis, MO). Bovine serum albumin (BSA), glycine, sodium chloride, sodium phosphate and sodium acetate were purchased from Sigma and ethanol, methanol and acetonitrile were obtained from Merck (Germany). Other chemicals used in this study were of analytical reagent grade. Distilled and demineralised water was used throughout.

Activated Fractogel Azlactona EMD was purchased from Merck.

2.2. Buffers

Coupling buffer pH 7.2, phosphate 0.1 M. NaCl 150 mM. Glycine–HCl buffer 0.2 M pH 8 and pH 2. Buffer HAc/NaAc 0.1 M pH 4. Buffer PBS 0.1 M pH 7.

2.3. Instrumentation

The measurements were performed with a Merck-Hitachi liquid chromatography consisting of an L-6200 pump, an UV-visible detector and a D-6000 interface. IA column was directly connected to the chromatographic system. A RP-18 Chromalit (4.6 mm × 100 mm) column (Merck) was used to obtain calibration curve of standards. Wavelength of detector was fixed at 200 nm.

A Superformance column (10 mm × 150 mm) manufactured by Merck (Darmstad, Germany) was used as the immunoaffinity cartridge. The temperature of the system was controlled to 10 °C using and immersion circulating bath.

2.4. Preparation of the immunosorbent

The IgG fraction of rabbit polyclonal anti-triclopyr antibodies was used to prepare the immunosorbent. Production of antisera against triclopyr was described elsewhere [34]. Briefly: polyclonal antibodies raised against triclopyr were prepared by conjugation of triclopyr to bovine serum albumin (BSA) to be used as antigen. Because a covalent peptidic bond is formed between the carboxy group of the triclopyr molecule and the free ε-amino groups of the protein, the epitopes to be recognized by the antibody must be probably the *N*-pyridinic and the three chloro attached to the benzenic ring. A new Zealand female rabbit was immunized with 300 mg of the conjugate, the first suspension was emulsified with 3 ml of Freund's complete adjuvant. The first antiserum collected was obtained 50 days after the first injection, and the serum was separated by centrifugation and stored at −20 °C. Purification was performed by ammonium sulphate precipitation.

The anti-triclopyr polyclonal antibodies were covalently bonded to Azlactona [36,37] gel following manufacture's instruction (Merck). Briefly, the immobilisation buffer (PBS, pH 7.2, 150 mM NaCl) was mixed at 10 °C during 3 h. Each ml of wet gel needs 3 mg antibody and 20 ml PBS. The extent of antibody binding was monitored by determination of the decrease in optical density of the supernatant at 280 nm. Coupling efficiency was 75.8% corresponding to 2.27 mg antibody per ml wet gel. According to the calculated coupled efficiency and considering about a 20% of specific anti-triclopyr Ab may be present in the IgG fraction of purified antisera, we could estimate a theoretical column capacity of 37 μg of triclopyr. Inactivation of remaining active groups in gel was performed with glycine buffer (pH 8, 0.2 M). The obtained immunosorbent was repeatedly washed using three different buffers: HAc (pH 4, 0.1 M), glycine (pH 2.5, 0.2 M) and PBS (pH 7, 0.1 M).

After preparation, the immunosorbent was stored at 4 °C in PBS containing 0.2% azide.

2.5. Preparation of the immunoaffinity column

The column used (10 mm × 150 mm) (Merck) was carefully prepared to operate at moderately high pressure. To obtain a stable packing bed, a gel compression of 30% is adequate to be used at moderately high pressures LC conditions.

The percentage of compression (PC) is

$$\left[\frac{\mathrm{VR/VC}}{\mathrm{VR}}\right] 100 = \mathrm{PC}$$

VR is the void column volume = $\pi r^2 h$ = 11.8 ml for a 150 mm length column and VC the compressed volume = 100VR/(100 − PC) = 16.8 ml.

We can calculate now the volume of suspended gel (70%) needed to fill the column as follows:

$$\text{gel volume} = \frac{\mathrm{VC}}{0.7} = 24\,\text{ml}.$$

2.6. Affinity chromatography

The analytical procedure was completed in four steps:

1. *Loading of the sample*. Triclopyr solutions in PBS, pH 7.2, covering the range 0.002–2.40 μg were injected in the chromatographic system. A flow rate of 0.5 ml min^{-1} of PBS, pH 7.2 was used. Injection volume was 40 μl.

2. *Washing*. Ten millilitres of PBS, pH 7.2, at 0.5 ml min^{-1} during 20 min.
3. *Elution*. Fifteen millilitres of water:ethanol (30:70, v/v) at 1 ml min^{-1}.
4. *Regeneration*. Forty millilitres PBS, pH 7.2, at 0.5 ml min^{-1}.

The obtained retention time for the eluted triclopyr was 12.31 ± 0.21 min.

2.7. HPLC procedure

LC conditions were as follows: TCP standards in PBS solution (pH 7.2) were injected (10 μl) in the HPLC system. Elution were performed with water:acetonitrile (50:50, v/v) at 1 ml min^{-1} flow rate. Wavelength of detector was fixed at 200 nm.

3. Results and discussion

3.1. Capacity of the IA column

The amount of antibody immobilised was 6.71 mg antibody/g of silica support, or 44 nmol antibody/g silica support.

The capacity of the column was determined by loading triclopyr samples in PBS spiked at three levels (0.05, 0.01 and 1 μg). Triclopyr was never detected after loading and washing steps. The bound fraction was eluted following the general procedure (15 ml of water:ethanol (30:70, v/v) at 1 ml min^{-1}).

Recoveries obtained are within 80–110% in every case, indicating that experimental binding capacity is 1 μg or greater.

The high capacity before column saturation takes place allows us, for routine applications, total immobilisation of triclopyr in a wide range of concentrations. Therefore, a complete elution of the analyte gives the possibility of direct quantitation of triclopyr without the need of a LC column on line with the IA column or ulterior quantitation of triclopyr by an alternative technique after collection of the fraction containing the analyte. This fact simplifies the methodology and performs in two single steps (retention and elution) purification, concentration and quantitation of triclopyr containing samples.

3.2. Immunoaffinity chromatography

Sample application, washing conditions and elution of the samples were obtained after many trials with different combinations of solvent mixtures.

Injection of samples in the IA column was performed in the volumes range between 40 and 500 μl. We found that PBS (pH 7.2) diluted samples at a flow rate of 0.5 ml/min were adequate to the chromatographic procedure. A washing step using 10 ml PBS do not elutes analyte from the IA column and clean it from matrix constituents retained by non-specific adsorptions.

Elution step is critical and several mobile phases as eluent were assayed. For analytes of low molecular weight is recommended that the use of organic modifiers such as ethanol or methanol instead of pH modifiers give the best results.

Table 1
Effect of mobile phase composition

Triclopyr added (μg)	Eluent	Recovery (%), $n=3$	Retention time (min)
0.6	EtOH (70%)	87.3	35.24
	MeOH (70%)	86.2	46.52
0.025	EtOH (70%)	87.0	35.64
	MeOH (70%)	74.9	46.77

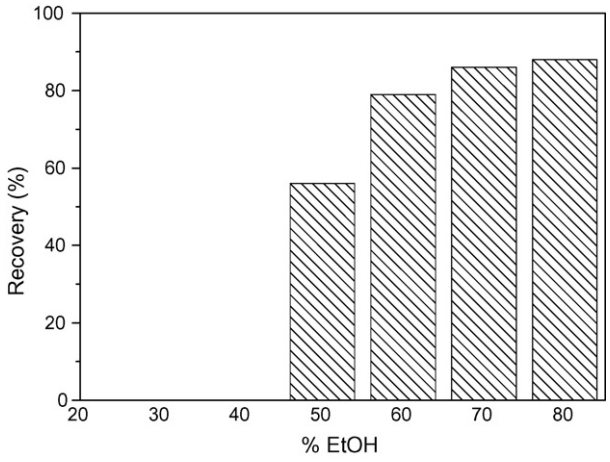


Fig. 1. Effect of percentage of ethanol in the elution step.

The effect of 70% mixtures water:ethanol and water:methanol as eluent in the percentage of recovery and retention time of triclopyr has been studied at two concentration levels (0.6 and 0.025 μg). Table 1 shows the results obtained in recovery assays using as eluent ethanol/water and methanol/water (70:30, v:v). From this, it can be seen that a lesser polar solvent (ethanol) gives little best recovery values and considerable shorter retention time than methanol.

The effect of percentage of ethanol in the recovery values were studied in the range 50–80%. In Fig. 1 are plotted recovery of triclopyr against different percentages of ethanol:water. From this data we decide the elution of analyte by a 70:30 (v:v) ethanol:water solution. The elution of triclopyr was carried out at a flow rate of 0.5 ml/min. Fig. 2 shows the chromatogram obtained in the IA column 15 cm long. 0.016 μg triclopyr was injected in a volume of 2 ml and flow rate of 0.5 ml/min. Obtained retention times are in the range 12.31 ± 0.31 min (three measurements).

3.3. Calibration curves, recovery assays and reproducibility

Calibration of triclopyr was performed directly with the IA column and in a reversed phase column (RP-18) to compare the obtained results. In both columns were injected standard solutions of triclopyr in two concentration ranges (0.002–0.025 and 0.1–2.4 μg triclopyr). Fig. 3(A and B) shows the obtained results. Regression values for four points adjusts were: Y (area) $= 0.2352X$ (μg) $+ 9 \times 10^{-6}$ ($R^2 = 0.9966$) for 0.002–0.250 range, and $Y = 0.1547X$ (μg) $- 0.0075$ ($R^2 = 0.9996$) for

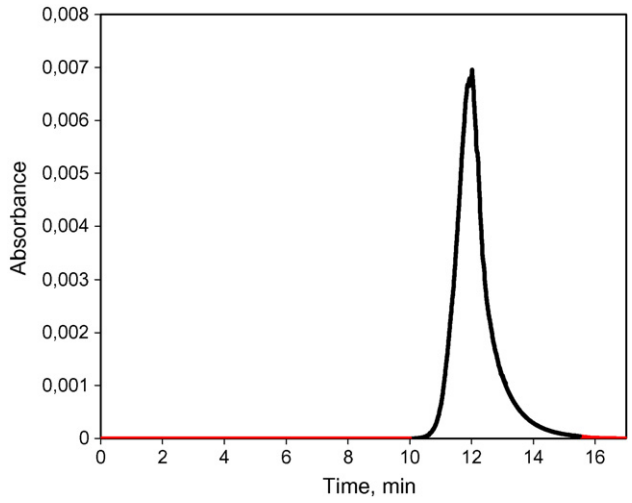


Fig. 2. Standard elution profile of 0.016 μg triclopyr. Flow rate 0.5 ml/min.

0.10–2.40 range. Calibration curves with RP-18 column show similar adjust parameters but higher slopes, as expected if some losses of analyte occur in the IA column.

Recovery assays of several samples containing triclopyr within the concentration ranges studied were carried out using the IA column and submitted to the experimental procedure. The obtained results are shown in Table 2, in which can be observed that recoveries above 80% are obtained in every case. It must be pointed out that recovery values were obtained by interpolation with the standard curves constructed with data obtained in the LC column, in that case "real" values of triclopyr found were used. Table 2 also shows that relative standard deviations are below 10% in every case, excepting at the assayed level of 0.002 μg triclopyr added.

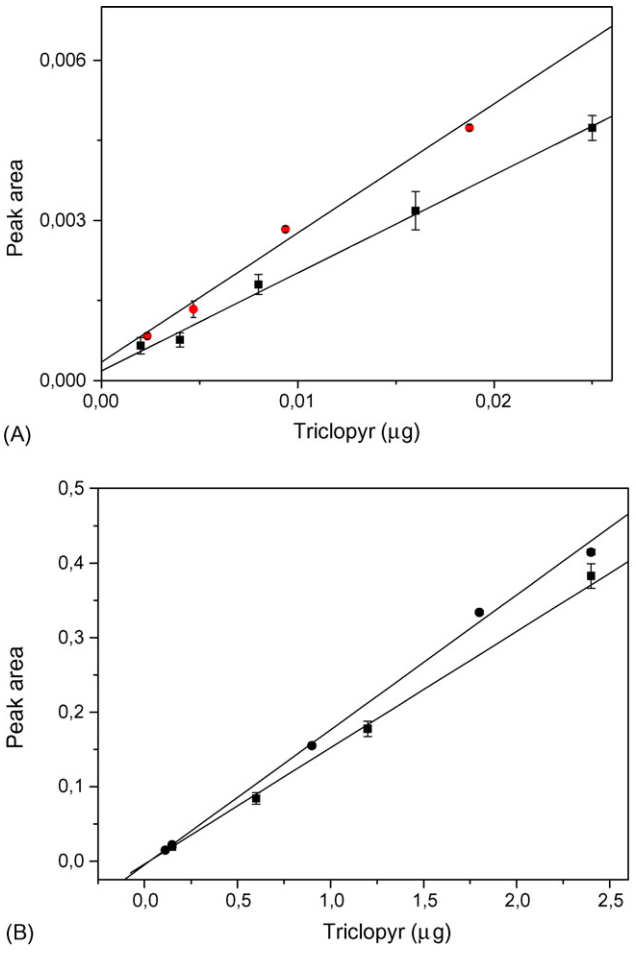


Fig. 3. Calibration curves: (A) concentration range: 0002–0.025 μg triclopyr; (B) 0.1–2.4 μg triclopyr. (■) IA column; (●) standard RP-18 column.

Table 2
Recovery assay of triclopyr

Triclopyr added (μg)	Triclopyr found (μg) ± standard deviation (relative standard deviation, %), $n = 3$	Recovery (%) ± standard deviation
0.0020	0.002 ± 0.002 (100)	110 ± 73
0.0040	0.0032 ± 0.0003 (9.4)	80 ± 9
0.016	0.013 ± 0.001 (7.7)	81 ± 8
0.025	0.021 ± 0.002 (9.5)	84 ± 9
0.15	0.13 ± 0.01 (7.7)	87 ± 5
0.60	0.52 ± 0.04 (7.7)	87 ± 8
1.20	1.05 ± 0.07 (6.7)	87 ± 7
2.40	2.19 ± 0.06 (0.5)	91 ± 3

3.4. Cross reactivity of the IA column

The affinity of compounds with structure closely related to triclopyr can be expected to be moderately high and this compounds can cause interferences in the quantitation of triclopyr.

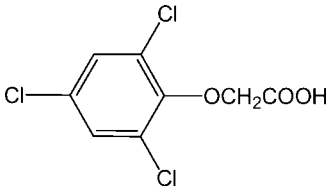
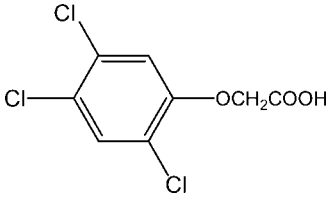
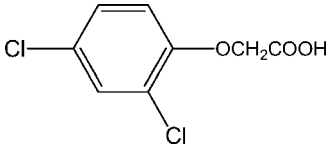
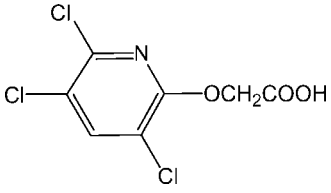
An initial experiment was realized in which the potential interferents were loaded in the IA column and submitted to the experimental procedure. Retention times were measured and then recovery values of triclopyr evaluated over mixtures prepared with the same concentration of triclopyr and interferent. Table 3 shows the results obtained. As can be seen MCPA and 2,4-D are not retained and 2,4,5-T is eluted at retention time about a half of that of triclopyr. In this case interference of 2,4,5-T can be eliminated because the difference in retention times.

3.5. Column reusability and durability

The use of immunoaffinity columns for sample clean-up and quantitation of analytes in only one operation is attractive for routine analysis. However, the cost of an IA column in time and effort is high and the reusability of the column is an important operational parameter that must be evaluated.

After 30 uses the binding efficiency of the triclopyr IA column maintains the initial performances, obtaining recovery values ranging in 80%. Durability of the prepared column was monitored by loading triclopyr (0.15 μg) and performing the recommended procedure. After measuring recovery values and storing the column at 4 °C, the procedure was repeated 30 times during an interval of time of 2 months. Fig. 4 shows triclopyr recoveries against number of uses, corresponding to the interval of 2 months. As can be seen, durability of column is as least 2 months. Obtained recoveries are grouped in a range between 80

Table 3
Cross reactivity of the immunoaffinity column

Structure	Name	Elution time	%Recovery triclopyr
	MCPA	Not retained	100.0
	2,4,5-T	2.9 min	94.4
	2,4-D	Not retained	100.0
	Triclopyr	12.3 min	100.0

and 110% in every case, excepting in three points, that can be associated to the change in initial environmental conditions after storage (temperature and conditioning of the stationary phase).

3.6. Application

Recovery experiments were carried out with tap water samples fortified at three concentration levels of triclopyr (1, 10 and 50 μg ml^{-1}, corresponding to 0.04, 0.4 and 2 μg triclopyr when injecting 40 μl of each sample). Injections have been made by triplicate. Results obtained were ordered in Table 4.

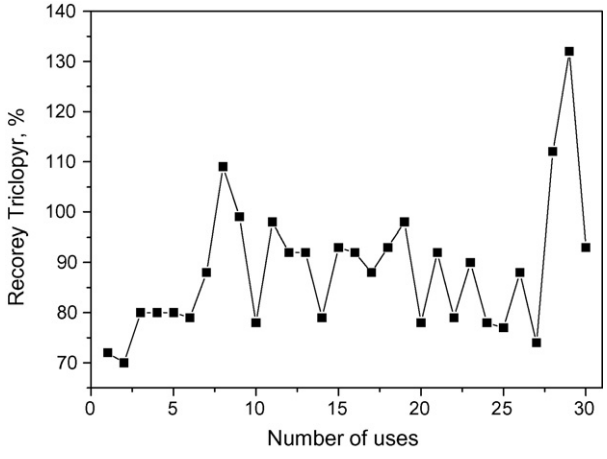


Fig. 4. Elution efficiency of a ticlopyr immunoaffinity column over time.

Table 4
Recovery of triclopyr in tap water samples fortified

Fortification concentration of samples (μg ml^{-1})	Found concentration of sample (μg ml^{-1}), $n=3$	R.S.D. (%)	Recovery (%)
1.0	0.89 ± 0.02	2.75	89
10.0	8.5 ± 0.2	1.95	85
50.0	44.5 ± 0.8	1.75	89

4. Conclusions

Triclopyr IA column probe to be and efficient chromatographic phase to clean-up and quantitates traces of triclopyr by means a single step chromatographic operation. Recovery values are between 80 and 110% and the use of the column is efficient as least 30 times. Since no interfering peaks from the matrix or contaminants are showing up, the analysis can be very rapid and simple.

Acknowledgement

The authors thank financial support for this work from grant CTQ2004-07778 from Spain's DGICyT.

References

[1] A. Visconti, M. Pascale, J. Chromatogr. A 815 (1998) 133.
[2] W.L. Shelver, G.L. Larsen, J.H. Huwe, J. Chromatogr. B 705 (1998) 261.
[3] C.K. Holtzapple, E.J. Pishko, L.H. Stonker, Anal. Chem. 72 (2000) 4148.
[4] M.A. Concejero, R. Galve, E. Abad, J. Rivera, M. de Frutos, Anal. Chem. 73 (2001) 3119.
[5] M.M. Rhemrev-Boom, M. Yates, M. Rudolph, M. Raedts, J. Pharm. Biomed. Anal. 24 (2001) 825.
[6] M.A. Concejero, E. Abad, J. Rivera, B. Herrador, M.J. Gonzalez, M. de Frutos, J. Sep. Sci. 27 (2004) 1093.
[7] J. Yan, M.P. Zhao, Y.Z. Li, J. Sep. Sci. 28 (2005) 1163.
[8] V. Pichon, A.I. Krasnova, M.-C. Hennion, Chromatographia 60 (2004) S221.
[9] W. Clarke, A.R. Chowdhuri, D.S. Hage, Anal. Chem. 73 (2001) 2157.
[10] N. Delaunay, V. Pichon, M.-C. Hennion, J. Chromatogr. B 745 (2000) 15.
[11] H. Fennet, E. Beltran, B. Gadji, J.F. Cooper, M.C. Coste, J. Agric. Food Chem. 49 (2001) 1293.
[12] A.E. Prince, T.S. Fan, B.A. Skoczenski, R.J. Bushway, Anal. Chim. Acta 444 (2001) 37.
[13] E. Watanabe, Y. Yushimura, Y. Ynasa, H. Nakazawa, Anal. Chim. Acta 433 (2001) 199.
[14] Z. Wu, J. Li, L. Zhu, H. Luo, X. Xu, J. Chromatogr. B 755 (2001) 361.
[15] D.S. Hage, J. Chromatogr. B 715 (1998) 2.
[16] V. Pichon, M. Bouzige, M.-C. Hennion, Anal. Chim. Acta 376 (1998) 21.
[17] J.M. Van Emmon, C.L. Gerlach, K. Kbowman, J. Chromatogr. B 715 (1998) 211.
[18] V. Pichon, M. Bouzige, C. Miege, M.-C. Hennion, Trends Anal. Chem. 18 (1999) 219.
[19] D.S. Hage, Clin. Chem. 45 (1999) 593.
[20] Z. Tang, H.T. Karnes, Biomed. Chromatogr. 14 (2000) 593.
[21] D. Tsikas, J. Biochem. Biophys. Meth. 49 (2001) 705.
[22] M.-C. Hennion, V. Pichon, J. Chromatogr. A 1000 (2003) 29.
[23] K.R. Salomon, C.S. Bowhey, K. Liber, G.R. Stephenson, J. Agric. Food Chem. 36 (1998) 1314.
[24] K.C. Ting, C.S. Lee, J. Chromatogr. A 690 (1995) 119.
[25] K. Woodburn, W.R. Green, H.E. Westerdahl, J. Agric. Food Chem. 41 (1993) 2172.
[26] H.M. Koch, J. Angerer, J. Chromatogr. B 759 (2001) 43.
[27] C. Aprea, A. Betta, G. Catenacci, A. Lotti, S. Magnaghi, A. Barisano, V. Passini, I. Pavan, G. Sciarra, V. Vitalone, C. Minoia, J. AOAC Int. 82 (1999) 305.
[28] J.R. Ormand, D.A. McNett, M.J. Bartels, J. Anal. Toxicol. 23 (1999) 35.
[29] K.A. Brzak, D.W. Harms, M.J. Bartels, R.J. Nolan, J. Anal. Toxicol. 22 (1998) 203.
[30] A.W. Abu-Qare, M.B. Abou-Donia, J. Chromatogr. Sci. 39 (2001) 200.
[31] A.W. Abu-Qare, M.B. Abou-Donia, J. Anal. Toxicol. 25 (2001) 275.
[32] A.W. Abu-Qare, M.B. Abou-Donia, J. Chromatogr. B 754 (2001) 533.
[33] J.V. Sancho, O.J. Pozo, F. Hernandez, Rapid Commun. Mass Spectrom. 14 (2000) 1485.
[34] F. Garcia Sanchez, A. Navas Diaz, A.F. Gonzalez, J. Lovillo, Anal. Chim. Acta 439 (2001) 131.
[35] E. Watanabe, R. Hocino, Y. Kanzaki, H. Tokumoto, H. Kubo, H. Nakazawa, J. Agric. Food Chem. 50 (2002) 3637.
[36] J.K. Rasmussen, S.M. Heilmann, L.R. Krepski, K.M. Jensen, J. Mickelson, K. Johnson, React. Polym. 16 (1992) 199.
[37] K. Ertekin, S. Alp, C. Karapire, B. Yenegül, E. Henden, S. Içli, J. Photochem. Photobiol. A 137 (2000) 155.

Available online at www.sciencedirect.com
ScienceDirect
Talanta 71 (2007) 1136–1143
Talanta
www.elsevier.com/locate/talanta

Improvement of prediction ability of PLS models employing the wavelet packet transform: A case study concerning FT-IR determination of gasoline parameters

Rodrigo Neves Figueiredo dos Santos [1], Roberto Kawakami Harrop Galvão [1], Mario Cesar Ugulino Araujo [*,2], Edvan Cirino da Silva [2]

Universidade Federal da Paraíba, CCEN, Departamento de Química, Laboratório de Automação e Instrumentação em Química analítica/Quimiometria (LAQA), Caixa Postal 5093, CEP 58051-970, João Pessoa, PB, Brazil

Received 4 May 2006; received in revised form 2 June 2006; accepted 3 June 2006
Available online 24 July 2006

Abstract

The wavelet packet transform (WPT) is a variant of the standard wavelet transform that offers greater flexibility in the decomposition of instrumental signals. Although encouraging results have been published concerning the use of WPT for signal compression and denoising, its application in multivariate calibration problems has received comparatively little attention, with very few contributions reported in the literature. This paper presents an investigation concerning the use of WPT as a feature extraction tool to improve the prediction ability of PLS models. The optimization of the wavelet packet tree is accomplished by using the classic dynamic programming algorithm and an entropy cost function modified to take into account the variance explained by the WPT coefficients. The selection of WPT coefficients for inclusion in the PLS model is carried out on the basis of correlation with the dependent variable, in order to exploit the joint statistics of the instrumental response and the parameter of interest. This WPT-PLS strategy is applied in a case study involving FT-IR spectrometric determination of four gasoline parameters, namely specific mass (SM) and the distillation temperatures at which 10%, 50%, 90% of the sample has evaporated. The dataset comprises 103 gasoline samples collected from gas stations and 6144 wavelengths in the range 2500–15000 nm. By applying WPT to the FT-IR spectra, considerable compression with respect to the original wavelength domain is achieved. The effect of varying the wavelet and the threshold level on the prediction ability of the resulting models is investigated. The results show that WPT-PLS outperforms standard PLS in most wavelet-threshold combinations for all determined parameters.
© 2006 Elsevier B.V. All rights reserved.

Keywords: Wavelet packet transform; Multivariate calibration; PLS regression; FT-IR spectrometry; Gasoline analysis

1. Introduction

The wavelet transform (WT) is a multiresolutional analysis tool that has found several applications in analytical chemistry [1], such as signal denoising [2], database compression [3], localization of inflection points [4], and multivariate calibration [5,6]. An extension of WT that has also been investigated in the literature [7–16] is the wavelet packet transform (WPT) [17], which offers more flexibility for analytical signal representation and feature extraction [18]. Similarly to WT, the applications of WPT have involved signal compression [8] and denoising [9–11]. Applications in pattern recognition and classification have also become popular [12–16].

In the context of multivariate calibration, either linear or nonlinear, the use of WPT has received comparatively little attention, with very few contributions reported in the literature [19,20]. In [19], WPT was employed at the input stage of an artificial neural network for simultaneous kinetic determination of Cu(II), Fe(III), and Ni(II). In [20], WPT was employed for

* Corresponding author. Tel.: +55 83 3216 7438; fax: +55 83 3216 7437.
E-mail address: laqa@quimica.ufpb.br (M.C.U. Araujo).
[1] Present address: Divisão de Engenharia Eletrônica, Instituto Tecnológico de Aeronáutica, Brazil.
[2] Present address: Universidade Federal da Paraíba, CCEN, Departamento de Química, Laboratório de Automação e Instrumentação em Química Analítica/Quimometria (LAQA), Brazil.

0039-9140/$ – see front matter © 2006 Elsevier B.V. All rights reserved.
doi:10.1016/j.talanta.2006.06.023

noise extraction prior to PLS regression for spectrophotometric determination of Ni(II), Cd(II), Cu(II) and Zn(II) with xylenol orange and cetyltrimethyl ammonium bromide in synthetic samples. The range 492–650 nm was employed with a 2 nm resolution. The WPT coefficients kept in the regression procedure were selected on the basis of a hard thresholding method [21] based on the coefficient magnitudes.

In the present paper, the use of WPT for feature extraction prior to PLS regression is investigated in a case study concerning the simultaneous determination of four quality parameters of gasoline by FT-IR spectrometry. The matrix involved in this application is considerably more complex than the metal solutions studied in [20]. Moreover, as compared with the UV–vis spectra in [20] (80 wavelengths), the FT-IR spectra have a much larger number of variables (6144 wavelengths), which presents a more challenging task in terms of feature extraction. Furthermore, rather than selecting the WPT coefficients on the basis of their magnitude, the selection is based on correlation with the dependent variable (gasoline parameter in each PLS model). Therefore, the joint statistics of the instrumental response and the parameter of interest are exploited, which is of relevance given the nature of the problem (regression). The effect of varying the threshold on the prediction ability of the resulting PLS model is also investigated.

The gasoline parameters under consideration are specific mass (SM) and the distillation temperatures at which 10%, 50%, 90% of the sample has evaporated (T10%, T50%, T90%). The determination of these parameters is required by the Brazilian national fuel authority (Agência Nacional de Petróleo, Gás Natural e Biocombustíveis, ANP) as part of fuel quality control. The specific mass is directly related to the total energy content of a sample with given mass or volume. Deviations from normal values may point to contaminations. The distillation temperatures depend on the volatility features of the fuel and are used to verify whether light and heavy fractions are within allowed limits. Volatility is the main determinant of the tendency for a hydrocarbon mixture to generate potentially explosive vapours. It facilitates cold starts and also affects engine performance because of its influence on fuel evaporation in the admission collectors and cylinders before and after combustion. Small T10% values indicate good volatility for engine start-up, whereas small T50% values favour acceleration performance. The T90% temperature is associated to the content of fuel constituents with high boiling points. High T90% values may contribute towards better fuel economy and antiknock features, but excessively high values may lead to the formation of deposits in the combustion chamber and gum in the fuel admission system.

It is worth noting that the relation between infrared absorbance and the physical parameters is not based on a fundamental linear law (such as Beer's law, which arises in the context of spectroscopic determination of absorbent species). However a large body of empirical evidence [22–29] suggests that linear PLS regression may be appropriate for FT-IR or NIR determination of physical parameters in petroleum products, provided that the resulting model is employed within the calibration limits.

2. Background and theory

2.1. Notation

Matrices are represented by bold capital letters, vectors by bold lowercase letters, and scalars by italic characters. Elements of a sequence or vector are denoted by italic characters with a subscript index. A vertical bar (|) represents the concatenation of two vectors. The hat symbol (∧) indicates a predicted value.

2.2. Filter bank implementation of the discrete wavelet transform (DWT)

As described in the wavelet literature [1,18], the DWT of a data vector $\mathbf{x}_{1\times J}$ can be calculated in a fast manner by using a filter bank of the form depicted in Fig. 1a. The basic structure of the filter bank comprises a low-pass/high-pass filter pair followed by a down-sampling operation, which consists of discarding every other point of the filter outputs. The filters can be chosen such that the overall transformation is invertible, thus preserving the information content of signal **x**. The output of the low-pass channel can be further decomposed by successive filter pairs up to a given number *Nit* of iterations. The final result of the decomposition of **x** is a vector $\mathbf{t} = [\mathbf{c}(Nit)|\mathbf{d}(Nit)|\mathbf{d}(Nit–1)|\cdots|\mathbf{d}(1)]$, in which sequences **c**(*s*) and **d**(*s*) are termed approximation and detail coefficients at the *s*th decomposition level, respectively. The filter bank can also be represented in a binary tree diagram, as shown in Fig. 1b. In this diagram, the filtering and down-sampling operations are represented by branches (low-pass filtering pointing to the left and high-pass filtering pointing

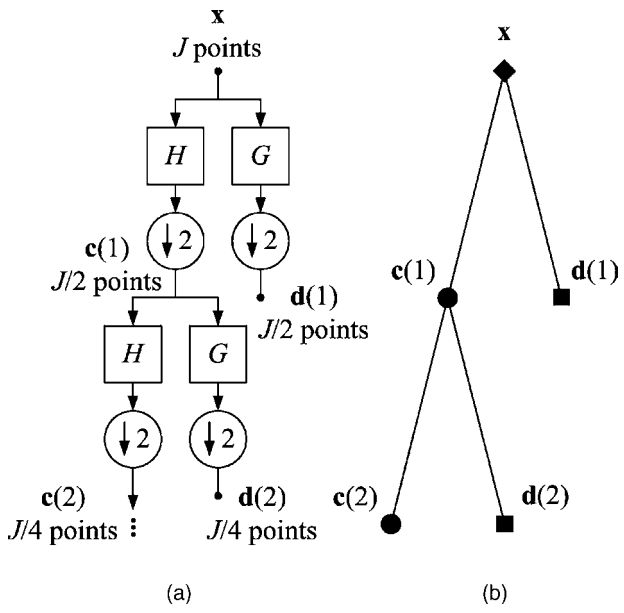


Fig. 1. (a) Filter bank implementation of the discrete wavelet transform. *H* and *G* represent low-pass and high-pass filters, respectively. ↓2 denotes the down-sampling operation. The approximation and detail coefficients at the *s*th decomposition level are denoted by **c**(*s*) and **d**(*s*), respectively. (b) Schematic tree representation of the filter bank. The root note (original signal), the approximation coefficients, and the detail coefficients are represented by symbols (♦), (■), and (●), respectively.

to the right), whereas the approximation and detail coefficients correspond to nodes.

2.3. Wavelet packet transform

In WPT, additional flexibility is gained by iterating the filtering/down-sampling operations on the high-pass (detail) nodes of the filter bank. However, in this case, the analyst if faced with the problem of determining the best sequence of low-pass/high-pass operations, which amounts to optimizing the structure of the decomposition tree. The complexity of such an optimization problem is considerable because of the large number of possible trees that can be generated for a given number of decomposition levels. In fact, the number N_s of different trees with at most smax levels follows the recursive relation $N_{smax} = 1 + (N_{smax-1})^2$ with $N_0 = 1$ [17]. For smax = 6, for instance, there are more than 2.1×10^{11} possible trees.

A computationally simple algorithm to find the best decomposition tree for a given signal was proposed by Coifman and Wickerhauser [17]. This algorithm follows a "bottom-up" dynamical programming procedure, starting from a complete tree with the maximum height established by the analyst. Subtrees are replaced or not by their common root on the basis of local optimality tests. Such a procedure leads to the optimal tree provided that the cost C to be minimized is an additive function, that is

$$C(\mathbf{t}) = \sum_{j=1}^{J} C(t_j) \quad (1)$$

where t_j are the elements of vector $\mathbf{t}$ resulting from the decomposition of $\mathbf{x}$. In this context, a cost function usually employed for the purpose of signal compression is the Shannon entropy defined as

$$C(\mathbf{t}) = -\sum_{j=1}^{J} t_j^2 \log(t_j^2) \quad (2)$$

where the sum is carried out over the nonzero WPT coefficients. By minimizing such an entropy cost, the energy of the signal becomes concentrated in a few coefficients, whereas the remaining approach zero and can be discarded.

In [20], this cost was adopted to optimize the tree with respect to the mean spectra of the calibration set. The SURE (Stein's unbiased risk estimation) criterion [30] was then applied to determine an appropriate threshold level. Thereafter, each spectrum in the data set was decomposed by the optimized tree, the coefficients smaller (in absolute value) than the threshold were discarded and the spectrum was reconstructed by using the inverse WPT. The spectra reconstructed in this manner were then used to build a PLS model.

2.4. Criteria adopted for tree optimization and selection of WPT coefficients

The classical algorithms for tree optimization and threshold selection described above were developed for signal compression problems. Multivariate calibration has two distinctive features that should be taken into account:

(a) the calibration database comprises several spectra (not just a single one);
(b) information regarding a dependent variable (property of interest **y**) is available.

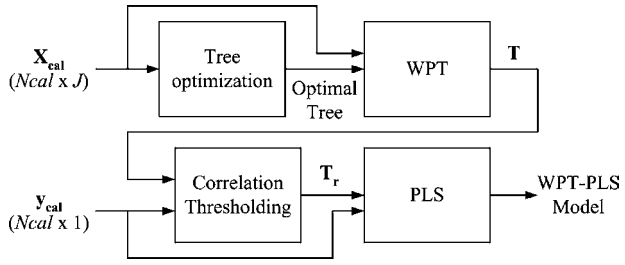


Fig. 2. WPT-PLS procedure. $\mathbf{X_{cal}}$ and $\mathbf{y_{cal}}$ denote the instrumental response matrix and the vector of property values in the calibration set, respectively. Tree optimization is carried out by using a modified entropy cost that takes into account the variance of the WPT coefficients. **T** and $\mathbf{T_r}$ denote the matrices of WPT coefficients before and after the thresholding operation.

In order to consider (a), the entropy cost function was modified in the present work in order to compress the variance of the calibration data (rather than the energy of a single spectrum) into a small number of WPT coefficients. For this purpose, the following expression was adopted for the cost:

$$C(\mathbf{T}) = -\sum_{i=1}^{\text{Ncal}} \sum_{j=1}^{J} (t_{i,j} - \bar{t}_j)^2 \log[(t_{i,j} - \bar{t}_j)^2] \quad (3)$$

where $\mathbf{T}(\text{Ncal} \times J)$ is the matrix of transformed calibration spectra, $t_{i,j}$ is the jth WPT coefficient of the ith spectrum and $\bar{t}_j$ is the average value of the jth column of **T**.

After the tree has been optimized, a subset of the WPT coefficients is selected on the basis of the correlation with the dependent variable, which is similar to the mutual information criterion described in [31]. Those coefficients that display a correlation coefficient (as observed in the calibration set) smaller than a given threshold are discarded. Thereafter, instead of reconstructing the spectra, the reduced matrix of WPT coefficients is directly employed to build a PLS model, as in [32]. It is worth noting that the reconstruction step would not introduce or remove information and therefore the PLS regression can be carried out in the wavelet domain. Such a modelling procedure, which is summarized in Fig. 2, will be henceforth termed WPT-PLS.

3. Experimental

3.1. Data set

The data set employed in this study consists of 103 gasoline samples collected from gas stations that are representative of the Pernambuco and Alagoas states in Brazil. The gasoline contained approximately 25% v/v ethanol, in conformity with

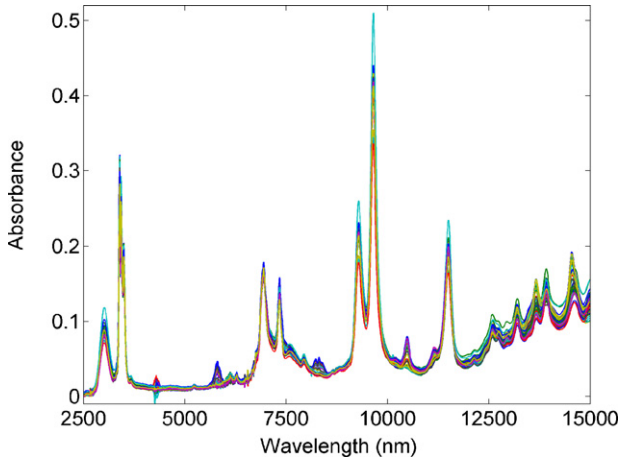


Fig. 3. FT-IR spectra of the gasoline samples.

the standard defined by ANP. The samples were stored in amber glass flasks under refrigeration at 5 °C.

The reference values for specific mass and distillation temperatures (T10%, T50%, T90%) were obtained according to the methods recommended by the American Society for Testing and Material (ASTM D 4052 and ASTM D 86, respectively).

The spectra were acquired with an FT-IR Perkin Elmer Spectrum GX spectrometer fitted with an ATR probe (Axiom Analytical, model DPR-210XY). The spectra were acquired at room temperature (22 °C) as the average of 16 scans, using a spectral resolution of 2 cm^{-1} in the range 2500–15000 nm. As a result, each spectrum consisted of 6144 points, as shown in Fig. 3.

3.2. Modelling and validation

The variables were mean-centered prior to the modelling procedures. A preliminary PLS analysis was carried out to sort the 103 samples into calibration, validation and prediction sets. On the basis of the resulting scores, the data set was divided into 63 calibration, 20 validation and 20 prediction samples. The validation and prediction samples were selected to cover the **X** and **Y** overall variation, while avoiding extreme points in the **X** and **Y** spaces.

PLS modelling and WPT decompositions were carried out with the Matlab 6.5 software, by using lab-made programs. In

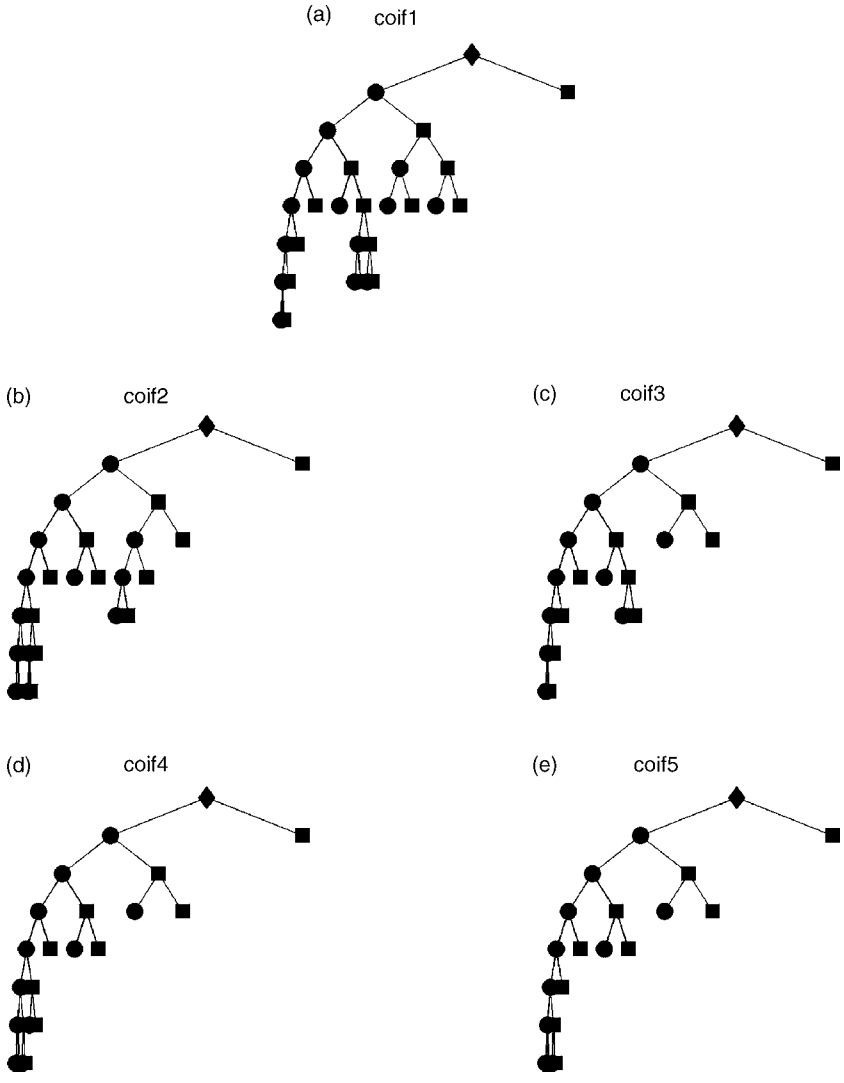


Fig. 4. Optimal trees obtained for the Coiflet family.

Table 1
PLS results

Property	Number of latent variables	RMSEP
SM	4	1.9 kg/m^3
T10%	5	0.7 °C
T50%	5	0.4 °C
T90%	11	1.6 °C

the PLS calibration, an appropriate number of latent variables (r) for each gasoline property was determined on the basis of the error obtained in the validation set. The criterion of Haaland and Thomas was applied to find the optimum point in the curve of prediction error sum of squares (PRESS) *versus* r [33,34]. Such a criterion consists of employing an F-test to determine the smallest value of r for which PRESS(r) is not significantly larger than the global PRESS minimum. An F-ratio probability of 0.75 is adopted, as suggested elsewhere [35]. The number of latent variables obtained in this manner was also adopted in the WPT-PLS models.

Eighteen wavelets were compared in the WPT-PLS modelling, as in [20]: nine from the Daubechies family (db4, db6, db8, db10, db12, db14, db16, db18, db20), four from the Symlet family (sym5, sym6, sym7, sym8), and five from the Coiflet family (coif1, coif2, coif3, coif4, coif5). The low-pass and high-pass filters for db$N$, sym$N$ and coif$N$ have length 2N, 2N, and 6N, respectively. The maximum number of decomposition levels in the wavelet tree was set to seven. This limit was established because at each tree node at level seven, the 6144 points in the spectrum are reduced to 48 WPT coefficients. Therefore, an additional decomposition would lead to sequences of 24 coefficients, which are shorter than some of the filters employed in the study. Filtering was carried out by using circular convolution. The correlation threshold for discarding WPT coefficients was established as a fraction of the single largest correlation coefficient (with the dependent variable **y**) observed among the WPT coefficients.

The results for each gasoline parameter were compared in terms of the root-mean-square error in the prediction set (RMSEP) defined as

$$\mathrm{RMSEP} = \sqrt{\frac{1}{N_\mathrm{p}}\sum_{i=1}^{N_\mathrm{p}}(y_\mathrm{p}^i - \hat{y}_\mathrm{p}^i)^2} \quad (4)$$

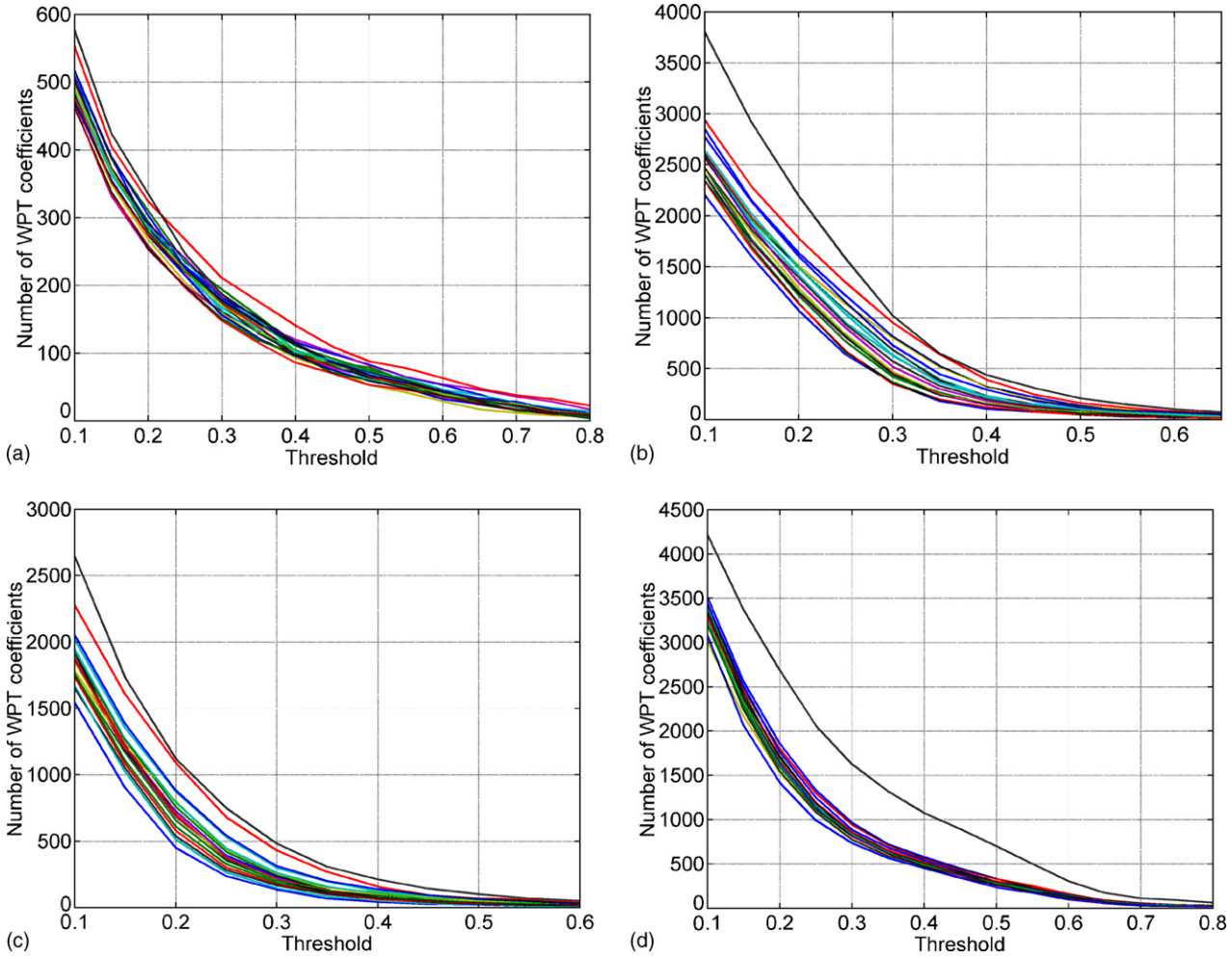


Fig. 5. Number of WPT coefficients remaining after the thresholding operation as a function of the threshold level for (a) specific mass; (b) T10%; (c) T50%, and; (d) T90%. The graphs display the curves for the 18 wavelets employed in the study.

where y_p^i and $\hat{y}_p^i$ are the reference and predicted values of the parameter under consideration in the ith prediction sample and $N_p = 20$ is the number of prediction samples.

4. Results and discussion

Table 1 summarizes the results obtained by conventional PLS modelling.

For illustration, Fig. 4 depicts the optimal wavelet packet trees obtained for the Coiflet family. As can be seen, as the filter length is increased (from coif1 to coif5), branches on the high-pass side of the tree (right-hand side) are removed and new branches are introduced on the low-pass side. Such a finding can be explained by noting that shorter filters have worse frequency selectivity and therefore there is a "spill-over" of information into the high-pass side of the tree. Such information needs to undergo a further refinement (that is, additional filtering iterations), which leads to the appearance of more branches on the high-pass side. On the other hand, it is worth noting that shorter filters have a better resolution in the wavelength axis. Because of such a trade-off between frequency selectivity and wavelength resolution, it is worth investigating the use of wavelet filters of different lengths.

Fig. 5 presents the number of WPT coefficients remaining after the thresholding operation as a function of the correlation threshold level. The threshold was increased in 0.05 increments starting from 0.10 up to the value where the number of remaining coefficients is insufficient to build a PLS model with the specified number of latent variables (as shown in Table 1). As can be seen, considerable compression with respect to the original wavelength domain (6144 spectral variables) can be achieved. The overall behaviour is similar for the 18 wavelets, with the exception of coif1, which leads to a larger number of WPT coefficients, specially for T10% and T90% (upper curves in Fig. 5b and d. Such a finding can be ascribed to the small length (six points) and consequently poor frequency selectivity of the low-pass and high-pass coif1 filters, which are the shortest among those considered in the study.

Fig. 6 presents the RMSEP values resulting from combinations of wavelet and threshold level in WPT-PLS. It can be noticed that smaller RMSEP values (darker grey) are generally

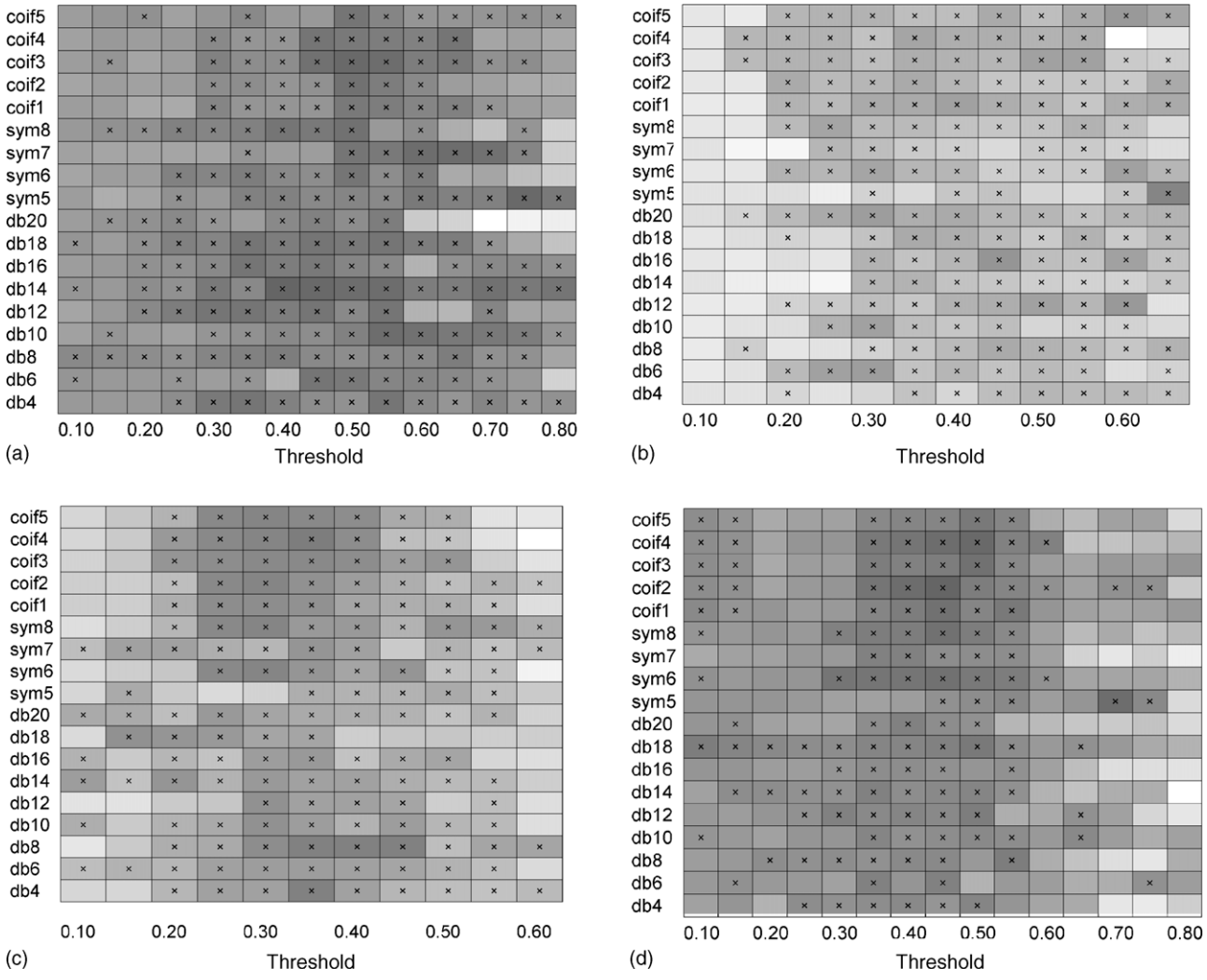


Fig. 6. RMSEP values obtained for (a) specific mass; (b) T10%; (c) T50%, and; (d) T90% as a function of the wavelet and threshold level employed in WPT-PLS. Darker grey levels correspond to smaller RMSEP values. The crosses (×) indicate wavelet-threshold pairs for which WPT-PLS resulted in an RMSEP smaller (taking into account the precision of the reference method) than PLS.

Table 2
Best WPT-PLS results for a threshold level of 0.50

Property	Wavelet	Number of WP coefficients	RMSEP
SM	coif3	68	1.3 kg/m^3
T10%	coif3	53	0.5 °C
T50%	coif3	38	0.3 °C
T90%	coif4	303	1.1 °C

obtained for intermediate threshold levels. In fact, if a small threshold is employed, information that is not related to the parameter of interest is included in the modelling process. On the other hand, if the threshold is too high, relevant information may be lost. For most cases (indicated by crosses in Fig. 6), the RMSEP obtained with WPT-PLS is smaller than the corresponding value for PLS. If an intermediate threshold level of 0.50 is adopted, for instance, the best WPT-PLS results are those shown in Table 2.

By comparing the RMSEP in Table 2 with the corresponding values in Table 1, it can be seen that improvements were obtained for all properties. Interestingly, the best results in this case were attained by using similar wavelets: coif3 for SM, T10%, T50% and coif4 for T90%. Moreover, if coif3 was also used for T90%, the RMSEP for this property would increase by a very small amount (from 1.1 °C to 1.2 °C).

It is worth noting that the WPT-PLS models in Table 2 were built by using only a small fraction of the total number of coefficients (6144). The largest number of WPT coefficients was required for T90%. Such a finding is in agreement with the conventional PLS modelling, in which T90% also required the largest number of latent variables, which suggests that more sources of variability affect this particular property.

5. Conclusions

The results of the case study presented in this paper indicate that the use of the wavelet packet transform coupled with an appropriate thresholding technique may lead to considerable improvements in the prediction ability of PLS models. Unlike [20], such improvements were now demonstrated in a large-scale analytical problem involving a complex fuel matrix, an extensive dataset of real samples and spectra with a very large number of variables.

Further investigations could extend the scope of this study to other instrumental techniques, as well as matrix types. From a theoretical point of view, algorithms for the optimization of the wavelet packet tree may be developed to take into account the joint statistics between instrumental response (**X**) and parameter values (**y**). Furthermore, variable selection techniques other than simple thresholding (such as genetic algorithms [36], simulated annealing [37] and the successive projections algorithm [38]) could be employed to take into account multivariate effects in the selection of WPT coefficients. Finally, additional studies concerning the use of wavelet packets with nonlinear modelling techniques, such as artificial neural networks [19], could be carried out.

Acknowledgments

This work was supported by CNPq (grants Universal 475204/2004-2, Pronex 015/98 and research fellowships) and CAPES (PROCAD 0081/05-1 and scholarships). The authors also wish to thank Dr. Fernanda Araujo Honorato and Prof. Maria Fernanda Pimentel of the Departamento de Engenharia Química of the Universidade Federal de Pernambuco, Brasil for providing the gasoline sample spectra and the reference values for the properties considered in this study.

References

[1] B. Walczak, Wavelets in Chemistry, Elsevier Science, New York, 2000.
[2] L. Pasti, B. Walczak, D.L. Massart, P. Reschiglian, Chemom. Intell. Lab. Syst. 48 (1999) 21.
[3] A.K.M. Leung, F.T. Chau, J.B. Gao, T.M. Shih, Chemom. Intell. Lab. Syst. 43 (1998) 69.
[4] V.L. Martins, L.F. Almeida, S.L. Castro, R.K.H. Galvão, M.C.U. Araújo, E.C. Silva, J. Chem. Inf. Comp. Sci. 43 (2003) 1725.
[5] P.J. Brown, T. Fearn, M. Vannucci, J. Am. Stat. Assoc. 96 (2001) 398.
[6] R.K.H. Galvão, G.E. José, H.A. Dantas Filho, M.C.U. Araujo, E.C. Silva, H.M. Paiva, T.C.B. Saldanha, E.S.O.N. Souza, Chemom. Intell. Lab. Syst. 70 (2004) 1.
[7] A.K.M. Leung, F.T. Chau, J.B. Gao, Chemom. Intell. Lab. Syst. 43 (1998) 165.
[8] B. Walzac, D.L. Massart, Chemom. Intell. Lab. Syst. 38 (1997) 39.
[9] B. Walzac, D.L. Massart, Chemom. Intell. Lab. Syst. 36 (1997) 81.
[10] H.W. Tan, J. Chemom. 13 (1999) 543.
[11] X.G. Shao, W.S. Cai, Anal. Lett. 32 (1999) 743.
[12] A.K.M. Leung, B. Walczak, B. Bogaert, D.L. Massart, Anal. Chem. 68 (1996) 1742.
[13] E.R. Collantes, R. Duta, W.J. Welsh, W.L. Zielinski, J. Brower, Anal. Chem. 69 (1997) 1392.
[14] M. Cocchi, R. Seeber, A. Ulrici, Chemom. Intell. Lab. Syst. 57 (2001) 97.
[15] M. Cocchi, C. Durante, G. Foca, D. Manzini, A. Marchetti, A. Ulrici, Chemom. Intell. Lab. Syst. 71 (2004) 129.
[16] A. Antonelli, M. Cocchi, P. Fava, G. Foca, C.G. Franchini, D. Manzini, A. Ulrici, Anal. Chim. Acta 515 (2004) 3.
[17] R.R. Coifman, M.V. Wickerhauser, IEEE Trans. Inf. Theory 38 (1992) 713.
[18] M.V. Wickerhauser, Adapted Wavelet Analysis from Theory to Software, A.K. Peters, Natick, MA, 1994.
[19] S. Ren, L. Gao, Anal. Bioanal. Chem. 378 (2004) 1392.
[20] L. Gao, S. Ren, Spectrochim. Acta A 65 (2005) 3013.
[21] D.L. Donoho, IEEE Trans. Inf. Theory 41 (1995) 613.
[22] D. Ozdemir, Petroleum Sci. Tech. 23 (2005) 1139.
[23] C.C. Felicio, L.P. Bras, J.A. Lopes, L. Cabrita, J.C. Menezes, Chemom. Intell. Lab. Syst. 78 (2005) 74.
[24] F.A. Honorato, R.K.H. Galvão, M.F. Pimentel, B.B. Neto, M.C.U. Araújo, F.R. Carvalho, Chemom. Intell. Lab. Syst. 76 (2005) 65.
[25] C.E. Boschetti, A.C. Olivieri, J. Near Infrared Spec. 12 (2004) 85.
[26] M.V. Reboucas, B.D. Neto, J. Near Infrared Spec. 9 (2001) 263.
[27] Z.M. Wang, W.Y. Hua, Z.K. Wei, H.H. Zhang, H.Z. Wu, Spec. Spectral Anal. 19 (1999) 684.
[28] G.E. Fodor, R.A. Mason, S.A. Hutzler, Appl. Spec. 53 (1999) 1292.
[29] J.M. Andrade, D. Prada, S. Muniategui, P. Lopez, Fresenius J. Anal. Chem. 355 (1996) 723.
[30] C. Stein, Ann. Stat. 9 (1981) 1135.
[31] B.K. Alsberg, A.M. Woodward, M.K. Winson, J.J. Rowland, D.B. Kell, Anal. Chim. Acta 368 (1998) 29.
[32] J. Trygg, D.L. Svante Wold, Chemom. Intell. Lab. Syst. 42 (1998) 209.
[33] D.M. Haaland, E.V. Thomas, Anal. Chem. 60 (1988) 1193.

[34] J. Moros, F.A. Inon, S. Garrigues, M. de la Guardia, Anal. Chim. Acta 538 (2005) 181.
[35] B.X. Li, D.M. Wang, C.L. Xu, Z.J. Zhang, Microchim. Acta 149 (2005) 205.
[36] R. Leardi, J. Chemometrics 15 (2001) 559.
[37] A. Aulinger, J.W. Einax, A. Prange, Chemom. Intell. Lab. Syst. 72 (2004) 35.
[38] M.C.U. Araujo, T.C.B. Saldanha, R.K.H. Galvão, T. Yoneyama, H.C. Chame, V. Visani, Chemom. Intell. Lab. Syst. 57 (2001) 65.

Available online at www.sciencedirect.com
ScienceDirect
Talanta 71 (2007) 1375–1381
Talanta
www.elsevier.com/locate/talanta

Speciation of selenium(IV) and selenium(VI) in environmental samples by the combination of graphite furnace atomic absorption spectrometric determination and solid phase extraction on Diaion HP-2MG

Kadriye O. Saygi [a], Esra Melek [a], Mustafa Tuzen [a], Mustafa Soylak [b,*]

[a] *Gaziosmanpasa University, Faculty of Science and Arts, Chemistry Department, 60250 Tokat, Turkey*
[b] *Erciyes University, Faculty of Science and Arts, Chemistry Department, 38039 Kayseri, Turkey*

Received 23 March 2006; received in revised form 24 June 2006; accepted 6 July 2006
Available online 14 August 2006

Abstract

A simple solid phase extraction procedure for speciation of selenium(IV) and selenium(VI) in environmental samples has been proposed prior to graphite furnace atomic absorption spectrometry. The method is based on the solid phase extraction of the selenium(IV)–ammonium pyrrolidine dithiocarbamate (APDC) chelate on the Diaion HP-2MG. After reduction of Se(VI) by heating the samples in the microwave oven with 4 mol l^{-1} HCl, the system was applied to the total selenium. Se(VI) was calculated as the difference between the total selenium content and Se(IV) content. The experimental parameters, pH, amounts of reagents, eluent type and sample volume were optimized. The recoveries of analytes were found greater than 95%. No appreciable matrix effects were observed. The adsorption capacity of sorbent was 5.20 mg g^{-1} Se (IV). The detection limit of Se (IV) (3sigma, $n = 11$) is 0.010 μg l^{-1}. The preconcentration factor for the presented system was 100. The proposed method was applied to the speciation of selenium(IV), selenium(VI) and determination of total selenium in natural waters and microwave digested soil, garlic, onion, rice, wheat and hazelnut samples harvested various locations in Turkey with satisfactory results. In order to verify the accuracy of the method, certified reference materials (NIST SRM 2711 Montana Soil, NIST SRM 1568a Rice Flour and NIST SRM 8418 Wheat Gluten) were analyzed and the results obtained were in good agreement with the certified values. The relative errors and relative standard deviations were below 6 and 10%, respectively.
© 2006 Elsevier B.V. All rights reserved.

Keywords: Selenium; Speciation; Solid phase extraction; Diaion HP-2MG; Atomic absorption spectrometry

1. Introduction

Selenium is an essential nutrient and necessary for human being. Selenium, present in soil, water and all living organisms, plays an important role in environmental and health studies [1–3]. Selenium is often deficient in the natural diets of domestic animal species. Se deficiency is associated with disease conditions and general impairment of the immune system. Supplementation of selenium to humans already consuming the RDA (recommended dietary allowance) may help to prevent certain cancers [4–6]. The inorganic selenium species most frequently found in waters and soils are selenite (Se(IV)) and selenate (Se(VI)). In this regard, a method for speciation is needed because selenium availability for plankton uptake, mobility in soil and toxicity in biota depends on the oxidation state of this element [4]. Beside the total content of selenium, the chemical form in which selenium is present is also most important due to the differences in bioavailability and toxicity of the different forms [5–7].

Various instrumental techniques including UV–vis spectrophotometry [8,9], voltammetry [10], X-ray fluorescence [11], high-performance liquid chromatography atomic fluorescence spectrometry [12], voltammetry [12,13], gas chromatography [14], atomic absorption spectrometry [15–18], etc., have been used for the determination of selenium. The levels of the selenium in the environmental samples are generally lower than detection limits of these techniques. The influences of the matrix components of the real samples are another problem in these determinations. For many of these techniques, it is not possible to determine different oxidation states of

* Corresponding author. Tel.: +90 352 4374 901; fax: +90 352 4374 933.
E-mail address: soylak@erciyes.edu.tr (M. Soylak).

0039-9140/$ – see front matter © 2006 Elsevier B.V. All rights reserved.
doi:10.1016/j.talanta.2006.07.008

the selenium species [19–21]. In order to solve these problems, preconcentration–separation techniques including solvent extraction [22], coprecipitation [23,24], ion-exchange [3,25,26], etc., have been proposed.

Solid-phase extraction is being utilized for preconcentration–separation and also speciation of heavy metals at trace levels due to its flexibility, economical and environment-friendly, absence of emulsion, speed and simplicity, sampling in the field, safety and ease of automation [27–29]. The application of solid phase extraction for the selenium species is a popular subject of the analytical chemistry [4,11,14,30–33]. Speciation of inorganic selenium in natural water samples was performed by Pyrzynska et al. [4]. The procedure was including solid phase extraction of selenium species on alumina microcolumn and their graphite furnace atomic absorption spectrometric determinations. A speciation procedure for selenium species have been reported by Castilla et al. [11]. The selenium species were determined by X-ray fluorescence spectrometry after sorption on activated carbon with 1-pyrrolidinecarbodithioic acid. Larraya et al. [31] have been proposed a speciation procedure for Se(VI) and Se(IV) based on the solid phase extraction of Se(IV) on activated alumina and reduction of Se(VI) to Se(IV) and determination by HG-AAS. Ferri and Sangiorgio [32] have been reported a solid phase extraction procedure on Chelex-100 resin for selenium speciation in polluted waters. The separation and preconcentration of Se(IV)/Se(VI) species by selective adsorption onto nanometer-sized titanium dioxide and determination by graphite furnace atomic absorption spectrometry have been performed with successfully results by Li and Deng [33].

Diaion adsorption resins as a class of macroporous polymeric gas chromatographic stationary phases provide large surfaces that exhibit strong adsorptive properties towards analytes that cover a wide range of hydrophobicity [34]. Diaion HP-2MG is relatively new resin for the solid-phase extraction of traces of heavy metal ions [35,36]. It is methacrylic ester copolymer, and has relatively hydrophilic nature. Its surface area, mesh size and pore size are 500 $m^2\ g^{-1}$, 25–50 mesh and 170 Å, respectively.

In the presented work, a rapid and easy speciation procedure for selenium(IV), selenium(VI) and total selenium in environmental samples by solid phase extraction on Diaion HP-2MG and their graphite furnace atomic absorption spectrometric determination has been proposed.

2. Experimental

2.1. Reagents and solutions

All chemicals used in this work, were of analytical reagent grade and were used without further purification. Deionised water (Milli-Q Millipore 18.2 MΩ cm^{-1} resistivity) was used for all dilutions. All the plastic and glassware were cleaned by soaking in dilute HNO_3 (1 + 9) and were rinsed with distilled water prior to use. The element standard solutions used for calibration were produced by diluting a stock solution of 1000 mg l^{-1} of the given element supplied by Sigma and Aldrich. Stock solutions of diverse elements were prepared from high purity compounds. The calibration standards were not submitted to the preconcentration procedure.

An ammonium pyrrolidine dithiocarbamate (APDC) solution (0.1%, w/v) was prepared by dissolving the requisite amounts of APDC in water/ethanol (75%/25%, v/v)). The solution was discharged 1 day. Diaion HP-2MG is purchased from Supelco (no.: 1–3601). In order to remove organic and inorganic contaminants, the resin was washed successively with methanol, distilled water, 1 mol l^{-1} HNO_3 in acetone, distilled water, 1 mol l^{-1} NaOH and distilled water.

0.1 mol l^{-1} HCl was used for pH 1. Phosphate buffer solutions ($H_2PO_4^-/H_3PO_4$) were prepared by mixing of appropriate volumes of 1 mol l^{-1} sodium dihydrogene phosphate and phosphoric acid solutions for pH 2, 2.5 and 3. Acetate buffer solutions (CH_3COO^-/CH_3COOH) were prepared by mixing of appropriate volumes of 1 mol l^{-1} acetic acid and 1 mol l^{-1} sodium acetate solutions for pH 4 and 5. NIST SRM 2711 Montana Soil, NIST SRM 1568a Rice Flour and NIST SRM 8418 Wheat Gluten standard reference materials were used in the experiment.

2.2. Instruments

A Perkin-Elmer AAnalyst 700 atomic absorption spectrometer equipped with HGA graphite furnace and with deuterium background corrector was used. For graphite furnace measurements, argon was used as inert gas. The operating parameters for working elements were set as recommended by the manufacturer given in Table 1. Pyrolytic-coated graphite tubes (Perkin-Elmer part no.: B3 001264) with a platform were used. Samples of 20 μl plus 10 μl of mixture of 0.015 mg Pd + 0.010 mg $Mg(NO_3)_2$ as matrix modifier during the study were injected into the furnace using Perkin-Elmer AS-800 autosampler. The signals were measured as peak areas. The absolute sensitivity is defined by the mass of an element, which gives a peak absorbance of 0.0044; it was found 22 pg for Se. The range of the calibration standards for selenium on graphite furnace atomic absorption spectrometric determinations was 0–50 μg l^{-1}. The correlation coefficient of the calibration curves were generally 0.999.

A pH meter, Sartorius pp-15 Model glass-electrode was employed for measuring pH values in the aqueous phase. Milestone Ethos D closed vessel microwave system (maximum pressure 1450 psi, maximum temperature 300 °C) was used.

Table 1
Instrument settings and analytical conditions for GFAAS determination of selenium

Wavelength (nm)	196
Slit width (nm)	2
Argon flow (ml min^{-1})	250
Atomization site	Pyrolitic/platform
Reading time (s)	5
Heating program temperature (°C (ramp time (s), hold time (s)))	
Drying 1	100 (5, 20)
Drying 2	140 (15, 15)
Ashing	1100 (10, 20)
Atomization	2100 (0, 5)
Cleaning	2600 (1, 3)

A short glass column with an inner diameter of 10 mm and a length of 100 mm, equipped with porous frits, was filled up to a height of about 25 mm with a suspension of 600 mg of Diaion HP-2MG resin in water. Prior to use; the resin was preconditioned with 10 ml of related buffer solution. After each experiment, the column was rinsed with water and stored for the next experiment.

2.3. Recommended analytical procedure for Se(IV)

The speciation method for selenium was tested with model solutions. Forty millilitre of solution containing 0.50 μg of Se(IV) ion was added 10 ml of buffer solution and 3.0 ml of APDC solution. The column was preconditioned by passing buffer solution. Selenium(IV)–APDC solution was passed through the column at a flow rate of 5 ml min^{-1}. The sample solution was permitted to flow through the column under gravity. After passing of this solution, the column was rinsed twice with 15.0 ml of buffer solution. The adsorbed chelate on Diaion HP-2MG was eluted with 8–10 ml portion of 1 mol l^{-1} HNO_3 in acetone. The eluent was evaporated over a hot plate to near dryness. The residue diluted to 5.0 ml with 1 mol l^{-1} HNO_3. The eluent was analysed for the determination of selenium by graphite furnace atomic absorption spectrometer.

2.4. Reduction of Se(VI) to Se(IV) and determination of total selenium

In order to reduction of selenium(VI) to selenium(IV), the procedure given by Ferri et al. [37] was applied to model solutions and natural water samples. Appropriate amount of concentrated hydrochloric acid was added to the solutions to give 4 mol l^{-1} as final acid concentration. Then the microwave program of 3 min for 250 W, 5 min for 450 W, 5 min for 650 W, vent: 8 min was performed. After reduction of Se(VI) to Se(IV), the method given in Section 2.3 was applied to the determination of the total selenium. The level of Se(VI) is calculated by difference of total selenium and Se(IV) concentrations.

2.5. Analysis of the real samples

2.5.1. Application to microwave digested samples

Digestion conditions for microwave system for the samples were applied as 2 min for 250 W, 2 min for 0 W, 6 min for 250 W, 5 min for 400 W, 8 min for 550 W, vent: 8 min [38,39].

NIST SRM 2711 Montana Soil, NIST SRM 1568a Rice Flour and NIST SRM 8418 Wheat Gluten standard reference materials (250 mg) were digested with 6 ml of HNO_3 (65%), 2 ml of H_2O_2 (30%) (6 ml of concentrated HCl and 2 ml of concentrated HNO_3 for Montana soil) in closed microwave digestion system and diluted to 50.0 ml with deionized water. A blank digest was carried out in the same way. Then the preconcentration procedure given above was applied to the final solutions.

In order to digestion of garlic, onion, rice, wheat and hazelnut samples, 1.0 g of sample was digested with 6 ml of concentrated HNO_3 and 2 ml of H_2O_2 (6 ml of concentrated HCl and 2 ml of concentrated HNO_3 for soil samples) in microwave system. After digestion of the samples, the volume of the digested sample was made up to 50.0 ml with distilled water. The blanks were prepared in the same way as the sample, but omitting the sample. The preconcentration procedure given above was applied to the samples.

2.5.2. Application to natural water samples

Tap water from Tokat City, River water from Greenriver-Tokat, Sea water from Blacksea analyzed were collected in pre-washed (with detergent, doubly de-ionised distilled water, dilute HNO_3 and doubly de-ionised distilled water, respectively) polyethylene bottles. The water samples were filtered through a cellulose membrane filter (Millipore) of 0.45 μm pore size. The pH of the samples was adjusted to 2.0 with buffer solution. Then the speciation procedure given above was applied to the samples. The levels of selenium in the samples were determined by graphite furnace atomic absorption spectrometry.

3. Results and discussion

The speciation method is based on sorption of selenium(IV) on Diaion HP-2MG resin as APDC complexes. The influence of several experimental parameters including pH, amounts of APDC, eluent type, sample volume, etc., on the sorption efficiency of selenium(IV) was studied.

3.1. Influences of pH

The effects of pH of the aqueous solution on the recoveries of Se(IV) and Se(VI) on Diaion HP-2MG as APDC complexes in the pH range of 1.0–5.0. The results were depicted in Fig. 1. Selenium(IV) was quantitatively recovered in the pH range of 1.0–2.5. Selenium(VI) was recovered lower than 10% at pH range of 1.5–2.5. This result shows that the speciation of selenium (IV) and selenium (VI) is possible at the pH range of

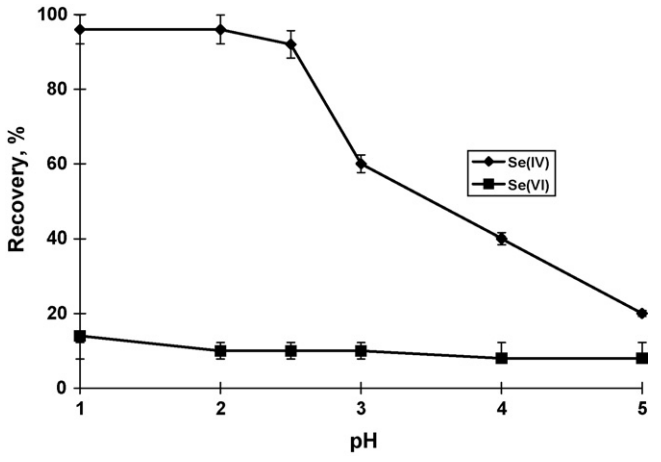


Fig. 1. Effects of pH on the speciation Se(IV) and Se(VI) on Diaion HP-2MG ($N = 3$, eluent: 1 mol l^{-1} HNO_3 in acetone).

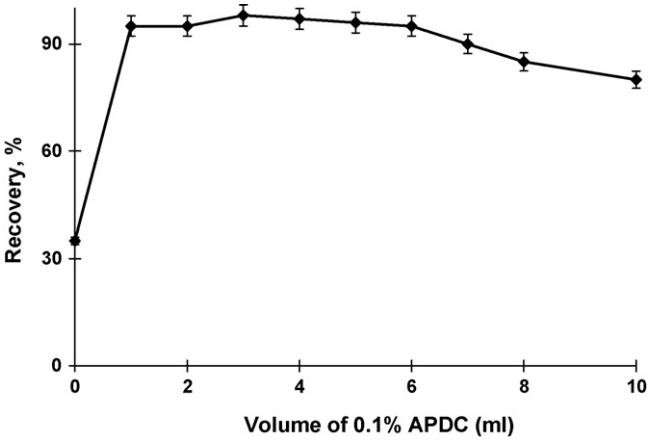


Fig. 2. Effects of APDC on the adsorption of Se(IV) on Diaion HP-2MG ($N = 3$, eluent: 1 mol l^{-1} HNO_3 in acetone).

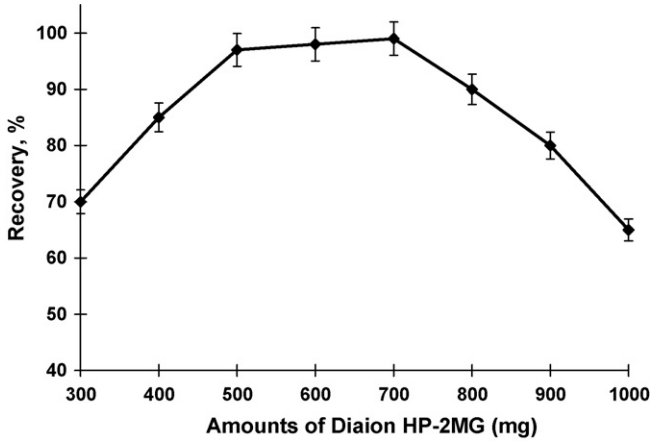


Fig. 3. Influences of Diaion HP-2MG on the sorption of Se(IV) ($N = 3$, eluent: 1 mol l^{-1} HNO_3 in acetone).

1.5–2.5. All the further works were performed for solid phase extraction of selenium(IV) as APDC complexes at pH 2.0.

3.2. Effects of amounts of APDC

The influences of amounts of ammonium pyrrolidine dithiocarbamate (APDC) on the recoveries of selenium(IV) on Diaion HP-2MG were also examined. The results were given in Fig. 2. Selenium(IV) was recovered at 35% without APDC. The recoveries of Se(IV) increased reached quantitative values (95%) with 1.0 ml of 0.1% (w/v) APDC. The recoveries decreased after 6.0 ml of 0.1% (w/v) APDC. For all subsequent works 2.0 ml of APDC was used.

3.3. Eluent

Several preconcentration papers about trace heavy metals employing polymeric adsorbents use nitric acid and hydrochloric acid as well as nitric acid and hydrochloric acid in acetone as eluent [37–41]. In the presented work also nitric and hydrochloric acids and nitric acid in acetone were tested as eluent for Se(IV)-Diaion HP-2MG system by using model solutions containing 0.50 μg of Se(IV). The results were given in Table 2. Quantitative recovery values for Se(IV) were obtained with only 5.0–10.0 ml of 1 mol l^{-1} HNO_3 in acetone. For all further works, 5.0 ml of 1 mol l^{-1} HNO_3 in acetone was used as eluent.

Table 2
Effects of various eluents on the Se(IV)-Diaion HP-2MG system (eluent volume: 10 ml, $N = 3$)

Eluent	Recovery of selenium(IV) (%)[a]
0.5 mol l^{-1} HCl	47 ± 3
1 mol l^{-1} HCl	50 ± 2
2 mol l^{-1} HCl	70 ± 3
0.5 mol l^{-1} HNO_3	40 ± 3
1 mol l^{-1} HNO_3	55 ± 3
2 mol l^{-1} HNO_3	65 ± 3
Acetone	90 ± 4
1 mol l^{-1} HNO_3 in acetone	97 ± 3

[a] Mean ± standard deviation.

3.4. Effects of amounts of Diaion HP-2MG

In order to obtain quantitative retention of selenium(IV), an appropriate amount of Diaion HP-2MG should be used in the adsorption step, For this reason, the effects of the amount of Diaion HP-2MG were examined. The solutions used contained 0.50 μg of Se(IV) at pH 2. The amount of Diaion HP-2MG was varied in the range of 300–1000 mg. The sorbed metals were then eluted by 1 mol l^{-1} HNO_3 in acetone. The results were given in Fig. 3. Se(IV) was quantitatively retained on the column containing 500–700 mg of Diaion HP-2MG. An excess amount of Diaion HP-2MG also prevents the quantitative elution of analytes by 10 ml volume of eluent. When a higher amount of Diaion HP-2MG was used, recoveries of selenium(IV) increased with increasing volume of eluent. In this study, 600 mg of Diaion HP-2MG was ideal for the preconcentration of Se(IV).

3.5. Flow rates of sample and eluent solutions

It is expected that sample solutions can be passed through the Diaion HP-2MG column at a higher flow rate without sacrificing the recoveries because a large volume of sample solution is needed in the preconcentration. The effect of the flow rate of the sample and eluent solutions on the recoveries of Se(IV) on the resin was examined in the range of 2.0–10.0 ml min^{-1}. The results were depicted in Fig. 4. The flow rate of the sample and eluent solutions had no obvious influence on the quantitative recoveries of Se(IV) at the range of 2.0–5.0 ml min^{-1}. 4.0 ml min^{-1} was chosen as the flow rate of the sample and eluent solutions in subsequent experiments.

3.6. Effect of the sample volume on Se(IV) sorption

In order to obtain high preconcentration factor, the effect of sample volume on the sorption behavior of selenium(IV) was investigated by passing 25–1000 ml of solutions containing

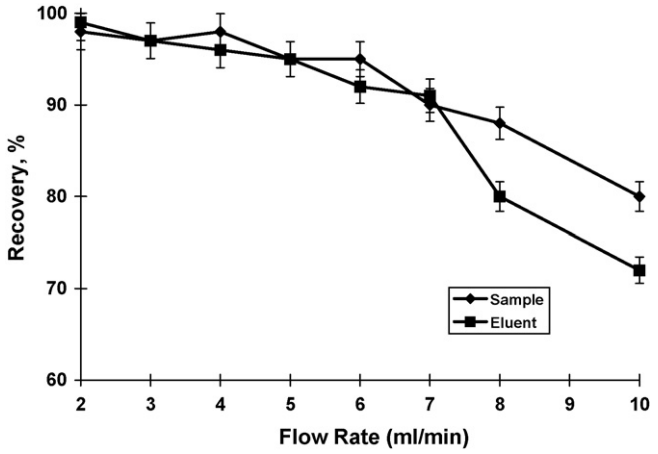


Fig. 4. The influences of flow rates of sample and eluent solutions on the recoveries of selenium (IV) ($N = 3$).

0.50 μg selenium (IV) ion and comparing the percentage of Se(IV) sorption (Fig. 5). The sorption of selenium(IV) ions was not affected by sample volume between 25 and 500 ml. At the higher volumes, the recoveries for Se(IV) was not quantitative. Thus, a sample volume in this range could be used in our procedures. The preconcentration factor is calculated by the ratio of the highest sample volume (500 ml) and the lowest eluent volume (5 ml). The preconcentration factor was 100.

3.7. Effect of divers ions

In order to assess the possible analytical applications of the recommended speciation–preconcentration procedure, the effect of some foreign ions which interfere with the determination of selenium(IV) ion or/and often accompany analyte ions in various real environmental samples was examined with the optimized conditions. The results are summarized in Table 3. The recoveries of Se(IV) in these studies were higher than 95%. Tolerable limit was defined as the highest amount of foreign ions that produced an error not exceeding 5% by the combination of the column solid phase extraction and atomic absorption spectrometric determination methods. As it is seen, large numbers of ions used have no considerable effect on the determination of Se(IV).

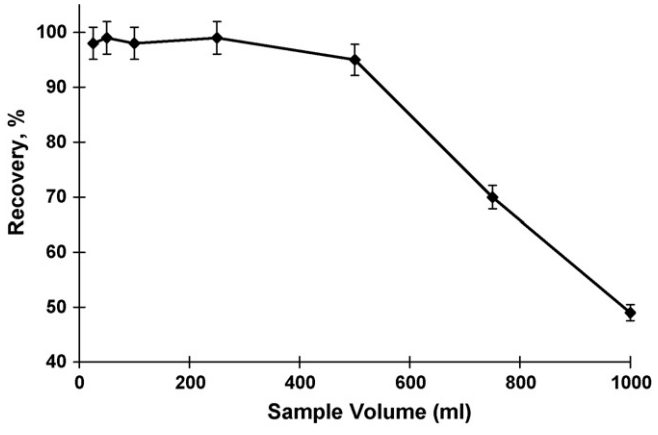


Fig. 5. The effect of sample volume on the retentions of Se(IV) as APDC chelates on Diaion HP-2MG ($N = 3$, eluent: 1 mol l^{-1} HNO_3 in acetone).

Table 3
Influences of some ions on the recoveries of selenium on the Diaion HP 2MG ($N = 4$, sample volume: 40 ml)

Ions	Added as	Concentration of ion (mg l^{-1})	Recovery of selenium[a] (%)
Na^+	NaCl	20000	95 ± 3
K^+	KCl	5000	100 ± 3
Ca^{2+}	$CaCl_2$	3000	98 ± 2
Mg^{2+}	$MgCl_2$	3000	99 ± 3
Cl^-	NaCl	20000	95 ± 2
F^-	NaF	1000	98 ± 3
SO_4^{2-}	Na_2SO_4	2000	96 ± 3
NO_3^-	KNO_3	3000	100 ± 2
PO_4^{3-}	Na_3PO_4	1000	99 ± 3
Ag^+	$AgNO_3$	50	97 ± 3
Cu^{2+}	$CuSO_4$	25	99 ± 4
Ni^{2+}	$NiSO_4$	50	95 ± 3
Cd^{2+}	$Cd(NO_3)_2$	100	98 ± 3
Fe^{3+}	$FeCl_3$	25	96 ± 3
Mn^{2+}	$MnSO_4$	50	97 ± 3
Co^{2+}	$CoSO_4$	100	95 ± 2
Zn^{2+}	$ZnSO_4$	100	96 ± 4
Pb^{2+}	$Pb(NO_3)_2$	100	98 ± 4
Al^{3+}	$Al_2(SO_4)_3$	100	97 ± 4

[a] Mean ± standard deviation.

The influences of the concentration of selenium(VI) as diverse ion on the adsorption of selenium(IV) were also investigated. The results were given in Table 4. The recoveries of Se(IV) were quantitative till 100 mg l^{-1} of Se(VI). After 100 mg l^{-1} of Se(VI), recovery values for Se(IV) were not quantitative.

3.8. Determination of total selenium

In order to determination of total selenium, test solutions that contain different amounts of selenium(IV) and selenium(VI) were prepared. Then reduction of selenium(VI) ions to selenium(IV) in the test solutions were performed by the reduction procedure given by Ferri et al. [37]. Then the procedure given in Section 2.3 was applied to these solutions. The results are given in Table 5. Quantitative recovery values were obtained for these solutions. The results show that the proposed method could be applied for the determination of total selenium in aqueous solutions.

Table 4
Effects of Se(VI) as diverse ion on retentions of Se(IV) on Diaion HP 2MG ($N = 4$, sample volume: 50 ml (Se(VI) is added as Na_2SeO_4)

Concentration of Se(VI) (mg l^{-1})	Recovery of selenium[a] (%)
25	99 ± 3
50	97 ± 3
100	96 ± 3
250	85 ± 4
500	60 ± 3

[a] Mean ± standard deviation.

Table 5
Determination of total selenium in spiked test solutions (volume: 50 ml, $N=4$)

Added ($\mu g\,l^{-1}$)		Found ($\mu g\,l^{-1}$)			Recovery (%)[a]		
Se(IV)	Se(VI)	Se(IV)	Se(VI)	Total Se	Se(IV)	Se(VI)	Total Se
0	20	–	19.8 ± 0.4	19.8 ± 0.5	–	99 ± 4	99 ± 4
5	15	4.8 ± 0.2	14.8 ± 0.6	19.6 ± 0.4	96 ± 2	99 ± 3	98 ± 4
10	10	9.9 ± 0.4	9.7 ± 0.3	19.6 ± 0.4	99 ± 3	97 ± 2	98 ± 3
15	5	14.7 ± 0.5	4.9 ± 0.2	19.6 ± 0.5	98 ± 4	98 ± 2	98 ± 3
20	0	19.5 ± 0.4	–	19.5 ± 0.4	98 ± 3	–	98 ± 3

[a] Mean ± standard deviation.

3.9. Adsorption capacity

In order to study the adsorptive capacity of Diaion HP-2MG, batch method was used. To 0.1 g resin was added 50 ml of solution containing 1.0 mg of Se(IV) at pH 2.0. After shaking for 1 h, the mixture was filtered. Ten millilitre of the supernatant solution was diluted to 100 ml. Then selenium content was determined by atomic absorption spectrometry. The capacity of sorbent was found as 5.20 mg g^{-1} Se (IV).

3.10. Figure of merits

The detection limit (LOD) of the present work was calculated under optimal experimental conditions after application of the preconcentration procedure to blank solutions. The limit of detection for selenium(IV) based on 3 times the standard deviations of the blank ($k=3$, $N=21$) was 0.010 $\mu g\,l^{-1}$. The precision of the determination of Se(IV) was evaluated under the optimum conditions mentioned above. For this purpose, the procedure was repeated 10 times for Se(IV). It was found that the recovery of Se(IV) was 98 ± 2 at 95% confidence level.

3.11. Application

The speciation procedure presented was applied to the speciation of Se(IV) and Se(VI) in natural water samples from a tap water from Tokat City, a river water from Greenriver and a sea water sample from Blacksea. Various amounts of selenium species were also spiked to these water samples. The results were given in Table 6. A good agreement was obtained between the added and measured analyte amounts. These results confirm the validity of the proposed method. The presented method could be applied successfully for the separation, preconcentration and speciation of trace amounts of selenium in both spiked and water samples.

The method was applied to NIST SRM 2711 Montana Soil, NIST SRM 1568a Rice Flour and NIST SRM 8418 Wheat Gluten standard reference materials after microwave digestion for total selenium. The results were given in Table 7. The results are in good agreement with the certified values for selenium. Also the application of the proposed procedure for total selenium was performed to the microwave digested environmental samples given in Table 7. The relative standard deviations for solid samples were in the range of 2.8–8.3%.

Table 6
Determination Se(IV), Se(VI) and total selenium in some natural water samples ($N=4$)[a]

Samples	Added ($\mu g\,l^{-1}$)		Found ($\mu g\,l^{-1}$)			Recovery (%)			Relative error (%)		R.S.D. (%)	
	Se(IV)	Se(VI)	Se(IV)	Se(VI)	Total Se	Se(IV)	Se(VI)	Total Se	Se(IV)	Se(VI)	Se(IV)	Se(VI)
Tap water	–	–	0.09 ± 0.003	0.06 ± 0.004	0.15 ± 0.01	–	–	–	–	–	3.3	6.7
from Tokat	1.0	3.0	1.1 ± 0.02	3.1 ± 0.1	4.2 ± 0.1	101 ± 1	101 ± 2	101 ± 2	+0.9	+1.3	1.8	3.2
City	3.0	1.0	3.1 ± 0.1	1.1 ± 0.03	4.2 ± 0.1	100 ± 2	104 ± 2	101 ± 2	+0.3	+3.6	3.2	2.7
	3.0	3.0	3.1 ± 0.1	3.1 ± 0.1	6.2 ± 0.1	100 ± 3	101 ± 2	101 ± 3	+0.3	+1.3	3.2	3.2
	2.0	1.0	2.1 ± 0.1	1.1 ± 0.5	3.2 ± 0.2	98 ± 3	99 ± 2	98 ± 3	−1.6	−1.6	5.1	4.8
River water	–	–	0.12 ± 0.01	0.18 ± 0.01	0.30 ± 0.02	–	–	–	–	–	8.3	5.6
from	1.0	5.0	1.1 ± 0.1	5.2 ± 0.2	6.3 ± 0.3	98 ± 3	100 ± 3	100 ± 3	−1.8	+0.4	9.1	3.8
Greenriver,	5.0	1.0	5.1 ± 0.2	1.2 ± 0.1	6.3 ± 0.2	100 ± 2	102 ± 1	100 ± 2	−0.4	+1.7	3.9	8.3
Tokat	5.0	5.0	5.1 ± 0.3	5.2 ± 0.3	10.3 ± 0.7	100 ± 2	100 ± 3	100 ± 3	−0.4	+0.4	5.9	5.8
	3.0	2.0	3.1 ± 0.1	2.1 ± 0.1	5.2 ± 0.4	99 ± 2	96 ± 2	98 ± 2	−0.6	−3.8	3.2	4.8
Sea water	–	–	0.22 ± 0.01	0.27 ± 0.02	0.49 ± 0.03	–	–	–	–	–	4.5	7.4
from	1.0	5.0	1.2 ± 0.1	5.2 ± 0.3	6.4 ± 0.4	98 ± 3	99 ± 1	99 ± 3	−1.7	−1.3	8.3	5.8
Blacksea	5.0	1.0	5.2 ± 0.3	1.2 ± 0.1	6.4 ± 0.3	100 ± 1	95 ± 2	99 ± 2	−0.4	−5.8	5.8	8.3
	5.0	5.0	5.2 ± 0.2	5.3 ± 0.2	10.5 ± 0.9	100 ± 2	100 ± 2	100 ± 2	−0.4	+0.6	3.8	3.8
	3.0	2.0	3.2 ± 0.1	2.2 ± 0.1	5.4 ± 0.4	99 ± 3	99 ± 2	98 ± 3	−0.6	−3.2	3.1	4.5

[a] Mean ± standard deviation.

Table 7
The level of total selenium in the standard reference materials and some real samples after application of the presented procedure ($N = 4$)

Sample	Concentration ($\mu g\, g^{-1}$)	RSD (%)	Certified value ($\mu g\, g^{-1}$)	Relative error (%)
NIST SRM 2711 Montana Soil	1.48 ± 0.09	6.1	1.52	−2.6
NIST SRM 1568a Rice Flour	0.36 ± 0.01	2.8	0.38	−5.3
NIST SRM 8418 Wheat Gluten	2.50 ± 0.10	4.0	2.58	−3.1
Soil from Tokat City	1.05 ± 0.05	4.8		
Garlic	0.052 ± 0.003	5.8		
Onion	0.021 ± 0.001	4.8		
Rice	0.15 ± 0.01	6.7		
Wheat	0.080 ± 0.005	6.3		
Hazelnut	0.12 ± 0.01	8.3		

Uncertainty at 95% confidence limit.

4. Conclusion

The preconcentration, speciation method for selenium(IV) and selenium(VI) is simple, quick and has good selectivity. Six hundred milligram of Diaion HP-2MG resin can be used all throughout the works without any loss in recovery values. The preconcentration factor was 100 for 500 ml of sample volume and 5.0 ml of final volume. The speciation procedure presented is comparable for the procedure in literature [18,20,28,30,42] with quantitative recovery values and lower detection limit for selenium species. The procedure presented was applied to the speciation of Se(IV) and Se(VI) in the various environmental samples with satisfactory results.

Acknowledgement

The authors would like to thank the Scientific and Technological Research Council of Turkey (TUBITAK) for financial helps (Project No.: 104T448). The authors are also grateful for the financial support of the Unit of the Scientific Research Projects of Gaziosmanpasa University and the Unit of the Scientific Research Projects of Erciyes University.

References

[1] B.D. Wake, A.R. Bowie, E.C.V. Butler, P.R. Haddad, Trends Anal. Chem. 23 (2004) 491.
[2] K. Pyrzynska, Chem. Anal. 40 (1995) 677.
[3] M. Bueno, M. Potin-Gautier, J. Chromatogr. A 963 (2002) 185.
[4] K. Pyrzynska, P. Drzewicz, M. Trojanowicz, Anal. Chim. Acta 363 (1998) 141.
[5] W. Aeungmaitrepirom, A. Hagege, Z. Asfari, L. Bennouna, J. Vicens, M. Leroy, Tetrahedron Lett. 40 (1999) 6389.
[6] C.S. Nomura, P.R.M. Correia, P.V. Oliveira, E. Oliveira, J. Braz. Chem. Soc. 15 (2004) 75.
[7] P. Bermejo-Barrera, A. Moreda-ineiro, A. Bermejo-Barrera, J. Anal. At. Spectrom. 15 (2000) 121.
[8] Z.J. Gong, X.S. Zhang, G.H. Chen, X.F. Xiao, Talanta 66 (2005) 1012.
[9] M.B. Melwanki, J. Seetharamappa, Turk. J. Chem. 24 (2000) 287.
[10] K.S. Kumar, K. Suvardhan, L. Krishnaiah, P. Chiranjeevi, Helvetica Chim. Acta 88 (2005) 343.
[11] M.I. Castilla, Y. Cortazar, J.V.L. Cosin, Agrochimica 39 (1995) 233.
[12] M. Potin-Gautier, F. Séby, M. Astruc, Anal. Bioanal. Chem. 351 (1995) 443.
[13] M. Ochsenkuhn-Petropoulou, F. Tsopelas, Anal. Chim. Acta 467 (2002) 167.
[14] E. Dimitrakakis, C. Haberhauer-Troyer, Y. Abe, M. Ochsenkuhn-Petropoulou, E. Rosenberg, Anal. Bioanal. Chem. 379 (2004) 842.
[15] Z. Mester, P. Fodor, Anal. Chim. Acta 386 (1999) 89.
[16] R. Saraymen, M. Soylak, L. Elci, M. Doğan, Fresen. Environ. Bull. 6 (1997) 694.
[17] J. Cvetković, T. Stafilov, D. Mihajlović, Fresen. J. Anal. Chem. 370 (2001) 1077.
[18] M.S. Dundar, H. Altundag, J. Food Comp. Anal. 17 (2004) 707.
[19] V.M.C. Dias, S. Cadore, N. Baccan, J. Anal. At. Spectrom. 18 (2003) 783.
[20] K. Pyrzynska, Anal. Lett. 31 (1998) 1777.
[21] F.Z. Kucukbay, M. Demir, Turk. J. Chem. 25 (2001) 341.
[22] M.N. Pathare, A.D. Sawant, Anal. Lett. 28 (1995) 317.
[23] Y. Kashiwagi, E. Kokufuta, T. Kawashima, Anal. Sci. 13 (1997) 623.
[24] T.P. Rao, M. Anbu, M.L.P. Reddy, C.S.P. Iyer, A.D. Damodaran, Anal. Lett. 29 (1996) 2563.
[25] J.L. Gomez-Ariza, J.A. Pozas, I. Giraldez, E. Morales, Analyst 124 (1999) 75.
[26] P.E. Carrero, J.F. Tyson, Analyst 122 (1997) 915.
[27] Y.K. Aktas, Fresen. Environ. Bull. 14 (2005) 993.
[28] S. Baytak, A.R. Turker, B.S. Cevrimli, J. Sep. Sci. 28 (2006) 2482.
[29] N. Manouchehri, A. Bermond, Anal. Chim. Acta 557 (2006) 337.
[30] Y. Cai, M. Cabanas, J.L. Fernandezturiel, M. Abalos, J.M. Bayona, Anal. Chim. Acta 314 (1995) 183.
[31] A. Larraya, M.G. Cobofernandez, M.A. Palacios, C. Camara, Fresen. J. Anal. Chem. 350 (1994) 667.
[32] T. Ferri, P. Sangiorgio, Anal. Chim. Acta 321 (1996) 185.
[33] S.X. Li, N.S. Deng, Anal. Bioanal. Chem. 374 (2002) 1341.
[34] http://www.diaion.com/ accessed December, 2005.
[35] M. Soylak, Quim. Anal. 20 (2002) 175.
[36] M. Soylak, İ. Narin, M.A. Bezerra, S.L.C. Ferreira, Talanta 65 (2005) 895.
[37] T. Ferri, S. Rossi, P. Sangiorgio, Anal. Chim. Acta 361 (1998) 113.
[38] M. Tuzen, M. Soylak, L. Elci, Anal. Chim. Acta 548 (2005) 101.
[39] M. Tuzen, K. Parlar, M. Soylak, J. Hazard. Mater. 121 (2005) 79.
[40] M. Ghaedi, M.R. Fathi, F. Marahel, F. Ahmadi, Fresen. Environ. Bull. 14 (2005) 1158.
[41] V.A. Lemos, D.R. Vieira, C.G. Novaes, M.E. Rocha, M.S. Santos, R.T. Yamaki, Microchim. Acta 153 (2006) 193.
[42] K. Suvardhan, L. Krishnaiah, K. Suresh Kumar, D. Rekha, B. Jayaraj, S. Ramanaiah, P. Chiranjeevi, Chemosphere 62 (2006) 899.

Available online at www.sciencedirect.com
ScienceDirect
Talanta 71 (2007) 1263–1267
Talanta
www.elsevier.com/locate/talanta

Studies on controlled potential coulometric determination of gallium in sodium perchlorate and sodium thiocyanate

H.S. Sharma [a,1], T.K. Bhardwaj [b], P.C. Jain [b,2], S.K. Aggarwal [a,*]

[a] *Fuel Chemistry Division, Bhabha Atomic Research Centre, Trombay, Mumbai 400 085, India*
[b] *Chemistry Department, Meerut College, Meerut 250 001, India*

Received 16 May 2006; received in revised form 23 June 2006; accepted 23 June 2006
Available online 8 August 2006

Abstract

Controlled potential coulometric (CPC) studies were carried out for developing a method to determine gallium at milligram levels, in the mixed supporting electrolyte medium (4 M $NaClO_4$ + 0.5 M NaSCN), employing stirring mercury as a working electrode. Investigations for optimization of working electrode potentials, quantity of charge, level of background current and electrolysis time for achieving quantitative reduction of Ga(III) to Ga and its oxidation back to Ga(III), were undertaken. Effect of gallium content and interference of zinc in of gallium determination were also studied. The developed methodology was employed for the determination of gallium in pure Ga as well as in synthetic U + Ga mixture solutions. Accuracy and precision values of better than 0.5% were obtained at 1–2 mg levels.
© 2006 Elsevier B.V. All rights reserved.

Keywords: Gallium; Uranium; Zinc; Sodium thiocyanate; Controlled potential coulometry

1. Introduction

Alloys and compounds of Group three metals are important owing to their utilization in electronic and optical devices and also in medical applications [1–5]. Physical properties of semiconductor materials greatly depend upon the stoichiometric composition as well as on the level of trace impurities present. Accurate and precise determination of gallium content is, therefore, an essential requirement in compound semiconductor materials such as Ga–As and also in standard reference materials of Pu–Ga alloy for chemical characterization of nuclear fuels. The subject of analytical methodologies adopted for chemical characterization has been reviewed [6–9]. Atomic absorption spectrometry, neutron activation analysis, atomic emission spectrometry, mass spectrometry, etc. can be employed for the determination of gallium. Utility of these techniques for routine applications is restricted due to non-availability of suitable standards and difficulties encountered due to matrix interference, in addition to high instrumentation cost and longer analysis time. On the other hand, the interference effect from matrix and coexisting elements in chemical methods can be suppressed by resorting to suitable chemical treatment or by separation. Besides, in chemical methods such as electrogravimetry and coulometry, chemical assay reference materials are not required. An indirect constant current coulometric method has been reported previously for the precise and accurate determination of gallium and arsenic in Ga–As compound semiconductor material. Ga^{3+} ions present in the dissolved sample aliquot were allowed to react with EDTA and the excess of EDTA was determined by titrating against Hg^{2+} ions generated electrolytically from a gold electrode plated with mercury. The end-point of EDTA-Hg^{2+} titration was detected amperometrically [6,8]. In the constant-current coulometric method, mean error of +0.03% with a relative standard deviation of 0.11% is reported, for a set of four gallium determination, at 20 mg level. Anodic stripping voltammetric (ASV) methods have also been employed in the past for the determination of gallium at trace and ultra-trace levels with a reproducibility of 2–3% [10–12]. However, ASV methodologies are not adequate for achieving accuracy and precision of better than 1%, required for the characterization of high purity Ga–As semiconductor alloys and standard reference materials containing gallium. Controlled potential coulometry (CPC) is

* Corresponding author. Tel.: +91 22 25593740; fax: +91 22 25505151.
E-mail addresses: drhssharma@yahoo.com (H.S. Sharma), skaggr@magnum.barc.ernet.in (S.K. Aggarwal).
[1] Tel.: +91 22 25594576; fax: +91 22 25505151.
[2] Tel.: +91 121 2575782.

0039-9140/$ – see front matter © 2006 Elsevier B.V. All rights reserved.
doi:10.1016/j.talanta.2006.06.030

a well-established technique in our laboratory and is employed for precise and accurate determination of uranium and plutonium in nuclear fuel materials [13–16]. In CPC, potential applied to the working electrode is held constant at the desired value electronically, which makes it highly selective as compared to constant-current coulometric method. Besides, an additional technique for the detection of end-point of coulometric titration is not required in CPC and this also makes it more advantageous as compared to constant current coulometric method. Cyclic voltammetric studies of Ga(III)/Ga electrode process recently carried out in our laboratory have shown that the electrode process is highly irreversible in 1 M $NaClO_4$ and becomes closer to reversible and diffusion controlled in the mixed electrolyte medium of 4 M $NaClO_4$ + 0.5 M NaSCN, at static mercury drop electrode (SMDE) [17]. It was, therefore, considered interesting to explore the possibility of employing CPC for precise and accurate determination of gallium at milligram levels.

2. Experimental

2.1. Apparatus, electrodes and reagents

An indigenous Controlled Potential Coulometer from Santronics India Ltd., Mumbai, coupled with Coulometric Cell and Synchronous Motor from PARC, USA, was employed in the present studies. Triple distilled mercury was used as a working electrode, platinum wire gauze and saturated calomel electrode (SCE) were respectively employed as counter and reference electrodes. The three electrodes were kept in separate compartments in the coulometric cell. Stock solution of gallium was prepared by dissolving high purity BDH grade gallium metal in aqua-regia followed by evaporating near to dryness and redissolving the residue in 0.1 M HCl. To ensure complete removal of nitrate, heating to near dryness and redissolving the residue in 0.1N HCl was repeated twice. Gallium concentration in the stock solution was determined by isotope dilution–thermal ionization mass spectrometry. Sodium perchlorate and sodium thiocyanate used were of AR grade from Fluka. The electrolyte mixture of sodium perchlorate containing sodium thiocyanate (4 M $NaClO_4$ + 0.5 M NaSCN), is referred to as mixed electrolyte in the text and all potentials referred to in the work are with reference to SCE.

2.2. Coulometric procedure

In a 50 mL capacity coulometric cell, 10 mL each of purified mercury and mixed supporting electrolyte were taken. The mercury surface-electrolyte solution interface was continuously stirred with a glass stirrer attached to the Synchronous Motor at 1600 rpm and high purity argon gas of Iolar grade II, having 6 ppm of oxygen, was purged over the electrolyte solution to remove the oxygen present initially from working solution and also to restrict entry of traces of oxygen in to the solution during the course of coulometric experiments. The blank experiments were initially run by applying reduction and oxidation potentials, prior to conducting actual run of redox cycle for Ga(III) reduction and Ga oxidation. Known amount of gallium solution, on weight basis, was taken directly in the coulometric cell. Ga(III) present in the solution was reduced to Ga at the optimized controlled potential until the background current reached to a low constant value. The reduced gallium was oxidized back to Ga(III) at an optimized controlled potential.

2.3. Separation of gallium from uranium

Known amount of U + Ga mixture solution on weight basis was added to an equilibration tube having 5 mL of 7 M HCl. The solution was equilibrated with 5 mL of isopropyl ether for 5 min and was allowed to stand for phase separation. The organic phase was transferred to a clean and dry conical flask. In order to achieve quantitative separation of gallium, two more extractions with isopropyl ether were carried out and the organic phase was combined in the same conical flask. Ether was air evaporated to dryness and residue containing gallium was redissolved in the mixed electrolyte for controlled potential coulometric experiments. The presence of NO_3^- ions in uranium solution interferes in quantitative extraction of gallium from aqueous phase. It was, therefore, essential to convert the U + Ga mixture to chloride form prior to extraction of gallium.

3. Results and discussion

3.1. Optimization of experimental conditions for exhaustive electrolysis

CV studies performed in our laboratory previously showed that Ga(III)/Ga electrode process in mixed electrolyte medium (4 M $NaClO_4$ + 0.5 M NaSCN) at SMDE is diffusion controlled and close to reversibility. Electro-reduction of Ga(III) occurs at −0.820 V and is a slow electrode process as compared to electro-oxidation of Ga which occurs at −0.800 V [17]. In view of this, CPC studies were first carried out for the optimization of potentials for quantitative reduction of Ga(III) to Ga and then oxidation of Ga to Ga(III), in the mixed electrolyte medium at stirring mercury electrode. In the reduction step, potentials more negative compared to −0.820 V, in the range of −0.90 to −1.05 V, were applied and a reduction potential of −0.95 V was found to be the most optimum. Potentials more positive than −0.800 V were applied to study quantitative electro-oxidation of Ga to Ga(III) and an oxidation potential of −0.6 V was found to be optimum. Achieving minimum and stable background current for 1–2 min, in the reduction as well as in the oxidation step, was the guide line adopted for detecting the end-point of exhaustive electrolysis. In the present studies, as will be seen below, the level of background current observed in the reduction step was much higher compared to the reported values of coulometric blanks.

Table 1 presents data comprising of integrated charge (Q), background electrolysis current (I) and electrolysis time (T) for reduction and oxidation steps of some representative coulometric blanks. The coulometric blanks were recorded for 10 mL of mixed electrolyte under stirring condition of mercury–solution interface. It can be seen that the Q values obtained in oxidation cycle are much lower as compared to those in reduction cycle and

Table 1
Controlled potential coulometric data, charge (Q), background current (I) and electrolysis time (T) of some representative blanks in 4 M $NaClO_4$ + 0.5 M NaSCNM

S.no.	Reduction cycle			Oxidation cycle		
	Q (mC)	I (μA)	T (min)	Q (mC)	I (μA)	T (min)
Bl-1	550	191	15	3.1	0	2
Bl-2	504	90	17	1	0	2
Bl-3	673	215	15	0.4	0	1
Bl-4	550	191	15	3.1	0	2

the background current approaches to zero in about 2 min. Our past experience on U and Pu coulometry [15,16] showed that the background current for reduction at −0.325 and +0.3 V versus SCE, in 1 M sulfuric acid, respectively, for mercury and platinum electrode are in the range of 10–20 μA. It may be mentioned that the reduction potential employed in the present studies, −0.95 to −1.0 V, is higher and closer to the hydrogen evolution reaction. Higher level of background current observed in the reduction step was attributed mainly to the hydrogen evolution.

Fig. 1(a) and (b) shows typical coulograms and depict variation of electrolysis charge as well as current as a function of time for the electro-reduction of Ga(III) to Ga and electro-oxidation of Ga to Ga(III), respectively. It can be seen that the electro-reduction current initially shoots to about 14 mA within 25 s and shows an exponential decreases to a value of about 1 mA after 1400 s and remains stable afterwards. Higher level of background current was attributed to the hydrogen evolution reaction at potential of −0.95 V. This is also supported by reduction coulogram shown in Fig. 1(a), where the integrated current (coulombs) is observed to increase even after 1400 s. It can be seen in Fig. 1(b) that the initial oxidation current is about five times higher as compared to the reduction current observed in Fig. 1(a) and the background electrolysis current falls to almost zero after 300 s. This suggests that the amount of Ga(III) reduced in the reduction step is quantitatively oxidized back to Ga(III) in oxidation step and that oxidation is a much faster electrode process as compared to reduction. This corroborates our CV

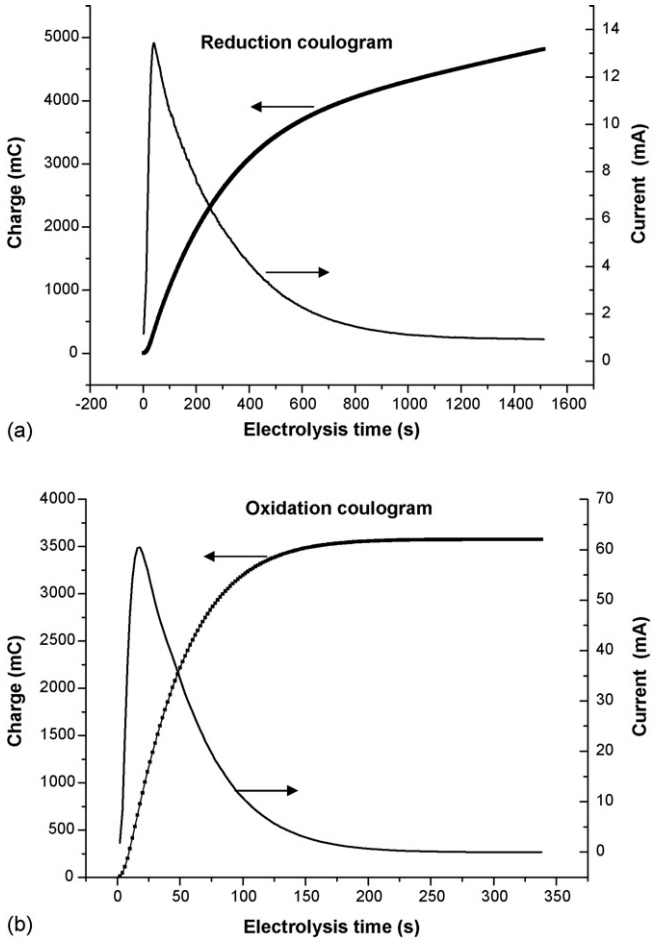


Fig. 1. Electrolysis charge (Q) and current (I) as a function of electrolysis time for (a) Ga^{3+} reduction and (b) Ga oxidation, in mixed electrolyte medium at mercury electrode.

results that Ga electro-oxidation is faster as compared to electro-reduction of Ga(III) in mixed electrolyte medium.

In Table 2, CPC data obtained by applying increasing negative reduction potentials in the range −0.95 to −1.05 V and an optimized oxidation potential of −0.6 V are presented. Weight

Table 2
Controlled potential coulometric data of reduction and oxidation steps during gallium determination

S.no.	Aliquot weight (g)	Reduction data				Oxidation data				Ga analysed	
		E (V)	Q (mC)	I (A)	t (min)	E (V)	Q (mC)	I (A)	t (min)	mg	mg/g
1	0.184	−0.95	6443.7	0.177	18	−0.6	6247	0	5	1.50	8.18
2	0.4548	−0.95	15720	0.373	19	−0.6	15356.7	0	5	3.70	8.13
3	0.2602	−0.95	10311.4	0.91	33	−0.6	8828.2	0	4	2.13	8.17
4	0.2505	−0.95	10198.2	0.701	42	−0.6	8479.6	0	7	2.04	8.15
5	0.1053	−1	4816.8	0.929	25	−0.6	3576.5	0	6	0.86	8.18
6	0.2165	−1	12809.6	2.387	33	−0.6	7361.5	0	6	1.77	8.19
7	0.2287	−1.05	4567.2	0.600	27	−0.6	7773.1	0	8	1.87	8.19
8	0.2438	−1.05	9726.6	0.827	33	−0.6	8235.8	0	9	1.98	8.14
9	Mean value										8.17 ± 0.02
10	Expected value										8.18 ± 0.001
11	In presence of 4 μg of Zn										8.17 ± 0.01 (5)[a]

[a] Replicate analysis.

of gallium solution taken for quantitative electrolysis along with Q, I and T values for the reduction and the oxidation steps are also included in the table. It can be seen that background current I in reduction step is significantly higher compared to that obtained in blank experiments, as given in Table 1. As the gallium solution is acidic, the pH of the supporting electrolyte medium reduces on adding a gallium aliquot and this results in the increase of background current. Almost zero background current similar to that obtained for blanks was obtained in the oxidation step, in relatively much shorter electrolysis time. This suggests that Ga(III) reduced in the reduction step is quantitatively oxidized at relatively faster rate at −0.6 V. This is an interesting and favourable observation and suggests that the charge obtained in the oxidation step is almost free from background corrections and can be taken for calculation of gallium content in the aliquot. Gallium concentration calculated from the oxidation charge data is presented in the last column of Table 2. It can be seen that an accuracy and precision values of about 0.3% are achieved at 1–3 mg levels of gallium. In order to investigate the effect of gallium content on accuracy, gallium determinations were carried out at different levels and the results obtained are presented in Table 3. It can be seen from the data that a difference of 0.5% with respect to expected value is achieved up to 0.5 mg of gallium present in the aliquot, however, the agreement becomes poor for gallium determination at levels below 0.5 mg of gallium. As the concentration of gallium in working solution is in mg/g, the gallium content becomes smaller with the decrease of sample solution weight (aliquot weight). The repeatability/reproducibility of the determined value of gallium content decreases with the decrease of gallium content because of errors involved in preparation of working sample solution, transfer of sample solution into the coulometric cell, variation in coulometric blank due to sample addition, error in current integration and weighing. It should be mentioned here that the errors involved due to blank contribution and charge integration at low electrolysis current becomes significantly higher at lower sample content. We have observed similar effect in plutonium determination by CPC at microgram levels [15].

3.2. Interference of zinc and determination of gallium in synthetic U + Ga mixtures

Zinc is recognized as a potential interfering element in gallium determination as its reduction potential is closer to the reduction potential of Ga(III) and is likely to come mainly from the supporting electrolyte. In view of this, we recorded CV's of

Table 3
Effect of gallium content on accuracy of gallium determination

Set no.	Ga present (mg) (A)	Ga determined (mg) (B)	B/A ratio
I	1.505	1.505	1
II	0.845	0.843	0.998
III	0.528	0.526	0.996
IV	0.467	0.465	0.996
V	0.323	0.316	0.978
VI	0.152	0.135	0.888

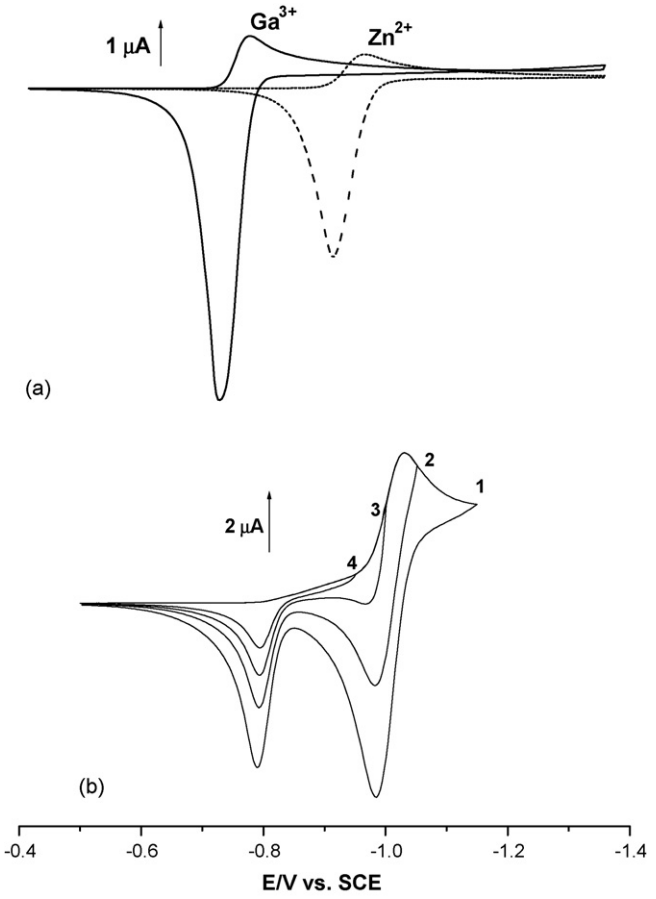


Fig. 2. CV's of 2.5 mM each of (a) Ga^{3+}(—) and Zn^{2+} (- - -), recorded separately and (b) $Ga^{3+} + Zn^{2+}$ mixture, recorded at decreasing cathodic potential limits: (1) −1.15 V, (2) −1.05 V, (3) −1.00 V, and (4) −0.95 V, at SMDE in mixed electrolyte medium. Potential of SMDE was cycled at a scan rate of 50 mV s^{-1}.

Ga(III) and Zn(II) separately as well as of Ga(III) + Zn(II) mixture in the mixed electrolyte medium, under similar experimental conditions at SMDE. It can be seen from Fig. 2(a) that Ga(III) is reduced at −0.850 V and Zn(II) at −1.02 V versus SCE showing a separation of about 200 mV in the reduction potentials. As the reduction potentials optimized for gallium determination are in the range of −0.95 to 1.0 V, Zn(II) interference in gallium determination is expected. In order to investigate this, we recorded CV's of Ga(III) + Zn(II) mixture having decreasing cathodic potential limit, in mixed electrolyte and are shown in Fig. 2(b). It can be seen that Ga(III) reduction peak is not well defined and thus is difficult to fix the potential at which Zn(II) reduction onsets. It can also be seen in the reverse scan of Fig. 2(b) that anodic current due to oxidation of Zn as well as Ga are observed to decrease with the decrease of cathodic potential limit in the cyclic voltammogram and the anodic peak due to Zn oxidation almost disappears when the cathodic potential is terminated at −0.95 V. This illustrates that −0.95 V is the optimum potential for selectively reducing Ga(III) in presence of Zn(II). In order to substantiate this, determination of gallium at 1–2 mg levels was carried out in presence of 4 μg of zinc, equivalent to about 2000–4000 PPM level in U–Ga alloy. As can be seen in Table 2, accuracy and precision of about 0.3% was achieved.

Table 4
Results of gallium determination in synthetic U + Ga mixture solutions

Ga in U + Ga mixture (%)	Ga present (mg/g) (*A*)	Ga determined (mg/g) (*B*)	*B*/*A* ratio
50	2.872	2.869 ± 0.001 (5)[a]	0.999
10	5.956	5.951 ± 0.001 (5)	0.999
2	5.006	5.001 ± 0.001 (5)	0.999

[a] Replicate analysis.

Gallium determination was also carried out in synthetic U + Ga mixture solutions. Ga + U synthetic mixture solutions having varying concentration of gallium 2.872 mg/g for 50% Ga + U mixture, 5.956 mg/g for 10% Ga + U mixture and 5.006 mg/g for 2% Ga + U mixture solutions were prepared by mixing appropriate contents of gallium and uranium from their respective stock solutions. Gallium could be determined directly in 1:1 Ga + U synthetic mixture solution. However, in solutions having more than 50% of uranium, interference of uranium in the determination of gallium was observed. At −0.95 V, U(VI) and Ga(III) are reduced simultaneously, and due to stronger hydrolysis tendency of U(IV), turbidity in the mixed electrolyte medium was observed. Gallium was, therefore, determined after separating it from uranium by solvent extraction with isopropyl ether, as described previously. Results of gallium determination in Ga + U synthetic mixture solution are presented in Table 4.

4. Conclusions

CPC studies presented here provide a simple methodology for determining gallium in the mixed electrolyte medium of 4 M $NaClO_4$ + 0.5 M NaSCN with a precision and accuracy of better than 0.5%, at milligram levels in presence of zinc as interfering element. To the best of our knowledge, this is the first report on controlled potential coulometric determination of gallium in synthetic Ga + U mixture solutions having varying concentration of gallium in the mixed electrolyte medium directly in the presence up to of 50% uranium and after separation of gallium in solutions having uranium above 50%. The insights gained in our study regarding the optimization of experimental parameters for the determination of gallium would provide guidelines for developing CPC methodology for the determination of gallium in gallium based semiconductor materials.

Acknowledgements

The authors are thankful to Dr. V. Venugopal, Director of RC & I Group at BARC, for his interest in this work. TKB thanks BARC authorities for allowing to work in FCD, BARC.

References

[1] R.K. Willardson, A.C. Beer (Eds.), Semiconductors and Semimetals: III–V Compound Semiconductors and Semiconductor Properties of Superionic Materials, vol.26, Academic Press, Boston, MA, 1988.
[2] X. Xu, R.P. Vaudoand, G.R. Brandes, Opt. Mater. 23 (2003) 1.
[3] A. Rodrigrez, J. Romero, J.A. Garcia-Vazquez, A. Sousa, J. Zubieta, D.J. Rose, K. Maresca, Inorg. Chim. Acta 281 (1998) 70.
[4] L.J. Baker, M.J. Taylor, Polyhedron 13 (1994) 251.
[5] P.L. Wallace, P.K. Hosmer, J.C. Walden, W.L. Haugen, X-ray Spectrom. 7 (4) (1978).
[6] S.C. Abhramas, J.L. Bern, J. Res. NBS A Phys. 8 (1977) 1.
[7] M.H. Yang, M.L. Lee, J.J. Shen, H.L. Hwang, Mater. Sci. Eng. B 12 (1992) 253–260.
[8] M.R. Brozel, III–Vs Rev. 10 (6) (1997) 32–34.
[9] S. Kayastha, N. Raje, T.P.S. Asari, R. Parthasarthy, Anal. Chim. Acta 370 (1998) 91–103.
[10] P. Cofre, G. East, C. Aguirre, Talanta 39 (1992) 621.
[11] G. East, P. Cofre, Talanta 40 (1993) 1273.
[12] M.J.G. Gonzalez, O.D. Renedo, M.A.A. Lomillo, M.J.A. Martinez, Talanta 62 (2004) 457.
[13] J.E. Harrar, Electroanalytical Chemistry, vol. 8, Marcel Dekker, New York, 1975.
[14] W.D. Shults, Talanta 10 (1963) 833.
[15] H.S. Sharma, N.B. Khedekar, S.G. Marathe, H.C. Jain, Nucl. Technol. 89 (1990) 399.
[16] N. Gopinath, J.V. Kamat, H.S. Sharma, S.G. Marathe, H.C. Jain, Bull. Electrochem. 10 (1989) 805.
[17] H.S. Sharma, T.K. Bhardwaj, P.C. Jain, S.K. Aggarwal, Ind. J. Chem. 44A (2006) 643.

Available online at www.sciencedirect.com
ScienceDirect
Talanta 71 (2007) 1424–1429
Talanta
www.elsevier.com/locate/talanta

Short communication

Development and validation of a HPLC method for the determination of voriconazole in pharmaceutical formulation using an experimental design

G. Srinubabu [a,*], Ch. A.I. Raju [a], N. Sarath [b], P. Kiran Kumar [c], J.V.L.N. Seshagiri Rao [b]

[a] *Center for Biotechnology, College of Engineering, Andhra University, Visakhapatnam 530003, India*
[b] *Department of Pharmaceutical Sciences, College of Engineering, Andhra University, Visakhapatnam 530003, India*
[c] *Department of Pharmaceutical Analysis, Rolands Institute of Pharmaceutical Sciences, Bhermpur, Orissa, India*

Received 8 February 2006; received in revised form 28 April 2006; accepted 28 April 2006
Available online 10 January 2007

Abstract

A rapid and sensitive RP–HPLC method with UV detection (260 nm) for routine analysis of voriconazole in a pharmaceutical formulation (Vfend®) was developed. Chromatography was performed with mobile phase containing a mixture of acetonitrile and water (50:50, v/v) with flow rate was of 1.0 ml min^{-1}. Quantitation was accomplished with internal standard method. The procedure was validated for linearity (correlation coefficient = 0.9999), accuracy, robustness and intermediate precision. Experimental design was used for validation of robustness and intermediate precision. To test robustness, three factors were considered. Percentage of acetonitrile in mobile phase, flow rate and p^H; an increase in the flow rate results in a decrease of the drug found concentration, while the percentage of organic modifier and p^H have no important effect on the response. For intermediate precision measure the variables considered were: analyst, equipment and number of days. The R.S.D. value (0.45%, $n = 24$) indicated a good precision of the analytical method. The proposed method was simple, highly sensitive, precise and accurate and retention time less than 4 min indicating that the method is useful for routine quality control.
© 2007 Published by Elsevier B.V.

Keywords: Voriconazole; HPLC; Validation; Robustness testing; Experimental design

1. Introduction

Voriconazole is designated chemically as (2*R*,3*S*)-2-(2,4-difluorophenyl)-3-(5-fluoro-4-pyrimidinyl)-1-(1H-1,2,4-triazol-1-yl)-2-butanol with an empirical formula of $C_{16}H_{14}F_3N_5O$ and a molecular weight of 349.3 (Fig. 1). This antifungal agent is a derivative of fluconazole, having one triazole moiety replaced by a fluoropyrimidine ring and a methyl group added to the propanol backbone [1]. This change in structure results in a potent and wide-spectrum activity against various mold species including *Aspergillus* [2]. In common with other azole antifungal agents, such as fluconazole and itraconazole, its primary mode of action is by inhibition of the fungal cytochrome P450-dependent 14α-sterol demethylase, an essential enzyme in ergosterol biosynthesis [3]. Voriconazole shows a greater selectivity for the fungal enzyme than for the corresponding rat liver enzyme as compared ketoconazole and itraconazole [4]. Voriconazole is moderately lipophilic (log $D_{7.4} = 1.8$) and a single diastereomer with *R*- and *S*-stereochemistry by virtue of two chiral centers (2*R*, 3*S*) as shown in Fig. 1. Human pharmacokinetic data for voriconazole have been published by Purkins et al. [5]. A few methods were reported for the determination of voriconazole in human serum [6–8], and in aqueous humor [9], reports regarding the determination of impurities [10] and separation of stereoisomers [11] also appear in literature. So far, no systematic HPLC method has been reported for determination of voriconazole in pharmaceutical injections. This paper reports a rapid and sensitive HPLC determination method with UV detection, useful for routine quality control of voriconazole in pharmaceutical formulations. The method was validated by parameters such as linearity, accuracy, precision and robustness. Experimental design was used for validation to evaluate the robustness and intermediate precision.

* Corresponding author. Tel.: +91 891 2844933/91 891 2535316; fax: +91 891 2755324.

0039-9140/$ – see front matter © 2007 Published by Elsevier B.V.
doi:10.1016/j.talanta.2006.04.042

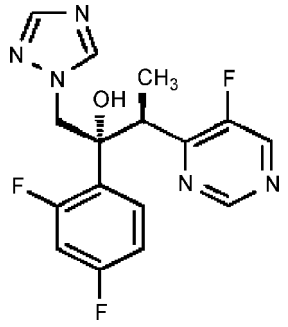


Fig. 1. Structure of voriconazole.

2. Experimental

2.1. Apparatus

Two different HPLC systems were used for the study. The corresponding specifications were provided below.

HPLC system 1: the HPLC 1 apparatus was a Waters chromatographic system equipped with an injection valve (Rheodyne 033381); Waters 2487 UV dual λ absorbance detector was used. A reversed-phase C_{18} column (25 cm × 4.6 mm i.d., particle size 5 μm). Peak area integration was performed using Breeze software.

HPLC system 2: The HPLC 2 apparatus was a Shimadzu chromatographic system with two LC-10AT VP pumps, variable wavelength programmable UV–vis detector SPD-10A, VP CTO, -10 AS VP column oven (Shimadzu) A reversed-phase C_{18} column (25 cm × 4.6 mm i.d., particle size 5 μm; YMC, IMC, Wilmington, NC, 28403, U.S.A.) and the HPLC system was monitored by software "Class-VP series version 5.03 (Shimadzu)". A model SL-164 UV–vis spectrophotometer (Elico Ltd., India) was employed for spectrophotometric study.

The experimental design and statistical analysis of the data were performed, by statistica [15] data analysis software system, with using central composite design (CCD) and 16 runs for robustness study.

2.2. Reagents

HPLC grade acetonitrile, potassium dihydrogenphosphate (A.R. grade) and orthophosphoric acid (A.R. grade) was obtained from Quiligens (Mumbai, India). Pure sample of drug and internal standard were obtained from Sun pharmaceuticals Ltd., India. Ultra pure water was obtained using a Milli-Q® UF-Plus apparatus (Millipore) was used to prepare all solutions for the method. The determination of voriconazole in commercial formulation was carried out (Vfend®) 250 mg vials, which are to be constituted with water before use.

2.3. Preparation of the standard solution

An accurately weighed sample (100 mg) of voriconazole reference standard was transferred to a 100 ml volumetric flask and dissolved in triple distilled water to make a solution (1 mg ml^{-1}). From this solution, a working standard solution of 100 μg ml^{-1} of strength was prepared from this dilution of 5, 10, 20, 30, 40, and 50 μg ml^{-1} were made in 10 ml volumetric flasks with the mobile phase here in every standard solution contains 5 μg ml^{-1} of famciclovir internal standard. To carry out the assay aliquots of voriconazole solution equal to 10,20,30,40 and 50 μg ml^{-1} were accurately withdrawn.

2.4. Calibration procedure

The calibration curve was plotted with five concentrations of the standard solution 5–50 μg/ml solutions and chromatography was repeated thrice for each dilution. The linearity was evaluated by linear regression analysis, which was calculated by the least square regression method. Before injecting solutions, the column was equilibrated for at least 30 min. with the mobile phase flowing through the system. Quantitation was accomplished using an internal standard method. Five determinations were carried out for each solution. Peak area ratios were recorded for all the solutions. The correlation graph was constructed by plotting the peak area ratios obtained at the optimum wavelength of detection versus the injected amounts.

2.5. Chromatographic conditions

The mobile phase was a mixture of acetonitrile and water (50:50, v/v) and flow rate was 1.0 mL min^{-1}. The UV detector wavelength was set at 256 nm and the temperature was set at 23 ± 1 °C.

3. Results and discussion

The applied chromatographic conditions permitted a good separation of voriconazole 10 μg ml^{-1} and the internal standard famciclovir 5 μg ml^{-1} (Fig. 2), no drug decomposition was observed during the analysis. The LC method was validated for the parameters reported below.

3.1. System suitability

The chromatographic separation, as explained above was carried out with HPLC 1 to evaluate the chromatographic param-

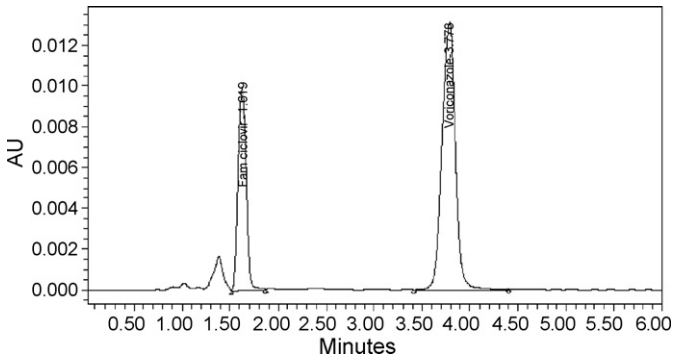


Fig. 2. Chromatogram of a solution containing voriconazole at the described chromatographic conditions.

eters (capacity factor (K'), asymmetry of the peaks, tailing factor and resolution between two consecutive peaks). In Fig. 2 representative chromatogram was shown, which corresponds to the chromatographic separation of these substances. The capacity factor (K') of the first peak was 3.6 and second was 5.1, the resolution factor was 1.6, results obtained for asymmetry of the peak and tailing factor parameters were the following 0.781 and 0.645, respectively, for IS famciclovir, 0.424 and 0.852 for voriconazole, respectively.

It was concluded that the developed method is the optimum according to the studied parameters. The capacity factor obtained is within the accepted values, above 2 for the first peak and less than 10 for the second peak. The tailing factor to be controlled was within the limits established by these guidelines. Lastly, good resolution was obtained between two consecutive peaks in the developed method. Therefore, this method can be applied to its intended purpose with no problems, its suitability being proved.

3.2. Stability of the solution

Results obtained in the study of the solution (both reference and sample solution) where it can be noticed that solutions were stable for 48 h, as during this time the results does not decrease below the minimum percentage (96%).

3.3. Linearity

Voriconazole and internal standard were chromatographed using the mobile phase. The linearity of peak area responses versus concentrations was studied from 5 to 50 μg ml^{-1} for voriconazole. A linear response was observed over the examined concentration range. The results are tabulated Table 1.

3.4. Accuracy and repeatability

Accuracy was studied using three different solutions, containing 10, 20 and 30 μg ml^{-1} of voriconazole. Recovery data are reported in Table 2. The obtained values were within the range of 99.45 and 100.50%, mean R.S.D.% was 0.53%, satisfying the acceptance criteria for the study. The system repeatability was calculated from five replicate injections of voriconazole at the analytical concentration of about 10 μg ml^{-1}; the R.S.D.% found was 0.79.

Table 1
Results of the data analysis for the quantitative determination of voriconazole by the proposed method

Statical parameter	HPLC
Concentration range (μg/ml)	5–50
Regression equation	$y = 0.31949x - 0.08903$
Correlation coefficient (r)	0.9999
Stand error on estimation (S_e)	0.09693
Standard deviation on slope (S_b)	0.00235
Standard deviation on intercept (S_a)	0.05383
Limit of detection (LOD) (μg/ml)	0.55
Limit of quantification (LOQ) (μg/ml)	2

Table 2
Accuracy for voriconazole

Concentration (μg ml^{-1})	Recovery (%)[a]	R.S.D. (%)
10	99.45	0.25
20	100.27	0.53
30	99.82	0.82
Mean	99.84	0.52

[a] Mean of five determinations.

3.5. Robustness

As defined by the ICH, the robustness of an analytical procedure refers to its capability to remain unaffected by small and deliberate variations in method parameters [12,13]. In order to study the simultaneous variation of the factors on the considered responses, a multivariate approach using design of experiments is recommended in robustness testing. A response surface method was carried out to obtain more information and to investigate the behavior of the response around the nominal values of the factors. Response surface methodology (RSM) has the following advantages: (a) to allow a complete study where all interaction effects are estimated; and (b) to give an accurate description of an experimental region around a center of interest with validity of interpolation [14,16,17]. Generally the large numbers of experiments required by standard designs applied in RSM discourage their use in the validation procedure. However, if an analytical method is fast and requires the testing of a few factors (three or less), a good choice for robustness testing may be the central composite design (CCD), widely employed because of its high efficiency with respect to the number of runs required. A CCD in k factors requires 2^k factorial runs, $2k$ axial experiments, symmetrically spaced at $\pm\alpha$ along each variable axis, and at least one center point [18]. Two to five center repetitions are generally carried out in order to know the experimental error variance and to test the predictive validity of the model [19]. In order to study the variables at no more than three levels (-1, 0, $+1$), the design used in robustness testing of voriconazole was a central composite design (CCD) with $\alpha = \pm 1$ [16,20]. Three factors were considered: percentage v/v of acetonitrile (x_1); flow rate ml min^{-1} (x_2) and p^H (x_3). The experimental domain of the selected variables is reported in Table 3. The ranges examined were small deviations from the method settings and the corresponding responses in the peak area ratio considered (Y) were observed. A three-factor CCD requires 16 experiments, including two replicates of the center point. The experimental plan and the corresponding responses are reported in Table 4. All experiments were performed in randomized order to minimize the effects of uncontrolled factors that may introduce a bias on the response. A classical second-degree model with a cubic

Table 3
Chromatographic conditions and range investigated during robustness testing

Variable	Optimized value	Range investigated
Mobile phase (ACN/buffer)	50:50	45/55–55/45
Flow rate (ml min^{-1})	1.0	0.8–1.2
p^H	3.0	2.5–3.5

Table 4
Experimental plan for robustness testing and obtained responses

No. exp.	Acetonitrile (%)	Flow rate (ml min^{-1})	p^{H}	Peak area ratio
1	45	0.8	2.5	2.15
2	55	0.8	2.5	2.18
3	45	1.2	2.5	1.95
4	55	1.2	2.5	1.84
5	45	0.8	3.5	2.13
6	55	0.8	3.5	2.14
7	45	1.2	3.5	1.86
8	55	1.2	3.5	1.92
9	45	0.8	3	1.91
10	55	1.2	3	2.00
11	50	1.0	3	1.95
12	50	1.0	3	2.11
13	50	1.0	2.5	2.14
14	50	1.0	3.5	2.16
15	50	1.0	3	2.16
16	50	1.0	3	2.15

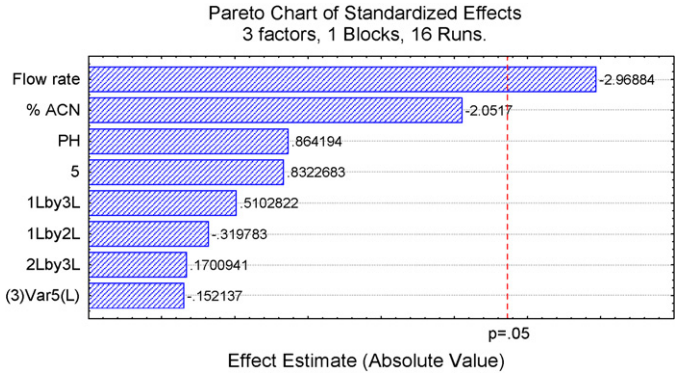
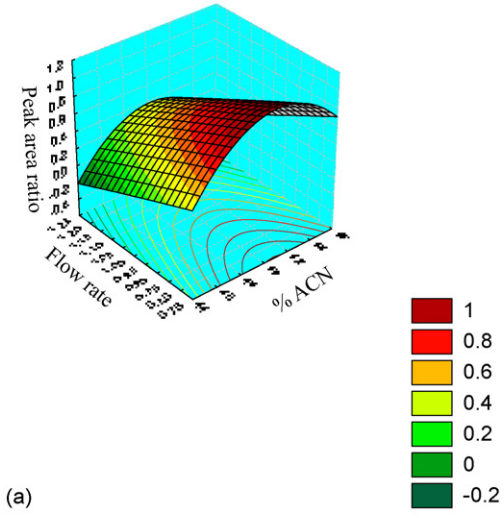
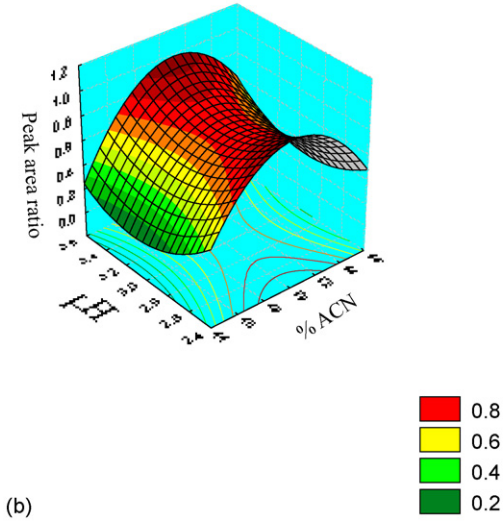


Fig. 3. Representative graphic to show the influence of variables studied in the response of voriconazole.





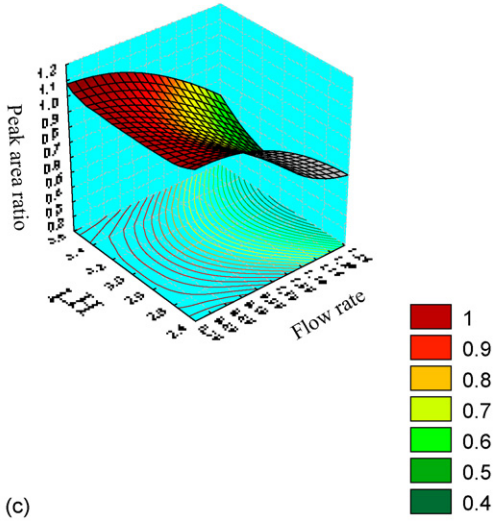


Fig. 4. Three-dimensional plot of the response surface for Y (found drug peak area ratio). (a) Variation of the response Y as a function of x_1 (% acetonitrile) and x_2 (flow rate); fixed factor: x_3 (p^{H}) = 3.0. (b) Variation of the response Y as a function of x_1 (% acetonitrile) and x_3 (p^{H}) fixed factor: x_2 (flow rate) = 1.0 ml min^{-1}. (c) Variation of the response Y as a function of x_2 (flow rate) and x_3 (p^{H}); fixed factor: x_1 (% acetonitrile) = 50% v/v.

Table 5
ANOVA results

Parameter	SS	MS	F	P
ACN (%)	0.007	0.007	0.692	0.432
Flow rate (ml/min)	0.095	0.095	8.813	0.020
p^H	0.002	0.003	0.023	0.883

experimental domain was postulated. Experimental results were computed by statistica [15]. The coefficients of the second-order polynomial model were estimated by the least squares regression. The equation model for Y (found peak area ratio) was as follows:

$$Y = 2.0950000 + 0.02791x_1 - 0.12875x_2 - 0.09958x_3 - 0.0050x_1^2 + 0.05502x_2^2 - 0.011250x_3^2 + 0.01875x_1x_2 + 0.00750x_1x_3 + 0.00625x_2x_3$$

The factor flow rate (x_2) was significant for the regression model assumed.

The model was validated by the analysis of variance (ANOVA). The statistical analysis showed (Table 5) that the model represents the phenomenon quite well and the variation of the response was correctly related to the variation of the factors. Fig. 3 shows the influence of each of the variables studied in the voriconazole as a response where none of them exceeds the limit except the flow rate as shown in the paerto graph. The interpretation of the results has to start from the analysis of the whole model equation rather than from the analysis of the single coefficients. It is important for the response surface study, to consider also the factors whose coefficients are statistically non-significant. For this reason the analysis of the response surface plot is necessary. As shown in Fig. 4(a)–(c), the analysis produces three-dimensional graphs by plotting the response model against two of the factors, while the third is held constant at a specified level, usually the proposed optimum. Fig. 3a shows a graphical representation of the isoresponse surface for variation of percentage of ACN (x_1) and flow rate (x_2), while the p^H (x_3) is maintained constant at its optimum of 3.0. An increase in the flow rate results in a decrease of the observed peak area ratio (Y), while the percentage of organic modifier had no important effect on the response. Analogous interpretation may be derived by examining Fig. 4c that plots the factors flow rate (x_2) versus p^H (x_3). In Fig. 4b, where the factor flow rate is maintained constant, the method can be considered robust for the studied experimental response. In conclusion, by examining the ANOVA results and analysis of response surface confirms that Y is not robust for factor x_2, thus a precautionary statement should be included in the analytical procedure for this factor.

3.6. Intermediate precision

The intermediate precision is a measure of precision between repeatability and reproducibility and it should be established according to the circumstances under which the procedure is intended to be used [21]. The analyst should establish the effects of random events on the precision of the analytical procedure.

Table 6
Experimental plan for intermediate precision testing and obtained responses

No. exp.	Analyst	Instrument	Day	Peak area ratio
1	Analyst 1	HPLC 1	Day 1	2.085
2	Analyst 1	HPLC 1	Day 1	2.087
3	Analyst 1	HPLC 1	Day 1	2.086
4	Analyst 2	HPLC 1	Day 1	2.086
5	Analyst 2	HPLC 1	Day 1	2.087
6	Analyst 2	HPLC 1	Day 1	2.085
7	Analyst 1	HPLC 2	Day 1	2.12
8	Analyst 1	HPLC 2	Day 1	2.15
9	Analyst 1	HPLC 2	Day 1	2.13
10	Analyst 2	HPLC 2	Day 1	2.14
11	Analyst 2	HPLC 2	Day 1	2.23
12	Analyst 2	HPLC 2	Day 1	2.18
13	Analyst 1	HPLC 1	Day 2	2.08
14	Analyst 1	HPLC 1	Day 2	2.082
15	Analyst 1	HPLC 1	Day 2	2.079
16	Analyst 2	HPLC 1	Day 2	2.079
17	Analyst 2	HPLC 1	Day 2	2.085
18	Analyst 2	HPLC 1	Day 2	2.14
19	Analyst 1	HPLC 2	Day 2	2.15
20	Analyst 1	HPLC 2	Day 2	2.11
21	Analyst 1	HPLC 2	Day 2	2.09
22	Analyst 2	HPLC 2	Day 2	2.16
23	Analyst 2	HPLC 2	Day 2	2.11
24	Analyst 2	HPLC 2	Day 2	2.10

The intermediate precision is obtained when the assay is performed by multiple analysts, using multiple instruments, on multiple days, in one laboratory [12]. In order to study these effects simultaneously, a multivariate approach was used.

The considered variables included analysts (1 and 2), equipment (HPLC 1 and 2) and days (1 and 2). The considered

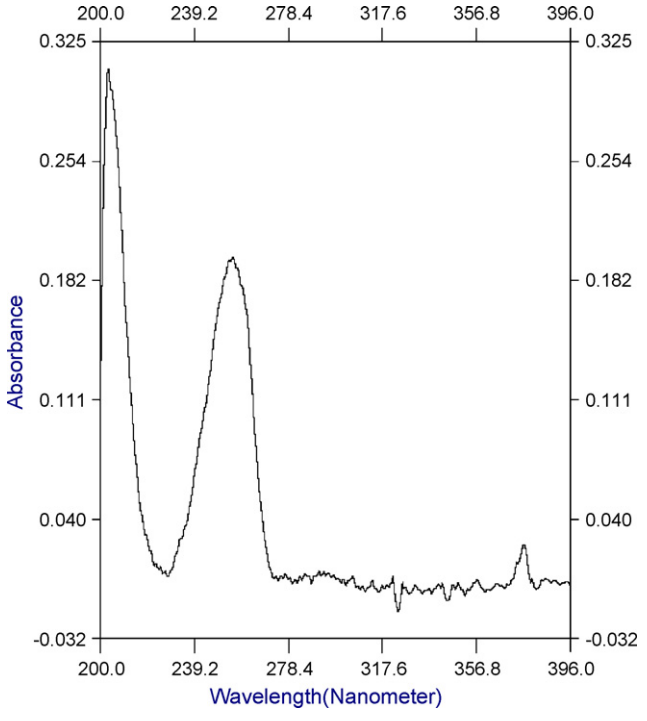


Fig. 5. UV spectrum of voriconazole 10 μg ml^{-1} concentration.

response was the found drug peak area ratio. A linear model ($y = b_0 + b_1x_1 + b_2x_2 + b_3x_3$) was postulated and a 2^3 full factorial design was employed to estimate the model coefficients. Each experiment was repeated three times in order to evaluate the experimental error variance. The analyses were carried out in a randomized order according to the experimental plan reported in Table 6. The concentration of voriconazole was about 10 μg ml^{-1}. No considered factor was found significant for the regression model assumed. The R.S.D. found (0.45%, $n = 24$) was acceptable, indicating a good precision of the analytical procedure.

The proposed method was compared to the UV spectrophotometry (Fig. 5) to verify the results obtained from HPLC. A calibration equation was obtained in the concentration range of 10–50 μg ml^{-1} and at the wavelength of 256 nm by using water as a blank. The relation between absorbance (A) and concentration of voriconazole (C) was [$A = 1854C - 0.0267$; $r = 0.9998$]. The injection vial analysis results were found to be 9.6 ± 0.2 (mean ± S.D.; $n = 6$) by UV spectrophotometry [22]. High reproducibility and insignificant differences between the two methods were obtained at the 95% probability level for t- and F-test of significance of $1.75 < 2.57$ and $1.11 < 5.05$, respectively.

4. Conclusion

The proposed high-performance liquid chromatographic method has been evaluated over the linearity, precision, accuracy, and specificity and proved to be convenient and effective for the quality control of voriconazole in pharmaceutical dosage forms. The measured signal was shown to be precise, accurate, and linear over the concentration range tested (5.0–50.0 μg ml^{-1}) with a correlation coefficient better than 0.9999. The proposed method was further compared with an UV procedure proposed by us and proved to be more accurate and precise. Moreover, the lower solvent consumption along with the short analytical run time of 4.0 min leads to a cost effective and environmentally friendly chromatographic procedure. Thus, the proposed methodology is rapid, selective, requires a simple sample preparation procedure, and represents a good procedure of voriconazole in vials.

Acknowledgements

The authors thank to M/s Sun pharmaceuticals Ltd., India for providing pure drugs to develop the method, Dr. K. Rama Krishna, UGC research awardee, Department of Chemistry, Andhra for his help during the work.

References

[1] K. Richardson, A.S. Bell, R.P. Dickinson, S. Narayanaswami, S.J. Ray, in: Program and Abstracts of the 35th Interscience Conference on Antimicrobial Agents and Chemotherapy, San Francisco, CA, September 17–20, 1995. The American Society for Microbiology, Washington, DC, p. 124 AF69.
[2] M. Murphy, E.M. Bernard, T. Ishimaru, D. Armstrong, Antimicrob. Agents Chemother. 41 (1997) 696–698.
[3] H. Sanati, P. Belanger, R. Fratti, M. Ghannoum, Candida krusei Antimicrob. Agents Chemother. 41 (1997) 2492–2496.
[4] G.W. Pye, G.P. Oliver, P.F. Troke, in: Program and Abstracts of the 35th Interscience Conference on Antimicrobial Agents and Chemotherapy, September 17–20, 1995, San Francisco, CA. The American Society for Microbiology, Washington, DC, p. 125 AF72.
[5] L. Purkins, N. Wood, P. Gharamani, K. Greenhalgh, M.J. Allen, D. Kleinermans, Antimicrob. Agents Chemother. 46 (2002) 2546–2553.
[6] H. Egle, R. Trittler, A. Koenig, K. Kuemmerer, Fast. J. Chromatogr. B: Anal. Technol. Biomed. Life Sci. 814 (2) (2005) 361–367.
[7] B.G. Keevil, S. Newman, S. Lockhart, S.J. Howard, C.B. Moore, D.W. Denning, Therap. Drug Monit. 26 (6) (2004) 650–657.
[8] F. Pehourcq, C. Jarry, B. Bannwarth, Biomed. Chromatogr. 18 (9) (2004) 719–722.
[9] L. Zhou, R.D. Glickman, N. Chen, W.E. Sponsel, J.R. Graybill, K.W. Lam, J. Chromatogr. B: Anal. Technol. Biomed. Life Sci. 776 (2) (2002) 213–220.
[10] R. Ferretti, B. Gallinella, F. La Torre, L. Zanitti, Chromatographia 47 (11–12) (1998) 649–654.
[11] P.K. Owens, A.F. Fell, M.W. Coleman, J.C. Berridge, Enantiomer 4 (2) (1999) 79–90.
[12] International Conference on Harmonisation, Topic Q2B, Validation of Analytical Methods: Methodology. The Third International Conference on Harmonization of Technical Requirements for Registration of Pharmaceuticals for Human Use (ICH), Yokohama, Japan, 1997.
[13] Y. Vander Heyden, A. Nijhuis, J. Smeyers-Verbeke, B.G.M. Vandeginste, D.L. Massart, J. Pharm. Biomed. Anal. 24 (2001) 723–753.
[14] D.K. Lin, J. Quality Technol. 31 (1999) 61–66.
[15] Stat soft, Inc., Statistica data analysis system, Statistica software east 2300, 14th street, Tulsa, OK 74104, 2001.
[16] K.K. Hockman, D. Berengut, Chem. Eng. 102 (1995) 142–148.
[17] H. Fabre, J. Pharm. Biomed. Anal. 14 (1996) 1125–1132.
[18] R. Ragonese, M. Mulholland, J. Kalman, J. Chromatogr. A 870 (2000) 45–51.
[19] G.A. Lewis, D. Mathieu, R. Phan-Tan-Luu, Pharmaceutical Experimental Design, Marcel Dekker, New York, 1999.
[20] S. Pinzauti, P. Gratteri, S. Furlanetto, P. Mura, E. Dreassi, R. Phan-Tan-Luu, J. Pharm. Biomed. Anal. 14 (1996) 881–889.
[21] J. Ermer, H.-J. Ploss, J. Pharm. Biomed. Anal. 37 (2005) 859–870.
[22] G. Srinu Babu, Ch. A.I. Raju, UV-Spectrophotometric Determination of Voriconazole in Bulk and Its Formulation, Asian J. Chem. 19 (2007) 1625–1627.

Available online at www.sciencedirect.com
ScienceDirect
Talanta 71 (2007) 1434–1437
Talanta
www.elsevier.com/locate/talanta

Short communication

Enantioselective potentiometric membrane electrodes based on C_{60} fullerene and its derivatives for the assay of L-Histidine

Raluca-Ioana Stefan-van Staden *, Bhajan Lal, Luxolo Holo

Department of Chemistry, University of Pretoria, Pretoria 0002, South Africa

Received 7 December 2005; received in revised form 5 May 2006; accepted 31 May 2006
Available online 7 July 2006

Abstract

Novel enantioselective, potentiometric membrane electrodes (EPMEs) based on carbon paste impregnated with C_{60} fullerene (I), (1,2-methanofullerene C60)-61-carboxylic acid (II), diethyl(1,2-methanofullerene C60)-61-61-dicarboxylate (III) and tert-butyl(1,2-methanofullerene C60)-61-carboxylic acid (IV) are reported. Response characteristics showed that the proposed electrodes could be reliably used in the assay of L-Histidine (L-His), with the best enantioselectivity and time-stability exhibited by fullerene derivatives. The surfaces of the electrodes are stable and easily renewable by simply polishing on an alumina paper. All proposed electrodes proved to be successful for the determination of the enantiopurity of histidine as raw material and of its pharmaceutical formulation.
© 2006 Elsevier B.V. All rights reserved.

Keywords: Enantioselective, potentiometric membrane electrodes; Enantioanalysis; C_{60}; L-Histidine

1. Introduction

Chiral recognition became an area of considerable research interests because of its importance in almost all fields of biological, chemical and pharmaceutical sciences [1]. The most used methods for chiral discrimination are chromatographic and electrochemical methods. The advantages of sensors over chromatographic methods are: direct assay of the enantiomer without any prior separation, high sensitivity and enantioselectivity, rapidity, accuracy and precision of analytical information, as well as low cost of analysis [2].

The discovery of C_{60} has stimulated a large activity in chemistry. Since fullerenes were discovered in 1985 [3,4], their derivatives were used by numerous researchers for pharmaceutical research [5–8].

Introduced by Ruzicka and Tjell in 1970 [9], carbon paste based selective electrodes were used for determination of various inorganic ions such as sodium, silver, copper, iron, nickel, chromium, zirconium, nitrate, perchlorate and fluoroborate [10]. Since 1998, carbon paste was used as matrix for the design of the enantioselective, potentiometric membrane electrodes [2].

L-Histidine (L-His)(Fig. 1) is an essential component of many proteins. Its residue is often found at the active site of enzymes [11]. L-Histidine acts as a neurotransmitter or neuromodulator in mammalian central nervous system, including retina [12,13]. It can minimize internal bleeding from microtrauma [14].

Electrochemical methods for the determination of trace amount of histidine [15–17] were proposed, but none of them described the enantioanalysis of histidine. Several other methods based on capillary electrophoresis [18–20], colorimetry [21], fluorimetry [22] and chromatography [23–27] were used for the analysis and enantioanalysis of histidine, but they are not always as simple and accurate as electroanalysis.

A new application of the C_{60} fullerene and its derivatives is presented in this paper: C_{60} fullerene (I), (1,2-methanofullerene C60)-61-carboxylic acid (II), diethyl(1,2-methanofullerene C60)-61-61-dicarboxylate (III) and tert-butyl(1,2-methanofullerene C60)-61-carboxylic acid (IV) were used for the design of enantioselective, potentiometric membrane electrodes (EPMEs) for enantioanalysis of L-Histidine.

2. Experimental

2.1. Reagents and materials

C_{60} fullerene (I), (1,2-methanofullerene C60)-61-carboxylic acid (II), diethyl(1,2-methanofullerene C60)-61-61-dicarbox-

* Corresponding author. Tel.: +27 12 4202510; fax: +27 12 3625297.
E-mail address: Raluca.Stefan@chem.up.ac.za (R.-I. Stefan-van Staden).

0039-9140/$ – see front matter © 2006 Elsevier B.V. All rights reserved.
doi:10.1016/j.talanta.2006.05.088

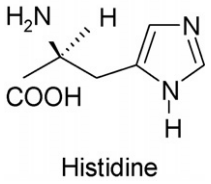


Fig. 1. L-Histidine.

ylate (III) and tert-butyl(1,2-methanofullerene C60)-61-carboxylic acid (IV) were supplied by Fluka (Buchs, Switzerland). Phosphate buffer of pH 5.40 was supplied by Merck (Darmstadt). Food supplement, energy booster, immunity modulator, capsules (containing 0.72 g L-Histidine and Vitamin C, Vitamin B6, Ca, Mg, Na, K) were supplied by Hypo-Plus Naturals, Onderstepoort, South Africa.

Deionized water from a Modulab system (Continental Water Systems, San Antonio, TX, USA) was used for all solutions preparations. The L- and D-Histidine solutions necessarily in the characterization of the enantioselective potentiometric membrane electrodes were prepared from standard L-His and D-His solutions (10^{-2} mol/L), respectively, by serial dilutions. All standard and diluted solutions were buffered with phosphate buffer (pH 5.40 mol/L) from Merck (Darmstadt, Germany) (1:1, v/v, buffer:deionized water).

2.2. Apparatus

A 663 VA Stand (Metrohm, Herisau, Switzerland) connected to a PGSTAT 100 (Eco Chemie, Utretch, Netherlands) and software version 4.9 were used for all potentiometric measurements. An Ag/AgCl (0.1 mol/L KCl) electrode served as reference electrode in the cell.

2.3. Recommended procedure: direct potentiometry

The potentiometric method was used for the potential determination of each standard solution (10^{-10} to 10^{-3} mol/L, pH 5.40). The electrodes were placed in the stirred standard solutions and graphs of E (mV) versus pL-His were plotted. The unknown concentrations of L-His were determined from the calibration plots.

2.4. Uniformity content test

Each of ten capsules (0.72 g histidine/capsule) was placed in a 250 mL volumetric flask and dissolve in a 1:1 deionized water:buffer (pH 5.4) solution. The unknown concentration was determined using the direct potentiometric method.

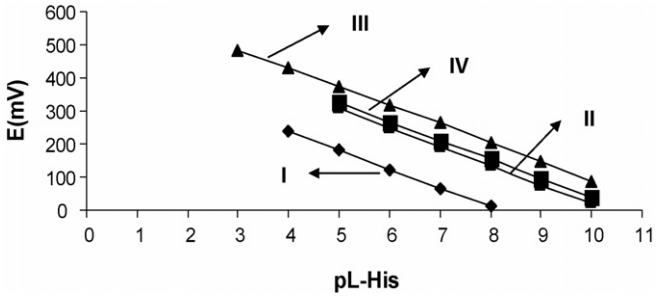


Fig. 2. Calibration graphs of EPMEs based on: I, fullerene (I); II, fullerene (II); III, fullerene (III); IV, fullerene (IV).

2.5. Electrodes design

Paraffin oil and graphite powder were mixed in a ratio of 1:4 (w/w) followed by the addition of chiral selector—fullerene (I), (II), (III) or (IV) to carbon paste. A certain quantity of carbon paste free of chiral selector was prepared and it was placed into a plastic pipette peak leaving 3–4 mm empty in the top to be filled with the carbon paste that contains the chiral selector. The diameter of the potentiometric, enantioselective membrane electrode and the thickness of the membrane were 3 mm. Electric contact was obtained by inserting an Ag/AgCl wire in the carbon paste. 0.1 mol/L of KCl was used as internal solution. The surface of the electrodes was wetted with deionised water and polished with alumina paper (polishing strips 30144-001, Orion) before using them for each experiment. The carbon paste prevents the leaching of the chiral selector from the membrane into solution. When it was not in use, the electrode was immersed in a 10^{-3} mol/L L-His solution.

3. Results and discussion

3.1. Electrodes response

The response characteristics exhibited by the proposed electrodes towards the L-His are summarized in Table 1. For all the calibration graphs (Fig. 2), the potentiometric membrane electrodes showed linear and near-Nernstian responses for L-His, with correlation coefficients for the equations of calibration of 0.9997 (I), 0.9999 (II, IV) and 0.9998 (III), respectively. The lowest limit of detection as well as the wider linear concentration range were recorded for the electrode based on fullerene (III)

Table 1
Response characteristics of the enantioselective, potentiometric, membrane electrodes based on C_{60} fullerenes

EPME based on	Slope (mV/decade of concentration)	Intercept, E° (mV)	Linear concentration range (mol/L)	Detection limit (mol/L)
I	56.8	465.8	10^{-8}–10^{-4}	6.3×10^{-9}
II	57.7	601.9	10^{-10}–10^{-5}	3.7×10^{-11}
III	56.0	652.4	10^{-10}–10^{-3}	2.2×10^{-12}
IV	57.5	602.4	10^{-10}–10^{-5}	3.3×10^{-11}

All measurements were made at room temperature; all values are the average of 10 determinations.

Table 2
Potentiometric selectivity coefficients for the proposed electrodes

Interfering species (J)	K_{sel}^{pot}			
	EPME based on			
	I	II	III	IV
D-His	4.0×10^{-3}	4.3×10^{-3}	2.2×10^{-3}	2.4×10^{-3}
Polyvinylpyrolidone	3.7×10^{-3}	5.7×10^{-3}	3.4×10^{-3}	5.7×10^{-3}
Creatine	3.2×10^{-3}	$\ll 10^{-4}$	2.9×10^{-3}	1.8×10^{-3}
Creatinine	4.6×10^{-3}	6.2×10^{-3}	2.7×10^{-3}	5.3×10^{-3}

All measurements were made at room temperature; all values are the average of 10 determinations.

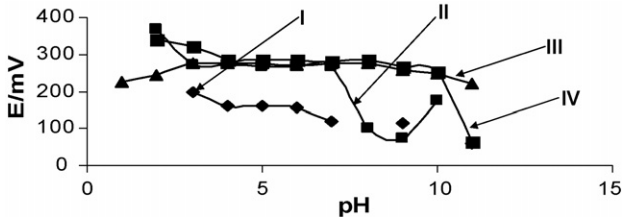


Fig. 3. The influence of pH on the response of the enantioselective, potentiometric membrane electrodes (L-His = 10^{-5} mol/L); for enantioselective, potentiometric electrodes based on: I, fullerene (I); II, fullerene (II); III, fullerene (III); IV, fullerene (IV).

while the best response was recorded for the electrode based on fullerene (II). The low detection limits are due to the utilization of a 0.1 mol/L KCl solution as internal solution in the electrodes design.

D-His on the other hand, showed non-Nernstian response.

The response of the EPMEs was 10 s for concentrations of L-Histidine higher than 10^{-5} mol/L and 1 min for concentrations of L-Histidine lower or equal with 10^{-5} mol/L. All electrodes displayed good stability and reproducibility over the 3 months test period (R.S.D. < 0.1%), when they were used every day.

3.2. Effect of pH on the response of the electrodes

The influence of pH on the response of the proposed electrodes was checked by recording the emf of the cell for solutions containing 10^{-5} mol/L L-His at different pH values. These solutions were prepared by adding very small volumes of HCl/NaOH solution (0.1 or 1 mol/L of each) to a L-His solution. The plots of E (mV) versus pH (Fig. 3) indicate that the response of the electrodes does not depend upon the pH in the following ranges: 4.0–6.0 [I] 3.0–7.0 [II], 3.0–8.0 [III] and 5.0–8.0 [IV], respectively. The wide range of pH can be explained by the equal capacity of protonated and neutral form of L-Histidine to interact with the specified fullerene.

3.3. Selectivity of the electrodes

The selectivity of the potentiometric membrane electrode was checked using mixed solutions method over compounds that may interfere in purity and enantiopurity tests of pharmaceutical formulations of L-Histidine. The concentrations of interfering ions and L-His were 10^{-4} and 10^{-5} mol/L, respectively. The values of potentiometric selectivity coefficients, K_{sel}^{pot}, shown in Table 2 demonstrated the enantioselectivity and selectivity properties of the proposed electrodes for the assay of L-His. Inorganic cations such a Na^+, K^+ and Ca^{2+} do not interfere in the analysis of L-His ($K_{sel}^{pot} \ll 10^{-4}$).

3.4. Analytical applications

The response characteristics as well as the selectivity and enantioselectivity of the proposed electrodes made them useful for the determination of enantiopurity of histidine raw material and for performing the content uniformity test of L-His capsules (food supplement, energy booster, immunity modulator and capsules).

Recovery tests of L-His in the presence of D-His were performed. The results proved that the electrodes are suitable for enantioanalysis of L-Histidine (Table 3), when the ratio between L- and D-His has got any value. No differences between the recovery values when the ratios L:D were 1:9 and 1:99.9 were recorded.

Table 3
Determination of L-His in the presence of D-His

L:D (mol/mol)	L-Histidine, recovery (%)			
	EPME based on			
	I	II	III	IV
2:1	99.50 ± 0.02	99.92 ± 0.02	99.60 ± 0.02	99.99 ± 0.01
1:1	99.50 ± 0.02	99.90 ± 0.01	99.99 ± 0.01	99.40 ± 0.02
1:2	99.99 ± 0.03	99.98 ± 0.02	99.89 ± 0.03	99.80 ± 0.02
1:4	99.50 ± 0.02	99.95 ± 0.02	99.98 ± 0.02	99.98 ± 0.01
1:9	99.52 ± 0.02	99.94 ± 0.01	99.98 ± 0.02	99.98 ± 0.02

All measurements were made at room temperature; all values are average of 10 determinations.

Uniformity content test was performed for Food supplement, energy booster, immunity modulator and capsules. The results obtained with the proposed electrodes: $96.4 \pm 0.1\%$ (I), $97.0 \pm 0.1\%$ (II), $96.53 \pm 0.02\%$ (III) and $96.7 \pm 0.3\%$ (IV), respectively are comparable with those obtained using the method proposed by Abdel-Latef ($97.0 \pm 0.2\%$) [25,26].

4. Conclusions

This paper describes new enantioselective, potentiometric membrane electrodes based on C_{60} fullerene (I), (1,2-methanofullerene C60)-61-carboxylic acid (II), diethyl(1,2-methanofullerene C60)-61-61-dicarboxylate (III) and tert-butyl(1,2-methanofullerene C60)-61-carboxylic acid (IV) as chiral selectors, for enantioanalysis of L-Histidine. The simple, fast and reproducible construction of the electrodes assures the reliable response characteristics. The good selectivity and enantioselectivity of designed electrodes is allowed to perform the enantiopurity test of L-His raw material as well as the uniformity content test of the pharmaceutical formulation (Food supplement, energy booster, immunity modulator and capsules).

Acknowledgement

The authors are thankful to National Research Foundation for their support.

References

[1] H.Y. Aboul-Enein, I.W. Wainer, The Impact of Sterochemistry on Drug Development and Use, Marcel Dekker, NY, USA, 1997.
[2] R.I. Stefan, J.F. Staden, H.Y. Aboul-Enein, Electrochemical Sensors in Bioanalysis, Marcel Dekker, NY, USA, 2001.
[3] C.N.R. Rao, R. Seshadri, A. Govindaraj, R. Sen, Mater. Sci. Eng. R: Rep. 15 (1995) 209.
[4] H.W. Kroto, J.R. Heath, S.C. O'Brien, R.F. Curl, R. Smalley, Nature 318 (1985) 162.
[5] K. Okuda, T. Mashino, M. Hirobe, Bioorg. Med. Chem. Lett. 6 (1996) 539.
[6] T. Mashino, D. Nishikawa, K. Takahashi, N. Usui, T. Yamori, M. Seki, T. Endo, M. Mochizuki, Bioorg. Med. Chem. Lett. 13 (2003) 4395.
[7] M. Orfanopoulos, S. Kambourakis, Tetrahedron Lett. 36 (1995) 435.
[8] E. Nakamura, H. Tokuyama, S. Yamago, T. Shiraki, Y. Sugiura, Bull. Chem. Soc. Jpn. 69 (1996) 2143.
[9] J. Ruzicka, J.C. Tjell, Anal. Chim. Acta 49 (1970) 346.
[10] J. Jezkova, J. Musilova, K. Vytras, Electroanalysis 9 (1997) 1433.
[11] T.E. Creighton, Encyclopedia of Molecular Biology, vol. 2, Wiley, New York, 1999, p. 1147.
[12] G.N. Chen, X.P. Wu, J.P. Duan, H.Q. Chen, Talanta 49 (1999) 319.
[13] Y. Kusakari, S. Nishikawa, S. Ishiguro, M. Tamai, Curr. Eye Res. 16 (1997) 600.
[14] D.F. Horrobin, M.S. Mandu, M. Oka, R.O. Morgan, S.C. Cunnane, A.I. Aly, T. Ghayur, M. Schweitzer, R.A. Karmali, Med. Hypothesis 5 (1979) 969.
[15] L.Z. Wang, X.L. Zhang, Chin. J. Anal. Chem. 21 (1993) 569.
[16] J.C. Moreira, A.G. Fogg, Analyst 115 (1990) 41.
[17] X.L. Zhang, C.S. Ma, L.A. Deng, Chin. J. Anal. Chem. 6 (1995) 783.
[18] P. Tuma, E. Samcova, P. Balynova, J. Chromatogr. B 821 (2005) 53.
[19] S. Zhao, Y.M. Liu, Anal. Chim. Acta 426 (2001) 65.
[20] M.J. Heravi, Y. Shen, M. Hassanisadi, M.G. Khaledi, Electrophoresis 26 (2005) 1874.
[21] S. Lata, A. Reichel, R. Brock, R. Tampe, J. Piehler, J. Am. Chem. Soc. 127 (2005) 10215.
[22] X. Li, H. Ma, S. Dong, X. Duan, S. Liang, Talanta 62 (2004) 367.
[23] S.W. Hovorka, T.D. Williams, C. Schoneich, Anal. Biochem. 300 (2002) 206.
[24] A. Namera, M. Yashiki, M. Nishida, T. Kojima, J. Chromatogr. B 776 (2002) 49.
[25] H.E. Abdel-Lafef, J. Pharm. Biomed. Anal. 17 (1998) 1267.
[26] H.E. Abdel-Lafef, M.M. Ayad, E.A. Taha, J. Pharm. Biomed. Anal. 18 (1999) 1021.
[27] Z.P. Yang, W.S. Hancock, T.R. Chew, L. Bonilla, Proteomics 5 (2005) 3353.

Available online at www.sciencedirect.com
ScienceDirect
Talanta 71 (2007) 1304–1311
Talanta
www.elsevier.com/locate/talanta

Effect of insignificant bias and its uncertainty on the coverage probability of uncertainty intervals
Part 2. Evaluation for a found insignificant experimental bias

Vaclav Synek *

Faculty of the Environment, Jan Evangelista Purkyně University, Kralova vysina 7, CZ-40096 Usti nad Labem, Czech Republic

Received 28 December 2005; received in revised form 7 June 2006; accepted 30 June 2006
Available online 9 August 2006

Abstract

This paper continues in studying the coverage probability of uncertainty intervals. It particularly investigates the uncertainty intervals determined in compliance with the GUM and EURACHEM Guide in case of the results uncorrected for the systematic error, since the experimental bias has been found insignificant. The problem is solved for known values of the experimental bias, its standard uncertainty and the overall standard uncertainty. The obtained findings given in graphs and tables show that coverage probability of the uncertainty intervals defined by expanded uncertainty about the uncorrected results can considerably fall below the chosen level of confidence; this depression depends only on the ratio of the bias and the overall uncertainty. The bias uncertainty does not directly influence this depression, it only determines whether the bias is significant or not and thereby determines whether the results will be corrected or not. The paper proposes three methods how to remove this coverage probability reduction: to apply a higher level of confidence in the significance test, to correct the results with the insignificant but too high biases and to compute the uncertainty intervals defined by some type of the uncertainties enlarged with the insignificant bias.
© 2006 Elsevier B.V. All rights reserved.

Keywords: Bias; Correction for systematic error; Coverage probability; Level of significance; *t*-Test; Uncertainty

1. Introduction

Part 1 of this work [1] investigates the coverage probability of the uncertainty intervals determined in compliance with the ISO "Guide to the Expression of Uncertainty in Measurement" (GUM) [2] and the EURACHEM/CITAC document "Quantifying Uncertainty in Analytical Measurement" (EURACHEM Guide) [3], i.e. which are defined by expanded uncertainty about the measured results. These documents require generally the results to be corrected for all recognised and significant systematic effects. It means that when the bias of the measurement has not been found significant, the results need not be corrected with it. Part 1 shows that owing to this approach the real coverage probabilities of the uncertainty intervals defined about the uncorrected results can be lower the chosen level of confidence (usually 0.95) and that this reduction depends on the true bias (true overall systematic error), the uncertainty of the experimental bias and the overall uncertainty. The obtained results correspond with the results and conclusions published by Maroto et al. [4] and O'Donnell and Hibbert [5]. The problem is studied with two different approaches, firstly for only those experimental biases, which are insignificant according to the *t*-test (approach of paper [4]), secondly for all possible experimental biases, both significant and insignificant (approach of paper [5]). However, there is a common defect of both previous approaches. The coverage probability is quantified for given values of the true bias, which are in fact unknown. It means that the coverage probability is evaluated from the view of 'omniscient god', who knows the true bias. Of course, this point of view enables to compute the coverage probability of the uncertainty interval for a presupposed analytical method or a given method defining this interval, but it does not suit a seeking analyst, who knows an experimental bias determined for his real analytical method. The analyst can choose a proper way how to compute the uncertainty intervals of his results only according to the determined experimental bias and not on the basis of the unknown true bias. It means that the studied coverage probability of uncertainty intervals should be expressed as a function of merely knowable quantities. This

* Tel.: +420 475 309 151; fax: +420 475 284 185.
E-mail address: synek@fzp.ujep.cz.

0039-9140/$ – see front matter © 2006 Elsevier B.V. All rights reserved.
doi:10.1016/j.talanta.2006.06.038

point of view let us return to the origin approach used in the papers by Maroto et al. [4,6], which takes into account only the insignificant experimental biases, because the analyst knowing a really observed experimental bias can obviously decide whether it is significant or not. When supposing a value of the true bias he can merely determine the probabilities with which the significant or insignificant experimental biases will occur.

2. Derivation of equations and computations

The conclusions in Part 1 say that the coverage probability of uncertainty intervals can be affected with the true bias, δ, the bias uncertainty, $u(b)$, and the overall uncertainty u (more exactly with their ratios $\delta/u(b)$ and $u(b)/u$). In this part for comparison's sake, it will be suitable to express the coverage probability as a function of such quantities, which are analogical from the new viewpoint to those quantities in Part 1; i.e. the experimental bias, b, and the quantities $u(b)$ and u (ratios $b/u(b)$ and $u(b)/u$).

The unknown true bias δ of an applied measurement process is estimated by an experimental bias of b, which has been determined in the trueness study with a bias uncertainty of $u(b)$. This value b can be regarded as a value randomly drawn from the population of all possible values, which has a normal distribution with a mean of δ and a standard deviation of $u(b)$. The probability that a given value b will be determined depends on the unknown value of the true bias and can be expressed by using the probability density function of that distribution, but here this function is applied reversely. In this function, the variable is the estimated true bias δ and the determined values of b and also $u(b)$ are constants for a given case; the function is denoted by $L(b, u(b), \delta)$—see Appendix (e.g. [7–9]). The probability (an infinitesimal probability $\mathrm{d}p$) that the estimated value of the true bias could be from the interval between δ and $\delta + \mathrm{d}\delta$ when the value b has been determined as the experimental bias (i.e. the probability that the given value b of the experimental bias could have occurred at random provided the value of the estimated true bias had been between δ and $\delta + \mathrm{d}\delta$) can be expressed

$$\mathrm{d}p = L(b, u(b), \delta)\,\mathrm{d}\delta \tag{1}$$

Besides the mentioned parameter (not statistical) b and $u(b)$ other needed parameters characterising the applied measurement process are known. They are the standard uncertainty combined from the uncertainty components reflecting all random errors of the process, σ, and the overall uncertainty of the measurement u combined from $u(b)$ and σ (see Part 1). (The mathematical relationships, which have already been given in Part 1, are not usually repeated in this part, they are only referenced to Part 1.) With these four known parameters (only three of them are mutually independent) and with that presuppose value of δ, the coverage probability of a chosen type of uncertainty interval can be computed for the results obtained on real samples with the given measurement process. When the experimental bias has been found as insignificant by the t-test (see Part 1), in compliance with EURACHEM Guide [3] this uncertainty interval should be defined by expanded uncertainty U about the uncorrected results. However, in this paper also other types of uncertainty intervals are studied (see below). The coverage probability of such an interval for the measurement of a real sample, i.e. probability that the given interval contains the true value of the measurand, μ, depends on the true bias δ. Since the real δ value is not known and only its estimate b is known, this coverage probability can be expressed as a function of the presupposed δ values, which can be estimated by the given b with different probabilities; an individual coverage exists to each value of δ. This individual probability depends also on the given case, i.e. on the computed type of uncertainty interval, values of b, u and σ or $u(b)$ and of course on the level of confidence α for the uncertainty interval. This function is denoted by ICP(b, u, σ, α, δ) here. Now by analogy with the computations in Part 1 a mean coverage probability, denoted by MCP, for the given case can be quantified. It must be computed as a weighted mean value from those individual coverage probabilities for all possible values of δ that can be estimated by the found experimental bias b. The whole range of these δ values is from $-\infty$ to ∞; and the weights are those infinitesimal probabilities (see Eq. (1)). The total sum of these weights must equal 1 (probability that a found experimental bias estimates a value of δ, which is from the range between $-\infty$ and ∞). The equation computing the MCP can be expressed like this

$$\begin{aligned}\mathrm{MCP} &= \int_{-\infty}^{\infty} \mathrm{ICP}(b, u, \sigma, \alpha, \delta)\,\mathrm{d}p \\ &= \int_{-\infty}^{\infty} \mathrm{ICP}(b, u, \sigma, \alpha, \delta) L(b, u(b), \delta)\,\mathrm{d}\delta \end{aligned} \tag{2}$$

(By analogy with Part 1 MCP is computed according to the total probability law again—see Appendix A in Part 1.)

This obtained MCP equation was specified for the same five types of uncertainty intervals as in Part 1 (see Appendix). The four types from them are defined about uncorrected results (1) with U, (2) with U(bias), (3) with SUMU and (4) with U_e(95%) and the last (5) type is defined by expanded uncertainty U about corrected results with the insignificant bias b, though they should not be corrected. (The equations to compute the uncertainty intervals by the U(bias), SUMU and U_e(95%) methods are given in Part 1.) The resulting integrals were solved numerically for some chosen values of those determining parameters (b, $u(b)$ and u or σ). The values of b as a parameter can be chosen from the range of the values insignificant according to the t-test, i.e.–$tu(b) \le b \le tu(b)$.

This presented evaluation of the coverage probability of uncertainty intervals takes into account that the overall uncertainty u is combined from the two basic component $u(b)$ and σ and that the experimental bias b can estimate more possible values of the true bias δ with the uncertainty $u(b)$. This approach was transferred from Part 1, where the evaluation of the coverage also considers the inside structure of u and by analogy considers the given true bias δ to be estimated with more possible experimental biases b. Both parts differ in the view at the bias. The proceeding presented here works with a practical variable – experimental bias while the proceeding in Part 1 works with a theoretical and unknowable variable – true bias. The calculations in both studies are conducted by analogy, which should enable

an easy comparison of the obtained results. However, the evaluation from the viewpoint applied in this paper can be also solved in a simpler way. Such solution has been used, e.g. in paper [10]. It considers the experimental bias b to be a point estimate of δ and ignores the inside structure of the overall uncertainty u. In this case, the bias uncertainty $u(b)$ is needful only to the bias significance test.

3. Results and their discussion

Fig. 1 shows the results obtained with the values of uncertainties from Case 1 of paper [4] (i.e. $u(b) = 0.70$, $\sigma = 1.5$, $u = 1.655$) and $b = 1.4$. This value of b represents the maximum insignificant value in this case since the applied t quantile was 2 (exactly 1.96; the t-test was considered two-tailed, at the usual level of significance $\alpha = 0.05$ and for very high degrees of freedom). Line 1 depicts the relationship between the function $L(b, u(b), \delta)$ and δ. Lines 2–4 depict the relationships between the possible values of δ and the individual coverage probabilities of the uncertainty intervals defined by those investigated methods (only the case of the intervals defined by the $U_e(95\%)$ method is not represented). Line 2 demonstrates the case when the obtained results are corrected with the given experimental bias though this bias is not significant. When the value of δ is close to b, the results corrected with this b are corrected properly. After this correction they approach the true values μ and consequently the uncertainty intervals defined by U about them have a high ICP (higher than 0.95). Such intervals are very probable since there is a high probability that the values of b and δ will be similar (maximum of $L(b, u(b), \delta)$—curve 1). Under these circumstances the mean coverage probability is determined mainly by the intervals that have high values of ICP. On the other hand the intervals defined by U about uncorrected results (line 3) can have such high ICP only when the value of δ is near to zero and therefore the correction is not necessary. However, there is only a low probability to find nearly significant experimental bias ($b = 1.4$) while the true bias δ is negligible; therefore the probability of such intervals is low (see line 1). The true bias δ, which can be estimated by b equalling 1.4 with a high probability, has to have a value close to 1.4 and such a bias would need to be corrected, because without this result correction the uncertainty intervals defined by U have a low ICP (about 0.89). Under these circumstances, the mean coverage probability is mainly determined by the intervals with low ICPs. When under the given conditions the analyst does not correct results and in spite of the fact he would like to get the mean coverage probability with a minimum of 0.95, he should compute some different uncertainty intervals, e.g. the wider intervals defined by U(bias) method (line 4).

The curves in Fig. 2 illustrate the relationships between the parameter $b/u(b)$ and the coverage probabilities computed as MCP for the uncertainty intervals obtained with all investigated methods (the values of uncertainties are from Case 1 of paper [4] again). Since the applied equations give the same results for b and $-b$ (even functions), the investigated range of $b/u(b)$ can be only from 0 to 2 (positive insignificant biases). Line 3 shows the case when the coverage probability is independent on $b/u(b)$ and equals always 0.95. It is valid for three types of uncertainty intervals: (1) when the uncertainty intervals are defined by expanded uncertainty U about the results corrected with the insignificant experimental biases; (2) when the uncertainty intervals limited about the uncorrected results are defined by SUMU or also (3) by $U_e(95\%)$ method. The findings for the first two cases are in agreement with the results obtained in Part 1 in which the mean coverage probabilities were considered for the distribution of all possible experimental biases b under given values of δ and $u(b)$. However, the results for the latter case differ from those obtained in Part 1. When the $U_e(95\%)$ uncertainty intervals are evaluated from this new viewpoint they give such coverage probabilities as the $U_e(95\%)$ method definition in paper [10] expected. Curve 2 shows the mean coverage probabilities when U(bias) method is applied. The coverage probabilities are higher than 0.95 and for higher values of $b/u(b)$ they approach a maximum of 0.975, which is associated with relatively large extensions

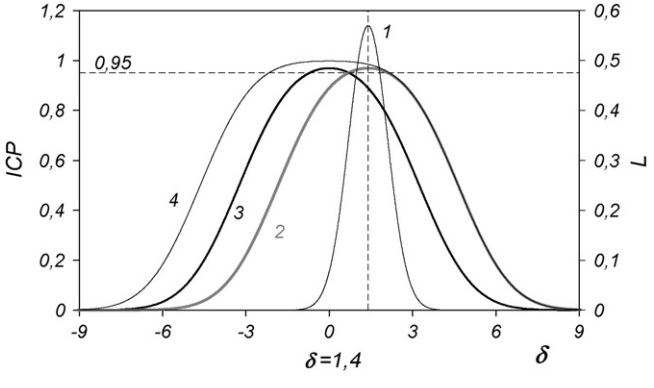


Fig. 1. The individual coverage probability (ICP) of the uncertainty intervals obtained by different computation methods for all possible true biases δ, which can be estimated by a certain value of experimental bias b vs. the given value of δ and 1: the corresponding function (L) expressing the probability density of these potential values of δ; conditions $b = 1.4$ (the largest insignificant b), uncertainties for Case 1 from [4]. The uncertainty intervals were defined: 2: SUMU method and U about corrected results, 3: U about uncorrected results, 4: U(bias) method.

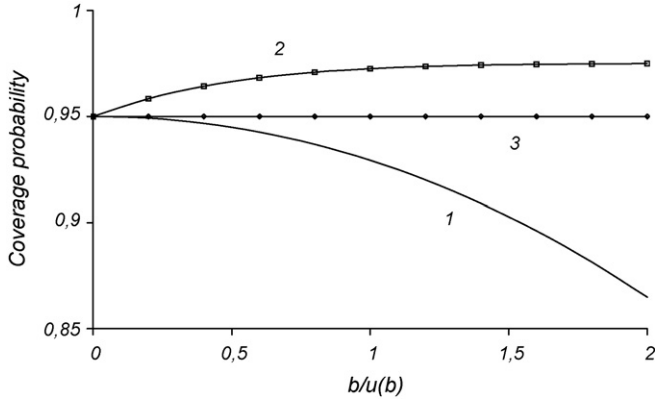


Fig. 2. The mean coverage probabilities of the uncertainty intervals computed with different methods vs. the insignificant experimental bias b normalized by its uncertainty $u(b)$ (uncertainties of Case 1 from [4]); all possible values of the systematic error estimated by the given insignificant experimental bias were taken into account. The uncertainty intervals were defined: 1: U about uncorrected results, 2: U(bias) method, 3: U about corrected results and also SUMU or $U_e(95\%)$ method.

Table 1
Coverage probability of the uncertainty intervals defined by 1.96u about uncorrected results obtained by a biased analytical method - dependence on the method characteristics—b: experimental bias; $u(b)$: experimental bias uncertainty; u: overall combined uncertainty; σ: combined uncertainty of all random effects

$b/u(b)$	$u(b)/u$						
	0.1	0.2	0.3	0.4	0.5	0.6	0.7
0.0	0.9500	0.9500	0.9500	0.9500	0.9500	0.9500	0.9500
0.2	0.9500	0.9498	0.9496	0.9493	0.9489	0.9483	0.9478
0.4	0.9498	0.9493	0.9483	0.9471	0.9454	0.9434	0.9410
0.6	0.9496	0.9483	0.9463	0.9434	0.9396	0.9350	0.9296
0.8	0.9493	0.9471	0.9434	0.9382	0.9315	0.9232	0.9134
1.0	0.9489	0.9454	0.9396	0.9315	0.9209	0.9078	0.8923
1.2	0.9483	0.9434	0.9350	0.9232	0.9078	0.8888	0.8661
1.4	0.9478	0.9410	0.9296	0.9134	0.8923	0.8661	0.8348
1.6	0.9471	0.9382	0.9232	0.9019	0.8741	0.8396	0.7985
1.8	0.9463	0.9350	0.9160	0.8888	0.8533	0.8094	0.7574
2.0	0.9454	0.9315	0.9078	0.8741	0.8299	0.7756	0.7119
2.2	0.9444	0.9275	0.8988	0.8577	0.8040	0.7384	0.6625
2.4	0.9434	0.9232	0.8888	0.8396	0.7756	0.6981	0.6101
2.6	0.9422	0.9185	0.8779	0.8199	0.7448	0.6552	0.5556
$u(b)/\sigma$	0.101	0.204	0.314	0.436	0.577	0.750	0.980

Different values $b/u(b)$ and $u(b)/u$ with the same product b/u give the same values of coverage probability.

of the uncertainty intervals (see paper [10]). Curve 1 shows the coverage probabilities of the uncertainty intervals defined by expanded uncertainty U about the uncorrected results. These coverage probabilities are less than 0.95 as soon as the experimental bias differs from zero. They decrease when the parameter $b/u(b)$ increases; for the maximum insignificant $b/u(b)$ (i.e. 2) the coverage approaches a value of 0.865. The differences from the presupposed level of confidence are less than those indicated by Maroto et al. [4], nevertheless they are very disturbing.

The uncertainty intervals calculated in agreement with the GUM [2] and EURACHEM Guide [3] in case of insignificant experimental biases were studied in detail with some selected values of parameters $b/u(b)$ and $u(b)/u$ (see Table 1). The investigated range of parameters $b/u(b)$ was from 0 to 2.6 (for the two-tailed t-test and very high degrees of freedom and at $\alpha = 0.01$ the quantile $t = 2.576$). The table indicates the same findings as Part 1 that the depression of coverage probability depends on both followed parameters. When the level of $u(b)/u$ is 0.4 or higher the coverage probability can fall below 0.90 for the insignificant values of b at the usual level of significance $\alpha = 0.05$ ($b/u(b) \leq 2$). In compliance with the conclusions of Part 1 the parameter $u(b)/u$ seems to be very important in these investigated relations. It is a question how high this ratio can be in some extreme but real analytical circumstances.

The maximum value of $u(b)/u$ applied by Maroto et al. [4] is 0.42 (valid also for Figs. 1 and 2) can be regarded as a realistic maximum estimate when the trueness study is based on a certified reference material (with about five replicates in the trueness study). This parameter can be higher only because of a higher value of the uncertainty of the certified value or a higher number of the replicates in the observations of the routine samples. However, if the trueness study is based on a reference method or a standard additions method [3] then this ratio can be higher; with similar uncertainties of both methods and under the conditions of Case 1 [4] the ratio would be about 0.55 ($u(b) = \sqrt{1.5^2/5 + 1.5^2/5} = 0.95$, $u = \sqrt{0.95^2 + 1.5^2} = 1.77$, $u(b)/u = 0.95/1.77 = 0.54$). For $b/u(b) = 2$ and $u(b)/u = 0.5$ Table 1 shows that the coverage probability equals 0.83. In the real example given in paper [10] the value of $u(b)/u$ is even 0.67 because the uncertainty of the certified value is relatively much higher than it was presupposed in Case 1. These figures confirm that values of $u(b)/u$ above 0.4 are not at all exceptional.

4. Effect of the parameter $u(b)/u$ on the coverage probability

As stated above, paper [10] studies the coverage probability of the same types of uncertainty intervals as this present paper but it applies a different and simpler approach. In that paper, the coverage probability is investigated with respect to the mutual relation of only two variables: the experimental bias b and the overall standard uncertainty u (denoted by u_c there); the investigated parameter is their ratio b/u. The approach applied in this present paper studies the coverage probability changes considering parameters $b/u(b)$ and $u(b)/u$, i.e. considering three variables in mutual relations. As a matter of fact with the additional variable $u(b)$ it takes into account the magnitude proportion of the uncertainty components arising from random effects (combined uncertainty σ) and systematic effects (combined uncertainty $u(b)$), i.e. the proportion in which they contribute to the common overall combined uncertainty; $u(b)/u = \sqrt{1/(1 + \sigma^2/u^2(b))}$. When from the date obtained in the validation process the experimental bias b was computed as a sufficient estimate of δ (e.g. [8,9]) (in our case of the normal distribution a sufficient estimator of the population mean δ is the sample mean) then the quantity $u(b)/u$ can give no addition information about δ and both approaches to the coverage evaluation should give the same results. However, a simple comparison of the obtained results

is not possible since the older paper [10][1] uses the parameter b/u and this present paper works with the parameters $b/u(b)$ and $u(b)/u$ (by analogy with $\delta/u(b)$ and $u(b)/u$ in Part 1). If parameters b/u and $u(b)/u$ had been applied in this paper the agreement could have appeared immediately.

The results of both approaches can be compared by using the plots in Fig. 2 of this paper and in Fig. 1 of paper [10]. The curves in Fig. 2 showing the relationship between the coverage probabilities and $b/u(b)$ are similar to the ones in Fig. 1 [10], which shows the relationship between the coverage probabilities and b/u. For both compared approaches, the SUMU and U_e(95%) methods with the uncorrected results and the expanded uncertainty U about the corrected results give uncertainty intervals always with the expected value of coverage probability, i.e. 0.95. Neither $b/u(b)$ nor b/u influences the coverage of these types of intervals. The comparison of both approaches in case of the intervals obtained with the U(bias) method and the intervals defined with the expanded uncertainty U about the uncorrected results shows that the coverage for these types of intervals depends on b/u but does not depend on $b/u(b)$. For both given methods defying the uncertainty intervals both these approaches to the coverage probability evaluation give the same coverage when the value of b/u in the older approach equals the value of $b/u(b)u(b)/u$ in the new approach. (The applied equations are given in Appendix; the differences between the results obtained with Eqs. (5) and (10) or Eqs. (7) and (11) were in the seventh decimal places.) It means when there are two uncertainty intervals of the same type (e.g. U about uncorrected results) obtained from different values of b, $u(b)$ and u but with the same ratio b/u (i.e. with the same product $b/u(b)u(b)/u$) their coverage probabilities equal. Table 1 confirms it: e.g. $b/u(b) = 2.0$ and $u(b)/u = 0.3$ on one hand and $b/u(b) = 1.0$ and $u(b)/u = 0.6$ on the other hand give the coverage probability equal to 0.9078. It can be seen that the coverage probabilities of all types of the investigated uncertainty intervals do not depend on the value of $u(b)$ they can depend on the values of b and u.

When the coverage probability of an uncertainty interval, obtained with one of those studied methods, is assessed by using only known and knowable parameters, this coverage probability is sufficiently determined by the experimental bias b and the overall uncertainty u, or more exactly by their ratio. The experimental bias uncertainty $u(b)$ is a redundant parameter in this assessment. When involved into account it only uselessly complicates the problem solution. Nevertheless it is an important parameter, because it determines the statistical significance or insignificance of b and consequently, it determines which of those types of uncertainty intervals is applied by the analyst. In this way – indirectly – it affects the coverage probability of the obtained uncertainty interval. (It also means that the complicated numerical computations of MCP under general Eq. (2) have turned out to be practically unnecessary. It only served to prove that the coverage probability computations taking into account all possible values of δ estimated with given values of b and $u(b)$ led to the same results as the computations taking into account only the point estimate of δ with the given value of b).

[1] Paper [10] studies possibilities to replace the result correction in case of significant experimental biases by a modification or an enlargement of the uncertainty intervals, i.e. it investigates the coverage probability of uncertainty intervals because of a different aim than this paper.

Table 2
The coverage probability of the uncertainty intervals defined by $1.96u$ about the uncorrected results depends only on parameter b/u (first two columns)

b/u	Coverage probability	$u(b)/u$ at α (t-quantile)		
		0.10 (1.64)	0.05 (1.96)	0.01 (2.58)
0.4	0.931	0.243	0.204	0.155
0.5	0.921	0.304	0.255	0.194
0.6	0.908	0.365	0.306	0.233
0.7	0.892	0.426	0.357	0.272
0.8	0.874	0.486	0.408	0.311
0.9	0.853	0.547	0.459	0.349
1.0	0.830	0.608	0.510	0.388
1.1	0.804	0.669	0.561	0.427
1.2	0.776	0.730	0.612	0.466
1.3	0.745	0.790	0.663	0.505
1.4	0.712	0.851	0.714	0.544
1.5	0.677	0.912	0.765	0.582

The last three columns give the critical values of $u(b)/u$, which decide on the experimental bias significance for a given value of b/u and at a given level of significance α (second line). When for a measurement procedure the value of $u(b)/u$ is higher than the critical value, the bias is found insignificant. Then all results determined by this procedure are not corrected and the coverage probability of the obtained uncertainty intervals falls to the value determined by the parameter b/u (b: experimental bias; $u(b)$: its uncertainty; u: overall uncertainty).

When an analyst has determined values of b, $u(b)$ and u for an applied analytical method, he tests the obtained experimental bias significance by the t-test. If the ratio $b/u(b)$ is lower than the t quantile corresponding to the chosen level of confidence α and the given degrees of freedom the tested b is insignificant. Then in compliance with the EURACHEM Guide [3] the analyst will compute the uncertainty intervals defined by U about the uncorrected results obtained with that analytical method for routine samples. The coverage probability of these uncertainty intervals depends on the ratio b/u and it can be found in Table 2.

This table also expresses the indirect effect of the ratio $u(b)/u$ on the coverage probability (in Part 1 this effect is shown as evident). The table gives the minimum possible values of $u(b)/u$, which can make a found experimental bias b insignificant at a given level of significance. They are determined by using this inequality

$$\frac{u(b)}{u} \geq \frac{b}{u}\frac{1}{t} \tag{3}$$

which can be obtained by a modification of the t-test. Suppose the ratios b/u and $u(b)/u$ are known for an analytical method. The given value of b/u in the first column and the proper level of significance for the t-test in the second line determine the critical value of $u(b)/u$. If the given ratio $u(b)/u$ for the analytical method is higher than this critical value or equals it, the determined bias is insignificant. The coverage probability of the uncertainty intervals defined by U about the uncorrected results is given in the second column. For example, if b/u equals 1.1 and the chosen level of significance is 0.05, the bias will be found insignificant provided $u(b)/u$ is higher than or equals 0.561. In this case,

the coverage probability of the uncertainty intervals defined by expanded uncertainty U about the uncorrected results will just fall to 0.804. When an elevated significance level is applied in the t-test, e.g. $\alpha = 0.1$, the experimental bias with $b/u = 1.1$ will not be found insignificant unless the parameter $u(b)/u$ reaches or oversteps a level of 0.669. This value of $u(b)/u$ seems to be very extreme and the cases with such large values of this parameter will not be too frequent (see above). When the ratio $u(b)/u$ determined for the analytical method is smaller than the critical value from Table 2, the determined bias is significant and the analyst will correct his results for systematic error. Then the coverage probability of the computed uncertainty intervals defined by U about the corrected results will equal 0.95.

5. How to proceed when a high but nevertheless insignificant bias has occurred

It is evident that the coverage probability of the uncertainty intervals computed with the studied method depends on the chosen level of confidence and on the method of the computation. The previous investigations confirm that the coverage probability for some types of the intervals can also depend on the parameter b/u. This parameter especially affects the coverage probability of the intervals defined by U about uncorrected result. When values of b/u are high the coverage of these intervals will considerably fall below the chosen level of confidence. Papers [4] and [6] and Part 1 also report the parameter $u(b)/u$ to influence the coverage probability. However, from the viewpoint presented here, the parameter $u(b)/u$ does not influence the coverage probability for a given type of uncertainty interval. It only determines which type of uncertainty interval should be computed and then at a given value of b/u the coverage probability is unambiguously defined. A high value of $u(b)/u$ causes that the experimental bias b, which is high with respect to u, will not be found significant in the t-test. Then in compliance with the EURACHEM Guide [3] the analyst does not correct the measured results for the systematic error and computes the uncertainty intervals defined with U about the uncorrected results, i.e. those intervals with the especially low coverage probability at the high value of b/u. There are also other options what to do with such extraordinary values of $u(b)/u$ and b/u. The analyst can decide not to follow the EURACHEM Guide direction and to correct the results with this insignificant experimental bias. In this way he obtains the uncertainty intervals defined by U about the corrected results, which have the coverage probability equalling the chosen level of confidence. Another alternative is not to correct the result and to compute some type of the uncertainty interval modified with the bias; these intervals have also satisfied coverage probabilities. There is a question now, when such a high but nevertheless insignificant experimental bias has occurred how to optimally define a suitable type of uncertainty interval.

One solution can be to raise the significance level at the t-test, e.g. to $\alpha = 0.1$. This precaution was proposed by O'Donnell and Hibbert [5]. The t-test with a higher level of significance will reveal some highest experimental biases as significant, though they would have been insignificant at the usual level of significance, and consequently these biases will be applied in the correction for systematic error. (I think that it is not necessary to require the same significance level for the t-test and for the uncertainty interval.) With $\alpha = 0.1$ the coverage probability for example cannot fall below 0.89, 0.85 and 0.80 unless the parameter $u(b)/u$ exceeds 0.43, 0.55 and 0.67, respectively (see Table 2). Of course, on the other hand when at this higher level of significance an experimental bias is significant with respect to its own uncertainty but negligible with respect to the overall uncertainty, the correction may be ignored. However, it is true that this elevation of significance level cannot eliminate the depression of coverage probability when the parameter $u(b)/u$ is extremely high (see, e.g. the above mentioned example from paper [10] with $u(b)/u = 0.67$).

A more reliable way would be to correct the results by all the experimental biases, which are too high with respect to the overall uncertainty, regardless of their significance or insignificance according to the t-test. It seems that the bias significance can be evaluated from two points of view. On one hand it can be proved by the t-test that an experimental bias differs significantly from zero with respect to its uncertainty. Consequently, the systematic error estimated by the experimental bias is proved at a given significance level, so it is sensible to correct each result by this bias for it. On the other hand the usual omission of the correction with an insignificant experimental bias, which is at the same time too high with respect to the overall uncertainty, causes a significant depression of the coverage probability of the uncertainty intervals defined by U (see Table 2). This depression of coverage probability can also be a reason for the correction of the results with the given experimental bias. In Part 1, it has already been stated that the GUM allows to interpret significance in this way since it asks to correct all systematic effects significant in size relatively to the required accuracy of a measurement [2]. From this point of view when the uncertainty intervals defined by U are applied, this rule could be recommended: provided that the ratio b/u is too high so that the coverage probability of these intervals about the uncorrected results would fall below, e.g. 90 or 85 or even 80% (see Table 2; this value would have to be nailed down) the results shall be corrected with this value of b regardless of its contingent insignificance under the t-test.

However, an analyst can assume this correction of each measured result with such an insignificant experimental bias to be unreasonable, since this bias disappears in the uncertainty of its own determination and therefore its value is not trustworthy. Then it is possible to include this bias in the uncertainty interval with one of the studied method as Maroto et al. [4,6] suggested, either with the SUMU or U_e(95%) or maybe with the U(bias) method (the last method gives redundantly wide intervals with a higher coverage probability). However, this third solution has also its own weak point. When the U_e(95%) or U(bias) method would be used this solution can cause this paradox: The results have been obtained by two different analytical methods, both with the same values of their overall uncertainty but one with an insignificant bias and the second one with a significant bias. The first and the better method, since without any proved systematic error, would give results with a higher uncertainty (U(bias) or U_e(95%)), while the worse method, since with a proved and

therefore corrected systematic error, would give results with a lower uncertainty (U).

6. Conclusion

Part 2 studies the effect of experimental bias on coverage probability in the same way as Part 1, i.e. by using the method of probability calculus. In compliance with the origin papers by Maroto et al. [4,6] it takes into account only the insignificant experimental biases but it looks at the problem from a different angle of view. The coverage probability is computed for a given found insignificant experimental bias that estimates the systematic error (true bias) of an applied analytical method. The obtained results let the analyst make a decision according to his really measured experimental bias.

The coverage probabilities of the uncertainty intervals computed strictly according to the EURACHEM Guide [3] considerably fall below the chosen level of confidence (0.95) provided that the experimental bias is high with regard to the overall uncertainty but nevertheless insignificant with respect to its own uncertainty. The coverage probability depression is a consequence of the fact that the results are not corrected with such large bias. It is proved that this reduction directly depends only on the ratio of the bias and the overall uncertainty. The bias uncertainty affects the coverage probability only indirectly. It determines whether the large bias is found significant or insignificant and thereby determines whether the uncertainty intervals will be defined by U about corrected results (intervals without any reduction of coverage) or about uncorrected result (intervals with the reduction of coverage). When contrary to the EURACHEM Guide the obtained results are corrected with the large but insignificant bias, the uncertainty intervals defined by U have the right coverage probability (0.95).

The coverage probability reduction could be moderated by application of a higher level of significance at the t-test, because then the insignificant biases could not be so high. It could be completely remove by the correction with all biases that are high with respect to the overall uncertainty, regardless of their significance or insignificance according to the t-test. The third way how to solve this problem is to compute the uncertainty intervals modified with those high but insignificant biases (e.g. by using the SUMU, U_e(95%) or U(bias) methods). None of these three suggested solutions is ideal.

At the end of this work, it is necessary to stress that its conclusions for the values of $b/u(b)$, b/u and $u(b)/u$ do not mean that the experimental bias, its uncertainty or perhaps the overall uncertainty should be increased in order that a higher coverage probability of uncertainty interval could result. Of course, the applied analytical method should have the highest possible trueness and precision under given conditions.

Appendix A

The equations to compute the mean coverage probabilities can be derived by the particular expressions of the term ICP(b, u, σ, α, δ) in Eq. (2). The general expression of ICP is

$$\mathrm{ICP} = \Phi\left(\frac{-\delta + U_-}{\sigma}\right) - \Phi\left(\frac{-\delta - U_+}{\sigma}\right) \tag{4}$$

where Φ denotes the cumulative distribution function of the normal distribution and terms U_- and U_+ generally denote the left and right sides of all studied types of uncertainty intervals (they can be replaced by their particular expressions given in Part 1). For the investigated cases these integrals can be obtained

(1) U about uncorrected results—substituted from Eq. (3) in Part 1:

$$\mathrm{MCP} = \int_{-\infty}^{\infty}\left[\Phi\left(\frac{-\delta + 1.96u}{\sigma}\right) - \Phi\left(\frac{-\delta - 1.96u}{\sigma}\right)\right] \times L(b, u(b), \delta)\,\mathrm{d}\delta \tag{5}$$

(2) SUMU about uncorrected results and also U about corrected results—substituted from Eq. (9) in Part 1:

$$\mathrm{MCP} = \int_{-\infty}^{\infty}\left[\Phi\left(\frac{-\delta + 1.96u + b}{\sigma}\right) - \Phi\left(\frac{-\delta - 1.96u + b}{\sigma}\right)\right] L(b, u(b), \delta)\,\mathrm{d}\delta \tag{6}$$

(3) U(bias) about uncorrected results—substituted from Eq. (7) in Part 1:

$$\mathrm{MCP} = \int_{-\infty}^{\infty}\left[\Phi\left(\frac{-\delta + 1.96u + |b|}{\sigma}\right) - \Phi\left(\frac{-\delta - 1.96u - |b|}{\sigma}\right)\right] L(b, u(b), \delta)\,\mathrm{d}\delta \tag{7}$$

(4) U_e(95%) about uncorrected results—substituted from Eq. (16) in Part 1:

$$\mathrm{MCP} = \int_{-\infty}^{\infty}\left[\Phi\left(\frac{-\delta + 1.96u + E|b|}{\sigma}\right) - \Phi\left(\frac{-\delta - 1.96u - E|b|}{\sigma}\right)\right] L(b, u(b), \delta)\,\mathrm{d}\delta \tag{8}$$

The applied value of the coverage factor (1.96) means that the level of confidence for the uncertainty intervals is 0.95. The term $L(b, u(b), \delta)$ in these equations has to be replaced by

$$\frac{1}{\sqrt{2\pi u^2(b)}}\exp\left(-\frac{(b-\delta)^2}{2u^2(b)}\right) \tag{9}$$

This function expresses the probability density of a normally distributed experimental biases. Here, it is a function of the unknown statistical parameter δ (mean of the distribution of all possible values b) while the given known experimental bias b (a value randomly taken from that distribution) is a fixed quantity during the computation. Such function is called the likelihood function [7–9]. In the function which is called the probability density function, the mean of the distribution (statistical parameter) is an invariable and the random quantity is the variable,

for which this function determines the probability density. Such function was applied in Part 1.

The solutions of the integrals given above were sought numerically by using the trapezoid rule on PC with program Microsoft Excel.

The alternative equations to compute the coverage probabilities, CP, which take into account only the parameter b/u, were derived in paper [10]. The equations applied in this paper are

U about the uncorrected results :

$$\mathrm{CP} = \Phi\left(\frac{b}{u} + 1.96\right) - \Phi\left(\frac{b}{u} - 1.96\right) \tag{10}$$

$$U(\text{bias}): \qquad \mathrm{CP} = \Phi\left(2\frac{b}{u} + 1.96\right) - \Phi(-1.96) \tag{11}$$

References

[1] V. Synek, Talanta (2006) in press.
[2] ISO, Guide to the Expression of Uncertainty in Measurement, International Organisation for Standardisation, Geneva, 1993.
[3] L.R. Ellison, M. Rősslein, A. Williams (Eds.), EURACHEM/CITAC Guide, Quantifying Uncertainty in Analytical Measurement, second ed., 2000.
[4] A. Maroto, R. Boqué, J. Riu, F.X. Rius, Accred. Qual. Assur. 7 (2002) 90.
[5] G.E. O'Donnell, D.B. Hibbert, Analyst 130 (2005) 721.
[6] A. Maroto, R. Boqué, J. Riu, F.X. Rius, Analyst 128 (2003) 373.
[7] Wikipedia, the free encyclopedia, http://en.wikipedia.org/wiki/Likelihood_function, modified June 12, 2005.
[8] C. Clapham, The Concise Oxford Dictionary of Mathematics, second ed., Oxford University Press, Oxford, 1996, p. 159.
[9] J. Anděl, Matematická Statistika, SNTL, Praha, 1978, p. 267.
[10] V. Synek, Talanta 65 (2005) 829.

Available online at www.sciencedirect.com
ScienceDirect
Talanta 71 (2007) 1198–1204
Talanta
www.elsevier.com/locate/talanta

Enzymatic oxidation of *tert*-butylcatechol in the presence of sulfhydryl compounds: Application to the amperometric detection of penicillamine

Angel A.J. Torriero [a,*], Hugo D. Piola [a], Noelia A. Martínez [a], Nancy V. Panini [a], Julio Raba [a], Juana J. Silber [b]

[a] *Departamento de Química, Facultad de Química, Bioquímica y Farmacia, Universidad Nacional de San Luis, Chacabuco y Pedernera 5700, San Luis, Argentina*
[b] *Departamento de Química, Universidad Nacional de Río Cuarto Agencia postal No 3, 5800 Río Cuarto, Córdoba, Argentina*

Received 16 March 2006; received in revised form 6 June 2006; accepted 9 June 2006
Available online 25 July 2006

Abstract

The high sensitivity that can be attained using an enzymatic system and mediated by 4-*tert*-butylcatechol (4-TBC) has been verified by on-line interfacing of a rotating biosensor and continuous flow/stopped-flow/continuous-flow processing. Horseradish peroxidase, HRP, [EC 1.11.1.7], immobilized on a rotating disk, in presence of hydrogen peroxide catalyzed the oxidation of 4-TBC, whose back electrochemical reduction was detected on glassy carbon electrode surface at −150 mV. Thus, when penicillamine (PA) was added to the solution, these thiol-containing compounds participate in Michael type addition reactions with 4-TBC to form the corresponding thioquinone derivatives, decreasing the peak current obtained proportionally to the increase of its concentration. The highest response for PA was obtained around pH 7. This method could be used to determine PA concentration in the range 0.02–80 μM ($r = 0.998$). The determination of PA was possible with a limit of detection of 7 nM, in the processing of as many as 50 samples per hour. The HRP-rotating biosensor was successfully applied to the determination of PA in pharmaceutical formulations.
© 2006 Elsevier B.V. All rights reserved.

Keywords: Penicillamine; Glassy carbon; Biosensor; Horseradish peroxidase; 4-*tert*-Butylcatechol

1. Introduction

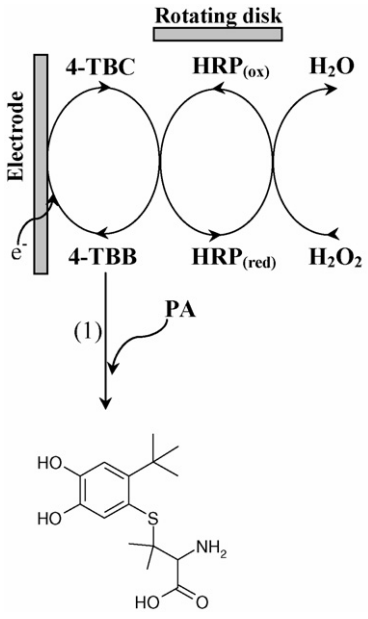
Penicillamine (2-amino-3-mercapto-3-methylbutanoic acid) (PA) is an unphysiological sulfur-containing amino acid that belongs to the aminothiols family. This compound is derived from hydrolytic degradation of penicillin [1,2] but it does not have antibiotic activity. It exists in D- and L-enantiomeric forms that show different biological and toxicological properties. D-PA (*S*-isomer) is a highly potent therapeutic agent used for many years in the treatment of various illnesses. It is the drug of first choice for patients with Wilson's disease [3], an autosomal recessive disorder of copper transport [4]. It is able to enhance the urinary excretion of others heavy metals such as lead, arsenic, mercury and zinc and therefore, is used as an oral chelating agent to treat conventional heavy metals intoxication [5]. It is also used as antifibrotic agent to treat scleroderma [6] and as antirheumatic drug to treat patients with active rheumatoid arthritis [7]. D-PA reduces excess of cystine excretion in cystinuria, another rare inherited disease affecting the active transport of the diamino acids cystine, ornithine, lysine and arginine across the renal tubule and the small intestine [8]. Mechanisms of action of D-PA in mentioned diseases are various. It is a reductive chelating agent [9], it appears to inhibit collagen deposition by interfering with the intramolecular cross-linking of mature collagen [10], it has immunomodulatory-anti-inflammatory properties [11–13] and it is able to make dimers through disulfide interchange or direct reaction with other physiological thiols [14]. For example, in cystinuria, D-PA-cysteine disulfide formation, which is a dimer more soluble than cystine, prevents the clinical manifestation of the pathology [14]. This suggests that it may also represent a potential drug for the hyperhomocyst(e)inemia and hypercyst(e)inemia treatment, two independent risk factors for atherosclerosis and cardiovascular disease [15,16].

* Corresponding author. Tel.: +54 2652 42 5385; fax: +54 2652 43 0224.
E-mail address: torriero@unsl.edu.ar (A.A.J. Torriero).

0039-9140/$ – see front matter © 2006 Elsevier B.V. All rights reserved.
doi:10.1016/j.talanta.2006.06.027

Several methods have been proposed for the determination of D-penicillamine including high performance liquid chromatography with pre or post column derivatization [17–19], calorimetry [20], fluorometry [21,22], spectrophotometric [23–25], chemiluminescene [26], capillary electrophoresis [27,28] and NMR spectrometry [29]. One of the important limitations of LC techniques is the fact that this thiol lacks sufficient UV absorption so a pre or post-column derivatization procedure is normally required [26]. Electrochemical methods are an alternative for the D-penicillamine determination because they are cheap, simple, fast and sensitive. Mercury and mercury amalgam [30,31] have been extensively used for thiol-compound determination, however, mercury has limitations due to its toxicity and the rapid deterioration of the electrode response [32]. A chemically modified electrode [33] has been also used to determine D-penicillamine but its use in flow injection analysis is limited because it needs particular mechanical and chemical stability towards the flowing solution. Recently, the boron-doped diamond thin film (BDD) electrode has emerged as a unique electrode material for several electrochemical applications, especially in electroanalysis [34].

To the best of our knowledge, no study with enzymatic biosensor behavior for PA has been reported. Thus, in this paper, we present and discuss for the first time the electrochemical and enzymatic reaction for PA determination, resulting in a single, fast and inexpensive analytical method as well as very sensitive devise based on HRP-rotating biosensor systems. The measuring principle of this biosensor for the detection of PA is shown in Scheme 1. Horseradish peroxidase (HRP) in the presence of H_2O_2 catalyses the oxidation of 4-*tert*-butylcatechol (4-TBC) [35] whose electrochemical reduction back was obtained at peak potential of −150 mV. Nevertheless, when thiol-containing compound is added to the solution, readily undergo reaction with quinone derivative (4-*tert*-butylbenzoquinone, 4-TBB), through the Michael type addition, decreasing the peak current obtained proportionally to the increase of thiol-containing compound concentration.



Scheme 1.

The initial reaction in the sequence (4-TBC⇆4-TBB) is well established [36–38] with NMR, pulse radiolysis and a number of electrochemical techniques used to probe the mechanism. A substantial body of research has also been compiled which documents the possible physiological consequences of such reactions [39–41]. The potential analytical utility offered by the second step (1) as a method of detecting PA is explored in this paper.

2. Experimental

2.1. Reagents and solutions

All reagents used, were of analytical reagent grade. The enzyme horseradish peroxidase, HRP, [EC 1.11.1.7] Grade II, were purchased from Sigma Chemical Co., St. Louis. The concentration of HRP was determined spectrophotometrically using the Soret extinction coefficient of 102 $mM^{-1}\,cm^{-1}$ at 403 nm (181 IU mg^{-1}). Glutaraldehyde (25% aqueous solution) and hydrogen peroxide were purchased from Merck, Darmstadt. 3-Aminopropyl-modified controlled-pore glass, 1400 Å mean pore diameter and 24 $m^2\,mg^{-1}$ surface area, was from Electro-Nucleonics (Fairfield, NJ) and contained 48.2 $\mu mol\,g^{-1}$ of amino groups. 4-*tert*-butylcatechol and penicillamine were purchased from Sigma Chemical Co., St. Louis. 4-*tert*-butylcatechol (0.1 M) and penicillamine (0.01 M) were prepared through the dissolution of the appropriate salt in deionized water and generally used within 1 h. All other reagents employed were of analytical grade and used without further purifications. All solutions were prepared with ultra-high-quality water obtained from a Barnstead Easy pure RF compact ultra pure water system, and the samples were diluted to the desired concentrations using a 10 ml Metrohm E 485 burette.

2.2. Flow-through sensor/detector unit

The main bodies of the amperometric-rotating bioreactor were made of Plexiglas. The design of the flow-through chamber containing the rotating enzyme biosensor and the detector system was described previously [42]. Briefly, glassy carbon electrode (GCE) is on the top of the rotating biosensor. The rotating biosensor is a disk of Teflon in which a miniature magnetic stirring bar (Teflon-coated Micro Stir bar from Markson Science, Inc. Phoenix, AZ) has been embedded. Typically, a sensor disk carried 1.4 mg of controlled-pore glass on its surface. Rotation of the lower sensor was effected with a laboratory magnetic stirrer (Metrohm E649 from Metrohm AG Herisau, Switzerland) and controlled with a variable transformer with an output between 0 and 250 V and maximum amperage of 7.5 A (Waritrans, Argentina.). Amperometric detection was performed using a BAS LC-4C potentiostat and BAS 100 B/W (electrochemical analyzer Bioanalytical System, West Lafayette IN) was used to voltammetric determinations. The potential applied to the GCE for the functional group detection was −150 mV versus Ag/AgCl/3.0 M NaCl reference electrode BAS RE-6, and a

Pt wire counter electrode. At this potential, a catalytic current was well established.

A pump (Gilson Minipuls 3 peristaltic pump, Gilson Electronics, Inc. Middleton, WI) was used for pumping, sample introduction, and stopping of the flow. The pump tubing was Tygon (Fisher AccuRated, 1.0 mm i.d., Fisher Scientific Co., Pittsburgh, PA) and the remaining tubing used was Teflon, 1.00 mm i.d. from Cole–Parmer (Chicago, IL).

All pH measurements were made with an Orion Expandable Ion Analyzer (Orion Research Inc., Cambridge, MA) Model EA 940 equipped with a glass combination electrode (Orion Research Inc.).

2.3. Horseradish peroxidase immobilization

The rotating disk biosensor (bottom part) was prepared by immobilizing HRP on 3-aminopropyl-modified controlled-pore glass (APCPG). The APCPG, smoothly spread on one side of a double-coated tape affixed to the disk surface, and was allowed to react with an aqueous solution of 5% w/w glutaraldehyde at pH 10.00 (0.20 M carbonate) for 2 h at room temperature. After washing with purified water and 0.10 M phosphate buffer of pH 7.00, the enzyme (10.0 mg of enzyme preparation in 0.50 ml of 0.10 M phosphate buffer, pH 7.00) was coupled to the residual aldehyde groups in phosphate buffer (0.10 M, pH 7.00) overnight at 5 °C. The immobilized enzyme preparation was finally washed with phosphate buffer (pH 7.00) and stored in the same buffer at 5 °C between uses. The immobilized HRP preparations were perfectly stable for at least one months of daily use.

2.4. Sample preparation for HRP-rotationg biosensor assay

A mass of powder of one capsule of penicillamine (Cuprimine 250 mg, Sidus Lab.; Cupripen 250 mg, Interpharm Lab.) was transferred to 100 ml volumetric flask and dissolved in 0.1 M phosphate buffer (pH 7). The flask was sonicated for 2 min and filled with 0.1 M phosphate buffer, pH 7.0. A small amount of non-dissolving excipients settled at the bottom of the flask. Then, suitable aliquots of the supernadant was further diluted with 0.1 M phosphate buffer (pH 7) to obtain a final concentration of 2.5 μM.

2.5. Preparation of synthetic capsule samples

Synthetic capsule samples were prepared in 100 ml calibrated flasks by spiking a placebo (mixture of capsule excipients) with accurately calculated amount of PA. Hereafter, the procedure described for the sample preparation was followed.

3. Results and discussion

3.1. Electrooxidation of 4-tert-butylcatechol in the absence and presence of PA

Cyclic voltammetry of a 1 mM solution of 4-*tert*-butylcatechol (4-TBC) in an aqueous solution containing 0.10 M phosphate buffer pH 7.0 as supporting electrolyte, shows one anodic (A_1) and a corresponding cathodic peak (C_1) which corresponds to the transformation of 4-TBC to *o*-benzoquinone and vice-versa within a quasi-reversible two-electron process (Fig. 1, curve a). A peak current ratio (Ip^{C_1}/Ip^{A_1}) of nearly unity, particularly during the repetitive recycling of potential, can be considered as a criterion for the stability of *o*-quinone produced at the surface of the electrode under the experimental conditions. In other words, any hydroxylation [43–46] or dimerization [47,48] reactions are too slow to be observed on the time scale of cyclic voltammetry. The oxidation of 4-TBC in the presence of PA as a nucleophile was also studied. Fig. 1, curve b, shows the cyclic voltammogram obtained for a 1 mM solution of 4-TBC in the presence of 2.5 mM PA. The voltammogram exhibits an anodic peak at 220 mV versus Ag/AgCl/3M NaCl, and the cathodic counterpart of the anodic peak A_1 has disappeared.

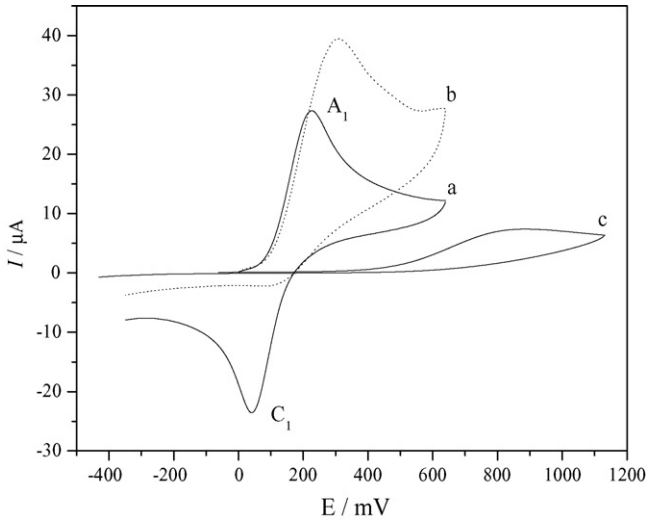


Fig. 1. Cyclic voltammograms of 1 mM 4-TBC: (a) in the absence; (b) in the presence of 2.5 mM PA; (c) 1 mM PA in the absence of 4-TBC, at glassy carbon electrode (3 mm diameter) in aqueous solution containing 0.1 M phosphate buffer (pH 7.00). Scan rate: 100 mV s^{-1}; *T*: 25 ± 1 °C.

The influence of increasing PA concentration on the electrochemical behavior of 4-TBC was investigated and the responses recorded are shown in Fig. 2. The height of the oxidation peak was found to increase with increasing additions of PA with the loss of the corresponding reduction peak consistent with the ECE type mechanism proposed in Schemes 1 and 2. The increase in the oxidation peak height is attributed to the oxidation of 4-TBC–PA adducts that have arisen through the electrochemically initiated reaction previously detailed in Scheme 1. The successive decrease in the height of the 4-TBC reduction peak can be ascribed to the fact that increasing concentration of PA serve to scavenge the oxidized form of 4-TBC such that on the reverse sweep there is little available for electro-reduction.

Given that the direct oxidation of this thiol at the electrode does not occur within the potential window studied (Fig. 1, curve c), the increase in the magnitude of the 4-TBC oxidation peak can be attributed solely to the re-oxidation of the 4-TBC–PA adduct.

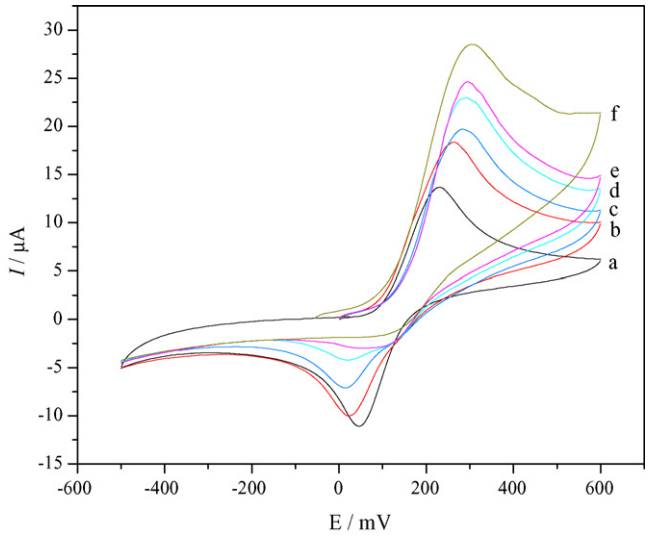


Fig. 2. Typical voltammograms of 0.5 mM 4-TBC at a glassy carbon electrode (3 mm diameter) in aqueous solution containing 0.1 M phosphate buffer (pH 7.00) at various PA concentrations, C_{PA}: (a) 0.0; (b) 0.09; (c) 0.17; (d) 0.29; (e) 0.37; (f) 0.67 mM. Scan rate: 100 mV s^{-1}, T: 25 ± 1 °C.

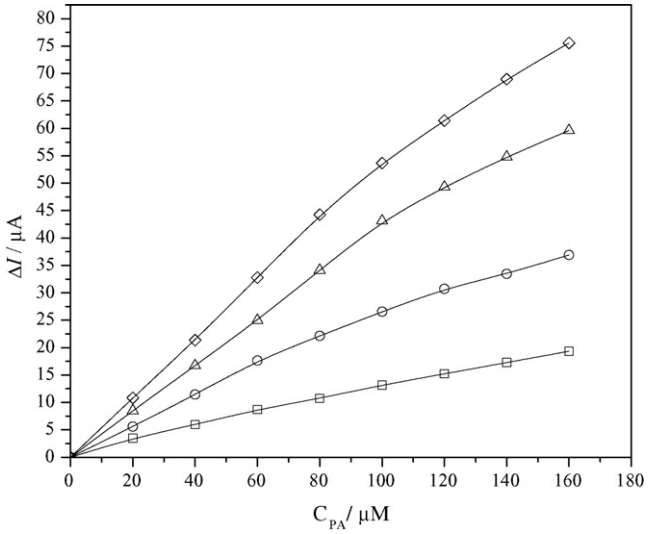
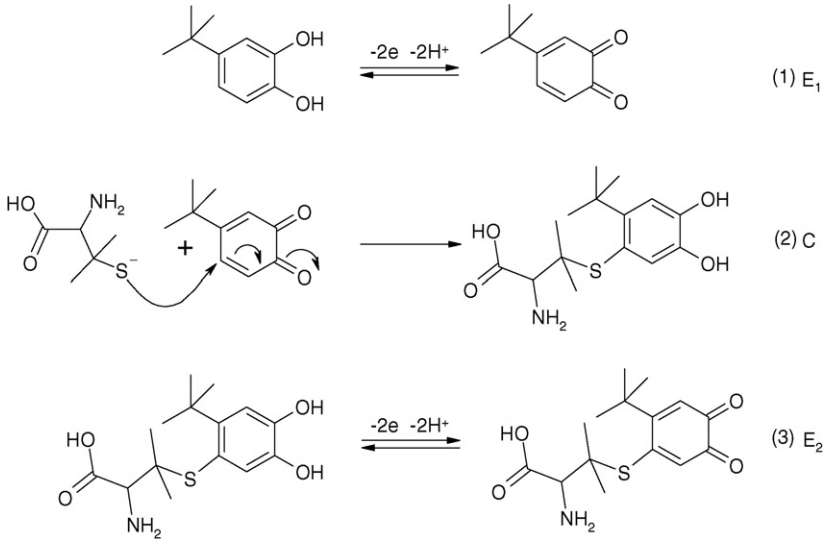


Fig. 3. Influence of pH on the magnitude of the oxidation signal for 1.00 mM 4-TBC in the presence of several penicillamine concentrations, using phosphate buffer (□) pH 4, (◯) pH 5, (△) pH 6 and (◊) pH 7.

3.2. *Effect of pH and H_2O_2 concentration*

The influence of pH on peak potential (Ep) of the reaction was assessed through examining the electrode response to 4-TBC–PA obtained in solutions buffered between pH 4 and pH 8. The position of the redox couple was found to be dependent upon pH with a shift of 61 mV pH^{-1} indicative of an n electron n proton behavior with n likely to be two [49]. A quantitative evaluation of the 4-TBC change peak current (ΔI) response to increasing additions of PA as a function of solution pH is highlighted in Fig. 3. The ΔI reported hereafter is the difference between the reduction current (from addition of 4-TBC) and the current due to the addition of PA (from addition of 4-TBC + PA). The response was found to decrease steadily as the acidity of the solution is increased. This can be attributed to the fact that as the solution pH is lowered, the thiol functionality will be increasingly protonated (PA RSH, pK_a ~7.9) and hence the nucleophilic character of the thiol moiety diminished. Increasing the pH clearly improves the response but an operational limit is reached once neutral conditions prevail. Alkaline solution severely compromises the enzyme stability as well as the response as the increased presence of nucleophilic hydroxyl ions compete with the less prevalent thiol. Therefore, the pH value used was 7.00 in 0.1 M phosphate buffer in concordance with the steadier pH of the enzyme.

The effect of H_2O_2 concentration may be observed easily varying H_2O_2 concentration from 2.5×10^{-5} to 5.0×10^{-3} M, for 20 µM 4-TBC solutions and several concentrations of HRP, whilst maintaining a constant 4-TBC concentration [42]. At low H_2O_2 concentration, 0.025 mM, a lineal relation can only be seen when the enzymes concentrations are low, losing this lin-



Scheme 2.

earity as the enzymatic concentration increases. This change occurs because the H_2O_2 concentration is insufficient to generate maximum catalytic activity. With 0.1 mM H_2O_2 concentration, a perfect linearity within the concentration range studied is obtained. With 0.5 mM H_2O_2 concentration, the linearity is lost to low concentrations. This is due to the fact the HRP is inactivated in excess of H_2O_2. At higher H_2O_2 concentration, such as 5 mM, inhibition by conversion of the initial enzyme by H_2O_2 into E_3 is observed throughout the entire HRP concentration range studied. In this case linearity is observed but the catalytic current obtained is less significant than in the optimal case.

3.3. Effect of biosensor rotation and continuous-flow/stopped-flow operation

The implementation of continuous-flow/stopped-flow programming and the location of two facing independent biosensors [42], permits: (a) utilization of relatively low enzyme loading conditions (b) instantaneous operation under high initial rate conditions, (c) easy detection of accumulated products, and (d) reduction of apparent Michaelis-Menten constant, K'_M. A more complete reagent homogenization is achieved, because the cell works as a mixing chamber by facilitating the arrival of substrate at the active sites and the release of products from the same sites. The net result is high values of current (Fig. 4). The main advantages of this system are its simplicity, and the ease with which it can be applied to the determination of PA at low levels.

As observed earlier [50], if the sensor in the cell is devoid of rotation, there is practically no response. If a rotation of 900 rpm is imposed on the sensor located at the bottom of the cell (with immobilized HRP), the signal is dramatically enlarged. The trend indicates that, up to velocities of about 900 rpm, a decrease in the thickness of the stagnant layer improves mass transfer to and from the immobilized enzyme active sites. Beyond 900 rpm, the current is constant, and chemical kinetics controls the overall process. Therefore, a rotation velocity of 900 rpm was used.

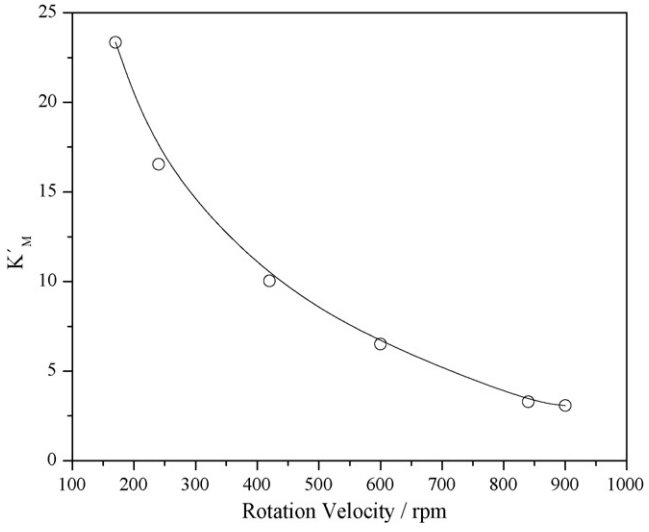


Fig. 4. The K'_M values for the system obtained at six different rotation velocities and stopping the flow for 1 min during measurement. The K'_M values were determined as discussed in the text; T: 20 ± 1 °C.

Table 1
Effect of sample size[a]

Sample size (μl)	I (μA)	Linear regression, standard deviation
50	5.82	±0.26
75	27.99	±0.19
100	50.92	±0.11
125	68.60	±0.26
150	72.35	±0.14
175	72.43	±0.29
200	72.60	±0.36

Solution containing 0.1 mM H_2O_2, 1.0 mM 4-TBC in 0.1 M phosphate buffer, pH 7.00. Flow rate, 1.00 ml min^{-1}.

[a] The current was measured under stopped-flow conditions. Each value of current is based on triplicate of six determinations.

Table 2
Intra- and Inter-day precision and accuracy ($n = 5$)

	Intra-day			Inter-day		
$C_{nominal}$ (μM)	0.60	5.20	21.80	0.60	5.20	21.80
Mean C_{found} (μM)	0.62	5.19	21.82	0.59	5.17	21.78
C.V. (%)	1.35	0.77	0.97	0.45	0.84	1.21
Bias (%)	3.22	0.19	0.10	1.70	0.60	0.10

Table 3
Specificity results of the HRP-rotating biosensor[a]

Sample no.	Pure sample 2.50 (μM)	Synthetic capsule sample ($n = 5$) X (μM)
1	2.51	2.51
2	2.48	2.48
3	2.51	2.50
4	2.49	2.48
5	2.52	2.51
6	2.48	2.48
X	$2.49 \pm 7 \times 10^{-3}$	$2.49 \pm 6 \times 10^{-3}$
S.D.	0.02	0.01
C.V. (%)	0.80	0.41

[a] X (μg ml^{-1}), mean ± S.E., standard error; S.D., standard deviation; C.V., variation coefficient.

Table 4
Determination by the developed method of amount of PA contained in commercial formulations

Sample No	Cuprimine (Sidus Lab.) (g/capsule)	Cupripen (Interpharm Lab.) (g/capsule)
1	250.10	249.91
2	249.95	249.87
3	250.05	250.10
4	249.90	250.15
5	249.87	249.89
6	249.98	250.04
7	250.12	249.94
8	250.09	250.08
X	250.01	249.98
S.D.	0.09	0.11

Table 5
A comparison of previous methods for determining penicillamine

Detection method	Matrix	Response time (min)	Linear range (μM)	Detection limit (μM)	Ref.
Square-wave voltammetry	Pharmaceutical preparations	<1	0.10–2.5	0.08	[51]
Capillary electrophoresis	Plasma	10	0.1–48	2×10^{-4}	[28]
Differential pulse voltammetry	Pharmaceutical preparations	<1	0.4–500	0.1	[52]
Spectrophotometry	Pharmaceutical preparations	<1	37.5–402	6.7	[53]
Amperometric	Pharmaceutical preparations	<1	0.5–50	0.01	[54]
Spectrophotometric	Pharmaceutical preparations	1.15	25–300	–	[23]
Amperometric	Pharmaceutical preparations	1	0.02–80	7×10^{-3}	Proposed method

3.4. Effect of cell volume and sample size

Depending on the volume of the cell in contact with the sensors, the overall process becomes controlled by diffusion (large volumes) or by the chemical kinetics of the enzyme-catalyzed reactions (small volumes). The cell volume was changed from 150 μl to 1 ml by removing the O-rings between the upper and lower half of the cell. The measured current, as expected, decreased linearly with an increase in cell volume, due to the dilution effect favored by rotation, and the fact that the measured current is directly proportional to bulk concentration. The smallest cell volume of 150 μl was adopted for further studies.

The measured current increased lineally with sample size up to 150 μl in a cell with a volume of 150 μl. For convenience a sample size of 150 μl was used. Sensitivity is almost tripled in the range between 50 and 150 μl (Table 1).

3.5. PA measurement with HRP-rotating biosensor

The working potential was selected using the same cyclic voltammogram showed before (Fig. 1a) for the couple 4-TBB/4-TBC at a GCE in phosphate buffer. For potentials values below −150 mV, the cathodic current became independent of the applied potential; therefore, this value was chosen as working potential. Furthermore, at this potential, a less contribution of the electroactive interferences is expected.

The performance of the HRP-rotating biosensor for the measurement of reduced thiols concentrations was characterized. For PA measurement, the following procedure was used: (a) a baseline current was established with the buffer solution; (b) a solution containing 1 mM 4-TBC and 0.1 mM H_2O_2 were injected in the rotating biosensor; (c) the flow was detained and the disk was rotated to 900 rpm, thus, a large reduction current was observed due to the quinone derivative and after 1 min, the flow was started again; then (d) a solution containing 1 mM 4-TBC, 0.1 mM H_2O_2, and several PA concentrations were injected in the rotating biosensor; (e) the flow was detained and the disk was rotated to 900 rpm and the reduction current was measurement. The addition of PA resulted in a current decrease. After 1 min, the flow was started again. A PA calibration plot was obtained by plotting ΔI versus PA concentration. A linear relation, $\Delta I\,(\mu A) = 8.7 \times 10^{-3} + 0.543$ [CPA], was observed between the ΔI and the PA concentration in the range of 0.02 and 80 μM (rotation 900 rpm). The correlation coefficient for this type of plot was typically 0.998. Detection limit (DL) is the minimal difference of concentration that can be distinguished from the signal of the pure 4-TBC solution. The DL was calculated as the amount of PA required to yield a net peak that was equal to three times the S.D. of the pure 4-TBC signal. In this study, the minimal difference of concentration of PA was 7 nM. Reproducibility assays were made using repetitive standards solutions ($n = 5$) containing 1.0 mM 4-TBC, 0.1 mM H_2O_2 and 10 μM PA; the percentage standard error was less than 3%.

The proposed method was applied to the determination of PA capsules. The precision of the method was obtained on the basis of intra-assay using standard addition. The intra- and inter-day precision (C.V.%) and accuracy (bias%) of the assay procedure were determined by the analysis of five samples at each lower, medium and higher QC concentration in the same day and one sample at each QC concentration in 5 different days, respectively (Table 2). There are no significant differences in the results, indicating that the analysis of PA capsules by the proposed method is reproducible.

Excipients frequently added to dosage forms are povidone, starch, lactose, sodium starch glycollate, magnesium stearate, hydroxymethylpropyl cellulose, talc, titanium oxide, and polyethylene glycol. The response of the analyte with excipients and PA was compared with the response of pure PA. It was found that assay results were not changed. Therefore, excipients commonly found in typical pharmaceutical preparations did not interfere with the quantization of PA present as active principle. In Table 3 the results are showed.

The developed method for the PA determination was applied to two different commercial preparations (Table 4). There is no need any extraction procedure before HRP-rotating biosensor analysis.

4. Conclusions

The usefulness of enzyme biosensor used for the determination of very low concentrations of PA was demonstrated. The biosensor developed in this work is found to be more sensitive than other techniques previously developed (Table 5). This type of detection (addition reaction on co-substrates) shows good promise in pharmacological sensing. Also, this biosensor is able to operate as a fast, selective and sensitive detection unit when is incorporated into a FIA system, and provides a fast and cost effective solution to the realization of quantitative information at extremely low levels of PA concentrations.

Acknowledgements

The authors wish to thank the financial support from the Universidad Nacional de San Luis and the Consejo Nacional de Investigaciones Científicas y Técnicas (CONICET). One of the authors (A.A.J.T) acknowledges support in the form of a fellowship from the Consejo Nacional de Investigaciones Científicas y Técnicas (CONICET).

References

[1] J.M. Walshe, Mov. Disord. 18 (2003) 853.
[2] D.A. Joyce, Baillieres Clin. Rheumatol. 4 (1990) 553.
[3] J.M. Walshe, Am. J. Med. 21 (1956) 487.
[4] B. Sarkar, Chem. Rev. 99 (1999) 2535.
[5] S.R. Gooneratne, D.A. Christensen, Vet. J. 153 (1997) 171.
[6] E.C. LeRoy, M. Trojanowska, E.A. Smith, Clin. Exp. Rheumatol. 9 (1991) 173.
[7] I.A. Jaffe, Am. J. Med. 75 (1983) 63.
[8] A.D. Stephens, J. Inherit. Metab. Dis. 12 (1989) 197.
[9] J. Peisach, W.E. Blumberg, Mol. Pharmacol. 5 (1969) 200.
[10] C.M. Herbert, K.A. Lindberg, M.I. Jayson, A.J. Bailey, Lancet 303 (1974) 187.
[11] W.H. Deutsch, J.F. Morton, Science 125 (1957) 600.
[12] R.R. Singh, A.N. Malaviya, R. Malaviya, M. Sharma, R. Shandilya, V. Taneja, S.D. Khare, D. Beri, A. Kumar, N.K. Mehra, J. Assoc. Phys. India 42 (1994) 201.
[13] R. Munro, H.A. Capell, Br. J. Rheumatol. 36 (1997) 104.
[14] D.J. Perrett, Rheumatol. Suppl. 7 (1981) 41.
[15] S.S. Kang, P.W. Wong, K. Curley, Pediatr. Res. 16 (1982) 370.
[16] S.S. Kang, P.W. Wong, P.B. Glickman, C.M. MacLeod, I.A. Jaffe, J. Clin. Pharmacol. 26 (1986) 712.
[17] J. Russell, J.A. McKeown, C. Hensman, W.E. Smith, J. Reglinski, J. Pharm. Biomed. Anal. 15 (1997) 1757.
[18] E.P. Lankmayr, K.W. Budna, K. Muller, F. Nachtmann, F. Rainer, J. Chromatogr. 222 (1981) 249.
[19] D. Beales, R. Finch, A.E.M. McLean, M. Smith, I.D. Wilson, J. Chromatogr. 226 (1981) 498.
[20] A.A. Al-Majed, J. Pharm. Biomed. Anal. 21 (1999) 827.
[21] T.P. Ruiz, C. Martinez-Lozano, V. Tomas, C.S. de Cardona, J. Pharm. Biomed. Anal. 15 (1996) 33.
[22] A.A. Al-Majed, Anal. Chim. Acta 408 (2000) 169.
[23] F.E.O. Suliman, H.A.J. Al-Lawati, A.M.Z. Al-Kindy, I.E.M. Nour, S.B. Salama, Talanta 61 (2003) 221.
[24] M.S. García, C. Sánchez Pedreño, M.I. Albero, V. Rodenas, J. Pharm. Biomed. Anal. 11 (1993) 633.
[25] P. Viñas, J.A. Sánchez Prieto, M. Hernández Cordoba, Microchem. J. 41 (1990) 2.
[26] Z. Zhang, W.R.G. Baeyens, X. Zhano, G.V.D. Weken, Anal. Chim. Acta 347 (1997) 325.
[27] M. Wronski, J. Chromatogr. B 676 (1996) 29.
[28] A. Zinellu, C. Carru, S. Sotgia, L. Deiana, J. Chromatogr. B 803 (2004) 299.
[29] S.E. Ibrahim, A.A. Al-Badr, Spectrosc. Lett. 13 (1980) 471.
[30] D.L. Rabenstein, G.T. Yamashita, Anal. Biochem. 180 (1989) 259.
[31] G.T. Yamashita, D.L. Rabenstein, J. Chromatogr. 491 (1989) 341.
[32] S. Zhang, W. Sun, W. Zhang, W. Qi, L. Jin, K. Yamamoto, S. Tao, J. Jin, Anal. Chim. Acta 386 (1999) 21.
[33] G. Favaro, M. Fiorani, Anal. Chim. Acta 332 (1996) 249.
[34] O. Chailapakul, E. Popa, H. Tai, B.V. Sarada, D.A. Tryk, A. Fujishima, Electrochem. Commun. 2 (2000) 422.
[35] C. Ruan, Y. Li, Talanta 54 (2001) 1095.
[36] C.J. Cooksey, K. Jimbow, E.J. Land, P.A. Riley, Melanoma Res. 2 (1992) 283.
[37] M.J. Picklo, V. Amarnath, D.G. Graham, T.J. Montine, Free Radic. Biol. Med. 27 (1999) 271.
[38] H.T. Deng, G.J. van Berkel, Electroanalysis 11 (1999) 857.
[39] T.J. Montine, M.J. Picklo, V. Amarnath, W.O. Whetsell, D.G. Graham, Exp. Neurol. 148 (1997) 26.
[40] D. Nemathollai, H. Goodarzi, J. Electroanal. Chem. 517 (2001) 121.
[41] D. Nemathollai, H. Goodarzi, Electrochim. Acta 50 (2005) 3648.
[42] E. Salinas, A.A.J. Torriero, M.I. Sanz, F. Battaglini, J. Raba, Talanta 66 (2005) 92.
[43] L. Papouchado, G. Petrie, R.N. Adams, J. Electroanal. Chem. 38 (1972) 389.
[44] L. Papouchado, G. Petrie, J.H. Sharp, R.N. Adams, J. Am. Chem. Soc. 90 (1968) 5620.
[45] T.E. Young, J.R. Griswold, M.H. Hulbert, Melanin. I.J. Org. Chem. 39 (1974) 1980.
[46] A. Brun, R. Rosset, J. Electroanal. Chem. 49 (1974) 287.
[47] D.I. Stom, S.N. Suslov, Biofizika 21 (1979) 40.
[48] M.D. Ryan, A. Yueh, C. Wen-Yu, J. Electrochem. Soc. 127 (1980) 1489.
[49] W.J. Albery, Electrode Kinetics, Clarendon Press, Oxford, 1975.
[50] A.A.J. Torriero, E. Salinas, F. Battaglini, J. Raba, Anal. Chim. Acta 498 (2003) 155.
[51] S. Shahrokhian, S. Bozorgzadeh, Electrochim. Acta, available online.
[52] S. Shahrokhian, A. Souri, H. Khajehsharifi, J. Electroanal. Chem. 565 (2004) 95.
[53] B. Gómez-Taylor Corominas, J. Pferzschner, M. Catalá Icardo, L. Lahuerta Zamora, J. Martínez Catalayud, J. Pharm. Biomed. Anal. 39 (2005) 281.
[54] N. Wangfuengkanagul, O. Chailapakul, Talanta 58 (2002) 1213.

Available online at www.sciencedirect.com
ScienceDirect
Talanta 71 (2007) 1268–1275
Talanta
www.elsevier.com/locate/talanta

Optimisation of the separation of herbicides by linear gradient high performance liquid chromatography utilising artificial neural networks

Anh T.K. Tran [a], Ross V. Hyne [b], Fleur Pablo [b], W. Roy Day [a,b], P. Doble [a,*]

[a] *Department of Chemistry, Materials and Forensic Science, Centre for Ecotoxicology, University of Technology Sydney, P.O. Box 123, Broadway, NSW 2007, Australia*
[b] *Department of Environment and Conservation (NSW), Centre for Ecotoxicology, P.O. Box 29, Lidcombe, NSW 1825, Australia*

Received 4 April 2006; received in revised form 26 June 2006; accepted 26 June 2006
Available online 14 August 2006

Abstract

An artificial neural network (ANN) was employed to model the chromatographic response surface for the linear gradient separation of 10 herbicides that are commonly detected in storm run-off water in agricultural catchments. The herbicides (dicamba, simazine, 2,4-D, MCPA, triclopyr, atrazine, diuron, clomazone, bensulfuron-methyl and metolachlor) were separated using reverse phase high performance liquid chromatography and detected with a photodiode array detector. The ANN was trained using the pH of the mobile phase and the slope of the acetonitrile/water gradient as input variables. A total of nine experiments were required to generate sufficient data to train the ANN to accurately describe the retention times of each of the herbicides within a defined experimental space of mobile phase pH range 3.0–4.8 and linear gradient slope 1–4% acetonitrile/min. The modelled chromatographic response surface was then used to determine the optimum separation within the experimental space. This approach allowed the rapid determination of experimental conditions for baseline resolution of all 10 herbicides. Illustrative examples of determination of these components in Milli-Q water, Sydney mains water and natural water samples spiked at 0.5–1 μg/L are shown. Recoveries were over 70% for solid-phase extraction using Waters Oasis® HLB 6 cm^3 cartridges.
© 2006 Elsevier B.V. All rights reserved.

Keywords: Artificial neural network (ANN); Polar herbicides; HPLC; Photodiode array; Solid-phase extraction

1. Introduction

The use of herbicides for crop protection is common throughout Australia [1,2]. The most prolific of these are simazine and atrazine, with over 3000 t used annually. In addition, over 1000 t of other classes of chemicals including phenoxy acids, benzoic acids and pyridines are also used annually. The herbicides 2,4-D and its derivatives, along with MCPA, are the major herbicides within this group [1]. Prolonged use is of concern because it may lead to pollution of surface and ground waters [1].

Australia's National Medical Research Council recommends concentrations of herbicides in drinking water should not exceed 0.1–2 μg/L. These concentrations approach the detection limits of current methods of analysis that often employ solid-phase extraction [3–6] to preconcentrate the target herbicides prior to analysis by gas chromatography (GC) or high performance liquid chromatography. Analysis of very polar herbicides such as dicamba, MCPA, 2,4-D and triclopyr by GC requires derivatisation [7–9]. This extra complexity can be a source of additional error and lengthens the total analysis time. HPLC offers an alternative method of analysis in which the polar herbicides do not require derivatisation. The HPLC is often coupled to MS, allowing sensitive and unambiguous identification [10,11]. Where an MS detector is not available an ultraviolet (UV) or photodiode array detector (PDA) is frequently employed [12,13]. MS detection may also be used simultaneously with UV or PDA detection to confirm herbicide identity [14].

Common herbicides consist of groups of differing chemical properties. These include acids, bases and neutrals with vastly differing polarities. Therefore, separation of mixtures of these groups for screening purposes has been challenging. Chiron et al. [10] reported that the acidic herbicides 2,4-D, MCPA were separated when the pH of the mobile phase was 2.9. Manipulation of selectivity by increasing the pH of the mobile for separation of more neutral compounds resulted in the co-elution of these

* Corresponding author. Tel.: +61 2 9514 1792; fax: +61 2 9514 1460.
E-mail address: Philip.Doble@uts.edu.au (P. Doble).
URL: http://www.forensics.edu.au.

0039-9140/$ – see front matter © 2006 Elsevier B.V. All rights reserved.
doi:10.1016/j.talanta.2006.06.031

herbicides. This was overcome via application of a high resolution LC column of length 25 cm and a particle size of 4 μm [10,12], resulting in significant increases in analysis time.

Di Corcia et al. [11] reported separations of 39 acidic and non-acidic pesticides including 2,4-D, simazine, atrazine, diuron, and metolachlor by HPLC with MS detection. These separations were optimised with a constant linear gradient and variation of the mobile phase pH. Although this method eventually arrived at suitable separation conditions, a large number of experiments were required. Furthermore, it was difficult to be sure that the separation was at the global optimum.

An alternative method to determine a separation optimum whilst also keeping the number of experiments to a minimum is to employ a multivariate approach in which the mobile phase parameters are changed according to an experimental design. This approach relies upon determination of factors that affect the separation, and design of experiments to interpolate the chromatographic response surface within the experimental space using a suitable mathematical technique [15]. Once the chromatographic response surface has been calculated the choice of the optimum is straightforward. One such approach is to employ an artificial neural network (ANN). The theory of ANNs has been described in several papers [16–18] and the use of ANNs to model gradient chromatographic response surfaces has been reported previously. Shan et al. [19] employed ANNs to predict analyte retention times for a range of amino acids at various pH values and linear gradient conditions. The authors modelled each analyte with a separate ANN resulting in an average error of 1.6% between the predicted and experimental retention times. Kaliszan et al. [20] employed an ANN for the a priori prediction of gradient retention times based on analyte structures. The authors conclude the prediction allowed for the first approximation of gradient retention for a new analyte.

This paper reports the optimisation of the linear gradient separation of 10 herbicides consisting of a mixture of acids, bases and neutrals employing a single ANN within an experimental space determined from a small number of scouting experiments. The method was applied to the analysis of the target herbicides in various water samples after solid-phase extraction.

2. Experimental

2.1. Apparatus and chromatographic conditions

Separations were performed on two instruments, either:

(a) Waters 2690 Separation Module equipped with a model 996 Photodiode Array Detector (Waters Corporation, Milford, MA, USA); or
(b) Waters 600 Controller equipped with a Waters 717 plus Autosampler and Waters 2487 Dual λ Absorbance Detector (Waters Corporation, Milford, MA, USA).

The development and optimisation of the method was performed on instrument (a); the method was applied to natural water samples using instrument (b). This was necessary as the research was performed at two different laboratories.

The void volume was approximately the same for each system at 1.6 min at 1 mL/min. Small differences in retention times were observed on each of the instruments due to different dead volumes and differences in gradient generation. However, this did not affect the overall resolution of the separations significantly.

The analytical column was a Zorbax StableBond C18 column, 150 mm × 4.6 mm i.d., 5 μm (Agilent Technologies, Sydney, Australia). Waters Oasis® HLB 6 cm^3 cartridges were obtained from Waters (Waters Australia, Sydney, Australia). Natural water samples were filtered with 0.45 μm mixed cellulose esters membranes (Millipore, Bedford, MA, USA). The extractions were performed with a SPE-12 vacuum glass manifold (Supelco, Bellefonte, PA, USA).

2.2. Reagents and procedures

All mobile phases were prepared in water treated with a Millipore Milli-Q (Bedford, MA, USA) water purification system. Mobile phases were degassed by vacuum filtration through a 0.45 μm polyvinylidene fluoride (HVLP 04700) filter (Millipore, Bedford, MA, USA). Stock solutions of herbicides were prepared individually by weighing and dissolution in methanol (MeOH). All stock solutions were stored at 4 °C.

All chemicals were of analytical reagent grade unless otherwise stated.

Dichloromethane, HPLC grade acetonitrile (ACN) and methanol (MeOH) were obtained from Crown Scientific (Sydney, Australia). Ammonium formate and formic acid were purchased from Asia Pacific Specialty Chemicals Limited (Crown Scientific, Sydney, Australia).

Simazine, chlomazone and bensulfuron-methyl were purchased from Riedel-de Häen (Seelze, Germany) and all other herbicides were obtained from Chem Service (Alltech Associates Pty, Sydney, Australia). Table 1 details the structure and relevant chemical data for each herbicide.

2.3. Experimental design

An experimental design approach was taken in which factors that affected the selectivity of the separation were identified [15]. These experiments investigated various mobile phases at various pH values and linear gradients of MeOH or ACN. ACN was the preferred solvent for subsequent experiments due to superior resolution of the analytes. Formate was chosen as the preferred buffer for a several reasons. Firstly, the phenoxy acetic acid herbicides have pK_a values from 2 to 4 [21], so manipulation of the pH of the mobile phase around this value was expected to have significant effects upon selectivity. Secondly, the pH of the mobile phase could be easily set to any desired pH within the above range via mixing of two separate solutions of ammonium formate and formic acid. Such a setup allows the pH to be controlled via appropriate solvent mixing using the HPLC system (see Table 2). Thirdly, formate buffers are compatible with MS detection, allowing the possibility of this method to be transferred to a HPLC–MS.

Table 1
Structure and chemical data of target herbicides

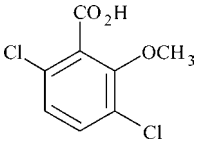
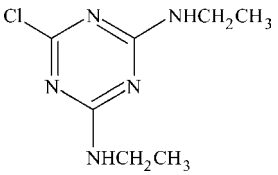
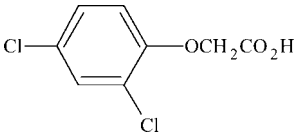
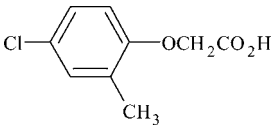
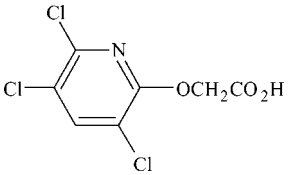
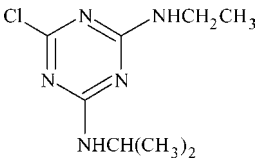
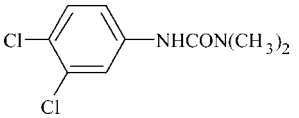
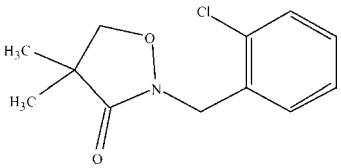
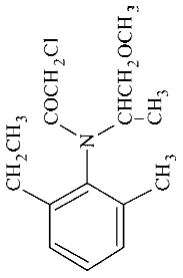
Chemical	IUPAC name	Formula	MW	Structure	pK_a	log K_{ow}	Water solubility (mg/l)
Dicamba	3,6-Dichloro-*o*-anisic acid	$C_8H_6Cl_2O_3$	221.0		1.97 (acid)	−1.88 (pH 6.8)	6100 (25 °C)
Simazine	6-Chloro-N^2,N^4-diethyl-1,3,5-triazine-2,4-diamine	$C_7H_{12}ClN_5$	201.7		1.62 (base)	2.1 (25 °C)	6.2 (pH 7, 20 °C)
2,4-D	(2,4-Dichlorophenoxy)acetic acid	$C_8H_6Cl_2O_3$	221.0		2.73 (acid)	0.04–0.33 (pH 5)	23180 (pH 7, 25 °C)
MCPA	4-Chloro-2-methylphenoxy)acetic acid	$C_9H_9ClO_3$	200.6		3.07 (acid)	−0.71 (pH 7, 25 °C)	273.9 (pH 7, 25 °C)
Triclopyr	3,5,6-Trichloro-2-pyridyloxyacetic acid	$C_7H_4Cl_3NO_3$	256.5		3.97 (acid)	−0.45 (pH 7)	8100 (20 °C)
Atrazine	6-Chloro-N^2-ethyl-N^4-isopropyl-1,3,5-triazine-2,4-diamine	$C_8H_{14}ClN_5$	215.7		1.7 (base)	2.5 (25 °C)	33 (pH 7, 22 °C)
Diuron	3-(3,4-Dichlorophenyl)-1,1-dimethylurea	$C_9H_{10}Cl_2N_2O$	233.1			2.85 (25 °C)	36.4 (25 °C)
Clomazone	2-(2-Chlorobenzyl)-4,4-dimethyl-1,2-oxazolidin-3-one	$C_{12}H_{14}ClNO_2$	239.7			2.5	1100

Table 1 (*Continued*)

Chemical	IUPAC name	Formula	MW	Structure	pK_a	log K_{ow}	Water solubility (mg/l)
Bensulfuron-methyl	α-(4,6-Dimethoxypyrimidin-2-ylcarbamoylsulfamoyl)-*o*-toluic acid	$C_{16}H_{18}N_4O_7S$	410.4		5.2 (acid)	0.62 (pH 7, 30 °C)	120 (pH 7, 25 °C)
Metolachlor	2-Chloro-6′-ethyl-*N*-(2-methoxy-1-methylethyl)aceto-*o*-toluidide	$C_{15}H_{22}ClNO_2$	283.8			2.9	488 (25 °C)

These scouting experiments demonstrated that significant selectivity changes occurred when the pH of the mobile phase was around the pK_as of the phenoxy acids, with ACN providing the best resolution of the analytes. Based on these results, an experimental space of pH 3.0–4.8, and linear gradients of 1–4% ACN/min was chosen as appropriate for modelling using an artificial neural network.

A series of experiments were performed in duplicate (using instrumentation (a)) within this experimental space in accordance with Table 2 to generate a chromatographic response surface.

The pH measurements were performed by passing the effluent from the detector over a pH metre. The pH metre was accurate to two decimal places.

2.4. Artificial neural network model of response surface

Trajan Neural Networks, version 6.0 (Trajan Software, Durham, UK) was used for constructing the artificial neural networks. All other calculations were performed using Microsoft Excel 2000.

The pH and the slope of the gradient were used as inputs, and the retention time of each of the herbicides was used as outputs. These experiments were based on a factorial design [15], with iterative training of the various ANN architectures using the following general approach. Initially, five experiments were performed in duplicate; at high and low values for pH and linear gradient slope; and one in the middle of the experimental space. These five experimental points were used as training data for a heuristic determination of the best ANN architecture of lowest error. That is the software automatically changed the number of nodes from 2 to 10 in the hidden layer to find an ANN architecture that described the chromatographic response surface with the lowest error. The training algorithms were combinations of back propagation (100 epochs) and conjugate descent (150–200 epochs). Three layer multilayer perceptron and radial basis function networks were investigated.

The ANN of lowest error constructed in this manner was then used to identify an optimum by calculation of minimum peak pair resolution. At this predicted optimum, actual retention times were compared against the predicted retention times. If poor agreement resulted indicating that the ANN had over-learnt, the newly generated data was used as either training or verification points to construct new ANNs to describe the chromatographic response surface. The verification points were not used train the ANN, but were used as a check for good predictability of retention times. Poor agreement between the predicted values and the verification points indicated over-learning. This procedure was followed until there was good agreement between predicted and actual retention times. This approach arrived at an optimum separation after nine experiments.

The retention times of each herbicide were predicted by the ANNs throughout the experimental space by inputting a grid pattern of the experimental space. The pH was inputted in the range of 3.0–4.8 at increments of 0.1 pH units, and the slope in the range of 1–4% at increments of 0.1%.

Table 2
Experimental conditions

Experiment	ANN	pH	Slope (% ACN/min)	Time (min)	%A ACN	%B H_2O	% C 20 mM HCOOH	% D 20 mM $HCOONH_4$
1	Training	3.01	1.00	0	20	50	27	3
				50.0	70	0	27	3
				50.1	20	50	27	3
				62.0	20	50	27	3
2	Verification	3.01	2.00	0	20	50	27	3
				25.0	70	0	27	3
				25.1	20	50	27	3
				37.0	20	50	27	3
3	Training	3.01	4.00	0	20	50	27	3
				12.5	70	0	27	3
				12.6	20	50	27	3
				24.5	20	50	27	3
4	Training	3.66	1.00	0	20	50	15	15
				50.0	70	0	15	15
				50.1	20	50	15	15
				62.0	20	50	15	15
5	Verification	3.66	1.33	0	20	50	15	15
				37.5	70	0	15	15
				37.6	20	50	15	15
				50.0	20	50	15	15
6	Training	3.66	2.00	0	20	50	15	15
				25.0	70	0	15	15
				25.1	20	50	15	15
				37.0	20	50	15	15
7	Training	3.66	4.00	0	20	50	15	15
				12.5	70	0	15	15
				12.6	20	50	15	15
				24.5	20	50	15	15
8	Training	4.80	1.00	0	20	50	3	27
				50.0	70	0	3	27
				50.1	20	50	3	27
				62.0	20	50	3	27
9	Training	4.80	4.00	0	20	50	3	27
				12.5	70	0	3	27
				12.6	20	50	3	27
				24.5	20	50	3	27

The resolution was calculated for each of the peak pairs from the predicted retention times utilising the standard resolution equation [22]. It was assumed that the peak widths were approximately the same throughout the chromatogram, so the resolution calculation was reduced to the difference between the retention times of each of the adjacent peaks. A resolution map was constructed with the minimum peak pair resolution at each condition. The minimum peak pair resolution was chosen as it gives a simple measure of the overall resolution of the separation, with the largest value on the response surface representing the greatest spread of the peaks.

2.5. Solid-phase extraction

Waters Oasis® HLB 6 cm^3 cartridges were used for extraction of the herbicides in three types of water (Milli-Q water, Sydney mains water and natural water obtained from South Creek, Sydney). Each cartridge was conditioned with 5 mL methanol and then washed with 10 mL Milli-Q water. One litre aliquots of Milli-Q water and Sydney mains water were extracted unfiltered. Aliquots of the natural water samples (500 mL) were filtered through 0.45 μm mixed cellulose esters membranes. Five molar formic acid was added dropwise (ca. 1%, v/v) to each of the samples to yield a pH of 3. Sodium chloride (10 g/L) was added to aid in the recoveries of the herbicides. The samples were then loaded onto the cartridges via a vacuum manifold at approximately 10 mL/min. The excess of water was removed by opening the valves and letting air to pass through the cartridge for 15–30 min. The herbicides adsorbed on the cartridges were eluted with 5 mL of methanol. After reducing to near dryness under a nitrogen stream, the samples were reconstituted in the mobile phase to a final volume of 1.00 mL. This final solution was then injected into the HPLC (using instrumentation (b)).

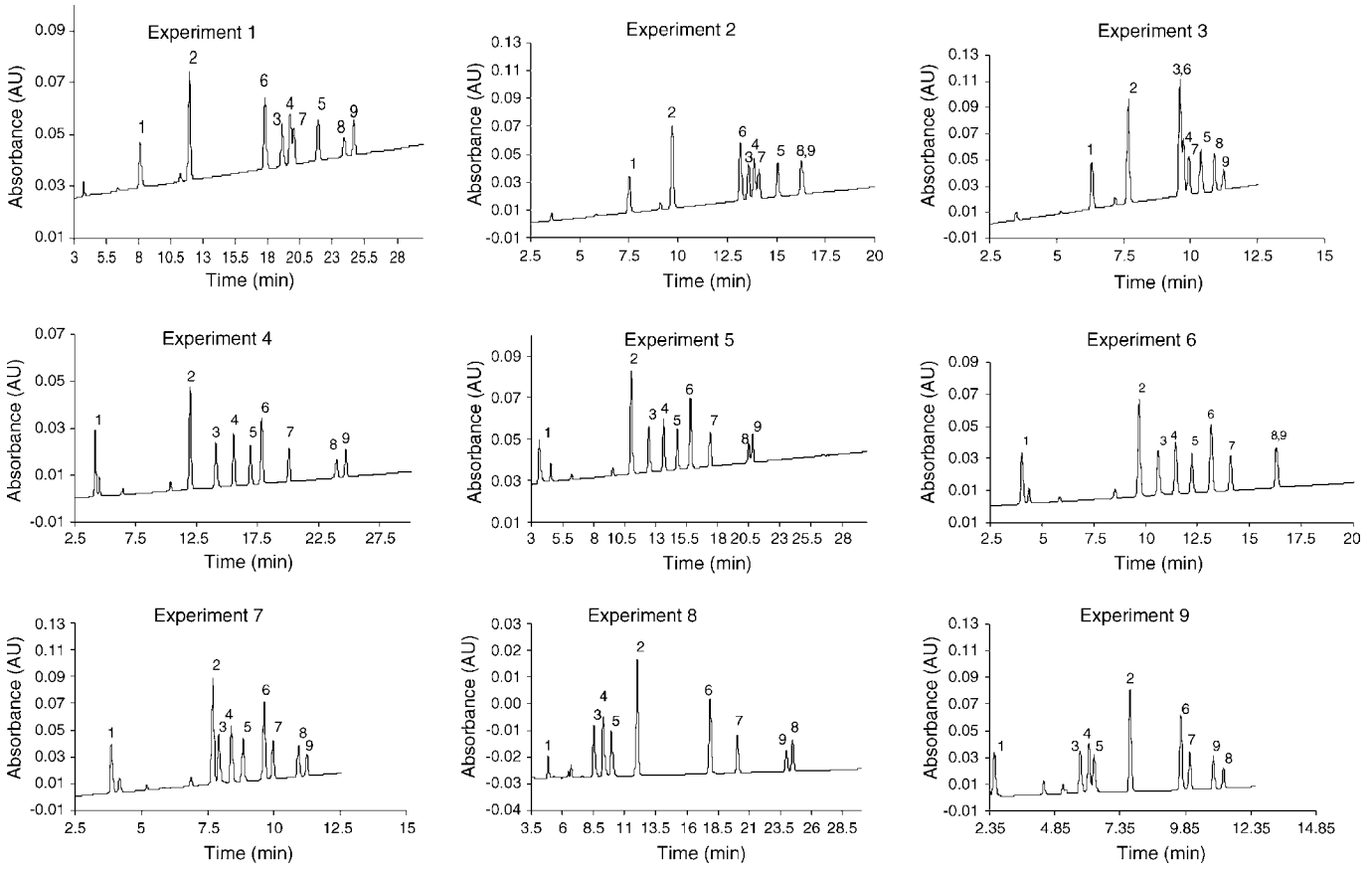


Fig. 1. Chromatograms of the herbicides at each of the experimental conditions. (1) Dicamba, (2) simazine, (3) 2,4-D, (4) MCPA, (5) triclopyr, (6) atrazine, (7) diuron, (8) clomazone and (9) bensulfuron-methyl. The experimental conditions are given in Table 1.

3. Results and discussion

3.1. Optimisation of the separation using an ANN

Fig. 1 shows nine chromatograms obtained at each of the experimental points to demonstrate selectivity changes within the experimental space. Peak 10, metolachlor was omitted from the optimisation process as it always eluted last and was clearly separated from the rest of the target herbicides. From visual inspection of these chromatograms a number of trends can be drawn.

Increasing the slope of the linear gradient from 1% to 4% ACN/min, whilst maintaining a constant pH (Experiments 1–3, 4–7, and 8–9), reduced the retention of all of the herbicides, without changing the elution order. Increasing the pH from 3.01 to 4.80, whilst maintaining a constant slope of 1 (Experiments 1,4 and 8) clearly show large selectivity changes for the acid herbicides, namely dicamba (1), 2,4-D (3), MCPA (4), triclopyr (5) and bensulfuron-methyl (9). Little effect on the neutral herbicides (clomazone (8)), and basic herbicides (atrazine (6) and simazine (2)) was observed. Similar trends were evident at other constant slopes and varying pH values.

Manipulation of these parameters to obtain a global optimum via a trial and error approach would be a significant and time-consuming challenge. Therefore, each of the experimental points was used to train a number of ANN architectures via a heuristic approach as described in 2.4. The best performing ANN was a multilayer perceptron of architecture 2:9:9. The training error was 0.015 root mean square (RMS) and the verification (select) error was 0.017 RMS. The agreement of these two errors strongly indicated the ANN had not over-learnt and provided good predictive performance as shown in Fig. 2, which illustrates the correlation between observed and predicted retention times of each of the herbicides for all data points from Experiments 1 to 9. The correlation was excellent with an r^2 value of 0.9982 and a slope close to 1. This demonstrates that the ANN was performing well in its description of the chromatographic response

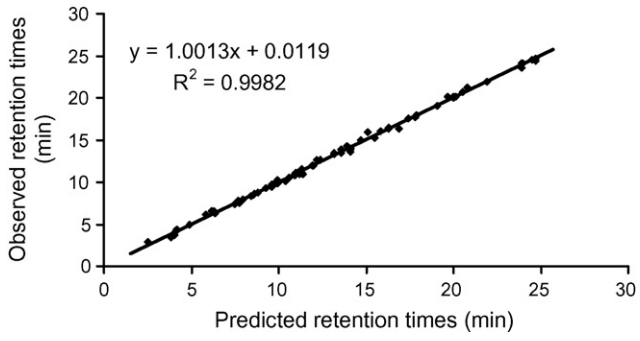


Fig. 2. Correlation of observed retention times vs. ANN predicted retention times for all data points from Experiments 1 to 9.

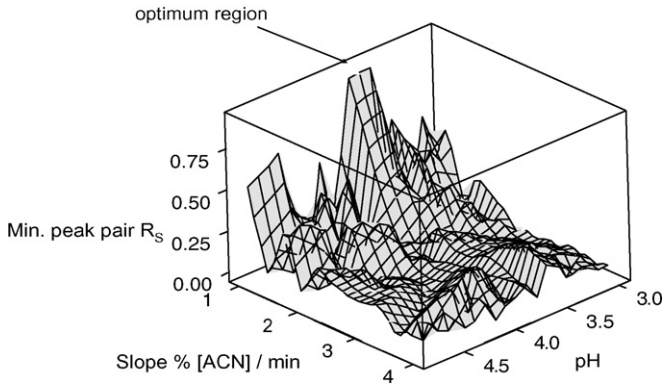


Fig. 3. The minimum peak pair resolution response surface predicted by the ANN.

surface. An ANN exhibiting perfect predictability would result with an r^2 value of 1 and slope of 1.

This ANN was used to construct a minimum peak pair resolution response surface throughout the experimental space, shown in Fig. 3. From this response surface, an optimum was clearly evident in the pH range of 3.6–3.8, and a gradient of 1% ACN/min.

The herbicide standard was run under these conditions resulting in complete separation of all of the acidic, basic and neutral components, and is shown in Fig. 4 (instrumentation (a)).

3.2. SPE preconcentration

Residual herbicides in natural waters can be of concern at low ppb (μg/L) levels. PDA detection lacks sufficient sensitivity to detect the herbicides of interest at such low levels. Waters Oasis® HLB cartridges were identified as suitable solid-phase extraction devices due to their hydrophilic and lipophilic characteristics [23]. It was expected that these cartridges could recover the acidic, basic and neutral components of the herbicide mix. The method of extraction was based upon that developed by Freitas et al. [24], with some minor modifications. The pH was of the sample solutions were decreased from 4 to 3 to ensure the extraction of dicamba, which has an octanol–water partition coefficient ($\log K_{ow}$) of −1.88 at pH 6.8 and a pK_a of approximately 2 [21]. However, this reduction in pH increased the co-extraction of humic and fulvic acids. In addition, 10 g/L of NaCl was added to aid in the recoveries [25,26].

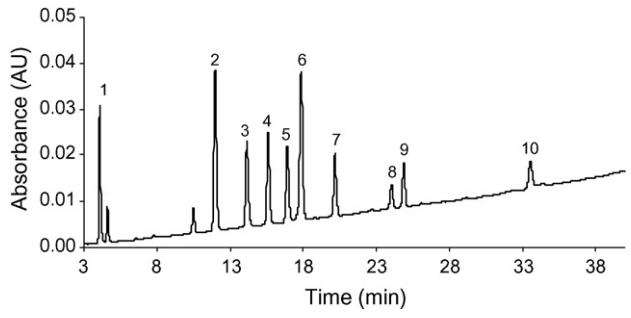


Fig. 4. Separation of a mixed herbicide standard at level 5–10 μg/L under the optimum separation conditions (instrumentation (a)): pH 3.72 buffer, 1% [ACN]/min, gradient from 20% acetonitrile to 60% acetonitrile in 40 min, flow-rate 1 mL/min, 10 μl injection, PDA 230 nm detection.

Table 3
Mean % recoveries for 0.5 to 1.0 μg/L concentration of analytes in different aquatic matrices using SPE

Herbicide	% Recovery ± % R.S.D.		
	Milli-Q water ($n=2$)	Sydney mains water ($n=4$)	South Creek water ($n=3$)
Dicamba	104 ± 2	87 ± 2	61 ± 7
Simazine	100 ± 1	91 ± 2	93 ± 3
2,4-D	102 ± 1	86 ± 11	104 ± 10
MCPA	99 ± 1	90 ± 5	84 ± 3
Triclopry	101 ± 1	85 ± 6	93 ± 6
Atrazine	100 ± 1	96 ± 2	83 ± 6
Diuron	94 ± 1	87 ± 3	90 ± 9
Clomazone	84 ± 1	81 ± 4	71 ± 8
Bensulfuron-methyl	72 ± 3	60 ± 2	82 ± 6
Metolachlor	107 ± 5	83 ± 2	87 ± 6

Recoveries for 0.5–1 μg/L (0.5 μg/L for atrazine and simazine, and 1 μg/L for other compounds) of the analytes spiked into Milli-Q water, Sydney mains water and South Creek water samples are shown in Table 3. The recoveries were over 70% for all of compounds.

Recoveries for Sydney mains and South Creek waters were somewhat lower than the recoveries for Milli-Q water. The most likely reason was the high concentration of humic acids present in the natural water samples. Humic acids consist of a mixture of complex macromolecules that have polymeric phenolic structures with the ability to chelate with metals, especially iron. These complexes may be trapped on the cartridges, and may aggregate with target herbicides.

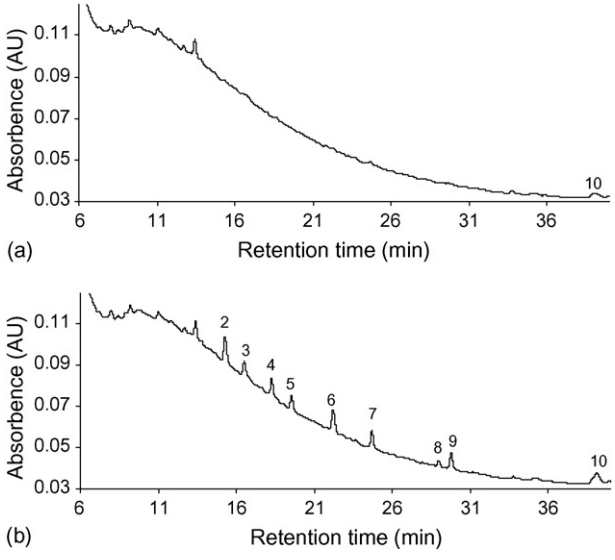


Fig. 5. (a) HPLC of 500 mL South Creek water blank and (b) HPLC of 500 mL South Creek water spiked with mixed herbicide standard, 0.5–1 μg/L, under the same optimum separation conditions after SPE preconcentration (instrumentation (b)), 100 μL injection, UV 230 nm detection. (1) Dicamba, (2) simazine, (3) 2,4-D, (4) MCPA, (5) triclopyr, (6) atrazine, (7) diuron, (8) clomazone, (9) bensulfuron-methyl and (10) metolachlor.

Fig. 5(a) shows a natural water sample obtained from South Creek, NSW Australia analysed on instrumentation (b) after preconcentration. The presence of metolachlor (peak 10) was detected. The sloping baseline was most likely due to the presence of humic acids. Fig. 5(b) shows the same water sample spiked with the target herbicides at 0.5–1 μg/L, again after preconcentration. Peak 1, dicamba eluted at the beginning of the chromatogram with retention time at 4.08 min (not shown). The differences in retention times of the herbicides in Figs. 4 and 5 are due to the different instrumentation.

3.3. Analytical performance

The detection limits of HPLC–UV system with respect to the compounds investigated were determined by analysing standard solutions at decreasing concentrations. Calibration curves were constructed for each of the herbicides over the range of 0.01–3.0 μg/L in Sydney mains water and analytes were preconcentrated by SPE. From the chromatograms obtained, S/N (signal/noise) ratios (high/high) were calculated for each analyte. The limit of detection (LOD) after SPE preconcentration based upon a signal to noise ratio of 3:1 were 0.05 μg/L for atrazine and simazine; 0.10 μg/L for diuron, bensulfuron-methyl and clomazone; 0.15 μg/L for 2,4-D, MCPA, trichlopyr and metolachlor in 1 L of Sydney mains water.

4. Conclusions

Linear gradient separations of a mixture of acidic, basic and neutral herbicides were accurately modelled with an ANN. This model allowed the construction of the chromatographic response surface from nine experiments. The response surface clearly showed the best separation occurred in the pH range of 3.6–3.8, and a gradient of 1% ACN/min. These conditions baseline resolved all of the target herbicides. This approach significantly reduced the method development time and number of required experiments when compared against traditional trial and error methods.

SPE with Waters Oasis® HLB cartridge gave good recoveries for the target herbicides (>70%) with the exception of dicamba (61% in natural water) and was sufficient to detect the herbicides at the required concentrations.

Acknowledgements

This work was supported by the Ministry of Education and Training of Vietnam, project no. 322. Support from Agilent Technologies is gratefully acknowledged.

References

[1] AATSE, Pesticide Use in Australia, Australian Academy of Technological Sciences and Engineering, Victoria, Australia, 2002, p. 310.
[2] B.W. Simpson, G.F. Haydon, Pesticide Usage Study in the Murrumbidgee Irrigation Area of New South Wales 1998, Department of Natural Resources, Queensland, Brisbane, Australia, 1999.
[3] M.C. Bruzzoniti, C. Sarzanini, E. Mentasti, J. Chromatogr. A 902 (2000) 289.
[4] M.-C. Hennion, J. Chromatogr. A 885 (2000) 73.
[5] M.E. Leon-Gonzalez, L.V. Perez-Arribas, J. Chromatogr. A 902 (2000) 3.
[6] H. Sabik, R. Jeannot, B. Rondeau, J. Chromatogr. A 885 (2000) 217.
[7] J. Hodgeson, J. Collins, W. Bashe, J. Chromatogr. A 659 (1994) 395.
[8] M.I. Catalina, J. Dalluge, R.J.J. Vreuls, U.A.T. Brinkman, J. Chromatogr. A 877 (2000) 153.
[9] S. Ollers, H.P. Singer, P. Fassler, S.R. Muller, J. Chromatogr. A 911 (2001) 225.
[10] S. Chiron, E. Martinez, D. Barcelo, J. Chromatogr. A 665 (1994) 283.
[11] A. Di Corcia, M. Nazzari, R. Rao, R. Samperi, E. Sebastiani, J. Chromatogr. A 878 (2000) 87.
[12] A. Balinova, J. Chromatogr. A 728 (1996) 319.
[13] V. Pichon, C.C.D. Coumes, L. Chen, S. Guenu, M.-C. Hennion, J. Chromatogr. A 737 (1996) 25.
[14] R. Jeannot, H. Sabik, E. Sauvard, E. Genin, J. Chromatogr. A 879 (2000) 51.
[15] J.N. Miller, J.C. Miller, Statistics and Chemometrics for Analytical Chemistry, 5th ed., Pearson Prentice Hall, p. 181.
[16] S. Agatonovic-Kustrin, R. Beresford, J. Pharm. Biomed. Anal. 22 (2000) 717.
[17] J.E. Madden, N. Avdalovic, P.R. Haddad, J. Havel, J. Chromatogr. A 910 (2001) 173.
[18] T. Vasiljevic, A. Onjia, D. Cokesa, M. Lausevic, Talanta 64 (2004) 785.
[19] Y. Shan, R. Zhao, Y. Zhang, W. Zhang, Y. Tian, J. Sep. Sci. 26 (2003) 1541.
[20] R. Kaliszan, T. Baczek, A. Bucinski, B. Buszewski, M. Sztupecka, J. Sep. Sci. 26 (2003) 271.
[21] C.P.S. Tomlin, The Pesticide Manual: A World Compendium, 13th ed., British Crop Protection Council, Alton, UK, 2003, p. 1344.
[22] V. Meyer, Practical High-Performance Liquid Chromatography, John Wiley, 2004.
[23] Oasis® Applications Notebook: Agrochemical Food Pharmaceuticals Forensics Environmental, Waters Oasis® Sample Extraction Products, Waters, 2003, p. 200.
[24] L.G. Freitas, C.W. Gotz, M. Ruff, H.P. Singer, S.R. Muller, J. Chromatogr. A 1028 (2004) 277.
[25] A. Balinova, J. Chromatogr. 643 (1993) 203.
[26] R. Carabias-Martinez, E. Rodriguez-Gonzalo, E. Herrero-Hernandez, F.J. Sanchez-San Roman, M.G. Prado Flores, J. Chromatogr. A 950 (2002) 157.

Available online at www.sciencedirect.com
ScienceDirect
Talanta 71 (2007) 1031–1038
Talanta
www.elsevier.com/locate/talanta

Electrochemical detection of phenolic estrogenic compounds at carbon nanotube-modified electrodes

D. Vega, L. Agüí, A. González-Cortés, P. Yáñez-Sedeño *, J.M. Pingarrón

Department of Analytical Chemistry, Faculty of Chemistry, University Complutense of Madrid, 28040 Madrid, Spain

Received 3 April 2006; received in revised form 23 May 2006; accepted 26 May 2006
Available online 22 June 2006

Abstract

The use of a carbon nanotube-modified glassy carbon electrode (CNT-GCE) for the LC–EC detection of phenolic compounds with estrogenic activity is reported. Cyclic voltammograms for phenolic endocrine disruptors and estrogenic hormones showed, in general, an enhancement of their electrochemical oxidation responses at CNT-GCE attributable to the electrocatalytic effect caused by CNTs. Hydrodynamic voltammograms obtained under flow injection conditions lead to the selection of +700 mV as the potential value to be applied for the amperometric detection of the phenolic estrogenic compounds, this value being remarkably less positive than those reported in the literature using other electrode materials. Successive injections of these compounds demonstrated that no electrode surface fouling occurred. A mobile phase consisting of a 50:50 (v/v) acetonitrile:0.05 mol l^{-1} phosphate buffer of pH 7.0 was selected for the chromatographic separation of mixtures of these compounds, with detection limits ranging between 98 and 340 nmol l^{-1}. Good recoveries were obtained in the analysis of underground well water and tap water samples spiked with some phenolic estrogenic compounds at a 14 nmol l^{-1} concentration level.
© 2006 Elsevier B.V. All rights reserved.

Keywords: Carbon nanotube-modified electrodes; Phenolic estrogenic compounds; Amperometric detection; Liquid chromatography

1. Introduction

Nowadays, it is well known that some pesticides and industrial products called endocrine-disruptors chemicals (EDCs) exhibit hormones-like behaviour [1–3]. The effects of EDCs on human reproduction is probably due to their ability to mimic the function of natural estrogens as well as to disrupt the synthesis and metabolism of such hormones by binding the hormonal receptors. Some alkyl phenols produced in a high extent in many industrial applications have been identified as xenoestrogens. Examples are disinfectants such as hydroxybiphenyls, or bisphenols, i.e. BPA used for the fabrication of polycarbonate packages. Besides EDCs, natural or synthetic estrogens used for birth control that are excreted by women, such as 17α-estradiol (EE2) or β-estradiol (E2) are also matter of concern due to their environmental impact. Recently, the European Commission elaborated a list of prioritary endocrine disruptors, and the admissible concentration limits as diary doses were fixed, in a first approximation, in 15 mg/kg [4].

Gas chromatography is the commonly used technique for trace analysis of estrogenic phenols [5–9]. GC–MS provides useful analytical information for the identification and quantification of these compounds. However, the required sample treatment procedures, which involve pre-purification, fractionation, hydrolysis and derivatization, limit its application for complex real samples. Liquid chromatography coupled with mass spectrometry (LC–MS) has demonstrated to be a useful technique for the analysis of phenolic estrogenic compounds in environmental and biological samples [10–13]. Also, fluorescence [14] and UV [15] have been used as detection modes. HPLC with coulometric detection has been successfully applied for the determination of bisphenol A (BPA) in human serum [16] and urine [17]. This detection mode implied the use of multi-electrodes due to the good selectivity that can be achieved by profiting from the differences in the redox behaviour of phenol derivatives at the electrode array, each electrode being maintained at a different potential value. Amperometric detection has also been employed, and so the analysis of river waters containing a mixture of EDCs and estrogenic phenols was accomplished

* Corresponding author.
E-mail address: yseo@quim.ucm.es (P. Yáñez-Sedeño).

0039-9140/$ – see front matter © 2006 Elsevier B.V. All rights reserved.
doi:10.1016/j.talanta.2006.05.071

by using a glassy carbon electrode (GCE) at +1.0 V, after preconcentration by SPME [18].

Electrochemical studies of alkyl phenols with estrogenic properties have been recently reported. The voltammetric behaviour of xenoestrogens 4-nonylphenol (NP) and BPA at a platinum electrode has been compared with that of β-estradiol and other natural hormones [19]. Moreover, the electrooxidation of BPA was also studied at a glassy carbon electrode [20]. Carbon fiber electrodes were used to carry out the electrochemical removal of NP [21] and BPA [22]. Finally, an amperometric tyrosinase biosensor in which the enzyme was entrapped within a poly(thionine) film, has been used to detect phenolic endocrine disruptors [23].

As a consequence of the unique electronic and conducting properties of carbon nanotubes (CNTs), modified electrodes with CNTs have demonstrated to improve the electroanalytical performance of different species [24,25]. Concerning electrooxidation of phenols, it is well known that phenoxy radicals and non-conducting/passivating polymeric materials are produced causing an irreversible fouling at glassy carbon electrode surface [26]. However, using CNT-modified electrodes, an improvement in the stability of voltammetric and amperometric responses of such compounds [27], and an enhancement of the electron-transfer kinetics for catecholamines and NADH [28,29] has been observed.

In this article, we report on the development of a method for the determination of phenolic estrogens based on the amperometric monitoring of their oxidation responses at CNTs-modified glassy carbon electrodes. A high sensitivity, together with a good repeatability of the measurements and a good reproducibility of the responses obtained with different modified electrodes have been achieved. The method has been applied to the analysis of spiked water samples containing low concentration levels of these compounds previous separation by HPLC.

2. Experimental

2.1. Apparatus and electrodes

Voltammetric measurements were carried out with a BAS 100B potentiostat provided with a BAS C2 EG-1080 cell stand. A Metrohm 6.084.010 glassy carbon electrode (3 mm Ø) modified with carbon nanotubes or unmodified, was used as working electrode. Carbon paste (CPE) and carbon felt (CFE) electrodes prepared as reported previously [30,31], and a BAS MF 2013 Pt electrode (1.6 mm Ø), were also used for comparative studies. The reference electrode was a BAS MF 2063 Ag/AgCl 3 M electrode, and a BAS MW-1032 Pt wire was used as the auxiliary electrode. BAS VC-2 10 ml electrochemical cells were also used. Chromatographic and flow injection experiments were performed using a Knauer 1000 Smartline pump provided with a Knauer 5000 Smartline Manager stand, and a Knauer A 1357 injection valve provided with a 50 μl coil. A Luna C_{18} (150 mm × 4.6 mm i.d., 5 μm particle size) (Phenomenex) chromatographic column was used. The flow-cell was a Metrohm EA-1096 wall-jet cell provided with a Ag/AgCl reference electrode and a gold counter electrode. The potential values applied were controlled by means of a BAS Epsilon Multichannel detector, and the Chromgraph 1.0.01 software (Liquid Chromatography Control Software) from BAS was used to record data.

2.2. Reagents and solutions

Stock 5.0×10^{-2} mol l^{-1} solutions of bisphenol A (BPA), 2-hydroxybiphenyl (OPP), 4-nonylphenol (NP), 2,3-dimethylphenol (DMP), 17α-ethynylestradiol (EE2), β-estradiol (E2), estriol (E3), estrone (E1) and 4-terbutylphenol (TBP) (Sigma, 99%), were prepared in acetonitrile (SDS, HPLC reagent grade). More diluted solutions were prepared by suitable dilution with the supporting electrolyte solution. A 0.05 mol l^{-1} phosphate buffer solution of pH 7.0 or a 0.1 mol l^{-1} Britton–Robinson buffer solution were used as the supporting electrolytes. Other solvents and chemicals used were of analytical reagent grade and water was obtained from a Millipore Milli-Q purification system. Multi-wall carbon nanotubes (MWCNTs, 30 ± 15 nm Ø), with a 95% purity were obtained from NanoLab (Brighton, MA), and were used without any pretreatment.

2.3. Procedures

2.3.1. Preparation of the CNTs-modified GCE

Prior to the modification, the glassy carbon electrode surface was polished with 0.3 μm alumina slurries, rinsed thoroughly with double distilled water, sonicated 30 s into water and 30 s into acetone, and dried in air. One milligram of CNTs was dispersed with the aid of ultrasonic stirring for 45 min in an aqueous 0.1% Nafion solution. A 10 μl aliquot of this dispersion was dropped on the GC electrode surface and then the solvent was evaporated under an infrared heat lamp.

2.3.2. HPLC with amperometric detection at the CNT-GCE

Chromatographic separation of mixtures of estrogenic and xenoestrogenic compounds were performed using a 50:50 acetonitrile–0.05 mol l^{-1} phosphate buffer of pH 7.0 as the mobile phase, which was previously filtered through a 0.1 μm membrane. A flow rate of 0.8 ml min^{-1} and an injection volume of 50 μl were used. A detection potential of +0.7 V versus Ag/AgCl was applied.

2.3.3. Determination of estrogenic phenols in water samples

Water (500 ml) spiked with bisphenol A, 2,3-dimethylphenol, 17α-ethynylestradiol and 4-terbutylphenol, at a 14 nmol l^{-1} concentration level for each compound, was treated with 1% methanol and acidified to pH 6 with HCl. Then, the sample was passed through C_{18} and styrene divinyl benzene (SDB) disks which were previously conditioned with 10 ml acetonitrile, 10 ml methanol and 20 ml distilled water successively. The C_{18} disk was set on top of the SDB disk; the sample was percolated at a flow rate of 50 ml min^{-1}, and eluted with three portions of 3.0 ml acetonitrile. The SPE eluate was evaporated to dryness under nitrogen atmosphere and the dried residue was reconstituted in 500 μl of acetonitrile.

3. Results and discussion

3.1. Voltammetric behaviour of phenolic estrogenic compounds at CNT-GCE

Fig. 1 shows the comparison of cyclic voltammograms obtained at a CNT-GCE and at an unmodified GCE for 1.0×10^{-4} mol l^{-1} solutions of OPP (A), BPA (B) and NP (C) in 0.05 mol l^{-1} phosphate buffer of pH 7.0. As it can be seen, OPP and BPA exhibit well-defined oxidation peaks at +575 mV (OPP) and +590 mV (BPA) versus Ag/AgCl, at the CNT-GCE, whose peak currents are considerably larger than those obtained at the bare GCE. Moreover, a slight potential shift towards less positive potentials is also observed with the CNT-GCE (see Table 1). In addition, the cyclic voltammogram for OPP showed a small cathodic peak at +267 mV preceded by a shoulder at +350 mV. Background voltammograms (dotted line) showed a slightly higher capacitive current at the CNT-GCE, which becomes more evident at more positive potential values. However, at the potential values at which the oxidation peaks are developed, the difference in capacitive current between both electrodes is practically negligible. On the contrary to that observed for OPP and BPA, the oxidation peak obtained for NP at the CNT-GCE, with an E_p value of +606 mV, was poorly defined and the peak current was smaller than that at the bare GCE.

Table 1
Peak potential values (V) and current densities per concentration unit (μA cm^{-2} mol^{-1} l) (in brackets) for the voltammetric oxidation of some phenolic xenoestrogens at different electrode materials

Electrode	BPA	OPP	NP
CNT-GCE	+0.59[a] (1.0×10^6)	+0.58[a] (1.1×10^6)	+0.60[a] (2.1×10^5)
GCE	+0.62[a] (3.5×10^5)	+0.65[a] (3.5×10^5)	+0.60[a] (3.2×10^5)
PtE [19]	+0.90[b] (1.0×10^5)		+1.05[b] (1.7×10^5)
CPE	+0.60[a] (4.1×10^5)	+0.61[a] (6.1×10^5)	+0.59[a] (4.2×10^5)
CFE [31]	+0.54[a] (3.8×10^6)	+0.60[a] (2.2×10^6)	+0.51[a] (9.3×10^6)

Peak potentials obtained by CV vs. Ag/AgCl.
[a] 0.05 mol l^{-1} PBS pH 7.0.
[b] 0.05 mol l^{-1} TBAP/H_2O/acetonitrile (50:50).

Cyclic voltammograms recorded for other phenolic endocrine disruptors and estrogenic hormones: 2,3-dimethylphenol (DMP), 4-terbutylphenol (TBP), 17α-ethynylestradiol (EE2), β-estradiol (E2) and estriol (E3), at both CNT-GCE and unmodified GCE, are displayed in Fig. 2. As it can be seen,

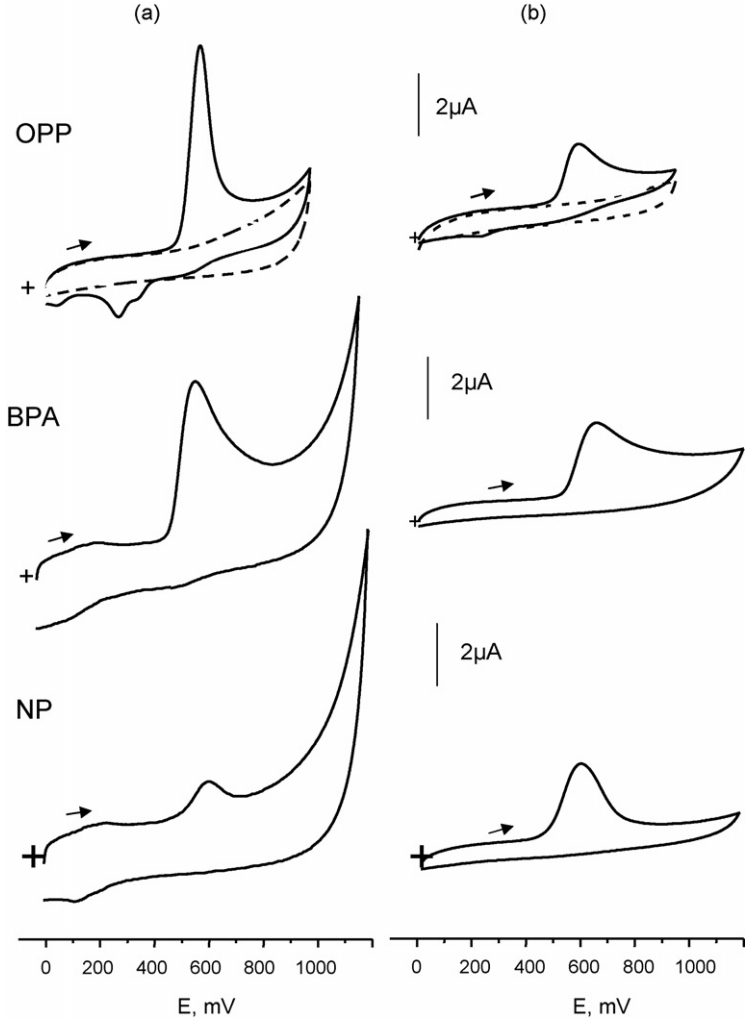


Fig. 1. Cyclic voltammograms at a CNT-GCE (a) and at a bare GCE (b) for 1.0×10^{-4} mol l^{-1} 4-hydroxybiphenyl (OPP), bisphenol A (BPA) and 4-nonylphenol (NP) in 0.05 mol l^{-1} phosphate buffer solution of pH 7.0. (- - -) Background voltammograms; $v = 50$ mV s^{-1}.

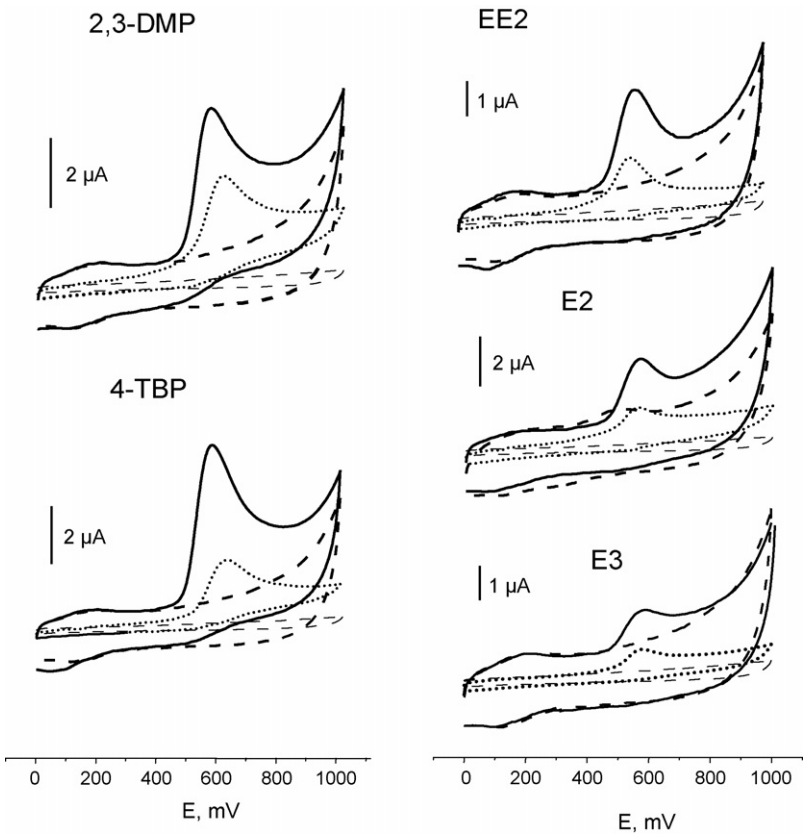


Fig. 2. Cyclic voltammograms at a CNT-GCE (—) and at a bare GCE (···) for 1.0×10^{-4} mol l^{-1} 2,3-dimethylphenol (2,3-DMP), 4-tertbutylphenol (4-TBP), 17α-ethynylestradiol (EE2), β-estradiol (E2) and estriol (E3) in 0.05 mol l^{-1} phosphate buffer solution of pH 7.0; (- - -) and (– – –) background voltammograms at CNT-GCE and GCE, respectively.

modification of the electrode surface with CNTs produced an enhancement of the electrochemical oxidation response for these compounds, particularly in the case of DMP and TBP.

Voltammetric parameters for OPP, BPA and NP at the CNT-GCE were also compared with those experimentally obtained or reported in the literature using other different electrode materials (Table 1). The structures of these phenols are presented in Fig. 3. BPA also showed an irreversible behaviour at Pt, carbon felt (CF) or carbon paste (CP) electrodes, the oxidation process involving one phenol moiety of the molecule with an overall transfer of two electrons and two protons followed by dimerization of the phenoxonium ion formed [19]. A similar irreversible behaviour is found for NP, which was also observed at CF [31], CP and Pt [32] electrodes. The more reversible electrochemical behaviour of OPP at the CNT-GCE was similar to that observed at other electrodes such as CF [31] or CP, and can be attributed to the oxidation of the phenolic compound to the corresponding quinone, which is subsequently reduced in the cathodic sweep. The oxidation peak potential values obtained by cyclic voltammetry, as well as the current density values per concentration unit ($I_p = i_p/AC$, where i_p is the oxidation peak current in μA, A the geometric electrode surface area in cm^2 and C is the concentration of the phenolic compound in mol l^{-1}) are summarized in Table 1. As it can be seen, the E_p values for each compound are relatively similar at the different electrode materials in phosphate buffer solution of pH 7.0. However, the current densities calculated at the CNT-GCE for BPA and OPP are approximately one order of magnitude higher than those obtained at bare GC, Pt or CP electrodes, and similar to those observed at carbon felt electrodes, which are quasi-three-dimensional electrodes with a high surface area at which practically quantitative electrolysis of the compounds is produced [31]. The enhanced current density obtained at the CNT-GCE is attributable to the electrocatalytic effect caused by CNTs towards the oxidation processes of the phenolic compounds, which is due to the structural characteristics and high conductivity of this material [26].

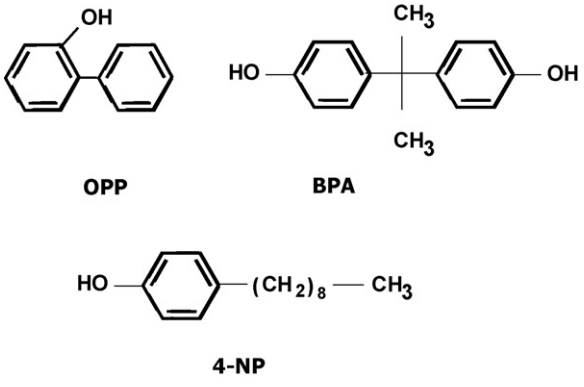


Fig. 3. Chemical structures of 2-hydroxybiphenyl (OPP), bisphenol A (BPA) and 4-nonylphenol (NP).

Regarding NP, the differences in its voltammetric behaviour with respect to BPA and OPP must be commented. As observed in Table 1, modification of the electrode surface with CNTs did not give rise to an enhancement in the current density when compared with other electrode materials, and, indeed this parameter was much lower that that measured at carbon felt electrodes. However, we have demonstrated recently [31] that the oxidation of NP at the CF electrode leads to a practically quantitative transformation of the compound to an NP oxidation product polymerized film which is accumulated on the electrode surface. The high tendency of NP to form this polymerized film can explain the inhibition of the electrocatalytic properties of the CNTs layer.

The effect of pH on oxidation peak current and peak potential values for OPP, BPA and NP at the CNT-GCE was checked over the pH range 2.0–12.0 using 0.1 mol l^{-1} Britton–Robinson buffer as supporting electrolyte. As expected, peak potential values shifted towards less positive values when the pH increased as it is usual for the oxidation of phenolic compounds. Fig. 4 shows the linear dependence ($r = 0.999$) found for OPP between pH 2.0 and 10.0, with a slope value of −61.7 mV. In the case of NP, this linear behaviour was observed between pH 2.0 and 7.0 ($r = 0.998$), with a slope value of −56.8 mV. These slopes values are consistent with the exchange of two electrons and two protons in the electrochemical oxidation of these compounds at the CNT-GCE. In the case of BPA, a linear E_p versus pH dependence was also observed over the 2.0–10.0 pH range ($r = 0.994$), but the slope value, −42.9 mV, moves away from the theoretical value, thus indicating a somewhat different oxidation mechanism as commented before. The intercept values of the two linear ranges obtained from the corresponding E_p versus pH plots (see Fig. 4 for OPP) should be related to the pK_a values of the phenolic compounds. So, the intercepts were 10.0, 9.9 and 7.0 for OPP, BPA and NP, respectively, which agree fairly well with literature data for their respective pK_a values (10.01, 9.8 and 7.2) [33,34]. On the other hand, peak current values also showed a decrease with increasing pH, similarly to that reported for phenolic compounds at different electrode materials. Therefore, in order to achieve a compromise between acceptably large peak currents and low detection potentials, a pH value of 7.0 was selected for the amperometric detection of these compounds.

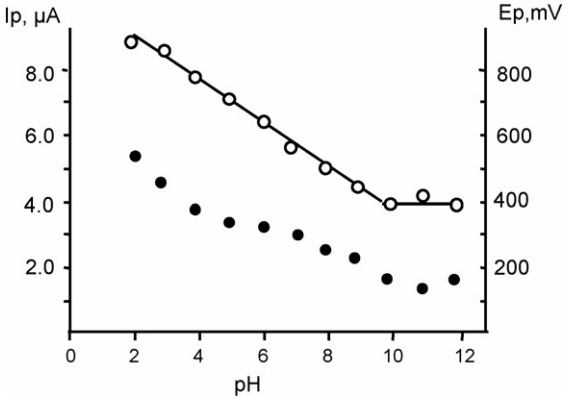


Fig. 4. Influence of pH on peak current (●) and peak potential (◯) values obtained by cyclic voltammetry at a CNT-GCE for 1.0×10^{-4} mol l^{-1} OPP.

The influence of the potential scan rate on the OPP, BPA and NP oxidation peaks was tested over the 2–5000 mV s^{-1} range, and for a phenolic estrogenic compound concentration of 5.0×10^{-5} mol l^{-1} in 0.05 mol l^{-1} phosphate buffer of pH 7.0. For BPA and NP, E_p values shifted to more positive values as the scan rate increased. However, OPP E_p values remained practically constant (with an absolute difference of 23 mV) between 2 and 100 mV s^{-1}, which is in good agreement with the more reversible electrochemical behaviour observed for this compound. Furthermore, a linear i_p versus $v^{1/2}$ plot was obtained for OPP in this scan rate range ($r = 0.997$), which is consistent with a diffusion control of the oxidation process. Similarly, a linear i_p versus $v^{1/2}$ plot was also obtained for NP ($r = 0.992$) in the 2–100 mV s^{-1} range. However, the use of faster scan rates for both compounds produced a deviation from this linearity, with higher i_p values with increasing v, which suggested the contribution of adsorption at these higher v values. In the case of BPA, a linear i_p versus v plot ($r = 0.997$) was obtained over the 2–2000 mV s^{-1}, with a slope value of the log i_p versus log v plot of 1.2. These results revealed that an adsorption process is involved in the electrochemical oxidation of BPA at CNT-GCEs.

In conclusion, it can be said that the oxidation mechanisms of OPP, BPA and NP at CNT-GCE show some differences attributables to their different structure. So, OPP exhibits a behaviour typical of the oxidation of phenolic compounds to the corresponding quinone, which is reduced in the reverse sweep. Furthermore, the oxidation current has demonstrated to be diffusion controlled. Concerning NP, its structure permits the formation of a quinoid derivative, but not the quinone because there is only an aromatic ring p-substituted. Such an oxidation process is also diffusion controlled. After this process, the quinoid derivative can suffer polymerization at the electrode surface. In the case of BPA, its structure does not allow the formation of a double bond to form the quinoid derivative. Therefore, the only possibility is polymerization after formation of the phenoxonium ion. This is supported by the adsorptive behaviour observed for this compound when the scan rate is varied.

3.2. Amperometric detection at the CNT-GCE

Flow injection with amperometric detection at the CNT-GCE, using OPP, BPA and NP as target compounds, was evaluated. Firstly, hydrodynamic voltammograms were constructed by measuring the corresponding peak current values at different applied potentials, after injection of 50-μl aliquots of 1.0×10^{-4} mol l^{-1} OPP, BPA or NP solutions into a carrier solution consisting of a 0.05 mol l^{-1} phosphate buffer of pH 7.0–acetonitrile (50:50) mixture (Fig. 5). This carrier solution was selected because it constituted an appropriate mobile phase for the chromatographic separation of estrogenic and xenoestrogenic compounds (see below). As it can be observed, well-defined sigmoidal shape plots were obtained for the three compounds, with peak current "plateaux" for potential values higher than +0.7 V. Moreover, very stable background currents were found over the whole potential range checked. According to these results, +700 mV was selected as the potential value to be applied for the amperometric detection of the phenolic

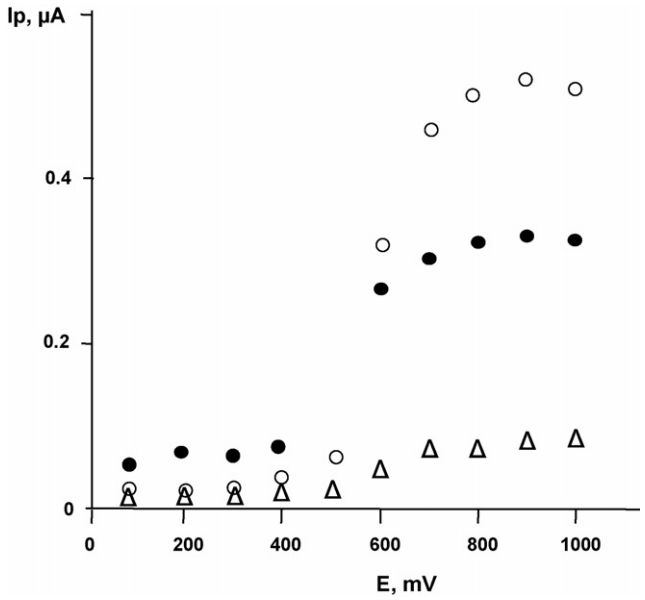


Fig. 5. Hydrodynamic voltammograms obtained by flow injection with amperometric detection at a CNT-GCE after injection of 50 μl aliquots of 1.0×10^{-4} mol l^{-1} OPP (◯), BPA (●) and NP (△) solutions into a carrier consisting of a 0.05 mol l^{-1} phosphate buffer of pH 7.0–acetonitrile (50:50) mixture.

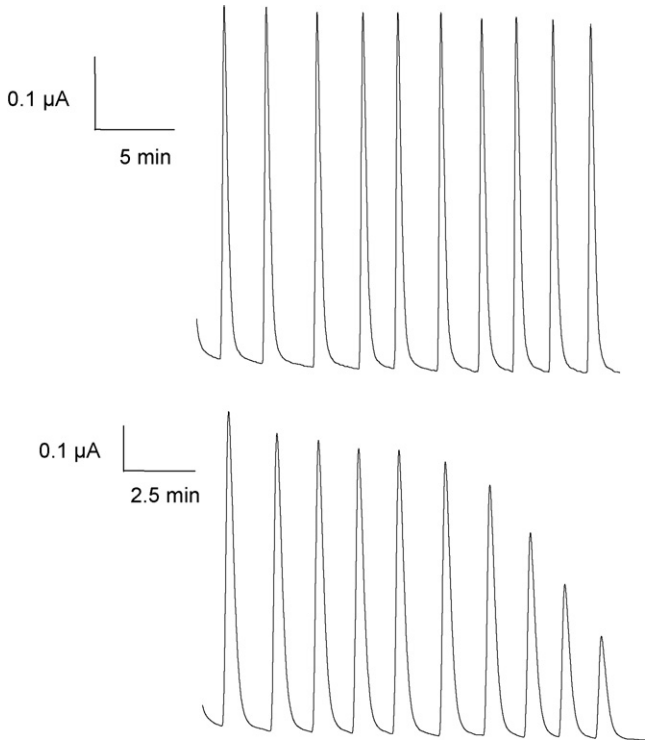


Fig. 6. Successive flow injection amperometric responses obtained at a CNT-GCE (a) and at a bare GCE (b) after injections of 50 μl of 1.0×10^{-4} mol l^{-1} OPP. Carrier solution as in Fig. 4; flow rate, 0.6 ml min^{-1}.

estrogenic compounds at CNT-GCE. It should be remarked that this value is considerably less positive than that reported in the literature for the amperometric detection of these phenolic compounds. For example, it is 300 mV less positive than that used for the determination of a mixture of estrogenic phenols in river waters at a conventional glassy carbon electrode, after a chromatographic separation [18].

The repeatability of the amperometric flow responses at this potential value was checked by successive injections of 50 μl of 1.0×10^{-4} mol l^{-1} OPP, BPA and NP and compared with that obtained at a bare GCE. As an example, fiagrams obtained for ten successive injections of OPP are displayed in Fig. 6. As it can be seen, reproducible amperometric signals were achieved using the CNT-GCE, with a R.S.D. value for i_p of 1.7% ($n = 10$). However, a continuous decrease of i_p is observed at the unmodified electrode, as a consequence of the surface fouling by the electrode reaction products under potentiostatic conditions. The anti-fouling properties of CNT-modified electrode surfaces are so corroborated. Similar results were obtained for BPA and NP, with R.S.D. values for i_p ($n = 10$) of 2.2 and 2.5%, respectively.

3.3. LC–EC detection at the CNT-GCE

HPLC with isocratic elution using a C_{18} reversed-phase column was employed to develop a method for the determination of several estrogenic compounds. The use of this stationary phase was recommended in the literature for the chromatographic separation of this type of compounds [16–18]. The mobile phase used to investigate the separation of mixtures of these compounds consisted of an acetonitrile:0.05 mol l^{-1} phosphate buffer solution of pH 7.0. Firstly, the influence of the acetonitrile percentage on the separation of BPA, DMP, EE2 and TBP, which were selected because of their differences in polarity, was evaluated. As expected, both the retention time and the peak current for these compounds decreased with the increase in the acetonitrile percentage over the whole range studied (10–60%, v/v). As a compromise between adequate retention times for the less polar compounds and a good sensitivity, when peak areas are measured, a mobile phase with a 50% (v/v) acetonitrile was selected.

The effect of the mobile phase flow rate was tested in the 0.2–1.0 ml min^{-1} range. As expected, both retention time and peak width decreased as the flow rate increased for all the compounds. However, a lower resolution was observed for the higher flow rates. Therefore, as a compromise, a flow rate of 0.6 ml min^{-1} was chosen for further work. Under these conditions, retention times of 9.5, 10.4, 12.5 and 16.7 min were obtained for BPA, DMP, EE2 and TBP, respectively. Fig. 7a shows a chromatogram obtained for a mixture of these compounds at a concentration of 1.0×10^{-5} mol l^{-1} each. Although there is not baseline resolution for BPA and DMP, their correct quantification is possible, as it will be demonstrated below. Fig. 7b shows the chromatogram for a mixture of six estrogens and xenoestrogens at the same concentration level. As it can be observed an adequate resolution, as well as retention times in a convenient range were achieved.

Calibration graphs constructed for BPA, DMP, EE2 and TBP using the peak areas as the analytical signals, exhibited the analytical characteristics summarized in Table 2. The detection limits were calculated according to the $3s_b/m$ criterion, where m is the slope of the calibration graph for each analyte and s_b was

Table 2
Analytical characteristics of the calibration graphs for different phenolic estrogens obtained by HPLC with amperometric detection at CNT-GCE

Species	Linear range (μM)	Slope (μC M^{-1} × 10^5)	Intercept (μC)	r	R.S.D.[a] (%)	Detection limit[a] (μM)
BPA	0.3–100	1.53 ± 0.02	−0.09 ± 0.08	0.999	3.4	0.098
DMP	0.5–100	1.45 ± 0.03	0.1 ± 0.1	0.996	2.9	0.171
EE2	1.0–100	0.70 ± 0.01	0.10 ± 0.07	0.994	3.2	0.340
TBP	1.0–100	0.82 ± 0.02	0.07 ± 0.04	0.998	3.0	0.308

[a] For peak areas (n = 5) at a concentration of 1.0×10^{-5} mol l^{-1} each.

estimated as the standard deviation (n = 10) of the peak area values obtained for the lowest concentration of the corresponding range of linearity. Using this criterion, detection limits ranging between 98 nM (BPA) and 340 nM (EE2) were achieved. The detection limit obtained for BPA can be compared with those reported in the literature for this compound using fluorescence [14] and MS [11] detection. By applying the S/N = 3 criterion, the limits of detection reported were 1 and 0.1 ng ml^{-1}, respectively. Using this same criterion, the detection limit for BPA with amperometric detection at the CNT-GCE is 0.6 ng ml^{-1}, which is comparable to that obtained using the much more expensive MS detection mode, thus demonstrating the suitability of the electrochemical approach at the modified electrode for the determination of low concentrations of phenolic estrogens.

The usefulness of the chromatographic method with amperometric detection at the CNT-GCE for the determination of phenolic estrogens was evaluated by analysing different water samples spiked with these compounds. The sample treatment described in Section 2 is a modification of that proposed by Cargouët et al. for the treatment of surface water for the determination of estrogenic compounds by GC–MS [35]. Underground well water and tap water samples were adequately collected and stored at 4 °C, and extraction of phenols was accomplished in a maximum period of time of 48 h. These water samples were spiked with BPA, DMP, EE2 and TBP at a 14 nmol l^{-1} concentration level of each compound. Solid phase extraction using C_{18} and SDB disks was employed in order to extract non-polar and polar or moderately polar compounds, respectively. Moreover, a blank sample prepared with spiked Milli-Q water was also analyzed. As described in Section 2, a 500-ml sample volume was processed through the disks in all cases, and eluted with acetonitrile. Aliquots of 50 μl from the analytical solution in acetonitrile containing the phenolic estrogenic compounds were injected into the chromatographic system. The results obtained are summarized in Table 3. As it can be seen, recoveries were satisfactory, independently of the type of water analyzed, thus demonstrating the suitability of the method for the determination of phenolic estrogenic compounds in this type of samples.

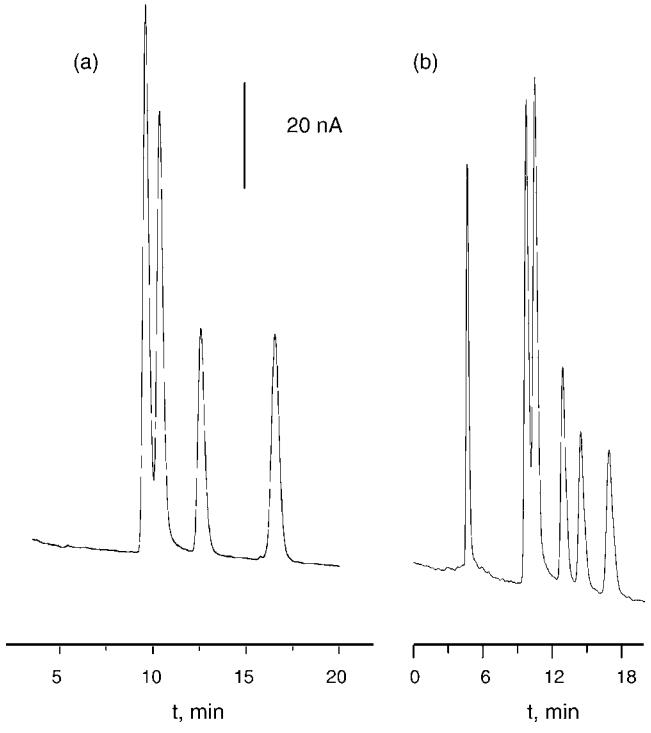


Fig. 7. Chromatograms obtained with amperometric detection at a CNT-GCE for a mixture of BPA, DMP, EE2 and TBP (a), and of E3, BPA, E2, EE2, E1 and TBP (b) at a concentration of 1.0×10^{-5} mol l^{-1} each. Mobile phase, 50:50 acetonitrile–0.05 mol l^{-1} phosphate buffer of pH 7.0; flow rate, 0.6 ml min^{-1}.

Table 3
Recovery studies of EDCs in spiked water samples using HPLC with amperometric detection at CNT-GCE

Compound	Well water	Tap water	Milli-Q water
BPA	97 ± 10	98 ± 2	102 ± 8
DMP	100 ± 6	93 ± 7	93 ± 7
EE2	88 ± 6	100 ± 6	100 ± 6
TBP	96 ± 1	98 ± 7	99 ± 3

Mean values from three determinations.

4. Conclusions

Modification of glassy carbon electrodes with carbon nanotubes produced an enhancement of the electrochemical oxidation responses obtained for phenolic estrogenic compounds. This allowed amperometric detection of these compounds at the CNT-GCE to be performed at an applied potential considerably lower than those previously reported using conventional electrode materials. Moreover, no significant fouling of the modified electrode surface was observed. This improved electroanalytical performance was profited to develop an HPLC–EC method with a high sensitivity for the determination of several estrogenic compounds in different water samples.

Acknowledgements

Financial support from the Ministerio de Educación y Ciencia (Project BQU 2003-00365) and PR27/05-13860-BSCH is gratefully acknowledged

References

[1] C. Sonnenschein, A.M. Soto, J. Steroid Biochem. Mol. Biol. 65 (1998) 143.
[2] H. Fang, W.D. Tong, L.M. Shi, R. Blair, R. Perkins, W. Branham, B.S. Hass, Q. Xie, S.L. Dial, C.L. Moland, D.M. Sheehan, Chem. Res. Toxicol. 14 (2001) 280.
[3] M. Petrovic, E. Eljarrat, M.J.L. de Alda, D. Barceló, Trends Anal. Chem. 20 (2001) 637.
[4] A. Boenke, C. Searle, T. Karjalainen, Anal. Chim. Acta 473 (2002) 161.
[5] M.J. Bartels, K.A. Brzak, G.A. Bormett, J. Chromatogr. B 703 (1997) 97.
[6] J.H. Kim, Anal. Sci. Technol. 12 (1999) 248.
[7] H.G.J. Mol, S. Sunarto, O.M. Steijger, J. Chromatogr. A 879 (2000) 97.
[8] S.D. Richardson, Anal. Chem. 74 (2002) 2719.
[9] R.B. Geerdink, W.M.A. Niessen, U.A.T. Brinkman, J. Chromatogr. A 975 (2002) 65.
[10] A.C. Bellfroid, A. Van der Horst, A.D. Vethaak, A.J. Schafer, G.B.J. Rijs, J. Wegener, W.P. Cofino, Sci. Total Environ. 225 (1999) 101.
[11] S.N. Pedersen, C. Lindholst, J. Chromatogr. A 864 (1999) 17.
[12] T. Benijts, W. Lambert, A. De Leenheer, Anal. Chem. 76 (2004) 704.
[13] N. Yoshioka, Y. Akiyama, K. Teranishi, J. Chromatogr. A 1022 (2004) 145.
[14] B. Saad, N.H. Haniff, M.I. Saleh, N.H. Hashim, A. Abu, N. Ali, Food Chem. 84 (2004) 313.
[15] R.D. Thompson, J. AOAC Int. 84 (2001) 815.
[16] K. Inoue, K. Kato, Y. Yoshimura, T. Makino, H. Nakazawa, J. Chromatogr. B 749 (2003) 17.
[17] K. Ouchi, S. Watanabe, J. Chromatogr. B 780 (2002) 365.
[18] A. Peñalver, E. Pocurull, F. Borrull, R.M. Marcé, J. Chromatogr. A 964 (2002) 153.
[19] M.M. Ngundi, O.A. Sadik, T. Yamagushi, S.-I. Suye, Electrochem. Commun. 5 (2003) 61.
[20] H. Kuramitz, Y. Nakata, M. Kawasaki, S. Tanaka, Chemosphere 45 (2001) 37.
[21] H. Kuramitz, M. Matsushita, S. Tanaka, Water Res. 38 (2004) 2331.
[22] H. Kuramitz, J. Saitoh, T. Hattori, S. Tanaka, Water Res. 36 (2002) 3323.
[23] E. Dempsey, D. Diamond, A. Collier, Biosens. Bioelectron. 20 (2004) 367.
[24] A. Merkoci, M. Pumera, X. Llopis, B. Pérez, M. del Valle, S. Alegret, Trends Anal. Chem. 24 (2005) 826.
[25] J. Wang, M. Li, Z. Shi, N. Li, Z. Gu, Electroanalysis 14 (2002) 225.
[26] P.I. Iotov, S.V. Kalcheva, J. Electroanal. Chem. 442 (1998) 19.
[27] J. Wang, R.P. Deo, M. Musameh, Electroanalysis 15 (2003) 1830.
[28] P. Zhang, F.-H. Wu, G.-C. Zhao, X.-W. Wei, Bioelectrochemistry 67 (2005) 109.
[29] M. Musameh, J. Wang, A. Merkoci, Y. Lin, Electrochem. Commun. 4 (2002) 743.
[30] J. Manso, L. Agüí, P. Yáñez-Sedeño, J.M. Pingarrón, Anal. Lett. 37 (2004) 887.
[31] L. Agüí, P. Yáñez-Sedeño, J.M. Pingarrón, Electrochim. Acta 51 (2006) 2565.
[32] O. Hammerich, B. Svensmark, in: H. Lund, M.M. Baizer (Eds.), Organic Electrochemistry. An Introduction and a Guide, Marcel Dekker, Inc., New York, 1991, p. 616.
[33] J.A. Zimmermann, J.M. Ballard, H. Wang, A. Wu, K.A. Gallager, Int. J. Pharm. 267 (2003) 113.
[34] R. Carabias-Martínez, E. Rodríguez-Gonzalo, P. Revilla-Ruiz, J. Chromatogr. A 1056 (2004) 131.
[35] M. Cargouët, D. Perdiz, A. Mouatassim-Souali, S. Tamisier-Karolak, Y. Levi, Sci. Total Environ. 324 (2004) 55.